

**GROWTH. KNOWLEDGE. NEW GENERATION.**  
NEW CONCEPTS • MORE INTERACTION • [WWW.GPD.FI](http://WWW.GPD.FI)



## CONFERENCE PROCEEDINGS

**#GPD2017**

**ALL EYES  
ON GLASS.**

**GLASS PERFORMANCE DAYS 2017  
JUNE 28 - 30, 2017. TAMPERE, FINLAND**

1 2 3 4 5 6 7 8 9 10 11 12 13 14 15 16 17 18 19 20 21 22 23 24 25





# CONFERENCE PROCEEDINGS

#GPD2017

**ALL EYES  
ON GLASS.**

**GLASS PERFORMANCE DAYS 2017  
JUNE 28 - 30, 2017. TAMPERE, FINLAND**



The authors of signed contributions are solely responsible for the statement and opinions expressed in them.

Copyright 2017  
by Glass Performance Days  
Glaston Finland Oy  
All rights reserved

Glass Processing Days, Glass Performance Days and the GPD logo are trademarks of Glaston Finland Oy

[www.gpd.fi](http://www.gpd.fi)

Published by  
Glass Performance Days

Glaston Finland Oy  
Vehmaistenkatu 5  
33730 Tampere  
Tel. + 358 10 500 500  
Fax. +358 10 500 6190  
[www.glaston.net](http://www.glaston.net)

ISBN: 978-952-5836-06-6  
Layout Jenga Markkinointiviestintä  
Printed in Finland  
Hämeen kirjapaino, Tampere



## A Quarter Century of Glass Innovation

Welcome to the 25th Anniversary of the Glass Performance Days. Celebrating 25 years could mean celebrating tradition. In a way we do that too, but on the other hand our tradition is really one of change and constant development. The escalating clock-speed of progress in the glass industry is of course always well reflected in its leading Conference. We can really claim to have been an active advocate of change and the adoption of new technology all along. In saying that, we do not refer to the Conference Organizers as a body, but to our entire global industry and its pioneering personalities – GPD Session Chairmen, Program Committee, lecturers and participants. Other conferences have followed in our proven GPD footsteps, but we can proudly claim to have held our position as the leading catalyst in the business – for a Quarter Century!

Our June 28-30, 2017 Conference again pushes the spirit of development further towards new horizons. The contents have been renewed, the modular structure of the Conference broadened and the very concept of this Glass Summit has been remodeled to reflect the pace of our times. Cases in point: The Step Change Approach for attracting startup organizations, the Ambassadorial Program to transfer technology and learning between generations and the Open Space Conference Concept, including a New Venue and new conferencing technology to increase awareness and involvement of participants. No more closed doors! Many more open (glass) windows.

The way in which we aim to bring together proven glass specialists with newcomers, mentors and investors is an innovation in itself. We apply the experiences of the dynamic world of information technology in an application for the art of glass construction. The sky is the limit!

Yours truly,

Jorma Vitkala  
Chairman of the Organizing Committee of  
the Glass Performance Days

## Platinum sponsors



## Gold sponsors



## Silver sponsors



The conference is supported by the following trade fairs and associations:



[www.glasstec-online.com](http://www.glasstec-online.com)

[www.bau-muenchen.com](http://www.bau-muenchen.com)



## GPD Glass Performance Days 2017 • Workshops • June 27, TUESDAY

|   |  |  |  |
|---|--|--|--|
| 8:00  | Registration   |  |  |
| <b>WORKSHOP 1</b>   | <b>WORKSHOP 2</b>  | <b>WORKSHOP 3</b>  |  |
| 9:00–17:00  | 9:00–17:00   | 9:00–17:00   |  |
| <b>What did we get during last 25 years in the flat glass industry (1992–2017) and what we could expect for tomorrow?</b><br>Bernard Jean Savaëte, BJS. Différences | <b>Critical issues in glass chemical strengthening</b><br>Guglielmo Macrelli, Isoclima SpA   | <b>Optimizing Cutting and Grinding</b><br>Peter Pokoern, Bohle AG<br>Michael Emonds, Aachener Chemische Werk   |  |
| <b>WORKSHOP 4</b>   | <b>WORKSHOP 5</b>  | <b>WORKSHOP 6 (Held in Helsinki)</b>   |  |
| 9:00–18:00  | 9:00–17:00   | 9:00–18:00   |  |
| <b>An introduction &amp; advanced instruction on the vacuum insulated glazing</b><br>Cenk Kocer, University of Sydney   | <b>Architectural Glass Quality</b><br>Mikko Suomi, Ayrox<br>Janne Aittokallio, Glaston<br>Riku Färm, Glaston<br>Mauri Saksala, Sparklike<br>Markus Klein, Sugarus GmbH | <b>Facades in High Rise Buildings – Architects &amp; Structural Engineers</b><br>Leon Jacob, Jacob & Associates Pty Ltd.<br>Peter Smithson and Mr. Oliver Ng, BG & E Facades<br>Keith Boswell and Ms. Lisa Follman SOM<br>James Carpenter James Carpenter Design Associates Inc.<br>Thomas Henriksen Mott McDonald |  |

## GPD Glass Performance Days 2017 • Workshops • June 28, WEDNESDAY

|   |   |  |   |  |  |
|---|---|--|---|--|--|
| 8:00  | Registration  |  |   |  |  |
| <b>WORKSHOP 1</b>   | <b>WORKSHOP 2</b>   | <b>WORKSHOP 3</b>  | <b>WORKSHOP 4</b>   | <b>WORKSHOP 5</b>  |  |
| 9:00–13:00  | 9:00–15:00  | 9:00–14:00   | 9:00–15:00  | 9:00–14:00   |  |
| <b>The introduction to glass tempering process and properties of tempered glass</b><br>Antti Aronen, University of Sydney   | <b>Glass surface: Alterations and treatment</b><br>Michael Emonds, Chemetall GmbH (part of BASF group)<br>Edda Rädlein, TU Ilmenau<br>Reinhold Senft, Grafotec Spray Systems GmbH   | <b>Testing, rheological modelling and design of interlayer materials in laminated safety glass</b><br>Miriam Schuster & Michael Kraus, Technical University Darmstadt & University of German Armed Forces Munich | <b>Anisotropy</b><br>Glass Innovation Institute:<br>Martin Regon, Olavi Uusitalo<br>Jorma Vitkala | <b>Serving Clients and Community through International Standards for Quality and Environment (ISO-9001, ISO-14001)</b><br>Lisett Guevara Gulnick, McGrory Glass, Inc.  |  |
| <b>WORKSHOP 6</b>   | <b>WORKSHOP 7</b>   |  | <b>WORKSHOP 8</b>   | <b>WORKSHOP 9</b>  |  |
| 9:00–13:00  | 9:00–15:40  |  | 9:00–15:00  | 9:00–15:00   |  |
| <b>Glass Design: A comparison of standards</b><br>Urmilla Sowell, Glass Association of North America<br>Bill Lingnell, Lingnell Consulting<br>Julia Schimmelpenningh, Eastman Chemicals<br>Stephen Morse, Texas Tech University<br>Geralt Siebert, Uni. of German Armed Forces Munich | <b>Advances in Coatings for Glass and Plastics</b><br>Dmitriy Bernt, NSG Pilkinton Glass<br>Sener Oktik, SISECAM<br>Wang Shijie, Institute of Materials Research and Engineering Singapore<br>Guenter Bräuer, Fraunhofer IST<br>Karel Spee, Solliance/TNO<br>Gerhard Schottner, Fraunhofer ISC<br>Georg Ockefuss, Viavi Solutions<br>Koichi Suzuki, Fraunhofer FEP & SurFtech Transnational Co., Ltd. |  | <b>How will UX Design effect Automotive Glazing?</b><br>Michael Robinson, ED Design srl.          | <b>Innovative Structural Silicone Bonding Technologies: Optimizing Transparency and Performance in Facade Systems</b><br>Larry Carbary & Valérie Hayez, Dow Corning Corporation<br>Lisa Rammig, Eckersley O'Callaghan<br>Bruno Kassnel-Henneberg, Glas Troesch<br>Michael Ludvik, M.Ludvik & Co. |  |

## Opening and Keynote speakers JUNE 28, 16:00, Tähti Areena

### Jorma Vitkala

Chairman of the Organizing Committee

### James Carpenter

Founder, James Carpenter Design Associates Inc.

### Michael Robinson

CEO & Design Director, ED Design srl.

### Bernard Savaëte

Founder, BJS. Différences

### Esko Aho

Executive Chairman of the Board, East Office of Finnish Industries, Former Prime Minister of Finland

### Peng Shou

CBMC

### Stephanie Akkaoui Hughes

Founder, AKKA Architects

Panel Discussion

20:00 Get Together party, Tähti Areena

# GPD Glass Performance Days 2017 • Program • June 29, THURSDAY

|                |  |   |  |
|----------------|--|---|--|
| 8:00           | Registration   |   |  |
|                | <b>Glass &amp; Sustainability</b>  | <b>Facade Engineering</b>   | <b>Structural Glass Applications</b>   |
|                | <b>Session Chairs:</b><br>Wim Stevels, Eastman Chemical Company  | <b>Session Chairs:</b><br>Lawrence Carbarry,<br>Dow Corning Corporation<br>Graham Dodd, Arup Materials Consulting   | <b>Session Chairs:</b><br>Ingo Stelzer, Kuraray<br>Michael Ludvik, M. Ludvik & Co  |
| 9:00           | <b>Active BIPV Glass facades: current trends of innovation, between new semantics and technological possibilities</b> Erika Saretta, University of Applied Sciences and Arts of Southern Switzerland | <b>Towards a More Consistent Design of Laminated Glass</b><br>Michael Dunham, Arup  | <b>Shaping Ultra-Thin Glass</b><br>Sophie Pennetier, ARUP  |
| 9:25           | <b>Innovative BIPV façade on administrative building in Klaipeda, Lithuania</b><br>Tomas Lenkimas, Glassbel EU   | <b>Verification of Insulating Glass Units in Modern CW Facades</b><br>Michael Elstner, AGC Interpane  | <b>Probabilistic Study of Wind-Temperature Interaction: An Initial Study Towards Optimized Structural Assessment of Glass Components</b> Manuel Santarsiero, <a href="#">Eckersley O'Callaghan</a> |
| 9:50           | <b>Numerically simulating the impact of hail in photovoltaic</b> Ivo Draganov, University of Ruse  | <b>Next generation calculation method for structural silicone joint dimensioning</b><br>Valerie Hayez, <a href="#">Dow Corning Corporation</a>                  | <b>Glass Constructions Under Extreme Boundary Conditions</b> Barbara Siebert, Dr. Siebert Consulting Engineers   |
| 10:15          | <b>COFFEE BREAK, ONE-ON-ONE MEETINGS</b>   |   |  |
| 11:00          | <b>Thermal and Hygrothermal Performance Monitoring of Advanced Insulation Materials Used in Curtain Wall Spandrel Panels</b><br>Stanley Yee, <a href="#">Dow Corning Corporation</a>                 | <b>Glazed Multilayered Building Envelopes</b><br>Martien Teich, seele GmbH  | <b>Hybrid Glass Structures</b><br>Peter Lenk, Arup   |
| 11:25          | <b>Deconstructing the Thermal Performance of a Window: How to achieve better performing façades</b> Helen Sanders, Technoform Glass Insulation NA, Inc.  | <b>Structural Glass Connections</b><br>Carles Teixidor, Bellapart SAU   | <b>New Concept of Horizontal Structural Elements in Glass: Self bearing "Pi" Shape Plate.</b> Jesús M. Cerezo, ENAR, ENVOLVENTES ARQUITECTONICAS   |
| 11:50          | <b>Qualifying and quantifying thermal comfort in highly glazed spaces</b><br>Medina Deliahmedova, Lund University  | <b>All-glass Pavilions</b> Geralt Siebert, Uni. of German Armed Forces Munich   | <b>Enabling Crystal Clear Façades</b><br>Valerie Hayez, <a href="#">Dow Corning Corporation</a>  |
| 12:15          | <b>Do's &amp; Don'ts of Building Facades</b><br><b>Session Chairs:</b> Leon Jacob, Jacob Associates  | <b>STEP-CHANGE, LUNCH, ONE-ON-ONE MEETINGS</b>  |  |
| 13:45          | <b>The Building Façade Concept:</b><br>Keith Boswell – SOM Architects  | <b>The Futurium Berlin – Large Scale SSG Rain Screen Facades without Mechanical Restraints: from Design to Installation</b><br>Jan Wurm, Arup                   | <b>Production and Testing of Kiln-Cast Glass Components for an Interlocking, Dry-Assembled Transparent Bridge</b> Telesilla Bristogianni, TU Delft, Faculty of Civil Engineering and Geosciences   |
| 14:10          | <b>The Specifications and Material Compatibility</b> Peter Smithson & Oliver Ng - BG & E Facades Pty. Ltd.   | <b>The Increasing Demand for Cyclone Resistant Glazing Solutions in the Asia-Pacific Region</b> Dario Trabucco, The Council on Tall Buildings and Urban Habitat | <b>The Strength of Aged Glass</b><br>Mauro Overend, University of Cambridge  |
| 14:35          | <b>The Manufacture and Supply of the Façade Components</b> Leon Jacob, Jacob & Associates Pty Ltd.   | <b>Glass Fins with Embedded Titanium Inserts for The Façades of The New Medical School Of Montpellier</b><br>Jordi Torres, Bellapart S.A.U.                     | <b>Sandwich Design of Mechanically Efficient and Structurally Slim Vision Panels</b> Carlos Pascual, University of Cambridge - Glass & Façade Technology Research Group                            |
| 15:00          | <b>COFFEE BREAK, ONE-ON-ONE MEETINGS</b>   |   |  |
| 15:45          | <b>A Case Study of Design and Collaboration</b><br>Ms Lisa Follman - SOM Architects  | <b>Structural Glass in Building Restoration. Europe? S Tower Entrance Hall. Madrid. Spain</b><br>Miguel Núñez, ENAR   | <b>Deformations in Fragments of Tempered Glass - Experimental and Numerical Investigation</b><br>Jens H. Nielsen, Technical University of Denmark  |
| 16:10          | <b>A Case Study – Unitized façade system designed with a highly transparent façade of low G-value combined with blast requirements.</b> Thomas Henriksen, Mott Macdonald                             | <b>Cost and Energy Saving Potential of Glass Façade Construction</b><br>Timo Saukko, Finnglass  | <b>Exploring The Potential of Free Standing Glass Columns Assembled from Stacked Interlocking Cast Elements</b> Telesilla Bristogianni, TU Delft, Faculty of Civil Engineering and Geosciences     |
| 16:35          | <b>Quality Assurance to the Science of Performance and Durable Façades</b><br>Sami Hui, Hong Kong Façade Association   | <b>Channel Glass on Pier 17: A Case Study</b><br>Sameer Kumar, SHoP Architects  | RESERVED   |
| 17:00          | <b>BREAK, ONE TO ONES, HAPPY HOUR</b>  |   |  |
| 19:30<br>23:00 | <b>CONFERENCE DINNER @ Solo Sokos Hotel Torni Tampere, Paja Congress Center</b>  |   |  |

| Research & Development   | Tempering / Preprocessing   | Quality Management  |
|--|---|---|
| <p><b>Session Chairs:</b><br/>Jens Schneider, Darmstadt TU<br/>Jan Belis, Ghent University<br/>Christian Louter, Delft TU</p>  | <p><b>Session Chairs:</b><br/>Francis Serruys,<br/>Saint-Gobain Building Glass Europe<br/>Miika Appelqvist, Glaston Finland Oy</p>                                      | <p><b>Session Chairs:</b><br/>AMETEK Land<br/>FeneTech Inc.</p>   |
| <p><b>Influence of the Distribution of Residual Stress on Strength Tests</b><br/>Jürgen Neugebauer, University of Applied Sciences FH-Joanneum</p>                                       | RESERVED  | <p><b>Roller Wave &amp; Milli Diopter, but what can we see and how does it Look?</b><br/>Hannes Spiss, TNG - Europe</p>   |
| <p><b>Biaxially Curved Glass? Determination of Strength using the Coaxial Double Ring Test</b> Steffen Müller-Braun, TU Darmstadt - Institute of Structural Mechanics And Design</p>     | <p><b>On Safety of Heat-Soaked Thermally Toughened Glass Panes</b><br/>Andreas M Kasper, Saint-Gobain HRDC</p>  | <p><b>The Psychology of Perception, Threshold, And Emotion in Interior Glass Design</b><br/>Jim Gulnick, Mcgrory Glass, Inc.</p>                                      |
| <p><b>Identification of A Rheological Model for Viscoelastic Materials in Structural Engineering</b> Michael Kraus, Uni. of German Armed Forces Munich, Miriam Schuster TU Darmstadt</p> | <p><b>Controlling Anisotropy</b><br/>Francis Serruys, Saint-Gobain Building Glass Europe</p>  | <p><b>Comparison Between Quality Requirements in Norms and Actual Client Expectations</b> Romas Zvirzdinas, GLASSBEL BALTIC UAB</p>                                   |
| <b>COFFEE BREAK, ONE-ON-ONE MEETINGS</b>   |   |   |
| <p><b>Influence of Weathering on Post-Fracture Performance</b><br/>Caroline Butchart, <a href="#">Eckersley O'Callaghan</a></p>  | <p><b>Infrared Temperature Measurement of Thermally Tempered Low Emissivity Glass</b><br/>Mark Bennett, <a href="#">AMETEK Land</a></p>                                 | <p><b>XX(X)L Glass - Quality Control, Logistics &amp; Insurance</b><br/>Dirk Schulte, APG International, Inc.</p>   |
| <p><b>Full-surface and non-destructive quality control and evaluation by using photo elastic methods</b><br/>Benjamin Schaaf, RWTH Aachen Uni.</p>                                       | <p><b>Effects of Non-Uniform Heat Transfer on Glass Quality in A Tempering Process</b> Reijo Karvinen, Tampere University of Technology</p>                             | <p><b>Infrared Temperature Measurement in The Glass Industry</b><br/>Peter Droegmoeller, <a href="#">AMETEK Land</a></p>  |
| <p><b>Experimental and Numerical Studies on Blast Resistance of Laminated Glass</b><br/>Suwen Chen, Tongji University</p>  | <p><b>Haze, Anisotropy, Clarity and Interference Effects (HACI) evaluation</b><br/>Louis Moreau, AGNORA</p>   | <p><b>Non-contact Glass Temperature Measurement – the Correct Adaptation of IR Thermometers and Cameras to Different Applications</b> Ingo Stahlkopf, Optris GmbH</p> |
| <b>STEP-CHANGE, LUNCH, ONE-ON-ONE MEETINGS</b>   |   |   |
| <p><b>Blast performance of point fixed assemblies utilizing crystal clear TSSA</b><br/>Lawrence Carbary, <a href="#">Dow Corning Corporation</a></p>                                     | <p><b>Automating flat glass tempering process</b><br/>Miika Appelqvist, <a href="#">Glaston Finland Oy</a></p>  | <p><b>Solutions for Closed-Loop Process Control of Low Glass Production for Architecture, Automotive and Smart Applications</b><br/>Marcus Klein, SURAGUS GmbH</p>    |
| <p><b>Transparency in Glass Connections – a Case Study</b> Lisa Rammig, Eckersley O'Callaghan, TU Delft</p>  | <p><b>Thermally Processed Glass: Correlation Between Surface Compression, Mechanical and Fragmentation Test</b> Ennio Mognato, Stazione Sperimentale Del Vetro Scpa</p> | <p><b>From Color to Chemometrics: Strategies to Determine Coating Thickness and Quality</b> Chris Hellwig, Carl Zeiss Spectroscopy</p>                                |
| <p><b>The Application of Glass as A Bracing Element</b> Daniel Neumer, Universität Der Bundeswehr München</p>  | <p><b>ASTM E1300 Uniform Load Strength Reduction Factor not Required for Ceramic Enameled Glass A.</b> William Lingnell, Lingnell Consulting Services</p>               | <p><b>Taking control of anisotropy in tempering process: the new way</b><br/>Riku Farm, <a href="#">Glaston Finland Oy</a></p>  |
| <b>COFFEE BREAK, ONE-ON-ONE MEETINGS</b>   |   |   |
| <p><b>Engineering and Applications of the Bundled Glass Column</b> Faidra Oikonomopoulou, TU Delft, Faculty of Architecture and The Built Environment</p>                                | <p><b>Proven Roller Stability in Advanced Tempering Process</b><br/>Jean Denis Nicolas, Vesuvius</p>  | <p><b>Anisotropy and White Haze On-Line Inspection System</b><br/>Kai Vogel, Viprotron GmbH</p>   |
| <p><b>Applied Machine Learning in Structural Glass Design</b><br/>James Griffith, Arup</p>   | <p><b>The Importance of an Integrated Software ERP Solution in The Glass Processing Industry</b><br/>Horst Mertes, <a href="#">FeneTech Inc.</a></p>                    | <p><b>Electromagnetic Shielding Effectiveness of Glazing Components</b><br/>Eric Stein, Viracon</p>   |
| <p><b>Is current sizing of float glass structures too much conservative?</b><br/>Gianni Royer Carfagni, University of Parma, Italy</p>   | <p><b>Criticities in Glass Chemical Strengthening</b><br/>Guglielmo Macrelli, Isoclima SpA</p>  | RESERVED  |

BREAK, ONE TO ONES, HAPPY HOUR

CONFERENCE DINNER @ Solo Sokos Hotel Tornio Tampere, Paja Congress Center

# GPD Glass Performance Days 2017 • Program • June 30, FRIDAY

|  |  |   |   |
|--|--|---|---|
| 8:00   | Registration   |   |   |
|  | <b>Smart Glazing</b>   | <b>Facade Contractor's Forum</b>  | <b>Complex Geometry</b>   |
|  | <b>Session Chairs:</b><br>Valerie Hayez, Dow Corning Corporation<br>Juha Liettjä, Glaston Oy   | <b>Session Chair:</b><br>Saverio Pasetto, Skanska   | <b>Session Chairs:</b> Benjamin Beer,<br>Meinhardt Façade Technology<br>Oliver Hans, Schueco  |
| 9:00   | <b>Smart Glazings -Lessons from the Past 25 years for Future Technologies and Market Trends</b><br>Stephen Selkowitz, LBNL   | <b>Glass specifications for visual acceptance in architectural applications</b><br>Hans Jansen, Scheldebouw                       | <b>The consequences of panelisation on visual inconsistency of curved glazed façades</b> Neesha Gopal,<br>Meinhardt Facade Technology               |
| 9:25   | <b>Liquid Crystal Window Technology? Crystal Clear Vision for Architecture</b><br>Martin Zitto, <a href="#">Merck KGaA</a>   | <b>Haute Couture for a Curtain wall: Serrated glass in façade application</b><br>Mathias Klaiber, Josef Gartner GmbH              | <b>Approaching Curved Annealed Glass</b><br>Timo Bühlmeier, Josef Gartner GmbH  |
| 9:50   | <b>The Potential of Structured Switchable Glazing</b><br>Walter Haase, University of Stuttgart   | <b>Curved glass in the building skin: Case studies and lessons learned</b><br>Marc Zimmer, Frener & Reifer GmbH/Srl               | <b>Integral design: free geometry, hybrid construction</b> Lutz Schöne, LEICHT<br>Structural Engineering and Specialist Consulting GmbH             |
| 10:15 COFFEE BREAK, ONE-ON-ONE MEETING STEP-CHANGE   |  |   |   |
| 11:00  | <b>Smart glazing and adaptive facades: what can we simulate?</b><br>Fabio Favoino, <a href="#">Eckersley O'Callaghan</a>   | <b>New Glass dimensions: large glass panes and their challenges in façade applications</b><br>Mathias Klaiber, Josef Gartner GmbH | <b>Free-Form Cold-Bent Façades and All-Glass Structures - Design and Value Engineering Challenges</b> Benjamin Beer,<br>Meinhardt Façade Technology |
| 11:25  | <b>Switchable Glazing Heliotrope</b>   | <b>Fabrication Technology for Hybrid Glass Metal Panels</b><br>Peter Eckardt, Seele GmbH  | <b>Structural Silicon Joints in Cold-bent SSG units</b><br>Viviana Nardini, Sika Services AG  |
| 11:50  | <b>Transparent Solarcells</b><br>Next Energy Technologies Inc  | <b>Glass Sandwich Facades</b><br>Martien Teich, Seele GmbH  | <b>Chaoyang Park Plaza Tower: Design and Construction of complex geometry façade</b><br>Hui Yu, RFR Shanghai  |
| 12:15  |  |   | <b>Systematically Unique Facade Geometry</b><br>Oliver Hans, Schueco  |
| 12:40  |  |   | LUNCH, ONE-ON-ONE MEETINGS  |
|  | <b>IGU &amp; Window Technology</b><br>Session Chairs: TBA  |   |   |
| 13:25  | <b>Architect Forum</b><br>Session Chairs: TBA  | <b>INVITED SPEAKER</b><br><b>Vacuum Insulating Glass? Past, Present and Prognosis</b><br>Richard Collins, University of Sydney    |   |
| 13:45  | <b>Recent Trends in Architectural Design of Transparent Facades</b> Marcin Brzezicki,<br>Wroclaw University of Science and Technology                                | <b>A Novel Glass Spacer for Vacuum Insulated Glazing</b><br>Cenk Kocer, University of Sydney                                      | <b>Beauty and The Beast: The Wilshire Grand's Façade Design in LA's Seismic Zone 4 Reality</b><br>Tammy Jow, AC Martin                              |
| 14:10  | <b>30 Years of Structural Design Innovations in Glass</b> Mick Eekhout, Octatube Space Structures B.V.   | <b>Vacuum Insulated Glazing Under the Influence of a Thermal Load</b><br>Antti Aronen, University of Sydney                       | <b>Structurally shaped glasses for the new library of Caen</b><br>Jacques Raynaud, Elioth   |
| 14:35  | <b>Glass Imagined and Realized: Case Studies of the Aesthetic Qualities and Possibilities of Glass in Architectural Design.</b><br>Daniel Vos, Heintges & Associates | <b>The Development of Synergy on Vacuum Glass</b><br>Jiang Yi, Beijing Synergy Vacuum Glazing Technology Co., Ltd.                | <b>Banco Popular HQ - Auditorium</b><br>Miguel Angel Ruiz, Martifer Metallic Constructions  |
| 15:00 COFFEE BREAK, ONE-ON-ONE MEETINGS, STEP-CHANGE |  |   |   |
|  |  |   | <b>Coatings Technology and Applications</b><br>Session Chairs: TBA  |
| 15:30  | <b>Glass Specification Challenges in London</b><br>Russell Cole, Arup Façade Engineering   | <b>Laser-Grown Bumps on Window Glass</b><br>Alexander Streltsov, Corning Incorporated   | <b>Breakthrough in Building Glass: High Energy Efficiency Coatings Through Laser Annealing.</b><br>Jean-Philippe Schweitzer, Saint-Gobain           |
| 15:55  | <b>New Solutions for Edge-Enamelling of Sputter Coatings</b><br>Ralf Greiner, Guardian Thalheim GmbH   | <b>Analysis of The Uncertainties In Acoustic Of IGU: A Comparison In Between Products and Labs</b><br>Fabien Dalzin, Saint-Gobain | <b>Next Generation of High Throughput Architectural Glass Coaters</b><br>Christoph Häusler, Von Ardenne GmbH  |
| 16:20  | CLOSING CEREMONY<br>Speaker <b>Stephanie Akkaoui Hughes</b> • Panel discussion   |   |   |
| 19:30 –UNTIL DAWN                                    | FAREWELL PARTY @ Hatanpään Kartano, Hatanpään puistokuja 1, 33900 Tampere  |   |   |

# GPD Glass Performance Days 2017 • Program • June 30, FRIDAY

| Arch Challenges & Solutions   | Laminated Glass  | Market Trends   |
|---|--|---|
| <b>Session Chairs:</b><br>Enrico Cutri, Dow Corning<br>Bjorn Sanden, Kuraray  | <b>Session Chairs:</b><br>Bernd Koll, Kuraray  | <b>Session Chairs:</b><br>Peter Dixen<br>A+W Software GmbH  |
| <b>Sustainable Facade Design for Glazed Buildings in a Blast Resilient Urban Environment</b> Guido Lori, Permasteelisa                        | <b>Testing of Glass Laminates for Edge Stability</b> Julia Schimmelpenningh, <a href="#">Eastman Chemical Company</a>          | <b>USA: Market Trends and Drivers</b><br>Urmilla Sowell, GANA   |
| <b>Glass Appearances - Expectations Regarding a Material, Driving Projects and Upcoming Solutions</b><br>Stefan Goeddertz, Herzog & de Meuron | <b>Edge Stability and Potential Cause of Blemishes in Laminated Safety Glass</b><br>Vaughn Schauss,<br><a href="#">Kuraray</a> | <b>Minimum energy performance requirements for window replacement in the 28 EU member states</b><br>Cédric Janssens, Glass for Europe |
| <b>Structural Silicone Glazing: Life Expectancy of more than 50 Years?</b><br>Sigurd Sitte, <a href="#">Dow Corning GmbH</a>                  | <b>Post-Lamination Response of Warm-Bent Laminated Glass</b><br>Gabriele Pisano, University of Parma, Italy                    | <b>Applicability of design thinking to the construction industry</b><br>Olavi Uusitalo, Holmark                                       |

## COFFEE BREAK, ONE-ON-ONE MEETING STEP-CHANGE

|  |   |  |
|--|---|--|
| <b>Silicone Opacifiers For Spandrel Glass Applications: Risk Mitigation In Thermal Stresses</b> Chris Fronsoe, ICD High Performance Coatings | <b>Thermal Radiation Against Forced Convection Heating in Flat Glass Lamination Oven</b><br>Mikko Rantala, <a href="#">Glaston Finland Oy</a> | <b>Digitalization in the Glass</b><br>Bernhard Saftig, <a href="#">Siemens</a>   |
| <b>Structural glass sandwich panels</b><br>Graham Dodd, Arup   | <b>Testing of adhesion on laminated glass using photometric measurements</b><br>Peter Hof, TU Darmstadt - MPA Darmstadt                       | <b>The Past, Present and Future of Glass Fabrication</b> Alex Ochoa, <a href="#">FeneTech Inc.</a>                         |
| <b>Tall self-supporting Load Bearing Glass Structures</b> Gennady Vasilchenko-Malishev, Malishev Engineers Ltd.                              | <b>Which Interlayer for Which Application?</b><br>Bjorn Sanden,<br><a href="#">Kuraray Europe GmbH - Trosifol</a>                             | <b>Coatings Glass market. Russia, Far East, Turkey &amp; Middle east – ICCG</b><br>Dmitriy Bernt, Sener Optik, Wang Shijie |

## LUNCH, ONE-ON-ONE MEETINGS

|  |  |  |
|--|--|--|
| <b>Counter Selective Glazing for a Passive Building Concept</b><br>Felix Weber, Arup   | <b>Effect of Different Sources of Interlayer Modulus Data for Glass Design: The Structural PVB Case</b><br>Wim Stevels, <a href="#">Eastman Chemical Company</a> | <b>The "Internet of Things" in Glass Processing</b><br>Peter Dixen, A+W Software GmbH  |
| <b>La Maison Des Fondateurs? Load Bearing Interlocking Glass Spiral as Building Structure</b> Philippe Willareth, Dr. Lüchinger + Meyer Bauingenieure AG | <b>Enhanced Structural Integrity of Laminated Glass Balustrades</b><br>Malvinder Singh Rooprai,<br><a href="#">Kuraray India Pvt. Ltd.</a>                       | <b>Glass in Transportation</b><br><b>Session Chairs:</b><br>Juha Artama, NSG Group<br>Juha Karisola, Glaston Finland Oy              |
| <b>Exciting Architectural Case Studies from All Around the World</b><br>Sandro Casaccio, <a href="#">Kuraray</a>   | <b>On The Causes of Optical Defects in Laminated Glass</b><br>Jan Belis, Ghent Universit   | <b>Developing New Technologies with Vehicle Manufacturers</b><br>Juha Artama, NSG Group  |
|  |  | <b>In Glass Laminated Displays (For Special Vehicles)</b><br>Joe Pimenoff, Beneq   |
|  |  | <b>Energy Efficiency of Different Windscreen Bending Furnaces</b><br>Juha Karisola, <a href="#">Glaston Finland Oy</a>               |
|  |  | <b>Patented Moiré Optical Distortion Measurement Supports Evolution of Automotive Glass</b><br>Jens Kayser, ISRA SURFACE VISION GmbH |

## COFFEE BREAK, ONE-ON-ONE MEETINGS, STEP-CHANGE

|  |   |  |
|--|---|--|
| <b>Challenging Project Development with Implementation of Innovative AR Coating</b><br>Anastasija Sutkina, Glassbel Baltic     | <b>Architectural Acoustic Glazing</b><br>Hengyi Ju, <a href="#">Eastman Chemical Company</a>  | <b>New Possibilities for Windshield Bending</b><br>Reinhold Senft, Grafotec Spray Systems GmbH |
| <b>The Development of Stainless Steel Based Warm Edge Spacer Systems</b><br>Gerhard Reichert, Polymer Extrusion Technology LLC | <b>Recent developments of laminating films as contribution for energy efficient buildings and facades</b> Steffen Bornemann, Folienwerk Wolfen GmbH | <b>New Era in Digital Printing On Glass</b><br>Yariv Ninyo, Dip-Tech                           |

## CLOSING CEREMONY

Speaker **Stephanie Akkaoui Hughes** • Panel discussion

FAREWELL PARTY @ Hatanpään Kartano, Hatanpään puistokuja 1, 33900 Tampere

# Contents

|   |      |
|---|------|
| Index of presenters in alphabetical order | XVI  |
| Conference Programme day by day           | X    |
| Tuesday                                   | V    |
| Wednesday                                 | V    |
| Thursday                                  | VI   |
| Friday                                    | VIII |
| Posters                                   | 427  |

## June 29, THURSDAY

### Glass and Sustainability 1

|   |   |
|---|---|
| Active BIPV Glass Facades: Current Trends of Innovation<br><i>Erika Saretta • University of Applied Sciences and Arts of Southern Switzerland</i> | 2 |
| Qualifying and quantifying thermal comfort in highly glazed spaces<br><i>Medina Deliahmedova • Lund University</i>                                | 8 |

### Do's and Don'ts of Building Facades 13

|  |    |
|--|----|
| 111 Main Enclosure   Responding to Extreme Performance Criteria<br><i>Lisa Follman • SOM Architects</i>  | 14 |
| Unitised Façade System Designed with a Highly Transparent Façade of Low G-value Combined with Blast Requirements:<br>20 Farringdon Street a Case Study<br><i>Thomas Henriksen • Mott Macdonald</i> | 20 |

### Facade Engineering 27

|   |    |
|---|----|
| Towards a More Consistent Design of Laminated Glass<br><i>Michael Dunham • Arup</i>   | 28 |
| Verification of Insulating Glass Units in Modern Curtain Wall Facades<br><i>Michael Elstner • AGC Interpane</i>   | 39 |
| Next Generation Calculation Method for Structural Silicone Joint Dimensioning<br><i>Valerie Hayez • Dow Corning Corporation</i>   | 46 |
| Double-Skin Facades: Characteristics and Challenges for an Advanced Building Skin<br><i>Fabian C. Schmid • Seele GmbH</i>   | 47 |
| Structural Glass Connections<br><i>Carles Teixidor • Bellapart S.A.U.</i>   | 51 |
| All-glass Pavilions<br><i>Geralt Siebert • Uni. of German Armed Forces Munich</i>   | 55 |
| The Futurium Berlin: Ventilated Façade System with Structurally Bonded Textured Glass - Durability Testing Under Climatic Influences and Mechanical Loads<br><i>Jan Wurm • Arup</i>               | 58 |
| Cyclone Resistant Glazing Solutions in the Asia-Pacific Region: a Growing Market to Meet Present and Future Challenges<br><i>Dario Trabucco • The Council on Tall Buildings and Urban Habitat</i> | 64 |

|  |            |
|--|------------|
| Glass Fins with Embedded Titanium Inserts for The Façades of The New Medical School Of Montpellier<br><i>Jordi Torres • Bellapart S.A.U.</i>   | 70         |
| Structural Glass in Building Restoration. Europe's Tower Entrance Hall. Madrid. Spain<br><i>Miguel Núñez • ENAR</i>  | 71         |
| Cost and Energy Saving Potential of Glass Facade Construction<br><i>Timo Saukko • Finnglass</i>  | 74         |
| <b>Structural Glass Applications</b>   | <b>75</b>  |
| Shaping Ultra-Thin Glass<br><i>Sophie Pennetier • ARUP</i>   | 76         |
| Probabilistic Study of Wind-Temperature Interaction: An Initial Study Towards Optimized Structural Assessment of Glass Components<br><i>Manuel Santarsiero • Eckersley O'Callaghan</i>               | 81         |
| Glass Constructions Under Extreme Boundary Conditions<br><i>Barbara Siebert • Dr. Siebert Consulting Engineers</i>   | 85         |
| Hybrid Glass Structures<br><i>Peter Lenk • Arup</i>  | 90         |
| New Concept of Horizontal Structural Elements in Glass: Self bearing "Pi" Shape Plate<br><i>Jesús M. Cerezo • ENAR, ENVOLVENTES ARQUITECTONICAS</i>  | 95         |
| Production and Testing of Kiln-Cast Glass Components for an Interlocking, Dry-Assembled Transparent Bridge<br><i>Telesilla Bristogianni • TU Delft, Faculty of Civil Engineering and Geosciences</i> | 101        |
| The Strength of Aged Glass<br><i>Mauro Overend • University of Cambridge</i>   | 107        |
| Mechanically Efficient and Structurally Slim Vision Panels<br><i>Carlos Pascual • University of Cambridge - Glass &amp; Facade Technology Research Group</i>   | 109        |
| Deformations and Strain Energy in Fragments of Tempered Glass - Experimental and Numerical Investigation<br><i>Jens H. Nielsen • Technical University of Denmark</i>                                 | 114        |
| <b>Research &amp; Development</b>  | <b>115</b> |
| Influence of the Distribution of Residual Stress on Strength Tests<br><i>Jürgen Neugebauer • University of Applied Sciences FH-Joanneum</i>  | 116        |
| Biaxially Curved Glass with Large Radii – Determination of Strength using the Coaxial Double Ring Test<br><i>Steffen Müller-Braun • TU Darmstadt - Institute of Structural Mechanics And Design</i>  | 120        |
| Parameter Identification Methods for Visco – and Hyperelastic Material<br><i>Michael Kraus • Uni. of German Armed Forces Munich, Miriam Schuster • TU Darmstadt</i>                                  | 121        |
| Influence of Weathering on Post-Fracture Performance<br><i>Caroline Butchart • Eckersley O'Callaghan</i>   | 122        |
| Full-surface and Non-destructive Quality Control and Evaluation by Using Photoelastic Methods<br><i>Benjamin Schaaf • RWTH Aachen Uni</i>  | 130        |
| Blast Performance of Point Fixed Assemblies Utilizing TSSA<br><i>John Kimberlain, Lawrence Carbary • Dow Corning Corporation</i>   | 135        |
| Transparency in Glass Connections – a Case Study<br><i>Lisa Rammig • Eckersley O'Callaghan, TU Delft</i>   | 140        |

|   |     |
|---|-----|
| Design and Experimental Testing of the Bundled Glass Column<br><i>Faidra Oikonomopoulou • TU Delft, Faculty of Architecture and The Built Environment</i> | 141 |
| Applied Machine Learning in Structural Glass Design<br><i>James Griffith • Arup</i>   | 143 |
| Is Current Sizing of Float Glass Structures too much Conservative?<br><i>Gianni Royer Carfagni • University of Parma, Italy</i>                           | 148 |

## Tempering / Preprocessing

153

|  |     |
|--|-----|
| News from an Old Theme: Spontaneous Cracking of Thermally Toughened Safety Glass<br><i>Andreas M Kasper • Saint-Gobain HRDC</i>                                      | 154 |
| Controlling Anisotropy<br><i>Francis Serruys • Saint-Gobain Building Glass Europe</i>  | 157 |
| Effects of Non-uniform Heat Transfer in a Tempering Process on Glass Quality<br><i>Reijo Karvinen • Tampere University of Technology</i>                             | 161 |
| Haze, Anisotropy, Clarity and Interference Effects (HACI) Evaluation<br><i>Louis Moreau • AGNORA</i>   | 167 |
| Thermally Processed Glass: Correlation Between Surface Compression, Mechanical and Fragmentation Test<br><i>Ennio Mognato • Stazione Sperimentale Del Vetro Scpa</i> | 169 |
| ASTM E1300 Uniform Load Strength Reduction Factor not Required for Ceramic Enamelled Glass<br><i>A. William Lingnell • Lingnell Consulting Services</i>              | 176 |
| Critical Issues in Glass Chemical Strengthening<br><i>Guglielmo Macrelli • Isoclima SpA</i>  | 180 |

## Quality Management

185

|  |     |
|--|-----|
| The Psychology of Perception, Threshold, and Emotion in Interior Glass Design<br><i>Jim Gulnick • Mcgrory Glass, Inc.</i>  | 186 |
| Non-contact Glass Temperature Measurement – the Correct Adaptation of IR Thermometers and Cameras to Different Applications<br><i>Ingo Stahlkopf • Optris GmbH</i> | 191 |
| From Color to Chemometrics: Strategies to Determine Coating Thickness and Quality<br><i>Chris Hellwig • Carl Zeiss Spectroscopy</i>                                | 193 |
| Anisotropy and White Haze On-Line Inspection System<br><i>Kai Vogel • Viprotron GmbH</i>   | 195 |
| Electromagnetic Shielding Effectiveness of Glazing Components<br><i>Eric Stein • Viracon</i>   | 197 |

# June 30, FRIDAY

|  |            |
|--|------------|
| <b>Smart Glazing</b>   | <b>205</b> |
| Potential of Structured Switchable Glazing<br><i>Walter Haase • University of Stuttgart</i>  | 206        |
| Smart Glazing in Intelligent Buildings: What Can We Simulate?<br><i>Fabio Favoino • Eckersley O'Callaghan</i>  | 212        |
| <b>Architect Forum</b>   | <b>221</b> |
| Recent Trends in Architectural Design of Light-permeable Facades<br><i>Marcin Brzezicki • Wroclaw University of Science and Technology</i>                               | 222        |
| Glass Innovations for Dutch Architecture' for GPD 2017<br><i>Mick Eekhout • Octatube Space Structures B.V.</i>   | 228        |
| Glass Imagined and Realized: Case Studies of the Aesthetic Qualities and Possibilities of Glass in Architectural Design<br><i>Daniel Vos • Heintges &amp; Associates</i> | 236        |
| Glass Specification Challenges in London<br><i>Russell Cole • Arup Facade Engineering</i>  | 244        |
| High-quality Edge Enameling for Architectural Glass<br><i>Ralf Greiner • Guardian Thalheim GmbH</i>  | 248        |
| <b>Facade Contractor's Forum</b>   | <b>253</b> |
| Fabrication Technology for Hybrid Glass Metal Panels<br><i>Stefan Marinitsch, Peter Eckardt • Seele GmbH</i>   | 254        |
| Face and Surface – Glass-Sandwich-Facades, the all-in-one Solution<br><i>Martien Teich • Seele GmbH</i>  | 259        |
| <b>IGU &amp; Window Technology</b>   | <b>263</b> |
| Vacuum Insulating Glass – Past, Present and Prognosis<br><i>Richard Collins • University of Sydney</i>   | 264        |
| A Novel Glass Spacer for Vacuum Insulated Glazing<br><i>Cenk Kocer • University of Sydney</i>  | 268        |
| Vacuum Insulated Glazing Under the Influence of a Thermal Load<br><i>Antti Aronen • University of Sydney</i>   | 273        |
| Laser-Grown Bumps on Window Glass<br><i>Alexander Streltsov • Corning Incorporated</i>   | 280        |
| Analysis of the Uncertainties in Acoustic Insulation Performance of DGU: a Comparison in-between Products and Laboratories<br><i>Fabien Dalzin • Saint-Gobain</i>        | 284        |

## Complex Geometry

287

- The Consequences of Panelisation on Visual Inconsistency of Curved Glazed Façades  
*Neesha Gopal • Meinhardt Facade Technology* 288
- Approaching Hot Bent Annealed Glass  
*Timo Bühlmeier • Josef Gartner GmbH* 294
- Free-Form Shape Cold-Bent Structural Silicone Glazed Façades - Design Concept and Challenges  
*Benjamin Beer • Meinhardt Façade Technology* 300
- Structural Silicon Joints in Cold-Bent SSG Units  
*Viviana Nardini • Sika Services AG* 309
- Chaoyang Park Plaza Tower: Design and Construction of Complex Geometry Façade  
*Hui Yu • RFR Shanghai* 314
- Systematically Unique Facade Geometry  
*Oliver Hans • Schueco* 324
- Beauty and The Beast: The Wilshire Grand's Façade Design in LA's Seismic Zone 4 Reality  
*Tammy Jow • AC Martin* 328
- Banco Popular HQ - Auditorium, Madrid (Spain)  
*Miguel Angel Ruiz • Martifer Metallic Constructions* 331

## Architectural Challenges & Solutions

335

- Sustainable Facade Design for Glazed Buildings in a Blast Resilient Urban Environment  
*Guido Lori • Permasteelisa* 336
- Structural Silicone Glazing: Life Expectancy of more than 50 Years?  
*Sigurd Sitte • Dow Corning GmbH* 338
- Silicone Opacifiers For Spandrel Glass Applications: Risk Mitigation In Thermal Stresses  
*Chris Fronsoe • ICD High Performance Coatings* 346
- Structural Glass Sandwich Panels  
*Graham Dodd • Arup* 351
- Tall Self-supporting Load Bearing Glass Structures  
*Gennady Vasilchenko-Malishev • Malishev Engineers Ltd.* 354
- Counter Selective Glazing for a Passive Building Concept  
*Felix Weber • Arup* 356
- La Maison Des Fondateurs – Load Bearing Interlocking Glass Spiral as Building Structure  
*Philippe Willareth • Dr. Lüchinger + Meyer Bauingenieure AG* 357
- Exciting Architectural Case Studies from All Around the World  
*Sandro Casaccio • Kuraray* 363

## Laminated Glass

365

- Testing of Glass Laminates for Edge Stability  
*Julia Schimmelpenninck • Eastman Chemical Company* 366
- Edge Stability and Potential Cause of Blemishes in Laminated Safety Glass  
*Vaughn Schauss • Kuraray* 371

|  |            |
|--|------------|
| Post-Lamination Response of Warm-bent Laminated Glass<br><i>Laura Galuppi, Gianni Royer Carfagni • University of Parma, Italy</i>  | 375        |
| Thermal Radiation Compared with Forced Convection Heating in Flat Glass Lamination Oven<br><i>Mikko Rantala • Glaston Finland Oy</i>   | 379        |
| Testing of Adhesion on Laminated Glass Using Photometric Measurements<br><i>Peter Hof • TU Darmstadt - MPA Darmstadt</i>   | 386        |
| Which Interlayer for Which Glazing Application?<br><i>Bjorn Sanden • Kuraray Europe GmbH - Trosifol</i>  | 390        |
| Effect of Different Sources of Interlayer Modulus Data for Glass Design: The Structural PVB Case<br><i>Wim Stevels • Eastman Chemical Company</i>  | 393        |
| Enhanced Structural Integrity of Laminated Glass Balustrades<br><i>Malvinder Singh Rooprai • Kuraray India Pvt. Ltd.</i>   | 397        |
| On The Causes of Optical Defects in Laminated Glass<br><i>Jan Belis • Ghent Universit</i>  | 401        |
| Architectural Acoustic Glazing – Fundamentals of Sound Transmission and Acoustic Interlayers<br><i>Hengyi Ju • Eastman Chemical Company</i>  | 402        |
| Recent Developments of Laminating Films as Contribution for Energy Efficient Buildings and Façades<br><i>Steffen Bornemann • Folienwerk Wolfen GmbH</i>  | 406        |
| <b>Market Trends</b>   | <b>411</b> |
| Minimum Energy Performance Requirements for Window Replacement in the 28 EU Member States<br><i>Cédric Janssens • Glass for Europe</i>   | 412        |
| Applicability of Design Thinking to the Construction Industry<br><i>Olavi Uusitalo • Holmark</i>   | 415        |
| The Advantages of Digitalization in the Glass Industry<br><i>Bernhard Saftig • Siemens</i>   | 419        |
| <b>Glass in Transportation</b>   | <b>421</b> |
| New Possibilities for Windshield Bending<br><i>Reinhold Senft • Grafotec Spray Systems GmbH</i>  | 422        |
| <b>Posters</b>   | <b>427</b> |
| The Effective Stiffness of Broken Laminated Glass. A Homogenized Approach<br><i>Gianni Royer Carfagni • University of Parma, Italy</i>   | 428        |
| Simple Statistics Shows that Heat-treated Glass is much Stronger than Expected<br><i>Gianni Royer Carfagni • University of Parma, Italy</i>  | 433        |
| Zaryadye Park, Glass Grid Shell Roof<br><i>G. Vasilchenko-Malishev • Malishev Engineers</i>  | 436        |
| Will the US Impose Tariffs on Imported Flat Glass Again?<br><i>Olavi Uusitalo • Holmark</i>  | 442        |
| Analysis of Float Glass' Development by Design Envelope<br><i>Olavi Uusitalo • Holmar</i>  | 446        |
| Approaching Free Energy<br><i>Jim Gulnick • McGroary Glass, Inc.</i>   | 451        |
| Morphological and Structural Features of the Gold Nanolayer on the Glass Surface Modified by Surface Ion Exchange and Chemical Etching<br><i>Olga Sidelnikova • Institute of Solid State Chemistry and Mechanochemistry, Novosibirsk, Russia</i> | 455        |

# Index of presenters in alphabetical order

|   |                    |   |          |   |             |
|---|--------------------|---|----------|---|-------------|
| Alexander Streltsov<br><i>Corning Incorporated</i>  | 280                | Guglielmo Macrelli<br><i>Isoclima SpA</i>                               | 180      | Mikko Rantala<br><i>Glaston Finland Oy</i>  | 379         |
| Andreas M Kasper<br><i>Saint-Gobain HRDC</i>  | 154                | Guido Lori<br><i>Permasteelisa</i>                                      | 336      | Neesha Gopal<br><i>Meinhardt Facade Technology</i>  | 288         |
| Antti Aronen<br><i>University of Sydney</i>   | 273                | Hengyi Ju<br><i>Eastman Chemical Company</i>                            | 402      | Olavi Uusitalo<br><i>Holmark</i>  | 415,442,446 |
| Barbara Siebert<br><i>Dr. Siebert Consulting Engineers</i>  | 85                 | Hui Yu<br><i>RFR Shanghai</i>   | 314      | Olga Sidelnikova<br><i>Institute of Solid State Chemistry and<br/>Mechanochemistry, Novosibirsk, Russia</i> | 455         |
| Benjamin Beer<br><i>Meinhardt Façade Technology</i>   | 300                | Ingo Stahlkopf<br><i>Optris GmbH</i>                                    | 191      | Oliver Hans<br><i>Schueco</i>   | 324         |
| Benjamin Schaaf<br><i>RWTH Aachen Uni</i>   | 130                | James Griffith<br><i>Arup</i>   | 143      | Peter Hof<br><i>TU Darmstadt - MPA Darmstadt</i>  | 386         |
| Bernhard Saftig<br><i>Siemens</i>   | 419                | Jan Belis<br><i>Ghent Universit</i>                                     | 401      | Peter Lenk<br><i>Arup</i>   | 90          |
| Bjorn Sanden<br><i>Kuraray Europe GmbH - Trosifol</i>   | 390                | Jan Wurm<br><i>Arup</i>   | 58       | Philippe Willareth<br><i>Dr. Lüchinger + Meyer Bauingenieure AG</i>   | 357         |
| Carles Teixidor<br><i>Bellapart S.A.U.</i>  | 51                 | Jens H. Nielsen<br><i>Technical University of Denmark</i>               | 114      | Ralf Greiner<br><i>Guardian Thalheim GmbH</i>   | 248         |
| Carlos Pascual<br><i>University of Cambridge - Glass &amp; Facade<br/>Technology Research Group</i> | 109                | Jesús M. Cerezo<br><i>ENAR, ENVOLVENTES ARQUITECTONICAS</i>             | 95       | Reijo Karvinen<br><i>Tampere University of Technology</i>   | 161         |
| Caroline Butchart<br><i>Eckersley O'Callaghan</i>   | 122                | Jim Gulnick<br><i>Mcgrory Glass, Inc.</i>                               | 186, 451 | Reinhold Senft<br><i>Grafotec Spray Systems GmbH</i>  | 422         |
| Cédric Janssens<br><i>Glass for Europe</i>  | 412                | John Kimberlain<br><i>Dow Corning Corporation</i>                       | 135      | Richard Collins<br><i>University of Sydney</i>  | 264         |
| Cenk Kocer<br><i>University of Sydney</i>   | 268                | Jordi Torres<br><i>Bellapart S.A.U.</i>                                 | 70       | Russell Cole<br><i>Arup Facade Engineering</i>  | 244         |
| Chris Fronsoe<br><i>ICD High Performance Coatings</i>   | 346                | Julia Schimmelpenningh<br><i>Eastman Chemical Company</i>               | 366      | Sandro Casaccio<br><i>Kuraray</i>   | 363         |
| Chris Hellwig<br><i>Carl Zeiss Spectroscopy</i>   | 193                | Jürgen Neugebauer<br><i>University of Applied Sciences FH-Joanneum</i>  | 116      | Sigurd Sitte<br><i>Dow Corning GmbH</i>   | 338         |
| Daniel Vos<br><i>Heintges &amp; Associates</i>  | 236                | Kai Vogel<br><i>Viprotron GmbH</i>                                      | 195      | Sophie Pennetier<br><i>ARUP</i>   | 76          |
| Dario Trabucco<br><i>The Council on Tall Buildings and Urban<br/>Habitat</i>                        | 64                 | Lisa Follman<br><i>SOM Architects</i>                                   | 14       | Stefan Marinitsch<br><i>Seele GmbH</i>  | 254         |
| Ennio Mognato<br><i>Stazione Sperimentale Del Vetro Scpa</i>  | 169                | Lisa Rammig<br><i>Eckersley O'Callaghan, TU Delft</i>                   | 140      | Steffen Bornemann<br><i>Folienwerk Wolfen GmbH</i>  | 406         |
| Eric Stein<br><i>Viracon</i>  | 197                | Louis Moreau<br><i>AGNORA</i>   | 167      | Steffen Müller-Braun<br><i>TU Darmstadt - Institute of Structural<br/>Mechanics And Design</i>              | 120         |
| Erika Saretta<br><i>University of Applied Sciences and Arts<br/>of Southern Switzerland</i>         | 2                  | Malvinder Singh Rooprai<br><i>Kuraray India Pvt. Ltd.</i>               | 397      | Tammy Jow<br><i>AC Martin</i>   | 328         |
| Fabian C. Schmid<br><i>Seele GmbH</i>   | 47                 | Manuel Santarsiero<br><i>Eckersley O'Callaghan</i>                      | 81       | Telesilla Bristogianni<br><i>TU Delft, Faculty of Civil Engineering<br/>and Geosciences</i>                 | 101         |
| Fabien Dalzin<br><i>Saint-Gobain</i>  | 284                | Marcin Brzezicki<br><i>Wroclaw University of Science and Technology</i> | 222      | Thomas Henriksen<br><i>Mott Macdonald</i>   | 20          |
| Fabio Favoino<br><i>Eckersley O'Callaghan</i>   | 212                | Martien Teich<br><i>Seele GmbH</i>                                      | 259      | Timo Bühlmeier<br><i>Josef Gartner GmbH</i>   | 294         |
| Faidra Oikonomopoulou<br><i>TU Delft, Faculty of Architecture and<br/>The Built Environment</i>     | 141                | Mauro Overend<br><i>University of Cambridge</i>                         | 107      | Timo Saukko<br><i>Finnglass</i>   | 74          |
| Felix Weber<br><i>Arup</i>  | 356                | Medina Deliahmedova<br><i>Lund University</i>                           | 8        | Valerie Hayez<br><i>Dow Corning Corporation</i>   | 46          |
| Francis Serruys<br><i>Saint-Gobain Building Glass Europe</i>  | 157                | Michael Dunham<br><i>Arup</i>   | 28       | Vaughn Schaus<br><i>Kuraray</i>   | 371         |
| Gennady Vasilchenko-Malishev<br><i>Malishev Engineers Ltd.</i>                                      | 354, 436           | Michael Elstner<br><i>AGC Interpane</i>                                 | 39       | Viviana Nardini<br><i>Sika Services AG</i>  | 309         |
| Geralt Siebert<br><i>Uni. of German Armed Forces Munich</i>   | 55                 | Michael Kraus<br><i>Uni. of German Armed Forces Munich</i>              | 121      | Walter Haase<br><i>University of Stuttgart</i>  | 206         |
| Gianni Royer Carfagni<br><i>University of Parma, Italy</i>  | 148, 375, 428, 433 | Mick Eekhout<br><i>Octatube Space Structures B.V.</i>                   | 228      | William Lingnell<br><i>Lingnell Consulting Services</i>   | 176         |
| Graham Dodd<br><i>Arup</i>  | 351                | Miguel Angel Ruiz<br><i>Martifer Metallic Constructions</i>             | 331      | Wim Stevels<br><i>Eastman Chemical Company</i>  | 393         |
|   |                    | Miguel Núñez<br><i>ENAR</i>   | 71       |   |             |

# Active BIPV Glass Facades: Current Trends of Innovation

Erika Saretta, Pierluigi Bonomo, Francesco Frontini  
ISAAC DACD SUPSI

## Keywords

1=BIPV 2=Glass façade 3=Solar energy  
4=Innovation trends

## Abstract

On the path towards the implementation of nearly zero-energy buildings, as stated by the European Commission, the integration of photovoltaics technology in buildings (BIPV) has been proven to be very interesting in order to achieve the energy goals. In detail, the use of glass BIPV modules is constantly improving due to the fact that they can replace almost every conventional material of the building envelope and they can actively contribute to the building energy balance. But, is the transfer of PV in architecture only a matter of energy? Certainly not. Along with the multi-functionality of the building skin, BIPV today involves a new aesthetics in contemporary architecture. Thanks to innovative possibilities in glass development and customization for BIPV solution, a wide range of architectural languages arises in current applications, ranging from the visible semantics of solar cells to the technological mimicry. The aim of this paper is to describe the current researches and trends of innovation in the use of BIPV glass for building facades, through the discussion of some pilot case studies collected by the Swiss BIPV Competence Center ([www.bipv.ch](http://www.bipv.ch)) in the framework of different projects. Moreover, this study will create a platform for a primary discussion aimed to describe the innovative factors concerning the technological transfer of the PV glazing elements in the built environment.

## Introduction – BIPV and glass

The use of a material in architecture, in the course of building history, has always been enriched with something other than simple technological innovation, including a symbolic spirit, expressing its own linguistic value, the change and the design power. In the common imaginary, for example, glass is the material that can express a sense of constructive and perceptual lightness, which peculiarities

result in the physical dematerialization of the architectural object and in obtaining a perceptual and psychological transparency. When we hear about photovoltaics, however, the image that is invoked in our mind is a blue or black element that usually seems to “overload” the aesthetical image of a building. Even though a PV element has the basic role to produce renewable energy, this is not the main aspect concerning the “innovation in architecture”.

The combination of glass and photovoltaics, despite their different appearance and materiality, seems to match well in terms of both aesthetics and functionality of the building skin and the “BIPV glass” market is expected to grow in the forthcoming years [1]. Moreover, both in architecture and research perspective, there are many products, flagship buildings, research projects and some arising innovation trends that represent drivers for a successful transfer of BIPV glass into the real built environment. Since a lot of requirements are more and more needed for a high-quality architectural project also compliant with challenging energy levels, these “innovation trends” can be interpreted as the “meeting points” between different fields: architecture, construction products, glass facades and energy. In accordance with this perspective, the authors will investigate and show some of the innovative drivers that arose out of lighthouse projects in Switzerland.

## Innovation trends and some implementations into real buildings

The origin of BIPV is a pioneering experimentation conducted in architecture in 1978-82: a glazed surface of a residential unit in Munich designed by Thomas Herzog in collaboration with Fraunhofer ISE that is still today an undiscussed reference on both PV technology and integrated design approach. Since 1990s, the trends of BIPV has increased worldwide both in terms of research and industrial projects for improving BIPV products/processes and applications in buildings. For instance, one of the first BIPV glass façade has been realized in 1991 in the Public Utilities Building of Aachen (Germany) where PV cells have been included into insulation glass panels, which have been used to replace the existing 20-years-old southern façade. The combination of PV cells

and glass can also provide several advantages in technical terms, such as lower potential induced degradation (PID), higher mechanical resistance and better reliability than traditional PV modules [2]. For instance, the presence of glass on both front and rear sides of the PV module allows a lower humidity and moisture penetration, reducing in such a way the PID mechanism. However, not only technical advantages can be identified for BIPV glass, since nowadays several new concepts and solutions are arising to allow the realization of active BIPV glass facades. In order to provide a clear – but not exhaustive – vision of some of these concepts and solutions, the innovation trends for BIPV glass are presented as the results of the “meeting points” between different disciplines/fields.

Specifically, the authors have identified four main trends of innovation: optimization of aesthetics and efficiency (**energy and architecture**); transformation of ideas into real products (**architecture and construction**), development of technological BIPV solutions (**construction products and glass facades**) and development of active BIPV facades (**glass facades and energy**).

## Energy and architecture: aesthetics and efficiency

The increased interest in nearly zero-energy buildings, as defined by the European Directive (REF), has led attention to the building envelope as a multifunctional and adaptive interface to be designed appropriately in order to the one hand reduce building energy consumptions (with more efficient solution) interacting with the outdoor conditions, such as winds, humidity and solar radiation and on the other hand produce local renewable energy. Moreover, the increased attention in solar buildings has created also an interest in the new role of BIPV facades, as active elements of the building skin. To allow architects new design opportunities for the aesthetical language of PV, researchers and module manufacturers are developing customized BIPV glass modules in terms of performance and visual appearance. In such a way, for example, PV cells can be camouflaged behind coloured patterns that completely dissimulate the original materiality of the PV cells. However, this involves a “shading” over the PV cells and a consequent reduction

of the energy production, that needs to be carefully optimized in order to obtain an energy efficient customization of the BIPV modules. Namely the challenge to optimally balance the aesthetical quality with the energy and electrical efficiency, reliability and safety is one of the drivers of innovation. Different customization techniques can be identified in the current developments:

- **glass surface techniques:**

- Sandblasting: technique that consists in spraying sand at high velocities on the front glass surface, creating milky white patterns and sketch. Within the EU project ConstructPV [3], different BIPV glass modules have been designed and realized with this technique, paying attention to the balance between costs, energy output and visual effects (fig. 1). Other examples of BIPV glass modules realized with sandblasting are the ones designed by SolarGlasLabor [4], where additional colouring techniques are used (fig. 2).

- Silk-screen printing: process that allows to print special ink on the glass surfaces in order to obtain a drawing. An interesting example of silk-screen printing has been developed by Ertex, that developed a process to obtain homogeneous BIPV glass modules in appearance [5]. In the framework of the EU project SmartFlex [6], a novel digital ceramic-based printing has been developed, enabling to print high definition pictures (up to 720 dpi) on the glass (fig. 3). Also in this case, the optimization of the aesthetics and energy outputs has been investigated in order to provide efficient BIPV glass solutions. Another example of multi-colours ceramic digital printing on BIPV glass has been developed by the Lucerne University of Applied Sciences (fig. 4), where a specially developed method ensures that, despite the use of different colours, no partial shading and losses of more than 20% result [7].

- Satin finish and glass printing: a satin finishing on the outer glass surface is combined with the silk-printing on the inner side. Therefore, there is a reduction of the glass transparency and a resulting coloured matte surface. Nevertheless, the treatment is carefully developed in order to allow light radiation to hit the PV cells, even though they are not visible.

- **use of special solar filters:**

- scattering and reflection filters: this technique has been developed by CSEM [8]. On the glass pane a front selective filter is applied. This is capable to reflect and diffuse the visible spectrum providing a white appearance, while the infrared

part is transmitted and converted into electricity. In such a way, there is an efficiency reduction of about 40% in comparison to a traditional module.

- spectrally selective coating: thanks to a special sputtering process, SwissINSO SA obtained coloured BIPV glass modules. For example, the conversion efficiency of these modules with white coating is 11.4%, instead of 19.1% of standard modules [9]. The coloured coating is a thin-film deposited on the front surface by chemical etching and it allows to realize different colours such as grey, terracotta, blue, bluish-green, green and yellow.

All of these techniques are carefully used in order to optimized the visual effect and the efficiency of the photovoltaic production, since there is a reduction of the incident light on the PV cells. It's interesting to remark a double approach: on one hand a high-tech development has created new techniques and materials (mainly transferring them from high-tech research fields such as material science or physics and optics) and on the other hand a transfer of techniques already used in the building industry has been adopted to customize the front glass. It's also relevant to consider that in some cases some aspects such as the design/production flexibility, the building performance and the cost-effectiveness still remain challenges to be achieved in order to ensure a feasible market penetration. What it is important to highlight is that some of the above-mentioned customizable BIPV glasses have been already implemented into real buildings. In some cases, these are lighthouse projects but also some private projects are arising, as a proof of a nascent market for customizable BIPV glass in a cost-effective and affordable way for the building market. In table 1, some Swiss buildings with innovative BIPV glass concepts are briefly explained, including the customization glass technique, the energy performance, the whole façade cost and the modules manufacturer.

### Architecture and construction: from ideas to building skin elements

Today we can image a solar module that is completely recognizable within the urban environment, expressing its own materiality and language, rather than completely camouflaged with another appearance. In any case when such a novel and customized BIPV glass module is envisioned and designed, the next step is the characterization and testing to assess its performances, behaviour and reliability. In the case of BIPV, the modules should be compliant both with electro-



Figure 1 ConstructPV module- UNSTUDIO design [3]



Figure 2 SolarGlasLabor module [4]



Figure 3 SmartFlex modules [6]



Figure 4 HSLU modules [7]

|   |   |  |
|---|---|--|
| <p style="writing-mode: vertical-rl; transform: rotate(180deg);"><b>Sandblasting</b></p>                    |  <p>Figure 5 Autarkic MFH, Brütten.<br/>Source: umweltarena.ch</p>              | <p><b>Autarkic Multi-Family House – Brütten [14]</b></p> <ul style="list-style-type: none"> <li>• the BIPV glass modules are thin-film modules with a matte outer surface obtained thanks to a sandblasting treatment and with different sizes to fit the shape of the building envelope</li> <li>• the module are glued to vertical back-profiles by means of SSG to be hung to the rear back-ventilated façade substructure</li> <li>• Façade cost = about 600 CHF/m<sup>2</sup></li> </ul>  |
| <p style="writing-mode: vertical-rl; transform: rotate(180deg);"><b>Silk-screen printing</b></p>            |  <p>Figure 6 MFH Chrüzmatte, Aesch.<br/>Source: Schweizer Solarpreis 2016</p>  | <p><b>Multi-Family House Chrüzmatte – Aesch [15]</b></p> <ul style="list-style-type: none"> <li>• the BIPV glass modules are 2,04x3.32m and they are hung on the facade by means of pre-mounted back-rails (generally already used for glass facades)</li> <li>• the modules have been subjected to a silk-screen printing in order to provide continuity to the wood façade elements and provide a homogeneous visual effect</li> <li>• Module manufacturer: Ertex Solar</li> </ul>   |
| <p style="writing-mode: vertical-rl; transform: rotate(180deg);"><b>Satin finish and glass printing</b></p> |  <p>Figure 7 PEB Renovation, Zürich.<br/>Source: Gasser Fassaden Technik</p> | <p><b>Plus-Energy Building Renovation – Zürich [16]</b></p> <ul style="list-style-type: none"> <li>• 18 different formats of frameless BIPV glass modules have been used to fit the whole building envelope as panels of an aluminium rear-ventilated façade construction, using back-rails (SSG-bonding on glass module)</li> <li>• Glass panes have been treated in order to obtain an anti-reflective and matte surfaces. Colour in the range from grey to anthracite with performance values of 109.2 W/m<sup>2</sup></li> <li>• Façade cost = 800 to 900 CHF/m<sup>2</sup></li> <li>• Module manufacturer: PVP Photovoltaik GmbH</li> </ul> |
| <p style="writing-mode: vertical-rl; transform: rotate(180deg);"><b>Selective coating</b></p>               |  <p>Figure 8 Solar Silo, Basel.<br/>Source: BFE-SUPSI</p>                    | <p><b>Solar Silo – Basel [17]</b></p> <ul style="list-style-type: none"> <li>• Crystalline framed standard-size BIPV glass modules are integrated as tile roof and 2 different formats for frameless BIPV glass modules are used as cladding panels of the rear-ventilated façade</li> <li>• Reduction of efficiency depending on the colour: -4.6% grey, -6.2% blue, -5.4% green, -10.8% gold, in comparison to a traditional PV module without the coloured solar filter</li> <li>• Façade cost = 780CHF/m<sup>2</sup></li> <li>• Module manufacturer: Antec/Kromatix Solarglas</li> </ul>   |

Table 1 Swiss buildings with innovative “aesthetics and energy” concepts.

technical standards set in the IEC framework and the relevant building standards as established in the European Construction Product Regulation CPR 305/2011[10] and local building authorities. This means that the BIPV system should be capable to perform as a traditional building skin element, as well as to produce an adequate electrical output in its expected life. In order to foster this concept, two European standards have been developed and published in 2016, the EN 50583:2016 "Photovoltaics in buildings" part 1 and part 2 [11]. With regard to BIPV glass module, there is also another international standard proposal– the ISO/DIS 18178:2014 "Glass in building. Laminated solar PV glass" [12] and, moreover, solar glass represents a topic in the Guidance for European Structural Design of Glass Components [13]. This is mainly due to the fact that BIPV glass modules have some peculiarities (e.g. cells, electrical wirings, operating conditions...) that should be taken into account differently than a conventional glass panel. Specifically, in the case of customized BIPV glass modules characterized by the above-mentioned customization techniques, it is fundamental to guarantee the durability of the glass treatments. Indeed, BIPV glass modules are subjected to twofold stresses: internal thermal stress within the encapsulant due to the increase of temperatures due to the electricity production of PV cells (up to 60°C in operating conditions during summertime) and external stresses due to outdoor weather conditions such as rain, temperature variations, humidity and hail, therefore it is necessary to ensure the maintenance of the module appearance during their expected life or during the expected façade life (as an even better option) by

means of dedicated aging tests. This means that a BIPV module, due to its peculiarities as a multifunctional element, should be characterized, tested and assessed according to a specific multidisciplinary approach integrating (not just adding) both building and energy/electrical aspects, in terms of performance, aesthetics, costs, etc.

**Construction and glass: technological BIPV solutions**

In the BIPV glass innovation field, one driving factor can be represented by the development of new solar glasses to integrate as functional elements of the building envelope, namely a construction product. Indeed, in accordance with the EN 50583-2, a BIPV system should also be capable to "form a construction product providing a function as defined in the European Construction Product Regulation CPR 305/2011". Therefore, not only BIPV glass module should be designed but the whole building skin system (modules and substructures), that constitute the building envelope engineering. A multidisciplinary approach is the key-challenge. In this framework, the BIPV glass "domain" such as some manufacturers should refer to the knowledge and expertise of the glazed facade domain to properly develop and manufacture a component to be used as part of the building skin – e.g. some basic design principles concerning the mechanical safety such as avoid excess load in correspondence of continuous supports along the edges or avoid constrained supports such as rigid clamps. On the other hand, the BIPV glass "domain" can also give some inputs to the glass facade "domain" since there are some peculiarities

that should be taken into account in the glass/façade design to ensure a reliable and optimal energy/electrical behaviour, such as the improved residual resistance due to the presence of PV cells interconnectors [18] or the stiffness effect of the junction box glued to the glass pane by means of sealant. Moreover, the use of BIPV glass elements – especially for glazed opaque facades – has led attention also to the development and testing of fastening systems with back-rails and adhesive elements to make invisible the mounting substructures and provide a homogeneous view of the glass façade (e.g. Structural Sealant Glazing), that have to guarantee the mechanical stability and resistance under the operating conditions. The importance of a strict correlation of the BIPV glass behaviour with the building skin technological solution is arisen also from the mechanical test activities developed within the SmartFlex project [6], where an "integrated approach" to evaluate the mechanical behaviour of laminated BIPV glass have been proposed [19]. Moreover, another experience concerning mechanical tests have been performed by SUPSI also on a real BIPV façade system developed for the recladding of the Plus-Energy multi-family house in Chiasso (table 2). Indeed, in the first design option, even though the modules were mounted onto the metal substructure with a safety clamping system, the cladding PV module failed because of its high deflection from the substructure. Then, the second design option – consisting in the use safety clamps and the gluing of the cladding panel onto the rear metal profiles– succeeded [20] due to the greater rigidity and the proper connection with the BIPV glass element. Therefore, some of the previous examples, demonstrate that innovative

| <b>BIPV technological solutions</b>  | <b>Active facade</b>   | <b>Active façade</b>  |
|--|--|---|
|  |  |  |
| <p><i>Figure 9 PEB, Chiasso. Source: BFE-SUPSI</i></p>                             | <p><i>Figure 10 ETH-HoNR building, Zürich. Source: ETH [20]</i></p>                  | <p><i>Figure 11 CSEM façade, Neuchâtel Source: BFE-SUPSI</i></p>                      |
| <p>Cold façade: glued BIPV glass modules</p>                                       | <p>BIPV dynamic façade</p>   | <p>Bifacial façade</p>  |

Table 2 Swiss buildings with innovative concepts

solutions can arise often just from the investigation of the most reliable and optimal solutions to integrate a BIPV glass modules in a conventional technical system of the building envelope, also in a specific case study.

## Glass and energy: active facades

Since glass has been used as a building envelope material in last two centuries, it provides a sense of de-materialization of the building envelope and lightness of the architecture. In 1960's the idea of energy savings has firstly led to the development of the insulating glass unit to reduce thermal dispersions and, more recently, to the development of special adaptive and complex systems, such as high-performance filters to reflect a portion of the light spectrum or thermochromic elements capable to blocks parts of solar radiation. Also thanks to the Energy Performance of Buildings Directive, published in 2010, the building envelope has been identified as the smart interface between indoor and outdoor environment that can assume an additional function: the active energy generation thanks to integrated solar systems (photovoltaics and/or solar thermal).

In this framework, some innovative façade concepts can be identified, such as the adaptive solar facades and the "bifacial" facades. An example of the former concept has been developed by the ETH team [21] in order to realize BIPV solar shadings moved by pneumatic actuators in order to control the visibility and transparency of the rear façade (table 2). The latter concept takes advantages from the recent development of bifacial photovoltaic glass modules, which can produce solar energy thanks to the direct sun radiation on the front side and the reflected radiation on the rear side. In such a way, a second bifacial PV screen can be integrated in the building envelope in order to exploit also the light reflected by the inner façade (e.g. in double skin facades). The CSEM building in Neuchâtel is a Swiss example reference that has been designed in 2015, for a total of 633 m<sup>2</sup> and an expected annual energy production of about 50 - 60 MWh (table 2).

## Conclusion and summary

Considering the relevant role of PV technology in the current energy policies at European and international level, a reflection about the innovation process affecting the building field is crucial. This study has been developed in order to present some main innovation trends in the use of architectural BIPV glass for building facades. A lot of approaches and developments in terms of manufacturing techniques and real case-studies have been discussed. To sum up, from the recent references and products, these requirements

calling for further developments arose from:

- the need of new BIPV glass products to support a high-quality architectural project in the field of nearly-zero energy buildings;
- the request of reliability for such products, according to both the electrical and building field;
- the complete functional/performance integration into the building envelope system,
- the combination of building energy concepts and the façade engineering field.

Of course, although we attempted to provide evidence on some driving principles and trends of innovation, undoubtedly a number of aspects remain still to be investigated and call for future research. What is interesting to note is that some innovation trends are already on the path to be implemented in Swiss buildings. This is also due to the fact that BIPV glass facade are already competitive today in terms of cost [23], when compared to conventional glass façades, so that a "BIPV façade" can today also represent an alternative to a conventional building envelope. Solar energy can represent an opportunity for the glass industry, not only for semi-transparent parts but also for opaque facades.

In conclusion, in recent years, the efforts in the development of glass facades have led to spectacular building glass envelopes that are capable to represent resistance but, at the same time, weightless, even though this can seem an oxymoron. Today, building glass envelope has the chance to achieve a wider goal that is represented by its active contribution in the sustainability domain without losing the architectural elegance of glass.

## References

- [1] N-Tech Research. (2015). BIPV Glass Markets 2015-2022
- [2] Wei, Q., Wu, C., Liu, X., Zhang, S., Qian, F., Lu, J., Lian, W., Ni, P. (2016) The Glass-glass Module Using n-type Bifacial Solar Cell with PERT Structure and its Performance, Energy Procedia, Volume 92, 2016, Pages 750-754, ISSN 1876-6102, <http://dx.doi.org/10.1016/j.egypro.2016.07.054>
- [3] EU Project ConstructPV, available at: <http://www.constructpv.eu/>
- [4] Geissler, A., Fornaro, P., Bianco, A. (2016). Visual Design of PV-Modules – a Crucial Factor for Façade Application Acceptance. Proceedings of the 32nd European Photovoltaic Solar Energy Conference and Exhibition, pp. 2470 - 2475, ISBN: 3-936338-41-8, doi: 10.4229/EUPVSEC20162016-6DO.7.2
- [5] Dieter, M. (2016). Nursery + e kita in Marburg – solar architecture at its best. In Jens Schneider and Bernhard Weller (Eds.), Engineered Transparency 2016: Glass in Architecture and Structural Engineering (349-354). Ernst&Sohn.
- [6] EU Project SMART-FleX, available at: <http://www.smartflex-solarfacades.eu/>
- [7] Gebäudehülle - Technik & Trends. (2016). Schön viel Strom Produzieren.
- [8] Escarré, J., Li, H.-Y., Sansonnens, L., Galliano, F., Cattaneo, G., Heinstejn, P., Nicolay, S., Bailat, J., Eberhard, S., Ballif, C., Perret-Aebi, L.-E. (2015) When PV modules are becoming real building elements: White solar module, a revolution for BIPV. 2015 IEEE 42nd Photovoltaic Specialist Conference (PVSC), New Orleans, LA, 2015, pp. 1-2. doi: 10.1109/PVSC.2015.7355630
- [9] Mertin, S., Hody-Le Caër, V., Joly, M., Scartezzini, J.-L., Schüller, A. (2011) Coloured coatings for glazing of active solar thermal façades by reactive magnetron sputtering. Proceedings CISBAT 2011, Lausanne, Switzerland.
- [10] Regulation N° 305/2011 Of The European Parliament and of the Council European – Construction Product Regulation
- [11] EN 50583-1:2016, Photovoltaics in buildings – Modules; EN 50583-2:2016, Photovoltaics in buildings – Systems
- [12] ISO/DIS 18178:2014, Glass in building – Laminated solar PV glass
- [13] Feldmann, M., Kasper, R., Abeln, B., Cruz, P., Belis, J., Beyer, J., Colvin, J., et al. (Eds.). (2014). Guidance for European structural design of glass components: support to the implementation, harmonization and further development of the Eurocodes. EUR. Luxembourg: European Union
- [14] "Autarkes Mehrfamilienhaus Brütten: Einmal ohne Netzanschluss bitte!", available at: <http://www.ee-news.ch/de/article/33698/autarkes-mehrfamilienhaus-brutten-einmal-ohne-netzanschluss-bitte>
- [15] "Ernst Schweizer: Symbiose von Holz- und Photovoltaikfassade", available at: <http://www.ee-news.ch/de/erneuerbare/article/32992/ernst-schweizer-symbiose-von-holz-und-photovoltaikfassade>
- [16] Bundesamt für Energie BFE. (2016) Leuchtturm Photovoltaik Fassade an PlusEnergieBau Sanierung Zürich
- [17] Steike, G., Menn, C., Geissler, A. (2016). Transformation eines Kohlesilos zum Solarkraftwerk mit farbigen PV-Modulen und Second-Life Speicher. 19. Status-Seminar "Forschen für den Bau im context von Energie und Umwelt". Zürich
- [18] Hemmerle, C. (2017). Solar PV Building Skins: Structural Requirements and Environmental Benefits. Journal of Façade Design And Engineering, 5(1), 93-105. doi:<http://dx.doi.org/10.7480/jfde.2017.1.1528>
- [19] Saretta, E., Bonomo, P., Frontini, F. (2016). Laminated BIPV glass: approaches for the integration in the building skin. In Jens Schneider and Bernhard Weller (Eds.), Engineered Transparency 2016: Glass in Architecture and Structural Engineering (363-372). Ernst&Sohn. Print ISBN: 978-3-433-03187-2
- [20] Frontini, F., Friesen, T., von Ballmoos, C., Di Gregorio, S. (2014). Palazzo Positivo: renovation of a residential building in Switzerland with BIPV facades. In: 29th European PVSEC, 2014, Amsterdam. (In Press)
- [21] ETH Adaptive Solar Façade, available at: <http://www.systems.arch.ethz.ch/research/active-and-adaptive-components/asf-adaptive-solar-facade.html>
- [22] Nagy, Z., Svetozarevic, B., Jayathissa, P., Begle, M., Hofer, J., Lydon, G., Willmann, A., Schlueter, A. (2016) The Adaptive Solar Façade: From concept to prototypes, Frontiers of Architectural Research, Volume 5, Issue 2, June 2016, Pages 143-156, ISSN 2095-2635, <http://dx.doi.org/10.1016/j.foar.2016.03.002>
- [23] Frontini, F., Bonomo, P., Chatzipanagi, A., Van den Donker, M., Verbene, G., Sinapis, K., Folkerts, W. (2015) Building Integrated Photovoltaics. Report 2015. Technical Report

## Acknowledgements

Authors would like to thank prof. Dr. Stephen Wittkopf from Hochschule Luzern for his support concerning the analysis of innovative coloured photovoltaic modules.

The research leading to these results received funding from the European Community's Seventh Framework programme (FP7/2007-2013) under grant agreement no 295981 [[www.constructpv.eu](http://www.constructpv.eu)] and it has been also developed in the framework of the project ACTIVE INTER-FACES - Holistic strategy to simplify standards, assessments and certifications for building integrated photovoltaics (#153849) founded by the Swiss National Science Foundation SNF. ActiveInterfaces.

# Qualifying and quantifying thermal comfort in highly glazed spaces

Medina Deliahmedova, Inform Design AB,  
Lund University  
Harris Poirazis, Inform Design AB  
Henrik Davidsson, Lund University

## Key words

1=Thermal comfort;2= glazed buildings;  
3= adaptive model (AM);4= PMV

## Abstract

This paper aims to answer a simple and elemental question: how do we qualify and quantify thermal comfort in highly glazed spaces with diverse occupants' use and expectation? And, how can designers achieve enhanced occupant experience with passive measures, minimizing the use of HVAC systems in such spaces? In this study variables, such as air and radiant temperatures, air velocity, relative humidity and direct solar component were identified as the "working tools" in order to create different indoor environments that fulfil expectations and serve the building's function. Parameters such as adaptability, occupants' expectation and duration of stay within each space are also affecting the acceptance levels of thermal comfort. The study includes the existing standards and comfort models and synthesizes this knowledge to develop a "hands on" method that will help designers meet the comfort expectations of diverse spaces with respect to the vision and the functionality of the building. As a result, an excel based tool was developed that can help designers in understanding thermal comfort and the important affecting variables, leading to appropriate measures for avoiding thermal discomfort and fulfilling the set performance requirements. The tool was used on a case study, where thermal comfort limits were examined for different types of spaces.

## Introduction

The lack of methodology for assessing thermal comfort in non-standard spaces can often be recognized when dealing with non-conventional buildings. The lack of appropriate methods that feed

comfort assessments is even more evident when it comes to highly glazed spaces, as the effect of the direct solar component is a significant factor in those space, but is neglected by standard methods for assessing thermal comfort. This generates a question as to whether comfort is appropriately assessed when using Dynamic Thermal Modelling tools. Furthermore, this generated one more question: are there any tools that can assist the designer size potential discomfort in early design stages? Often, the design process is based on the principle of try and error, where the design is tested through a simulation program and if it doesn't fulfill the specified comfort requirements the process needs to start again. But how can we bring the knowledge of thermal comfort into the early design process so that it can help designers find an appropriate design solution?

## Problem formulation - case study

The initiation of this project idea came when examining microclimates for a fully glazed tropical park in south of Sweden. Within this project, it was essential to provide enhanced occupant comfort in various types of spaces such as entrance areas, cafeteria, cinema and most importantly the exhibition areas. In the latter spaces, specific plants and animals would need to co-exist, while the environment needs to simultaneously be pleasant for the visitors. Although this project is somewhat extreme, the questions that arose can easily be applicable to any building with spaces with different function and design. Some of those questions are: Which is the appropriate comfort model for the different types of spaces? Can the same model be used for accessing thermal comfort in diverse spaces with different occupant use e.g.in an entrance space and in a cinema hall or in an atrium and in an office space?

## Background theory

It has been demonstrated that the main environmental parameters that influence

perception of thermal comfort are air temperature, mean radiant temperature (MRT), relative humidity (RH) and air velocity ( $v_a$ ) [10]. Furthermore, the activity level and clothing level can also significantly affect comfort [10].

Those parameters are used in a model called PMV [5] that has been widely used to evaluate thermal comfort in buildings and has also been included in European and International Standards [3], [4], [11]. The model uses the theory of human thermal regulation and is calibrated according to results of experiments from climate chambers [5].

However, the approach used to develop the PMV model have been criticized, because it considers human beings to be passive recipients of the thermal conditions [7]. Adaptive comfort model was developed, that considers the "human factor" or in other words the ability of people to adapt to their environments, thus being able to function in wider range of environmental conditions [9]. The model is derived from statistical data, comparing the outdoor temperature to the comfortable indoor operative temperature and differentiating between conditioned and non-conditioned buildings [9].

Another model, called Universal Climate Index (UTCI), was developed in recent years, that uses computer model for human response to thermal environment [2]and [6]. The index is an equivalent of the air temperature in Celsius of a reference environment that is providing the same thermal sensation as the actual environment [2]. It is mostly used to describe outdoor thermal comfort. International and European standards that address thermal comfort in buildings have adopted the PMV model for assessment of thermal comfort in standard buildings. The adaptive model is recommended only for non-conditioned buildings or parts of the year when the building is not conditioned. The standards do not deal with outdoor or semi external spaces. Several studies have led to conclusions that the standard recommendations cannot be used, when thermal comfort is assessed in not standard spaces such as entrance areas or highly glazed atria ([11] and [12]). It is suggested that in such

spaces adaptive model is appropriate regardless if the space is conditioned or not. Wider comfort limits are also considered acceptable compared to the ones stated in the standards [8].

**Method**

In this project a methodology was developed and formed into an excel based tool, that can help designers to improve their understanding of thermal comfort and the implication of different parameters to it [13]. Different comfort models were used to predict the thermal expectations in various types of spaces, the focus was set to transitory and highly glazed ones, as they are not well covered in the standard recommendations for thermal comfort. The tool through an iterative process can potentially help designers to set the right performance requirements of the building envelope and find appropriate set points for control mechanisms used in the building. The tool developed within this work uses thermal comfort models – predicted mean vote (PMV), adaptive model (AM), an extended AM for transitory spaces and UTSI, to set the limitations for the environmental parameters that affect the human perception of thermal comfort namely - air temperature, MRT, RH and air velocity. Variables as activity and clothing level are also considered.

Algorithm for finding appropriate comfort model was developed, based on the existing literature, that considers also factors as space type, adaptation possibilities, duration of occupation and connection to exterior. The algorithm suggests two options: 1) appropriate comfort model according to the literature; and 2) the standard recommended model, see Figure 1. In the figure with black outline are presented the steps taken to identify the comfort model that is recommended by the standards. In case the standards do not cover the type of space in question the value “---” is given. In the figures with blue outline are the steps necessary to determine a suitable comfort model based on the background literature review. In green outline are the steps taken to define the type of AM to be used, when it is suitable or standard recommended, where AMT is adaptive model for transitory space, AMN is adaptive model for non-conditioned spaces and AMC is adaptive model for conditioned spaces.

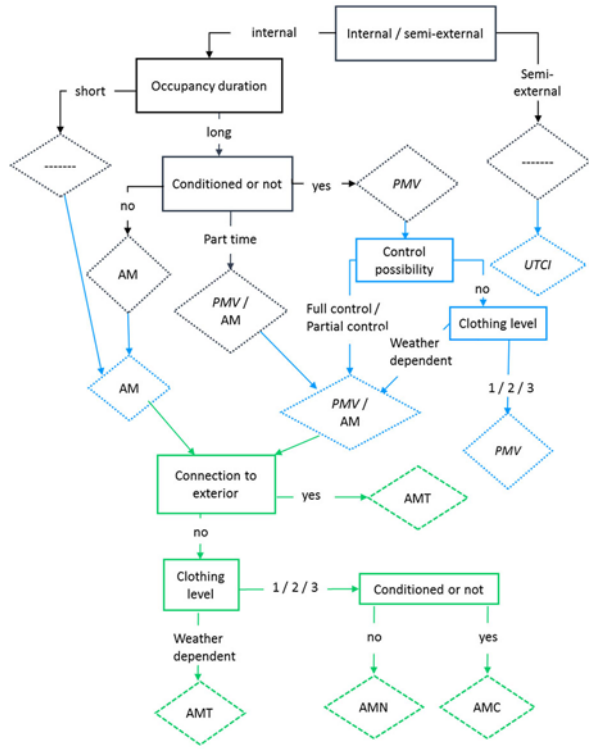


Figure 1. Algorithm for selecting appropriate comfort models

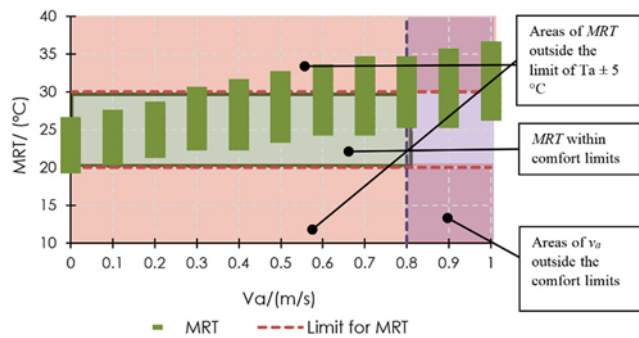


Figure 2. Example of informative graph, presenting MRT and  $T_a$  for given  $v_a = 0.1 \text{ m/s}$  and  $RH = 50\%$

Further the excel tool gives the users possibility for varying each of the environmental parameters and examine their effect to the thermal comfort, according to the different models. With changing one environmental parameter, visual graphs are automatically created to inform the user about the comfort limits of each parameter. The first informative graph, see Figure 2, presents MRT and  $v_a$  for given  $T_a$  and in the case of PMV and UTCI also given RH. In this case the MRT and  $v_a$  for  $T_a = 25 \text{ }^\circ\text{C}$  and  $RH = 50\%$  are presented. The green bars of the graph represent the MRT values for different  $v_a$  that result in comfortable conditions. The area highlighted in green is the area where MRT is within the limit of  $T_a \pm 5 \text{ }^\circ\text{C}$ . The areas highlighted in light red include values of MRT that are within the comfort limits according

to the models, but are outside the limit of  $T_a \pm 5 \text{ }^\circ\text{C}$ . The purple area of the graph indicates that the air velocity is higher than the limit for comfort of 0.8 m/s. From the graph, it can be read for the given  $T_a$  what the limits are for MRT at which for example natural ventilation can be sufficient and when it is necessary to add solar control in order to reduce the MRT.

The second informative graph, Figure 3, presents MRT and  $T_a$  for given  $v_a$  and in the case of PMV and UTCI also given RH. In this case combinations of MRT and  $T_a$  are presented, for  $v_a = 0.1 \text{ m/s}$  and  $RH = 50\%$ . In this graph the limits for MRT of  $T_a \pm 5 \text{ }^\circ\text{C}$  are shown with red lines. The green area shows values of MRT within this limit. The light red areas show MRT values that would still result in comfort conditions, but are outside the limit

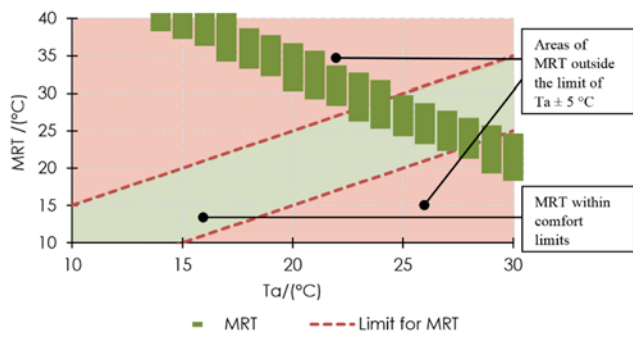


Figure 3. Example of informative graph, presenting MRT and  $v_a$  for given  $T_a = 25^\circ\text{C}$  and  $RH = 50\%$

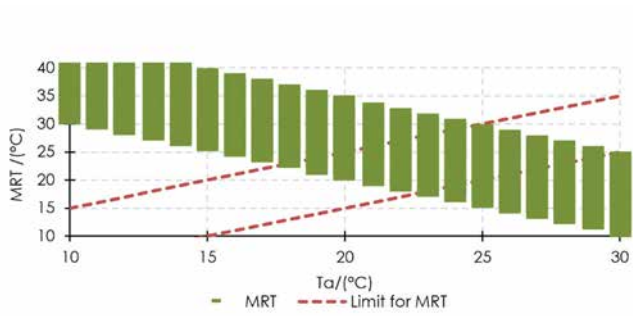


Figure 4. MRT and air temperature for air velocity of 0.1 m/s

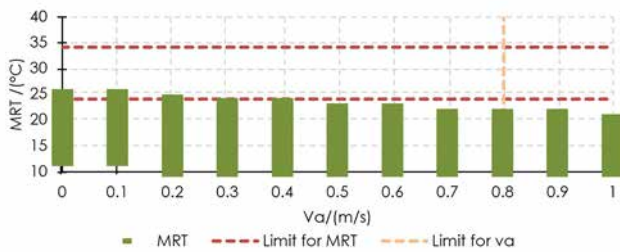


Figure 5. MRT and air velocity for air temperature of  $29^\circ\text{C}$

of  $T_a \pm 5^\circ\text{C}$ . This can inform the designer of the possibility to use passive measures as shading devices or solar gains, and when active heating or cooling needs to be applied. The comfort limits are set according to EN 15251 and ISO 7730.

Within this study different areas were chosen from the case study, described above. In this paper, only the entrance space will be presented to demonstrate the value of the developed tool.

The characteristics of the space were as follows: space type – internal; part time conditioned; limited adaptation possibility; short duration of occupation and connected to exterior.

## Results

The comfort models, recommended by standards for this space, are PMV for the part of the year when the space is conditioned and AM when it is not. However, based on the literature review the algorithm created has suggested that an extended AM for transitory spaces can be used to describe the comfort limits throughout the whole year.

When examining different combinations of environmental parameters using the developed method, it was observed that for air velocity of 0.1 m/s the minimum value of the air temperature that falls within the comfort limits is  $18^\circ\text{C}$  and the maximum is  $29^\circ\text{C}$ , demonstrated in Figure 4. For these values of air temperature, the MRT can be  $23^\circ\text{C}$  and  $24^\circ\text{C}$  respectively. The largest spans for MRT are from  $18^\circ\text{C}$  to  $28^\circ\text{C}$  and from  $19^\circ\text{C}$  to  $29^\circ\text{C}$ , indicated in Figure 4 by the green bars, corresponding to air temperature of  $23^\circ\text{C}$  and  $24^\circ\text{C}$  respectively. These results show that air temperature as low as  $18^\circ\text{C}$  can be compensated by higher MRT.

To consider the risk of overheating and possible measures to prevent it, air temperature of  $29^\circ\text{C}$  was considered. The combinations of MRT and air velocity, that would result in comfort conditions, were examined, see Figure 5. The span of permissible air velocity for this air temperature is from 0 to 0.2 m/s, with MRT of  $24^\circ\text{C}$  to  $25^\circ\text{C}$ . Since the air temperature is rather high, lower MRT values are needed to achieve comfort, which would result in bigger difference between MRT and the air temperature than it is considered appropriate by the standards. Thus, lower air temperature is required to have a better chance to avoid overheating only with varying the air velocity or the MRT. In practice this means that the air temperature should be lower than  $29^\circ\text{C}$  so that natural ventilation and shading will

be able to have positive effect on the thermal comfort. If the air temperature exceeds this level a cooling system needs to be considered with lower set point to achieve acceptable thermal conditions.

## Conclusions

Through a case study it was demonstrated that the method can be valuable for building designers in understanding thermal comfort and the effect of different environmental parameters as air temperature, mean radiant temperature, air velocity and relative humidity. The method can help designers in finding appropriate measures for avoiding thermal discomfort, by defining the limits for each environmental parameter. It can be useful especially for nonstandard and highly glazed spaces in finding the appropriate comfort model, as those spaces often cannot be assessed properly by the standard comfort models.

The tool is flexible in a way that it allows designers to dynamically change all parameters, explore their limits and find combinations that provide comfort conditions. The tool is also valuable as it uses standard recommendations to derive comfort limits as described in EN 15251 and ISO 7730 and also gives alternative solutions taking into consideration the latest scientific knowledge.

## References

- [1] ASHRAE, 2004. Thermal Environmental Conditions for Human Occupancy - ANSI/ASHRAE Standard 55. s.l.:American Society of Heating, Refrigerating and Air-Conditioning Engineers, Inc..
- [2] Blazejczyk, K. et al., 2010. Principals of the New Universal Thermal Climate Index (UTCI) and Its Application to Bioclimatic Research in European Scale. *Miscellanea Geographica*, Volume 14, pp. 91-102.
- [3] EN 15251, 2007. Indoor Environmental Input Parameters for Design and Assessment of Energy Performance of Buildings Addressing Indoor Air Quality, Thermal Environment, Lighting and Acoustics. Brussels: European Committee for Standardization.
- [4] EN ISO 7730, 2005. Ergonomics of the thermal environment – Analytical determination and interpretation of thermal comfort using calculation of the PMV and PPD indices and local thermal comfort criteria. Brussels: European Committee for Standardization.
- [5] Fanger, P. O., 1970. Thermal comfort. Copenhagen: Danish Technical Press.
- [6] Fiala, D., Lomas, K. j. & Stohrer, M., 2001. Computer Prediction of Human Thermoregulatory and Temperature Responses to a Wide Range of Environmental Conditions. *International Journal of Biometeorology*, Volume 45, pp. 143-159.
- [7] Halawa, E. & van Hoof, J., 2012. The Adaptive Approach to Thermal Comfort: A Critical Overview. *Energy and Buildings*, Volume 51, pp. 101-110.
- [8] Hui, B. S. C. M. & Jie, J., 2014. Assessment of thermal comfort in transitional spaces. Kowloon, Hing Kong, Proceedings of the Joint Symposium

- 2014: Change in Building Services for Future
- [9] Nicol, F., Humphreys, M. & Roaf, S., 2012. *Adaptive Thermal Comfort: Principles and Practice*. London: Taylor and Francis group.
- [10] Parsons, K. C., 2003. *Human thermal environments*. second ed. London: Taylor and Francis group.
- [11] Pitts, A., 2010. Occupant acceptance of discomfort in an atrium building: to sweat or to shiver?. London, Department of Architecture and Planning, Sheffield Hallam University.
- [12] Pitts, A., 2013. Thermal Comfort in Transition Spaces. *Buildings*, Volume 3, pp. 122-142.
- [13] Deliahmedova, M. Examination Of Adaptive Thermal Comfort Models For Appropriate Assessment Of Thermal Comfort In Transitory And Semi-External Spaces, Lund, Department of Energy and Building Design, Lund University

# 111 Main Enclosure | Responding to Extreme Performance Criteria

Lisa Follman, Associate  
Skidmore, Owings & Merrill, LLP

## Abstract

111 Main presented a unique challenge of façade design. A 35' tall all-glass storefront designed and constructed in a market that had no prior experience with glass of that scale, and almost three feet of vertical movement between the glass storefront and the tower above. The design and execution of a structural glass façade required input and expertise from a wide range of professionals, including the Architect, Engineer, Specialty Glass Engineer and Builder. By assembling the core team of specialists, the Owner achieved their goal of developing an exceptional and iconic building in the heart of Salt Lake City, Utah.

## Project Overview

111 Main is a 24-story speculative office tower located at the corner of South Main and E 100 South Street in the heart of downtown Salt Lake City, Utah, and only blocks away from Temple Square, the historic headquarters of the Church of Jesus Christ of Latter-day Saints. The building is connected on the

ground floor to the Eccles Theatre, a new 2,500 seat performing arts center built concurrently to the 111 Main tower, and is directly across the street from City Creek Center, a 20-acre mixed use development with retail, commercial and residential program completed in 2012. (Refer to Figure 1.)

Design of 111 Main was nearly complete when the project was acquired by City Creek Reserve, Inc. (CCRI). CCRI is the real estate investment portfolio of the Church of Jesus Christ of Latter-day Saints and a major developer of commercial real estate in Salt Lake City, Utah. CCRI's recent developments include the City Creek Center.

In the years leading up to their acquisition of the project, CCRI had made significant investments in the revitalization of downtown Salt Lake City. CCRI viewed the 111 Main project as an opportunity to create a landmark building within this newly re-energized downtown corridor.

## Site Complexities

The 111 Main tower is the cornerstone of a city block identified by the Salt Lake City

Redevelopment Agency (RDA) as the ideal location for a new performing arts center. Contained within this city block was a 90,000 square-foot (8,360 square-meter) L-shaped property owned by the RDA. The majority of this property was intended for use by the new performing arts center. A portion of the property was to be sold to the 111 Main development team for construction of a new office tower.

Economic feasibility of the office tower required a 21,000 square-foot (1,950 square-meter) footprint. However, to accommodate essential program elements, the new performing arts center required a footprint of nearly 75,000 square-feet (6,970 square-meter). For the tower project to move forward, a 21,000 square-foot (1,950 square-meter) tower floor-plate would need to be constructed on a 15,000 square-foot (1,390 square-meter) site.

The northern edge of the building is aligned with the property line along 100 South Street. Above Level 5, the southern edge of the building is suspended approximately 47.5 feet (14.48 meters) over the southern property line. The performing arts center encroaches 45 feet (13.72 meters) into the tower footprint between

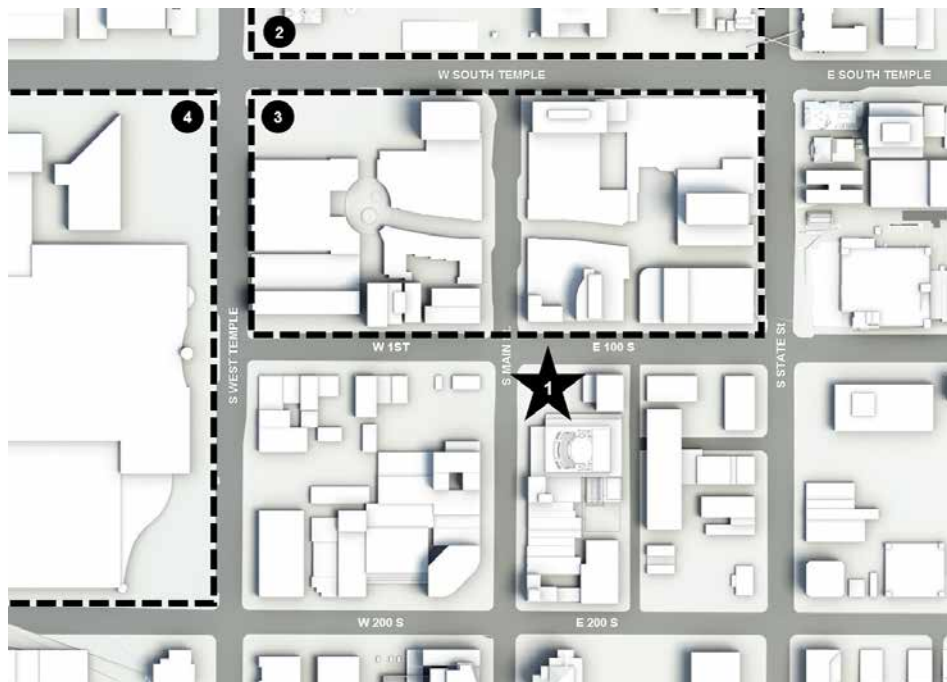


Figure 1 – Site Plan: 1. 111 Main Tower; 2. Temple Square; 3. City Creek; 4. Museum and Convention Center

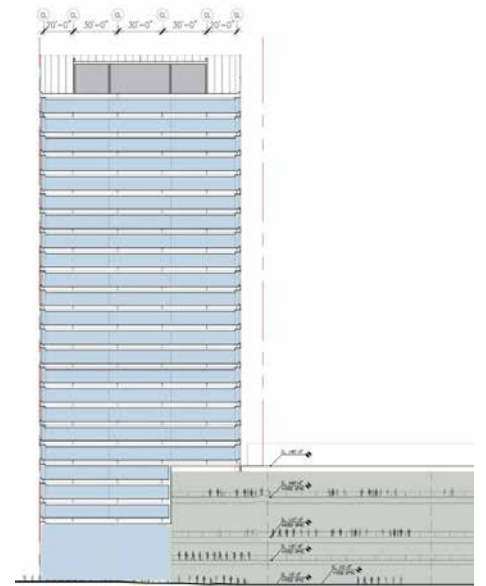


Figure 2 – Section Diagram

the ground floor and Level 5. CCRI acquired air rights from the RDA, and SOM Architects and Structural Engineers conceived a building with rooftop trusses to suspend the southern lease span of the tower over the new five-story performing arts center. (Refer to Figure 2.)

## Building Form

The tower has a rectangular form beginning at Level 5 and continuing up the full height of the building. The tower footprint is a 155 foot (47.24 meter) by 135 foot (41.15 meter), 21,000 square-foot (1,950 square-meter) rectangle. Levels 3 and 4 create a 155 foot (47.24 meter) by 87.5 foot (26.67 meter) rectangle, justified to the northern edge of the tower above. Level 2 is a mechanical level enclosed by intake and exhaust louvers, and setback 2.5 feet (0.76 meters) from the property lines along the west and north. The ground floor is 37 feet (11.28 meters) tall and has a footprint of 14,000 square-feet (1,300 square-meters).

## Structural Performance

Salt Lake City is located in Seismic Design Category D, near the active Salt Lake Segment of the Wasatch Fault Zone. As a result, the building is designed to accommodate severe seismic activity. With an above grade building height of 387 feet (118 meters) the building structure was designed using a performance-

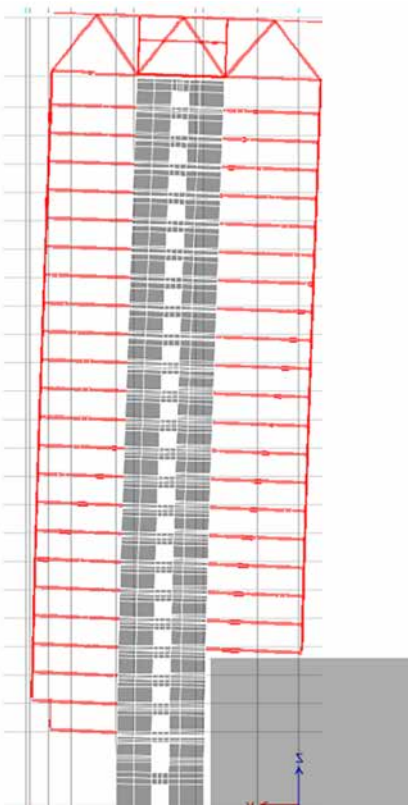


Figure 3 Structural Section Diagram

based seismic design procedures, which required additional independent peer reviews.

The building foundation is driven steel HP-piles, reaching depths over 100 feet (30.48 meters) below grade, supporting a central reinforced concrete core. The reinforced concrete core extends from 18 feet (5.5 meters) below grade up to the mechanical penthouse level (Level 25) at 351 feet (107 meters) above grade. The mechanical penthouse level consists of a two-way steel truss system suspending 18 perimeter columns. The perimeter columns along the south reach down to Level 5. In order to create a balanced system, on the west, north and east the perimeter columns reach down to Level 2. All floors of the tower are supported from the suspended perimeter columns, which are supported by two-way steel truss system at the roof. Gravity loads are transferred from the hat trusses to the top of the reinforced concrete core walls using six steel spherical structural bearings.

The two-way steel truss system at the roof supports 23 suspended levels on the west, north and east, and 20 suspended levels on the south. The reinforced concrete core walls are the only connection between the tower and the foundation, and account for the transfer of all gravity, wind, and seismic loads.

The building's unique structural design combined with the anticipation of severe seismic activity result in significant differential movements, mostly between Level 1 and Level 2. At this location design of the exterior enclosure and building systems were required to accommodate significant movement: vertical movement up to 32 inches (81.3 centimeters), parallel movement up to 3.3 inches (8.4 centimeters), and perpendicular movement up to 3.3 inches (8.4 centimeters). (Refer to Figure 3.)

## Building Design: General

There were three fundamental principles that served to guide the design of the 111 Main tower: transparency, visual depth and performance. Transparency was engaged as the primary means of connecting the building and its occupants to the site, at the human scale in response to the dense urban setting, and at the environmental scale in response to its geographic location in a valley bordered by the Wasatch and Oquirrh mountain ranges. Visual depth is used in the massing and the design and detailing of exterior enclosure as a juxtaposition to the transparency. The visual depth of the exterior enclosure creates a presence in the skyline and on the street that is constantly changing and invites people

closer to explore the building. Performance requirements included accommodation of challenging movements from the building structure, an emphasis on human health and comfort, and an understanding of the regional market and tenant demands. At each step in the design process these principles were rigorously considered and articulated in the resolution of building systems and exterior enclosures.

## Exterior Enclosure Design: Tower Enclosure

The primary building exterior enclosure is comprised of a unitized curtain wall. Typical units are 5 feet (1.5 meters) wide by 13.75 feet (4.19 meters) tall, corner units are 7.5 feet (2.3 meters) wide by 13.5 feet (4.1 meters) tall, and the floor to ceiling vision glazing is 9.42 feet (2.87 meter) tall. At Level 24 the typical units are 5 feet (1.5 meters) wide by 15.75 feet (4.8 meters) tall, the corner units are 7.5 feet (2.3 meters) wide by 15.75 feet (4.8 meters) tall, and the floor to ceiling vision glazing is 12.75 feet (3.9 meters) tall. The wide corner units combined with floor to ceiling vision glazing serve to maximize transparency, especially at the corners, offering occupants breathtaking and unobstructed views of the surrounding valley and mountain ranges.

A shadow box at the spandrel features a series of horizontal aluminum extrusions painted to accentuate the shadows they create. At each of the vertical mullions there are 10-inch deep (25.4 centimeter) glass fins with a custom frit pattern. The horizontal lines and the depth of the shadow box combined with the vertical lines and the depth of the glass fins are used to create visual depth in the façade. (Refer to Figure 4.)



Figure 4 Tower Curtain Wall

Located in a dry and arid climate at an elevation of approximately 4,250 feet (1,295 meters) above sea level, the building systems and exterior enclosures are required to accommodate significant temperature swings (basis of design was an outside cooling condition of 97.4°F [36.3°C] and an outside heating condition of 9.3°F [-12.6°C]) to maintain an indoor space temperature of 72°F (22.2°C). 42,935 square-feet (3,990 square-meters) of the exterior enclosure faces due south, 39,815 square-feet (3,700 square-meters) faces east and west, and 47,200 square-feet (4,385 square-meters) faces due north. With an average of 70% window to wall ratio, it was important to minimize solar heat gain. A gray tinted 0.375 inch (9.52 millimeter) float glass on the outer lite of the insulated glazing unit was installed with a Low-E coating on the #2 surface.

For occupant comfort, glass deflection was limited to a maximum of 1 inch (25.4 millimeters) at the center of the vision area. Because wind loads in some areas were in excess of 65 miles per hour (105 kilometers per hour) the insulated glazing unit was comprised of a 0.375 inch (9.525 millimeter) outer lite, 0.5 inch (12.7 millimeter) air space, and a 0.375 inch (9.525 millimeter) outer lite.

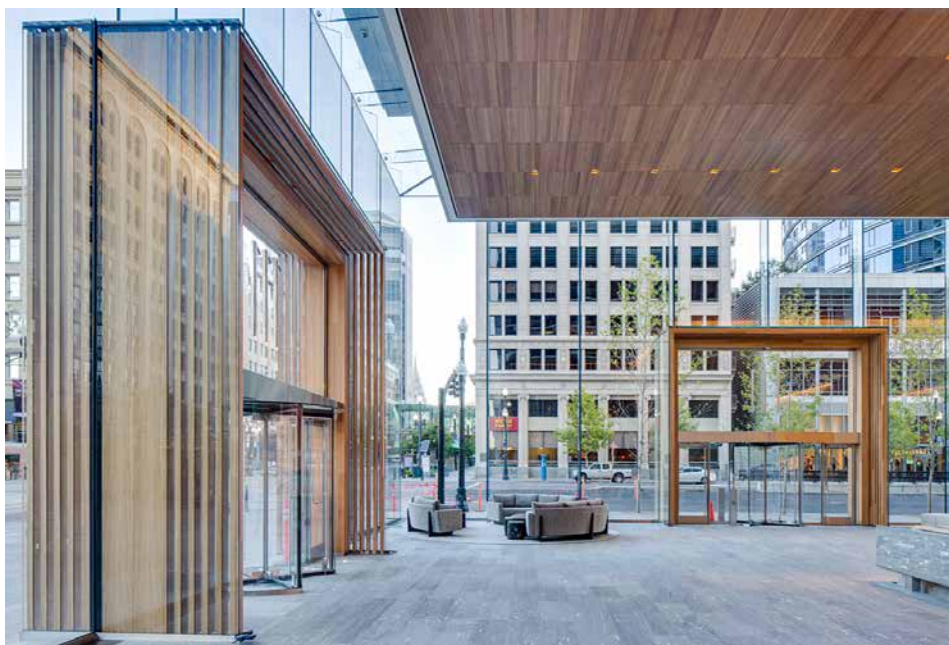


Figure 6 Lobby Interior

The anticipated seismic drift between any two of the typical floor slabs of the tower, spaced at 13.75 foot (4.2 meter) apart, is 3.3 inches (83.8 millimeters). Seismic drift is accommodated in the unitized curtain wall through a combination of sliding and tilting of the units. Further complicating the design of the unitized curtain wall, the construction schedule required that installation of the unitized curtain wall begin well before the building loads were transferred from temporary shoring to the rooftop trusses. This required an unusually large amount of adjustment to be designed into unit to unit joinery at the curtain wall anchors. (Refer to Figures 5A and 5B.)

### Building Design: Ground Floor Lobby

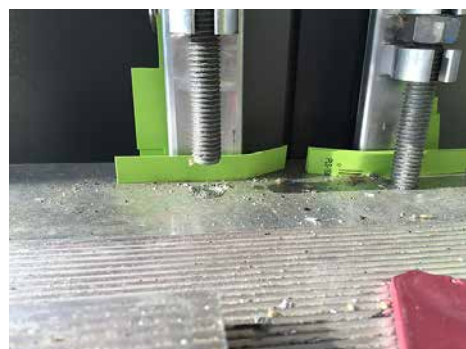
It was important to CCRI that the L-shaped lobby at the base of the 111 Main tower be a public, open and active space. The design of the ground floor lobby was conceived of as a living room for the city, a large space that functions at a human scale by offering a place to gather, lounge and repose. Along the southern edge of the lobby there is a large 29.5 foot (9 meter) wide by 32.5 foot (9.9 meter) tall interior glass storefront, the bottom 10.5 feet (3.2 meters) of which slides open providing a direct connection between the tower lobby and the great hall of the adjacent performing arts center. At the opposite end of the L-shaped lobby is a café, also open to the tower lobby. The connections to the performing arts center and the café – in combination with a 40 foot (12.2 meter) long water feature, a 36 foot (11 meter) by 19.5 foot (5.94 meter) tall media wall art installation, and a collection of couches, tables and chairs – serve to inspire public

curiosity and engagement within the space, and encourage free-flow through the lobby.

### Exterior Enclosure Design: Lobby Enclosure

To promote the lobby's connection to its urban context and inspire public use, the lobby exterior enclosure along public ways on the north and west was designed to be a transparent all-glass façade. Except at the entries, the storefront is constructed of only one material – laminated ultra-clear glass. Using this single material and a generous 10 foot (3 meter) by 35 foot (10.7 meter) module the number of material intersections is minimized and each detail is carefully crafted to support the principles of transparency and visual depth. (Refer to Figure 6.)

Because the building structure is suspended from the roof, the 37 foot (11.28 meter) tall ground floor is column-free. The all-glass lobby exterior enclosure is gravity supported at grade resulting in extreme differential movement between the enclosure and the tower above. The all-glass exterior enclosure is required to accommodate +14 inches (35.6 centimeters) and -18 inches (45.7 centimeters) of vertical movement between the base of the suspended tower and the ground, and 3.3 inches (8.4 centimeters) each of parallel and perpendicular movement. Focused on the principles of transparency and visual depth, cumbersome and opaque expansion joints were replaced with a system design able to accommodate these movements.



Figures 5A and 5B Performance Mockup

The primary elements of the all-glass lobby exterior enclosure are described below, and are as follows:

1. Typical plan detail
2. Corner plan detail
3. Pivot section detail
4. Corner section detail at skylight
5. Lobby enclosure return
6. Lobby entrance portals

**1. TYPICAL PLAN DETAIL:** Spaced at 10 feet (3 meters) on center, each of the laminated glass stabilization fins consists of four 0.5 inch (12 millimeter) sheets of ultra-clear low iron glass. The laminated glass stabilization fins are set behind the laminated glass face panels to provide a continuous line of resistance to positive and negative wind loads and eliminate the need for visible metal fittings. The laminated glass face panels are 10 feet (3 meters) wide by 35 feet (10.7 meters) tall. Each laminated glass face panel consists of two 0.5 inch (12 millimeter) sheets of ultra-clear low iron glass. Glass manifestation is provided in the form of a horizontal line of small white rectangles that are screen printed onto the #2 surface of each laminated glass face panel. The laminated glass face panels and the laminated glass stabilization fins are cantilevered from the ground in an 8 inch (20.32 centimeter) deep steel channel.

A continuous vertical line of black structural silicone adheres the laminated glass face panels to the laminated glass stabilization fins. The use of black silicone is visually recessive in elevation, and the use of large glass panels with a minimal number of materials at the intersecting joinery reinforces the principle of transparency.

At the base of the all-glass lobby exterior enclosure, nestled between each of the laminated glass stabilization fins, is a series of linear trench heaters. The trench heaters force warm air up the interior side of the all-glass exterior enclosure reducing condensation.

**2. CORNER PLAN DETAIL:** The lobby exterior enclosure has three glass corners, one at the main building corner, and two where the enclosure returns to meet the building. Because the laminated glass corner panels at the corner act to support one another, there are no laminated glass stabilization fins at the corners of the all-glass lobby enclosure. The converging 10 foot (3 meter) by 35 foot (10.7 meter) laminated glass face panels are mitered and joined with a 0.75 inch (19 millimeter) black silicone joint. This joint configuration allows the laminated glass corner panels to support each other in shear, deform in a seismic event, and provides ultimate transparency.

**3. PIVOT SECTION DETAIL:** While the all-glass lobby exterior enclosure is laterally supported by a laminated glass purlin joined to the tower, the vertical movements anticipated between the all-glass lobby exterior enclosure and the tower suspended above required that the enclosure be isolated from the tower. In order to satisfy these opposing criteria the glass roof of the all-glass lobby exterior enclosure was designed to act as a movement joint.

The 6 foot (1.8 meter) wide laminated glass skylight panels consists of two 0.5 inch (12 millimeter) sheets of ultra-clear low iron glass. The laminated glass skylight panels are supported every 10 feet (3 meters) by a laminated glass purlin. The laminated glass purlin consists of four 0.5 inch (12 millimeter) sheets of ultra-clear low iron glass. Designed around a mortise and tenon joint, on one end of the laminated glass purlin the outer two layers of laminate are held back, and at the top of the laminated glass stabilization fins the inner two layers of the laminate are cut short. The laminated glass purlin is spliced into the laminated glass stabilization fin and joined with a stainless steel pin. The other end of the laminated glass purlin is pinned to a concealed linear guide rail. The guide rail is mounted to the base of the tower, allowing for free movement between the all-glass lobby exterior enclosure and the tower above. The laminated glass skylight panel is joined to the laminated glass face panel with a 1.63 inch (41.4 millimeter) black silicone joint, and to the laminated glass purlin with a 0.75 inch (19.05 millimeter) black silicone joint. (Refer to Figure 7.)

Similar to the typical plan details, the relatively thin and singular black silicone joints recede in elevation. The stainless steel pin, the laminated glass stabilization fin and laminated glass purlin are shaped to express the rotational movements they have been designed to accommodate.

**4. CORNER SECTION DETAIL AT SKYLIGHT:** The moment where a number of complex movements converge, the all-glass skylight corner was designed to encourage the laminated glass skylight corner panels to shift above or below one another in a seismic event. The laminated glass skylight corner panels are trapezoidal in shape. The panel is orthogonal and parallel to the building at the front and back edges, and at the laminated glass stabilization fin located 10 feet (3 meters) away from the corner. On the corner edge, the laminated glass skylight corner panels are cut at an angle to meet the building above. To encourage one laminated glass skylight corner panel to slide up and over the adjacent laminated glass skylight corner panel, the joint between the two laminated glass skylight



Figure 7 Pivot Section Detail

corner panels was required to be cut at a 30 degree angle. Because a 30 degree angle exceeds glass fabrication standards, the edge of each of the laminated glass skylight corner panels was cut at a 45 degree angle. The mitered edge was finished to receive a custom stainless steel shape designed to transition the 45 degree angle of the laminated glass skylight corner panel to the 30 degree angle required to encourage one laminated glass skylight corner panel to slide up and over the adjacent panel. The custom stainless steel shape was shop applied to the mitered edge of each of the laminated glass skylight corner panels. The exposed portion of the cast stainless steel shape is approximately 0.75 inch (1.9 millimeter) wide, and is aligned with the vertical 0.75 inch (1.9 millimeter) silicone joint at the vertical corner panels. There are thin black silicone lines on either side of the exposed portion of the cast stainless steel shape. (Refer to Figure 8.)



Figure 8 Skylight Corner

A 0.375 inch (9.5 millimeter) wide silicone joint separates the two laminated glass skylight corner panels. The primary water line is a silicone sheet bridging over the top of the two laminated glass skylight corner panels, adhered with a silicone sealant at the edge of each of the laminated glass skylight corner panels.

**5. LOBBY ENCLOSURE RETURN:** The east and south property lines are shared lot lines. The ground floor exterior enclosure along these shared lot lines consists of reinforced concrete, CMU block, and steel framed walls, all clad with aluminum panel or cement plaster and cantilevered from the ground. At both the northeast and the southwest corners of the building the all-glass lobby exterior enclosure returns to meet an aluminum clad wall assembly. Because the adjacent wall assemblies are isolated from the base of the suspended tower using conventional seismic joints, it was necessary also to isolate the all-glass lobby exterior enclosure from these adjacent wall assemblies.

On the southwest corner the 35 foot (10.7 meter) tall laminated glass return panel is terminated behind an aluminum clad wall at a 12 inch (30.48 centimeter) wide by 2 inch (5.08 centimeter) deep vertical steel tube cantilevered from the ground and connected to the base of the tower with a concealed linear guide rail. The laminated glass return panel is captured in a continuous built-up steel channel mounted on the vertical steel tube, and running the full height of the laminated glass return panel. The vertical steel tube is isolated from the adjacent aluminum-clad wall assembly by 4 inches (10.16 centimeters) in all directions to accommodate the anticipated differential movement between these two assemblies. Vertical aluminum panel clad hinged seismic joints are provided on both the interior and exterior sides of the laminated glass return panel, and a 18 inch (45.72 centimeter) tall slot is provided above the laminated glass return panel and built-up steel channel to accommodate vertical movement. The laminated glass skylight panel is held back from the face of wall by approximately 1 inch (2.5 centimeters). An angled horizontal joint in the aluminum panel tracks the line of the laminated glass skylight panel, and a silicone sheet is adhered to the edge of the laminated glass skylight panel on one end, and to the waterproofing membrane behind the aluminum clad panels on the other.

The laminated glass return panel on the northeast corner is resolved in much the same way as the laminated glass return panel on the southwest, except that the laminated glass

return panel on the northeast corner is only 20 feet (6.1 meters) tall and is set on top of a 10 foot (3 meter) tall steel framed entry portal.

The execution of an all-glass expression of the lobby exterior enclosure returns was essential to the resolution of both aesthetic and performance considerations. The all-glass expression of the southwest and northeast corners created an additional dimension – the all-glass lobby exterior enclosure was given a cubic form further articulating its transparency. By terminating the all-glass lobby exterior enclosure into an adjacent wall assembly parallel to the laminated glass face panels, visual depth was achieved and used to emphasize the transparency of the all-glass lobby exterior enclosure. Additionally, by implementing details similar to those already used at the all-glass lobby exterior enclosure main building corner and lateral supports, the number of unique details was minimized and the need for additional and complex movement joints was eliminated.

**6. LOBBY ENTRANCE PORTALS:** The two public lobby entrance portals, one on 100 South Street and one on Main Street, are constructed of glass, steel and wood. Two modules wide, a structural steel frame was designed to support two of the lobby exterior enclosure laminated glass face panels and the three laminated glass stabilization fins supporting them. On the exterior side of the steel frame, two 2.5 foot (0.76 meter) deep by 20 foot (6.1 meter) tall laminated glass side panels support a 2.5 foot (0.76 meter) deep by 20 foot (6.1 meter) wide laminated glass lintel. On the interior side of the steel frame, two 5 foot (1.52 meter) deep by 20 foot (6.1 meter) tall laminated glass side panels support a 5 foot (1.52 meter) deep by 20 foot (6.1 meter) wide laminated glass lintel. The four laminated glass side panels consist of three 0.5 inch (12 millimeter) sheets of ultra-clear low iron glass. The two laminated glass lintel panels consist of three 0.5 inch (12 millimeter) sheets of ultra-clear low iron glass and one 0.3 inch (8 millimeter) sheet of ultra-clear low iron glass. The steel frame, laminated glass side panels and laminated glass lintel panels serve to define the 20 foot (6.1 meter) wide by 20 foot (6.1 meter) tall by 7.5 foot (2.29 meter) deep lobby entrance portal.

Transparency at the lobby entrance portal is achieved by using solid materials judiciously, and by engaging the laminated glass panels to support solid materials when possible. Given the transparent nature of the all-glass lobby exterior enclosure, bringing prominence to the building entrance portals within the urban context was a key criteria for the design of the

enclosure. It was the introduction of wood, a quarter sliced California Eucalyptus, which served to set the entrance portals apart from the adjacent all-glass lobby exterior enclosure and to add an inviting warmth to the façade.

Visual depth of the entrances is reinforced by passing through a series of ten wood wickets. There are four exterior wood wickets, one wood-clad steel wicket, and five interior wood wickets. The exterior and interior wood wickets measure 2.5 inch (6.35 centimeter) by 6 inch (15.24 centimeter) and are constructed of solid California Eucalyptus. They are spaced at approximately 5.5 inches (14 centimeters) on center. The wood-clad steel wicket houses the structural steel frame that supports the all-glass lobby exterior enclosure above and the large 20 foot (6.1 meter) wide by 10 foot (3 meter) tall laminated glass transom panel.

The four exterior wood wickets and five interior wood wickets are mechanically fastened to continuous concealed stainless steel hardware. At the lintel, the continuous concealed stainless steel hardware is mechanically fastened to the laminated glass lintel panel and adhered to the underside of the laminated glass lintel panel with a continuous line of structural silicone. At each end of the lintel, there is a mechanical connection to the continuous concealed stainless steel hardware that supports the vertical wood of the exterior and interior wood wickets. The continuous concealed stainless steel hardware that supports the vertical wood of the exterior and interior wood wickets is then adhered to the laminated glass side panels with a continuous line of structural silicone. At their bases, the wood wickets are held 2.5 inches (6.35 centimeters) off of the ground to express their how they are supported, and to avoid degradation of the wood by keeping out of water at grade and allowing air to flow freely below. By engaging the laminated glass panels to support the exterior and interior wood wickets the need for additional solid materials reaching out to support them is eliminated. The lobby entrance portals appear solid from across the street, but completely transparent from within.

To further reinforce the transparency and visual depth created by the exterior and interior wood wickets, and to eliminate visibility from the outside of the entrance portals of the 2.5 inches (6.35 centimeters) wide structural silicone lines used to adhere the stainless steel hardware, a natural wood veneer was captured inside of the laminated glass side and lintel panels. Because this had not been done before, the design team worked closely with the contractor, the specialty glass engineer and the

glass manufacturer to research and develop a means for achieving this assembly. Along the way, issues such as veneer substrate, veneer finish, reduced structural contact area of the interlayer, and instability of a 10 foot (3 meter) long by 2.5 inch (6.35 centimeter) wide length of veneer during the lamination process were revealed and addressed through a series of fabrication samples and full scale mockups.

## Acknowledgements

The 111 Main project, and the unique opportunities it provided were made possible by the vision of the ownership team at City Creek Reserve, Inc.. Other key players in the success of the 111 Main tower included my fellow SOM Architects and Engineers, Okland Construction Company, Steel Encounters, Inc., Eckersley O'Callaghan Engineers, Sedak, and a number of local associate Architects and Engineers. By assembling this core team of specialists, CCRI realized their goal of developing an exceptional and iconic building in the heart of Salt Lake City, Utah.

Also, a special thanks to my mentor of more than a decade, Keith Boswell, for his tireless devotion to the practice of architecture and support of my work.

# Unitised Façade System Designed with a Highly Transparent Façade of Low G-value Combined with Blast Requirements: 20 Farringdon Street a Case Study.

Authors and companies:

Thomas Henriksen 1,  
Ben Daykin 2,  
Cindy Prophet 3,  
Ana Ruiton 4,  
1 Mott Macdonald  
2 Mott Macdonald  
3 Mott Macdonald  
4 Mott Macdonald

## Keywords:

1=g-value 2=Frit 3=façade 4=Glazed  
5=coating 6=daylight

## Abstract:

Today's architectural demand for transparency has been developed to attain maximum daylight saturation which is aimed to improve the well-being of users and maximise interaction with the outside. However, transparency also needs to be combined with the requirements of moderating heat gains (achieving low g-value). This becomes a challenge with current available passive glass coating solutions and the increasingly strict regulatory restrictions that are aimed at limiting window sizes.

In this paper, 20 Farringdon Street, a London based project is the case study that demonstrates how a high transparency façade can be realised by utilising solar control and thermal control glass coatings in combination with optimised frit as part of a single insulated glass unit. This has been designed to increase occupant comfort in the perimeter zone of the building. The glazing solution has the additional benefit of fulfilling the project requirement to reduce the overall energy usage of the building. A further stipulation on this façade has also been the requirement for blast resilience, which has added complexity to the façade design, and has created an additional restraint to the design process. This paper will demonstrate how it is possible to combine complex coatings with frit and containment laminates to arrive at a fully glazed building envelope that will meet today's architectural demands.



Figure 1.1. Farringdon Street is approximately aligned along a north-south axis and is lined with tall mixed-use buildings (Denton Corker Marshall, London).

## 1. Introduction:

20 Farringdon Street is a new 11 storey steel frame building, which incorporates office accommodation on eleven upper floors and a Public House on the ground floor. The building is in the City of London, on the east side of Farringdon Street, approximately 500m north of the River Thames (Figure 1.1). The lead architects of the project are Denton Corker Marshall (DCM) working with Mott MacDonald as the façade consultants and Waterman Building Services (WBS). The glass suppliers for the project are Guardian Glass and Interpane.

The proposed façade is predominantly floor to ceiling curtain wall glazing that wraps around the three sides of the building, creating a light, bright desirable, contemporary office environment and appearance to the scheme (Figure 1.2 and 1.3). The ground and upper 3 floors are set back from the main façade line and benefit from the addition of terraces to east and west (Figure 1.4). The architectural intent for levels 9 – 11 to have a different visual appearance from main levels 2-8, therefore the dark grey upper floors appear chiselled from a single monolithic block.



Figure 1.2 and 1.3. A lightweight cladding wrap on 3 sides to visually connects the building from Farringdon Street around to Fleet Place (Denton Corker Marshall, London).



Figure 1.4. The upper levels are set-back from the main facade line to create terraces as well as architectural modelling appropriate for the site location (Denton Corker Marshall, London).

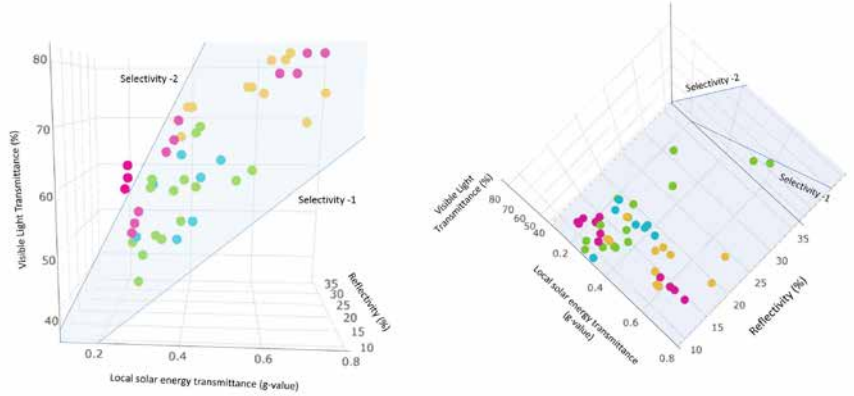


Figure 3.1: Visible light transmission against solar energy transmittance and Reflectivity (Mott MacDonald).

## 2. Glass Build-up

The proposed systems for the case study building all feature laminate glazing on at least one leaf (Figure 2.1). This option provides better blast-resistance than Anti-Shatter Film (ASF) and Bomb Blast Net Curtains (BBNC)<sup>1</sup>, subject to suitable frame fixing into the adjacent structure (Figure 2.2).

## 3. Solar Performance Requirements

High quality daylight levels are required for contemporary office accommodation in order to create a pleasant visual environment leading to a feeling of wellbeing. However, the visible light transmission must be balanced against solar heat gain.

A façade that has a high percentage of glazing requires careful consideration to achieve the correct balance regarding glass performance.

Control of the solar heat gain and daylight glare control need to be strongly considered. The project required g-value for the façade was determined by the building services engineer, this was in line with British Council for Offices (BCO) specification 2014. BCO requirements for daylighting stipulate a daylight factor (DF) between 2% and 5%. The stipulated façade g-value (Table 3.1) was 0.15. For levels 02-08 which are fully glazed without a spandrel, the resultant g-value of the glass is 0.15 also. Levels 09-11 include an insulated spandrel panel; therefore, the resultant g-value of the glass is 0.20.

| Floor        | g-value |
|--------------|---------|
| Ground to 01 | 0.23    |
| Level 02-08  | 0.15    |
| Level 09-11  | 0.20    |

Table 3.1. Maximum g-value requirements

It is needed to select glass that achieves the required g-value and still provide a sufficient level of light through the façade (light transmission – VLT). This is known as a ‘high selectivity glass (VLT/g-value)’. The graph below (Figure 3.1) shows the relationship between g-value and light transmittance of the glass types currently available on the market (colour dots). When the glass g-value is lowered, the amount of visible light transmitted is also lowered. It can be seen that for a certain g-value, several glasses may be available with varying light transmissions and vice versa.

### High Selectivity Glass (VLT/g-value).

To achieve such a low g-value whilst still allowing a relatively large percentage of VLT, high selectivity glasses were considered. It is clear that achieving g-value of 0.15 with just the glass coating/tint would result in a light transmission of approximately 25% or lower (Figure 3.1).

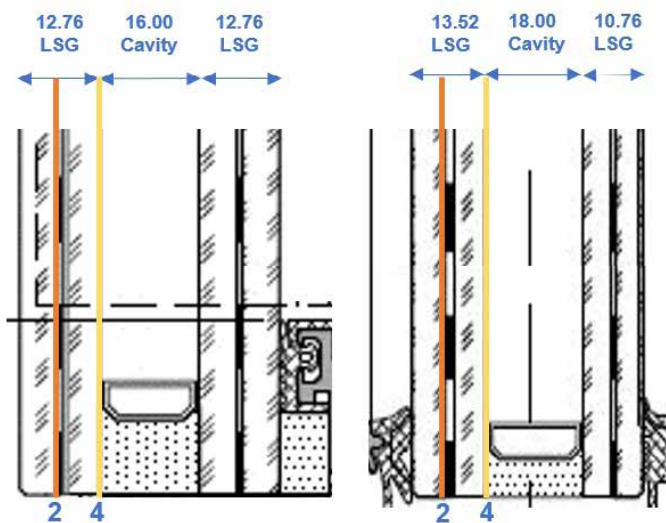


Figure 2.1: Images of laminate glass build-up. Left: levels 02 – 08. Right: Levels 1, 09-11 (Mott MacDonald).

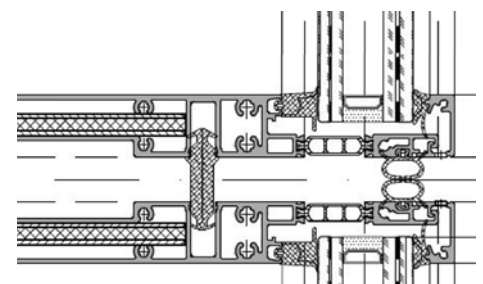


Figure 2.2: DGU mullion connection (Mott MacDonald).

| Glass Coating            | g-value | Frit density (%) | Light transmittance- VLT (%) |
|--------------------------|---------|------------------|------------------------------|
| Guardian SNx 50/23       | 0.23    | 0                | 50                           |
| Interpane Ipasol 50/27   | 0.27    | 0                | 50                           |
| Pilkington Suncool 50/25 | 0.27    | 0                | 50                           |

Table 4.1: High selectivity glass from three glass suppliers (Mott Macdonald study).

| Glass                    | Target g-value | Frit density (%) | Light transmittance VLT (%) |
|--------------------------|----------------|------------------|-----------------------------|
| Guardian SNx 50/23       | 0.15           | White 80%        | 22                          |
|                          |                | Grey 35%         | 32                          |
| Interpane Ipasol 50/27   |                | White 55%        | 26                          |
|                          |                | Grey 50%         | 24                          |
| Pilkington Suncool 50/25 |                | White N/A        | White N/A                   |
|                          |                | Grey 55%         | 24                          |

Table 4.2: Comparison study of glass options (Mott MacDonald)

This is considered too dark for an office environment and would greatly reduce the occupants connection with the outside.

An approach was to select a high selectivity glass that allowed approximately 50% VLT. With a selectivity of at least 2, this would result in a g-value of approx 0.25. The addition of a ceramic frit to the glass would be investigated to lower the g-value to 0.15, and, although anticipated frit density would be high, its position on the glass could be controlled to allow the vision area of the glass to remain frit free and so still achieve clear views and relatively high VLT.

#### 4. Glass Coatings

High performing double/triple silver glass coatings were investigated from several of the major glass suppliers in the UK. The three glass coatings further investigated were: Guardian SNx 50/23<sup>3</sup>, Interpane Ipasol 50/27<sup>4</sup> and Pilkington Suncool 50/25<sup>5</sup> (Table 4.1).

##### Ceramic Frit

Ceramic frit is a relatively simple and economic solution to lowering the g-value, it has the advantage that the density can be varied throughout a panel so that vision areas can remain relatively clear.

Frit colour concerns both architecture and performance. A white frit becomes a much more noticeable feature of the façade and can define the architecture. Whereas a grey frit is a more subtle addition but can also dull the appearance of a glazed façade.

From a performance perspective, a grey frit has increased performance over a white frit in regards to reducing the solar heat gain as the

darker frit absorbs a higher proportion of the heat and radiates it outward.

The surface position of the frit within the IGU also affects both aesthetic and performance; for the fritting to be most effective in reducing solar gains, it should be located on the outer leaf of the double-glazed unit.

The table below (Table 4.2) shows the density of white frit and grey frit required to achieve the required g-value of 0.15 from the three glass suppliers.

#### 5. Manufacturer's Limitations

##### Achieving U-value

With the application of 35% ceramic frit to the Guardian glass, the 0.15 g-value requirement can be achieved. The Interpane and Pilkington glass have much larger frit requirement at 50% to achieve the 0.15 g-value but they do not meet the light transmittance requirement of minimum 32%.

##### Coating Position

The fritting and solar control coating are most effective on the outer leaf. Pilkington and Interpane can produce monolithic glass with both the frit and solar control coating on the same surface (surface #2). However, Guardian do not recommend applying frit to the same surface as their SNx 50/23 coating; they would require a laminated construction to the outer leaf with the fritting on surface #2 and their triple silver solar coating on surface #4.

##### Aesthetic Limitations

The architect required grey silicone in levels 02- 08 which would have given a more monolithic appearance but Guardian Glass

could not manufacture grey silicone bonding due to manufacture restrictions.

#### 6. Façade solution options

Due to manufacturing limitations in achieving the required g-value, additional design solutions (Figure 6.1) were explored to lower the percentage of frit on the façade by adding a spandrel into the external pane configuration (Option C and D, Figure 6.1). The study of a spandrel addition (Figure 6.2) showed that, as the solar radiation is no longer being transmitted through the spandrel area, the glass itself did not have to perform to the same level. Therefore, g-value of the façade could be relaxed from 0.15 to 0.20, as the proposed glass is now 80% rather than 100%. As shown in Figure 6.2 by including 20% of spandrel, the white frit could be reduced to a more sensible level and the light transmittance can be increased.

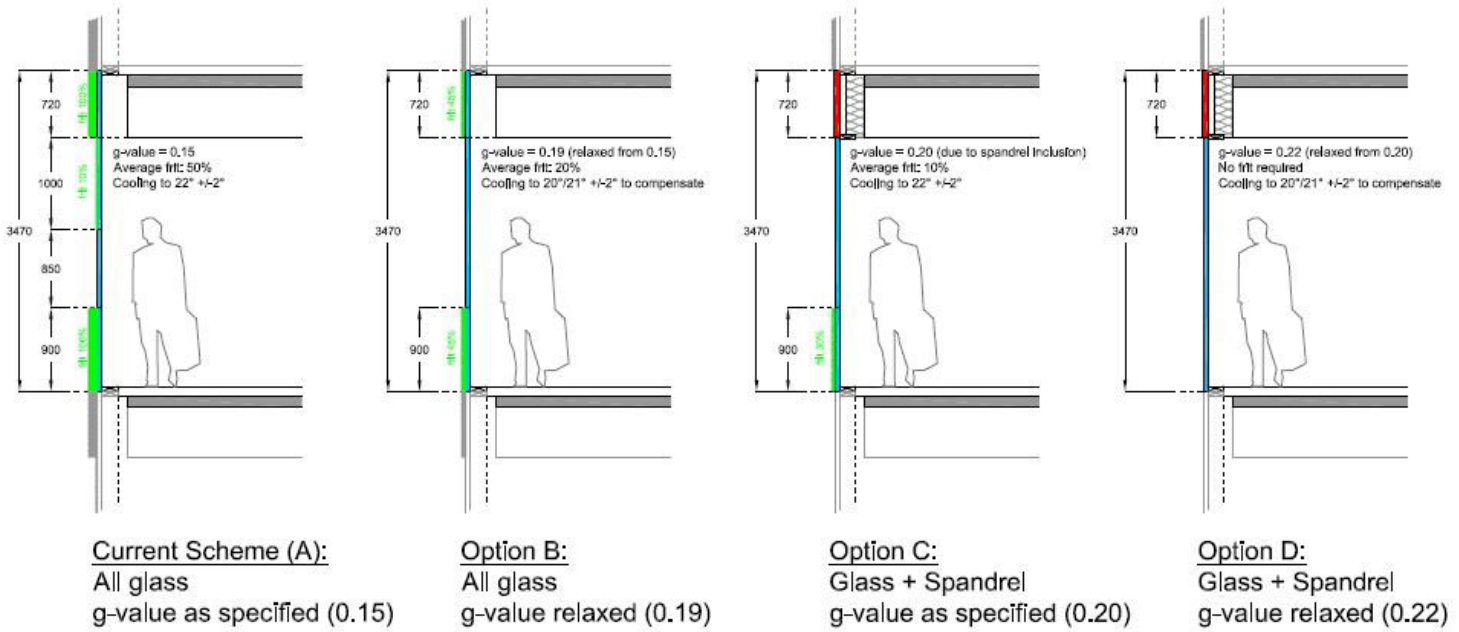


Figure 6.1: Façade study options (Mott MacDonald).

| Options                  | Curtain wall unit configuration |                   |               |                               |  |   |             |  |
|--------------------------|---------------------------------|-------------------|---------------|-------------------------------|--|---|-------------|--|
|                          | Description                     | % of vision glass | % of spandrel | Inclusive of internal blinds? | g-value (solar heat gain) of glass                         | Approximate % of fritting required to achieve g-value | Frit colour | Average resultant visible light transmission through glass |
| <b>A: Current Scheme</b> | All glass                       | 100%              | 0%            | YES                           | 0.15<br>g-value as per WBS model                           | 50%   | White       | 31%  |
| <b>Option B</b>          | All glass                       | 100%              | 0%            | YES                           | 0.19<br>g-value 'relaxed' from 0.15 (has M&E implications) | 20%   | White       | 41%  |
| <b>Option C</b>          | Includes spandrel               | 80%               | 20%           | YES                           | 0.20<br>g-value as per WBS model                           | 10%   | White       | 43%  |
| <b>Option D</b>          | Includes spandrel               | 80%               | 20%           | YES                           | 0.22<br>g-value 'relaxed' from 0.20 (has M&E implications) | 0%  | N/A         | 48%  |

Figure 6.2: Curtain wall unit configuration options (Mott MacDonald).

As can be seen below in Figure 6.3, the pane options including spandrel have a better thermal performance to Part-L requirement, contribute to the targeted BREEAM Excellent rating and improve the base acoustics performance scheme.

| Options                  | Performance                    |   |   |  |   |  |  |               |                        |  |
|--------------------------|--------------------------------|---|---|--|---|--|--|---------------|------------------------|--|
|                          | Lighting loads                 | Perimeter cooling loads (to achieve BCO and Part L improvement) | Approximated overall cooling increase compared to Option A +allow 30% diversity to solar gain | Thermal Comfort Controllability Compare to Base Scheme | Contribution to Part L improvement compared to option A | Daylight Factor (for BCO and BREEAM point) | Thermal performance (U-value tp Part L requirement)? | Glare Control | BREEAM point for glare | Acoustics Performance (floor floor flanking) |
| <b>A: Current Scheme</b> | As per current energy model    | 22° +/-2°   | -   | -  | Incorporated currently                                  | Requires daylighting study to be conducted | ✓  | Controlled    | Can be targeted        | Acoustically weak                            |
| <b>Option B</b>          | Reduced loads over base scheme | 22° +/-2°   | 6.30%   | Acceptable   | Small negative - lighting offset cooling energy         |  | ✓ (no change)  | Controlled    | Can be targeted        | No change over base scheme                   |
| <b>Option C</b>          | Reduced loads over base scheme | 22° +/-2°   | 1.40%   | Acceptable   | Small negative - lighting offset cooling energy         |  | ✓ (better performance)                               | Controlled    | Can be targeted        | Improvement over base scheme                 |
| <b>Option D</b>          | Reduced loads over base scheme | 22° +/-2°   | 1.60%   | Acceptable   | Small negative - lighting offset cooling energy         |  | ✓ (better performance)                               | Controlled    | Can be targeted        | Improvement over base scheme                 |

Figure 6.3: Façade study options performance (Mott MacDonald).

### 7. Conclusion / Glass Performance Summary

The decision to include spandrels rather than 100% glass offers better performance on various fronts. Two glass types were selected (Table 7.1) due to their best performance against manufacture limitations. A sensible level of frit was impossible to achieve without the inclusion of a spandrel which lowered the overall g-value target. Guardian's glass was selected for the black frit area of the façade only due to its low g-value. The white frit area of the façade was appointed to Interpane.

#### Final Frit pattern selection

Various studies were undertaken by the Architect and these were tested to understand which were considered the most lettable. The final selection for frit pattern on Level 00, 01, 09-11 was Black, 6mm vertical stripes with 6mm spacing at low level with 5% coverage (Figure 7.1). On Levels 02-08 white 2mm dots frit with 15% coverage was selected as the most appropriate (Figure 7.2).

| Floor               | Glass     | g-value | Frit                   | Light transmittance (%) |
|---------------------|-----------|---------|------------------------|-------------------------|
| Level 00, 01, 09-11 | Guardian  | 0.20    | 5% black (6mm stripes) | >45                     |
| Level 02-08         | Interpane |         | 15% white, (2mm dot)   | >32                     |

Table 7.1: Final Thermal Performance (Mott MacDonald)



Figure 7.1: Glass Sample of 5% fritting, 5 mm vertical black stripes. Guardian SNX 50/23. (Denton Corker Marshall, London)



Figure 7.2: Glass Sample of 7,5% fritting, 2 mm white dots + grey edge Stopray Ultraselect 50. Interpane. (Denton Corker Marshall, London)

## Acknowledgements:

Special thanks to Clive Atkinson for his and support in writing this paper and to the architects for their collaboration.

## References:

- [1] CPNI
- [2] BCO Guide to Specification 2014
- [3] Guardian Glass, Sunguard Extra Selective SNX 50/23 Datsheet
- [4] Interpane, Ipasol 50/27 Datasheet
- [5] Pilkington, Suncool 50/25 Datasheet

# Towards a More Consistent Design of Laminated Glass

Michael R. Dunham, M.S., P.E., Arup  
Yoojin Kim, B.S., Arup  
Kateri Knapp, M.S., Arup

## 1. Keywords

Glass, Glass Design, Laminated Glass, Glass Failure Prediction Model, Design Standards, Utilization Method

## 2. Abstract

Laminated glass design methods and codes are inconsistent both regionally and globally, particularly when subjected to loads of different durations and temperatures. Many codes and standards incorrectly treat the time and temperature dependence of interlayer stiffness or ignore it altogether. Five design standards for laminated glass from around the world are compared, and a new method is proposed to combine the effects of loads of different durations and temperatures.

## 3. Introduction

Design standards around the world treat glass, and particularly laminated glass, in very different ways. Although building codes always vary across borders, the way that laminated glass is designed across the world varies more than other building materials such as steel and concrete. Since both glass strength and laminated glass stiffness vary with time, it is necessary to develop a method of dealing with loads of different durations acting on a piece of glass.

An easy and accurate method of analyzing laminated glass is important so that the design engineer can have confidence in the safety and reliability of the structure. Properly sizing the glass thickness is also important to the owner and contractor with respect to economy of material.

Although other building materials have time dependent deflection characteristics (stretch of cables, steel relaxation, concrete creep) the time-dependent properties of laminated glass are both geometric and structural. Both the probability of breakage and the structural stiffness of a laminated piece of glass change with time. It's for this reason that there is not a consensus on how to treat the material.

## 4. Problem Statement

This paper's objective is to propose a new method of laminated glass design based on a simple utilization check that takes into account the structural system change that occurs with both temperature and time. This method proposes that each load be applied to the glass individually and analyzed assuming geometric non-linearity. Once results are obtained for each load state, the deflections are summed to determine a total deflection and the stress utilizations are summed to determine a total utilization. Analyzing the loads individually allows both load duration and temperature to be taken into account for each load state. Summing the utilizations rather than the stresses allows the designer to use different stress limits for each load, depending on the duration.

In addition to this new method for laminated glass design, a general survey of current approaches is undertaken in order to better understand the state of practice in laminated glass design. The following five glass standards from around the world as well as the Utilization Method are used to design the same laminated glass panel and the approaches are compared.

### 4.1 ASTM E1300 – United States

The general approach of ASTM E1300 is to design glass panels such that under the design load conditions the glass has a probability of breakage of 8/1000. This is done by determining the load resistance of a given panel from design charts which are derived from the Glass Failure Prediction Model. The charts assume a load duration of 3 seconds and an interlayer temperature of 50°C. Loads of longer duration can be factored up to an equivalent 3 second load. There are methods of taking loads of different duration and temperature into account included in the appendices, which is what the Utilization Method is based on.

### 4.2 AS 1288 – Australia

AS 1288 uses an allowable stress based approach in which the stress in a panel is checked against an allowable stress determined by taking into account different aspects of the glass panel under consideration. Laminated glass is assumed to be either fully

monolithic for short term loads, or fully layered for long term loads. There are no provisions for taking different temperatures or load durations into account.

### 4.3 BS 5516-2 – United Kingdom

BS 5516-2 is similar to ASTM E1300 in that the load resistance of a panel is read from a chart, but unlike E1300 there is no way to take into account loads of different durations. Additionally, design charts are not provided for heat-strengthened glass, and there is no provision for temperature.

### 4.4 DIN 18008 – Germany

DIN 18008 is similar to AS1288 with respect to approach, but no composite action of the interlayer can be used without special approvals. There are no provisions for loads of different duration or temperature.

### 4.5 prEN 16612 – Provisional European Norm

prEN is also an allowable stress approach but like the appendices of ASTM E1300 the effective thickness method is used in order to take into account loads of different temperatures and durations. However, like in E1300, there is no method given for combining the effects.

### 4.6 Design Example

In order to compare these standards a common design example will be used. A skylight is chosen for the example because it is the most common application for glass panels subject to loads of different durations. For the purposes of the design examples herein, the following panel will be designed:

Geometry: 2.0m x 2.0m panel, horizontal placement  
Aspect Ratio: 1.0  
Heat treatment: both lites Heat-Strengthened  
Glass Make-up: 4mmHS / 1.52mm PVB / 4mm HS  
Slenderness:  $b/t = 2000/9.52=210$   
Support Conditions: 4-side simply supported

In order to compare design standards with respect to glass design, the initial loads are assumed to be the same. Any differences in regional approach to wind loads and snow loads is therefore ignored. However any differences in design approach with

respect to load factors, safety factors, etc. will be observed. Therefore, the following serviceability limit state loads are assumed:

Wind load: 1.0kPa

Snow load: 1.0kPa

For the purposes of this paper all glass thicknesses will be referred to by the nominal thickness (e.g. 4mm) but the minimum allowable thickness as shown in Table 1 will be used in all calculations (e.g. 3.78mm). It should be noted that DIN proposes to use the nominal thickness in calculations rather than the minimum thickness and account for the difference between nominal and minimum with the material safety factors.

| Nominal and Minimum Glass Thicknesses |                        |
|---------------------------------------|------------------------|
| Nominal Thickness [mm]                | Minimum Thickness [mm] |
| 2.0                                   | 1.8                    |
| 2.5                                   | 2.16                   |
| 2.7                                   | 2.59                   |
| 3.0                                   | 2.92                   |
| 4.0                                   | 3.78                   |
| 5.0                                   | 4.57                   |
| 6.0                                   | 5.56                   |
| 8.0                                   | 7.42                   |
| 10.0                                  | 9.02                   |
| 12.0                                  | 11.91                  |
| 16.0                                  | 15.09                  |
| 19.0                                  | 18.26                  |
| 22.0                                  | 21.44                  |
| 25.0                                  | 24.61                  |

Table 1 Nominal and Minimum Glass Thicknesses as per ASTM E1300-16

## 5. Calculation Methodology

Since the objective of this paper is a comparison of codes and the description of a novel design method, little space is devoted to showing the actual steps of stress and deflection calculation. Because the chosen design example is a simple 4-side supported plate, equations can be used to closely approximate the non-linear behavior of the plates with respect to deflection and stress. For stress calculations the methodology presented in prEN 16612 will be used as follows:

$$\sigma_{max} = k_1 \cdot \frac{A \cdot p}{t^2} \quad (Eqn. 1)$$

Where

$$k_1 = \frac{1}{4} \sqrt{\frac{1}{z_2} + \frac{p^{*2}}{z_3^2 + (z_4 \cdot p^*)^2}} \quad (Eqn. 2)$$

$$p^* = \left(\frac{A}{4 \cdot t^2}\right)^2 \cdot \frac{p}{E} \quad (Eqn. 3)$$

$$z_2 = 24 \cdot \frac{1}{AR} [0.0447 + 0.0803(1 - \exp(-1.17(AR - 1)^{1.073}))] \quad (Eqn. 4)$$

$$z_3 = 4.5(AR - 1)^2 + 4.5 \quad (Eqn. 5)$$

$$z_4 = 0.585 - 0.05(AR - 1) \quad (Eqn. 6)$$

And

$A = \text{area (mm}^2\text{)}$

$AR = \text{aspect ratio } \left(\frac{\text{long side}}{\text{short side}}\right)$

$E = \text{Young's Modulus (N/mm}^2\text{)}$

$p = \text{design load (N/mm}^2\text{)}$

$t = \text{glass thickness (mm)}$

The stress derived from these equations will be compared to the allowable stress in the method specific to the design standard being considered.

For deflection calculations ASTM E1300

Appendix X1 will be used as follows:

$$w = t \cdot \exp(r_0 + r_1 \cdot x + r_2 \cdot x^2) \quad (Eqn. 7)$$

$$r_0 = 0.553 - 3.83(AR) + 1.1(AR)^2 - 0.0969(AR)^3 \quad (Eqn. 8)$$

$$r_1 = -2.29 + 5.83(AR) - 2.17(AR)^2 + 0.2067(AR)^3 \quad (Eqn. 9)$$

$$r_2 = 1.485 - 1.908(AR) + 0.815(AR)^2 - 0.0822(AR)^3 \quad (Eqn. 10)$$

$$x = \ln\left(\ln\left(\frac{p \cdot A^2}{E \cdot t^4}\right)\right) \quad (Eqn. 11)$$

The deflections derived from these equations will be compared to a limit of L/60 for all design standards. Because deflection limits can be a subjective criteria and the objective is to compare quantitative indices, the limit criterion is set to the same value for each code, despite in some cases disagreeing with the standard considered.

## 6. Calculations

### 6.1 ASTM E1300

The basic procedure for designing according to ASTM E1300 is as follows:

- Determine the design loads and combine loads of different durations as per Appendix X5 if applicable
- Determine the Non-Factored Load (NFL) from appropriate chart (A1.29-35)
- Determine the Glass Type Factor (GTF)
- Multiply the NFL by the GTF to get the Load Resistance (LR)
- Verify that the LR is greater than the design load combination
- Determine the deflection from the appropriate chart (A1.29-35)

The load combinations as per ASCE 7-05 are:

- 1)  $1.0D + 1.0W$  (Eqn. 12)
- 2)  $1.0D + 1.0S$  (Eqn. 13)
- 3)  $1.0D + 0.75W + 0.75S$  (Eqn. 14)

As per Appendix X5 of E1300, the equivalent 3-second load of a 1kPa 30-day load is:

$$S = \frac{1kPa}{0.43} = 2.326kPa \quad (\text{Eqn. 15})$$

Therefore, loadcase 3 governs and the design load is:

$$P = 0.2kPa + 0.75 \cdot 1.0kPa + 0.75 \cdot 2.326kPa = 2.695kPa \quad (\text{Eqn. 16})$$

Next the NFL is determined from the appropriate chart:

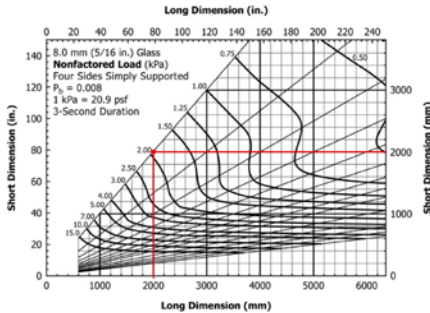


Figure 1 Non-Factored Load chart for 8mm laminated glass

It can be seen from the chart that the NFL = 1.9. Next the GTF is determined from the appropriate table:

TABLE 1 Glass Type Factors (GTF) for a Single Lite of Monolithic or Laminated Glass (LG)

| Glass Type | GTF                       |                              |
|------------|---------------------------|------------------------------|
|            | Short Duration Load (3 s) | Long Duration Load (30 days) |
| AN         | 1.0                       | 0.43                         |
| HS         | 2.0                       | 1.3                          |
| FT         | 4.0                       | 3.0                          |

Figure 2 ASTM E1300 Table 1 - Glass Type Factors

Since all loads are converted to 3s load, the GTF = 2.0 for Heat Strengthened glass.

Next determine the LR:

$$LR = GTF \cdot NFL = 2.0 \cdot 1.9kPa = 3.8kPa \geq 2.695kPa \quad (\text{Eqn. 17})$$

Next the deflection is read from the appropriate chart. In order to do this the following number is needed:

$$\text{Load} \times \text{Area}^2 = 2.69kPa \cdot (4m^2)^2 = 43.1kN - m^4 \quad (\text{Eqn. 18})$$

As per Figure 3, for an aspect ratio of 1.0, the deflection = 25.5mm.

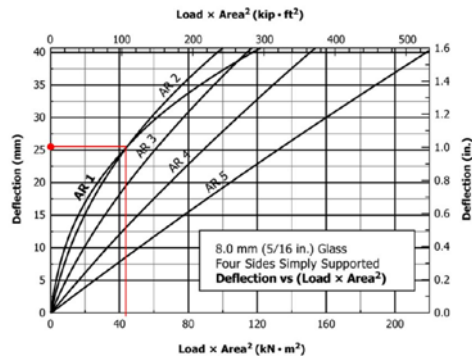


Figure 3 Deflection chart for 8mm laminates

$$\Delta_{all} = \frac{L}{60} = \frac{2000mm}{60} = 33.33mm > 25.5mm \quad (\text{Eqn. 19})$$

## 6.2 AS 1288

The basic procedure for design according to AS 1288 is as follows:

- Determine the loading as per AS 1170.1, 1170.2, and 1170.3
- Determine the design load combinations according to AS/NZS 1170.0
- Determine the annual probability of exceedance for the relevant ultimate limit states
- Ensure the glass does not exceed the maximum allowable size as per AS 1288
- Determine the design action effect  $S^*$  resulting from the strength limit state design loads by elastic structural analysis.
- Determine the nominal capacity  $R_u$  as determined from clause 3.3.2 and compare to the design action effect
- Check Deflection

The applicable strength combination cases are:

- 1)  $1.35G$  (Eqn. 20)
- 2)  $1.2G + 1.0W_u$  (Eqn. 21)
- 3)  $1.2G + 1.0S_u$  (Eqn. 22)

The applicable serviceability cases are:

- 4)  $1.0G$  (Eqn. 23)
- 5)  $1.0W_s$  (Eqn. 24)
- 6)  $1.0S_s$  (Eqn. 25)

Where:

- $G$  = self weight
- $W_s$  = Service wind action
- $S_s$  = Service snow action
- $W_u$  = Ultimate wind action
- $S_u$  = Ultimate snow action

As per AS/NZS 1170.0, the annual probability of exceedance for wind and snow loads on a category 2 (normal) structure with a 50yr design life are:

$$W_u = 1/500$$

$$S_u = 1/150$$

The 1.0kPa wind and snow loads must be factored up by the appropriate values to get to the ultimate limit state loads required above. For Australia the following chart is given for wind speed return periods.

**TABLE 3.1**  
**REGIONAL WIND SPEEDS**

| Regional wind speed (m/s)      | Region          |                    |                  |                         |                         |
|--------------------------------|-----------------|--------------------|------------------|-------------------------|-------------------------|
|                                | Non-cyclonic    |                    |                  | Cyclonic                |                         |
|                                | A (1 to 7)      | W                  | B                | C                       | D                       |
| $V_1$                          | 30              | 34                 | 26               | $23 \times F_C$         | $23 \times F_D$         |
| $V_5$                          | 32              | 39                 | 28               | $33 \times F_C$         | $35 \times F_D$         |
| $V_{10}$                       | 34              | 41                 | 33               | $39 \times F_C$         | $43 \times F_D$         |
| $V_{20}$                       | 37              | 43                 | 38               | $45 \times F_C$         | $51 \times F_D$         |
| $V_{25}$                       | 37              | 43                 | 39               | $47 \times F_C$         | $53 \times F_D$         |
| $V_{50}$                       | 39              | 45                 | 44               | $52 \times F_C$         | $60 \times F_D$         |
| $V_{100}$                      | 41              | 47                 | 48               | $56 \times F_C$         | $66 \times F_D$         |
| $V_{200}$                      | 43              | 49                 | 52               | $61 \times F_C$         | $72 \times F_D$         |
| $V_{250}$                      | 43              | 49                 | 53               | $62 \times F_C$         | $74 \times F_D$         |
| $V_{500}$                      | 45              | 51                 | 57               | $66 \times F_C$         | $80 \times F_D$         |
| $V_{1000}$                     | 46              | 53                 | 60               | $70 \times F_C$         | $85 \times F_D$         |
| $V_{2000}$                     | 48              | 54                 | 63               | $73 \times F_C$         | $90 \times F_D$         |
| $V_{2500}$                     | 48              | 55                 | 64               | $74 \times F_C$         | $91 \times F_D$         |
| $V_{5000}$                     | 50              | 56                 | 67               | $78 \times F_C$         | $95 \times F_D$         |
| $V_{10000}$                    | 51              | 58                 | 69               | $81 \times F_C$         | $99 \times F_D$         |
| $V_R (R \geq 5 \text{ years})$ | $67-41R^{-0.1}$ | $104-70R^{-0.045}$ | $106-92R^{-0.1}$ | $F_C (122-104R^{-0.1})$ | $F_D (156-142R^{-0.1})$ |

Figure 4 Table 3.1 from AS/NZS 1170.2

Since wind pressure varies with the square of the velocity, and since the serviceability wind return period is 25 years, the assumed 1.0kPa serviceability load must be factored as follows assuming Region B to arrive at an ultimate limit state wind load:

$$W_u = W_s \cdot \frac{V_{500}^2}{V_{25}^2} = 1.0kPa \cdot \frac{57^2}{39^2} = 2.14kPa \quad (\text{Eqn. 26})$$

A similar exercise for snow loads is possible by using ASCE 7 conversion factors of 0.8 and 1.2 to convert the 50 year snow load to the 25yr and 100yr snow load respectively. Using those data points to derive a logarithmic equation for return period, the equation for converting the 25 year snow load to the 150 year load is as follows:

$$S_u = S_s \cdot \frac{0.2885 \cdot \ln(R_u) - 0.1288}{0.2885 \cdot \ln(R_s) - 0.1288} = 1.0kPa \cdot \frac{0.2885 \cdot \ln(150) - 0.1288}{0.2885 \cdot \ln(25) - 0.1288} = 1.67kPa \quad (\text{Eqn. 27})$$

Which leads to the following design loads:

$$P_{d1} = 1.2 \cdot G + 1.0 \cdot W_u = 1.2 \cdot 0.2kPa + 1.0 \cdot 2.14kPa = 2.38kPa \quad (\text{Eqn. 28})$$

To be checked with the laminated glass acting monolithically.

And

$$P_{d2} = 1.2 \cdot G + 1.0 \cdot S_u = 1.2 \cdot 0.2kPa + 1.0 \cdot 1.67kPa = 1.91kPa \quad (\text{Eqn. 29})$$

To be checked assuming no composite action between panels. Using equation 1 the following design action effects are obtained:

$$S_{s-1} = 24MPa$$

$$S_{s-2} = 35MPa$$

Next, determine the nominal capacity of the glass as follows:

$$S^* \leq \varphi \cdot R_u \quad (\text{Eqn. 30})$$

$$R_u = c_1 \cdot c_2 \cdot c_3 \cdot f'_t \cdot X \quad (\text{Eqn. 31})$$

Where:

$$\varphi = 0.67$$

$$c_1 = \text{glass type factor} = 1.6 \text{ for HS glass}$$

$$c_2 = \text{surface type factor} = 1.0 \text{ for untreated glass}$$

$$c_3 = \text{load duration factor} = 1.0 \text{ for wind, 0.5 for snow and deadload}$$

$$f'_t = \text{characteristic tensile strength of the glass} = -9.85 \cdot \ln(t) + 71.34 \text{ MPa}$$

$$X = \text{geometric factor}$$

Therefore:

$$R_{u\text{-wind}} = 62.4 \text{ MPa} > 24 \text{ MPa} \quad \text{OK}$$

$$R_{u\text{-snow}} = 31.2 \text{ MPa} < 35 \text{ MPa} \quad \text{NG!}$$

Next check the deflections with equation 7 as per loadcase equations 23-25.

Since  $W_s = S_s > G$ , the snow load deflections will govern since they are to be analyzed assuming no composite action of the interlayer. Therefore, using equation 7 to analyze a 4mm panel subjected to 0.5kPa yields:

$$\Delta_{\text{snow}} = 20 \text{ mm} \leq 33.3 \text{ mm} \quad \text{OK}$$

### 6.3 BS 5516-2

The basic procedure for design according to BS 5516 is as follow:

- Determine the wind and snow load
- Based on the wind, snow, and assumed deadload, determine the design loadcases for both deflection and stress
- Determine the effective area of the glass based on the gross area and the aspect ratio
- Choose glass thickness based on charts using the effective area and the factored load
- Check deflections using the factored deflection load and the glass thickness determined from stress analysis

The ultimate limit state loadcases are as follows for positive downward pressure. The higher of either:

$$1) 0.6p_w + 2.6(p_s + p_{di}) \quad (\text{Eqn. 32})$$

Or

$$2) 1.0p_w + 2.6(0.6p_s + p_{di}) \quad (\text{Eqn. 33})$$

Where

$$p_w = \text{Wind pressure}$$

$$p_s = \text{Snow load}$$

$$p_{di} = \text{Deadload including self weight}$$

Therefore, for the assumed glass make-up:

$$0.6 \cdot 1.0 \text{ kPa} + 2.6(1.0 \text{ kPa} + 0.2 \text{ kPa}) = 3.72 \text{ kPa} \quad (\text{Eqn. 34})$$

Or

$$1.0 \text{ kPa} + 2.6(0.6 \cdot 1.0 \text{ kPa} + 0.2 \text{ kPa}) = 3.08 \text{ kPa} \quad (\text{Eqn. 35.})$$

So use 3.72kPa for the stress calculation.

In order to read the required glass thickness from the charts, first determine the effective area.

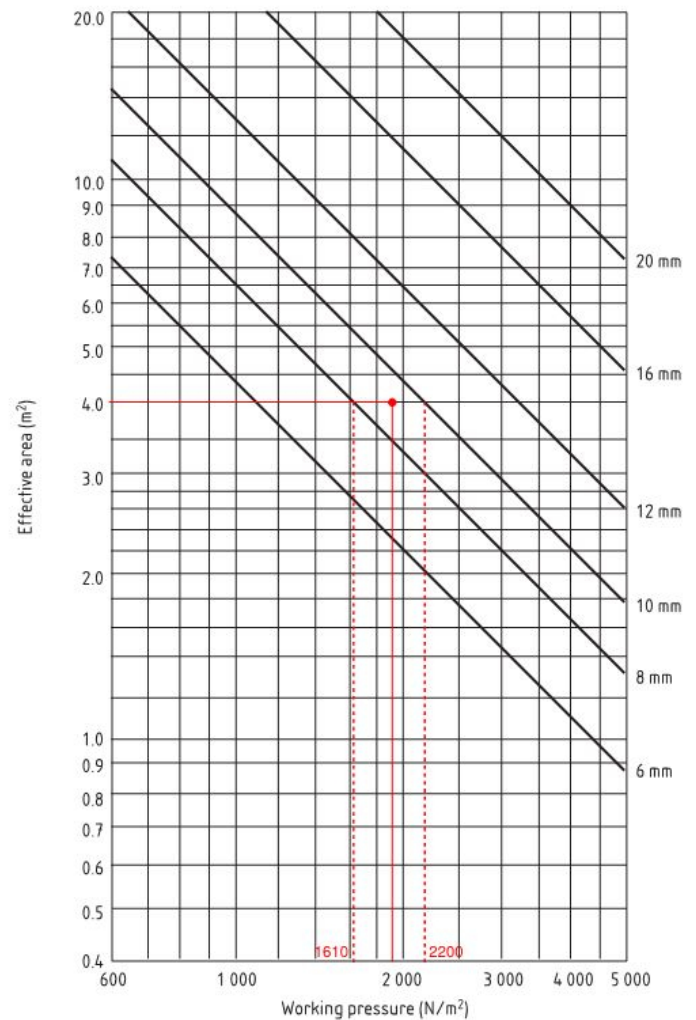


Figure 5 BS 5516 design chart for annealed laminated glass

$$A_e = A \cdot F \quad (\text{Eqn. 36})$$

$$A = a \cdot b \quad (\text{Eqn. 37})$$

$$F = \frac{4r}{(AR + 1)^2} \quad (\text{Eqn. 38})$$

Where

$a$  = long dimension of the glass panel

$b$  = short dimension of the glass panel

$AR$  = aspect ratio

$F$  = shape factor

$A$  = gross area of the glass panel

$A_e$  = effective area of the glass panel

Therefore:

$$A_e = a \cdot b \cdot \frac{4 \cdot AR}{(AR + 1)^2} = 2m \cdot 2m \cdot \frac{4 \cdot \frac{2m}{2m}}{\left(\frac{2m}{2m} + 1\right)^2} = 4m^2 \quad (\text{Eqn. 40})$$

Because BS5516 does not provide a design chart for heat-strengthened laminated glass, the following assumptions must be made in order to use the charts:

1) Stress varies linearly with load

2) Heat-strengthened glass is twice as strong as annealed glass

Although neither of these assumptions is completely accurate, it will allow the selection of a glass thickness for comparison purposes here. Based on the above assumptions, enter the chart with ½ of the load calculated in equation 34.

The chart shows that a 5mm/pvb/5mm laminate would be adequate as indicated by the location of the red dot in Figure 5 between the 8mm and 10mm lines. The dotted lines on the left and right represent the maximum capacity of an 8mm and a 10mm laminate with a 4.0m<sup>2</sup> effective area respectively. If those lines are traced down to the working pressure, it can be seen that the capacity of an 8mm heat-strengthened laminate with a 4.0m<sup>2</sup> effective area is 1.61kPa. This means that the 8mm laminate would have a utilization of:

$$U = \frac{3.72kPa/2.0}{1.61kPa} = 115\% \quad \mathbf{N.G.}! \quad (\text{Eqn. 41})$$

Next check the deflections per the following loadcases:

$$1) 0.6p_w + 1.0p_s + 1.0p_{di} \quad (\text{Eqn. 42})$$

Or

$$2) 1.0p_w + 0.6p_s + 1.0p_{di} \quad (\text{Eqn. 43})$$

Which are equivalent since  $p_w = p_s$ .

Therefore, the serviceability limit state load is  $+0.6 \cdot 1.0kPa + 1.0kPa + 0.2kPa = 1.8kPa$

And using equation 7, the deflection is:

$$\Delta = 21mm < 33.33mm \quad \mathbf{OK} \quad (\text{Eqn. 44})$$

## 6.4 DIN 18008

The basic procedure for designing according to DIN 18008 is:

- Determine the load actions
- Determine the load-bearing resistance
- Determine the load action effect and check it is lower than the load-bearing resistance
- Check that serviceability criteria are not exceeded

First determine the load actions.

The ultimate limit state loadcase is:

$$F_{d-ULS} = 1.35G + 1.5W + 1.5 \cdot 0.6S \quad (\text{Eqn. 45})$$

The serviceability limit state loadcase is:

$$F_{d-SLS} = 1.0G + 1.0W + 0.5S \quad (\text{Eqn. 46})$$

Where

$F_d$  = the design value of the combination of actions

$G$  = the value of permanent actions (e.g. self-weight)

$W$  = wind load

$S$  = snow load

Based on the above the Design Actions are as follows:

$$F_{d-ULS} = 1.35 \cdot 0.2kPa + 1.50 \cdot 1.0kPa + 1.50 \cdot 0.60 \cdot 1.0kPa = 2.67kPa$$

$$F_{d-SLS} = 0.2kPa + 1.0 \cdot 1.0kPa + 0.5 \cdot 1.0kPa = 1.7kPa$$

Next determine the load-bearing resistance as follows:

$$R_d = \frac{k_c \cdot f_k}{\gamma_M} \cdot 1.1 \quad (\text{Eqn. 47})$$

Where:

$R_d$  = the design value of the load bearing resistance

$k_c$  = the factor to take into account the type of structure. Unless specified otherwise,  $k_c = 1.0$  shall apply

$f_k$  = the characteristic value of the tensile bending strength = 70MPa for HS glass per EN1863 – 1

$\gamma_M$  = the partial safety factor for the material.

For thermally toughened glass (including Heat Strengthened),  $\gamma_M = 1.5$  shall be used.

1.1 factor is a strength increase factor allowed per DIN 18008 for laminated glass recognizing that it is unlikely that both lites would be of low quality/strength. Therefore:

$$R_d = \frac{1.0 \cdot 70MPa}{1.5} \cdot 1.1 = 51.37MPa$$

$$E_d \leq R_d \quad (\text{Eqn. 48})$$

Where:

$E_d$  = the design value of the effect (stresses)

$R_d$  = the design value of the load – bearing resistance (stresses)

According to DIN 18008, favorable shear interaction between the individual panes of glass shall not be taken into account. Therefore, each pane will resist half the load.

Using equation 1 to analyze the panel for a  $2.67/2 = 1.33\text{kPa}$  load yields:

$$E_d = 48\text{MPa} \leq 51.4\text{MPa} \quad \text{OK}$$

Using equation 7 to analyze the following load:

$$F_{d-SLS} = \frac{1.7\text{kPa}}{2} = 0.85\text{kPa}$$

Yields:

$$E_d = 26\text{mm} < 33.33 \quad \text{OK} \quad (\text{Eqn. 49})$$

## 6.5 prEN 16612

The basic design procedure according to prEN 16612 is as follows:

- Determine the design actions
- Combine the loads to determine the design combination
- Determine the glass strength
- Determine the effective thicknesses for stress and deflection calculations
- Analyze the glass using the effective thickness and compare the design action result to the glass strength and deflection limits

The governing loadcases are similar to DIN 18008, but with lower load factors which take into account that these are infill panels rather than main structure.

The ultimate limit state loadcase is:

$$F_{d-ULS} = 1.1G + 1.1W + 1.0 \cdot 0.6W \quad (\text{Eqn. 50})$$

$$F_{d-ULS} = 1.1 \cdot 0.2\text{kPa} + 1.1 \cdot 1.0\text{kPa} + 1.1 \cdot 0.6 \cdot 1.0\text{kPa} = 1.98\text{kPa}$$

The serviceability limit state loadcase is:

$$F_{d-SLS} = 1.0G + 1.0W + 0.2S \quad (\text{Eqn. 51})$$

$$F_{d-SLS} = 1.0 \cdot 0.2\text{kPa} + 1.0 \cdot 1.0\text{kPa} + 0.2 \cdot 1.0\text{kPa} = 1.4\text{kPa}$$

Next determine the strength of the panel:

$$f_{g;d} = \frac{k_{mod}k_{sp}f_{g;k}}{\gamma_{M,A}} + \frac{k_v(f_{b;k} - f_{g;k})}{\gamma_{M,v}} \quad (\text{Eqn. 52})$$

Where:

$f_{g;k}$  = the characteristic value of the bending strength =  $45\text{N/mm}^2$

$\gamma_{M,A}$  = the material partial factor for annealed glass

$k_{mod}$  = load duration factor

$k_{sp}$  = glass surface profile factor

$\gamma_{M,v}$  = the material partial factor for surface prestress

$f_{b;k}$  = the characteristic value of the bending strength of prestressed glass

$k_v$  = the factor for strengthening of prestressed glass

$$k_{mod} = 0.663 t^{-\frac{1}{16}} \quad (\text{Eqn. 53})$$

where t is the load duration in hours

For a 5 second wind gust:

$$k_{mod} = 0.663 \left(\frac{5}{3600}\right)^{-\frac{1}{16}} = 1.0$$

For snow load for 3 weeks:

$$k_{mod} = 0.663 (504)^{-\frac{1}{16}} = 0.45$$

$$\gamma_{M,A} = 1.8$$

$$\gamma_{M,v} = 1.2$$

For float glass,  $k_{sp} = 1$

For heat strengthened glass,  $f_{b;k} = 70\text{MPa}$

Assume horizontal toughening,  $k_v = 1.0$

$$f_{g;d-wind} = \frac{(1.0)(1)(45)}{1.8} + \frac{1(70 - 45)}{1.2} = 45.8\text{MPa}$$

$$f_{g;d-snow} = \frac{(1.0)(0.45)(45)}{1.8} + \frac{1(70 - 45)}{1.2} = 32.1\text{MPa}$$

Next determine the effective thickness for deflection:

$$h_{ef,w} = \sqrt[3]{\sum_k h_k^3 + 12\omega \left[ \sum_i h_k h_{m,k}^2 \right]} \quad (\text{Eqn. 54})$$

and for stress:

$$h_{ef,\sigma,j} = \sqrt[3]{\frac{(h_{ef,w})^3}{(h_j + 2\omega h_{m,j})}} \quad (\text{Eqn. 55})$$

Where:

$\omega$  = the interlayer shear transfer coefficient

$h_k, h_j$  = the thicknesses of the glass plies

$h_{m,k}, h_{m,j}$  = the distances from the midplane of glass plies k and j, respectively, from the mid-plane of the laminated glass

Since snow load and wind load are equivalent, the snow load leading case will govern since it will have a smaller effective thickness.

$$h_{ef,w} = \sqrt[3]{\sum_k h_k^3 + 12\omega \left( \sum_i h_k h_{m,k}^2 \right)}$$

$$= \sqrt[3]{3.78^3 + 3.78^3}$$

$$= 4.76\text{mm}$$

$$h_{ef,\sigma,1} = h_{ef,\sigma,2} = \sqrt[3]{\frac{(h_{ef,w})^3}{(h_j + 2\omega h_{m,j})}}$$

$$= \sqrt[3]{\frac{(4.76\text{mm})^3}{(3.78\text{mm})}}$$

$$= 5.34\text{mm}$$

The resultant maximum surface stress as per equation 1 =  $38.24\text{MPa} > 32.1\text{MPa}$  **NG!**

The maximum deflection as per equation 7 =  $27.55\text{mm} < 33.33\text{mm}$  **OK**

## 6.6 Utilization Method

The basic procedure of the Utilization Method is as follows:

- Determine the serviceability level loads and the corresponding temperature and duration
- Determine the effective thickness of the assumed glass make-up for each of the load states (load, temperature, duration combinations) as per Appendix X9 of ASTM E1300
- Determine the applicable loadcases as per ASCE 7
- Calculate the stress and deflection for each individual factored load
- Compare each individual stress result with the allowable stress for that load duration to determine a utilization for that load

- Do the same for deflection
- Sum the stress and deflection utilizations as per the loadcases and verify that all are less than 100%.

It should be noted that for non-linear calculations as the load increases, so does the percentage of the load resisted by membrane action rather than bending action. So for non-linear calculations, n times the stress due to load P is greater than the stress due to load nP. Therefore, the method described above is conservative.

ASTM E1300 recommends the following load durations and temperatures:

Wind: 50°C, 3 seconds

Snow: 23°C, 30 days

Since wind will be combined with snow and occurring at the same time, it is not possible that it is occurring at 50°C, so use 23°C for both wind and snow.

No recommendations are given for deadload, so assume 50°C and a duration of 10 years.

The equations for determining effective thickness as per X9 of ASTM E1300 are as follows.

For deflection:

$$h_{ef,w} = \sqrt[3]{h_1^3 + h_2^3 + 12 \cdot \Gamma \cdot I_s} \quad (\text{Eqn. 56})$$

For Stress:

$$h_{ef1,\sigma} = \sqrt{\frac{h_{ef,w}^3}{h_1 + 2 \cdot \Gamma \cdot h_{s,2}}} = h_{ef2,\sigma} \text{ for equal laminates} \quad (\text{Eqn. 57})$$

Where:

$$\Gamma = \frac{1}{1 + 9.6 \cdot \frac{E \cdot I_s \cdot h_v}{G \cdot h_s^2 \cdot a^2}} \quad (\text{Eqn. 58})$$

$$I_s = h_1 \cdot h_{s,2}^2 + h_2 \cdot h_{s,1}^2 \quad (\text{Eqn. 59})$$

$$h_{s,1} = \frac{h_s \cdot h_1}{h_1 + h_2} \quad (\text{Eqn. 60})$$

$$h_{s,2} = \frac{h_s \cdot h_2}{h_1 + h_2} \quad (\text{Eqn. 61})$$

$$h_s = 0.5(h_1 + h_2) \cdot h_v \quad (\text{Eqn. 62})$$

And:

$h_v$  = interlayer thickness = 1.52mm

$h_1$  = glass ply 1 minimum thickness = 3.78mm

$h_2$  = glass ply 2 minimum thickness = 3.78mm

$E$  = Glass Young's modulus = 71,700MPa

$a$  = length of the short edge of the glass plate

$G$  = interlayer shear modulus

$\Gamma$  = shear transfer coefficient

Based on the above, the effective thicknesses are as follows:

| Load Type | Duration | Temperature | Effective Thickness |
|-----------|----------|-------------|---------------------|
| [name]    | [time]   | [°C]        | [mm]                |
| Dead      | 10yrs    | 50          | 5.52                |
| Snow      | 30days   | 23          | 6.82                |
| Wind      | 3sec     | 23          | 8.73                |

Table 2 Effective thickness for deflection calculations as per ASTM E1300 X9

| Load Type | Duration | Temperature | Effective Thickness |
|-----------|----------|-------------|---------------------|
| [name]    | [time]   | [°C]        | [mm]                |
| Dead      | 10yrs    | 50          | 6.27                |
| Snow      | 30days   | 23          | 7.58                |
| Wind      | 3sec     | 23          | 8.89                |

Table 3 Effective thickness for stress calculations as per ASTM E1300 X9

ASCE 7 serviceability loadcases which involve dead, snow, and wind load are as follows:

- 1) 1.0D (Eqn. 63)
- 2) 1.0D + 1.0W (Eqn. 64)
- 3) 1.0D + 1.0S (Eqn. 65)
- 4) 1.0D + 0.75W + 0.75S (Eqn. 66)

Since wind and snow are the same magnitude, equation 66 will govern the design. Therefore, using equations 1 and 7 the following results are obtained.

| Load Type | Action | Duration | Temperature | Effective Thickness | Action Effect |
|-----------|--------|----------|-------------|---------------------|---------------|
| [name]    | [kPa]  | [time]   | [°C]        | [mm]                | [mm]          |
| Dead      | 0.20   | 10yrs    | 50          | 5.52                | 8.69          |
| Snow      | 0.75   | 30days   | 23          | 6.82                | 14.29         |
| Wind      | 0.75   | 3sec     | 23          | 8.73                | 9.69          |

Table 4 Deflection calculations

| Load Type | Action | Duration | Temperature | Effective Thickness | Action Effect |
|-----------|--------|----------|-------------|---------------------|---------------|
| [name]    | [kPa]  | [time]   | [°C]        | [mm]                | [MPa]         |
| Dead      | 0.20   | 10yrs    | 50          | 6.27                | 4.87          |
| Snow      | 0.75   | 30days   | 23          | 7.58                | 10.52         |
| Wind      | 0.75   | 3sec     | 23          | 8.89                | 9.27          |

Table 5 Stress calculations

The maximum allowable surface stress to be used with independent stress analysis for heat strengthened glass is 46.6 MPa as per X6 of ASTM E1300 assuming a 3 second load duration and a probability of breakage of 8/1000.

Appendix X4 of ASTM E1300 provides a table to convert the 3s load resistance of glass panels to different durations.

Therefore, the allowable stresses and the utilizations are as follows:

| Duration  | Factor |
|-----------|--------|
| 3 sec     | 1.00   |
| 10 sec    | 0.93   |
| 1 min     | 0.83   |
| 10 min    | 0.72   |
| 1 hr      | 0.64   |
| 12 hrs    | 0.55   |
| 1 day     | 0.53   |
| 1 week    | 0.47   |
| 1 month   | 0.43   |
| 1 year    | 0.36   |
| Long term | 0.31   |

Table 6 Values for load resistance duration conversion from ASTM E1300 X4

| Load Type    | Action | Duration | Temperature | Effective Thickness | Action Effect | Limit | Utilization |
|--------------|--------|----------|-------------|---------------------|---------------|-------|-------------|
| [name]       | [kPa]  | [time]   | [°C]        | [mm]                | [MPa]         | [MPa] | [%]         |
| Dead         | 0.20   | 10yrs    | 50          | 6.27                | 4.87          | 14.45 | 34          |
| Snow         | 0.75   | 30days   | 23          | 7.58                | 10.52         | 20.04 | 53          |
| Wind         | 0.75   | 3sec     | 23          | 8.89                | 9.27          | 46.6  | 20          |
| <b>TOTAL</b> |        |          |             |                     |               |       | 106         |

Table 7 Stress Utilization for 4mm/PVB/4mm panel

And the allowable deflections and the utilizations are:

| Load Type    | Action | Duration | Temperature | Effective Thickness | Action Effect | Limit | Utilization |
|--------------|--------|----------|-------------|---------------------|---------------|-------|-------------|
| [name]       | [kPa]  | [time]   | [°C]        | [mm]                | [mm]          | [mm]  | [%]         |
| Dead         | 0.20   | 10yrs    | 50          | 5.52                | 8.69          | 33.33 | 26          |
| Snow         | 0.75   | 30days   | 23          | 6.82                | 14.29         | 33.33 | 43          |
| Wind         | 0.75   | 3sec     | 23          | 8.73                | 9.69          | 33.33 | 29          |
| <b>TOTAL</b> |        |          |             |                     |               |       | 98          |

Table 8 Deflection Utilization for 4mm/PVB/4mm panel

Therefore the panel is slightly over-utilized for stress.

## 7. Results

Table 9 shows the results of the initial stage of the calculation – defining the design loads. As can be seen in the table, despite starting with the same initial loads of 1kPa wind and snow the final serviceability and ultimate limit state design loads differ quite substantially across standards.

| Standard           | SLS Dead Load | SLS Snow Load | SLS Wind Load | Ultimate Limit State |                  |                  |               | Serviceability Limit State |                  |                  |               |
|--------------------|---------------|---------------|---------------|----------------------|------------------|------------------|---------------|----------------------------|------------------|------------------|---------------|
|                    |               |               |               | DL Factor            | Snow Load Factor | Wind Load Factor | Design Action | DL Factor                  | Snow Load Factor | Wind Load Factor | Design Action |
| [name]             | [kPa]         | [kPa]         | [kPa]         | [#]                  | [#]              | [#]              | [kPa]         | [#]                        | [#]              | [#]              | [kPa]         |
| ASTM E1300 - 2016  | 0.2           | 1.0           | 1.0           | 1.00                 | 1.74             | 0.75             | 2.69          | 1.00                       | 1.74             | 0.75             | 2.69          |
| AS 1288: 2006      | 0.2           | 1.0           | 1.0           | 1.20                 | 1.67             | 0.00             | 1.91          | 0.00                       | 1.00             | 0.00             | 1.00          |
| BS 5516: 2004      | 0.2           | 1.0           | 1.0           | 1.30                 | 1.30             | 0.30             | 1.86          | 1.00                       | 1.00             | 0.60             | 1.80          |
| DIN 18008-1: 2010  | 0.2           | 1.0           | 1.0           | 1.35                 | 1.50             | 0.90             | 2.67          | 1.00                       | 1.00             | 0.50             | 1.70          |
| prEN 16612: 2013   | 0.2           | 1.0           | 1.0           | 1.10                 | 1.10             | 0.66             | 1.98          | 1.00                       | 1.00             | 0.20             | 1.40          |
| Utilization Method | 0.2           | 1.0           | 1.0           | 1.00                 | 0.75             | 0.75             | 1.70          | 1.00                       | 0.75             | 0.75             | 1.70          |

Table 9 Design actions for a 4mm/PVB/4mm panel

These design actions were then applied to the panels in the manner prescribed by the respective standard, the results of which are shown in Table 10.

| Standard           | Ultimate Limit State |        |          |     | Serviceability Limit State |        |       |     |
|--------------------|----------------------|--------|----------|-----|----------------------------|--------|-------|-----|
|                    | Design Action        | Effect | Limit    | U   | Design Action              | Effect | Limit | U   |
| [name]             | [kPa]                | [MPa]  | [MPa]    | [%] | [kPa]                      | [mm]   | [mm]  | [%] |
| ASTM E1300 - 2016  | 2.69                 | n/a    | 3.80 kPa | 71  | 2.69                       | 25.5   | 33.3  | 77  |
| AS 1288: 2006      | 1.91                 | 34.9   | 29.7     | 118 | 1.00                       | 20.8   | 33.3  | 62  |
| BS 5516: 2004      | 1.86                 | n/a    | 1.61 kPa | 115 | 1.80                       | 20.1   | 33.3  | 60  |
| DIN 18008-1: 2010  | 2.67                 | 47.8   | 51.4     | 93  | 1.70                       | 26     | 33.3  | 78  |
| prEN 16612: 2013   | 1.98                 | 38.2   | 32.2     | 119 | 1.40                       | 27.6   | 33.3  | 83  |
| Utilization Method | 1.70                 | n/a    | varies   | 106 | 1.70                       | 32.7   | 33.3  | 98  |

Table 10 Overall results - 4mm/PVB/4mm panel

## 8. Discussion

As can be seen from Table 10, the approach and results of the various analyses vary substantially. For example the stress utilization varies from 71% to 119%. There is even more spread in the deflections; a range of 12.6mm is a variation of 63%! In comparing the standards the following discrepancies and areas of future code development were noted.

### 8.1 ASTM E1300

ASTM E 1300 recognizes the time dependency of the allowable glass stresses and accounts for this by providing factors which can be used to convert longer term loads into the 3 second loads used for design. This is not true for deadload however, as highlighted in an example given in the standard in which the deadload is simply subtracted from the load resistance without first factoring it – this is akin to assuming that deadload only acts for 3 seconds. Since this standard is also the least conservative in terms of stresses (with the resulting stress limited glass make-up only 3mm/PVB/3mm) that is a potentially unsafe assumption, especially for heavy glass make-ups. Additionally all design charts in E1300 have been developed assuming a temperature of 50°C, so there is no way to account for temperature in the calculations. The appendices present stresses to be used with independent stress analysis as well as a method to determine effective thickness which takes into account temperature and load duration. The Utilization Method presented herein is a way to utilize these appendices in a rational design procedure.

### 8.2 AS 1288

AS 1288 does not take into account any subtlety when dealing with the interlayer shear interaction of laminated glass. For short term loads the panel acts monolithically and for long term loads the system is treated as layered. Therefore, temperature effects and different interlayer properties cannot be taken into account. This results in inaccurate deflection calculations. Similarly there are two catchall values (1.0 for short term, 0.5 for long term) for factoring glass allowable stress according to load duration.

### 8.3 BS 5516

BS 5516 was the least complete of the standards that were reviewed. It does not contain any provisions for accommodating loads of different durations, temperatures, or even glass of different heat-treatments than annealed. It is not stated how one should treat laminated glass with respect to interlayer shear transfer.

### 8.4 DIN 18008

DIN 18008 does not allow any shear transfer through the interlayer regardless of the load duration, but instead gives a blanket 10% increase in the safety factor for laminated glass. Like AS1288 this results in inaccurate deflection calculations. It also does not reduce the strength of heat-treated glass for longer duration loads.

### 8.5 prEN 16612

prEN 16612 is a draft document meant to address the inconsistencies in the national codes regarding glass design and it does take load duration effects on glass strength

as well as temperature effects into account. However, like other approaches it does not properly account for combining loads of different durations since the resulting different structural systems are not considered. It is otherwise the most complete standard studied.

### 8.6 Utilization Method

The Utilization Method is based on the charts and appendices of ASTM E1300. The method relies on the assumption that probabilities of breakage for individual load states (load, duration, and temperature) can be summed to arrive at an overall probability of breakage, or utilization rate. By doing this one can take into account the different allowable stresses and stiffnesses associated with loads of different durations and temperatures. Linearly summing the deflections obtained from a non-linear analysis of different load states is conservative as it neglects some membrane action that will occur in the actual condition. It does however give a more accurate picture of deflection than other methods studied. Because the calculated deflections are conservative, the deflection limit criterion should be considered carefully when the panel thickness is governed by deflection.

## 9. Future Work

For this study only loads which have the same distribution were studied. For roof panels, maintenance loads can also be a design concern and it could be studied how to incorporate point loads into the Utilization Method. Further finite element analysis which utilizes a time history and load application in several steps could also be undertaken

to test the validity of this method. However, ultimately the best test of the validity of any of the methodologies would be a medium term physical test which could measure the stress and deflection of a panel over a period of one or two months at a specific controlled temperature.

## 10. Conclusion

The results of this study show that there is inconsistency across regions in the design methodology of laminated glass and that each code or standard has its own faults. Because most of these standards were developed for vertical glazing which rarely sees loads of different durations in combination, this area of code development seems to be lacking. The Utilization Method proposed herein is a conservative but more accurate and consistent method of designing laminated glass. Given that non-linear plate bending equations can be put into spreadsheet form, the entire design process can be automated. Ultimately, for laminated glass subjected to loads of different duration or temperature, the benefit of the Utilization Method is that it offers a more rational design process than current standards.

## 11. References

- [1] AS/NZS 1170.0: 2002: Structural design actions – Part 0: General Principles (2002)
- [2] AS/NZS 1170.1: 2002: Structural design actions – Part 1: Permanent, imposed and other actions (2002)
- [3] AS/NZS 1170.2: 2011: Structural design actions – Part 2: Wind actions (2011)
- [4] AS/NZS 1170.3: 2003: Structural design actions – Part 3: Snow and ice actions (2003)
- [5] AS 1288-2006: Glass in buildings – Selection and installation (2006)
- [6] ASCE/SEI 7-05: Minimum Design Loads for Buildings and Other Structures (2006)
- [7] ASTM E1300-16: Standard Practice for Determining Load Resistance of Glass in Buildings (2016)
- [8] BS 5516-2: 2004: Patent glazing and sloping glazing for buildings – Part 2: Code of practice for sloping glazing (2004)
- [9] BS EN 1990: 2002: Eurocode - Basis of Structural Design (2002)
- [10] BS EN 1991-1-1: 2002: Eurocode 1: Actions on structures – Part 1-1: General actions - Densities, self-weight, imposed loads for buildings (2002)
- [11] BS EN 1991-1-3: 2003: Eurocode 1: Actions on structures – Part 1-3: General actions - Snow loads (2003)
- [12] BS EN 1991-1-4: 2005: Eurocode 1: Actions on structures – Part 1-4: General actions - Wind actions (2005)
- [13] DIN 18008-1: 2010-12: Glass in Building – Design and construction rules – Part 1: Terms and general bases, English translation (2010)
- [14] prEN 16612: 2013: Glass in building – Determination of the load resistance of glass panes by calculation and testing (2013)
- [15] prEN 16613: 2013: Glass in building – Laminated glass and laminated safety glass – Determination of interlayer mechanical properties (2013)

# Verification of Insulating Glass Units in Modern Curtain Wall Facades

## Authors

Florian Döbbel<sup>1</sup>, Michael Elstner<sup>2</sup>  
<sup>1</sup>Sika Services AG Building Systems & Industry  
<sup>2</sup>AGC Interpane

## Keywords

unitized curtainwall, finite element analysis (FEA), insulating glass units, case study, climatic loads, ASTM E1300, load sharing

## Abstract

ASTM E1300 is the main US standard for determining the load resistance of glass in buildings. The safety concept is based on a "Failure Prediction Model (FPM)". Depending on the application, the accepted probability of glass breakage can vary and is typically less than 0.008 for vertical glazing. Normally verification of glass is done against wind loads and for rectangular units only. In modern Curtain Walling facades, irregular shapes and the additional impact of linear or concentrated loads on the glass units are demands not yet covered by FPM of ASTM E1300. Considering relevant load sharing between inner and outer lite as well as climatic effects caused by the enclosed gas volume in hermetically sealed IG units is required for a reliable glass design. For proper verification and evaluation of various influences, use of an "Allowable Stress Design" is advisable. Taking into account the static fatigue of annealed glass the load duration is a dominant factor for determining the relevant allowable stress. Relevant load case combinations are mentioned in IBC and ASCE, but just for typical loads within the building sector. The structural analysis of insulating glass units requires taking into account probable interaction of internal and external loads. While wind loads are determined for load duration of 3s, live loads and climatic effects can act in a period of several minutes, hours or years.

This paper shows an approach of combining loads with different load durations based on the safety concept of ASTM E1300 and how to combine load types which are not explicitly mentioned in that standard. In conclusion, the proposal of appropriate load case combinations and relevant load durations leading to an "Allowable Stresses Design" is presented.

## 1. Introduction

Standard practice for determining the existing load resistance of specific glass units used in buildings, especially in windows, is found in ASTM E1300 [2]. Procedures described in [2] also cover determination of load resistance and maximum lateral deflection for glass types combined in sealed insulating glass units. Focusing on common practice, the procedures of [2] are applicable for rectangular insulating glass units, simply supported on four sides and exposed to uniform lateral loads of short and long duration. An approximation of the behavior and probability of fracture of various types of glass combined in sealed IG units as well as a proportional assumption of load sharing between inner and outer lite of double glazed IG units is stated in appendixes X2 and X3 of [2], which is sometimes a conservative approach but not in any case. Appendix X5 provides an approximate technique to combine various lateral uniform loads of different load duration. However, all assumptions given by [2] are very limited in terms of shape, edge support, load effects and sufficient evaluation of combined types of glass. State-of-the-art applications of insulating glass in Unitized Curtain Walling and Structural Sealant Glazing require effective evaluation methods of special shapes, loads and boundary conditions along with a reliable combination of various loads acting concurrently but in different directions, with different load durations and concentrated on different areas of a glass unit. For these cases more accurate calculation methods are needed as internal loads have to be taken into account for an IG unit and capable procedures for evaluating separated and combined effects have to be discussed.

## 2. Design Loads and Load sharing

Various types of loads and combinations of loads have to be taken into account for the design of architectural glass in facades according to [1]. Most relevant are those like:

- Wind loads (3s gust), both acting positive (inward) and negative (outward)
- Dead load components of inclined (inward or outward sloped) IG units
- Barrier loads (horizontal line load, concentrated load and uniform load representing human impact)

In practice there are additional internal load effects existing if insulating glass units are used. ASTM E1300 is using a load share factor between the lites of an IG unit, but does not address the internal "climatic effect", deeper described in the next section. Within this section, the rules of load sharing between inner and outer glass shall be presented, first.

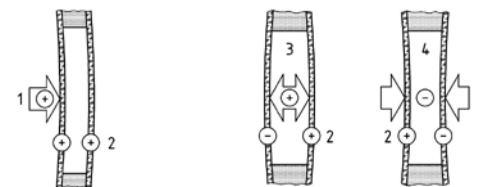


Figure 1: Sharing of external loads and acting of internal loads according to [3].

Lites of an IG unit are not only linearly bonded around the perimeter. They are also connected by the gas volume enclosed in the hermetically sealed cavity. This coupling effect causes load sharing between the connected lites. A simplified approach widely used in engineering practice and mentioned in [2], appendix X3 is determining the correct proportional stiffness of inner and outer glass. Actually, an accurate approach of load sharing (ref. to Table 2) has to respect the shape and the dimension of the IG unit and the direction of the relevant loading as stated in [3] and [5], too. Covering all the relevant influences Prof. Feldmeier introduced an insulating glass factor  $\varphi$  which depends on the length of the shorter glass edge  $a$  and the characteristic length  $a^*$ .  $a^*$  is representing characteristic properties of the IG unit like aspect ratio  $B_v$  (ref. to Table 1), dimension of the hermetically sealed cavity  $t_{\text{cavity}}$  and stiffness of the two lites (outer lite  $t_1$ , inner lite  $t_2$ ). The equations to determine these factors are shown in (1).

E - Young's modulus glass - 71 700 MPa  
 pB - barometric pressure - 100 kPa

$$\varphi = \frac{1}{1+(a/a^*)^2}; \quad a^* = \sqrt{\frac{E}{p_0} \times \frac{t_1^3 \times t_2^3 \times t_{cavity}}{(t_1^3 + t_2^3) \times B_v}}; \quad \delta_1 = \frac{t_1^3}{t_1^3 + t_2^3}; \quad \delta_2 = \frac{t_2^3}{t_1^3 + t_2^3}. \quad (1)$$

| a / b          | 1.0    | 0.9    | 0.8    | 0.7    | 0.6    | 0.5    | 0.4    | 0.3    | 0.2    | 0.1    |
|----------------|--------|--------|--------|--------|--------|--------|--------|--------|--------|--------|
| B <sub>v</sub> | 0.0194 | 0.0237 | 0.0288 | 0.0350 | 0.0421 | 0.0501 | 0.0587 | 0.0676 | 0.0767 | 0.0857 |

a – length of the shorter glass edge, b – length of the longer glass edge

Table 1. Coefficient B<sub>v</sub> according to [3] and [5].

| Loading                | Load direction               | Load component taken by the outer lite                      | Load component taken by the inner lite                      |
|------------------------|------------------------------|---|---|
| Negative wind pressure | Pressure onto the inner lite | $w_{n,1} = (1-\varphi) \times \delta_1 \times w_{n,total}$  | $w_{n,2} = (\varphi\delta_1 + \delta_2) \times w_{n,total}$ |
| Positive wind pressure | Pressure onto the outer lite | $w_{p,1} = (\delta_1 + \varphi\delta_2) \times w_{p,total}$ | $w_{p,2} = (1-\varphi) \times \delta_2 \times w_{p,total}$  |

Table 2. Load components bases on load sharing according to [3] and [5].

### 3. Climatic Effects in hermetically sealed units

Insulating glass units are hermetically sealed systems. This means that gas (air or inert gases like argon and krypton) is enclosed in the space between at least two or more lites. It is an isochoric condition. This means that the volume is remaining constant, as shown in [2].

$$\frac{p}{T} = \text{const.} \quad (2)$$

Climatic effects imply internal load effects caused by the expansion of the gas volume. The expansion of the enclosed volume is confined by the inner and the outer lite. Due to the fact that the lites are not absolutely rigid, the actual state is balanced between an isochoric and an isobaric limit state. The individual loading depends on the external conditions and the geometrical properties. Geometrical properties are the dimension of the cavity, the dimension of the IG unit and the thickness of the inner and the outer lite. External conditions include

- Variation of atmospheric pressure  $\Delta p_{atm}$ ,
- Variation of temperature of the enclosed gas  $\Delta T$  and
- Variation of elevation  $\Delta H$ , which can result an increasing pressure in the cavity.

Variations acting on the glass and the edge seal are also related to changed conditions between production of the IG unit just as the edge seal and conditions after installation or during service life. The relevant isochoric limit state  $p_0$  can be determined according to [3]. The geometrical properties are embedded into the insulating glass factor  $\varphi$  determined in (1). The product of isochoric pressure and insulating glass factor in (4) results in the internal load  $P_{climatic}$  acting as the maximum

climatic load effect on the inner and the outer lite as well as on the edge seal of the IG unit.

$$p_0 = (\Delta T \times 0.34 \text{ kPa/K}) + \Delta p_{atm} + (\Delta H \times 0.012 \text{ kPa/m}). \quad (3)$$

$$P_{climatic} = \varphi \times p_0. \quad (4)$$

While larger IG units are mainly affected by wind loads or other externally imposed loads the impact of climatic effects becomes more and more decisive for smaller and narrow units. In some cases, climatic load effects for the smaller IG units are much higher than wind load impacts relevant for the larger units. That makes it important to not just consider the largest IG units for a proper glass and secondary seal design. Taking into account climatic load effects and considering smaller IG units is significantly important for the entire glass design, a durable edge sealing system and a final IG configuration which meets all demands on safety and life expectancy.

### 4. Allowable Surface stress in accordance with ASTM E1300

The glass failure prediction model (FPM) that serves as a basis for the non-factored load (NFL) charts of ASTM E1300 [2] assumes that the probability of glass breakage is a function of the distribution and severity of stress-raising surface discontinuities and the distribution of surface tensile stresses over the glass area. If the maximum stress levels on two lites with different dimensions and thicknesses are the same, the lite with the maximum stress distributed over the bigger area is more likely to fail. It is not appropriate to base the structural adequacy of glass used in buildings solely on its modulus of rupture as determined through the testing of small-scale laboratory specimens. The verification approach of [2] is based on the load resistance (LR) determined

as a uniform lateral load. LR is composed of a non-factored load (NFL) representing a maximum applicable load (3-seconds duration, probability of breakage  $\leq 0.008$ , monolithic annealed glass) taking into account surface conditions, glass thickness as well as glass dimensions and of the glass type factor (GTF) representing the appropriate glass type and the relevant load duration. This procedure becomes more complex if laminated glass (LG), insulating glass (IG) or even the combination of more than one load acting concurrently with different load durations, has to be considered. Depending on the specific case, additional load sharing factors (LS), lite probability factors (p) and combination of load effects and load duration according to [2], X5.1 have to be respected. LR is going to be determined for each lite, while the lower of all load resistance values is decisive. In case of combined loads q and LR are determined for an equivalent 3-seconds duration, shown in [5].

$$LR_i = NFL_i \times GTF_i \times LS_i; \quad q \leq LR_i. \quad (5)$$

More and more there is demand for designing and verifying glass units of irregular shape or composition, not 4-sided simply supported or even exposed to non-uniform load impacts and load combinations. In these cases, more flexible and accurate calculation techniques such as finite element, finite difference or standard engineering mechanics formulas have to be used to determine maximum surface stress and deflection taking into account specific boundary conditions.

Different from FPM used in [2] most common engineering practices and tools are based on allowable stress design (ASD). Covering design of special glass shapes and loads on an adequate level of safety and confidence ASTM E1300 gives some indications for the approximate maximum surface stress to be used with an independent stress analysis in appendix X6. Mostly conservative allowable surface stress values for a 3-seconds duration load and a probability of breakage  $\leq 0.008$  are mentioned in [2], X6.2 with 23.3 MPa (3 380 psi) for annealed float glass, 46.6 MPa (6 750 psi) for heat-strengthened glass and 93.1 MPa (13 500 psi) for fully-tempered glass. X6.3 requires calculating the maximum surface stress in a glass lite using rigorous engineering analysis, which takes into account large defections, like non-linear finite element analysis. In general, non-linear effects get more significant for the verification of continuously supported glass units the bigger the glass deflection in relation to the glass thickness and the closeness of the aspect ratio to quadratic shape. The calculated surface stress has to be less than the maximum allowable stress.

The maximum allowable surface stress is a function of area (A), load duration in seconds (d), surface flaw parameter (k), probability of breakage (Pb) and an exponent that characterizes the weakening effect due to sub-critical crack growth (n). All of these parameters can be considered as properly represented by the allowable surface stress according to [2], X6.2. The equation mentioned in X6.2 must be verified in each individual case or within a proper structural design considering different loads and their combination factors. Parameters, which still could be adapted to the specific cases and glass types are the load duration (d) and the exponent n differentiated in [8], Note 2 for different glass types, using  $n = 16$  for annealed float glass,  $n = 32$  for heat-strengthened glass and  $n = 48$  for fully-tempered glass. Another important point is a suitable evaluation of fritted glass. [8], Note 1 gives a general recommendation for disruptive surface treatments stating an allowable stress reduction factor of 0.5 but with a remarks to consult the glass manufacturer. [9] summarizes a useful study. Based on its conclusions an allowable stress reduction factor of 0.6 is sufficient and reliable.

$$\sigma_{\text{allowable}} [d,n] = \frac{\sigma_{\text{allowable}} [2], X6.2}{\sqrt[n]{d/3}} \quad (6)$$

Representing the effective conditions, always the minimum glass thickness in accordance with ASTM C1036 is relevant. In case of a European glass manufacturer or float glass supplier the minimum glass thickness

according to EN 572 should be taken into account. For annealed glass, the assumed values for Young's modulus and Poisson's ratio are 71.7 GPa (10.4e6 psi) and 0.22, respectively. Based on [2] the PVB interlayer is allowed to be considered with a shear modulus of 0.40 MPa at temperatures up to +50 °C (122 °F) and for 3-seconds load duration.

| Load Duration | 3 s   |        | 60 s  |        | 600 s (10 min) |        | 43 200 s (12 hours) |        | 473 040 000 s (>> 1 year) |       |
|---------------|-------|--------|-------|--------|----------------|--------|---------------------|--------|---------------------------|-------|
|               | [MPa] | [psi]  | [MPa] | [psi]  | [MPa]          | [psi]  | [MPa]               | [psi]  | [MPa]                     | [psi] |
| AN            | 23.30 | 3 380  | 19.32 | 2 803  | 16.73          | 2 427  | 12.81               | 1 858  | 7.16                      | 1 039 |
| HS            | 46.60 | 6 750  | 42.44 | 6 147  | 39.49          | 5 720  | 34.55               | 5 004  | 25.84                     | 3 742 |
| HS, fritted   | 28.00 | 4 050  | 25.46 | 3 688  | 23.69          | 3 432  | 20.73               | 3 003  | 15.50                     | 2 245 |
| FT            | 93.20 | 13 500 | 87.54 | 12 683 | 83.46          | 12 089 | 76.35               | 11 059 | 62.90                     | 9 111 |
| FT, fritted   | 55.90 | 8 100  | 52.52 | 7 610  | 50.08          | 7 254  | 45.81               | 6 635  | 37.74                     | 5 466 |

Table 3. Allowable surface stress for different load duration and glass types based on [6].

| Nominal Thickness or Designation |       | Minimum (calculation) Thickness acc. to ASTM C1036 |       | Minimum (calculation) Thickness acc. to EN 572 |       |
|----------------------------------|-------|--|-------|--|-------|
| [mm]                             | [in.] | [mm]   | [in.] | [mm]   | [in.] |
| 4.0                              | 1/8   | 3.78   | 0.149 | 3.8  | 0.150 |
| 5.0                              | 5/32  | 4.57   | 0.180 | 4.8  | 0.189 |
| 6.0                              | 3/16  | 5.56   | 0.219 | 5.8  | 0.228 |
| 8.0                              | 1/4   | 7.42   | 0.292 | 7.7  | 0.303 |
| 10.0                             | 5/16  | 9.02   | 0.355 | 9.7  | 0.382 |
| 12.0                             | 1/2   | 11.91  | 0.469 | 11.7   | 0.461 |

Table 4. Nominal and minimum glass thicknesses according to ASTM and EN standard.

### 5. Combination of relevant loads

ASCE Code 07 [4] is the basic rule for minimum design loads and relevant load combinations in buildings and other structures. The challenge is to define an approach for a proper IG unit design respecting these rules and basic design principles as well as recognizing that both wind loads and climatic effects are leading impacts for capable dimensioning of glass thickness and secondary seal bite. Actually, climatic conditions, alternating temperatures and different elevations of production site and installation site create expansion or contraction of the enclosed gas space, an effect that is not specifically described in [4]. But assuming that [4] is defining the combination of permanent loads (named as dead load), variable loads (mainly wind load) and self-straining loads (put as system-implemented load, like climatic effects, only affecting the IG unit itself), we can split the climatic effect summarized in equation (3) into different components differentiated regarding load duration and combined action. While

effects caused by the difference of elevation  $\Delta H$  separately create a permanent impact, the combined action of  $\Delta H$ , temperature difference  $\Delta T$  and difference of atmospheric pressure  $\Delta p_{\text{atm}}$  is an effect alternating during the course of a day or the combination of climatic effect and wind is in total a short-term combination. Furthermore, [4], section 2.4.4 states that it's unlikely that the maximum effect of self-straining loads occurs simultaneously with the maximum effect of other variable loads. A combination with 0.75 of the maximum effects is recommended. Table 5 takes into account all summarized aspects for a proper combination of wind load and climatic effects in vertically installed IG units.

| LC | Combination  | Load Duration |
|----|--|---------------|
| 1  | 1.0 negative wind pressure +<br>1.0 effect of maximum difference of elevation between installation and production ( $\Delta H$ )   | 3 sec         |
| 2  | 1.0 negative wind pressure +<br>1.0 effect of minimum difference of elevation between installation and production ( $\Delta H$ )   | 3 sec         |
| 3  | 1.0 positive wind pressure +<br>1.0 effect of maximum difference of elevation between installation and production ( $\Delta H$ )   | 3 sec         |
| 4  | 1.0 positive wind pressure +<br>1.0 effect of minimum difference of elevation between installation and production ( $\Delta H$ )   | 3 sec         |
| 5  | 0.75 negative wind pressure +<br>0.75 climatic effects at "summer conditions" (difference of atmospheric pressure ( $\Delta p_{atm}$ ) and difference of gas space temperature between service and production ( $\Delta T$ )) +<br>1.0 effect of relevant difference of elevation between installation and production ( $\Delta H$ ) | 3 sec         |
| 6  | 0.75 negative wind pressure +<br>0.75 climatic effects at "winter conditions" (difference of atmospheric pressure ( $\Delta p_{atm}$ ) and difference of gas space temperature between service and production ( $\Delta T$ )) +<br>1.0 effect of relevant difference of elevation between installation and production ( $\Delta H$ ) | 3 sec         |
| 7  | 0.75 positive wind pressure +<br>0.75 climatic effects at "summer conditions" (difference of atmospheric pressure ( $\Delta p_{atm}$ ) and difference of gas space temperature between service and production ( $\Delta T$ )) +<br>1.0 effect of relevant difference of elevation between installation and production ( $\Delta H$ ) | 3 sec         |
| 8  | 0.75 positive wind pressure +<br>0.75 climatic effects at "winter conditions" (difference of atmospheric pressure ( $\Delta p_{atm}$ ) and difference of gas space temperature between service and production ( $\Delta T$ )) +<br>1.0 effect of relevant difference of elevation between installation and production ( $\Delta H$ ) | 3 sec         |
| 9  | 1.0 climatic effects at "summer conditions" (difference of atmospheric pressure ( $\Delta p_{atm}$ ) and difference of gas space temperature between service and production ( $\Delta T$ )) +<br>1.0 effect of relevant difference of elevation between installation and production ( $\Delta H$ )                                   | 12 hours      |
| 10 | 1.0 climatic effects at "winter conditions" (difference of atmospheric pressure ( $\Delta p_{atm}$ ) and difference of gas space temperature between service and production ( $\Delta T$ )) +<br>1.0 effect of relevant difference of elevation between installation and production ( $\Delta H$ )                                   | 12 hours      |
| 11 | 1.0 effect of maximum difference of elevation between installation and production ( $\Delta H$ )   | >> 1 year     |
| 12 | 1.0 effect of minimum difference of elevation between installation and production ( $\Delta H$ )   | >> 1 year     |

Table 5. Load combinations representative for proper design of vertical insulating glass units

## 6. Case study: 33 Tehama, San Francisco, CA, USA

The approach described above has been used for verification of glass design in several projects in the US. The following project helps to compare the normal procedure of ASTM E1300 [2] and an allowable stress design including combined action of wind load and climatic effects. Relevant for the glass design of the project was not just the estimation of wind loads expected for different zones of the building façade but also a comprehensive thermal analysis including thermal glass stress analysis, calculation of the maximum temperatures of glass components and primary seal as well as the minimum and maximum temperature of the enclosed gas space. These temperatures are basically needed for calculating expected climatic effects.

33 Tehama Tower in San Francisco is a 35-story apartment high-rise building under

construction. Its completion is expected in 2017. Due the thermal requirements, the spandrel units were identified as IG units with very high air space temperatures. As mentioned above, small and narrow units can create very high climatic effects. For typical spandrel units one has the accumulation of both extraordinary high temperature and inappropriate small glass dimensions. The units of GD-6, as a best practice example, were considered in a smaller dimension 100% utilized by climatic effects and in a maximum dimension showing 27% utilization due to the impact of negative wind pressure or even 42% utilization caused by positive wind pressure creating the maximum surface stress on the fitted (disruptively treated) surface of the inner lite. While bigger units are mainly restricted by limitation of deflection, the huge utilization of smaller units caused by climatic effects isn't recognized by the standard procedure of [2]. Boundary conditions taken into account for glass verification of the spandrel units GD-6:

- Production site (Lauenfoerde, Germany): 97 m [318 ft] a.s.l.
- Installation site (San Francisco, CA, US): 5 m [16 ft] a.s.l.
- Installation height: 123 m [420 ft]
  
- GD-6: Spandrel unit, insulating glass make-up
  - Outer lite: 6 mm [1/4 in.] Planibel Clearlite ipasol Neutral 48/27 # 2, fully tempered & heat soaked
  - Space: 20 mm [3/4 in.] air, aluminum spacer, black
  - Inner lite: 6 mm [1/4 in.] Planibel Clearlite, fritted, RAL 7035 # 4, fully tempered & heat soaked
  
- Dimensions (width x height)
  - Smaller span: 997 mm x 391 mm [39.3 in. x 15.4 in.]
  - Maximum span: 1505 mm x 3452 mm [59.3 in. x 135.9 in.]
  
- Wind load (3 sec): -2.155 kPa / +1.915 kPa [-45 psf / +40 psf]
- Continuously simply supported
  
- Internal shadow box make up
  - Internal backup: 63 mm [2 1/2 in.] distance, air, not ventilated
  - Insulation: 50 mm [2 in.], R = 1,43 m<sup>2</sup>K/W
  - Steel back pan: 1 mm [1/32 in.]
  - 200 mm [7 7/8 in.] air, not ventilated, R = 0.18 m<sup>2</sup>K/W acc. to ISO 6946
  - 20 mm [3/4 in.] sub ceiling or floor, R = 0.1 m<sup>2</sup>K/W
  
- Isochoric pressure
  - Climatic effects, summer ( $\Delta T_{\text{cavity}} \leq 80\text{K}$ ;  $\Delta p_{\text{atm}} \geq -2\text{kPa}$ ;  $\Delta H_{\text{altitude}} \leq 30\text{m}$ ): +29.6 kPa [+618 psf]
  - Climatic effects, winter ( $\Delta T_{\text{cavity}} \geq -24\text{K}$ ;  $\Delta p_{\text{atm}} \leq 4\text{kPa}$ ;  $\Delta H_{\text{altitude}} \geq 15\text{m}$ ): -12.0 kPa [-251 psf]

ASTM E1300 [2] is a simplified concept. Direct comparison of values determined according to [2] with values from a non-linear finite elements analysis is not reliable. Producing a direct comparison between failure prediction model FPM and allowable stress design ASD the type factors for insulating glass stated in [2], X2.2 were neglected. Furthermore, any disruptive effect of the ceramic frit was not taken into account, as Table 7 is a comparison of concepts but does not represent any verification. Wind pressure and climatic effects were evaluated separately. In step 1 maximum surface stress of the glass units was calculated on a single glass unit respecting the load sharing factors of [2]. In step 2 the more accurate load sharing concept of Table 2 was applied to the determination of load resistance LR according to [2]. Based on this modification a comparison with the simulation of a full IG model was more feasible. Additionally, only minimum glass thickness according to ASTM C1036 was used for comparing the results at similar conditions.

Table 7 shows a good approximation of utilization determined according to FPM and ASD. In general, a more accurate concept of load sharing factors, as given in Table 2 and shown in step 2, is advisable for smaller units. For bigger units a significant influence of surface area on the load resistance is considered in the FPM of [2] but neglected for the allowable surface stress values according to [2], X6.2. This could have an impact on design and resistance of larger annealed glass lites. For commercial façade units and SSG application it is common to use tempered or heat-strengthened glass so glass dimensions or accepted loads are mainly limited by allowable deflection and the utilization of allowable surface stress and usually far away from 100 %. In conclusion, allowable surface stress values defined in [8], X6.2 are conservative for smaller IG units and sufficient for larger ones. But a suitable are appropriate limitation of glass deflection is an important design condition, too.

| GD-06: Spandrel, Maximum Span  |                        |                        |                 |                 |                           |                                     |                        |                        |                 |                 |                           |                      |
|--|------------------------|------------------------|-----------------|-----------------|---------------------------|-------------------------------------|------------------------|------------------------|-----------------|-----------------|---------------------------|----------------------|
| Glass dimension: 1505mm x 3452mm; Glass make-up: 6mm FT & HST / 20mm Air / 6mm FT & HST, fritted on #4 |                        |                        |                 |                 |                           |                                     |                        |                        |                 |                 |                           |                      |
| Wind load (U.L.S, 3sec): -2.155 / +1.915 kPa   |                        |                        |                 |                 |                           | Climatic effects, summer: 29.6 kPa  |                        |                        |                 |                 |                           |                      |
|  |                        |                        |                 |                 |                           | Climatic effects, winter: -12.0 kPa |                        |                        |                 |                 |                           |                      |
| Load case  | Outer glass            |                        |                 |                 |                           |                                     | Inner glass            |                        |                 |                 |                           |                      |
|  | principle stress [MPa] | allowable stress [MPa] | utilization [%] | deflection [mm] | allowable deflection [mm] | limitation ratio [%]                | principle stress [MPa] | allowable stress [MPa] | utilization [%] | deflection [mm] | allowable deflection [mm] | limitation ratio [%] |
| LC1*   | 24.8                   | 93.20                  | 27              | -24.8           | 25.4                      | 98                                  | 25.2                   | 93.20                  | 27              | -25.1           | 25.4                      | 99                   |
| LC2*   | 24.7                   | 93.20                  | 27              | -24.7           | 25.4                      | 97                                  | 25.2                   | 93.20                  | 27              | -25.2           | 25.4                      | 99                   |
| LC3*   | 23.5                   | 93.20                  | 25              | 22.7            | 25.4                      | 89                                  | 23.5                   | 55.90                  | 42              | 22.7            | 25.4                      | 89                   |
| LC4*   | 23.5                   | 93.20                  | 25              | 22.8            | 25.4                      | 90                                  | 23.5                   | 55.90                  | 42              | 22.6            | 25.4                      | 89                   |
| LC5*   | 24.4                   | 93.20                  | 26              | -24.8           | 25.4                      | 98                                  | 17.8                   | 93.20                  | 19              | -16.1           | 25.4                      | 63                   |
| LC6*   | 19.8                   | 93.20                  | 21              | -18.8           | 25.4                      | 74                                  | 22.9                   | 93.20                  | 25              | -22.7           | 25.4                      | 89                   |
| LC7*   | 16.0                   | 93.20                  | 17              | 13.7            | 25.4                      | 54                                  | 23.3                   | 55.90                  | 42              | 22.8            | 25.4                      | 90                   |
| LC8*   | 21.4                   | 93.20                  | 23              | 20.5            | 25.4                      | 81                                  | 18.6                   | 55.90                  | 33              | 16.9            | 25.4                      | 67                   |
| LC9  | 6.3                    | 76.35                  | 8               | -6.6            | 25.4                      | 26                                  | 6.3                    | 45.81                  | 14              | 6.6             | 25.4                      | 26                   |
| LC10   | 2.6                    | 76.35                  | 3               | 2.7             | 25.4                      | 11                                  | 2.6                    | 76.35                  | 3               | -2.7            | 25.4                      | 11                   |
| LC11   | 0.1                    | 62.90                  | 0               | -0.1            | 25.4                      | 0                                   | 0.1                    | 37.74                  | 0               | 0.1             | 25.4                      | 0                    |
| LC12   | 0.0                    | 62.90                  | 0               | 0.0             | 25.4                      | 0                                   | 0.0                    | 37.74                  | 0               | 0.0             | 25.4                      | 0                    |

\* non-linear FE Analysis

| GD-06: Spandrel, Smaller Span  |                        |                        |                 |                 |                           |                                     |                        |                        |                 |                 |                           |                      |
|--|------------------------|------------------------|-----------------|-----------------|---------------------------|-------------------------------------|------------------------|------------------------|-----------------|-----------------|---------------------------|----------------------|
| Glass dimension: 997mm x 391mm; Glass make-up: 6mm FT & HST / 20mm Air / 6mm FT & HST, fritted on #4 |                        |                        |                 |                 |                           |                                     |                        |                        |                 |                 |                           |                      |
| Wind load (U.L.S, 3sec): -2.155 / +1.915 kPa   |                        |                        |                 |                 |                           | Climatic effects, summer: 29.6 kPa  |                        |                        |                 |                 |                           |                      |
|  |                        |                        |                 |                 |                           | Climatic effects, winter: -12.0 kPa |                        |                        |                 |                 |                           |                      |
| Load case  | Outer glass            |                        |                 |                 |                           |                                     | Inner glass            |                        |                 |                 |                           |                      |
|  | principle stress [MPa] | allowable stress [MPa] | utilization [%] | deflection [mm] | allowable deflection [mm] | limitation ratio [%]                | principle stress [MPa] | allowable stress [MPa] | utilization [%] | deflection [mm] | allowable deflection [mm] | limitation ratio [%] |
| LC1  | 2.2                    | 93.20                  | 2               | -0.2            | 7.8                       | 2                                   | 4.4                    | 93.20                  | 5               | -0.3            | 7.8                       | 4                    |
| LC2  | 1.6                    | 93.20                  | 2               | -0.1            | 7.8                       | 2                                   | 5.0                    | 93.20                  | 5               | -0.4            | 7.8                       | 5                    |
| LC3  | 3.9                    | 93.20                  | 4               | 0.3             | 7.8                       | 4                                   | 2.0                    | 55.90                  | 4               | 0.1             | 7.8                       | 2                    |
| LC4  | 4.4                    | 93.20                  | 5               | 0.3             | 7.8                       | 4                                   | 1.5                    | 55.90                  | 3               | 0.1             | 7.8                       | 1                    |
| LC5  | 35.7                   | 93.20                  | 38              | -2.5            | 7.8                       | 33                                  | 30.7                   | 55.90                  | 55              | 2.2             | 7.8                       | 28                   |
| LC6  | 12.6                   | 93.20                  | 14              | 0.9             | 7.8                       | 12                                  | 17.6                   | 93.20                  | 19              | -1.3            | 7.8                       | 16                   |
| LC7  | 31.1                   | 93.20                  | 33              | -2.2            | 7.8                       | 28                                  | 35.6                   | 55.90                  | 64              | 2.5             | 7.8                       | 32                   |
| LC8  | 17.2                   | 93.20                  | 18              | 1.2             | 7.8                       | 16                                  | 12.7                   | 93.20                  | 14              | -0.9            | 7.8                       | 12                   |
| LC9  | 45.8                   | 76.35                  | 60              | -3.3            | 7.8                       | 42                                  | 45.8                   | 45.81                  | 100             | 3.3             | 7.8                       | 42                   |
| LC10   | 18.5                   | 76.35                  | 24              | 1.3             | 7.8                       | 17                                  | 18.5                   | 76.35                  | 24              | -1.3            | 7.8                       | 17                   |
| LC11   | 0.6                    | 62.90                  | 1               | 0.0             | 7.8                       | 1                                   | 0.6                    | 37.74                  | 1               | 0.0             | 7.8                       | 1                    |
| LC12   | 0.0                    | 62.90                  | 0               | 0.0             | 7.8                       | 0                                   | 0.0                    | 37.74                  | 0               | 0.0             | 7.8                       | 0                    |

Table 6. Maximum surface stress and deflection for load cases of Table 5. The first table shows the results for a linear calculation and the second one for a non-linear calculation based on a Finite Element Analysis. Grey mark indicates the decisive load case.

| Glass Type  | Step of Comparison   | Failure Prediction Model FPM  | Allowable Stress Design ASD  |
|---|--|---|--|
| <b>Smaller Span</b><br>997 mm x 391 mm [39.3 in. x 15.4 in.]<br>6 mm [1/4 in.] FT & HST<br>20 mm [3/4 in.] air<br>6 mm [1/4 in.] FT & HST   | Step 1<br>Load sharing acc. to [2]<br>Negative wind load:<br>-2.155 kPa [-45 psf]          | LSF1 = LSF2 = 2.00<br>NFL = 11.1 kPa<br>GTF1 = GTF2 = 36<br>LR = 11.1 kPa x 3.6 x 2.00<br>LR = 79.92 kPa          | LSF1 = LSF2 = 2.00<br>$\sigma_{min} = 3.62 \text{ MPa}$<br>$\sigma_{max} = \sigma_{min} = 93.2 \text{ MPa}^*$<br>$\sigma_{max,1} = \sigma_{max,2} = 118.8 \text{ MPa}^{**}$                                  |
|   | Utilization step1  | 2.155 / 79.92 = 2.7 %   | 3.62 / 93.2 = 3.9 % *<br>3.62 / 118.8 = 3.1 % **   |
|   | Step 2<br>Load sharing acc. to Table 2<br>Negative wind load:<br>-2.155 kPa [-45 psf]      | LSF1 = 3.78<br>LSF2 = 1.36<br>NFL = 11.1 kPa<br>GTF1 = GTF2 = 3.6<br>LR = 11.1 kPa x 3.6 x 1.36<br>LR = 54.35 kPa | Full IG model<br>$\sigma_{min} = 1.96 \text{ MPa}$<br>$\sigma_{max} = 5.28 \text{ MPa}$<br>$\sigma_{min} = \sigma_{max} = 93.2 \text{ MPa}^*$<br>$\sigma_{max,1} = \sigma_{max,2} = 118.8 \text{ MPa}^{**}$  |
|   | Utilization step 2   | 2.155 / 54.35 = 4 %   | 5.28 / 93.2 = 5.7 % *  |
|   |  |   |  |
| <b>Bigger Span</b><br>1500 mm x 3450 mm [59.1 in. x 135.8 in.]<br>6 mm [1/4 in.] FT & HST<br>20 mm [3/4 in.] air<br>6 mm [1/4 in.] FT & HST | Step 1<br>Load sharing according to [2]<br>Negative wind load:<br>-2.155 kPa [-45 psf]     | LSF1 = LSF2 = 2.00<br>NFL = 0.89 kPa<br>GTF1 = GTF2 = 3.6<br>LR = 0.89 kPa x 3.6 x 2.00<br>LR = 6.41 kPa          | LSF1 = LSF2 = 2.00<br>$\sigma_{min} = 24.83 \text{ MPa}$<br>$\sigma_{max} = \sigma_{min} = 93.2 \text{ MPa}^*$<br>$\sigma_{max,1} = \sigma_{max,2} = 80.9 \text{ MPa}^{**}$                                  |
|   | Utilization step 1   | 2.155 / 6.41 = 33.62 %  | 24.83 / 93.2 = 26.7 % *<br>24.83 / 80.9 = 30.7 % **  |
|   | Step 2<br>Load sharing according to Table 2<br>Negative wind load:<br>-2.155 kPa [-45 psf] | LSF1 = 2.01<br>LSF2 = 1.99<br>NFL = 0.89 kPa<br>GTF1 = GTF2 = 3.6<br>LR = 0.89 kPa x 3.6 x 1.99<br>LR = 6.38 kPa  | Full IG model<br>$\sigma_{min} = 24.85 \text{ MPa}$<br>$\sigma_{max} = 25.13 \text{ MPa}$<br>$\sigma_{min} = \sigma_{max} = 93.2 \text{ MPa}^*$<br>$\sigma_{max,1} = \sigma_{max,2} = 80.9 \text{ MPa}^{**}$ |
|   | Utilization step 2   | 2.155 / 7.08 = 30.4 %   | 24.97 / 93.2 = 26.8 % *<br>24.97 / 80.9 = 30.9 % **  |
|   |  |   |  |

\* Conservative allowable surface stress values for a 3s duration load stated and probability of breakage  $\leq 0.008$  in [2], X6.2.

\*\* Specific allowable surface stress values acc. to [2], equation X6.1, additionally considering influences of glass dimension, glass thickness, aspect ratio and stress distribution on the probability of breakage.

Table 7. Comparison of FPM concept of ASTM E1300 [2] and ASD concept based on a non-linear finite elements analysis for wind load.



Figure 2: Project renderings (© Hines Constructions & Invesco)

## Conclusion

The above-discussed concept and the presented project example show that "Allowable Stress Design" is a useful and suitable practice for finding and verifying a capable glass design as well as including much more significant boundary conditions than provided by the standard procedure used in ASTM E1300 [2]. Important considerations for proper design are not just a suitable link between FPM and ASD, but also a reliable concept of combining different loads with different load durations. The draft given in Table 5 is specifically considering load effects on vertical IG units. Essential for proper and sustainable design of IG units is an appropriate concept for determining climatic effects caused by the interaction of the enclosed gas space and external environment as well as respecting effective load sharing between inner and outer lites of a double glazed unit. Here, ASTM E1300 [2] shows some inadequacy, especially regarding smaller and midsize glass dimensions, which can be heavily affected by climatic effects and which clearly show a load sharing behavior different from the simplified approach of [2]. For larger glass units, especially those composed of tempered and heat-strengthened glass, the verification based on ASD should be completed by evaluation and limitation of maximum glass deflection.

It should be mentioned that in the European design codes are based on the principle of partial safety specific combination factors. The limit state design approach requires taking into account safety and combination factors for the values of applied stress as well as for the resistance value of the glass product. Both safety factors for the stress and resistance

value are separated and represent the specific statistical deviation for loading and material.

Regardless from other international glass codes, this paper describes an approach keeping the systematic of the existing North American standards ASTM E1300 and ASCE 07. Thanks also to Permasteelisa North America regarding their expert support and their support regarding the case study, as they have done the curtain wall cladding.

## References

- [1] Glazing-Manual-50th-Anniversary-Edition, Glazing Association North America (GANA), 2009.
- [2] ASTM E1300 – 12a:1: Standard Practice for Determining Load Resistance of Glass in Buildings, 2012.
- [3] DIN 18008-2: Glass in Building – Design and Construction Rules, Part 2: Linearly Supported Glazings, 2010.
- [4] ASCE/SEI 7-10: Minimum Design Loads for Buildings and other Structures, American Society of Civil Engineers, Structural Engineering Institute, 2010.
- [5] Feldmeier, F.: Insulating Units Exposed to Wind and Weather – Load Sharing and Internal Loads, GPD Glass Processing Days, Tampere, pp. 633-636, 2003.
- [6] Morse, S. M.; ASCE; A. M.; Norville, H. S.: Relationship between Probability of Breakage to Maximum Principles Stress in Window Glass, Journal of Architectural Engineering© ASCE, March 2010.
- [7] Haldimann, M.; Luible, A.; Overend, M.: Structural Engineering Documents 10, Structural Use of Glass, International Association for Bridge and Structural Engineering, 2008.
- [8] ASTM E2751/E2751M – 13: Standard Practice for Design and Performance of Supported Laminated Glass Walkways, 2013.
- [9] Maniatis, I.; Elstner, M.: Investigations on mechanical strength of enameled glass, Challenging Glass Conference 5, International Conference on the Architectural and Structural Application of Glass, Delft, 2016.

- [10] Doebbel, F.; Elstner, M.; Patterson, M.; Davis, W.: Optimized Secondary Seal of Insulating Glass Units for Structural Sealant Glazing Application, GlassCon Global Conference Proceedings 2014, Philadelphia 2014.

# Next Generation Calculation Method for Structural Silicone Joint Dimensioning

Pierre Descamps, Valerie Hayez\*, Mahmoud Chabih

\*valerie.hayez@dowcorning.com. Dow Corning Europe SA, Parc Industriel Zone C, rue Jules Bordet, B-7180 Seneffe, BELGIUM

**Extended Abstract** (The complete contribution will be published in the Glass Structures and Engineering journal)

Bonding of glass onto aluminum frames, known as Structural Silicone Glazing (SSG), has been applied for more than 40 years on facades with various improvements of the technology being made over time. Silicone sealants are used in this application because of their unique resistance to weathering (UV, temperature, moisture, ozone). They also provide resistance to water ingress and thermal insulation. Their structural role is to sustain wind loads and to accommodate for differential thermal expansion of different bounded substrates.

Historically, silicone joint dimensioning is calculated with a simplified equation implemented in various standards for structural glazing. This equation assumes homogeneous stress distribution along the sealant bite whilst high local stress peaks, structure deformation or material ageing are included in a global safety factor. New trends in commercial buildings include the use of large dimensions glass panes, higher complexity of façade designs and stronger engineering performance requirements such as high windloads above 5000Pa. These trends have recently challenged the conventional methods of joint dimensioning, since using the simplified equation for these projects results in economically unacceptable large bite sizes. Furthermore, increasing joint bite will not necessarily increase the safety factor as the simplified relationship neglects important factors such as the joint rotation due to glass pane bending. Increasing the sealant design stress is an option to decrease the bite but this solution is limited and also requires a better understanding of stress distribution as well as joint failure mechanisms).

This explains the recent increased interest to use Finite Element Analysis (FEA) to help designing SSG and joint dimensions. In FEA, the geometry is divided in small volume elements interconnected by points call

nodes. Applying energy conservation to the whole system, via strain energy calculation at small element level, local stress and/or local deformation can be predicted.

However, there is no technical guideline or standardized method explaining how to use FEA in structural joint dimensioning. Without such guidance, calculations carried-out by different engineering offices may lead to different absolute values of the maximum local stress. The outcome of FEA model is highly sensitive to the accuracy of input data such as the parameters of the hyperelastic model selected for the sealant. The stress volume distribution is also highly mesh dependent, especially close to the interfacial region between the sealant and the substrate. This is more particularly true because even being easily deformable, silicone sealant is a nearly incompressible material.

Finally, even if the maximum local stress or strain in joint volumes are calculated in an accurate way, we do not know the acceptable value a joint can sustain while ensuring long term durability of façade systems. In fact, there is no unanimous approach on how to define a "rupture" criteria from local stress and to determine what the best model to predict material failure is. Several criteria like principal stress, Von Mises stress or maximum deformation energy are possible. Hence it is difficult to use a local stress distribution for predicting failure in a macroscopic joint and consequently use this information for joint dimensioning.

An alternative approach is to use FEA results to simulate observable (or engineering) joint deformation because this variable has a lower sensitivity to mesh configuration. Indeed, observable deformation results from the integral of the strain energy over the whole joint volume hence local high stress values which are highly mesh sensitive are averaged. Joint deformation calculated using FEA for one particular façade can be compared to H-bar testing results for test pieces having the same geometry and more particularly similar joint aspect ratio  $R$  (defined as the ratio between joint bite  $W$  and joint thickness  $e$ ).

While calculating engineering joint deformation with FEA creates a more direct link with sealant performances measured on test pieces, carrying out a FEA model remains an expensive procedure, requiring investment in FEA software acquisition and engineering

resources to run simulations. Hence this methodology is difficult to extend to small/medium size façade makers who would prefer using a simple "manual" calculation method. The goal of this paper is not to provide a direct contribution to the effort of joint behavior understanding, but to propose an improved mathematical relationship making a direct correspondence between a joint included in a façade system and the behavior of a test piece. A history of the mathematical relations of joint dimensioning is presented, explaining their limit of validity and why it is important to move to a new relationship including additional physics effects like joint rotation which were neglected previously and which represent more accurately the joint behavior. Very rough assumptions have been made for its derivation to keep it simple. Validation of the proposed relationship for large windload is carried out by confronting predictions with physical measurements and the results from FEA modeling. The improved relationship was deduced assuming first a linear material. To optimize the correlation between FEA and the equation for larger elongations, an extension of the improved linear model to accommodate non-linear behavior is proposed, assuming a Neo-Hookean model. All the studies described in this paper were carried out using properties and experimental characterization of Dow Corning® 993 Structural Glazing Sealant, which is a two-component neutral alkoxy curing silicone formulation specifically developed for the structural bonding of glass, metal and other building components.

# Double-Skin Facades: Characteristics and Challenges for an Advanced Building Skin

Dr.-Ing. Fabian C. Schmid\*, Dipl.-Ing. Dr. techn. Stefan Marinitsch\*, Dr.-Ing. Martien Teich\*

\*seele GmbH, Gutenbergstraße 19, 86368 Gersthofen, Germany

## Keywords

1=façade 2=double skin 3=self-conditioning  
4=closed cavity 5=lightweight structures  
6=glazing

## 1 Relevance of double skin facades in today's industry

The construction typology of the curtain wall arose with Joseph Paxton's Crystal Palace and accelerated in the 20th century. Separating a building's enclosing wall from its structure enabled an independent development of façade and structure, greater flexibility in design and incredible lightness of buildings. [1-3] Initially, growing demands on user comfort, energy efficiency and maintenance were managed by technical advances in the performance of glazings, materials, jointing elements, and air conditioning. Advances in precision manufacture allowed the development of unitised systems, realizing cost and programme benefits through prefabrication and preassembly. These developments influenced the classical massive wall constructions. Multi-layer or cavity walls were adapted to increase flexibility by separating cladding and structure, gaining advantages through pre-assembled panels. [1-3] Figure 1 shows the mentioned construction typologies in principal.

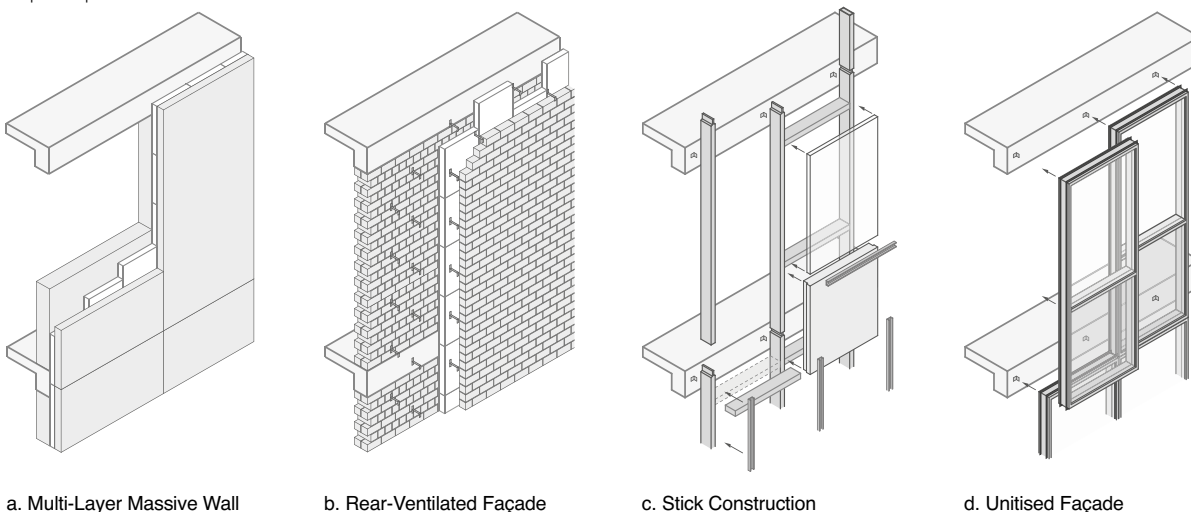
Triggered by the energy crisis in the 1970's, it was tried to increase user comfort in high-rise buildings through natural ventilation. Rising demands for noise protection made double skin facades popular. This typology however was developed in the early days of the 20th century with the production hall of Steiff in Giengen on the Brenz, Germany and the Hallidie Building in San Francisco. [5] Double skin facades usually use two layers of glass that air can flow in the intermediate cavity. Natural ventilation of the cavity, a fan supporting air circulation, or mechanical driven ventilation flaps are necessary to exclude overheating and condensation. The different and manifold parts make stick, double skin and unitised systems one of the more costly elements of a building. [3] Unitised facades dominate the curtain wall market especially for high-rise buildings because of the time saving on site, advantages for installation access, cost-savings by a semi-automated production for many equal units, and the quality improvements through pre-assembled products in a factory. Stick systems are typically used for low-rise buildings, entrance areas, or smaller developments. [1-3] The improvement of curtain wall systems is related to the advancements made on frames, fillings, and sealants. Dimensions, durability, and anchoring techniques are improved to realise lighter constructions, allowing increased element sizes up to 3.2 x 15 m. Fabrication technology allows the production of bigger pane sizes, client-specific geometries, combinations of multilayer laminated safety

glass or insulation glass and glass setups with different functional coatings. [1,6] Desktop studies and calculations allow the assessment of the structural and physical performance during design.

As outlined before, a main driver for the ongoing development was an increasing awareness for energy saving. Improvements in coatings and double and triple layer insulation glass reduced the thermal losses through the transparent areas of a building. This impacts as side-effect the visual quality of glazed facades. The cavity of double skin systems operates as thermal buffer and reduces the need for eye-catching coatings. Double skin facades using natural ventilation for high-rise buildings had advantages in user comfort and a greater transparency.

On contrary, double skin facades are faced with higher maintenance and cleaning cost. In design, increased wall zoning requirements lead to a reduced floor area available for usage and rent. [5] Ongoing challenges are energy performance, the upcoming need to reduce the resource consumption, and to balance economical and user comfort demands in the most beneficial way. Different site conditions and holistic evaluation of economical, ecological and social aspects leads to a very multidimensional design task choosing the most reasonable solution.

The integration of the double skin concept within a unitised system is one of the latest developments. They are closely related to room-high box-type windows and exclude some major disadvantages of classical double



a. Multi-Layer Massive Wall

b. Rear-Ventilated Façade

c. Stick Construction

d. Unitised Façade

Figure 1: Multilayer, rear-ventilated, stick and unitised construction alternatives [4]

skin concepts. An individual exchange of units is possible as well as reduced cleaning efforts to gain comparable maintenance cost to classical curtain wall systems. The minimized width of the construction increases lettable floor space. Modern unitised double skin facades combine opaque and glazed multilayer constructions.

## 2 Concepts of double skin facades

Double Skin Façade is a generic term for transparent, translucent or opaque constructions, which typically use decoupled layers of construction elements or material. Two main constructive principals of curtain walls are used for double skin façades. Stick systems are dominated typically by natural ventilated concepts. Unitised systems are dominated by box type windows, which have the possibility to clean the interior panes, or by closed-cavity and self-conditioning facades, which reduce the cleaning effort for the interior panes.

Concepts integrate heating, ventilation, air conditioning, shading, and sound insulation, reducing energy consumption and increasing user comfort. Functions, typically realised with energy consuming indoor installations, are moved into the façade to gain benefits of natural heat buffering and ventilation. Double skin facades serve various façade orientations, different climatic conditions and site-specific requirements.

Beside the constructive principals, three separation concepts between cavity and interior space can be described. Buffer systems [Figure 2a] establish a conditioned air system without an interaction. The air conditioning is realised by natural or mechanical ventilation. Extract-Air-Systems [Figure 2b] use the warm exhaust air of the interior space to increase constantly the temperature of the cavity. A mechanical

ventilation system is used for the rooms. Exchange-Air-Systems [Figure 2c] use natural ventilation within the cavity to guide tempered air into the rooms and extract the used air for a constant exchange process. Figure 2 shows the different separation concepts in principal. The air streams within the different separation concepts are driven either mechanically or naturally. Natural ventilated systems need careful design considering changing climatic conditions. Mechanically driven solutions are more robust in this regard, but need controlling and installation. Temperature and humidity conditions can be managed by mechanical driven openings, by fans, or air conditioning units.

The ventilation solutions vary in accordance to their assigned function. First, a second glass layer in front of the exterior cladding of a building [Figure 3a] is discussed. Ventilation openings are required at the bottom and the top of the outer pane to exclude an overheated construction. This typology utilizes multiple ventilation options. A corridor façade uses vertical or horizontal separations between the cladding sectors. Ventilation openings are spaced evenly to ensure used and heated air is mixed before re-entry in the cavity. The naturally driven shaft box façade guides the warm air into a combined shaft, possessing better thermodynamic properties with no negative influences through an exchange with used air. Mechanical driven systems [Figure 3d] may use a centralized vent for the whole façade or share the installation with the conventional air conditioning system. Box window facades [Figure 3b] combine several advantages of windows. Story-high window elements are used as units. Each unit is accessible using typically an interior opening element and an external glass panel. Ventilation openings are installed at the bottom

and top of each window for naturally ventilated alternatives. Mechanically driven systems [Figure 3e] use decentralized air conditioning units integrating the room's heating and cooling system in the façade. Box window facades enable the most individual adaptation of climatic and air conditioning characteristics for each window element. In addition, flexibility is gained on each floor and new room configurations can be established easier. The disadvantages are cleaning effort and cost. Integrating functions like air conditioning, natural lighting or light control into the façade increase the complexity and increase the design effort. [8]

Self-Conditioning Facades [Figure 3c] and Closed Cavity Façades [Figure 3f] reduce the constructive width compared to other unitised double skin systems. Constant filtration and sealed cavities makes cleaning of the interior panes obsolete. The gained floor space, reduced maintenance and integrated shading devices provide a competitive setting in comparison to triple glazed units with interior or exterior shading devices. Closed Cavity Systems can manage climatic conditions with the need of pipework and a mechanical ventilation system. Self-Conditioning Facades need a detailed assessment for every project to ensure performance over time.

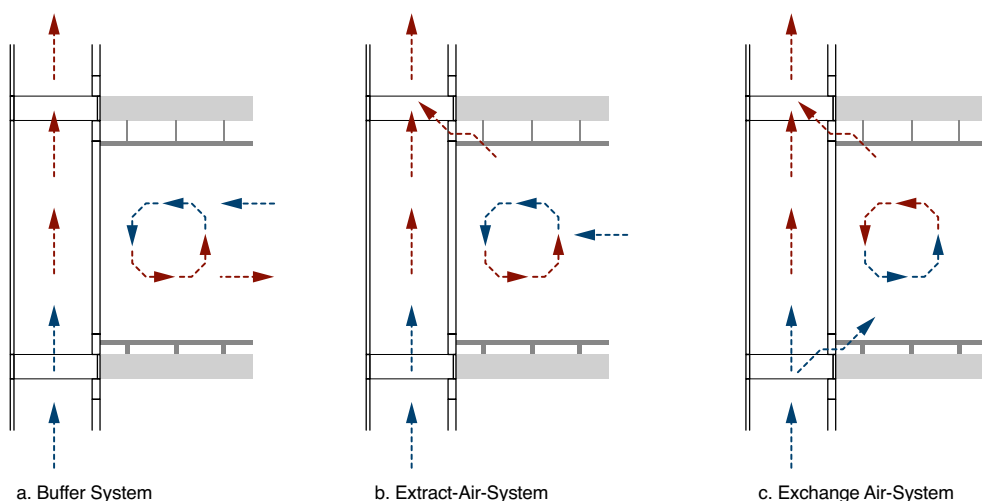


Figure 2: Double skin façades with different separation concepts between cavity and interior [7]

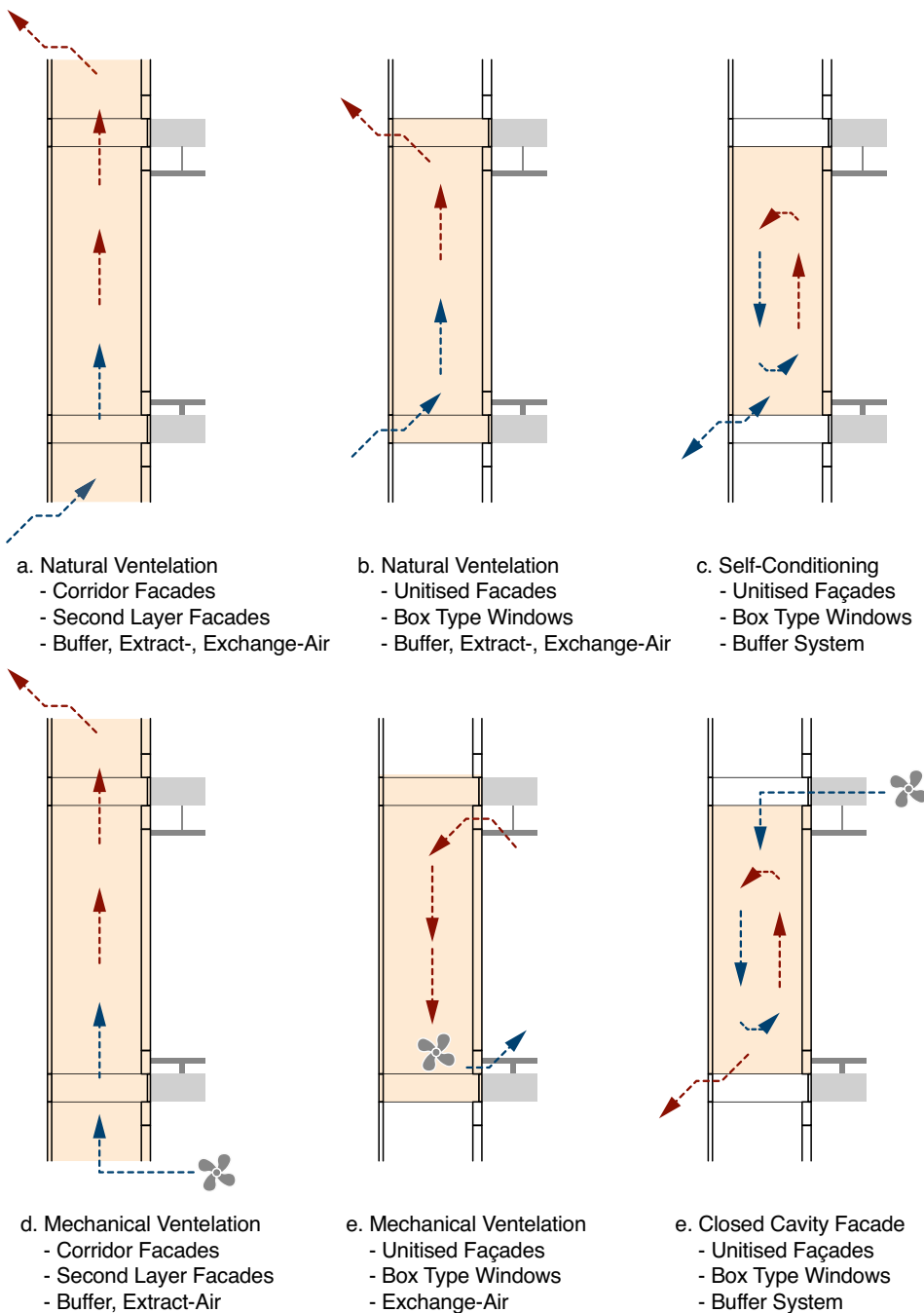


Figure 3a: Double skin façades with different ventilation concepts (part 1)  
 Figure 3b: Double skin façades with different ventilation concepts (part 2)

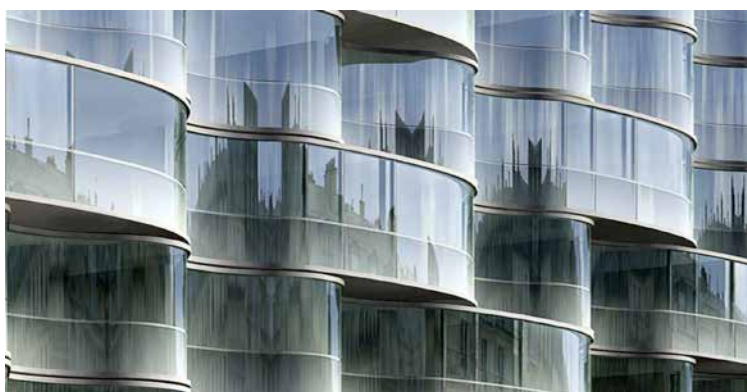


Figure 4: Curved and Self-Conditioned Glazing for the Wagram Hotel, Paris [9]

### 3 limiting cases and challenges for unitised systems

For both constructions, the geometries are limited to sizes and shapes of huge glass structures. Glass tubes, flat and curved panes can be used with pane sizes up to 3,2 x 15 m and curvatures typical for hot bended panes. (Figure 4).

For closed cavity facades pressurised air supply or a ventilation system is used adopting the concept of pressurized multilayer ETFE-foil cushion constructions. Dried, filtered and sometimes tempered air is used for the cushion constructions in order to manage condensation. Mechanically driven vents or compressors, stainless steel pipework and valves are used as air supply system. Filtration and exclusion of any contaminations of the supply air is essential in order to ensure a performing cavity condition. The system performance can be adjusted to a more tolerant or a more effective configuration for the glazed façade variante. Tightness of the elements and the pipework, an adjusted flow rate between 3 and 40 l/h·m<sup>3</sup> can fulfil the project specific demands in different climate zones.

Self-conditioning facades adopt the concept of pressure equalized insulated glass, using natural ventilation without mechanical aid. Pressure compensation and air exchange is achieved by coupling the cavity to the exterior. The air exchange is necessary to balance the vapour conditions and control condensation. The conditioning of the cavity is self-regulating during its entire service life. It is balanced by the coordinated interaction between the thermal properties of the façade and fluid-mechanical effects in the cavity and outside. The conditioning takes place with a minimal exchange of air not affecting the thermal performance significantly. The design of a passive façade requires a precise understanding of the prevailing conditions regarding climate, micro-climate and site conditions. Relevant parameters are interior, exterior and cavity air temperatures as well as surface temperatures including their dew point temperatures. The exterior and cavity humidity are relevant for the hydrothermal conditions, the resulting dew point and the surface temperatures. The factors are shown in a schematic section in Figure 5. [5,10,11]

Designing for these parameters lead to a reliable and autonomous system. Critical situations for these systems are cooling phases during clear summer nights. High temperatures and high levels of humidity over the course of the day and a steep temperature drop over night due to clear sky radiation

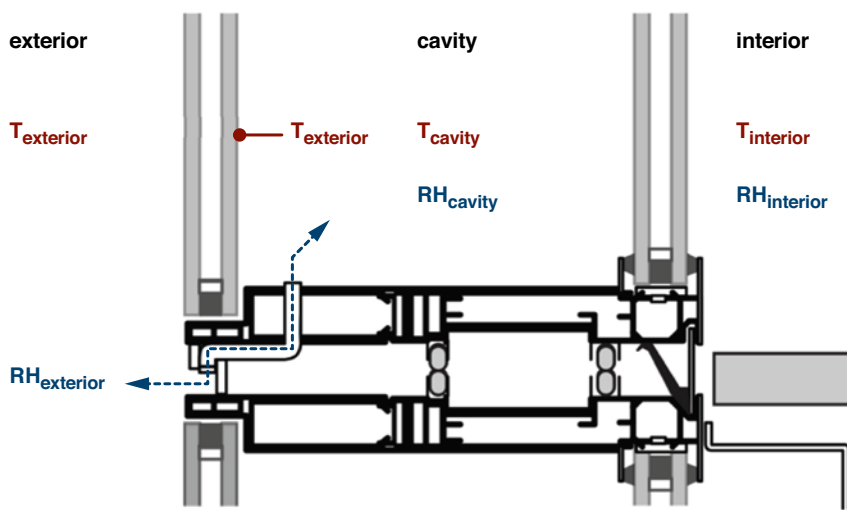


Figure 5: Schematic Drawing with Relevant Physical Factors [10,11]

define the most relevant threshold. Tests showed that the effect of the temperature drops can be influenced through system design. A continuous offset between surface temperature of the inner glass panes and the dew point is necessary. [5,10,11] Closed Cavity Systems realize this offset between surface temperature and dew point through a flow rate with dried air.

A general issue for unitised buffer systems is its material usage especially when designing for integrated sunscreens. [12] The influence of elevated temperatures on used components and the compatibility of materials especially the used plastics needs to be considered during design.

The disadvantages of both systems require an continuous development with additional marketable technological solutions. The concept of closed cavity systems would be strenghtend greatly by avoiding mechanical ventilation and pipework. The required design of self-conditioning facades on the other hand is costly and complex. Buffer technologies using drying agents for humidity and phase change materials for temperature management are investigated in order to establish a natural ventilated but robust alternative.

Focus on environmental, architectural and social quality is needed in addition to the insulation properties of an assembly. A major issue of the future is resource consumption. A typical self conditioning façade emits two times and a closed cavity façade three times more greenhouse gas equivalent than a spandrel and double-glazing curtain wall reference over its lifetime. [14] Thus, energy and material flow analysis will gain importance. The design should inform the decision-making processes of the future in order to detect critical production steps or material choices early. [15]

## 6 Conclusion

An increasingly systematised approach within the planning process is required. Advanced double-skin façades like the self-conditioned or closed cavity system challenge the traditional glazed façade structures. The self-conditioning concept demonstrates, that passive systems require a sound understanding of the system parameters and physical relations to operate the façade safely, saving energy whilst reducing maintenance effort. Closed cavity systems are a typical active concept, which can serve different requirements through an easily adaptable mechanical solution. Both systems need to integrate shading solutions, lighter concepts and alternative insulation glass façades. [8] Advanced façades need to be improved constantly and need to be assessed regarding their suitability for various climate change scenarios as well. Extreme weather conditions might occur earlier as predicted. These increased demands regarding the planned and built environment must be balanced with additionally resources and energy. [8]

## References

- [1] Herzog, T.; Krippner, R.; Lang, W. (2004): façade manual, Birkhäuser.
- [2] Knaack, U.; Klein, T.; Bilow, M. et al. (2014): Façades: Construction Principals, Birkhäuser.
- [3] Crosbie, M. (2005): Curtain Walls: Recent Developments by Cesar Pelli, Birkhäuser.
- [4] Schmid, Fabian C. (2015): Methodological and Systematic Design of Future Façade Solutions, Springer.
- [5] Khoraskani, R. A. (2015): Advanced Connection Systems for Architectural Glazing, Springer International Publishing AG.
- [6] Schittich, C, Staib, G., Balkow, D. et al. (2006): Glass Manual, Birkhäuser.
- [7] Boake, T., Harrison K., Collins, D. et al. (2003): Understanding the General Principles of the Double Skin Façade System, University of Waterloo.
- [8] Schmid, F.; Marinitsch, S. (2016): Methods and

Technologies for Advanced Building Skin Design; Advanced Building Skins 2016 Bern.

[9] Seele GmbH

[10] Cseh, X. (2013): Numerical Modelling of Unpressurized Double-Skin Façades, Bauhaus-Universität Weimar.

[11] Fraunhofer Institut für Bauphysik (2014): Research Report.

[12] Rehner, C. (2014): Bauphysikalische Betrachtung von textilen Sonnenschutzelementen in einem geschlossenen, druckentspannten Fassadensystem, Augsburg: Hochschule Augsburg.

[14] Souviron, J. (2016): Producing Transparency: An Energy and Material Flows Analysis of Glazing and Membrane Façades and their Potential of Hybridisation, Ecole Nationale des Ponts et Chaussées Paris.

[15] Sobek, W.; Schäfer, S. (1996): On the Seam: Joining Components made of Different Materials, in: Deutsche Bauzeitung 130/1996.1, S. 106–114.

# Structural Glass Connections

Carles Teixidor, Jordi Torres, Francesc Arbós Bellapart s.a.u.

## Keywords

1=Structural glass 2=Embedded laminated connection 3=Metal insert 4=lonomer

## Abstract

In the last decade there has been a trend in Architecture to design façades in which all structural elements are made of glass. This trend has also extended to other parts of the building such as rooflights, staircases, etc. However, popularity should not hide the fact that this type of construction is delicate due to the intrinsic fragile nature of glass combined with the stress concentrations that appear in connections. Careful design and construction are required in order to deliver a safe and durable product to the client.

Recently, the authors have been involved in a number of such structural glass projects. The aim of this paper is to show some of the connections that were employed in these projects and to discuss the techniques used for their structural analysis, design and construction.

## Introduction

In the last decade there has been a growing trend in Architecture to incorporate into buildings some iconic all-glass elements, such as entrance façades, rooflights, staircases, etc. These are aimed at reaching the highest level of transparency, thus the use of any structural material other than glass is to be minimised. Despite the existence of some remarkable pioneering works in the 1990's, such as the glass bridge in Rotterdam by Dirk Jan Postel, it was not until 2006 that this type of construction became increasingly popular thanks to the opening of the Apple store in the 5<sup>th</sup> avenue of New York with its well-known glass cube and staircase.

However, popularity should not hide the fact that this type of construction is delicate due to the stress concentrations that appear in connections that glass, being a perfectly elastic and fragile material, is unable to redistribute. These stress concentrations may be caused by either the existence of holes or notches on glass, the bonding of metal parts that create sudden stiffness changes on the panel surface,

or simply by the application of a significant force on a small glass area. This results in connections most often governing the design of structural glass components.

Recently, the authors have been involved in a number of such structural glass projects, from a government building in London, to an educational building in Montpellier, an office building in Madrid and a number of retail shops around the globe. A discussion on some of the connection details and design methods employed in these projects follows.

## The importance of global modelling

The previous section has emphasized the importance of connections in the design of structural glass components. But the first step in a proper design of a connection is to know with certitude the forces being applied to it. Therefore, the design of a structural glass façade should always start with the definition of a structural scheme with clear load paths that remove any ambiguity in the determination of the loads applied to each connection. However, the complexity of modern projects often require to complement these structural schemes with sufficiently accurate numerical models with the aim of capturing any second order effects that may have skipped the initial manual calculations or to take into account the load transfer between adjacent glass panels through structural silicone joints, etc.

As a simple example of the latter, fig.1 shows the use of structural silicone joints to reduce the wind deflection of the central two-side supported flat glass panels (measuring 2.5 x 8.0 m approx.) by transferring part of the wind load to the side panels which have a significantly higher bending stiffness due to their curvature. In this case, the flat glass panels were able to resist the factored wind load alone, but the deflection requirements in service could only be met by considering the façade to behave (partially) as a single panel.

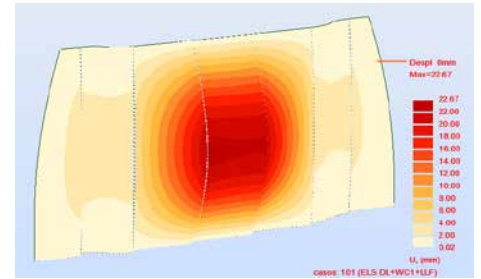


Figure 1 Out-of-plane displacement of a simple façade with structural silicone joints under wind suction.

## Structural silicone modelling and design

The projects that led to the publication of this paper made extensive use of structural silicone bonds for three different functions:

- To make compatible the out-of-plane deflection of adjacent glass panels under wind load, as shown in fig.1.
- To provide cross-bracing in the plane of the façade, specially in glass pavillions where two glass façades are connected at an angle, or where the façade is subject to in-plane seismic loads.
- To avoid the distortion of the façade under small relative displacements of the supporting structure.

In order to properly capture the stresses and strains in each structural silicone joint of a façade, these are included in the global structural model by means of a series of beam elements connecting the glass panels together at constant distances in the range of 100-200 mm (fig.2).

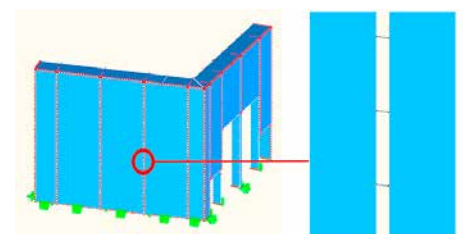


Figure 2 Modelling of the structural silicone joints.

The stiffness of each silicone joint is to be studied by means of finite element models that take into account the actual geometry of the bond and the nonlinear behaviour of the specific silicone product for the range of strains under consideration.

The reader is warned against using certain silicone stiffnesses published by silicone manufacturers which may correspond to tensile tests on dumbbell specimens or to joints with aspect ratios of about 1:2, typically found in curtain walling applications. Deeper joints may show significantly higher stiffnesses, specially in tension and compression, and possibly higher stresses than those expected if the above values were used.

In the projects mentioned above, two-dimensional plane strain finite element analyses were performed for each joint geometry considering the hyperelastic material model of the sealant, which was supplied by the silicone manufacturer. Tension, compression and out-of-plane shear were analysed at different levels of stress within the acceptable range. The stiffness of the joint under in-plane shear was assumed to be similar to that of out-of-plane shear. Figure 3 shows the results of such analysis for a 50x30mm joint subject to out-of-plane shear. Note that the response in the considered range of forces/displacements is almost perfectly linear, thus a single value of effective shear modulus could be found. Linearity was slightly worse in tension and compression.

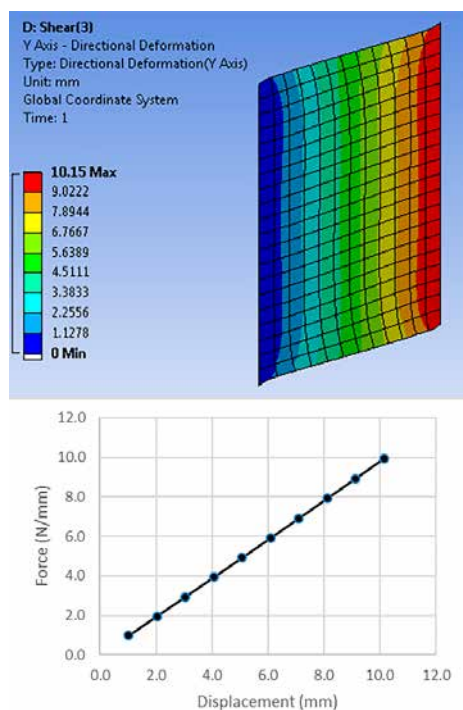


Figure 3 Stiffness of a 50x30mm silicone butt joint in shear.

The design strength of a structural silicone bond may be obtained from the European Technical Assessment (ETA) of the product. However, the values shown in the ETA are normally affected by a safety coefficient of 6 that is intended to be used in combination with the simplified methods of analysis shown in ETAG 002 [1]. For more accurate analysis

methods such as the one discussed in this paper, the use of lower safety coefficients is possible. Dow Corning recommends a safety coefficient of 4 in this situation [2]. Finally, it is necessary to take into account the interaction of axial and shear stresses in order to obtain a design method that can be applied in practice. Back in 1989 Sandberg and Ahlborn [3] suggested an elliptical interaction for silicone joints under short-term loads. Currently, silicone manufacturers can provide slightly modified expressions that improve the accuracy of the former and take into account the concurrent application of short- and long-term loads.

### Stiffness of the supporting structure

Sometimes the deformation expected in the building structure to which a façade is connected may not be compatible with the façade design, creating excessive stresses in glass joints or even collisions between panels. This was the case of an entrance hall to an office building in Madrid, in which two structural glass façades made up of laminated glass panels with a typical size of 3.0 x 10.0 m (b x h) were to be installed on a hybrid steel and concrete slab built in the 1980's. Obviously, the supporting slab had to be reinforced to meet the new loading conditions and to provide a sufficiently stiff base for the new glass façade. In spite of the reinforcement, the façade showed to be highly sensitive to deformations at the base, which created excessive stresses in the vertical structural silicone joints and detachment of some glass panels from one of their support pads in some circumstances. In this case, the use of elastic supports along the bottom edge of the panels (fig.4) permitted to accommodate the slab deflections making them compatible with the structural silicone bonds and avoiding detachment of glass from its support pads for all considered load combinations. Most often, Belleville springs are adequate for the construction of such elastic supports in which relatively high forces and small displacements need to be accommodated. They provide a relatively linear response along their full working length.

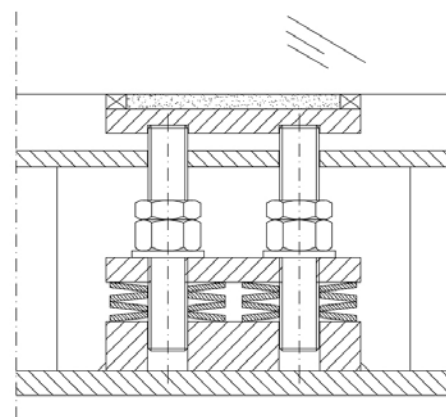


Figure 4 Elastic supports on the bottom edge of the façade panels.

A different approach was used in a retail shop in the Middle East in which a 12m tall façade on a concrete slab was made relatively insensitive to the slab displacements by supporting the weight of the cladding panels with a single resin pad located at the centre of their bottom edge. The in-plane rotation of the panel was impeded only by the structural silicone joints along the vertical edges of the panel whereas out-of-plane displacements were blocked mechanically. The differential vertical displacement between adjacent panels produced a shear displacement at vertical joints that had to be accommodated by the structural silicone.

### Embedded metal inserts

Another common characteristic of the projects discussed in this paper is the use of adhesive connections in which a metal part is embedded in a glass laminate. In this case, a laminate with a minimum of three glass plies is necessary, with the central ply having a notch that accommodates the metal insert. The bond is provided by the interlayer adhering to both glass and metal during the lamination process. Therefore, the interlayer must have sufficient strength and good affinity with metals, which makes it a perfect application for a ionomer interlayer like SentryGlas. Besides the obvious visual advantages of these connections, arising from the transparency of the adhesive and unobtrusiveness of the metal parts, their mechanical behaviour is quite complex even under the simplest loading conditions such as a pull-out force. As discussed in [4], a pull-out force on the metal insert is transferred to glass by shear on the lateral surfaces, shear on the top and bottom surfaces and tension on the frontal surface (fig.5). The distribution of the force between these mechanisms depends on their relative stiffnesses. At room temperature and under short term loads, the displacement of the interlayer on the front surface in a direction perpendicular to the force is significantly

restrained by the adjacent interlayers and glass panels. This fact, combined with a relatively high Poisson ratio, leads to the force being mainly transmitted by the front surface to the inner glass ply. This mechanism also exists at higher temperatures and for longer load durations, but it is less significant due to the lower lateral constraint provided by a softer interlayer.

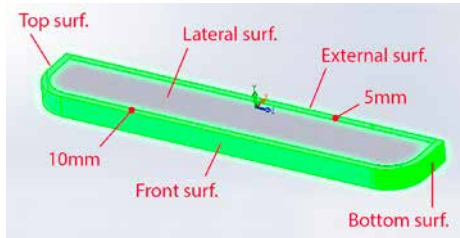


Figure 5 Typical metal insert. Nomenclature and delaminated surfaces considered in ULS (in green)

In addition to the stresses produced by the applied forces, there may be some residual stresses as a result of the lamination process. The difference in the thermal expansion coefficient and the specific heat between glass and metal produces some differential displacements during the cooling phase of the autoclave cycle. To the authors' knowledge, a quantification of this effect is not yet available in the literature. However, it is well known that metals with physical properties quite similar to glass (titanium alloys) are easier to laminate than, for instance, typical stainless steel grades.

The combination of relatively high stresses in the frontal bond resulting from external forces and some unknown residual stresses may produce delamination in this area. In fact, the region more prone to delaminate is the curved transition between the frontal and the top/bottom surfaces, which is subject to a combination of tensile and shear forces. Delaminations in these areas appearing spontaneously during the first week after lamination have been observed occasionally. The numerical prediction of the strength of embedded laminated connections is an active field of research. The recent publication of the excellent PhD thesis of M. Santarsiero [6] and some related scientific publications [4-9] has shed some light on this issue. However, the results shown in these publications cannot be directly used for design for the following reasons:

- a) All results are based on average values obtained from testing. Average strengths are totally correct in a scientific work but cannot be used for design.
- b) All tests are performed on glass-to-stainless steel connections. Thus, lab test results in these publications need to be cross

checked if other metals (e.g. titanium alloys) are used, although important differences in bond strength are not expected.

c) A method to account for the simultaneous application of tensile and shear stresses, together with the existence of both deviatoric and volumetric stresses is proposed in the thesis. This method needs to be further verified with physical tests before being applied for design.

d) A quantification of the residual stresses resulting from the lamination process and their relaxation with time and temperature is still an open field for research.

Until further information on this subject is available, the following design approach for the adhesive bond is suggested:

- a) Use the embedded adhesive connections to transfer short term loads exclusively.
- b) Determine the design strength of the bond in pure tension and pure shear by testing, for the intended temperatures and load durations. The design strength is the characteristic strength as per Eurocode 0 (5%-percentile of the distribution of strengths with 75% confidence) divided by a material factor obtained from [10]. The following interaction expression was obtained from Peters [11] and adapted to this application. Note that it ignores the existence of hydrostatic stresses.

$$U = \left[ \left( \frac{\sigma_{t,Ed}}{\sigma_{t,Rd}} \right)^2 + \left( \frac{\tau_{Ed}}{\tau_{Rd}} \right)^2 \right]^{1/2} \leq 1$$

The Generalized Triaxial Model (GTM) proposed by Santarsiero and Louter [6, 7] may be a more adequate approach.

c) Analyse the embedded connection in Ultimate Limit State (ULS) with sufficiently accurate finite element models considering the frontal, top and bottom surfaces, together with a 10mm strip on the lateral surfaces, to be completely delaminated (fig 5). In addition, a 5mm strip on the lateral surface adjacent to the outer edge is not considered to participate in the force transfer as adhesion may be affected by environmental influences, as shown in [12]

Therefore, only the central part of the lateral surfaces participate in the force transfer in ULS. This area is mainly subject to shear stresses, although some tensile stresses may also be present due to the deformation of the outer glass plies.

- d) Cross check numerical results with some physical tests of the final connections. With regard to the design of glass, the scenario in which no delaminations exist in ULS should be considered for the determination of the maximum stresses in the central glass ply. At the same time, the scenario of maximum delamination as noted above is to

be considered for the design of the outer glass plies.

Obviously, stresses on glass arising from bending of the panel (in addition to pull out forces) should also be taken into account. These may be quite relevant in long glass fins or beams with metal inserts on their tensile fibre, where the notches created to accommodate the insert produce significant stress concentrations.

In some circumstances, it is possible to take advantage of the metal inserts to help alleviating stress concentrations due to bending of the glass panels. For instance, in the entrance hall of an office building in Madrid (currently in construction) significant stress concentrations occurred around inserts of the cladding panels. These are 10+15+10mm laminates with a 1.52mm SentryGlas interlayer and a typical size of 3x10 m (b x h) fixed continuously along their bottom edge and at four points along their vertical edges by means of titanium inserts connected to internal glass fins. Only out-of-plane wind loads are transferred through the inserts by means of a clamping system.

Significant stress concentrations were found on glass and on the interlayer due to the high curvature of the panel around point fixings combined with the sudden stiffness change at the top and bottom edges of the insert. Stresses could be significantly alleviated by extending the height of the inserts from the initial 240mm up to 400mm in order to locate the transition from metal to glass in an area of small curvature, as shown in fig.6.

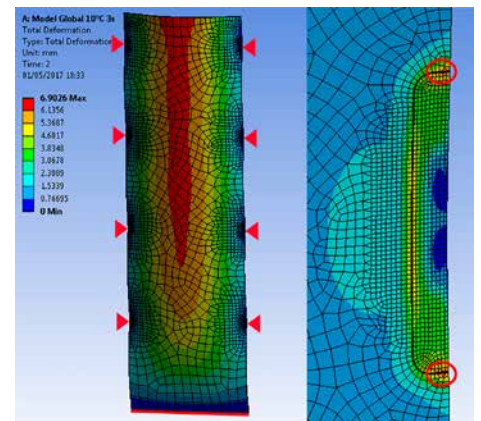


Figure 6 Deflections on a 3x10m cladding panel and distribution of stresses on the interlayer around metal inserts. For a 400mm long insert, these max. stresses are acceptable.

## Conclusions

This paper has described some connection designs used in a number of recent structural glass projects, together with the techniques used for their structural analysis and design. A number of topics which require further research have also been identified, specially in

the field of embedded laminated connections. Research organisations are encouraged to progress on these topics which have a clear industrial interest.

## References

- [1] ETAG 002 "Guideline for European Technical Approval for Structural Sealant Glazing Kits (SSGK). EOTA, 2012
- [2] Design stress for DC structural silicones, Dow Corning GmbH, 2015
- [3] Sandberg L.B., Ahlborn T.M. "Combined stress behaviour of structural glazing joints". J.Struct.Eng. 115 (1989) p.1212-1224
- [4] Santarsiero M., Louter C. "Embedded and point laminated adhesive connections for glass structures: parametric non-linear numerical investigations". Proceedings of Glass Performance Days 2013
- [5] Santarsiero M., Louter C. "Preliminary studies on the mechanical behaviour of thick embedded laminated connections. Proceedings of Glass Performance Days 2015
- [6] Santarsiero M. "Laminated connections for structural glass applications" PhD thesis n° 6828. École Polytechnique Fédérale de Lausanne. December 2015
- [7] Santarsiero M., Louter C. "Failure criteria for SentryGlas ionomer and TSSA silicon: a theoretical introduction to a novel Generalized Triaxial Model (GTM)" Proceedings of Challenging Glass 5. Ghent, 2016
- [8] Santarsiero M., Louter C., Nussbaumer A. "Laminated connections for structural glass applications under shear loading at different temperatures and strain rates" Construction and Building Materials 128 (2016) p.214-237
- [9] Santarsiero M., Louter C., Nussbaumer A. "Laminated connections for structural glass components: a full scale experimental study". Glass Struct. Eng. 2017
- [10] "Guide to the structural use of adhesives" The Institution of Structural Engineers. London, 1999
- [11] Peters S. et al. "Ganzglastreppen mit transparenten SGP-Klebeverbindungen – Konstruktion und statische Berechnung" Stahlbau 76 (2007), Heft 3
- [12] Gallizia M., Scheers J., Arbos F., Teixidor C. "Point fixed SentryGlas overhead glazing: 11 years ageing performance" Proceedings of Challenging Glass 4. Lausanne, 2014

# All Glass Pavilions

Geralt Siebert

University of self-defense forces Munich,

geralt.siebert@unibw.de

Tobias Herrmann

Ingenieurbüro Dr. Siebert, Germany, the@ing-

siebert.de

Barbara Siebert

Ingenieurbüro Dr. Siebert, Germany, the@ing-

siebert.de

## Abstract

In 2015 a pavilion mainly built of glass was finished. The building contractors themselves planned it as a transparent extension of their detached house to the garden. The structural system consists on one hand of a glazed steel frame with four stanchions rigidly fixed to the base plate and connected by four transoms at the top and on the other hand of two laterally load-bearing glass attachments. These are made of vertical load-bearing glass walls and a horizontal glass roof, which are connected among each other by structural sealants. Together with an anchor profile that is completely hidden in the joint gap, the glass elements are also acting as bracing elements. Specifications of the building authorities called for a structural concept of the pavilion's glass attachments for different states of destruction. In addition extensive requirements had to be fulfilled to obtain a special building permit for the structural sealants. The project is an outstanding example for the possibilities in constructing with glass. It combines the structural features of a load bearing all glass building with state-of-the-art joint techniques.

## Keywords

All glass building, Structural sealant, Glass joint technique

## General

In early 2015, a cuboid pavilion with glass walls and glass roof was completed in the northeast of Munich. It is a free-standing extension of a single house to the garden. The pavilion can be both garden side accessed through large sliding glass elements, as well as from the main building by a short walkway. The building is 8.6 m long, 5.8 m wide and 4.2 m high. It was designed by the owners Hildegard Rasthofer and Christian Neumaier. The latter was also responsible for the execution.



Fig. 1 view from inside ([www.master-ateliers.com](http://www.master-ateliers.com))

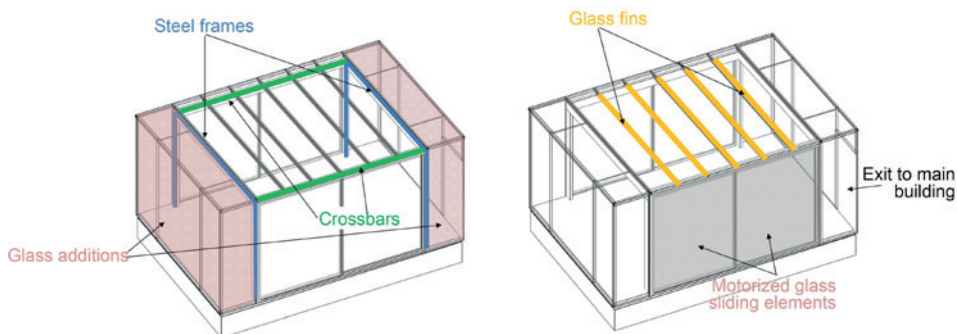


Fig. 2a) and b) Main components of the pavilion

## The structure

Two steel frames made of welded rectangular tubes are connected with crossbars in the corners and form the core of the structure. The four columns are connected rigidly via anchor plates and steel anchors with the floor slab made of reinforced concrete. The main axes of the steel frames are each offset by about 1.25 m from the short sides of the building inward. In these areas glass walls and roof glazing form self-supporting building envelopes (the additions) attached to the steel structure. Both consist of one roof panel and four wall panels respectively. In the wall-roof joint a ring anchor of stainless steel is hidden, which firstly embraces the roof panel and bears it horizontally. Secondly it serves as a mechanical securing for the glass walls against wind suction.

The walls between the steel frames are made of floor to ceiling, motorized glass sliding elements. The roof panels are supported in this area by glass fins.

## The glazing

The fixed glass wall panels consist of a 77.5 mm thick 3-pane insulated glass unit (IGU) having inside a laminated safety glass (LSG) from twice heat-soaked fully tempered glass. The latter takes over the functions of a primary load-bearing structure:

Bearing the vertical loads from the supported roof panes

Working as a bracing element for horizontal loads in case of failure of another panel

The largest glass wall is about 3 meters wide, 4 meters high and weighs more than two

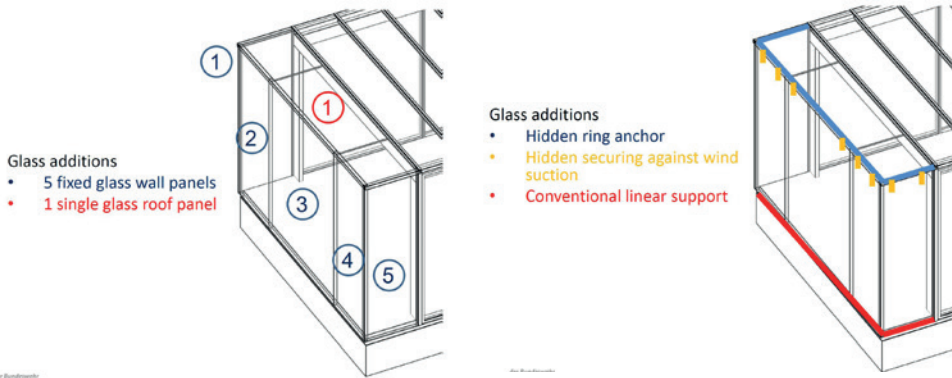


Fig. 3a) and b) Structural elements of the glass additions.

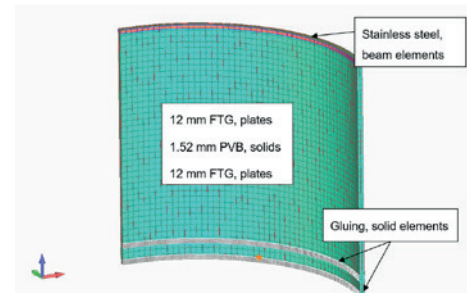


Fig. 4 Section through joint between glass wall and roof panel

tons. The fixed vertical glazing is mounted conventionally on the lower edge and glued to the roof panel on the top edge via structural sealant. The joints between the wall panels are also sealed with silicon.

The 5.4 m long and up to 1.3 m wide roof panels also consist of 3-pane insulated glass units. The bottom layers are laminated safety glass made of heat strengthened glass. In case of the glass additions, these act together with the ring anchors as horizontal bracing elements. Only here the edges of the horizontal glazing are structurally bond to the wall panels. The other edges are fixed mechanically by pressure plates.

The LSG-glass fins are only 280 mm high with a length of 5.35 m and consist of four layers of heat-soaked fully tempered glass. Their ends are each seated in a steel socket welded to the cross bar, which serves as a non-displaceable and torsional stiff support. A U-profile is bond to the top edge of the fins and forms the basis for a metal channel in which the screws of the roof pressure plates are anchored.

In the IGU factory bonding of the individual layers in the glass edge seal took place using Dow Corning's structural silicon DC 993.

Because the top and vertical edges of the glass walls are not braced by pressure plates, the sealant is stressed by wind suction and pressure differences between air space and atmosphere. Because the individual layers were supported vertically on the bottom edge by plastic blocks, no shear forces have to be considered from the dead load.

First, the glass walls were erected and aligned on site. Thereafter, the ring anchors and roof panels were placed. The joints between ring anchors and glass were sealed with structural two-component silicon DC 993, too. The joints were designed for the resultant of wind suction and dead weight of the roof panel according to ETAG 002.

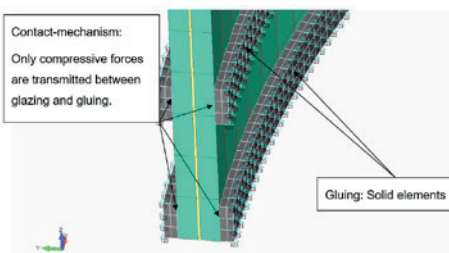


Fig. 5 Glass fin with socket detail

### Structural sealant glazing

In this construction, two types of structural bonding can be distinguished, also with regard to place of manufacture:

Edge seal of insulating glass units: Factory bonding

Assembling of the different IGUs: On site bonding

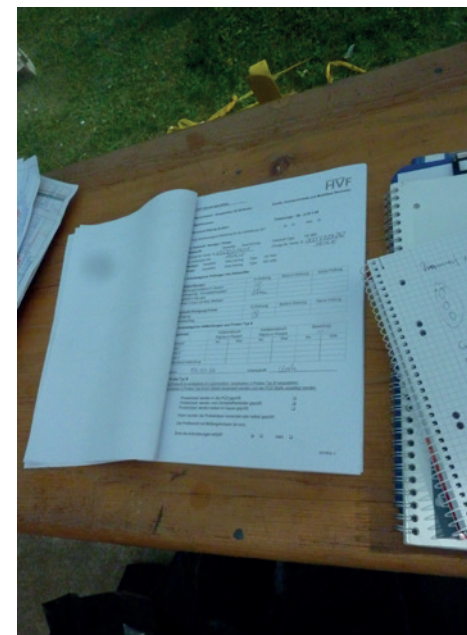


Fig. 6a), b) and c) Blending, controlling and documentation for each cartridge during on-site-bonding



Fig. 7a) and b) Sealing of glass wall joint and finished façade (www.master-ateliers.com)



Fig. 8 View from outside

## Rules and regulations

For the construction project a special building permit had to be obtained. The bonds are different from the currently valid general building approvals for structural sealant glazing systems. In addition, there are glass walls and glass fins outside the field of application of current German standard DIN 18008.

In two expert opinions that have been used as a basis for granting the special building permit, the respective differences were evaluated. For the structural bonding in the edge seal of the insulating glass panes, a certificate of conformity was demanded on the basis of a factory production control and an external inspection beyond. Such a certificate was required for the on-site-bonding, too. The adhesive Dow Corning DC 993 is approved by the European Technical Approval ETA-01/0005. However, the application in glued all-glass constructions requires a further general national building approval or, as here a special building permit. In the related expert opinion, among other things, the different substrates were evaluated for their adhesion behavior: Enamelled and not enamelled fully tempered and heat strengthened glass  
Aluminum extruded profile  
Stainless steel ring anchor

Further it was checked to what extent the seal dimensions correspond to the specifications of the ETAG 002.

The second report deals with the glazing as part of the main structure. There the effects of different destruction states were analyzed. This included an assessment of the residual strength of the bonded horizontal glazing and the stability of the glass additions in case of failure of one or more layers of glass. The walls and roof panels of the glass additions provide multi-layer glass assemblies. Only their inward LSG layers are used for tasks of the main structure, as these are connected via the ring anchor and the structural seal. In the case of a hard impact from the outside, two monolithic glass layer will protect the relevant LSG. A hit from the inside can cause breakage of the inner LSG-ply at most. Structural calculation must ensure a sufficient load bearing capacity for this extraordinary scenario. Even in the unlikely case of the complete failure of one entire wall or roof panel, the remaining IGUs provide an acceptable stability due to the ring anchor and the bracing interlayers. And also for the glass fins corresponding scenarios have been gone through and evaluated. It could be shown that two of the four LSG-plyes are enough to withstand the supported loads using reduced safety factors of extraordinary limit state.

## Conclusion

The complexity of the project required a close collaboration between supervision, consultants, experts and testing laboratories, inspection and certification bodies. The meetings proceeded intensively and on a very high level. Particularly important is the expert care of the client by experienced structural engineers and inspection services. It is certainly not too often that the owners of such a complex project signed at the same time responsible for the design and its execution. For the developed joint technology in the all-glass additions a patent has been applied for.

## References

- [1] Siebert, G., Maniatis, I., Herrmann, T.: Klebungen mit Silikon – Bemessung und Anwendungsbeispiele. In: Glas im konstruktiven Ingenieurbau 13, Conference proceedings, Hochschule München (2015)
- [2] ETAG 002 – Part 1: European Technical Approval Guideline - Structural Sealant Glazing Systems - SSGS; Supported and Unsupported Systems, first edition 1999, last amendment: May 2012
- [3] DIN 18008: Glass in Building - Design and construction rules, Parts 1 to 6; published 2010 to 2015
- [4] T., Siebert B.: A Glass Pavillon. Challenging Glass 5. Ghent, June 2016
- [5] Siebert G., Maniatis I., Herrmann, T.: Ein Glaspavillon für den Garten

# The Futurium Berlin: Ventilated Facade System with Structurally Bonded Textured Glass - Durability Testing Under Climatic Influences and Mechanical Loads

Dr.-Ing. Jan Wurm, Arup Deutschland  
 Ing. Nicolo Guariento, Arup Deutschland  
 Prof. Dr.-Ing. Jens Schneider, Schütz Goldschmidt Schneider (SGS), Heusenstamm, Germany  
 Dr.-Ing. Jonas Hilcken, Schütz Goldschmidt Schneider (SGS), Heusenstamm, Germany  
 Dipl.-Ing. Jens Kleuderlein, Schütz Goldschmidt Schneider (SGS), Heusenstamm, Germany

## Keywords

1=Rainscreen 2=Textured Glass 3=Structural Sealant Glazing (SSG) 4=Ageing Effects

## Abstract

The opaque areas of the Futurium in Berlin designed by Richter Musikowski Architects are clad with an innovative pre-fabricated rainscreen system. The smooth and shimmering homogeneous skin resembles a space ship landed next to the river Spree. The installed facade features a diagrid with pre-fabricated cassettes of 0,5 m<sup>2</sup> size combining translucent textured glass with a folded reflector on the back. The variations of the position of reflector and screen pattern on the front of the glass lead to subtle transformations. The application of the structurally bonded, heat treated textured glass without mechanical fixings is the result of a close collaboration between all stakeholders. The final solution of this innovative and cost-effective solution is based on extensive testing simulating ageing effects with samples simultaneously exposed to climatic influences and mechanical loads. The development of the cassette system with its sub-structure, fixing system and joint design was a complimentary process to the building design phases and showcases a successful strategy for implementing a product development approach in façade engineering.

## 1 Introduction

The "Futurium" designed by Richter Musikowski Architects [1] located at the River Spree will act as an international platform to bring together relevant parties

and individuals from Government, Science, Industry and the Public to discuss all issues regarding the future. The project was procured by Bundesanstalt für Immobilienaufgaben as a Private Public Partnership with BAM Deutschland AG as general contractor. Arup Deutschland was commissioned by Richter Musikowski architects during scheme design and by BAM during detail design to develop the façade solution [2]. SGS provided expert opinion [3] for the approval of the structural sealant glazing (SSG) and the structural calculation for the ventilated façades [4]. The specialist contractor for the ventilated facade was AL Promt.

The building is up to 22 m high and fully accessible by the public around its perimeter [5]. It is oriented north south with its ends creating overhangs marking the public entrances (see Figure 1). With the building mainly hosting exhibition spaces and functional rooms, the core is a monolithic concrete structure with openings cut in only for allowing access on ground floor and windows for offices located on upper floors of east and west facades. With a glazing-percentage of approx. 20% the project is representational for contemporary cultural buildings with an increasing area of opaque façade areas that reflect stringent energy efficiency codes.

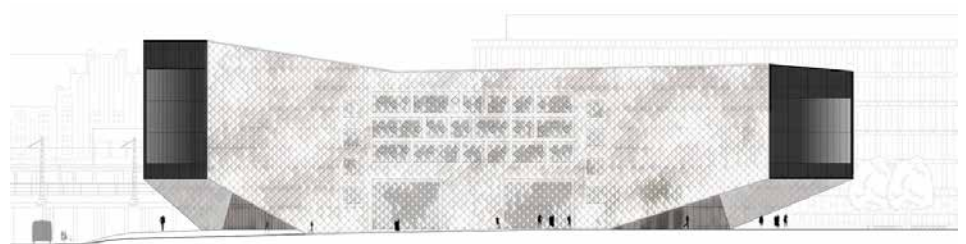


Figure 1 West Elevation Futurium © Richter Musikowski Architekten



Figure 2 East Façade during Installation © Richter Musikowski Architekten

Ventilated façade systems are in general the first choice to play on the opaque areas due to both the proven and robust building physics performance and high design freedom. Over the past years architects have been pushing the limitations of rain screen facade systems by exploring less regular penalization and joint patterns and introducing folded and curved panels [6]. The façade design of the Futurium presents a new development stage as it combines a visual complexity and depth with a modular ventilated façade system that allows a seamless integration of doors and windows.

## 2 Development of Rainscreen Cassette System

### 2.1 Objectives

The façade design is elemental in drawing together the faceted building volume and emphasizing its sculptural effect. The strong homogenizing effect is achieved by the dia-grid penalization of the façade intersecting with the edges of the building volume and the regular small tile sizes of 0,7 m x 0,7 m. The diamond pattern extends across the entire west, south east and north east façades including areas with vision glass and soffits above the entrance areas.

The architects visual objective was to create a smooth and shimmering external skin with its individual panels transforming into radiant facets under direct sun light displaying and enforcing the changing light conditions across the day. No visible mechanical fixings should counteract the abstract geometric qualities and the joint width should be limited to max. 15mm. The bonded edges of the glass should be as invisible as possible.

### 2.2 Cassette System

The design team developed a panelized and prefabricated cassette comprising textured glass on the outside, an adapter frame and a folded metal tray from brushed stainless steel on the back. The textured glass with its translucent and soft reflective surface features a partial white screen print on surface one. An anodised U-shaped aluminium adapter profile is continuously bonded to all edges of the glass facilitating the implementation of hidden toggle fixings for transferring wind loads to the dia-grid substructure. A grey screen print along glass edges conceals the structural silicone joints (see Figure 3). The diagonal folds in the metal tray of 1 mm polished stainless steel creates an undulated reflective surface behind the veil of the textured translucent glass capturing direct sun light and projecting it back, illuminating the glass from the back.

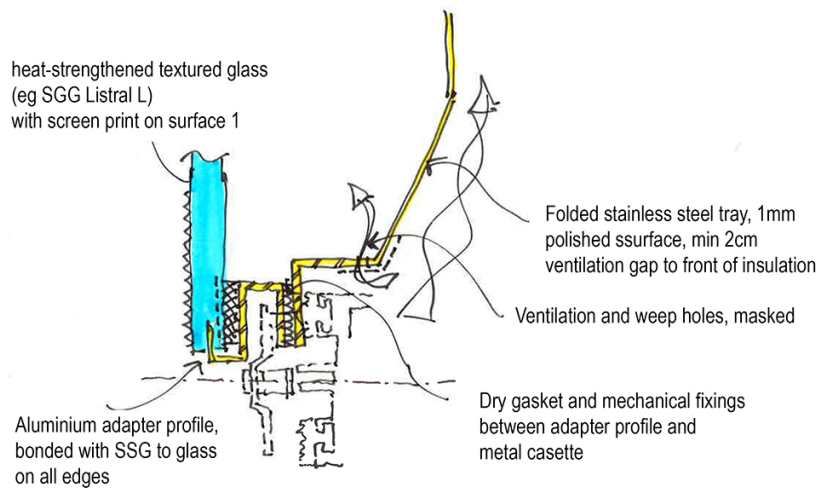


Figure 3 Concept Sketch Cross Section Cassette

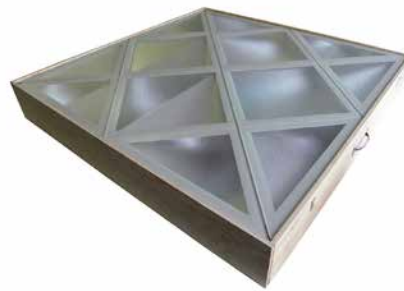


Figure 4 Mock-up during Scheme Design development - Scale 1:2 © Richter Musikowski Architekten



Figure 5 Close-up of 1:1 mock-up with dry gaskets instead of wet sealed joints © Richter Musikowski Architekten

There are four main cassette types:

- Type 1: Standard cassettes on vertical facades (approx. 2500 m<sup>2</sup>, ca. 5000 panels)
- Type 2: Cut cassettes around perimeter of vertical facades (approx. 200 m<sup>2</sup>, ca. 500 panels)
- Type 3: Overhead cassettes on soffits above entrance zones (approx. 1200 m<sup>2</sup>, ca. 2500 panels)
- Type 4: Cut cassettes around perimeter of soffits (approx. 100 m<sup>2</sup>, ca. 400 panels)

With over 7500 regular units, the development of the cassette followed a process similar to the development of an industrial product. After the definition of the core characteristics, performance requirements and basic structural configuration the detail design emerged through a systematic investigation and evaluation of options. From the sampling of materials over a series of mock-ups to the manufacturing of prototypes, in depth multi-disciplinary technical investigations informed the decision making process. A key challenge was the fixing system and build-up of the textured glass.

### 2.3 Desk Study Glazing Options

To address German building regulations requiring the mechanical fixing of structurally bonded glass panels located 8 m and more above ground corresponding to ETAG Type I [7], the concept design featured hidden metal clips interlocking with the glass edges through machined grooves then known as Steindl Classics G1 System [8]. By the time of detail design in 2014/15 Steindl had gone in arbitration and alternative procurement options were investigated:

- A: Monolithic textured glass with concealed metal clip (Type I ETAG)
- B: Laminated safety glass with textured glass on outside with metal clip (Type I ETAG)
- C: Monolithic textured glass with no mechanical restraints (Type II ETAG)
- D: Laminated safety glass with textured glass on outside with no mechanical restraints (Type II ETAG)

All options based on use of heat-strengthened glass for all plies.

### 2.3.1 Option A

A monolithic build-up would require the use of heat strengthened glass for upper floors to ensure sufficient post fracture integrity. The glass thickness would need to be 10 mm or 12 mm thick to accommodate the groove. Due to the limited mechanical strength of textured glass and its large tolerances of  $\pm 1$  mm the implementation of a controlled temper stress level along the grooved edges is highly questionable [9,10]. The considerable associated technical risk would require a detailed analysis of the stress levels from tempering and loading around the grooves and mechanical tests with 1:1 specimen to demonstrate a safe application affecting cost and program.

### 2.3.2 Option B

The metal clips interlock with a groove along the heat treated float glass of min 8 mm thickness while the front ply of the textured glass serves as pure aesthetic layer of 4 mm to 6 mm thickness. The technical risks of Option A are mitigated, however the question on the actual temper stress level along the machined edges remains requiring a series of tests and strict quality assurance during production. The textured glass should be as thin as possible to limit tolerances and reduce risk of delamination. As higher temperature levels during service can be expected, use of an Ethylenvinylacetat (EVA-) interlayer might be required as EVA unlike Polyvinylbutyral (PVB) provides a minimum shear modulus even at elevated temperatures.

### 2.3.2 Option C

As with Option A the textured glass would need to be heat-strengthened for upper floors, a thickness of 6 mm would be sufficient to withstand wind loads. While this principal build-up would in principle be acceptable to authorities outside Germany, the use of structurally bonded glass without mechanical fixings is in general not approved as sufficient and reliable data on the impact of mechanical and cyclic loading on the simultaneous ageing and deterioration of the structural silicon over time does not exist.

### 2.3.3 Option D

The use of laminated glass allows the integration of two glass surfaces with a ceramic screen print meeting the architects' design intent. The build-up is also more robust than heat-strengthened monolithic glass.

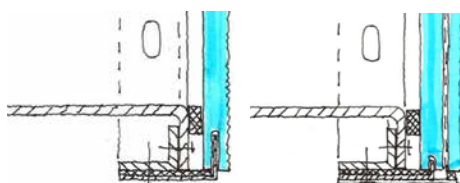


Figure 6 Sketch section bottom glass edge of Option A (left) and Option C (right)

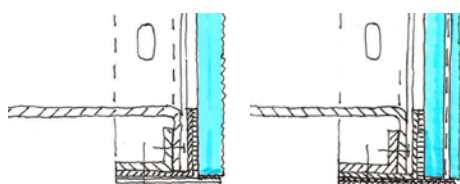


Figure 7 Sketch section bottom glass edge of Option B (left) and Option D (right)

## 2.4 Discussion

From a technical point of view the use of metal clips is the least favourable option. Also Option C and D allow use of thinner glass and are more cost-effective. Commercially the clips add cost of approx. 10 € per glass unit while the use of laminated glass instead of monolithic glass add approx. 30 € per glass unit. Allowing the highest architectural design flexibility and safety level, Option D was recommended based on the assumption that the long term mechanical performance of the SSG under simultaneous ageing can be demonstrated. With a total length of 2,8 m structural silicone joints per panel of an area of only 0,5 m<sup>2</sup> the risk of a complete failure of the silicone seal leading to the drop of a panel is low, however authorities asked for experimental evidence. Standard ageing tests according to ETAG 002 had to be combined with mechanical loading representing the expected service loads during life time of 30 years [7, 11, 12].

## 3 Thermal Study (Arup)

### 3.1 Objectives

A specific issue of the cassette design was the heat build-up in the cavity. The temperature levels inside the cassette not only influence mechanical loading due to thermal expansion as a key parameter for ageing effects, but also impact on durability of laminated potentially glass due to delamination. In order to assess the maximum temperature the laminated glass could be exposed to and associated risk of delamination a dynamic thermal analysis has been carried out.

The following build-up of the cassette was assumed:

- 4 mm textured glass laminated with 6 mm float glass (Energy transmittance: 73% / Energy Absorption: 20%). Approximately 50% of the surface of the glass present fritted dots, white on the front and silver on

the back.

- 20 mm cavity
- Highly reflective steel panel (Reflectivity: 55% / Absorptivity: 45%)
- Ventilation
- Insulation

Because of the high transparency of the textured glass, most of the incident solar radiation will be absorbed by the steel back panel. Even if the steel panel can reflect most of the incident solar radiation, the limited air velocity of the back ventilation can lead to a significant overheating of the back ventilated façade and to possible delamination of the external glazing.

As the maximum temperature is determined by the mutual effect of the external air temperature and the infrared radiation due to the absorption of the solar radiation by the steel back panel the aims of the analysis were:

- Calculate the maximum solar radiation on the different façade orientations, taking into consideration the shading effect of the surrounding buildings.
- Calculate the temperature distribution in the build-up of the back-ventilated façade for the worst case scenarios of maximum solar radiation.
- Recommend suitable interlayer material.

### 3.2 Method

The analysis has been carried out for the west, north-east and south-east facades featuring the ventilated façade system.

The analysis has been carried out with EnergyPlus 8.4, based on a sketch-Up 3D-Model [13]. The temperature distribution within the façade build-up has been calculated with the software WIS 3.01 SP2 [14]. The 3D-Model included also the volumes of the surrounding buildings, in order to evaluate their shading effect.

### 3.3 Results

The results of the analysis confirm that the temperature of the façade construction is the results of the mutual effect of the external air temperature and the incident solar radiation, absorbed by the steel back panel. However, since the peaks of incident solar radiation occurs when the air temperature is relatively low and most of the radiation can be reflected by the steel back panel, the worst-case scenarios are represented by the hours of the year when the maximum air temperature is reached.

In particular, on the South-East façade the peak solar radiation reaches 925 W/m<sup>2</sup> at the beginning of April, when the air temperature do not exceed 20°C. However, in the middle of June an external air temperature of 28°C, together with a peak incident solar radiation of approximately 720 W/m<sup>2</sup>, heat up the steel

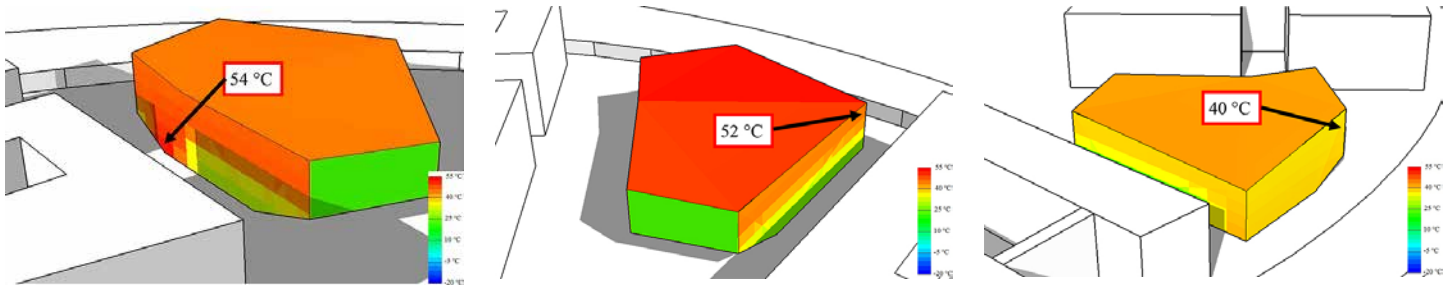


Figure 8 Max. Surface temperature levels west façade on 30 June 5pm (left), south east façade on 16 August 10 am and north east façade on 16 June at 8 am.

back panel to a surface temperature of 54°C. Because of the air movement in the cavity between laminated glass and back panel, the glass will reach a maximum temperature of 42°C.

The temperatures of the glass calculated in the other analysed façade faces never exceed 40°C.

As standard PVB-interlayer can resist up to a temperature of 60°C with sufficient mechanical properties it's use for this application would not be critical with respect to risk of delamination, however use of EVA was specified.

#### 4 Examination of durability under complex loading

##### 4.1 General

The vertical façades of the Futurium are Type II structural sealant glazing systems. The individual glazings have mechanical supports for the transfer of the dead load but do not have any mechanical fixings or retaining devices, which could hold the glass in place in case of failure of the structural sealant. Although the cassettes in the horizontal overhead areas have retaining devices, the self-weight of the glazing must be transferred to the sub-structure by the SSG joint only. This corresponds to a type IV glazing according to ETAG 002 [7]. The glazing consists of laminated glass with EVA. Since only the inner panes are supported by the SSG joint and retaining devices are only located in the horizontal areas, the outer panes of the laminated glass are only supported by the intermediate EVA layer. Here, only the experimental investigations with respect to the durability of the SSG joints simultaneously exposed to climatic influences and mechanical loads are described in detail.

##### 4.1 Test procedure

To investigate the durability of the SSG joint a multistep verification method was used, which was developed within the framework of a research project [11, 12]. In contrast to the previously harmonized European method by ETAG 002 [13], in which different influences on the durability and the mechanical strength are

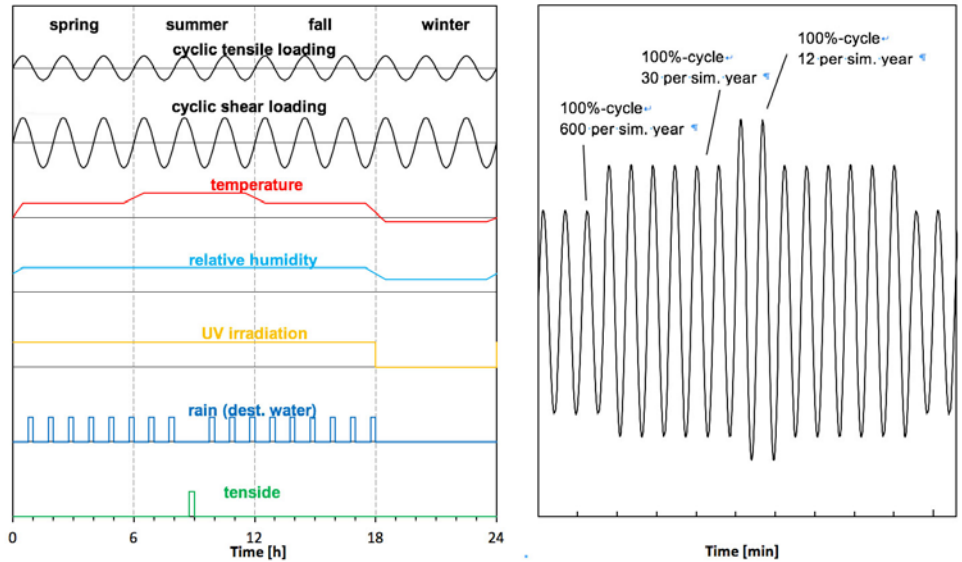


Figure 9 Schematic representation of the load of one simulated year (left) and the cyclic tensile and shear loading of one period (right)

examined separately, mechanical, climatic and chemical influences are tested in combination. For the applied verification method, a representative system sample is subjected to a cyclic mechanical test under changing climatic conditions. The representative system sample consists out of a stainless steel profile, a glass pane and the SSG joint. The materials of these parts are the identical materials which are used for the façades of the Futurium. The length of the steel profile and the SSG joint is 400 mm. The glass pane has a width of 245 mm and a length of 400 mm. The SSG joint (6 mm x 12 mm) was arranged at the edge of the stainless steel profile. In the tests, two representative system samples were tested. Both samples could be fixed next to each other in the tests setup and could be tested simultaneously. In addition, one sample was added to the tests, which was exposed only to the climatic and chemical influences.

In the experiment, one year in service is simulated in one experimental day [12]. In order to simulate the usual service life for buildings of 50 years, the experiments are carried out over a period of 50 days. The simulated year is divided into four periods

according to the seasons, in which different climatic loadings are applied simultaneously with a cyclic mechanical load. In Figure 9, the schematic representation of the loading of a experimental simulated year is shown. The temperature loading was defined according to the thermal simulation [2] presented in section 3 and according to EN 1991-5 [15]. The maximum temperature during the simulated summer was set to  $T = 60^{\circ}\text{C}$ , during the simulated winter to  $T = -20^{\circ}\text{C}$ . Additionally, the samples were periodically sprinkled with distilled water to simulate rain events and irradiated with a power of  $20 \text{ W/m}^2$  in the simulated seasons spring, summer and fall. For one rain event per year instead of distilled water a tenside solution was used as chemical load of the sample [11, 12].

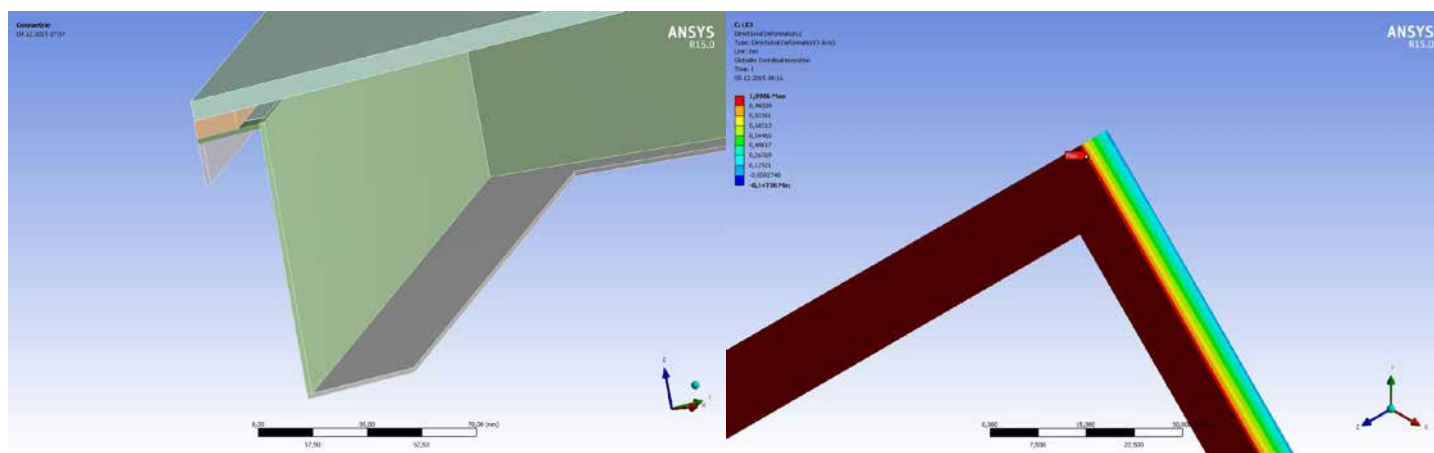


Figure 10: Finite Element calculation to define the cyclic tensile and cyclic shear loading of the combined durability test

The applied cyclic tensile and shear loading of the durability test was defined by a detailed finite element calculation, wherein the cassette was modelled in full detail with volume elements and loads from self-weight, wind (suction, pressure) and temperature (summer, winter) were investigated. According to these calculations, the maximum shear deformation was set to 1.14 mm and the maximum tensile deformation to 0.30 mm for the deformation controlled tests. These values include both full design loads as well as an increase by a factor of 2.14 by which the small sample size is considered.

For the evaluation of the material strength, the material properties of the SSG joint in the initial state and in the final state after complex loading were investigated by tests as defined in ETAG 002 [7].

### 4.3 Results

Both test specimens subjected to the durability test with complex loading have passed the test. However, during the experiments a reduction of the resulting force could be determined in tensile direction as well as in shear direction. This decrease in stiffness of the SSG joint can be attributed to microscopical material deterioration and the Mullins effect. In Table 1, a comparison of the strength and elongation values of tensile and shear tests according to ETAG 002 [7] in initial and final state is given. The increasing elongation at failure proves the decrease in stiffness.

The strength values in final state are lower than in initial state. Nevertheless, the design strength values determined from the strength test in the final state after complex loading with a partial safety factor of 6 are sufficient to transfer the loads acting on the façades [4]. The ratio between technical stresses from loading and technical strength after ageing is about 15%.

| Parameter                        | Initial state | Final state (after climatic & mechanical loading) | Final state (climatic loading only). |
|----------------------------------|---------------|---|--------------------------------------|
| Tensile strength (ETAG 002)      | 1,15 MPa      | 0,84 MPa  | 1,25 MPa                             |
| Elongation at failure (ETAG 002) | 0,38          | 0,53  | 0,49                                 |
| Shear strength (ETAG 002)        | 1,08 MPa      | 0,67 MPa  | 1,02 MPa                             |
| Elongation at failure (ETAG 002) | 1,36          | 1,47  | 1,43                                 |

Table 1 Comparison of the results (mean values) of tensile and shear tests according to ETAG 002 in initial and final state after simultaneous exposition to climatic influences and mechanical loading

## 5 Conclusions

The cassette design with clearly defined mechanical interfaces based on a single design basis for over 7500 panels, still enabling a large degree of freedom and flexibility for aesthetics could be achieved. This approach required an in-depth technical analysis for optimizing the system design and glass configuration leading to cost savings in the final design.

The durability of the SSG joints for the façade of the Futurium was tested by a new testing method [11, 12], in which climatic influences and mechanical loads act cyclically and simultaneously on large scale samples to simulate the service life for a defined time period. The test results shows that the SSG joints in this project could be classified as sufficiently durable regarding a simulated service life of 50 years. For usual building projects, the new test method seems to be too time consuming and complex to be applied each time. Nevertheless, further scientific research and experiments should be carried out in order to compare the results with cyclic fatigue tests for different load levels, boundary conditions and climatic influences to study the

deterioration and failure mechanisms of SSG joints systematically.

## 6 References

- [1] <http://www.richtermusikowski.com/kultur/haus-der-zukunft-berlin/>
- [2] Arup Deutschland GmbH: „Haus der Zukunft – Variantenbewertung Fassade, Rev C“, 21st June, 2015
- [3] SGS Ingenieurdienstleistungen im Bauwesen GmbH: Gutachterliche Stellungnahme 1118/2015.15.03 zur Structural Glazing Fassade BV Haus der Zukunft“, Heusenstamm, May 2nd, 2017
- [4] SGS Ingenieurdienstleistungen im Bauwesen GmbH: „Statische Berechnung 1147/2016.22.01 der Fassadenkonstruktion des BV Haus der Zukunft, Berlin“, Heusenstamm, September 27th, 2016.
- [5] <https://www.futurium.de/>
- [6] [http://www.fvhf.de/Fassade-bilder/docs/Prospekte/FVHF\\_Doku\\_Fassadenpreis\\_2013.pdf](http://www.fvhf.de/Fassade-bilder/docs/Prospekte/FVHF_Doku_Fassadenpreis_2013.pdf)
- [7] EOTA, ETAG 002: Guideline for European technical approval of Structural Sealant Glazing Kits (SSGK), June 2013
- [8] European Technical Approval Steindl Glassics G1 (ETA - 08/0099), 13th May 2013
- [9] DIN EN 572-5: Glass in building. Basic soda lime silicate glass products. Patterned glass, July 2012
- [10] Schneider J., Hof P., Block, C.: Fastening of Glass Panes with Undercut Anchors. Numerical tempering simulation, experiments, load-bearing capacity. Proceedings of the 2nd International Colloquium on Modelling of Glass Forming and Tempering (M.G.F.T.), University of Valenciennes,

France, 23.01.-25.01.2002, pp. 247-254

[11] Bundesanstalt für Materialforschung und -prüfung (BAM): „Schlussbericht zum MNPQ Projekt 22/10 „Entwicklung und Validierung einer innovativen, qualitätsgesicherten Befestigungstechnologie für Glasfassaden mit Hilfe eines neuartigen Untersuchungsverfahrens“, Berlin, June 30th, 2015

[12] Recknagel, C.: Potential of Dynamic-Mechanical Analysis Toward a Complementary Material and System Testing Approach for Structural Glazing,” Journal of ASTM International, Vol. 9, No. 4, 2012, pp. 1-17

[13] EnergyPlus 8.4.0, Release September 30th 2015

[14] Window Information System (WIS) version 3.0.1 with service pack SP2, Release October 2006

[15] EN 1991-1-5: Eurocode 1: Actions on structures - Part 1-5: General actions - Thermal actions

## 8 Acknowledgements

Michael Vahlert (Partnerschaften Deutschland); Jan Musikowski, Christoph Richter, Sebastian Haufe (Richter Musikowski Architekten); Andreas Jorsch, Ralf Rykarski (BAM Deutschland); Christoph Recknagel (Bundesanstalt für Materialforschung und -prüfung); Alexander Morgenroth (SteindlGlas); Charlotte Heesbeen, Frank Walter, Dirk Regenspurger (Arup Deutschland GmbH)

# Cyclone Resistant Glazing Solutions in the Asia-Pacific Region: a Growing Market to Meet Present and Future Challenges

Dario Trabucco<sup>1</sup>  
 Angela Mejorin<sup>1</sup>  
 Will Miranda<sup>1</sup>  
 Reisuke Nakada<sup>2</sup>  
 Christoph Troska<sup>2</sup>  
 Ingo Stelzer<sup>2</sup>

<sup>1</sup>CTBUH - The Council on Tall Buildings and Urban Habitat / IUAV University of Venice  
<sup>2</sup>Kuraray Trosifol® World Of Interlayers

## Keywords

1=Typhoon-resistant glazing 2=Windborne debris 3=Curtain wall 4=High-rise buildings 5=Refuge 6=Climate changes

## Abstract

The Asia-Pacific region has seen unprecedented growth over the past decade, both in terms of economy and population. As the growth in this area occurs, the demand for additional high density residential and office space has also increased, resulting in record numbers of high-rise buildings being constructed. The development of the built environment in this region has largely occurred in coastal areas, which are increasingly vulnerable to disastrous storms, specifically cyclones, also known as typhoons in Asia and as hurricanes in the US. The Asia-Pacific region is the most disaster prone in the world, and since 1980, these climate-change-induced disasters have been consistently increasing in both frequency and severity. These events can be of such magnitude that the economic stability and growth of highly-populated areas can be threatened. Currently, the curtain wall is seen as the primary barrier to protect a tall building and its occupants from these external threats, in addition to controlling a buildings internal climate and lighting.

This research will examine the buildings that have been affected by cyclone events, buildings that are currently at risk, and steps that have already been taken to combat these threats. Next, projections of future threats will be made, which will emphasize the need for advancements in cyclone resistant glazing technologies and standards. Through these advancements, tall buildings could not only avoid major damage during cyclone events, but

also serve as a refuge for local residents.

## Introduction

The research project "Cyclone-Glazing and Façade Resilience for the Asia-Pacific Region" has been conducted by the Council on Tall Buildings and Urban Habitat, thanks to a research grant received from Kuraray Trosifol® World of Interlayers. The bond between the contemporary skyscrapers' architectonic image and glazed construction is evident. The performances of glass are rising with these buildings, guaranteeing users' safety. Current, state-of-the-art cyclone-resistant façade technology requirements in the Asia-Pacific region have been investigated. In this area of the world, megacities are developing to address the demand for additional residential and office space, which calls for the construction of high-rise buildings. High-wind storms, called typhoons in the region, represent a serious threat to the economic stability and growth of these markets, and can often claim a high toll of lives when they occur. The building's envelope is a critical component to its performance during a windstorm. Damage to glazed enclosures, caused by windborne debris during a typhoon, represents a significant contributor to the post-event recovery costs.

The aim of the research was exploring the norms and standards of the major tall building markets within the Asia-Pacific region in order to propose a new general guideline for the design of typhoon-resistant façades in those countries in the future.

The research in this paper focuses on the some of the countries that are the most prone to typhoons in the Asia-Pacific region.

## Asia Pacific Region Environmental Vulnerabilities

The World Bank Group in its October 2016 "Reducing Vulnerabilities" East Asia and Pacific Economic Update [1] has shown that both the frequency and severity of disasters in East-Asia Pacific region have been rising since 1980. Over this period, more than 3.5 billion people have been affected by natural disasters, and the region has sustained some US\$525 billion in losses (nearly a quarter of total global

losses from natural disasters). Although the number of fatalities have not followed a linear trend, the total number of disasters and the amount of people affected in the EAP region between 1980 and 2015 have been constantly rising. The data also shows a growth in the frequency and intensity of atmospheric events. This data means that CTBUH has to work with building solutions and technologies in order to reduce the affected population. The World Risk Report [2] has created a World Risk Index, which characterizes the disaster risk for 173 countries. The risk index takes into account natural hazards and the social sphere.

This is calculated on:

- the exposure to natural hazards;
- susceptibility: likelihood of suffering harm;
- coping capacities: the capacity for a country to reduce negative consequences;
- adaptive capacities: the capacity for a country to develop long-term strategies for societal change.

The research community has to increase the amount of proposed technical and societal improvements for the Asia Pacific countries, in order to reduce the negative consequences of natural disasters. Currently, 7 of the 10 most at-risk countries in the world are located in the Asia Pacific region (11 in the top 20) and the East Asia and Pacific region is the most disaster prone in the world [3].

Furthermore "Sustaining Resilience" East Asia and Pacific Economic Update of April 2017 [4] indicates that most of the small Pacific Island Countries are experiencing moderate to strong growth but they are at the same time vulnerable to natural disasters and climate change. More or less every year, these countries are hit by natural disasters. In the "Pacific Possible" program of research on long-term economic opportunities, vulnerability will remain high even with an increased policy focused on disaster risk management. This high level of vulnerability could undermine the development of these countries [5].

Almost all of the standards developed for wind speed and wind pressures for cyclone events are based on a predictive model. This model does not take into account the strongest event in a deterministic manner but in a statistical

one. The research community does not have the recorded data from all historical cyclone events. The development of the model has sped up in recent years, taking into account the increasing number of these natural events due to climate changes [6].

### “Cyclone-Glazing and Façade Resilience for the Asia-Pacific Region” Research Project

The research methodology has been developed according to the following three steps:

- identification of the severity of the problem presence of tall buildings in typhoon prone areas;
- identification of existing codes – design and test requirements for typhoon resistant façades;
- comparison of Asia-Pacific codes on the matter, and comparison with the most advanced international codes and best practice in the western countries.

The output of the Research is a concise tool for public administrations, for private consultants operating in the Asia Pacific market, for insurance companies, and at the very least, for façades professionals operating in typhoon prone countries field. It is a matrix examining the similarities and differences between international, US, and Asia-Pacific countries codes and standards for cyclone resistant glazing systems. Technical performance requests, local market minimum requirements in designing, testing, commissioning, and acceptance processes for fast emerging economies is shown. This means identifying what is missing in each regional code and how the various requirements available can be merged to generate a new region wide guideline for typhoon prone façade resilience in the Asia-Pacific Region, which identifies different levels of technical performance in the specific theme.

Typhoon resilience is the capacity for a building to protect its properties and provide safety to occupants during tropical storm events. The social conditions of analyzed fast emerging countries is highlighted though this tool that photographs the current situation, in order to be able to propose actions to be taken for the future.

### Identification of the Severity of the Problem – Tall Buildings in Typhoon Prone Areas

The risk to tall buildings in the Asia-Pacific region due to typhoon events has been examined in detail country-by-country. CTBUH manages and implements the Skyscraper Center [7], the world’s largest database on tall buildings with entries on more than

13,000 buildings above 100 meters in height (and more than 25,000 tall buildings total). The geographic location of such buildings have been compared with the Geographic Information System (GIS) data of past typhoon events to identify how many tall buildings have suffered from typhoon events in the region (see Figure 1), and how many are located in an area that has been struck by a typhoon in the past and therefore is likely to be hit by extreme winds in the future.

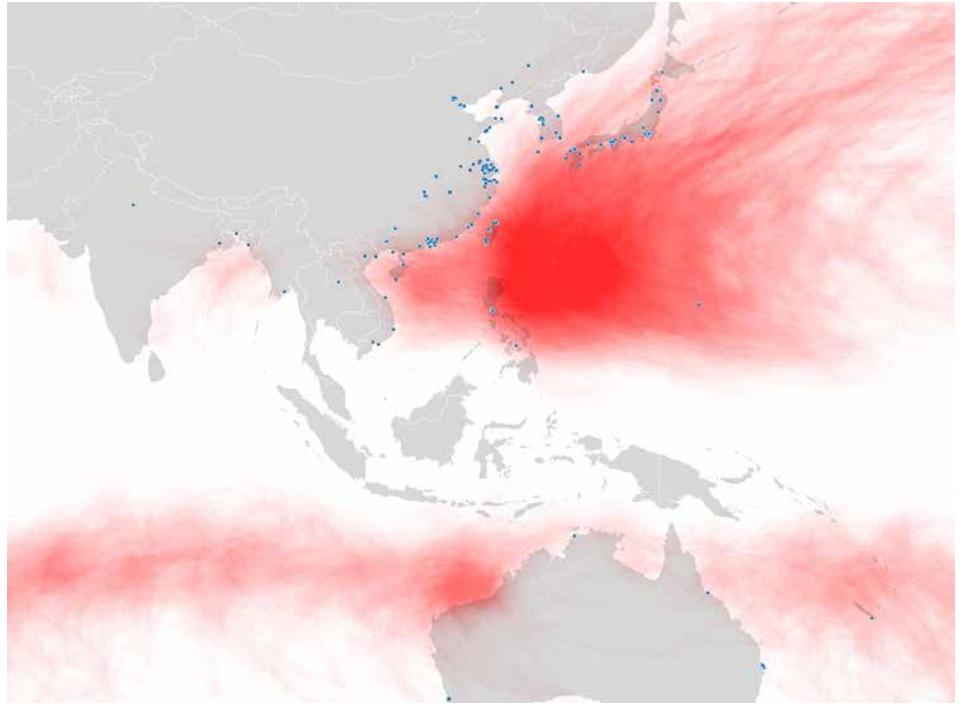


Figure 1 Tall buildings and past typhoon events.

Utilizing the GIS modeling of past typhoon events and tall building’s locations, the following information was extracted for the selected Asia-Pacific countries:

- amount of tall buildings affected by typhoon events in the past;
  - amount of tall buildings in the same prone areas that could be affected now;
  - amount of tall buildings in the same prone areas that could be affected in the near future.
- 1,772 buildings have experienced a typhoon, resulting in at least 16,500 total instances that buildings have been affected by 234 unique typhoon events in the past 45 years (336 of the 1,772 buildings have experienced a severe typhoon event with wind speeds greater than 150km/h).

|             | Total population (2014) | Urban population (2014) | GDP per capita (US\$) | Annual average of typhoon events | Deaths due to typhoon events (annual averages) | Economic loss due to typhoon events (annual averages) (,000 US\$) | Tall buildings affected by typhoon event in the past | Tall buildings in typhoon prone area - existing | Tall buildings in typhoon prone area - under construction |
|-------------|-------------------------|-------------------------|-----------------------|----------------------------------|--|---|--|---|---|
| Australia   | 23,130,900              | 89.15%                  | \$67,458.36           | 1.74                             | 6  | \$ 911,507.18   | 68   | 169   | 24  |
| Bangladesh  | 156,594,962             | 32.75%                  | \$957.82              | 3.17                             | 685  | \$ 109,308.20   | 2  | 4   | 5   |
| China       | 1,357,380,000           | 53.17%                  | \$6,807.43            | 9.63                             | 722  | \$ 4,356,162.59   | 286  | 1433  | 451   |
| Hong Kong   | 7,187,500               | 100.00%                 | \$38,123.52           | 0.78                             | 0  | \$ 30.97  | 569  | 808   | 13  |
| India       | 1,252,139,596           | 31.94%                  | \$1,498.87            | 3.63                             | 397  | \$ 1,012,917.68   | 5  | 19  | 7   |
| Japan       | 127,338,621             | 92.49%                  | \$38,633.71           | 3.32                             | 96   | \$ 3,239,414.10   | 469  | 557   | 14  |
| New Zealand | 4,470,800               | 86.22%                  | \$41,555.83           | 0.32                             | 1  | \$ -  | 5  | 10  | 0   |
| Philippines | 98,393,574              | 44.63%                  | \$2,765.09            | 9.23                             | 1,430  | \$ 1,310.93   | 72   | 121   | 44  |
| South Korea | 50,219,669              | 82.25%                  | \$25,976.95           | 1.03                             | 12   | \$ 89,336.50  | 213  | 357   | 27  |
| Taiwan      | 23,361,753              | 77.00%                  | \$22,598.00           | 2.44                             | 30   | \$ 60,723.99  | 76   | 99  | 11  |
| Thailand    | 67,010,502              | 47.94%                  | \$5,778.98            | 1.03                             | 6  | \$ -  | 0  | 0   | 0   |
| Vietnam     | 89,708,900              | 32.31%                  | \$1,910.51            | 3.41                             | 157  | \$ 409,541.76   | 7  | 70  | 47  |

Table 1 Asia-Pacific countries' tall buildings development and typhoon effects.

More than double the amount of buildings (3,647) are now built in these same areas that have experienced a typhoon event in the past (4,290 buildings are completed or currently under construction in these areas). This shows that the magnitude of the problem is increasing as a mix of increased number of tall buildings and severity of typhoon events. The list of countries analyzed in the research is shown in Table 1. It reports data about: local population; economy; effect of typhoon events; tall buildings in typhoon prone areas by each country [8] [9].

Data shows that there are no complete or under-construction tall buildings that are in areas that have experienced a typhoon event in the past 30 years in Thailand. That being said, the data analyzed by CTBUH does not take into account climate change, which is shown from the various parties as a principal contributor to these disaster increasing in frequency and severity. Thus, the buildings that are in these areas that have not experienced past events

could very well experience a typhoon in the future. In this country the total amount of tall buildings currently complete or under-construction is 165.

The summarized output of the GIS analysis for the Asia Pacific countries is displayed in Table 2. The total amount of Asia-Pacific tall buildings analyzed was 6,618 , and more than a half of those are located in typhoon-prone area (4,290).

### Developed Countries Existing Codes and Standards Requirements for Typhoon Events Prone Façades

Australia (1975, following Cyclone Tracy) followed by the US (1994, following Hurricane Andrew) were the first developers of codes and standards requirements for typhoon prone regions.

In 1992, Hurricane Andrew hit the coast of Florida left 65 dead and \$26 billion in damage to local buildings, especially to their envelopes.

In the following years, curtain wall provisions were added to Florida Building Code [10], which included the strengthening of building openings and glass surfaces to limit damage caused by high velocity windborne debris. This code represents the most demanding building codes in the US when it comes to impact-resistance of façade systems from cyclone events.

The Florida Building Code regulates façades performance requirements with the Testing Application Standard [11] procedures (TAS 201-94, TAS 202-94, TAS 203-94 specified in the Florida Building Code). These standards provide the most stringent testing requirements on the research topic in the US. The Miami-Dade County best practice includes the product approval program with the Notice of Acceptance (NOA). These are set forth by Miami-Dade County for all construction trades and the Florida Product Approval organize the owner's product acceptance [12].

|                                 | Deaths due to typhoon events (annual averages) | Economic loss due to typhoon events (annual averages) (,000 US\$) | Tall buildings affected by typhoon event in the past | Tall buildings in typhoon prone area - existing | Tall buildings in typhoon prone area - under construction | Tall buildings in typhoon prone area - total number | Tall buildings in typhoon prone area never affected by typhoon event in the past | Tall buildings - total number for Asia Pacific analyzed countries |
|---------------------------------|--|---|--|---|---|---|--|---|
| Asia Pacific analyzed countries | 3,543  | \$10,190,253.88   | 1,772  | 3,647   | 643   | 4,290   | 2,518  | 6,618   |

Table 2 Asia-Pacific tall buildings in typhoon prone area – 4,290 constructions.

In the ASCE 7-10 [13], the wind zone map is shown to identify the windborne debris regions and the boundary hurricane-prone regions. ASTM E1886 [14] and ASTM E1996 [15] requirements, or local standards requirements when more stringent, have to be followed by buildings constructed in US areas affected by hurricanes. ASTM standards dictate the glass composition for the building envelope, as well as, the air infiltration control during a disaster event [16] [17].

There are some differences between the wind zone map represented in ASCE 7-05 [18] and in ASCE 7-10. In ASCE 7-05 the wind speed is lower than in the ASCE 7-10. This reflected the definition of a safer wind speed map based on climate changes, but in the last edition of ASCE 7-16 wind speed maps represent reduced wind speeds for much of the country and clarify the special wind study zones, including new maps for Hawaii [19].

The International Code Council regulates areas in 130 mph wind zones and higher [20], which are identified as wind borne debris regions and in which it defines the required debris missile resistance. International Building Code's references [21] are the ASTM E1886 and the ASTM E1996 standards.

The International Standard ISO 16932 [22] defines the destructive-windstorm resistant security glazing requirements and it has its references in the ASTM standards and in Australian technical requisites developed in the last decades, which are well rooted as best practices for the Asia-Pacific countries.

### Asia-Pacific Countries Codes and Standards Requirements for Typhoon Events Prone Façades

Australia and New Zealand are the Asia-Pacific's most advanced countries in terms of the existence of codes and standards requirements for typhoon resilient façade design and construction. While test and performance requirements in Australia and New Zealand are well identified, they differ from the best practices in the US. The 2011 edition of AS/NZS 1170.2 'Wind Actions' [23] included significant increases to speeds for the large missile (4 kg mass of timber) tests [24], which are now higher than those specified in the US. However cyclic pressure testing following missile impact testing which has long been a requirement for roofing and façade panels in buildings in cyclone prone areas is not a requirement for typhoon glazing certification. The effect of cyclic pressures on the glazing construction component is well representative of the meteorological phenomenon of the typhoon event and has been identified in the US as a critical part of the testing protocol for missile impacted

glazing. In other Asia-Pacific countries different kinds of approaches have been identified for building codes and standard minimum design requirements. The straight input to refer at international or US standards for typhoon resistant glazing systems is given to Asia-Pacific codes users in some cases [25]. In some other cases foreign countries' codes has been translated in local languages and locally adopted (i.e., the National Structural Code of the Philippines [26] is based on ASCE7-05 and is asking for the requirements specified in ASTM E1886 and ASTM E1996).

However there are circumstances in which these countries' wind maps haven't been updated in accordance with the increasing in the intensity of typhoon events due to last recorded disasters. There are Asia-Pacific countries without their own wind map although

the standard authority translated and adopted a foreign code [27], but regional wind maps exist in region wide internationally recognized wind maps [28].

Many analyzed countries have been affected by typhoons every year in the past decades, but they still don't have typhoon resilience construction safety requirements. If there are not specific codes for typhoon resistant façades it is commonly possible to use every more restrictive foreign code for wind, pressure cycling, debris resistance, in order to secure storm disaster façade resilience.

From the various parties consulted by CTBUH, it is evident that a major problem faced by contractors operating in the Asia Pacific region is that bids for new projects can be over-exhaustive and contain a generic list of codes. It is up to the responsibility of the contractor to decide which one to comply with. Many foreign

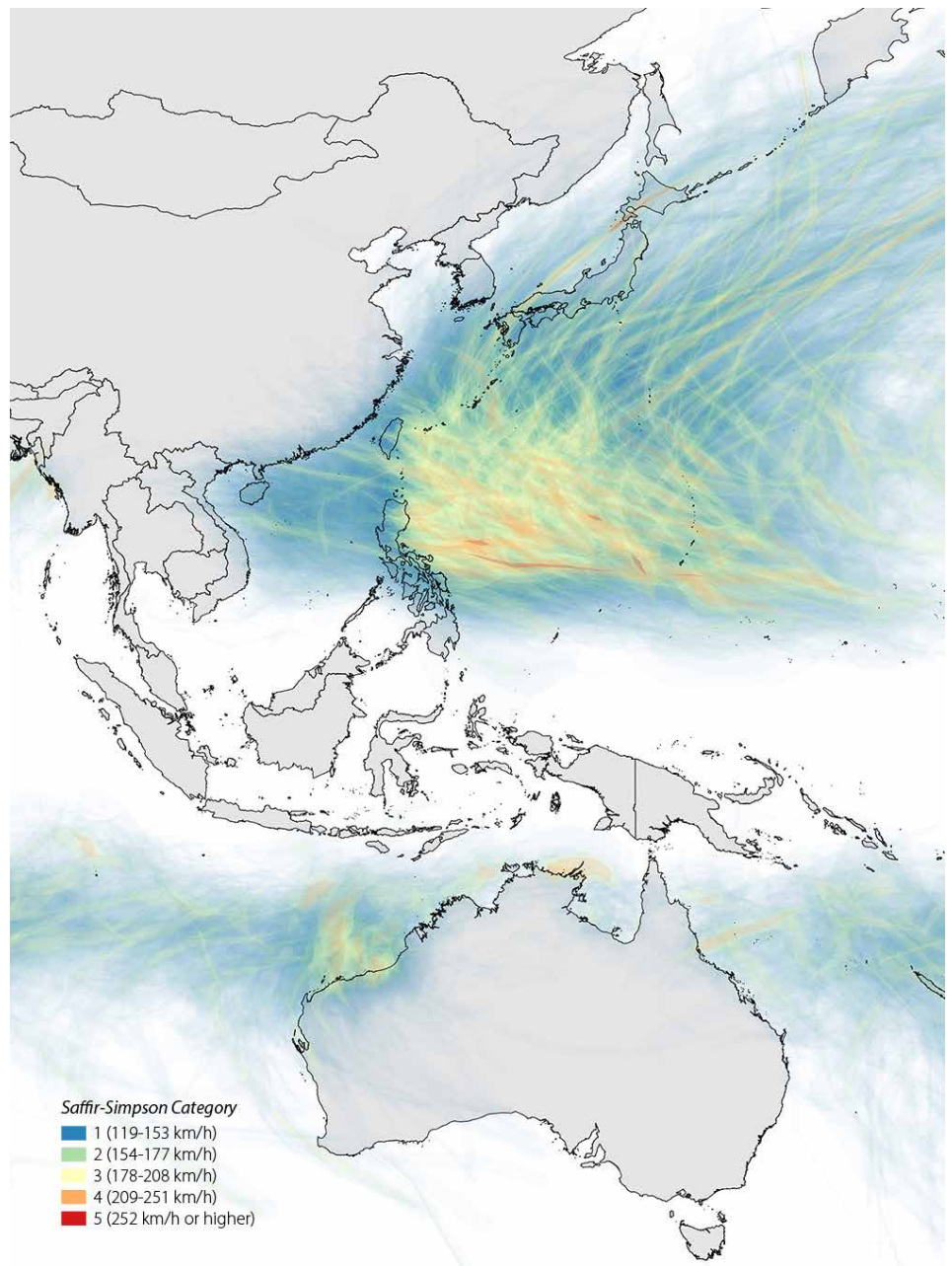


Figure 2 Typhoon events from 1970 - 2015 according to wind speed.



Figure 3 Biloxi. Despite the apparent integrity of the building envelope of MGM Mirage's Beau Rivage Hotel and Casino, after hurricane Katrina there were many extensive damages.

countries, the US, and international codes are frequently mentioned and, in most cases, no test requirements are needed for façade construction authorization process.

### Typhoon Events Prone Façades – Generic Problems and Gaps in Standards

Façade resilience is needed to provide adequate safety during a typhoon event. This characteristic aims to primarily avoid broken glass. In Thailand requirements, from 1997 the glass in the external façade of high-rise buildings must be laminated safety glass [29]. This requirement is not directly related to typhoon resistance, but has an indisputable repercussion on environmental effects due to typhoon events. Australian Standard AS 1288-2006 Amendment 2 [30] in 2011 also recognizes the potential danger represented by the spontaneous breakage of toughened glass. Heat soaked toughened glass or laminated glass is required in buildings above a height of 5 meters. It is the only code to recognize the potential danger represented by spontaneous breakage of toughened glass. The laminated glass composition used in typhoon resistant glass must resist both the design wind load and the missile impact specified by codes. The thickness of the glass lites in the laminated glass is determined by the wind load and the interlayer type. However, resistance to penetration by missile impact is determined by the interlayer type and the thickness of the interlayer. The interlayer thickness relates to missile impact speed, not

to design wind load. The purpose of ASTM E1886 and ASTM E1996 is related with the safeguard of human life and of public/private property. Building envelope failure caused by a typhoon event can have consequences on interior damage, internal pressurization, interruption of business during the renovation period, and can cause potential mold problems. One of the gaps identified by this research, and confirmed by technical experts, is the need for improved testing of windows for wind driven rain over current international and US standard test methods. While the US standards for resistance to windborne debris and wind pressure cycling are adequate, the one area where improvement is needed is regarding wind driven rain. There are many standards related to this performance of the building envelope, but they are not required for cyclone prone region façades testing [31] [32] [33].

### Conclusions

The purpose is to sensitize Asia-Pacific governments on security issues for typhoon resistant façades. If the local directives are not in line with the identified best practice, the most desirable result is that a maximum time is given by local authorities themselves to align these requirements to the most developed countries on the specific issue. Skyscrapers concentrate in a small plant area, a large amount of inner surface and a huge amount of façade surface, compared to conventional constructions. This building typology has always represented

a symbol – for a company, for the society, a landmark in the city. This kind of construction has to follow the best practice for typhoon resistant glazing because in addition to interior damage, the potential effects to the external area due to storms is invaluable (glass breakage, internal objects downfall). For rapidly developing Asia Pacific countries, tall buildings best ambition is to have a new image in the collective function, serving as a refuge for local residents during disaster events [35] [36].

### References

- [1] World Bank Group, 2016b. "Reducing Vulnerabilities" East Asia and Pacific Economic Update (October 2016). World Bank, Washington, DC.
- [2] Comes, M. et al., 2016. World Risk Report 2016. Edited by Bündnis Entwicklung Hilft (Alliance Development Works) and United Nations University – Institute for Environment and Human Security (UNU-EHS), 2016.
- [3] United Nations Office for Disaster Risk Reduction www.unisdr.org/
- [4] World Bank Group, 2017. "Sustaining Resilience" East Asia and Pacific Economic Update (April 2017). World Bank, Washington, DC.
- [5] World Bank Group, 2016a. "Growing Challenges" East Asia and Pacific Economic Update (April 2016). World Bank, Washington, DC.
- [6] Zhou, Y., Kijewski, T., and Kareem, A., 2002. Along-Wind Load Effects on Tall Buildings: Comparative Study of Major International Codes and Standards. Journal of Structural Engineering, pp. 788-796.
- [7] The Skyscraper Center www.skyscrapercenter.com
- [8] Global Risk Data Platform www.grid.unep.ch
- [9] PreventionWeb www.preventionweb.net
- [10] International Code Council, Florida Building Code – Buildings, 5th Edition, 2014.
- [11] International Code Council, Florida Building Code – Test Protocols for High-Velocity Hurricane Zones, 5th Edition, 2014.
- [12] Miami-Dade County, 2012. Notice Of Acceptance (NOA) General Submittal Information. Department of Regulatory and Economic Resources – Product Control Selection.
- [13] American Society of Civil Engineers, ASCE/SEI 7-10, 2013. Minimum Design Loads for Buildings and Other Structures.
- [14] ASTM E1886-13a, 2013. Standard Test Method for Performance of Exterior Windows, Curtain Walls and Storm Shutters Impacted by Missile(s) and Exposed to Cyclic Pressure Differentials.
- [15] ASTM E1996-14a, 2014. Standard Specification for Performance of Exterior Windows, Curtain Walls and Storm Shutters Impacted by Windborne Debris in Hurricanes.
- [16] ASTM E283-04, 2012. Standard Test Method for Determining Rate of Air Leakage Through Exterior Windows, Curtain Walls, and Doors Under Specified Pressure Differences Across the Specimen.
- [17] ASTM E330-14, 2014. Standard Test Method for Structural Performance of Exterior Windows, Doors, Skylights and Curtain Walls by Uniform Static Air Pressure Difference.
- [18] American Society of Civil Engineers, ASCE/SEI 7-05, 2006. Minimum Design Loads for Buildings and Other Structures.
- [19] American Society of Civil Engineers www.asce.org
- [20] International Code Council, ICC 600, 2014.

Standard for Residential Construction in High-Wind Regions.

[21] International Code Council, International Building Code, 2015.

[22] ISO 16932, 2006. Glass in building - Destructive-windstorme-resistant security glazing - Test and classification.

[23] AS/NZS 1170.2-2011, 2016. Structural design actions - Part 2: Wind actions. Incorporating Amendments No. 1, 2, 3 and 4 to Australian/New Zealand Standard.

[24] Cyclone Testing Station, 2017. Technical Note No. 4 - Simulated Windborne Debris Impact Testing of Building Envelope Components (Version 4). Cyclone Testing Station, James Cook University, Australia.

[25] Bangladesh National Building Code, 2004.

[26] Association of Structural Engineers of the Philippines C101-10, 2010. NSCP National Structural Code of the Philippines.

[27] SNI 03-1727, 2013. Minimum load for the design of buildings and other structures. Standard National Indonesia.

[28] HB 212-2002, 2016. Design Wind Speeds for the Asia-Pacific Region. Australian Standards.

[29] Republic of Thailand, 1997. Law Regulation No. 48, Clauses 27-28, 1997. Minister of Interior. Issued Under Building Control Regulation 1979.

[30] AS 1288-2006, 2016. Glass in buildings - Selection and installation. Incorporating Amendment No. 2 of November 2011 to Australian/New Zealand Standard.

[31] ASTM E331-00, 2016. Standard Test Method for Water Penetration of Exterior Windows, Skylights, Doors, and Curtain Walls by Uniform Static Air Pressure Difference.

[32] ASTM E2268-04, 2016. Standard Test Method for Water Penetration of Exterior Windows, Skylights, and Doors by Rapid Pulsed Air Pressure Difference.

[33] AAMA 520-12, 2012. Voluntary Specification for Rating the Severe Wind-Driven Rain Resistance of Windows, Doors and Unit Skylights.

[34] Lieut. Commander Mark Moran, 2005 September 11. Location: Mississippi, Biloxi. Looking east down Beach Blvd (Hwy 90). Beau Rivage at right, Hard Rock Casino with trademark guitar visible at top center. NOAA's National Weather Service (NWS) Collection, Image ID wea02506.

[35] Mori, H., 2015. Developing Tall Buildings and Urban Spaces, in Japan and Elsewhere. In: CTBUH Conference Proceeding of CTBUH 2015 New York Conference, pp. 122-131.

[36] Judah, I., Cousins, F., 2015. The Resilient Urban Skyscraper as Refuge. In: CTBUH Conference Proceeding of CTBUH 2015 New York Conference, pp. 230-237.

## Acknowledgments

The paper authors gratefully thank Kuraray Trosifol® World Of Interlayers, Phillip Davies, Richard Davis, Volker Gehl, David Chi and this research's international peer reviewer team.

# Glass fins with embedded titanium inserts for the façades of the new Medical School of Montpellier

Authors:

Jordi Torres

Núria Guitart

Carles Teixidor

Bellapart, Les Preses, Spain

## Keywords:

Façade; Structural Glass Component; Laminated Embedded Connections; Glass Fin; Pull-Out Test; Full-Scale Tests; Construction

**Extended Abstract** (The complete contribution will be published in the *Glass Structures and Engineering journal*)

The new Medical School of Montpellier, designed by François Fontès, is enclosed by several façades stiffened by the use of glass fins up to 12.71 meters high. The main façade assures the monumentality of the institution with its length of more than 65 meters. The façade glass panels, with a maximum size of 3.8x2.8m, are piled transferring the dead load to the bottom panels through plastic setting blocks. The façade panels are fixed with patch-fittings bolted to titanium inserts embedded in the vertical glass fins. The structural system is designed to resist seismic actions and to accommodate the displacement of the main structure under an earthquake scenario. The stability to lateral buckling and under seismic loads is guaranteed by a system of cables and rods which transmits the in-plane forces to the main structure. The stability to lateral buckling and under seismic loads is guaranteed by a system of cables and rods which transmits the in-plane forces to the main structure. The post-breakage behaviour of the multilaminated heat-strengthened glass panels and the design of the façade guarantee the stability even under very aggressive accidental scenarios.

The adhesion between the embedded metal connections and glass depends strongly on the fabrication tolerances, in terms of perimetral dimensions and thickness. The glass fins with embedded titanium connections were verified in terms of strength by means of detailed numerical simulation of the insert zone. Due to the existence of the embedded connection, the stress concentrations on glass around the notch of the inner panels were dimensioning (Figure 1).

The stability of the glass fins was checked by means of the so-called non-linear buckling analysis and a stability checks based on

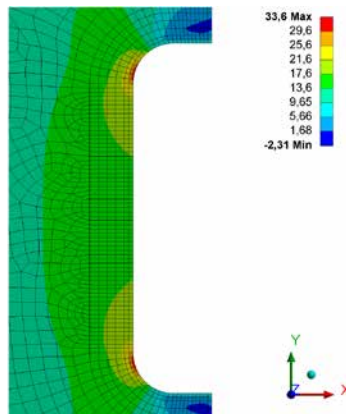


Figure 1. Maximum principal glass stress on inner glass panels [MPa]

Eurocodes. In the second method, the critical buckling load was calculated with a rectangular and monolithic shell model. The numerical analyses were completed with pull-out tests at room temperature of aged specimens in order to determine the resistance of the adhesive connections (Figure 2). All samples have shown delaminations along the edges of the inserts. None of these delaminations are relevant in terms of the resistance of the embedded connection because they appeared inside the zones already considered unbonded in the numerical simulations. In the specimens in which the glass failure was produced before the bolts collapse, the crack origin was located around the curved edge of the inner panels as predicted by the numerical simulations. A full-scale glass fin was submitted to a three-point bending test to validate the design. The glass fin was loaded until the first crack above 2xULS. The crack was produced around the embedded connection located near the mid-span of the glass fin (Figure 3). After the first crack, the in-plane force was increased again until ULS loading. Although, the crack grew significantly, the glass fin showed a very good post-breakage stability without any sign of collapse. The construction of the façades of the new Medical School of Montpellier started on February 2016. After erecting the steelwork, the glass fins were installed successfully between May and November 2016, with a maximum installation rate of 4 fins per day. The works were finished by February 2017 (Figure 4).



Figure 2. Pull-out test setup

## Acknowledgments

The authors would like to thank François Fontès and the team of Fontès Architecture. In addition, the CSTB and SOCOTEC teams, specifically Mrs. Orand and Mr. Valem. Also, we would like to thank the glass supplier, Sedak GmbH. Finally, the authors would like to thank the team of Bellapart: R.Brugués, L.Estupiña, P.Guerold, M.Millastre, J.F. Portal, J. Pereira and G. Robert, which have been working hard in this project.



Figure 3. Glass fin after the first failure

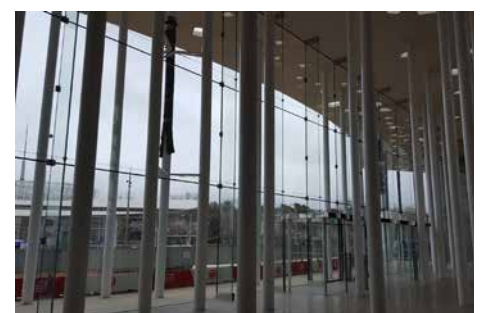


Figure 4. Main façade almost finished

# Structural Glass in Building Restoration. Europe's Tower Entrance Hall. Madrid. Spain

Miguel Angel Nuñez Diaz  
ENAR. Architectural Envelopes

Jesús M. Cerezo Miguel  
ENAR. Architectural Envelopes

## Keywords

1= Refurbishment 2=Structural Glass  
3= Sentryglass

## Abstract

Currently in Spain the building's restoration is world of rehabilitation of office buildings is at boiling point. Many of these restorations are made to adapt the building to legislation and to implement improvements in energy efficiency, but also to give them a new exterior image. This new image intends to be present and with a technological design without great design performances.

In this new image, use of structural glass is a perfect idea because it involves a minimal intervention with little visual impact, and current and technological elements.

This is the case of the new hall Torre Europa in Madrid that shows as a free dihedral glass composed of mullions 10 m high on which a horizontal beam glass stabilizes the assembly is arranged, and which transmits the loads the main building structure.

The enclosure is made with laminated glass full height and 3 m wide which are stabilized by metal inserts to the mullions themselves, having revolving doors of access 5.50 m high. At the top as closing a skylight glass composed of 12 m long x 1.50 m wide is available.

The project is owned by INFINORSA, and was conducted by the British architects RTKL with the Spanish study LKS. The facade has been consulting by ENAR and the project has been awarded for construction Bellapart.

## Introduction

In Madrid North's area, there is an area called AZCA, created in the 70's of last century, where the financial center of the city is located. In this area, many of Madrid's office buildings have been built since then. Nowadays, other business areas have been built, but this area is still the most valued and emblematic for this type of office, where are among other buildings like the Picasso Tower of Yamsaki and the

BBVA Tower of Sáinz de Oiza.

The existing buildings in this area date from the same period between the 70s and 80s of the last century, and therefore these buildings need to carry out an update, in terms of benefits, regulations and image. This is the case of the Torre Europa Building.

Torre Europa is an emblematic building of this area of Madrid, located at the corner of the AZCA complex right in front of the Santiago Bernabeu stadium, with the facade in the Paseo de la Castellana. The building is a tower of 121 m of height built by the architect Miguel Oriol and Ybarra between years 1975 and 1985, property at present of the company Infinorsa. The property has decided to make a complete rehabilitation of the building, including interior works, changing the air conditioning systems and eliminating the interior fancoils so that the glass is liberated from floor to ceiling, and also on the outside to give the building a new image more technological and current, according to the new times. For this reason, Infinorsa has counted with the team of English architects RTKL, along with the collaboration of the Spanish study LKS.

## General description of the refurbishment

The current building has a spiral-shaped plant with a central core in which are the vertical communication and the general services, leaving the rest of the plant without other elements. The structural system proposed also contributes to this idea, since it has no intermediate pillars inside the office, the structural elements being centered in the central core and in the perimeter, outside the building. The pillars are prefabricated elements of Steel reinforced concrete. The pillars award a very characteristic image to the building in Madrid.

In the lower part an Access hall is situated tangent to the building, as an element added to the own building. This vestibule consists of a fully glazed element with vaulted elements and glass roof, made with an aluminum curtain wall system over steel structure. The exterior glasses are very darks with very little transparency, giving the building an old image that is inconsistent with the new Actual trends. The facade proposal made by the architecture study, RTKL, focuses on two main actions:

- Access update. The absolute remodeling of

the access hall is proposed, incorporating in addition an upper canopy of metallic structure that will be situated in the outside perimeter of the building.

- Pillar cladding. It is planned to update the building's image by placing a textured stainless steel exterior over the prefabricated concrete pillars and the emergency staircase of the building.
- In this article we will focus on the upgrade of the entrance hall of the building.

## Description of the design

The refurbishment of Hall access involves the complete demolition of existing access for the construction of a new lobby with greater transparency and a more current and technological aspect. To get this new image, the architect choose a solution in structural glass, without other structure.

The access is made under a canopy of metallic structure that unifies the lower area of the main facade of the building, this canopy is supported in an area supported by pillars on the ground floor, while in another area there are hanged on the building to free the bottom zone from pillars.

The entrance hall is situated in the area closest to the building and it is attached to it to allow its enclosure as shows figure 1. The hall is closed at the top by a skylight that is supported on the metal structure of the canopy, and on its vertical facades by structural glass enclosures supported on the ground floor slab, independently.

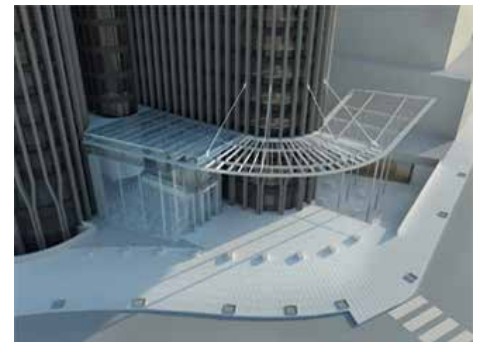


Figure 1 Exterior image of the project

The access is located in the north facade of the hall with two revolving doors of great dimensions that are included in the own facade.

At the bottom of the east facade, to the area of Paseo de la Castellana, there will be a sheet of water inside and outside the building that will allow the reflection of the building itself and the facade itself, dematerializing the support of the same.

In the transition with the existing building, and between the vertical facades and the upper skylight, ventilation louvres are introduced in case of fire to guarantee the evacuation of smoke from the hall because it is an escape way.

This zone of louvres is set back from the rest of the façades, so that the facades will be more exposed to the exterior, simulating a perfect glass cube, vertical facades and horizontal enclosure. The vertical glass is 10 m high below the upper roof of the canopy, which rises 1.50 m above, leaving in the middle the zone of louvres. The façade will have a dimension of approximately 11.00 m wide by 10.00 m high, divided into 3,00 m wide glass with corner glass of approximately 1.20 m.

The revolving access doors are integrated into the exterior facades, ie in the area of the glass cube, with a height of 5.50 m and a diameter of 3.00 m, with two side doors that will allow the evacuation of the building.

## Structural Behaviour

The proposed structural behaviour for access aims to separate the movements of the building and the canopy from the movements of the ground floor and access, to avoid possible differential movements between the two elements. In this way, the vertical enclosure of the access must be self-supporting and stable, transmitting the reactions to the ground floor and punctually to the building but without assuming the movements of it.

The upper part of the vestibule, that is to say the cover and the zone of louvres will depend structurally of the canopy, and therefore of the building, whereas the zone of the facades will depend on the slab of ground floor, taking in the strip of louvres the necessary expansion joint between both systems.

## Roof Area

The roof area must support both wind stresses that collect the façade of the main building and throws towards the bottom and snow loads and maintenance overloads.

The roof is supported on a framework of lacquered steel beams, as a continuation of the outer canopy. The framework is composed of two main longitudinal beams parallel to the main facade of the building, on which transverse beams are arranged every 3,00 m approximately. The main beams are supported

on pillars on the ground floor of the building and on the first floor slabs of the Tower itself. A structure of glass beams is located at the top of each piece of steel beams on the upper part of the beams is provided every 1.50 m, which always is supported on the longitudinal beams, whether or not they coincide with the steel cross beams of the main structure. These beams have a span between supports variable of approximately 7.00 m, and with variable cantilever from 1.50 to 2.00 m in length, with a maximum dimension of beams of 12.00 m on its side longer.

The beams have trapezoidal shape to give slope to the skylight and allow the water to be evacuated, so that the lower part is horizontal coincident with the main metal structure of the canopy and the top have the necessary inclination.

The anchors will allow the expansion and movement of the beams, without constraints, avoiding the vertical displacement in both pressure and suction, and will have elements of stiffening to avoid the movements perpendicular to the beam itself to achieve the general bracing of the skylight.

Over the glass beams will be placed the glasses of horizontal roof, which will be double glazing that will work supported on the previous ones.

The skylight extends outwards, outside the vertical walls, with a canopy over the access area. In this area the structural solution is the same as in the interior zone, but a cantilevered glass will be provided from the last perpendicular beam, being continuous with the previous glass.

From the metal structure of the upper part of the canopy a light steel structure is lifted to support the area of exutorios, which also hangs from the upper part.

## Lower Cube area

The area of the cube must support wind loads in the vertical walls, in addition to the horizontal live loads.

In this area structural glass is used, all the facades and the horizontal trim element will be made of glass without any other type of main structure.

The lower part consists of a trihedron composed of the two vertical facades, with the upper horizontal element, which is supported directly on the lower floor of the ground floor. The vertical walls have vertical stiffening glass fins that also support the horizontal stresses of glass located in the joints between glasses every 3.00 m.

Both vertical faces and glass fins are embedded in the lower part, while in the upper part they are stabilized together by a horizontal "L" shaped beam that joins and stiffens both

square facades, forming the self-supporting trihedron. All the set that stabilized to the main building by two points in the corner of the trihedron, that transfer the efforts to the main building.

The horizontal beam is attached to both the vertical glass fins and the vertical glass, and in the corner between both facades. At the two ends of the cube a larger dimension glass fin is arranged as a closure of the assembly that reaches the inside part of the louvres. This beam has a steel element in its interior that gives it vertical inertia to avoid the vertical deformation of the horizontal element, as well as to achieve the transfer of shear in the area of attachment and in case of breakage of any of the sections.

These points of fixing to the building are made up with a cantilevered beam to support the horizontal stresses, with a pillar supporting the weight of the beam itself, and which helps to support the vertical enclosure of louvres side walls.

In the area of the doors, in addition to the supporting structure of glass are added stainless steel frames to support the upper windows and the transmission of stress through the doors' holes.

## Calculation Made

The calculation justification for the different elements is done from different scenarios:

- Overall operating model
- Timely model of the elements separately
- Detail model of fastening elements.

In these scenarios it is necessary to take into account the hypothesis of the breakage of some of the elements to avoid the collapse of the structure, to take into account these criteria in the constructive solution to be developed.

The overall model is made by a bar system, verifying that both tensions and compressions are below the admissible values of the glass (according to pr UNE EN 16612), and the overall deformations of the assembly are checked to check the structural viability.

The calculation of the main elements is done by a program of finite elements specialized in glass to be able to guarantee the union between the different materials.

The detail models are also made with a finite element program to guarantee the minimum dimensions of the elements to be realized.

This third part will be developed later by the contractor hired to carry out the work, in this case Bellapart, which will also provide possible solutions to the problems encountered.

## Proposed construction solution Superior Zone. Skylight

The area of the upper skylight is solved with laminated glass beams 10.10.10 mm with a stainless steel plate glued on its upper part on which a standard skylight head with its EPDM rubbers is arranged which will guarantee the operation and the sealing of the system. A double continuous glazing throughout its length is made up of an outer tempered glass of 10 mm with greater resistance to withstand hail or falling elements and an inner laminated safety glass 6 + 6 mm fall, all of them are low iron to avoid the green color of the glasses. The fixing of the glasses is done by means of a stainless steel outer cover. The evacuation of water is done towards the area of the building, where a continuous gutter is arranged which coordinates with the drainage of the building itself.

In the lower part of the skylight there is a strip of louvres that Works in case of fire. These louvres have an approximately 1,50 m in height, coinciding with the actual cutting of the roof. The louvres will be of pivoting glass slats and will have motorization hidden in the vertical uprights of fixation. The louvres will be laminated glass 5 + 5 mm without elements between joints between louvres to guarantee a greater transparency of the enclosure.

## Bottom area. Glass Cube

The vertical glass is made with 12 + 12 + 12 mm monolithic laminated glass laminated with SGP to provide the assembly with greater stiffness and greater post-break safety. These glasses are embedded in the lower part with stainless steel anchors, which must also be compatible with the waterproofing trim and bottom water sheet.

The inner glass fins will also be embedded in their lower part on anchors of galvanized steel with three-dimensional regulation as shows figure 2. The fixing between the glass fins and the anchors is made by stainless steel screws with inner bush. To guarantee the position of the holes, a resin with characteristics of strength and hardness higher than the glass itself will be used.



Figure 2 Bottom detail

The connection between the inner vertical glass vertical and the vertical glass is done by Titanium elements laminated with the glass itself thanks to the use of the SGP. The connection is made by inner clips that are introduced through the joint between glasses as shows the figure 3. In the corner glasses also a connection between the glass of the enclosure and the lateral glass fin with screwed fasteners is made, in addition to using structural silicone glue strings.

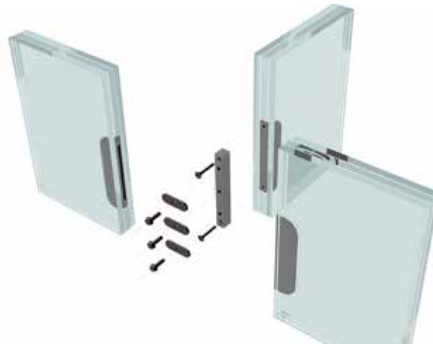


Figure 3 Intermediate connection

The upper joint of the glass fins with the horizontal top glass beam is also made with titanium inserts on both sides and then with countersunk screws, all without external elements to guarantee the watertightness of the assembly in the horizontal part as shows figure 4.



Figure 4 Upper joint

The upper horizontal element will have a horizontal continuity profile of stainless steel that is screwed to the different glasses to achieve the transfer of the efforts between them, as well as stabilizing element with the own building. This element will be able to support the tensions created by this beam in case of breakage of some section of the beam, as well as connecting element for the replacement of glasses separately. On the other hand, this element serves as flexible

connection between the lower part of the hub and the top cover.

In the access area, the doors of the building are arranged, which will also be fixed on the inner structural glass fins, supported on the stainless steel frames in the same way, through the joints between glass and elements.

## Solution to build. Problems of refurbishment

For the execution of the project has been contracted the company facade Bellapart, which has begun the development of its own construction project as an evolution of the architectural project delivered. The project carried out by Bellapart respects the design and structural criteria set out in the submitted project, but makes a series of changes to improve its implementation and to adapt to its philosophy of work.

Additionally, in the beginning of the work, since it is a refurbishment, it has been discovered that there are elements in the building that do not correspond to the elements expected in the architectural project, such as that the ground floor slab does not have the Resistance required and the execution of reinforcements is necessary.

For all this, a series of changes have been made in the project, approved by all parties for its correct execution.

## Conclusions

As main conclusions after the realization of the project of rehabilitation with structural glass we can obtain the following conclusions:

- Structural glass can be an important design element in the rehabilitation, since it throws a novel and technological image, according to the required changes of image.
- The transparency and low presence of structural glass elements as a restoration enclosure, lead to an easy coexistence between them and existing buildings.
- Rehabilitation works have a high degree of uncertainty that can change the criteria at the beginning of the work.

## Acknowledgements

INFINORSA. Owner  
RTKL & LKS. Architect Office  
BOVIS. Project Manager  
BELLAPART. Contractor

# Cost and Energy Saving Potential of Glass Façade Construction

Timo Saukko  
Finnglass Oy

## Keywords

1=Electrically heated glass 2=Cost savings glass façade construction 3=Energy savings glass façade

## Abstract

There is remarkable temperature difference between glass surface and indoor air when temperature is normal winter day temperature in Nordic Countries. Cold surface makes cold wall effect and cold air natural convection. With glass facades in cold climates traditionally has been used radiators or fan coils to improve winter time indoor conditions. Besides of current solutions, there are no guaranteed solution to prevent coldness and cold draught inside building.

Fan coils and radiators heat façade up to 55°C during cold winter day. This makes heat loss double compared to system where glass surface temperature is heated with electricity to room temperature 21°C. Remarkable energy can be saved by using electrically heatable glass in facades in Nordic climate conditions. Radiators and fan coils needs space from floor area which is very costly and fan coils/ radiators needs investment. Glass facades in cold climates can be made remarkable lower costs with electrically heatable glass. Pure façade purchase cost with electrically heatable glass is more expensive than façade without heatable glass, when only pure façade costs are compared. When also necessary compensative HVAC system and space savings are taken account, huge savings can be reached. Savings from reduced floor space and savings coming from missing fan coils / radiators will make electrically heated glass façade superior compared to non-active glass façade. Total saving from this new façade can be up to 50%.

Energy aspect and traditional solutions Traditionally there have been used fan coils or radiators in a front of glass façade to prevent cold draught and cold wall effect. Radiators are used mostly for the preventing cold draught and heating. In cold winter day even 55°C hot water is feed to radiator. This means that radiator surface is hot accordingly and heats air. So even 50°C hot air is fed against glass façade. This will double heat loss through glass façade on this area /1/.

Fan coils are used for preventing cold wall effect, heating and cooling depending weather and indoor conditions. If it is used for preventing cold wall effect and heating, then even 55°C hot air is blown against façade glass surface. This means that heat loss is double compared to situation that glass surface is heated to room temperature.

Case where fan coils are used for building cooling is not always perfect solution due to fact that modern solar control glass and low-iron glasses are not heavily absorbing heat. By blowing cold air it is impossible to stop heat radiation coming from sun. As modern glasses are not absorbing heat façade cooling just increases energy consumption of the cooling. The more façade is cooled, the more heat is coming in due to bigger temperature difference between outside and inside.

Energy aspect and electrically heated glass Electrically heated glass can be used to compensate heat loss through facades. Inner glass surface is heated to room temperature by using small electrical current. Even 20-30W/m<sup>2</sup> is enough to compensate heat loss through glass façade /i/. Glass surface temperature is controlled with sensor and thermostat. Heat is produced uniformly in whole glass area and then temperature differences are minimized. As glass surface is heated to room temperature, there will not be any thermal difference between glass surface temperature and room temperature. Therefore there are no temperature asymmetries in winter and neither cold draught. Glass surface is heated

just to room temperature and this brings energy savings compared to fan coils and radiators. Important factor is that by using electrically heated glass building can be constructed smaller with same utilities. This bring additional saving due that there are less cubic meters to be heated.

Construction costs of fan coils and radiators vs. electrically heated glass Big public building costs easily 10 000Eur/m<sup>2</sup> in Nordic countries. Cost of fan coils without installations are 1500-4000Eur/m. With fan coils normally 0,5-1,0m bottom area is lost in front of glass façade. Cost of radiators purchase is not handled separately. Additional cost of electrically heated glass in façade is estimated 200Eur/m<sup>2</sup> compared to non heated insulating glass. It can be seen from table 1. that as huge floor area can be saved, then also huge cost saving can be achieved. In any case initial investment cost saving is in 5 m height glass façade 70% compared to fan coils. Biggest saving is coming from floor area reduction with same functionality of the building.

## Summary

Electrically heated glass increases façade construction cost 200Eur/m<sup>2</sup> (per façade square meter). As building is planned in the beginning so that electrically heated glass is used, then impact of glass façade cost to total building construction costs can be reduced minimum 70% compared to traditional solutions. Biggest saving is coming from floor area reduction with same functionality. Second biggest saving is coming from device investment costs. Also energy consumption of the building can be reduced by using electrically heated glass.

| Investment cost (Eur/m)   |           | Cost of floor area (Eur) | Total investment cost (Eur) |
|---------------------------|-----------|--------------------------|-----------------------------|
| Electrically heated glass | 1000      | 0                        | 1000                        |
| Fan coils                 | 1500-4000 | 1500-10000               | 3000-14000                  |

Table 1. Comparison of investment cost, including devices and floor area, when glass façade height is 5m. Installation costs are excluded.

# Shaping ultra-thin glass

Sophie Pennetier  
Mark Bowers  
Guillaume Evain  
Arup  
BIG Architects

## Keywords

1 = Ultra-thin glass, 2 = Cold bent glass,  
3 = Sculpture

## Abstract

Ultra-thin glass is neither a new product nor new to the building environment. It is yet very little utilized in translucent facades for stiffness, detailing and cost reasons. This paper describes the elaboration of a cold bent ultra-thin glass sculpture, from concept to procurement, with explorations worth the eye of the façade designers. The design tools, FE analysis and testing procedure and fabrication of the glass elements are documented.

## 1 Introduction

In the building environment, transportation, household or artistic applications, glass is generally formed by slumping process, at temperatures exceeding 600 deg.C. The works described herein are based on the elastic deformation of the glass, which means that the glass is shaped without the use of heat but only by application of a sustained loading. This engages the glass structurally, not only as a rigid body transferring load like in the audacious Serres de la Villette by Peter Rice and RFR but where the glass compounds are subject to permanent internal bending forces like in other project RFR projects, such as the Avignon and Strasbourg railway stations. The present work, of a much smaller scale, is

a sculpture made of cold bent 200 µm glass strips, where the stability and the rigidity of the system is ensured by the internal bending forces of the glass, locked into the strips connected to one another. The sculpture measures 750mm by 750mm on plan and 700mm in height. This project demonstrates how an iterative analysis of the geometry and the internal forces can result into a rigid free form system, a process that is scalable to the built environment.

The use of thin glass in the built environment has many advantages. A stiff and thin glass façade system allows for the reduction of the glass weight supported by the superstructure, impacting transportation costs and energy demands as a result. The durability of glass in a chemical or corrosive environment and to UV is an asset, it is scratch resistant and hermetic, compared to other thin materials such as polycarbonate or ETFE, and ultimately the optical clarity of the glass is unequalled. Until now, thin glass products such as Corning Gorilla and Willow glass are used in the building environment within a laminate compound, mainly for interior flat applications such as wall cladding (Corning Inc, 2016). This article presents the fundamentals of glass cold bending, the properties of the thin glass product used for the project, the elaboration of the geometry, the structural analysis and the fabrication.

## 2 Cold bent glass

Cold bending a glass element consists of deforming it elastically, without the use of heat. Maintaining the bending force is required to keep the curvature of the glass element. The geometry resulting from the elastic deformation of flat elements is called a

developable surface. This requires no distortion of the original flat element, as discussed in further detail in chapter 4.

Cold bending is particularly interesting in the built environment for the reason that it does not require any heating process. The bending process can occur in factory or on site, at virtually at any ambient temperature.

The façades of several architectural projects comport cold bent glass panels, such as the Avignon train station in France or the IAC Headquarters in New York (respectively Figure 1 and Figure 2). For these two projects, glass sheets were assembled in Insulated Glass Units (IGU) and the limiting component wasn't the glass itself but the shear of the primary seal of the IGU. This limitation lead to larger curvature radii than the one the glass sheets alone could sustain. Here the geometry allows to keep each strip in place and the structure stable only because of to the connection to the adjacent glass pieces.

Glass warm bending – also called two step bending, cold-lamination bending, lamination bending – consists of piling up sheets of glass and interlayer(s), bending the stack onto a support jig and then laminating it in autoclave. When the initial bending force is removed and the laminate removed from the jig, the shear in the interlayer prevents the assembly from completely flattening. The use of the term warm for this fabrication process derives from the fact that the lamination process requires to heat up the compound to ensure the adhesion of the interlayer to the glass. The lamination temperature, which depends on the interlayer material and pressure is approximately 80 to 140 deg.C which which is well below the softening temperature of glass, which exceeds 600 deg.C. Given the relative softness of certain interlayers, the glass laminate may partially



Figure 1,2,3 – Cold bent glass architectural projects precedents (left to right) : Strasbourg Railway station (2011, AREP+Dutilleul)  
IAC Headquarters (2007, Gehry architects) Strasbourg Railway station (2007, AREP+Dutilleul)

spring back. (Knippers, Filduth, Badassini, Pennetier, 2014) propose a time history study of warm bent laminates.

The glass panels of the Strasbourg train station have been curved using this process (Figure 3).

### 3 Ultra-thin glass

Architectural glass sheets in facades range in thicknesses between 2 and 22 mm. Thin glass refers to 2 to 6mm thickness and ultra-thin is proposed for smaller thicknesses, from of 25  $\mu\text{m}$  to 2mm excluded.

Whereas most of the architectural glass for facades is soda-lime glass produced on a float line, thinner glass products such as Corning's Gorilla Glass and Willow Glass and AGC's Leoflex have a different chemical composition and different fabrication process.

Gorilla glass is composed of aluminosilicate.

It is produced in thickness ranging from 0.2 to 0.7mm by a proprietary fusion-draw process. Gorilla is then chemically tempered in potassium chloride, which provides a surface compression stress preventing crack propagation.

Willow glass, used for the project discussed herein, is an alkali-free boroaluminosilicate glass (Corning Inc, 2016). It is fabricated by a proprietary overflow process (Corning Inc, 2016). In this process, the glass in fusion overflow out of a gutter on both sides down and fuses at the bottom point of the gutter (see Figure 4).

Unlike Gorilla glass, Willow glass is not chemically tempered and present a breakage pattern similar to the one of annealed glass, shattering in long thin pieces. Willow glass is named after the shape of the overflow used during the fabrication.

Willow glass is produced in sheets up to 1100 by 1200mm or spools of 1300mm wide, 300 meter long. The minimum bend radius, depending on handling and surface weathering, is 90mm for the 100  $\mu\text{m}$  nominal thickness and 180mm for the 200  $\mu\text{m}$  nominal thickness (Corning Inc, 2016).

Combining these bending radii to the bending charts provided by Corning (Corning inc, 2016) a design value of 40 MPa was extrapolated and retained for the design of the sculpture. In the built environment, material reduction factors should be used, concomitantly with reduction factors associated with (for example but not limited to) shape, size, load duration.

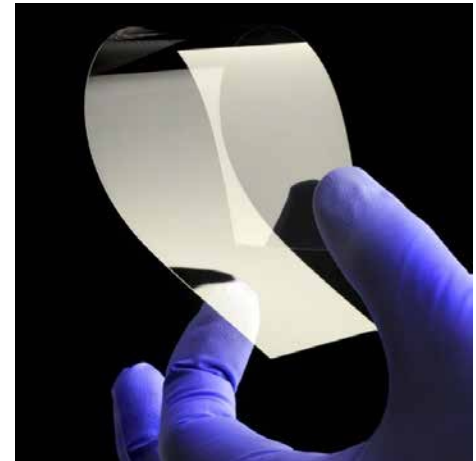


Figure 4,5,6 – Left to right: Corning proprietary fusion-draw process, Willow pattern and Willow glass

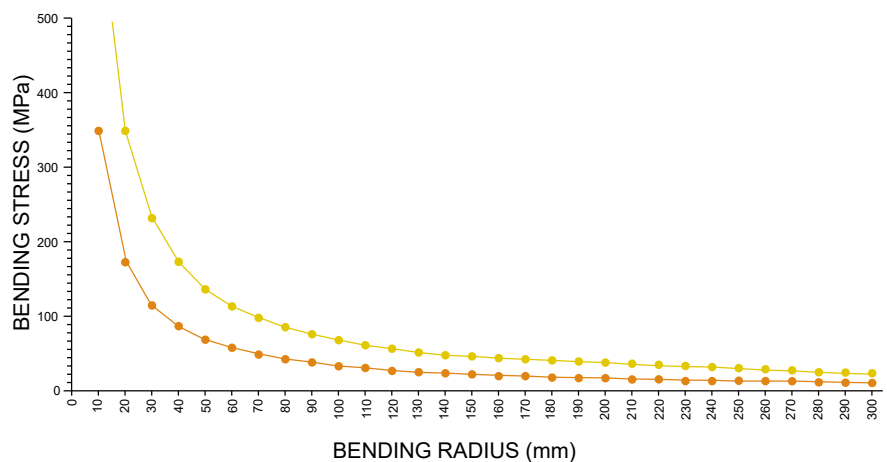


Figure 7 – Bending stress of Willow glass

## 4 Geometry

The deformation of inextensible flat sheets results in a developable surface. It is a specific case of ruled surface, which does not only apply to inextensible materials. For example, a hyperbolic paraboloid is a ruled surface which can be built from the translation in space of straight lines, it can be built with extensible nylon fabric but not from paper.

Developable surfaces comprise of cylinders, cones and tangent surfaces of spaces curves (Pottman and al) as shown in Figure 8. Conical shapes are ordinarily described by a planar curve and apex point. In the context of this sculpture, we used a variation of conical shapes defined by a space curve and apex point for each of the elements constituent of the geometry.

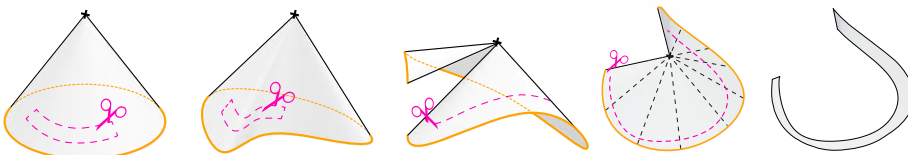


Figure 8 – Trims of developable surfaces

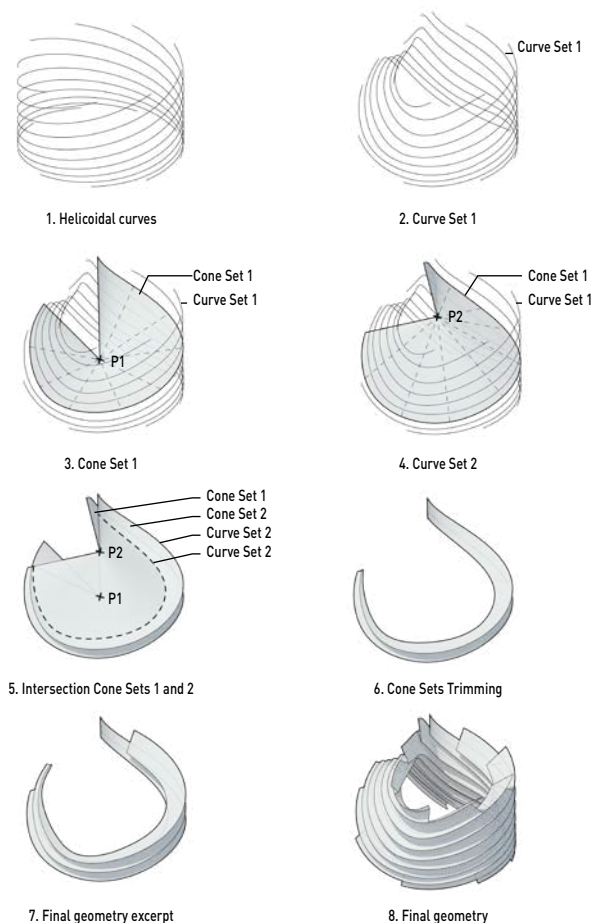


Figure 9 – Geometric principles

Figure 9 illustrates each step through the generation of the geometry for this project. At first, a set of helicoidal curves were created and distorted smoothly to create desired guide curves (Curve Set 1). The resulting curves are free form and do not comply with any geometrical rule, apart from the fact that they need to not overlap.

A first set of cones (Cone Set 1) was generated from each curve to an apex point P1 placed within the helicoidal set of curves (Curved Set 1). A second set of cones (Cone Set 2) was generated from each curve to an apex point P2 located above P1 so that every adjacent surface intersects each other. The Curve set 2 is defined by the intersection of the two sets of cones. Lastly, the two cone sets were trimmed by the Curve Set 2, creating the final developable surfaces used for the sculpture. A parametric model allowed the fine tuning of the geometry in order to control the local radius of curvature.

## 5 Analysis

This project being a sculpture, it was at firstly analyzed to sustain gravitational and bending forces.

An iterative process involving the round trip between maximum bending stresses assessment and the geometry adjustment was performed in a 3D modeling software packages (Rhino and Grasshopper). Since each strip is in pure bending, the principal curvature and bending stress can be derived from Eq. 1 and Eq. 2 below.

$$M = EI/R \text{ (Eq.1)}$$

$$s = Et/2R \text{ (Eq.2)}$$

With E : Young's modulus of elasticity (N/mm<sup>2</sup>)

I : Moment of inertia (mm<sup>4</sup>)

R : Curvature radius (mm)

t : Glass thickness (mm)

Figure 10 shows a mapping of the principal curvature along one strip of glass.

When required, the construction points and generative curves of the strips geometry were adjusted in order to maintain a maximum stress of 35 MPa. This value, which is smaller than the allowable stress extrapolated in chapter 3, was arbitrarily set for the first iterative process, allowing additional reserve capacity for the effects gravity loading and potential buckling effects. Ultimately, the FE analysis proved that the effect of gravity was negligible for this specific geometry, scale and glass thickness.

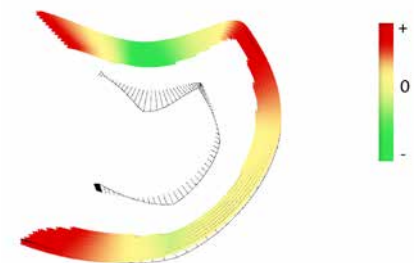


Figure 10 – Principal curvature mapping (only one strip shown for clarity)

After the parametric study has been performed, the strips were flattened and imported into a finite element analysis software (Strand7). For the analysis, a Young's modulus of elasticity of 75 GPa and a Poisson's ratio of 0.225 were used. Each strip was composed of approx. 200 plate elements of max. 20mm width. The thickness of the material was 200 μm. The model totaled 2560 plate elements. Each strip was initially flat and tied by links to the nodes of its final position (see Figure 11). A staged non-linear static analysis was then used to deform gradually the strips while the bending stress increase was monitored.

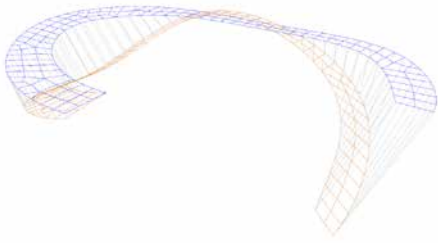


Figure 11 – Links used for imposing displacement on mesh nodes from flat (above) to bent (below)

Figure 12 shows the analysis steps. The glass strips are imported as flat geometry in the FE Analysis environment and shrink links pull them into position. At the last stage, when the glass strips are cold bent into position, adjacent nodes at the ridges are coupled together by stiff spring links and the load redistributes between the glass elements. The maximum stresses under bending case and after assigning gravity to the structure were below the maximum allowable stresses, with maximum at supports locations.

## 6 Models

For the fabrication, the 3D geometry was flattened and laid out on sheets. Two study models were built prior to the final construction of the sculpture. A desk model and a full-scale model. Figure 13 shows the fabrication steps of a scaled model made of 0.5mm thick PETG plastic strips and assembled by hand with tape. The first plastic scaled model, an assembly 130 x 130 in plan by 100mm high assembly of 20mm large strips, served as communication tool and a first proof of the fabrication sequence.

The second full scale model was fabricated with 1mm PETG foils. It was used as a template for the adjustment of the supports and jigs used for the glass sculpture. The full scale fabrication sequence was validated with this model. The connection detailing and assembly are not discussed herein.

## 7 Glass cutting process

The glass elements were provided and CNC cut by Coresix Inc, based in Virginia (USA). The fabrication pictures show in order: unrolling the Willow glass spool, the CNC cutting operation, strips cuts for testing and calibration of the tooling (the microscopic evaluation is not pictured), the breaking out of the final pieces, the final C shaped pieces and one piece bent by an operator. The cutting process used to cut the glass pieces is called scribe and break. It is a similar process to standard glass cutting, despite the

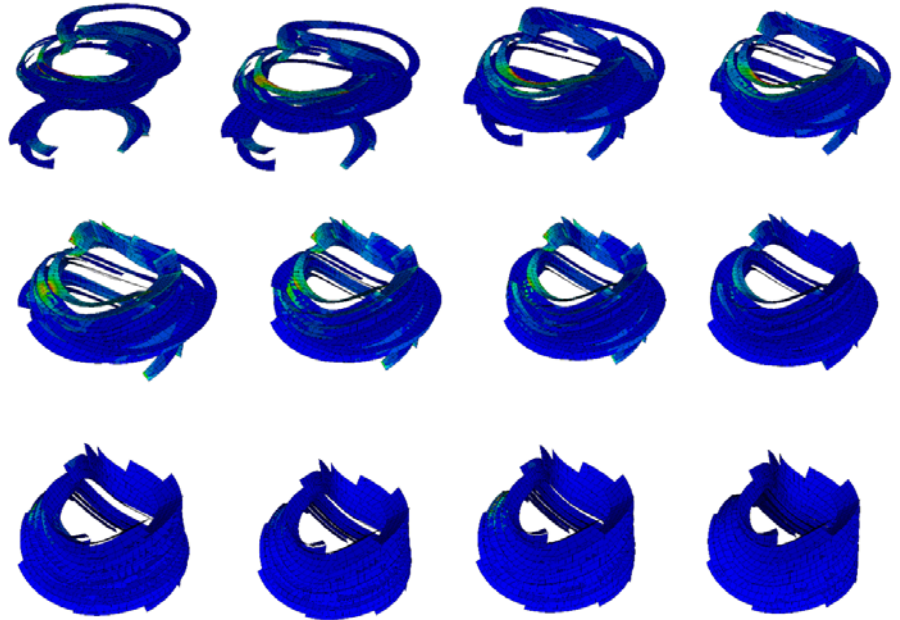


Figure 12 – Staged analysis



Figure 13 – PETG model fabrication



Figure 14 – PETG model

small thickness of the glass. The scribing is performed by rolling a small diamond wheel on the glass creating a small crack, or vent. Then the sheet of glass is handled by an operator which breaks it at the location of the vent. This process can be used for pieces of a couple millimeter overall size.

## 7 Conclusion

At the time of the publication of this article, the connection detail connecting the glass pieces is still under testing consideration. The design, fabrication and manipulation of the glass elements for the sculpture is a proof of concept of the design process for ultra-thin cold bending to form a small structure with tight curvature for both base flat shape cuts and bending radii. Given its relatively small size and the fact that, as a sculpture, it is not designed to resist climatic or seismic loads, the current design comports assumptions which does not make it directly scalable. The final geometry, the thickness of the glass, the connections between strips and to the ground will need to be re-evaluated.

However, it is obvious to the practitioners that the geometrical rules, the geometry to finite element analysis workflow and curved cuts fabrication knowledge capitalized on this project can be used for larger scale.

This work was supported by the 2016 Fellowship from the Metropolitan Contemporary Glass Group, Urban Glass Brooklyn and Arup.

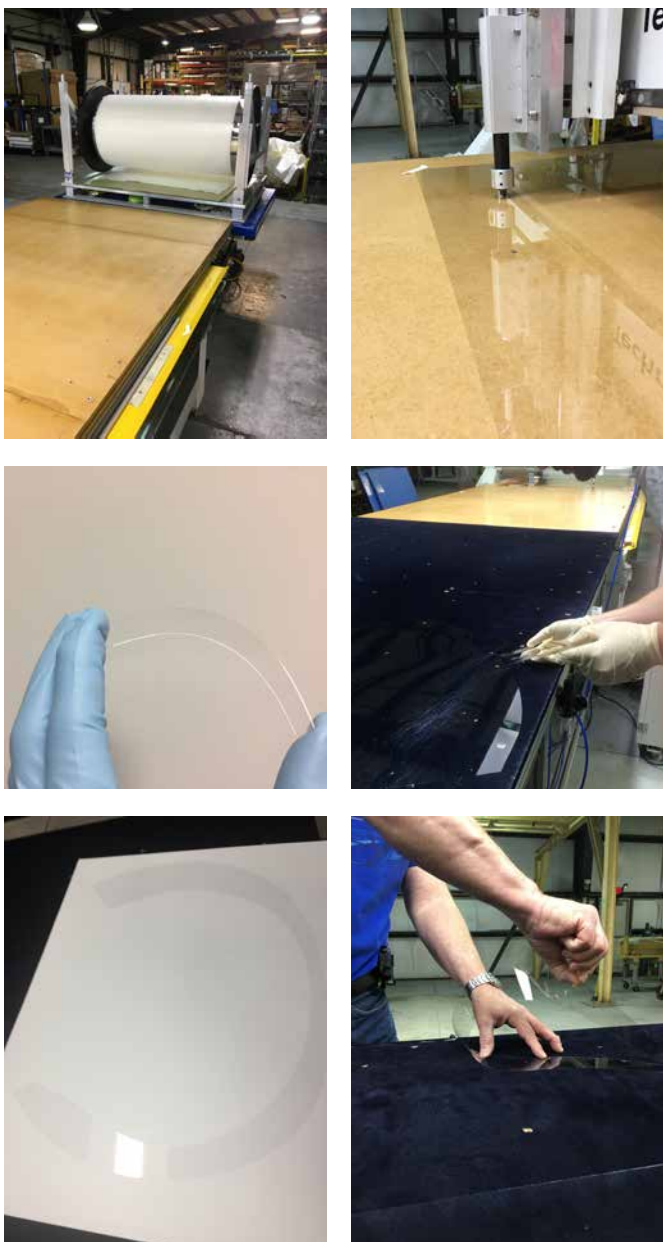


Figure 15 – Glass sculpture fabrication images

## Acknowledgments

The authors would like to thank Corning Inc for their technical support and Coresix Inc for providing and cutting the glass.

This work is supported by the 2016 Jerry Raphael Fellowship from the Metropolitan Contemporary Glass Group and by Arup liA# 13618 - Use of thin glass in the built environment.

## Conflict of interest statement

On behalf of all authors, the corresponding author states that there is no conflict of interest.

## References

- Corning Inc: Willow Glass Fact Sheet [https://www.corning.com/media/worldwide/cdt/documents/Willow\\_2014\\_fact\\_sheet.pdf](https://www.corning.com/media/worldwide/cdt/documents/Willow_2014_fact_sheet.pdf) (accessed on 13/02/2017)
- Corning Willow Glass Laminates website <https://www.corning.com/worldwide/en/innovation/corning-emerging-innovations/corning-willow-glass.html> (accessed on 13/02/2017)
- Neugebauer, J.: Determination of Bending Tensile Strength of Thin Glass. *Challenging Glass 5* (2016)
- T. Fildhuth, J. Knippers, F. Bindji-Odzili, N. Baldassini, S. Pennetier: Recovery behaviour of laminated cold bent glass – Numerical analysis and testing. *Challenging Glass 4* (2014)
- H. Pottmann, A. Asperl, M. Hofer, A. Kilian: *Architectural Geometry* (2007)



Figure 16 – Final sculpture rendering image

# Probabilistic Study of Wind-temperature Interaction: an Initial Study Towards Optimized Structural Assessment of Glass Components

Manuel Santarsiero<sup>1</sup>, PhD, Ing., MEng, BEng.  
Eckersley O'Callaghan

## Keywords

1=Structural performance assessment  
2=Probabilistic study 3=Wind 4=Temperature

## Abstract

The structural assessment of laminated components over the entire design life is rather complex, especially if compared to mainstream construction materials. This is because the structural performance of laminated components strongly depends on several parameters, such as temperature. However, limited guidance is provided by code and standards on the relevant boundary conditions to be considered for each relevant scenario. This work presents a study on a probabilistic approach for the structural assessment of laminated components. More in detail, the interaction between maximum wind and glass temperature is analysed by means of probabilistic methods. The results show that historical data exhibits a stochastic behaviour characterized by a variable variance as a function of multiple dimensions. It is also shown that probabilistic models need to be used to perform realistic safety assessment over the design life of the components.

## Introduction and motivations

The last decades of architecture have been characterized by a large demand for transparency. This trend has led to a significant advancement in glass technology and to a large use of structural components made of glass. Columns, fins, beams, and large load-bearing panels made of laminated glass are no longer exceptions, with dimensions that can nowadays reach 18m. However, the mechanical response of laminated components is rather complex, especially if compared to standard construction materials. It indeed exhibits a non-linear behaviour that depends on several parameters,

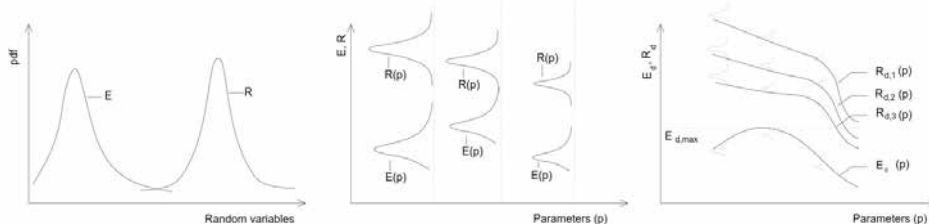


Figure 1. Schemes of probabilistic approaches for safety and performance assessment of structural components.

such as time<sup>2</sup>, surface area, edge length, edge type, toughening process, residual stress and temperature.

The latter plays a major role on the mechanical performance of laminated components subject to bending stresses. This is because laminated components are composed by several glass layers, which are bonded together with laminated interlayer polymers to transfer shear stresses between panels. The structural behaviour of laminated components therefore depends on the structural response of these interlayers. Due to their polymeric-viscoelastic nature, their behaviour is characterized by complex non-linear response, which is a function of several parameters. Moreover, the stiffness values of the interlayer, i.e. storage modulus, loss modulus and phase angle, are some of the main parameters affected by temperature variations.

Generally speaking, the structural assessment of structural components is performed by means of a probabilistic comparison of action and their effects (E) to the performance capacity of the components (R). In particular, the assessment is performed ensuring that the objective function<sup>3</sup> is larger than zero over the design life. To do so, adequate scenarios and boundary conditions needs to be defined for each relevant action (e.g. wind load, snow load, dead load, etc.). In that regards, when performing structural assessment of laminated components, load duration and temperature values should be defined for each relevant loading scenario. It is therefore essential to establish appropriate and realistic boundary conditions to be considered for each loading scenario, given the non-linear

response of laminated components described above.

Limited studies are available in literature on the subject [1]–[6]. Limited indications are also provided by current design standards on the appropriate temperatures and others boundary conditions to be considered for each different scenario. The available approaches tend to be either conservative or not accounting for the actual project specific boundary conditions. In addition, they usually make use of deterministic or empirical assumption on the interaction between different stochastic variables. Based on the above considerations, it is instead essential to establish sensible and realistic temperature values to be considered when performing the performance assessment against, for example, design wind loads (or other scenarios like condensation or thermal shock risk assessment).

Based on the above, structural engineers are therefore called either to make empirical assumptions based on their engineering judgment or to perform structural assessments based on extremely conservative assumptions. This, often, has a large impact on the design, construction and costs of glass components. In addition, it does not allow to perform a realistic and correct assessment of the actual reliability level of structural systems.

It is therefore suggested a methodology to establish the appropriate design scenarios is used in the structural assessment of laminated components. It requires a systematic method to evaluate the actual boundary conditions to be considered for different relevant scenarios when performing structural performance

<sup>1</sup> manuel@eocengineers.com

<sup>2</sup> More specifically on the stress time-history, due to the static fatigue phenomenon

<sup>3</sup> In this work, the objective function involve the mechanical performances of laminated glass panel and loadings. However the method here proposed can be more generally used also for non-structural objective function, e.g. probabilistic assessment of thermal shock, condensation and performance optimization of envelop with passive and adaptive systems).

assessments. This should be based on probabilistic approaches and models that (i) account for the stochastic nature of the actions and (ii) allow to perform realistic assessment of structure reliability over the entire design life. This work therefore aims to provide a first initial contribution to this topic. More in detail, an overview of the method is first presented in the following section. Then, a simple application example is presented, the results of which are analysed and discussed. Finally, conclusions and future consideration are given.

## Methodology

This section presents a short overview of the proposed probabilistic methodology. Firstly historical data from weather station is collected. Data set should contain the stochastic variable of interest such as air temperature, wind 3-second gust speed, radiation, relative humidity, snow depth, etc. measured over certain time frame. Data is post-processed, filtered and low quality measurements are excluded. Historical data should be collected for a relatively large period. However, the time period does not necessary need to be equal or larger than the target return period. Shorter time frame could be considered, as long as statistical tests show a satisfactory representativeness of the population.

Data is then post processed and analysed. Frequency and distribution analyses are performed to evaluate the stochastic behaviour of the random variables under consideration over time. The correlation between variables, such as maximum wind speed and air temperature, is also analysed using probabilistic approach. Radiation data is then analysed and continuous analytical function are to be derived to compute the temperature in the glass component.

Finally, the full set of post-processed data is used to derive a full probabilistic non-linear model. The model is (i) defined over several dimensions (e.g. time, temperature, etc..) (ii) capable of account for variable variance over the dimensions and (iii) capable to take into account different values of exceeding probability and confidence interval. The structural assessment can then be performed either by means of interaction curves at selected exceedance probability or by full probabilistic approach. Given the analytical complexity of the probabilistic models and the scale of the data sets to be analysed (usually in the order of several millions values), the algorithms and method described above are implemented in Python scripts.

## Analysis and discussion

In this section, the analysis and results of the proposed method are briefly discussed by means of a simple example. As the objective of this study is to give a brief overview of the method rather than specific values (which are dependent on the location), the data presented in this section are normalized with respect to the maximum values.

Figure 2 shows the behaviour of the temperature and the 3-seconds gust wind speed (here simply indicated as wind speed for the sake of brevity) measurement over time. More specifically, the graphs show data for San Francisco (US) between 1<sup>st</sup> of December 1948 to the 30<sup>th</sup> March 2017 (approx. 68 years of data, above 10 millions data points). From the graphs it can be observed that the behaviour of maximum wind speed and temperature data shows a typical stochastic nature over time. Moderate values are indeed occurring with high frequency, while extreme values are observed with low frequency. Statistical extreme value analysis is therefore needed to provide a more quantitative evaluation of these data.

Figure 3 shows then frequency histograms of the maximum 3-second wind speed and maximum temperature data. As expected, maximum wind speed and maximum temperature values show typical behaviour of non-linear extreme distributions. In particular, the right-hand tails of the populations appear to be statistically more spread than the left-hand side. The population seems to follow a non-symmetric probability density function, with mode and medial on the left-side of the mean.

The graph of Figure 4 collects the maximum wind values plotted against the corresponding temperature measured over time. Several observations can be made from this graph. Firstly, it is observed that the maximum wind speed is not occurring at temperature value equal to the maximum temperature measured of over the entire time-frame of the historical data. Large wind speeds are indeed generally occurring at temperature values lower than maximum one. If compared to the extreme maximum value, the wind speed generally decreases at high and low temperature. It can also be seen that the frequency of low wind speed is considerably lower than then

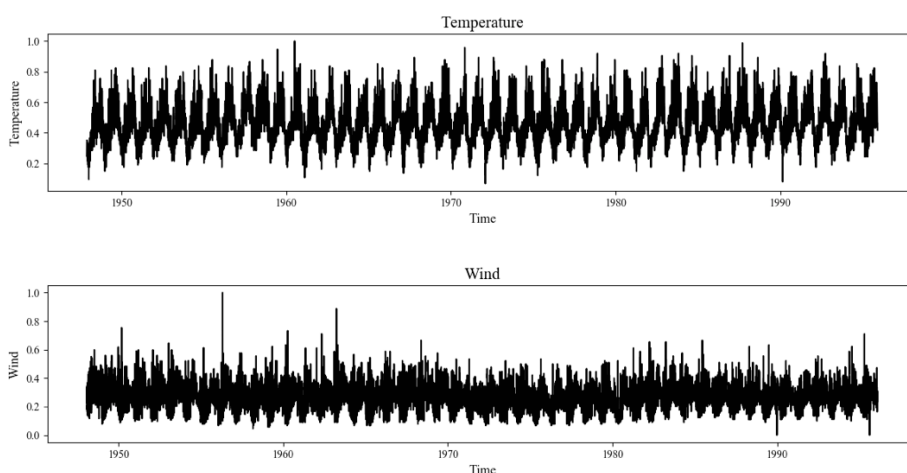


Figure 2. (top) normalized temperature and (bottom) normalized 3-sec gust wind speed over time.

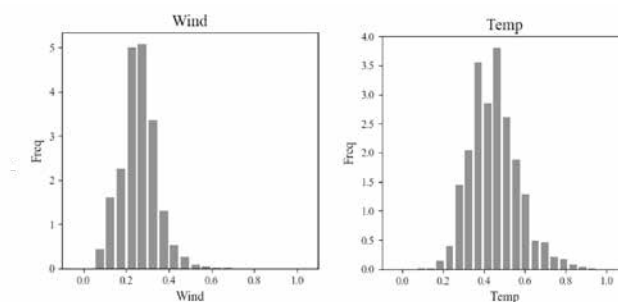


Figure 3. Frequency plot for (left) normalized maximum 3-sec gust wind speed and (right) maximum air temperature.

maximum one occurring across the full range of temperature. Therefore, it is apparent the hypothesis of maximum values of temperature and wind occurring at the same time is not theoretically correct, it is very conservative and above all, it does not allow for a uniform level of exceedance probability. In addition, it can also be observed that an 'envelope approach, (which would consider for instance a maximum envelope of the data set) would not be appropriate or correct. This is because (i) the results would be dependent on the time-frame used to collect historical data (ii) it is deterministic (iii) it is extremely sensitive to outliers and (iv) does not provide an homogeneous level of reliability. Instead, data should be used to determine the probabilistic behaviour of the stochastic variables and the structural assessment should be performed at homogeneous exceedance probabilities over the multi-dimensional domain.

From these graphs it can also be observed that to describe correctly the stochastic nature of these variables, a probabilistic non-linear model, that is able to account for a variable variance over the multi-dimensional space of the problem (e.g. wind-temperature-radiation in this example) is needed. From Figure 4, indeed, it can be seen that the stochastic nature of the random variables varies at different location of the considered space. In order to evaluate more in detail how the variance of the stochastic variables behaves data is now further post-processed and plotted in Figure 5 focusing on the effect of temperature.

The graphs of Figure 5 show that the stochastic behaviour of the maximum wind speed changes as a function of the temperature<sup>4</sup>. It can be observed that, for this example, the average of values decreases at high temperature, with maximum values occurring between 10°C and 20°C. As for the average, maximum and minimum values also vary with the temperature.

Figure 5 also shows that (in addition to mean, maximum and mean values) the statistical nature of the population distribution, and how it is spread over the domain, changes at different temperatures. The derivation of a probabilistic interaction between these stochastic variable, should therefore implement a non-linear variable variance over the multi-dimensional space. Consequently, both position, shape and scale parameters of the probability density function exhibit non-linear variability behaviour. For this type of problem extreme distributions usually are used (however any type probability

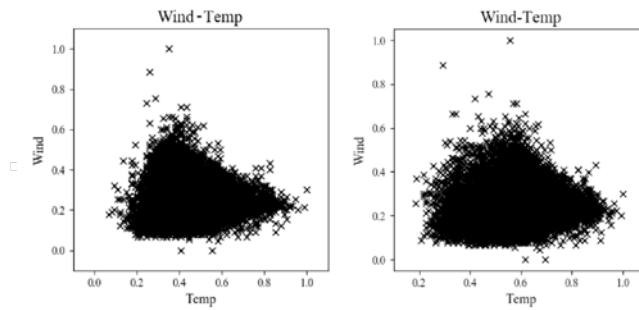


Figure 4. Normalized 3-sec maximum gust wind-speed and corresponding (left) air temperature (right) glass temperature.

density function can be implemented). The more appropriate type of probability density function (e.g. Log-Normal, Gumbel, three-parameters-Weibull and many others) is then selected as the one that provide best performance in term of statistical tests and residuals analysis.

The following step is to account the effects of other relevant boundary conditions (for example the solar radiation), which also changes with time. This step allows to convert the air temperature, and the correspondent radiation over time, into the temperature of the laminated components. First, an analytical equation that describes the radiation over time of a specific component is derived<sup>5</sup>. Then, given the appropriate boundary conditions, the temperature in the glass component is

computed over time (see Figure 6). This can be done by means of (i) simplified indications provided by standards and guide lines (ii) simplified method that allows to compute the components temperature considering an equivalent monolithic components as performed in [4] and (iii) by more advanced analytical and/or numerical approach. The probabilistic model can then be derived over the different dimensions, e.g. time, temperature, wind speed, radiation, etc. This allows then to compute the interaction curves that can then be used to perform the structural assessment of the laminated components. More specifically, the actions (e.g. wind) and their effects can be estimated as a function of the different considered scenario ensuring an homogeneous exceeding probability<sup>6</sup>.

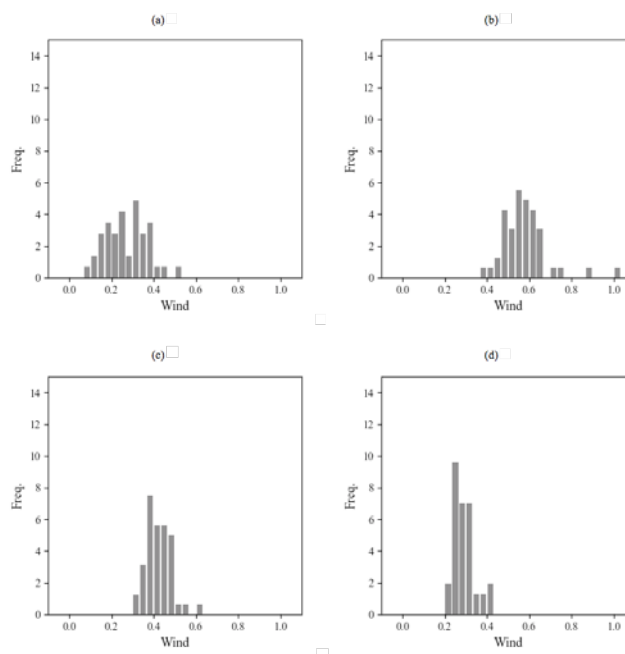


Figure 5. Yearly maximum 3-sec gust wind speed at different values of air temperature  $T$ : (a)  $T < 10^\circ\text{C}$  (b)  $10^\circ\text{C} < T < 20^\circ\text{C}$  (c)  $20^\circ\text{C} < T < 30^\circ\text{C}$  and (d)  $T > 30^\circ\text{C}$ .

<sup>4</sup> As well as for other parameters, study not here reported for the sake of brevity.

<sup>5</sup> This can be done either by simplified equations (which takes into account simply the panel orientation) or by advanced simulation technique (which simulate for both reflection and shadow effect due to surrounding surfaces).

<sup>6</sup> This is often defined by national code and standards, and depends on many parameter as type of building, importance of the construction, class of consequences, etc..

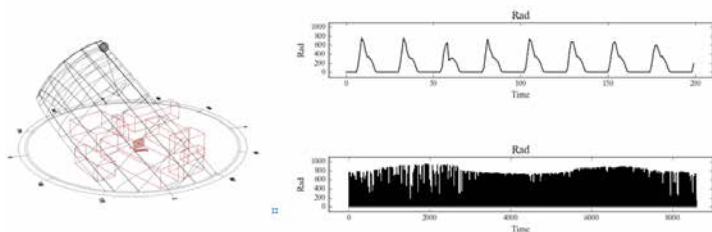


Figure 6. Example of the solar radiation computation over time that accounts for surrounding constructions and their surfaces properties.

This is done computing objective curves of the event under consideration as function of temperature at given exceeding probability<sup>7</sup>. Note that this computation depends the stochastic nature and distribution of the models, which varies from point to point in the multi-dimensional space, as shown in the one-dimensional example above shown in Figure 5. Given the target exceeding probability, the correspondent average recurrence interval (sometimes also indicated as return period) can also be computed.

The curves should be computed taking into account, not only the exceeding probability of the event, but also the target confidence interval. More specifically, a one-side asymmetric confidence intervals estimate should be implemented. It is important to note that confidence interval can be often estimated by means of closed form equation when the population can be described by normal distribution or other simple distributions. However, when extreme-distributions are used, or when the distribution is a-priori un-know, the complexity of the computation increases significantly<sup>8</sup>.

Figure 7 shows an example of probabilistic interaction curves computed at different exceedance probabilities as a function of temperature. This allows a realistic evaluation of the actions and related effects on laminated components for each relevant scenario to be performed. The process described above should then be repeated for each<sup>9</sup> panel or components to ensure the entire structural system satisfy the performance required for the entire design life.

Finally, it is worth mentioning that an alternative approach would be the full probabilistic method. This would represent the most accurate approach for the structural assessment as it allows computation of the total probability of failure over the entire design life of the system. The assessment is performed making use of the analytical probabilistic expressions of both action and resistance. The total probability of failure is then computed as function of time and the assessment is performed ensuring that the computed probability is lower than acceptable limits<sup>10</sup> over the entire design life. This approach can be sometimes computationally expensive and as such tends not to be widely adopted in structural engineering.

## Conclusion

This work presents a first study on a probabilistic approach for the structural assessment of laminated panels. In details, the interaction between maximum wind and glass temperature is analysed by means of probabilistic approach. The study shows that data exhibits a stochastic behaviour characterized by a variable variance over multiple dimensions such temperature and time. It is also shown that probabilistic models need to be used to perform realistic safety assessment over the design life of the components. The preliminary results

presented in this study should only be considered as an example, with the aim to provide a brief overview of the methodology. More detailed analysis is to be performed with certified data to complete an extensive scientific study. It should be noted that the proposed probabilistic approach is applied to wind and temperature stochastic variables. However, given its general validity, it can be applied to different type of variables, problems or performance assessment objective functions (e.g. probabilistic assessment of thermal shock, condensation and performance optimization of envelope with passive and adaptive systems).

## References

- [1] F. Wellershoff, "Bemessungsschubmodulwerte für Verbundglasscheiben," *Stahlbau*, vol. 76, pp. 177–188, 2007.
- [2] N. Grammou and J. Schneider, "Investigation of correlation between snow, wind and temperature during periods of snow .pdf," in *Challenging Glass 4 & COST Action TU0905 Final Conference*, 2014.
- [3] P. Lenk, V. Marinov, and L. Rammig, "Structural glass envelops - Implementation of environmental studies into viscoelastic analysis," *J. Facade Des. Eng.*, 2014.
- [4] A. Baldini, L. Rammig, and M. Santarsiero, "A systematic methodology for temperature assessment in laminated glass components," in *Engineered Transparency*, 2016.
- [5] M. Santarsiero, "Laminated connections for structural glass applications," Thesis Dissertation, École Polytechnique Fédérale De Lausanne - EPFL, 2015.
- [6] G. Sedlacek, K. Blank, W. Laufs, and J. GÜsgen, *Glas im Konstruktiven Ingenieurbau*. Berlin: Verlag Ernst & Sohn, 1999.
- [7] M. Santarsiero, C. Louter, and A. Nussbaumer, "Laminated connections for structural glass applications under shear loading at different temperatures and strain rates," *Constr. Build. Mater.*, vol. 128, pp. 214–237, 2016.

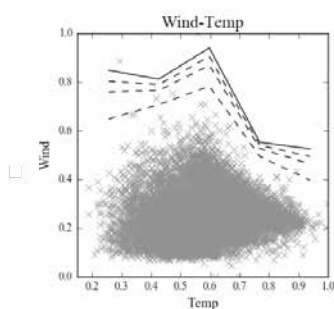


Figure 7. Interaction probabilistic curves at different exceeding probabilities:  $2.00E-2$ ,  $3.33E-3$ ,  $1.43E-3$ ,  $5.88E-4$ .

<sup>7</sup> Following the algorithm developed in [5] and adopted in [7].

<sup>8</sup> In such cases closed solutions are usually more complex to derive analytically. This can be done by means of different methods can be used, such as the one used in [5]

<sup>9</sup> Indeed, each panel is potentially subjected to different radiation values at any point in time (thus to different temperature). This can be due to different location, inclination, adjacent surfaces etc.

<sup>10</sup> This is often defined by national code and standards, and depends on many parameters as type of building, importance of the construction, class of consequences, etc.

# Glass Constructions Under Extreme Boundary Conditions

Barbara Siebert

Dr. Siebert Consulting Engineers, Munich, Germany, Contact: [bsi@ing-siebert.de](mailto:bsi@ing-siebert.de)

Tobias Herrmann

Dr. Siebert Consulting Engineers, Munich, Germany, Contact: [bsi@ing-siebert.de](mailto:bsi@ing-siebert.de)

## Abstract

Building with glass as structural element becomes more and more common. Under special boundary conditions like in alpine areas or near the coast this might become a challenge concerning design and execution at the building site. Important points are the climatic conditions in alpine and maritime regions, like extreme wind loads, extreme pressures for insulating glass units due to the difference in altitude, salt water near the sea, narrow installation situations and a narrow time slot. Basics and applications of glass constructions in these extreme boundary conditions are presented. Two summit stations with glass applications, the Nebelhorn (2224m) and the Zugspitze (2962m) and a pavilion located in the Baltic Sea are presented.

## Keywords

Glass, railings, facades, curved glass, insulating glass unit, structural analysis.

## 1 Introduction

Glass as a building material is used in a multitude of new applications like modern glass façades or transparent railings. New ways of fixing the glass and almost a boundless freedom in size and shape offer a plentitude of solutions for these issues. From the architect's point of view glass balustrades and facades in alpine regions should be as transparent as possible (magnificent view), but simultaneously they have to act as a protective barrier and load bearing element (enormous loads). The situation is similar with buildings in touristic areas near the sea. Experienced structural engineers can satisfy both sides of the same coin.

## 2 Glass as structural element

Glass is used more and more as structural element. Structural element means that the

glazing is exposed to actions like wind, snow, line loads, impact and climatic loads in case of insulation glazing. This requires for almost all glass constructions like facades, railings and canopies a careful design and structural analysis.

Glass is a brittle material. Hence it is very important to consider stress peaks, e.g. resulting from the constraint with point fittings or internal corners. Bonded connections have to be analysed in a close to reality structural model.

By means of a temper process, the strength of the glass can be increased. Three levels of prestressing are commonly distinguished:

- annealed glass (float glass) with a tensile strength of 45 MPa,
- heat strengthened glass (HSG) with a tensile strength of 70 MPa and
- fully tempered glass (FTG) with a tensile strength of 120 MPa.

Enamellings reduce the above characteristic values.

Apart from above bending strength the different behaviours of breakage and the different remaining load carrying capacities must be taken into account. Usually laminated safety glass (LSG) is used (two or more layers of glass with an elastic interlayer made of PVB) to increase safety in case of breakage. But PVB is not the only interlayer material for laminated safety glass, other interlayers with different properties are offered, too. E.g. the ionoplast interlayer behaves very stiff and it is not as sensitive towards increasing temperatures as ordinary PVB interlayers. FTG is breaking into very small fragments resulting in a poor remaining load carrying capacity. It can be increased by the use of above mentioned stiff interlayer.

As the use of glass in structural engineering is a quite new subject, only a few regulations and design rules exist so far. With the German standard DIN 18008 more applications are regulated, based on fracture mechanics and in line with the current concept of partial safety factors [2], [3], [4], [5], [6], [7]

## 3 Boundary conditions in alpine areas

In alpine and maritime areas, specific boundary conditions must be taken into account:

Extreme weather conditions with high wind and snow loads.

- Difficult access to the building site.
- In case of insulated glass units (IGU) extreme differences of air pressure and temperature between manufacturing and installation site.
- High UV radiation might cause problems of aging of bonds and sealants.
- High salt water content might cause problems of corrosion of metal parts.
- Potential problems of delamination of laminated glass due to moisture.
- Potential problems of infiltration of moisture and snow to the substructure.

## 4 Summit station "Nebelhorn"

The summit station of the mountain cableway "Nebelhornbahn" is situated next to the town Oberstdorf, Germany at an altitude of 2224 m above sea level. The station was rebuilt in summer and autumn 2016. The building itself is a timber construction with partially curved facades and curved balustrades. The area of the Nebelhorn is famous for skiing in winter and hiking in summer.

The architect's plan of Hermann Kaufmann ZT GmbH shows an organic, very transparent shape made of timber, glass and a bronze-coloured cladding, see Figure 1.



Figure 1. Rendering ([www.hermann-kaufmann.com](http://www.hermann-kaufmann.com))

### 4.1 Glass Elements

The glass railing is situated on two floors along the terraces of the building, see Figure 2.

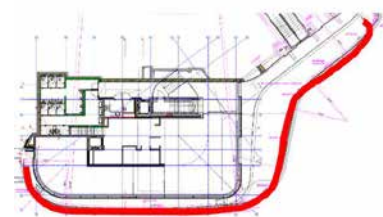


Figure 2. Floor plan of ground floor with railing (red)

The smallest radius of the balustrade's curved glass is 870 mm, the maximum radius 6970 mm. A laminated safety glass with two layers of fully tempered glass and a 1.52 mm-thick PVB interlayer was used. At the plane areas laminated safety glass with a 1.52 mm-thick ionoplast interlayer was applied. The clamped glass balustrade is situated on a small base, to protect the glazing at its base, see Figure 3. The overall height of the balustrade of about 1.5 m is higher than building regulations would require. But besides its function as protective barrier it also serves as a wind shield for the visitors of the terrace. The façade consists of fully framed insulated glass units of which some work as sliding doors.

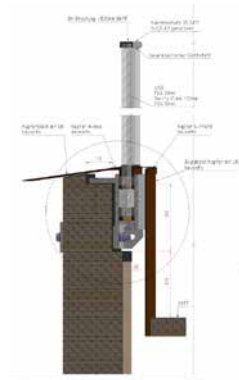


Figure 3. Vertical section through railing (StahlGlasbau Dann GmbH, Kempten)

## 4.2 Structural analysis and impact

### 4.2.1 Railing

The special feature of this project was the curved glass. There are some advantages but also disadvantages with this kind of glazing, see Table 1.

| Rating   | Explanation  |
|----------|--|
| positive | In case of monolithic glazing small deflections  |
| positive | High load capacity if supported properly   |
| negative | In case of insulation glazing stiffness causes very high climatic loads.                             |
| negative | Curved glazing is in Germany often an unregulated construction. A special permit might be necessary. |
| negative | Elaborate framing  |

Table 1. Curved glass

The wind speed was examined in an expert report with a speed of 50 m/s. The resulting wind loading was 4.7 kN/m<sup>2</sup>. According to Eurocode EN 1990 in combination with DIN 18008-1 the following load sets were

considered for the balustrades:

$$\text{LC 1: } 1.35 g_k + 1.5 q_k + 0.9 w_k \quad [1]$$

$$\text{LC 2: } 1.35 g_k + 1.05 q_k + 1.5 w_k \quad [2]$$

Due to the high wind loads and the low line load's impact height the load-case LC 2 is dominating.

In addition, it is necessary to consider partial destroyed glass panes as an accidental design situation.

$$\text{LC 3: } 1.0 g_k + 1.0 q_k + 0.2 w_k \quad [3]$$

The curvature of the glazing was considered in a finite element analysis, so was the glued constraint situation. The latter is often applied in case of curved balustrades, because otherwise inevitable tolerances of the clamping structure would cause constraint forces in the glass.

Another topic was the anchorage on the wooden substructure. Beside the problems of the analysis it was very important to avoid penetration of snow or rain into the base point of the railing.

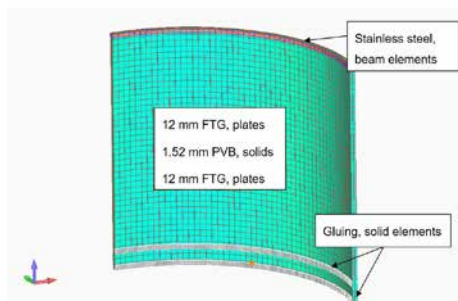


Figure 4. Finite-element analysis

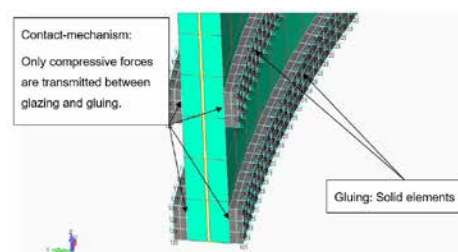


Figure 5. Finite-element analysis

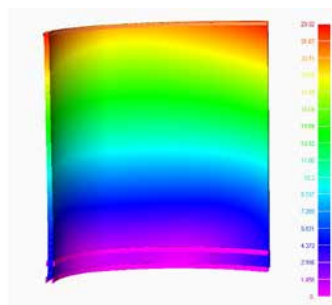


Figure 6. Plot of deformation

### 4.2.2 Post-breakage behaviour

Beside the load carrying capacity of the intact glazing a remaining load carrying capacity has to be established. It must be ensured that a glass construction cannot collapse

(immediately) in case of breakage, so that the safety of pedestrians, e.g. pushing against a glass facade is guaranteed. Depending on the kind of application the verification of residual resistance is done with different testing or numerical methods. If it is safe to assume that at least one glass layer of the LSG remains intact, because it is protected from all accessible sides, a numerical proof is possible. The reduced loads of LC 3 must be carried by the remaining layer alone. However the edges of the glazing – particularly in the case of balustrades – often are not protected enough against hard impacts. These entire broken elements also must provide a sufficient residual load carrying capacity. As a reliable numerical simulation of broken LSG is not possible (yet), full scale tests and/or expert reports are unavoidable.

The behaviour after breakage of a glass pane depends on many factors. The kind of glass (thermally toughened or heat strengthened glass), the kind of lamination between the glass panes (PVB, ionomer or cast-in-place resin) and the kind of fixture are the main influences.

### 4.2.3 Impact

Dynamic actions in the form of impact loads have to be considered, too. German standards allow three kinds of verification:

- Comparison to approved systems
- Verification by calculation
- Verification by testing

Curved glazing is excluded from the first two methods. Therefore pendulum tests or at least expert`s surveys have to be charged.

### 4.2.4 Curved Facade

The resulting pressure in the space between the panes and the mechanical stress to the edge seal is very high.

Under a uniform load bent glass behaves much stiffer than flat glass panes. For the so called "climatic loads" apply almost isochoric conditions (Volume = const.).

According to the DIN 18008-1 [8] it is not allowed to consider a beneficial shear connection in the edge seal. So it is often necessary to consider two cases in the calculation:

- Only radial joint of glass panes (stiff or elastic)

- Additional shear transfer in the edge seal

Aspects like elastic constraint influence of the spacer, consideration of the gluing (intact or with delamination), consideration of the kind of sealing material and many others were very important to investigate. Especially the sealing material plays an important role in the calculation. E.g. a polymer has a nonlinear behavior. The stiffness depends on the geometry, the temperature, the strain-rate and

the ageing. The question is, if it is necessary to implement all these phenomena to the calculation.

Because of the extreme difference of air pressure and temperature between production plant and installation site, valves in the space between the panes are necessary during transport to the summit. The manufacturer allowed the valves to be opened for 10 minutes without having severe influence on the gas-filling.

#### 4.2.5 Prefabrication

To reduce the time in the cold areas on the top of the mountain as much as possible, time for setup was shifted to the workshop. The elements of glass-plates glued in the substructure were prefabricated (Figure 7). The width of the elements was optimized due to the performance of the helicopter.



Figure 7. Prefabrication (StahlGlasbau Dann GmbH Kempten)

#### 4.2.6 Installation

For installation, a very narrow timeslot was given. Reasons are the following:

- Early start of winter with temperatures below zero degree Celsius
- Minimisation of operation breakdowns of the cableway between high season in summer and high season in Winter
- Many project members and trades on a very narrow building site

The glass elements were transported to the middle station "Seealpe" by truck, the final step of transportation was done by helicopter (Figure 8). Because of the high cost for the helicopter, it was very important to optimize the size and weight of the prefabricated elements.



Figure 8. Transportation by helicopter (StahlGlasbau Dann GmbH Kempten)



Figure 9. Installation at 2224m above sea level (StahlGlasbau Dann GmbH Kempten)

#### 4.2.7 Finished project

The project was finished in time in autumn 2016.

Figure 10 to Figure 13 show the completed project with the railing and the façade.



Figure 10. Building from the outside



Figure 11. Railing



Figure 12. Building from the outside



Figure 13. Part of the façade

## 5 Summit station "Zugspitze"

The summit station of the "Zugspitze" is situated near the town Garmisch-Partenkirchen at 2962 m above sea level. A new cableway including a renovated and partially rebuilt building on the peak is under construction at present. It is the highest situated building site at Germany. The project will be completed in 2017.

### 5.1 Glass Elements

The façade consists of different glass sizes of double and triple insulated glass units (IGU). Structural analysis

The wind pressure was examined in an expert report with up to 5.4 kN/m<sup>2</sup>, the snow-load on the terrace is given with 15 kN/m<sup>2</sup>.

For the structural design of IGU, the climatic loads have a main influence. According the DIN standard the following formulas apply accordingly:

Summer :

$$\Delta T = T_{\text{Space,Summer}} - T_{\text{prod}} + \Delta T_{\text{Absorptionsgrad}} + T_{\text{sunprotection}} = 39^{\circ}\text{C} - 19^{\circ}\text{C} + \Delta T_{\text{Coating}} + T_{\text{sunprotection min. 20 K}} \quad (4)$$

Winter:

$$\Delta T = T_{\text{Space,Winter}} - T_{\text{prod}} = 2^{\circ}\text{C} - 27^{\circ}\text{C} = 25 \text{ K} \quad (5)$$

Next step is the approximate calculation of the volumetric coefficient with a linear relationship between variation of volume and load:

$$\Delta V = v \cdot p \quad (6)$$

All the formulas for IGU's can be found in DIN 18008-1 and DIN 18008-2 [2], [3]

## Installation

For installation, also a very narrow timeslot was given:

- Early start of winter with temperatures below zero degree Celsius, snowfall also in summer possible.
- Many project members and trades on a very narrow building site



Figure 14. Snow in July ([www.zugspitze.de](http://www.zugspitze.de))

The glass elements were transported to the summit with a second existing cable car from the Austrian side of the mountain.



Figure 15. Building site ([www.zugspitze.de](http://www.zugspitze.de))

The current situation on the building site at early spring 2017 can be seen in Figure .



Figure 16. Building site ([www.zugspitze.de](http://www.zugspitze.de))

## 6 The teahouse in the Baltic sea

The Teahouse is situated in the Baltic Sea near the small touristic town Timmendorfer Strand, only accessible over a pedestrian bridge.

The impacts of wind and seawater on the building are very high; this had to be taken into account during design of the building and the transparent parts: Large Façade Areas, also with function as anti drop device, accessible glassing – scarcely above the water surface, railings inside and a wind protection outside are all made of glass. The teahouse was designed by Schubert architects, Hamburg inspired by the Japanese Architecture.



Figure 17. Building site teahouse – outside



Figure 18. Building site teahouse - outside

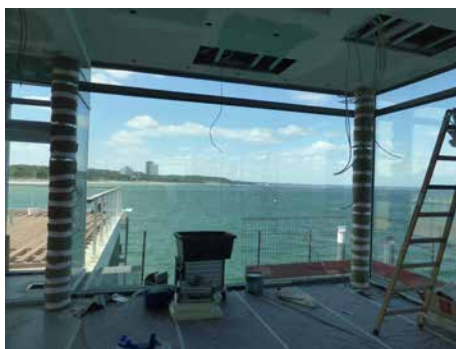


Figure 19. Building site teahouse - inside

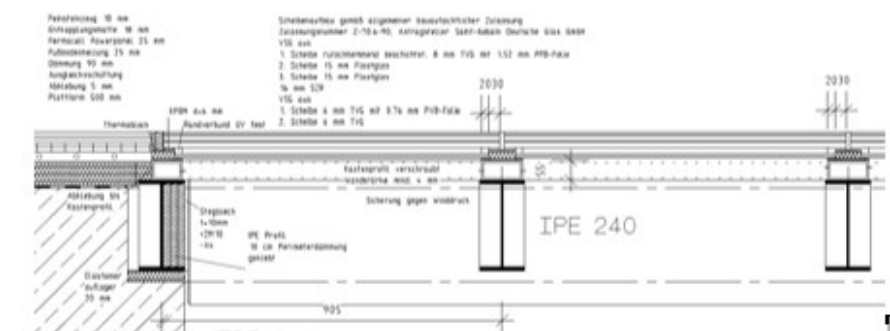


Figure 20 accessible glazing

## 6.1 Façade

The façade is situated in the ground floor and the first floor of the building. The IGU's are acting as anti drop device and have dimensions of 4630mm x 2730mm. Because of the exposed situation wind zone 3 is obligatory.

The glass set up is from inside to outside:

- A laminated safety glass with two 8mm layers of fully tempered, heat-soaked glass and a 0,76 mm-thick PVB interlayer
  - 14mm cavity
  - 10mm layers of fully tempered, heat-soaked glass
- The load carrying posts are shifted to the inside, from the outside only the transparent cover is visible.

## 6.2 Accessible glazing

The accessible floor has dimensions of 4760mm x 3300mm in two areas. 10 glass elements with the dimension of 850mm x 1545mm (area 1) and 800mm x 1545mm (area 2) are situated direct above the surface of the water.

Details and the glass set up can be seen in Figure 20.

The analysis was done according DIN 18008 [1]. The ground floor is used as a restaurant, so a load of 5,0 kN/m<sup>2</sup> and alternately a single point load was considered (Table 2, Table 3).

| LK | Load combination             | Limit state                |
|----|------------------------------|----------------------------|
| 1  | $1,35 \cdot g$               | Ultimate limit state       |
| 2  | $1,35 \cdot g + 1,5 \cdot q$ | Ultimate limit state       |
| 3  | $1,35 \cdot g + 1,5 \cdot Q$ | Ultimate limit state       |
| 4  | $1,0 \cdot g + 1,0 \cdot q$  | Serviceability limit state |
| 5  | $1,0 \cdot g + 1,0 \cdot Q$  | Serviceability limit state |

Tabelle 2 all glass panes intact

| LK | Load combination            | Limit state          |
|----|-----------------------------|----------------------|
| 6  | $1,0 \cdot g$               | Ultimate limit state |
| 7  | $1,0 \cdot g + 1,0 \cdot q$ | Ultimate limit state |
| 8  | $1,0 \cdot g + 1,0 \cdot Q$ | Ultimate limit state |

Tabelle 3-upper layer broken

### 6.3 Windscreen

The additional mounted windscreen with high wind loads up to  $2,2 \text{ kN/m}^2$  has dimensions of  $1400\text{mm}$  (width) x  $1500\text{mm}$  (height). A laminated safety glass of  $2 \times 8\text{mm}$  fully tempered, heat soaked glass was used. Main problem was the mounting with highly corrosion resistive anchoring rods in the bridge to the tea house (figure 21, 22).



Figure 21 Wind screen

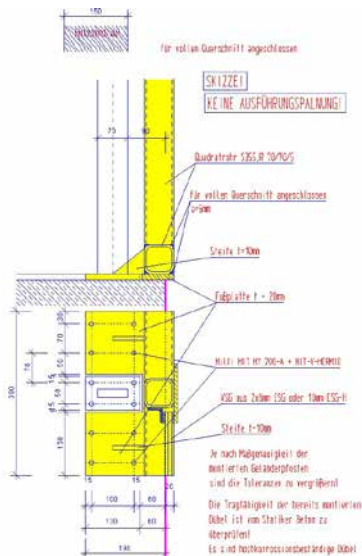


Figure 22 Connection to the bridge

### 7 Conclusions

Constructions at exceptional locations are often challenging but worth one's while. Extreme boundary conditions and sophisticated demands of the client have to be considered. Experience in the field of structural use of glass, extensive knowledge on the current glazing technologies, state-of-the-art manufacturers and engineering expertise led to the presented impressive solutions.

### 8 References

- [1] ETAG 002: Guideline for European Technical Approval for Structural Sealant Glazing Systems (SSGS)
- [2] DIN 18008-1: 2010-12: Glas im Bauwesen – Bemessungs- und Konstruktionsregeln – Teil 1: Begriffe und allgemeine Grundlagen
- [3] DIN 18008-2: 2010-12: Glas im Bauwesen – Bemessungs- und Konstruktionsregeln – Teil 2: Linienförmig gelagerte Verglasungen
- [4] DIN 18008-2: 2011-04: Glas im Bauwesen – Bemessungs- und Konstruktionsregeln – Teil 2: Linienförmig gelagerte Verglasungen, Berichtigung zu DIN 18008-2: 2010-12
- [5] DIN 18008-3: 2013-07: Glas im Bauwesen – Bemessungs- und Konstruktionsregeln – Teil 3: Punktförmig gelagerte Verglasungen
- [6] DIN 18008-4: 2013-07: Glas im Bauwesen – Bemessungs- und Konstruktionsregeln – Teil 4: Zusatzanforderungen an absturzsichernde Verglasungen
- [7] DIN 18008-5: 2013-07: Glas im Bauwesen – Bemessungs- und Konstruktionsregeln – Teil 5: Zusatzanforderungen an begehbbare Verglasungen
- [8] Herrmann, T.; Siebert, B.: Energetische Sanierung Hypo-Hochhaus – Gebogene 3-fach Isolierverglasung der neuen Doppelfassade. Stahlbau Sonderheft Glasbau April 2014, Ernst & Sohn Verlag Berlin
- [9] Siebert, B., Herrmann, T.: Glass balustrades and facades on pedestrian bridges, 9th German – Japanese Bridge Symposium in Kyoto. September 2012 in Kyoto
- [10] Feldmeier, F.: Bemessung von Dreifach-Isolierglas. In: Stahlbau Spezial 2011 – Glasbau. Ernst & Sohn, Berlin 2011.
- [11] Siebert, B., Pistora A. Teehaus am Timmendorfer Strand. Glasbau 2015. Ernst und Sohn Verlag

### 9 Acknowledgements

We would like to thank the company StahlGlasbau Dann GmbH ([www.dann-gmbh.de](http://www.dann-gmbh.de)) for providing the pictures of the installation.

# Hybrid Glass Structures

Dr Peter Lenk  
Arup, London, UK

## Keywords:

Glass, Hybrid, Holistic, Design

## Abstract

Façade transparency is becoming an increasingly significant design factor for both client and architect, which has aesthetic and comfort implications. On the other hand, both parties are also expecting smaller, more slender structural elements that are challenging in terms of code compliance. Both aims may be satisfied using Hybrid Glass Structures (HGS). Combining glass panels with another structural material could contribute to the total structural performance of a building, with efficiencies that allow for material savings and a reduction in construction time. Guidelines outlining HGS on the analysis, basis of design, methodology and constructability are currently considered inconsistent. This paper intends to review existing projects that include HGS in order to assess the adequacy of the structural scheme and materials used. Commonly, materials consist of steel/stainless steel or fibre reinforced polymers. This paper will include a literature review opening up to a broader state-of-the-art review to develop knowledge on this theme. An example of existing structures with numerical studies are presented and the potential benefits of HGS quantified.

## 1 Introduction

Engineers are expected to propose the efficient use of natural and human resources to a design problem specified by the client in their brief, architectural intent and national / international regulations and code of practice. A problem is never trivial and design space is multi-parameter; engineering judgment is as important as technical knowledge. In the current, competitive climate, consultants are asked to deliver original designs with, perhaps, a controversial performance brief. More often than not, design consultants offer their clients a multidisciplinary and global service to provide a holistic design approach. As such, a multidisciplinary team of experts (from many fields of expertise) will cooperate closely to develop a bespoke solution. It is

important for engineers to drive innovation and research in growing areas of the construction business that allow for quick and effective answers to client demands, while at the same time developing solutions that are sustainable, practical and deliverable. This topic is explored in more detail in [4].

The concept of combining materials to produce desirable characteristics that differ from those possessed by the individual materials themselves is not a new concept. Wilkinson and Monier's 19<sup>th</sup> Century composite of iron bar embedded in concrete is still a concept used widely in the construction industry today. It is worth noting that in composite materials, the individual component materials remain separate and distinct.

Materials can be categorised according to their characteristic properties and for each subcategory advantages and disadvantages can be listed as per particular design situation.

## 2 Performance criteria

As mentioned earlier, the engineer is responsible for compliance with client, architecture brief and design codes of practice. Efficiency can be measured by total material use per unit volume, but cost tends to be used to compare different schemes. This is because the quantity surveyor will incorporate scheme complexity such as procurement, constructability, access and maintenance and risks associated with above activities alongside with material costs. Innovative (or complex) design concepts such as HGS require upstream investment and development to 'mainstream' it as reliable structural solution that may be disseminated to all the involved parties within the construction environment, and hence reduce costs.

This study has identified five main aspects where schemes comprising of glass in combination with other material(s) have been a success story. Precedents have been gathered from past projects and projects being currently developed.

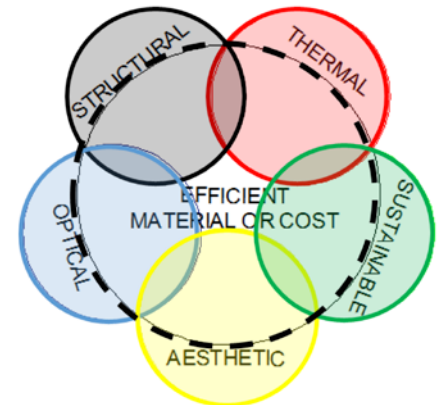


Fig 1 Performance criteria

### 2.1 Structural

Outlined below are key structural qualities when designing with structural glass. Further information can be found in [5]:

- Redundancy – duplication of critical component to increase reliability of system;
  - Passive: extra strength, no. of elements
  - Active: prevents overstressing
- Ductility – ability of relatively high energy absorption capacity due to the material yielding;
- Robustness – ability of system to cope with change without being damaged to an extent disproportionate to original cause;
- Resilience – ability to absorb or avoid damage without suffering complete failure and recover within reasonable cost or time;

Improving in service performance or post failure behaviour of HGS could be achieved on an elementary level:

- Reinforced with steel, timber, FRP, GRP glass edges, to increase strength, stiffness from rectangular flat plate to T, I sections. Such reinforcement may switch failure mode of the HGS component from brittle to ductile.
- Lamination of glass panes with interlayers and polycarbonate sheets is well known technique to increase redundancy of the element.
- Edge rods, profiles, may contain failed element and as such improve robustness of the glass element. Concept successfully proposed by Dodd [3] on the Constitution Bridge in Manchester where measures to increase public safety was required.

On a material level, glass may be combined with other materials that complement the lacking characteristic properties of glass. Particular attention to the differential thermal expansion and thermal capacity of the materials shall be given, as well as the magnitude and distribution of connection forces between components and failure mode prediction. After the literature review we summarised materials considered by researchers and designers as:

- Metals - Stainless steel, Aluminium, Titanium; [12], [13]
- Hard and soft timber, Engineered timber composites; [8], [9]
- Polymers, and cement based materials as FRP, GFRP, GFRC; [10], [11]

Glass in structural systems can differ in form; planar, single or double curved geometry have been explored. Internal composition of the structural form is closely linked with geometrical orientation. Short summary of possible structural systems are outlined:

- Predominantly bending structures, with a structural skeleton spaced further apart consisting from flat 1D or 2D elements. Concept often used to maximise transparency, however potentially resulting in larger elements which may hinder visual perception;
- Diffused glass structure with a smeared metal skeleton. Traditional greenhouses of 19<sup>th</sup> century are considered highly transparent despite the relatively closely spaced steel bars;
- Sandwich glass elements; [6]
- Membrane;
- Compression; (glass bricks)
- Shear walls and stability elements (reinforcing diaphragm in tensile nets or traditional steel frames).

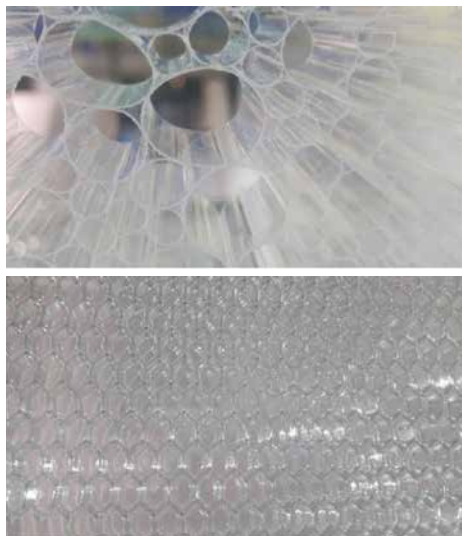


Fig 2 Examples of material inside insulated glass panel cavity a.) PVC, b.) Aluminium honeycomb

## 2.2 Thermal

With the increasing financial and environmental cost of the energy, designers are focusing their efforts on improving thermal performance of building envelopes. Another increasingly important parameter to consider in the design is the shading coefficient as reducing cooling demands is a high priority of envelopes comprising of high ratio between transparent and opaque areas. A shading device may be integrated into the structural system and recently dynamic shading components or switchable glass was researched by many teams with new exciting products emerging on the market.



Fig 3 PV Cells and switchable glass example

Over past years we have developed and perfected our envelope detailing to mitigate energy loss. Today we are investing our efforts in harvesting some of the energy to create energy passive buildings. Some examples of the latest generation of PV cells thermo /photo chromic glass are presented on figure above. Interesting prototype of Glasstex arch was built by a team led by Jan Wurm and Ralf Herkrath in 2002 for the Glasstec fair in Dusseldorf. The design was motivated by evenly distributed light to prevent overheating as such desire to integrate solar shading into the structural concept was developed. The structural system is a complex cable stabilised compression glass arch with bottom tension cables connected with fabric shades and longitudinal forces. Similar concepts to integrate shading devices into the cavity of insulated glass units was outlined in [7]. The micro louvers in the glazing cavity help to provide Sun and glare protection. Z-profiles can be employed to optimise solar shading and provide full protection when sun is high in the sky.

## 2.3 Sustainability

The graphical data illustrated on figure below shows the embodied carbon of a variety of typical façade materials. Additional fabrication processes of annealed glass such as heat treatment, heat soaking, lamination, edge polishing and coating can more than double the embodied carbon footprint of the final product. However it is expected that above processes will improve product performance and as such reduce operational carbon footprint.

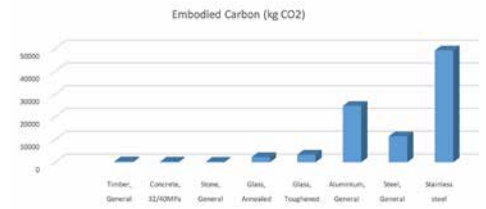


Fig 4 Embodied carbon footprint per kg of typical materials

## Stick System Curtain Wall Embodied Carbon (kg CO<sub>2</sub>)

■ Embodied ■ Transport ■ Operational

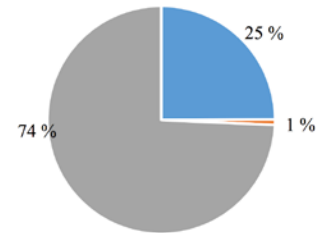


Fig 5 Total carbon footprint for typical stick system

## 2.4 Optical

The visual performance of glass may be specified as either transparent, opaque, or both/in-between. Furthermore, the transparency of glass may (appear to) be dynamic. Optical quality, distortions and reflections shall be reviewed as they may have an influence on the perception of the final product.

## 2.5 Aesthetic

Glass, when combined with other materials, is a unique solution with unlimited possibilities for clients, architects and engineers. Aspects such as natural/artificial light, reflection and shadows are usually considered in conceptual design stages. Furthermore, the process of combining materials should strive to enhance structural integrity. The concept of total transparency is challenged by increasingly prominent environmental requirements that are in favour of an alternative concept of diffused transparency. In diffused glass structures, a holistic approach of 'layering' (and where possible, integrating functions) helps to minimise cost and develops a product with desirable properties.

## 3 Selected applications

### 3.1 Structural IGU Panel

Architects are intrigued by uninterrupted views and as such often tend to specify facades without vertical mullions or horizontal transoms. In this particular example, architectural intent is to provide maximum

transparency between opaque elements by omitting framing in the visual zone. This provided the engineer with a challenge to design floor to floor glazing panels which are 3 side supported with the middle panel only two side supported top and bottom. Displacement compatibility at the edge was a considerable issue here. To avoid increasing glass thickness and thus cost and weight to the primary structure, all panels were connected with a structural silicone. Structural silicone is stiff enough to transfer shear forces from the 'softer' middle (two side supported) panel to the stiffer three side supported panels and as such equalise system deformations. However, to limit out of plane edge deformations to the acceptable industry limit of  $L/175$  and reducing durability risks of the insulated glass units, two sets of two glass panes of 12mm thick laminated glass were required. This is around 50% more glass than on a typical curtain wall system (per  $m^2$  of elevation) with mullions.



Fig 6 Internal view from the office floor with exterior decorative glass fins

As briefly touched on earlier, researchers and industry focus on connecting both inner and outer glass panes together to benefit from the increase of inertia moment. The shear coupling co-efficient introduced by interface slippage can be theoretically calculated. The build-up offers improved structural performance. Such structural insulated glass units must be designed to withstand climatic loads. Alternatively units can be pressure equalised and connected to the external desiccant container to mitigate climatic stress and water condensation within the cavity. This strategy was successfully used in many projects including the recent Berkeley Hotel, development in London completed by Bellapart and design by our colleagues from Arup. [6] Our initial studies focused on the development of the edge connections between the outer and inner pane of the insulated glass units using finite element analysis. Traditionally, this seal is semi-structural and usually consists of an Aluminium spacer bar filled with desiccant, butyl adhesive and structural silicone (predominantly acting as a secondary seal to prevent moisture ingress and air/gas leakage.) Triple insulated units are becoming increasingly common in order to increase the thermal performance of building envelopes. Larger spacing between outer and inner glass panes in the triple insulated panels may significantly increase structural performance of the element.

Effect of the edge bonding has been parametrically studied on the array of panels. In this paper we will only present results for panel with 2m width and 3.35m length. Connection edge stiffness with elements of generic stiffness of  $E=100\text{mm}$ ,  $\nu=0.45$ ,  $t=25\text{mm}$  have been considered in this example and results presented in the graphs below. In addition, three conditions were studied where connections between outer and inner glass panes were considered on short, long and both edges of the panel. Peak shear forces in the connection element are presented on the figure below. While the peak shear force for short and long connection is almost equal 3.8 kN, 3.7 kN respectively, a smaller shear force of 3.2 kN was calculated located in the shorter edge for both edges.

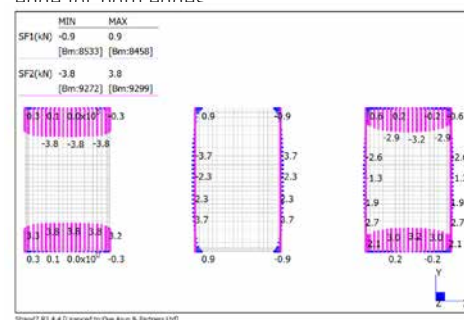


Fig 10 Distribution of shear forces in the edge connection elements a.) short edge, peak force of 3.8 kN, b.) long edge, peak force of 3.7kN, c.) both edges, peak force 3.2kN

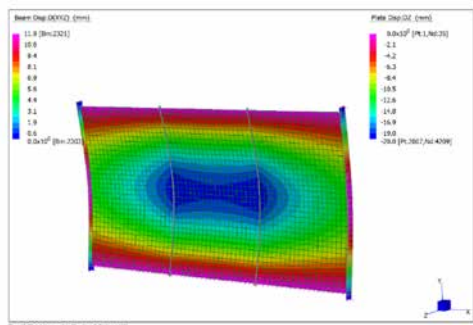


Fig 7 Structural system of silicone bonded 2 and 3 way supported panels

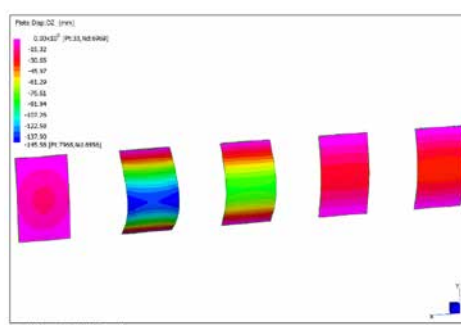


Fig 9 Panel deformation from left to right, Connection stiffness  $E=100\text{MPa}$   
 a. four side supported panel, standard system  
 b. two side supported panel, no composite action between glass panels  
 c. two side supported panel, partial composite action, connection modelled with spring element  
 d. two side supported panel, partial composite action, connection modelled with plate element  
 e. two side supported panel, partial composite action, connection modelled with volumetric element

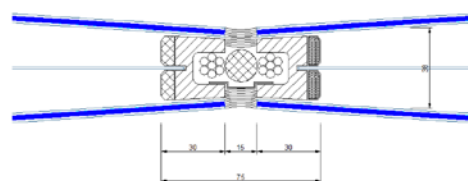


Fig 8 Conceptual detail of triple insulated curved panel made from thin laminated glass

Deformation analysis of the above panel revealed that short edge connections contribute least to the overall panel stiffness with peak mid panel deformation of 59.3mm. The long edge connection provided slightly improved composite action with peak deformation of 51.7mm, while if all edges were connected the deformation peak was 35.8mm. The above results are graphically presented below.

From discussions with the Architect, it was clear that the width of the bond on the long edges should be kept to a minimum as those are key visual obstructions, while the less active bond on the short edge could be potentially increased in depth as it is usually hidden within the top and bottom connection within the opaque panels between ceiling and floor. As such the top connection was modified and depth increased to 75mm. Decrease in overall deformation from 35.8mm to 28.9mm was noticed, not as dramatic as hoped for. However, a further study will be required to understand this phenomenon in greater detail and as such optimise this concept for practical application. The following graph summarises deformations and neutral axis stress. It is clear

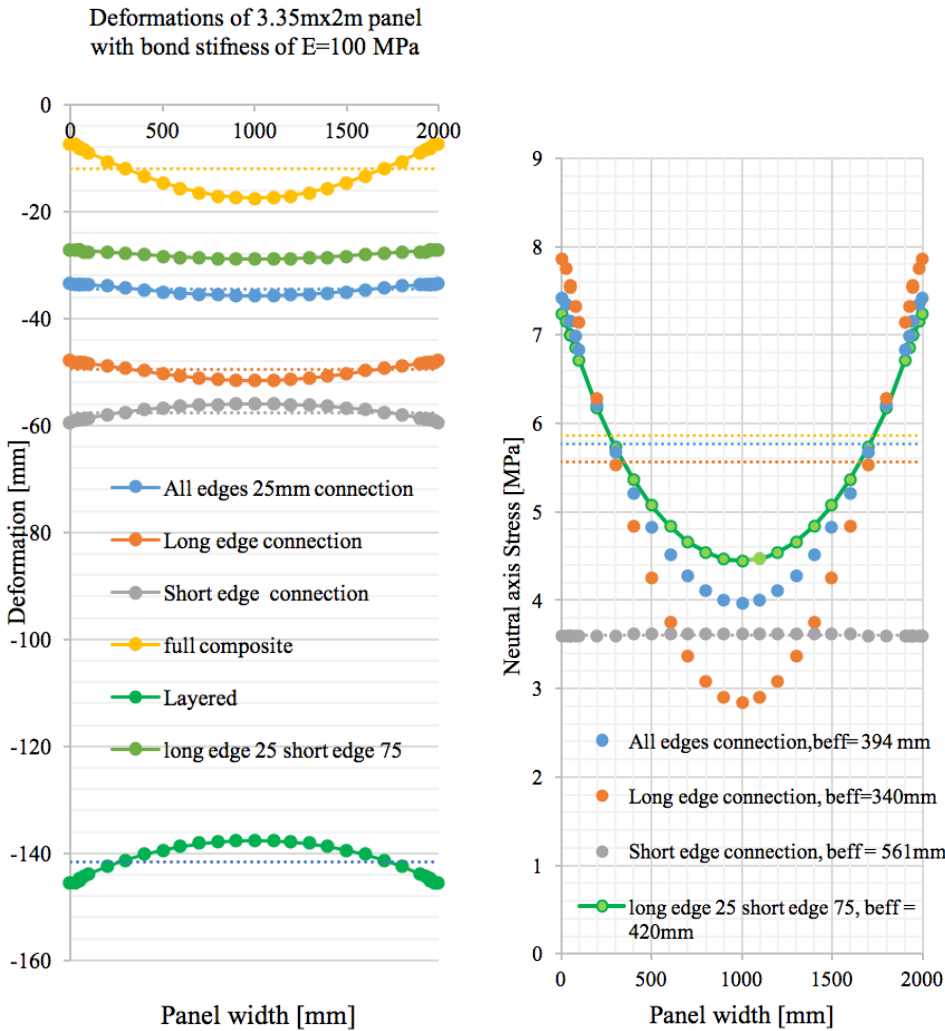


Fig 11 Analysis results

- a. Deformation plot at mid span through panel width
- b. Neutral stress plot at mid span through panel width



Fig 12 Glass pavilion mock up and detail



Fig 13. Material selection, Timber, Traditional glass laminate, thin glass

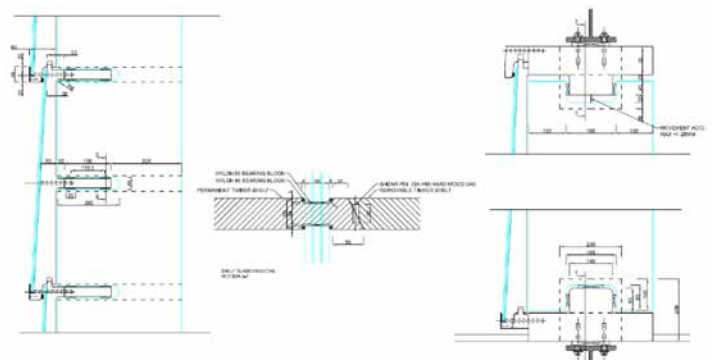


Fig 14. Concept details

from the neutral axis glass stress plot that a very linear stress distribution is noticeable in the case of the short edge connection. Longer effective width of 561mm was calculated as well in comparison to the effective width of 420mm for the modified all edge condition. The methodology as outlined in [1] and [2] was used to calculate effective width of the structural insulated panel.

### 3.2 Glass / Timber Pavilion

London based architectural studio Friend & Co. won a competition for the new V&A shop with a 6m tall glass pavilion. A main volume is ground supported with a top vertical movement joint to accommodate floor movements. This volume initially comprised of a 6.0m tall, 400mm deep glass fins spaced up to 1200mm from each other. Glass fins were designed as simply supported beams. However, due to the fast track program and long procurement time of the jumbo size glass components available from mainland Europe only, a late design change was introduced to reduce fin size to approximately 3.5m. A second smaller volume attached to the main volume is a 3m tall by approximately 2.5m x 2.5m size in plan. This volume is top hung. As such separation via a movement joint was specified. Again, glass fins as primary structural elements were value engineered after tender stage.

A non-traditional combination of glass and timber was envisage by the architect. From a strength perspective, both C24 softwood and D40 hardwood would be capable of safely transferring loads. However tight deflection limits limited material selection.

One potential issue was the shelf dimension at 400mm. This is on the extreme end of the dimensions available for a solid piece of timber. Typically hardwoods come in larger dimensions (being larger diameter trees) but this depended on availability within the UK market, Alternatives were outlined, namely engineered timber products such as LVL, or glued connections of multiple solid timber planks.

Timber shelves are connected to the glass fins via extremely narrow glass notches. Due to the high stress concentrations at fin notches, heat strengthened glass was specified. Triple laminated glass consisting of 12mm thick panes were considered to provide enough bearing to the timber. Polished edges are specified for the glass fins which are particularly difficult due to the notch shape. The pavilion is clad from outside with glass shingle. Annealed glass is specified to deliver superb visual quality and lightweight appearance. Thin glass laminate was proposed in the early design stages. However due to the procurement time traditional double laminate consisting from 3mm thick glass was ultimately installed.

A series of finite element analyses were carried out to justify the feasibility of the scheme. Global deformations of the global system were within few millimetres. The glass fin was analysed with shell elements and notches of 200x 40mm were explicitly modelled to check local stress concentrations in the glass. It should be noted that good quality of workmanship – glass polish in this zone was achieved.

#### 4 Conclusions and summary

Examining previous Arup projects and projects recently built by others, it was realised that the concept of hybrid glass structures should be reviewed from a wider perspective. Key areas were identified that our clients have been interested in when designing with structural glass. Clients are now interested in holistic design (i.e. combination of multiple performance criteria's rather than structural excellence only.) This requirement is what will define hybrid glass structures of the future. The knowledge from this paper has been disseminate on current Arup Facade Engineering projects.

#### Acknowledgements

Invest in Arup fund 077359-54, Chris Noteboom, Patrick Rogers, Luis Soares Martins, James Griffith, Vladimir Marinov, and Graham Dodd

#### References

- [1] Amadio, C., Fragiaco M., 2002 Effective width evaluation for steel–concrete composite beams *Journal of Constructional Steel Research* 58 (2002) 373–388
- [2] Bin Zou, et al, 2011 Evaluation of effective flange width by shear lag model for orthotropic FRP bridge decks, *Composite Structures* 93 (2011) 474–482
- [3] Dodd, G., Reed, L. 2014, Anchoring Triangular Glass Panels to Prevent Collapse, *Challenging Glass 4 Conference on Architectural and Structural Applications of Glass*, Bos, Louter, Belis (Eds.), 2014.
- [4] Lenk, P., 2016. : *Designing with Structural Glass*, *Challenging Glass 5 Conference on Architectural and Structural Applications of Glass*, Bos, Louter, Belis (Eds.), Ghent University, 2016.
- [5] Lenk, P. Honfi, D., 2016. *Resilience, Damage Tolerance & Risk Analysis of a Structure Comprising Structural Glass, engineered transparency*, Dusseldorf 2016
- [6] Teixidor, C., 2010, *Glass – Honeycomb Composite Panels*, *Challenging Glass 2 Conference on Architectural and Structural Applications of Glass*, Bos, Louter, Veer (Eds.), TU Delft 2010.
- [7] Wurm, J., 2007, *Glass Structures*, Birkhäuser, Germany 2007
- [8] Kozłowski M., E. Serrano E., Enquist B., *Experimental investigation on timber-glass composite I-beams*, *Challenging Glass 4 & COST Action TU0905 Final Conference – Louter, Bos & Belis (Eds) 2014*
- [9] Antolic D., et al, *Laminated Glass Panels in Combination with Timber Frame as a Shear Wall in Earthquake Resistant Building Design*, *Challenging glass 3 conference on architectural and structural applications of glass*, 2012
- [10] Valarinho L., et al., *Numerical simulation of transparent glass-GFRP composite beams using smeared crack models*, *Proceeding of the 6th International Conference on Fibre-Reinforced Polymer (FRP) Composites in Civil Engineering (CICE 2012) Rome 2012*,
- [11] Louter Ch., et al., *Structural Glass Beams with Embedded Glass Fibre Reinforcement*, *Challenging Glass 2 – Conference on Architectural and Structural Applications of Glass*, Bos, Louter, Veer (Eds.), TU Delft 2010
- [12] Bos, F.P., *Stainless steel reinforced and post-tensioned glass beams* Pappalettere, C (Ed.), *International conference on experimental mechanics / icem12 / advances in experimental mechanics*, Bari 2004
- [13] Feldmann, M., Abeln, B., Richter, C., *Experimental and Numerical Studies of the Non-linear Structural Behaviour of Bonded Steel-glass-façade elements Subjected to Multi-axial Loading*, *2nd International Conference on Structural Adhesive Bonding*, Porto 2013

# New Concept of Horizontal Structural Elements in Glass: Self-bearing $\pi$ Shape Plate

## Authors

Cerezo, Jesús M. [1]; Nuñez, Miguel A. [2]; Lauret, Benito [3]; Marco, José M. [4]  
ENAR, Envoltentes Arquitectónicas [1, 2]; UPM [3]; Ariño Duglass [4]

## Keywords

Structural glass; Pre-stressed glass; walkway glass, post-breakage glass beam.

## Abstract

A new design of structural glass application is presented, based on a horizontal self-bearing and pre-stressed glass solution. Our main objectives were to design, develop manufacture and test a completely transparent slender walkway, having the particularity of being self-bearing. The starting point for the design has been the good behaviour of pre-stressed beams in terms of load capacity. Special care has been taken during the design state to fulfil five safety requirements: resistance, retention, redundancy, post-breakage resistance and standard regulations. For the design and verification of the model, analytic structural calculation as well as a finite element model have been carried out. The effect of different pre-stress loads and buckling behavior of the element has been studied, obtaining the relationship between load capacity, deflections, maximum tensional stress in the glass and design parameters. [1] Finally, a full glass prototype has been manufactured and tested. During the loading stage, test deformation and the evolution of stress in glass has been monitored and measured using a polariscope. The glass element has been led to breakage to validate the expected data of the design phase and obtain relevant information regarding the post-breakage behaviour. Load was increased up to 2.5 times design load to reach the breakage state and to hold 1.4 times the design load once reached the collapse state for 12 hours.

## Introduction

This research is the result of several years of study of glass beams, analyzing the problems with the brittle breakage and the safe post-breakage behaviors.

The aim of this study is the design of a self-bearing pre-stressed glass element that achieves the features of maximum transparency and keeps a post-breakage capacity to be used in the field of architecture. For this purpose, there will be inserted a pre-stressed reinforcement steel [2] and a ribbed section shape (that results from an optimized and evolved design). (See Figure 1)

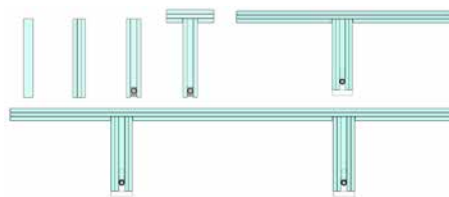


Figure 1

## Design and geometry

The solid beam as concept is only used as a calculation model. Laminated beam will be used as many examples of skylight glass beams enhancing its transparency. Reviewing the state-of-the-art, we can say that the insertion of a pre-stressed reinforcement element will provide a safe breakage beam and a bigger load capacity [3] and against breakage. In the first step of the evolved design, the beam will be compound of several laminated glass plies to keep them joined and to include a redundant or sacrifice leaf in case of breakage. The intermediate glass leaf is trimmed to place a steel rod. This rod will receive a strain of tensile from both ends that compresses the glass plies conferring bigger resistance (increasing the compressed areas and decreasing the tensile areas); otherwise, it increases the safety due to the reinforced steel rod that avoids glass fragments falling down. Because of the pre-stress applied, these fragments will be held together. The effect of pre-stressing in the laminated section provides lateral buckling; in order to avoid this effect a T shape will be obtained with an a bespoke recess in the joint detail. This T shape will increase the inertia. The design will be optimized if the intermediate glass leaf is trimmed with a longitudinal curve shape to avoid the deflection due to the dead loads when the pre-stressing is applied. The linear gap confines the rod laterally. (See Figure 2)



Figure 2

On the other hand, if the wings of the T become bigger to support a uniform distributed load a problem could arise in the joint knot between the horizontal and vertical element obtaining an unstable element as well; to avoid this issue, the section of the T shape is doubled in TT shape solving the problem [4]. In this case, the moment diagram would work as a continuous beam over the ribs (and therefore in a very optimized way) getting a better stability as a prefabricated element easy to transport and install.

Finally, the design could be improved by adding an anti-slip layer of thin glass with more impact resistance (3mm toughened plate). Also, it can be used as a sacrifice layer to be removed when scratched or broken. It would be better if all glass layers were low-iron glass. The self-bearing prefabricated element has a modular character to create slabs. There can be attached elements in 2 directions over a net of 6x6 m. The ribs are located in such a way that the distances between them are the same when more elements are joined. (See Figure 3)



Figure 3

The isostatic glass slab weight is on the top of the pyramid in respect to the slenderness and lightness parameters regarding other slabs for the same loads. (See Figure 4)

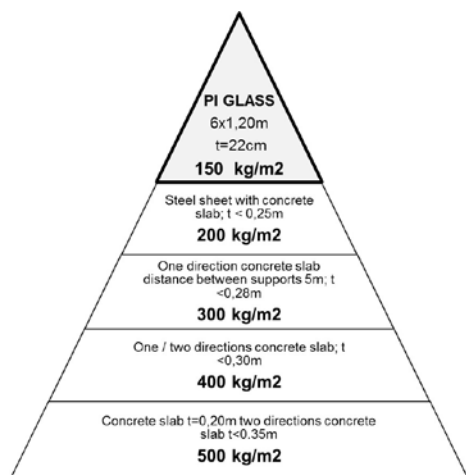


Figure 4

The general geometry is 6.00mX1.2m, length due to the common length of fabrication and width because of half width of a box of a truck. The height of the element does not have precedent in this kind of structural glass element, L/30, reducing the height and the effect of buckling [5]. Other researches use double height, around L/15. (See Figure 5)

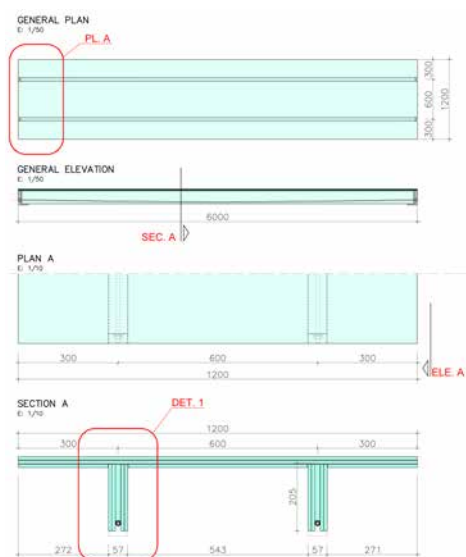


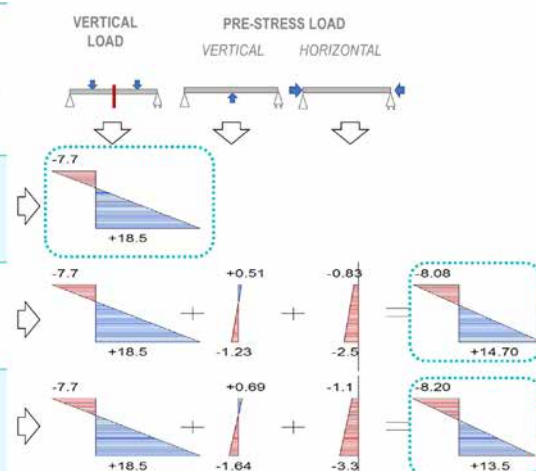
Figure 5

### Hypothesis and bases of calculation

We have adopted the bases of calculation for the glass plate for all the methods of calculation, so they will be performed for the scale 1:2 which will be the scale of the test sample: The dead load of the n glass plate at scale 1:2 is 1,10kN and the live load is 5kN/m<sup>2</sup>. The limit of the deflection will be L/500 since we need to ensure the feeling of stability. The admitted calculation strain according to prEN 16612 will be 14.25 Mpa, according to the type of glass (annealed glass), the surface treatment (without treatment), the type of load

| PRE-STRESS (kN) | INFERIOR STRAIN (Mpa) | UPPER STRAIN (Mpa) |
|-----------------|-----------------------|--------------------|
| 0               | +18,5                 | -7,7               |
| 7,50            | +14,7                 | -8,1               |
| 10,0            | +13,5                 | -8,2               |

Figure 6



(permanent), and the lasting of time (load with peaks as much as 11 hours continuously). To justify the change of the scale in the 3 methods we have to hold the hypothesis that glass always breaks at the same strain in any scale and the deflections are proportional for the same loads. For simulating the uniform distributed load will be replaced by 2 supports located at L/4 from the ends to obtain a similar moment with a deflection that varies less than 10%.

### Checking by analytic calculation

For the analytic calculation, the element is simplified to half section "T" shaped with the same properties in terms of geometry, thickness and compression efforts on the ribs. The hypothesis in this case is that the glass board and ribs are working together monolithically as a single element..

#### Hypothesis

|                           |                        |
|---------------------------|------------------------|
| Distance between supports | L= 3.00 m              |
| Width of load             | B= 0.60 m              |
| Distributed load          | q= 5 kN/m <sup>2</sup> |
| Linear load               | q= 3 kN/m              |
| Point load                | F = 4.5 kN             |
| Position of load (L/4)    | a= 0.75 m              |
| Pre-stress                | N1= 7.5kN; N2= 10 kN   |
| Vertical load             | V1= 0.15kN; V2= 0.2kN  |

#### Geometry data

|                      |                            |
|----------------------|----------------------------|
| Height of beam       | H1= 100 mm                 |
| Width of beam        | b1= 30 mm                  |
| Height of glass pane | H2= 10 mm                  |
| Width of glass pane  | b2= 300 mm                 |
| Inertia              | Ix= 706.25 cm <sup>4</sup> |
| Resistance module 1  | W1= 91.13 cm <sup>3</sup>  |
| Resistance module 2  | W2= 217.3 cm <sup>3</sup>  |
| Area                 | A= 60 cm <sup>2</sup>      |
| Elasticity Modul     | E=73,000 Mpa               |

For developing the analytic calculation, we start with a vertical load and a normal compression load on the ribs. This compression load is

performed through a tensile rod with a curved shape, generating a vertical force against the vertical load. (See Figure 2) If the efforts of these actions are included in the strain graphics of the "T" shaped beam sections, we obtain the results shown below on the left where tensile strain decreases with pre-stressing to improve the glass behavior. (See Figure 6)

### Checking by FEM simulation

For FEM simulation there have been performed several hypothesis and premises to be close to the real test. The load is modeled on a surface of 2 cm in the whole width of the board and the total load is distributed on this surface. The supports are simulated on a lower line on the ribs to avoid distortions in the results; there will be single supports allowing the turns and limiting the 3 displacements in one of the ends and 2 displacements in the opposite one to allow the expansion and the action of the pre-stressing. For simulating the pre-stressing, load is located on the surface of the section of both ends. The strains will be monitored at the middle point of the upper surface of the board, in the lower area of the ribs and the deflections related to different load steps for the 3 cases of comparison:

Without compression, compression of 15kN and compression of 20 kN. The data for the design load is 9kN. (See Figure 7)

| PRE-STRESS (kN) | INFERIOR STRAIN (MPa) | UPPER STRAIN (MPa) | DEFOR-MATION (mm) |
|-----------------|-----------------------|--------------------|-------------------|
| 0               | +19,0                 | -7,8               | -3,7              |
| 7,50            | +16,7                 | -7,6               | -3,3              |
| 10,0            | +13,5                 | -7,5               | -2,8              |

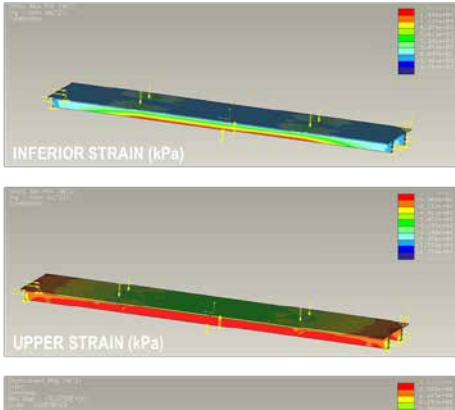


Figure 7



Figure 8

### Checking by tests

First of all, we make several changes to adapt the glass plate to scale 1:2., based on the results of the state-of-art [6].

Glass: Extra clear is replaced by clear float

Glass board: laminated 10+10+10 is replaced by 10+5 allowing the curing of the UV adhesive through the 10mm monolithic glass.

Ribs: Glass pane 19 is replaced by 10 because it is the more similar thickness and it allows the insertion of an 8mm rod.

Layer/ Adhesive: SGP layer is replaced by PVB and UV adhesive.

Tensile rod: S275JR steel Ø16mm rod is changed by Ø8mm rod.

The square shoes of support and pre-stressing keep proportional in thickness and geometry.

Assembly n glass plate: The glass ribs will be located in the boxes of the glass board keeping a perpendicular manner and will be adhered with Panacol Vitricol UV. The lamp used is Panacol S 255 WT with the same brand of Vitralit. This UV adhesive reach stresses up to 23 MPa.

After this, we have to pre-stress the Ø8mm tensile rods locating them into the gap created of 10mm and pre-stressing against the square shoes. In this case, the misaligned problems will be multiplied if the design of the ending elements are very complex. Pre-stressing of 7.5kN and 10kN are applied in each tensile rod that means 3/5 and 4/5 of its elastic limit.

To perform the test we have designed a self-bearing and a test bench.

The measurement devices will be as follows: a load cell with digital screen, a comparator clock with articulated arm, a digital caliper, a polarimeter with specific software and a hydraulic jack as load applicator. (See Figure 8)

Finally, the test process with the load phase in the elastic period was performed as follows: The n glass plate with dimensions 3.00m X 0.60m will support a uniform distributed load of 5 kN/m<sup>2</sup> that means a single load of 9 kN split in two single loads at 1/4 and 3/4 from the ends with several steps of loads along 3 minutes by load step. After this, the load will be increased up to 9 kN x 1.5 = 13.5 kN as safety test.

There will be performed 3 load tests with 3 different conditions: pattern test without pre-stress, 15kN pre-stress test (7.5kN each tensile rod) and 20 kN pre-stress test (10kN per tensile rod). In each of the 3 tests, several data there will be monitored: the lower stress

in the middle of the span in one of the ribs, the upper strains on the glass board and the deflection.

### Extracted results

#### Results of tensile on the low point of the rib

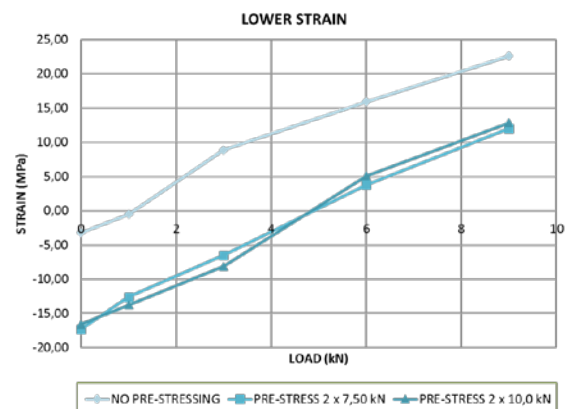
The gap between the yellow graphic and the orange and red ones is due to the first step of pre-stress.

However, there is a short difference between two pre-stressed steps, that means it would have been suitable to apply increase the difference between pre-stress loads for improving the results.

In the case of a non-pre-stressed beam, it has not been carried out a safety test because there was a big breakage risk overcoming the calculation resistance. (see Figure 9)

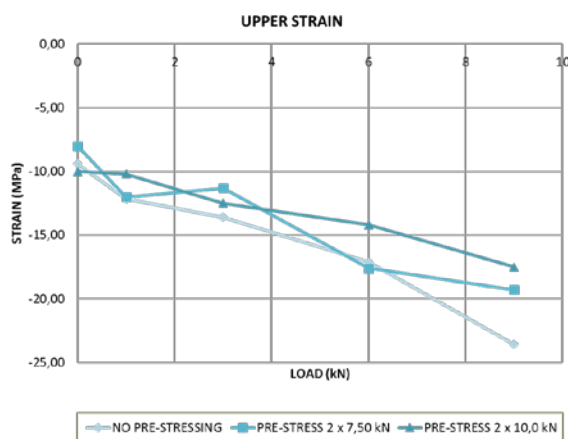
| LOAD (kN) | LOWER STRAIN  |                        |                        |
|-----------|---------------|------------------------|------------------------|
|           | NO PRE-STRESS | PRE-STRESS 2 x 7,50 kN | PRE-STRESS 2 x 10,0 kN |
|           | TEST          | TEST                   | TEST                   |
| 0         | -3,2          | -17,3                  | -16,58                 |
| 1         | -0,5          | -12,6                  | -13,75                 |
| 3         | 8,9           | -6,5                   | -8,10                  |
| 6         | 15,9          | 3,8                    | 5,10                   |
| 9         | 22,6          | 12                     | 12,83                  |
| 13,5      |               | 21,85                  | 16,50                  |

Figure 9



| UPPER STRAIN |               |                        |                        |
|--------------|---------------|------------------------|------------------------|
| LOAD (kN)    | NO PRE-STRESS | PRE-STRESS 2 x 7,50 kN | PRE-STRESS 2 x 10,0 kN |
|              | TEST          | TEST                   | TEST                   |
| 0            | -9,4          | -8                     | 0                      |
| 1            | -12,15        | -12                    | -10,2                  |
| 3            | -13,6         | -11,3                  | -12,5                  |
| 6            | -17,1         | -17,6                  | -14,2                  |
| 9            | -23,57        | -19,3                  | -17,5                  |
| 13,5         | -             | -24,4                  | -20,7                  |

Figure 10

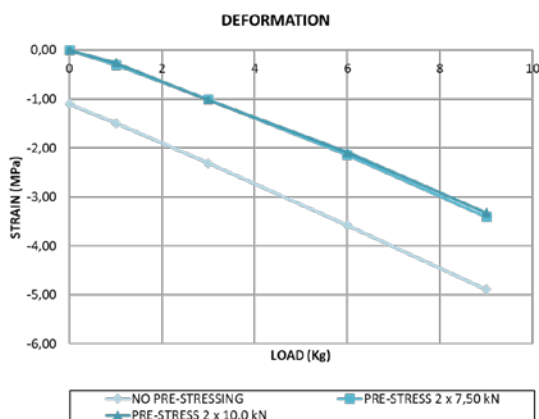


### Results of tensile from the upper point over the glass board

There has been checked the stress on the laminated glass board according to the polarimeter: it is 7 MPa due to the pressure and temperature in the laminated process. The highest value of the compression stress is exactly from ribs without pre-stress because this is not balanced for any compression in the lower part and therefore it has highest values in tensile stress (below) and compression stress (upper). (See Figure 10)

| DEFORMATION |               |                        |                        |
|-------------|---------------|------------------------|------------------------|
| LOAD (kN)   | NO PRE-STRESS | PRE-STRESS 2 x 7,50 kN | PRE-STRESS 2 x 10,0 kN |
|             | Test media    | Test media             | TEST                   |
| 0           | -1,08         | 0                      | 0                      |
| 1           | -1,49         | -0,3                   | -0,26                  |
| 3           | -2,31         | -1,01                  | -1,02                  |
| 6           | -3,58         | -2,14                  | -2,09                  |
| 9           | -4,89         | -3,405                 | -3,32                  |
| 13,5        | 0             | -5,175                 | -5,16                  |

Figure 11



### Results of deflections

The deflection in the case of non-pre-stress is almost 50% in respect to the pre-stressed ones and there is a short difference between them. The constant created between the lines is almost parallel and is due to the contra deflection acquired in the process of pre-stress. (See Figure 11)

### Differences among test results with different pre-stress

Pre-stress improves mainly lower tensile stress and therefore also its resistance and breakage risk. The effect of pre-stressed causes a reduction of the upper stresses that means improving these stresses. Deflections are also improved giving stiffness and stability feeling.

The big jump of improving in the lower stress and deformation are achieved in great amount with the first step of pre-stressing. The second step of pre-stressing confirms the trend but does not improves according to pre-stress increasing. (See Figure 12)

| Load = 9 kN            | TEST                  |                    |                  |
|------------------------|-----------------------|--------------------|------------------|
|                        | INFERIOR STRAIN (MPa) | UPPER STRAIN (MPa) | DEFORMATION (mm) |
| NO PRE-STRESS          | 22,60                 | -23,57             | -4,89            |
| PRE-STRESS 2 x 7,50 kN | 12,00                 | -19,30             | -3,41            |
| PRE-STRESS 2 x 10,0 kN | 12,83                 | -17,50             | -3,32            |

Figure 12

### Post-breakage behaviour (non-elastic period)

This test of post breakage behavior is performed with a simulation of uniform distributed load (4 points) with a 20 kN of pre-stressing (10 kN per rib). There are different phases in the breakage and also there are 2 rules from the state-of-the-art that says than with the first crack in the lower part in a test of 4 point is considered breakage; when the first crack appears in the upper part of the board that is considered collapse. We are going to differentiate 3 phases: elastic period until breakage, and non-elastic period with breakage with loadbearing for some time and with collapse with loadbearing for some time. In the first step the deflections are proportional to the loads in the elastic period: The design load of 9 kN is reached with deflection of 3.3 mm. The safety load (1.5 x 9=13.5kN) is reached with deflection of 5.2 mm

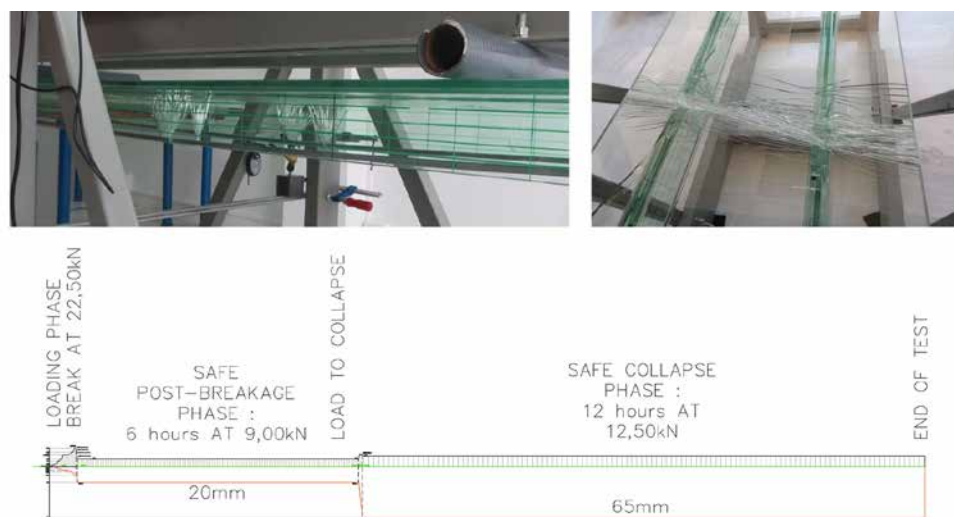


Figure 13

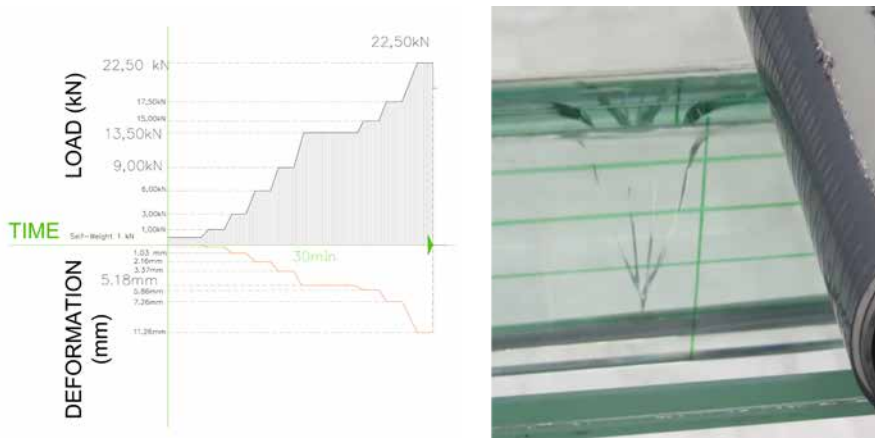


Figure 14

The breakage is reached up to 22.5 kN (2.5 times design load) when the first crack appears in the lower part of the rib. (See Figure 13)

### Breakage phase

This crack in "V" shape is repeated until 3 times in an identical way in the same rib. This crack is characteristic extending in horizontal in the upper area because is the more compressive area.

The crack does not reach the upper area and the reinforcement steel rods avoid the element from going down. Once the safety load is reached (22.5 kN) and cracks appear sequentially in the same way, so at the same time the element is going unloading until the stabilization at the load of 9 kN (the design load by coincidence) with a deflection of 20 mm (6 times bigger than without breakage) and keeping in this way for 6 hours when we decided to lead it to the collapse. (See Figure 14)

### Collapse phase

After post-breakage phase, the phase of collapse begins when the first crack appears on the upper surface of the board [7]; this is considered unsafety. That means although the sample was not collapsed keeping itself due to the adherence of glass panes and the rods of pre-stressed with all the layers broken, it is considered unsafety.

In the test, the first crack on the horizontal surface appears at the load of 15 kN; in that moment, we stopped applying the load and decreased until 12.5 kN where it will be kept by itself with a deflection 65 mm for 12 hours; in that moment we considered the end of the test. In this final figure, we can see how the test sample has finished the test after the loads supported and the lack of the visible collapse holding a load of 1.4 times the design load with an extension of deflection [8] of L/50 approximately. (See Figure 15)

### Conclusions and summary:

#### General

The prefabricated PI shaped glass plate has demonstrated its ability and safety post-breakage to become a reliable element for applying in the field of architecture. The structural element achieved gets bigger transparency with less glass due to a slender section more optimized thanks to pre-stressing.

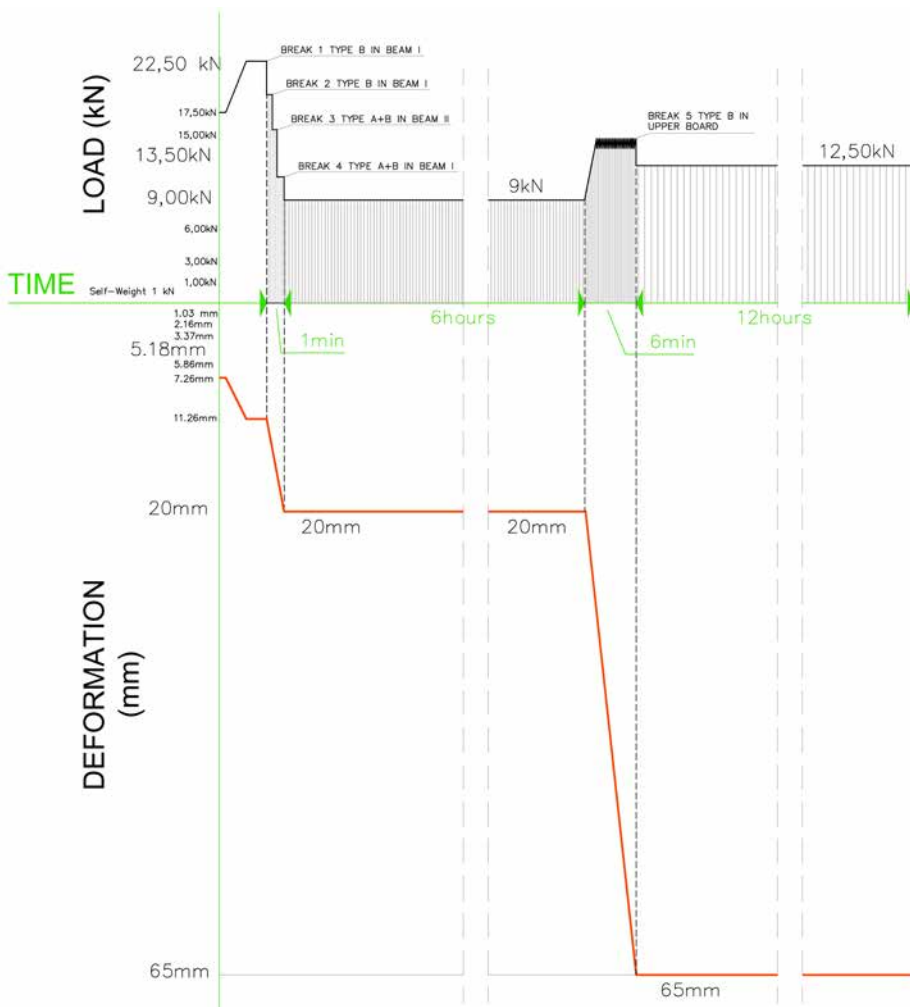


Figure 15

## Methodological conclusions

The test at scale confirms the analytic calculation results and the results coming from the FEM simulation within the elastic period and therefore the method is right. Test let to characterize the post-breakage behavior, impossible from the analytic study.

## From materials

The adhesive technology and its efficiency has been demonstrated without increasing unknowns even in the limit situation of breakage keeping the UV adhesive unalterable. Steel alternatives with more resistance will imply a more slender design.

## Structural range

The pre-stressing designed improves the strains and the deflections of the glass plate and it is a way to optimize the sections achieving greatest slender.

The weight per square meter is lighter for supporting the same load than the lightest steel or concrete slab.

## Experimental range

The results have demonstrated safety against the breakage when is applied a pre-stressing decreasing the tensile at the lower area and getting smaller deflections.

It is possible to increase the pre-stressing if we improve the quality or even if the section of the rod is increased.

Since the breakage has reached 2.5 times the design load, with this result, we have achieved a safety collapse under our point of view.

The box in the lower part of the board has controlled the lateral buckling of the ribs coming from due to compression effect and the deflection due to the loads.

It is significant the importance of keeping the design load of 9.00kN/m<sup>2</sup> since the breakage for 6 hours and keeping for 12 hours the collapse phase with 1.4 times the design load. Finally, it has been shown a high level of breakage safety and we have achieved to take a little step forward against the brittleness of glass [9]. (See Figure 16)



Figure 16

## References:

- [1] AMADIO, C., & BEDON, C. (2010). Buckling of laminated glass elements in out-of-plane bending. *Engineering Structures*(32), 3780-3788.
- [2] CUPAC, J., MARTENS, K., NUSSBAUMER, A. ET AL. *Glass Struct Eng* (2017) 2: 3. doi:10.1007/s40940-017-0038-5
- [3] BOS, F. P.; VEER, F.A.; HOBBELMAN, G.J. ; LOUTER, P.C. (2008). Stainless steel reinforced and post-tensioned glass beams. Recuperado el 7 de Abril de 2008
- [4] VEER, F. (2007). Walking on air, designing and engineering a glass bridge. *Glass Performance Days* (pp. 244-246). Tampere, Finland: GPD.
- [5] LOUTER, C., BELIS, J., VEER, F., & LEBET, J. (2012). Structural response of SG\_Laminated reinforced glass beams; experimental investigations on the effects of glass type. *Engineering Structures* (36), 292-301.
- [6] LOUTER, C. (2007). Experimental research on scale 1:4 models of an 18m reinforced glass beam, part i. *Glass Performance Days 10th International Conference on Architectural and Automotive Glass*. Tampere, 87-92.
- [7] LOUTER, C. (2013). Reinforced and Post-tensioned Glass Beams. Tampere: GPD.
- [8] MARTENS, K.; CASPEELE, R.; BELIS, J (2015). Development of composite glass beams – A review. DOI: <https://doi.org/10.1016/j.engstruct.2015.07.006>
- [9] MARTENS, K.; CASPEELE, R.; BELIS, J (2015). Development of Reinforced and Posttensioned Glass Beams: Review of Experimental Research. DOI: [http://dx.doi.org/10.1061/\[ASCE\]ST.1943-541X.0001453](http://dx.doi.org/10.1061/[ASCE]ST.1943-541X.0001453)

## Acknowledgements:

The authors gratefully acknowledge the support provided by Ariño Duglass, Laguna Belvis and ENAR team.

# Production and Testing of Kiln-cast Glass Components for an Interlocking, Dry-assembled Transparent Bridge

## Authors

Telesilla Bristogianni 1, Faidra Oikonomopoulou 2, Fred A. Veer 2, Ate Snijder 2, Rob Nijssse 1,2  
 1 TU Delft, Civil Engineering and Geosciences  
 2 TU Delft, Faculty of Architecture

## Keywords

Cast glass, interlocking components, kiln-casting, glass bridge, dry-assembled transparent load-bearing structures

## Abstract

A pedestrian glass bridge, located at the TU Delft campus site, is being designed by the TU Delft Glass & Transparency Group. Specifically, the arch-formed bridge consists of cast, dry-assembled, interlocking glass components. To validate the shape of the components, glass mock-ups in 1:2 scale have been kiln-cast and tested. This paper follows the elements' production process from the 3D milled MDF model and the construction of disposable moulds via the lost-wax technique, to the kiln-casting at 940°C with the "flowerpot method". Steps are taken towards the refinement of the production technique, with emphasis in minimizing the occurrence of air bubbles, surface flaws and internal stresses that can reduce the load-bearing capacity of the components. Polarisation techniques are employed to define the residual stress distribution of the cast elements as well as to map the consolidated flow of molten glass and the areas of inhomogeneity or non-cohesion. The structural performance of the components and their interlocking behaviour are studied by conducting shear tests on three series comprising three glass bricks with a transparent PU interlayer in-between. The fracture patterns of the specimens are analysed and correlated with the flaws and internal stresses resulting from the kiln-casting process.

## 1. Introduction

The high compressive strength of glass renders the material suitable for load-bearing applications in structures subjected to compression. In that sense, and inspired by



Figure 1 Aspect of the Glass Masonry Bridge and the brick shape

the logic of the Roman arches, a completely transparent glass masonry bridge has been designed by Snijder et al. [1], to be located at the Green Village at TU Delft. The potential of glass masonry systems, comprising adhesively bonded solid glass bricks is well demonstrated by the completion of the Crystal Houses in Amsterdam in 2016 [2]. Developing this innovative glass system a step further, the bridge circumvents the need for an adhesive connection between the glass bricks. Thus it is composed of curved interlocking cast glass components, compressed together to form a stable arch (Figure 1). In-between the glass bricks, a transparent Polyurethane (PU) rubber interlayer is placed, to avoid stress concentrations. Such dry-connections allow for the easy assembly and disassembly of the structure and favour the reuse and/or easy recycling of the individual components. These design decisions result in a more sustainable application of structural glass.

Previous research by [1], [3], [4] led to the current interlocking brick shape that limits the contact of the bricks to the upper and bottom zone of the bridge. This choice leads to a minimum generation of tensile forces in the case of asymmetrical loading. The current paper focuses on the study of the interlocking

behaviour of these components. For the purposes of the presented research, a series of glass components have been kiln-cast at the TU Delft Glass & Transparency Laboratory in scale 1:2 and tested in shear. The production of these components differs from the conventional hot-pour casting process which will be used for the final bricks for the bridge, as in kiln casting the glass is cast at a lower temperature and thus with a higher viscosity. The paper studies the production process, to determine the influence on the strength and structural behaviour of the bricks.

## 2. Production of the components

### 2.1. Mould production

Disposable investment moulds are prepared for the casting of the glass specimens. The lost-wax technique is- at this initial development stage- preferred, as it allows for the fast and low-cost production of moulds, and thus the easy experimentation with various shapes. The process consists of a series of steps (Figure 2), starting with the accurate milling of the desired brick model in medium-density fibre board (MDF). Based on the MDF model, a silicone counter-mould is produced that serves for the shaping of the brick model in wax. An investment slurry consisting of



Figure 2 Production steps from MDF mould to final glass model

| B 270® i Ultra-White Glass by Schott |               |               |                 |
|--------------------------------------|---------------|---------------|-----------------|
| Before casting                       |               | After casting |                 |
| Compound name                        | Content (wt%) | Content (wt%) | Difference in % |
| SiO <sub>2</sub>                     | 71.802        | 71.883        | 0.081           |
| Na <sub>2</sub> O                    | 10.138        | 9.629         | -0.509          |
| K <sub>2</sub> O                     | 6.275         | 6.122         | -0.153          |
| CaO                                  | 5.168         | 5.575         | 0.407           |
| ZnO                                  | 2.198         | 2.452         | 0.254           |
| Al <sub>2</sub> O <sub>3</sub>       | 2.083         | 1.777         | -0.306          |
| TiO <sub>2</sub>                     | 1.765         | 1.622         | -0.143          |
| Sb <sub>2</sub> O <sub>3</sub>       | 0.403         | 0.444         | 0.041           |
| MgO                                  | 0.041         | 0.042         | 0.001           |
| BaO                                  | 0.03          | 0.286         | 0.256           |
| Cl                                   | 0.022         | -             | -               |
| S                                    | 0.018         | 0.058         | 0.04            |
| Er <sub>2</sub> O <sub>3</sub>       | -             | 0.043         | -               |
| P <sub>2</sub> O <sub>5</sub>        | 0.017         | 0.014         | -0.003          |
| Fe <sub>2</sub> O <sub>3</sub>       | 0.016         | 0.018         | 0.002           |
| ZrO <sub>2</sub>                     | 0.008         | 0.009         | 0.001           |
| SrO                                  | 0.006         | 0.008         | 0.002           |
| Rb <sub>2</sub> O                    | 0.005         | 0.005         | 0               |
| NiO                                  | -             | -0.004        | -               |
| CuO                                  | -             | 0.004         | -               |
| PbO                                  | 0.005         | 0.003         | -0.002          |

Table 1 Composition of B 270® before and after kiln-casting

1 part water to 2.8 parts Crystalcast M248- a powder mixture of Cristobalite, Quartz and Gypsum [5]- is poured around the wax and left to cure. The steaming out of the wax model results in a heat-resistant mould, suitable for glass casting up to 900°C temperature. After the casting is completed, the mould is removed by submerging it in to water, which dissolves down the investment material. A more detailed description of the above process is described in [6].

## 2.2. Selected type of glass

The selected glass for the castings is B 270® i Ultra-White Glass by Schott, an optical highly transparent crown glass used for optical applications [7]. Zschimmer [8] stresses the importance of such potash-lime-silica systems -the base of crown glass- in glass technology, due to their lack of colour when compared to typical soda-lime-silica systems. The glass used is shaped in the form of lenses of 70mm diameter.

The exact glass composition is analysed with a Panalytical Axios Max WD-XRF spectrometer and the data are evaluated via SuperQ5.0i/Omnia software. As seen in [Table 1] Zinc oxide is also included in the recipe, a compound contributing, as well, in the colourlessness of the glass [8].

[Figure 3] provides insight to the viscosity of the glass used as a function of the temperature. In short we encounter the softening point at 724°C, the annealing point at 541°C and the glass's strain point at 511°C [9]. The forming temperature starts from 827°C.

| Firing no                             | 10  |       |     |     |     | 11     |       |                      | 14                   |  | 19 |  |
|---------------------------------------|-----|-------|-----|-----|-----|--------|-------|----------------------|----------------------|--|----|--|
| Brick number                          | a   | b     | 1   | 2   | 3   | a      | c     | c                    | f                    |  |    |  |
| Position in the kiln (door at bottom) |     |       |     |     |     |        |       |                      |                      |  |    |  |
| Flowerpot arrangement                 |     |       |     |     |     |        |       |                      |                      |  |    |  |
| Distance flowerpot-mould (mm)         | 40  | 40    | 30  | 30  | 40  | 0      | 0     | 25                   | 40                   |  |    |  |
| Diameter of flowerpot (mm)            | 20  | 20    | 14  | 14  | 14  | 12, 14 | 12    | 14                   | 14                   |  |    |  |
| Air bubbles                           |     |       |     |     |     |        |       |                      |                      |  |    |  |
| Air-bubble size (mm)                  | ≤ 3 | ≤ 2,5 | ≤ 1 | ≤ 1 | ≤ 1 | ≤ 1    | ≤ 1,5 | ≤ 1 (2 bubbles: 3,5) | ≤ 1 (2 bubbles: 3,5) |  |    |  |
| Surface crystallisation               | no  | no    | yes | yes | yes | no     | no    | no                   | no                   |  |    |  |
| Internal stresses (front side)        |     |       |     |     |     |        |       |                      |                      |  |    |  |
| Internal stresses (concave side)      |     |       |     |     |     |        |       |                      |                      |  |    |  |

Table 2 Variables and results regarding Firings 10, 11, 14 and 19

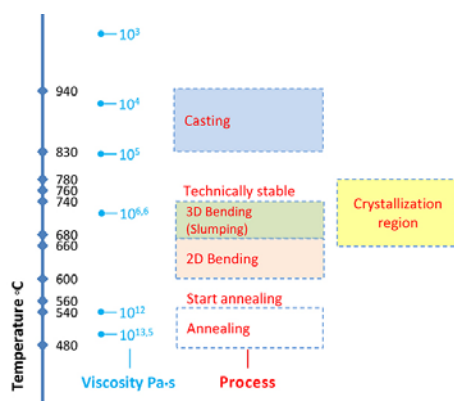


Figure 3 Viscosity of B 270® glass as a function of temperature

## 2.3. Casting set-up and firing schedules

The glass bricks studied in this paper are produced by kiln-casting [Figure 4]. This production technique employs a single kiln for the melting of the glass into the moulds and for the subsequent annealing process. As the investment moulds remain in the kiln throughout the whole process, they define the maximum heating rate (50°C/hr) and maximum temperature (900°C) that can be reached [10]. These specifications are tested by the authors and adjusted up to a heating rate of 75°C/hr and a maximum temperature of 950°C. The maximum temperature reached corresponds to a glass of 10<sup>5</sup> dPa•s viscosity [9]. This viscosity value is considerably higher than in the hot-pour casting method, which is planned for the final production of the bricks. Indeed in such a method, viscosities of around 10<sup>3</sup> dPa•s or less are achieved [11],

to guarantee a homogeneous and air-bubble free mixture. Questions are therefore raised regarding the homogeneity, cohesion and strength of the glass components produced by the kiln-casting method. The above mentioned aspects will be examined below. The "flowerpot" casting method is employed for the feeding of the glass into the moulds. This method suggests the positioning of terracotta flowerpots filled with glass above the moulds. At forming temperatures, the glass drops down through the flowerpot hole and fills the mould [Figure 5].



Figure 4 Kiln-casting method



Figure 5 Glass flowing from the flowerpot down to the mould

| Firing schedule 10 |             |                | Firing schedule 11 |             |                | Firing schedule 14 |             |                | Firing schedule 19 |             |                |
|--------------------|-------------|----------------|--------------------|-------------|----------------|--------------------|-------------|----------------|--------------------|-------------|----------------|
| Temperature (°C)   | Ramp (°C/h) | Dwell time (h) | Temperature (°C)   | Ramp (°C/h) | Dwell time (h) | Temperature (°C)   | Ramp (°C/h) | Dwell time (h) | Temperature (°C)   | Ramp (°C/h) | Dwell time (h) |
| 25                 |             |                | 25                 |             |                | 25                 |             |                | 25                 |             |                |
|                    | 50          |                |                    | 75          |                |                    | 50          |                |                    | 50          |                |
| 750                |             | 2              | 750                |             | 2              | 350                |             | 1              | 750                |             | 1              |
|                    | 50          |                |                    | 75          |                |                    | 50          |                |                    | 50          |                |
| 850                |             | 2              | 850                |             | 1              | 750                |             | 1.5            | 850                |             | 1              |
|                    | 30          |                |                    | 40          |                |                    | 50          |                |                    | 50          |                |
| 950                |             | 7              | 940                |             | 28.5           | 850                |             | 2              | 940                |             | 8              |
|                    | -160        |                |                    | -160        |                |                    | 30          |                | open door          |             | -260           |
| 870                |             | 1              | 870                |             | 2              | 940                |             | 9              | 617                |             |                |
| open door          |             | -105           | open door          |             | -113           | open door          |             | -160           |                    | -160        |                |
| 606                |             |                | 616                |             |                | 870                |             | 2              | 560                |             | 6              |
|                    | -160        |                |                    | -160        |                | open door          |             | -125           |                    | -2          |                |
| 580                |             | 4              | 580                |             | 4              | 600                |             |                | 540                |             | 12             |
|                    | -2          |                |                    | -2          |                |                    | -160        |                |                    | -2          |                |
| 540                |             | 12             | 540                |             | 12             | 560                |             | 12             | 510                |             | 12             |
|                    | -2          |                |                    | -2          |                |                    | -2          |                |                    | -2          |                |
| 510                |             | 12             | 510                |             | 12             | 540                |             | 12             | 480                |             | 6              |
|                    | -2          |                |                    | -2          |                |                    | -2          |                |                    | -30         |                |
| 480                |             | 4              | 480                |             | 4              | 510                |             | 12             | 300                |             | 0              |
|                    | -30         |                |                    | -30         |                |                    | -2          |                | 150                |             | 0              |
| 300                |             | 2.5            | 300                |             | 2.5            | 480                |             | 4              | 20                 |             | 0              |
|                    | -30         |                |                    | -30         |                |                    | -30         |                |                    | -30         |                |
| 150                |             | 0              | 150                |             | 0              | 300                |             | 2.5            |                    |             |                |
|                    | -25         |                |                    | -25         |                |                    | -30         |                |                    |             |                |
| 20                 |             | 0              | 20                 |             | 0              | 150                |             | 0              |                    |             |                |
|                    |             |                |                    |             |                |                    | -25         |                |                    |             |                |
|                    |             |                |                    |             |                | 20                 |             | 0              |                    |             |                |

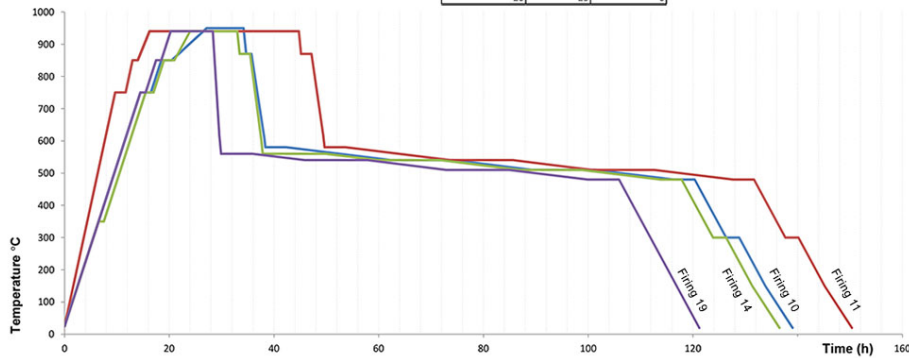


Table 3 Firing schedules 10, 11, 14 and 19

Four firings- Firing 10, 11, 14 and 19- are conducted for the production of the glass bricks, using a ROHDE ELS 200 S Kiln with 5-sided heating. Different variables regarding the casting set-up are presented in [Table 2]. The position of the mould in the kiln, the number of used flowerpots, the distance of the flowerpots from the mould and the radius of the flowerpot hole are documented so that their influence to the final product is examined. The four firing schedules followed are presented in [Table 3]. Although the schedules are mainly similar, a few alternations do occur between them. Regarding the heating up of the moulds and glass, Firing 10 has the slowest process, lasting 27hrs while Firing 11 has the fastest, lasting 16hrs. At top temperature, Firing 11 has a considerably higher dwell, reaching 28.5 hrs while the rest of the firings have a dwell between 7-9hrs. Regarding the temperature drop from the forming temperature to the annealing point, in Firing 10, 11 and 14, this occurs in two steps, one from 940°C to 870°C at -160°C/hr rate (including 1-2hrs dwell at 870°C) and a second step at approx. -105 to 125°C/hr rate (executed by consecutively opening and closing the kiln door). In Firing 19, the intermediate step at 870°C is avoided, and the cooling down occurs at a -260°C/hr rate (aided by the opening of the kiln door). Finally, in Firings 10 and 11, the annealing soak starts at 580°C while in Firings 14 and 19 it starts lower, at 560°C. In Firing 19, the annealing soak time is half that applied in Firing 14.

### 3. Assessment of the cast components

#### 3.1. Contamination

An X-ray fluorescence (XRF) analysis is conducted with a Panalytical Axios Max WD-XRF spectrometer on a glass specimen resulting from Firing 11. The resulting composition, seen in [Table 1] is compared to the original glass recipe. The difference in content of the main compounds is not exceeding the percentage of  $\pm 0.5$ , therefore significant alternations in the glass recipe are not observed. Impurities due to contamination from the Crystalcast mould do appear, in percentages below 0.05, namely Nickel Oxide ( $\text{NiO}=0.004\%$ ), and Copper Oxide ( $\text{CuO}=0.004\%$ ). The content of Barium Oxide ( $\text{BaO}$ ) and Sulfur (S) is also increased due to contamination from the mould. Especially interesting is the presence of Erbium Oxide ( $\text{Er}_2\text{O}_3=0.043\%$ ) after casting. This is an expensive element often used in soda-lime silicate glasses as a luminescent dopant or to create optical amplifiers [12], [13]. Since optical glass lenses are used for melting, it is possible that Erbium

traces exist in the original recipe and were not traced in the XRF test. An XRF analysis of the Crystalcast is required to define which of the above impurities are indeed attributed to the investment material.

#### 3.2. Air-bubble entrapment

In [Table 2] the distribution and sizing of the entrapped air is seen. It can be observed that the most influential parameters for the size and spreading of the air-bubbles is the size of the flowerpot hole and its distance from the mould. The least air-content is seen in Firing 14, where the minimum flowerpot hole diameter and distance from the mould is found. This can be explained if we focus on the melting and pouring process, as this occurs from the flowerpot to the mould [Figure 6]. First, the glass starts to melt from the boundaries of the flowerpot towards its interior. As the lenses start to fuse together, big bubbles are formed due to the initial existing voids from the stacking of the lenses. Then, the molten glass- with the big bubbles present- starts to flow down the mould and mix with the existing air, creating a new series of big bubbles. The more the level of the molten glass rises in the mould, the less the impact the glass has when dropping and thus the smaller the created air-bubbles. Considering the above, the reduction of the path to be travelled by the molten glass stream (flowerpot closer to the mould) creates less turbulence and thus less air-bubbles. This is also the case with a smaller stream diameter (smaller flowerpot hole). Moreover, a small flowerpot hole prevents the big bubbles formed in the flowerpot to pass through together with the glass. In Firing 14, the use of two smaller flowerpots instead of one bigger further contributes, as less voids occur while stacking the glass lenses inside the smaller pots. The increase of the dwell time at top temperature seems to be less decisive than the above variables in the content of air. This is observed in the samples of Firing 11 -kept at top temperature for approx. 20hrs more than the other samples- that still have a high content of air-bubbles. In Firing 19- the only firing that has one abrupt cooling stage directly from 940°C to 617°C at -260°C/hr rate- an intense swirling of miniature air-bubbles is seen. It should be noted that this firing schedule also

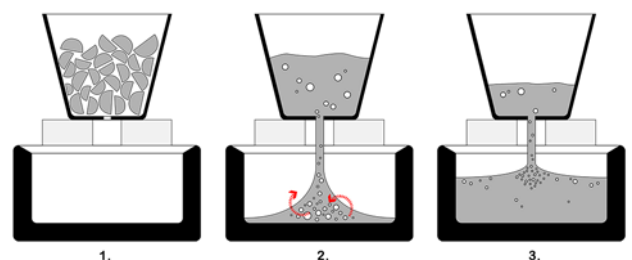


Figure 6 Air-entrapment during kiln-casting

has the fastest heating rate from the start of the forming temperature towards the top temperature. This fast heating implies that the glass is dropping in a faster rate and while larger differentiations in the temperature of the melt occur. This is expected to intensify the swirling of the molten glass inside the mould. Moreover, the fast cooling abruptly "freezes" the air-bubbles in place. At the top surface of both bricks, two bubbles of larger diameter were about to escape when they got trapped in the glass by the abrupt cooling. This shows that similar bigger bubbles (caused at the initial melting step) that existed in the samples of the other firings had enough time to escape with a slower cooling rate. In principle, such bubbles have a bigger volume that creates a bigger upward force, making their escape easier than in the case of the smaller bubbles (that even after 28.5hrs at 940°C in Firing 11, they were still present). Finally, the position of the moulds in the kiln has negligible influence in the formation of air-bubbles.

### 3.3. Surface crystallization

Crystallization at the top surface is only observed in the samples of Firing 11. This crystallization appears in the perimeter of the bricks, where the glass surface is in contact with the mould. The nucleation is thus linked to the mould material and possibly to the contamination of the air circulating inside the kiln. Although the dangerous crystallization zone of B 270 glass is empirically located between 780-660°C, the prolonged presence of the samples at top temperature and the extra hour of dwell at 870°C seems to affect the growth from the nuclei. As the temperature range of crystallisation can differ with the nucleating agent [14] an analysis of the percentage of crystallinity should be conducted in order to identify the present crystal.

### 3.4. Internal stresses

A qualitative estimation of the strain concentration and the uniform stress regions is made by projecting a polarized white light source behind the bricks and photographing them with a crossed circular polarized filter. Areas subjected to stress exhibit optical birefringence, causing the polarized light beam to exert the glass object with a phase difference that corresponds to the presence of isochromatic fringes [15]. In [Table 2] the results of the polarized pictures can be seen and compared. In general, regardless the firing schedule, the location of the moulds in the kiln, and the number of flowerpots used, all bricks seem to have the same stress distribution [Figure 7]. The geometry of the brick is thus catalytic in the arrangement of these stress regions. The polarized images suggest that these regions are linked with the manner the

molten glass is flowing from the flowerpot stream inside the specific shape of the mould. This is especially evident when studying the polarized images of the concave side of the bricks [Figure 8]. The regions imply that the flowing glass mass - due to its relatively high viscosity at the top temperature- does not entirely cohere throughout the total volume, resulting thus to the occasional appearance of fusion lines/strips. The described layering is particularly evident in the bricks of Firing 19 that are abruptly cooled to the annealing point. Regarding the quantity of the stresses, the bricks of Firing 10, as well as the bricks 11-1 and 19c have higher internal stresses. Other factors -for example the location of the moulds in the kiln and therefore their proximity to the kiln-door, the heating elements or other moulds- seem to interfere with the cooling schedule of the bricks, causing the observed irregularities. The samples presented in this paper are not sufficient for drawing conclusions on the exact effect of these factors.



Figure 7 Typical stress zones after the kiln-casting of the bricks (Polarized image)

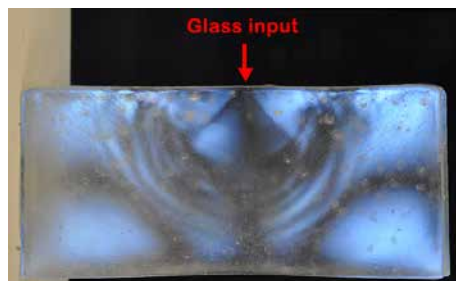


Figure 8 The polarized images show the flow patterns of the glass

## 4. Experimental validation

### 4.1. Experimental set up

The bricks with the least internal stresses, layering and air-bubbles are chosen for the shear experiment. Regarding the experimental set up, three glass bricks with a 2mm thick PU rubber sheet of hardness 70A in between, are framed by two steel L-shaped frames [Figure 9]. The frames are fixed on the base of a Zwick Z100 displacement controlled universal testing machine. Two extra steel plates welded at the frames prevent the side bricks from moving downwards. In between the compression head and the middle brick, an aluminium profile is placed that fits the dimensions of the brick. Loose acrylic parts shaped to match the brick's geometry are placed on the one side for support. The L frames are bolted together until the bricks are fixed in place. Between the horizontal surfaces of the glass components and the elements of the setup, 2mm thick sheets of neoprene are placed. Three shear tests are conducted until failure, with a displacement speed of 10mm/min. The bricks are lit with white polarized light and photographed during the experiment with a crossed circular polarisation filter.

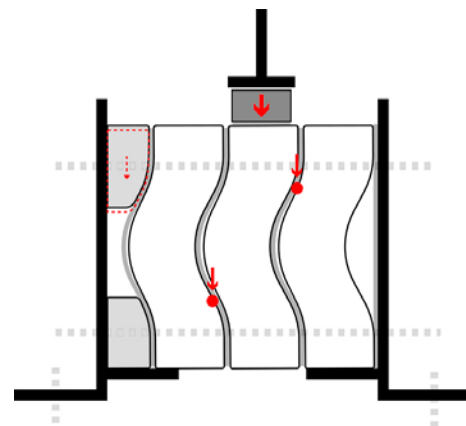


Figure 9 Experimental set-up

### 4.2. Results

In [Figure 10] the load is plotted versus the displacement. Since the contact area between the bricks is limited to their upper and lower part, two point loads develop at the side bricks [Figure 9] during the loading of the middle brick. All tests terminate with the failure of the brick on the right that is confined between the middle glass brick and the L-shaped frame. The loose acrylic parts in contact with the brick on the right allow, in fact, for minor adjustments in the position of this brick and therefore the development of a more favourable load case. The point load acting on the right brick subjects it to bending, creating a zone of tension at its concave surface, from where eventually all bricks start to crack. In [Figure 11], the gradual increase of the number of isochromatic fringes in proportion to the

increase of the external loading can be seen [16]. In [Figures 12] the correlation between the areas where the isochromatic fringes appear during the experiments and the fracture zone of the bricks is seen. In addition, the fracture patterns are linked with the initial polarized images of the bricks, to determine possible defects that could affect the crack path. It is observed that within the weakest zone dictated by the load case, possible flaws found in the glass from the casting become the origins of fracture. This is particularly evident in Test 2/ Brick 14a, where the crack originates from an impurity cluster combined with an air-bubble. Such clusters are not directly observed in the other two cracked bricks (11-3, 14c) which could explain why these bricks failed at double the load. Regarding the path of the cracks, they tend to follow fusion lines and internal stress regions found in the initial polarized images. In brick 11-3 (side view) for example, the crack spread corresponds to a cone region formed exactly below the flowerpot. In the case of brick 14a, when removing the initially attached flowerpot, a damaged glass zone around the terracotta traces was created, which acts as an attraction to the crack path. In [Figures 13] a wave is seen at the crack travelling through brick 11-3 and 14c. Such local deviations can be caused by internal stresses or inhomogeneities [17]. Areas of lower fracture toughness could occur due to the kiln-casting process, introducing weaker zones that divert

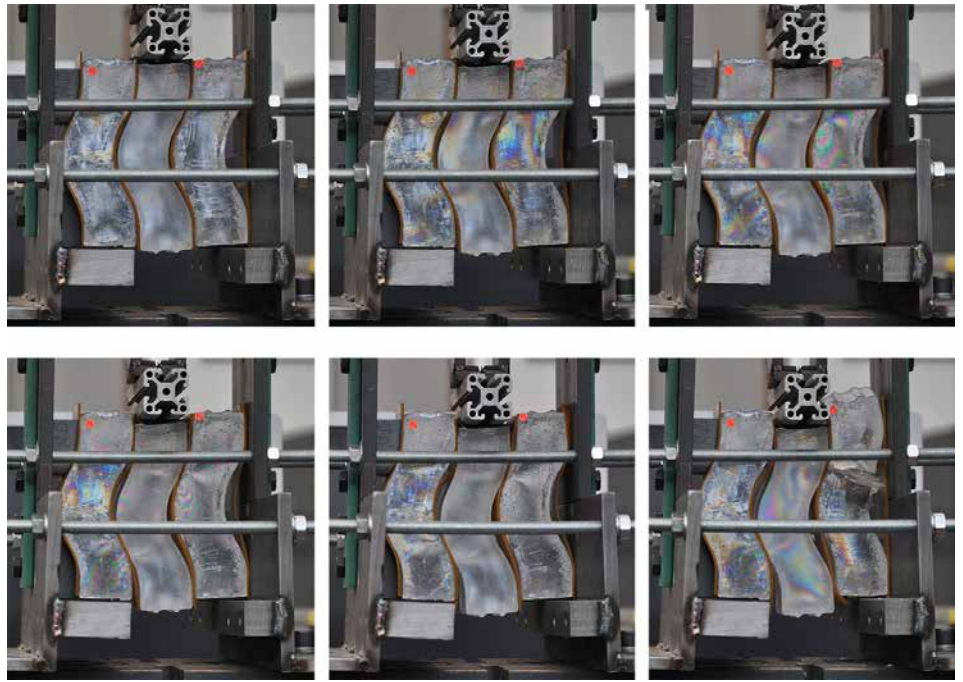


Figure 11 Polarized pictures of Test 1, showing the increase of the stresses developed in the glass

Figure 12 Superposition of the fracture paths of the broken bricks and the polarized images of the bricks before and during testing (prior to failure)

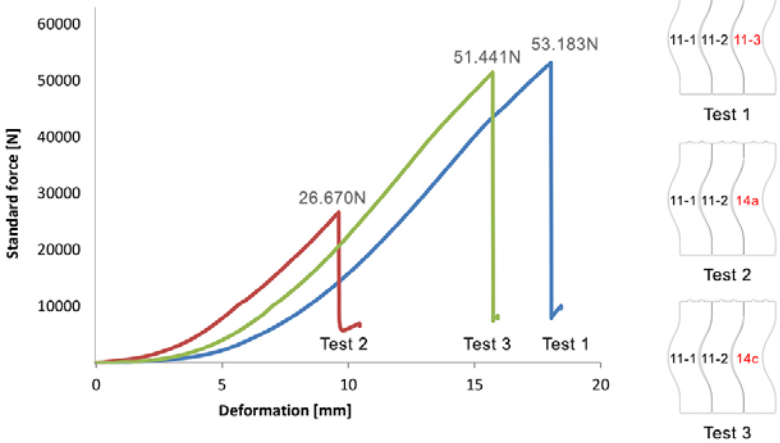
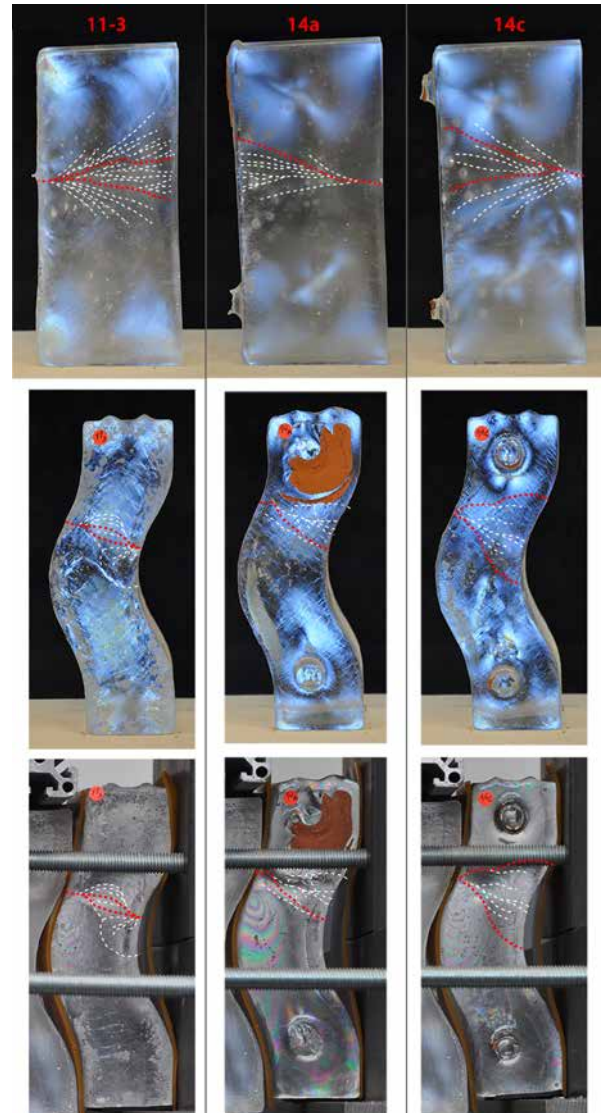


Figure 10 Load versus displacement diagram

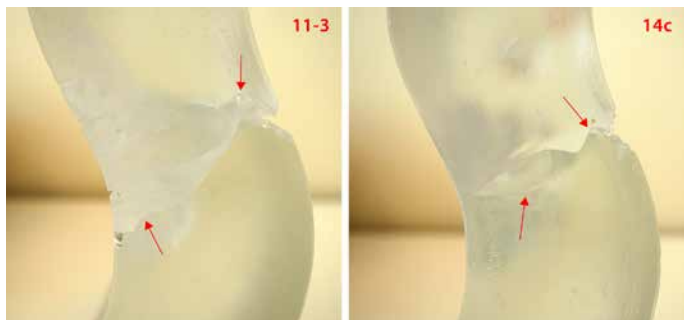


Figure 13 Fracture paths of bricks 11-3 and 14c

the crack. An indentation test should be conducted to define possible differences in the fracture toughness along the glass mass.

## 5. Conclusions

In this paper, interlocking kiln-cast glass components are produced and tested, to define their structural performance. The analysis of the kiln-casting method and its results highlights the influential factors on the quality of the glass components. The process can be optimized when a slower heating rate is adopted, in combination with the use of smaller flowerpots placed directly above the moulds. This is crucial, as flaws generated during the casting stage can initiate failure when subjected to tension. The polarized images of the bricks indicate zones of fusion and inhomogeneity in the glass, due to casting at a relatively high viscosity. Upon brick failure, these are considered weak zones that attract the path of the crack. The kiln-cast bricks -produced for the first experimental phase- form therefore the worst case scenario, as the final hot-poured bricks are not expected to contain these flaws in such extent. Nonetheless, the governing factor in the failure mode of the bricks is the applied load case. In that sense, questions arise whether the partial contact of the bricks at their bottom and top surface- which introduces point loads- is desired. The redesign of the bricks so they achieve full contact along their height could enhance the structural performance of the system and should be experimentally validated in the next research phase.

## References

- [1]. Snijder, A., Smits, J., Bristogianni, T. & Nijse, R., Design and Engineering of a Dry Assembled Glass Block Pedestrian Bridge in Challenging Glass 5, B.L. Belis, Editor. 2016: Ghent.
- [2]. Oikonomopoulou, F., Bristogianni, T., Veer, F., and Nijse, R., The construction of the Crystal Houses façade: challenges and innovations. Glass Structures & Engineering, 2017: p. 1-22.
- [3]. Sombroek, I., Structural cast glass; A research process of design and experiment towards a feasible geometry for a cast glass element, in Architecture and The Built Environment. 2016, TU Delft.
- [4]. Aurik, M., Structural Aspects of an Arched Glass Masonry Bridge, in Civil Engineering and Geosciences 2017, TU Delft.
- [5]. SRS. MSDS Glass Investment Powder. 2003; Available from: [http://artisanfoundry.co.uk/product\\_info.php?products\\_id=131](http://artisanfoundry.co.uk/product_info.php?products_id=131).
- [6]. Bristogianni, T., Oikonomopoulou, F. Veer, F. A. & Nijse, R., Design and production of a structural cast glass element for a transparent dome. in Proceedings of the 6th International Conference on Structural Engineering, Mechanics and Computation, SEMC 2016. 2016. Cape Town, South Africa: CRC Press.
- [7]. SCHOTT. B 270@ i Ultra White Glass. 2013; Available from: [\[glass/ultra-white-glass-b-270-i/index.html\]\(http://www.schott.com/advanced\_optics/english/products/optical-materials/thin-glass/ultra-white-glass-b-270-i/index.html\).](http://www.schott.com/advanced_optics/english/products/optical-materials/thin-</a></li></ol></div><div data-bbox=)

- [8]. Zschimmer, E., Chemical Technology of Glass, ed. M. Cable. 2013, Sheffield, UK: Society of Glass Technology.
- [9]. KNIGHT, OPTICAL. Technical / Sheet Glasses TSG-B270. Available from: <http://www.knightoptical.com/technical-library/sheet-and-technical-glasses/>.
- [10]. Gold, Star. Gold Star Powders. Available from: [www.siamcasting.com/download/SCP.pdf](http://www.siamcasting.com/download/SCP.pdf).
- [11]. SCHOTT, Technical Glasses, Physical and Technical Properties. 2014: Germany.
- [12]. Krsmanović, R., Bertoni, G. & Van Tendeloo, G. Structural Characterization of Erbium doped LAS Glass Ceramic Obtained by Glass Melting Technique. in Eighth Yugoslav Materials Research Society Conference "YUCOMAT 2006". 2006. Herceg-Novi.
- [13]. Lægsgaard, J., Dissolution of rare-earth clusters in SiO<sub>2</sub> by Al codoping: A microscopic model. Physical Review B (Condensed Matter and Materials Physics), 2002. Vol. 65(No. 17): p. p. 174114.
- [14]. Thieme, K., Avramov, I. & Rüssel, C., The mechanism of deceleration of nucleation and crystal growth by the small addition of transition metals to lithium disilicate glasses. Scientific Reports, 2016. 6: p. 25451.
- [15]. McKenzie, H.W., & Hand, R.J., Basic Optical Stress Measurement in Glass. 2011, Sheffield, UK: Society of Glass Technology.
- [16]. Post, D., Photoelasticity, in Manual on Experimental Stress Analysis, J.F. Doyle, Phillips, J. W. & Post, D., Editor. 1989, Society for Experimental Mechanics: Michigan.
- [17]. Quinn, G.D., Fractography of Ceramics and Glasses. 2007: National Institute of Standards and Technology.

## Acknowledgements

The authors would like to thank Hein van de Water (SiO<sub>2</sub>) and Dawn Bendick (Inside Out Glass Studios) for their guidance on the mould-making and kiln-casting process, Lida Barou (CiTG, TU Delft) for assisting with the artwork, Kees Baardolf (BK, TU Delft) for the experimental set-up, Remko Siemerink (BK, TU Delft) for the milled MDF model, Ruud Hendriks (3mE, TU Delft) for the XRF analysis, and Clarissa Justino de Lima (CiTG, TU Delft) for her insight in glass chemistry.

# The Strength of Aged Glass

Kyriaki Corinna Datsiou\*, Mauro Overend

Glass and Façade Technology Research Group,  
Department of Engineering, University of  
Cambridge, Cambridge CB2 1PZ, UK

**Extended Abstract** (The complete contribution will be published in the *Glass Structures and Engineering Journal*)

Glass is known for its excellent durability, but the strength of glass is very sensitive to the characteristics of its surface, which is known to accumulate damage during its service life. There is however, a lack of strength data on weathered or aged glass, particularly on thermally or chemically treated glass.

This study [1] addresses the paucity of data on aged toughened glass by evaluating the decrease in strength of toughened glass caused by erosion of 20-year equivalent natural ageing. The first part implements a method, recently developed by the authors [2] to select suitable parameters for the artificial erosion of glass. These parameters are subsequently used in a carefully calibrated sand trickling test [2] to produce surface damage equivalent to erosive action of 20 years of natural weathering on different types of glass namely: soda-lime-silica annealed (AN), soda-lime-silica fully toughened (FT) and alumino-silicate chemically toughened (CT) glass.

The soda-lime-silica glass specimens are tested destructively in their as-received (AR) and artificially aged (SA) form in a conventional coaxial double ring set-up. During the testing of thin chemically toughened glass it was found that significant stress concentrations are generated in the vicinity of the loading ring that disrupt the equibiaxial state of stress within the loading ring area. Therefore, an improved coaxial double ring set-up that involves the introduction of a spreader plate between the glass specimen and the loading ring, is developed in this study for the destructive testing of thin chemically toughened glass. Additionally, fractography is subsequently used in all types of glass to measure the critical flaw size induced by the sand abrasion. The strength data are analysed statistically and the design strengths for each glass type are obtained. Unsurprisingly, it is found that, as-received chemically toughened glass is the strongest, followed by fully toughened glass

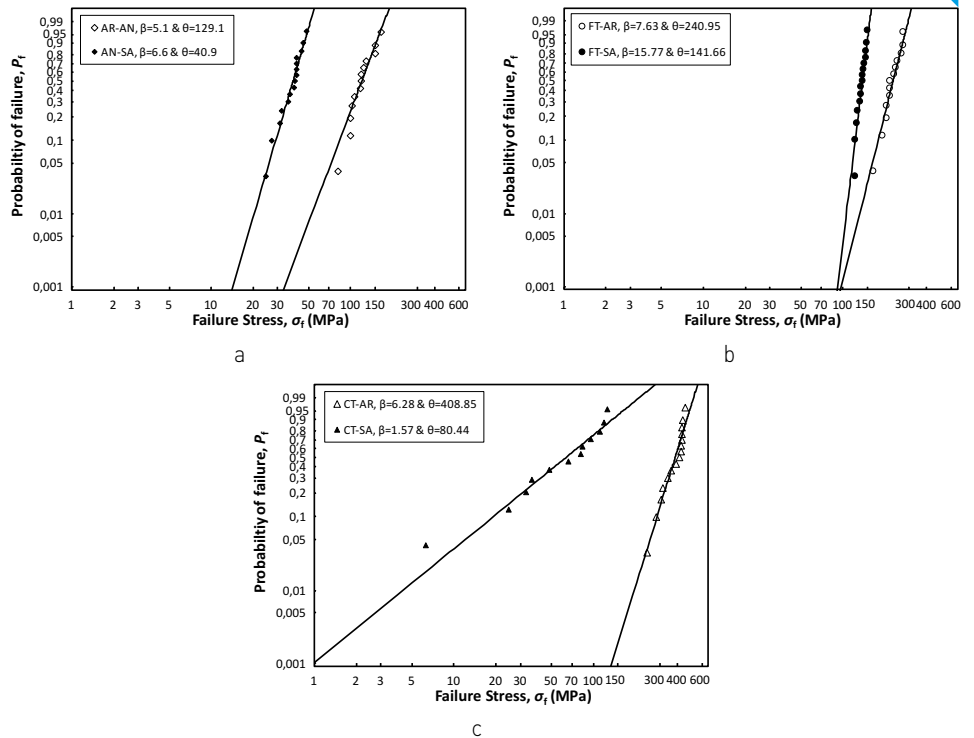


Fig. 6: Cumulative distribution functions of strength for (a) annealed glass (as-received and artificially aged); (b) fully toughened glass (as-received and artificially aged) and; (c) chemically toughened glass (as-received and artificially aged)

and subsequently annealed glass (Fig. 1a-c). The strength of as-received fully toughened glass (FT-AR) and chemically toughened glass (CT-AR) is 191% and 321% respectively larger than annealed glass (AN-AR) at mean probabilities of failure ( $P_f=0.50$ ). Strength reduction is evident in all types of glass after sand abrasion, with fully toughened glass providing the best post-aged performance. In particular, annealed glass suffers a 61% and 68% reduction in strength for  $P_f=0.008$  and  $P_f=0.50$  respectively after artificial ageing (Fig. 1a). Fully toughened glass has a better response than annealed glass after artificial ageing showing a reduction of 19% and 40% in as-received strength for  $P_f=0.008$  and  $P_f=0.50$  respectively (FT-SA, Fig. 1b). This better performance is a result of the residual surface stress and the relatively large case depth of fully toughened glass. Whereas, chemically toughened glass has the worst performance among all types of glass despite its high degree of toughening; it suffered a 98% and 83% reduction in as-received strength for  $P_f=0.008$  and  $P_f=0.50$  respectively (CT-SA, Fig. 1c). Additionally, the strength of sand abraded chemically toughened glass at low probabilities

of failure is even lower than that of annealed sand abraded glass. Fractographic results show that the degree of toughening in the glass affects the erosion resistance, with chemically toughened glass outperforming the other glasses in this respect. In particular, it is found that the average critical flaw depths after sand abrasion are as follows:  $472\mu\text{m}$  ( $132\mu\text{m} \leq a < 1370\mu\text{m}$ ) for annealed glass,  $127\mu\text{m}$  ( $72\mu\text{m} \leq a < 218\mu\text{m}$ ) for fully toughened glass and  $96\mu\text{m}$  ( $71\mu\text{m} \leq a < 132\mu\text{m}$ ) for chemically toughened. This implies that the degree of toughening (i.e. the amount of residual surface stress) has an effect on the critical flaw depth for the same artificial ageing procedure and thereby, the erosion resistance of glass i.e. higher residual surface stress results in smaller flaw depths under the same ageing conditions. Typical micrographs of the critical flaws are shown in Fig. 2a-i, representing the largest, average and smallest flaw for each type of glass, all of which are exposed to the same controlled artificial ageing regime.

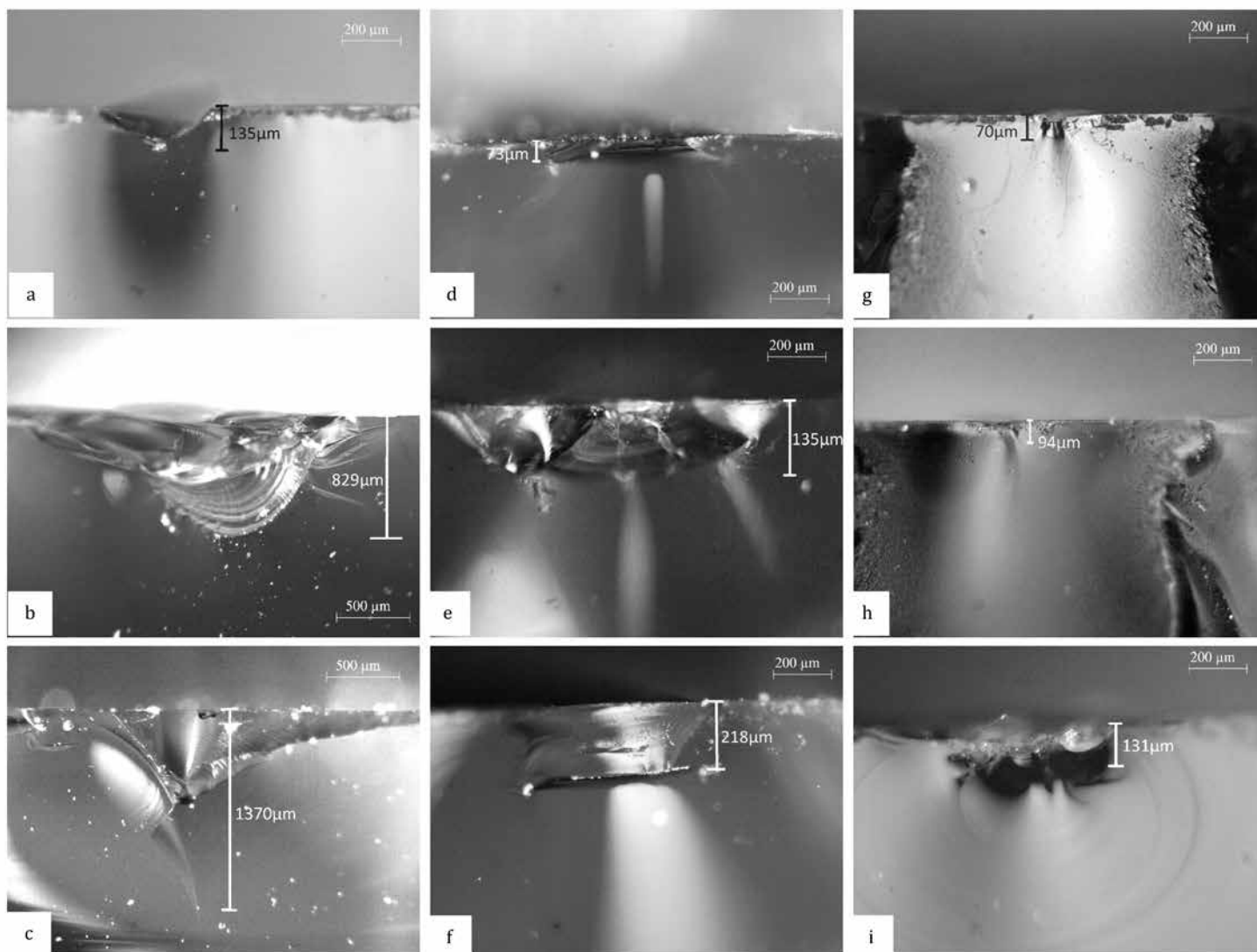


Fig. 7: Critical flaws (of max, average and min depths) in sand abraded: (a-c) annealed; (d-f) fully toughened and; (g-i) chemically toughened glass.

## References

- [1] K.C. Datsiou, M. Overend, The strength of aged glass, *Glass Structures & Engineering*, 2017.
- [2] K.C. Datsiou, M. Overend, Artificial ageing of glass with sand abrasion, *Construction and Building Materials*, vol. 142, pp. 536–551, 2017.

# Mechanically Efficient and Structurally Slim Vision Panels

Carlos Pascual<sup>1</sup>, Shelton Nhamoinesu<sup>2</sup>, Mauro Overend<sup>1</sup>

<sup>1</sup>Glass and Façade Technology Research Group. Department of Engineering, University of Cambridge, Trumpington Street, Cambridge CB2 1PZ, United Kingdom.

<sup>2</sup>Wintech Façade Engineering Consultancy Ltd, Wobaston Road, Wolverhampton WV9 5HA, United Kingdom.

## Keywords

1=Adhesively-bonded sandwich structure, 2=composite action, 3=glass, 4=numerical modelling, 5=analytical modelling, 6=post-fracture response.

## Abstract

Glass panes adhesively-bonded to structural profiles allow for the design of stiff, robust and transparent sandwich structures. In beam applications this is often achieved by bonding glass webs to glass fibre-reinforced polymer (GFRP) or steel flanges. However in glazing panel applications, e.g. vision panels of building envelopes, the need for transparency requires a swap in the position of these components: i.e. GFRP or steel core profiles are used to separate glass face sheets. Very limited research exists on the mechanical response of sandwich vision panels. The objectives of this paper are to study their shear and post-fracture responses as a function of the core material and the adhesive employed for bonding core and face sheets. Four-point bending tests were performed on short-span GFRP-glass and steel-glass sandwich panels bonded with epoxy and acrylic adhesives respectively. The deflections at collapse of both panels were large due to the progressive shear failure of GFRP profiles and the shear plasticity of the acrylic adhesive. Post-fracture capacities of more than 50% of the load at first fracture were achieved in all panels. Numerical modelling and a novel analytical tool are presented to evaluate the mechanical response of adhesively-bonded vision panels.

## 1. Introduction

Glazed curtain wall systems are made of insulated glazing units (IGUs) supported by rectilinear frames (e.g. metallic mullions spanning from floor to floor). The connection between the IGUs and the frames has a relatively low shear stiffness and therefore rotates independently of its substrates rather than bend with them – resulting in low shear transfer and low composite action between IGUs and mullions. Glazed curtain wall systems are therefore function-separated layered systems: the structure (mullions) provides stiffness and load-bearing capacity, whereas the façade (IGUs) behaves as infill vision panels providing transparency and thermal insulation. Despite the development of high-tech and high performance IGUs and support frames, the inherent function separation of the façade assembly produces structural inefficiency (reduced composite action), architectural constraints (visual obstructions and thermal bridges due to metallic mullions) and economic cost (non-profitable indoor space occupied by large mullions).

A slimmer, lighter and mechanically-efficient envelope system can be designed by merging façade and structure into a single composite component: a multifunctional sandwich vision panel. In this configuration the structural profiles are sandwiched in between and structurally bonded to fully toughened glass panes – see Figure 1a for a conceptual mock-up. The high shear stiffness of the adhesive layers and of the core profiles constrains them to bend together with the glass face sheets producing therefore high composite action in the system. The structural efficiency of this component provides an opportunity to reduce the overall depth of traditional curtain walls and therefore the core profile can be thinner and lighter than traditional mullions. Weight can be further reduced by using glass fibre-reinforced polymer (GFRP) core profiles instead of metallic ones – and this has the additional benefit of reducing thermal bridges through the envelope due to the low thermal conductivity of the composite material compared to metals.

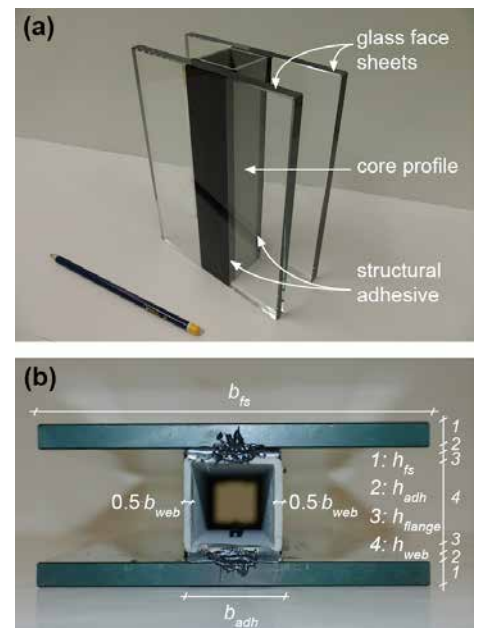


Fig 1. (a) Mock-up of the multifunctional vision panel merging façade and structure into a single sandwich component, and (b) geometrical parameters defining the cross section of the sandwich panels presented in this paper (subscripts  $fs$  and  $adh$  refer to face sheet and adhesive respectively).

Bonding core profiles to outer glass face sheets is not a new idea. In the last decade, experimental investigation on the bonding of GFRP profiles to glass panes has been performed by Peters [1] and Wurm [2] – however very limited research on the modelling of the mechanical response was produced in these studies. More recently, extensive experimental work has been complemented with detailed analytical and numerical modelling at the University of Cambridge by Nhamoinesu [3] and Pascual et al. [4]. The objective of this paper is to present the salient research performed at Cambridge and illustrate the pre-fracture and post-fracture behaviour of GFRP-glass and steel-glass sandwich panels subjected to transverse (out-of-plane) loads. Four-point bending experiments are presented for short-span (460 mm) adhesively-bonded GFRP-glass (with epoxy adhesive) and steel-glass (with acrylic adhesive) panels. Analytical and numerical models to capture their mechanical response are presented.

## 2. Experimental investigation

Two adhesively-bonded sandwich configurations were investigated: GFRP-glass (epoxy adhesive) and steel-glass (acrylic adhesive) composite panels – the former configuration has a GFRP pultruded core profile and the latter has a steel core profile. In addition a GFRP-glass layered sandwich panel was also investigated. The materials, four-point bending experimental set-up and experimental results of these panels are described below.

### 2.1. Materials and geometry of panels

Seven sandwich panels were fabricated: three GFRP-glass composite panels, three steel-glass composite panels and one GFRP-glass layered panel. The face sheets of all the panels consist of fully toughened soda-lime-silica glass manufactured to BS EN 12150-2 [5] and measuring 150 x 500 x 10 mm<sup>3</sup>. The sandwich cores were made of a 500-mm length profile made of GFRP or steel and having a rectangular-hollow section. The GFRP pultruded profiles were produced by Exel Composites (38 x 38 x 3 mm<sup>3</sup>) and the mild steel E275 profiles were manufactured to BS EN 10305-3 [6] (30 x 10 x 1.5 mm<sup>3</sup>). Epoxy adhesive DP490 from 3M (2-mm thickness) and Araldite A2047 from Huntsman (3-mm thickness) were used respectively to bond GFRP profiles and steel profiles to glass face sheets. In the following text the six composite panels are labelled according to the core, adhesive and face sheet material, i.e. GFRP-DP490-glass and steel-A2047-glass panels. The cross-sectional dimensions of the two composite sandwich panel configurations are given in Table 1 according to the geometrical parameters defined in Figure 1b – the layered GFRP-glass panel was identical to the GFRP-DP490-glass composite panel except that the adhesive layers were replaced by low friction spacers. The elastic and shear moduli,  $E$  and  $G$ , of the materials in all the panels are given in Table 2. The properties of the polymeric materials, i.e. GFRP and adhesives, exclude viscous effects and were estimated as follows: 1) for GFRP from burn-off and three point bending tests [4], 2) for adhesive DP490 from single-lap shear specimens (Figure 2a) [4], 3) for adhesive A2047 based on compression-relaxation tests on adhesive cylinders (Figure 2b) [3] – the stress-strain laws adopted here for the two adhesives are shown in Figure 2c (the Poisson's ratio of DP490 and A2047 are 0.38 and 0.43 respectively [3]). Unlike glass, steel and adhesives (all isotropic), GFRP is highly orthotropic and properties in Table 2 correspond to the pultrusion direction ( $E$ ) and the core-web plane ( $G$ ) – properties in other directions are given in previous work [4].

| Sandwich panel    | Core              |                   |                      |                      | Adhesive layers   |                   | Face sheets      |                  |
|-------------------|-------------------|-------------------|----------------------|----------------------|-------------------|-------------------|------------------|------------------|
|                   | Webs              |                   | Flanges              |                      | $b_{adh}$<br>(mm) | $h_{adh}$<br>(mm) | $b_{fs}$<br>(mm) | $h_{fs}$<br>(mm) |
|                   | $b_{web}$<br>(mm) | $h_{web}$<br>(mm) | $b_{flange}$<br>(mm) | $h_{flange}$<br>(mm) |                   |                   |                  |                  |
| GFRP-DP490-glass  | 6                 | 32                | 38                   | 3                    | 38                | 2                 | 150              | 10               |
| steel-A2047-glass | 3                 | 7                 | 30                   | 1.5                  | 30                | 3                 | 150              | 10               |

Table 1. Cross-section dimensions of the two configurations of adhesively-bonded sandwich panels according to geometrical parameters defined in Figure 1b.

| Sandwich panel    | Core              |                  | Adhesive layers             |                             | Face sheets |           |
|-------------------|-------------------|------------------|-----------------------------|-----------------------------|-------------|-----------|
|                   | $E$ (GPa)         | $G$ (GPa)        | $E$ (GPa)                   | $G$ (GPa)                   | $E$ (GPa)   | $G$ (GPa) |
| GFRP-DP490-glass  | 26.5 <sup>a</sup> | 3.0 <sup>a</sup> | 135·10 <sup>-3</sup>        | 49·10 <sup>-3</sup>         | 72          | 29.5      |
| steel-A2047-glass | 210 to 0          | 80.8 to 0        | (543 to 0)·10 <sup>-3</sup> | (190 to 0)·10 <sup>-3</sup> | 72          | 29.5      |

Table 2. Elastic and shear moduli ( $E$  and  $G$ ) of the materials in the core, adhesive layers and face sheets in the two configurations of adhesively-bonded sandwich panels. Note: <sup>a</sup>properties in the longitudinal direction ( $E$ ) and core-web plane ( $G$ ) as required for analytical modelling – orthotropic properties in other directions required for finite element modelling are given in Pascual et al. [4]

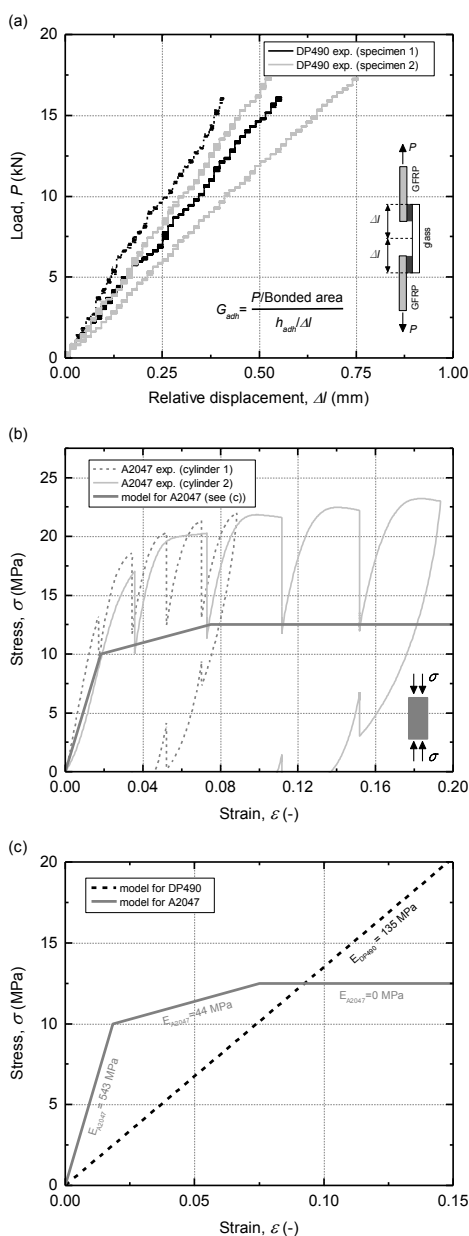


Fig 2. Stiffness of adhesives investigated in (a) single-lap shear tests for DP490 (bonded areas of 50x25 mm<sup>2</sup>) [4] and (b) compression-relaxation tests for A2047 [3], and (c) stress-strain laws adopted for the two adhesives.

### 2.2. Experimental set-up

The shear response of the seven sandwich panels was evaluated in four-point bending tests. The span of all panels was  $L = 460$  mm and the span-to-depth,  $L/h$ , were 7 (GFRP-glass layered and GFRP-DP490-glass panels) and 13 (steel-A2047-glass panel). The loading configuration is shown schematically in Figure 3a and the values of the shear-span BC ( $L_a$ ) and half bending-span AB ( $L_b$ ) are given in Table 3. The loads were applied on the panels by means of a 150-kN electromechanical testing machine (Instron 5500R) fitted with a steel load distribution frame which included two steel rollers (see Figure 3b to 3d). The experiments were displacement controlled at a rate of 0.25 mm·min<sup>-1</sup> (GFRP-glass layered and GFRP-DP490-glass panels,  $L/h = 7$ ) and 0.5 mm·min<sup>-1</sup> (steel-A2047-glass panel,  $L/h = 13$ ) and performed at ambient laboratory conditions ( $23 \pm 5$  °C and  $50 \pm 10\%$  RH) – low loading rates were selected to produce low strain rates and therefore avoid viscous effects in the polymeric materials of the panels, and to this end the loading rate was lower for the panels with lower span-to-depth ratio. The applied loads,  $2P$ , and the mid-span deflections,  $w_A$ , were measured respectively by the 150-kN load cell fitted in the Instron machine and a LVDT transducer located below the bottom glass face sheet (see Figure 3a).

| Sandwich panel    | $L/h$<br>(-) | $L$<br>(-) | $L_a$<br>(mm) | $L_b$<br>(mm) | $D_{global}$<br>(N.mm <sup>2</sup> ) | $D_{local}$<br>(N.mm <sup>2</sup> ) | $U$<br>(N)        |
|-------------------|--------------|------------|---------------|---------------|--------------------------------------|-------------------------------------|-------------------|
| GFRP-DP490-glass  | 7            | 460        | 80            | 150           | $1.50 \cdot 10^{11}$                 | $3.65 \cdot 10^9$                   | $6.09 \cdot 10^5$ |
| steel-A2047-glass | 13           | 460        | 50            | 180           | $3.86 \cdot 10^{10}$                 | $2.14 \cdot 10^9$                   | $5.53 \cdot 10^5$ |

Table 3. Span-to-depth, spans and global and local flexural rigidities and shear stiffness of the two adhesively-bonded sandwich panel configurations.

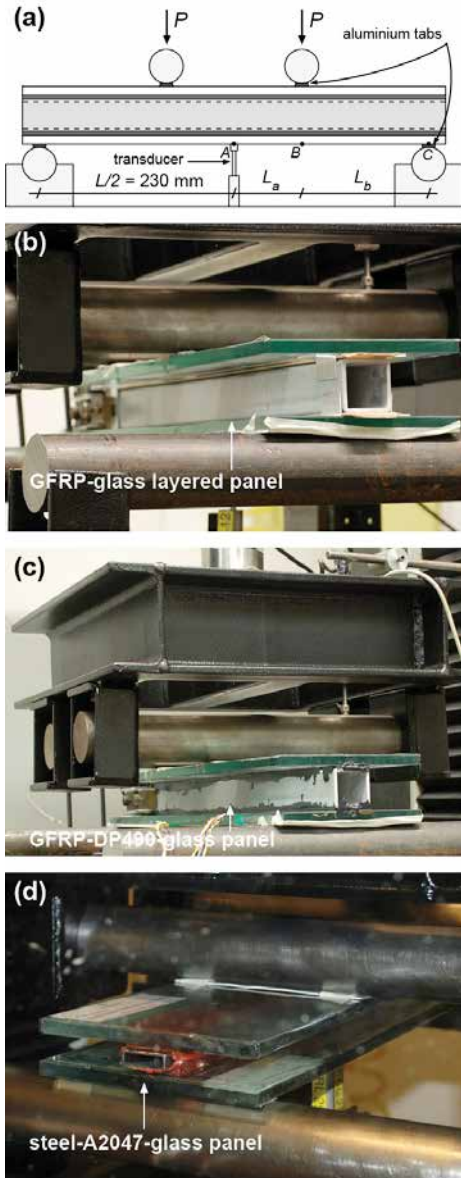


Fig 3. (a) Schematic view of the four-point bending experimental set-up, and four-point bending tests performed on (b) GFRP-glass layered panel, (c) GFRP-DP490-glass panel and (d) steel-A2047-glass panel.

### 2.3. Experimental results

The seven  $2P-w_A$  experimental curves of the panels are shown in Figure 4a (GFRP-glass layered and GFRP-DP490-glass panels) and Figure 4b (steel-A2047-glass panel). The response of the GFRP-glass layered panel was linear up to the fracture of the top glass face sheet that occurred at about 14 kN (and 7-mm mid-span deflections) (see Figure 5a and 5b).

The resisted load abruptly reduced due to this fracture and then increased linearly in a reduced stiffness path up to about 11 kN (and 8-mm mid-span deflections) that produced the fracture of the bottom glass face sheet (see Figure 5c). The stiffness and load-bearing capacity of this layered panel were significantly outperformed by the three GFRP-DP490-glass panels. The response of these composite panels was almost linear up to loads between 20 kN and 30 kN (and at mid-span deflections of around 3 mm) that produced the longitudinal shear failure of the pultruded core profiles close to the supports (see Figure 5d). The resisted loads reduced due to the local shear failure of the profiles and then subsequently increased on a reduced stiffness path to around 27 kN producing the fracture of the bottom glass face sheets (Figure 5e). This fracture produced an abrupt reduction in the resisted loads. As the loads subsequently increased on a significantly reduced stiffness path up to around 15 kN, the top glass face sheet fractured (Figure 5f) – corresponding mid-span deflections were of around 17 mm to 24 mm.

The three  $2P-w_A$  experimental curves of steel-A2047-glass panels exhibited a linear response (0a in Figure 4b) up to about  $2P = 10$  kN and 2-mm mid-span deflections. Then the curves exhibited a significant non-linearity (ab) between 10 kN and 20 kN indicating a relevant reduction in the stiffness of the panels which was attributed to adhesive plastification. An almost linear response (bc) was then observed up to about 31 kN that produced the fracture of the bottom glass face sheet – corresponding mid-span deflection were of about 12.5 mm (Figure 5g). The resisted loads reduced abruptly due to this fracture (cd) and subsequently increased on a reduced stiffness path (de) up to about 16 kN to 18 kN producing the fracture of the top glass face sheet (see Figure 5h) and corresponding to mid-span deflections of about 14 mm to 17 mm. After the failure of both face sheets a residual deformation was observed in the core profiles indicating plastic deformations in the steel material (see Figure 5i).

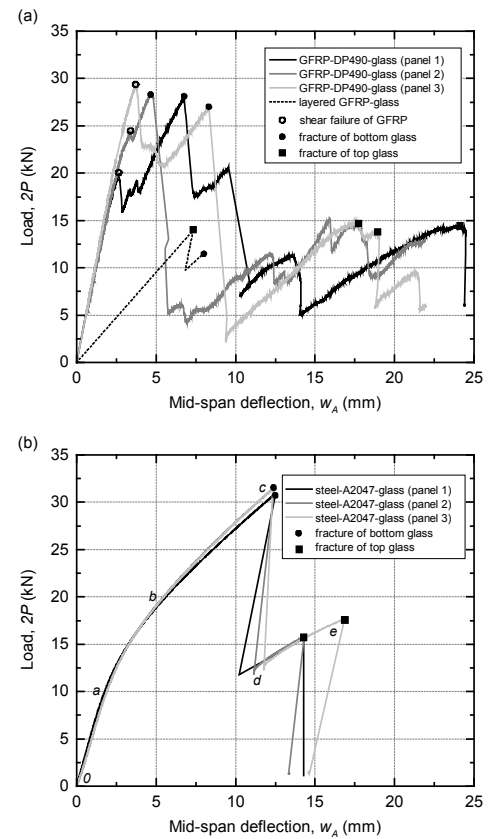


Fig 4. Experimental load-deflection curves of (a) GFRP-glass layered and GFRP-DP490-glass panels and (b) steel-A2047-glass panels (letters refer to points of interest discussed in the text).

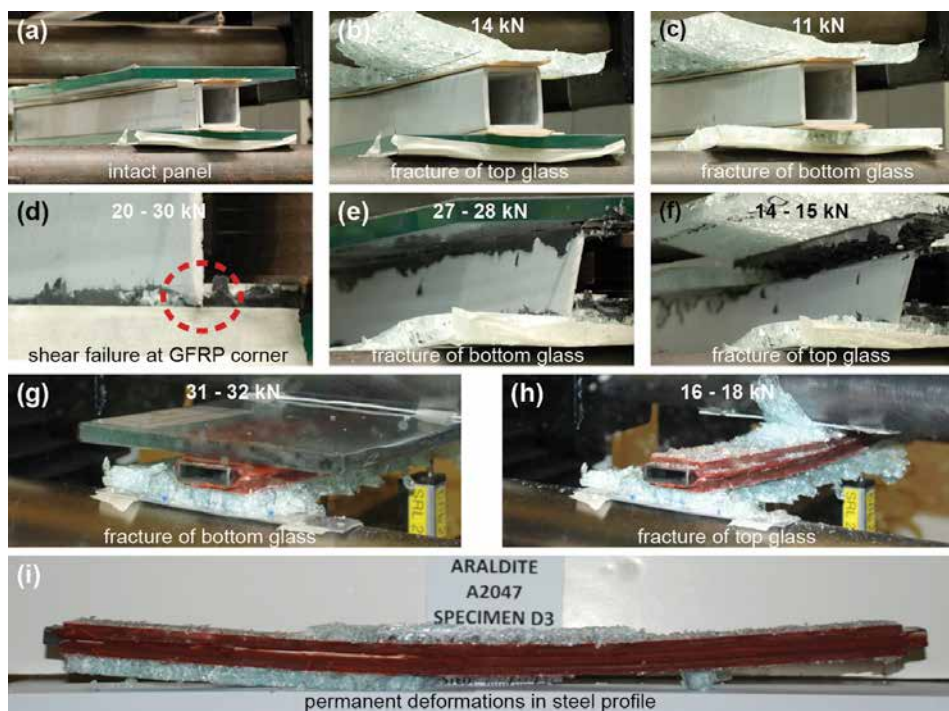


Fig 5. Progressive failure of GFRP-glass layered panel shown at (a) intact state, (b) failure of top glass and (c) failure of bottom glass, of GFRP-DP490-glass panel at (d) GFRP profile close to a support, (e) bottom glass, (f) top glass, and of steel-A2047-glass panel at (g) bottom glass and (h) top glass and (i) permanent deformations in steel core profile.

### 3. Modelling

In this section the load-deflection responses ( $2P-w_A$  curves) of the un-fractured composite panels were modelled numerically (finite element models) and analytically (solutions developed by Pascual et al. [4]) and the predictions were compared to the experimental results.

#### 3.1. Numerical

Three-dimensional finite element models of the four-point bending experiments on the GFRP-DP490-glass and steel-A2047-glass panels were developed using Ansys Mechanical APDL v16.2 software. The geometry of the panels, i.e. spans and cross-section dimensions, are defined in Tables 1 and 2 – only one quarter of the panels were modelled as the panels are by-symmetric (Figure 6). A fine mapped orthogonal meshes of SOLID45 elements was adopted – details on the meshing criteria can be found in Pascual et al. [4]. The strain-stress responses of the materials were considered as: linear elastic (for glass, GFRP and adhesive DP490), elastic perfectly plastic (for steel, i.e. yield stress of 275 MPa) and trilinear elasto-plastic (for adhesive A2047 as shown in Figure 2c). The numerically predicted  $2P-w_A$  curves of the panels are shown in Figure 7 together with the experimental results (un-fractured state). For the GFRP-DP490-glass panels, the numerical prediction was linear and showed an excellent matching of stiffness (slope of the

curves) with respect to the tested panels. For the steel-A2047-glass panels, the numerically predicted response was highly non-linear largely due to the non-linearity of the adhesive response. Up to  $2P = 20$  kN, the stiffness obtained in the numerical simulation matched well with the test results, however above this load the numerical response underestimated the stiffness by about 35% - which indicated that the adhesive stiffness at large strains (considered here as  $E_{A2047} = 0$  MPa) may have been underestimated.

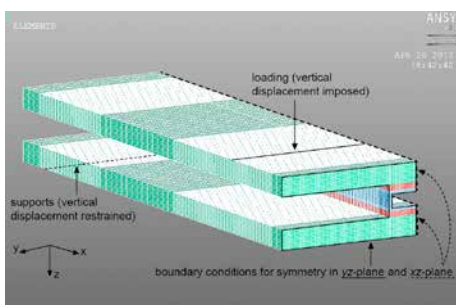


Fig 6. Geometry, mesh and boundary conditions considered for finite element model of the sandwich panels subjected to four-point bending loads (the graphical representation of this figure corresponds to steel-A2047-glass panel).

#### 3.2. Analytical

A novel analytical model for predicting the deflections and strains produced by four-point bending loads on adhesively-bonded sandwich panels (with thick face sheets and

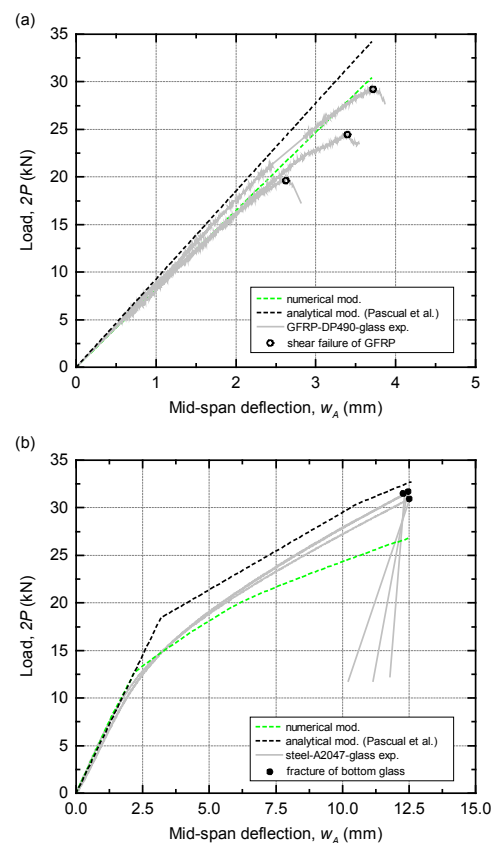


Fig 7. Applied loads ( $2P$ ) vs. mid-span deflections ( $w_A$ ) obtained experimentally, numerically and analytically for (a) GFRP-DP490-glass panels and (b) steel-A2047-glass panels (results are shown up to displacements producing the first fracture in GFRP or glass components).

shear-deformable adhesive layers and cores) was recently developed by Pascual et al. [4]. This model considers that all materials behave linearly and that the structural response of the panel result from the contribution of two mechanisms: 1) a local response in which cross-sections of the core and face sheets bend about their respective centroidal axes, and 2) a global response in which the sandwich cross-section bends as a whole about the global centroidal axis. Shear deformations are also associated to these mechanisms and the geometrical compatibility of bending and shear deformations depends on a mechanical parameter,  $a^2$ , relating shear stiffness to bending rigidity and is given by [4]:

$$a^2 = \frac{U}{D_{local} \cdot \left(1 - \frac{D_{local}}{D_{global}}\right)} \quad (1)$$

where  $D_{local}$  and  $D_{global}$  are the flexural rigidities of the local and global mechanism respectively and  $U$  is the shear stiffness of the sandwich panel – the values of these mechanical properties for the two configurations of composite panels presented in this paper are given in Table 2. The analytically predicted  $2P-w_A$  curves for

the composite panels studied here are shown in Figure 7. For the GFRP-DP490-glass panels, the predicted response was linear and matched well with the experimental results – experimental stiffness was overestimated by about 10%. For the steel-A2047-glass panels, analytical predictions were more complex to calculate because the adhesive response was trilinear (see Figure 3a). The analytical model was therefore applied in three independent stages as a function of the average shear stress in the adhesive layer across the shear-span  $BC$ : 1)  $E_{A2047} = 543$  MPa was considered until an average shear stress of 10 MPa was reached in the shear-span, 2)  $E_{A2047} = 44$  MPa was then considered up to an average stress of 12.5 MPa and 3)  $E_{A2047} = 0$  MPa was then considered. The predicted response was essentially bilinear and was in good agreement with the experimental results although the gradual decrease of stiffness for  $10 \text{ kN} < 2P < 20 \text{ kN}$  could not be captured analytically (see Figure 7b). This result indicates that the response of the tested panels may have been governed by a bilinear response of the adhesive ( $E_{A2047} = 543$  MPa and  $E_{A2047} = 44$  MPa with plastification at about 10 MPa shear stress) and that  $E_{A2047} = 0$  MPa may have not been reached during the experiments.

#### 4. Discussion

The sandwich configuration presented in this research produces composite glass panels with high levels of robustness and load-bearing capacity: the deflections at collapse obtained here were 5 times higher than those at first failure of GFRP core profiles (about 3 mm) or at first plastification of A2047 adhesive (about 2 mm) and collapse loads were significantly high and more than 50% of the maximum capacity of the panels (see Figure 4). In addition the sandwich configuration presented in this paper generates the composite action between the structural glass face sheets and therefore achieves high levels of structural stiffness in the panels. The composite action in terms of deflections,  $\eta$ , can be defined as:

$$\eta = \frac{w_{\text{layered},A} - w_A}{w_{\text{layered},A} - w_{\text{monolithic},A}} \cdot 100\% \quad (2)$$

where  $w_{\text{layered},A}$  and  $w_{\text{monolithic},A}$  are respectively the mid-span deflections that would be obtained if very shear-flexible adhesives, i.e.  $G_{adh} \rightarrow 0$  (layered panel), and shear-rigid adhesives, i.e.  $G_{adh} \rightarrow \infty$  (monolithic panel) were employed and  $w_A$  is the mid-span deflection obtained for the particular adhesive (shear modulus  $G_{adh}$ ) for which the composite action is investigated. According to equation 2, and applying the novel analytical model to

predict deflections [4], the adhesives used in this study have generated a composite action,  $\eta$ , in the order of 90% and outperform structural silicones ( $2\% < \eta < 7\%$ , see Figure 8).

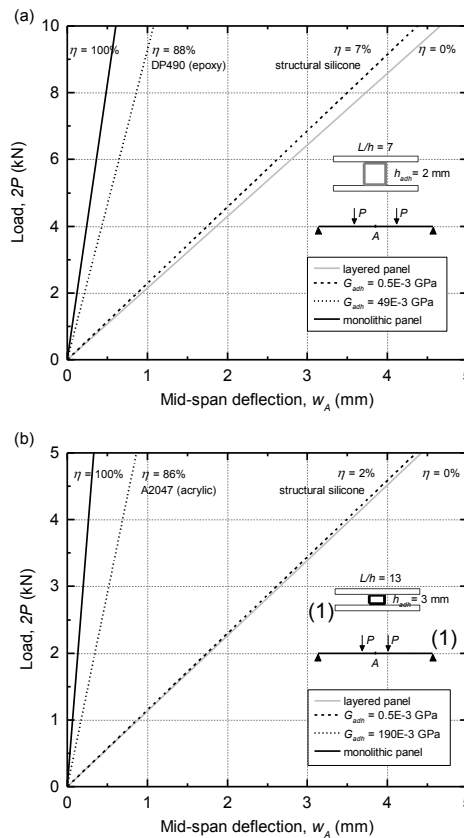


Fig 8. Applied loads ( $2P$ ) vs. mid-span deflections ( $w_A$ ) predicted analytically in the elastic response region for (a) GFRP-DP490-glass panels and (b) steel-A2047-glass panels bonded with structural adhesives and typical structural silicone (layered and monolithic panel responses are plotted for comparison).

From the analytically predicted response of steel-A2047-glass panels, it has been inferred that the adhesive response in the tested panels might have been essentially bilinear – instead of the trilinear material law obtained in the tests performed in adhesive cylinders (see Figure 2b). This can be attributed to the confinement of the adhesive in the panels (together with its high Poisson's ratio of 0.43) which may have prevented the second plastification ramp ( $E_{A2047} = 0$  MPa) and may have produced a sustained elastic modulus of about  $E_{A2047} = 44$  MPa for strains above 0.075. Research is still in progress concerning the mechanical response of the structural adhesives employed in this research as well as models to capture the progressive failure of adhesively-bonded sandwich panels.

#### 5. Conclusions

Novel glass components combining structure and façade into a single sandwich panel have been tested under four-point bending loads and have been numerically and analytically investigated. The following conclusions were obtained:

- Sandwich structures made of structural glass face sheets separated and structurally bonded to composite or metallic core profiles produce stiff and strong vision panels. The stiff structural adhesives used in this study activate composite actions (in terms of deflections) of about 90% and outperform structural silicones.
- Deflections at final collapse of the composite panels were of at least 5 times higher than those at first failure and collapse loads were about 50% of the maximum capacity of the panels indicating robustness in the sandwich configuration.
- A numerical and a novel analytical model have been successfully used to model the responses of the composite panels. To improve further the accuracy of the models and capture also the post-fracture behaviour, research has to be done concerning the non-linear response of adhesives and the fracture of glass in the proposed sandwich configuration.

#### References

- [1] Peters S. Kleben von GFK und Glas für baukonstruktive Anwendungen [PhD Thesis]. Germany: Universität Stuttgart; 2006.
- [2] Wurm J. Glass structures: design and construction of self-supporting skins. Basel: Birkhauser; 2007.
- [3] Nhamoinesu S. Steel-glass composite panels [PhD Thesis]. UK: University of Cambridge; 2015.
- [4] Pascual C, Montali J, Overend M. Adhesively-bonded GFRP-glass sandwich components for structurally efficient glazing applications. Compos Struct 2017;160:560-573.
- [5] BS EN 12150-2. Glass in building – thermally toughened soda lime silicate safety glass (part 2). London: British Standards Institution; 2004.
- [6] BS EN 10305-3. Steel tubes for precision applications – technical delivery conditions (part 3). London: British Standards Institution; 2002.

# Deformations and Strain Energy in Fragments of Tempered Glass: Experimental and Numerical Investigation

Jens H. Nielsen,  
Technical University of Denmark, Department  
of Civil Engineering

Marie Bjarrum,  
NIRAS

## Keywords

1=Tempered Glass, 2= Fragment, 3= Strain Energy, 4=Topology measurements, 5= FEM simulation

**Extended Abstract** (The complete contribution will be published in the *Glass Structures and Engineering journal*)

The present paper is an abstract of the paper with the same title and authors published in *Glass Structures & Engineering*.

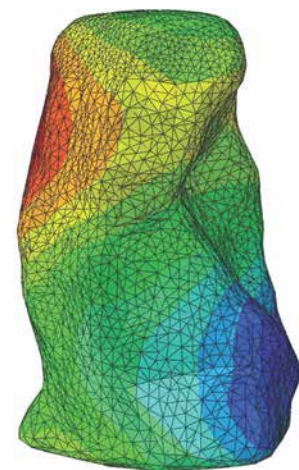
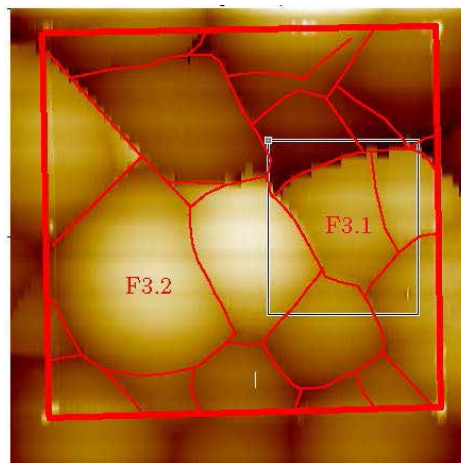
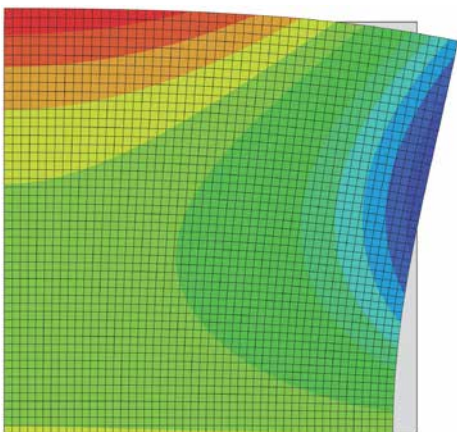
One of the most characteristic features of tempered glass is its ability to fragmentize completely upon failure. It is well-known that the phenomena has something to do with the amount of residual stresses stored in the glass and for many years, the size of these fragments have been used for characterizing

weather the glass was tempered (toughened) or not. With the introduction of stiff interlayers also the post failure capacity of laminated tempered glass might be affected by the expansion of the fragments which might increase their ability to interlock and thereby increase the post failure capacity.

Even though the use of the phenomena have been quite vital for the glass community a satisfying theory for predicting the fragment size have not yet been proposed.

The present work is providing some of the building blocks for establishing such theory, namely an investigation of how much of the stored energy is left in the fragment after failure. This is investigated both numerically and experimentally by measuring the deformations of a fragment. The investigation compares and discusses the FEM models for predicting the remaining strain energy and compares with novel experimental results.

In short, the investigation measures the surface deformation of a single fragment after failure which is compared to a FE-model of the same fragment geometry found by means of a 3D scanning. The investigation demonstrates a feasible procedure for experimental investigation.



# Influence of Distribution of Residual Stress on Strength Tests

Jürgen Neugebauer <sup>1</sup>,  
Irma Kasumovic <sup>2</sup>,  
Ivo Blazevic <sup>2</sup>

<sup>1</sup> University of Applied Sciences FH-Joanneum,  
<sup>2</sup> Josef Ressel Centre for thin glass technology  
for structural glass applications

## Keywords

1=stress distribution, 2=residual stress,  
3=defects, 4=flexural bending strength

## Abstract

In several standards such as EN 1288 test scenarios for the determination of strength of glass is described. On the one hand there is the ring-on-ring test for the determination of the strength of glass without and on the other hand there is the four-point-bending test for the determination of the strength of glass with the influence of the edge strength. All these tests are described having perfect conditions. For example, glass is homogeneous or test set-ups are without any imperfections. One interesting part is the distribution of the residual stress through the thickness and along the surface. Residual stress is caused by thermal or chemical pre-stress of glass. In case of heat strengthened or fully tempered glass photo-elastic studies of the stress distribution showed that the distribution along the surface is not homogeneous. This not constant distribution is shown in a grey pattern, which can be visualized with the principle of polarized light. This paper is a discussion about this grey pattern, imperfections and measured stress with the help of SCALP stress measurement device. This investigation helps to understand much better the reason of the location of the origin of fracture.

## 1. Introduction

### Thermal treatment

Thermal treatment is a typical process of pre-stressing, according EN 12150 [1] or EN 1263 [2], of glass in which the glass is moved on rollers forwards into the heating zone and is heated up above the transition point. After this heating phase, the glass is blown off with air. During the phase of cooling to ambient temperature, glass is permanently moved forwards and back-wards on rollers up to the end

of the furnace. The thinner the glass the bigger so-called roller waves can occur.

For this reason, the Austrian company LISEC has investigated a process in which the glass is transported on air cushion. This technique gives the possibility to pre-stress thinner glass by thermal treatment without roller waves.

## Chemical treatment - Ionic Exchange

Another possibility to pre-stress the glass is chemical treatment according EN 12337 [3]. The glass is immersed into molten potassium nitrate. At a temperature of approx. 370 - 450°C the effect of ionic exchange takes place. The smaller sodium ions diffuse from the glass into the liquid potassium nitrate and the larger potassium ions penetrate into the glass matrix. Due to the larger ionic diameter of potassium ions, compressive stresses in the close up range of the surface result. The depth of penetration the so-called case depth is around 30 - 100 µm. [4]

## 2. Test scenarios for determination of ultimate bending strength

In case of thin glass with a thickness less than 2 mm the values for ultimate bending strength, which are the basis for a structural design, are still missing. Therefore, a couple of different test scenarios were investigated for their applicability for determination of ultimate bending strength of thin glass. Due to the application one has to differ between test scenarios with and without the influence of the edge strength (edge quality) - the so-called edge effect. In the following a couple of possible test scenarios were investigated.

### Ring-on-ring test - EN ISO 1288

The test set-up is performed by placing the glass sample on a circular steel reaction-ring (supporting ring) and applying on its upper surface a load transmitted through a steel loading-ring, until the glass breaks. The purpose of this test is to achieve a uniform tensile stress field inside of the loading ring that is independent of edge effects. As described in NEUGEBAUER [5] these in EN 1288 described test scenarios fail for thin glass.

### Silicon pad/ pressure pad

As a possible of improvement of the ring-on-ring test a silicon-pad or pressure-pad on

ring test was investigated. The test set-up is performed by placing the glass sample on a circular steel reaction ring (supporting ring) and applying on its upper surface a load transmitted through a silicon or pressure pad instead of the loading ring, until the glass breaks. The advantage of such test setup is that in the centre of the glass a homogenous stress distribution arises. [5]

### Four-point bending test

In case of thin glass large deflections result and the bearing forces are not longer vertical but inclined. The glass pane distributes its bearing force only by contact and eventually by friction between glass and rubber (EPDM). Due to the thinness no breakage of these thin glass panels can eventually be reached, because of slip from bearing pins due to bowstring effect (distance of pins is constant but ends of panes move towards) or on some testing machines reach of maximum piston stroke. [5]

### Bending with axial force

The value for the ultimate bending strength can for example be determined with a kind of a stability test. With a force  $F$  and eccentricity  $e$  the maximum stress can be determined according the theory of large deformations. Instead of inducing bending by loading perpendicular to test specimen an alternative concept applies the load in plane of the test specimen with bending due to deflection. [5]

### Bending with constant radius

Instead of introducing the load in plane as described above it is also possible to apply the load with a rotation of the shorter opposite edges and a reduction of the distance between the supporting hinges, as described NEUGEBAUER [5]. With an accurate adjustment of the length of bowstring (distance between the supporting hinges) of the arched bent glass sample and the applied rotation a constant stress distribution on nearly the whole bent edges (excluding a small zone at the straight edges where the rotation is introduced) arises. [5]

## 3. Stress distribution on surface

### Anisotropy

In general, the phenomenon of anisotropy can be defined as a characteristic of the material, that has directionally dependent behaviours of the material for example like tensile strength,

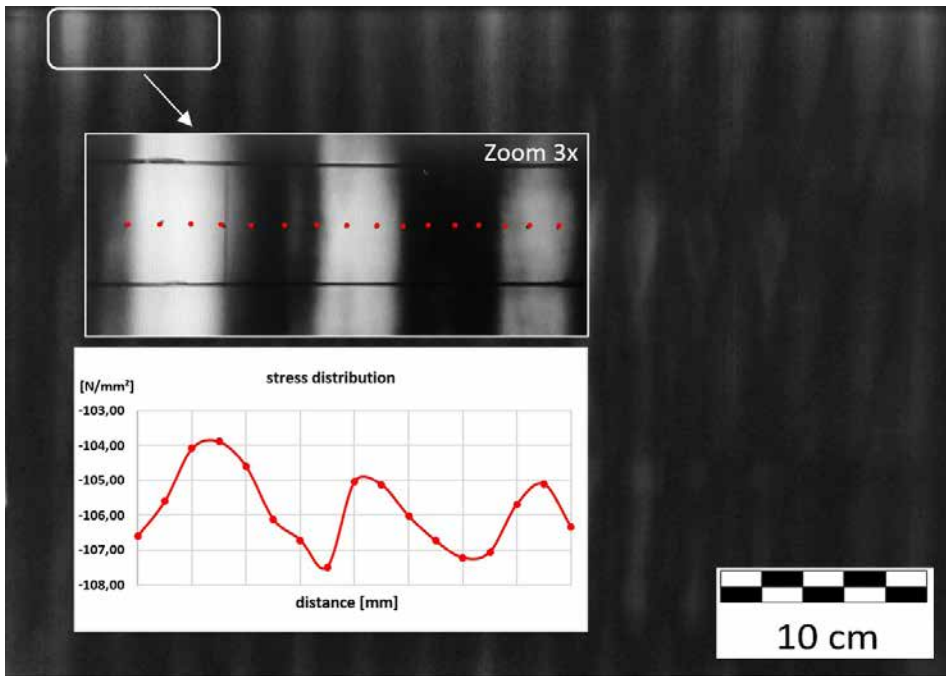


Figure 1 Distribution of residual stress of fully tempered glass

conductivity or refractive index. In case of glass, the anisotropy effect results from the presence of polarized light in the natural environment, the birefringent property the anisotropy of the refractive index of glass (photoelasticity) and mechanical stresses in the glass due to the thermal pre-stressing process. [6].

To understand this behaviour much better pre-stressed glass was investigated with the help of the physic principle of polarisation. In case of fully tempered glass a so-called "zebra pattern" arises, the picture is shown in figure 1 below. This 8 mm glass is pre-stressed in a conventional tempering furnace on rollers. In certain points the residual stress on the surface were measured with help of SCALP measurement device.

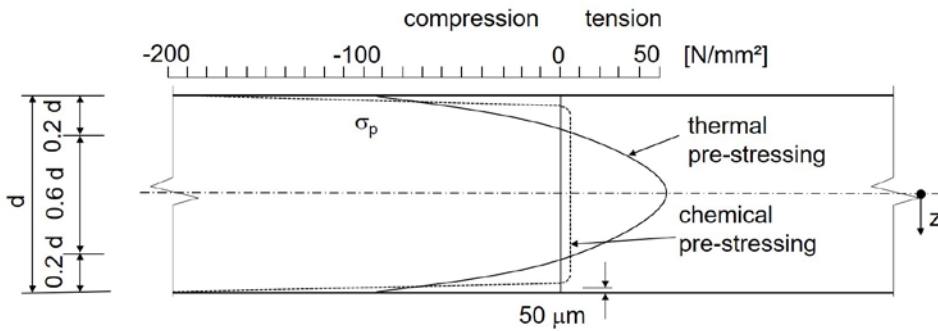


Figure 2 Distribution of residual stress of thermally and chemically pre-stressed glass

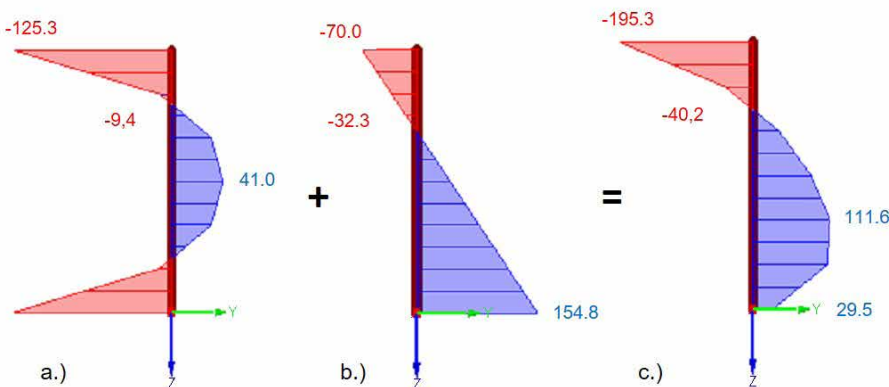


Figure 3 FE-simulation of distribution of residual stress glass without surface defects

As shown in the diagram in figure 1 above the measured residual stress in not homogenous along the surface. The level of stress is varying in a range of maximum and minimum. In this case the compressive stress at the surface was measured between  $s = -102.8$  and  $-107.5$  MPa. For the discussion of the determination of the ultimate bending strength these distributions, caused by tempering processes, have to be taken into account.

Not only the distribution along the surface has an influence on the bending strength the distribution through the thickness has to be taken into account as well.

#### 4. Stress distribution through thickness

The stress distribution through the thickness of glass is characterized with a zone of compression stress at the surface and a tension stress in the core of the glass pane.

A comparison of a fully tempered and a chemically pre-stressed glass is shown in figure 2 left. In general, a chemically toughened soda lime glass has a surface compression stress with around  $\sigma = -300$  MPa, but the compression zone is with 50 mm very thin. Special aluminium silicate glass can be pre-stressed up to  $\sigma = -1000$  MPa. In comparison to the chemically treated glass a fully tempered glass has a residual stress of around  $\sigma = -120$  MPa, but a thickness of the compression zone of around  $0.2d$  (20% of the thickness). The tension stress in the core is much smaller than in case of thermally tempered glass.

Such a stress distribution could be modelled with the help of finite element programs.

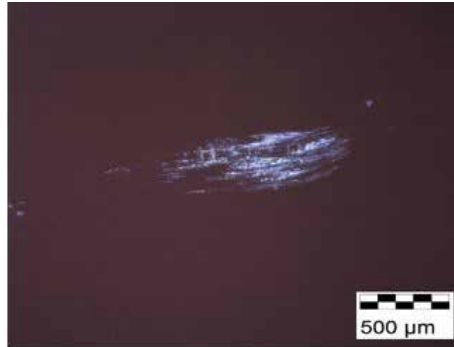
Figure 3 shows in (a.) the stress distribution of a fully tempered glass with a surface pressure of  $\sigma = -125.3$  MPa and a tensile stress of  $\sigma = 41$  MPa in the core of the glass pane. In the same figure the illustration (b.) shows the stress distribution due to a loading according a test scenario with a pressure pad as described in chapter 2 before. This distribution results from pure bending with  $\sigma = \pm 112.4$  MPa and a constant stress distribution due to membrane forces  $\sigma = + 42.4$  MPa (tension). The residual stress and the stress due to the loading have to be added. The result of this superposition is shown in figure 3 (c.) beside.

## 5. Defects

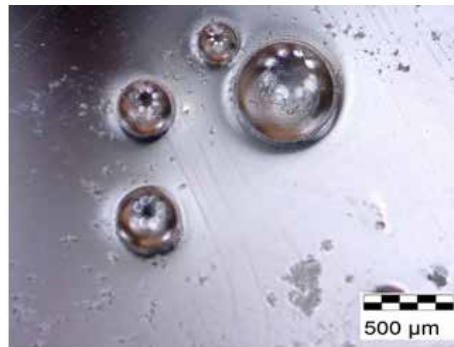
The theoretical strength of glass is given at around 10,000 MPa in different literatures. In contrast to the theoretical strength the measured bending strength of, for example, annealed glass is around 80 MPa.

This enormous reduction of the strength of the glass results from imperfections on the surface (e.g. cracks, scratches) and in the glass matrix (e.g. NiS inclusions - as the origin of fracture due to volume change of NiS) itself. Figure 4 below shows some examples for defects on the surface (a. and b.), at the edge (c.) or in the glass matrix itself (d.). Such defects can arise from the very first beginning of the production of glass e.g. on the floatglas line, during the manufacturing of glass products due to handling or in the lifetime of glass e.g. cleaning.

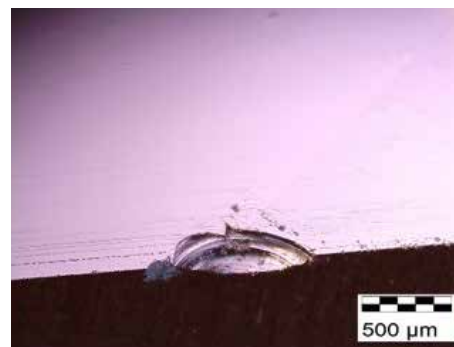
Defect a.) in figure 4 below shows simply scratches due to wrong cleaning work and defect b.) shows bubbles on the surface which occurred during the glass production. Defect c.) is an edge defect which is being caused by wrong edge finishing and defect d.) shows a bubble (inclusion) in the glass matrix which occurred during the glass production.



a.)



b.)



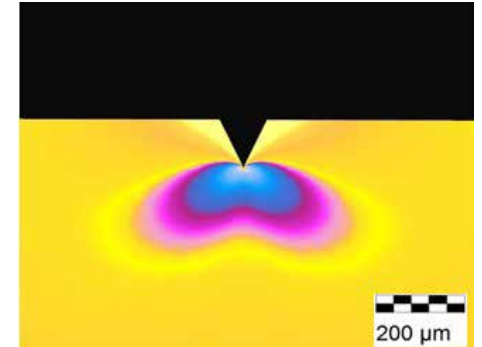
c.)



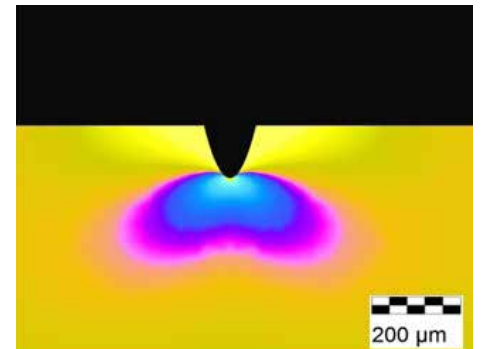
d.)

Figure 4 Defects

In the following discussion in this paper a surface flaw before the pre-stressing process is assumed. For a better understanding a stress distribution in the close up area of the surface flaws were deeper investigated. As a result of this analysis the following stress distribution in the near field of the bottom of the flaws is shown in figure 5 below.



a.)



b.)

Figure 5 Investigation of surface defects with help of finite element model

Figure 5 shows the stress concentration of the principle stress  $\sigma_1$  of two simplified types of surface flaws, a very sharp bottom of the flaw (a.) and a rounded out bottom of the flaw (b.). The depth of the flaws is assumed with 0.1 mm for further investigations. At the bottom of the flaws stress concentrations arise. This phenomenon is described in several publications like in SCHULA [7] or GROSS [8]. In these publications an analytic approach with the following equation 1 for the determination of the stress distribution in the near field of the bottom of the surface flaw is given.

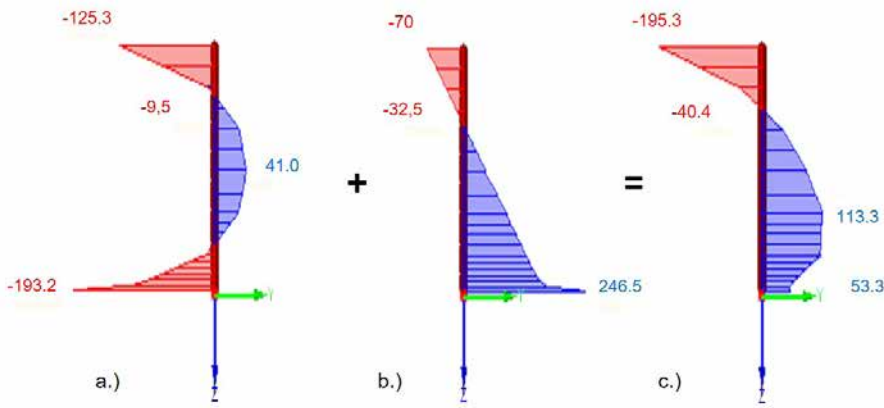


Figure 7 FE-simulation of distribution of residual stress glass with surface defects

With the following assumptions, as assumed for the finite element simulation, nearly the same stress distribution could be determined as with the finite element model. The distance from the location of interest to the midpoint M of the rounding is given with  $r = 0,03 \text{ mm}$  and the angle  $\varphi$  is perpendicular to the surface of the glass ( $\theta = 0$ ).

The diameter of the rounding of the bottom of the surface is assumed with  $\rho = 5 \mu\text{m}$ . This simplification with a tip radius of  $5 \mu\text{m}$  is an assumption for the above described investigation, but microcracks can be also very "sharp" with a radius on an atomic scale. The stress field without a defect is assumed with  $\sigma = -125.3 \text{ MPa}$ , as described in chapter 4. For the determination of the stress concentration factor  $K_I$  the geometry factor  $Y$  is given with  $Y = 1,1215$  for long surface flaws.

The stress  $\sigma_{yy}$  in the closed up area in direction parallel to the surface (as shown in figure 6 above) was calculated with  $\sigma_{yy} = -186.4 \text{ MPa}$ , which coincide very well with the stress, which was determined with help of finite elements, with  $\sigma = -193.2 \text{ MPa}$ , as described in the next chapter below.

### 6. Stress distribution with surface defects

This additional influence of the surface flaws is furthermore investigated with a simulation with the help of a finite element program. At the bottom of the flaw a stress concentration due to the thermal pre-stressing arises with  $\sigma = -193.2 \text{ MPa}$  in comparison to the upper surface without a defect ( $\sigma = -125.3 \text{ MPa}$ ), as shown in figure 7 (a.).

$$\begin{Bmatrix} \sigma_{xx} \\ \sigma_{yy} \\ \tau_{xy} \end{Bmatrix} = \frac{K_I}{\sqrt{2 \cdot \pi \cdot r}} \begin{Bmatrix} \cos(\theta/2) \cdot [1 - \sin(\theta/2) \cdot \sin(3 \cdot \theta/2)] \\ \cos(\theta/2) \cdot [1 + \sin(\theta/2) \cdot \sin(3 \cdot \theta/2)] \\ \cos(\theta/2) \cdot \sin(\theta/2) \cdot \cos(3 \cdot \theta/2) \end{Bmatrix} + \frac{K_I}{\sqrt{2 \cdot \pi \cdot r}} \begin{Bmatrix} -(\rho/2 \cdot r) \cdot \cos(3 \cdot \theta/2) \\ (\rho/2 \cdot r) \cdot \cos(3 \cdot \theta/2) \\ -(\rho/2 \cdot r) \cdot \sin(3 \cdot \theta/2) \end{Bmatrix} \quad (1)$$

The following figure 6 supports the explanation of the input data for the equation 1 as described above.

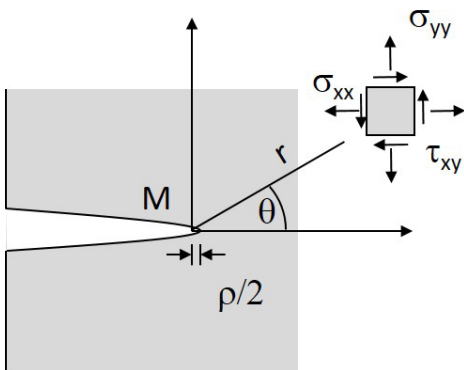


Figure 6 Sketch of a surface flaw for the explanation of equation 1[7]

The same effect of stress concentration arises due to the loading, as shown in figure 7 (b.). As described in previous chapter 4 both stress distributions were added and the result is shown in figure 7 c.).

### 7. Summary

For the determination and of the ultimate bending strength and a better understanding of the nature of the fracture mechanism it is crucial to combine the information about the stress distribution along the surface and through the thickness, the stress distribution due to loading and the influence of the defects on the surface and in the glass matrix. With the knowledge of all these components it is possible to predict the location of the origin of fracture.

### 8. Acknowledgements

The paper is a result of the research project "Josef Ressel Centre for thin glass technology for structural glass applications" funded by the Austrian Christian Doppler Research Association.

### 9. References

- [1] EN 12150; Glass in buildings – Thermally toughened soda lime silicate safety glass
- [2] EN 1863; Glass in building — Heat strengthened soda lime silicate glass
- [3] EN 12337; Glass in buildings – Chemically strengthened soda lime silicate glass
- [4] Neugebauer J.; Movable Canopy, conference proceedings, Conference proceedings; Glass Performance Days, Tampere, Finland, 2015
- [5] Neugebauer J.; Investigation of different test set scenarios for determination of ultimate bending stress of thin glass; Conference proceedings; Engineered Transparency; Düsseldorf; 2016
- [6] Illguth M., Schulera C., Bucak Ö.; The effect of optical anisotropies on building glass façades and its measurement methods; Frontiers of Architectural Research 4; 119–126; Elsevier; 2015
- [7] Schula S.; Charakterisierung der Kratzanfälligkeit von Gläsern im Bauwesen; Doctoral Thesis; Darmstadt; 2014
- [8] Gross D., Seelig T.; Bruchmechanik; Springer-Verlag Berlin Heidelberg; 2011

# Biaxially Curved Glass with Large Radii – Determination of Strength Using the Coaxial Double Ring Test

Steffen Müller-Braun<sup>1</sup>, Jens Schneider<sup>2</sup>

<sup>1</sup>Technische Universität Darmstadt, Germany -  
Institute of Structural Mechanics and Design

<sup>2</sup>Technische Universität Darmstadt, Germany -  
Professor for Structural Mechanics and Design

## Keywords

curved glass, coaxial double ring test, bending  
strength of glass, annealed glass, spherically  
curved glass

**Extended abstract** (The complete  
contribution will be published in  
the Glass Structures & Engineering  
journal)

The coaxial double ring test is used for  
determining the surface strength of flat glass  
e.g. as it is described in existing standards.  
The main idea of this test setup is to generate

a defined area of surface tensile stress, which  
is uniform in all directions within the load ring.  
Thus, the orientation of surface flaws does  
not influence the test results. Furthermore,  
the defined area with uniform stress allows a  
statistical evaluation with regard to the flaw  
distribution and therefore a prediction for  
deviating area sizes is possible.

For biaxially curved glass, the generation  
of such an area of uniform tensile stress is  
not easily possible in a test setup. However,  
for large radii of curvature and low glass  
thicknesses it is possible to flatten the  
specimen during the test and to generate an  
area of uniform tensile stress with increasing  
load.

In Fig. 1 the developed FE Model is shown.  
For spherically curved glass the load ring and  
the support ring are completely adapted to  
the specimen. In this case, geometrical non-  
linear effects have to be taken into consideration to

determine a threshold of the bending radius  
up to which this test setup is practicable.  
In the case of biaxially curved glass the  
specimen adapts at two points to the load ring  
and support ring (Fig. 1 a)). Thus, additional  
structural nonlinear effects superimpose  
the stress distribution. In Fig. 2 the result  
of a simulation of a glass plate with a large  
difference of the two radii is shown. For this  
geometry, it is not possible to generate an  
area of uniform tensile stresses within the  
load ring, because of the afore-mentioned  
effects. With the use of parametric studies,  
thresholds for the radii of biaxially curved  
glass are determined in which the coaxial  
double ring test provides good results. The  
investigations are focused on the common  
glass thickness of 4 mm. Furthermore,  
the nonlinear behaviour regarding the  
determination of the maximal main tensile  
stress is examined.

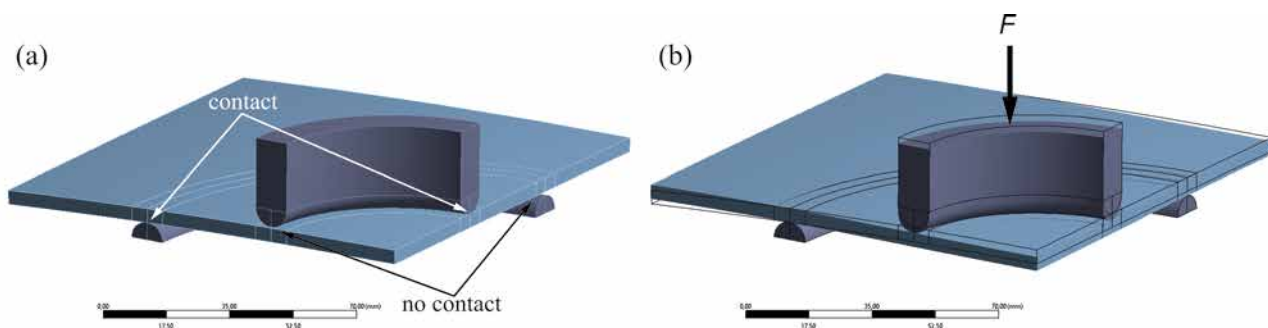


Fig. 1 Biaxially curved glass with large radii, which is flattened during the experiment and thus completely adapts to the load ring and support ring, without load (a), loaded (b)

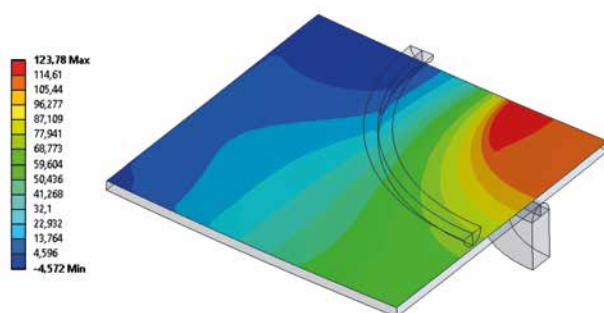


Fig. 2 Maximum principal tensile stress (MPa),  $R_x = 2000$  mm,  $R_y = 10000$  mm,  
 $F = 3232$  kN, view from below, thickness of glass  $t = 4$  mm

# Parameter Identification Methods for Visco – and Hyperelastic Material

Michael A. Kraus<sup>1</sup>, Miriam Schuster<sup>2</sup>  
Johannes Kuntsche<sup>3</sup>, Geralt Siebert<sup>4</sup>,  
Jens Schneider<sup>5</sup>

<sup>1</sup> University of German Armed Forces Munich, Germany - Institute and Laboratory for Structural Engineering

<sup>2</sup> Technische Universität Darmstadt, Germany - Institute of Structural Mechanics and Design

<sup>3</sup> ProfessorPfeiferandPartner - Ingenieurbüro für Tragwerksplanung

<sup>4</sup> University of German Armed Forces Munich, Germany - Professor for Structural Design and Building Physics

<sup>5</sup> Technische Universität Darmstadt, Germany - Professor for Structural Mechanics and Design

**Extended abstract** (The complete contribution will be published in the Glass Structures & Engineering journal)

Many materials in modern civil engineering applications, such as interlayers for laminated safety glass, are polymer-based. These materials are showing distinct viscoelastic

(strain-rate) and temperature dependent behaviour. In literature, different mathematical representations of these phenomena exist. A common one is the 'Prony-series' representation, which is implemented in many state-of-the-art Finite-Element-Analysis-Software to incorporate linear viscoelastic material behaviour. The Prony-parameters at a certain reference temperature can either be determined by relaxation or retardation experiments in the time domain or with a steady state oscillation in the frequency domain in the so called 'Dynamic Mechanical Thermal Analysis' (DMTA) followed by a 'Time-Temperature-Superposition-Principle' (TTSP). However, present research shows that polymeric materials also may need to have constitutive equations which include hyperelasticity (nonlinear stress-strain behaviour in a quasi-static condition) when undergoing large deformations and which also may respect the Mullins- or Payne-Effect, so that the material model should be expanded for a more realistic representation in numerical simulations.

A novel method for the whole identification process for a numerical material model in terms of a linear Generalized Maxwell model (Prony-series) based on experimental data will be presented (**Figure 1**). Furthermore, material parameters for different hyperelastic material models based on experimental investigations will be shown (e.g. **Figure 2**) and compared. Future research activities as well as extensions of the presented novel method are also highlighted within this paper.

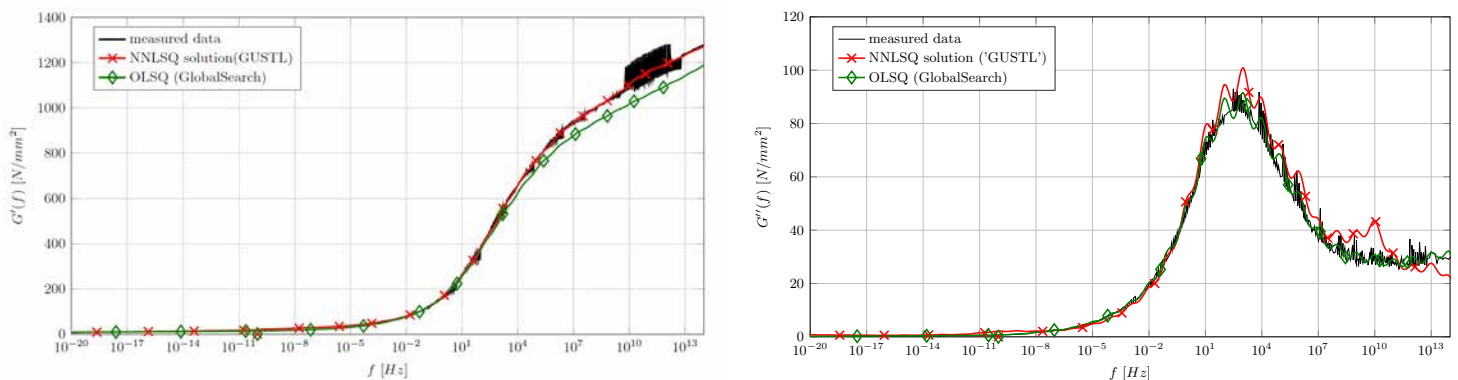


Figure 1: Parameter identification for viscoelastic behaviour – generalized Maxwell Model

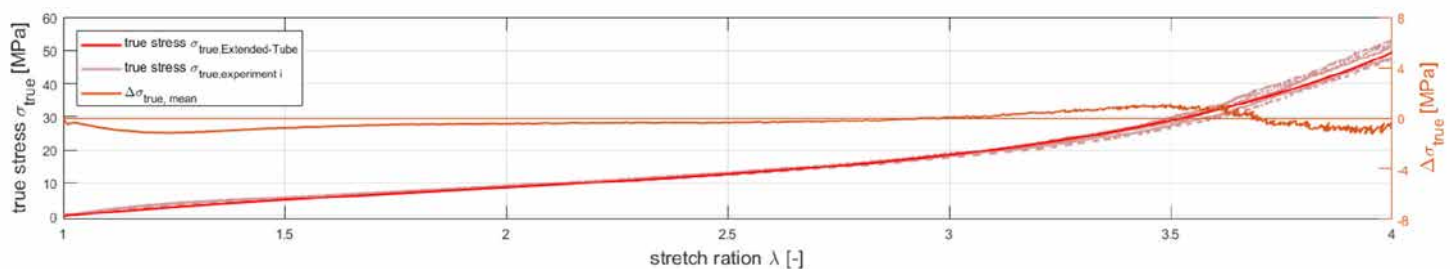


Figure 2: Parameter identification for hyperelastic behaviour – Extended Tube

# Influence of Aging on Post-Fracture Performance

Caroline Butchart<sup>1</sup>

Mauro Overend<sup>2</sup>

1. Eckersley O'Callaghan

2. University of Cambridge, Department of Engineering, UK

## Keywords

1=Laminated Glass 2=Post-fracture

3=Adhesion 4=Durability

## Abstract

Laminated glass deteriorates with time when subject to different environmental conditions. In this work, the impact of different environmental conditions on post-fracture performance is investigated by means of through-crack tensile tests on small scale PVB laminates. The changes in interlayer stiffness, adhesion and tear resistance after exposure to 3 different environmental conditions are recorded and compared to newly manufactured specimens. It was found that each environmental condition was detrimental to performance in different ways, but for each weathering condition investigated a significant deterioration was noted.

## 1. Introduction

Laminated glass deteriorates with time: appearance, light transmittance, mechanical properties and even chemical composition can all change when subject to different environmental conditions. The consequence of this deterioration on the post-fracture performance is unquantified, and consequently weathering is not specifically included in material safety factors for post-fracture design.

There has been some research into the impact of weathering in laminated glass. Much of this has been directed by interlayer manufacturers towards the prevention of visual defects. Recently research has been conducted into the deterioration of mechanical properties after weathering, predominantly for unfractured glass. The impact of weathering on post-fracture glass is different to that of unfractured glass. Before fracture, the role of the interlayer is to transfer shear only. After glass fracture, the interlayer carries both tension and shear, and must maintain adhesion to the glass, as such this topic warrants investigation beyond

the pre-fracture case.

Weathering can occur either before fracture, i.e. during the lifespan of the glass, or after fracture for example glass breakage in a humid or wet environment. Weathering after fracture is a separate topic not addressed within this work, but was published as part of a separate study [1].

This work investigates the impact on post-fracture performance of different environmental conditions by means of through-crack tensile tests on small scale PVB laminates. The changes in interlayer stiffness, adhesion and tear resistance are recorded and compared to newly manufactured specimens. It was found that each environmental condition affected post-fracture performance in different ways, but in all cases deterioration was significant and warranted further, larger scale study.

## 2. Existing Literature

The existing body of research can be divided into three categories: 1) That focussing on visual deterioration; 2) studies investigating change in the mechanical performance of unfractured glass, and 3) studies from the adhesive community which investigate deterioration of adhesion under different environmental exposures. Each topic is addressed in turn below.

The largest body of research into weathering has been conducted by interlayer manufacturers. The aim of which is predominantly to develop their interlayers and lamination techniques to resist visual defects. In 1998 accelerated weathering procedures for the assessment of visual performance was standardised in Europe by EN ISO 12543-4 [2, 3]. Three accelerated weathering procedures are prescribed: high temperature, high humidity and exposure to UV. Laminates must be able to withstand these procedures without occurrence of visual defects. There is no requirement for assessment of the mechanical performance after these weathering procedures.

Delincé [4] investigated changes in the shear stiffness of PVB and SG after artificial exposure to UV and high humidity. Specimens were subject to the artificial weathering procedures outlined in EN ISO 12543-4. After weathering, the specimens were tested in shear and four-point bending and compared to a reference

set of non-weathered specimens. They found that exposure to both UV and humidity increased the stiffness of PVB marginally for the shear specimens, but decreased the stiffness in the four-point bending specimens. Sackmann [5] also performed shear tests on PVB laminates exposed to humidity and UV-radiation. They found that UV-radiation reduced the shear modulus by about 10%, whilst humidity exposure reduced the shear modulus by as much as 50%. The reader is also directed to detailed studies conducted by Ensslen [6] who conducted shear tests on both naturally and artificially weathered specimens; Serafinavicius [7] who conducted four-point bending tests on specimens subject to the artificial weathering procedures prescribed in EN 12543-3; and Kothe [8, 9] who investigated changes in the glass transition temperature after different weathering procedures. Recently there has been some work into the durability of interfacial adhesion. Additionally, the literature is supplemented well by research conducted on glass-specific adhesives. Louter [10] investigated changes in adhesion in steel-glass composite beams bonded with an SG interlayer after exposure to humidity and thermal cycling weathering procedures. Louter found that adhesion was reduced in specimens which had been exposed to humidity, but could not conclude if thermal cycling affected adhesion. Both Delincé [4] and Sackmann [5] found that both humid environments and high UV radiation caused a reduction in adhesion for PVB-glass laminates, whilst Goebel [11] found no reduction in adhesion in glass-EVA laminates after exposure to salt spray for 28 days.

## 3. Weathering Procedures

In this work 3 different environmental exposures were investigated and compared to nominally identical newly-manufactured specimens. The 4 testing categories are summarised in table 1.

Two accelerated weathering procedures were investigated alongside one "natural" weathering procedure. These were compared to tests conducted on nominally identical, newly manufactured specimens. The two accelerated weathering procedures that seek to simulate the effects of long term exposure to high temperatures and high humidity environments respectively. The procedures

outlined in BS EN 12543-4 were followed for both conditions. This standard prescribes accelerated weathering procedures developed specifically for PVB glass laminates.

**High Temperature:** Specimens were heated in a convection oven from room temperature to 100 °C over a period of 30 minutes. The specimens were then held at 100 °C for a further 16 hours before being allowed to cool at room temperature. Once fully cooled, the specimens were tested within 24 hours.

**High Humidity:** Specimens were held above water in a sealed chamber heated to 50 °C for a period of 2 weeks. This creates a relative humidity of 100% within the chamber. Specimens were subsequently tested at ambient conditions (21 °C; 45% RH) within 3 hours of removal from the chamber.

**Naturally weathered:** Specimens were placed in an external environment in Cambridge, UK, for a period of 1 year (10th March 2013 - 10th March 2014). The specimens were positioned on a west facing surface inclined at 20° to the horizontal in an area with no shade. A sloped surface was utilised to prevent soaking of the specimens during heavy rain-fall. These conditions by no means represent a worst-case scenario, but indicate whether weathering should be a consideration for all glazing, or if it is relevant only to extreme environments.

## 4. Experimental Work

Through crack tensile (TCT) tests were conducted on 200 mm x 50 mm laminated glass specimens as shown in figure 1. The specimens were manufactured from two layers of 6 mm annealed soda-lime-silica glass, laminated with a 0.76mm Saflex RB41 PVB interlayer. A dotted grid was printed on one side of the interlayer. The lamination process was representative of standard production techniques.

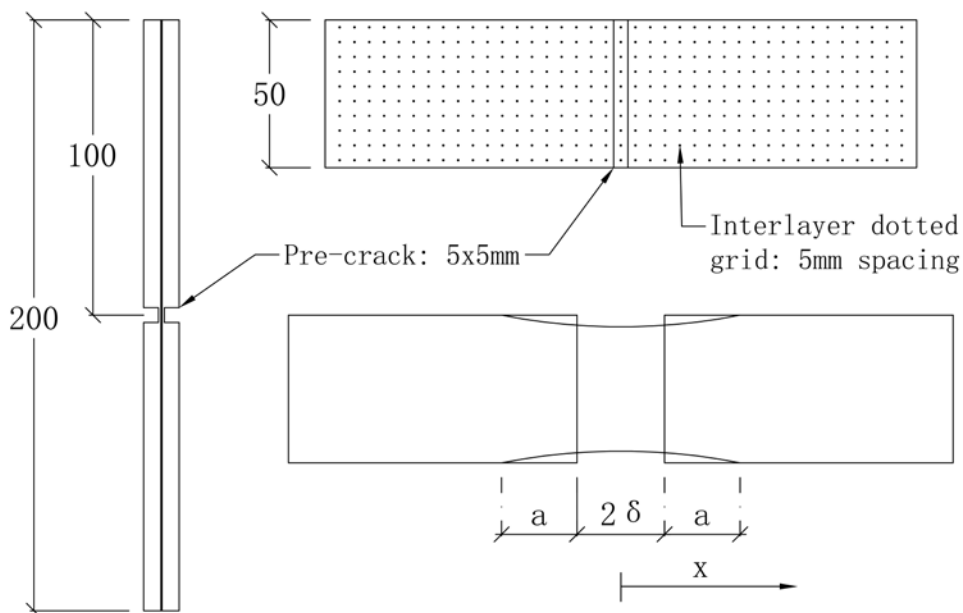


Figure 1 Test Specimens

| Test Category      | No. tests | Label    |
|--------------------|-----------|----------|
| As-New             | 5         | AN-(1-5) |
| High Temperature   | 5         | HT-(1-5) |
| High Humidity      | 5         | HH-(1-5) |
| Natural Weathering | 5         | NW-(1-5) |

Table 1 Testing regime.

The TCT specimens in the naturally weathered group were placed in an external environment in Cambridge, UK, for a period of 1 year (10th March 2013 - 10th March 2014). The specimens were positioned on a west facing surface inclined at 20° to the horizontal in an area with no shade. A sloped surface was utilised to prevent soaking of the specimens during heavy rain-fall. These conditions by no means represent a worst-case scenario, but indicate whether weathering should be a consideration for all glazing, or if it is relevant only to extreme environments.

The TCT test was initially developed by Sha et. al. [12], and has since been used widely as a simple and controlled method of assessing post-fracture performance. The test set-up is shown in figure 2: the glass is clamped rigidly in an Instron 5500R universal testing machine. A tensile force is applied to the 2-ply laminate which has a single, coincident fracture in each glass ply. The applied load is transferred across the glass fracture by the polymer interlayer which elongates, and delaminates from the glass surfaces. The specimens fail by tearing of the interlayer or by excessive delamination between the glass and the interlayer. A pre-crack was created by grinding a 5 mm wide and ≈ 5 mm deep channel across the mid-line of each glass ply in figure 1. This process left 1mm of glass intact on either side of the polymer interlayer. The pre-crack was formed after the weathering procedure, in order to ensure that the test was a true representation of weathering occurring before glass fracture.

Slip at the interface between glass and test rig was eliminated by bonding pure aluminium plates on the glass in the region to be clamped. Whilst the test specimens were placed a small, but constant tension was applied. This prevented compressive forces causing buckling of the slender 'pre-crack'. Once secured the remaining 1 mm of glass was fractured in tension, immediately prior to testing. This significantly reduced the occurrence of damage to the interlayer. A displacement rate of  $2\delta = 0.264$  mm/s was applied across the fracture such that the interlayer stretched and delaminated. This speed corresponds to that used during a previous study at the University of Cambridge. Applied force was recorded by the universal testing machine. Distortion of the dotted grid was captured using a high-definition video camera at 25 frames/second. The images were analysed using the open source digital image correlation (DIC) software by Eberl [13]. Finally, the delamination front was captured throughout the duration by a portable digital microscope.

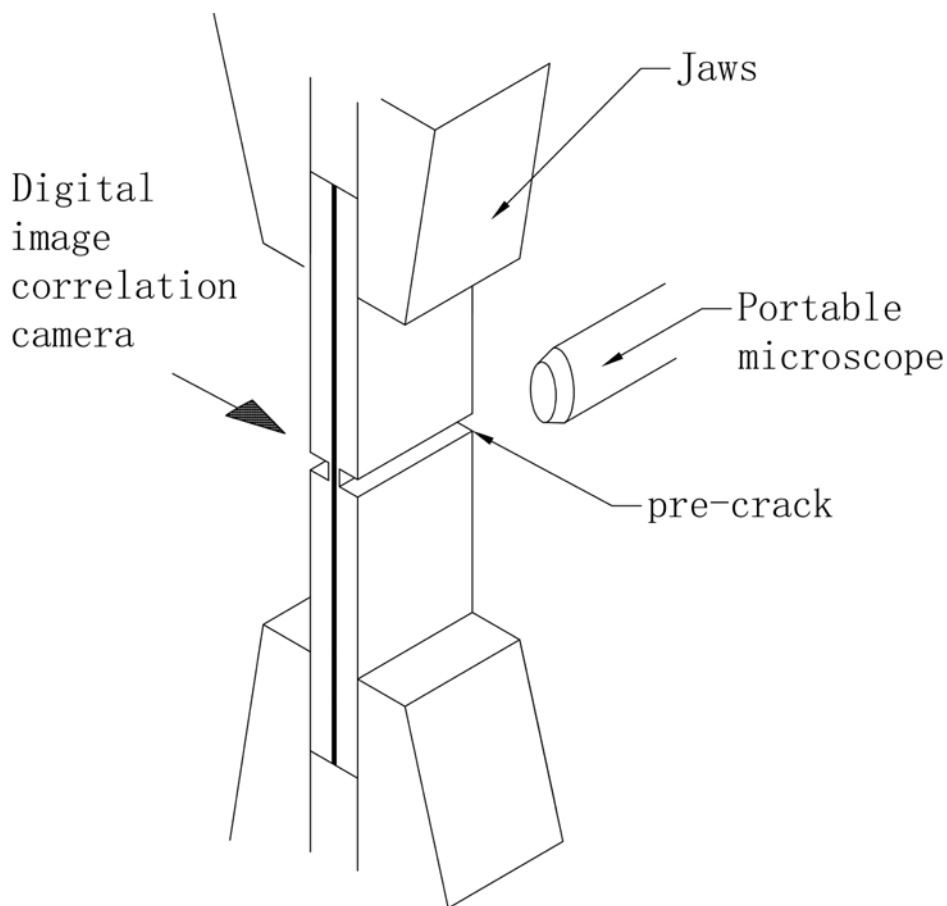


Figure 2 a) Schematic of test rig, and b) image taken during testing.



## 5. Results

### 5.1 Response of as-new specimens

The response of the newly manufactured specimens is shown in figure 3. It can be divided into three distinct phases:

- (i) Linear phase, with forces increasing to an average peak of 275 N. This phase is labelled as (i) in figure 3. The response is interrupted by a discontinuity at 160 N caused by movement in the test rig. During this phase the length of initially un-bonded interlayer stretches; little to no delamination occurs
- (ii) Steady-state phase during which delamination commences and continues at a roughly constant rate. The force also remains constant. This phase, labelled as (ii) in figure 3, continues until approximately 3 mm total displacement
- (iii) Failure phase - beyond displacements of  $2\delta = 3$  mm the response varies between specimens. This has been noted previously by Ferretti [14].

Three different failure methods were observed: specimens 2 and 4 failed in tension across the delaminated interlayer; specimens 1 and 5 failed by slip between glass and jaws, both specimens exhibited large interlayer deformation prior to failure. Specimen 3 failed by interlayer tearing. This tearing occurred early in the test before significant delamination. This is attributed to a damaged interlayer, caused during glass fracture.

### 5.2 Response after High Temperature pre-conditioning

The force-displacement response of the specimens which were pre-conditioned with the high-temperature accelerated weathering procedure can be seen in figure 4. These specimens also show an initial linear response, with a peak force of 340 N. Beyond the linear phase, each specimen responded differently. As previously reported by Ferretti [14], TCT test responses are frequently very varied, even for newly-manufactured specimens.

The high temperature specimens showed a stiffer response than newly-manufactured, forces were higher and delaminated lengths smaller. Ink from the dotted grid transferred from PVB to glass, making digital image correlation difficult. Failure occurred by local tearing in specimens 1 and 2; slip at the glass-jaw interface in specimen 3; delamination in specimen 4; and global tension in specimen 5. The failure mechanisms were not significantly different to newly manufactured.

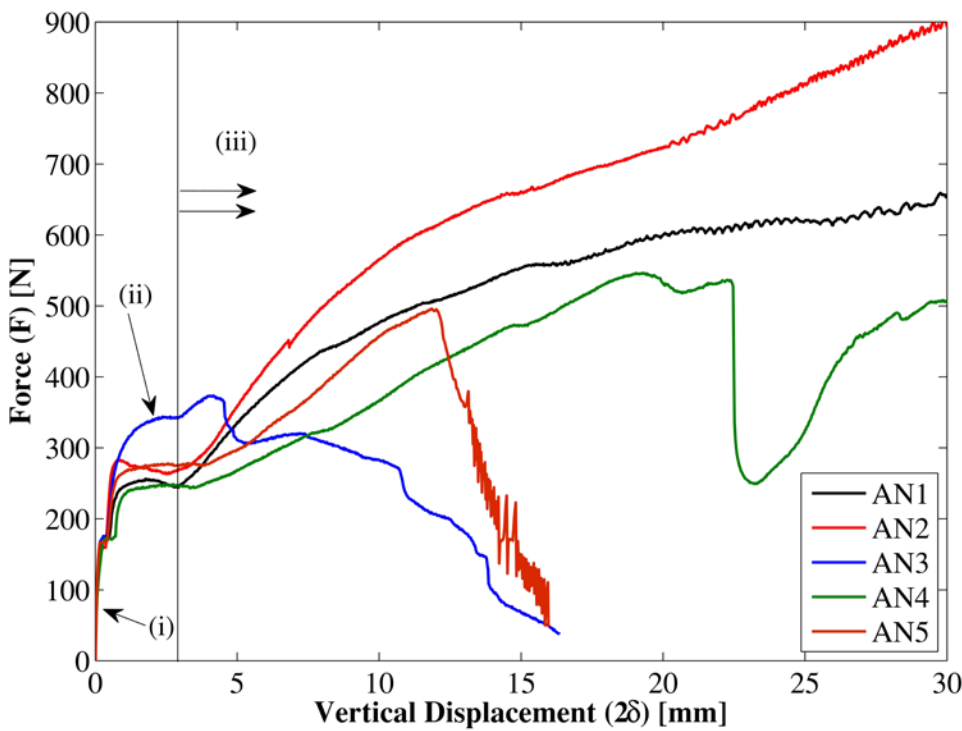


Figure 3 Force displacement response of the newly manufactured specimens.

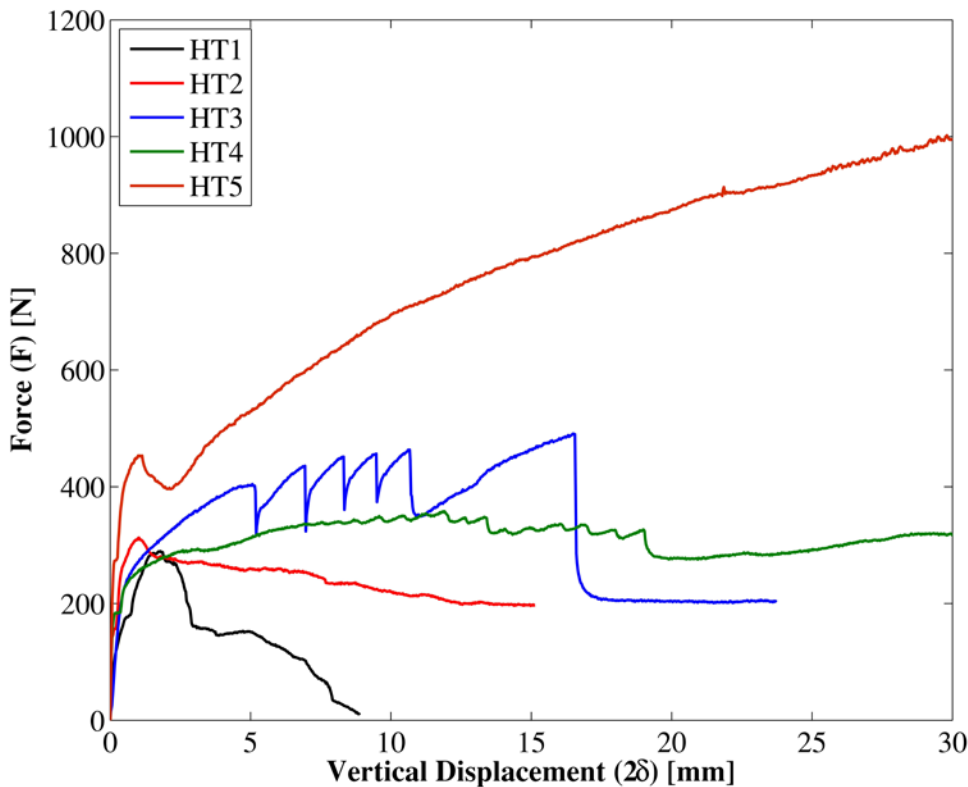


Figure 4 Force displacement response for specimens subject to high-temperatures.

### 5.3 Response after High Humidity pre-conditioning

The force-displacement response of the specimens which were pre-condition with the high-temperature accelerated weathering procedure can be seen in figure 5. The response is markedly different to both the as-new and high-temperature categories. After the initial stretching phase, the steady-state delamination phase occurred at approximately 115 N. The delamination phase continued for significantly longer than the as-new and high-temperature specimens: specimens 1 and 5 remained in the steady-state delamination phase throughout the entire test duration.

### 5.4 Response after Naturally Weathering

The naturally weathered specimens exhibited a lower load-carrying capacity than the as-new specimens. Steady state delamination occurred at just under 200 N, compared to 115 N in the high-humidity tests, and 275 N in the as-new specimens. The response can be seen in figure 6. Specimens 2-5 showed some uneven delamination and then tore. In previous categories, tearing was only seen when no delamination occurred, and it was attributed to interlayer damage. Specimens 2-5 all tore after delamination, suggesting a significant reduction in interlayer tear resistance.

### 5.5 Results Comparison

Figure 7 shows a summary of the test data for each weathering category. In image (a) the average steady state force as recorded during phase 2 of the test is shown. It is clear that the high humidity environment reduces the force required to delaminate the PVB interlayer. This is consistent with previously published results [1]. In figure 7(b) the average initial stiffness of each weathering category is shown. The stiffness is calculated for the linear phase (phase 1 in figure 3) only. This stiffness is recorded before significant delamination and is therefore a measure of the effect of weathering on the bulk interlayer shear modulus. Again, the humid environment was found to be severely detrimental to performance.

In figure 7(c) the interlayer strain causing delamination is shown. This was calculated using digital image correlation software to measure strain in the first delaminated row (see figure 7(e)), This represents interlayer strain before significant creep and can be used to assess adhesive strength after weathering. Figure 7(d) shows the delamination rate before onset of tearing. A consistent response is seen across all categories. This is a strong indicator that adhesion is strain-governed as opposed to stress-governed. Finally, DIC was used to determine the interlayer strain profile at failure.

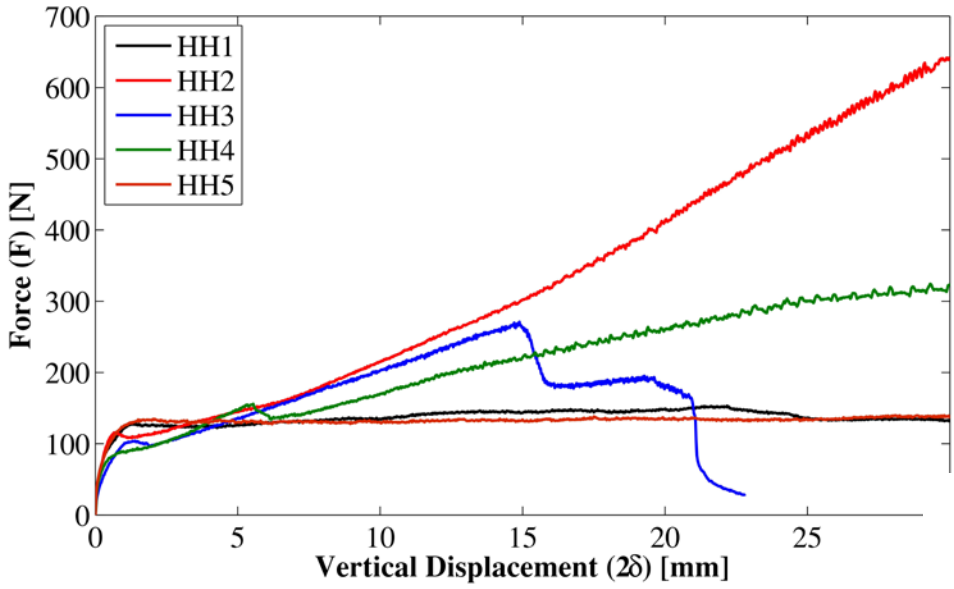


Figure 5 Force displacement response for specimens subject to high-humidity.

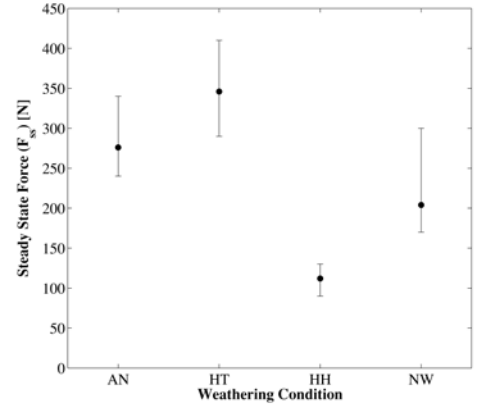


Figure 7a

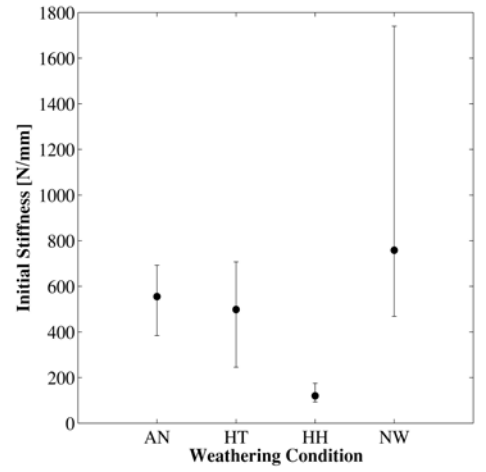


Figure 7b

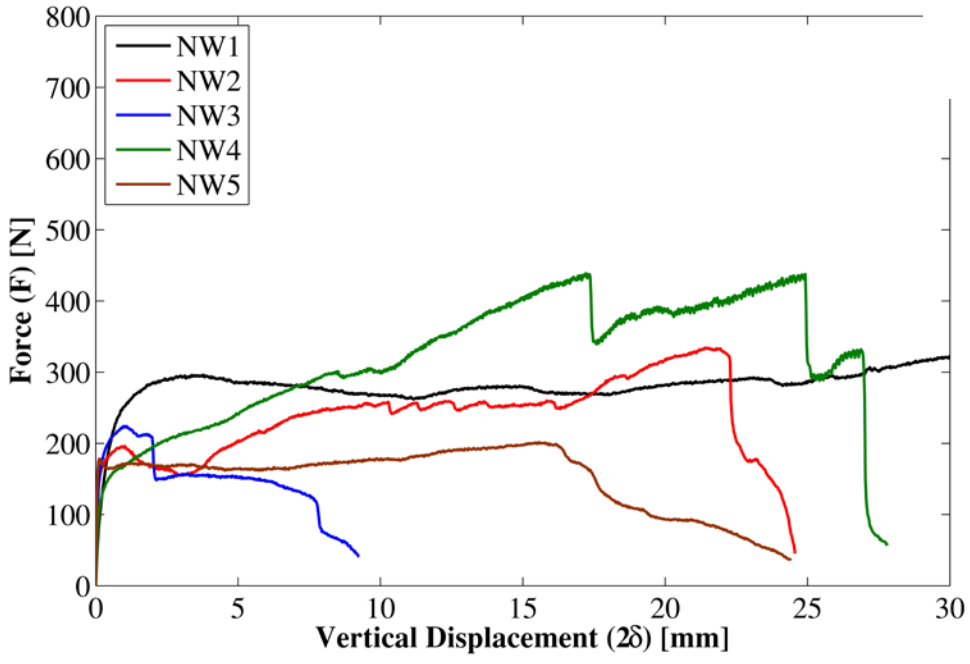


Figure 6 Force displacement response for specimens subject to natural weathering

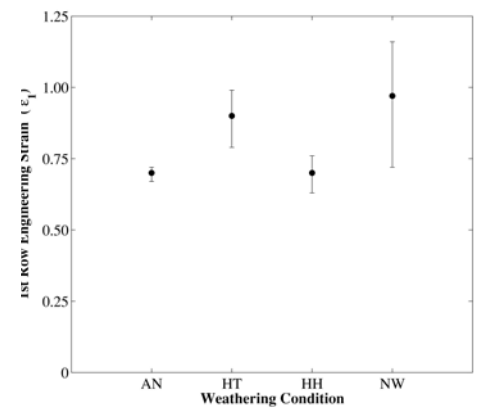


Figure 7c

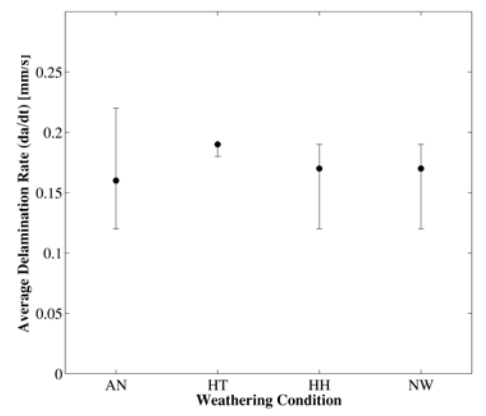


Figure 7d

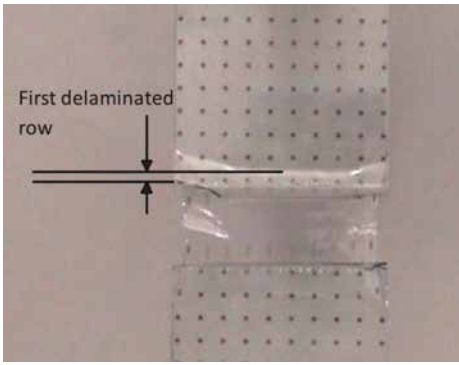


Figure 7 (a to e) Summary of test data for all weathering conditions, average and data range  
 a) Steady state force, b) Initial stiffness, c) Decohesion strain, d) Delamination rate before onset of tearing, e) Material length considered for calculation of decohesion strain

The results can be seen in figure 8. In Figure 8 the strain profile represents a snap shot in time at the point of TCT specimen failure. The distance  $x$  represents distance, measured vertically from the specimen midline. The findings of all tests are summarised in table 2.

### 6. Discussion

The results show that the post-fracture performance is changed for each weathering condition investigated. Different weathering procedures influence interlayer bulk behaviour, interfacial adhesion, and tear resistance in different ways.

**Exposure to high temperature:**

High temperature led to an increase in steady state force without a corresponding increase in bulk interlayer stiffness. This indicates that temperature has no effect on the bulk interlayer but increased the interfacial adhesion. Unfortunately, increased adhesion is well known to increase susceptibility to tearing.

**Exposure to high humidity:**

High humidity led to significant reduction of interlayer stiffness. This is in agreement with the observed reduction in steady state force. It appeared that there was no change in the adhesion causing strain. This contrasts with earlier published results [1], and implies that the reduction in stiffness is sufficiently high to govern global post-fracture behaviour.

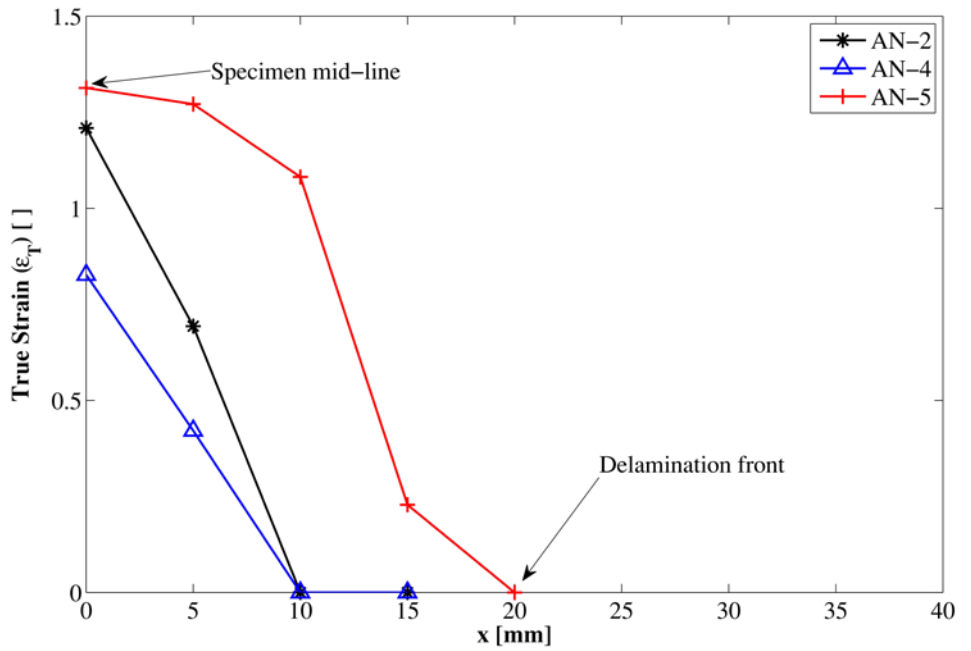


Figure 8a

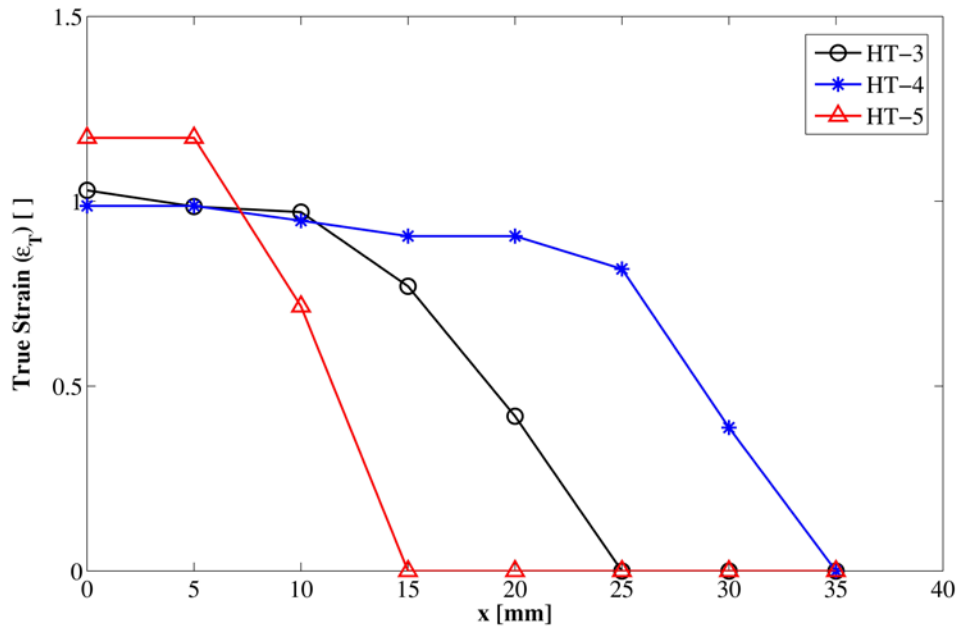


Figure 8b

| Weathering Procedure | Fss      | Stiffness | Adhesion  | Tear resistance |
|----------------------|----------|-----------|-----------|-----------------|
| High Temperature     | Higher   | No change | High      | No change       |
| High Humidity        | Very Low | Lower     | No change | N/A             |
| Naturally Weathered  | Lower    | Higher    | Very high | Very low        |

Table 2 Summary of findings

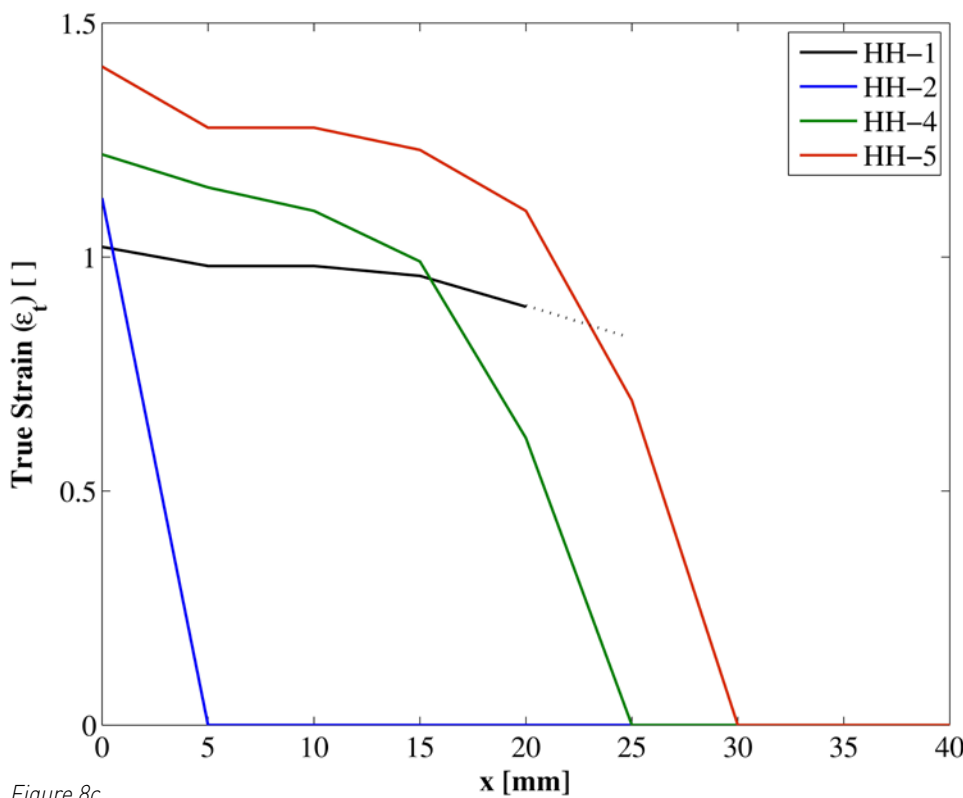


Figure 8c

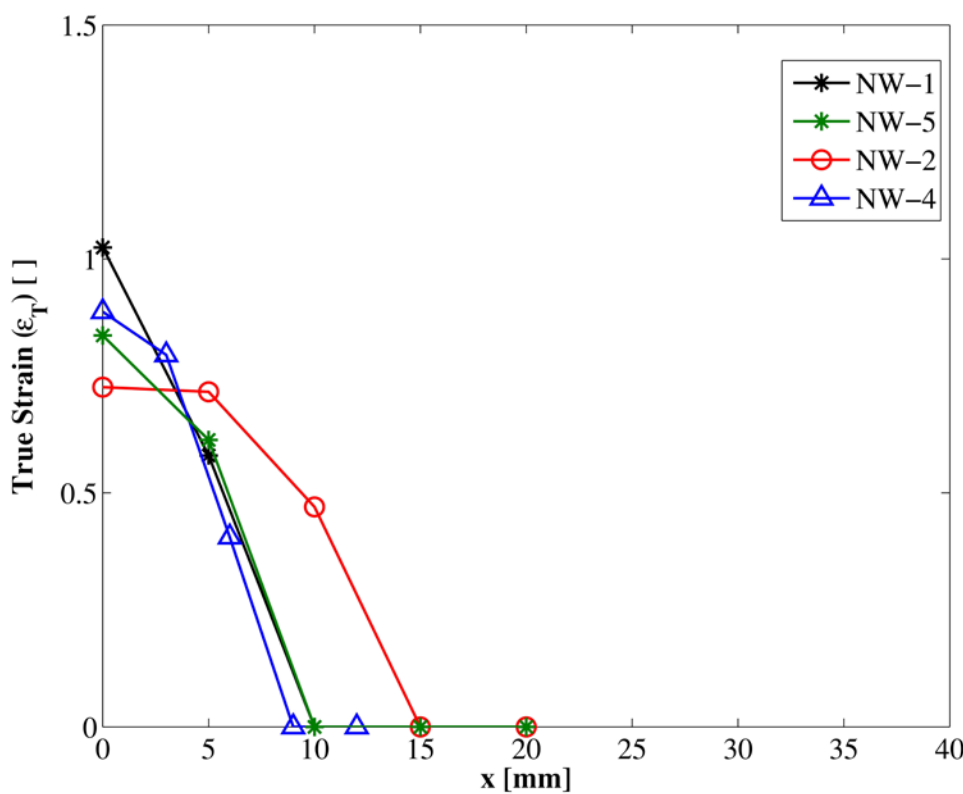


Figure 8d

**Exposure to natural weathering:**

The specimens exposed to natural weathering recorded lower forces than those observed in the newly manufactured specimens. Conversely, both stiffness and interfacial adhesion were found to be higher than as new. This infers that the energy was being dissipated by other means – probably local large strain mechanisms that eventually led to the early tearing witnessed in this category.

These findings are reflected in the strain profile at failure shown in figure 8. The area below the strain profile curve combined with the steady state force, indicate energy dissipated by interlayer strain. The intersection with the x-axis shows the total delamination at failure. More energy was dissipated as strain for the specimens which underwent high-temperature weathering. Both the area under the curve and steady state force are higher than newly manufactured. The observed high adhesion strength limited energy dissipated by delamination. Conversely, the total delaminated length was also higher, this suggests some increase in resistance to tearing. The specimens exposed to high temperatures, also exhibited a more symmetrical and even delamination; this could also account for the increase in total delamination. There is an increase in area under the curve for the high humidity tests, however this is matched with a reduction in steady state force and increased test duration. From the strain profile alone it is difficult to decompose the global behaviour into the constituent bulk and adhesive parts.

The strain profile of the naturally weathered specimens shows that little energy is dissipated in both global deformation and interlayer delamination. Instead the energy is dissipated in local large strain mechanisms which eventually lead to tearing.

## 7. Conclusions

All weathering procedures investigated here caused a change in the post-fracture response. Humidity was found to decrease interlayer stiffness. High temperatures increased adhesion which could lead to premature tearing. The naturally weathered specimens showed a significant decrease in tear resistance.

The work highlights the need for further study, in particular for the need to investigate the post-fracture performance of full scale, naturally weathered laminates from a variety of real-world environments.

It is impossible to perform a quantitative assessment of the impact of weathering from lab based research on small scale specimens. The qualitative results presented here require real world data to inform:

- 1) Influence of specimen size
- 2) Relationship between accelerated weathering procedures outlined in BS EN 12543 and "real-world" environments.

## Acknowledgements

The authors would like to thank Interpane for providing the samples for this work, and also to thank Eckersley O'Callaghan for their time and guidance.

## References

- [1] C. Butchart and M. Overend, "Influence of Moisture on the Post-Fracture Performance of Laminated Glass," Glass Performance Days, Finland, June 2013.
- [2] CEN. BE EN ISO 12543-4:2011 Glass in building - Laminated glass and laminated safety glass - Part 4: Test methods for durability, 2011.
- [3] Norbert Wruk. A New ISO Standard for Laminated Glass. Glass Processing Days 1999
- [4] D. Delincé, J. Belis, Gauthier Zarmati, and Benoit Parmentier. Structural behaviour of laminated glass elements – a step towards standardization. In Glass Performance Days 2007, pages 658–663, Finland, June 2007.
- [5] Vincent Sackmann, Christian Schuler, and Holger Gräf. Testing of Laminated Safety Glass. In ISAAG 2004, pages 1–8, 2004.
- [6] Frank Ensslen. Influences of laboratory and natural weathering on the durability of laminated safety glass. In Glass Performance Days 2007, volume 2, pages 584–590, Tampere, 2007.
- [7] T Serafinavicius, Jean-Paul Lebet, Christian Louter, A Kuranovas, and T Lenkimas. The effects of environmental impacts on durability of laminated glass plates with interlayers (SG, EVA, PVB). In Challenging Glass 4 & COST Action TU0905 Final Conference, pages 455–462, 2014.
- [8] Michael Kothe and Bernhard Weller. Influence of environmental stresses to the ageing behaviour of interlayer. In Challenging Glass 4, pages 439–446, 2014.
- [9] Bernhard Weller and Michael Kothe. Ageing Behaviour of Polymeric Interlayer Materials and Laminates. In Glass Performance Days 2011, pages 240–243, 2011.
- [10] Christian Louter, Jan Belis, Fred A. Veer, and Jean Paul Lebet. Durability of SG-laminated reinforced glass beams. In Glass Performance Days 2011, pages 343–347, Tampere, 2011.
- [11] Horst Goebel. Laminated safety glass with EVA-based densely cross-linked interlayer: Durability, mechanical and optical properties. In Glass Performance Days 2013, pages 232–234, 2013
- [12] Y. Sha, C.Y. Hui, E.J. Kramer, P.D. Garrett, and J.W. Knapczyk. Analysis of adhesion and interface debonding in laminated safety glass. Journal of Adhesion Science and Technology, pages 49–63, 1997.
- [13] C. Eberl. Digital Image Correlation and Tracking, 2006. URL: <http://www.mathworks.co.uk/matlabcentral/fileexchange/12413-digital-image-correlation-and-tracking>.
- [14] Daniele Ferretti, Marco Rossi, and Gianni Royer-carfagni. Through-cracked-tensile delamination tests with photoelastic measurements. In Challenging Glass 3, number June 2012.

# Full-surface and Non-destructive Quality Control and Evaluation by Using Photoelastic Methods

Benjamin Schaaf<sup>1</sup>, Pietro Di Biase<sup>1</sup>, Markus Feldmann<sup>1</sup>, Christian Schuler<sup>2</sup>, Steffen Dix<sup>2</sup>,

<sup>1</sup>RWTH Aachen University, Institute of Steel Construction, Mies-van-der-Rohe-Str. 1, 52074 Aachen, Germany

<sup>2</sup>University of Applied Science Munich, Laboratory for Steel and Light Alloy Construction, Karlstr. 6, 80333 Munich, Germany

## Keywords

Anisotropy, Thermally toughened glass, Algorithm, Full-surface quality control, Photoelasticity

## Abstract

In the last years contentions about anisotropies (stress birefringence, which can cause visible appearances within the glass) among customers and manufacturers occurred when using glass products, such as heat-strengthened (HS) or fully tempered glass (FT). Findings from recent research activities show that anisotropies have to be evaluated in various aspects. Furthermore, it is mandatory to rate anisotropies using a suitable assessment method. Within this article, RWTH Aachen University (RWTH) and University of Applied Science Munich (HSM) present two non-destructive methods, based on photoelasticity, for a full-surface evaluation. It is shown in particular that both methods are suitable for an objective evaluation of anisotropy. Firstly, a method to determine the edge membrane stresses is demonstrated, followed by the visualization and research of anisotropy within the glass pane.

## 1. Introduction

In the course of the production of thermally pre-stressed glass products, a non-homogeneous distribution of the impressed prestressing within the surface of the glass pane can occur due to uneven cooling. If the prestress in all directions is locally unequal, the effect of the so-called stress birefringence results in visible iridescence phenomena, which often can be seen as grey to coloured stripes or spot patterns over the surface of the glass pane [cf. Figure 1]. This phenomenon is also described as anisotropy. However, in [1]



Figure 1 - Facade with tempered glass panes, left strong anisotropies and right low anisotropy, no polarising filters used (Luxembourg)

and [2] anisotropies are not characterized as a defect, but as a physical effect of thermally pre-stressed glasses.

The intensity of the anisotropies depends on the inhomogeneity of the thermally impressed prestress: the higher the anisotropy, the more iridescences can appear [4]. When (partially) polarised light occurs anisotropies can be optically detected. The higher the degree of polarisation, the better iridescence can be detected [5].

Polarised light is part of the natural environment and occurs by scattering and by reflection. The degree of polarisation of the light depends on several parameters, such as sun position or reflection angle. In a current research project the objective of research is to evaluate the glass quality by the basic requirements like strength, fracture and optics in a non-destructive way. The project also includes the development of an evaluation algorithm for the calculation of the anisotropy as well as a measurement method for the determination of the edge membrane stress. One of the big advantages of the method is the 100% anisotropy evaluation of the surface by excluding unavoidable geometrical induced anisotropies like edges, corners or holes / bores [cf. Figure 2].

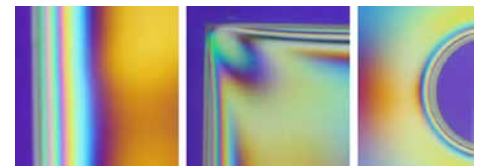


Figure 2 - Examples of geometrically induced anisotropies: edge, corner and bore

In this paper, first of all, the physical basis of anisotropy is discussed. Subsequently, the measurement method for the two-dimensional detection and description of the anisotropy in thermally pre-stressed glass panels is presented, compared with an already existing analysis method and, finally, first results are presented.

## 2. Physical basics

### 2.1 Circular polariscope

One method to study anisotropies in thermally toughened glass is by the use of so-called polariscopes. Within the scope of the performed investigations a circular polariscope was used. Circularly polarised light has no constant direction of oscillation and is, therefore, direction-independent. The setup of the used circular polariscope includes two polarisers and two so-called quarter-wave plates, which consist of birefringent material. The first quarter-wave plate is placed directly after the polariser, the second is placed in front

of the analyser. The polariser initially produces linearly polarised light, which, after passing through the first quarter wave plate, undergoes a circular polarisation. When entering the birefringent specimen (e.g. tempered glass), the light vector is decomposed into two components depending on the directions of the principal stresses. After exiting the specimen a retardation  $s$  can be detected (as shown in Figure 3). The circularly polarised light is again linearly polarised by the second quarter-wave plate and, finally, passes the analyser [6].

The resulting retardation  $s$  depends on the value of the differences of the principal stresses at a given point. The stress difference and the retardation are linked by the specimen's thickness  $d$  and the so-called photoelastic constant  $C$ .

$$s = C \cdot (\sigma_1 - \sigma_2) \cdot d \quad (1) \quad \text{Figure 3 - Functionality of a circular polariscope}$$

If, in addition, the path difference is referred to the wavelength ( $s/\lambda$ ), the phase shift  $\delta$  is obtained, which yields to the so-called main equation of photoelasticity:

$$\delta = \frac{C}{\lambda} (\sigma_1 - \sigma_2) \cdot d \quad (2)$$

If a birefringent medium, e.g. tempered glass, is viewed in a polariscope with monochromatic light, black lines occur due to interference. These black lines are called isochromats of 0<sup>th</sup>, 1<sup>st</sup>, 2<sup>nd</sup>, etc. order, depending on the magnitude of the phase shift. Isochromats indicate ranges in the test specimen which have the same principal stress difference  $\sigma_1 - \sigma_2$ . When using white light (compound of light with different wavelengths) these effects occur separately for each wavelength. Only the light of a certain wavelength is extinguished and the isochromats appear in the complementary colour of the extinguished light [6].

## 2.2 Edge characteristics

Tempered flat glass panes can be categorized into four zones by their stress distribution [7]. The plate surface with a sufficient distance from the edges and bores forms zone 1. The impressed pretension  $\sigma_1 = \sigma_2$  in this region is reflected by a parabolic profile over the thickness. When approaching the edge of the plate (zone 2),  $\sigma_1$  perpendicular to the edge assumes the value zero, as illustrated in Figure 4. This effect leads to the fact that, by means of different stress-optical methods, the mean compressive stress  $\sigma_2$  (edge membrane stress) can be determined since the second unknown  $\sigma_1$  is omitted from the principal equation of stress optics.

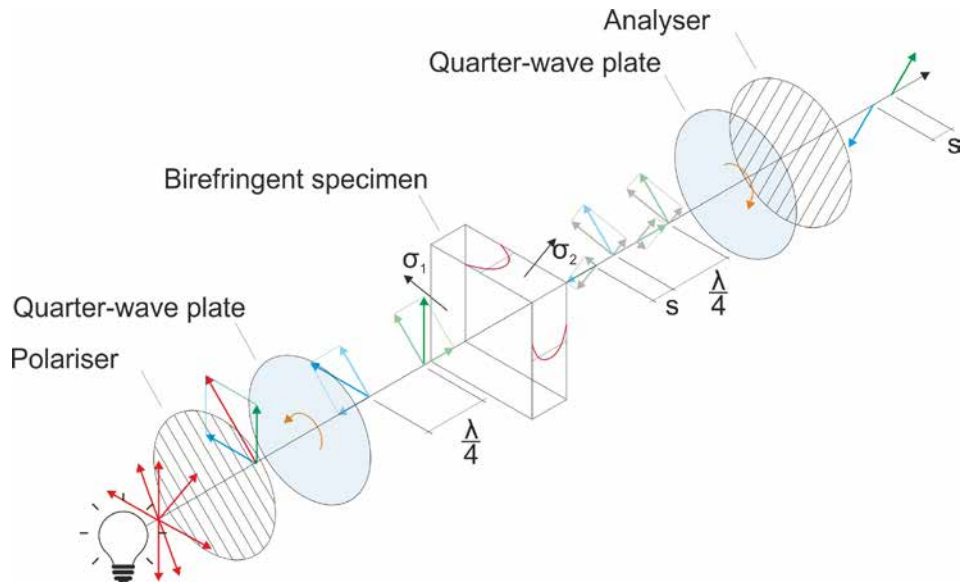


Figure 3 - Functionality of a circular polariscope

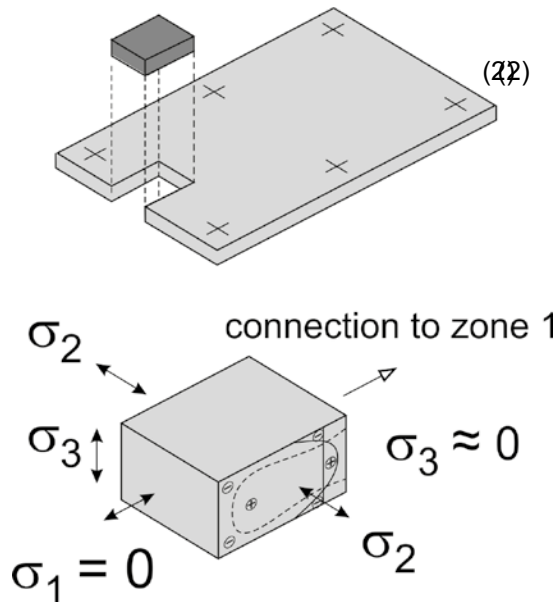


Figure 4 - Stress distribution near edge (zone 2)

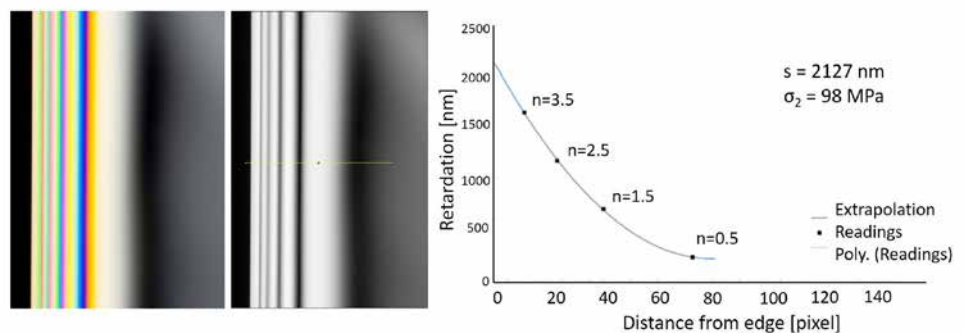


Figure 5 - Polarisering filter image RGB (left) and monochrome (centre), determination of the retardation  $s$  (right)

### 3. Analytical methods for the evaluation

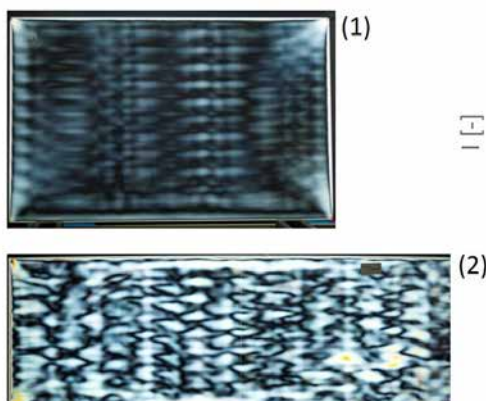
RWTH and HSM independently developed different analysis methods to determine stress differences in the plane of the glass in order to evaluate objectively the resulting anisotropies. In addition, a measuring method of the HSM is presented in order to study the edge compressive stress of thermally toughened glass by means of digital polarising filter images.

#### 3.1 Method HSM

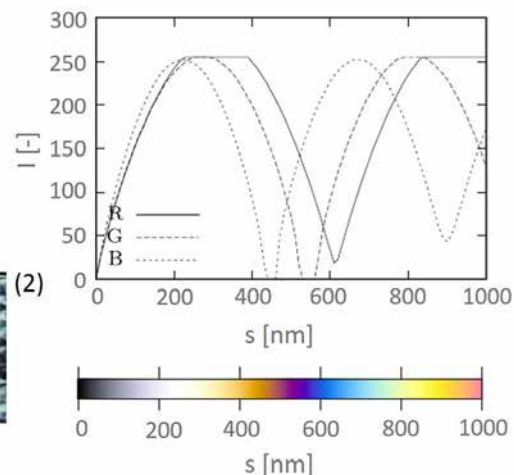
The analysis methods described here are based on the principles for determining the isochromatic order from polarising filter images by means of computer algorithms, as described in [8]. First, a method to determine the average edge membrane stress is explained. The determination of the stress  $\sigma_2$  on a free edge of a component by simply counting the isochromatic order is a known method, which can also be found in [6]. The method used requires a monochromatic light source or the division of the digital image (white light) into the three colour channels red, green and blue (RGB). Counting orders always starts from load-free or isotropic places. In the circular polariscope in combination with white light, these spots are dark (in contrast to the higher-order coloured isochromates). For a precise determination of the edge membrane stress  $\sigma_2$ , the wavelength of the light has to be known. A telecentric lens in combination with a white light source was used for laboratory tests to create polarising filter images (cf. Figure 5), which the location of the isochromates can be taken from. With the order  $n$  and the known wavelength  $\lambda$  of the light used, the associated retardation is determined for each isochromat by multiplication of the order with the wavelength. Since the maximum and minimum brightness alternate by half an order, a further point can be found between two isochromats. The retardation  $s$  is determined by extrapolation of the supporting points as show in Figure 5. By means of the principal equation of photoelasticity and the knowledge that the principal stress  $\sigma_1$  at the edge is zero, the edge membrane stress  $\sigma_2$  can be obtained as a quotient of the retardation  $s$  and the product of the glass thickness  $d$  and photoelastic constant  $C$ .

The second analysis method, which has been tested at the HSM for the first time in 2014, can be used to determine the path difference in the glass surface for each pixel [3]. The digital evaluation of isochromatic images is the basis for the determination of a quantifiable, objective measurement for anisotropies in thermally toughened glasses.

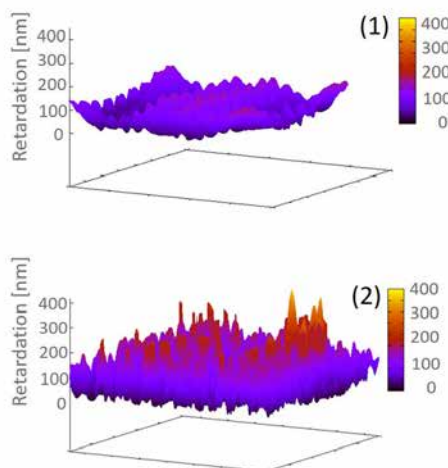
### 1. Polarising filter image



### 2. Calibration basis



### 3. Evaluation & visualisation



### 4. Statistical methods

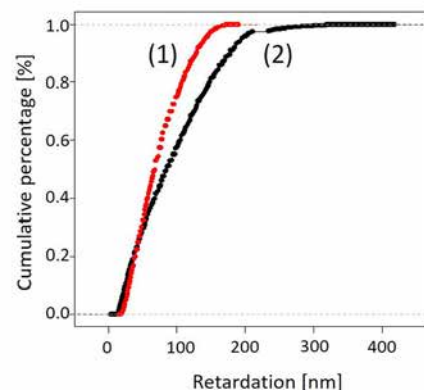


Figure 6 – Order of the method used at HSM

The sequence of the measurement method, as shown in Figure 6, starts with the recording of digital polarising filter images in the dark field of a circular polariscope. In order to obtain a correlation between colour and path difference, it is mandatory to calibrate the used camera, polariser and light source. The calibration procedure is described in detail in [8] and is based on the implementation of a Babinet-Soleil compensator into the beam path. Thus, it is possible to assign path differences to RGB intensities by increments 10 nm, which then can be split in 1-nm-increments by means of a further calculation. With the use of the calibrated polarising filter image the path difference of each pixel can be obtained by using an analysis software. The algorithm compares the colour of each pixel of the image with the colour of the calibration base; the best match is calculated using the error sum [3] [8]. The results of the analysed image can be shown in terms of 3D plots. Further stochastic evaluation methods offer a possible tool for the evaluation of anisotropies.

#### 3.2 Method RWTH

The analysis method developed by RWTH is a database solution for the two-dimensional analysis of anisotropies in the tempered glass. First of all, polarising filter images in the dark field are recorded with the physical setup shown in Figure 3, in order to gain the state of prestress distribution. Subsequently, the existing colour spectrum is measured, colour-conspicuous spots are marked on the generated polarising filter images as well as on the glass pane (cf. Figure 7) and the prestresses along the principal stress directions ( $\sigma_1$  and  $\sigma_2$ ) [7] are determined locally using SCALP-04 by Glass Stress Ltd.

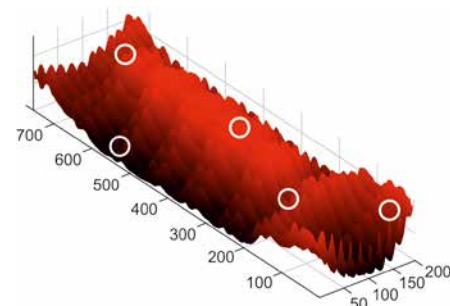


Figure 7 - Red value distribution over the glass pane

Since the principal stress directions of the test specimen can vary within test specimens, it is necessary to determine them in advance. The measurements are carried out both from the air and from the tin side of the glass pane and then combined into a single curve. From the resultant parabola, the integrals of the principal stresses and the corresponding retardations are calculated by using the main equation of photoelasticity. Subsequently, the corresponding colour in the polarising filter image is then assigned to each point and its associated retardation which results from the local measurement. The determined data points serve as support points for generating a database.

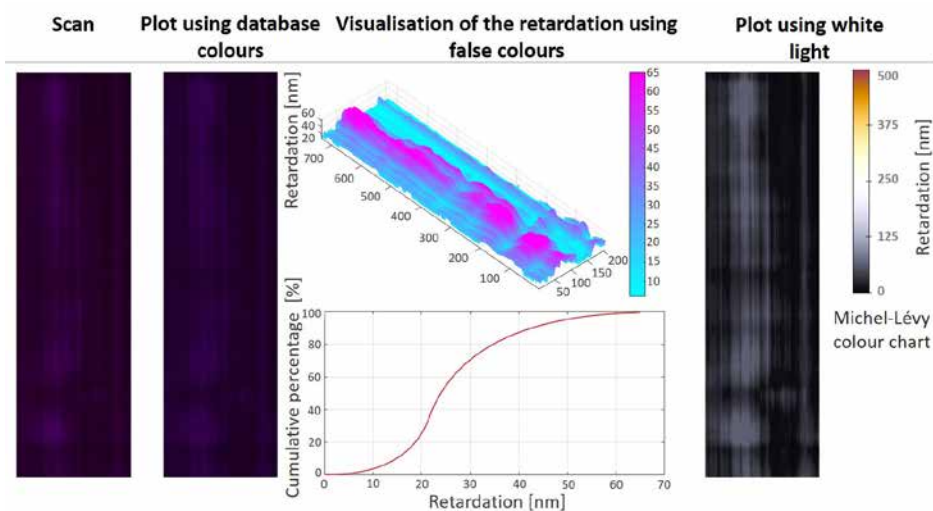


Figure 8 - Result output of the evaluation algorithm

An analysis algorithm was developed to analyse the full-surface of glass panes for anisotropy. The algorithm analyses every pixel of the polarising filter images with respect to their colour and assigns a corresponding retardation by using the previously generated database. A plot with database colours is generated for visual comparison and control purposes. The anisotropy within the surface of the glass pane is presented in a 3D plot of the retardation distribution in false colours, as shown in Figure 8, to highlight areas of high anisotropy due to differences in colour and height component. Since white light is not necessarily required to be used to generate polarising filter images, a plot simulates a virtual polarising filter image in white light according to the colour chart of Michel-Lévy [10].

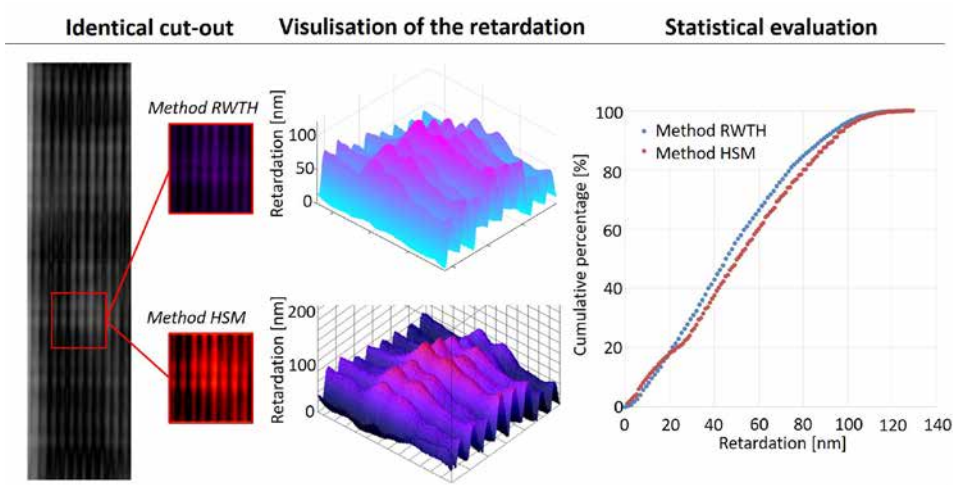


Figure 9 - Comparison of the two evaluation methods

A first step towards the objective evaluation of thermally toughened glass is the detection of the distribution of the anisotropy over the surface. In this respect, the program calculates the cumulative percentage of the retardation distribution and presents this in a graph. It should also be mentioned that an objective assessment is possible only if the underlying conditions are known in the context of the detection of the anisotropy.

### 3.3 Comparison

In order to compare both full-surface analysis methods, here an example is shown, that studies the same section of a polarising filter image of a thermally toughened glass pane. The evaluation was carried out with regard to the distribution and amount of the retardations over the cumulative percentage. It can be seen in Figure 9 that the two surface graphs are very similar in shape and structure. Light spots within the polarising filter image indicate a higher retardation than dark spots, which is correctly mapped in the evaluation of both methods and results in a wave-like surface of the 3D plots. With a maximum value of 129.0 nm determined by

the HSM method as compared to a maximum determined retardation of 126.5 nm by the method of RWTH, the peak values of both methods are very close to each other (deviation 0.98%). Deviations may result due to measurement inaccuracies and the calibration of both methods. In addition, the cumulative percentage curves resulting from the relative frequency distribution are very close to each other for both methods, especially with regard to the gradients of the curves. Overall, it can be observed that the peak values analysed show a good conformity.

## 4. Conclusion and summary

Within the scope of this article, two independently developed approaches for a full surface detection of anisotropies of thermally toughened glass products are described and compared. Furthermore, a method for the determination of the edge membrane stress is presented. It is found that the two methods for the analysis of anisotropy show a good

agreement within the measurement results. In this case, the statistical evaluation presented can be used as a basis for a possible evaluation of anisotropy. However, a general assessment criterion is not yet defined, but criteria for assessing anisotropies are currently being developed by the glass industry.

In order to be able to integrate the obtained results for the detection of anisotropies in the production process of thermally toughened glass products, the aim of a research project between SoftSolution GmbH and VitroDUR GmbH is to develop an online procedure for quality assurance in cooperation with RWTH and the HSM. The quality of the stress distribution over the glass surface as well as the degree of prestressing should be reliably determined and documented.

## 5. References

- [1] EN 12150: Glass in buildings - Thermally toughened soda lime silicate safety glass, 2015
- [2] EN 1863: Glass in buildings - Heat strengthened soda lime silicate glass, 2012
- [3] Illguth, M.; Schuler, C.; Bucak, Ö.: The effect of optical anisotropies on building glass façades and its measurement methods. *Frontiers of Architectural Research*, DOI 10.1016/j.foar.2015.01.004, 2015.
- [4] Bucak, Ö.; Feldmann, M. et al.: Reproduzierbare und prüfbare Erhöhung der Qualität und damit der Leistungsfähigkeit thermisch vorgespannter gebogener Gläser. ZIM Endbericht, 2010 (unpublished)
- [5] Feldmann, M.; Kasper, R.; Di Biase, P.; Kremens, T.; Bucak, Ö.; Illguth, M.; Wahlers, L.; Reckow, J.; Kubiak, R.: Qualitätskontrolle von ESG und TVG – Einsatz der Spannungsoptik. In: *Der Stahlbau*, Heft 3/12, Ernst und Sohn, DOI 10.1002/stab.201201533, 2012
- [6] Föppl, L.; Mönch, E.: *Praktische Spannungsoptik*. Springer-Verlag Berlin, 3. Auflage, ISBN 978-3-540-05534-1, 1972
- [7] Feldmann M.; Kasper, R.; Langosch, K.: *Glas für tragende Bauteile*. Werner Verlag, ISBN 978-3-8041-1626-9, 2012
- [8] Ramesh, K.: *Digital Photoelasticity: Advanced Techniques and Applications*. Springer Verlag, Berlin und New York, ISBN 978-3-54066-795-7, 2000
- [9] Feldmann, M.; Schuler, C. et al.: *Methoden zur Erfassung und Analyse von Anisotropien bei thermisch vorgespannten Glasprodukten*. Konstruktiver Ingenieurbau. Bundesanzeiger Verlag GmbH Köln, 01/2017
- [10] Sörensen, B.: *A revised Michel-Lévy interference colour chart based on first-principles calculations*, 2012

## 6. Acknowledgements

This work was developed within the framework of the research project "Gläsernes Glas" funded by the German Federal Ministry of Economics and Energy (ZF4053101GM5 and ZF4051701GM5) within the framework of the Central Innovation Program "Mittelstand" (ZIM). The authors would like to thank all project partners for the good cooperation.

# Blast Performance of Point Fixed Assemblies utilizing TSSA

Jon Kimberlain

Lawrence D. Carbery

Dow Corning Corporation, a Wholly Owned Subsidiary of the Dow Chemical Company

## Abstract

Architectural preferences for commercial building continue towards increased transparency resulting in large lites of glass with minimal visual obstruction. Point fixed glazing systems meeting this architectural desire are popular especially in entry or common areas at ground level. Recent technology advances have allowed the use of super high strength adhesives to attach these large lites to fittings without the requirement of drilling through glass.

The typical ground floor location increases the probability that the system must function as a protective layer for occupants of the building above and beyond the typical wind loading requirements. Some testing has been completed on drilled point fixing systems but not on the adhesive method.

The purpose of this paper is to document mock-up testing using a shock tube with an explosive charge to simulate blast loads onto adhesively bonding transparent assemblies. The variables include pre-defined blast loads from ASTM F2912 [1] performed on lites laminated with SGP ionomer interlayer.

The study, a first of its kind, enables the ability to quantify potential blast performance for use in large scale testing and building design. Four 60mm (2.36") diameter TSSA fittings were attached to lites 1524 x 1524mm (60" x 60"). Four assemblies loaded to 48.3 kPa (7 psi) or less showed no breakage or effect on TSSA and glazing. Five assemblies were loaded above 62 kPa (9 psi), and four of the five showed glass breakage resulting in glazing displaced from the opening. In all cases, TSSA remained attached to the metal fittings and no failure, adhesive or cohesive, was noted. The testing shows that this tested TSSA design is capable of an effective safe system, according to AAMA 510-14, at loads of 48.3 kPa (7 psi) or less. The data generated here can be used for engineering the system of TSSA to meet specified loads.

## Bio

Jon Kimberlain is a Senior Application Specialist in Dow Corning High Performance Building at Dow Performance Silicones . Lawrence D. Carbery is the Industry Scientist in Dow Corning High Performance Building at Dow Performance Silicones and ASTM Fellow.

## Introduction

Structural silicone attachment of glass panels has been used for nearly 50 years to enhance the aesthetics and performance of modern architecture [2][3][4][5]. The attachment method allow smooth uninterrupted facades with a great deal of transparency. Architectural desires for increased transparency has resulted in the development and use of cable net walls and bolted point supported facades. Architecturally challenging iconic buildings will include the modern technology of the day and must meet the local codes and standards for construction and safety.

Transparent Structural Silicone Adhesive (TSSA) was studied and presented as an alternative to drilled bolted fittings to support glass [6][7]. The crystal clear adhesive technology with strength, adhesion and durability has a set of physical properties that allow façade designers to engineer attachment systems in unique and novel ways. Circular, rectangular, and triangular fittings to meet aesthetics and structural performance are easily engineered. TSSA is cured in an autoclave alongside of laminated glass being processed. When the material is removed from the autoclave cycle, 100% proof testing can be completed. This quality assurance benefit is unique to TSSA as it provides immediate feedback on the structural integrity of the assembled pieces.

Conventional Structural Silicone materials have been studied for impact resistance [8] and blast mitigation [9]. Wolf et al provided data generated at the university of Stuttgart

that showed increased tensile and elongation of structural silicone materials under extreme strain rates of 5m/s (197in/s) when compared to the quasi-static strain rates specified in ASTM C1135 [10] to indicate a strain dependent relationship on physical properties. As TSSA is a highly elastic material, with higher modulus and strength compared to structural silicone, it is expected to follow the same general behavior. Although lab testing at high strain rates was not conducted, it was expected that the high strain rates in a blast would not affect the strength.

Bolted glass connections have been tested to blast mitigation standards [11] and presented at Glass Performance Days in 2013. The visual results clearly showed the advantage of mechanical retention of the glazing after glass breakage. This will be a challenge for a purely adhesively attached system.

## Test Specimens: Fabrication and Quality Assurance

Frames were fabricated from American Standard Steel Channels of dimension 151mm deep x 48.8 mm wide x 5.08mm web thickness (6" x 1.92" x 0.20") commonly referred to as a C 6" x 8.2# channel. The C Channels were welded together at the corners and a 9mm (0.375") thick triangular section was welded in the corners, set back from the face of the frame. An 18mm (0.71") hole was drilled in the plate so that a 14mm (0.55") diameter bolt could be easily inserted into it.

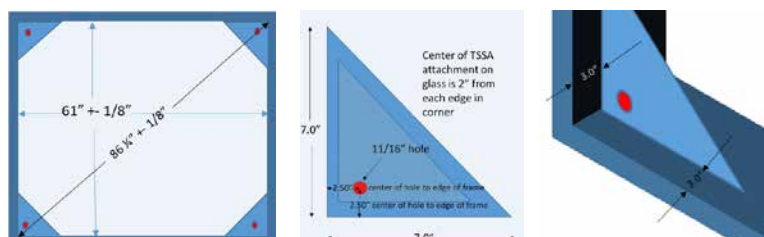


Figure 1 (A) (B) (C): Steel frame elevation and dimensions



Figure 2: Glass with TSSA attachment set into

The 60mm (2.36") diameter TSSA metal fittings were placed 50mm (2") from each corner. Four fittings were applied to each piece of glass to make everything symmetrical. A unique feature of TSSA is the fixture can be placed close to the edge of glass. Drilled fittings into glass for mechanical retention have specific dimensions from the edge that have to be incorporated into the design and the holes must be drilled before tempering.

The close dimension to the edge enhances the transparency of the finished system while allowing reduced spider attachments as the moments on typical spiders are lower.

The glass chosen for the project was two layers of 6mm (1/4") tempered clear 1524mm x 1524mm (5' x 5') laminated with Sentry Glass Plus (SGP) ionomer interlayer 1.52mm (0.060"). TSSA discs 1mm (0.040") thick were applied to a primed stainless steel fittings 60mm (2.36") in diameter. The primer is designed to enhance the adhesion durability to stainless steel and is a combination of silane and titanate in solvent. The metal discs were pressed onto the glass with a measured force of 0.7 MPa (100 psi) for one minute to provide wetout and contact. The assembly was put into an autoclave that reached 11.9 Bar (175 psi) and 133 C° (272°F) so that the TSSA would achieve a 30 minute soak time in the autoclave required for cure and adhesion.

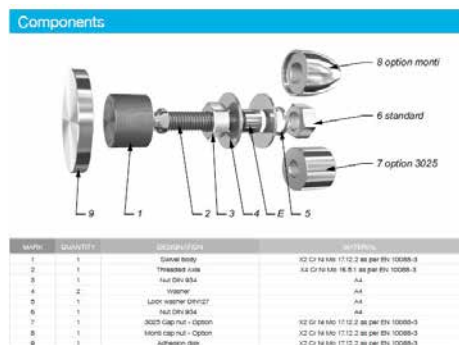


Figure 3: Exploded details of R1006 TSSA fitting by Sadev

After the autoclave was finished and cooled, each TSSA fitting was inspected, and then torqued to 55Nm (40.6 ft-lb) to demonstrate a proof load of 1.3 MPa (190 psi). The fittings used for the TSSA were supplied by Sadev and identified as R1006 TSSA fittings.

The body of the fittings were assembled onto the cured pucks on the glass and the assembly was lowered into the steel frame. The nuts on the bolts were adjusted and secured so that the exterior glazing was flush with the exterior of the steel frame. The 13mm x 13mm (1/2" x 1/2") joint about the perimeter of the glass was sealed with two part structural silicone so that testing to pressure loading could commence the next day.

Testing was conducted utilizing a shock tube at the University of Kentucky Explosives Research Laboratory. The shock tube consists of a reinforced steel body with capability to install up to 3.7m by 3.7m units on the face. The shock tube is driven by the use of explosives placed along the length the tube to simulate both the positive and negative phase of a blast event [12][13]. The entire glass and steel frame assembly were placed into the shock tube for testing as shown in Figure 4.



Figure 4: Frame and glazing installed into the shock tube

Four pressure sensors were mounted inside the shock tube so that the pressure and impulse could be accurately measured. Two digital video camcorders and a digital SLR camera were used to document the test. A MREL Ranger HR high speed camera located adjacent to the window outside the shock tube captured the test at 500 frames per second. A deflection laser recording at 20 kHz was set adjacent to the window to measure deflection at the center of the window.

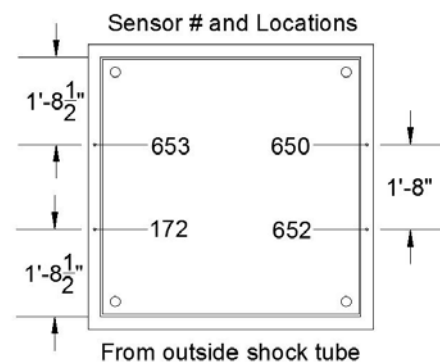


Figure 5 (A) (B): Pressure sensors location inside the shock tube.

Four frame assemblies were tested a total of nine times. If the glass did not leave the opening, the assembly was retested at a higher pressure and impulse. The target pressure and impulse is recorded along with the glass deflection data in each case. Each test was then also given a rating based on the Voluntary Guide Specifications for Blast Hazard Mitigation for Fenestration Systems, AAMA 510-14 [14].

## Results and discussion

As mentioned above four frame assemblies were tested till the glass was removed from the opening from the blast.

The first test was targeted to reach 69 kPa @ 614 kPa-ms (10 psi A 89 psi-msec) impulse. Under the applied load, the glazing shattered and released from the frame. The Sadev point fittings had TSSA adhered to the broken tempered glass. The glazing left the opening after it had roughly 100mm (4") of deflection as the tempered glass shattered.

| Frame #1 |              |                  |            |                     |                    |
|----------|--------------|------------------|------------|---------------------|--------------------|
| Test #1  |              |                  |            |                     |                    |
|          | Pressure kPa | Impulse kPa-msec | Deflection | AAMA 501-14 Ratings |                    |
| 1        | 64.061       | 519.198          |            | ISC Performance     | 5                  |
| 2        | 69.449       | 582.946          |            | ISC Protection      | Low                |
| 3        | 73.952       | 539.386          |            | ISC Hazard          | High               |
| 4        | 79.717       | 547.568          |            | UFC Protection      | Below AT Standards |
| AVE      | 71.8         | 547.3            | -100 mm    | ASTM F 1642         | High Hazard (N/A)  |
| Target   | 69           | 614              | glass fail |                     |                    |

Table 1: Frame 1 results



Figure 6: Glass breakage at ~4" of deflection, Frame 1, Test 1



Figure 7: Glass shards adhered to the TSSA and weatherseal

Frame 2 was tested three times with increased consecutive loading. The results showed no failures till the pressure approached 69 kPa (10 psi). Measured pressures of 44.3 kPa (6.42 psi) and 45.4 kPa (6.59 psi) did not affect the integrity of the assembly. At the measured pressure of 62 kPa (9 psi) the deflection of the glass caused breakage and the glazing left the opening. All TSSA fittings had broken tempered glass attached to them as identical to Figure 7

| Frame #2 |              |                  |              |                     |               |
|----------|--------------|------------------|--------------|---------------------|---------------|
| Test #2  |              |                  |              |                     |               |
|          | Pressure kPa | Impulse kPa-msec | Deflection   | AAMA 501-14 Ratings |               |
| 1        | 41.077       | 146.481          |              | ISC Performance     | 1             |
| 2        | 45.000       | 194.296          |              | ISC Protection      | Safe          |
| 3        | 44.350       | 154.884          |              | ISC Hazard          | None          |
| 4        | 46.648       | 152.924          |              | UFC Protection      | High          |
| AVE      | 44.3         | 162.1            | -50 + 25 mm  | ASTM F 1642         | No Break (H1) |
| Target   | 28           | 193              | glass intact |                     |               |

| Frame #2 |              |                  |              |                     |               |
|----------|--------------|------------------|--------------|---------------------|---------------|
| Test #3  |              |                  |              |                     |               |
|          | Pressure kPa | Impulse kPa-msec | Deflection   | AAMA 501-14 Ratings |               |
| 1        | 41.944       | 264.882          |              | ISC Performance     | 1             |
| 2        | 45.421       | 316.400          |              | ISC Protection      | Safe          |
| 3        | 45.681       | 296.437          |              | ISC Hazard          | None          |
| 4        | 48.840       | 276.465          |              | UFC Protection      | High          |
| AVE      | 45.5         | 288.5            | -56 + 20 mm  | ASTM F 1642         | No Break (H1) |
| Target   | 40           | 283              | glass intact |                     |               |

| Frame #2 |              |                  |            |                     |                    |
|----------|--------------|------------------|------------|---------------------|--------------------|
| Test #4  |              |                  |            |                     |                    |
|          | Pressure kPa | Impulse kPa-msec | Deflection | AAMA 501-14 Ratings |                    |
| 1        | 57.003       | 502.630          |            | ISC Performance     | 5                  |
| 2        | 58.825       | 516.429          |            | ISC Protection      | Low                |
| 3        | 64.730       | 558.354          |            | ISC Hazard          | High               |
| 4        | 68.609       | 511.734          |            | UFC Protection      | Below AT Standards |
| AVE      | 62.3         | 522.3            | -100 mm    | ASTM F 1642         | High Hazard (N/A)  |
| Target   | 69           | 614              | glass fail |                     |                    |

Table 2: Results of Frame 2: tests 2, 3 and 4

Frame 3 was tested two times with increased consecutive loading. The results showed no failure till the pressure approached the targeted 69 kPa (10 psi). Measured pressures of 48.4 kPa (7.03) psi did not affect the integrity of the assembly. A data acquisition failure did not allow deflection to be taken, however visual observations from video suggest that that Frame 2 test #3 and Frame 4 Test #7 are similar in deflection. At the measured pressure of 64 kPa (9.28 psi) the deflection of the glass measured at 190.5 mm (7.5") caused breakage and the glazing left the opening. All TSSA fittings had broken tempered glass attached to them as identical to Figure 7.

| Frame #3 |              |                  |              |                     |               |
|----------|--------------|------------------|--------------|---------------------|---------------|
| Test #5  |              |                  |              |                     |               |
|          | Pressure kPa | Impulse kPa-msec | Deflection   | AAMA 501-14 Ratings |               |
| 1        | 42.732       | 274.742          |              | ISC Performance     | 1             |
| 2        | 46.230       | 302.839          |              | ISC Protection      | Safe          |
| 3        | 49.040       | 286.852          |              | ISC Hazard          | None          |
| 4        | 55.858       | 281.470          |              | UFC Protection      | High          |
| AVE      | 48.5         | 286.5            | NO Data      | ASTM F 1642         | No Break (H1) |
| Target   | 40           | 283              | glass intact |                     |               |

| Frame #3 |              |                  |            |                     |                    |
|----------|--------------|------------------|------------|---------------------|--------------------|
| Test #6  |              |                  |            |                     |                    |
|          | Pressure kPa | Impulse kPa-msec | Deflection | AAMA 501-14 Ratings |                    |
| 1        | 57.003       | 545.263          |            | ISC Performance     | 5                  |
| 2        | 59.942       | 539.831          |            | ISC Protection      | Low                |
| 3        | 65.784       | 552.694          |            | ISC Hazard          | High               |
| 4        | 73.274       | 547.525          |            | UFC Protection      | Below AT Standards |
| AVE      | 64.0         | 546.3            | -190 mm    | ASTM F 1642         | High Hazard (N/A)  |
| Target   | 69           | 614              | glass fail |                     |                    |

Table 3: Results of Frame 3: tests 5 and 6

Frame 4 was tested three times with increased consecutive loading. The results showed no failure till the pressure approached the targeted 10 psi the second time. Measured pressures of 46.8 kPa (6.79) and 64.9 kPa (9.42 psi) did not affect the integrity of the assembly. The glass was measured to deflect 100mm (4") during test #8. It was anticipated that this loading would cause the glass to break, however an additional data point was able to be taken. During test #9, the measured pressure of 65.9 kPa (9.56 psi) deflected the glass 190.5 mm (7.5") and caused breakage and the glazing left the opening. All TSSA fittings had broken tempered glass attached to them as identical to Figure 7. The fittings were easily removed from the steel frame without any apparent damage in all cases.

| Frame #4 |              |                  |              |                     |               |
|----------|--------------|------------------|--------------|---------------------|---------------|
| Test #7  |              |                  |              |                     |               |
|          | Pressure kPa | Impulse kPa-msec | Deflection   | AAMA 501-14 Ratings |               |
| 1        | 44.010       | 269.654          |              | ISC Performance     | 1             |
| 2        | 46.807       | 263.274          |              | ISC Protection      | Safe          |
| 3        | 47.749       | 280.309          |              | ISC Hazard          | None          |
| 4        | 48.793       | 272.122          |              | UFC Protection      | High          |
| AVE      | 46.8         | 271.3            | -75 + 37mm   | ASTM F 1642         | No Break (H1) |
| Target   | 40           | 283              | glass intact |                     |               |

| Frame #4 |              |                  |              |                     |               |
|----------|--------------|------------------|--------------|---------------------|---------------|
| Test #8  |              |                  |              |                     |               |
|          | Pressure kPa | Impulse kPa-msec | Deflection   | AAMA 501-14 Ratings |               |
| 1        | 58.489       | 548.737          |              | ISC Performance     | 1             |
| 2        | 60.324       | 497.495          |              | ISC Protection      | Safe          |
| 3        | 64.447       | 540.664          |              | ISC Hazard          | None          |
| 4        | 76.662       | 566.533          |              | UFC Protection      | High          |
| AVE      | 65.0         | 538.4            | -100 + 37 mm | ASTM F 1642         | No Break (H1) |
| Target   | 69           | 614              | glass intact |                     |               |

| Frame #4 |              |                  |            |                     |                    |
|----------|--------------|------------------|------------|---------------------|--------------------|
| Test #9  |              |                  |            |                     |                    |
|          | Pressure kPa | Impulse kPa-msec | Deflection | AAMA 501-14 Ratings |                    |
| 1        | 60.057       | 553.237          |            | ISC Performance     | 5                  |
| 2        | 62.521       | 529.429          |            | ISC Protection      | Low                |
| 3        | 68.531       | 563.739          |            | ISC Hazard          | High               |
| 4        | 72.553       | 553.551          |            | UFC Protection      | Below AT Standards |
| AVE      | 65.9         | 550.0            | -190 mm    | ASTM F 1642         | High Hazard (N/A)  |
| Target   | 69           | 614              | glass fail |                     |                    |

Table 4: Results of Frame #4

The TSSA remained intact for each test. When the glass remained intact, there was no visual change in the TSSA after the testing concluded. The High speed video showed the glass breaking at the mid points of the span, and then leaving the opening.



Figure 8 (A) (B) (C): Glass Failure at test 4, 6, and 9



Figure 9: Glass at max deflection at test 8.

From the figures 8 and 9 comparing glass failure to none, it is interesting to note that the pattern of fracture in the glass occurs in section away from the adhesive point of attachment indicating that the unbound section of glass is reaching a bending point that has rapidly approached the embrittlement yield point in the glass versus the section that are held adhesively. This suggests that the broken plate in these sections is likely moving mostly in shear during the testing. In combination with this principle and the observation that the failure mode appears to be embrittlement in the glass thickness at the interface of the adhesive, the control of the deflection by increased glass thickness or other means should improve the performance as stated loads are increased.

Frame 4 Test #8 was a pleasant surprise at the test facility. While the nonbreaking of the glass allowed the frame to be tested again, this large load was held intact by the TSSA and the perimeter weatherseal. The design windload for this TSSA system using 4 60mm attachments supporting the glazing for both live and permanent loads is 2.5 kPa [50 psf]. This is a moderate design with desirable architectural transparency that exhibited extreme loading and the TSSA remained intact.

## Conclusions and Recommendations

This study was undertaken to determine if adhesive attachment of glazing systems has some sort of inherent danger or flaw in low level specified blast performance

requirements. It is clearly evident that the simple system of 60mm TSSA fittings applied close to the edge of the glazing has performance up to the breakage of the glass. When glass is designed to resist breakage, TSSA is a viable method of attachment to provide a level of protection while maintaining the architectural desire for transparency and openness.

Based upon the standard, ASTM F2912-17, the window assembly tested meets a hazard level of H1 at a specification level of C1.

The fittings used in the study, Sadev R1006, were unaffected.

Tempered glass used in this study was the "weak link" in the system. Once the glass broke, the TSSA and the perimeter weatherseal were unable to retain the bulk of the glazing because small shards of glass remained on the silicone materials.

From perspective of design and performance, TSSA adhesive systems have now been proven to provide a high level of protection in blast rated façade assemblies in the initial levels of blast performance specification as noted by widely accepted industry standards. The tested façade indicates a clear performance difference in hazard classification for loads between blast loads of 41.4 kPa (6 psi) and 69 kPa (10 psi). Of importance, though, is that the difference in hazard classification is not attributed to a failure in adhesive as indicated by the cohesive mode of failure of the adhesive and glass shards between the hazard thresholds. Based on observations, properly sizing the glass to minimize deflection to prevent embrittlement due to bending and increased shear response at the interface of attachment appears to be a critical factor in performance. Future designs may be able to incorporate reduced hazard levels at higher loadings through increased glass thickness, location of the point fixation relative to edge and increased contact diameter of the adhesive.

## References

- [1] ASTM F2912-17 Standard Specification for Glazing and Glazing Systems Subject to Airblast Loadings, ASTM International, West Conshohocken, PA, 2017, <https://doi.org/10.1520/F2912-17>
- [2] Hilliard, J. R., Parise, C. J., and Peterson, C. O., Jr., Structural Sealant Glazing, Sealant Technology in Glazing Systems, ASTM STP 638, ASTM International, West Conshohocken, PA, 1977, pp. 67-99.
- [3] Zarghamee, M. S., Schwartz, T. A., and Gladstone, M., "Seismic Behavior of Structural Silicone Glazing," Science and Technology of Building Seals, Sealants, Glazing and Waterproofing, Vol. 6, ASTM STP 1286, J. C. Myers, Ed., ASTM International, West Conshohocken, PA, 1996, pp. 46-59.
- [4] Carbary, L. D., A Review of the Durability and Performance of Silicone Structural Glazing Systems, Glass Performance Days, Tampere Finland, June 2007 conference proceedings pp. 190-193
- [5] Schmidt, C. M., Schoenherr, W. J., Carbary L. D., and Takish, M. S., "Performance Properties of Silicone Structural Adhesives," Science and Technology of Glazing Systems, ASTM STP1054, C. J. Parise, Ed., American Society for Testing and Materials, Philadelphia 1989, pp. 22-45
- [6] Wolf, A.T, Sitte, S., Brasseur, M., J., and Carbary L. D., "Preliminary Evaluation of the Mechanical Properties and Durability of Transparent Structural Silicone Adhesive (TSSA) for Point-Fixing in Glazing" Fourth International Symposium on Durability of Building and Construction Sealants and Adhesives, Journal of ASTM International, published online August 2011, Volume 8, Issue 10 (November 2011), JAI 104084, available at [www.astm.org/DIGITAL\\_LIBRARY/JOURNALS/JAI/PAGES/JAI104084.htm](http://www.astm.org/DIGITAL_LIBRARY/JOURNALS/JAI/PAGES/JAI104084.htm).
- [7] Clift, C., Hutley, P., Carbary, L.D., Transparent Structural Silicone Adhesive, Glass Performance Days, Tampere, Finland, June 2011, conference proceedings pp. 650-653
- [8] Clift, C., Carbary, L.D., Hutley, P., Kimberlain, J., "Next Generation Structural Silicone Glazing" Journal of Facade Design and Engineering 2 (2014) 137-161, DOI 10.3233/FDE-150020
- [9] Kenneth Yarosh, Andreas T. Wolf, and Sigurd Sitte "Evaluation of Silicone Sealants at High Movement Rates Relevant to Bomb Mitigating Window and Curtainwall Design" Journal of ASTM International, Vol. 6, No. 2 Paper ID JAI101953
- [10] ASTM C1135-15 Standard Test Method for Determining Tensile Adhesion Properties of Structural Sealants, ASTM International, West Conshohocken, PA, 2015, <https://doi.org/10.1520/C1135-15>
- [11] Morgan, T., Advances in Explosion Resistant Bolt Fixed Glazing, Glass Performance Days, June 2103, Conference proceedings pp 181-182
- [12] ASTM F1642/F1642M-17 Standard Test Method for Glazing and Glazing Systems Subject to Airblast Loadings, ASTM International, West Conshohocken, PA, 2017, [https://doi.org/10.1520/F1642\\_F1642M-17](https://doi.org/10.1520/F1642_F1642M-17)
- [13] Wedding, William Chad, and Braden T. Lusk. "Novel method to determine blast resistant glazing system response to explosive loading." Measurement 45.6 (2012): 1471-1479.
- [14] "Voluntary Guide Specification for Blast Hazard Mitigation for Vertical Fenestration Systems" AAMA 510-14.

# Transparency in Glass Connections – a Case Study

Lisa Rammig, Eckersley O'Callaghan, TU Delft

## Keywords

Structural glass, glass connections, curved glass, transparent adhesives, glass slide

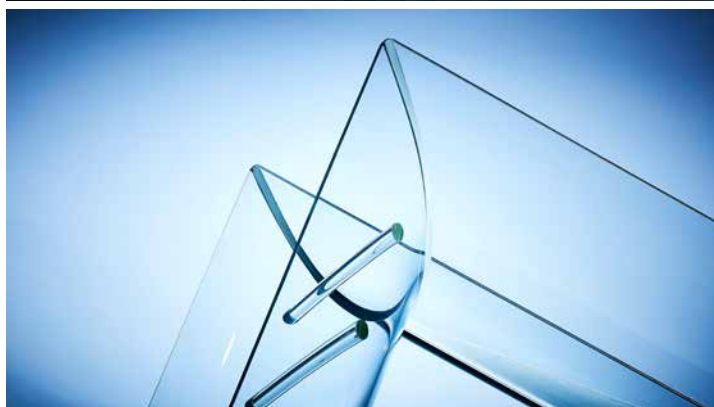
## Abstract

The transparency of glass structures is fascinating and daunting at the same time. The emotional distrust towards a transparent material opposes the rational knowledge that the material would be sufficiently strong to form a structure.

Recently, glass has increasingly been used as a structural component. However, its inherent brittleness still requires opaque metal connections to transfer loads, which commonly are stainless steel or titanium. These connections define contemporary glass architecture – firstly, because they are immediately apparent in a transparent structure and, secondly, as they are part of the engineering design language. However, designers and architects are still aiming to increase the transparency of building envelopes and structures, hence there is a strong demand to reduce the visibility of structural connections in glass.

In particular, glass staircases have gained popularity in recent years, forming transparent structural features within buildings. Due to the loads they have to carry, coupled with safety regulations, these structures traditionally consist of many layers of glass, laminated into thick packages and then connected with opaque metal fittings.

This paper discusses a novel approach to transparent connections for treads on a case study project- not a staircase but a glass slide with glass treads, bonded to the curved glass stringer with a transparent structural silicone creating a minimal and entirely transparent glass structure.



# Design and Experimental Testing of the Bundled Glass Column

F. Oikonomopoulou<sup>1\*</sup>, E.A.M. van den Broek<sup>1</sup>, T. Bristogianni<sup>2</sup>, F. A. Veer<sup>1</sup>, R. Nijssen<sup>1,2</sup>

<sup>1</sup> Department of Architectural Engineering + Technology, Faculty of Architecture and the Built Environment, Delft University of Technology, Delft 2628 BL, the Netherlands

<sup>2</sup> Department of Structural Engineering, Faculty of Civil Engineering and Geosciences, Delft University of Technology, Delft 2628 CN, The Netherlands

\* contact: [f.oikonomopoulou@tudelft.nl](mailto:f.oikonomopoulou@tudelft.nl)  
\_tel: +31(0)641140976

**Abstract** (The complete contribution will be published in the *Glass Structures & Engineering* journal)

In this paper, a transparent bundled glass column is presented as a promising solution for diaphanous compressive members. Owing to the high compressive strength of glass and its most characteristic attribute, transparency, a glass column is capable of transferring compressive loads while allowing for space and light continuity. Several different all glass columns have been explored in the past, nevertheless, they are seldom applied in construction. Reasons include complications in fabrication, absence of statistical strength data but above all lack of a built-in safety system due to the inherent brittleness of glass. The goal of this research is to develop a glass bundled column in a scale relevant to buildings that can safely carry loads, have a high visual result and be easily manufactured. Towards this aim, the paper presents an overview of the research conducted by the authors from the design concept to the manufacturing, engineering and experimental testing of full-scale prototypes.

The concept of the bundled column is in itself simple: Multiple glass bars are bonded together by a colourless adhesive, forming a composite yet unified cross-section. To investigate the feasibility of the bundled column for real applications, first a production method is developed for manufacturing specimens in a scale relevant to buildings with guaranteed consistency in their structural and visual performance. Initially, different glass rod configurations, adhesives and bonding techniques were explored in search of a combination that would (a) ensure the desired coupling degree of the individual rods, (b)

achieve minimum visual flaws and (c) result to an easy and standardized manufacturing method. The final column consists of a central, star-shaped, hollow CONTURAX<sup>®</sup> profile with 17(±2.00) mm inner and 30(±2.00) mm external diameter adhesively bonded by a clear, UV-curing adhesive to 6 DURAN<sup>®</sup> rods of Ø 22(±0.45) mm diameter. All used rods are standardized, extruded borosilicate profiles, 1500 mm in length by SCHOTT.

The degree of coupling between the individual rods is investigated through experimental testing of a series of prototypes of 500 mm length [A<sub>1</sub> series]. The consistent, high failure stress of approximately 500 MPa suggests that the high shear stiffness of the selected adhesive enables the bundle to behave as a single monolithic unit under the anticipated compressive forces.

The employed extruded profiles are standardized up to 1500 mm length. Thus, longer prototypes are made by adapting the splice lamination principle: To prevent the introduction of weaker zones, each column is segmented in such a way that the connection points spiral up along its height. In order to evaluate the degree of influence of the splice lamination joint, alternative connection types (a small gap, an adhesive connection and an insert of a 2mm thick aluminium disc) are experimentally tested in a series of 470 mm long [A<sub>2</sub>] specimens. The results point out that specimens with aluminium discs in the split joints performed the closest to the monolithic variant.

Next, three series of prototypes [B<sub>1</sub>, B<sub>2</sub> and C<sub>1</sub>] up to 2.4 m in height are made and tested in compression to investigate the failure behaviour and structural performance of the designed column. Custom-made metal caps with an inlayed lead layer are mounted to each column's ends to prevent the direct contact of glass with the steel surface of the machine. With the aim of securing a more gradual and thus safer failure, a post-tensioned steel tendon is introduced to one of the 2.4 m long series [C<sub>1</sub>] and experimentally evaluated.

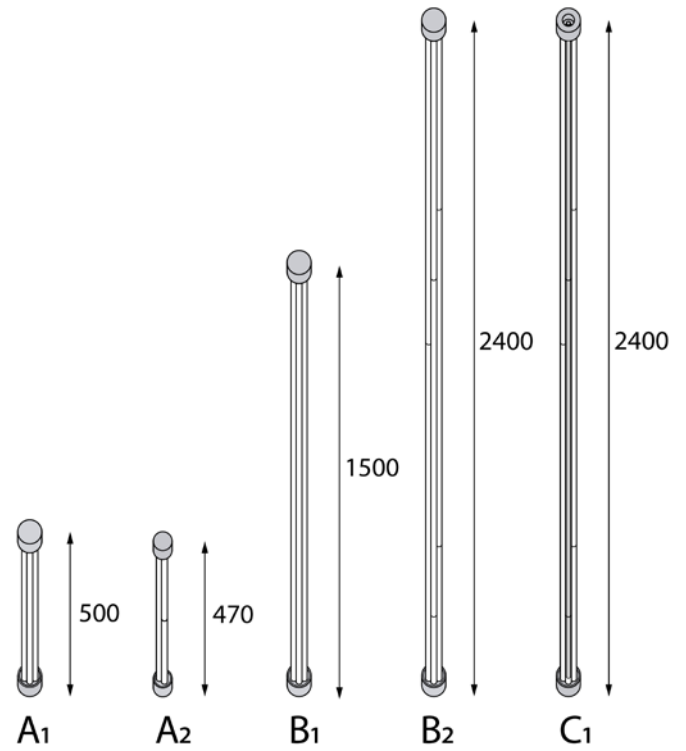
The results demonstrate that the chosen adhesive and rod configuration enable the designed column to perform monolithically under loading and fail by buckling in values close to the theoretical buckling force of the corresponding solid bundle. The spliced joints and eccentricities occurring during fabrication seem to have only a minor influence on the

resulting stresses.

Nevertheless, all specimens without post-tensioning failed in a complete way without maintaining any post-breakage load-carrying capacity; thus not providing a safe failure behaviour.

In contrast, the post-tensioned specimens present a more consistent and visible failure and a narrow load spread, suggesting that post-tensioning allows for a more predictable failure, which in turn provides increased structural reliability. After failure, the post-tensioned specimens preserved a limited load-bearing capacity, attributed mainly to the tendon. In this direction, the steel tendon can in the future be engineered to provide an alternative, built in load path that can reduce the consequences of failure. Yet, the specimens of this series demonstrated a lower load-bearing capacity, which is ascribed to the insufficient cooperation between the tendon and the glass, due to inevitable manufacturing tolerances. By optimizing the contact between tendon, sheathing and the glass bundle, the lateral movement of the glass bundle leading to eccentricity can be constrained, resulting in higher failure loads.

Overall, the results indicate that the bundled glass column can be an elegant solution of sufficient compressive strength in the search of a transparent, load-bearing component. With the aim of applying the bundled glass column in future structures, further work will focus on the development of the top and bottom connections as well as on improving the post-tensioning mechanism towards a safer and stronger all-glass column. The presented glass column design is first applied in the truss elements of a temporary pedestrian 14 m long bridge at the TU Delft campus.



Left: Realized 1.5m long prototypes of the bundled column by the authors  
 Right: Illustration of all specimen series tested in compression (length dimensions in mm)



Rod configuration of the final bundled column design.

# Applied Machine Learning in Structural Glass Design

James Griffith  
Vladimir Marinov  
Giulio Antonutto  
Arup

## Keywords

1 = Machine Learning  
2 = Artificial Intelligence  
3 = Glass  
4 = Structural design  
5 = Optimisation

## Abstract

Machine learning, a type of artificial intelligence, is becoming increasingly prevalent in everyday life. Email spam filters, autonomous cars, and speech recognition all rely on machine learning algorithms to function accurately and efficiently. Such algorithms allow computers to find trends in data without explicit programming or problem awareness, allowing them to make predictions when exposed to new inputs.

This paper explores the potential of this technology to assist in the field of structural glass design. Supervised regression multi-layer neural networks and classification algorithms are trained on a database of computational structural glass solutions generated parametrically in Grasshopper and Strand7. Once trained, the algorithm's accuracy is assessed and used to predict glass build-ups for a rectangular plate with uniform pressure. Thickness classification accuracies of greater than 80% are achieved in all cases. When used in combination with experienced structural engineers, such intelligent predictors have the potential to offer benefits in early stage design, allowing rapid and accurate assessment of glass and consideration of the wide variety of design drivers involved in structural glass design.

## Introduction

As with other technical fields, fundamental engineering problems can be formulated and automated based on their mathematical principles. The principles of computer aided design (CAD) have long been outdated and we have progressed into the domain of computer "generated" design. As designers and engineers we are increasingly more reliant on

computational power not only to solve technical problems but to generate the designs in the first place. Architects and designers resort to computational design as a means of exploring a multitude of solutions which are sub-optimal with increasingly wider range of parameters, including solar, thermal, structural, views and aesthetics.

Currently, despite the computer advances, expertise in design and engineering has been provided by individual human input. As a result most problems are solved through the prism of personal experience and judgment. In this human experience, learning is critical. While this works well on an individual basis, the power of the collective experience cannot be mobilised due to the knowledge having to be passed on. With this emphasis on the quality of learning, we flag the importance of learning as a principle in digital design. Furthermore, the principle of computer learning can be applied to any task for which basic parameter data can be gathered and stored in a logical way.

Machine learning is the definition of a series of algorithms originating in computer science and mathematics, specifically in the subset of artificial intelligence. For the purposes of applied engineering it can be described as self-teaching algorithms that are trained on a set of data gathered in the course of a process. The algorithms make future predictions by extrapolating from past-experience. For well-defined, trivial engineering problems there may be little benefit in their application, but the algorithms have unparalleled potential to solve very complex problems. As our problems become more reliant on numerical analysis and integration of disciplines, the separation of individual aspects of a problem will become more difficult. As we evolve further to solve those complex problems entirely in the digital domain we will need to classify, record and discretise as much of the input and output information as possible. Machine learning uses this information, stored in large organised databases to create predictive mathematical models based on the analysis of this data. In Figure 1 the data for a two dimensional problem can be analysed and a function can be fitted to represent the data based on a set of criteria.

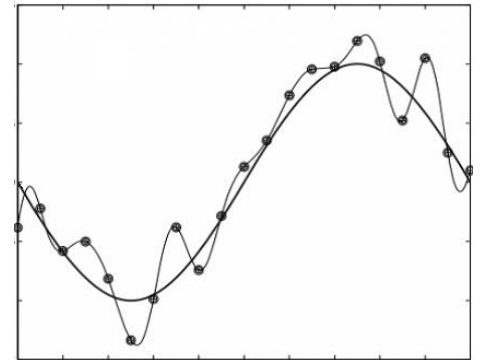


Figure 1: Curve fitting to a set of data points

## Applied Machine Learning in Other Industries

Two transferable examples are highlighted below illustrating how applying machine learning could offer value to companies and clients throughout the design chain of the glass industry.

- i. Google DeepMind: Minimising data centre cooling loads  
By harvesting data collected from thousands of sensors within their data centres, Google DeepMind trained neural networks to predict energy use, future temperatures and future pressures in their data centres. When run on live data centres, this machine learning system was able to consistently demonstrate a 40% reduction in the energy used for cooling [1].
- ii. Otto: Predictive inventory management  
Otto, a German based e-commerce company, have trained a deep learning algorithm to predict what customers will purchase before they order. By analysing 3 billion past transactions and over 200 variables, the algorithm is able to predict with 90% accuracy what will be sold in the next 30 days. It purchases around 200,000 items automatically each month with no human intervention. As a result, Otto's surplus stock has reduced by one fifth, customers get their products sooner, and product returns have reduced by over 2 million items per year [2].

## Methodology

### Problem Outline

While machine learning is successfully used to solve complex optimisation problems, its use in the field of structural and façade engineering is not yet explored. The work presented here aims to prove the suitability of this technique in the field of structural glass. A common design task in structural glass is to find the minimum thickness of a four-side supported rectangular plate for given stress and deflection limits. This problem is well understood, with analytical solutions documented in Rourke [3]. As such, it provides a well bounded, restricted domain, comparative example to illustrate and validate the suitability of machine learning methods for this particular design situation. The complexity of the problem can be generalised to include more parameters and constraints in the future.

The problem outline is: "Predict **thickness** for a given **width, height, pressure** and **glass type**."

### Data Harvesting

Machine learning requires vast amounts of data to train any predictive algorithms to a high degree of accuracy. Here lies a challenge for applying the technology for structural design; in many structural engineering firms the data from past projects is in multiple formats (eg: hand calculations, Excel spreadsheets, finite element models etc), saved in a myriad of different locations, and with no clear demarcation of which solutions were deemed successful and approved for the final design.

As such, curating an organisation's past project information into a format suitable to train machine learning algorithms on was deemed beyond the scope of this paper. Instead, an alternative approach to generate new datasets was adopted using parametric design methods. A model of the problem was setup parametrically in Grasshopper, allowing variation of plate width, height, thickness and applied pressure. This was converted into a model suitable for finite element analysis using Geometry Gym [4]. With the Strand7 Application Programmable Interface (API) scripted in Python, the finite element model could be solved in Strand7 Finite Element software.

Finally, the peak stresses and deflections were extracted automatically and saved in a database along with their corresponding input parameters. With this fluid parametric design setup, a database of 1080 models was generated, each corresponding to the inputs and results extracted from a uniquely

generated finite element model. The workflow is illustrated in Figure 2, with input data in Table 1.

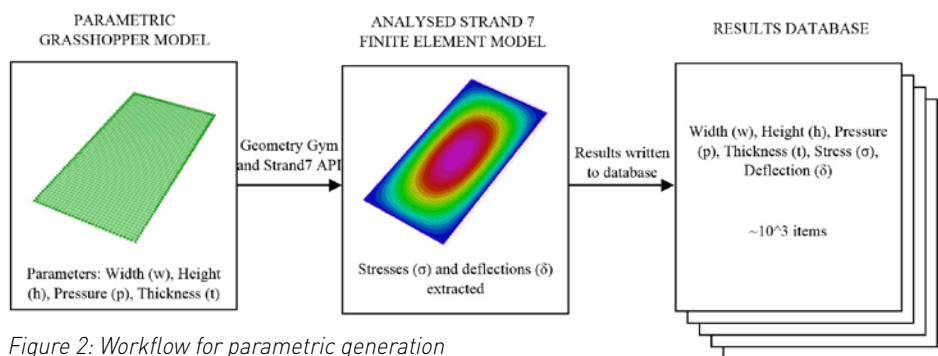


Figure 2: Workflow for parametric generation of results database

| Inputs           | Range                            |
|------------------|----------------------------------|
| Width            | 1000, 2000, 3000 mm              |
| Height           | 1000 to 15000 in steps of 1000mm |
| Thickness        | 3, 4, 5, 6, 8, 10, 12, 15 mm     |
| Uniform Pressure | 500, 1000, 1500 Pa               |

Table 1: Range of input values for database generation

### Application of Codified Design Limits

In order for the learning algorithm to generate code-compliant designs, limits from design codes need to be applied. The ASTM E1300-12a allowable edge stresses for seamed edges for 3 second load durations were chosen and summarised in Table 2.

| Glass Type                                    | Limits    |
|---|-----------|
| Annealed Glass Allowable Edge Stress          | 18.3 MPa  |
| Heat Strengthened Glass Allowable Edge Stress | 36.5 MPa  |
| Fully Toughened Glass Allowable Edge Stress   | 73.0 MPa  |
| Deflection                                    | Span / 65 |

Table 2: Design limits from ASTM E1200-12a

These limits can be adjusted depending on the code chosen, and applied at two distinct locations in the machine learning process; before, or after the training of the algorithm. The locations of where these limits are applied lend themselves to two distinct groups of machine learning algorithms.

## Method 1: Regressive Machine Learning Algorithm

In the first method, a regressive learning algorithm can be trained on the database, mapping the inputs (width, height, thickness and pressure) to outputs (stress and deflection). With regression algorithms, the inputs map to a continuous set of outputs. Once trained, the predictor is used to generate a value of stress and deflection for a given input set. Codified limits are then applied to this prediction, iterating through thicknesses until a viable optimum is found. The flow of this logic is illustrated in Figure 3.

The machine learning was conducted using Matlab r2017a's 'Neural Network Toolbox' [5]. A two layer multi-neuron feed-forward neural network with sigmoid hidden neurons and a linear output neuron was trained on the parametrically generated database. The database was segmented into 50% training data, 25% validation data and 25% testing data. The training data is used to train the network weights using Bayesian Regularisation Backpropagation incorporated into a Levenberg-Marquardt optimisation. The validation set provides a measure of generalisation, and the testing set an independent measure of network performance.

The effect of varying the network hyperparameters, in particular the number of hidden neurons was explored.

## Method 2: Classification Machine Learning Algorithm

The second approach uses a supervised classification algorithm to map inputs directly to thicknesses. To achieve this, the codified limits are applied on the initial database (Figure 4); finding the minimum thickness for a given width, height and pressure that satisfies the deflection and stress limits. These minimum thicknesses are then stored in a new database. As the values of glass thickness fall into distinct categories (3, 4, 5, 6, 8mm etc), a classification machine learning algorithm can be trained to predict which label to 'tag' the input data with, corresponding to a particular glass thickness.

The advantages of this method are that no iterative loops are required when the predictor is called, increasing speed of prediction. Additionally, the predictor here has no awareness of stresses or deflections; it simply is able to identify trends in the input data based on past experience to classify the query with an appropriate thickness.

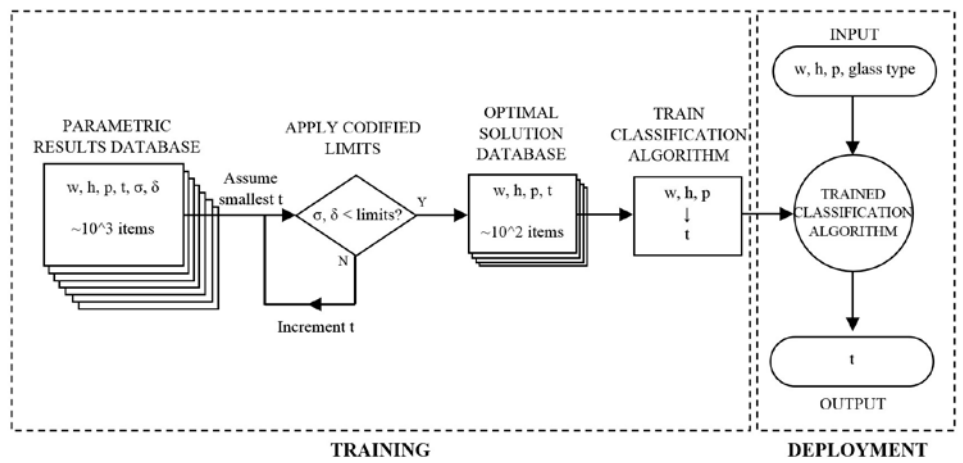


Figure 3: Training and deployment methodology for regression learning algorithm

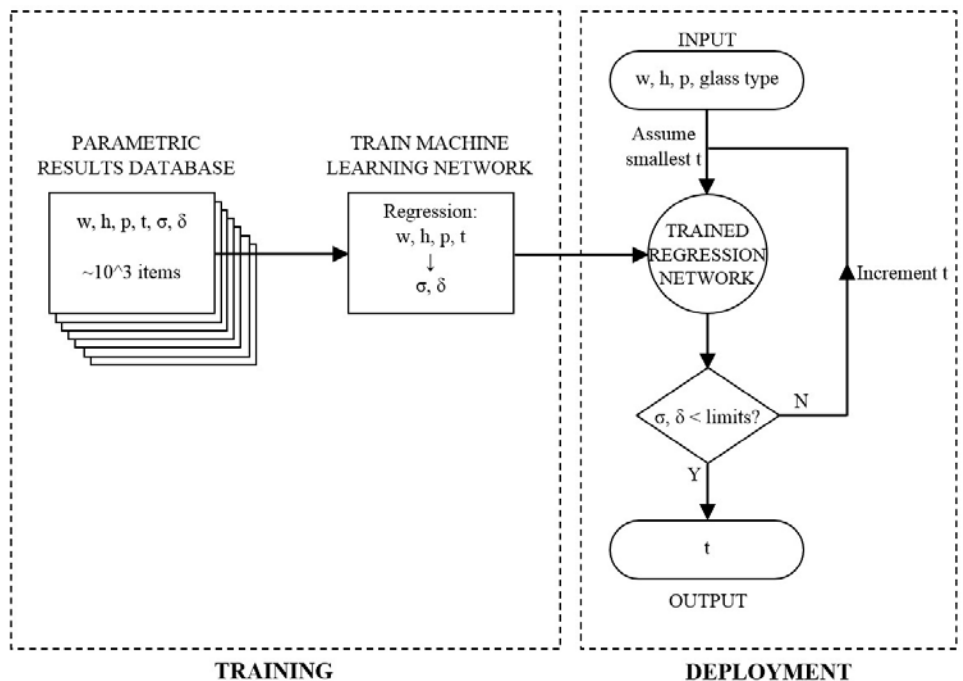


Figure 4: Training and deployment methodology for classification learning algorithm

The machine learning was conducted using Matlab r2017a's 'Neural Network Toolbox.' A variety of classification algorithms were trained, including Support Vector Machines, Logistic Regression and Discriminant Analyses. It was found that weighted k-nearest neighbour and Ensemble Boosted Trees performed best on this dataset, with 5 fold cross-validation. These were therefore used for the rest of the investigation.

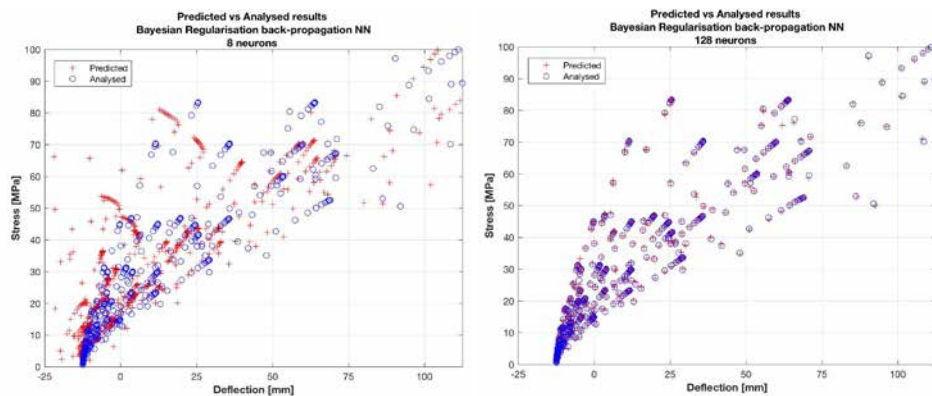
## Results and Discussion

### Regression Algorithm Solutions

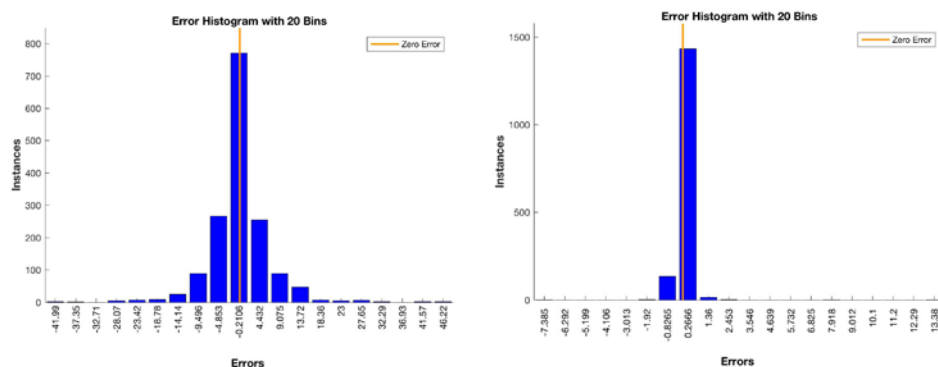
The performance of the trained and validated neural network is illustrated in Figures 5 and 6, using all of the datapoints for illustrative purposes. The effect of increasing the number of hidden neurons from 8 to 128 neurons

provides significant performance gains, moving the initially scattered predictions crosses to within the circle of the analytical solution. This suggests 8 neurons provided too few hyperparameters to capture the four-to-two-dimensional mapping of the dataset, underfitting the data.

A comparison of the error histogram (Figures 7 and 8) for the two sets illustrates the reduction in error margin that a larger network provides; reducing the deviation of the approximately normally distributed errors. It should be noted that the error is approximately symmetric about its mean, showing the solution is equally likely to be above (conservative design) as below (unsafe design).



Figures 5 & 6: Predicted [cross] vs analysed [circle] results for 8 neuron (left,  $R = 0.99213$ ) and 128 neuron (right,  $R = 0.99995$ ) regression neural network.



Figures 7 & 8: Error histograms for 8 neuron (left) and 128 neuron (right) regression neural networks

Figure 9 illustrates the improvement in network performance with more hyperparameters. 25 distinct networks were trained with 8, 80 and 128 neuron hidden layers, and their average performance taken. The underfitted 8 neuron network performs worse, but an 80 neuron network has a similar average performance and reduced deviation in comparison to a 128 neuron network. This is due to the increased complexity of the 128 neuron network overfitting the data, resulting in an increased generalisation error when exposed to new test data.

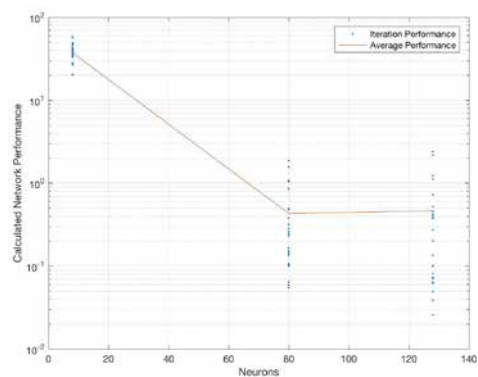


Figure 9: Improvement in average network performance of 25 trained networks with 8, 80 and 128 neurons in hidden layer

### Classification Algorithm Solutions

The results from the classification algorithm are shown in Figures 10 to 12 for annealed, heat strengthened and fully toughened glass. The predicted thickness (x axis) is compared against the analytically derived optimum thickness (y axis) meaning a perfect prediction would fall on the "y = -x" diagonal. The algorithms correctly identify the analytical solution in over 80% of the cases. As in the regression algorithm, the error tends to be distributed either side of the diagonal, demonstrating the susceptibility to conservative and unconservative solutions. As the training data was a subset of the parametrically generated database, each algorithm only had approximately 100 data points to train a three- to one-dimensional mapping. It is anticipated that with larger datasets, more accurate predictions could be achieved.

### Example Predictions

To demonstrate the efficacy of the predictors in a more tangible manner to a glass designer, 5 random problems were generated. The glass thicknesses predicted by the regression and classification algorithms are compared to the analytical solution in Table 3. For added complexity, Example 4 includes an inverted aspect ratio where width is greater than height and Example 5 includes a wind pressure outside of the range of training data.

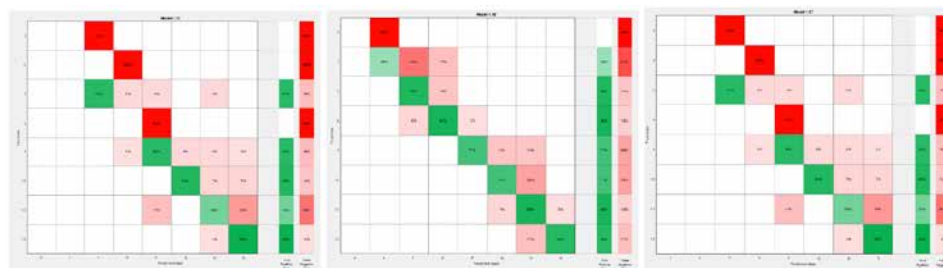


Figure 10 to 12: Classification confusion matrices with (from left to right) Annealed (80.4% accuracy), Heat Strengthened (81.2% accuracy) and Fully Toughened (82.1% accuracy)

| # | Width / mm | Height / mm | Pressure / Pa | Glass Strength | Thickness / mm      |                    |                        |
|---|------------|-------------|---------------|----------------|---------------------|--------------------|------------------------|
|   |            |             |               |                | Analytical Solution | Regression Network | Classification Network |
| 1 | 2730       | 8740        | 1090          | HS             | 12                  | 15 (+3mm)          | 15 (+1mm)              |
| 2 | 1540       | 3560        | 1030          | FT             | 8                   | 10 (+2mm)          | 10 (+2mm)              |
| 3 | 1400       | 7150        | 510           | AN             | 8                   | 8 ()               | 5 (-3mm)               |
| 4 | 2860       | 910         | 980           | FT             | 5                   | 8 (+3mm)           | 6 (+1mm)               |
| 5 | 580        | 14470       | 1670          | AN             | 5                   | 6 (+1mm)           | 6 (+1mm)               |

Table 3: Five examples comparing analytical solutions with machine learning predictions

As these 5 examples indicate, both networks perform favourably against the analytical solution. In all but one case, the networks predict exact or conservative solutions. It is anticipated that more training data, particularly for the classification network, will help improve the accuracy of predictions.

## Conclusions and Future Work

This paper demonstrates the feasibility of training machine learning algorithms on structural data and their potential application as a predictive tool in early stage design work. Trained regression and classification networks on datasets of  $10^3$  and  $10^2$  entries respectively demonstrate accuracies of greater than 80% in comparison to the exact analytical solutions.

Fine-tuning of the network hyper-parameters can adjust the accuracy of the results, with under- and overfitting data resulting in increased generalisation errors.

To train accurate machine learning algorithms, large datasets are required to reduce the error below an acceptable level, which may extend beyond the data harvesting capability of most engineering practices. As such, the method applied in this paper of parametrically generated result databases may have wider applicability. A rule of thumb of 'one order of magnitude of data for every input parameter' is likely to provide sufficient accuracy.

Future work includes extending the algorithms to consider multiple load cases, (such as point and line loads which do not have direct analytical solutions) and developing algorithms for double and triple glazed units with climatic loading and laminated panes. The ability to incorporate 'soft' design parameters (such as visual quality or post breakage safety) as well as hard (adhering to codified design limits) allow machine learning algorithms to assist in design decision making, and allow the algorithms to provide more wide ranging considerations than a purely analytical solution would offer.

## References

- [1] Evans, R. and Gao, J. (July 2016) DeepMind AI Reduces Google Data Centre Cooling Bill by 40% [online] Available at: <https://deepmind.com/blog/deepmind-ai-reduces-google-data-centre-cooling-bill-40> [Accessed 3 May 2017]
- [2] The Economist (April 2017) How Germany's Otto uses artificial intelligence [online & print] Available at: <http://www.economist.com/news/business/21720675-firm-using-algorithm-designed-cern-laboratory-how-germanys-otto-uses> [Accessed 3 May 2017]
- [3] Young, W. and Budynas, R. (2011) Roark's Formulas for Stress and Strain 8th Ed. McGraw Hill Companies
- [4] Mirtschin, J. (2017) GeometryGym [online] Available at: <https://geometrygym.wordpress.com/> [Accessed 3 May 2017]
- [5] Matlab (2017) Neural Network Toolbox [online] Available at: <https://uk.mathworks.com/products/neural-network.html> [Accessed 3 May 2017]

# Is Current Sizing of Float Glass Structures too much Conservative?

Gabriele Pisano<sup>1</sup>,  
Gianni Royer Carfagni<sup>1,2</sup>,  
1 Department of Engineering and Architecture,  
University of Parma, Italy.  
2 Construction Technologies Institute - Italian  
National Research Council (ITC-CNR), Milano,  
Italy

## Keywords

1=Glass strength 2=Heat-treated glass  
3=Weibull 4=Statistics 5=Failure 6=Verification  
formulae

## Abstract

Structural design of float glass elements is performed as a rule with the semi-probabilistic approach by defining partial factors for glass strength, calibrated with full probabilistic methods on paradigmatic case-studies. Although the most used statistics for float-glass strength is the 2-parameter Weibull's (2PW), we show that it fails to interpret the left-hand-side tail of the population of experimental data, associated with small failure probabilities. The tails govern the calibration of partial factors, since the probability of failure admitted for a construction work are very small; but the 2PW statistics leads to a very conservative design. Contrariwise, from experiments a lower bound for float-glass strength, attributable to modern factory production controls, is recognizable. Moreover, we show through modelling that corrosion/abrasion do not imply the decay of strength below a certain limit, thus inducing a lower dispersion in the data. Therefore, we propose to use generalized Weibull statistics, among which the left-truncated Weibull distribution, to better interpret the tail of the population. Partial material factors calibrated with the novel approach are considerably lower than with the 2PW statistics. Noteworthy savings can be achieved with this refined statistical approach to interpret float-glass strength.

## Introduction

The role of architectural glass has changed during the last decades, by expanding from that of window panes to load-bearing structural components. Glass strength is sensitive to surface flaws, unavoidably

present because of the production process, later handling and aging. Glass panes are generally produced with the process patented by Pilkington in the 1950s, following which glass paste is poured on a bed of molten tin so to form a floating panel. The temperature is gradually reduced from 1100°C down to 600°C and, then, the glass sheet passes through a lehr on steel rollers where it is cooled. The rapidity of the cooling process makes the difference between heat-strengthened glass and fully-tempered glass, i.e., in heat-strengthened glass the cooling process is slower than in tempered glass. A consequence of such production process consists of the fact that different-in-type defectiveness scenarios will be present on the "air-side" and on the "tin-side" surfaces. Additional flaws are due to the cutting process. However, glass has to meet certain aesthetic and optical requirements: this is why the panels that present major defects are usually discarded by strict factory production controls. In any case, the defectiveness scenario may change during service life because of corrosion and abrasion phenomena.

Fracture is due to the unstable propagation of a dominant crack when the combination of its size and the stress normal to its surface reach a critical value (mode I). It is clear that shape, size and distribution of surface flaws have a strongly random nature, so that glass strength turns out to be a high non-deterministic size-dependent value. In fact, the higher the area under tensile stress, the higher is the probability of finding a critical crack. Moreover, the fact that micro-cracks open in mode I makes glass strength dependent upon the type of stress state. If the stress is equibiaxial, the principal tensile component is always orthogonal to the crack plane, but in other states one has to evaluate the normal stress to the crack plane. Hence, the corresponding probability of fracture occurrence will be lower than for the case of an equibiaxial state. The Weibull model (Weibull, 1951), which is based on the weakest-link-in-the-chain rationale and assumes that flaws are randomly-orientated, non-interacting and shear-insensitive, is generally favored for interpreting the population of glass strengths. The most widely-used distribution for structural design is certainly the two-parameter Weibull (2PW) statistics, which can provide reliable estimates of the expected

mean and standard deviation but, as demonstrated in (Pisano<sup>2</sup>, 2015), cannot well interpret the tails of the statistical population. For what concerns design of structural glass components, the failure probabilities considered acceptable depend upon the consequences of the failure itself. Such probabilities are prescribed by structural standards; in particular, the Eurocode EN1990 (EN1990) indicates the accepted probabilities of failure for three Classes of Consequences (CC), varying from  $1.335 \times 10^{-5}$  (CC1), to  $1.305 \times 10^{-6}$  (CC2) and  $9.96 \times 10^{-8}$  (CC3) in one year. By reasonably assuming that actions can be statistically modelled, the target probability scenario is defined on the basis of glass characteristic resistance and partial material factors  $\gamma_m$ , which are calibrated by comparison, on paradigmatic examples, of the failure probability obtained through convolution of cumulative probability for glass strength and probability density function for the actions (complete probabilistic method – level III). As mentioned above, 2PW distribution cannot provide an accurate interpretation of the left-hand-side-tail of the statistical population of glass strength, Hence, the use of such statistics leads to very high material factors  $\gamma_m$  (Badalassi, 2014) which are not in agreement with the values suggested by empirical approaches and practical experience. Arguments were presented in (Ballarini 2016a) that support the existence of a lower bound for glass strength attributed to the aforementioned factory production controls, which leads to a truncation of the population of crack sizes. It is reasonable to assume that the dominant crack is semicircular and its surfaces are perpendicular to the surface. The assumption of a right-skewed distribution of flaw size implies that the distribution of the material strength must be left-skewed. Hence, denoting with  $c_{0,max}$  the maximum radius of cracks initially present on glass surfaces, the lower bound for glass strength is given by

$$\sigma_0 = \frac{K_{Ic}}{\gamma(\pi c_{0,max})^{0.5}}, \quad (1)$$

where  $K_{Ic} = 0.75 \text{ MPa m}^{0.5}$  is the nominal fracture toughness of soda-lime glass and  $\gamma=2.24/\pi$  is the shape factor for a thumbnail semicircular crack. Hence, such truncation suggests to use the Left-Truncated Weibull (LTW) distribution for interpreting the variability of glass fracture-stress. It will be shown that

the calibration of partial material factors  $\gamma_m$  through such statistics leads to values much lower than those obtained in (Badalassi,2014), closer to those generally adopted in the practice.

### Two-parameter weibull distribution (2PW) and left-truncated weibull distribution (LTW)

The two-parameter Weibull distribution (2PW) is "unbounded" since the failure stress domain is  $[0, +\infty)$ . The probability of failure for a loaded element, whose surface area  $A$  is under a generic tensile state of stress, reads

$$P_{f,W2} = 1 - \exp \left[ - \int_A \left( \frac{\sigma_{eq,W2}}{\eta_0} \right)^m dA \right] ;$$

$$= 1 - \exp \left[ - K_{2w} A \left( \frac{\sigma_{max}}{\eta_0} \right)^m \right], \quad (2)$$

where  $\sigma_{max}$  represents the maximum tensile stress on the stressed area,  $m$  and  $\eta_0$  are the shape and the scale parameters, respectively, whereas  $\sigma_{eq,W2}$  represents an equivalent stress field accounting for the distribution of tensile stress. Denoting with  $\sigma_1$  and  $\sigma_2$  the principal components of the tensile stress and  $\psi$  the angle between the direction of the maximum tensile stress  $\sigma_1$  and the normal to the surface of the dominant crack, the equivalent stress takes the form

$$\sigma_{eq,W2} = \left[ 2/\pi \int_0^{\pi/2} (\sigma_1 \cos^2 \psi + \sigma_2 \sin^2 \psi)^m d\psi \right]^{1/m}. \quad (3)$$

Thus, the effective area  $K_{2w}A$ , taking into account the effect of the type of stress on the probability of failure, becomes

$$K_{W2}A = A_{ef,W2} = \frac{\int_A (\sigma_{eq,W2})^m dA}{(\sigma_{max})^m}. \quad (4)$$

On the other hand, the left-truncated Weibull (LTW) distribution is obtained from a population obeying to a 2PW statistics when a selection is made, i.e., all experimental data lower than a certain threshold  $\sigma_0$  are rejected. LTW statistics is hence a "bounded" Weibull distribution, whose failure stress domain is  $[\sigma_0, +\infty)$ . The cumulative probability of failure becomes

$$P_{f,W_T} = 1 - \exp \left[ - \frac{\int_A (\sigma_{eq,W_T}^m - \sigma_0^m) dA}{\eta_0^m} \right]$$

$$= 1 - \exp \left[ - \frac{K_{WT} \sigma_{max}^m - \sigma_0^m}{\eta_0^m} A \right], \quad (5)$$

where the equivalent stress field  $\sigma_{eq,W_T}$  and the effective area  $K_{WT}A$  assume the same form as for the 2PW statistics, and hence they are given by equations (2) and (3), respectively. The supposed existence of a lower bound for glass strength is a major assumption that may be justified by the factory production controls.

### Evidence of the lower bound for glass strength

The results of the wide experimental campaign performed by the working group TC129/WG8 of CEN (European Committee for Standardization) were statistically analysed in (Pisano2, 2015).

Thirty samples, each one composed of approximately 25, 6 mm thick, specimens, were tested under coaxial double ring configuration according to the EN1288-2 standard [EN1288-2]. The 741 failure stress measurements, 340 for the air side and 341 for the tin side, were manipulated and rescaled to let them be representative of the ideal reference condition (equibiaxial stress state acting within an unitary surface) and, then, interpolated through several statistics. Such statistical analysis showed that the 2PW statistics clearly fails to interpret the experimental evidence for float glass; on the other hand LTW distribution provided excellent results, especially for the air-side strengths.

There are several contributions in the technical literature providing evidence that glass strength tends asymptotically to a nonzero lower limit, even after abrasion or degradation due to natural aging. For example, float glass plate pre-treated by dropping corundum on them were tested according to EN1288-2 standard [EN1288-2] by *Durchholz* et al. (*Durchholz* 1995), who showed that the lower measured strength was of the same order as that measured before the treatment, in any case much higher than that predicted by using a 2PW statistics. Remarkably, pre-damaging sensibly lowers the data dispersion and, at the same time, the difference in strength between air and tin side tends to vanish.

Another interesting experimental campaign is certainly that by *Madjoubi* et al. (*Madjoubi* 1999), who tested three sets of 50 specimens under four-point-bending after a certain time of exposure to sandblasting. Increasing the sandblasting time reduces glass strength, but after a certain time a constant level of strength is asymptotically reached, while standard deviation decreases. *Wang* et al. (*Wang* 2010), who observed that the maximum length of the long axes of flaw due to 20-min exposure to sandblasting was approximately 35  $\mu\text{m}$ , confirmed these experimental findings. Considering that the maximum crack length that does not affect the transparency of glass is of the order of 200-250  $\mu\text{m}$  (*Ballarini* 2016a), and that sandstorms certainly represent an extreme condition, it can be inferred that abrasion cracks are most likely smaller than the largest cracks allowed by factory production controls. Although cracks due to abrasion may lead to a decay of the lower limit as a consequence of an amplification of the stress intensity factor, *Ballarini* et al. [*Ballarini*

2016a] have showed that such amplification and, hence, the decay of the lower bound for glass strength, cannot go beyond a certain limit. Thus, the lower bound for glass strength may be reduced, but not annihilated, by abrasion/corrosion [*Ballarini* 2016a, *Ballarini* 2016b].

### Calibration of partial material factors through left-truncated weibull statistics. Comparison with 2-parameter weibull distribution.

The performance of a structure is given by the maximum allowed probability of failure. Collapse probability that are reputed to be acceptable are established by standard EN 1990 [EN1990] for buildings and other civil works. Three classes of consequences (CC1, CC2 and CC3) are defined on basis of the consequence of failure in environmental, social and economic terms. The partial material factors to be used in the structural design for any Class of Consequence are calibrated by comparing the results obtainable with methods of level III (full probabilistic) in paradigmatic case studies.

Let  $S$  represent the domain for actions,  $f_s$  the statistical distribution of the values  $s \in S$  and, by analogy,  $R$  the domain of the resistances and  $f_r$  the statistical distribution of the values  $r \in R$ . If actions and resistances are independent variables and their domains coincide  $r = s = x$ ,  $x \in X$ , the probability of failure  $P_f$  can be calculated from

$$P_f = P[R - S \leq 0] = \int_{-\infty}^{+\infty} F_R(x) f_s(x) dx, \quad (6)$$

where  $F_R(x)$  represents the cumulative distribution of strengths.

In general partial safety factors are provided that refer to the second Class of Consequence (CC2), whereas to pass to CC1 or CC3 a correction coefficient  $R_M$  is introduced. For what concerns the calibration of partial factors through the LTW statistics, the considered paradigmatic case studies are those of a 8mm-thick square glass plate of side 3000 mm, simply supported at the edges, under a uniformly distributed out-of-plane pressure, representative of wind on a façade panel or snow on a roof panel. The statistical models for the effects of the applied actions, essentially wind and snow, are consistent with those proposed in the EN 1991-1-4 [EN 1991]. The calibration procedure based upon the LTW statistics is reported in [*Ballarini* 2016b – section 3.3]. For such process the failure stress measurements, obtained by the working group TC129/WG8 of CEN are used. They are rescaled according to subcritical crack growth law [*Wiederhorn* 1970] so as to account for the duration of applied loads. The

effects of abrasion phenomena are considered by reducing the glass strength lower limit (Ballarini 2016b).

The parameters defining the action were made to vary until convolution integral (6) reached the target value for the probability of failure. Thus, once evaluated the design action, the maximum stress acting in the reference plate was evaluated via a structural analysis. Finally, the material partial factors  $\gamma_m$  were estimated through the verification formula in the semiprobabilistic approach of level I, by looking for equality in the inequality

$$\sigma_{max,\tau,d} - \sigma_{0,d} \leq \frac{K_{mod}\lambda_{A,\tau,WT}(f_{g,k} - \sigma_{0,k})}{R_M\gamma_m} \quad (7)$$

Here  $K_{mod}$  synthetically takes into account the phenomenon of subcritical crack growth, the coefficient  $\lambda_{A,\tau,WT}$  accounts for the effects of size and type of stress,  $f_{g,k} = 45$  MPa is the reference value for the characteristic strength of glass and  $\sigma_{0,k}$  represents the reference characteristic value of the lower bound for glass strength. The design value  $\sigma_{0,d}$  of the location parameter is taken of the form

$$\sigma_{0,d} = \frac{K_{mod}\lambda_{A,\tau,WT}\sigma_{0,k}}{R_M\gamma_m} \quad (8)$$

so to obtain a simple verification formula, i.e.

$$\sigma_{max,\tau,d} \leq \frac{K_{mod}\lambda_{A,\tau,WT}f_{g,k}}{R_M\gamma_m} \quad (9)$$

Results of the calibration process are shown in Table 1. The partial material factor obtained through a LTW statistics are compared with those obtained by Badalassi et al. (Badalassi 2014), who used a 2PW distribution for interpreting material strength variability.

| Load Case    | CC1 (2PW) | CC1(LTW) | CC2 (2PW) | CC2(LTW) | CC3 (2PW) | CC3(LTW) |
|--------------|-----------|----------|-----------|----------|-----------|----------|
| Wind, 3 sec  | 2.11      | 1.62     | 3.09      | 1.82     | 4.89      | 2.04     |
| Wind, 10 min | 2.27      | 1.61     | 3.2       | 1.81     | 4.97      | 2.04     |
| Snow, 1 mon  | 2.05      | 1.59     | 3.07      | 1.78     | 4.92      | 1.98     |

Table 1: Product of partial safety factors  $\gamma_m$  and coefficient  $R_M$  from the 2-parameter Weibull (2PW) and left-truncated Weibull (LTW) distribution for a 3 x 3 m<sup>2</sup> plate.

## Discussion and conclusion

The target failure probability of glass structures is guaranteed by partial material factors, which are calibrated by comparison with the full probabilistic approach (level III) on paradigmatic case studies. The results obtained by using a classical 2-parameter Weibull (2PW) distribution and a left-truncated Weibull (LTW) statistics are shown in Table 1. According to a recent study (Ballarini 2016a), the LTW statistics is able to interpret the

left-hand-side tail of the population of glass strength much better than the 2PW model, a very important property when considering low probabilities of failure likewise those representing target conditions in construction works. In particular, according to the LTW statistics, a lower bound for glass strength is provided, which is justified on basis of the strict production control phase (Ballarini 2016a). The hypothesis of a null location parameter (2PW statistics) provides a strongly conservative estimate, in particular for what concerns very low probability of failure (CC2 and CC3). Hence, the 2PW distribution provides much higher values of the partial factors than the LTW statistics. In particular, the values for  $\gamma_m$  are different but comparable for elements in class CC1, whereas the gap becomes striking for classes CC2 and CC3. The building industry and professional designers have always considered very conservative the values for partial factors obtained by Badalassi et al. (Badalassi 2014), because they are much higher than the coefficients traditionally used on the basis of experience and rules of practice. Even though one could argue that the 2PW statistics is on the safe side, its overly conservative nature sensibly reduces the competitiveness of glass in building market. On the other hand, the LTW statistics, which is able to well interpret the left-hand-side tail of the distribution, leads to lower partial material factors, which are comparable with those chosen according to the practice. Moreover, it is of interest to note that material partial factors obtained through the LTW distribution have been calibrated by taking

into account subcritical crack growth and abrasion phenomena, whereas this was not done by Badalassi et al. (Badalassi 2014). The calibrated values of  $R_M$ , which allow to pass from CC2 to CC1 or CC3, are recorded in Table 2. Observe that Eurocode EN1990 (EN1990) provides the multiplicative coefficient  $K_{FI}$  for the actions to pass from CC2 to CC1 ( $K_{FI} = 0.9$ ) or to CC3 ( $K_{FI} = 1.1$ ), and that such coefficient has exactly the same meaning of  $R_M$  when considering linear elastic structures. One finds from Table 1 that the LTW distribution gives results in excellent agreement with the procedure suggested by the Eurocode for all building materials, according to which the variation associated with  $R_M$  is approximately 10%. Industrial competitiveness in the globalized market asks for reliable and safe construction that at the same time comply with the issues of cost-effectiveness, energy savings and reduction of pollutant emission. The use of 2PW statistics for calibrating partial material factors may lead to an overly conservative design of structural elements made of glass, by causing material waste and raising costs. The proposed method, which is based upon a generalized Weibull statistics, can provide the theoretical base to solve such difficulty.

## References

Badalassi M., Biolzi L., Royer-Carfagni G., Salvatore W., 2014. Safety factors for the structural design of glass. *Construction and Building Materials* 55: 114-127.

Ballarini R., Pisano G., Royer-Carfagni G., 2016(a). The lower bound for glass strength and its interpretation with generalized Weibull statistics for structural application. *ASCE Journal of Engineering Mechanics* 142(12): 04016100, 20pp.

Ballarini R., Pisano G., Royer-Carfagni G., 2016(b). New calibration of partial material factors for the structural design of float glass. Comparison of bounded and unbounded statistics for glass strength. *Construction and Building Materials* 121: 69-80.

CEN-TC250, 2005. EN1990 – Eurocode 0 – Basis of Structural Design. European Standard.

CEN-TC250, 2005. EN1991 – Eurocode I – Actions on Structures – Part 1-4: General Actions. European Standard.

| Statistics | Wind, 10 min CC1 | Wind, 10 min CC3 | Wind, 3 sec CC1 | Wind, 3 sec CC3 | Snow, 1 mon CC1 | Snow, 1 mon CC3 |
|------------|------------------|------------------|-----------------|-----------------|-----------------|-----------------|
| 2PW        | 0.68             | 1.58             | 0.71            | 1.55            | 0.67            | 1.60            |
| LTW        | 0.89             | 1.12             | 0.89            | 1.13            | 0.89            | 1.11            |

Table 2: Values of  $R_M$  according to the 2-parameter (2PW) and the left-truncated (LTW) Weibull statistics.

- Durchholz M., Goer B., Helmich G., 1995. Method of reproducibly predamaging float glass as a basis to determine the bending strength. *Glass Science and Technology: Glastechnische Berichte* 68(8): 251-252.
- Madjoubi M., Bousbaa C., Hamidouche M., Bouaouadja N., 1999. Weibull statistical analysis of the mechanical strength of a glass eroded by sand blasting. *Journal of European Ceramic Society* 19(16): 2957-2962.
- Pisano G., Royer-Carfagni G., 2015. The statistical interpretation of the strength of float glass for structural application. *Construction and Building Materials* 98: 741-756.
- Wang Z., Liu L., Li X., Zhao L., 2010. An experimental method for analyzing environmental effects of blowing sands on glass abrasion. *Procedia Environmental Sciences* 2: 207-217.
- Weibull W, 1951. A statistical distribution function of wide applicability. *Journal of Applied Mechanics* 18: 293-297.
- Wiederhorn S.M., Bolz L.H., 1970. Stress corrosion and static fatigue of glass. *Journal of the American Ceramic Society* 53(10): 543-548.

## Acknowledgement

The authors acknowledge the partial support of the Italian *Dipartimento della Protezione Civile* under project ReLUIIS-DPC 2014-2018.

# News From an Old Theme: Spontaneous Cracking of Thermally Toughened Safety Glass

Andreas M Kasper, Saint Gobain HRDC

**Extended abstract** (The complete contribution will be published in the *Glass Structures & Engineering journal*)

The complete findings we below refer to are in course of publication in "Glass Structures & Engineering" as a (most probably two-part) peer-revised paper. Here, after introducing the problem, we only give a short summary of our conclusions.

## Introduction and problem statement

Spontaneous breakage of thermally toughened safety glass has been an issue since more than fifty years, and also the Heat Soak Test (HST) was invented a long time ago in order to make the glass safe against this defect. However, we have compiled facts and relevant new findings because the matter is still under discussion. In the 1990's and the beginning of the 2000's the "old HST" (e.g. following German DIN 18516) seemed to be insufficient because numerous spontaneous breakages were recorded on buildings even in Europe. The use of toughened glass in facades came more and more in vogue, so that not only the bare number of such sheets, but also the obvious lack in heat-soaking capacity demanded the amendment of the standard. After some R&D efforts, e.g. the collection of more than 1200 times-to-breakage in a number of refined HST ovens and their statistical evaluation, a new product was defined in EN 14179-1 (2006) named "Heat Soak Tested Thermally Toughened Safety Glass". This product is said to be safe because the heat-soaking procedure is meticulously prescribed; fraud or accidental malpractice seem to be excluded, and the product is expected to be as safe as possible in all actual conscience.

Luckily, after that, a R&D project that was carried out on our initiative at the Grenoble University in France (SIMaP institute = Science et Ingénierie des Matériaux et Procédés), that was, at the same time, the PhD study of O. YOUSFI. He showed that the HST might not

be as safe as we thought. Namely, YOUSFI found that above a certain compositional limit ( $x > 1.012$  in  $\text{NiS}_x$ ), the  $\alpha$  to  $\beta$  transformation of nickel sulphide cannot be completed if the temperature exceeds a certain limit ([3] YOUSFI 2010). This temperature limit is just  $280^\circ\text{C}$ , i.e. the lower (!) temperature during the holding time in HST defined in EN 14179-1(2006). His results were published, extensively discussed and some years later (in the frame of a general revision) integrated into said standard. The temperature level during holding time will newly be  $[260 \pm 10]^\circ\text{C}$ , i.e. in average 30 degrees lower than before, so that the temperature is safely below the critical limit identified by YOUSFI.

This should make the HST safer than before. Nevertheless, some people, thinking about ARRHENIUS' law that requires time prolongation on temperature decrease, started to discuss the holding time. Mainly in Germany where, since a long time, the Bauregelliste<sup>1</sup> requires doubling of the holding time in comparison with EN 14179-1(2006), ostensibly to reach a certain safety level corresponding to a component failure probability of less than  $10^{-6}$ , four hours of holding time are assertively defended.

We discuss this point of view under the light of our R&D results. In Part One of the paper ("Properties of nickel sulphide inclusions", under revision) we resume the real actual knowledge and experience on nickel sulphide inclusions, and we add previously unpublished facts from older findings from our archives whose relevance was misinterpreted or just not understood at the time of gathering them. Summarizing, after more than 50 years of R&D, we must say that still not everything is known and calculable in the very complicated theme of spontaneous breakage of toughened glass; through our present double paper we believe to make a big, maybe technologically deciding step forward again.

Part Two ("Statistical evaluation of breakage records", coming soon) will deal with statistic evaluation of several datasets. One among them was newly obtained in the frame of a nickel sulphide inclusion detection trial in China and Korea (C/K trial). Two datasets of sizes and positions of nickel sulphide

inclusions having caused breakages of toughened glass from both Heat Soak Test (HST) and from buildings were partly published in 1997 and 2001 already, but we continued accumulating data during the last 20 years. Today they seem sufficient for statistical evaluation, too.

## Summary of conclusions

The evaluation of a dataset obtained already in 1999 on 10 mm toughened Cathedral glass shows that not only nickel sulphide inclusions, but also refractory stones lead to breakage in HST. The general form of both time-to-breakage curves is nearly identical. This proves that the heating-up period of the HST, including the strong thermo-mechanical forces (temporary stress) induced into the glass, has a deciding influence on the breakages, and it obviously impacts more than the virtual nature of the inclusions causing the breakage. In particular, this makes clear that the  $\alpha$  to  $\beta$  transformation speed of the nickel sulphide inclusions is not the process determining the time to breakage in HST. This observation solves an enigma discussed since a long time, namely why the time-to-breakage curve in HST cannot be explained by the measured phase transformation speed of the different relevant  $\text{NiS}_x$  species.

In a trial at the Saint-Gobain laboratories in China and Korea we proved what beforehand was only assumed, namely that the distribution of nickel sulphide inclusions in raw glass is random, i.e. in average "flat". We even find some in the glass surface. Subject to Heat-Soak Test after thermal toughening, only 25% of these nickel sulphide inclusions lead to spontaneous glass breakage. An important conclusion from this is that a HST cannot eliminate every nickel sulphide inclusion; only the critical ones lead to breakage in HST, and they are probably the minority. In other words, the HST selects the "critical" ones from the total number.

The same would be true on buildings if unsoaked glass would be used. Also in this case, only the "critical" nickel sulphide inclusions can make the glass break. But in comparison, "criticality" has a quantitatively different

<sup>1</sup> List of building regulations. Only valid in Germany, it contains guidelines for building construction cases where an explicit normative regulation does not exist, in order to prevent too many case-by-case reviews.

Tab.1 List of "irrelevant" breakages estimated from different findings in the present paper

| Chapter | Keyword                         | Estimation result |         | Remark  |
|---------|---------------------------------|-------------------|---------|---|
|         |                                 | minimum           | maximum |   |
| 2.2.2.  | Crystallisation at forming      |                   | > 54%   | Additive to other effects   |
| 5.2.    | Thickness impact (HST)          |                   | > 90%   | All effects included  |
| 6.1.2.  | Position (HST-EU)               | > 64%             | > 85%   | Additive to other effects   |
| 6.2.2.  | Size (HST-EU) + Crystallisation |                   | > 99%   | Most important effects included   |
| 6.2.3.  | Size (HST-EU)                   | > 23%             | > 49%   | Most important effects included, but minimum estimation from mathematical-analytic evaluation |
|         |                                 | > 45%             | > 86%   |   |
| 6.2.4.  | Histograms (all)                |                   | > 57%   | Additive to other effects   |
|         | Average                         |                   | > 65%   |   |

meaning here. The external conditions are different between building and HST; the main relevant differences are in the temperature regime and in the fact that the glass in the HST is subject to strong transient thermo-mechanic stress as described above.

Consequently, breakages must be much more frequent in HST than (with hypothetically the same glass) on buildings.

This means that the HST following EN 14179-1(2006) sorts out much more glass panes than really necessary. Based on the statistical comparison of datasets from HST and buildings we are now able to estimate respective quotients.

Namely, because in the actual HST 80% of the breakages occur during the heating-up period [(1) KASPER-2000] and, following our estimations from different approaches (see **Tab.1**), approx. 1/3 only are "necessary", we can reasonably hypothesize that under the present HST conditions a holding time is completely needless for adequate safety of "Heat-Soak Tested Thermally Toughened Safety Glass". Under this hypothesis, if we really do the holding time, it's exclusively to further amend safety, but eventually even to such extend that is not really relevant in practice.

This is an important argument for why the existing estimations for the HST safety are under-estimating its real safety. The presumption that the breakage behavior in HST and on buildings would be the same is definitely not true.

As already mentioned, due to recent scientific findings, the conditions of the HST standard will officially be modified soon, probably still in 2017. Mainly, the holding temperature will be reduced from (in average) 290°C to 260°C. This is necessary in order to allow complete the a to b transformation of every potentially dangerous nickel sulphide inclusion, including the seldom ones with exotic over-stoichiometric composition. Therefore, temperature reduction will make the HST safer.

We can therefore conclude that a HST with the new holding temperature and the old holding time of two hours will be safer than before.

But, in order to reassure this, we would wish an independent recalculation to be done in order to be absolutely sure of this argument. Naturally, we claim this check to base on (or correlate with) the known facts, new findings and observations described in the present paper.

In short, what's new in our paper?

- Ideas on properties of nickel sulphide inclusions in glass depending on their detailed composition, including the presence of Ni9S8 and Ni3S4. Consequences from this on their criticality and the breakages on buildings and in the HST.
- Experimental proof (and first publication ever) that also refractory stones lead to breakages in HST, and that the time-to-breakage curve is – except for some minor details – an S-shaped curve like for nickel sulphide inclusions with even identical expansion. Conclusion that the time to breakage does not so much depend on the transformation kinetics of NiSx but on temperature heterogeneity in the HST oven. Obviously the HST puts strong thermo-mechanical stress onto the toughened glass. Therefore, except the really critical nickel sulphide inclusions, also inclusions being uncritical at ambient temperature lead to breakage, and the same is true for sufficiently big refractory stones.
- Experimental proof that the nickel sulphide inclusion repartition in raw glass is flat.
- Experimental proof that only a minority of the nickel sulphide inclusions factually existing in raw glass, but more than ca. 1/4, really leads to breakages in both HST-C/K and on buildings. Breakage rate in HST-EU is higher.
- Experimental and statistical proof that

the HST destroys much more glass than would break on buildings. "Criticality" of an inclusion is different under the different temperature conditions. Estimation for this to be one to two thirds of the breakages observed in HST, maybe even more.

- Proof that the safety of "Heat-Soak Tested Thermally Toughened Safety Glass" is actually strongly under-estimated. Out of the reasons enumerated above, the respective calculation is only a minimum estimation and needs independent revision.

To do's / open questions:

- New quantification of breakage probabilities based on fracture mechanics computer model and above-mentioned findings.
- Critical testing of hypotheses of the present paper by independent scientists. For this purpose, the authors offer to make available to every serious glass scientist every data set used in the present paper for own calculation, check and discussion.
- More measurements and evaluation of samples left from C/K trial in order to verify / falsify said hypotheses, and to allow more precise calculation.
- Eventually, re-calculation of position distribution curves for HST-EU and Building datasets applying more complicated fitting with more than one function, and correlation with size distributions if statistically feasible.
- Eventually, collection of new field data from HST, quantifying the times to breakage under the new temperature conditions.

In reference to practice, and in spite of this to-do list, one thing is sure. The actual safety estimation for the HST [(2) SCHNEIDER-HILCKEN-2012] is not totally invalid. It is strongly under-estimating the real safety, therewith fixing an exaggerating lower limit of the real safety. We have shown in the present paper that this safety estimation is an absolute worst-case scenario. Coarsely spoken, about two thirds of the breakages in HST are irrelevant and would not have led to breakages on buildings. Consequently it does not matter at all if the holding temperature is reduced by 30 degrees, or if the holding time is two or four hours. Our firm conviction is that the new conditions in EN 14179-1, including a scientifically founded reduction of the holding temperature and a limitation of the heating-up speed to three degrees per minute, will let us produce a Heat-Soak Tested Thermally Toughened Safety Glass that thoroughly fulfills all expected reliability demands for its typical applications in buildings.

The authors would like to thank J. Hilcken, A. Minne, F. Rubbert, J. Schneider and A. Schusser for fruitful discussion, H.W. Kuster for unbureaucratic leeway and S. Kasper for uncomplaining personal support.

## Reference list

(extended in "Glass Structures & Engineering")

KASPER-2000

Kasper, A.: Nickel sulphide: Supplementary statistical data of the heat soak test. *Glastech. Ber. Glass Sci. Technol.* 73(2000)no.11 pp.356-360

SCHNEIDER-HILCKEN-2012

Schneider, J., Hilcken, J., Kasper, A.: Ein Modell zur Bestimmung der Versagenswahrscheinlichkeit von heißgelagertem ESG. In: *Glasbau 2012* (ISBN978-3-433-03021-9), pp.171-184

YOUSFI-2010 a

Yousfi, O., P. Donnadieu, Y. Brechet, A. Crisci, A.

Kasper, F. Serruys: Composition and microstructure of nickel sulphide stones found in tempered glass.

*Verre*, 2010, 16, pp.30-35

# Controlling Anisotropy

Dr. Romain Decourcelle (1)  
Guillaume Kaminski (2)  
Francis Serruys (3)

(1) Saint-Gobain Glass France – CRDC  
(2) Eckelt Glas GmbH  
(3) Saint-Gobain Building Glass Europe

## Keywords

1 = Anisotropy 2 = Heat treated glass  
3 = Optical retardation 4 = Quantification

## Abstract

Although anisotropy is inevitable when heat treating glass a major breakthrough took place in the industry in 2016 by developing an on-line anisotropy visualisation equipment. The result is an on-line equipment capable of visualizing and quantifying the level of anisotropy of each single heat treated glass based on the photo-elastic theory. This allows a scientific way of quantifying the level of anisotropy. The use of this method to evaluate the level of anisotropy of each single heat treated glass allows also to guarantee the consistency of the produced glass with an approved mock-up glass in case of an architectural project.

## 1. Introduction

Anisotropy as shown in Figure 1 is also called 'iridescence' or 'leopard spots' or 'toughening marks' or 'quench marks' or 'Brewster Marks' or 'strain marks'.

The European Standard EN 12150 Glass in building – Thermally toughened soda lime silicate safety glass [1] [2] [3] describes anisotropy as follows:

### 9.2 Anisotropy (iridescence)

The toughening process produces areas of different stress in the cross section of the glass. These areas of stress produce a bi-refracting effect in the glass, which is visible in polarised light. When thermally toughened safety glass is viewed in polarised light, the areas of stress show up as coloured zones, sometimes known as 'leopard spots'. Polarised light occurs in normal daylight. The amount of polarised light depends on the weather and the angle of the sun. The bi-refracting effect is more noticeable either at a glancing angle or through polarised spectacles. The



Figure 1 Anisotropy visible on a façade.

phenomenon is a natural, physical property of toughened glass and cannot be eliminated.

And the ASTM C1048 – 12 Standard Specification for Heat-Strengthened and Fully Tempered Flat Glass [4] defines anisotropy as: 7.4 Strain Pattern—A strain pattern, also known as iridescence, is inherent in all heat-strengthened and fully tempered glass. This strain pattern may become visible under certain lighting and other conditions. It is a characteristic of heat-treated glass and should not be mistaken as discoloration, non-uniform tint or color, or a defect in the glass. The strain pattern does not affect any physical properties or performance values of the glass.

A visualization method has been developed allowing to improve the homogeneity of the heating and cooling of the glass during the heat treatment process by modifying the settings of the tempering oven parameters hence decreasing the stress differentials in the glass. A quantification based on the photo-elastic theory will allow to calculate the optical retardation. The result of the calculation will not only allow to better compare the overall anisotropy appearance of each single heat treated glass but also to specify the level which shall be reached.

## 2. Glass processing and anisotropy

Anisotropy is the inevitable consequence of the heat treatment process in order to obtain heat strengthened glass (HS) or thermally toughened safety glass also called fully tempered (FT) glass. This heat treatment process can be split into 3 parts i.e.

A/ The heating up of the glass in a furnace till a temperature of approximately 680°C

B/ Followed by the more or less sudden cooling of the glass in the quench in order to introduce stresses into the glass

C/ Cooling down

The process shall be controlled in such a way that the heating and cooling of the glass will be as homogeneous as possible.

The oscillation of the glass during the first phase of the cooling in the quench is critical.

An optimised cooling process shall be determined taking into account the cooling rate (HS or FT) and possible oscillation path.

The oscillation path is determined by the dimensions of the glass and the length of the cooling zone or quench. As the length of the quench is fixed and as the cooling rate for obtaining heat strengthened glass is lower compared to fully tempered glass, heat strengthened glass will show more anisotropy than fully tempered glass.

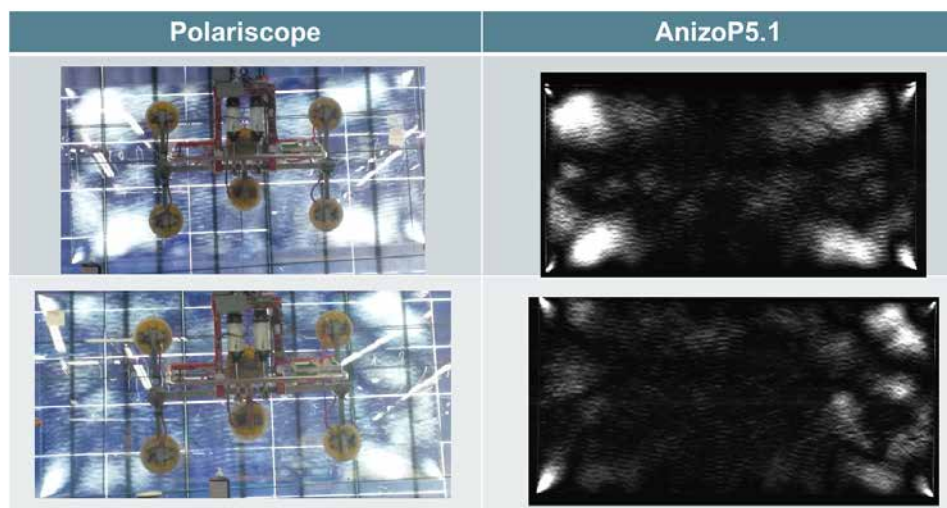


Figure 2 A 100% match of the visualisation of anisotropy obtained with the polariscope and the on-line visualisation equipment.

The same reasoning can be made for thicker heat treated glass i.e. the thicker the glass the longer it will take before the glass reaches a temperature below the glass transition temperature. Consequently the thicker the glass the higher the risk of having visible anisotropy.

The level of anisotropy is fixed once the heat treatment has been done.

### 3. Measures to control anisotropy

The optimisation of the heat treatment process can be evaluated by checking the level of anisotropy after the heat strengthening or tempering process. Ideally this is done for each glass pane. Therefore an on-line inspection equipment has been developed allowing to visualise the anisotropy of each pane coming out of the tempering equipment.

It was important that at first the on-line inspection gave exactly the same information as the picture obtained with the off-line equipment allowing to check the quality of the picture acquisition. Figure 2 shows the comparison between the pictures obtained with a polariscope off-line equipment versus the pictures obtained with an on-line visualisation equipment.

### 4. Acquisition of on-line anisotropy pictures

Many parameters are influencing the visualisation of anisotropy. The most important parameters are the type of light used – monochromatic light or white light – and the kind of polarising filter i.e. a linear or circular polaroid filter.

#### 4.1. Isoclinics

A beam of polarised light entering heat treated glass will be split into two principle axes as glass is subject to stresses after the heat treatment and consequently is behaving as a bi-refracting material. The principle axes are perpendicular one to the other and the light waves will travel at different speeds through the material hence one will be retarded with respect to the other when travelling through the heat treated glass. This retardation results in a phase difference between the two waves when exiting the glass.

If there is no phase shift, the screen will be black as the components will eliminate each other. However the screen will also be black if the direction of polarisation coincides with one of the principle stress axis as the

polarised light entering the glass will not be split although a non-homogeneous stress state may exist in the glass. These fringes, called isoclinics, are showing the points where the direction of the principal stress is the same but are independent of the magnitude of the stress. Consequently, isoclinics will not give any information related to the appearance of anisotropy.

#### 4.2. Circular polariscope

When monochromatic light is passing through a linear polariser, heat treated glass and a linear analyser which is at  $90^\circ$  to the polariser, two different fringes can be seen i.e. isoclinics and isochromatics. As isoclinics are not giving valuable information with respect to the appearance of anisotropy a circular polaroid filter shall be used. This optical arrangement will eliminate the isoclinics and keep the isochromatic fringes. These fringes may be considered as the location of all points having the same difference in principal stress. Eliminating the isoclinic fringes means that there is no distinctive direction for the polarised light beam. This is in opposition to the use of a linear polaroid filter where the light intensity changes with the orientation of the axis of polarisation (i.e. light intensity of the observed pattern will be maximised at a phase shift of half a wavelength).

#### 4.3. White light

White light is made up of many wavelengths. If such a light source is used in combination with a circular polaroid filter, a pattern of multi-coloured isochromatic fringes will be observed as shown in Figure 3.

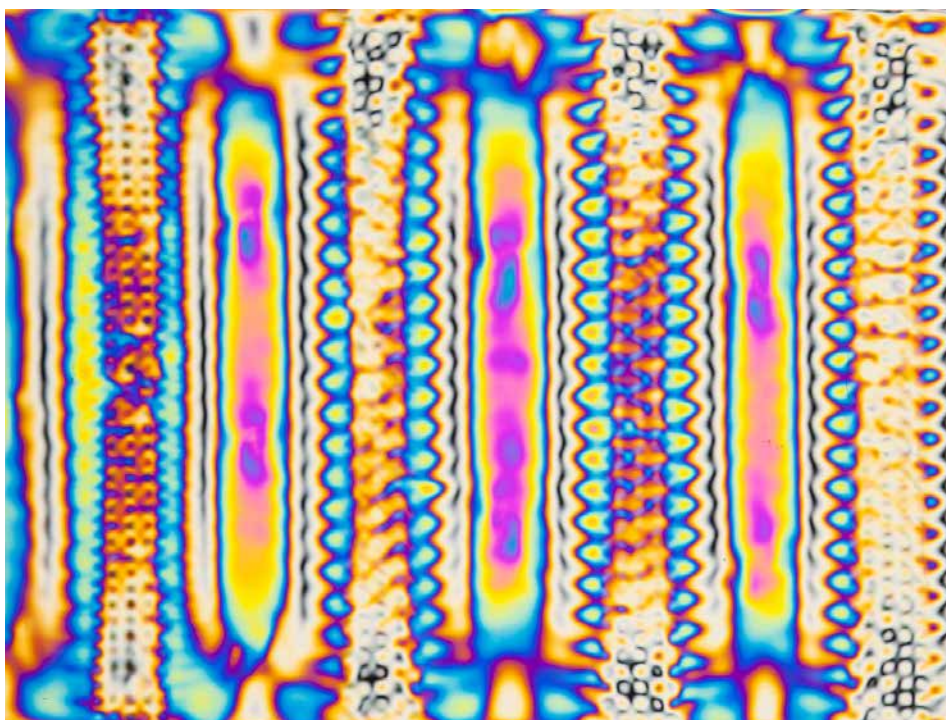


Figure 3 Multi-coloured fringes

The colour of the isochromatic fringes depends on which wavelengths are extinguished. It can be seen in Figure 4 that the higher the relative retardation, the more colour may be extinguished at the same time.

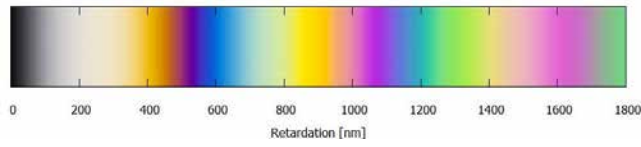


Figure 4 Colours extinguished for different relative retardation

## 5. Quantification

Since the quality of image acquisition technology has improved a lot over the past decade the optical retardation can be determined by using a method based upon the RGB-photoelasticity [5].

The source image coming from the on-line visualisation equipment is given in Figure 5. For each pixel of this image the retardation is determined by comparing the RGB value with the calibrated scale for the given system. This process results in the coloured Figure 6 showing the optical retardation in each point.

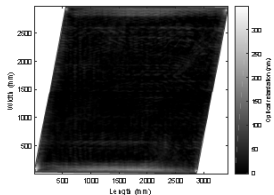


Figure 6 Image showing the optical retardation

From Figure 6 a graph (Figure 7) can be plotted showing the optical retardation in relation to the percentage of the glass surface. Example: 66% of the glass surface has an optical retardation below or equal to 50 nm. The steeper the curve, the less visible anisotropy as the optical retardation will be small indicating that the stress differential over the entire glass surface will be small i.e. the stress distribution will be more homogeneous.

From this curve a statistical evaluation can be made as given in table 1. The use of quantiles is recommended for benchmarking the level of anisotropy between different single heat treated glass panes of one or different batches. If the values of the optical retardation for the 5% and 95% quantiles are almost equal meaning that the curve is very steep, almost no anisotropy will be visible.

|                    |        |             |    |
|--------------------|--------|-------------|----|
| Maximum            | 349.00 | Quantile 5  | 0  |
| Mean               | 22.27  | Quantile 50 | 9  |
| Standard deviation | 32.06  | Quantile 95 | 97 |

Table 1 Statistical evaluation of the optical retardation [nm]

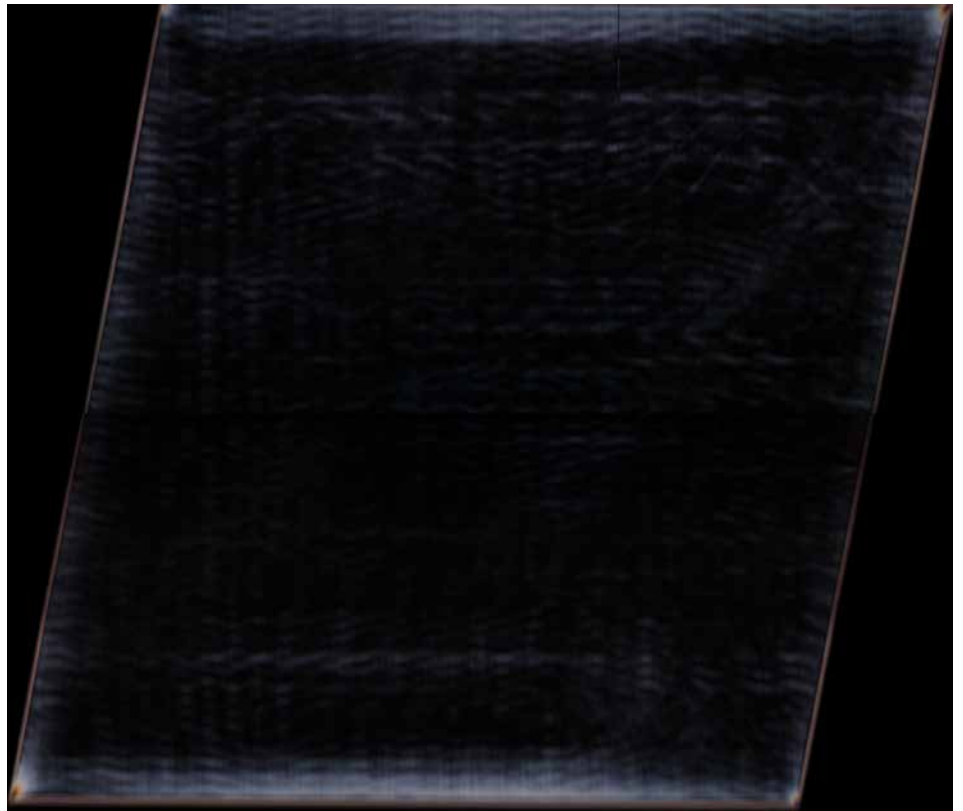


Figure 5 Source image obtained with the on-line visualisation equipment

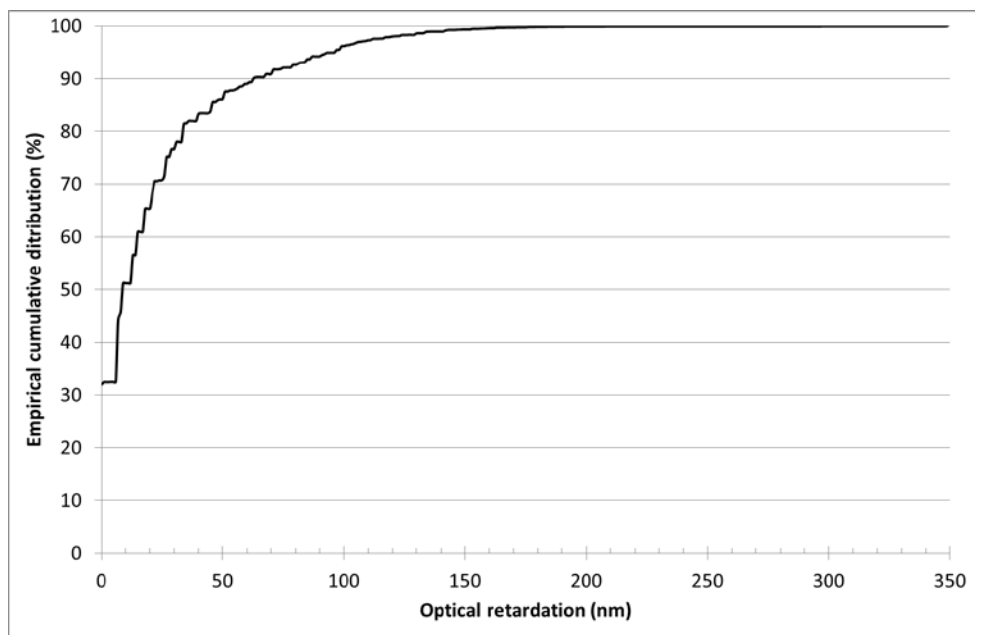


Figure 7 The optical retardation in relation to the glass surface.

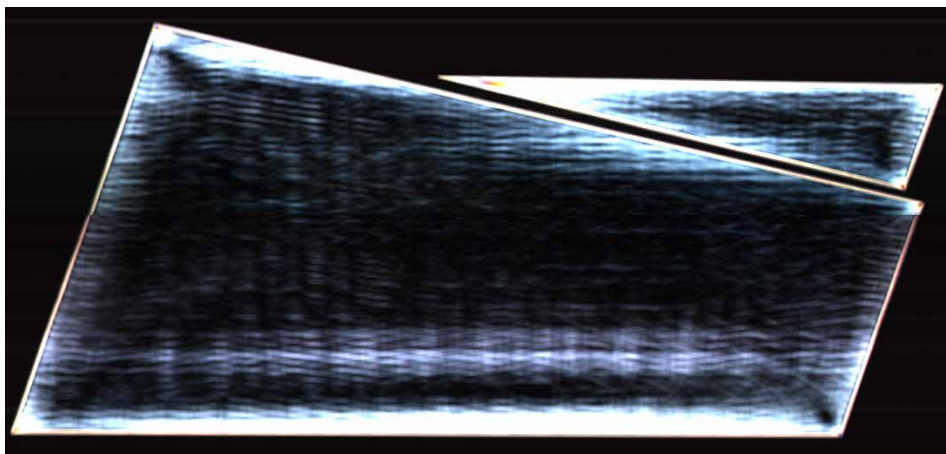


Figure 8 The impact of one pane on the other during the heat treatment on the consequent appearance of anisotropy.

As there will always be visible anisotropies along the edges of the glass one can decide whether to ignore the edge area or not depending on the future glazing method i.e. a captured system or a frameless system.

## 6. Financial impact

The sharp point of a triangle will always show critical anisotropy. Moreover the shape of the triangle is influencing the air-flow in the furnace and quench and affects the anisotropy of the bigger pane as shown in Figure 8. This means that when controlling the anisotropy during the heat treatment one must take into account that a pane may influence another pane if they are part of the same bed load. In some cases controlling the anisotropy will reduce the bed load. This in addition to an optimized oscillation speed etc. will reduce the output of the tempering line.

## Conclusions and Summary

As anisotropy free heat treated glass doesn't exist and as the environment is influencing the appearance of anisotropy it is recommended to evaluate the glass by means of a mock-up installed on or nearby the construction site. Once the mock-up has been approved, the continued production shall be controlled using an on-line visualization and quantification equipment allowing to compare the quality of the single heat treated glass with the quality of the approved mock-up. Furthermore a scientific approach based on the photo-elastic theory resulting in an objective quantification shall be used to specify the required and acceptable level of anisotropy. While specifying heat treated glass it must be taken into account that heat strengthened glass and/or thicker glass will show more anisotropy than fully tempered and/or thinner

glass. Even so it must be taken into account that a project with a lot of different dimensions and/or shapes will be more critical to have visible anisotropies compared to a project with huge series of glass having the same composition, dimension and shape.

Further measurements must be done to determine the additional cost for controlling the anisotropy during the heat treatment as the overall equipment efficiency is impacted by this process.

Finally measurement data shall be collected aiming at defining classes of anisotropy which potentially shall be standardized and become the reference.

## References

- [1] EN 12150 Glass in building – Thermally toughened soda lime silicate safety glass, 2015, 20
- [2] EN 1863 Glass in building - Heat strengthened soda lime silicate glass, 2011
- [3] EN 14179 Glass in building - Heat soaked thermally toughened soda lime silicate safety glass, 2016
- [4] ASTM C1048 – 12 Standard Specification for Heat-Strengthened and Fully Tempered Flat Glass, 2012,3
- [5] M. Illguth, C. Schuler, Ö. Bucak, The effect of optical anisotropies on building glass façades and its measurement methods, *Frontiers of Architectural Research* (2015) 4, 119 – 126
- [6] H.W. McKenzie & R.J. Hand, *Basic optical stress measurement in glass*, Society of Glass Technology, 2014

# Effects of Non-uniform Heat Transfer in a Tempering Process on Glass Quality

Antti Mikkonen<sup>1</sup>, Antti Aronen<sup>2</sup>, Mikko Rantala<sup>3</sup>,  
Reijo Karvinen<sup>1</sup>

<sup>1</sup> Tampere University of Technology, Finland

<sup>2</sup> The University of Sydney, School of Physics,  
Australia

<sup>3</sup> Glaston Finland Oy, Finland

## Keywords

1=Glass tempering, 2=Anisotropy, 3=Residual stress, 4=Non-uniform heat transfer, 5=Numerical models

## Abstract

Importance of heat transfer control on created residual stresses is well-known. Tempering of thin glasses has given new challenges not only to uniformity of heat transfer but also to energy consumption because very high heat transfer coefficients are required. Cooling is achieved by using arrays of high velocity small air jets located near the glass surface which create large variation of the local heat transfer coefficient. Simultaneously optical anisotropies which are seen as stripes or spots in glass panes are formed. These cannot be avoided in all light and viewing conditions even if cooling is uniform, but non-uniformity surely increases the effect. In this paper numerically calculated (CFD) local heat transfer results of impinging jets are presented and used as an input in the numerical modeling of residual stresses. Simple validation cases are presented for both the heat transfer and residual stresses. The solved residual stress distributions are then compared to anisotropy distributions of tempered glass panes with a plane polariscope.

## Introduction

In the glass tempering process heat transfer is the basis of the process. Glass is first heated above 600 °C and then cooled down below 450 °C in a couple of seconds to cause residual stresses to form in the glass. A stress profile where surface is under compression and mid-region is under tensile stress is formed. The temperature of the glass must be raised to a suitable level before cooling. Too hot temperature can cause roller waves or other local bending faults. Too low temperature prevents residual stresses from forming [1]. Uneven temperature field can cause

different bending faults or give uneven stress distribution over area.

The cooling rate must be high in order to cool down the glass fast enough to produce a sufficient residual stress level. In order to produce visually pleasant glass the cooling must also be uniform enough. Natural light from clear blue sky or from a reflection can be polarized and expose the uneven quality of the glass as visual defects called anisotropy. In industrial setting the inspection of glass panes can be done by using a plane polariscope [2]. Fig.1 shows extreme optical anisotropies of a tempered glass plate, less obvious patterns like this can be seen in car rear-windows with polarized sun glasses. They are caused by a stationary cooling jet arrangement. An example of normal tempered glass that was quenched while moving, is shown in Fig. 2. It is well known that uneven heat transfer causes uneven residual stresses, which in turn cause anisotropy. The details of the mechanism are, however, not well studied. Depending on the level of anisotropy the visual quality of the tempered glass can be kept good or bad. Also the location of glazing and amount of polarized light in that area affects the level visual defects [2].

In a tempering process the cooling nozzle system can consist of thousands of jets, which should be located in such a way that relatively uniform heat transfer over the surface area is obtained. However, the highest heat transfer is at the jet stagnation point area and it decreases when the distance from the stagnation point increases [3]. During cooling the glass moves first from the heating section to a cooling part, where the local heat transfer at each point of glass surface is changing over the time. This position change relative to nozzles makes heat transfer more uniform over the area and time. Due to movement, the local stress does not change significantly in the glass movement direction. However, the stresses perpendicular to the glass moving direction changes due to the differences in local heat transfer. This non-uniformity of forced convection in quenching causes stripes in the glass movement direction.

Uniform stress distribution is especially important in glasses which are made to be placed in architecturally important buildings, because polarized light occurs in normal daylight.

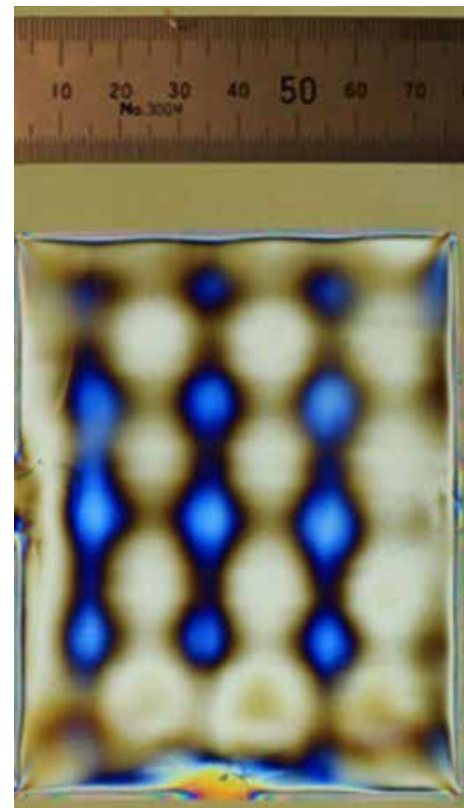


Figure 1. Anisotropy pattern of tempered glass without moving in quenching seen through polarized filters.

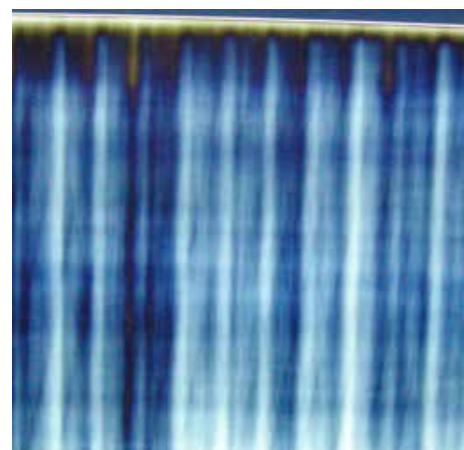


Figure 2. Anisotropy pattern of tempered glass produced by moving it in quenching seen through polarized filters.

In this paper local heat transfer of impinging small jets on surface heat transfer and residual stresses is studied. Convection heat transfer results are calculated using the open source CFD software OpenFOAM. Temperature distribution in a glass and residual stresses are

calculated using FEM in the Ansys software. Calculated heat transfer results are compared to measured results of a single jet in order to check the validity of modelling. Numerically obtained convective heat transfer coefficients are used in the modelling of a real tempering line with different jet arrangements. At the end, distributions of residual stresses are compared to anisotropy patterns of tempered glass panes measured with a plane polariscope.

## 2 Heat transfer

In order to solve the residual stress distribution in a glass plate a temperature distribution of the plate must first be solved. The glass is assumed to have a constant initial temperature before cooling. Only the calculation of cooling in a tempering process is dealt in this paper. The solution of cooling consists of two parts: heat conduction inside the glass and heat convection from the glass surface to air. Both are solved using numerical methods and include the local and temporal variation of heat transfer.

### 2.1 Conduction in glass plate

Temperature distribution and history in the glass plate with no internal sources is obtained from the following equation

$$\rho c_p \frac{\partial T}{\partial t} - k \frac{\partial^2 T}{\partial x_i^2} = 0 \quad (1)$$

where the thermal properties of glass, i.e. density  $\rho$ , specific heat  $c_p$  and thermal conductivity  $k$ , are temperature-dependent and isotropic. The effect of radiation in Eq.1 during cooling is very small and it is ignored. In order to solve the above heat conduction equation it is necessary to first solve the convective heat transfer coefficient from the glass surface by assuming that the heat transfer coefficient and glass surface temperature are not coupled together

$$h = \frac{q''}{T_w - T_{ref}} = - \frac{1}{T_w - T_{ref}} k \frac{\partial T}{\partial x_n} \quad (2)$$

where  $x_n$  is the surface normal direction,  $T_w$  and  $T_{ref}$  are the surface and cooling air temperatures. The heat transfer coefficient, Eq. (2), provides a boundary condition for Eq. (1) and is solved using the  $k$ - $\omega$ -SST turbulence model considered in the next section. Eq. (1) is solved using FEM of the Ansys 17 code [4]. The heat wall heat flux is solved from the energy equation in the CFD model, see next section.

### 2.2 Convection in glass-air interface

Convection is solved with the Finite Volume Method using the open source software OpenFOAM [5]. The validity of calculation is tested by comparing results to experimental data of a single jet in Fig. 3b.

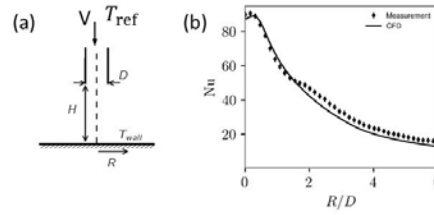


Fig.3. Schematic of a nozzle (a) and comparison of numerically modelled and measured Nusselt number  $Nu=hD/k_a$  (b)

The test case was chosen from Alimohammadi's paper [6] with  $Re=14000$ ,  $H/D=4$ , and  $D=13mm$ . The Nusselt number  $Nu=hD/k_a$ , where  $h$  is the convective heat transfer coefficient,  $D$  is the nozzle diameter and  $k_a$  is the thermal conductivity of air. Results and schematic figure of nozzle-plate system are given in Fig. 3. The nozzle height to nozzle diameter ratio  $H/D$  agrees well to the one used in tempering. The Reynolds number  $Re = VD/\nu$ , where  $V$  is the flow speed,  $D$  is the nozzle diameter and  $\nu$  is the kinematic viscosity of air, is roughly half of the one used in the tempering process. It can be seen that CFD predicts the heat transfer with good accuracy. All predicted Nusselt number fall within 15% range of the measured ones.

The convection results used in this paper for the residual stress modeling are produced using a 3D model. The cooling section jet array is made of repeating structures and only one of these structures needs to be included into calculations.

The glass surface is at a constant temperature of 500 °C roughly corresponding to the mean of the relevant glass temperature range for tempering. No wall functions are used for the glass surface because wall functions are not suitable for impinging jet flows.

Navier-Stokes equations for steady-state compressible flow are solved using Reynolds averaging for turbulence. Menter's  $k$ - $\omega$ -SST [7] model for turbulent kinetic energy is used

$$\frac{\partial(\rho k)}{\partial t} + \frac{\partial(\rho U_j k)}{\partial x_j} = \overline{P_k} - \beta^* \rho k \omega + \frac{\partial}{\partial x_i} \left[ (\mu + \sigma_k \mu_t) \frac{\partial k}{\partial x_i} \right] \quad (3)$$

and specific dissipation is solved from the equation

$$\frac{\partial(\rho \omega)}{\partial t} + \frac{\partial(\rho U_j \omega)}{\partial x_j} = \frac{\overline{\alpha P_k}}{\nu_t} - \beta^* \rho \omega^2 + \frac{\partial}{\partial x_i} \left[ (\mu + \sigma_\omega \mu_t) \frac{\partial \omega}{\partial x_i} \right] + 2(1 - F_1) \rho \sigma_{\omega 2} \frac{1}{\omega} \frac{\partial k}{\partial x_j} \frac{\partial \omega}{\partial x_j} \quad (4)$$

The model used in OpenFoam 4.0 [5] differs in detail from the one proposed by Menter [7]. Details are given in the the OpenFoam source code or in the paper by Mikkonen and Karvinen [8]. Ideal gas law is used as the equation of state and Sutherland's correlation is used for viscosity to include the effect of temperature. Heat convection at the glass surface is very sensitive to grid size and quality. A very fine grid size is used near the glass surface. Grid independency is studied by repeatedly refining the mesh. For a 3D calculation millions of cells are needed. For an introduction to impinging jet heat transfer, see the paper by Zuckerman and Lior [9].

### 3 Residual stress

The calculation of residual stresses due to tempering process is based on the thermo-mechanical model. For thermal stresses the temperature distribution has to be solved using the theory shown above in Chapter 2.1. The mechanical behavior of the glass during the cooling process based on the thermal strains and the viscoelastic behavior of the glass at different temperatures. The stress of the glass at each time can be calculated by using Eq. (5) [10].

$$\sigma_{ij}(t) = \delta_{ij} \int_0^t K(t-t') \frac{\partial(\bar{\varepsilon} - 3\varepsilon^{th})}{\partial t'} dt' + 2 \int_0^t G(t-t') \frac{\partial(e_{ij})}{\partial t'} dt' \quad (5)$$

Where  $\sigma_{ij}$  is the directional stress,  $K(t)$  is the bulk relaxation modulus as shown in Eq. (6),  $G(t)$  is the shear relaxation modulus as shown in Eq. (7), and are the strain components as shown in Eqs. (8) and (9) and is the thermal strain as shown in Eq. (10). In the mechanical model the temperature-dependent viscoelasticity and the structural relaxation are taken in consider [11].

$$K(t) = K_{\infty} + (K_0 - K_{\infty}) \sum_{p=1}^P w_{2p} \exp\left(-\frac{t}{\tau_{2p}}\right) \quad (6)$$

$$G(t) = G_0 \sum_{q=1}^Q w_{1q} \exp\left(-\frac{t}{\tau_{1q}}\right) \quad (7)$$

where subscript 0 is the initial value and  $\infty$  is the value at infinite time. In the weighting factors  $w$  and relaxation times  $\tau$  the subscript 1 is for the shear relaxation and 2 for the bulk relaxation.

$$\bar{\varepsilon} = \varepsilon_{xx} + \varepsilon_{yy} + \varepsilon_{zz} \quad (8)$$

$$e_{ij} = \varepsilon_{ij} - \delta_{ij} \frac{1}{3} \bar{\varepsilon} \quad (9)$$

$$\varepsilon^{th}(t) = (\alpha_l - \alpha_g) (T_f(t) - T_f(0)) + \alpha_g (T(t) - T(0)) \quad (10)$$

where  $\alpha_l$  is the thermal expansion coefficient for the liquid state and  $\alpha_g$  for the glassy state. Fictive temperature  $T_f$  is related to structural relaxation of glass [11]. A detailed theory of the model is in the literature [12].

In calculations Ansys 17.0 software is used [4], which is based on Finite Element Method (FEM). The calculation has to be done transient using different time steps over the whole cooling time to solve the residual stress. The model verification has been done in the thesis by Aronen [12] and compared to experimental results by Gardon [13], see Fig. 4, which both were obtained using uniform heat transfer coefficients over the area. Modeling results are the same as experimental results with low heat transfer coefficients, but with high heat transfer coefficients the modeling results are about 10 % lower compared to experimental results. It can be noted that internal stress measurements are not easy they can contain errors.

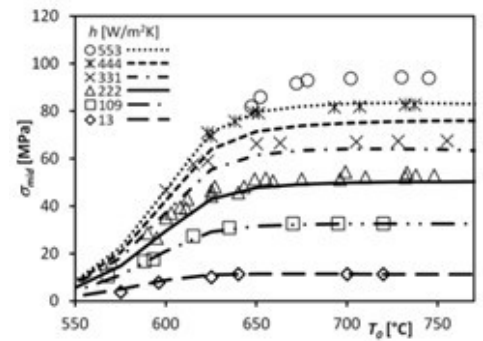


Figure 4. Comparison of experimental (points [13]) and calculated (lines [12]) results for mid-plane residual stresses with different initial temperatures and heat transfer coefficients. Glass thickness is 6.1 mm.

### 4 Anisotropy

The effect of the anisotropy can be explained with the principal stress differences. The photoelasticity is used to determine the stress field in transparent materials with an experimental method. In the stress-optic law the principal refractive indices are expressed as a function of principal stresses. The refractive index in direction 1 is presented in the Eq. (11). The equations in other directions are the same except for the subscripts in labeling [14].

$$n_1 = n_0 + C_1 \sigma_1 + C_2 (\sigma_2 + \sigma_3) \quad (11)$$

Parameter  $n_0$  is the refractive index of unstressed material and constants  $C_1$  and  $C_2$  are depending on material. For the plane stress the normal to plate stress  $\sigma_3 = 0$  and the light is passed through the plate in the direction 3. Then the stress difference  $\sigma_1 - \sigma_2$  is

studied. The relative retardation  $\delta$  is presented by the equation of Wertheim law and it is [14] Where  $C=C_1-C_2$  is photoelastic constant and  $d$  is the thickness of material. In the case that stress distribution is changing over the thickness the relative retardation can be integrated over the area [14].

$$\delta = (n_1 - n_2)d = C(\sigma_1 - \sigma_2)d \quad (12)$$

The plane polariscope, as presented in the Fig. 5, can be used to see the colorful anisotropy pattern. In the plane polariscope light is first polarized at the polarization filter. Polarized light passes through the glass with residual stresses where the relative phase shift of components of polarized light forms. Finally when polarized light with relative phase shift passes through the second polarization filter, which is rotated 90° comparing to the first filter.

$$\delta = C \int_d (\sigma_1(z) - \sigma_2(z)) dz \quad (13)$$

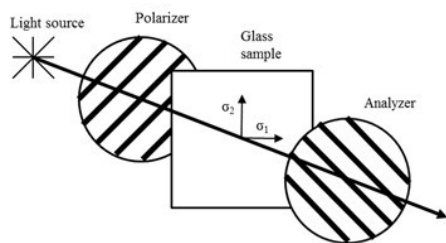


Figure 5. An illustration of the plane polariscope.

## 5 Computational and experimental results of tempered glass

### 5.1 Convective heat transfer in tempering

Using the nozzle geometry used in glass tempering machine cooling section, see Fig. 6, the heat transfer coefficients are calculated. The overpressure is 5000 Pa compared to the outside atmosphere pressure and jet velocity about  $V \approx 100$  m/s,  $H/D \approx 4$ , and  $D \approx 5$  mm. The used numerical methods are described in section 2.2 and expect for the geometry and over pressure are the same as used in the validation case in Fig. 3. The total length of a nozzle plate is 80 mm and plates are installed 120 mm apart from each other.

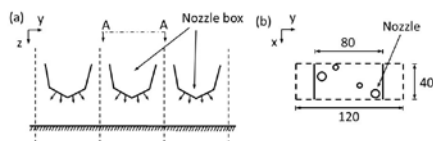
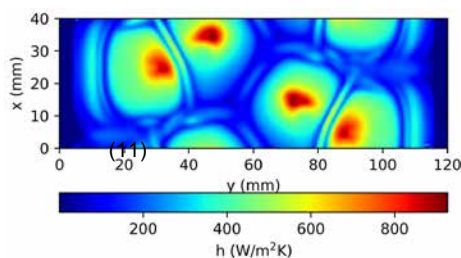


Figure 6. Schematic of the nozzles (a) and locations in nozzle plate (b).  
Figure 7. Distribution of heat transfer coefficient in section A-A of Fig. 6.



In Fig. 7 calculated heat transfer coefficient in the glass surface is shown. It can be seen that heat transfer of a nozzle array is qualitatively similar to heat transfer of a single nozzle shown in Fig. 3. Heat transfer is highest near the stagnation point where the jet hits the wall directly and decreases with increasing distance from the stagnation point. Heat transfer coefficients in Fig. 7 are used to calculate the temperature field for a moving glass, when the effect of jet locations is studied below. Under the supporting rollers, near the edges of the calculation domain in the y-direction, heat transfer is small because of near zero air velocities. The irregularities in the fields are caused by the transient nature of jets.

### 5.2 Residual stress distribution in glass

The stress distribution in glass after tempering process is calculated by using the convective heat transfer coefficient distribution solved above and shown in Fig. 7. The stress distribution has been solved for three different cases. In the first case (C1) the solved local heat transfer distribution repeats periodically. In the second case (C2) heat transfer distributions in sequential periods are shifted in the x-direction by the half width of the periodical distance. In the third case (C3) sequential periods are shifted in the x-direction by the quarter of the width. Illustration of these cases is shown in Fig. 8. The width of sequential period is 40 mm and length is 120 mm.

In the modelling the 3.85 mm thick glass moves relative to the quenching system continuously in one direction (y-direction) for 5 seconds with the speed of 450 mm/s. This corresponds approx. glass movement in a 2 m long chiller. After 5 seconds the cooling has changed to a uniform heat transfer coefficient (330 W/m<sup>2</sup>K) cooling and glass movement is stopped. Then glass is cooled close to room temperature. The change to uniform heat transfer coefficient is done to simplify the calculation. The beginning of the cooling is the most important and the change after 5 seconds does not effect on the residual stress distribution. Heat transfer is symmetric relative to the mid-plane. The size of modeled area, where residual stresses are considered, is 100 x 100 mm<sup>2</sup> as shown in Fig. 9. The initial temperature of the glass is 650 °C.

The material properties for glass used in the model are the same as used by Aronen [12]. The results show that the stress in 40 x 40 mm<sup>2</sup> size area in the center of modeled area varies significantly only in the x-direction, as shown in Fig. 10. The stress variations are due to the local variations in average heat transfer. The stress in the x-direction and the y-direction as also the stress difference along the x-direction with different nozzle systems at the surface and in the mid-plane are shown in the Figs 11 (surface) and 12 (mid-plane). These stresses are plotted along the dashed line shown in Fig. 10. Results show the clear influence of the shifting of the nozzle plates to uniform the local heat transfer and stress distribution. Results for Cases 1 and 2 can vary over 20 MPa between maximum and minimum stress in surface and 10 MPa at mid-plane. Case 3 is more uniform and the stress difference between maximum and minimum values is less than 5 MPa.

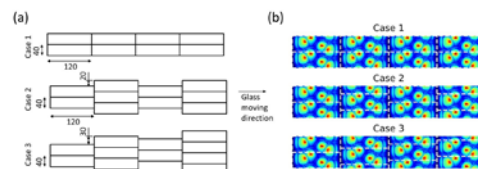


Figure 8. Illustration of periodic location of nozzles and comparison to heat transfer coefficient. (a) Schematics. (b) Heat transfer coefficients. Dimensions are in mm.

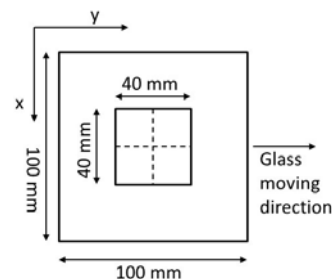


Figure 9. Modeled area in stress simulation.

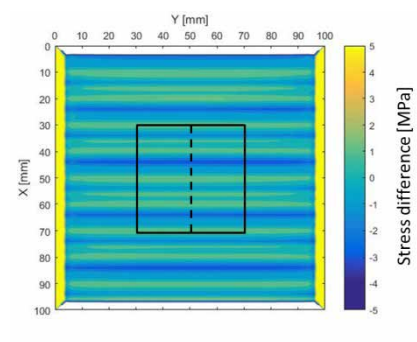


Figure 10. Stress difference  $\sigma_x - \sigma_y$  at the outer surface of 100 x 100 mm<sup>2</sup> area with Case 3 nozzle system. Square in the middle presents 40 x 40 mm<sup>2</sup> area. Results in Figs. 11 and 12 are presented along the dashed line.

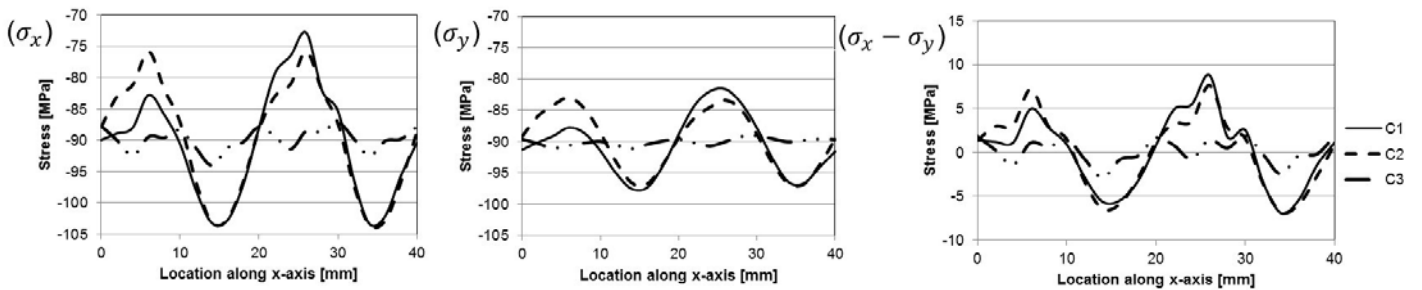


Figure 11. Compressive stress  $\sigma_x$ ,  $\sigma_y$ , and  $\sigma_x - \sigma_y$  on the glass surface along the dashed line in Fig. 10.

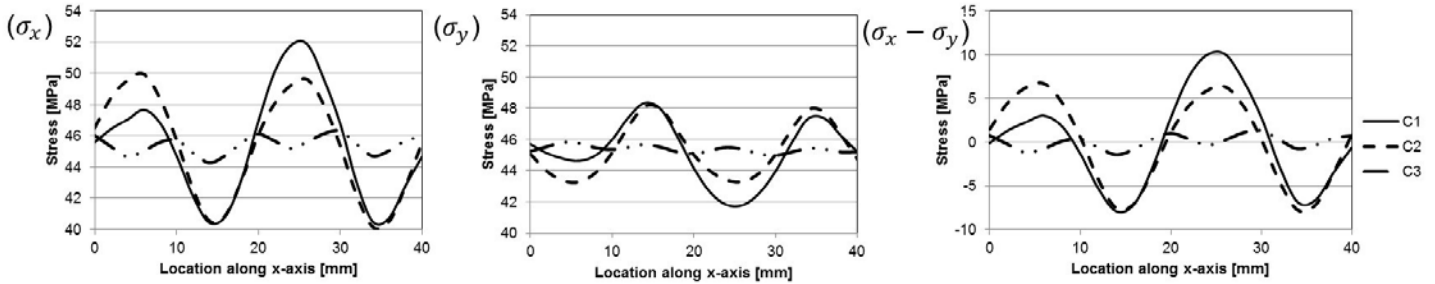


Figure 12. Tensile stress  $\sigma_x$ ,  $\sigma_y$ , and  $\sigma_x - \sigma_y$  on the glass mid-plane along the dashed line in Fig. 10.

### 5.3 Anisotropy observations in tempered glass

The modeled stress results are compared to real anisotropy distribution from a test sample shown in Fig. 13. In the experiment test sample of clear float glass with the size 585 x 800 mm<sup>2</sup> and the thickness 3.85 mm was tempered. Glass was first heated to about 630 °C and the cooled with nozzle cooling system similar to Case 3 in numerical results. The overpressure in a n air box was 5000 Pa and distance from nozzle to plate was 16 mm. In the cooling part, glass was moving with speed 450 mm/s. The stress on the surface was measured with the GASP surface stress polarimeter. Depending on the location stress was between 89-93 MPa. The visual anisotropy in the test sample is shown in Fig. 13. For the anisotropy distribution the polarization filters and the glass sample are oriented as in the Fig. 10. In Fig. 13, the main result to compare the numerical results and experimental results is the horizontal wide stripes which repeat regularly. In the enlarged area in Fig. 13 three regularly repeating horizontal stripes are shown. The width of one strip is about 40 mm, which is same to numerical results. The stress level in the anisotropy distribution is not available. However, by comparing the intensity differences in the enlarged area in the Fig. 13 to the intensity differences in the center of pane in the Fig. 13, the stress change due to nozzle location is smaller.

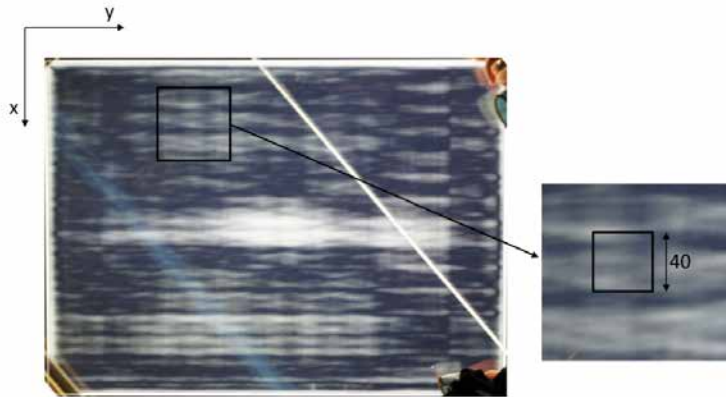


Figure 13. The anisotropy distribution of 585 x 800 mm<sup>2</sup> tempered glass plate. In the enlarged area on the right the 40 x 40 mm<sup>2</sup> is marked to present the similar area to one presented in Fig. 10.

## 6 Conclusions

Visual quality of the tempered glass without anisotropy is coming more and more important factor in tempered glass and tempering machine business. The most important factor to glass quality is the control of heat transfer, which should be uniform over the glass plate and symmetric over the mid-plane of the glass. This paper shows that with state-of-the-art CFD numerical methods it is possible to calculate the heat transfer during quenching. These heat transfer result can be used in FEM program to solve the residual stresses caused by the heat transfer. By comparing calculated residual stress distributions and visual observations of tempered glass with a plane polariscope similarities can be noted. With numerical methods the effect of the

nozzle placements on stress distribution can be studied and optimized. Though, the modeling and experimental results of residual stresses show similar behavior as anisotropy in tempered glass the stress level cannot be solved from anisotropy image.

## References

- [1] Aronen, A. Karvinen, R., Effect of initial temperature and cooling rate on residual stresses of tempered glass, Glass Structures & Engineering, under review.
- [2] Illguth, M., Schuler, C., Bucak, Ö., The Effect of Optical Anisotropies on Building Glass Façades and its Measurement Methods, Frontiers of Architectural Research, Vol. 4, pp. 119-126, 2015.
- [3] Holger, M., Heat and Mass Transfer between Impinging Gas Jets and Solid Surfaces, Advances in Heat Transfer, vol. 13, pp. 1-60, 1977.
- [4] ANSYS® Academic Research, Release 17.0
- [5] The OpenFOAM foundation, <http://www.openfoam.com>.

org/, version 4.0, 2017.

- [6] Alimohammadi, S., Murray, D., Persoons, T. Experimental Validation of a Computational Fluid Dynamics Methodology for Transitional Flow Heat Transfer Characteristics of a Steady Impinging Jet, ASME. Journal of Heat Transfer, Vol. 136, 2014
- [7] Menter, F. R., Kuntz, M., Langtry, R., Ten Years of Industrial Experience with the SST Turbulence Model, Turbulence, Heat and Mass Transfer, Vol. 4, pp.625 – 632, 2003.
- [8] Mikkonen, A., Karvinen, R., Heat Transfer of Impinging Jet: Effect of Compressibility and Turbulent Kinetic Energy Production, IX International Conference on Computational Heat and Mass Transfer, 23-26 May 2016 Cracow, Poland, 2016.
- [9] Zuckerman, N., Lior, N., Jet Impingement Heat Transfer: Physics, Correlations, and Numerical Modeling, Advances in Heat Transfer, Vol. 39, pp.565–631, 2006
- [10] Flügge, W., Viscoelasticity, 2nd ed., Springer-Verlag, Berlin, Germany, 1975.
- [11] Scherer, G., Relaxation in Glass and Composites, John Wiley & Sons, Inc., USA, 1986.
- [12] Aronen, A., Modelling of Deformations and Stresses in Glass Tempering, Dissertation, Tampere University of Technology, 2013.
- [13] Gardon, R., The Tempering of Flat Glass by Forced Convection, Proceedings VIIth International Congress on Glass, Brussels, Belgium, 1965.
- [14] Aben, H., Guillemet, C., Photoelasticity of Glass, Springer-Verlag, Germany, 1993.

## Acknowledgement

The authors acknowledge the Finnish Funding Agency for Technology and Innovation (Tekes) for partly funding this work during the program Energy Efficient Tempering of Thin Glasses for Solar Energy Next Generation Products. The authors also acknowledge the University of Sydney HPC service at The University of Sydney for providing HPC and software resources that have contributed to the research results reported within this paper.

# Haze, Anisotropy, Clarity and Interference Effects (HACI) Evaluation

Louis Moreau,  
AGNORA, Collingwood, ON, Canada

## Keywords

Haze  
Anisotropy  
Clarity  
Interference  
Ionoplast

## Abstract

As a manufacturer and supplier of monolithic, laminated and insulated glass panels to the high-end retail and business markets, we often produce larger panels that must use heat-treated components, ionoplast interlayers and multi-layer assemblies. This invariably produces HACI. All these phenomena are observable, but deemed inevitable, physical properties and inherent to manufacturing. We want to offer higher quality products and believe that we can improve those aspects. However, there are no instruments on the market to qualify and quantify HACI on large pieces of glass. We believe that a numerical, repeatable value is the base that will allow improvement in our process.

We launched a research program in conjunction with McMaster University to develop such an instrument. We will share our field observations and early experiments to detect and quantify these phenomena. This remains a work in progress. We see the GPD attendees as the ideal network of professionals to help us align our R&D with industry needs. Our goal is to establish a numerical model that will reflect the severity of the different HACI factors.

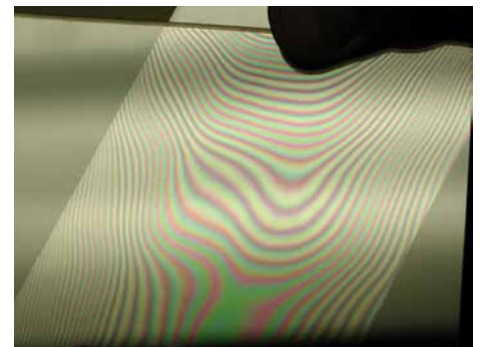


Photo 1-2-3-4

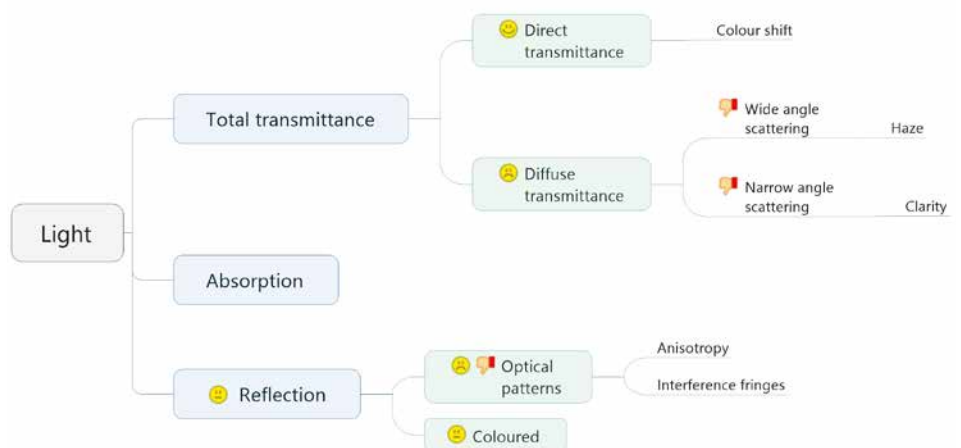


Photo 5

## What are we talking about?

### Anisotropy

Anisotropic material exhibits properties with different values when measured in different directions. The opposite behaviour is isotropy; vacuum and annealed glass are isotropic. Tempering glass creates heterogeneous stresses that cause birefringence, an optical property having a refractive index that depends on the polarization and propagation direction of light. These optical patterns become noticeable when polarized light is transmitted or reflected on the glass.

### Haze

Haze is more simply the scattering of light that creates a reduction in contrast of objects viewed through it. Haze is quantifiable. ASTM defines it as the percentage of transmitted light that is scattered so that its direction deviates more than a  $2.5^\circ$  angle from the direction of the incident beam (ASTM International, 2000). Coatings and ionoplast interlayers can create haze when crystalline structures build up in them. Haze is also pervasive in switchable privacy films.

## Clarity

Clarity is similar to haze, but pertains to scattering with a smaller angle.

## Interference

Interference fringes exist in insulating glass units and under sacrificial lites. They are the result of an interaction between colliding light waves. Because of reflections off the multiple glass surfaces, light waves divide and travel different paths, then recombine. When they recombine, interference fringes may be seen (PPG Industries, Inc., 2002).

## Regulation and standards

An exhaustive study of European and British standards and industry guidelines was presented at GPD 2015. "Anisotropy is clearly recognized as an inevitable effect of the heat treatment processes by current British Standards" (Pasetto, 2014). The same wording exists in North American standards C 1048. However, the Glass Association of North America (GANA) takes a more utilitarian approach than its European counterpart by suggesting the use of full size mock-ups viewed on-site to determine acceptable anisotropy levels (GANA, 2008).

## Stakeholders' opinion

Savario Pasetto exposed the results of a survey aimed at identifying the extent to which anisotropy is perceived as a defect and how it affects the façade industry in the same GPD presentation (Pasetto, 2014). The quality of the respondents and their distribution in all appropriate domains - Façade consultants, Façade contractors, Architects, Glass suppliers - make this survey relevant despite its small sample size (35). Apparently, the results show, the results show that most participants are aware of the phenomenon and would like to mitigate it. We think that the current state of technical capabilities, costs and liability influence the wording and possible standardization. Mr. Pasetto rightly note that "the development of anisotropy equipment is critical to analyze the stresses and their distribution and in turn optimize oven design" ... "the measuring equipment is also fundamental in defining objective acceptance and rejection parameters" (Pasetto, 2014).

## Design criteria for our inspection equipment

The randomness of field problems encountered showed that all glass need to be analyzed in their complete area. We already do this in our existing optical and defect scanners. 100% inspection is also the norm in the automotive glass industry. From our first set

of experiments, we can say that we need to analyze finished products:

- Individual components do not show all the story
- There is interaction of interference patterns that complexifies the heterogeneity
- Haze and Clarity are predominately caused with ionoplast lamination, thus exist only in complete laminates
- Interference fringes exist only in IGUs

Knowing the sheer size and weight of our products and the difficulty of manipulating them safely, we will have to integrate inspection after a washer. Vertical setup will minimize floor space and simplify logistics. Computation time is paramount, we want rapid Go/No-Go results independent of operator. Needless to say, these results and photos will be associated with individual pieces for traceability and reporting if required by the customer - as we do for HST records, for example.

We do not think we can measure all phenomena with a single setup. We will share all mechanical devices, but detection apparatus will be different. We are analyzing if a single high-intensity polarized light source could be used.

## Quantification

We want to develop and promote an industry standard, we don't want to work alone nor re-invent the wheel.

## Anisotropy

University of Applied Sciences Munich (UASM) has proposed a practical method based on a statistical evaluation of complete retardation array. Using p-quantile, they are able to output simple numerical values that look very promising (M. Illguth, 2015). This method was further developed by our session chair, and we are confident that Saint-Gobain Glass will publish more details on their work in enhancing UASM's method.

## Haze

Because we analyze on a large area and we are more interested in heterogeneity, our detection method will be very different from the ASTM D1003 (ASTM International, 2000). However, our objective is to be able to match the absolute value found with the results of the Unidirectional illumination: diffuse viewing method. Percent haze being calculated from the ratio of diffuse,  $T_d$ , to total luminous transmittance,  $T_t$ , as follows:

$$\text{haze, \%} = T_d / T_t \times 100$$

## Interference

We are not aiming at quantifying interference fringes. We think interference will be a by-product of our experimentation. In correct illumination, that phenomenon should be easily observable. As its origin is purely physical, a feedback loop to design parameters is the only recourse to minimize it.

## Conclusion and summary

We are embarking on a very interesting journey that will lead to quantifying phenomena that are deemed inevitable but, in our opinion, can be improved. In the long term, measuring HACI will lead to aesthetic improvements of large and complex glass panels. We believe HACI quantification has the same or even more influence on visual quality and transparency than current small punctual defect detection.

## References

- ASTM International. (2000). Standard Test Method for Haze and Luminous Transmittance of Transparent Plastics. ASTM D 1003-00.
- GANA. (2008). Quench Patterns in Heat-Treated Architectural Glass. GANA TD 05-0108.
- M. Illguth, C. S. (2015). The effect of optical anisotropies on building glass façades and its measurement methods. Munich, Germany: ScienceDirect.
- Pasetto, S. (2014). Anisotropy as a defect in U.K. architectural float heat-treated glass. Bath, UK: University of Bath.
- PPG Industries, Inc. (2002). Interference Fringes in Insulating Glass Units. Pittsburgh, PA: Glass Technical Document TD-118.

# Thermally Processed Glass: Correlation Between Surface Compression, Mechanical and Fragmentation Test

Ennio Mognato<sup>1</sup>, Stefano Brocca<sup>1</sup>, Alessandra Barbieri<sup>1</sup>

<sup>1</sup> Stazione Sperimentale del Vetro

## Keywords

Surface Compression, Bending Strength, Fragmentation, Thermally Treated

## Abstract

The paper correlates the data recorded in Stazione Sperimentale del Vetro, in many years. The aim is to define a correlation between the following parameters in heat treated glass:

1. bending strength tested according EN 1288-3 [1];
2. fragmentation tested according relevant Standards [2, 3, 4];
3. surface compression stress measured with laser Gasp [5]

For heat strengthened glass the fragmentation correlation due to the different crack path ("island" fragments instead of small fragments) is only related to conformity: C/NC. The research is the development of the previous ones [6, 7] carried out at Stazione Sperimentale Vetro, increasing the experimental data (up to 2016) considering in detail the emissivity of coated glass and extending also to enamelled glass. The correlation between surface compression stress and mechanical strength and fragmentation is relevant for the manufacturer, who may use surface pre-stress measurement as a means of product control.

## Introduction

Thermally treated glass is used in many applications and the range of glass products is quite wide considering coated glass and enamelled too.

Coated glass needs to respect energetic parameters: low-e, selective and reflective glass in function of the climatic zone and law requirements for specific projects.

In the recent years the enamelled glass has started to be request more and more for specific applications in which the designer would like to hide some elements or create an opaque surface or for artistic propose. The enamelled treatment could be applied uniformly on the whole surface or at specific

zones (i.e. along the glass pane edges), according to drawings (screen printing) or pattern (points, lines, strips). They are produced by applying and burning a coloured paint on glass surface; then the pane is thermally treated. The interaction between glass surface and paint is a tricky aspect due to the tensile stress that the frit induces at the interface and by the effect of pigment granules [8]; both weaken the surface of application. This aspect is taken in account by Standards reducing the minimum values for the mechanical strength [2, 3, 4]. In Italy a new Standard was published at the beginning of 2017 [9].

SSV carries out many experimental tests on these products. The data are collected to evaluate a correlation between the Surface Compression Stress (SC) and the other characteristics: Fragmentation (FR) and Flexural Bending Strength (FB). This database started in 2002 and it is still going on. The data reported in the present paper had been collected until the end of 2016 and had been organised as:

1. surface compression stress tested according [5]
2. bending strength tested according [1];
3. fragmentation tested according relevant standard [2, 3, 4];

The aim of this paper is to evaluate and extend the considerations carried out in the previous papers [6, 7, 10] to coated and enamelled glass. Furthermore heat strengthened glass data were considered, whereas fragmentation is considered in terms of conformity Y/N according [2] due to the different crack path ("island" fragments instead of small fragments).

The correlation between surface compression stress and mechanical strength and fragmentation is relevant for the manufacturer, who may use surface pre-stress measurement as a means of product control.

## Thermal process on heat treated glass

The soda lime silicate glass HS (conformity to [2]) or TT (conformity to [3, 4]) is a glass in which was induced permanent surface compressive stress through a controlled process of heating and cooling to increase mechanical and thermal strength; for TT product, in addition, to get the fragmentation

characteristics such as to limit the damage to people and/or things in case of its failure.

The heat transfer in the tempering process takes place through:

- Radiation (resistors in the pre-heating and heating)
- Conduction (contact with the rollers)
- Convection (important in the case of coated glass)

The convection plays a crucial role in the process with introduction of the low-e glass in the market: glass with high emissivity absorbs heat while one with low emissivity reflects it.

The presence of a face with lower emissivity may involve an asymmetrical heating and the resulting curvature of the pane at the end of the treatment, with unlikely no homogeneous residual stresses.

After heating, in the first instants of air blowing, the glass surface is cooled more quickly than the centre of glass pane and, in few seconds due to the low thermal conductivity, the temperature difference between the surface and the core of the pane reaches the maximum value. It is evinced that more energy is requested to temper thin glass than that for thicker one. The quenching step is obtained by forced blowing whose time depends on the glass thickness.

Undesired residual stress on glass surface may be caused mainly by:

- no uniformity of heating of pane in its plane and between the two surfaces
- different quenching speed from point to point of pane
- presence of holes, notches, that induce differential heating and quenching rate

It is necessary to control the process at every stage to avoid these problems.

## Measurement of residual stress in heat treated glass

The measure of residual stress has to be carried on by photoelastic measurement, which has been widely developed in the recent years. Nowadays, the main instruments are: 1) GASP, registered trademark of Strainoptics Technologies; 2) SCALP, developed by GlasStress Ltd.

The measurement is carried on to evaluate the SC and correlate this non-destructive measure with the FB or FR values carried out by destructive tests. Redner wrote many papers on this topic [11, 12, 13, 14, 15, 16]

explaining the features of the GASP instrument and its capability to be used in QC after glass tempering. Other authors proposed a new instrument (SCALP) based on scattered light polariscope technique [17, 18] evincing that the residual stress in tempered glass can be highly inhomogeneous, both locally and globally.

## Frame of the research

The research is developed according to test procedure reported in:

- EN 12150-1 [3] for thermally toughened glass, in the following named TT
- EN 14179-1 [4] for heat soaked thermally toughened glass, included in TT
- EN 1863-1 [2] for heat strengthened glass, in the following named HS

which prescribe fragmentation test (FR) and four point bending test (FB), according [1], after measurement of surface compression stress (SC), according to [5].

The value carried out from experimental data are:

- SC: surface compressive stress considered as mean value of five measure for each specimen;
- FR: number of fragments obtained according to [3, 4]
- FB: flexural strength calculated at collapse load, following the equation defined in [1].

The SC is correlated to FR and FB respectively. Up to day, the ASTM C1048:2012 [19] and ISO Standards [20, 21] specify a surface compressive stress requirement as showed in table 1; whereas the EN Standards define the bending strength limits and the minimum number of fragments as reported in table 2.

The assessment for FR differs between HS and TT glass because the crack path is

| Standard Reference      | Heat Strengthened                                 | Thermally Toughened                            |
|-------------------------|---|--|
| EN 1863-1:2012          | No value is indicated                             | --   |
| EN 12150-1              | --  | No value is indicated                          |
| EN 14179-1:2016         | --  | No value is indicated                          |
| ASTM C1048:2012         | 24±52 MPa<br>(thickness equal or lower than 6 mm) | 69 MPa   |
| ISO/DIS 22509 rev.:2016 | 25±55 MPa   | --   |
| ISO/FDIS 12540:2016     | --  | 80 MPa minimum for FB<br>90 MPa minimum for FR |

Table 1 Reference Value of Surface Compressive Stress

| Standard Reference      | Float and coated           | Enamelled                 |
|-------------------------|----------------------------|---------------------------|
| EN 1863-1:2012          | 70 N/mm <sup>2</sup> (FB)  | 45 N/mm <sup>2</sup> (FB) |
| EN 12150-1:2015         | 120 N/mm <sup>2</sup> (FB) | 75 N/mm <sup>2</sup> (FB) |
| EN 14179-1:2016         | 120 N/mm <sup>2</sup> (FB) | 75 N/mm <sup>2</sup> (FB) |
| Glass thickness 4÷12 mm | 40 TT (FR)                 | 40 TT (FR)                |
| 5 mm                    | 30 TT (FR)                 | 30 TT (FR)                |

Table 2 Minimum value of Bending Strength and number of fragments for TT

different. Therefore in case of HS glass the only indication of Conformity (C) or not (NC) has been considered to evaluate the minimum SC necessary to get it. In case of TT glass the number of particles have been considered according the count procedure of Annex C [3]. All the specimens were grouped as reported in tables 3 and 4, where the number of available tested specimens are reported for the two correlations.

EN Standards define B1 as coated glass with  $0.89 \geq \epsilon > 0.25$ . In this range a wide set of products exists and the heat treatment differs

greatly from glass to glass. For this reason the authors divided in B1 ( $\epsilon = 0.89$ ) and B1\_bis ( $0.89 > \epsilon > 0.25$ ), but also B1\_bis  $\epsilon$  range is too large.

Data are representative of thermally treated glass production in Italy, with some sampling from other European producers.

As data refers to different producers, it means the tempering process differs for ovens and their technology of heating and convention, as for tempering recipes related to glass thickness and type.

| Thickness (mm)-HS                | 4   |    | 5   |    | 6   |    | 8   |    | 10  |    | 12  |    | 15  |    | Total |     |
|----------------------------------|-----|----|-----|----|-----|----|-----|----|-----|----|-----|----|-----|----|-------|-----|
|                                  | C   | NC | C     | NC  |
| Float                            | 35  | 5  | 68  | 3  | 134 | 6  | 129 | 21 | 106 | 26 | 45  | 10 | --  | -- | 517   | 71  |
| B1: $\epsilon=0.89$              | --  | -- | 5   | 0  | 10  | 15 | 5   | 5  | 5   | 0  | 5   | 0  | --  | -- | 30    | 20  |
| B1_bis: $0.25 < \epsilon < 0.89$ | --  | -- | --  | -- | 5   | 0  | 5   | 0  | 5   | 5  | 5   | 0  | --  | -- | 20    | 5   |
| B2: $0.1 < \epsilon \leq 0.25$   | --  | -- | --  | -- | 20  | 0  | 5   | 0  | --  | -- | 0   | 5  | --  | -- | 25    | 5   |
| B3: $\epsilon \leq 0.1$          | --  | -- | 15  | 0  | 25  | 5  | 15  | 5  | 23  | 10 | 0   | 5  | --  | -- | 78    | 25  |
| Enamelled                        | --  | -- | 10  | 0  | 8   | 0  | 3   | 0  | 5   | 10 | --  | -- | --  | -- | 26    | 10  |
| Thickness (mm)-TT                | 4   |    | 5   |    | 6   |    | 8   |    | 10  |    | 12  |    | 15  |    | Total |     |
|                                  | C   | NC | C     | NC  |
| Float                            | 248 | 27 | 252 | 19 | 283 | 15 | 286 | 19 | 310 | 55 | 227 | 38 | 104 | 10 | 1710  | 183 |
| B1: $\epsilon=0.89$              | 30  | 0  | 20  | 0  | 95  | 0  | 65  | 0  | 30  | 0  | --  | -- | --  | -- | 240   | 0   |
| B1_bis: $0.25 < \epsilon < 0.89$ | 20  | 0  | 5   | 0  | 53  | 7  | 56  | 9  | 60  | 5  | --  | -  | --  | -- | 194   | 21  |
| B2: $0.1 < \epsilon \leq 0.25$   | 37  | 3  | 10  | 0  | 55  | 0  | 30  | 0  | 15  | 0  | 10  | 0  | --  | -- | 157   | 3   |
| B3: $\epsilon \leq 0.1$          | 99  | 12 | 25  | 0  | 92  | 13 | 136 | 14 | 85  | 10 | 13  | 2  | --  | -- | 450   | 51  |
| Enamelled                        | 30  | 0  | 14  | 0  | 15  | 0  | 7   | 3  | 25  | 0  | 5   | 0  | --  | -- | 96    | 3   |

Table 3. Number of specimens for SC vs FR

| Thickness (mm)-HS            | 4   |    | 5   |    | 6   |    | 8   |    | 10  |    | 12  |    | 15 |    | Total |    |
|------------------------------|-----|----|-----|----|-----|----|-----|----|-----|----|-----|----|----|----|-------|----|
|                              | C   | NC | C  | NC | C     | NC |
| Float                        | 19  | 0  | 57  | 0  | 102 | 0  | 87  | 0  | 83  | 0  | 31  | 2  | -- | -- | 379   | 2  |
| B1: $\epsilon=0.89$          | --  | -- | 3   | 0  | 8   | 0  | 5   | 0  | 3   | 0  | 3   | 0  | -- | -- | 21    | 0  |
| B1_bis: $0.25<\epsilon<0.89$ | --  | -- | --  | -- | 4   | 0  | 4   | 0  | 4   | 0  | 4   | 0  | -- | -- | 16    | 0  |
| B2: $0.1<\epsilon\leq 0.25$  | --  | -- | 13  | 0  | 24  | 0  | --  | -- | --  | -- | --  | -- | -- | -- | 37    | 0  |
| B3: $\epsilon\leq 0.1$       | --  | -- | 11  | 9  | 40  | 0  | 53  | 0  | 31  | -  | 2   | 0  | -- | -- | 137   | 9  |
| Enamelled                    | --  | -- | --  | -- | --  | -- | --  | -- | 17  | 0  | --  | -- | -- | -- | 17    | 0  |
| Thickness (mm)-TT            | 4   |    | 5   |    | 6   |    | 8   |    | 10  |    | 12  |    | 15 |    | Total |    |
|                              | C   | NC | C   | NC | C   | NC | C   | C  | C   | NC | C   | NC | C  | NC | C     | NC |
| Float                        | 119 | 0  | 140 | 1  | 162 | 1  | 146 | 2  | 221 | 1  | 145 | 2  | 82 | 0  | 1015  | 7  |
| B1: $\epsilon=0.89$          | 21  | 3  | 15  | 0  | 82  | 0  | 66  | 0  | 20  | 0  | --  | -- | -- | -- | 204   | 3  |
| B1_bis: $0.25<\epsilon<0.89$ | 15  | 0  | 4   | 0  | 33  | 1  | 40  | 0  | 52  | 0  | --  | -- | -- | -- | 144   | 1  |
| B2: $0.1<\epsilon\leq 0.25$  | 25  | 0  | 7   | 0  | 51  | 0  | 20  | 1  | 11  | 0  | 8   | 0  | -- | -- | 122   | 1  |
| B3: $\epsilon\leq 0.1$       | 81  | 0  | 25  | 0  | 90  | 1  | 126 | 4  | 95  | 1  | 23  | 5  | -- | -- | 440   | 11 |
| Enamelled                    | 70  | 5  | 30  | 0  | 24  | 0  | 4   | 0  | 50  | 4  | 7   | 0  | -- | -- | 188   | 9  |

Note: The FB specimens are lesser because, if the sampling did not pass FR, the test was stopped. For this reason the NC specimens are also limited.

Table 4. Number of specimens for SC vs FB

| Producer | Glass Type           | Tensile side | SC (MPa) |          | FB (N/mm <sup>2</sup> ) |          |
|----------|----------------------|--------------|----------|----------|-------------------------|----------|
|          |                      |              | Mean     | Dev. St. | Mean                    | Dev. St. |
| A        | 10 mm Clear Float TT | no roller    | 107.0    | 6.8      | 194.4                   | 23.8     |
|          |                      | roller       | 106.0    | 7.4      | 138.2                   | 8.3      |
| B        | 10 mm Clear Float TT | no roller    | 105.5    | 1.9      | 202.0                   | 26.8     |
|          |                      | roller       | 104.6    | 2.2      | 165.0                   | 18.1     |
|          | 10 mm Clear Float HS | no roller    | 43.7     | 2.4      | 129.8                   | 11.9     |
|          |                      | roller       | 43.8     | 0.9      | 81.7                    | 10.1     |

Table 5. Data of float glass

Another aspect concerns the rollers influence on glass bending strength. It is well known the influence of "tin" and "air" side referred to float glass due to the rollers effect during the annealing phase. Sometime this effect is also amplified when the "tin" side is placed in contact with tempering rollers and the process is not well controlled. The authors carried out specific tests on some producer plans to evaluated the roller effect both for float (Tab. 5) and enamelled glass panes concerning the bending strength.

In these two very extremely cases tempering roller effect is clearly evident. The SC values are equal inside the same sampling but the bending strength differs between "roller" and "no roller" side, independently from the "air" or "tin" side. In general the decrement of bending strength is coupled by a decrement of standard deviation: defects, introduced by the roller, reduce data dispersion. The correlations of this paper (see tables 9-11) will be also affected by this effect.

The enamelling process weakens the glass surface and this aspect is well known,

whereby the Standards define lower value of characteristic bending strength for enamelled glass, as reported in table 2. Usually the paint is applied on the "air" side and then the glass is processed bonding the paint to the glass surface. In this way the "tin" side is in contact with rollers. The enamelling process reduces the bending strength and the value dispersion too.

### Fragmentation vs Surface Compression

All the data of specimens (from 4 mm to 15 mm glass thickness) with recorded surface compressive stress and particles number were considered and the minimum acceptable value of SC to get the conformity was recorded and reported in table 6 in function of glass thickness and type for TT but with a certain degree of NC incidence. The data are plotted in figure 1 (float glass), 2a, b, c, d (coated glass), and 3 (enamelled glass).

The authors proposed in the previous paper a safety limit value of 90 MPa, independently

from glass thickness, considering only float glass. This value should be confirmed by the increment of test data for float, B1 and B2. It may be revised considering the coated b1\_bis, B3 and enamelled glass, which request higher SC to reach conformity; for these the value should be increased to 95 MPa (Tab. 7). Also at this limit values some specimens have high SC but they are not conform (see % incidence), especially for B3, where 100 MPa will reduce the NC incidence. The reason could be that the SC is measured at tin side and the SC should be not homogeneous along the glass thickness, giving NC fragmentation pattern.

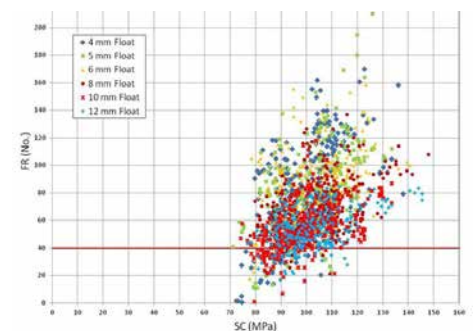


Figure 1. Correlation of surface compressive stress (SC) versus fragmentation (FR) for float glass

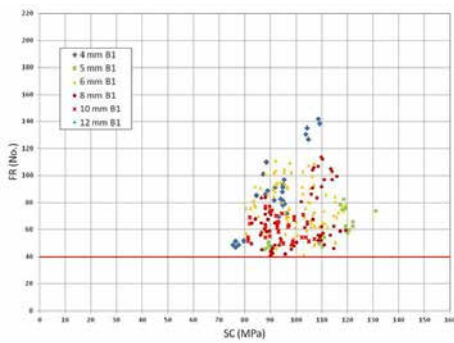


Figure 2a. Correlation of surface compressive stress (SC) versus fragmentation (FR) for B1 coated glass

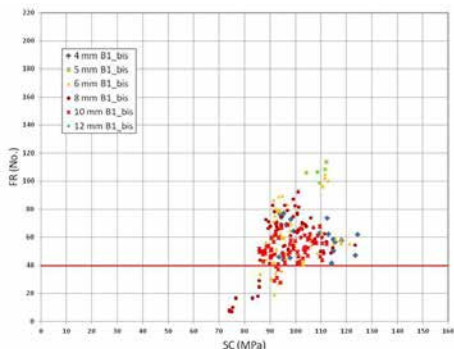


Figure 2b. Correlation of surface compressive stress (SC) versus fragmentation (FR) for B1\_bis coated glass

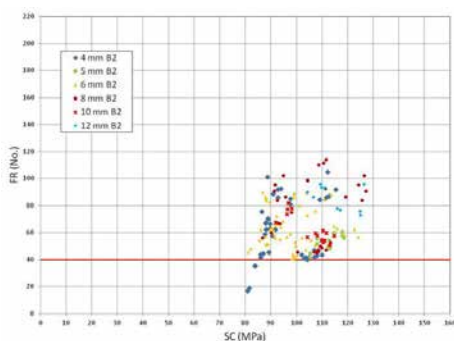


Figure 2c. Correlation of surface compressive stress (SC) versus fragmentation (FR) for B2 coated glass

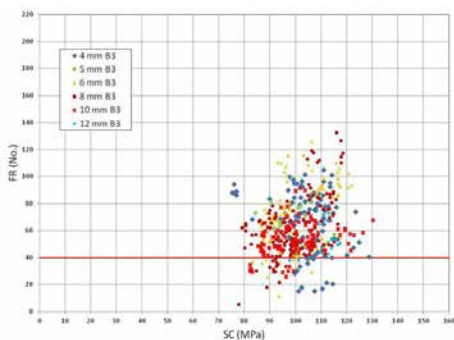


Figure 2d. Correlation of surface compressive stress (SC) versus fragmentation (FR) for B3 coated glass

|                                  | 4 mm    | 5 mm   | 6 mm    | 8 mm   | 10 mm   | 12 mm   | 15 mm   |
|----------------------------------|---------|--------|---------|--------|---------|---------|---------|
| Float                            | 80(7%)  | 80(6%) | 80(4%)  | 80(6%) | 80(14%) | 80(14%) | 80 (1%) |
| B1: $\epsilon=0.89$              | 75      | 88     | 81      | 83     | 81      | --      | --      |
| B1_bis: $0.25 < \epsilon < 0.89$ | 94      | --     | 87(10%) | 86     | 86(8%)  | --      | --      |
| B2: $0.1 < \epsilon < 0.25$      | 86      | --     | 81      | 87     | 92      | 104     | --      |
| B3: $\epsilon < 0.1$             | 99(11%) | 85     | 86(11%) | 79(9%) | 86(5%)  | 108     | --      |
| Enamelled                        | 96      | 97     | 97      | 91     | 96      | --      | --      |

Note: (%) incidence value of data in the limit SCvalue but NC to FR.

Table 6. Minimum value SC (MPa) vs conform FR for TT in SSV specimens

|                                  | Limit value SC | 4 mm | 5 mm | 6 mm | 8 mm | 10 mm | 12 mm | 15 mm |
|----------------------------------|----------------|------|------|------|------|-------|-------|-------|
| Float                            | 90             | 2    | 3    | 2    | 3    | 6     | 11    | 0     |
| B1: $\epsilon=0.89$              | 90             | 0    | 0    | 0    | 0    | 0     | --    | --    |
| B1_bis: $0.25 < \epsilon < 0.89$ | 95             | 0    | --   | 0    | 0    | 0     | --    | --    |
| B2: $0.1 < \epsilon < 0.25$      | 90             | 0    | --   | 0    | 0    | 0     | 0     | --    |
| B3: $\epsilon < 0.1$             | 95             | 11   | 0    | 6    | 1    | 4     | 13    | --    |
| Enamelled                        | 95             | 0    | 0    | 0    | 0    | 0     | --    | --    |

Table 7. Incidence value (%) of NC data for SC (MPa) vs FR in TT with the proposed SC value



Figure 3. Correlation of surface compressive stress (SC) versus fragmentation (FR) for enamelled glass

|                                  | 4 mm | 5 mm | 6 mm | 8 mm | 10 mm | 12 mm | 15 mm |
|----------------------------------|------|------|------|------|-------|-------|-------|
| Float                            | 67   | 65   | 62   | 63   | 58    | 60    | --    |
| B1: $\epsilon=0.89$              | --   | 60   | 51   | 56   | --    | --    | --    |
| B1_bis: $0.25 < \epsilon < 0.89$ | --   | --   | --   | --   | --    | --    | --    |
| B2: $0.1 < \epsilon \leq 0.25$   | --   | --   | 63   | --   | --    | --    | --    |
| B3: $\epsilon \leq 0.1$          | --   | 56   | 64   | 55   | 52    | --    | --    |
| Enamelled                        | --   | 61   | 71   | --   | 50    | --    | --    |

Table 8. Maximum value SC (MPa) vs conform FR for HS in SSV specimens

|                                  | 4 mm | 5 mm   | 6 mm | 8 mm | 10 mm | 12 mm   | 15 mm |
|----------------------------------|------|--------|------|------|-------|---------|-------|
| Float                            | 37   | 38     | 31   | 35   | 34    | 34[6%*] | --    |
| B1: $\epsilon=0.89$              | --   | --     | 48   | --   | --    | --      | --    |
| B1_bis: $0.25 < \epsilon < 0.89$ | --   | --     | 42   | --   | --    | --      | --    |
| B2: $0.1 < \epsilon \leq 0.25$   | --   | --     | 30   | --   | --    | --      | --    |
| B3: $\epsilon \leq 0.1$          | --   | 31     | 32   | 45   | 37    | --      | --    |
| Enamelled                        | --   | 50[5%] | --   | --   | 42    | --      | --    |

Note: (%) incidence value of data in the limit value but NC to FB.

\* Sampling with high SC but with "roller effect"

Table 9. Minimum value SC (MPa) vs conform FB for HS in SSV specimens

|                                  | 4 mm | 5 mm    | 6 mm   | 8 mm   | 10 mm   | 12 mm   | 15 mm |
|----------------------------------|------|---------|--------|--------|---------|---------|-------|
| Float                            | 81   | 79(<1%) | 79     | 83(1%) | 79(<1%) | 82(1%)  | 85    |
| B1: $\epsilon=0.89$              | 83   | 87      | 81     | 85     | 82      | --      | --    |
| B1_bis: $0.25 < \epsilon < 0.89$ | 88   | --      | 91[3%] | 87     | 86      | --      | --    |
| B2: $0.1 < \epsilon \leq 0.25$   | 87   | --      | 82     | 86(9%) | --      | --      | --    |
| B3: $\epsilon \leq 0.1$          | 78   | 88      | 85(1%) | 81(2%) | 82(1%)  | 99(18%) | --    |
| Enamelled                        | 94   | 94      | 95     | --     | 91[4%]  | --      | --    |

Note: (%) incidence value of data in the limit value but NC to FR.

Table 10. Minimum value SC (MPa) vs conform FB for TT in SSV specimens

In table 8 the data for HS are reported, considering conform and not specimens.

### Flexural Bending Strength vs Surface Compression

The data of specimens with SC and FB measurement were considered. All the glass thickness and side in tension were considered (tin, air, coated, un-coated, enamelled) although the SC is measured only at "tin" side, "un-coated" and "un-enamelled" side. Moreover the data were not segregated, considering specimens with both central and edge fracture origin.

All the data of specimens (from 4 mm to 15 mm glass thickness) with recorded SC and FB were considered and the values of SC were recorded and reported in table 9 for heat strengthened glass and table 10 for thermally toughened, in function of glass thickness and type.

In diagrams of figure 4, 5a, b, c, d and 6 the testing value are plotted, showing clearly the type of glass that were tested: heat strengthened and thermally toughened safety glass.

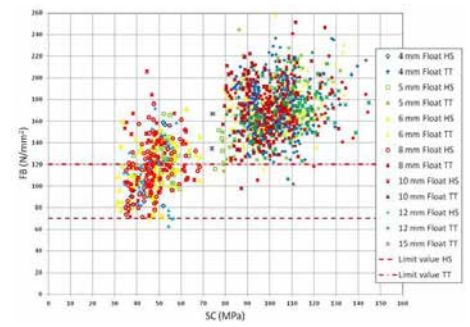


Figure 4. Correlation of surface compressive stress (SC) versus flexural bending (FB) for float glass.

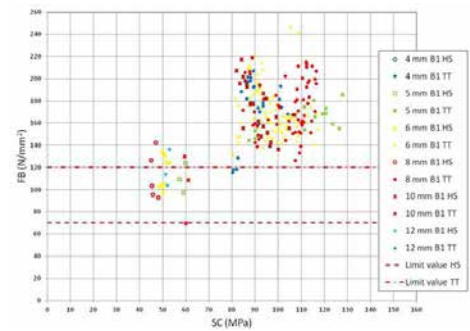


Figure 5a. Correlation of surface compressive stress (SC) versus flexural bending (FB) for B1 coated glass.

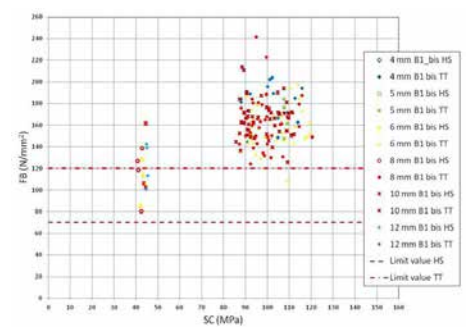


Figure 5b. Correlation of surface compressive stress (SC) versus flexural bending (FB) for B1 bis coated glass.

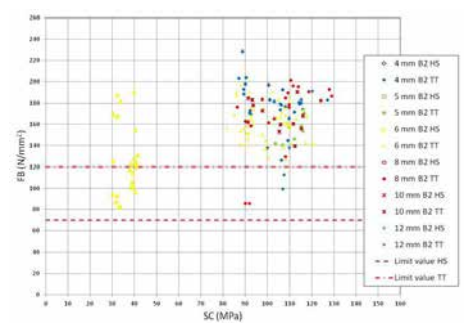


Figure 5c. Correlation of surface compressive stress (SC) versus flexural bending (FB) for B2 coated glass.

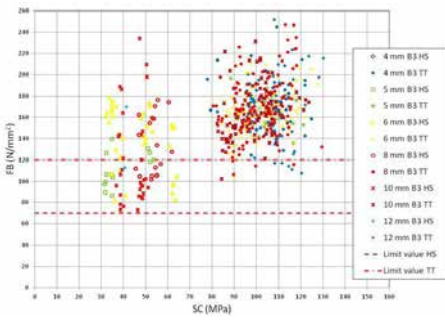


Figure 5d. Correlation of surface compressive stress (SC) versus flexural bending (FB) for B3 coated glass.

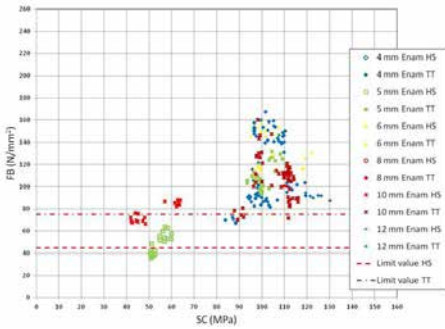


Figure 6. Correlation of surface compressive stress (SC) versus flexural bending (FB) for enamelled glass.

The limit value of SC that has to be reached to respect the characteristic strength value of thermally toughened (TT) safety glass can be confirmed to be 85 MPa for float glass and 90 MPa for coated glass; in case of enamelled glass this value should be increased to no less than 95 MPa (Tab. 11).

In the case of heat strengthened glass (HS), the SC value of 35 MPa for float glass can be confirmed. For coated glass the minimum founded SC value was between 30-50 MPa, whereas for enamelled glass it is 45 MPa (Tab. 12). Some specimens are not conform although the SC is high. As for the SC vs Fragmentation, this is due more to roller effect than non uniformity of SC along the glass thickness.

### Conclusions

The elaborated data goes across many years of laboratory tests on different type of glass (heat strengthened and thermally toughened safety, coated and uncoated as enamelled) provided by different producers in Italy and in Europe. The correlations between SC and FR or FB is accepted at Standard level (see ISO Standard) and it is useful during FPC (Factory Production Control) to evaluate the quality of process by a non destructive procedure. This procedure

|                              | Limit value SC | 4 mm | 5 mm | 6 mm | 8 mm | 10 mm | 12 mm | 15 mm |
|------------------------------|----------------|------|------|------|------|-------|-------|-------|
| Float                        | 85             | 0    | 0    | <1   | <1   | <1    | 1     | 0     |
| B1: $\epsilon=0.89$          | 90             | 0    | 0    | 0    | 0    | 0     | 0     | --    |
| B1_bis: $0.25<\epsilon<0.89$ | 90             | 0    | --   | 3    | 0    | 0     | 0     | --    |
| B2: $0.1<\epsilon\leq 0.25$  | 90             | 0    | --   | 0    | 9    | --    | --    | --    |
| B3: $\epsilon\leq 0.1$       | 90             | 0    | 0    | 1    | 1    | 0     | 17*   | --    |
| Enamelled                    | 95             | 0    | 0    | 0    | --   | 1     | --    | --    |

Note: \* Sampling with high SC but with "roller effect"

Table 11. Incidence value (%) of NC data for SC (MPa) vs FB in TT with the proposed SC value

| Glass Type                   | FR_HS       | FB_HS       | FR_TT       | FB_TT       |
|------------------------------|-------------|-------------|-------------|-------------|
|                              | Upper bound | Lower bound | Lower bound | Lower bound |
| Float                        | 60          | 35          | 90          | 85          |
| B1: $\epsilon=0.89$          | 55          | 50          | 90          | 90          |
| B1_bis: $0.25<\epsilon<0.89$ | 45          | 40          | 95          | 90          |
| B2: $0.1<\epsilon\leq 0.25$  | 55          | 30          | 90          | 90          |
| B3: $\epsilon\leq 0.1$       | 60          | 40          | 95          | 90          |
| Enamelled                    | 60          | 45          | 95          | 95          |

Table 12. SC value (MPa) respect FR and FB found in SSV testing

was defined as the measurements of surface compressive stress on tin side, as prescribed by EN 12150-2:2004 [22] for thermally toughened safety glass, EN 14179-2:2005 [23] for HST glass and EN 1863-2:2004 [24] for heat strengthened glass. The value has to be correlated to fragmentation density (for TT) and to flexural strength (for HS and TT). The not conform specimens were considered too, because they could occur in production and must be detected in the procedure.

The limit value of SC proposed by the authors based on their experimental data are reported in table 12.

### References

[1] EN 1288-3:2000, Glass in building - Determination of the bending strength of glass - Part 3: Test with specimen supported at two points (four point bending).  
 [2] EN 1863-1:2004, Glass in building - Heat strengthened soda lime silicate glass - Part 1: Definition and description.  
 [3] EN 12150-1:2015, Glass in building - Thermally toughened soda lime silicate safety glass - Part 1: Definition and description.  
 [4] EN 14179-1:2016, Glass in building - Heat soaked thermally toughened soda lime silicate safety glass - Part 1: Definition and description.  
 [5] ASTM C1279:2013, Standard Test Method for Non-Destructive Photoelastic Measurement of Edge and

Surface Stresses in Annealed, Heat-Strengthened, and Fully Tempered Flat Glass.  
 [6] Schiavonato M., Mognato E., Redner A.S., Stress measurement, fragmentation and mechanical strength, GPD, 2005.  
 [7] Mognato E., Barbieri A., Schiavonato M., Pace M., Thermally toughened safety glass: correlation between flexural strength, fragmentation and surface compressive stress, GPD, 2011, pp. 115-118.  
 [8] Hreglich S., Riduzione della resistenza meccanica del vetro sottoposto a processi di decorazione della sua superficie, Rivista della Stazione Sperimentale del Vetro, Vol. 5, 2008, pp. 7-10.  
 [9] UNI 11666:2017, Vetro per edilizia - Vetro verniciato per uso esterno - Requisiti estetici, di durabilità, meccanici e metodi di prova.  
 [10] Redner A.S., Mognato E., Schiavonato M., Correlation between strength and measured residual stress in tempered glass products, J. of ASTM Int., Vol. 2, No. 3, 2005.  
 [11] Redner A.S., On-line measurement of stresses and optical distortion of QC of tempered glass, GPD, 2003, pp. 388-390.  
 [12] Redner A.S., Automated measurement of edge stress in automotive glass, GPD, 2003, pp. 578-579.  
 [13] Feingold J. M. and Redner A.S., New PC-based scanners improve quality and productivity for glass fabricators, Int. Glass Review, Issue 1, 2003, pp. 63-66.  
 [14] Redner A.S., Hoffman B.R., Measuring stresses and optical distortion for QC of automotive glass, GPD, 1997, pp. 385-389.  
 [15] Redner A.S., Hoffman B.R., Detection of tensile stresses near edges of laminated and tempered glass, GPD, 2001, pp. 589-591.

- [16] Redner A.S., Bhat G.K., Precision of surface stress measurement test methods and their correlation to properties, GPD, 1999, pp. 169-171.
- [17] Anton J., Errapart A., Paemurru M., Lochegnies D., Hödemann S., Aben H., On the inhomogeneity of residual stresses in tempered glass panels, GPD, 2011, pp. 119-121.
- [18] Aben H., Anton J., Paemurru M., Öis M., A new method for tempering stress measurement in glass panels, GPD, 2013, pp. 216-217.
- [19] ASTM C1048 - 2012e1 Standard Specification for Heat-Strengthened and Fully Tempered Flat Glass
- [20] ISO/DIS 22509 rev.:2016 Glass in building - Heat strengthened soda lime silicate glass - Definition and description
- [21] ISO/FDIS 12540:2016 Glass in building - Tempered soda lime silicate safety glass
- [22] EN 12150-2:2005, Glass in building - Thermally toughened soda lime silicate safety glass - Part 2: Evaluation of conformity/Product standard.
- [23] EN 14179-2:2005, Glass in building - Heat soaked thermally toughened soda lime silicate safety glass - Part 2: Evaluation of conformity/Product standard.
- [24] EN 1863-2:2004, Glass in building - Heat strengthened soda lime silicate glass - Part 2: Evaluation of conformity/Product standard.

# ASTM E1300 Uniform Load Strength Reduction Factor not Required for Ceramic Enameled Glass

W. Lynn Beason, Ph.D., P.E. Michael S. Brackin, Ph.D., P.E. A. William Lingnell, P.E.

Beason Brackin & Associates, LLC Beason Brackin & Associates, LLC Lingnell Consulting Services

## Keywords

1=Glass 2=Ceramic Enameled Glass  
3=ASTM E1300 4=heat-strengthened 5=frit

## Abstract

Results of highly publicized testing have shown that in some cases, the mean strength of freshly manufactured enameled glass is less than the mean strength of analogous uncoated glass [1,2,3,4]. Therefore, it has been proposed by some [1,4] that a strength reduction factor be incorporated into ASTM E1300 "Standard Practice for Determining Load Resistance of Glass in Buildings" [5] for the design of enameled glass. Test results presented herein show that while the mean strength of freshly manufactured enameled glass appears to be reduced, the coefficient of variation is also significantly reduced. It is shown herein that the reduction in the coefficient of variation coupled with the fact that ASTM E1300 is based on the reduced strength of in-service glass combine to compensate for the apparent reduction of the mean strength of freshly manufactured enameled glass. These results show that there is no need to incorporate an enamel glass strength reduction factor in ASTM E1300 for the heat-strengthened glass examined. The behavior of enameled glass is complicated and it will require a substantial amount of additional research before changes to ASTM E1300 can be justified by technical considerations.

## Introduction

Recently, the uniform load resistance of enamel coated glass plates has become a topic of interest with respect to proposed changes to ASTM E1300. Of particular interest are reports that state that the breaking strength of enamel coated glass is reduced when compared to uncoated, freshly manufactured glass of the same type [1,2,3,4]. While it is clearly stated in the text of ASTM E1300 that the glass thickness selection criteria presented are referenced to the strength of in-service glass

and not the strength of freshly manufactured glass [5], there may be implications for the use of ASTM E1300 for the design of enamel coated glass plates. This controversy has largely been confined to enamel coated heat-strengthened (HS) glass.

Much of the controversy that has developed regarding the use of ASTM E1300 to specify the uniform load resistance of enamel coated glass is apparently the result of a lack of understanding that the glass thickness selection charts presented in ASTM E1300 are based on the performance of in-service glass and not freshly manufactured glass. Results of in-service glass strength tests conducted by Beason [6] showed that the strength of in-service glass is significantly less than freshly manufactured glass. Since this initial testing by Beason, additional testing has confirmed that the strength of in-service glass is in fact significantly less than that of freshly manufactured glass [7]. The in-service strength reduction has been reported to be as much as 50% when compared to freshly manufactured glass [7,8].

The fact that the strength of in-service glass is significantly less than that of freshly manufactured glass was one of the primary drivers for the original development of ASTM E1300. It is clearly stated in the Significance and Use section of ASTM E1300 that use of the practice assumes that "the surface condition of the glass is typical of glass that has been in service for several years, and is weaker than freshly manufactured glass due to minor abrasions on exposed surfaces" [5]. Therefore, if the applicability of ASTM E1300 to enamel coated glass is to be challenged, it must be on the basis of a comparison of the strength of enamel coated glass to the in-service strength of uncoated glass, as defined in ASTM E1300, and not the freshly manufactured strength of uncoated glass.

As stated above, most of the current controversy regarding the strength of ceramic enamel coated glass is focused on the performance of HS enamel coated glass. Therefore, it is important to have a clear understanding of the ASTM E1300 treatment of HS glass. Throughout most of the 20th century, glass thickness selection criteria presented in the United States incorporated a strength factor of 2.0 for HS glass. It was well understood in the glass design community

at the time that the 2.0 HS strength factor was based on linear stress analyses and the conservative assumption that the level of residual surface compression for heat-strengthened glass would meet the minimum required value of 3,500 psi.

At the time that ASTM E1300 incorporated glass thickness procedures for HS glass, full discussions and debates were conducted within ASTM to determine the best way to accomplish this. As a part of these discussions, results of research conducted by Beason were considered [9]. These results included glass thickness selection charts corresponding to in-service glass with minimum residual surface compressions of 3,500 psi. It was shown that the well-established HS strength factor of 2.0 provides a solid lower bound across the full range of glass sizes presented in ASTM E1300 [9]. Further, it was shown that for many glass geometries, a much higher HS strength factor could be justified [9]. This coupled with the fact that virtually all HS glass is fabricated with residual surface compressions that are significantly greater than the required minimum of 3,500 psi leads to the unavoidable conclusion that the ASTM E1300 treatment of HS glass is very conservative from a strength point-of-view. This fact was fully understood by those involved with the inclusion of HS glass in ASTM E1300. When statistical inferences are being made regarding the probability of breakage (POB) of glass, the two most important factors are central tendency and dispersion. Central tendency is usually quantified with the mean and dispersion is associated with the standard deviation. Of particular importance, in historic glass design procedures, is the ratio of the standard deviation to the mean. This statistic is usually termed the Coefficient of Variation (COV) and it tends to remain relatively constant for a particular type of glass, regardless of the geometries tested. Historically, glass designers conservatively assumed that the COV for annealed (AN) and HS glass are on the order of 20-25% and 15%, respectively [10]. The design strength associated with a specified POB reduces as the mean of the strength data reduces, and the design strength for a specified POB increases as the COV decreases. The glass thickness selection criteria presented in ASTM E1300 is based on the Glass Failure Prediction Model (GFPM) developed by Beason [11]. It is often erroneously assumed

that the GFPM is nothing more than the application of the well-known two parameter Weibull probability distribution function [12] as an alternative to the normal distribution function that was widely used in historic glass design procedures throughout the United States. However, the GFPM is actually based upon a relatively obscure statistical failure theory for brittle materials that was also developed by Weibull [13].

The GFPM incorporates two parameters,  $m$  and  $k$ , that represent the distribution and severity of flaws across the surface of a glass plate. It must be emphasized that these two parameters represent the occurrence and severity of surface flaws [11] and are not an inherent material property of glass that can be determined by testing small glass specimens in a controlled laboratory setting.

It can be shown that the  $m$  surface flaw parameter corresponds more directly to the COV, while the  $k$  surface flaw parameter corresponds more directly to the mean [14]. At the time that ASTM E1300 was introduced, the value of the  $m$  surface flaw parameter was set to 7 to reflect the historic understanding of the COV that was typically used for the design of AN glass and the value of  $k$  was adjusted to reflect the in-service reduction in mean strength [14]. As stated above, these surface flaw parameters represent the severity and distribution of surface flaws and not the type of glass. Since there is little scientific reason to believe that HS glass attracts a different type of in-service surface damage than AN glass, it seems logical to assume that there would be no distinction between the populations of surface flaws associated with in-service AN and in-service HS glass. Therefore, it is reasonable to use the in-service surface flaw parameters developed for AN glass to model HS glass provided that the residual surface compression is properly dealt with. If the GFPM is properly extended to the treatment of HS glass, it can be shown that the associated COV for HS glass reduces as the level of residual surface compression increases in a manner that is consistent with the historical design understandings discussed above.

The surface flaw parameters that are incorporated into ASTM E1300 are representative of the character and distribution of surface flaws that were selected in the ASTM consensus process to be typical of in-service exposures [14]. The exact values selected were not the result of a curve fit to a particular set of data. Rather, the ASTM E1300 surface flaw parameters reflected the central tendency and dispersion of a wide group of data developed by industry and public interest groups combined with the collective judgment of those involved in the ASTM consensus process [14]. It is well known now, and at the time that ASTM E1300

was introduced, that if freshly manufactured glass is tested and analyzed for the best-fit surface flaw parameters, the values would be significantly different than those used in ASTM E1300. This notwithstanding, the ASTM E1300 surface flaw parameters were fully discussed and established through the ASTM consensus process and provide a demonstrably conservative set of glass thickness recommendations that retain strong continuity with the United States historical glass design process [14].

As discussed above, there are multiple levels of conservatism built into ASTM E1300 with regard to the treatment of HS glass. The inherent conservatisms built into ASTM E1300 with respect to HS glass makes it highly unlikely that enamel coated glass will have a lower design strength than that represented in ASTM E1300.

### Full-Scale Test Results of Enamel Coated Glass Plates

The most direct procedure to determine if there are problems using ASTM E1300 to select the minimum thickness of enamel coated HS glass is to test a representative sample of full-scale, enamel coated HS glass plates and compare the design load thus determined to the corresponding design load presented in ASTM E1300. Either ASTM E1300 over predicts the strength of enamel coated HS glass or it under predicts the strength of enamel coated HS glass. Any other comparison procedure involves projections and extrapolations.

The first group of data discussed herein was collected by the writers. These data were developed by subjecting two sets of 40 x 60 x 1/4 in. glass plates with four-sides of continuous support to linearly increasing uniform lateral loads to failure. The test setup is shown in Figure 1. One set of specimens involved uncoated HS glass and the other set of specimens involved enamel coated HS glass with average thicknesses of 0.224 and 0.226, respectively. The enamel coating on the second set of glass was a full coat across the entire surface of the glass. All of the glass specimens tested were taken from the same batch of freshly manufactured glass. The glass plates were tested with the coated side in tension.



Figure 1. Uniform Lateral Load Test Machine.

The test statistic of primary interest was the 3-second equivalent duration breakage load for each glass plate. Standard understandings of "static fatigue" were used to convert the failure strength data measured to equivalent 3-second durations [8]. Statistical analyses were used to determine the equivalent mean 3-second breakage load, the associated standard deviation and COV, and the equivalent 3-second duration failure load corresponding to a POB of 8 lites per 1,000. These analyses were performed for both the coated and the uncoated specimens. Calculation of the equivalent 3-second duration failure load corresponding to a POB of 8 lites per 1,000 was accomplished using standard normal distribution assumptions. In addition, the residual surface compression was measured for each specimen. These data are presented in Table 1 [12].

|   | Uncoated Clear | Enamel Coated |
|---|----------------|---------------|
| Mean Residual Surface Compression (psi)   | 6086           | 6128          |
| Mean 3-second Duration Breakage Load (psf)  | 501            | 288           |
| Standard Deviation of 3-second Duration Breakage Load (psf)                         | 40.4           | 8.4           |
| Coefficient of Variation of 3-second Duration Breakage Load (%)                     | 8.1            | 2.9           |
| Sample Size   | 10             | 10            |
| 3-second Duration Load Corresponding to 8 lites per 1,000 Failure Probability (psi) | 403            | 268           |
| Ratio of Measured Design Pressure to ASTM E1300 Specified Load                      | 3.66           | 2.44          |

Table 1. Equivalent 3-Second Duration Breakage Load Statistics for 40 x 60 x 1/4 in. Heat Strengthened Glass Plates.

The information presented in Table 1 is extremely interesting. First, it can be observed that the mean 3-second duration equivalent failure load of the enamel coated specimens is about 43% less than that for the uncoated specimens. This strength reduction is on the order of that which has been reported for in-service glass as discussed above [7,8]. The COV of the uncoated specimens was determined to be 8.1%, while the COV for the coated specimens was determined to be 2.9%. This is a tremendous difference. As stated above, the COV for HS glass has been historically assumed to be closer to 15%

for design purposes. This means that the measured COV for enamel coated HS glass is about 5 times less than the COV that has historically been assumed for the design of uncoated HS glass. An extremely low COV tends to be an emerging characteristic of enamel coated HS glass that is supported by a wide range of testing [1,2,3,4].

As stated above, statistical techniques were used to estimate the loads corresponding to a POB of 8 lites per 1,000 assuming the data are normally distributed. It was found that the design load is 403 psf for the uncoated HS glass and 288 psf for the enamel coated glass. This means that the design load for the enamel coated HS glass is about 29% less than that for the uncoated glass. While this comparison is of some interest, it has no bearing on the use of ASTM E1300 for specifying the appropriate thickness of enamel coated HS glass.

If the glass thickness selection charts presented in ASTM E1300 are consulted, it is found that the in-service design load corresponding to a POB of 8 lites per 1,000 for a 40 x 60 x 1/4 in. AN glass plate is approximately 55 psf [5]. Then, if a factor of 2.0 is applied to this value, as directed for HS glass, it can be determined that the ASTM E1300 design load for a 40 x 60 x 1/4 in. HS glass plate is 110 psf [5]. If this information is combined with the data presented in Table 1, it can be shown that the measured design load for uncoated, 40 x 60 x 1/4 in. HS glass is about 3.7 times greater than is required by ASTM E1300. This is the case because of the inherent conservatism discussed above. In addition, it can be seen that while the enamel coated HS glass is weaker than freshly manufactured clear HS glass, it is still more than 2.4 times greater than it has to be to comply with ASTM E1300. It is difficult to imagine how this can be considered a problem. The second group of full-scale data discussed herein involved 38 x 76 x 1/4 in. glass plates with four-sides of continuous lateral support that were subjected to an increasing lateral pressure until failure [4]. These tests involved five different sets of specimens. The first set of glass specimens was uncoated HS glass. The other four sets of glass specimens had different patterns of enamel coatings. The second set had a dot pattern that covered 40% of the surface, the third set had a line pattern that covered 50% of the surface, the fourth set had a hole pattern that covered 60% of the surface, and the fifth set had a uniform coating with 100% coverage. Complete details of the specimens and testing methods are presented elsewhere by Berger et al. [4].

Berger et al. presented processed data including the mean equivalent 3-second breakage load, the associated standard deviation and COV, the percent reduction in

strength compared to uncoated glass, and the equivalent 3-second duration failure load corresponding to a POB of 8 lites per 1,000 for both the coated and the uncoated specimens. Calculation of the equivalent 3-second duration failure loads corresponding to a POB of 8 lites per 1,000 was accomplished by Berger et al. by calculating unique m's and k's for each data set. These data are presented in Table 2. [4]

|   | Uncoated Clear | Enamel Coated Dot Pattern 40% Coverage | Enamel Coated Line Pattern 50% Coverage | Enamel Coated Hole Pattern 60% Coverage | Enamel Coated Uniform 100% Coverage |
|---|----------------|--|---|---|-------------------------------------|
| Mean Residual Surface Compression (psi)   | 6222           | 5961                                   | 5816                                    | 6135                                    | 6628                                |
| Mean 3-second Duration Breakage Load (psf)  | 424            | 292                                    | 284                                     | 276                                     | 219                                 |
| Standard Deviation of 3-second Duration Breakage Load (psf)                         | 60.6           | 3.0                                    | 16.7                                    | 18.8                                    | 16.7                                |
| Coefficient of Variation of 3-second Duration Breakage Load (%)                     | 14.1           | 8.1                                    | 5.9                                     | 6.6                                     | 7.6                                 |
| Sample Size   | 26             | 27                                     | 27                                      | 26                                      | 27                                  |
| Percent Strength Reduction Compared to Clear Glass (%)                              | --             | 31                                     | 33                                      | 35                                      | 48.3                                |
| 3-second Duration Load Corresponding to 8 lites per 1,000 Failure Probability (psf) | 272            | 215                                    | 228                                     | 213                                     | 169                                 |
| Ratio of Measured Design Load to ASTM E1300 Specified Design Load                   | 3.25           | 2.58                                   | 2.73                                    | 2.55                                    | 2.02                                |

Table 2. Equivalent 3-Second Duration Breakage Load Statistics for 38 x 76 x 1/4 in. HS Glass Plates. [4]

If the glass thickness selection charts presented in ASTM E1300 are consulted, it is found that the in-service design load corresponding to a POB of 8 lites per 1,000 for a 38 x 76 x 1/4 in. AN glass plate is approximately 41.8 psf [5]. Then, if a factor of 2.0 is applied to this value, as directed for HS glass, it can be determined that the ASTM E1300 design load for a 38 x 76 x 1/4 in. HS plate is approximately 83.6 psf [5]. This means that the design load for the 38 x 76 x 1/4 in. uncoated HS glass is about 3.25 times greater than is required by ASTM E1300. In addition, it can be seen that while the enamel coated HS glass specimens are weaker than freshly manufactured, uncoated glass, the ratios of the reported design loads of the enamel coated HS glass specimens compared to that required by ASTM E1300 range from 2.02 to 2.58. Therefore, in the worst case situation, the enamel coated HS glass is more than 2.0 times stronger than it has to be to comply with the requirements of ASTM E1300. Again, it is difficult to imagine how this can be considered to be a problem.

## Conclusions

Presented above are the results of full-scale testing performed on two independent groups of enamel coated HS glass plates to evaluate their load resistance and compare these results to information presented in ASTM E1300. This testing involved one group of specimens tested by the writers, and one group of specimens tested by Berger et al. [4]. All glass tested was freshly manufactured HS glass. For both groups of glass plates tested, it was determined that the mean strengths of freshly manufactured enamel coated HS glass range from 29% to 48.3% less than the analogous mean strength of uncoated HS glass.

All glass design procedures in common use in the United States since the middle of the last century have incorporated central tendency and dispersion into the process to estimate either design stresses or design loads to meet a specified POB. In general the design strength corresponding to a specified POB, such as 8 lites per 1,000, is

directly proportional to the mean strength and inversely proportional to the COV of the strength data. Thus, as the mean strength decreases, the design strength decreases, and as the COV decreases, the design strength increases.

One observation that needs to be emphasized with respect to the performance of enamel coated HS glass, regardless of manufacturer or test organization, is that the attendant COV of enamel coated HS glass seems to be significantly less than is the case with uncoated HS glass and is substantially less than the COV traditionally assumed for the design of uncoated HS glass. This trend compensates to some extent for the reduction of the mean strength of enamel coated glass compared to uncoated glass.

The fundamental assumption incorporated in ASTM E1300 is that glass strength is referenced to the strength of in-service glass and not the strength of freshly manufactured glass [5]. Therefore, evaluation of the design strengths of the enamel coated glass must be made with respect to the in-service design strengths derived from ASTM E1300 and not the measured strengths of freshly manufactured glass.

Results of the full-scale plate tests presented herein shows that the measured design loads for enamel coated HS glass associated with a POB of 8 lites per 1,000 range from about 2.0 to 2.73 times greater than is required to be in compliance with ASTM E1300. Therefore, it is concluded that the types of enamel coated HS glass that were investigated by the two groups of independent researchers presented herein meet all requirements for ASTM E1300 and that a reduction factor is not warranted.

The only issue that is not addressed in the data presented herein is the effect of in-service exposures on the long-term strength of the enamel coated HS glass. Based upon the collective experience of the writers, it seems clear that the in-service strength reduction incorporated in ASTM E1300 is largely the result of the accumulation of mechanical damage over years of in-service exposure. This damage consists of scratches, pits, abrasions, etc. that occur as the result of things such as cleaning, human contact, windborne debris, etc. Further, the writers are not aware of any credible evidence that other noncontact in-service exposures such as UV exposure significantly reduce the strength of glass.

Whatever is responsible for the reduction in the mean failure strength of enamel coated glass, it is clear that once the enamel coating has been applied it provides a protective barrier over the coated surface that should make it more difficult for the glass surface to accumulate additional mechanical damage.

In addition, most enamel coated HS glass is used in spandrel applications where the coated surface is protected from in-service mechanical exposures that are believed to be the cause of the in-service strength reduction incorporated into ASTM E1300. At this time there is no credible evidence to suggest that the enamel coated glass surface will experience additional mean strength reductions with in-service exposure. Finally, before enamel coated glass plates of the type discussed herein fall out of compliance with ASTM E1300, the strength of the enamel coated HS glass would have to be reduced by another 50% as the result of in-service exposures. This does not seem realistic. Based upon information presented herein, it can be concluded, at this point, that there is no technically defensible reason to include a strength reduction factor in ASTM E1300 for the design of enamel coated HS glass that is subjected to uniform lateral pressure loads.

## References

- [1] Natividad, K., Fonseca, J.C., Erickson, B., Morse, S.M., and Norville, H.S. (2016), "Bending Tests of Heat Treated Glass with Ceramic Frit", *GlassCon Global*, pp165-172.
- [2] Maniatis, I. and Elstner, M. (2016), "Investigations on the Mechanical Strength of Enameled Glass", *Glass Struct. Eng.*, Springer, pp 277-288.
- [3] Elstner, M. and Maniatis, I. (2016), "Enameled Glass - New Research Studies *GlassCon Global*, pp 69-76.
- [4] Bergers, M., Natividad, K., Morse, S.M. et al. (2016), "Full Scale Tests of Heat Strengthened Glass with Ceramic Frit", *Glass Struct. Eng.*, Springer, pp 261-276.
- [5] ASTM Standard E1300, (2012), "Standard Practice for Determining Load Resistance of Glass in Buildings," E 1300, ASTM International, West Conshohocken, PA.
- [6] [Beason, W. L., \(1980\), "A Failure Prediction Model for Window Glass", Ph.D. Dissertation, Texas Tech University, Lubbock.](#)
- [7] Norville, S.H., and Minor, J.E., (1985), "Strength of Weathered Window Glass", *American Ceramics Society Bulletin*, Vol. 64, No. 11, pp 1467-1470.
- [8] Beason, W.L., and Lingnell, A.W., (2000), "Emerging Uses for Window Glass", *Emerging Materials for Civil Infrastructure - State of the Art*, ASCE, Reston, VA, pp 190-216.
- [9] Beason, W.L., (1993), "Development of a Failure Prediction Model for Heat-Treated Glass", Final Report submitted to Cardinal IG, W. Lynn Beason, Ph.D., P.E., Engineering Consultant, College Station, TX.
- [10] ASTM Standard E997, (1984), "Standard Test Method for Structural Performance of Glass in Exterior Windows, Curtain Walls, and Doors Under the Influence of Uniform Static Loads by Destructive Methods", E 997-84, Philadelphia, PA.
- [11] Beason, W.L. and Morgan, J.R., (1984), "Glass Failure Prediction Model", *Journal of Structural Engineering*, ASCE, Vol. 110, No. 2, pp 197-212.
- [12] Ostle, B. and Mensing, R.W. (1975), *Statistics in Research*, 3rd Edition, The Iowa State University Press, Ames, IA.
- [13] Weibull, W., (1939), "A Statistical Theory of the Strength of Materials, *Handlering NR 151*, Royal

Technical University, Stockholm.

[14] Beason, W.L. and Norville, H.S., (1989), "Development of a New Glass Thickness Selection Procedure", *Proceedings 6th U.S. National Conference on Wind Engineering*, Vol II, University of Houston, Houston, TX.

# Critical issues in glass chemical strengthening

Guglielmo Macrelli  
Isoclima SpA – R&D Department

## Keywords

1=Chemical strengthening 2=Ion Exchange  
3=Strength issues 4=Structural glazing

## Abstract

In structural glazing applications a growing attention is reserved to glass chemical strengthening by ion exchange. Superior optical quality and no limitations in thickness and shape are the most appealing characteristics of this strengthened glass product. Additionally, a significant higher level of surface compression can be introduced by the ion exchange process. Drawbacks related to consistency of strength either initially and during the product service life will be discussed. Crack initiation tendency will also be discussed in connection to glass chemical composition for both Soda Lime Silicate and Sodium Alumino Silicate glass. Processing drawbacks related to glass surface chemical attack together with effects on glass strengthening performances due to salt bath contamination will be presented.

## Introduction

In the glass science community, chemical strengthening of glass by ion exchange below glass transition temperature (herewith we will use the acronym CSG-IX) is a known subject since several decades [1]. Reviews of process fundamentals and final strength determination are available in the literature [1],[2],[3] and [4]. Examples of glazing products with CSG-IX can be found in a number of applications ranging from transportation (windscreens for aircraft cockpit, marine glazing, automotive and railway glazing), consumer electronics (displays for smartphones, tablets and TV), pharmaceutical and medical devices (ampoules and vials for injectors) and architectural special projects (self-bearing stairs, facades). A critical discussion of applications in structurally glazing has been recently presented [5] where it has been clearly indicated that final strength of CSG-IX is strongly depending from original surface quality of the glass (original surface flaws population distribution) and from the evolution of surface quality during the glass

article lifetime. In this discussion also a lack of international standardization for CSG-IX has been put in evidence.

Some areas of ignorance are still existing in some basic scientific understanding of stress build up and crack initiation and propagation in glass processed by ion exchange. Nevertheless, a reasonable mathematical model can be assumed [6],[7] as the presently best available for stress distribution in a glass strengthened by ion exchange. Equation (1) represents the stress field induced by the stuffing of the invading ions in the glass matrix.

$$\sigma(x,t) = -\frac{B \cdot E \cdot V}{1-\nu} \cdot \left[ \int_0^t R(t-t') \cdot \frac{\partial [c(x,t') - \overline{c(t')}]}{\partial t'} \cdot dt' \right] \quad (1)$$

It can be shown that, after some manipulations, equation (1) can be transformed into equation (2):

$$\sigma(x,t) = -\frac{B \cdot E \cdot V}{1-\nu} \cdot \left[ (c(x,t) - \overline{c(t)}) - \int_0^t \frac{\partial R(t-t')}{\partial t'} \cdot [c(x,t') - \overline{c(t')}] \cdot dt' \right] \quad (2)$$

Where:

- E (MPa) Young Modulus
- $\nu$  Poisson ratio
- B (m<sup>3</sup>/mol) Linear Network Dilatation Coefficient (Cooper Coefficient)
- V Varshneya factor
- c(x,t) (mol/m<sup>3</sup>) concentration of the invading ions

$$\overline{c(t)} = \frac{1}{d} \cdot \int_0^d c(x,t) \cdot dx \quad (\text{mol/m}^3) \text{ average concentration of the invading ions}$$

d(m) glass article thickness

R(t) Relaxation function

From equations (1) and (2) it is evident the key role of the concentration - c(x,t) - of invading ions in the calculation of residual stress field. The front coefficients in equations (1) and (2) is related to the induced value, by ion exchange, of surface compression at zero time. The elastic parameters (E = 70000 MPa and  $\nu=0.23$  for Soda-Lime glass) can be considered constants for all process duration. The Cooper coefficient (B) and the Varshneya factor (V) depends on glass chemical composition, equilibrium conditions at the glass / molten salt interface and glass thermal history. In the framework of the presented mathematical model it makes more sense to group all these

parameters in a single measurable one: the surface compression at zero time. For the type of glass of this study (Soda Lime Silicate), at the process temperature of 450°C, the surface compression at zero time can be taken from [8] as  $SC(0) = -744$  MPa. For a wide class of ion exchange processes, concentration can be reasonably represented by a “complementary error function”. The physical reason is related to the point that concentration of the invading ions is described by a diffusion process that can be considered [1], with an acceptable degree of approximation, following the Fick diffusion equation. The complementary error function is a known solution [1] to the Fick diffusion equation with constant diffusion coefficient.

$$c(x,t) = c_0 \cdot \operatorname{erfc}\left(\frac{x}{2\sqrt{D \cdot t}}\right) \quad (3)$$

where:

$c_0$  (mol/m<sup>3</sup>) equilibrium concentration at the glass surface ( $x=0$ ) assumed constant for all process duration

$D$ (m<sup>2</sup>/s) Diffusion coefficient

Substituting equation (3) into equation (1) it results equation (4):

$$\sigma(x,t) = \frac{B \cdot E \cdot V \cdot c_0}{1-\nu} \cdot \left[ \frac{2}{d} \cdot \sqrt{\frac{D}{\pi}} \cdot \int_0^t \frac{R(t-t')}{\sqrt{t'}} \cdot dt' - \frac{2}{\sqrt{\pi}} \cdot \int_{\frac{x}{2\sqrt{Dt}}}^{\infty} R\left(t - \frac{x^2}{4 \cdot D \cdot p^2}\right) \cdot e^{-p^2} \cdot dp \right] \quad (4)$$

When stress relaxation can be neglected then relaxation function  $R(t)=1$  and equation (4) results:

$$\sigma(x,t) = -\frac{B \cdot E \cdot V \cdot c_0}{1-\nu} \cdot \left[ \operatorname{erfc}\left(\frac{x}{2\sqrt{D \cdot t}}\right) - \frac{4}{d} \cdot \sqrt{\frac{D \cdot t}{\pi}} \right] \quad (5)$$

A theoretical analysis of strength after ion exchange in soda lime silicate glass as a function of the characteristic initial flaw depth ( $a$ ) has been presented [5]. That analysis was based on a first order linear stress field model originally introduced in [9] and modified in [10] to take into account central tension value. In the present study, the linear stress field approximation has been improved [11] considering also relaxation effects by the KWW (stretched exponential) relaxation function [8] and the analysis has been performed using equation (2) as stress field distribution. Figure 1 reports the main result of this theoretical improvement.

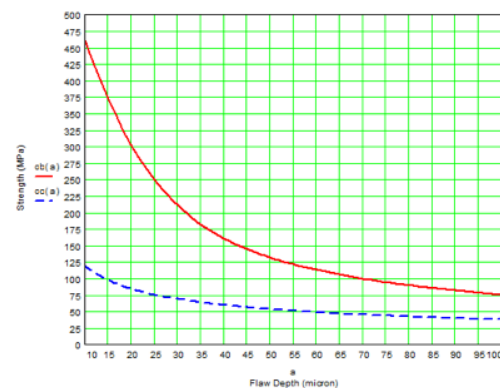


Figure 1 – Calculated Strength of a sodalime silicate glass as a function of critical surface flaw depth ( $a$ ).

Dotted blue curve: not strengthened glass, Continuous red curve: CSG-IX glass (IX process  $Cd=35$   $\mu$ m;  $SC= 450$  MPa)

Strength results for sodalime silicate glass with a specific surface quality selection and edge finishing procedures have been presented in [4] and [10]. In this study an experimental investigation will be presented for the same type of glass with far less accuracy in surface quality control and edge finishing procedures. Samples will be submitted to a very similar CSG-IX process. Results will be compared with former ones [4],[10] in order to evaluate the effects on strength of surface selection and edge finishing procedures.

Original glass strength and the capability of strength conservation during service life are connected to the initial crack formation probability and to the crack initiation and propagation tendency. Recent studies [12] indicate that initial crack formation probability depends on the glass chemical composition related to the forming network topology. The effectiveness of chemical strengthening by ion exchange to prevent crack initiation and propagation depends on compression layer depth and, again, glass chemical composition. Optimal glass matrices in respect to reduced initial crack formation and crack propagation tendency are Alkali Alumino Silicate and Alkali Boro-Alumino Silicates. This is probably related to their capability of getting deeper compression layer and more network topological connectivity in respect to Soda Lime glass matrices. The negatively charged fourfold [AlO<sub>4</sub>] network forming unit of these Alumino Silicate glass matrices results in a weaker bond with the alkali ions than with a non-bridging oxygen Alkali bond typical of Soda Lime Silicate glass. The weaker bond of the network with the Alkali ions increases ion exchange rate and leave a more connected structural network of the glass matrix. This has been demonstrated in [12] by the determination of crack formation probability

before chemical strengthening, by flexural strength of chemically strengthened pre-damaged glasses and by ball drop strength after chemical strengthening. In that study the compression layer depth of the investigated soda lime glass was very shallow:  $C_d=12\ \mu\text{m}$ . This value is quite comparable with original surface flaws depth (1-10  $\mu\text{m}$ ), nevertheless the effects of the chemical composition of the glass matrix on crack initiation and propagation were clearly evident.

In industrial applications of CSG-IX, the efficiency of ion exchange rate and the need to maintain an acceptable level of surface compression are related to the control of contaminants in the salt bath. Recent studies [13] indicates that both  $[\text{Na}^+]$  and  $[\text{Ca}^{2+}]$  influences negatively ion exchange rate, surface compression levels and final strength. The effect is remarkable for  $[\text{Ca}^{2+}]$  even in excess of few ppm leading to an almost complete process deactivation. Contamination from  $[\text{Na}^+]$ , coming from the process itself, is more affecting compression layer depth and surface compression although very relevant levels of contamination are needed to reveal substantial effects in strengthening. This means that in industrial application salt bath contamination is an issue to be carefully considered and recorded.

## Objective

The main objective of the present study is to evaluate strength of soda lime silicate float glass chemically strengthened by ion exchange when the glass articles have not been exposed to specific protocols in terms of surface quality selection and edge finishing. As mentioned above, similar results have been presented [10] for soda lime float glass with specific selection protocols for surface quality and edge finishing. The introduction of those selection and edge finishing protocols introduces additional costs for industrial products both for increased percentage of scrapes in initial selection and increased time work and tools arrangement in edge finishing (grinding and polishing wheels, reduced speed, increased cooling).

The evaluation will be performed at the same level of ion exchange parameters (compression layer depth,  $C_d$  and surface compression,  $S_c$ ), in order to evaluate the effect on strength of the surface selection and edge working procedures.

## Methods

Soda lime silica float glass samples with nominal thickness 10mm, dimensions 1100mm by 300mm have been chemically

strengthened by ion exchange in order to reach a compression layer depth of 35  $\mu\text{m}$  resulting in a surface compression of 450 MPa. Residual stress parameters (Compression layer depth and Surface compression) have been determined by Differential Surface Refractometry [9],[10]. Samples have been tested up to breakage by four points bending test according to EN 1288-3 in an automatic calibrated dynamometer at a load rate of 2 MPa/s. Test have been performed at room temperature ( $20 \pm 2\ ^\circ\text{C}$ ) with a relative humidity ranging between 40% and 50%. All tests have been performed with the tin side of the samples towards the loading rolls (compression side) so that for all samples air side results in tensile stress. Results have been evaluated in two ways: A) taking all thirty results with no consideration of the breakage position (with no exclusion of breakages outside of loading rolls): B) taking only the ones (twenty) with breakages origin in between the loading rolls. The practice to limit evaluation only for data with breakages within loading rolls (even though indicated in the standard), is questionable as it indicates a breakage occurred with a lower bending moment. Neglecting those results (breakages outside the bending rolls) may lead to an underestimation of critical issues in the product. For structural glazing application this occurrence should not be accepted.

## Results

Strength results for all thirty samples are reported in Figure 2, where they are compared with strength results previously determined [10] (reference) for the same type of glass, strengthened by ion exchange with very close parameters of residual stress but different protocols for surface quality selection and edge finishing. Ten out of thirty samples presented breakages outside the loading rolls while none of reference samples [10] presented this evidence. In Figure 3 the ten samples with breakages outside loading rolls have been excluded. It can be noticed that the data in Figure 2 present different slopes and a significant dispersion, this indicates different populations of surface flaws. This type of behavior in a fracture probability vs. strength plot is typical of pre-damaged (before ion exchange) surfaces [12]. Data in Figure 3 present a far better behavior in terms of homogeneity (not significant evidence of multiple slopes) while they exhibits a larger dispersion when compared with results of reference [10].

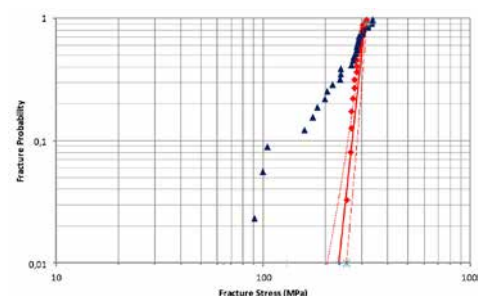


Figure 2 – Weibull plot of the results of reference [10] (red curve and symbols) compared to the results of the present study (blue indicators). Thirty results A) type with 10 samples with breakage origin outside loading rolls.

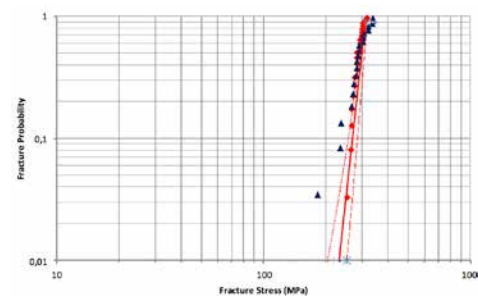


Figure 3 – Weibull plot of the results of reference [10] (red curve and symbols) compared to the results of the present study (blue indicators). Twenty results B) type with breakage origin within loading rolls.

It is quite evident, comparing Figure 2 with Figure 3, that the elimination of the results of breakages outside the loading rolls restores a reasonable behavior of the curve in terms of Weibull statistics. On the other side the elimination of those data, even though allowed by the standard, is not quite acceptable for structural glazing applications as it may hide serious strength issues.

The breakage origins of the eliminated 10 samples were identified as coming from the edges. A detailed observation with a simple magnification lens (15X magnification) revealed that the origin was coming from the corner to the surface of the grounded part of the flat polishing. On this basis, it can be concluded that the breakages with origins outside the loading rolls were likely generated by the different selected edge finishing. In Table 1 the characteristic breaking strength values ( $\bar{\sigma}_b$ ) have been evaluated considering in all cases a Weibull distribution. Confidence limits at 95% probability have been evaluated according to EN 12603 and the characteristic values are evaluated at 5% fractile. Expectation value and Variance have been calculated for the two parameters Weibull distribution as follows:

$$\bar{\sigma} = \theta \cdot \Gamma\left(1 + \frac{1}{\beta}\right) \quad (6)$$

$$\text{Var} = \theta^2 \cdot \left[ \Gamma\left(1 + \frac{2}{\beta}\right) - \Gamma^2\left(1 + \frac{1}{\beta}\right) \right] \quad (7)$$

| Series  | sb (MPa) | Expectation value (MPa) | $\sqrt{\text{Var}}$ (MPa) |
|---|----------|-------------------------|---------------------------|
| Reference samples [8] – Specific surface quality selection and edge finishing protocols | 230      | 288                     | 18                        |
| Results Series A – Present study – All data   | 103      | 248                     | 71                        |
| Results Series B – Present study – Breakage only within load rolls                      | 180      | 288                     | 38                        |

Table 1 – Characteristic breakage strength, expectation value and variance compared with reference [9]

Where:

- $\bar{\sigma}$  Expectation value of Weibull distribution
- Var Variance of Weibull
- $\Gamma(x)$  Gamma function
- $\theta$  (MPa) Weibull scale parameter
- $\beta$  Weibull modulus (shape parameter)

According to EN 12337-1, the acceptance qualification limit for the characteristic breaking strength for CSG is  $sb \geq 150$  MPa. Series A is below this limit, while series B is above this limit. On the basis of these results a critical problem rise up: is this CSG-IX glass qualified according to EN standards or not?

In Table 1 it is remarkable that expectation value for data series A is not dramatically distant from reference value. Expectation value of data series B is exactly the same of reference data. The main difference between characteristic breaking strength values of samples series of this study with that of reference is to be addressed to the significant higher dispersion (Variance), which is due to the lack of surface selection and edge finishing of the present samples compared to the reference ones.

## Conclusions and summary

Mathematical models of residual stress profile resulting from ion exchange in silicate glasses have been presented. On this basis strength reduction due to pre-damaged surfaces or damaged surface during service life can be evaluated as a function of most critical surface flaw depth.

Critical issues in glass chemical strengthening for structural application have been presented and put in evidence in terms of characteristic breakage strength values to be considered for product qualification. The cause of the inconsistencies has been addressed to surface damages occurred before and after the chemical strengthening leading to crack initiation and crack propagation. This

last argument open the discussion to the consideration of strength limits for the as produced article and strength degradation during the product service life. Design of glazing structure with chemically strengthened glass is possible but it shall carefully consider product qualification and product strength integrity with time and service conditions. The reduction in the characteristic breaking strength values recorded in this study when compared to the ones taken as reference [10] is mainly due to the significant dispersion of data generated by the reduction in selection protocols of surface quality and edge finishing.

According to the experimental results presented above, the product qualification according to EN standards can be questionable: it is strongly recommended not to underestimate potential risks due to part of production chain of the glass article (surface selection, edge finishing and polluted chemicals bath) leading to unexpected breakages (outside loading rolls) during product qualification.

## References

- [1] Varshneya, A.K.: Fundamentals of Inorganic Glasses, 2nd Edition [Sheffield, Society of Glass Technology] 2006
- [2] Gy, R.: Ion Exchange for glass strengthening. In Materials Science and engineering B, 149 159-165, 2008
- [3] Karlsson, S.; Jonson, B.: The technology of glass chemical strengthening – a review. In: Glass Technology: European Journal of Glass Science and Technology. Vol. 51, 2010, pp 41-54.
- [4] Macrelli, G.: Glass chemical strengthening by ion exchange: from ion exchange kinetics to strength determination. In Proceedings of Glass Performance Days 2015 406-410 – Tampere June 2015
- [5] Macrelli, G.: Critical evaluation of chemically strengthened glass in structural glazing applications. In Engineered Transparency 2016. Glass in Architecture and Structural Engineering. First Edition Edited by Jens Schneider, Bernhard Weller, Ernst & Sohn GmbH & Co. KG. 2016
- [6] Macrelli, G.: Some “unconventional” analytical solutions to diffusion equation in thermal ion exchange in silicate glass. Presented at the SGT100/ESG2016 Centenary conference, Sheffield UK September 2016
- [7] Shen, J.; Green, D.J.: Prediction of stress profiles in ion exchanged glasses. Journal of Non Crystalline Solids, 344 (2004) 79-87

- [8] 7. Varshneya, A.K., Olson, G.A., Kreski P.K., Gupta, P.K. Buildup and relaxation of stress in chemically strengthened glass. Journal of Non Crystalline Solids, 427 (2015) 91-97
- [9] Aben, H.; Guillemet, C.: Photoelasticity of glass, Berlin Heidelberg: Springer Verlag, 1993
- [10] Macrelli, G.; Poli, E.: Chemically strengthened glass by ion exchange: residual stress profile and strength evaluation. In Engineered Transparency. International conference at Glasstec, Dusseldorf (Germany), 2014, 231-240
- [11] Macrelli, G. Chemically strengthened glass by ion exchange: strength evaluation. To be published
- [12] Morozumi, H.; Nakano, H.; Yoshida, S.; Matsuoka, J.: Crack initiation tendency of chemically strengthened glass. International Journal of Applied Glass Science, 6 [1] 64-71 2015
- [13] Sglavo, V.M.: Effects of salt impurities on chemical strengthening of float glass by ion exchange. Presented at the SGT100/ESG2016 Centenary conference, Sheffield UK September 2016

# Automating Flat Glass Tempering Process

Miika Äppelqvist  
Glaston Finland Oy

## Keywords:

flat glass tempering process automation, supply chain digitalization, business logic

## Abstract

In the past 10 years, flat glass tempering process has taken relatively slow paced steps towards process automation. A handful of fully automated process have been done, however the technology is not yet suitable for meeting the needs of average glass processor who delivers glass to architectural segment.

The emerging technologies related to data collection, data analysis and integrated intelligence are already available and will change the pace of development. We see already now a very fast development for the next three years regarding tempering process automation.

This presentation goes through the current automation levels of tempering furnaces and presents the required steps for automating flat glass tempering process.

# The Importance of an Integrated Software Erp Solution in the Glass Processing Industry

Horst Mertes  
FeneTech Inc.

A completely integrated software ERP solution in a modern glass processing plant is essential to achieve complete automation. Only by closing the gaps between machinery and software and by eliminating island solutions an efficient flow can be achieved.

Complete automation is making factories smarter and requires constant innovation, which is the process of making something better by use of new original ideas, mainly in software technology. Through that new form of automation software control systems are applied to reduce labor, increase raw material usage and improve quality by repeatable work methods.

This process is changing the landscape of manufacturing. Modern and fully integrated software solutions furthermore coordinate the activity of the islands of automation created by the many talented machinery and system vendors. By deeply integrating and inter-connecting machinery and software in a factory a complete view of materials, status of all processes can be available to anyone, at any time.

# The Psychology of Perception, Threshold, and Emotion in Interior Glass Design

James R. Gulnick  
McGrory Glass, Inc., USA

## Abstract

This paper will discuss the psychology of perception, threshold, and emotion in interior glass design. Color theory and referenced material behind threshold will be presented, and the implication of threshold in the design and specification of glass in various architectural applications will be examined. Humans have the ability to discern color and contrast but there is a range of differences in colors and contrast that are not perceivable to the human brain. The signal strength between the differences has to be great enough for the mind to be able to conclude there is a difference. This phenomenon is known as threshold.

The emotional content of shapes and colors will also be investigated. What shapes and colors are most pleasing and how aesthetics impact the psychological state of occupants will be presented.

## Keywords

emotion, psychology, anti-reflective, threshold, architectural glass, perception, contrast, colour, shape

Situational attributes provided by environmental conditions impact the behaviour of individuals. The way people act can be significantly altered by involving authorized direction and providing an environment that reinforces the desired behaviour. It thus becomes ultimately important that the design of interior spaces highlights and supports the ideal conditions matching the culture, experience, or wanted outcomes of occupants and visitors. There is a level of integrity and responsibility that must fall upon the architect or designer in meeting both corporate and societal needs in keeping with the greater good.

## Experiments in Design Gone Wrong

In a series of controversial experiments, Milgram and others show that individuals tend to change the way they act due to situational variables that promote conformance and behavioural despite the dispositional attitudes present. Humans tend to give over their decision making power, logic, and reason to the control of a higher authority if put in certain authority/subordinate roles and provided with reinforcing environmental aesthetics, conditions, or situations.

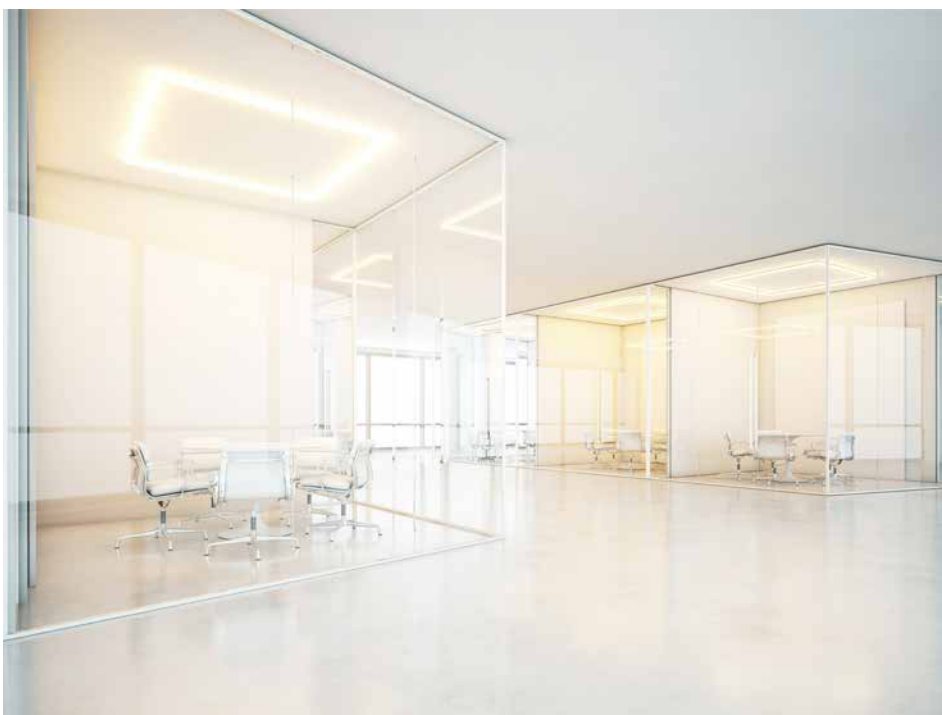
Milgram went through great efforts in his experiments to create a simulated shock machine in a laboratory setting that was so real looking that it fooled two electrical engineers (Russell, 2011).

In his experiments, Milgram would have a test participant issue a shock to an actor that appeared to be another test subject. The shock was fake, but the actor made it appear to be real. A doctor or facilitator wearing a lab coat, holding a clip board, and providing the official authorization to continue onward would prompt the test participant to issue greater levels of corrective shocks to a the actor.

Part of the success of the experiments has been as much the acting and sensationalized production as the study itself (Reicher & Haslam, 2011). The experiment shows how easily people are moved to do things that harm others and justify these actions through outside control. But, the experiment can also show authority how better to control the general public. Have we learned to be wary of authority, or have we gained useful insight into how authority can better control the public? Current research suggests continued support for control through environmental and authoritarian factors.

Navarick (2012) suggests that there are three stages in a decision making process of a participant in whether to withdraw from an experiment. The stages are priming (collecting evidence), decision (mental), and choice (action). Priming is where a person is affected by the situational factors such as aesthetics, design, colors, lighting, and the atmosphere created by the "set" and the people and processes within the environment. The situational priming is magnified by things such as salience of the evidence intuited through all the senses such as emotional experience, and visual, tactile, and auditory feedback. The decision stage is where the participant decides what to do next.

Another experiment utilizing authority and environmental situational factors to control the behaviour of test subjects was Zimbardo's infamous Stanford prison experiment. Students were randomly selected to play the role of guards or prisoners in a simulated prison environment. The prison guards



became tortuous and embodied the behaviours of the provided situation. Zimbardo was forced to stop the experiment by a graduate student as he and the participants had lost touch with reality and accepted the evils being perpetrated by the participants as tolerable behaviour in the given situation (McDermott, 2007).

## Design for Good

The experiments showed that situational experience and atmosphere overwhelmed innate dispositions to move people to the actions and behaviour that the authority wanted. Since, situation trumps disposition, is not it the role of architects and designers to help create the wanted emotional response in those visiting, working within, or simply viewing the building?

That being the case, perception, threshold, colour, and shape all are important variables in framing the human emotions derived from architectural designs and specifically in glass design. Glass can bring light, add clarity, provide colour, and create atmosphere through contrast, pattern, and shape. The simple synergy of space and its interaction with movement can tailor emotions and response. Creativity can be enhanced, performance benefited, and well-being safeguarded.

## Context and Content

Feature saliency or the quality of a feature being noticeable and impactful is inversely proportional to the frequency of a feature's appearance (Vasquez, 2010). Little things, sparse usage, and unique features make a big difference to observers. Redundancy of colour or shapes tend to cause lost impact and may be overwhelming.

The environment created with situational context effects neural processing and impacts social perception (Lieberman, 2006). When a building is designed with shapes and colours that move people to collaborative and positive outcomes, positive results ensue.

Emotional context of environment impacts the way humans perceive neutral faces (Mobbs, 2006). A welcoming building design will predispose occupants to being more receptive of each other. A receptive building, a receptive organization, and a well-received client.

## The Shape of Things

Certain shapes or features of designs are connected with protection, positive feelings, and feminine qualities whereas other shapes



or features of designs are associated with threat, negative feelings, and masculine characteristics (Palumbo, 2015). Both male and female participants found curved designs to be more nurturing and welcoming than angular shapes (Palumbo, 2015). Shapes of objects, patterns, and designs are important in creating environmental emotional context.

Storefronts may have harsh angularity further aggravated by shiny lights bouncing off the exterior glass. The sharp shapes and corners may create an emotional response opposite of what is wanted; avoidance of angular and straight edges innately seen as teeth, razors, or knives and provoking a flight or fight response from consumers.

Softening of hard surfaces and reduction of angularity becomes a solution. If the glass was not noticeable in the above example, then attention of the consumer could be brought into the store. A subconscious emotional welcome may be felt as the colours, curves, and features of the store would be forefront in the senses.

### Threshold: When does a Reflection Become Noticeable?

Humans have the ability to discern colour and contrast. For every light level, there is a range of colours and contrast differences that are unperceivable to the human brain. The signal strength between the differences has to be great enough for the mind to be able to conclude there is a difference. This phenomenon is known as threshold.

This threshold phenomenon is what sets anti-reflective glass types apart. Reflections

become unnoticeable when they cause a contrast or color deviance of less than 0.5%. In environments where the glass has been designed for high transparency, the light levels are similar on both sides. This is why it becomes important to utilize materials with the lowest reflectivity possible to minimize the chance for distraction.

One of the standard measurements in colour matching taken from the textile industry is delta E (dEcmc) which is a calculation combining lightness or contrast and colour variance (Hunt, 2004). While differences in contrast are more allowable than colour, there is an acceptable range set in commercial applications. Colour specialties industry standard treats a deviation of less than 0.5% dEcmc as being an indiscernible colour and contrast difference (Green, & MacDonald, 2002). However, not all eyes are the same. In regards to contrast, the difference in lightness and darkness, there needs to be greater than a 1% difference in order for humans to see an apparent difference nearly 100% of the time (Malm, 1999). According to Malm (1999), in cases of contrast level differences of less than 0.5%, the difference becomes not noticeable to nearly everyone:

- Under 0.5%, the reflection (contrasting light) becomes unseen
- Above 1.0%, the reflection (contrasting light) becomes 100% noticeable

## Contrast Threshold of 1%

The ability to detect contrast differences is based upon visual perception sensitivity and delineates the threshold between what is visible and invisible (Pelli & Bex, 2013). Since 1860, scientific tests and research have found and maintained that threshold contrast levels necessary for something to be seen is 1% for most objects within a wide variety of environments (Pelli & Bex, 2013). A thorough review of past measurements show that the threshold contrast has remained at 1% independent of dimensions and light levels (Pelli & Bex, 2013).

The simple test used for research of this phenomenon consists of two candles of the same light level being used to illuminate a screen or wall. One has a simple solid and opaque cylinder placed in front to cast a shadow on the screen. By varying the distance of candles from the screen until the shadow is perceived or not perceived the ratio of light between the unobstructed screen and the shadow cast on the screen can be calculated. The amount of light difference along the edge of the shadow is determined by the far candle with the opaque cylinder in front as the amount of light from a point source varies as a function of the inverse of the distance squared (Pelli & Bex, 2013). The measurement of threshold comes at the point when the observer can just barely see the shadow.

This technique consistently results in observation of a 1% threshold (Pelli & Bex, 2013). Other methods such as using a spinning disc with a black section of a slice that when spun created a black ring have also shown this 1% level as the threshold over a wide range of light levels (Pelli & Bex, 2013).

## Colour Threshold of .44% to .69%

Colour differences are detected similarly to differences in contrast but become noticeable when the perceived colour shifts (not just brightness level) enough to reach threshold. The human eye detects colours with differing specialised receptors which are excited by blue, green, and red wavelengths of light. Each receptor reacts similarly to colour and light level changes but follow the same general rules as threshold for contrast.

The required level of cone excitation change for threshold detection of colour signals remains equal for a given background excitation level (Jennings & Barbur, 2010). Each cone reacts independently of each other in the level necessary for detection enabling predictive modelling of detection thresholds necessary

for any specified background light level and colour (Jennings & Barbur, 2010).

S-cones are excited by blue wavelengths, M-cones are excited by green wavelengths, and L-cones are excited by red wavelengths. Research supports a significant and strong linear threshold relationship ( $r^2 = .90$  and  $.94$  respectively) between the M- and L- cone excitations changes required to differentiate between foreground and background colour and brightness levels (Jennings & Barbur, 2010). Blue cones are much less sensitive to excitation changes. The M (green) and L cones (red) required approximately .44% - .69% excitation change to reach threshold levels necessary to be detected (Jennings & Barbur, 2010).

Light is always reflecting from glass surfaces. The question is whether it is visible or invisible to the observer. When the level of reflection does not reach threshold, it is said to be invisible. The contrast threshold of 1% and the colour threshold of .44% - .69% interplay in the effect reflections have on the observer when looking through glass. When the reflection causes a combined light or colour level difference that reaches threshold, the reflection becomes noticeable. For simplification purposes, under .5% has been selected as below threshold for contrast and colour as represented in the findings of the referenced studies. Similarly, 1% threshold is presented as a level of contrast or colour difference where the change in level is apparent and seen by 100% of normal observers. It is important to understand these ranges in respect to reflection. The reflection is analogous to the light shadow cast by the far candle in the prior referenced example. Reflections cause changes in perceived light levels, contrast, or colours if they reach the threshold level.

## The Colour of Moods

### Colour Impacts Colour

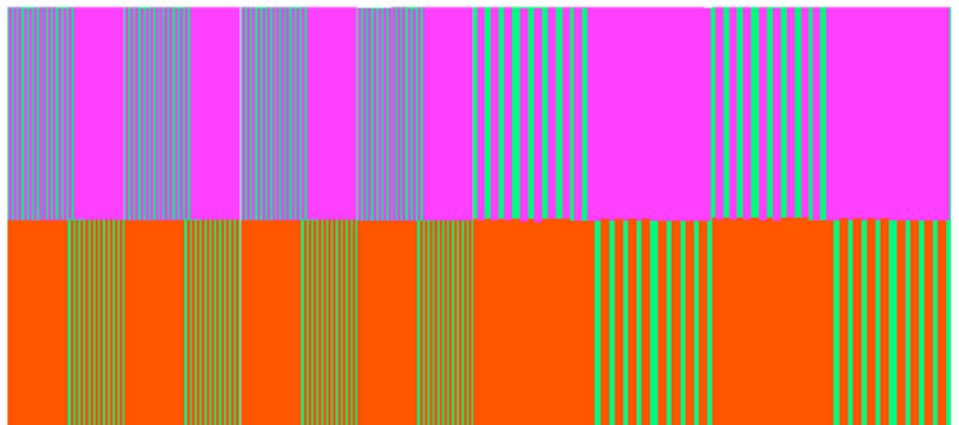
The impact on colour reflections is equal in significance to the impact of glass nuances which may render a colour slightly askew. The colour rendering index of glass is one of the measurements which compares how closely objects will be to their true colour when seen through the glass. Coatings, glass chemistry, and reflections may all have an impact on the perception of colour through the glass but most attention has only been paid to the colour change imparted by the physical glass itself and not the reflections.

Colours reflected from behind the observer may foul and obscure the true colours of the scene observed. There is not a measurement or index associated with this shift in perception relegated to coloured reflections but they are nonetheless important. For instance, a colour next to a colour affects its appearance.

A line may appear both blue and green depending on the colour next to it (Picture 1). The line is the same colour but the purple and orange colours frame the context in which the colour is viewed. The eye and mind automatically judge the line based upon the nearby reference changing what is seen. Reflections may also impact the colours seen through the glass in the same manner.

### Not a Reflection of You

Invisible storefronts create a unique aesthetic appeal. With reflection reduced by up to more than 16 times when compared to uncoated float glass, product displays pop and architectural designs transcend nature. The store blends effortlessly with its surroundings becoming one with the square. Foot traffic swells. As a natural result your client smiles.



Picture 1. Blue and Green Lines are the Same Colour

Views become breathless through anti-reflective glass. The type and application of anti-reflective coating can provide glare-free glass storefronts with visible light reflection ranging from less than 0.5% up to 4% as well as produce little to no discernable colour shift. Anti-reflective storefronts are available in monolithic, tempered or laminated, and insulated units. With large formats also available, the many fabrication options give unrivalled flexibility in aesthetically pleasing applications. Many glass fabricators stock and custom process anti-reflective glass to bring life to architectural designer creations. Imagine an environment where beauty flows effortlessly together without the harsh reflections of unforgiving float glass. Figure 1 is an example of how anti-reflective glass creates separation without reflection.



Figure 1. Anti-Reflective Glass Example

Today's anti-reflective coating technologies produce glass that limits glare and unsightly reflections in numerous unique applications. These high-tech coatings remove glass distractions from picture frame glass allowing the artwork to leap off the wall and become the focus of attention. Anti-reflective storefronts invite customer attention and welcome passers-by to come in and shop. When used in projection systems or displays, the light or visual media smoothly transmits through the glass capturing the viewer's attention without double images or visual light-front interference.

### Transparent Communication

Restaurants, boutiques, and image-conscious retail shops require their carefully-designed, visual display elements to be communicated in the most favourable light. Glass provides a weather-tight, physical barrier that still maintains a visual connection between the public and the store. Unfortunately, traditional glass also creates a secondary plane of focus

pulling attention away from what is in the store to the reflections on the glass surfaces.

Anti-reflective glass can virtually eliminate the reflection enabling the store's inner beauty to speak for itself. Traditional glass reflects 8% of the visible light. What does this really mean in real life? Only 92% of the outside light source reaches the inside of the storefront and provides a maximum potential for surface viewing through the same glass of 84.6% since 8% of light suffers from internal reflection on the way back out. Maximum illuminance becomes 100% when no glass separates the light source and the object and no glass or substance separates the object and the observer.

### Brightness and Reflection Issues

The relative brightness of typical outside ambient light is 10 to 300 times brighter than inside lighting on overcast and sunny days. Figure 2 indicates some common lighting situations and the relative brightness. The impact that the interior lighting has on noticeable reflectance is negligible for a majority of occurrences. And, when a store is lit up at night, the inner beauty of the store is released to the street in awe inspiring artistry especially with anti-reflective glass.

| Lighting Examples                | Relative Brightness |
|----------------------------------|---------------------|
| Bright Sunlight (Beach)          | 100000              |
| Diffuse indirect sunlight        | 20000               |
| Overcast day                     | 15000               |
| Jewelry Making, Small Models     | 1500                |
| Restaurant Food Prep             | 750                 |
| Workshop, Blueprint              | 750                 |
| Study, Bath, Kitchen             | 350                 |
| Torrential rains and dark clouds | 200                 |
| Dining, Entertaining             | 150                 |
| Walking Traffic                  | 65                  |

Figure 2. Relative Brightness of Common Lighting Situations

### Distractibility Index

The direct reflection ratio allows comparison of visible light-front distraction between differing solutions. This ratio of "reflection annoyance" can be measured and provide a "distractibility index" to compare different solutions. Simply put, the amount of reflection divided by the amount of maximum illuminance gives a ratio that is measured on a scale of 0 to ∞. Zero would indicate that there is no reflectance no matter how much light reaches the objects within the storefront and back out to the observer. Infinity would indicate a perfect mirror where all light is reflected at the glass storefront and no light reaches the objects within the storefront and back out to the observer.

How does anti-reflective glass impact the visual presence of a store, display, or building? When undistracted viewing is desired, finding a solution that provides the minimum colour, contrast, and brightness differential is the answer. In the real world, the architect and designer have limitless options at their fingertips. Figure 3 is a real life example of a storefront with a high performance anti-reflective coating that has visible light reflectance equal to only 0.5%. It allows display merchandise to be protected from the elements while the colours, textures, and beauty are breathtakingly presented without glare to distract.



Figure 3. Storefront with Anti-Reflective Glass

### Direct Reflection Ratio

DR = Direct Reflection (% of Source)  
MI = Max Illuminance (% of Source)  
DIR = DR/MI = Direct Reflection Ratio

As previously discussed, monolithic float glass has visible light reflectance of 8%. A maximum of 92% of the outside source light reaches the objects within the storefront. Additionally, the brightness of the image of the objects as seen by the outside observer has been reduced by another 8% as the light passes again through the glass and another 8% of the visible light reflects back into the store.

Now, let's calculate the ratio for a storefront with uncoated monolithic float glass:

DIR = DR/MI = Direct Reflection Ratio  
Direct Reflection Ratio = 8%/84.6% = 9.5%

In this example, the amount of reflection distracts the observer from the object displayed within the storefront. The direct reflection already peaks at a substantial 8%. But since the maximum illuminance is only 84.6%, the effect of the reflection is 9.5% of the value of maximum illuminance. When an object is brightly coloured the reflection annoyance is bad enough, but when a darker coloured object with fine detail and nuances is displayed, the "distractibility index" understates the problem.

Now, let's calculate the ratio for a storefront that uses monolithic anti-reflective glass as shown in the photo:

$$DIR = DR/MI = \text{Direct Reflectance Ratio}$$

$$\text{Direct Interference Ratio} = 0.5\%/99\% = 0.51\%$$

In this example, the lower amount of interference does not distract the observer from the object. The difference in "distractibility index" can be significant and the ability to see the item on display is increased dramatically. The two examples show a 1900% difference in harsh glare and bouncing light. Anti-reflective glass provides this type of benefit. The lower the direct reflection ratio of the anti-reflection glass, the higher the ability of the observer to focus on the objects displayed within the storefront.

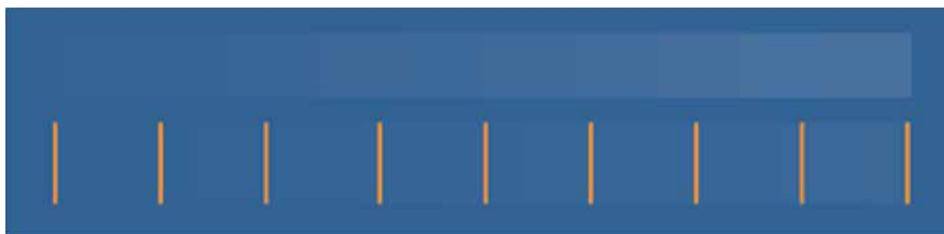


Figure 4. Left to Right Transition from 0% to 10% White and 0% to 4% White

## Summary

The long and the short of it is that anti-reflective glass is great when focus needs to be on the objects within the storefront, office, or display and not on the glass. Anti-reflective glass provides beauty by being invisible. It is most valuable when noticed the least. Anti-reflective glass allows more of what is being looked at to meet the eye.

| Type of Glass   | Reflectance | Max Illuminance | Direct Reflection Ratio |
|-----------------|-------------|-----------------|-------------------------|
| Anti-Reflective | 0.5%        | 99.0%           | 0.5%                    |
| Anti-Reflective | 1.0%        | 98.0%           | 1.0%                    |
| Anti-Reflective | 2.0%        | 96.0%           | 2.1%                    |
| Anti-Reflective | 4.0%        | 92.2%           | 4.3%                    |
| Float Glass     | 8.0%        | 84.6%           | 9.5%                    |
| Reflective      | 20.0%       | 64.0%           | 31.3%                   |
| Reflective      | 40.0%       | 36.0%           | 111.1%                  |
| Reflective      | 60.0%       | 16.0%           | 375.0%                  |
| Mirror          | 100.0%      | 0.0%            | ∞                       |

## Distractibility Index

This threshold phenomenon is what sets anti-reflective glass types apart. Reflections become unnoticeable when they cause a contrast or colour deviance of less than 0.5%. In environments where the glass has been designed for high transparency, the light levels are similar on both sides. This is why it becomes important to utilize the lowest reflectivity possible to minimize the chance for distraction. The difference between 1.0% and 0.5% may not seem like a lot, but it is the difference between a reflection being 100% perceived and nearly imperceptible. In other words, 0.5% is nearly 0% and 1% is 100% - a huge difference in perception for such a small difference in surface reflection.

Figure 4 shows a white block transition within the darker rectangle above. The left most line represents 0% reflectance/contrast whereas the far right line represents 4% for the transition with the line segments shown. 100% of people surveyed saw contrast differences above 1% (third line from the left). To the left of the second line, the white block became completely unseen.

the Milgram Paradigm: Tests of an Experimentally Derived Model of Defiance Using Accounts of Massacres by Nazi Reserve Police Battalion 101. *Psychological Record*, 62(1), 133-154.

Navarick, D. J. (2009). Reviving the Milgram Obedience Paradigm in the Era of Informed Consent. *Psychological Record*, 59(2), 155-170.

Palumbo, L., Ruta, N., & Bertamini, M. (2015). Comparing Angular and Curved Shapes in Terms of Implicit Associations and Approach/Avoidance Responses. *Plos One*, 10(10). doi:10.1371/journal.pone.0140043

Reicher, S., & Haslam, S. (2011). After shock? Towards a social identity explanation of the Milgram 'obedience' studies. *British Journal Of Social Psychology*, 50(1), 163-169. doi:10.1111/j.2044-8309.2010.02015.x

Russell, N. (2011). Milgram's obedience to authority experiments: Origins and early evolution. *British Journal Of Social Psychology*, 50(1), 140-162. doi:10.1348/014466610X492205.

Vazquez, E., Gevers, T., Lucassen, M., Weijer, J. V., & Baldrich, R. (2010). Saliency of color image derivatives: a comparison between computational models and human perception. *Journal of the Optical Society of America A*, 27(3), 613. doi:10.1364/josaa.27.000613

## References

Malm, W. C.: Introduction to Visibility. National Park Service and Colorado State Institute for Research on the Atmosphere, Fort Collins, Colorado, 1999.

Green, P., & MacDonald, L. W.: Colour Engineering: Achieving Device Independent Colour. Chichester: Wiley, 2002.

Hunt, R. W. G.: The Reproduction of Colour. Chichester, West Sussex, England: John Wiley & Sons, 2004

Jennings, B. J., & Barbur, J. L. (2010). Colour detection thresholds as a function of chromatic adaptation and light level. *Ophthalmic & Physiological Optics*, 30(5), 560-567.

Pelli, D. G., & Bex, P. (2013). Measuring contrast sensitivity. *Vision Research*, 9010-14.

Bocchiaro, P., & Zimbardo, P. G. (2010). Defying Unjust Authority: An Exploratory Study. *Current Psychology*, 29(2), 155-170. doi:10.1007/s12144-010-9080-z

Lieberman, M. D. (2006). Neural bases of situational context effects on social perception. *Social Cognitive and Affective Neuroscience*, 1(2), 73-74. doi:10.1093/scan/nsl015

McDermott, R. (2007). The lucifer effect: Understanding how good people turn evil - by philip zimbardo. *Political Psychology*, 28(5), 644-646. doi:10.1111/j.1467-9221.2007.00597.x

Mobbs, D., Weiskopf, N., Lau, H. C., Featherstone, E., Dolan, R. J., & Frith, C. D. (2006). The Kuleshov Effect: the influence of contextual framing on emotional attributions. *Social Cognitive and Affective Neuroscience*, 1(2), 95-106. doi:10.1093/scan/nsl014

Navarick, D. J. (2012). *Historical Psychology and*

# Non-contact Glass Temperature Measurement – the Correct Adaptation of IR Thermometers and Cameras to Different Applications

Ingo Stahlkopf,  
Torsten Czech  
Optris GmbH

## Keywords

1=Infrared, 2=Temperature, 3=thermometer,  
4=low-emissivity, 5=Linescan, 6=Quality

## Abstract

During the whole process of glass production and further treatment the temperature is one of the most important values to be measured, either directly for production control or for documentation or both of them.

For precise measurement the behavior of glass regarding IR-radiation must be known. There are influences from the ambient area as well as specific emissivity values of different glass types. Therefore, the right type of sensor or camera has to be chosen. In Figure 1 typical emission values for several types of glass are given.

As to see there are two ranges with relatively high emissivity peaks, around  $5\mu\text{m}$  and at  $7.9\mu\text{m}$ . That's the reason why most pyrometer, line scanners or IR cameras within the glass industry are working with such spectral filters, either at 5 or  $7.9\mu\text{m}$ . The high emissivity in this range means a low amount of reflections from the ambient.

For applications where not the surface temperature but the inner temperature shall be measured much shorter wavelength are needed. This can be the case for example in the float glass industry by measuring the glass in the float bath or behind. Another example is the internal temperature of glass drops within the container glass industry.

Figure 2 gives an example of improper measurement by comparing a long wavelength device which is working from  $7.5\text{--}13\mu\text{m}$  with a device working at  $7.9\mu\text{m}$ .

On the right side the image provides a calm temperature profile while on the left side

interferences created by reflections, certainly parts of the plant roof, clearly to see. That means in the end the left image would give a much uncertain temperature image compared to the  $7.9\mu\text{m}$  device.

The problem of reflections becomes even worse when coated glass comes into considerations. Due to the typically strongly reduced emissivity by the coating even measurements at specific wavelength cannot be done meaningful. In this case there is only one option left: measurement from below, where is no coating on the glass.

There are two different approaches:

1. Direct measuring with a proper device from below, which means it must be installable and in the best case it is able to measure the whole width of the glass.
2. The second approach is mainly depending on the level of low-emissivity coating. In some cases a solution can be found by using one pyrometer from below as reference pyrometer. The temperature reading of this reference pyrometer can be used as input value to the device which is still measuring from above, in most cases line scanners or IR cameras in line scanner mode. The accuracy of the measurement from the top then is increased.

Next to the emissivity in some applications the glass temperature itself means a challenge regarding precise temperature measurement. Right after the laminating process often the glass temperature is too cold to be measured by devices with 5 or  $7.9\mu\text{m}$ . In this case only long wavelength devices can be used which again means a higher potential risk of improper measurement due to reflections (Figure 2).

For all kind of noncontact temperature measurement of glass first of all the right choice of the spectral response is important which is mainly driven by the application. Secondly the installation must be done physically in a proper way. This includes the correct distance to ensure a proper field of view and the selection of the right protective accessories for high ambient temperatures. In a lot of installations where coated glass is measured it is still state of the art to use line scanners from top and a reference pyrometer from underneath. The innovative new approach of a scanning temperature measurement

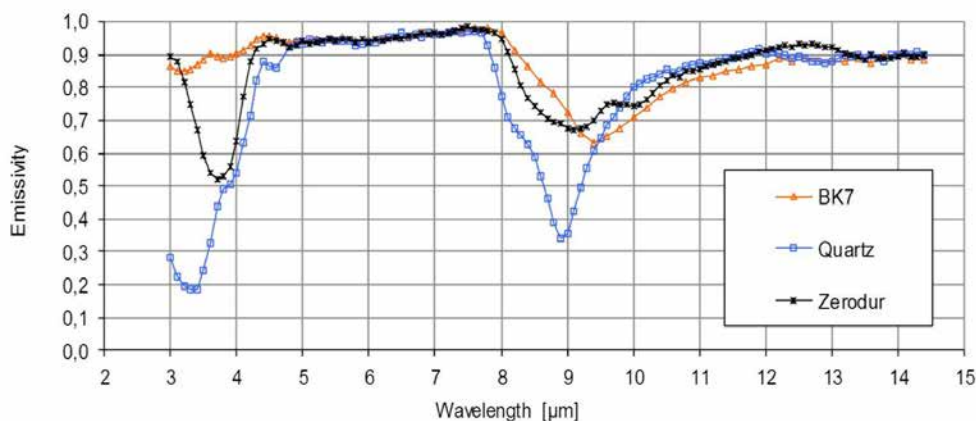


Figure 1: emissivity of different glass types

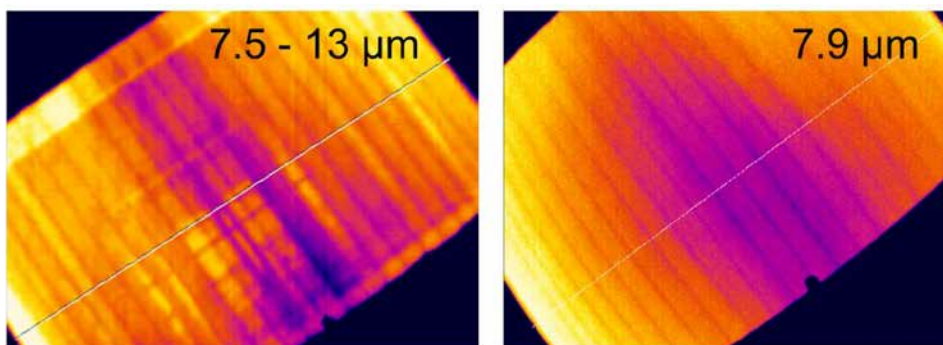


Figure 2: reflection of glass at different IR-spectral ranges

from underneath requires modern compact sized IR cameras which are able to operate in linescanning mode. The size of traditional line scanners does not fit in the small space between the tempering furnace and the cooling section. The whole installation effort is also reduced as for devices underneath usually no cooling are required.

# From Color to Chemometrics: Strategies to Determine Coating Thickness and Quality

Chris Hellwig, Torsten Büttner, Mario Krause  
 Carl Zeiss Spectroscopy GmbH, Jena  
 Keywords: inline process control; coating thickness; wet coating;

## Abstract

A well-known method to perform in-situ process control in the glass processing industry is the determination of color. Within this industry, most coating plants for glass or foils are equipped with visible wavelength range spectrometers. The use of visible spectrometer measurements are twofold, predicting the appearance and intended final color as well as the variation in color values as an indicator of applied layer thicknesses.

In order to determine complex layer designs, e.g. triple silver coatings, color variation might be a misleading layer thickness indicators. In these cases, physical attribute based calculation methods are used to determine the layer thickness based on the measured spectral data.

Demands for process monitoring and thus process capable metrology arises out of other applications such as wet coating on diffuse materials like paper. Neither color measurement nor thickness determination based upon interference are sufficient to provide stable process metrology results. Therefore, a method based on chemometric modeling was introduced to provide the machine operator with reliable process information. The talk will show how a combination of different process capable methods – color, physical, and chemometric models – helps the operator to stabilize coating processes and control the final product quality with a single equipment.

## Introduction

Monitoring the properties of coatings during the production process is a method to stabilize the process itself by ensuring the product quality in a very early stage. Thus, it enables the operator to optimize process parameters within seconds. In the last decades, different methods of inline capable direct measurement methods were introduced and used. This includes systems to measure the optical density (OD), sheet resistance

using eddy current sensors, monitoring a single wavelength reflected or transmitted intensity as well as measuring the spectral transmissivity and reflectivity.

Monitoring the optical density (OD), sheet resistance or single wavelength intensity requires knowledge of limit values for certain layers or layer systems. These limits are determined during the product development.

For more complex layer systems, broadband monitoring systems are used. Typically those systems include an in-situ spectrometer system. While these systems measure the full spectral characteristics of the layer it is necessary to extract specific spectrum information: This can be the wavelength of a local minimum in the spectrum, the integrated intensity over a wavelength range or the color values. These values are calculated using standardized and published methods [2].

Another widely used method to determine layer thickness is thin-film interference [3]. Here the interference patterns generated by two or more optical surfaces are used to calculate the optical thickness of the layers. Knowing the diffractive index of the material allows geometrical thickness calculation [4]

An extended overview of well-known methods for layer thickness evaluation is given in [1]. The methods described above are well known, stable and established in their fields of application, mainly the large area vacuum deposition of functional layers (architectural glass or metallization of plastic films for packaging foil).

For paper, film and foil converting application a wide range of sensors exists, including NIR (Near Infra-Red) reflectance and transmission measurement sensors, beta transmission and gamma backscatter gauges, X-Ray transmission and backscatter gauges as well as (optical density) OD sensors. Those sensors are used to determine coat weight, coating thickness, barrier layers, lamination quality and moisture.

In the past decades, a field of spectroscopy evolved: NIR spectroscopy with chemometric data analysis to derive information such as water content or proteins in food [7].

This talk does not cover the rigor of the mathematical techniques used in the analysis; such as; matrix algebra, analytic geometry, experimental design, calibration regression, linearity, design of collaborative laboratory studies, comparison of analytical methods, noise analysis, use of derivatives, analytical accuracy or analysis of variance that are the classical tools used in the science of chemometrics. Rather, small examples are used to illustrate some ways of working, mainly by using graphical analytical techniques.

Since we provide both - inline capable systems for large area coatings and systems for the food and agriculture industries - it is possible to combine techniques from both application fields in our system software. This allows the end user not only to decide which technology fits best - it is possible to combine the results. So we can provide not only the remaining moisture in a wet coating, which is needed for process control. We can also supply the color values or the coating thickness as well.

## Coating thickness prediction using color values

For simple layer designs, a correlation of the thickness and a color value may exist and this correlation needs to be found. This theoretical calculation can be performed prior to any real measurement. The results of these calculations for ZnO on glass are shown in Fig. 1. The data show a good correlation between thickness and the  $b^*$  value for this specific layer.

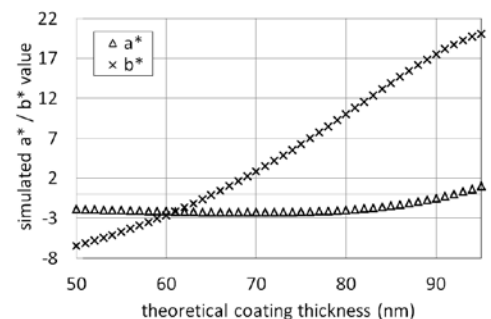


Fig. 1: Correlation of  $a^*/b^*$  and coating thickness of ZnO on glass calculated with the SCOUT modelling software.

For process control a 3rd order polynomial based on the data in Fig. 1 was used to calculate the coating thicknesses from the measured  $b^*$  values.

On six ZnO coated glass panes (S1– S6) the  $b^*$  values were measured and the predicted thickness results are shown in Fig. 2 for three of the samples.

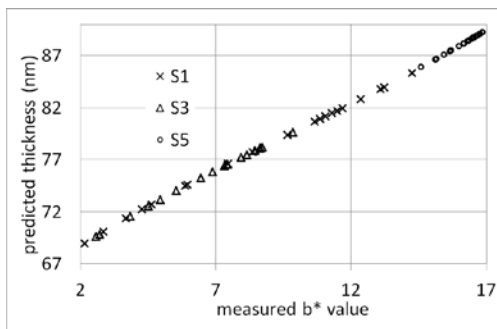


Fig. 2: Thickness results based on  $b^*$  measurements.

### Model based approaches

A simulation tool generates a simulated spectra based on the optical model of the coating system. This optical model is fitted to the measured spectra by varying some parameters of the optical model like layer thickness [6].

The example shows am silicone layer on a 23  $\mu\text{m}$  PET substrate. The model does not take the interference of the substrate material into account. Therefore, no fringes caused by the 23  $\mu\text{m}$  PET material are modelled in the simulated spectra. The optical and physical parameters of the model are fitted to yield simulated spectra that match the measured spectra. The best match was achieved with a silicone layer thickness of 186 nm.

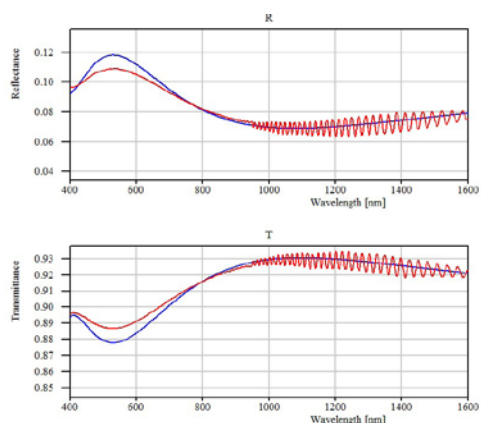


Fig. 3: Measured (red) and simulated (blue) reflection and transmission spectra for sample 2. The best match of simulated and measured data was achieved with a silicone layer thickness of 186 nm.

### Chemometric approaches

Coated paper samples were measured on a 45°: 0° diffuse reflectance probe connected to an NIR spectrometer with a spectral range of 1340 – 2000 nm. The setup was calibrated with a diffuse reference material. The paper samples' grammage values ranged from 0.19 to 4.14 g/m<sup>2</sup>. Each of the 13 samples was measured at three spots. The spectra of the samples with a grammage of 0.19, 1.80, and 4.14 g/m<sup>2</sup> were used to develop a calibration function (see Fig. 4).

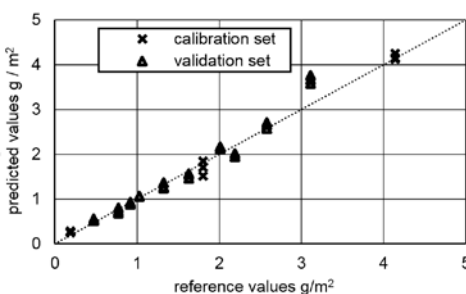


Fig. 4: Plot of the predicted grammage values for three calibration samples and 10 validation samples.

All other measurements were used for validation of the calibration function.

### Conclusion

The final product quality is defined as a combination of many features such as color appearance or coating thickness. Since inline spectrometers measure the full spectrum, these quality-related parameters can be evaluated in one single step. Extended range inline spectrometer systems allow chemometric prediction in the NIR range as well as color evaluation, even within a single measurement system.

It is shown that inline spectrometers are versatile and stable process-capable measurement systems to keep a production line under control and ensure the final product quality [8]. The data provided by such instruments can be used for direct monitoring of the production process. This speeds up the developing of new coatings or coating processes an inline process monitoring. An example is given in Fig. 5.

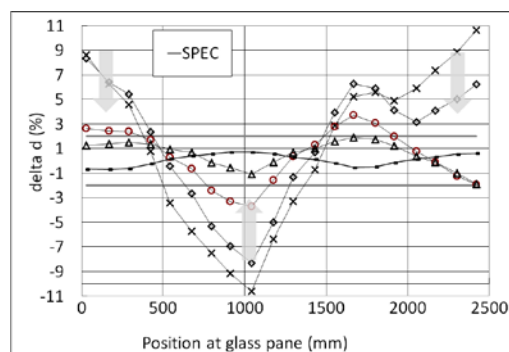


Fig. 5: Example of a cross section plots of coating thickness variation ( $d/\%$  of nominal value) for process monitoring (six different glass panes).

Because the quality of the measurement results is very stable and data collection is fast, they can be used as an input for automated control loops. However, this needs a close cooperation between process engineers, automation solution provider, and measurement system provider.

### References

1. Martina Lindner and Markus Schmid; Thickness Measurement Methods for Physical Vapor Deposited Aluminum Coatings in Packaging Applications: A Review. Coatings 2017, available online <http://www.mdpi.com/2079-6412/7/1/9/pdf> (accessed on 25.04.2017)
2. Gernot Hoffmann; CIE Lab Color Space; available online <http://docs-hoffmann.de/cielab03022003.pdf> (accessed on 25.04.2017)
3. Wikipedia.Org; Thin-film interference; available online [https://en.wikipedia.org/wiki/Thin-film\\_interference](https://en.wikipedia.org/wiki/Thin-film_interference) (accessed on 25.04.2017)
4. Carl Zeiss Spectroscopy; Basics of layer thickness measurement; available online <https://www.zeiss.com/spectroscopy/solutions-applications/layer-thickness-and-coating-measurement.html> (accessed on 25.04.2017)
5. Mark & Workman; Chemometrics in Spectroscopy, 1st Edition, Elsevier
6. Theiss; SCOUT spectrum simlatoon software; available online [http://www.mtheiss.com/download/scout\\_2.pdf](http://www.mtheiss.com/download/scout_2.pdf) (accessed on 25.04.2017)
7. Carl Zeiss Spectroscopy; Moisture Measurement; available online <https://www.zeiss.com/spectroscopy/solutions-applications/moisture-measurement.html> (accessed on 25.04.2017)
8. T. Büttner, C. Hellwig, J. Margraf; Process Monitoring with lab-like Certainty; Spectronet (2013)

### Acknowledgements

Thanks to Dr. G. Kleideiter from Grenzebach Maschinenbau GmbH for providing the method and measurement results for thickness prediction from color.

# Electromagnetic Shielding Effectiveness of Glazing Components

Eric Stein  
Viracon, Inc.  
800 Park Drive  
Owatonna, MN 55060  
507-444-3683  
estein@viracon.com

## Keywords

1=Radio Frequency 2= Attenuation  
3=Conductive Coatings 4=ASTM F3057-14  
5=Glass Façade

## Abstract

As wirelessly transmitted data has become widespread, the need to protect this data has also increased. The obvious first level of protection is to secure the network; however, this does not stop potential electronic eavesdroppers from seeing that the network exists. Utilizing Radio Frequency (RF) shielding glass within a building façade creates a Faraday cage, which keeps any wireless data contained so eavesdroppers won't know a network even exists. Prior to

2014, there was no standard method to test the electromagnetic shielding effectiveness of glazings. A version of the IEEE 299 standard was frequently used, which gave accurate results, but was modified using varying frequency ranges, antenna types/locations, enclosure environments, and glass sizes, each depending on the equipment at the specific test location. ASTM F3057-14 was developed to standardize the shielding effectiveness test method such that attenuation results focused on the glass itself and not the framing system, so product comparisons can now be made industry wide. Testing has been completed using both a modified IEEE method and the ASTM method for various RF shielding glass products. The results will show that incorporating a Fluorine-doped Tin Oxide (FTO) conductive coating result in higher attenuation than the addition of a film or use of a standalone Low-E coated product. Utilizing a conductive coating in combination with a Low-E coating also allows for improved thermal and solar performance while maintaining pleasant aesthetics.

## Introduction

Utilizing Insulating Glass Units (IGUs) within a building façade has well-known benefits, including occupant comfort, superior aesthetics, and energy efficiency. In addition to the aesthetic and energy-saving benefits, glass can be utilized for electronic eavesdropping protection. Electromagnetic shielding glass can provide protection in buildings where intercepting electronic information, such as cell phone conversations or wireless transmitted data networks, is a concern. The entire electromagnetic spectrum includes frequencies from 3 Hz to 300 EHz (10<sup>18</sup> Hz). The middle-upper end of this spectrum includes the infrared, ultraviolet, and visible frequencies, and most traditional coatings were designed to work in these frequency ranges to improve aesthetics and energy performance. The radio frequencies, on the lower frequency end of this spectrum, are where today's electronic devices operate, specifically between the 100 kHz and 20 GHz range. This lower frequency range is where the focus lies for RF shielding glass.

|                        |                     | ASTM F3057-14       | Modified IEEE 299 |
|------------------------|---------------------|---------------------|-------------------|
| <b>Unit Dimensions</b> |                     | 0.91 m x 0.91 m     | 0.3 m x 0.3 m     |
| <b>Aperture Size</b>   |                     | 0.86 m x 0.86 m     | 0.28 m x 0.28 m   |
| <b>Magnetic Field</b>  | Frequency Range     | 100 kHz to 20 MHz   | Not Tested        |
|                        | Antenna Type        | Loop                |                   |
|                        | Positions           | 3                   |                   |
|                        | Distance from Glass | 30.48 cm            |                   |
|                        | Measurements Taken  | >461 equally spaced |                   |
| <b>Electric Field</b>  | Frequency Range     | 1 MHz to 100 MHz    | 10 MHz to 100 MHz |
|                        | Antenna Type        | Dipoles/Monopoles   | Biconical         |
|                        |                     | Log Periodic        | Log Periodic      |
|                        | Positions           | 2 each              | 1 each            |
|                        | Distance from Glass | 183 cm              | 50cm              |
| Measurements Taken     | >461 equally spaced | 51 equally spaced   |                   |
| <b>Plane Wave</b>      | Frequency Range     | 100 MHz to 20 GHz   | 100 MHz to 18 GHz |
|                        | Antenna Type        | Horn                | Horn              |
|                        |                     | Log Periodic        | Log Periodic      |
|                        | Positions           | 2 each              | 1 each            |
|                        | Distance from Glass | 183 cm              | 100cm             |
| Measurements Taken     | >461 equally spaced | 142 equally spaced  |                   |

Table 1: Test Parameters for ASTM F3057-14 and Modified IEEE 299 standards

Shielding effectiveness, a material's ability to block RF, is referred to as "attenuation" and is measured in decibels (dB). Attenuation is measured for each individual frequency within a specific range. A higher attenuation correlates to a weaker signal, which means that more of the signal was blocked by the medium. Because the decibel is a logarithmic unit of measure, every single decibel increase in attenuation can have a big impact, meaning it is less likely for eavesdroppers to retrieve wireless data.

## Test Results

Prior to the development of the ASTM F3057-14 test method, a modified version of the IEEE 299 standard was frequently used to determine the shielding effectiveness of glazings. The IEEE 299 method was not developed for glass components; however, it still gave valid attenuation results with some modifications to the test, which may have included different antenna types, enclosure environments and glass sizes. This was a satisfactory way for an individual company to make comparisons between various coatings or products, but poor for industry-wide comparisons, as each company had a different test setup depending on its particular equipment parameters or specific frequencies of interest. ASTM F3057-14 was developed to standardize the test method such that attenuation results focus on the glass itself and not the framing system, so product comparisons can now be made industry wide. This test identifies a specific glass size, frequency range, antenna type, antenna position and data collection method. Table 1 compares differences between IEEE 299 parameters and parameters specified in the new ASTM F3057-14 standard.

The most important differences between the two tests are unit dimensions and aperture size, as the ASTM F3057-14 test size is three times as large as the IEEE 299 standard. Another important difference is the inclusion of the magnetic field component for the ASTM F3057-14 method. For the electric field and plane wave frequencies, however, there are only slight differences between each test setup.

Each of the modified IEEE 299 or ASTM F3057-14 tests are completed in a metal-enclosed chamber with a metal wall separating the chamber, creating two rooms. A transmitting antenna is placed in one room and a receiving antenna is placed in the other room. There is an opening, called the aperture, located on the metal wall that separates the two rooms. A signal loss is calculated from the transmitting antenna to the receiving antenna for the open aperture, and then repeated with the opening covered with metal, called the closed aperture. The difference in the measured attenuation through the open aperture and the closed aperture is called the dynamic range (DR), which is the theoretical maximum attenuation possible. The product being evaluated is then placed in the aperture and the same signal loss is calculated, which results in the attenuation of the product. Four different laminated samples and four different Tempered Laminated Insulated (TLI) unit samples were tested per the IEEE 299 method. Testing was repeated using one laminated sample and two different TLI unit samples per the ASTM F3057-14 method. Each of the TLI unit samples are variations of the CyberShield™ product, which was designed to incorporate a single Low-E coating for aesthetics and solar/thermal performance, combined with two layers of

DataStop™, a transparent FTO conductive coating incorporated in an inboard laminate for attenuation performance. An FTO Laminate, made with two plies of the transparent FTO conductive coating, was included to show the performance of the FTO coating by itself. The selected laminated samples were the most commonly used RF shielding products available on the market at the time of the study. A clear-clear laminate with no coating was also run as a control.

There were four different Low-E coatings tested, representing four different FTO TLI unit makeups, within the IEEE 299 test: one single Silver (VRE59), two double Silvers (VUE50 and VE2M), and one triple Silver (VNE63). These four Low-E coatings were purposely selected to determine differences in attenuation with an increasing number of Silver layers. For the ASTM F3057-14 test, only the two double Silver coatings (VUE50 and VE2M) were tested. The FTO laminate includes two layers of the FTO conductive coating that are standard in the FTO TLI units, however this sample is just the laminate and does not include an additional Low-E coating.

Two additional non-FTO products were also tested: Laminate 1 and Laminate 2. The Laminate 1 product incorporates two Low-E coatings, which are responsible for aesthetics, thermal and attenuation performance. The Laminate 2 product incorporates a film within the interlayer, which is responsible for aesthetics, thermal, and attenuation performance.

The makeups specified above are listed in Table 2. Note that the Laminate 1 product tested did not have edge deletion, which would be required for this product in any field installation due to the potential for degradation of the Low-E coating. This lack of edge deletion

| Test              | Sample    | Product             | Glass | #2 Surface | Edge Deletion | Spacer / PVB | #3 Surface | Edge Deletion | Glass | #4 Surface | Spacer / PVB | Glass | #6 Surface |
|-------------------|-----------|---------------------|-------|------------|---------------|--------------|------------|---------------|-------|------------|--------------|-------|------------|
| Modified IEEE 299 | Laminates | Laminate 1          | 6mm   | Low E      | None          | 0.76mm PVB   | Low E      | None          | 6mm   | N/A        |              |       |            |
|                   |           | Laminate 2          | 5mm   | RF Film    | 7mm Cutback   | 0.76mm PVB   | N/A        |               | 5mm   | N/A        |              |       |            |
|                   |           | Clear-Clear Control | 5mm   | None       | N/A           | 0.76mm PVB   | None       | N/A           | 5mm   | N/A        |              |       |            |
|                   |           | FTO Laminate        | 5mm   | FTO        | N/A           | 0.76mm PVB   | N/A        |               | 5mm   | FTO        | N/A          |       |            |
|                   | TLIs      | FTO Units           | 5mm   | VRE59      | 9.5mm         | 13.2mm Al    | N/A        |               | 5mm   | FTO        | 0.76mm PVB   | 5mm   | FTO        |
|                   |           |                     |       | VNE63      |               |              |            |               |       |            |              |       |            |
|                   |           |                     |       | VE2M       |               |              |            |               |       |            |              |       |            |
|                   |           |                     |       | VUE50      |               |              |            |               |       |            |              |       |            |
| ASTM F3057-14     | Laminate  | FTO Laminate        | 5mm   | FTO        | N/A           | 0.76mm PVB   | N/A        |               | 5mm   | FTO        | N/A          |       |            |
|                   | TLIs      | FTO Units           | 5mm   | 9.5mm      | 13.2mm Al     | N/A          |            | 5mm           | FTO   | 0.76mm PVB | 5mm          | FTO   |            |

Table 2: Sample Makeups for Each Test

may have resulted in an overestimate of attenuation performance for the Laminate 1 product. The FTO TLI units, the FTO Laminate, and the Laminate 2 product were tested as they would be installed in the field. The modified IEEE 299 test protocol was completed at Environ Testing Laboratory (currently Element Laboratory) in Minneapolis, Minnesota. The ASTM F3057-14 test protocol was completed at Advanced Programs, Inc. (API) in Columbia, Maryland. The attenuation results are split between the electric field and plane wave field for the modified IEEE 299 test, and between the magnetic field, electric field, and plane wave field for the ASTM F3057-14 test. An average attenuation for the total frequencies within each field is shown in the graph's legend, which provides an overall comparison by product type. However, for a true product comparison, the attenuation for each individual frequency is graphed. Since the plane wave field includes the largest frequency range, the x-axis is plotted on a logarithmic scale to better show the results below 1000 MHz. The attenuation data for the multiple antenna positions are averaged for each product within the ASTM F3057-14 test, with the standard deviation for each product listed in the text for each figure.

Figure 1 shows the results from the modified IEEE 299 test for the electric field. Note that the FTO TLI unit with the VUE50 coating does not have an average attenuation within this field because it was not tested below 35 MHz. The highest performing FTO TLI unit had a 4.7dB higher average attenuation than the FTO Laminate, which suggests that the addition of the Low-E coating increased the attenuation by 39%. Each of the FTO TLI units had an average attenuation within 1.9 dB of one another with a standard deviation of 1.0 dB, suggesting that the attenuation will be similar no matter what Low-E coating is applied for aesthetic, thermal and solar performance. Apart from a spike around 100 MHz, the control clear-clear laminate had very low attenuation, which validates the test results.

Figure 2 shows the results from the modified IEEE 299 test for the plane wave field. Some of the products tested had an attenuation that was higher than the dynamic range, so for these frequencies the product attenuation was reduced to the dynamic range. Each of the FTO TLI units and the Laminate 1 product were affected by this reduction in attenuation. Once again for the plane wave field, the highest performing FTO TLI unit had an attenuation that was 38% greater than the attenuation of the FTO Laminate, further showing the advantage of incorporating the Low-E coating. The average attenuation for the FTO TLI units

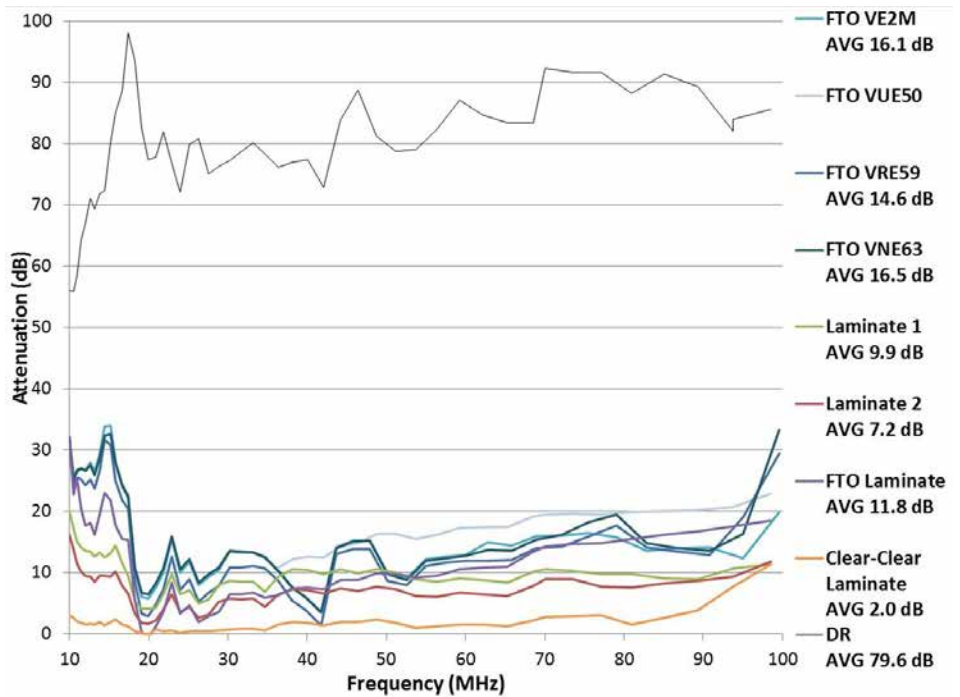


Figure 1: Modified IEEE 299 Attenuation for the Electric Field

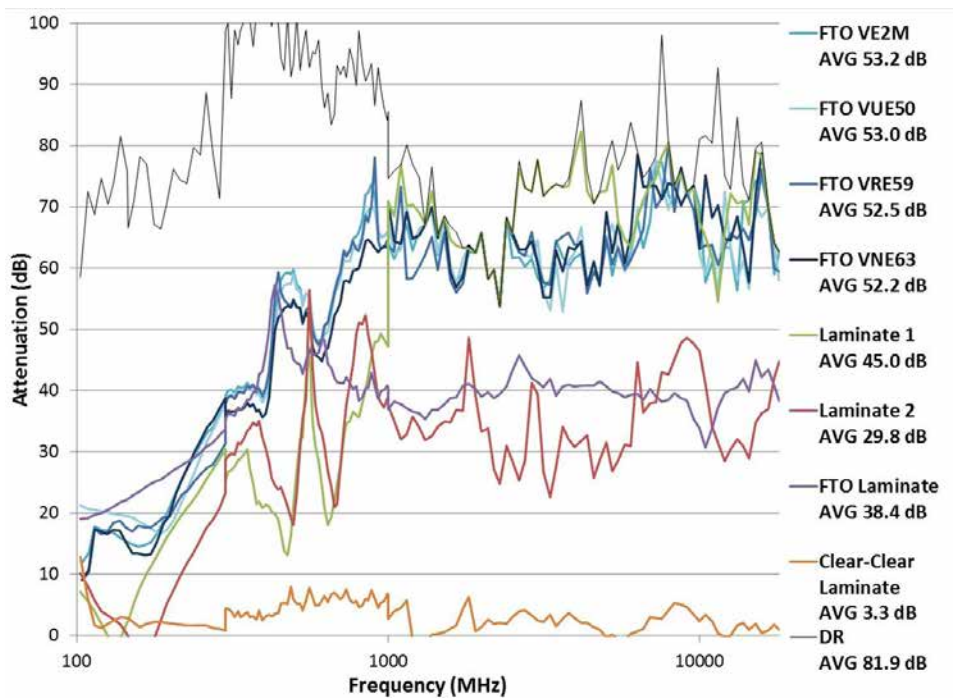


Figure 2: Modified IEEE 299 Attenuation for the Plane Wave Field

had an even tighter range for the plane wave field than the electric field, having an average attenuation within 1 dB of each other with a standard deviation of 0.46 dB. The similar result of each Low-E coating further suggests the specific coating type does not influence attenuation performance, as long as a Low-E coating is incorporated. As expected, the attenuation for the control clear-clear laminate remained well below 10 dB for most of the frequency range.

Figure 3 shows the results from the ASTM F3057-14 test for the magnetic field. The standard deviations between the three antenna positions for each FTO TLI units were: 0.57 dB for VE2M and 0.19 dB for VUE50, with a standard deviation of 1.18 dB for the FTO Laminate. As expected, the attenuation is lower for this frequency range, but the same trend holds true for the performance of the FTO TLI units versus the FTO Laminate, and the similar performance of each Low-E coating type.

Figure 4 shows the results from the ASTM F3057-14 test for the electric field. The standard deviations between the two antenna positions for each FTO TLI unit were: 0.06 dB for VE2M and 0.06 dB for VUE50, with a standard deviation of 0.13 dB for the FTO Laminate. The performance of the FTO Laminate was similar to the FTO TLI units within the electric field, which is in contrast to the results obtained when tested per the IEEE 299 protocol.

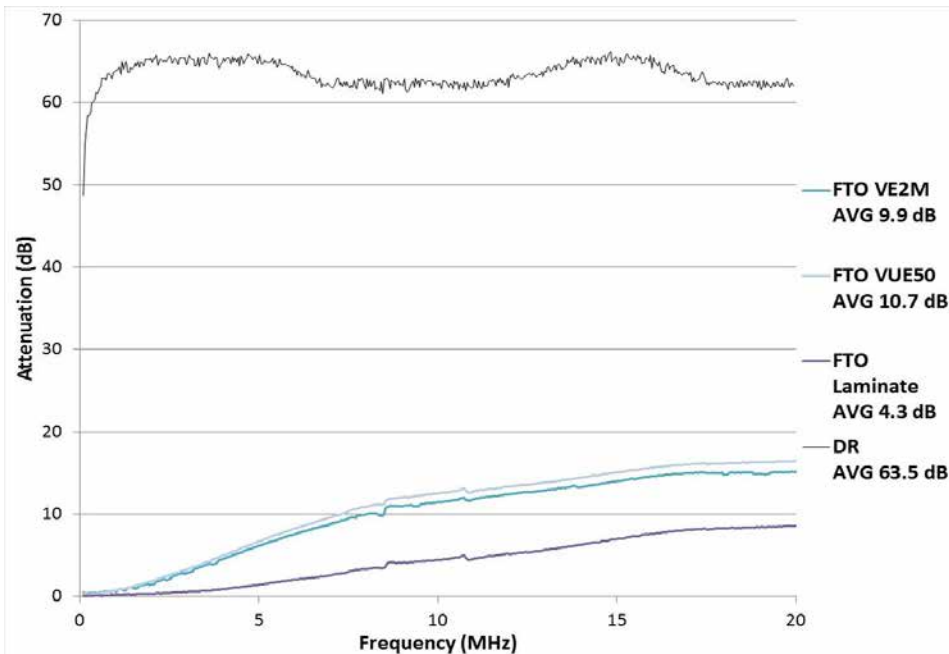


Figure 3: ASTM F3057-14 Attenuation for the Magnetic Field

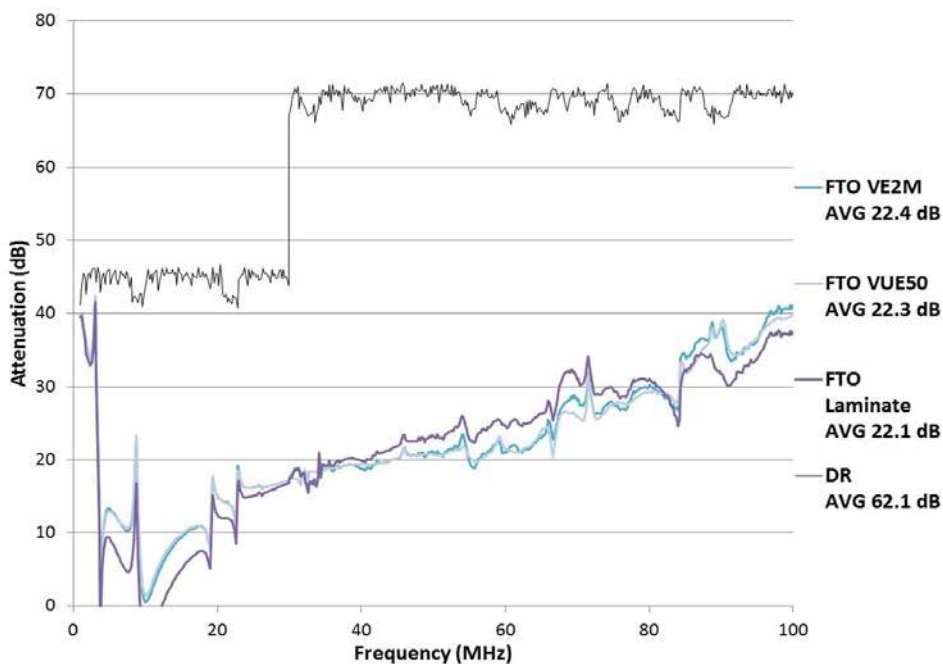


Figure 4: ASTM F3057-14 Attenuation for the Electric Field

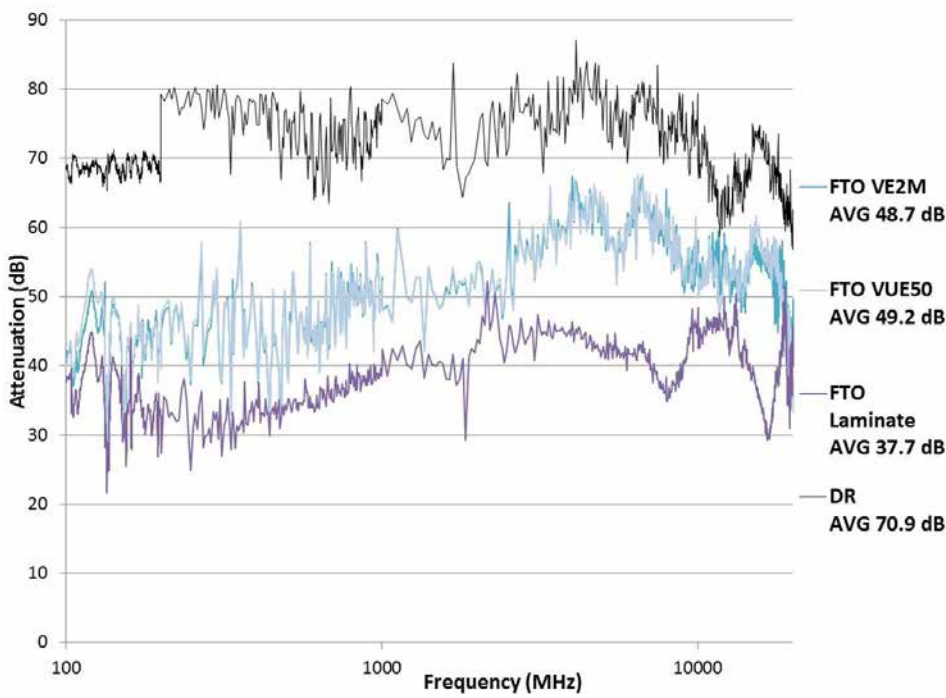


Figure 5: ASTM F3057-14 Attenuation for the Plane Wave Field

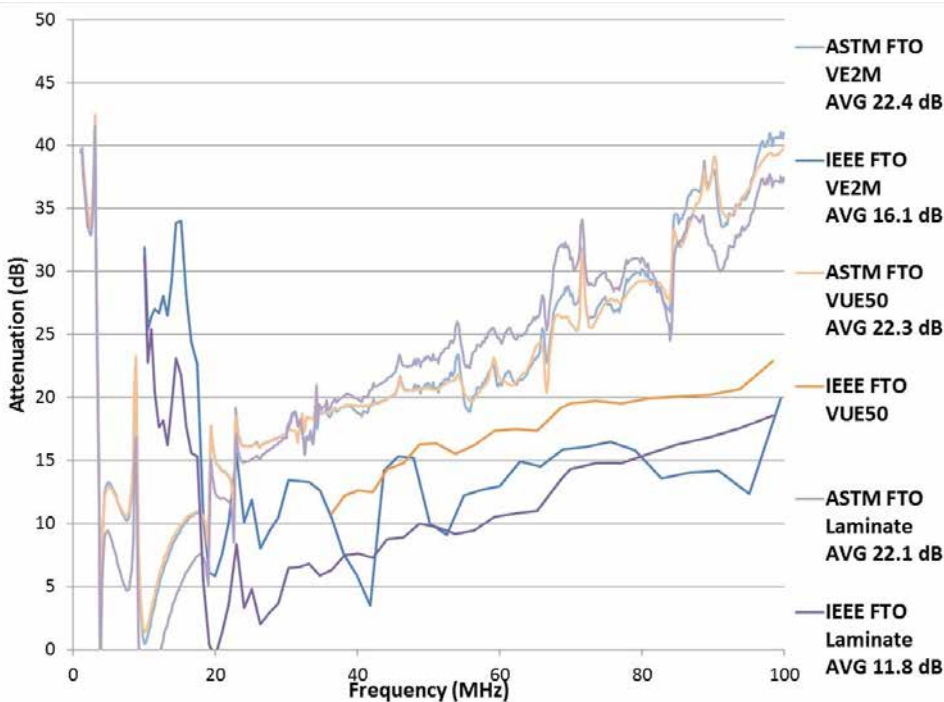


Figure 6: Comparison of the Modified IEEE 299 Results and the ASTM F3057-14 Results for the Electric Field

Figure 5 shows the results from the ASTM F3057-14 test for the plane wave field. The standard deviations between the two antenna positions for each FTO TLI unit were: 0.07 dB for VE2M and 0.51 dB for VUE50, with a standard deviation of 1.42 dB for the FTO Laminate. Once again, the highest performing FTO TLI unit had attenuation that was 30% greater than the attenuation of the FTO Laminate, further highlighting the importance of incorporating a Low-E coating.

Figures 6 and 7 show a comparison between the modified IEEE 299 results and the ASTM F3057-14 results. Figure 6 shows the electric field comparison, where the ASTM F3057-14 test resulted in consistently higher attenuation than the modified IEEE 299 test. Figure 7 shows the plane wave field comparison, where the ASTM F3057-14 test resulted in slightly lower attenuation than the modified IEEE 299 test. ASTM F3057-14 resulted in higher attenuation until approximately 300-500 MHz, when the IEEE 299 results started to exceed the ASTM attenuation levels. Overall, the averages for each test for the plane wave field were within 10% of each other for the FTO TLI units and within 2% of each other for the FTO Laminate.

As demonstrated, a properly selected glass product can have excellent RF shielding performance and can be effective at securing a building from potential electronic eavesdroppers. However, glass will never be as good at blocking RF signal as a fully-enclosed metal cage, so other important considerations must be taken into account when selecting a glass product, such as aesthetics, thermal and solar performance, visible light transmission, and reflective color. These attributes were calculated for the tested products and are shown in Figure 8, Figure 9, and Table 3. Color is an important selection criterion for architects with a general preference for neutral colors. Figure 8 shows the interior reflective film-side color, and Figure 9 shows the exterior reflective glass-side color. Table 3 shows the overall average attenuation for the electric and plane wave fields for both test methods, along with visible light transmission, thermal and solar performance numbers. For thermal and solar performance comparison purposes, this table also includes the corresponding insulating laminated unit performance for each coating without the FTO conductive coating within the FTO Laminate. Combining all of these results shows that when accounting for all variables in the glass selection process for anti-eavesdropping, a conductive coated product with a Low-E coating provides the best attenuation performance along with providing improved thermal and solar performance.

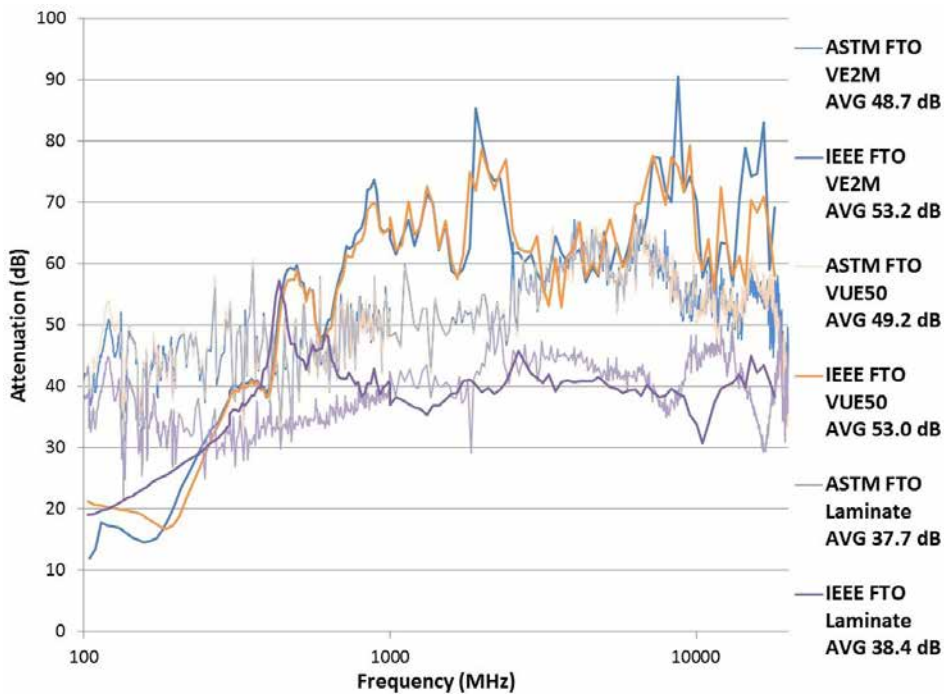


Figure 7: Comparison of the Modified IEEE 299 Results and the ASTM F3057-14 Results for the Plane Wave Field

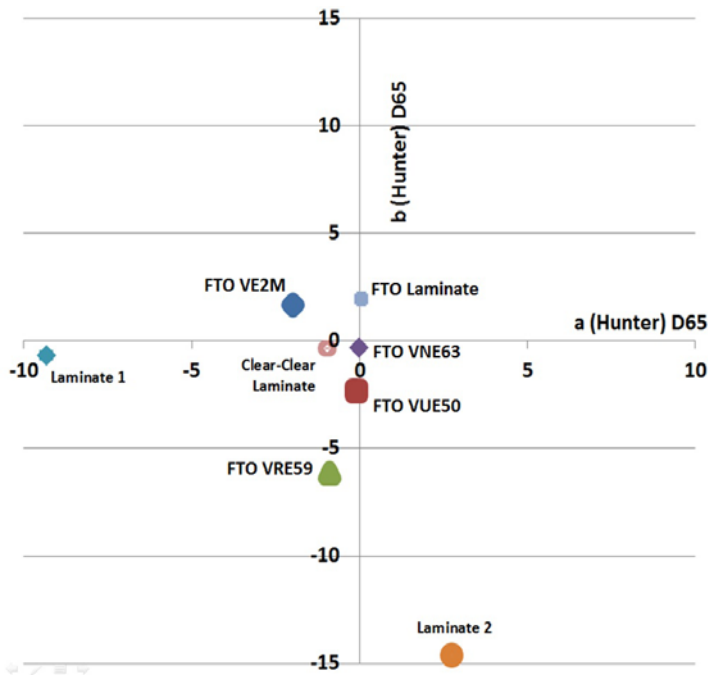


Figure 8: Interior Reflective Film-Side Measurement for Tested Products

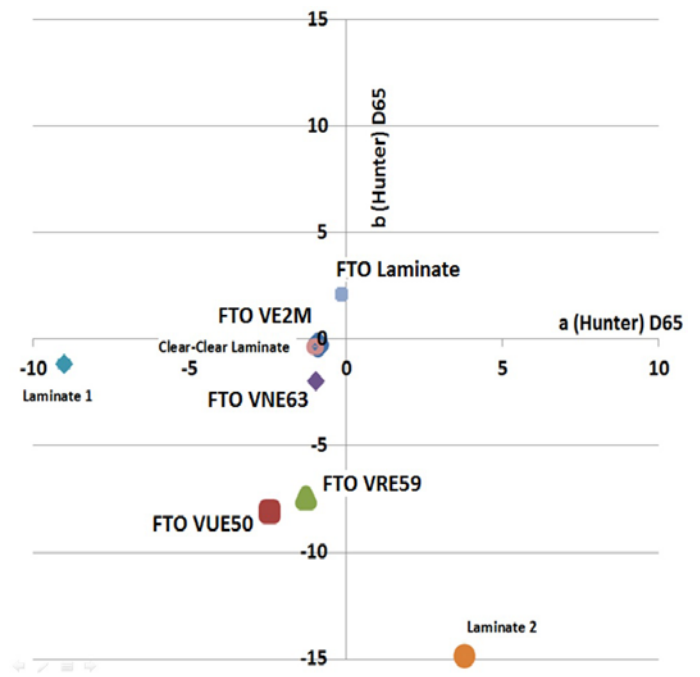


Figure 9: Exterior Reflective Glass-Side Measurements for Tested Products

| Product              | Average Attenuation (IEEE 299 Result, except where noted) |                   | Visible Light Transmission (%) | U-Value (Winter) | U-Value (Summer) | Solar Heat Gain Coefficient |
|----------------------|---|-------------------|--------------------------------|------------------|------------------|-----------------------------|
|                      | Electric Field (dB)                                       | Plane Wave (dB)   |                                |                  |                  |                             |
| FTO VE2M             | 19.3 <sup>1</sup>   | 51.0 <sup>1</sup> | 58                             | 0.23             | 0.20             | 0.33                        |
| Non-FTO VE2M         | N/A   | N/A               | 68                             | 0.29             | 0.26             | 0.37                        |
| FTO VUE50            | 22.3 <sup>2</sup>   | 51.1 <sup>1</sup> | 40                             | 0.23             | 0.20             | 0.22                        |
| Non-FTO VUE50        | N/A   | N/A               | 46                             | 0.28             | 0.25             | 0.25                        |
| FTO VRE59            | 14.6  | 52.5              | 44                             | 0.23             | 0.21             | 0.30                        |
| Non-FTO VRE59        | N/A   | N/A               | 51                             | 0.29             | 0.26             | 0.38                        |
| FTO VNE63            | 16.5  | 52.2              | 51                             | 0.23             | 0.20             | 0.25                        |
| Non-FTO VNE63        | N/A   | N/A               | 60                             | 0.29             | 0.25             | 0.33                        |
| Laminate 1           | 9.9   | 45.0              | 43                             | 0.97             | 0.88             | 0.25                        |
| Laminate 2           | 7.2   | 29.8              | 53                             | > 0.80           | > 0.80           | 0.30                        |
| FTO Laminate         | 17.0 <sup>1</sup>   | 38.1 <sup>1</sup> | 75                             | 0.62             | 0.49             | 0.56                        |
| Clear-Clear Laminate | 2.0   | 3.3               | 85                             | 0.95             | 0.86             | 0.71                        |

<sup>1</sup>Average of IEEE 299 and ASTM F3057-14 results.

<sup>2</sup>ASTM F3057-14 result only.

Table 3: Overall Average Attenuation for Each Product with Visible Light Transmission, Thermal and Solar Performance Numbers

## Conclusions

While the IEEE 299 test protocol has several important differences when compared to the ASTM F3057-14 test, the attenuation results from each method yields similar results. The ASTM F3057-14 test, however, is superior in the sense that the attenuation results are more focused on the glass due to the larger sample and aperture size. The larger size maximizes the dynamic range, minimizes variation in attenuation, and reduces the contribution from signal leakage around the perimeter. The ASTM F3057-14 test also standardizes the test parameters, making it possible to compare results for products tested by different manufacturers or at different labs. This makes comparisons between products more reliable and improves consistency industry wide. With less variation, a better determination can be made on which product to select for installations, and the end customer can be more confident that the product selected will perform as it did in the laboratory testing. A properly selected glass product can deliver good aesthetics, solar performance, and RF attenuation performance. Standardization of the RF test method will allow the customer to select the best anti-eavesdropping product for the building construction.

## References

1. ASTM F3057-14, "Standard Test Method for Electromagnetic Shielding Effectiveness of Glazings"
2. IEEE Std 299- final revision 2006, "Standard Method for Measuring the Effectiveness of Electromagnetic Shielding Enclosures"
3. CyberShield™ is a trademark of Viracon.
4. DATASTOPTM is a trademark of Pilkington.

# Taking Control of Anisotropy in Tempering Process: The New Way

Riku Farm  
Glaston Finland Oy

## Keywords:

Anisotropy, Iridescence, stress pattern, leopard spots, quench marks

## Abstract

Anisotropy is caused by stress differences in the glass which result from uneven heating and cooling of the glass in the tempering process. The phenomenon becomes visible when glass is viewed in polarized light – which is why anisotropy is especially visible for example when glass is installed by seaside or high in the mountains. In certain conditions anisotropy can become visible other venues as well.

Anisotropy is first and foremost a visual defect and it does not make glass weaker from a mechanical point of view. Laws, regulations and standards define requirements for safety glass regarding its mechanical strength. Hence, anisotropy is traditionally not considered as a defect from a regulatory point of view. However, anisotropy can effectively ruin a facade's appearance, which is why it should not be overlooked. A key factor here is also measurement technology that hasn't been able to provide reliable and fast measurements of all processed glasses.

Taking control of anisotropy has been a continuous headache for glass processors. By using latest machinery and technology it is possible to get better results regarding anisotropy – and solutions for controlling anisotropy are getting more and more sophisticated. In this session we will take a look of how anisotropy can be controlled and measured with latest technology.

# Potential of Structured Switchable Glazing\*

Walter Haase<sup>1</sup>, Marzena Husser<sup>1</sup>, Werner Sobek<sup>1,2</sup>

## Abstract

Glazed facade units must satisfy numerous criteria. In addition to allowing an unobstructed view of the exterior they should also provide protection from direct sunlight and the associated heat transfer. In order to optimize the performance of glazed facades under varying conditions, much effort has been directed towards the development of adaptive glazing systems based on smart materials or smart mechanisms. This article will outline the functional principles and visual properties of a liquid crystal based system.

By modifying conventional liquid crystal technologies used for display applications and upscaling the pixel size to an architectural meso scale a switchable glazing system with unique and promising characteristics was developed and investigated by the authors. The advantages and the most promising fields of application of this adaptive glazing system will be presented herein.

## 1. Introduction

The function of the building envelope is to act as the interface between the interior and exterior environments. The performance of the glazed sections of the facade is essential for providing the maximum possible comfort for the building occupants, while minimizing the energy and resource demands of the building. Since both the external climate conditions as well as the user demands from the interior vary considerably over time, an interface with constant properties is bound to be less than optimal. Instead, an adaptable "building skin" is required – one which can regulate light and energy flows and prevent glare effects to maintain the highest possible level of efficiency under all conditions.

## TN cell

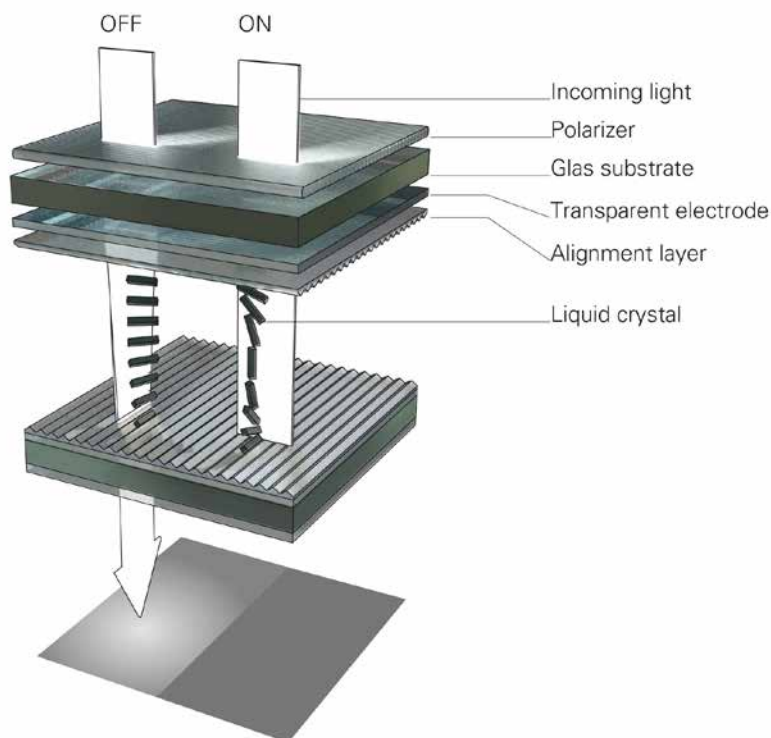


Figure 1. TN-cell with external polarizers – functional principle

Research and design have been underway for some time in the field of adaptive window elements for building envelopes, in both university and industrial settings. By modifying conventional liquid crystal technologies used for display applications and upscaling the pixel size to an architectural meso scale a switchable glazing system with unique and promising characteristics was developed and investigated by the authors.

## 2. Controllable Liquid Crystal Based TN-Glazing - properties

The vast majority of current large scale television displays is based on liquid crystal (LC) technology [1]. LC-displays (LCD) are substructured into hundreds of thousands of pixels which individually act as light valves

to control the transmittance of the screen's backlight. Each pixel comprises three sub-pixels equipped with red, green, and blue color filters. By altering its transmittance each sub-pixel can be controlled to produce the desired intensity of color and thereby display color images. The simplest technology to achieve displaying images (grayscale) is the twisted nematic liquid crystal cell (TN-cell). A very thin layer of nematic liquid crystals (only a few microns thick) is contained between two glass substrates. Two conductive layers are necessary on the inside surfaces of the substrates. So-called orientation layers at the boundary surfaces of the liquid crystals serve to selectively orient the rod-shaped crystals if no voltage is applied. If polarizers are applied to each substrate on the outside, it becomes possible to influence the transmittance of

\* Research supported by the Federal Institute for Research on Building, Urban Affairs and Spatial Development within the Federal Office for Building and Regional Planning, Germany (research project: "TN technology for architectural applications") and by Baden-Württemberg Stiftung GmbH, Germany (research project: "i<sup>3</sup>: intelligent, interactive, integrative solar control glazing")

<sup>1</sup> Institute for Lightweight Structures and Conceptual Design (ILEK), University of Stuttgart, Pfaffenwaldring 7 and 14, 70569 Stuttgart, Germany

<sup>2</sup> Werner Sobek Group GmbH, Albstraße 14, 70597 Stuttgart, Germany

light and energy. The polarizers are usually oriented at 90 degrees to one another. Through the application of a small voltage (~3-15 V) to the two conductive layers, the orientation of the liquid crystal molecules is affected and the intensity of the transmitted light can be controlled. The investigated TN-cell in "off" and "on" state is depicted in Figure 1.

The idea of scaling up the pixels of a TN-cell to dimensions suitable for architectural glazing applications is not new [2]. However, thus far it has not been possible to manufacture an adaptive window unit based on the TN-cell technology with sufficient long-term durability. The temperature- and UV-stability of the foil polarizers and their sensitivity to moisture have been the primary obstacles. Improvements on foil polarizers now seem to permit the use of TN-cell technology as an adaptive element of large scale glazing units [3][4].

As in conventional liquid crystal displays, the conductive layers of the TN-cell can be structured in a laser or photolithographic process. In this process the cell is subdivided into pixels that may be switched individually. Every pixel is connected to the control unit via a transparent conductive path (transparent wiring) which generates a thin gap between adjacent pixels. The conductive path cannot be darkened. Such a device is defined as TN-module.

Due to the filter effect of the polarizers and the reflection and absorption of the glazing itself, a TN-module reaches a maximum light transmittance of about 37 %, making it comparable to other sun protection glazing systems. Though, the pixel transmittance can be varied down to less than 1 %. The transmittance of the module is higher and greatly depends on the gap width and the total gap area of the module. Decreasing the gap area is therefore the aim for optimizing the pixel layout. The spectral transmittance of a single pixel of the TN-module, as measured with a spectrometer by the authors, is shown in Figure 2.

For optimizing the properties of the insulation glass unit (IGU) with integrated TN-modules, the fundamentals of energy flux through a window must be considered. Radiative heat flux represents approximately 2/3 of the energy flux within a window and is dependent on the material characteristics of window panes and coatings [5]. Due to the high absorptance of the switchable cell, it heats up to approximately 70 °C – 80 °C. In order to prevent heat transfer from the cell to the room, the application of additional glass coatings is advisable. On the basis of measurements in a sun simulator

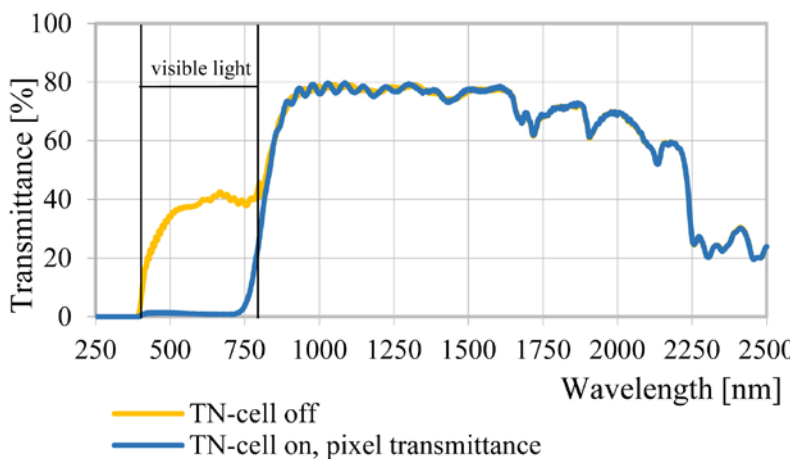


Figure 2. Spectral transmittance of a single TN-cell pixel with external polarizers

and simulations done with the software Window / Optics [6] it could be shown that the temperature of the inner pane of an insulation glass unit equipped with TN-modules and provided with a selective coating does not exceed the temperature of a common double glazing significantly [4].

### 3. Prototypes

The authors succeeded in manufacturing two prototypes of substructured switchable insulation glass units (SIGU) [7]. The functional components (TN-modules) were produced by the company BMG MIS GmbH Luminator Technology Group according to the specifications defined by the authors. The glass panes for the IGU were delivered by Okalux GmbH according to the layout defined by the authors. Appropriate mounting parts have been designed to fix the TN-modules to the inner surface of the outer glass pane of the IGU. Two different TN-module types have been investigated by the authors. TN-module type 1, as shown in Figure 3, exhibits

a pixel arrangement with 26 columns and 16 lines (amount of pixels: 416). The individual pixels may be driven in the „off“ or „on“ state. Different transmittance values of this type of glazing are to be achieved by displaying different image patterns. The vertical non-switchable pixel gaps mainly define the minimum overall transmission of the module. In these gaps, the contacting wires are guided to the control electronics, which is located at the upper module edge.

The slight reduction of the amount of pixels per module led to TN-module type 2 (Figure 4.). In 19 columns and 16 lines there are 304 individually controllable pixels which can be switched in 16 gray scale steps each. The pixel gaps could be reduced significantly for this type, which leads to an improved dark state of the glazing.

The spectral transmittance of one single pixel of both types of modules and the appropriate values for the modules are shown in TABLE 1. Spectral properties were measured using

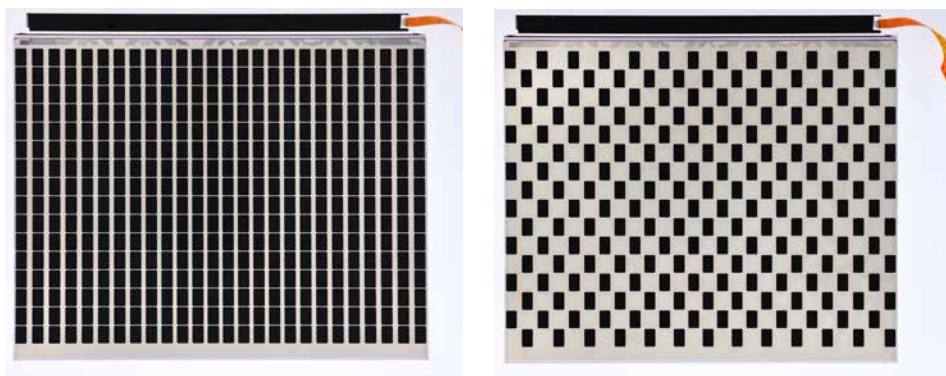


Figure 3. TN-module type 1: all pixels in "on" state (left), 50 % pixels in "on" state and 50 % pixels in "off" state (right)

a spectral photometer [see Figure 2]. Photometric (index: vis) and radiometric (index: sol) properties have been calculated then according to DIN EN 410 [8]. The minimal transmittance of module type 1 ( $T_{vis}=13\%$ ) is significantly higher than of module type 2 ( $T_{vis}=5\%$ ) [9]. Further development of the pixel layout aims at achieving a dark state of the module of about 2%. Daylight simulations [10] for Stuttgart confirmed that no further glare protection would be necessary for a TN-glazing with this darkening efficiency. Transmittance, Reflectance And Absorptance Values Of The Pixel Area And The Modules For Both Types Of Tn-Cells



Figure 4. TN-modul type 2: all pixels in "on" state (left), graded transparency (right)

#### 4. Facade test facility

For further investigation of the influence on the indoor climate, the energy consumption for room conditioning, the daylight provision and the glare protection, the SIGU equipped with TN-modules have been implemented in the south facade of a test building in Stuttgart-Vaihingen.

The two-storey timber building at the University of Stuttgart includes four test rooms with dimensions of 2.00 m x 4.20 m x 2.70 m (width x depth x height). Each of these rooms can be considered an independent office space. Crucial properties of the construction components of the test building are presented in TABLE 2.

The south facade of the building is designed for easy incorporation of different glazing units. Two test rooms are currently equipped with the switchable glazing units presented in this paper (cell type 1 in room 1, cell type 2 in room 2), as shown in Figure 5. The first insulation glazing unit was equipped with 45 modules of type 1 arranged in 9 lines and 6 columns of modules. The window size is 244 cm in height and 174 cm in width. This arrangement of the SIGU exhibits 18720 pixels. The SIGU in the second room was equipped with 54 TN-modules of type 2 with 16416 pixels.

The facade test facility is provided with measurement equipment for recording the outdoor and indoor conditions. Solar irradiation is detected by means of two pyranometers and a traceable pyrheliometer on the roof of the building. Other weather parameters are provided by a local weather station. For measurements of the visual and thermal conditions in the interior, illuminance sensors, thermocouples and humidity sensors are used. The measurement equipment for one of the test rooms is visualized in Figure 6.

|               | Single pixel |           | TN-module  |           |
|---------------|--------------|-----------|------------|-----------|
|               | <i>off</i>   | <i>on</i> | <i>off</i> | <i>on</i> |
| Module type 1 |              |           |            |           |
| $T_{vis}$     | 0.37         | 0.01      | 0.37       | 0.13      |
| $T_{sol}$     | 0.46         | 0.28      | 0.46       | 0.34      |
| $R_{vis}$     | 0.08         | 0.06      | 0.08       | 0.06      |
| $R_{sol}$     | 0.13         | 0.12      | 0.13       | 0.13      |
| $A_{vis}$     | 0.55         | 0.93      | 0.55       | 0.81      |
| $A_{sol}$     | 0.40         | 0.60      | 0.40       | 0.53      |
| Module type 2 |              |           |            |           |
| $T_{vis}$     | 0.37         | 0.01      | 0.37       | 0.05      |
| $T_{sol}$     | 0.46         | 0.28      | 0.46       | 0.30      |
| $R_{vis}$     | 0.08         | 0.06      | 0.08       | 0.06      |
| $R_{sol}$     | 0.13         | 0.12      | 0.13       | 0.12      |
| $A_{vis}$     | 0.55         | 0.93      | 0.55       | 0.89      |
| $A_{sol}$     | 0.40         | 0.60      | 0.40       | 0.58      |

Table 1. Transmittance, reflectance and absorptance values of the pixel area and the modules for both types of tn-cells

| Building structure component               |   | U-Value [W/m <sup>2</sup> K]<br>(EN ISO 6946) |
|--|---|---|
| Exterior wall                              | Wood frame construction with 120 mm wood fiber insulation, rear-ventilated timber façade        | 0.30  |
| Interior wall                              | Wood frame construction with 60 mm wood fiber insulation  | 0.48  |
| Roof                                       | Laminated timber with approx. 140 mm tapered insulation, waterproofing with PCV membrane strips | 0.19  |
| Storey ceiling                             | Wood frame construction with 60 mm wood fiber insulation  | 0.49  |
| Base plate, elevated (160 mm above ground) | Wood frame construction with 200 mm wood fiber insulation                                       | 0.21  |

Table 2. Construction characteristics of the façade test facility (rubnerhaus ag – s.p.a)

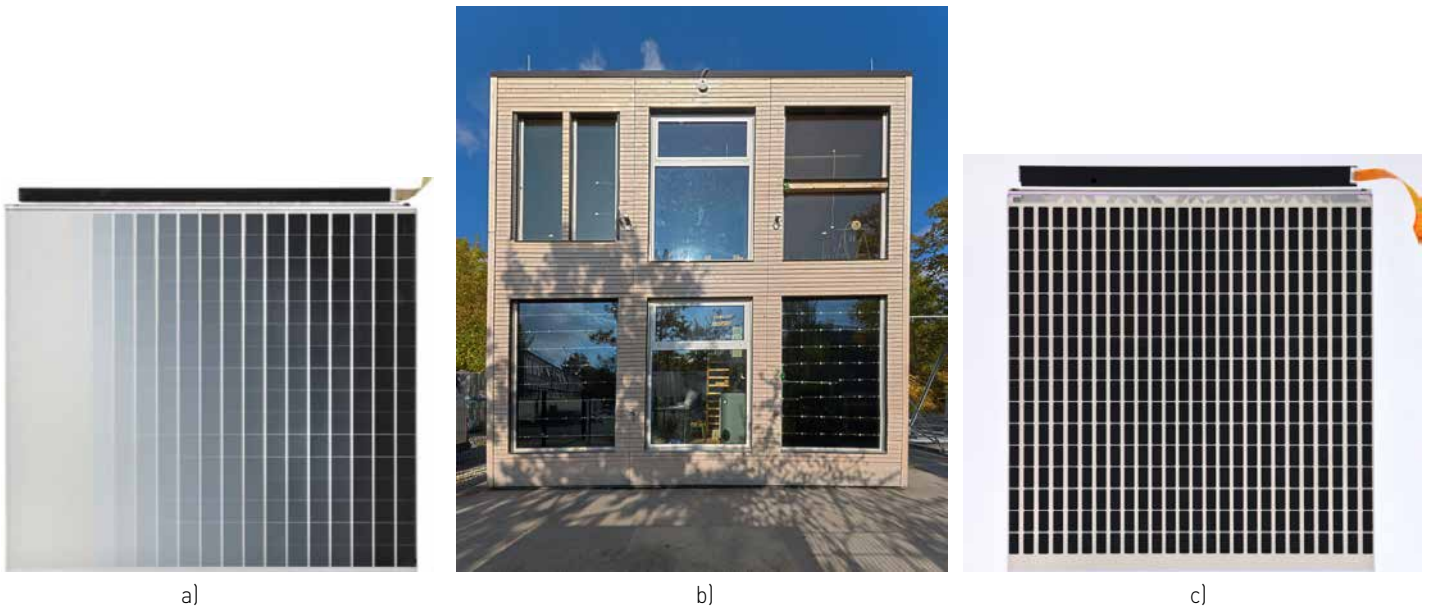


Figure 5. Facade test facility at the University of Stuttgart: b) south facade with substructured switchable glazing units in two test rooms on the ground floor (right: module type 1 a), left: module type 2 c)).

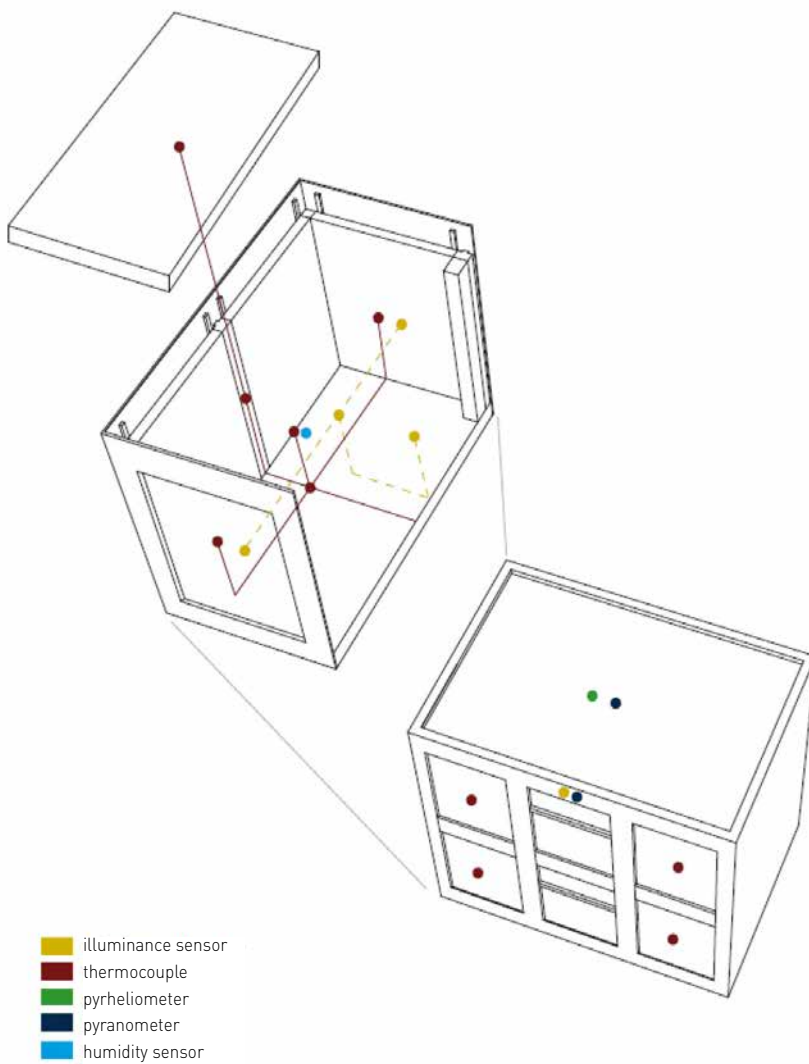


Figure 6. Measurement equipment of the facade test facility at the University of Stuttgart

## 5. The Concept of Control

The control strategy applied to each of the switchable glazing takes into account the feasibilities arising from the subdivision in individually controllable pixels and from the quick response time for switching a pixel. Switching times under different temperatures have been measured (TABLE 3). The response time depends on the applied voltage and temperature of the module. Even under low voltage and low temperatures switching from one transmittance state to another does not exceed 103 ms. The ability for tinting the glazing partially combined with the quick response time allow for controlling daylight and glare protection independently from one another. The high switching capacity allows for following the changes of outside conditions and ensuring the best possible indoor lighting situation. Glare protection may be achieved by tinting the appropriate areas of the glazing. Daylight provision may be adjusted by darkening or brightening the remaining areas as needed.

| Temperature [°C]    | -9    | 23   | 90  |
|---------------------|-------|------|-----|
| Switching time [ms] | 102,5 | 17,9 | 2,5 |

Table 3. Switching time of the investigated TN-Module at different temperatures

Glare protection is investigated by displaying a circular spot on the window. The algorithm for calculating the position of this spot takes into account the sun's movement and the occupant's position in the room.

First measures assumed a fix position of the inhabitant. Therefore, it was sufficient to update the positioning of the spot once a minute to ensure proper shading of the occupant's head. First tests of the SIGU with TN-modules of type 1 with this strategy have been started and led to promising results. The movement of the spot is shown in Figure 7. The shading effect on the direct sun radiation for the occupant is shown in Figure 8.

The irradiation intensity at the occupant's position will be measured using photometric and photographic methods during next steps of investigation. Currently, the reliability of the control strategy could be proved even though it is obvious that glare protection cannot be achieved completely with the TN-glazing of type 1 because of its too high transmittance in the dark state.

Improvements in shadowing efficiency are expected when investigating the TN-glazing of type 2 because of the lower transmittance in the dark state. The main advantage of the TN-glazing compared to other investigated glazing types is the possibility of sub-structuring the window area. It allows for an increase in light transmittance by only darkening the necessary spots. In addition, a window equipped with TN-modules offers the occupants a further option because it may also be used as an information display. This effect is shown in Figure 9. Even though the resolution is quite rough compared to LC-displays the potential of this type of glazing is clearly demonstrated.

## 6. Conclusion

Although both types of the TN-glazing exhibit lower maximum transmittance compared to electrochromic window technology, their performance is promising. First quantitative results will have to be confirmed during the following qualitative investigations of daylight and glare control, as well as their influence on reducing energy demands for room conditioning. Currently, the authors are implementing further control strategies into the facade test facility for in situ evaluations. Automatic detection of the occupant's position will ensure an enhanced flexibility of the glazing partitioning.

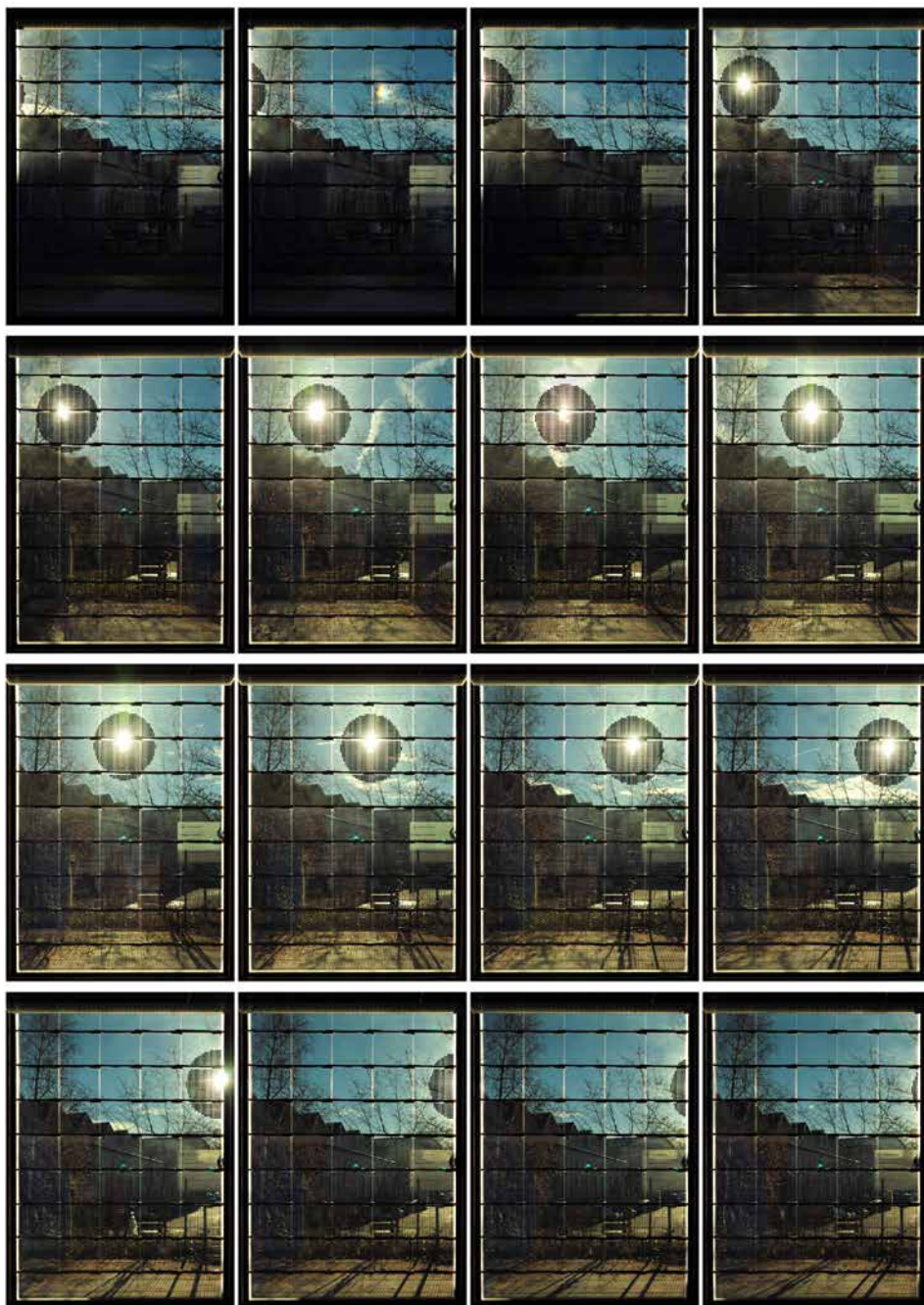


Figure 7. View from inside to outside with spot displayed before sun position (SIGU with TN-modules of type 1) to ensure shading of the occupant's head (8 th of Dec. 2016). Phot.: G. Metzger, ILEK



Figure 8. Shadow caused by spot on the glazing to prevent glare effect on occupant. Phot.: G. Metzger, ILEK



Displaying information on the SIGU with TN-modules of type 1. View from inside to outside. Phot.: G. Metzger, ILEK

## 7. Architectural potentials

In comparison to conventional facade solutions, the switchable, substructured TN-glazing developed by the authors shows significant advantages. It is characterized by a large switching range and a very short switching time. The possibility of implementing the switchable glazing units in standard framing systems, combined with their minimal connection requirements makes the system perfect for being applied into new building facades as well as for retrofitting existing buildings.

As shown within the first simulations [7], the TN-glazing has the potential to replace conventional insulating glazing units with external shading. The integration of sun and glare protection functions, complemented with an effective controlling, leads to a remarkable comfort improvement. The glare is the main comfort factor which can be influenced by the implementation of the TN-glazing. Moreover, a slight reduction of the building's energy demand is expected. Additionally to the reduction of cooling energy demand, the reduction of embodied energy and of the resources consumption, compared with common additive facade solutions, are remarkable advantages of the TN-glazing.

Waiving of additive solutions leads to an architecture of simplified expression and complex functionality. The sun protection is no longer a secondary device which has to fill out strictly defined boundaries. The possibility of darkening any required area of the glazing makes the facade flexible and changeable. The position of areas on the facade used for light and energy transmission and to enable visual contact to the outside can be flexibly redefined in dependence on actual needs [7]. The following Figure 10. illustrates several application options of the structured adaptive glazing in a fully glazed facade. The depicted flexibility is only one example for the expected wide application field of this system.

## 8. Acknowledgements

The work described herein was carried out in the framework of the following research projects: "TN technology for architectural applications", founded by the Federal Institute for Research on Building, Urban Affairs and Spatial Development within the Federal Office for Building and Regional Planning and "i<sup>3</sup>: intelligent, interactive, integrative solar control glazing", founded by the Baden-Württemberg Foundation. The construction of the facade test facility was supported by numerous industrial companies, above all by Rubner Haus



Figure 10. Application possibilities of the structured adaptive glazing in a fully glazed facade. Renderings: S. Leistner, ILEK

AG - S.p.A., Toshiba Klimasysteme Beijer Ref Deutschland GmbH, TWL-Technologie GmbH, Nimbus Group GmbH, Alcoa GmbH, Paul Bauder GmbH & Co. KG, Okalux GmbH. The companies BMG MIS GmbH and Okalux GmbH supported the manufacturing of the described prototypes. The authors wish to express their gratitude for this support.

## References

- [1] Chen, R. H.: Liquid Crystal Displays: Fundamental Physics and Technology, New York (2011)
- [2] Gläser, H.-J.: Abschirmvorrichtung für Fenster (Shielding for Windows), German patent DT 2155951, date of patent: 8 th March 1973.
- [3] Haase, W., Husser M., Kurz E., Rau L. "Schaltbare Verglasung auf der Basis von lyotropen und nematischen Flüssigkristallen (Switchable Glazing Based on Lyotropic and Nematic Liquid Crystals)", Project Report, Stuttgart, 2014.
- [4] Husser, M. et al., "Structured Sun Protection Glazing" in Proc. Engineered transparency. International Conference at glasstec, Düsseldorf, 2014.
- [5] Schittich, C. et al., Glass Construction Manual, Birkhäuser, Munich, 2007.
- [6] Lawrence Berkeley National Laboratory (LBNL), "Window Optics", <http://windowoptics.lbl.gov/> (Access on: 08 Mai 2017).
- [7] Husser, M., Haase, W., Hoß, P., and Sobek, W., "New Possibilities of Sun and Glare

- Protection with a Structured Switchable Glazing" in Proc. Challenging Glass 5, Ghent, 2016.
- [8] DIN EN 410 Glass in Building – Determination of Luminous and Solar Characteristics of Glazing, German Version EN 410: 2011.
- [9] Haase, W., Husser, M., & Sobek, W., "Potentiale strukturierter, schaltbarer Verglasungen (Potential of Structured Switchable Glazing)" in B. T. Weller, Glasbau. Ernst & Sohn GmbH & Co. KG., 2016.
- [10] Hoß, P., Simulation des Einflusses verschiedener klimatischer Randbedingungen auf die Regelungsstrategie schaltbarer Verglasungen und den Gebäudeenergiebedarf (Simulation of the Influence of Different Climate Conditions on the Building Energy Demands and on the Control Strategies for Switchable Glazing), Bachelor Thesis at ILEK, Stuttgart, 2015.

# Smart Glazing in Intelligent Buildings: What Can We Simulate?

Fabio Favoino<sup>a,b1</sup>, Luigi Giovannini<sup>c</sup>,  
Roel Loonen<sup>d</sup>

<sup>a</sup> Eckersley O'Callaghan Ltd, 236 Gray's Inn Road, WC1X 8HB London, UK

<sup>b</sup> Glass and Facade research group, University of Cambridge, Trumpington Street, CB2 1PZ Cambridge, UK

<sup>c</sup> Department of Energetics, Politecnico di Torino, Corso Duca degli Abruzzi 24, 10141 Torino, Italy

<sup>d</sup> Building Physics and Services, TU Eindhoven, Postbus 513 5600 MB, Eindhoven, the Netherlands

The integration of smart glazing and adaptive façade in buildings can lead to large performance improvements and added functionality compared to conventional static building envelope systems. This is achieved not only by embedding automatic/controllable (smart/active) switchable materials into the building envelope, but also including intelligence into the way the whole building is designed and operated.

Desk studies and Building Performance Simulation can be used to support the design process of these technologies and of the building integrating them, as well as to support product development aimed at building integration of novel switchable glazing technologies. Although BPS tools traditionally lag behind the development of novel technologies and adaptive building envelope systems, therefore it is not always possible or easy to evaluate in an accurate and comprehensive way the performance of building integrated switchable glazing technologies, and in general adaptive facades. In this paper we outline the main requirements for BPS of smart glazing. These include user interface requirements, models availability, integration of physical domains, integration and customisation of control strategies. We analyse possible BPS tools that could be used and their main advantages and drawbacks, and describe the latest advances for more integrated simulation methodologies and tools, included an ad-hoc developed simulation tools which aims at overcoming the main limitation of traditional BPS tools.

## Keywords

building performance simulation, smart glazing, adaptive facades

## 1. Introduction

The potential of smart (switchable or adaptive) glazing technologies to improve building performance is due to their ability to modulate their thermo-optical properties in response to external stimuli, enabling the modulation of the amount of solar radiation entering the indoor environment in response to transient boundary conditions (external, such as climate, or internal, such as occupants' requirements). The main purposes two adopt a switchable glazing are to improve:

- indoor environmental conditions in terms of visual (e.g. daylight utilization, glare discomfort, view to outside) and thermal (e.g. overheating in summer) comfort aspects, as well as privacy;
- building energy use and carbon emissions (by reducing heating, cooling and lighting energy use at the same time, by controlling these switchable glazing in an intelligent way).

Different materials and systems are used as functional layers to modulate thermo-optical properties in switchable glazing, including, chromogenic materials (e.g. thin-film metal compounds), liquid crystals and suspended particles. The main differences between various types of switchable windows can be summarized with the following features:

- Control mechanism:** referring to the terminology in (Loonen, 2013)), *extrinsic* control refers to the use of an external signal (i.e. electrochromic and liquid crystal devices, LCD), while *intrinsic* control refers to the essential feature of the material to vary its thermo-optical properties in an autonomous way in response to changing boundary conditions, e.g. as a function of temperature (i.e. thermochromic, thermotropic) or incident light (i.e. photoelectrochromic, photovoltachromic) etc..
- Wavelength range:** switchable windows can modulate thermo-optical properties in the whole solar spectrum, or only

in the visible part, non-visible part or independently in both parts of the solar spectrum (De Forest et al. 2017).

- Optical properties:** solar radiation can either be reflected to outside or absorbed by the smart glazing. Moreover, depending on the variation of the refractive index of the materials embedded in the functional layer, a switchable glazing could have a diffusive behavior when activated (as thermotropic and LC devices), contributing to reduce glare risk from direct solar radiation and to distribute light more uniformly in the indoor space, instead of maintaining the specular state.

Smart glazing compete with dynamic solar shading technologies on different aspects, from improved building performance, to building and component integration issues, control strategies, maintenance strategies, initial and operating costs etc.. Both smart glazing and dynamic solar shading technologies present different advantages and disadvantages, which may be generally valid or project specific. This comparison is not in the scope of this paper, although most of the considerations presented in this work regarding the evaluation of their performance can be applied to both.

Different types of switchable windows are commercially available on the market (Fig. 1 and 2). Baetens et al. (2010), Jelle et al. (2012) and Favoino et al. (2015) provide extensive overviews of the state-of-the-art in this field. Input data for switchable windows is available at glazing manufacturers such as View Inc, SAGE (electrochromics), Raven Windows (thermotropics), Merck (liquid crystals), and via the International Glazing Database (IGDB) that is linked to the LBNL Window software. In figure 1 the performance of established (continuous lines) and innovative (dashed lines) smart glazing technologies is compared to conventional static glazing (data points) in terms of thermo-optical properties (g-value on the x-axis and visible transmission on the y-axis), the main difference and advantage is that smart glazing (continuous and dashed lines) are able to modulate their properties between different states compared to conventional glazing, represented only by one set of properties (data point).

<sup>1</sup> Email: fabio@eocengineers.com, ff279@cam.ac.uk

Besides the capability of the switchable glazing to actively manage the solar radiation entering the built environment, it is the way it is controlled that finally determine which performance objective is improved and to which extent, as an adaptive behaviour itself does not automatically guarantee effective operations (Wickmans et al. 2005). In this context, Building Performance Simulation (BPS) a quantitative and true comparison between different materials (either adaptive or static), products and controls, by means of overall building performance metrics, i.e. total primary energy, comfort/discomfort indexes, overall indoor environmental quality and whole life value indicators etc.. However, simulation of smart glazing can be significantly more complex than performance prediction of conventional static facades, as existing simulation tools were not originally developed for this purpose.

The present paper aims at guiding professionals and researchers in understanding the issues related to BPS of smart glazing, and selecting the best suited models, tools and simulation strategies to suit their purposes.

## 2. Building Performance Simulation requirements for smart glazing

Most BPS tools stem from a time when variation of thermo-optical properties of building components and their control was not a primary consideration (Oh and Habert 2015), restricting the options for modelling switchable glazing and adaptive facades. The requirements and limitations of BPS tools to evaluate the performance of buildings integrating switchable glazing can be grouped into the following areas (Loonen et al. 2016):

### a) Multi-domain integration of performance evaluation

Switchable glazings influence both visual and thermal performance aspects of a building. The interactions between these physical domains need to be taken into account in an appropriate way, depending on the purpose of the evaluation (i.e. the building performance indicators under evaluation) and on the control mechanisms of the switchable glazing. Whenever a thermal/energy performance indicator need to be evaluated (i.e. building loads, building energy use, temperatures, thermal comfort etc...) together with a visual comfort indicator (i.e. glare index, light levels etc.) and/or the adaptation of the façade is triggered by a result in another physical domain, virtual physical models representing only one physical domains (i.e. only thermal or visual) or two

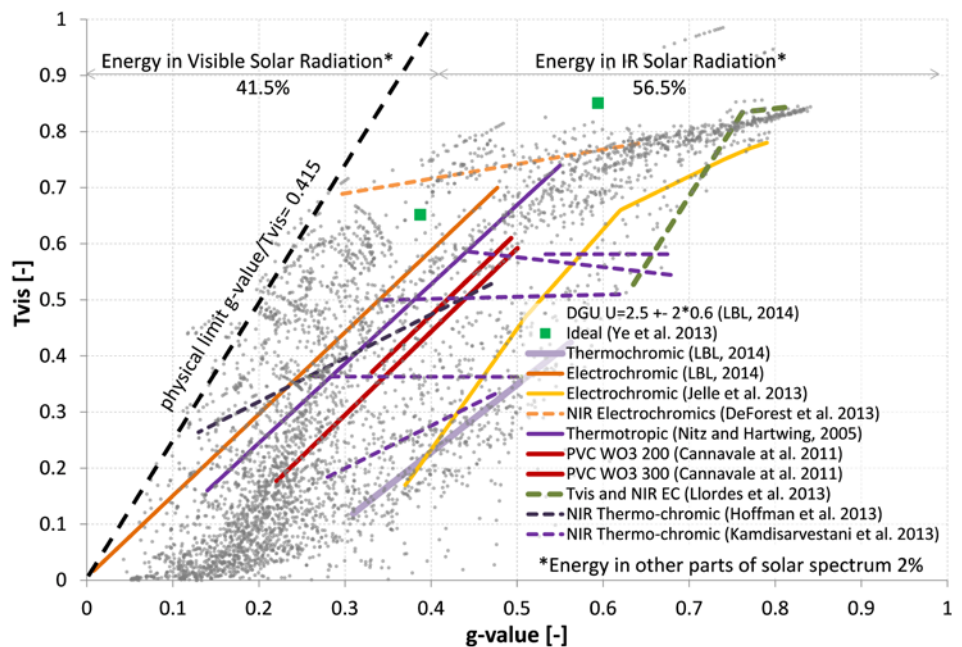


Figure 1. Comparison of switchable glazing integral solar properties compared with conventional double glazing units (grey data points) (Favoino 2015).

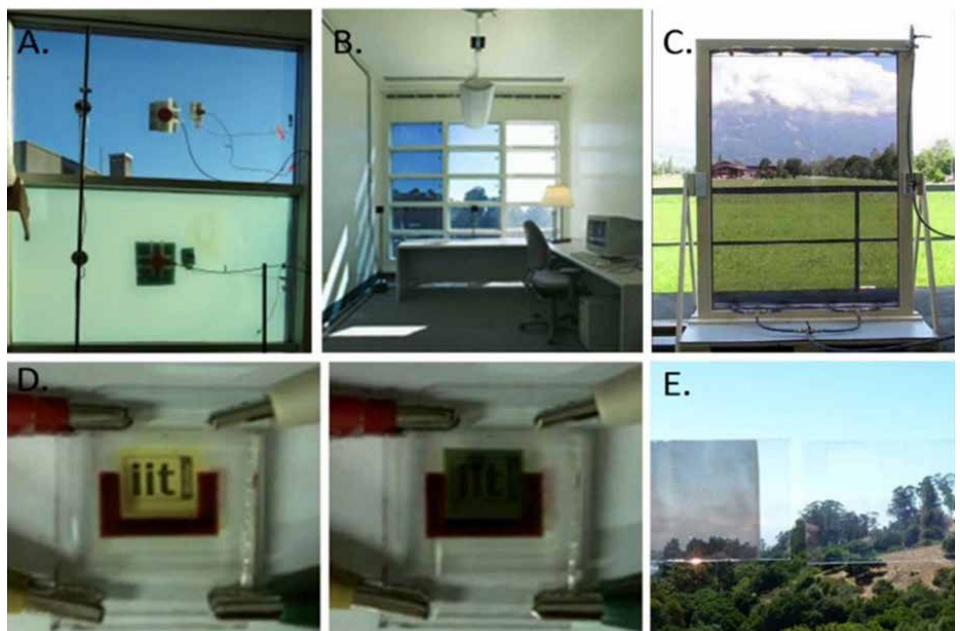


Figure 2. View of different smart glazing technologies: A) thermo-tropic, B) electro-chromic, C) Fluidglass, d) Photo-Volta-Chromic, e) Tunable Visible-Infrared Reflector.

independent physical domains (i.e. one thermal and one visual model independent from each other) cannot provide reliable results (Favoino et al. 2017) (cf. Section 4).

b) **User interface definition of switchable glazing:** Two types of modelling approaches can be distinguished: (i) application-oriented and (ii) general-purpose approach. **Application-oriented (AO)** indicates that the user can select a specific material / glazing model between the one already available in the BPS tool. Therefore the switching mechanisms and how it is triggered are already embedded

in the specific model, and users can activate it easily by means of the graphical user interface, but they are limited to the pre-sets available. The **general-purpose (GP)** features, on the other hand, are not restricted to a specific technology, but offer the user flexibility to define the way thermo-physical properties varies within the switchable glazing and/or their control mechanisms (either passive or active).

c) **Solution routines for transient heat conduction through building elements:** it is important that the switching of window properties happens during simulation

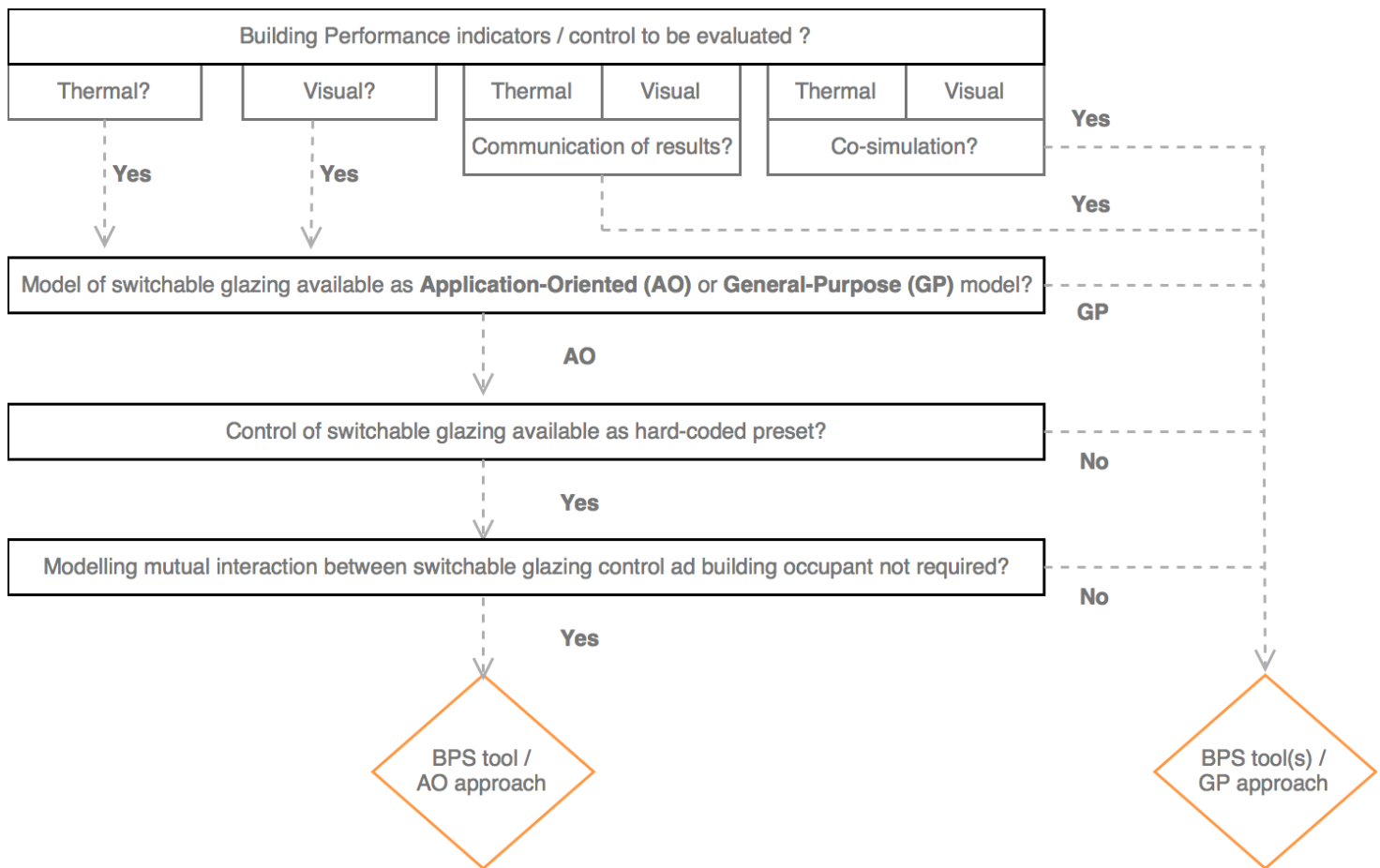


Figure 3. Proposed workflow to select BPS tools according to simulation requirements and characteristics of switchable glazing technology.

run-time, because the changing amount of solar radiation that enters the zones leads to a different transient thermal response of the space. Although the methods to solve heat transfer phenomena differential equations in BPS tools can only work with time-invariant thermo-physical properties (i.e. density, specific heat capacity, thermal conductivity), the models for calculating energy gains/losses through transparent portions of the building envelope, on the other hand, do not normally include thermal storage effects [Freire et al. 2011] several intensive studies have been carried out in order to reduce the energy consumption of buildings. One solution lies on whole building energy simulation that permits to enable the heat (and moisture. For this reason it is easier to take dynamically changing window properties into account.

- d) **Control strategies:** for AO options, the user can only select between the control strategies pre-coded in the BPS tools (hard-coded control), whether these are intrinsic (depending on a state of the material, i.e. glazing temperature) or extrinsic switchable glazing (depending on an external stimulus, i.e. room air temperature). Time-scheduled control is

generally available, but the user can only pre-define control actions as a function of time. Some BPS tools presents script-based control capabilities, allowing the user to code the preferred control strategy in the simulation tool, replicating and extending the hard-coded pre-set options to suit the specific control requirements of the switchable glazing. Hard-coded presets or script-based controls are extremely suitable for evaluating the performance of rule based controlled switchable glazing, this is by far the most adopted control option in the market [Oldewurtel et al. 2012], and many studies adopts this to test the performance of switchable glazing technologies [Jonsson and Ross, 2010; Fernandes and al. 2013]. More advanced control strategies for switchable glazing, such as advanced rule based or Model Predictive Control strategies, can only be evaluated by adopting script based control in combination with more advanced simulation strategies [Favoio et al. 2016, De Forest et al. 2017, cf. Section 4].

- e) **Occupant interaction:** scarce information and modelling capabilities is available to model the way individual occupants may want to control a specific switchable glazing technology. This capability requires

behavioural models that describe the interaction of building occupants with adaptive building envelope systems. Until now, such occupant interactions can only be implemented via script-based control approaches [Yan et al. 2015, Gunay et al. 2015].

Based on these requirements building designers and researchers need to assess the most appropriate tool and methodology to simulate switchable glazing to suit their purpose. In Figure 3 a flow chart diagram is used to guide this evaluation, to understand whether the switchable glazing under investigation can or cannot be simulated with current BPS tools, and which modelling approach should be used.

### 3. Implementation of smart glazing models and controls into BPS tools

As a result of their presence in the market, options for AO modelling of switchable glazing technologies are embedded in many of the widely-used simulation tools (EnergyPlus, ESPr, IDA ICA, IES VE and TRNSYS) Such implementations offer the possibility to control the properties of the building model's fenestration systems during simulation run-time.

### 3.1. Application oriented modelling capabilities

Most of extrinsically controlled switchable glazing, such as electrochromic, SPD and liquid crystal devices could be modelled in BPS tools with the AO approach, by defining different glazing states (each one with specific thermo-optical properties) and linking these with a pre-set hard coded control. The differences between the various implementations are the number of possible window states [e.g. on/off versus gradual transitions] and the simulation state variables that can be used for the control of adaptation [e.g. room temperature, ambient temperature and incident radiation].

Intrinsically controlled switchable glazing, such as thermotropic/chromic windows, are slightly more complicated to simulate than other switchable window types because of:

- a) intrinsic control: adaptation of the fenestration properties is directly triggered by window material temperature instead of a control signal that is based on more general simulation variables;
- b) hysteretic behavior: most thermochromic / thermotropic functional layers presents a different variation of thermal properties according to material temperature when undergoing heating or cooling (Warwick et al, 2013). This hysteresis can have a significant impact on the heating and cooling energy use of buildings (Warwick and Binions, 2014), although until no study

exists on the influence of this behavior also on thermal and visual comfort.

A provision for thermochromic window simulation is implemented in EnergyPlus since v3.1 and ESP-r. The input of these models consists of sets of glazing thermo-optical properties at various temperatures. During the simulation, the thermochromic layer temperature of the previous time step is automatically fed into a window control algorithm, which then selects the window properties that best match with the given temperature. In IDA ICE and Trnsys, it is also possible to model thermotropic/chromic windows, but a significantly higher level of work and expertise is required from the user side because a script for the control strategy needs to be manually developed by the simulation user. The hysteretic behavior of switchable window cannot be modelled in any BPS tools (Saedi et al., 2010), although some researchers developed a simplified approach to evaluate its effect (Warwick et al, 2013) by a two-step simulation process, aimed at developing a correlation between thermochromic window states (optical properties) and climate boundary conditions (i.e. solar irradiance on the glazing).

Figure 4 shows how 5 of the most adopted BPS tools implement AO modelling capabilities and control modelling capabilities. These tools (EnergyPlus, ESPr, IDA ICE, IES VE and TRNSYS) are selected as they present i) the largest user community among designer

and researchers, ii) extensive building envelope modelling capabilities and iii) they are widely validated. On the right of Figure 4 different switchable glazing technologies are represented and connected with the BPS tool which presents any AO modelling capabilities regarding that specific technology. While on the left hand side of Figure 4, the control options available in each simulation tool are outlined. Not all hard coded control options are available for all switchable glazing technologies, especially for intrinsic technologies (i.e. thermochromic glazing). This graphical representation will be hosted in a web based tool, allowing the user to define the switchable glazing technology and its control strategies and to identify to most suited simulation tool to fit his/her purpose, and vice-versa to select his/her preferred simulation tool and understand its modelling capabilities.

### 3.2. General purpose modelling capabilities

In order to overcome the limitations set by AO modelling approaches, researchers and designers oriented towards the tools allowing more GP modelling approaches. EnergyPlus, ESPr and TRNSYS allow the user to adopt the general oriented approach to simulate a smart glazing:

- a) **ESP-r**: this is a simulation tool with an open-source environment aimed at the research community. Since its first version, various groups have contributed general-purpose functionalities for

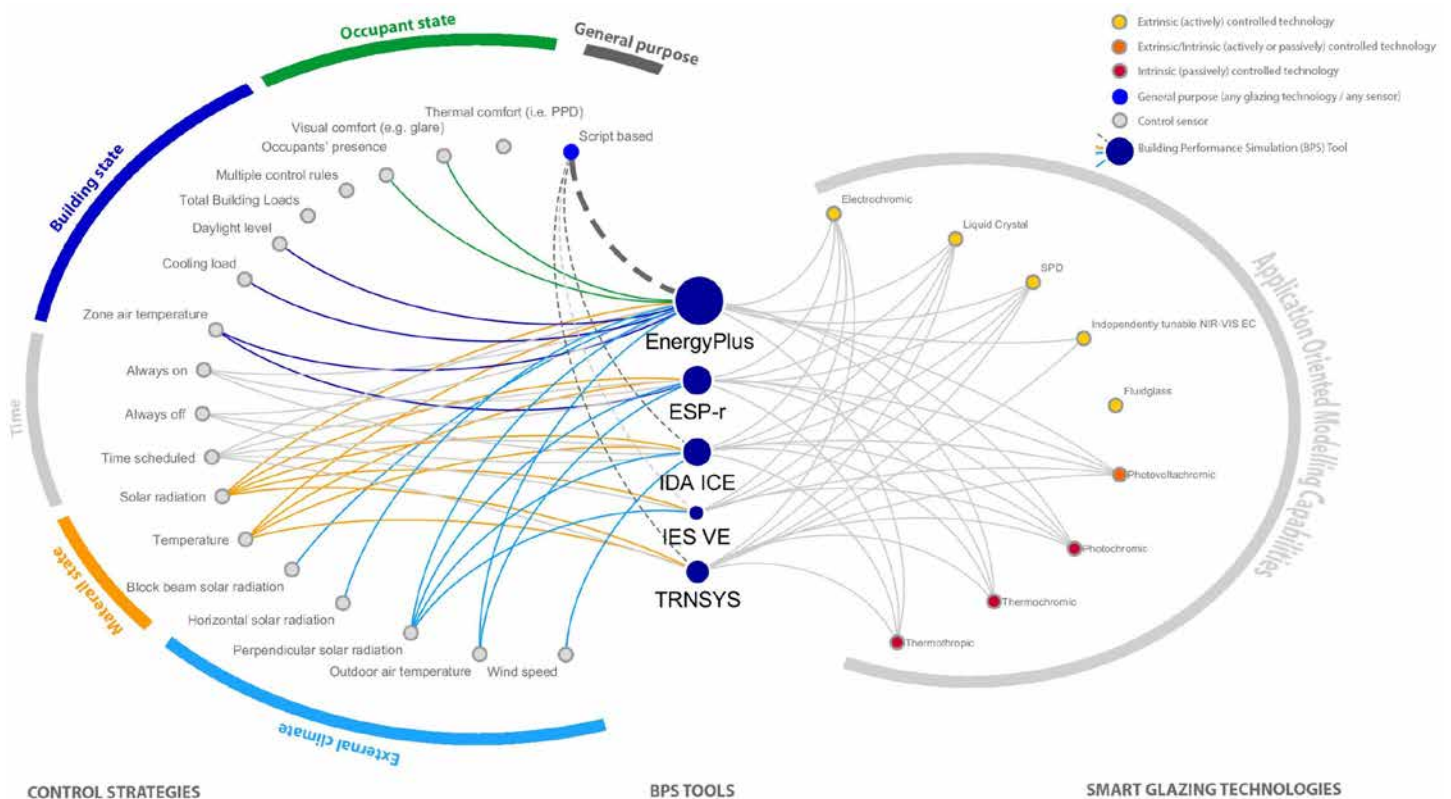


Figure 4. Implementation of Application Oriented modelling and control capabilities in existing BPS tools.

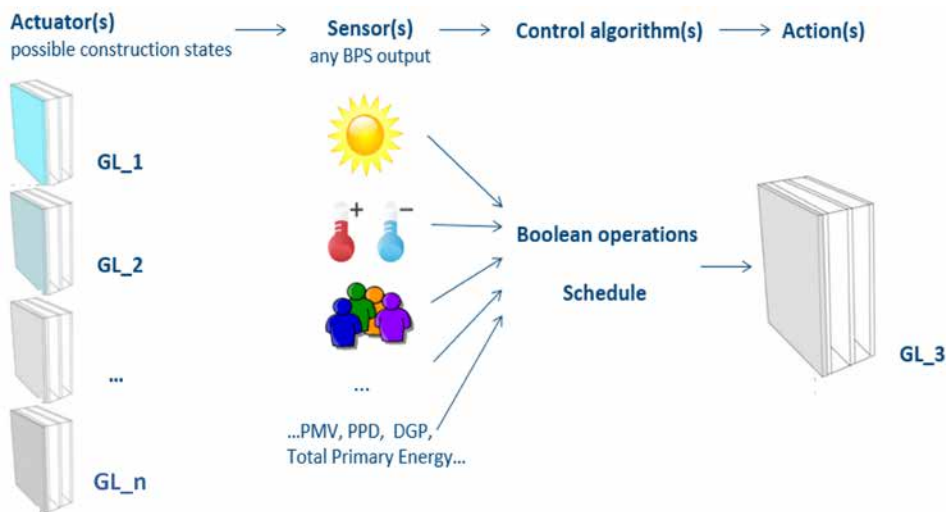


Fig 5. Modelling and simulation logic of the EMS-EnergyPlus "Surface construction state" actuator, TRNSYS Type 56 "WindowID" Actuator, ESPr "transparent multi-construction control".

liquid crystals, or shading devices), etc.. The logic of the "Construction State Actuator" of the EMS is schematized in Fig. 5, this is similar to the TRNSYS "WindowID" and ESPr "transparent multi-construction control" actuators. This logic is divided in four sequential steps defining: i) the actuators, in this case different glazings each one with the properties of one alternative state of the switchable glazing; ii) the sensors, identifying the boundary conditions whom the control of the switchable glazing will be controlled on; iii) the control algorithm, how the variation of the boundary conditions ultimately influence the variation of the switchable glazing states; iv) the actions, identifying which of the glazing state, which building services state (i.e. air flow or dimmable artificial lighting power) and which building occupant state (i.e. thermal comfort or visual comfort indicator) can be associated with each sets of boundary conditions.

#### 4. Limitations of current BPS tools and future outlook

Although switchable windows are one of the most mature adaptive façade technologies, when it comes to integration in building performance simulation tools, there are still some issues that require further research. Based on the presented review, the following points requires particular focus:

- few documentation is available on the validation of AO and GP modelling approaches for switchable glazing;
- many switchable window coatings have special angular-dependent optical properties that are different from regular specular glazing systems. It is not always straightforward to introduce such effects in building performance simulation tools;
- some switchable window technologies, especially electrochromic materials have a delay of 10 to 20 minutes between actuation and actual coloration of the window. This effect may have significant impact on window performance, particularly for visual comfort and glare; it is nevertheless not possible to take this effect into account in most simulation tools;
- it is currently not always possible to model the effects of windows that can independently control switching in various parts of the solar spectrum;
- some switchable window technologies, especially thermochromic / thermotropic materials have an hysteretic dependence of optical properties on temperature. This effect have significant impact on the window energy performance, and may have significant impact on thermal and visual

modeling adaptive facade technologies. The (i) transparent multi-layer construction control and (ii) special materials (Evans and Kelly 1996), allow a general purpose modelling of switchable glazing;

- TRNSYS:** the multi-zone building model (TYPE 56) is one out of a large number of possible system components. The variable window id option and a controllable bi-directional scattering distribution function (BSDF) (Hiller and Schöttl 2014) are directly implemented in TYPE 56. All other adaptive features in TRNSYS can be activated by manipulating (i.e. switching on/off or modulating) the connections to and from the TYPE 56 building model, via equations using either the graphical Simulation Studio or by editing text files;
- EnergyPlus:** of all software tools analysed, EnergyPlus has had the largest growth in adaptive facade modelling capabilities since it was developed. Most notably, these developments have been driven by the introduction of the EnergyPlus Runtime Language (Ellis, Torcellini, and Crawley 2007), aiming at replicating a real building Energy Management System (EMS). The system is based on the same elements of a real EMS – that is, sensors, control logics and algorithm, and actuators. In the latest release of the EMS system (US DOE, 2015) new actuators were introduced in order to control thermo-optical properties of the building envelope in a more flexible way. A control algorithm can be designed in the EMS, adopting the ERL programming language, in order to control any actuator, based on data from the sensors. Any output from EnergyPlus can be adopted as a sensor, together with outputs from any other independent virtual model, allowing the integration of results from other BPS tools (i.e. Radiance for daylight results).

In ESP-r only two states of the glazing could be modelled, while in ESP-r and TRNSYS only few simulation outputs could be used as a sensor for the control. EnergyPlus appears to be the most comprehensive and flexible tool to evaluate the performance of switchable glazing when building integrated. In fact within its EMS, the "Surface Construction State" actuator can be used to simulate variable thermo-optical properties, and therefore an adaptive glazing [Actuated Component Control Type: Construction State; Actuated Component Type: Surface]. This specific actuator allows to interchange during simulation runtime different constructions, characterised by different material properties, for the same building surface, according to a user specified control strategy. This GP modelling approach could be used to simulate the behaviour of switchable glazing, whereas different transparent constructions can be defined for each state the switchable glazing can assume during building operations, and an algorithm can be designed to control it according to the mechanisms triggering adaptation (i.e. phase/temperature change, electric signal, electron migration due to solar radiation etc.). By designing the control algorithm, the user could define either a novel intrinsically controlled smart glazing (controlled based on material states or climatic boundary conditions), or set-up a novel control for extrinsically controlled switchable glazing which is not included in BPS hard-coded pre-sets. In fact, in order to simulate other passive or active switchable glazing technologies, the control can be based on the signal from sensors such as: temperature of the construction element (thermo-chromic/tropic glazing); amount of solar radiation on the external side of the glazing (photo-chromic glazing); heating or cooling demand, amount of daylight in the indoor environment (for electrochromics and

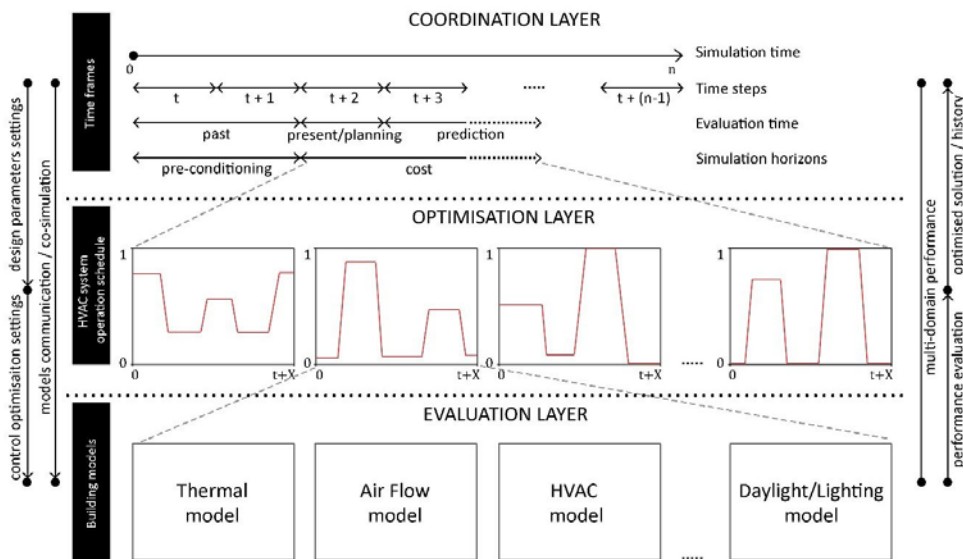


Figure 6. Architecture of advanced simulation strategies for switchable glazing.

by GP modelling approaches or by middle-ware software, while for co-simulation the use of a middle-ware software is essential (such as MATLAB or BCBTB, Wetter 2011). Optimisation middle-ware could be added to the simulation strategy to optimise the switchable glazing control strategy, as shown by Favoino et al. (2016). Figure 6 shows the usual architecture of advanced simulation strategies, involving i) a coordination layer (or software) for model communication or co-simulation; ii) an optional optimisation layer (software) to eventually optimise the control of the switchable glazing; iii) the evaluation layer constituted by the different building virtual models. The main limitation of advanced strategies is the additional work required to the modeller, to create the virtual building models in different physical domains and coordinate or exchange of information between these models by programming and scripting.

- comfort; although it is not possible to take this effect into account in any simulation tool;
  - f) it is not always straightforward and sometimes not possible to perfectly integrate the control of switchable glazing with the control of HVAC and artificial lighting systems;
  - g) the number of possible control strategies available for extrinsically controlled switchable window is very limited;
  - h) the implementation of novel smart glazing technologies and innovative controls by means of GP approaches require an extensive user expertise, due the lack of appropriate user interfaces allowing more efficient integration with the design process;
  - i) it is not possible to correctly evaluate the interaction between thermal and visual effect of controlling a switchable window within a single BPS tool, especially for technologies not implement in AO models or controls which are not hard-coded in the simulation tool already.
- In order to overcome most of these limitations, researchers have been adopting workarounds and simplified simulation strategies or more advanced simulation strategies.

#### 4.1. Simplified simulation strategies

The building integrating the switchable glazing can be represented by a series of independent building models, each one representing the building with the switchable glazing in a different glazing state (i.e. with different glazing thermo-optical properties). The results of the independent building models can then be combined at a post-processing stage in an attempt to capture the performance of a building integrating a dynamic component (i.e.

switchable glazing for which a model is not available yet), and/or to mimic more advanced building operations (Kasinalis et al. 2014; DeForest et al. 2013). This discrete approach works well for facade systems with long adaptation cycles (e.g. seasonal), but it cannot accurately model short-term adaptive building envelope dynamics, as it fails to account for the effect of delayed thermal response arising from the capacitance of building components (i.e. slabs, walls and internal partitions). These inaccuracies may eventually compromise decision-making based on simulation outcomes, but little information about this issue is reported in literature.

#### 4.2. Advanced simulation strategies

Whenever more than one physical domain need to be simulated at the same time (i.e. thermal and visual performance of a switchable glazing) the main approach is to integrate in a coordinated simulation strategy different BPS tools, enabling either the exchange of information between different models, or co-simulating the different models involved. Co-simulation, in particular, is a simulation strategy in which two or more simulators solve systems of coupled equations, by exchanging data during simulation run-time (Trcka et al. 2009). This strategy could become particularly important for performance prediction of switchable glazing, as it enables to (i) integrate the simulations over different interrelated physical domains (i.e. thermal and visual), (ii) evaluate emerging technologies for which models may not be directly available in the specific BPS tool used, and (iii) assess the potential of advanced control strategies of switchable glazing. In order to use these more advanced simulation strategies the exchange of information need to be enabled

#### 4.3. Current research activity and future work

Within the COST Action TU1403 – Adaptive Facade Network, which EOC is actively contributing to, the authors are developing an advanced simulation strategy and a graphical user interface to overcome most of the limitation of current BPS tools, based on a deep understanding and evaluation of the complexity of the requirements and capabilities of the simulation tools reviewed in this paper. This novel simulation tool aims at evaluating the building performance of switchable glazing (and adaptive facades in general) when integrated with buildings and their occupants in a more accurate and comprehensive way. It integrates EnergyPlus (thermal, airflow and HVAC simulation) with Radiance (daylight simulation) in a parametric environment (Grasshopper and Rhino), in order to be able to interface with 3D models and with the design process in a more efficient way. Figure 7 shows the Grasshopper interface of the simulation tool and some example results. The advanced simulation strategy adopted by this tool, was extensively validated and demonstrated in numerous publications, regarding: i) the definition of an ideal switchable glazing able to minimise building energy use (Favoino et al. 2015); ii) the assessment of innovative control for a novel photovoltachromic switchable glazing (Favoino et al. 2016); iii) the design and control optimisation of novel adaptive insulation technologies (Favoino et al. 2017).

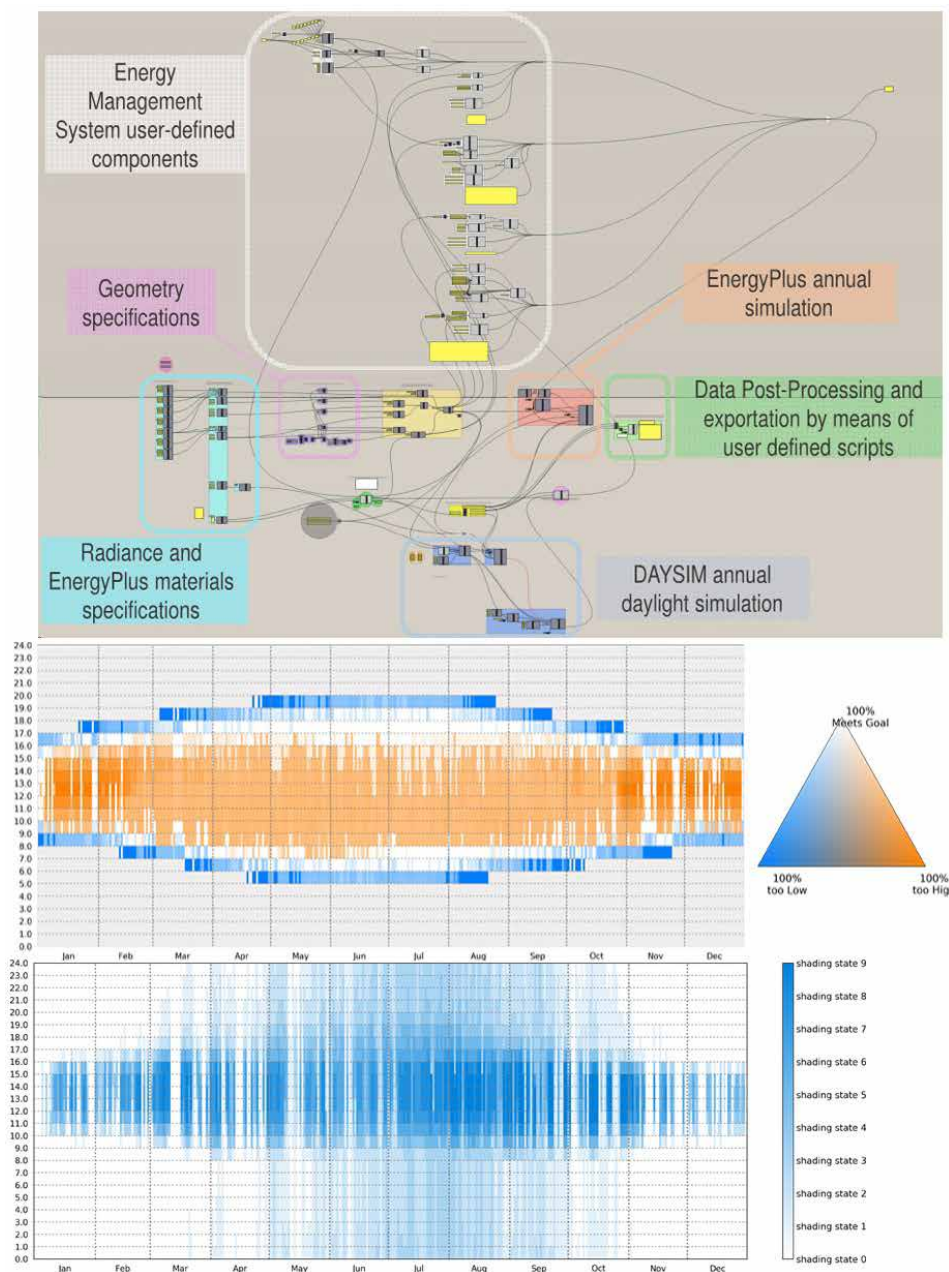


Figure 7. Top: Grasshopper Interface of the novel simulation tool for adaptive facade; Center: Goal based yearly results; Bottom: Resulting control of three state switchable glazing to meet performance goals.

The next steps of the research, by means of the developed simulation strategy and interface, are to:

- evaluate the effect of the hysteresis of thermochromic glazing on energy and visual comfort related aspects;
- evaluate the performance of novel switchable glazing [and innovative controls] on large scale projects;
- develop further the parametric graphic user interface to support general purpose modelling approaches and to provide a more efficient and user friendly way define advanced control via script based approaches.

## Conclusions

The presents paper provides an overview of the requirements and capabilities of Building Performance Simulation tools to evaluate the performance of building integrating switchable glazing. The modelling approaches capabilities of different Building Performance Simulation tools are analysed and compared with the requirements set from a technological point of view. Currently these tools offer an application-oriented approach, which restricts the modelling capabilities to the switchable glazing models and controls pre-coded in the specific simulation tool. Although some of them have started to present a more flexible modelling approach, named by the authors

“general purpose”, allowing flexibility to model switchable glazing and controls which are not ready available in the BPS tools interface. Nevertheless different issues need to be addressed in order to provide a comprehensive method and tool to evaluate building integrated switchable glazing, mainly regarding physical domain integrations, advanced control simulations and accuracy of specific switchable glazing models. These different issues are discussed and an ad-hoc developed simulation strategy and tool is presented, with the aim to address most of the limitations of current BPS tools, while supporting in a more efficient way the design process of building integrating switchable glazing and the product development of novel switchable glazing technologies.

## Acknowledgement

The authors would like to acknowledge the COST Action TU1403 – “Adaptive Facades Network” for providing excellent research networking opportunity.

## References

- Baetens R., Jelle B.P., Gustavsen A., [2010]. Properties, requirements and possibilities of smart windows for dynamic daylight and solar energy control in buildings: A state-of-the-art review, *Sol. Energy Mater. Sol. Cells*. 94, 87–105
- DeForest, N., A Shehabi, G Garcia, J Greenblatt, E Masanet, E.S. Lee, S. Selkowitz, and D.J. Milliron. (2013). “Regional Performance Targets for Transparent near-Infrared Switching Electrochromic Window Glazings.” *Building and Environment* 61 (March). Elsevier Ltd: 160–68.
- DeForest N., Shehabi A., Selkowitz S., Milliron D.J., A comparative energy analysis of three electrochromic glazing technologies in commercial and residential buildings, *Applied Energy*, Volume 192, 15 April 2017, Pages 95-109, ISSN 0306-2619, <https://doi.org/10.1016/j.apenergy.2017.02.007>.
- Ellis, P. G., Torcellini, P.A. and D. B. Crawley (2007). “Simulation of Energy Management Systems in EnergyPlus.” In *Proceedings of Building Simulation 2007*, 1346–53.
- Evans, M., and N. J. Kelly (1996). *Modelling Active Building Elements with Special Materials*. ESRU Occasional Paper, University of Strathclyde, Glasgow
- Favoino F., Overend M., Jin Q., [2015]. The optimal thermo-optical properties and energy saving potential of adaptive glazing technologies, *Appl. Energy* 156, 1-15.
- Favoino F., Fiorito F., Cannavale A., Ranzi G., & Overend M., [2016]. Optimal control and performance of photovoltachromic switchable glazing for building integration in temperate climates, *Applied Energy*, Volume 178, 15 September 2016, Pages 943-961, ISSN 0306-2619, <http://dx.doi.org/10.1016/j.apenergy.2016.06.107>.
- Favoino F., [2017]. *Building Performance Simulation of adaptive facades*, PhD thesis, University of Cambridge, UK.
- Favoino F., Jin Q., Overend M. [2017], Design and control optimisation of adaptive insulation systems for office buildings. Part 1: Adaptive technologies and simulation framework, *Energy*, Volume 127, 15 May 2017, Pages 301-309, ISSN 0360-5442

- Fernandes L.L., Lee E.S., Ward G., (2013). Lighting energy savings potential of split-pane electrochromic windows controlled for daylighting with visual comfort, *Energy and Buildings* 61, 8-20, ISSN 0378-7788, <http://dx.doi.org/10.1016/j.enbuild.2012.10.057>.
- Freire, R. Z., Mazuroski, W., Abadie, M.O., and N. Mendes (2011). "Capacitive Effect on the Heat Transfer through Building Glazing Systems." *Applied Energy* 88 (12): 4310-19. doi:10.1016/j.apenergy.2011.04.006.
- Gunay, H. B., O'Brien, W., & Beausoleil-Morrison, I. (2015). Implementation and comparison of existing occupant behaviour models in EnergyPlus. *Journal of Building Performance Simulation*, 1-46.
- Hiller, M., and P. Schöttl (2014). "Modellierung Komplexer Verglasungssysteme in Trnsys." In *Proceedings of BauSIM2014, the Fifth German-Austrian IBPSA Conference*, 387-94
- Hong, T., D'Oca, S., Turner, W.J.N., and S. C. Taylor-Lange (2015). "An Ontology to Represent Energy-Related Occupant Behavior in Buildings. Part I: Introduction to the DNAs Framework." *Building and Environment* 92: 764-77. doi:10.1016/j.buildenv.2015.02.019.
- Jelle B.P., Hynd A., Gustavsen A., Arasteh D., Goudey H., Hart R., (2012). Fenestration of today and tomorrow: A state-of-the-art review and future research opportunities, *Sol. Energy Mater. Sol. Cells*. 96, 1-28.
- Jonsson A., Roos A. (2010). Evaluation of control strategies for different smart window combinations using computer simulations, *Solar Energy* 84:1, 1-9, ISSN 0038-092X, <http://dx.doi.org/10.1016/j.solener.2009.10.021>
- Kasinalis C., Loonen R.C.G.M., Cóstola D., Hensen J.L.M., (2014). Framework for assessing the performance potential of seasonally adaptable facades using multi-objective optimization, *Energy Build.* 79, 106-113.
- Loonen, R.C.G.M., Trčka, M., Cóstola, D., Hensen, J.L.M., (2013). Climate adaptive building shells: State-of-the-art and future challenges, *Renewable and Sustainable Energy Reviews* 25: 483-493, ISSN 1364-0321
- Loonen, R.C.G.M., Favoino, F., Hensen, J.L.M. & Overend M, (2016). Review of current status, requirements and opportunities for building performance simulation of adaptive facades, *Journal of Building Performance Simulation*, DOI: 10.1080/19401493.2016.1152303
- Oldewurtel F., Parisio A., Jones C.N., Gyalistras D., Gwerder M., Stauch V., Lehmann B., Morari M., (2012). Use of model predictive control and weather forecasts for energy efficient building climate control, *Energy and Buildings*, 45, 15-27, ISSN 0378-7788, <http://dx.doi.org/10.1016/j.enbuild.2011.09.022>
- Oh, Sukjoon, and Jeff S. Haberl (2015). "Origins of Analysis Methods Used to Design High-Performance Commercial Buildings: Whole-Building Energy Simulation." *Science and Technology for the Built Environment* 4731 (October): 1-20. doi:10.1080/23744731.2015.1063958.
- Saeti, M., Piccirillo, C., Parkin, I.P., Binions, R., Ridley, I. (2010). Energy modelling studies of thermochromic glazing, *Energy Build.* 42, 1666-1673
- Trcka, M., J.L.M. Hensen, and M. Wetter (2009). "Co-Simulation of Innovative Integrated HVAC Systems in Buildings." *Journal of Building Performance Simulation* 2 (3): 209-30. doi:10.1080/19401490903051959.
- U.S. DOE (2015). "Application Guide for EMS Energy Management System - User Guide." [http://nrel.github.io/EnergyPlus/EMS\\_Application\\_Guide/EMS\\_Application\\_Guide/](http://nrel.github.io/EnergyPlus/EMS_Application_Guide/EMS_Application_Guide/).
- Warwick, M. , Ridley, I. and Binions, R., (2013). The Effect of Transition Hysteresis Width in Thermochromic Glazing Systems. *Open Journal of Energy Efficiency*, 2, 75-88. doi: 10.4236/ojee.2013.22011.
- Warwick, M.E.A., Binions, R., (2014). Advances in thermochromic vanadium dioxide films, *Journal of Material Chemistry A* 2, 3275-3292
- Wetter, M. (2011). "Co-Simulation of Building Energy and Control Systems with the Building Controls Virtual Test Bed." *Journal of Building Performance Simulation* 4 (3): 185-203. doi:10.1080/19401493.2010.518631
- Wickmans, A., Aschehoug, O., Hestnes, A. G., (2005). The intelligent Building Envelope - Concept and Qualifications, *Glass in Buildings Conference Proceedings*, Bath, UK.
- Yan, D., O'Brien, W., Hong, T., Feng, X., Gunay, H. B., Tahmasebi, F., & Mahdavi, A. (2015). Occupant behavior modeling for building performance simulation: current state and future challenges. *Energy and Buildings*, 107, 264-278

# Recent Trends in Architectural Design of Light-permeable Facades

Marcin Brzezicki, PhD marcin.brzezicki@pwr.edu.pl  
Faculty of Architecture, Wrocław University of Science and Technology, Wrocław, Poland

## Keywords

1=transparency 2=architecture theory 3=façade glazing 4=glass printing 5=glass coating

Contemporary architectural transparency (understood as the optical property of the material) is constantly being redefined and, over the last decade, new design trends have developed related to transparent façades in architecture. Those trends are the result of dynamic technological progress and of the advancement in the field of materials science. Transparency is no longer limited to specific functions [e.g. illumination of the interior], but has become a tool of formal expression itself. Apart from the standard understanding of transparency as the use of light-permeable materials in façade design one can find other innovative and creative interpretations. This paper defines and describes the most recent and distinct trends, including: (i)

redundant transparency – which employs innovative techniques to enrich the spatial depth of the façade; (ii) veiled transparency – which postulates advanced obstruction of transparency; (iii) multilayered transparency – which creates complex and daylight-responsive detailing; (iv) regulated transparency – which uses modern technologies to turn facades into light-valves; (v) perceptual transparency – which achieves the impression of transparency without the use of light-permeable materials.

## 1. Introduction

Contemporary architectural transparency (understood as the optical property of the material) is constantly being redefined and, over the last decade, new design trends have developed related to transparent façades in architecture. Those trends are the result of dynamic technological progress and of the advancement in the field of materials science. Contemporary trends in architecture are generally rooted in philosophy and reflect the prevailing social moods and transparency is not an exception. It must be stressed,

however, that the term transparency has been repeatedly redefined and often misused as a tool of political discourse by numerous authors (see Chapter 7 for more). Some authors also find general relationships with current human condition, as “transparency expresses the dichotomy between the visual interconnection and the isolation of the individuals in modern society” [8]. These authors assume that certain optical characteristics of transparent envelopes can be permanent. This is not true since the visual experience connected with viewing architectural glass greatly depends on the light. Glass walls are “both reflective and transparent depending on the time of day, angle of the sun, and weather” [2]. Therefore, when some lighting conditions change, the once established relationships are no longer valid. In an attempt to bring some objectivity to the issue of trends in architectural transparency, the author of this paper presents a different point of view that is based on a systematic morphological analysis. This analysis, however, might be somewhat subject to the author’s personal aesthetic preference.

| 1  | case study name               | year | number of light-perm. layers* |   |   | depth of penetration | light transmission |                |
|----|-------------------------------|------|-------------------------------|---|---|----------------------|--------------------|----------------|
|    |                               |      | 1                             | 2 | 3 |                      | homogenous         | heterogeneous  |
| 1  | B.-W. Landtag                 | 1962 |                               |   |   | 0                    |                    |                |
| 2  | Kunstmuseum Winterthur        | 1995 |                               |   |   | 0.3                  |                    |                |
| 3  | Bockenheimer Landstrasse      | 1998 |                               |   |   | 0.6                  |                    |                |
| 4  | Go-cart racing track in Delft | 2000 |                               |   |   | 12.0-18.0            |                    |                |
| 5  | CDU headquarters              | 2002 |                               |   |   | 12.0                 |                    |                |
| 6  | Bern Train Station            | 2003 |                               |   |   | 0.6-1.2              |                    |                |
| 7  | Deutsche Krankenversich.      | 2005 |                               |   |   | 0.3                  |                    |                |
| 8  | De Baljurk in Hague           | 2005 |                               |   |   | 0.9                  |                    | in small scale |
| 9  | Lightcube Office in Zurich    | 2006 |                               |   |   | 0.6                  |                    |                |
| 10 | Clinique du Parc              | 2007 |                               |   |   | 0.9                  |                    |                |
| 11 | Hôpital Jean Mermoz           | 2008 |                               |   |   | 0                    |                    |                |
| 12 | New Credit Suisse Backoffice  | 2012 |                               |   |   | 0.6                  |                    |                |
| 13 | Casuariestraat, DGMR          | 2012 |                               |   |   | 0.3                  |                    |                |
| 14 | Silesian Museum               | 2013 |                               |   |   | 6.0                  |                    |                |
| 15 | Headquarter Sotax AG          | 2013 |                               |   |   | 6.0                  |                    |                |
| 16 | Toni-Areal                    | 2014 |                               |   |   | 0.3                  |                    | in small scale |
| 17 | Uni Carl Vogt                 | 2015 |                               |   |   | 0.2                  |                    |                |
| 18 | Supreme Court in The Hague    | 2016 |                               |   |   | 0.6                  |                    |                |

\* the IGU unit was treated as a one layer, because of the short distance between the panes.

Table 1. The morphological analysis of case studies.

## 2. Methodology

The objective of the presented research project was to investigate and identify new trends in architectural design of transparent façades, identify their scope and devise models that illustrate sets of typical features in each trend. The identification of new trends is crucial not only for the architectural theory but also for the planning of glass production strategies and manufacturing of glass processing equipment, which can serve as practical tools in implementing certain visual solutions. The methodology is based on in-situ research of case studies – photographic documentation of existing buildings. Field observation is an essential component of the proposed scientific method and plays an important role in collecting data and formulating scientific insights. This paper is a brief presentation of the results of a large case study of over two hundred buildings, located in Europe and built between 1995-2016 (only 18 selected buildings are presented in the paper).

The case-study buildings were chosen based on the assumption that only the most representative examples are best suited to clearly illustrate the discussed trends. The characteristic features of the selected buildings most accurately portray these trends. It was also the author's intention to present European buildings that have different numbers of permeable façade layers. Since double leaf façades are quite popular in Europe, the number of presented buildings with two or more façade layers reflects this general trend.

By visiting and photographing the case-study buildings the author could formulate opinions based on his personal impressions. While this kind of aesthetic assessment is rather emotionally-driven than science-based, one must realize that a scientific method of objective appraisal of beauty has yet to be invented. The author's emotional assessment is counterbalanced by his analytical approach focused on identifying the technique, the materials that were used, and the optical results produced. For each studied case (see Tab. 1), the morphological analysis takes into account the following factors: (i) the number of transparent layers, (ii) the depth of penetration of the eye and (iii) homo- or heterogeneous light transmission through the façade.

## 3. Background

Architects approach transparency differently depending on their own attitude and that of the client. Some solutions are well-thought-out and serve as architectural manifestos, others are by-products of the chosen design technologies, e.g. double façades were initially

introduced to regulate the climate and handle the acoustics. Furthermore, transparency in architecture is still an important tool of political discourse when it is used by those authorities that associate optical transparency with institutional transparency. Paradoxically, the term transparency – rarely seen in the form of bona-fide visual manifestation in reality – has gained an additional meaning associated with “legitimacy, policy efficiency, and good governance, as well as a universal remedy against corruption” [5]. This politically-driven discourse is still present in architecture and – despite the fact that transparency has gained an identity of its own – is commonly used to justify the excessive use of glass in public buildings, for example, in the Supreme Court in the Hague (arch. by KAAAN Architecten, 2015), which has recently been reviewed as “more crystalline than transparent” [11] or the well-known CDU headquarters in Berlin (arch. Petzinka and Partners, 2001). Although the former building is extensively glazed at the street level, it only allows for a shallow penetration of its doubled glazed envelope on the top floors (see Fig 1, Fig 2). Such “glazing manifestos” have repeatedly been built around Europe since the 1960s, with Stuttgart's Landtag von Baden-Württemberg (arch. Horst Linde, 1961) as the originator of this trend. The most recent trends in architectural transparency seem to have shaken off this political burden by allowing visual and material



Fig. 1. Supreme Court in the Hague (arch. by KAAAN Architecten, 2015)



Fig. 2 CDU headquarters in Berlin (arch. Petzinka and Partners, 2001)

experiments to take a leading role in the creation of architectural space and of the user's impressions.

## 4. Trends in transparency

The following trends have been identified and defined by the author based on a general morphology of facades with emphasis on the number of glass layers (see Fig. and Table 1). This allowed for the isolation of five main trends, which are described in the four chapters that follow.

### 4.1 Redundant transparency

Redundant transparency is probably the most interesting trend to start with. This trend was identified and described by the author in 2014 in his paper titled Redundant transparency: the building's light-permeable disguise. Redundant transparency occurs when light-transmitting materials are used to “enrich the spatial depth of the spandrel region of a building's facade without affecting its main important function of bringing light into the building” [3]. The use of light-transmitting materials does not affect the illumination of a building but visually activates large areas of the façade that were previously relatively inert. Shallow space behind this “redundant” glazing adds the impression of depth to the previously flat part of the building. Originally, redundant transparency took the form of the so-called: (i) shadow-box, which consisted of a relatively shallow space behind glass, such as in the case of Deutsche Krankenversicherung headquarters in Cologne, Germany (arch: Störmer Murphy and Partners, 2005). This form later developed into much more complex solutions with entire buildings covered by



Fig. 3. Deutsche Krankenversicherung (arch: Störmer Murphy and Partners, 2005)



Fig. 4 Go-cart racing track in Delft (arch. Cepezed, 2000)

(ii) a “cloche”, which means bell-shaped glass. The cloche, defined as an additional transparent layer of the outer envelope, originated in buildings in the early 20th century e.g., Steiff Factory (arch. Richard Steiff, 1903). However, it became very popular as it proved to be surprisingly effective in shaping the microclimate in a building by mitigating the seasonal temperature differences. This was achieved by exploiting air circulation in the summer period and solar gain in the winter period. An excellent but not widely known example of this “cloche” solution is the glazed enclosure build over the go-cart racing track in Delft in Netherlands (arch. Cepezed, 2000).

#### 4.2 Veiled transparency, perceptual transparency

Although obstruction of transparency is not a new trend, it has recently gained in importance with the emergence of innovative technologies and materials that offer new formal solutions. This trend can be divided into two sub-trends, of which the first one has existed almost since the advent of glass while the second one is relatively new. Transparency can be interrupted (i) heterogeneously, when “light transmission is blocked by elements that are randomly or evenly scattered in front of, or on the pane’s surface” [4] or (ii) homogeneously, when a homogenous decrease in light intensity is experienced. Venetian blinds, perforated and meshed surfaces are examples of heterogeneous interruption, whereas various versions of translucent, hazy and foggy glazing represent the homogenous one.

Owing to many interesting discoveries that are being made in the field of materials science, heterogeneous interruption does not necessarily have to take the traditional form of obstructing device placed in front of the glass (like a shutter, roller or venetian blind). The same could be achieved by printing, laminating or depositing a thin layer on the surface of the glass. Examples of such solutions include the screen-printed glass in Hôpital Jean Mermoz

(arch. F.-H. Jourda, 2008), Clinique du Parc (arch. Xanadu, 2007) or small patches of reflective surface which create a pattern on the glazed façade of the Uni Carl Vogt in Geneva (arch. 3BM3, 2015) – see Fig. 5, 6, 7.



Fig. 5 Hôpital Jean Mermoz (arch. F.-H. Jourda, 2008)

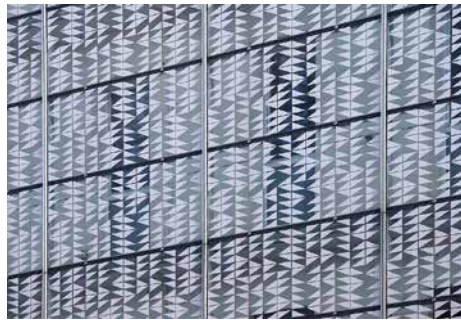


Fig. 6 Clinique du Parc (arch. Xanadu, 2007)



Fig. 7 Uni Carl Vogt in Geneva (arch. 3BM3, 2015)

Classical examples of veiling include the use of evenly translucent or foggy/ornamental glass that is embossed with a small-scale graphical or geometrical pattern. This type of material distorts the image transmitted through the glass and causes the elements behind it to appear hazy and foggy. Some architectural theoreticians notice the connection between this type of transparency and postmodernism and trace the beginning of this trend back to the writings of the French philosopher Jean Starobinski, who derives a foggy translucence from the ancient and archetypical “Poppea’s veil” [16]. Herbert Muschamp even says that “the skin of a building is not used to reveal but to hide” [9].

Light-scattering materials also behave differently on the optical level. The entire translucent pane emits scattered light and successfully blocks the image but lets the light to pass through. This is a feature of translucent light-permeable materials that changes the quality of light and thus gives a soft and hazy quality to the illumination. From an architectural perspective, translucency offers the unique possibility to dematerialize the building, to blur its boundaries and achieve visually different results in different daylighting scenarios. The Silesian Museum in Katowice (arch. Pysal Ruge Architekten, 2013) is a good example of the use of ornamental glazing embossed with the so-called frost-flower pattern, while the headquarters Sotax AG (arch. Itten+Brechtbühl, 2013) could serve as an example of the use of a uniformly translucent façade. The new Credit Suisse Backoffice (arch. Burckhardt+Partners, 2012) offers an even more exciting visual experience as the building is equipped with “recessed ribbon windows with translucent glass balustrade elements” [10] which make the areas where translucent panes are mounted seem out of focus, see Fig. 8, 9, 10.



Fig. 8 Silesian Museum in Katowice (arch. Pysal Ruge Architekten, 2013)



Fig. 9 Headquarter Sotax AG (arch. Itten+Brechtbühl, 2013)



Fig. 10 New Credit Suisse Backoffice (arch. Burckhardt+Partners, 2012)

Small-sized meshes or perforated surfaces (although typologically heterogeneous) are optically perceived as a homogenous decrease in transparency. This phenomenon of perceptual transparency occurs when the openings in such meshes or perforations are beyond the limits of the spatial acuity of the human eye. The perforated surface/mesh becomes evenly transparent. This perceptual phenomenon is eagerly used by architects as it produces the effect of transparency without the use of optically light-permeable materials. There are many solutions that take advantage of this technology ranging from a glittering mesh, such as the one on the façade of the De Baljurk in Hague (arch. Eric Vreedenburgh, 2005) to perforated metal sheets which not only create the effect of transparency, but simultaneously produce moiré fringes. This sometimes unwanted byproduct is especially visible in the expanded metal cladding of the recently refurbished Toni-Areal development in Zurich (arch. EM2N Mathias Müller und Daniel Niggli, 2014), see Fig 11, 12.



Fig. 11. De Baljurk in Hague (arch. Eric Vreedenburgh, 2005)



Fig. 12 Toni-Areal development in Zurich (arch. EM2N Mathias Müller und Daniel Niggli, 2014)

## 5. Multiplication

The multiplication of optical phenomena in façades was initially a side-effect of the deliberate use of an extra layer of glass in order to improve the thermal performance of windows. This “doubling” trend peaked in the mid-1990s with the development of the technology and methods of calculating air flow (computational fluid dynamics) and assessing the climatic performance of double facades, which in turn offered evidence supporting the choice of a given technology. Double façades also provided additional space for solar gain regulation devices (rollers or blinds) thus eliminating the need to use mirrored glass to control the insolation. This important change in technology allowed for the new optical characteristics to appear. Since daylight plays a key role in the perception of transparency of a building, the elusive appearance of its façade depends very much on the viewing conditions. This phenomenon has become the most interesting feature of new multiplied transparent walls. In their designs architects started incorporating the effects of multiplied optical phenomena, such as decreased transmission and overlaid reflections, in order to achieve rhythm, proportion and balance.

Optical phenomena are produced by all smooth surfaces. A single pane will both transmit, absorb and reflect light. Overlaid reflections lead to the formation of various optical illusions. As stated by Eve Blau, transparent walls “visually project spaces onto, through, and beyond one another” [2]. The key visual effects that deserve a brief mention include: (i) the apparent loss of image focus, i.e. a blurred reflection, such as in the Lightcube Office in Zurich (Fischer Architekten, 2006) where “material transparency of the walls” is converted “into perceptual opacity” [2], (ii) the varied reflections produced by positioning the glass panels at different angles, e.g. Casuariestraat, DGMR (arch. Fokkema Partners, 2011), (iii) apparent duplication of the elements of the structural frame, as the light is zigzagging between panels, e.g. the façade

of Bern Train Station (arch. Atelier 5, 2003). Under certain lighting conditions the reflection of the surrounding area can be so intense that it is very difficult or even impossible to see the double-skin façade, as in the case of the Bockenheimer Landstrasse office building (arch. KSP Architekten, 1998), see Fig. 13, 14, 15.



Fig. 13 Lightcube Office in Zurich (Fischer Architekten, 2006)



Fig. 14 Casuariestraat, DGMR (arch. Fokkema Partners, 2011)



Fig. 15 Bockenheimer Landstrasse office building (arch. KSP Architekten, 1998)

Notable buildings and concepts that are usually quoted by architecture critics, such as Tres Grande Bibliotheque proposal (OMA, 1997), Institute for Hospital Pharmaceuticals (Herzog de Meuron, 1995), and Kunstmuseum Winterthur (arch. Gigon & Guyer, 1995), represent the multiplication trend which, at some point, gave birth to the abovementioned redundancy trend.

## 6 Smart glazing

The emerging trend of regulated transparency is undoubtedly a novelty. Changing light transmission properties within the pane has been of interest to architects and engineers mainly because it can be used for microclimate regulation, but also because it helps to achieve a variety of visual, formal and architectural expressions. The optical results of the light flux regulation could be achieved by the application of various technologies. Optical transparency can be altered: (i) qualitatively by changing the

quality of transmitted light, as in the case of light-scattering PrivaLite glass by Sain Gobain, or (ii) quantitatively by changing the amount of transmitted light (e.g. by using suspended particle devices in transmission mode or by electrochromics, as in the case of Sage Glass). The character of the change introduces a new dimension in the discourse on altered architectural transparency: the dimension of time. Transparency regulation techniques differ in the amount of time that is required to complete the change of light-permeable properties of the pane. The change can occur within milliseconds or may still be hardly visible after several minutes. This inability to produce an instant change, as well as the price for square meter exceeding 500 EUR, are the main factors that limit the popularity of these technologies. As this technology advances, it is expected to overcome these limitations and become an important element of architectural practice. The first large-scale example of applying smart glass technology is the Chanel Ginza Façade (arch. Peter Marino Architect, 2004) store in Tokyo.

## 7. Discussion

When the subject of recent trends in architectural transparency is viewed from a broad, architectural perspective, several conclusions can be formulated. Based on the studied cases, trends in architectural transparency can be represented by schematic drawings that illustrate the number of the light-permeable layers and define the path of the light ray. The trends in transparency overlap as inspiration flows freely between designers, see Fig. 16.

Seeing that elements of artificial or authentic space stratification are present in almost every analyzed trend, the transparency superposition seems to be the most prominent. As Ch. Schittich notes: "superimposing layers of various kinds – printing, louvres, etc. – over a glass skin can produce further variations within the transitional zone" [14]. Those new elements which constitute the transitional zone could also be recognized as a case of "additive configuration of planes" as it is addressed

by A.-C. Schultz in her extensive research on architectural overlaying [15]. This observation has been confirmed by many researchers and it raises the question why the overlaying of numerous light-transmitting layers is so frequent?

What stimulates architects to search for new ways of utilizing light-transmitting materials might be depth of the façade. Pane superposition could be one of the ways to achieve this. "The plastic effect of the facade within its immediate surroundings is essentially created by the offsetting of the individual surfaces within the facade and the resulting shadows" [6]. Nina Rappaport also observes that the "wake of postmodern discourse [...] has created a need for a visual surface simulation and depth" [12]. Paradoxically, many architects – following Mies van der Rohe's statements that glass itself provides sufficient variability to the façade – simultaneously seek additional measures to spatially activate what is commonly seen as a "boring flat glazed wall". This is probably deeply rooted in human appreciation of beauty. For the vast majority of non-expert viewers only the sculptural aspects are recognized as aesthetically pleasing.

The multiplication of layers of glazing on the façade allows for the stratification of space and the differentiation of planes. It also produces effects that were previously absent e.g.: (i) it connects spaces visually without providing the spatial connection – thus avoiding exchange of air, (ii) it fastens elements to the glass – in technical terms – but they seem to be hanging "in the air" if viewed in certain lighting conditions, (iii) it sculpts with light creating space which is much more daylight-dependent. Glass layering can also be seen as a way of building up architectural space, or, as Yoshinobu Ashihara labels it, "space that is created centrifugally" [1].

Another reason might be the recent change in the function of the façade. In his influential book *Complexity and Contradiction in Architecture* from the early 1960s, Robert Venturi devised a new division of a building into its "volume" and its "façade" [17]. Terence Riley described a very similar mechanism of "shifting the objects meaning from its form to its surface" [13]. This "transformed the building from the monolithic form into the act of communication – a symbol, a message bearer" [7]. thus strengthening the role of the façade itself.

This, however, is not an entirely new approach. The façade has always been seen as more than mere protection against weather. It has symbolized prestige and power, first with the use of stone, now through glass and technology, which perform a similar function but offer easier and more direct

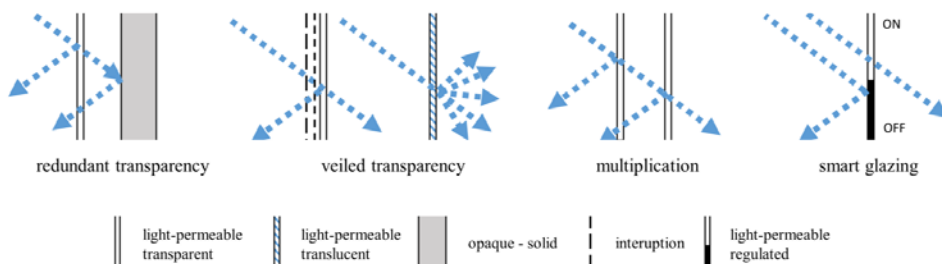


Fig. 16. Diagram of the studied transparency trends showing the facades in vertical section. Based on the general idea of Fig A 2.1.15 [6, p. 35].

communication. It is no longer necessary to be an expert in Greek mythology – as it was before – to understand the message of the architect. Now this information can be communicated more directly and understood by the observer. Media facades present the most recent type of information-infused transparency and, most probably, are paving the path to the future of the façade industry. New technologies also facilitate the communication of new architectural ideas to the audience, thus creating new social values and stronger relationships among the people.

## 8. Conclusion

This brief study of transparency trends identifies the main trends and opens the way for much more extensive study in the future. Judging from the abovementioned solutions, the increase in spatial depth of the façade is no longer an emerging trend, but has become a well-established practice. However odd it may seem, this trend coincides with an equally strong tendency of both image blurring and transmission interruption. Moreover, in many cases these trends reinforce each other or blend. Glazed façade design has now become more of an art than ever before. The demand for new technologies will stimulate innovation in the field, with possible focus on smart solutions in the near future.

## 9. Acknowledgment

This paper was funded by the Polish National Science Centre grant entitled: "New trends in architecture of transparent facades – formal experiments, technological innovations ", ref. no. 2014/15/B/ST8/00191.

## References

1. Ashihara, Y.: *The hidden order*. Tokyo. New York (1989)
2. Blau, E.: *Inventing New Hierarchies*, 2010 Laureates Essay for The Pritzker Architecture Prize, The Hyatt Foundation. 1-7., [http://www.pritzkerprize.com/sites/default/files/file\\_fields/field\\_files\\_inline/2010\\_essay\\_0.pdf](http://www.pritzkerprize.com/sites/default/files/file_fields/field_files_inline/2010_essay_0.pdf) (2010). Accessed 16 March 2017
3. Brzezicki, M., *Redundant Transparency: The Building's Light-Permeable Disguise*, *Journal of Architectural and Planning Research*. 31:4, 299-3014 (2014)
4. Brzezicki, M.: *Light-transmitting energy-harvesting systems. Review of selected case-studies. Engineered Transparency. International Conference at glasstec, Düsseldorf, Germany, (2016)*
5. Forssbaeck, J., Oxelheim L.: *The Oxford Handbook of Economic and Institutional Transparency*. Oxford University Press, Oxford (2015)
6. Herzog, T., Krippner, R., Lang, W.: *Facade construction manual (1st ed.)* Birkhauser, Basel (2004)
7. Mack, G.: *Buildings with Images [in:]*, *Architecture Landscape Urbanism 3: Eberswalde Library*, AA Publications (2000)
8. Montesinos, A.: *SANAA Figuration/configuration*, <http://www.experimentalfields.com/wp-content/uploads/2013/12/SANAA.pdf> (2014). Accessed 16 March 2017
9. Muschamp H., *Buildings that hide and reveal [in:]* Kipnis, J., Gannon, T.: *The Light Construction Reader*. Monacelli. 28-43 (2002)
10. *New Backoffice*, <http://www.burckhardtpartner.ch/en/references/items/new-credit-suisse-backoffice.html>, Accessed 16 March 2017
11. *Order, Clarity, Transparency: the Supreme Court in The Hague*, *Detail*, 6, 488-490 (2016)
12. Rappaport, N.: *Deep Decoration*. 30/60/90 *Architectural Journal*. 11, 95-105 (2006).
13. Riley, T.: *Light Construction. The Museum of Modern Art*, New York (1995)
14. Schittich Ch.: *New Glass Architecture – Not Just Built Transparency*. *Detail*, 3. 340-341 (2000)
15. Schultz A.-C.: *Time, Space and Material: The Mechanics of Layering in Architecture*. Edition Axel Menges, Fellbach (2015)
16. Starobinski, J.: *Le voile de Poppée, [in:]*, *L'oeil vivant: Essai*. Gallimard, Paris. 9-27 (1961)
17. Venturi, R.: *Complexity and Contradiction in Architecture*. The Museum of Modern Art, New York (1997)

# Glass Innovations for Dutch Architecture' for GPD 2017

Prof.dr.Mick Eekhout  
Chair of Product Development in Architecture,  
TU Delft; Founder and director of Octatube,  
Delft

## Keywords

Incremental innovations; cold bending / cold twisting

## Abstract

Continuous incremental innovations in a project-steered design & build organisation in the last three decades in material applications, details, structural systems and safety development with the aid of models, prototypes, small initial projects, certifications and applications in large projects.

## Introduction

As the main designer and principal of Octatube, Delft, The quest for innovative glass structures was constant in the last three decades. The strategy was mainly following smaller projects first, larger projects later, also preferably first in the Netherlands and later abroad. Looking over my shoulder innovations could be characterised as small innovative steps, incremental steps forward. But by continuing the innovative quest in the same time the glass world has changed from "nothing is possible and nothing allowed" to "Smart engineering can bridge the gap



Fig 1: Music dome in Haarlem clad with laminated annealed glass

between wild ideas and certification and trustworthy applications in projects".

## Laminated glass

As a designer I have always strived towards elegance by slender forms and detailing. As a covering material glass is most suited: it shows the elegance of the structure. So the

first glass clad dome was developed with Wiek Röling and was realised in 1984 as a music pavilion in a park in Haarlem, NL.

The cladding consisted of laminated annealed glass 3.3.1, which also appeared to be very vulnerable for vandalising youth. However the city guards this "jewel of architecture", as they call it, very closely and regularly vandalized panels were replaced.



Fig.2,3: Glass Music Hall, Amsterdam, outside and inside view



Fig. 4,5: Inside and outside of the OZ building with 52 x 16 m Quattro glass façade in Israel.

### Structurally loaded Quattro glass

The Glass Music Hall was opened in spring 1990. The first glass façade of frameless 'Quattro' glass. All glass panels suspended from the roof space frame structure through the glass itself, which was loaded in tension. The upper panels were heavily loaded. Their connections were friction connections: bolts in large glass holes with sand paper to increase the friction factor between glass and metal saucers.

Yet larger and more serious step forward was done in 1995 in the façade of the OZ-building in Ramat Gan, Israel, designed by Avram Yaski. The façade is 52 m high and 16 m wide. The deadweight of the glass is again suspended to the roof structure, not via the glass but via extra deadweight suspenders, diameters from 10 mm below to 20 mm at the upper side of the façade. Wind loadings has been taken by tensile rods, in the form of a bending moment line, a lens-shape both for compression as well as for suction of the façade. So the end result were double curved tensile trusses for inward and outward wind loading, 20 mm around. The trusses were anchored at each floor level, so that the reaction forces from the structure could be directly be connected to the concrete floors. Glass was laminated 6.6.2, fully tempered.

### Glued connections

The fully glued connections were first applied in 1994 for the roof structure of the Court of Justice in Maastricht. The gluing of these connections required a laboratory in which the glass panels could be cured for 24 hours under 40 degrees Celsius, in order to gain the required and analysed strength. Research and development led to a specific glueing process with certifications. Two years later similar glued connections were used not only for the roof, but also for the vertical facades in the Glass Museum Hall of the Prinsenhof in Delft, architect Mick Eekhout.



Fig.6: Prinsenhof museum hall, Delft, with glued Quattro connections in roof and facades.

In this system a number of atrium coverings have been realised based on a 3D-system of micro tensile trusses, at the time the lightest version of steel and glass structures. A similar system had been realised in the circular roof structure for the main office building of Santander in Madrid. A 30 m diameter bicycle wheel horizontally with a steel outer circular running rim RHS 350x350 x 12 mm, spokes of stainless steel of 20/25 mm diameter and a central vertical hub with many outriggers, architect Kevin Roche.

### Glazed light weight steel structures

In 2006 the design & build contract was signed for a high glass cube of 30 x 30 m, 21m high for the bank city of Santander near Madrid. The design was based on masts made of CHS tubes and cable stabilisations on both sides on outriggers, and the roof trusses in two directions were similar. The glass panels were 2.5 x 2.5 m<sup>2</sup>, on the top 2.5 x 3.5 m<sup>2</sup>. IGU's

as laminated fully tempered glass panels with solar coating. In this case Octatube, normally the design & build specialist, was also the main contractor in this case, architect Alphonso Millanes.



Fig.7: Circular bicycle roof 30 m diameter

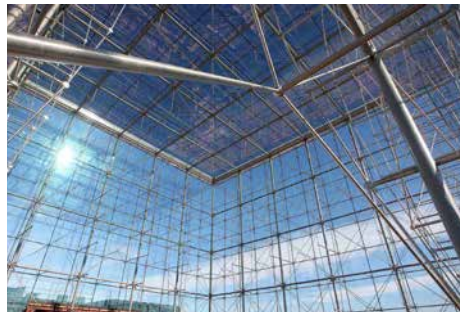


Fig. 8, 9: outside and inside of the glass cube with slender cable structure stabilisations



Fig. 13: Overview of the facades of INHolland

### Cold twisted glass panels

For the town hall of Alphen aan den Rijn (arch Erick van Eegeraat) cold twisted glass panels were developed for the first time, 2002. The structural engineers of Octatube analyzed the stresses in the glass panels and concluded that 25 % of the allowable stresses are consumed by diagonal bending stresses or twisting stresses and the remaining 75% was enough to withstand wind loadings, and on the top of the building, also snow loading. The spaghetti lintels were realized without major problems.



Fig. 12: Delft glass tramway and bus station in cold warped glass

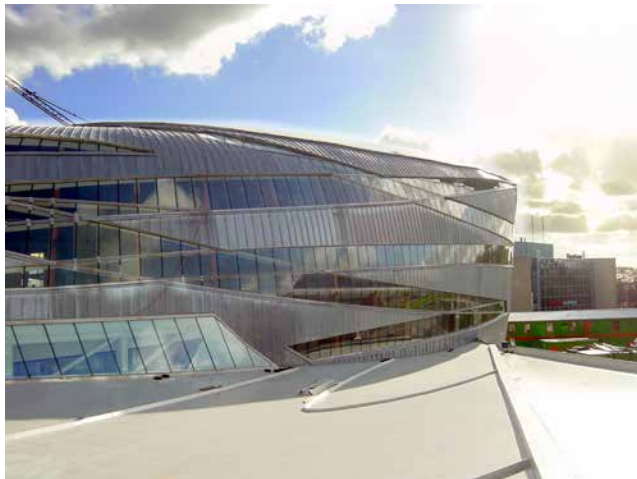


Fig. 10,11: Back side of the town hall with the cold twisted insulated laminated glass panels

One year later a graduation student from TU Eindhoven, Dries Staaks, devoted to analyse the process of cold twisting and came up with his theory, now called 'Staaks Theory of Cold Twisted Glass', published GPD 2004. A roof design for a bus and tram station in Delft was designed made by Mick Eekhout in the form of an undulating glass roof with twisted glass. The difference between flat glass and twisted panels was found in the width of the silicone seams.



### Cable stabilised glass facades

The INHolland polytechnic school in Delft owns a Composite Laboratory and required an experimental content of the glass facades. The initial idea was to use carbon fibre as spacers and carbon fibre tubes inside the inner glass space, through which Aramid cables would be fed from top of the façade panels to the bottom one of panels. The Aramid cables were thought to be fed through all successive glass panels, to be post-stressed and after that to act as the wind loading resisting cables. In the single cable principle, these cable had to be post-tensioned to a high degree, in equilibrium with the steel structure in the roof, from which the cables would be fed, architect Rijk Rietveld.

The glass supplier, AGC, reported the day before starting the glass panel productions that they did not trust the quick tests we had done and required much more testing, may be years in a row. Problem was the unknown adherence between the sealant, the metal spacer and the carbon fibre tubes. So we decided to run the cables on the inside space of the IGU's instead of through the inner spaces of the IGU's. It shows that the glass producers were very serious. The facades were 13 m high, two facades of 20 m long en one of 3.5 m long. It was decided that the small façade would be as originally designed and engineered. The two longer facades were made in the best possible way, with single Aramid cables running and post-stressed in carbon fibre tubes at the interior of the space, behind the glass panels.

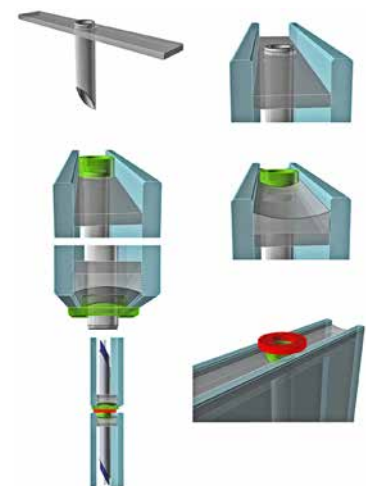
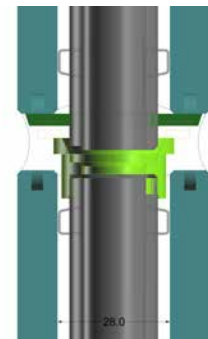


Fig. 14, 15: The detailing of the Aramid cable through the carbon fibre inside the inner space



Fig. 16: The experimental façade with the vertical Aramid cables inside of the IGU inner space.

The structural action of the facades, with single vertical post-stressed cables show a deflection of 300 mm inward in highest wind compressions and 300 mm outward in wind suction. The two longer 20 m long facades have a perpendicular common corner. In case of wind compression on both facades, the two façade would bed inward and would crash on each other. To prevent this, the corner lines of these two facades were cut off in a lens-formed silhouette. When both façades move inward simultaneously they do not touch each other. The lens-formed corner is closed off with a double insulated rubber membrane.

Following the experiment of the vertical cable facades of INHolland a new challenge was introduced with the design of the Market hall of Rotterdam designed by Winy Maas of MVRDV. The two identical facades measure 40 m wide and 34 m high. The structural design made by Royal Haskoning DHV provided already a good equilibrium between pre-stressed cables in 2 directions and a stiff concrete ring structure around the cable net and the lower concrete parking garage walls. Octatube was selected to detail, engineer, certificate and produce and realise the glass cable facades. The structural analysis showed a deflection in the centre of the cable net structure of 700 mm inward and 700 mm outward. The glass panels, measuring 1.5 x 1.5 m<sup>2</sup> would form dilatations at each of their vertical and horizontal seams. So the silicone sealant would be effective for water-tightness and for dilatation. The biggest problem were the glass panels in the four corner areas of the facades, where the glass panels are twisted during maximum wind loading. Here the experiences done with cold

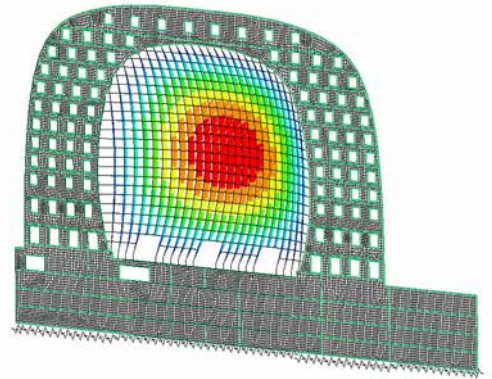


Fig. 17, 18: the Market hall with 2 x 700 mm deformation due to maximum wind loading.

twisting was helpful. The glass panels are laminated heat-strengthened glass panels 6.6.2

The exact positioning of the post-stressed cables was a challenge. Before execution a major problem was creep in the concrete structure of the surrounding walls. The post-stresses in the cables were chosen to be 25% higher than the analysed stresses, so that 25 % could devaluate due to the deformation in the concrete. This happens predominantly in the first two years. After 1.5 year the cables have been checked and 12 to 15% of the post-stress is already reduced.

The accuracy of the cable net was a major point of development during the process of building. Tolerances in the glass membrane were max 1 mm per cable and not more overall. The glass panels are prefabricated as standard size and they all had to fit. On the other hand the anchoring of the cables had to



allow for post-stressing of the cables and had to very accurate as well. We applied measuring and drilling of the front plates after casting in of the boxes. This was the only reliable method to obtain a high accuracy for the positioning of the cable anchors. The post-stressing of the cables was done in 5 sequences: 25, 50, 75 and 100 of the required cable-stresses respectively. The glass panels were chosen as 6.6.2 heat strengthened laminated glass. The attraction of the hall for buying visitors and tourists worked excellently: Rotterdam all of a sudden is internationally renowned as a Dutch hot-spot for tourists. Lonely Planet saw in 2015 Rotterdam saw the 'Best in Travel City 2016'. And Financial Times wrote in 2015: "Will Rotterdam's Markthal be equivalent of Bilbao's Guggenheim?"

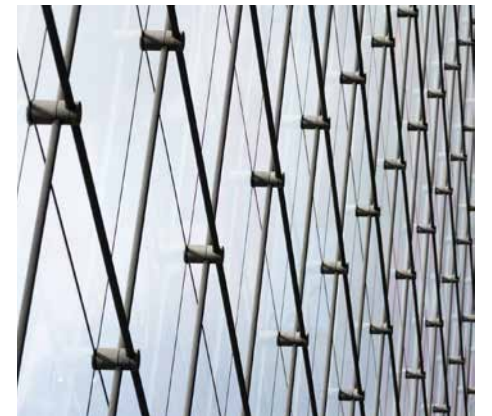


Fig. 19, 20: connections of the cable anchoring and the cable net



Fig. 21, 22: Resulting overview of the Markthal in Rotterdam

### Multi-innovative glass project

In September 2015 the Van Gogh Museum in Amsterdam has opened its new Glass Entrance. The architectural design is drawn by Kisho Kurokawa Architect & Associates and the detailed design by Hans van Heeswijk Architects and Octatube, complementing the curved and elliptical shape of the Kurokawa wing. The entrance is featured by a spheroidal glass roof with glass fins stabilizing the steel structure and a cold bent glass facade.

The shape of the glass roof is defined by turning around the spheroidal surface of the existing wing. The so created roof consists of insulated and laminated glass units all different in width and supported by 30 triple laminated glass fins with SentryGlas®Plus (SGP) interlayer, which are all optimized and unique in length and height. The largest glass fin is 12 metres long and 700 millimetres in height. The glass beams are supported by steel shoes connected to the main steel structure consisting of 400 millimetres circular hollow sections (CHS). This detail allows the glass

fins stabilised by the IGU roof panels to act like beams while supporting and stiffening the steel structure.

Due to the complex geometry, the many glass fin connections and extremely tight tolerances, the entire steel structure of 60 x 15 x 10 metres was pre-assembled surveyed and checked in the factory scale 1:1. The double glass roof units in the outer 1.3 metres wide perimeter are cold-twisted to fit in the roof's curved surface and outline. The curved outer facade consists of cold-bent insulated glass units fixed to 20 unique triple laminated glass fins with SGP, the longest being 9.4 metres. The smallest bending radius is 11.5 metres. When the term 'cold-bent glass' is used, 'cold' refers to the installation process at ambient temperature at which the glass is bent in a certain shape. PVB is a commonly used interlayer for laminated glass and its creep behaviour makes it a good choice for cold-bending. The cold-bent glass units are connected to glass fins for maximum transparency. The composition of the glass units consists of a laminated outer and inner

pane, both with two sheets of 5 millimetres heat-strengthened glass and 4 layers of PVB in between. Normally, fully tempered glass is chosen in case of cold-bent glass for its higher tensile capacity, but in this case heat-strengthened glass was chosen after detailed analysis, for the benefit of favourable post-failure characteristics. The actual bending of the flat insulated glass units to their curved pre-stressed cold-bent shape is done airborne, by an electrically operated bending machine combined with vacuum suckers. This multipurpose bending machine was developed as a combination of a regular glass vacuum lifting machine with two vacuum circuits, and an electrically driven bending mechanism. It was calibrated on site to accommodate the different bending radii. To connect the bent IGU to the substructure, at least the four corner bolts with clamps were tightened and then, the bending machine was released. This description shows that an obviously simple procedure of cold bending formed a real engineering challenge.

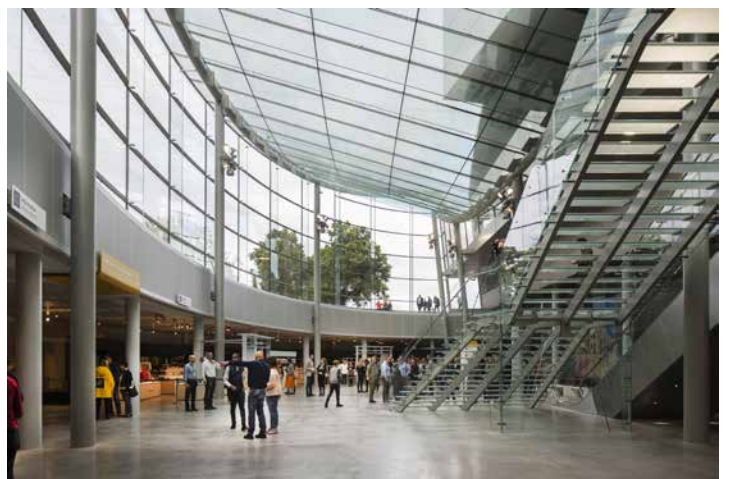


Fig. 23, 24: Exterior and interior photographs of the new Van Gogh Museum main entrance in Amsterdam.



Fig. 25: The cold bent glass facades of the Van Gogh Museum entrance forms a regularly curved facade

### After more than 20 years ‘Zappi’ has a material form and composition

In 1992 I started my professorship in TU Delft with ‘The Quest for Zappi’, the unbreakable glass material. It became a continuous development of safe glass structures with continuous innovations. An unbreakable glass material does not exist but the engineer can develop more safe, yet innovative and challenging structures. A number of these steps have been described in this article. The end of the quest was marked by the testing of a triple laminated glass fin of fully tempered glass. Glass fins are increasingly used, up to 12 m length, usually triple laminated. The glass fin of 6 m length was fully loaded (concrete tiles equivalent with the actual roof loading) and one after the other the three panes were broken. After the first pane was broken, nothing happened, nor after the second. After the third and central pane also was broken a slight sag was observed. We left the test for 4 weeks and the fin did not break, did not collapse. The glass beam proved to be reliable, even with fully broken panes. So for me this was the end of the Quest for Zappi. What would be the next ambition?

### The ecological ambition

All of the described projects and partial innovations in glass designs show that the consumption of glass has increased enormously in the last 25 years. It went from 8 mm in 1990 tot sometimes 60 mm in 2016. Glass facades became quite fashionable amongst architects in the last decades. They symbolize transparency in organizations and display also the structural composition of buildings. However, transparent glass facades require thick insulated glass units with a high amount of embedded energy per m<sup>2</sup>. This has an ecological consequence that in a few years will collide with the architectural aspirations. How to prepare the glass industry to avoid ecological damnation? The entire building chain contributes the embedded energy amount. How can this ecological investment be radically reduced, for example to 50% of the current amount over 5 years time? The ambition over the total chain of glass production and the use of half the embedded energy in the building envelope, would include a quest involving all related parties in the building process: the glass recyclers, the glass melters and float glass producers, the

glass production processors, the coaters, the glass panel manufacturers, the architects, the structural engineers, the façade engineers and façade producers, the norm committees, the governmental approving bodies, the investors, owners and users. The process would lead to an industry-wide collaboration on international scale. Expected results could be revolutionary new working methods caused by the coming transition process towards 50% of the energy in the total sum of the different related industries and stakeholders. The many stakeholders have to take over their own bit for further development. Some future-looking are already busy doing so on their own account and others have to be persuaded probably. All in openness and publicly available publications so that a co-operation, even collaboration on a grand scale could be possible.

This requires much co-operation between different players in a platform-approach for this sort of fundamental developments. Logically it will have to become a building branch wide approach with many different stakeholders involved, both on the producing, the designing, the engineering, the approving and the consuming side of facades. All parties have to be awakened and activated. This is a first attempt to initiate an ecological evolution in the usage of glass in all-glass facades based on extra thin glass usage and it will have its by-effects in other glass facades.

This master plan proposal for a platform R&D project leads to an integrated chain project. Ideally, it involves many different players. Beginning with the many different glass companies with external collaborations of architects, engineers, local authorities, norm institutions, building owners and users. Setting out the master strategy with the potential participants, the willingness of potential participants to really participate will show a subdivision of the total chain (master project)

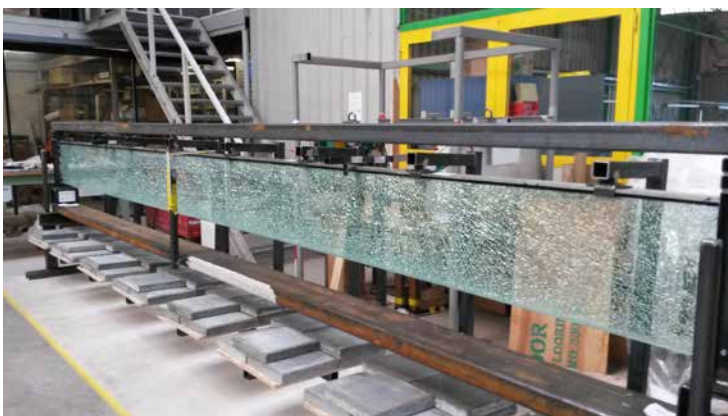


Fig. 26: Triple laminated glass fin with all three layers deliberately broken and fully loaded with concrete tiles as the deadweight and live load, kept up for 4 weeks without collapse. The material was broken, but the structure intact.

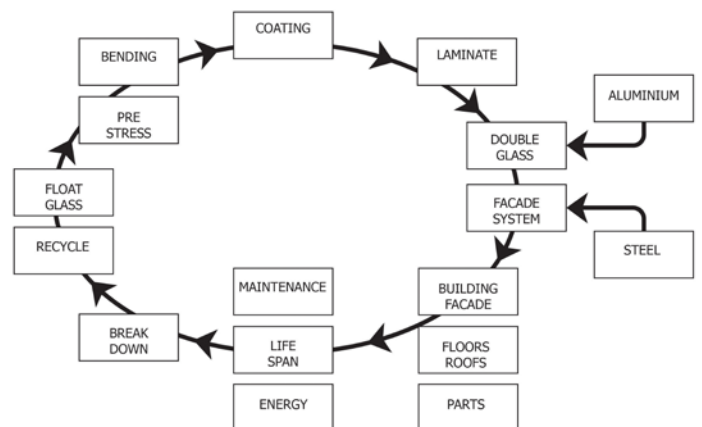


Fig. 27: Proposal for an industry-wide quest to develop 50% less glass content in all glass facades

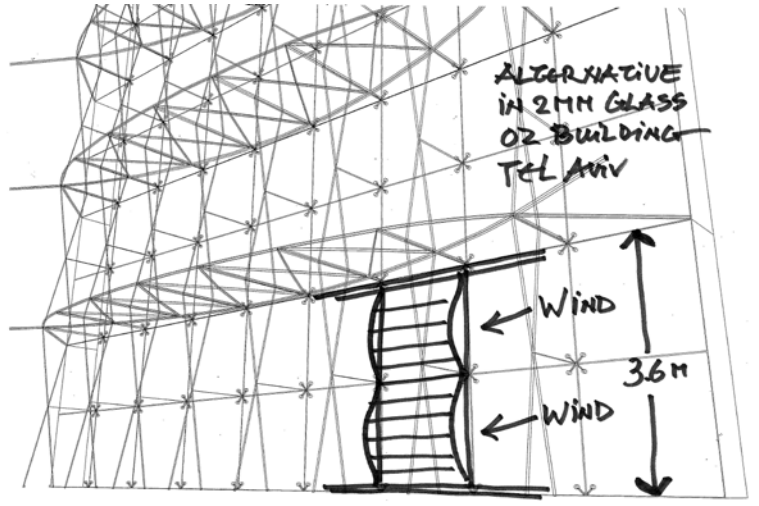
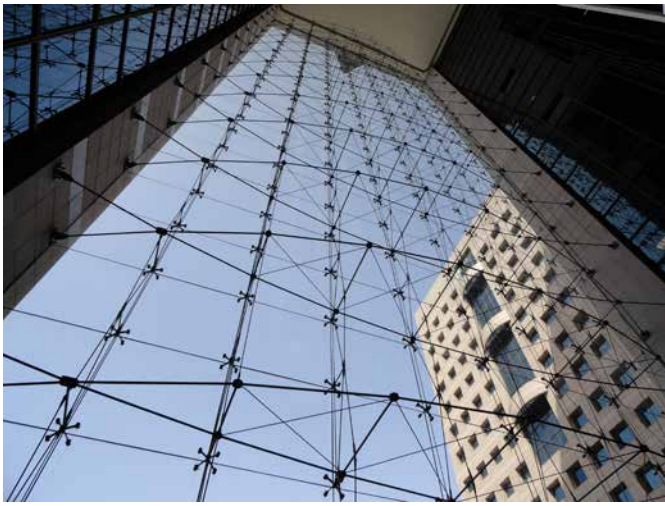


Fig 28, 29: OZ building façade in Tel Aviv, current and proposed situation

into separate links (separate projects) or pieces of links (connected projects). Individual targets will be set, identifying the most suited players and inviting the external players.

### New ambition for extra thin glass

The proposal of this considerations is to stop the increase in the glass consumption, to evaluate the alternative possibilities and to go back to a much lower, but for all concerned parties acceptable level of embedded energy consumption in all glass facades. In this proposals on different spots the possible use of extra thin glass is proposed. I have taken 3 different realized Octatube projects in which I have sketched for all three how extra thin glass could have been applied.

The first example is the 52 m high and 16 m wide frameless glass façade for the OZ building in Tel Aviv, realized by Octatube in 1995, see fig. 28 and 29. The load bearing structure was composed of horizontal tensile trusses, deadweight is brought upwards via deadweight suspenders to the roof structure. The glass panels 1.8 x 1.8m<sup>2</sup> were 8.8.2 laminated fully tempered glass panels with 4 corner holes for M16 bolts. The tensile trusses are located at the floor levels @3.6m. The intermediate node is stabilized by a zigzagging pair of tensile rods.

The second project is formed by the acoustical glass screens as suspended the Nieuwe Kerk (New Church, 1658), The Hague, arch Kees Spanjers. The long reverberation time of 5 to 7 seconds was o.k. for organ music, but not for the contemporary use of chamber music. For that reason a glass ceiling was provided and glass curtains. The curtains had to be removable in front of the organ so that also organ music would be heard in its full splendor.

The glass curtains were designed to be made in 2mm laminated extra thin glass, laminated to be safe, extra thin to be lightweight, easier for its mobility. The glass curtains are to be moved sideward into two halves in case the organ will be played.

The third project, the Fletcher hotel near Amsterdam, architects Benthem Crouwel, 2009, has a cylindrical shaft as a second skin (no ecological purpose, only esthetics) around hotel floors. See fig 31, 32. The laminated and screen printed glass panels were produced in China. Cold bending or laminated extra thin glass would have been quite easy in the horizontal direction in sizes of 1.5 x 3.0 m<sup>2</sup>. The middle support would push the flat panels into the curved shape and the metal clamp lines glued on the glass would ensure the horizontal



Fig. 30: Curved glass curtain in front of the 17<sup>th</sup> century organ which will be made sliding sideward.

post-stressing of the façade. The short turnbuckles between the vertical strips would ensure required post-stress situation of the glass panels.



Fig 31, 32: A2 Fletcher hotel in Amsterdam current and proposed situation

## Conclusion

In all shown developments and projects a certain degree of ambition, creativity and imagination caused 'wild ideas'. The engineering how to realize these ideas, combined with the sturdiness of the gained 'design & build' background (knowing about engineering as well as producing and building, including the responsibilities and liabilities) brought us in intensive research & development in the field of structures, material, elements, components and connections through many prototypes, mock-ups, real load testing and applications.

These were realized in smaller projects first, followed later by larger projects and export projects. 'Innovation' is not a fashionable word but is realized thanks to many adventures, some courage, some naivety (not wanting to know exactly what problems have to be overcome), and much suspicion (according to the 'Law of Murphy' everything can go wrong, certainly in combinations).

Some of the innovations are nowadays called 'moonshots', complicated stacks of multiple innovations influencing each other and hardly manageable. But all projects with technically innovative ingredients were positively realized, based on serious engineering and prototyping.

# Glass Imagined and Realized: Case Studies of the Aesthetic Qualities and Possibilities of Glass in Architectural Design

Daniel A. Vos,  
Chenyu Pu  
Heintges & Associates

## Keywords

1=Glass Materiality 2=Transparency  
3=Reflectivity 4=Acid Etch

## Abstract

As contemporary buildings increasingly use glass as a significant cladding material, architectural designers are focusing more on the aesthetic qualities of glass. While transparency was, and remains, the dominant attribute for most projects, many designs now use a more complete materiality palette encompassing reflectivity, color, and surface materiality. These aesthetic goals must be combined with sometimes-competing performance requirements (strength, impermeability, solar protection, thermal isolation, acoustic attenuation, and durability) and manufacturing capabilities.

In this paper, six case studies of recent projects are presented that exhibit qualities of transparency, reflectivity, color, and surface materiality, including design and fabrication challenges of meeting designers' and owners' expectations for their projects.

National Museum of African American History and Culture  
150 Greenwich, 4 World Trade Center  
The United Nations Secretariat Façade Replacement  
Barnard College Diana Center  
The Dutchess County Residence  
Reflections at Keppel Bay

## Introduction

As contemporary buildings increasingly use glass as a significant cladding material, architectural designers are focusing more on the aesthetic qualities of glass. While transparency was, and remains, the dominant attribute for most projects, many designs now use a more complete glass materiality palette encompassing reflectivity, color, and variation of surface. In the realization of glass facades, these aesthetic goals are influenced by both the performance requirements of the glass and contemporary



*Figure 1 National Museum of African American History and Culture  
Location Washington, D.C., United States  
Architect FAB/S Team (Freelon Adjaye Bond/SmithGroup)  
Owner Smithsonian Institution  
Completion 2016*



*Figure 2*

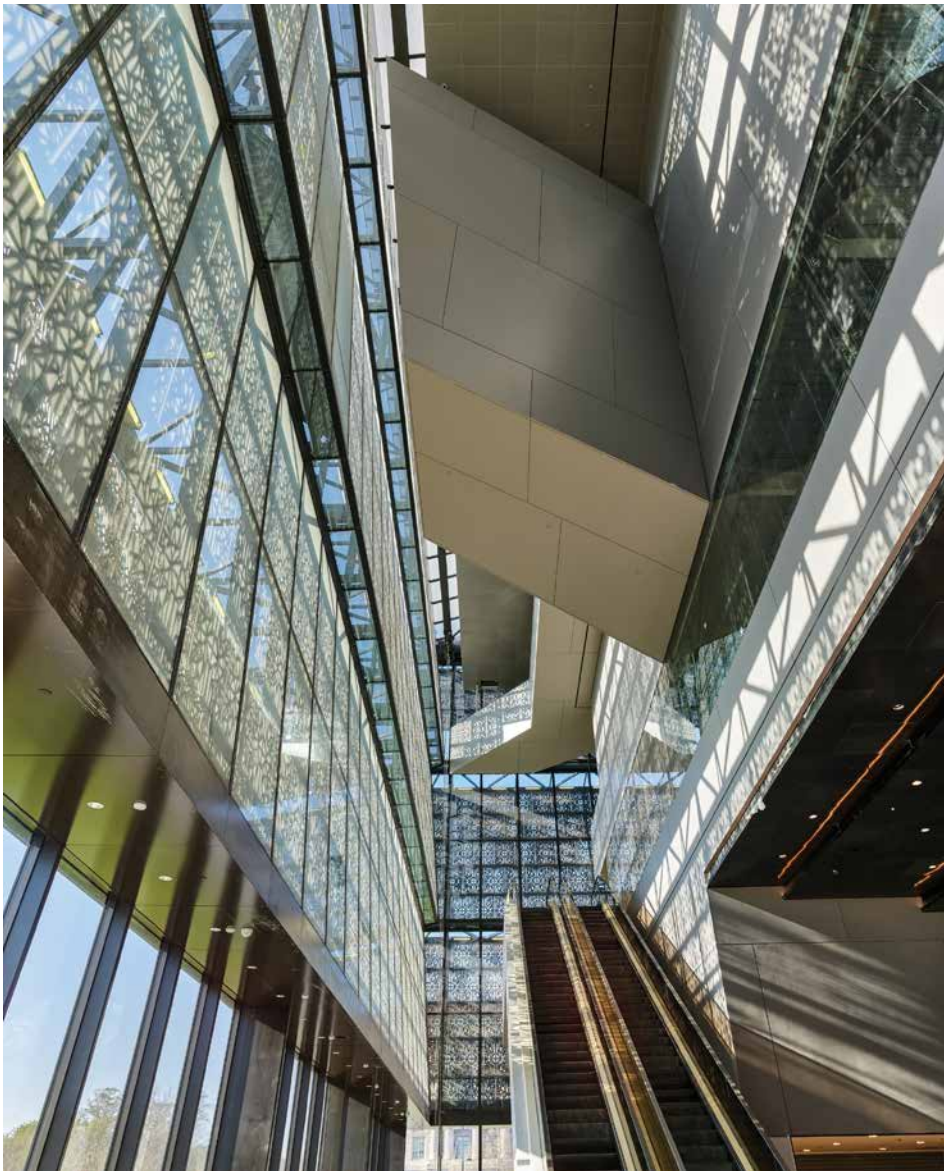


Figure 3



Figure 4 150 Greenwich Street (4 World Trade Center) Location New York, NY, United States  
 Architect Maki and Associates, Adamson Associates Architects Owner Empire State Development Corp., LMDC, Silverstein Properties Completion 2013

manufacturing capabilities for small and large-scale production. The following selection of projects are prime examples of designers expressing the architectural design of their projects by exploring the materiality of glass, while meeting engineering requirements and working within manufacturing limitations.

## Transparency

At the National Museum of African American History and Culture, Freelon Adjaye Bond/SmithGroup designed the building to be wrapped by a monumental exterior screen in the form of a crown or corona, a reference to a traditional Yoruban column capital. The three tiers express faith, hope, and resiliency, and the inclined 17-degree angle is a direct reference to the capstone of the adjacent Washington Monument.

A steel truss system supports both the Corona's exterior screen and interior glass from the zone in between these two layers. Upon entering the museum, a visitor sees a smooth, uninterrupted plane of glass, zig-zagging upward. The full height of the Corona is experienced through an atrium space on all four sides [Figure 3]. Glass sizes and structural modules were optimized to maximize the overall transparency.

The glass enclosure inboard of the Corona screen uses transparency to facilitate views, both from outside to inside, and from inside to outside. Solar shading of the all-glass envelope is accomplished through multiple measures. The Corona screen shades the glass façade, providing an initial reduction of solar heat gain and helping to avoid uncomfortable glare conditions. Next, the clear insulating glass units, framed in curtain wall units, incorporate a high-visible-light-transmittance, low-e coating, and a PVB laminate that filters out nearly all the unwanted ultraviolet light. Lastly, two densities of dot-pattern ceramic frit are incorporated. The horizontal skylights carry a denser frit pattern as they are not shaded by the Corona and receive a greater portion of the incident solar radiation. A lighter density of dot-pattern ceramic frit to the sloped glass inboard of the Corona. This frit helps the lighting in the zone between Corona screen and glass to achieve a soft glow at night, appropriate for the National Mall. The result is a uniform wash of light which highlights the texture of the screen's perforations.

The first floor and at the "lenses" the glass is designed for maximum transparency to invite visitors in and highlight views out. Here, the insulating glass is low-iron and larger in size. The transparent glass appears dark when viewed frontally from the exterior during the day because the light level outside is on



Figure 5



Figure 6



Figure 7

the order of 400 times brighter than inside the building [Figure 1]. This effect occurs on any similar “transparent” glass installation. However, in the early evening when the light levels inside and outside are more balanced, light from the interior of the museum spills out onto the mall and through the Corona [Figure 2]. Once inside, the situation is reversed. The glass appears most transparent during the day looking out onto the bright mall as shadows from truss components and screens enliven the gallery’s walls [Figure 3].

## Reflectivity

While the reflective glass high-rise tower typology has proliferated around the globe, especially in hot climates where solar protection is critical, rarely has the reflectivity of glass been used with as much architectural impact as at 4 World Trade Center. Fumihiko Maki’s minimalist design combines two interlocking prisms, and orients a shear planar façade rising 978 feet (298 meters) above the 9/11 Memorial Plaza and the footprints of the former World Trade Center buildings. While several different glass treatments were studied during the initial glass selection process, including ideas of muting the reflection with a subtle #1 surface frit, the final design direction was to optimize reflectivity: enough to mask the difference between vision and spandrel while providing sufficient visible light. A high performance, low-e coating was selected for its high reflectivity level of 46% with minimal coloration, and it was combined with low-iron glass so that the body tint of the glass would not affect the color of the reflections (note that the reflected light passes through the outer lite two times making the neutral tint of the glass critical). The aluminum frame curtain wall units removed all unnecessary glass joints with floor to floor modulation, eliminating all extraneous geometry to accentuate the flat plane of the façade.

The final effect is the dematerialization of the massive building by making it most apparent as reflection. In many daytime lighting conditions, the 61-story tower blends into the sky and its urban context, while the 35% visible light transmittance of the glass creates a comfortable interior lighting level. After the sun sets, a soft glow can be seen through the glass, but the reflections of adjacent buildings and the darkened sky remain the dominant appearance of the building itself.



Figure 8 United Nations Headquarters Location New York, NY, United States Architect Heintges & Associates Owner United Nations Capital Master Plan Completion 2015



Figure 9



Figure 10

## Color

The United Nations Headquarters in New York City was designed in 1947 by a collaborative group of architects, including Le Corbusier, Wallace K. Harrison, and Oscar Niemeyer, among others. The iconic International Style, 17-acre campus is composed of six buildings, with the tower form of the Secretariat rising above the nearby East River. The original Secretariat façade was revolutionary for its time, with interlocking unitized frames installed sequentially up the façade. Once the steel and aluminum units were in place, double-hung window sashes with heat absorbing blue-green PPG Solex® glass were installed in the vision area, and Aklo® heat absorbing blue-green, rolled, wire glass was installed at the spandrels in front of a black painted concrete masonry unit wall. The overall effect was a lattice of metal with horizontal bands of transparent glass at the vision areas and slightly darker glass at the spandrels.

Unfortunately, the glass tint was not sufficient to limit solar heat gain and glare, so soon after completion a reflective film was added to the east elevation, and years later to the west elevation. The unintended consequence was the loss of the designers' original intent of a transparent façade [Figure 8, 2007].

After many years of weathering, the UN undertook a complete campus renovation in 2006. Heintges & Associates was hired as both Design Architect and Specialist Consultant, tasked with restoring the integrity of the façades for all six of the campus buildings. For the Secretariat, extensive onsite testing proved that the wall was not repairable, and the UN moved forward with a replacement strategy that was faithful to the historic design intent, but upgraded to meet modern standards for performance, security, and sustainability. At the beginning of the design phases, the project team identified glass selection as critical to the success of the project: the challenge was to match the historic appearance of the original 6mm monolithic glass with a much thicker laminated insulating glass unit that would provide for improved performance, daylight comfort, solar heat gain control, thermal isolation, and security.

Physical samples of over 25 combinations of clear, low-iron, and tinted substrates with high-performance low-e coatings were compared to the appearance of the historic vision and spandrel glass [Figure 9]. Samples were monitored on the roof of the adjacent Library Building over several weeks with varying sky dome conditions, sun angles, and times of day, with concerns of color match, reflectance color shift, polarizing effects, etc., eliminating many of the products. From these, a full-scale



Figure 11 Spandrel glass reflection exceeds that of vision glass.



Figure 12 Trials of spandrel glass options with reduced reflectivity. From left to right along middle spandrel glass options: (1) simulation of historic monolithic glass, (2) insulating glass with clear inner lite, (3) and (4) insulating glass with gray inner lite and low-e coating. Note that appearance of (1) matches (3) and (4).

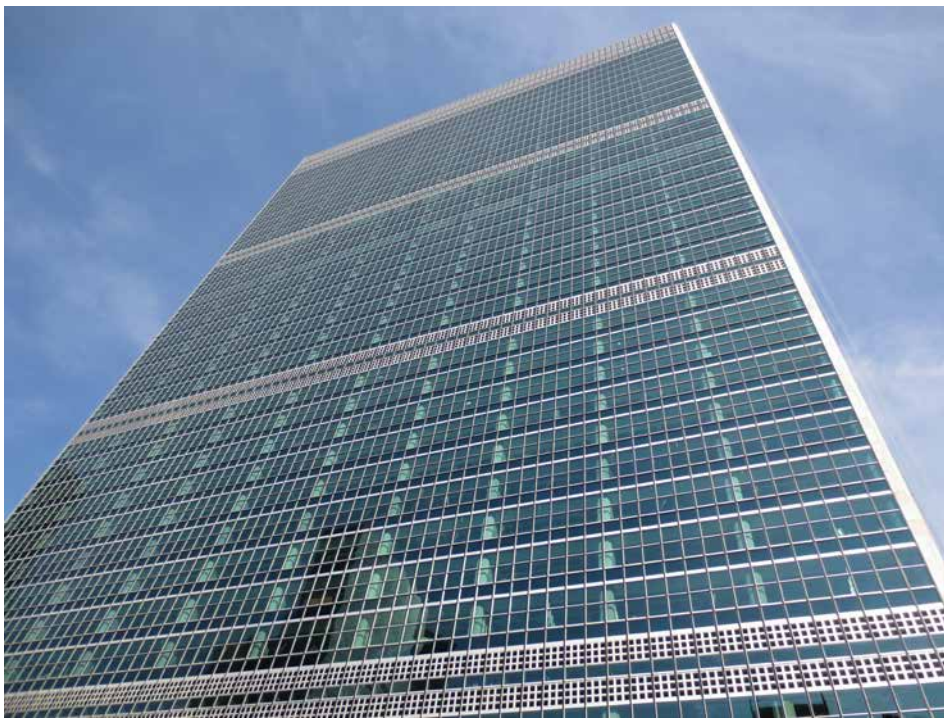


Figure 13

mockup was set-up on the campus to review the best three options for the vision glass, and a single type of laminated blue-green spandrel glass that matched the coloration and visible light transmittance of the original spandrel glass set in front of three different back pan colors. For comparison, the visual mockup also included simulations of the original monolithic vision and spandrel glass. Interior blinds and proposed lighting fixtures were also included, allowing the glass to be viewed in multiple lighting and shading conditions [Figure 10].

Based on the observations of color, reflectivity, and transmittance, a 33mm thick insulating glass unit with a tinted blue-green outer lite, high performance triple-silver low-e coating, and low-iron laminated inner lite was selected for the vision area. Visually it was the best match when compared to the simulated original, and it offered the best performance with an energy efficient solar heat gain coefficient of 0.24 and a comfortable interior light level with visible light transmittance of 51%.

The spandrel glass selection proved more difficult, and was a further illustration of the importance of color and the effect of reflection on our perception of the glass color. At the visual mockup, the façade contractor proposed a modification to include insulating glass at the spandrels to reduce risk of condensation within the shadowbox cavity. A clear inner lite was added to the specified composition of two different blue-green tinted substrates to replicate the tint of the original spandrel glass. Unfortunately, the clear inner lite increased the reflectivity of the overall glass composition from 6.1% to 9.2%, an increase of 50% more reflectivity. While this was not visible at the visual mockup due to the low viewing angle, it became readily apparent at the performance mock-up [Figure 11]. The increased reflectivity caused the spandrel zone to read as brighter than the vision glass, an inversion of the original intent of a dark spandrel zone separating transparent vision areas. Fifteen additional alternates were developed with various combinations of frits, low-e coatings and tinted substrates, and four were finally selected for review on the performance mockup. The successful solution incorporated a grey inner lite with a thermal low-e coating that further reduced reflection off the inner lite and a total reflectance level of 7.0%, meeting both the design intent of historically accurate color and the project performance requirements [Figure 12].

The final result of the glass selection process was the replacement of the façade in a manner faithful to the original design intent of transparent tinted vision glass and relatively darker bands of spandrel glass [Figure 13].



Figure 14 Barnard College Diana Center Location New York, NY, United States Architect Weiss/Manfredi Architects Owner Barnard College Completion 2010



Figure 15



Figure 16

## Surface Materiality

While transparency, reflectivity, and color are material properties of glass, none of them express the material surface of the glass architecturally. By etching the outermost surface of the glass, adding an opaque frit pattern, or other processes, architects materialize the glass surface itself as part of the architecture. The last three projects will explore three ways this has been achieved.

Weiss/Manfredi Architects designed a seven-story mixed-use building and student center to replace Barnard College's two-story McIntosh Center. A skeptical board of trustees, partial to the conventional brick-and-mortar buildings of the campus, was persuaded by an all-glass facade design that references the aesthetic red brick with glass that is essentially perceived as a masonry material.

Extensive samples and mock-ups tested the color of the façade's glass in various light conditions [Figures 15 and 16]. The result is a unitized system of transparent, fritted, and translucent glass over colored back panels. The acid-etched #1 surface evokes the look of opaque masonry while still reflecting light; the building's distinct color is created by a pale terra cotta-colored frit on the #2 surface, a bright red-painted back panel inboard, and bronze-colored aluminum panels at floor lines. Glass is structurally glazed into a bronze-colored aluminum frame, creating a warm effect that varies throughout the day and seasons.



Figure 17 Dutchess County Residence Location Dutchess County, NY, United States Architect Allied Works Architecture Completion 2011



Figure 19

On the eastern slopes of the Hudson River Valley, Allied Works Architecture designed a residence, guesthouse, and private gallery on a 400-acre property in Dutchess County, New York. The helical structure of the Main House is enclosed by a skin of transparent, translucent, and opaque panels that let views and natural light into the space while helping to protect an extensive art collection within.

The entire façade is composed of glass panels, some as transparent walls and openings that give striking views of the landscape to those inside, others as opaque cladding to conceal structural elements or interior walls for hanging art. The opaque panels are deeply carved and then acid-etched with vertical

stripes, redefining them as surface [Figure 18]. When darkness falls, the etched glass becomes a canvas for "Light House," a site-specific video installation by Doug Aitken that uses 360-degree projection to illuminate the glass with striking images of nature that make it pop from its surroundings, or almost camouflage it altogether on the landscape [Figure 19].



Figure 18

Reflections at Keppel Bay, located on the shoreline of Singapore's Keppel Harbor, consists of six curved residential towers ranging in height from 395 feet (120 meters) to 575 feet (175 meters). Studio Daniel Libeskind gathered the various buildings together to create an airy composition in glass and aluminum that is different from every angle. Since the forms of the towers were independent from the residential layout on the interior, it was important to the designers to blend out the regular vision glass areas with the grid of spandrel areas. A concept of pixilation was developed, requiring two distinct types of spandrel glass that would look different under any viewing angle. Since nearly all glass looks similar at very oblique angles due to the uniform surface, this required one type to have a surface treatment on the outermost face of the glass.

A full-scale visual mockup was erected on a nearby site to review 20 different options for the two needed spandrel glass types [Figure 21]. The eventual solution was a simple inversion: one type would be a true acid etch on the #1 surface, with a mirrored low-e coating on the innermost surface; and a second type that consisted of a "simulated acid etch" ceramic frit (translucent white) facing a laminate, and the same mirrored low-e coating on the innermost surface. The matte reflection of the first type causes it to go "dark" in direct light conditions and oblique viewing angles, and "light" in more diffuse light and perpendicular angles when reflecting bright scenes. The second type behaves just the opposite, looking "light" in direct light conditions and oblique viewing angles, and "dark" in diffuse light or in perpendicular viewing angles when reflecting bright areas. The result is a dynamic reading of the façade that continuously changes its pixilation as one moves around the towers, blending the gridded façades into uniformly pixilated surfaces.



Figure 20 Reflections at Keppel Bay Location Singapore Architect Studio Daniel Libeskind, DCA Architects Pte. Ltd. Completion 2011



Figure 21



Figure 22

## Glass Industry Development

Through careful selection, the architects and designers of the projects shown above have enhanced the architectural expression of their projects through the materiality of glass. To support these efforts, the glass industry will need to continue to develop current and future architectural glass products available on the market. For transparency, reduce anisotropy from heat treatment (make online anisotropy measurement standard), continue to improve solar selectivity of high performance, low-e coatings, and reduce the cost of anti-reflective coatings. For reflectivity, improve glass flatness for heat treated glass (transition industry to milidiopter distortion measurement). For surface, continue to develop other processes to modify the outer surface of the glass. And for all the material qualities, increase size capacity throughout the supply chain, especially during installation. With new tools and better quality at their disposal, façade designers will continue to push the architectural expressions of the materiality of glass.

## Conclusion

Creative designers are pushing façades to new and unexpected directions. We have seen this at the National Museum of African American History and Culture where transparency of the glass was critical for accentuating the Corona. At 4 World Trade Center, the expression of the glass as pure reflection enhanced the minimalist form, paying tribute to its memorial context. At the United Nations Secretariat, the original glass color was maintained and upgraded through a historically faithful replacement. And at the Barnard College Diana Center, the Dutchess County Residence, and Reflections in Singapore, the #1 surface of the glass was transformed from the glossy reflectivity we have come to expect into a matte surface that can receive light.

Our view is that more and more projects are seeking to express the full range of glass materiality as the glass industry continues to develop and support these initiatives. While transparency will likely continue as the dominant materiality to connect interior and exterior, reflectivity, color, and surface texture provide equally interesting areas of exploration for future projects.

# Glass Specification Challenges in London

Russell Cole  
Arup

## Abstract

The London property market has enjoyed a boom in construction since 2010 including many large developments of diverse typologies. There has been a broad trend over the past few years though has been towards a simplistic approach to glass specification and procurement. There are a few projects where more sophisticated latest glass products have been sought but more commonly glass is treated as a commodity. However there is also a significant population of projects that aim to achieve glass that achieves a high performance, looks good and has an attractive visual quality. Over the same time available glass products have multiplied and sourcing has become globalised from numerous sources in numerous geographies. This expanded supply has provided both opportunity and competition. However even though a wide range of products are available it is not unusual that developers, owners, designers and specifiers are disappointed with their glazing. This paper will explore some of the characteristics and drivers of this outcome and discuss how the glass industry and specifiers might play their parts and respond to give the customer what he wants.

## Introduction

Over the past few years, since 2010, London has enjoyed a building boom seeing a large number of developments particularly in the residential and commercial office sectors. Over this period however glass supply has developed certain characteristics, but it still seems that it is very difficult for a buyer to purchase high performance process glass with certainty that the visual quality of the glass is also of a high standard. This paper asks why this is the case and what can be done to achieve high performance to a high visual quality.

Parts of the London construction market aim to achieve very high quality properties, but clients in these sectors find themselves frustrated with the visual quality of the glass that is supplied to their projects. They aim for glazing that achieves a high performance but is also transparent, has a good colour rendition

and views and reflections are free of adverse distortions, but this is not typically achieved. Some particular issue are as follows:

- Poor reflections and flatness of reflections
- Distortions of view through and lack of transparency and clarity
- Discolouration colour consistency and Anisotropy
- Edge deletion
- Damage and scratches – which may be compliant to standards but are still considered defects by occupants
- Residual responsibility for any potential breaks due to critical NiS inclusions.

## Glass specification in the London market

The wave of construction in London has seen large developments and a significant number of tall towers that have not previously been a characteristic of the London market. The scale of projects and the volume of development has resulted in a rapid expansion of construction activity pulling in suppliers and sub-contractors from around the world. Although activity is tempered by Brexit there are still a lot of developments that are underway. The range of residential developments range from the ultra-prime residential developments of Mayfair and Chelsea in central London, through large tower developments in places such as Battersea and Stratford to lower cost and affordable properties throughout the city. Typically these are private developments although housing associations account for a significant portion. Similarly in the commercial sector there have been a number of iconic tower developments in and around the City of London and offices have also been developed throughout the central area of London and into places such as Kings Cross and Paddington. As the value of properties has increased so have expectations around the standard, quality, appearance and durability of the building increased. For offices in the City of London and residential developments in the West End have increasing been described as “super prime” and sometimes “ultra-prime”. As a result many projects have high standards in response to the expectations of purchasers and tenants. These are investors who are paying for some of the most expensive properties in the world (or at least they were until the pound dropped post-Brexit) and as such it is difficult for them

to accept anything substandard or imperfect. When it comes to glass they will expect clear, undistorted views, good colour rendition and their property will need to look neat and crisp from the exterior. Reflections in glass therefore will also need to be crisp. Similarly the glazing will need to perform well. Regulations will drive the thermal performance and light transmission of the glass and overheating needs to be avoided through solar control coatings. Similarly glass will play its part in controlling noise from outside and will form part of a window with a good security rating. And, of course, although there have been large increases in the value of properties those funding the projects will naturally aim to limit construction costs.

Often these high expectations in a not insignificant portion of the London construction were often not realized. The complexity of the glass specifications certainly added to the issue but visual quality appears difficult for a client to specify for various reasons as discussed below. The result in these cases has been disappointment with the clarity and consistency of the view through the building, a lack of transparency, the presence of distorted reflections and liabilities related to the performance of the glass that the owners have to carry.

Before exploring these more carefully the context of these specifications and resulting work need to be put into context.

## Typical Glass Procurement Practice

Given the scale and diversity of the London construction market there are a range of procurement models but the most common is described below used in this boom for projects in the central area.

Over the past few years the majority of projects have procured the building on a Design and Build model. In this the design responsibility for the whole project is passed to the main contractor at an appropriate stage. It is quite likely that the original design team (architects, engineers and specialists) will be novated to the main contractor to continue and finalise the design. Within this however some elements will be procured prescriptively, i.e. fully documented by the design consultants such as the structural concrete frame, whereas other elements will have a Contractor's Design Process (CDP). The latter is the most common

model for the façade elements where the design consultants will prepare design intent drawings and a performance specification for the main contractor, and their specialist sub-contractors, to propose appropriate solutions, e.g. systems, materials, finishes and products, including glass panels. Therefore the contractors have quite an influence over the supply chain and how it is eventually managed. Within this procurement chain the glass will most typically be specified either within the façade performance specification by a specialist façade consultant or a section L40 of the UK National Building Specification system. This specification would most typically be used by either a sub-contractor responsible for the entire building facade or if there are several then the supplier and installer of the windows and other glazing elements. As a result there are a number of parties that sit between the client and the glass processor. There are good reasons for this but all of these layers potentially add complexity and inhibit flexibility in the response to tenders.

One other aspect of recent procurement arrangements in central London has been the proliferation of PCSA (Pre-Construction Services Agreement) engagements also known as two stage tenders. Under these the main contractor and in some cases the sub-contractor are engaged independently during the project's detailed design stage, or Stage 4 under the RIBA Plan of Work 2013, to provide advice on the construction aspects of the project, to give them an early mobilization and in the case of the façade sub-contractor prepare their proposed details. Typically competitive tenders are used to select the PCSA (sub-)contractor including an estimate of the value of the main contract or sub-contract package. Later as the design develops the commercial aspects are refined, leading to a negotiated final price. Although there is the option for the client to then take the design to the market this is rarely the case. If the PCSA is well planned then the façade sub-contractors services can include firming up their proposed supply chain, including the source of the glass and samples and visual mock-ups can be prepared as part of the scope. This approach may be used by a team aiming to reach a higher quality standard or an unusual glass composition.

## Process for Better Glass

Where the project's ambition requires or very high standards are expected the project team may try to take particular measures to achieve glass of good quality. As alluded to above samples and visual mock-ups will feature in this approach, but before these can be procured the detailed specification of the glass



Figure 1 A glass sample viewing box in use in Fitzroy Square, London

needs to be determined. Standard glass samples 300mmx200/300mm are commonly used to assess clarity, tone and reflectivity of glass build-ups through the design stages of projects. On some projects viewing boxes are used to allow the project team to assess differences between samples in open air spaces whilst also modelling the inside to outside aspects of the glass.

Although representative these samples are too small to be tempered. Visual mock-ups are also a key factor. In these fully processed, full sized glass units can be viewed in context of the proposed façade and the expected appearance reviewed by the client and the design team. If there is an open book approach to the cost of glass with the sub-contractor then different products from a range of suppliers can be compared for their visual quality. Selection however can only be made on what is presented. Client teams at that point will then wish to set these panels as control samples for visual quality. This may or, more likely, may not be accepted by the sub-contractor or main contractor as there will be no associated commitment from the glass processor to maintain this visual standard. The glass viewed is likely to fall well inside of the flatness tolerances and therefore may not be representative of the full range of production. For an enhanced project though the client team through specifications will aim to tighten the various dimensional, appearance and flatness criteria to control the appearance of the glass. These may or may not survive the tendering process and will most likely be

challenged by all parties in the supply chain, who by contrast will aim to adhere to standards and industry norms.

## Drivers behind around the issue

Different players with the supply chain each have drivers that make the specification and procurement of performance glass with a high visual quality difficult.

### Clients

- Maintaining a competitive situation, leads avoiding specification of a sole supplier, avoiding changes to the specification after the award of tender, avoid situations that lead to poor negotiating positions
- Budget certainty as soon as possible, leads to using PCSA to obtain early budgets, require well defined tender documents, desire to lock in prices at an early stage
- Aim to transfers various risks to contractor that will include design, selection of materials, responsibility for workmanship
- Compliant with regulations and planning requirements – to avoid compromising the value of the development.
- Demonstrable compliance with standards and property market specification for space being constructed e.g. BCO, NHBC, etc. to position the development in the market sector
- Low maintenance in service which in relation to glass means that specification target avoiding occupant complaints, deterioration and breaks in service,

Architects (and these issues are also those of the clients)

- Aesthetics and standard of finish – these project the image of the development and allow it to achieve its potential returns
- Consistency of appearance
- Weathering

Main contractors and sub-contractors

- Working to maximize returns within the agreed price and finding opportunities to provide more to the project.
- Minimising risk and uncertainty generating a risk adverse culture that minimizes loose ends, avoid tests and other activities that are difficult to control, avoid subjective assessments and criteria, control the location and extent of VMU, minimising production / value add completed at risk, avoid fitness for purpose requirements,

Glass processing industry

- Avoidance of customization
- Improve efficiency of production and minimize wastage and potential for rejection of product.
- Speed and simplicity of production
- Limited responsibility and limit the extent of warranties.
- Reliance on standards and industry norms that they are confident that their production can meet.

## Outcome

Given the typical behaviours of different players in the supply chain as mentioned above even when the client and their design team are seeking to specify glass to a higher standard it is subverted in various ways. To control risk main contractors and sub-contractors will often seek to supply glass that is merely compliant with the relevant codes. These codes take a long time to produce and update and as they are developed by code committees comprising of all players in the industry the glass suppliers have a big influence to see that the standards set are not too challenging for their industry. To overcome the limitations or the lack of coverage of local codes facade consultants will include references and elements of other international standards, but this can end in confusion as within one national system the codes will cross refer making a mixture of codes difficult to manage. For instance ASTM glass codes allow different tolerances in glass thickness compared to Euro Norms making references to different codes potentially invalid.

Codes are supplemented by industry guides and standards, but these are often generated by one side of the industry and may not have universal acceptance. This can be further

complicated where glass processors are based overseas and therefore propose that their products follow their local codes and industry standards rather than those set out in the specification.

Finally many codes have only limited controls on visual aspects of glass, leaving some phenomena undefined. Also definitions can be ambiguous and the various criteria apply to each process in turn. As a result the cumulative effect of different impacts on the visual aspects of the glass units are not controlled or defined by the standards. And the codes only apply to units at the time of production and do not necessarily apply to the as installed or in service condition.

As a result currently there are no standards that can be adopted where higher standards are sought.

## The Way Forward

As noted above it would appear straight forward that the client should be able to procure what they want, i.e. high performance glass with a high visual quality, but for the reasons discussed above there are barriers. So how can the industry respond to cut through the issues?

A mixture of approaches can be envisaged that will probably have to work in tandem to unlock the problem. Essentially suppliers need the following:

- A clear definition of the requirements – how to define the various aspects of high visual quality?
- Agreed methods of measurement aligned to the definitions of visual quality
- A capability to control and avoid distortions during each of the glass processing stages
- Appropriate control and checks of visual quality that can be completed on the production line to avoid glass being returned.

If these can be addressed then suppliers, and those above them in the supply chain may have confidence that the required standard can be achieved.

Appropriate standards and definitions appears to be key. Subjective criteria are problematic and the only available standards are very broad and do not define the higher quality product that clients are seeking. Glass processors are targeting standards that easily exceed the established dimensional / flatness criteria, mainly to avoid returns, but these standards can sold to the client due to a lack of definition. One step forward would be an industry definition of higher visual quality glass. This would need to define either dimensional (measurable) criteria for flatness, thicknesses and other aspects that impact images viewed through or reflected by the glass. And these standards would need to apply to

the completed glass unit rather than each individual process to avoid the accumulation of distortions within a unit.

The alternative to dimensional criteria would be optical standards. These have been discussed within the industry for many years but are not being taken up. Are the barriers the complexity of the criteria or the need for the industry to invest in new measuring methods? Is it that methods for measuring glass are evolving quickly and no new methods can be established before an alternative is proposed? Clearly as the issues are generally related to visual aspects direct measurement of a distorted glass appears the best approach. If this was adopted then there would have to be investment by suppliers and education of all those parties within the supply chain.

As mentioned measurement methods are evolving as new equipment and perhaps more importantly sensors and ways of processing the data are available. Two particular technologies come to mind. Laser pin point surveys could be used to precisely map the surface of the glass to determine its shape. These results could be quickly assessed by software predicting the visual characteristics of the glass. Alternatively glass could pass in front of a viewing box with say a zebra board so a visual scanner can determine the degree of distortions to view through the glass. Introducing a new step in the production sequence to measure the quality of the glass will impact production rates and also result in glass being downgraded and potentially destroyed.

This raises an alternative strategy formed on the basis that the visual quality of glass cannot be controlled. In which case it needs to be managed in ways that naturally variable materials such as stone are handled, i.e. panels are in assessed, perhaps subjectively, for visual acceptability against a set of control samples. The panels are then either set a position on the façade or are graded and potentially scrapped if they do not meet the particular criteria of the locations. In addition to the cost of wasted units it would also be burdensome to manage especially on projects where repetition of sizes is low.

Behind all of these techniques is the ability of the glass processing industry to rise to the challenge. If wonderfully flat, undistorted insulated glass units could be produced without any compromise in performance then this would be a dead issue. But at the moment the way forward is unclear. Glass processing equipment is continuing to evolve and incorporate increasing numbers of controls and sensors that can adjust settings to give more reliable products.

We may not be far from a point where enough of the industry has confidence for instance

to halve the roller wave criteria established in codes for tempered glass around the world. Unfortunately at the moment there is no incentive for the industry to revise these specifications, but as discussed above this results in clients and specifiers being unable to procure glass to tighter tolerances. As noted above if a premium could be charged for glass produced to tighter tolerances then a change may occur.

# High-quality Edge Enameling for Architectural Glass

Ralf Greiner<sup>1</sup>, Artur Bechtloff<sup>2</sup>

1 Guardian Thalheim GmbH

2 Ferro GmbH

## Keywords

1=edge-enamel 2=ceramic paint 3=sputter coating 4=structural glazing

## Abstract

New solutions for edge-enameling of sputter coatings. System TEA is a specific ceramic paint application, jointly developed with the enamel manufacturer Ferro, for the combination with Guardian sputter-coated architectural glass. The technology creates a very stable and uniform ceramic surface. This new process opens up opportunities to provide high performance coated glass for a number of different applications such as structural glazing, all-glass corners, glass roofs or louvre windows. The process involves the enamel being applied directly onto the coating. During subsequent heating, the enamel dissolves the sputter coating and fuses with the glass to create a very strong bond – comparable to standard enamel on float glass. After cooling, the coating is fully embedded in the enamel.

## Introduction

The introduction of heat-treatable thermal insulating and solar control coated glass was a big step towards the improvement of customer service and flexibility in the realization of architectural glass projects. This led not only to new possibilities for the provision of tempered and heat-strengthened glass, but also to the possibility to bend coated glass and, depending on the type of coating, even to print on glass with suitable ceramic paints. Printing took place either over the entire surface in order to manufacture reflecting spandrel glass, or at the edge of the glass panes in order to conceal structural elements or to create suitable surfaces for structural bonding. However, the available ceramic paints are compatible only with a few types of coating. In addition to that a change of colour, in some cases clearly noticeable, is seen in particular with very transparent or silver-containing coatings; see fig. 1. On the other hand, new generations of coated glass (e.g. the so-called double and triple silver coatings) are not

usually compatible with ceramic paints. The consequence of this is that many applications can be realized only with a great deal of effort using conventional processing methods.

These applications include:

- structural bonding
- all-glass corners
- overhanging roof glazings
- glass louvre windows
- turn and tilt windows in all-glass facades.

The usual cut-to-size tempered and heat-strengthened glass necessary for this often also have to be elaborately coated, which is usually connected with long and unpredictable delivery times, quality risks and not least, high logistics expenditure. The removal of the coating at the edges of the glass by conventional grinding, either automatically directly on the cutting table or manually with the appropriate equipment, also usually leads to unsatisfactory results with regard to aesthetics and surface quality; see fig. 2. The amount of work necessary to remove the coating from large areas also incurs costs that are frequently significant.

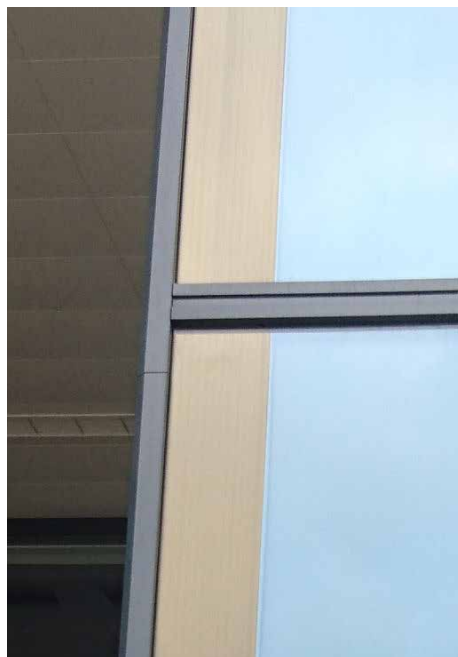


Fig. 1: Edge-printed coated glass with typical colour drifting

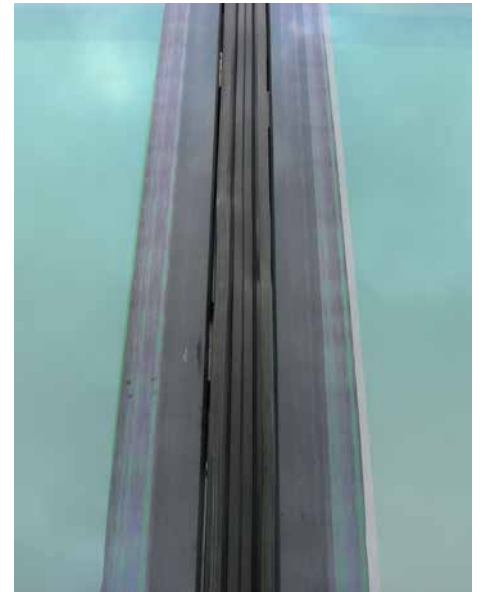


Fig. 2: Glass with edge deletion by grinding, showing typical grinding marks

## New processing technology

The "System TEA" technology (TEA = True Edge Application), developed in collaboration with Ferro, a leading manufacturer of ceramic paints for architecture, allows direct printing on coatings, including those of the latest generation. This method makes use of a completely new type of material-dissolving ceramic paint (enamel), which was conceived for use in combination with heat-treatable sputter coatings. During the firing process the coating is completely dissolved in the enamel. The System TEA enamel fuses with the glass and adheres very strongly – comparable to conventional ceramic paint on glass. After cooling, all constituents of the coating are chemically passivated, similar to colour pigments, and completely embedded in the enameling.

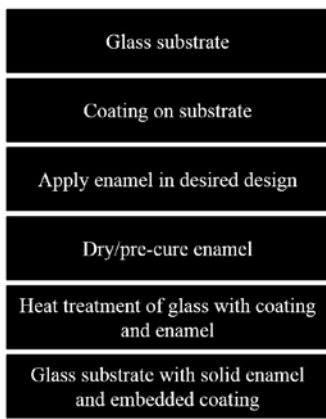


Fig. 3: System TEA – flow chart

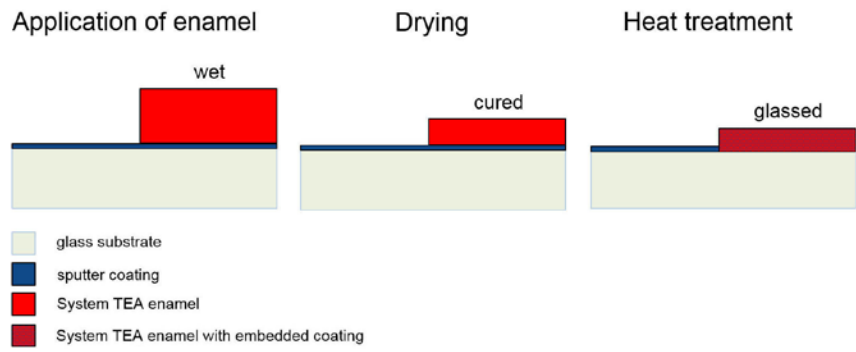


Fig. 4: System TEA – coating and enamel during processing

Due to the efficiency of the process, the number of processing steps is considerably reduced. The complete dissolving of the coating constituents by the ceramic paint makes it unnecessary to grind off the coating before enameling. This allows the omission of the work step that is most critical for the final product and which is frequently responsible for an unacceptable appearance and an inhomogeneous surface. At the same time, the technical risk for intended structural bonding is lowered.

### Application of the glass enamel and firing

A decisive criterion for the application of the paint is the most homogeneous enameling possible. The wet film thickness [measured directly after printing] should be at least 44 µm (see also System TEA data sheet from Ferro) in order to ensure the complete dissolving of the coating material. The wet film thickness should be checked by means of suitable measurements.

The coated surface can be printed on using various methods. The best results are achieved with the so-called roller coating technique. Wet film thicknesses > 70 µm are easily achievable here and the homogeneity of the enameling is typically very good. Another option is ceramic screen printing. Here the minimum wet film thickness must be ensured through the selection of an appropriate screen. Manual paint application using a hand roller is possible, but not recommended, since the uniformity of the enameling is very difficult to maintain.

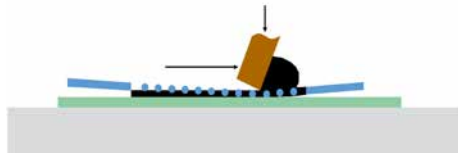


Fig. 6: Screen print technique (schematic representation)

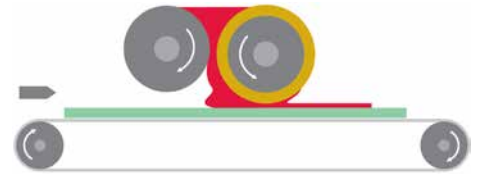


Fig. 7: Roller coating technique (schematic representation)

The subsequent drying process is equally decisive for an optimum result. Infrared or convection dryers are recommended for this. The glass temperature should be > 130 °C. It is important that the paint dries homogeneously and completely. The paint is fired during the normal heat treatment of the glass to make tempered or heat-strengthened glass. On account of the differing degrees of reflection for long-wave thermal radiation exhibited by the ceramic printed surface and the low-emission coating, the glass may warp during heating in the furnace and in the cooling area due to lateral temperature differences. These deformations depend on the width of the printed surface and the number of printed edges. A circumferential edge print in particular can lead to strong “bulging” of the glass in the furnace. The furnace parameters must therefore be adapted accordingly.

### Tests and analyses

Various tests were carried out on the end product. The aim was, firstly, to prove the coating-dissolving properties of the ceramic paint and, secondly, to test the properties of the enameled surface with respect to its suitability for the corresponding applications.

#### Proof of the coating-dissolving properties

In order to prove the coating-dissolving properties, samples were analytically examined by means of SEM (Scanning Electron Microscopy) / EDX (Energy-Dispersive X-ray spectroscopy) or WDX (Wavelength-Dispersive X-ray spectroscopy). In the process, all



Fig. 5: Determination of wet film thickness with a layer thickness gauge

materials and material combinations used in the Guardian coatings had to be accounted for. Therefore, different coatings were printed on and analyzed accordingly. The aim was to prove the complete removal of the coating constituents at the interface. In other words, the composition of the glass/enamel interface remains independent of the dissolved coating. In fact, relevant coating constituents such as silver (Ag) or dielectric coating elements could no longer be found at the interface using the methods described above. That applies both to the coated surface and to the cross section through to the glass surface. Amongst others, the coating SunGuard SNX 50/23-HT, consisting of a series of over 20 individual layers, was examined as an example.

From the analyses, the conclusion can be drawn that no change is detectable in the composition of the enamel paint in the System TEA due to the dissolved coating constituents. That applies both to the surface of the printed areas and to the profile cross-section. All elements of the various coatings were fully dissolved. The SEM photo in fig. 8 shows a typical interface between glass and System TEA enamel. The EDX analyses prove that there is a sliding transition of the Si concentration between the float glass and the enamel, which indicates good fusion. [2]

#### Adhesive behavior of structural silicone

An important reason for the development of the System TEA technology was the problem of undefined surfaces following the mechanical grinding off of sputter coatings. This can lead to unforeseen risks, especially for structurally bonded surfaces. Therefore, the following silicones were tested for structural bonding to the System TEA surface according to ETAG 002-1:

- Dow Corning DC 993 (passed)
- Dow Corning DC 3363 (passed)
- Sika SG 500 (passed)
- Sika IG-25 HM+ (test is still running)

The test specimens according to ETAG 002-1 were stored under changing temperatures and subjected to tension until failure. Moreover, the residual strength was tested after storage in water at a high temperature and UV exposure, after storage in moisture and NaCl environment, after storage in moisture and SO<sub>2</sub> environment and after storage in a cleaning agent solution. The requirements were met in each case.

In addition, the System TEA was adopted into the General Type Approval (AbZ) issued by the DIBt (Germany building authority) for the use of Dow Corning DC 993 in combination

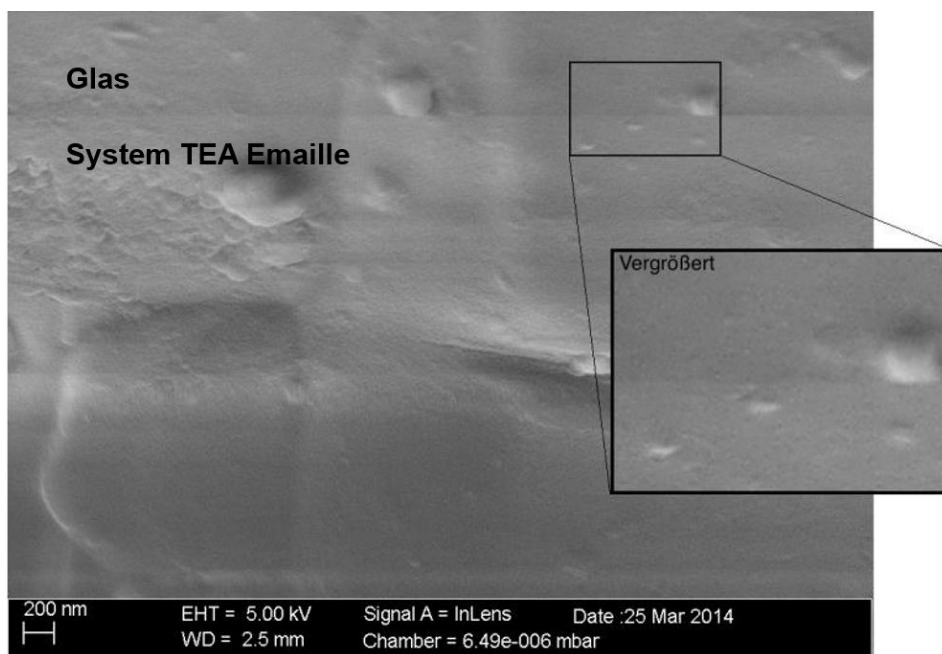


Fig. 8: SEM photo of glass with a SunGuard SNX triple-silver-coating and System TEA [2]

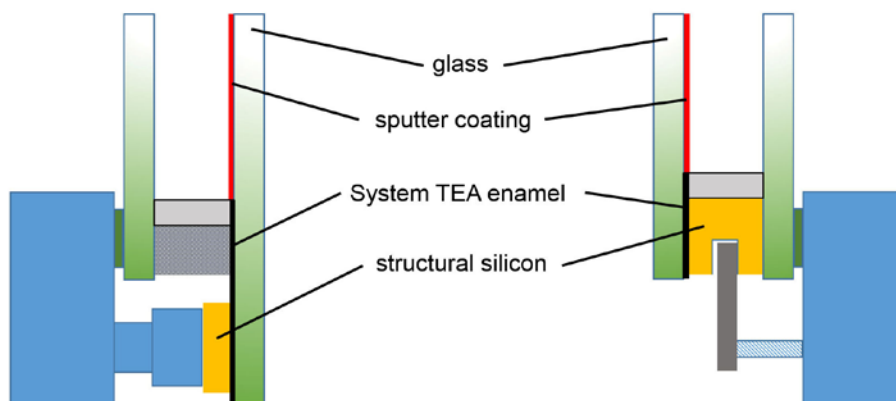


Fig. 9: System TEA in a structural application (left: stepped glass; right: toggle system)

with tempered, tempered heat-soaked and heat-strengthened glass in structural facade applications. The sputter coatings covered by the General Type Approval AbZ (Z-70.1-75) are listed there in the appendix. In order to obtain the data for a suitable production control within the scope of the General Type Approval, the following properties of the ceramic-printed surfaces were also determined:

- Scratch hardness (ISO 1518): no scratches detectable with adhesion test rod at  $\leq 16$  N pressure
- Porosity (ASTM C 1048-92): no penetration with isopropanol
- Degree of glass (DIN 67530): measured 126,7 (required: min. 110 at 60° angle) [3]

#### Proof of the properties of tempered heat-soaked glass

The objective was to prove that tempered, heat-soaked glass printed with glass enamel of the type System TEA with correspondingly dissolved sputter coatings conforms to the standard DIN EN 14179-1. The types of coated glass selected as examples were the SunGuard HD Neutral 67, a relatively simple solar protection glass, and the SunGuard SNX 50/23 HT, which is equipped with an extremely complex coating. Panes of glass in the thicknesses 6 and 8 mm were tested in each case. All panes tested met the requirements of the standard.

| Property                                       | Measured                    | Requirement |
|--|-----------------------------|-------------|
| Fragmentation (fragments within 50 mm x 50 mm) | 46 – 70 across all samples  | ≥ 40        |
| Bending strength [N/mm <sup>2</sup> ]          | 89 – 105 across all samples | ≥ 75        |

Table 1: Classification of panes of tempered and heat-soaked glass with System TEA enameling according to DIN EN 14179-1

## Summary and outlook

Today, glass enamel printing is used more and more frequently wherever structural elements have to be concealed, for example in the case of all-glass corners or louvre windows. The "System TEA" opens up opportunities for the use of edge-enameled, coated architectural glass. Using this new technology, visually homogeneous glass enamel surfaces can be created that are both mechanically and chemically stable. The surfaces of the System TEA always offer reliable and tested adhesive characteristics for the structural bonding of facade elements. At the same time an attractive, visually uniform outside appearance is achieved. The new method reduces the expenditure for production and logistics. On one hand it is possible to eliminate the laborious grinding off of the coating, which is often associated with poor quality while on the other hand heat-treatable coatings can be used instead of a logistically elaborate coating onto cut-to-size heat treated glass. All in all, it can be expected that the use of this technology will make a very big contribution to the improvement of the quality of enameled architectural glass in the future.

It is planned in the future to supplement the currently available colour black grey shades, amongst others. These would be used especially with grey structural sealants.

## Literature

- [1] Internat. Patent Application, Int. Publication Number: WO 2014/133929 A2 (24.02.2014) Title: "Window units made using ceramic frit that dissolves physical vapor deposition (PVD) deposited coatings, and/or associated methods"
- [2] Bahn, M.: Charakterisierung von Guardian Magnetronbeschichtungen bei Emaillierung mit einem neuartigen schichtauflösenden Email (CFDPC)", Bachelorarbeit, Köthen, May 2014
- [3] Ferro, Technical datasheet GSGF TEA Black 14 4400AL

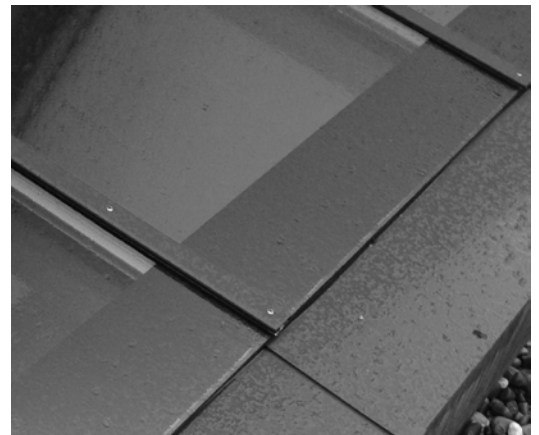


Fig. 10: Typical application for TEA enameling (left: all-glass systems; middle: louvre windows; right: roof glazing)

# Fabrication Technology for Composite Glass-metal Panels

Dipl.-Ing. Dr. techn. Stefan Marinitsch<sup>1)</sup>, Dipl.-Ing. Peter Eckardt<sup>1)</sup>, Dr.-Ing. Fabian Schmid<sup>1)</sup>, Dr.-Ing. Martien Teich<sup>1)</sup>,

<sup>1)</sup> seele GmbH, Gutenbergstraße 19, 86368 Gersthofen, Germany

## Abstract

Following a short overview outlining key design objectives, the fabrication process of an opaque composite glass panel is described in detail. The assembly is formed of ceramic coated, heat treated glass and smaller backing panels laminar bonded using a silicone adhesive. The backing panels are segmented forming multiple connection points. Whilst mainly focusing on fabrication technologies and the QA-QC procedures utilized, this paper will also discuss material properties and structural considerations to provide the reader with a comprehensive overview.

## Keywords

1=laminar bonding, 2=façade, 3=composite panel, 4=silicone adhesive

## Objectives

The composite panel was developed for a project specific requirement of cladding components to form a uniformly opaque and seamless glass surface. Mechanical fixings (Figure 1), protruding the glass surface or shining through a colored interlayer or ceramic print, have been agreed to be visually non-desirable. A further requirement is the necessity to utilize the composite in an overhead application. Consideration of the post-breakage behavior for glass in this configuration typically leads to laminated safety glass. In combination with mechanical fixings or supporting elements sufficient in size and or number, stability following damage needs to be ensured.

With the visual intent, project particulars and safety considerations in mind, the following design objectives have been formulated. They serve as a coarse road map for the product development process.

- The cladding system should provide a uniform opaque surface in sizes up to 15 m x 3.2 m.

- Visual continuity of the surface is paramount. The surface should not be disrupted by localized components (i.e. mechanical fixings).
- Any supporting structure should avoid or minimize local stress concentrations in the glass.
- As the glass is fully opaque, mirroring is expected. To ensure an unhasty visual experience, a small and/or uniform deflection of the glass is required. This is understood to be a mixed task, requiring structural (deflections due to loadings), fabrication (off site tolerances) and installation (on site tolerances) input.
- Any weight reduction will help to reduce seismic loadings and minimize the structural requirements for the supporting structure.
- In case of glass breakage sufficient system redundancy is needed.
- For cleaning and maintenance the glass may be accessible.
- Considering a quantity of approx. 30.000 m<sup>2</sup> fabrication ideally allow for an automated process.

By substituting one glass ply with an aluminum backing panel, bonded using a silicone adhesive, a weight reduction of over 30 % is possible. Silicone is selected as a suitable material to bond glass and aluminum backing panels. The laminar bonding provides redundancy in case of glass breakage and is able to transfer loadings safely. The system does not require additional mechanical fixings, providing a uniform surface (Figure 2). It is important to note that silicone in laminar application is outside current regulations (i.e. ETAG [1] or ASTM [2,3] or ASTM [2-4]).

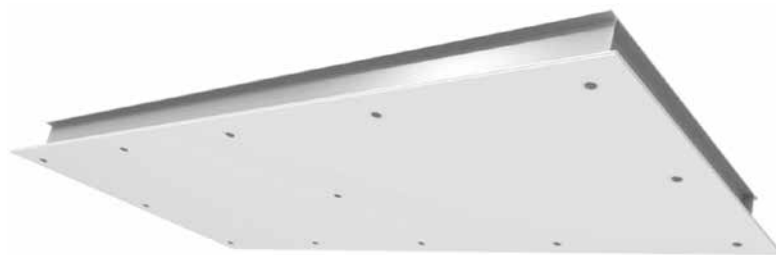


Figure 1 Overhead application with visible point fixings



Figure 2 Composite glass panel without visible mechanical fixings In Figure 3 the primary components of the assembly are shown. Ceramic coated, heat treated glass (i.) is bonded using laminar silicone (ii.) to multiple aluminum backing panels (iii.)

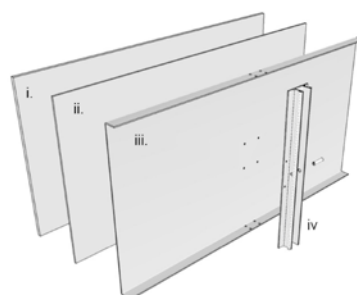


Figure 3 Build-up of the composite panel: i...glass, ii...silicone, iii...backing panel, iv...adapter profile

The size of the backing panels is limited to manage thermal expansion between the individual bonding partners. This approach allows the design to be optimized for silicone thickness, however with decreased backing panel sizes the amount of connection points increases. Every backing panel is attached to a supporting sub-structure via an adapter profile (iv.), mechanically fixed to the backing panel. Figure 4 shows a 15 x 3 m tall composite unit. The unit has up to 80 individual backing panels bonded to the surface.



Figure 4: 15x3m composite panel viewed from the panel side.

For the structural design of the glass panel, point loadings at the glass edge are identified as critical. The stress levels around the connection points are not critical for the glass.

### Silicone adhesive – material properties

For the intended use, a self-leveling silicone adhesive was developed. Processing times in mind, a two-component silicone was chosen. The material has been optimized for a laminar application. A variety of tests have been conducted to verify mechanical performance, long term flexibility, adhesion, curing parameters as well as pre-treatment options. This led to a design concept and application limits for selected bonding substrates and materials in direct contact with the adhesive. The silicone performance has been confirmed by independent laboratories on the basis of ETAG 002 [1], ASTM C 1184 [2] and ASTM C 920 [3]. These standards provided guidance when testing material behavior but require adaption to account for the intended laminar application. Lateral elongation is constrained, therefore the shear modulus is not equal a third of the Young's modulus as assumed for linear applications. In Table 1 key material properties derived by testing are summarized.

### Structural Design

The silicone layer is depicted using spring elements (Figure 4). These elements are based on the parameters and design values summarized in Table 1 and its thickness. The glass and the aluminum panels are modeled using shell elements.

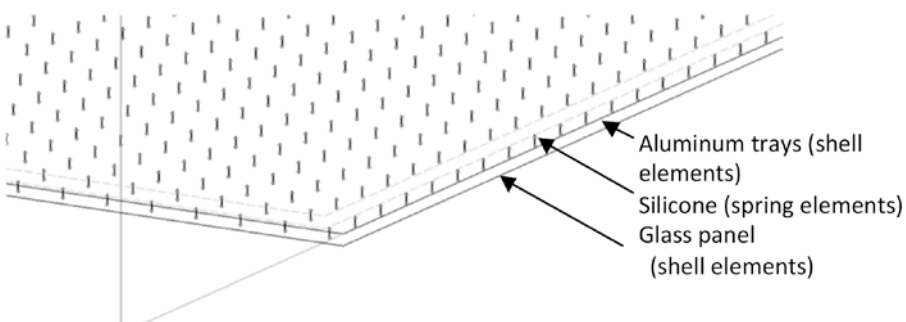


Figure 4 Principal of finite element model of composite panel to verify global structural performance

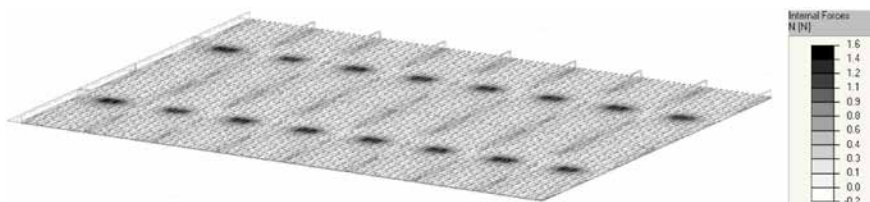


Figure 5 Internal load concentration in silicone spring elements in support area (example).

|   |                   | MPa   | Corresponding thickness of the silicone layer |
|---|-------------------|-------|---|
| Design value for short term tensile loading | $\sigma_{des}$    | 0.060 | approx. 6mm                                   |
| Design value for permanent tensile loading  | $\sigma_{\infty}$ | 0.006 | approx. 6mm                                   |
| Tensile Modulus at 12.5% elongation         | E                 | 2.40  | approx. 6mm                                   |
| Design value for short term shear loading   | $\tau_{des}$      | 0.030 | approx. 6mm                                   |
| Design value for permanent shear loading    | $\tau_{\infty}$   | 0.003 | approx. 6mm                                   |
| Shear modulus at 12.5% movement             | G                 | 0.30  | approx. 6mm                                   |

Table 1 Recommended design values for Sikasil® GS-687 for laminar bonding applications

The spring forces are converted to stresses using the area substituted by a spring element. As apparent in Figure 5 the stresses in the silicone are not evenly distributed due to the varying stiffness of the backing elements. The verification concept accounts for the interaction of normal and shear stresses for short- and long-term loading. This approach allows for a detailed structural check of all components against dead, wind, seismic, temperature and maintenance loadings. More details on the structural assessment and design limitations can be found in [5].

### Fabrication methods

The amount of backing panels provides the quantity of fixing points as every backing panel is required to transfer loadings back to the supporting structure in case of glass breakage. The fabrication process must allow for the positioning of the individual fixing points to tight tolerances. The maximum deviation of any point in the surface, measured from defined reference points was agreed to be within +/- 2 mm.

First concepts were trying to connect the panels via its folds to the supporting structure. Fabrication trials showed this approach to be hard to control. The selected design works on the basis of a connection pin, located in an adapter profile. The adapter profile is mechanically fixed to the aluminum tray. Using bespoke lifting frames, each holding a row of panels spanning over the short length of the glass it is possible to control the fixing point position within the required tolerances (Figure 7). Rotations of the aluminum panel do not influence the accuracy of the fixing point position.

The lifting frames require fabrication to tolerances smaller  $\pm 2\text{mm}$  as all equipment and fabrication tolerances will sum up and eventually exceed the agreed tolerances. For the lifting and positioning frames fabrication tolerances below 1mm, measured from its setting out points are required. The frames are equipped with adapters tying into the actual connection bolts and with pressure elements pressing the panels into the silicone bed to ensure a defined distance between outer glass surface and connection bolt (Figure 8). The distance between glass and aluminum is maintained using silicone

spacers, cast from the same silicone material used for the laminar application.

Whilst the lifting frame provides exact positioning for a row of panels, tolerances between adjacent frames require consideration as well. To ensure two neighboring frames are positioned within the agreed tolerances, processing tables are required (Figure 9). These tables are equipped with perimeter profiles receiving connector elements (Figure 10). These connector elements can be positioned along the machine bed within a 1/10 mm. Following positioning of the



Figure 7: Bespoke lifting frames, without (left) and populated with panels (right)



Figure 8: Image adapter elements for the connection bolts (left) and pressure elements (right)

adjustable connectors using a high precision measurement equipment the elements have been grout locked in position to eliminate the risk of position errors during mass production. The tables allow for exact positioning of the glass units, using setting out references. As glass in the sizes used for the process in itself is tolerance afflicted, a setting out edge has been agreed on. All glass tolerances have been pushed to defined joints. A flexible edge evacuation was designed, able to account for glass tolerances, minimizing any follow up works.

A bespoke silicone pump, designed for the processing of the laminar silicone was travelling along tracks to serve 16 processing tables (Figure 11). Following machine cleaning and positioning of the glass on the tables, the pump would apply the required amount of silicone. Once an area big enough for a positioning frame is applied, 2 operatives would place a frame on the machine bed and clamp it in position (Figure 12). This process was repeated till the glass was fully clad. To reduce cycle time for the lifts, 5 lifting frames

were combined to a process lift. The individual frames were connected with the same fast connectors used to secure the elements on the table. Once finished the composite panel was allowed to rest for 24 hours prior repositioning to allow the fabrication of a new unit. The described fabrication equipment allowed for an accurate positioning of the components within the allowable silicone processing time of 20 minutes. It was possible to successfully fabricate 1750 façade units in sizes 10-15 m x 3 m on the described fabrication line with prototype character.



Figure 9: Processing table



Figure 10: Adapter elements



Figure 11: Silicone pump



Figure 12: Lifting frames in service

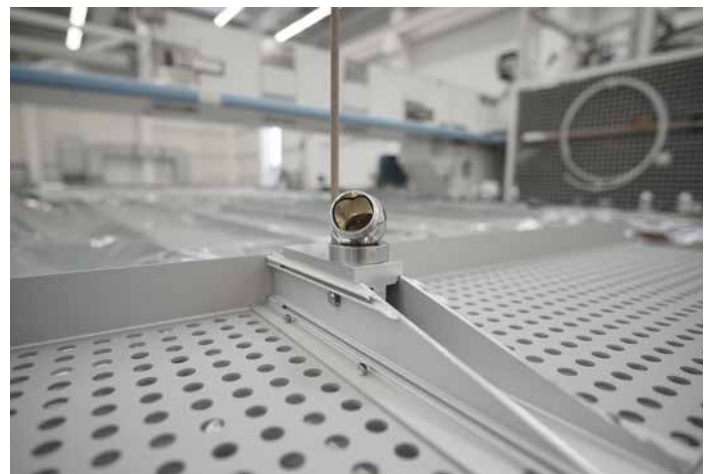
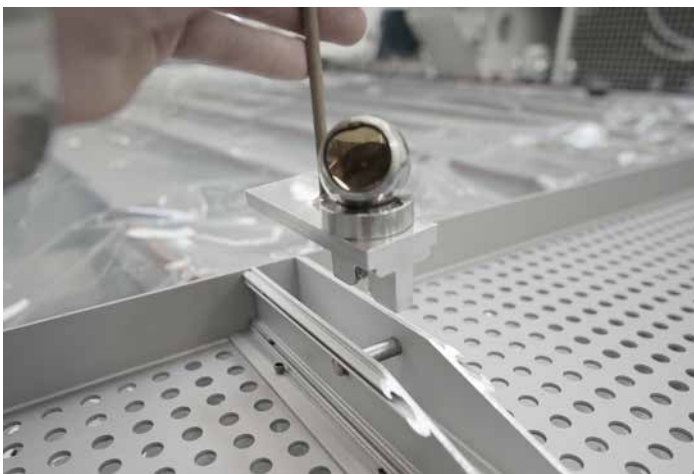


Figure 13: Check-measurement using custom targets

## Quality Assurance / Quality Control

Fabrication on large scale when utilizing new methods and materials needs a strict quality assurance and control system. To mitigate human error all manual cleaning processes have been replaced by automated approaches. The glass was machine washed, the aluminum panels were delivered packed from the anodizing plant and plasma treated prior processing.

All system relevant parameters (e.g. surface treatment method, adhesion, mechanical strength) are trialed and tested prior implementation into the process and checked in parallel to fabrication to ensure consistent quality.

Dimensional control is carried out on the composite element on the processing tables, measuring the actual bolt locations to identify deviations.

## Summary

The fabrication process for a composite glass panel has been described in detail. Key aspects considered in the development process were outlined. It has been shown that it is possible to develop and implement new technologies and methods on a project basis. When approaching new technologies an open mindset for all parties involved is paramount.

## References

- (1) EOTA ETAG 002-1, Structural Sealant Glazing Systems Part 1. 2012.
- (2) ASTM C 1184-13, Standard Specification for Structural Silicone Sealants. 2013.
- (3) ASTM C 920-11, Standard Specification for Elastomeric Joint Sealants. 2011.
- (4) ASTM C 1401-09a, Standard Guide for Structural Sealant Glazing. 2009.
- (5) Doebbel, F.; Müller, U.; Teich, M.; Marinitsch, S.: Nobel laminar silicone application. In: Challenging Glass 4 & COST Action TU0905 Final Conference. Lausanne, 2014, pp 347-352.

# Face and Surface – Glass-Sandwich-Facades, the all-in-one Solution

Dipl.-Ing. Hans Frey, iconic skin GmbH,  
Gersthofen, DE

Dr.-Ing. Martien Teich, iconic skin GmbH,  
Gersthofen, DE

## Abstract

Architecture is the creation of space, which is (typically) defined and expressed by walls. Walls separate inside and outside. Openings in the walls expose and express their structural depth, which has been a major design feature in the evolution of facade design. New materials and technology have ever been used for shaping a building's face, defining its appearance as the walls do with space. Glass-Sandwich-Facades are not conceived with new materials but are a new and innovative combination of proven components and technology – glass, structural adhesive, sandwich panels and window systems. This is a precise response to the ever more challenging boundary conditions of today's construction market.

## Keywords

1=Glass Sandwich Panel, 2=GSP®, 3=Glass Sandwich Façade, 4=warm façade

## 1 Introduction

### 1.1 Evolution of the wall

The theoretical and philosophical debate about shape, space and surface currently seems more intense than in recent years as the vanishing period of free-form extravaganza has led (and apparently mis-led many) to a sheer limitless vocabulary supported by new design and fabrication technologies. It's a kind of back to the roots movement, remembering the basic values of architecture and regaining the status of process owner in the design delivery. Architecture is the creation of space, which is (typically) defined and expressed by walls. Walls separate inside and outside. Walls have always been a defining element, including or excluding. With great thickness if fortified or for structural reasons a wall can develop an inner life, incorporate (subtractive) space. In the German language there are even two distinct phrases for a wall – Wand (from weaving) and Mauer (from masonry). Openings within the opaque walls, expressing the structural depth, have always been a key

design feature, connecting spaces, public and private, inside and outside. New materials and technology have ever been used for shaping a building's face, defining its appearance as the walls do with space. Gottfried Semper is only one of the many sources to be mentioned here, that theoretically and practically dealt with a wall's many different properties. A façade is a special wall, distinct from inner partitions by its special two and three dimensional treatment that provides for an expression radiating beyond its boundaries.

With the triumph of steel and glass the wall depth and amount of materials involved was reduced to a minimum, leaving such theories behind like Dom Hans van der Laan's 'Seven relationships of architectonic space', that defined a wall's thickness as a kind of DNA for a building [1]. The individual expression stood back for an aesthetic dominated by industrial products. No more technology leading to architecture, as Perret envisioned it. In a video tour of his 2014 Venice Architecture Biennale with the Guardian Rem Koolhaas complained about architecture having become a fiction. What is left to the architects would be only the remnant of a real wall, a thin screen in front of all the services pointing out at an exhibit "this is us and that is them" [2].

### 1.2 Designing with industrial products

In the early 1990s in response to the sheer unmanageable supply of industrial building products that focused on technology and market but not their design potential a studio for Constructive Design was established at the ETH Zurich by Hans Kollhoff. Its goal was to explore design options with industrial products in an experimental approach. For Kollhoff it was not about finding the right construction, that does not exist, but the interrelationship of architectural intent and constructive solution. Archithese, the Swiss journal, dedicated its May 1993 issue with the title 'ready-made. Designing with Industrial products' to that challenge [3]. It was about fighting the loss of architectural expression with the rise of technical perfection. As a main problem the distance between the building industry and the architectural world was identified. The Constructive Design studio's first highly influential designs, a series of experimental pavilions, ultimately resulted in a focus on the façade's surface, corners, openings and joints. The conclusion was that industrial

products were semi-finished components that are not ready for an instant application. In Kollhoff's view it is important that building products are not simply made for an individual styling but that develop their quality in an architectural application. Per Swiss architect Erwin Mühlenstein working with industrial or standard products will never create a short lived trend as designing and building with them requires a certain intellectual discipline and adaptation of the architectural expression to the respective technology [4].

### 1.3 Today's construction environment

From bid to building a design has to sustain many influences in the course of multiple developmental stages. Budgets are tighter than ever, thus decision making is delayed and bid processes are likewise lengthy and often involve several rounds. Too often building envelopes are the first target of a value engineering processes and this applies not only to challenging projects including innovations and exceptional design or construction elements. For a successful delivery of projects it has become paramount to look beyond scope boundaries and to consider market and feasibility at the very early design stage [5]. Once a design has finally evolved other challenges such as quality issues caused by price and time pressure as well as unskilled workforce must be coped with. That are all aspects that also a highly digitalised delivery process so many have become dependent on cannot resolve. As a consequence of that situation and based on more than 30 years of experience with the most challenging building envelopes and structures, iconic skin GmbH, which is part of the seele group, has developed a building product that helps overcome these issues - the Glass Sandwich Panel GSP®.

## 2 Status Quo of GSP® and the Glass-Sandwich-Façade GSF

### 2.1 GSP® Conception

The GSP® development was not about reinventing the wheel but it is a new and innovative combination of proven components and technology – glass, structural adhesive and sandwich panels [6].



Figure 2-1: Glass-Sandwich-Panel GSP® – Build-up (for vertical application)

6mm HS glass panels with full ceramic print are structurally bonded to lightweight and easy to handle sandwich panels. The bonding is carried out with strips of adhesive. Elements can be produced as long as 16,0m, with a width of up to 1,50m. The sandwich panel is the load bearing component and provides for impermeability as well as the excellent thermal and acoustical properties. However, the tremendous design potential lies within the glass panel with its perfect surface that provides for much more metaphysical depth than its physical 6mm thickness.

The unit can be fixed to frameworks or solid walls, the latter e.g. for renovations or upgrades. Because of the glass panel's opacity no bonding or other means of fixing are visible as the screws are concealed within the joints (Figure 2-2). If aesthetically or functionally required, the GSP® panels receive on their backside facing the interior a drywall system. In front of a solid wall the cavity between the two components is warm, as it is closed at the upper and lower perimeter with a permeable insulation.

### 2.2 Glass-Sandwich-Façade GSF

In combination with window systems GSP® becomes the Glass-Sandwich-Façade (Figure 2-3). As a warm system it provides for a near seamless and dry transition between the two main components, omitting problematic interfaces or connections requiring attention and maintenance throughout their life-span. The window profiles are fixed to GSP® with system compatible transfer profiles, which also take the loads of the windows (Figure 2-4). That principle allows for new applications as a secondary back-up structure is typically not necessary. In horizontal applications windows can span the full length of a panel. [7] Unlike a cold façade system that involves many layers and interfaces that need to be well coordinated from design to completion, the Glass-Sandwich-Façade is basically one element and layer that can be easily managed during design, bidding, fabrication and installation. With all components being pre-fabricated high levels of precision and quality are achieved and thus errors during the efficient installation period on site can be prevented. The easy handling throughout the whole delivery process is only one of the many



Figure 2-3: Glass-Sandwich-Façade GSF – GSP® merges with openings

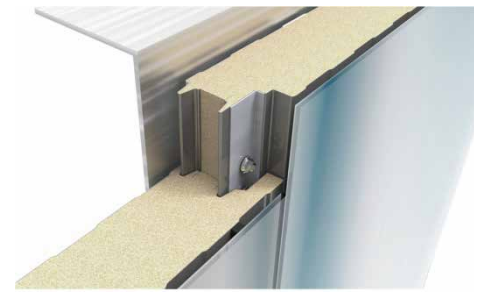


Figure 2-2: Glass-Sandwich-Panel GSP® – vertical fixation

sustainable and commercial advantages that continue beyond the completion date. The glass panels of GSP® can be e.g. exchanged in situ, without opening the building's physical barrier. And at the end of the life cycle GSP® can be more or less completely recycled. Whether a client looks for cost conscious aesthetics, the designers for aesthetics and individuality, a system processor or building operator look for a hassle free product – they all will find their objectives met with a Glass-Sandwich-Façade.

### 2.3 Configurations

GSP® panels are applied in either vertical or horizontal direction, creating a basic linear joint system. The joints can vary per floor or express the full building height. No other high-end cladding panel is available in that length. Adaptations and creation of movement can be achieved via the following design options that were initially presented at the BAU 2017 in Munich this year:

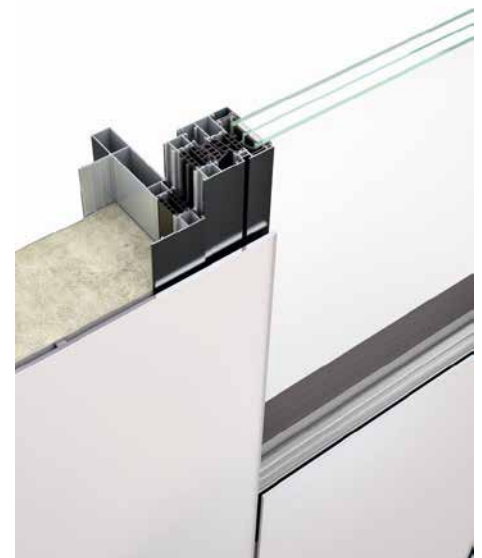


Figure 2-4: Glass-Sandwich-Façade GSF – Transition (HUECK Trigon GSP®)

- 2D Print GSP®
- 2D Pattern GSP®
- 2D Light GSP® lumen
- 3D Embrasure GSP®
- 3D Shingles GSP®multilam
- 3D Rotation GSP®
- 3D Material switch GSP®

The prime design feature is the glass panels' individualisation via ceramic printing – digitally, by roller or screen print. Or in a combination of them e.g. if signage or special imagery are desired. The advanced technology creates long lasting and colour-fast treatment that makes the product look the same all throughout the life cycle. Later changes or add-ons will match the other panels. A recent completion of a commercial project in Dortmund, Germany, involved a special dynamic design called 'Dortmund Crossing' conceived by artist Joerg Maxzin (Figure 2-5). 60 GSP® panels received illusory images with digital printing. Another 150 GSP® panels completing the curved glass ribbon surrounding the volume on the ground floor level were screen printed. A standard product became a case specific and identity creating application solely by treating the glass surface on one side.



Figure 2-5: Installation of 'Dortmund Crossing'

### 3 Summary

The presented product development is a precise response to the ever more challenging boundary conditions of today's construction market, budget conscious without compromising aesthetics. It shows that glass remains also in an opaque application an important enclosure material. GSP® is an all-in-one product with an easy to individualise surface that with or without plug-ins provides for a multitude of architectural expressions. It shows that industrial building products do not necessarily limit design options, but rather open a whole range of new opportunities if their basic properties are understood and reflected in the design concept from the beginning.

### 4 Literature

- [1] Van den Bergh, W.: Wand und Raum. In: der architekt, Düsseldorf: Bund Deutscher Architekten, 2016 [04], 35-40
- [2] Wainwright, O., Levene, D.: <https://www.theguardian.com/artanddesign/video/2014/jun/06/rem-koolhaas-fundamentals-venice-architecture-biennale-video>
- [3] Kollhoff, H., Baumann, D.: Experimentelles Entwerfen mit Industriebauprodukten. In: archithese 5.93, Zürich: archithese 1993, 46-47
- [4] Maurer, B.: Eternitgerecht Bauen. In: archithese 5.93, Zürich: archithese 1993, 24
- [5] Frey, H.: From bid to building. In: Glasbau 2016, Weller B., Tasche S. (eds.), Berlin: Ernst & Sohn, 2016, 33-45.
- [6] Teich, M., Mertel, H.: iconic skin glass sandwich panel. In: gpd proceedings book 2015, 13-15
- [7] Teich, M., Radner, W.: Glass Sandwich Facade – development of a new façade typology. In: Glasbau 2017, Weller B., Tasche S. (eds.), Berlin: Ernst & Sohn, 2017

# Vacuum Insulating Glass – Past, Present and Prognosis

Richard Collins  
University of Sydney

## Abstract

This paper reviews the history and current status of Vacuum Insulating Glass (VIG), and discusses future possibilities for this technology.

## Keywords

Vacuum insulating glass, vacuum glazing, thermal insulation

## General description of Vacuum Insulating Glass

Vacuum Insulating Glass (VIG), illustrated in Figure 1, is simply conventional insulating glazing (IG) with an evacuated space between the two glass sheets [1, 2, 3]. (Note: Due to space limitations, most of the references in this paper are to review papers, which contain source references.) VIG achieves high levels of thermal insulation using the same principles as the Dewar flask – the vacuum eliminates heat transfer between the two glass sheets due to gaseous conduction and convection, and radiative heat transfer is reduced to a low level by one or two internal transparent low emittance coatings.

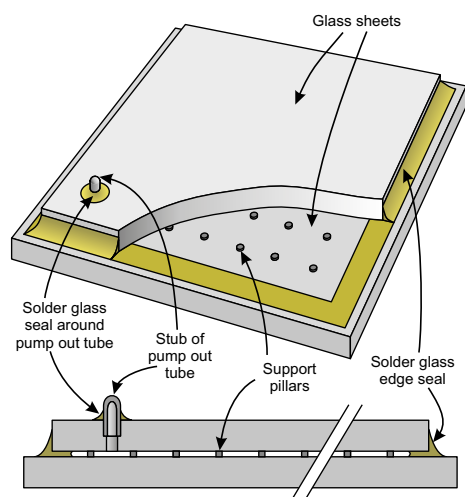


Figure 1 Schematic diagram of VIG

Highly insulating VIG must incorporate several features, including:

- A hermetic (leak free) seal around the edges of the two glass sheets;
- A high and stable thermally insulating internal vacuum (pressure below  $\sim 10^6$  atmosphere);
- An array of support pillars to maintain the separation of the glass sheets under the large forces due to atmospheric pressure (10 tonnes/m<sup>2</sup>);
- An internal transparent low emittance coating to reduce radiative heat flow to a low level; and
- An acceptable design compromise between the heat flow through the pillars and the mechanical stresses in the glass sheets near the pillars due to atmospheric pressure.

The VIG concept offers several significant attractive possibilities:

- Very high levels of thermal insulation can be achieved, in principle;
- The vacuum space is very thin, so the overall thickness of the structure is only slightly greater than the combined thickness of the two glass sheets;
- VIG should exhibit negligible degradation in the field due to gas permeation through the hermetic edge seal. VIG therefore has the potential to achieve very high reliability in practical installations.

## History

### 1913 - 1988

The concept of VIG was first described in a 1913 German patent by Zoller [4] only 20 years after the invention of the Dewar flask. This patent claims structures with multiple glass sheets, and internal supports consisting of "ribs, grooves, prisms, projections on the glass sheets, spheres or blocks made of thermally insulating material, and line supports crossing at an angle".

During the following 75 years, many attempts were made to develop this concept, virtually all of which were published only in the patent literature [3]. The claims in these patents relate to many aspects of the design and manufacture of VIG, including:

- Support pillars of many different designs and materials;
- Pillar arrays of various geometries;
- Flexible and rigid edge seals made with

solder glass and metal;

- Edge seals made by direct fusion of the two glass sheets;
- Ports and tubes for evacuating the internal volume;
- In-vacuum sealing of the edges;
- Contoured glass sheets;
- VIGs with multiple glass sheets; and
- VIGs with internal low emittance coatings.

### 1988 - 1994

Despite this extensive work over many decades, the first practical thermally insulating sample of VIG was not made until 1989 [5]. This was achieved in work that followed on from a 1988 Senior undergraduate project by Stephen Robinson, supervised by the author, at the University of Sydney School of Physics.

These first experimental samples were made using two heating steps, as shown in Figure 2. In the first step, a rigid edge seal was formed between the glass sheets by melting solder glass at a temperature above  $\sim 450^\circ\text{C}$ . During this step, solder glass was also melted to form the support pillars, and to seal a small, in-plane pump out tube to the edges of the glass sheets. After cooling, the sample was suspended from the pump out tube and evacuated. The internal surfaces of the sample were then outgassed during the second heating step at a much lower temperature. After cooling to room temperature, the pump out tube was melted and sealed. The existence of a thermally insulating vacuum was demonstrated using a rudimentary guarded hot plate apparatus [3, 5].

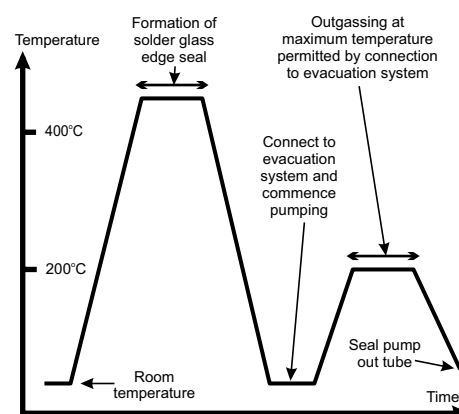


Figure 2 Two step manufacturing procedure for VIG

This achievement stimulated an extensive research and development program on VIG at the University of Sydney, involving several staff members and many students. During this program, which continues to this day, over 1000 laboratory VIG samples up to 1 m x 1 m in size were made, with centre-of-glazing U-values as low as 0.8 W m<sup>-2</sup> K<sup>-1</sup>. The innovations in VIG science and technology developed in this program were reported in many papers and patents.

New developments in production technology during this period include:

- Metal pillars, including designs that automatically orient correctly when placed on the glass sheet;
- A stepped edge around the periphery of the sample for deposition of the solder glass (Figure 1);
- A procedure for evacuating and sealing the sample using a cup that is sealed with an O-ring to the surface of one glass sheet around a pump out tube ([2] and Figure 3).

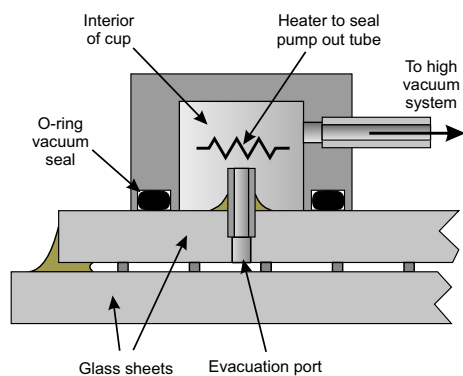


Figure 3 O-ring sealed evacuation cup

Achievements in VIG design and modelling over the whole research program include:

- Determination of the nature and magnitude of the stresses in the glass sheets due to atmospheric pressure and temperature differences, and experimental validation of these data [1, 2, 3 and 6];
- Development and validation of methods for calculating the heat flow through the VIG due to thermal conduction through the support pillars, gas conduction, radiation and edge effects [1, 2];
- A procedure for designing the pillar array that quantifies the tradeoffs between heat flow through the pillars and the stresses in the glass sheets near the pillars due to atmospheric pressure [2]; and
- Demonstration that the time necessary to evacuate the internal volume of a VIG through a small pump out tube or aperture need not be a limiting factor in the production process [2].

The program also developed several innovative measurement methods including:

- A small area (~1 cm<sup>2</sup>) guarded hot plate (GHP) apparatus for making accurate and absolute room temperature measurements of the separate heat flows due to the different relevant processes [7];
- Confirmation of the GHP data by measurements on large area samples at other laboratories [2].
- A method for measuring the overall thermal conductance of samples at elevated temperatures [2];
- Direct, non-perturbing measurement of the internal pressure in experimental VIG samples [8];
- Measurement of the outgassing rates of relevant gas species [8]; and
- Long term and accelerated ageing measurements that identified the physical processes and gas species that can cause vacuum degradation, and enabled vacuum degradation rates to be related to manufacturing procedures [8];

The program also included significant fundamental science:

- Measurement of extremely slow rates of the growth of cracks in glass under relatively low stresses, leading to the confirmation of the existence of a sub-critical limit of such growth [9];
- Extension of glass failure models to account for the sub-critical limit of crack growth [10]; and
- Development and validation of methods of calculating radiative heat flow between surfaces that incorporate the dependency of emittance on angle and wavelength [11].

From its inception, the University of Sydney took the view that it did not have the capability or resources to commercialise VIG, either in-house, or by a spin-off entity. The University's VIG research program therefore sought to understand the relevant science and technology, and to develop production-compatible designs and fabrication processes that would be useful to a potential commercial partner. The University also sought patent protection for relevant innovative concepts [3]. Finding a commercial partner proved to be very challenging, for many reasons. It was not known whether several of the necessary procedures for making highly insulating VIG could be realised in a production environment. In addition, because the VIG concept had been the subject of several previous unsuccessful development attempts, many thought that this new approach was also unlikely to succeed. Equally importantly, it was clear that commercial VIG technology would be expensive to develop, and that a manufacturing plant would require significant capital investment. Put simply, commercialisation of VIG appeared to be a high cost and high risk enterprise.

## 1994 to 2000

The first serious industry interest in the University of Sydney's VIG technology occurred in 1993 from Nippon Sheet Glass Group (NSG) in Japan. Around that time, Hideo Kawahara, Director of NSG Architectural Glass R&D Division, was considering the development of thin, moderately insulating glazings for the Japanese retrofit market. The VIG concept was directly relevant to that initiative. In 1994, the University and NSG entered into licensing and collaborative research agreements with the aim of developing a commercial VIG product. This commercial VIG development occurred at a time when the University's understanding of many of the relevant technical issues was quite incomplete. Several critical decisions relating to the design and method of manufacture of the product were therefore made on the basis of very limited information. Important matters in this category included the dimensions of the pillar array, particularly the pillar separation, and the level of bakeout required to achieve a stable internal vacuum. The decision to develop a batch manufacturing process, rather than a continuous one, was made because it provided more flexibility to implement any changes needed as a result of these uncertainties. After an intensive period of technology transfer and collaborative work, NSG built a pilot VIG production line at its Kyoto manufacturing plant. Most of the post-assembly part of the initial manufacturing process was modelled on the laboratory procedures developed at the University. The process involved two separate heating steps (Figure 2), and the samples were evacuated and sealed utilising a cup that was sealed around the pump out tube with an O-ring (Figure 3). The process also incorporated sophisticated glass handling techniques, and an innovative pillar placement technology that was specially developed by NSG for this application. The first commercial VIG product, Spacia, was launched by NSG in 1996. This was immediately followed by an expansion of the capability of the Kyoto production line. Shortly afterwards, NSG established a second, purpose-built VIG manufacturing plant at Ryuugasaki, near Tokyo. Over the following few years, the design of the NSG product and its method of manufacture evolved significantly. Some of the changes were made to improve the yield of the manufacturing process, as normally occurs in the early stages of any new production technology. Some changes were major, and were a direct consequence of the earlier limited understanding of important technical issues. At one stage, the entire post-assembly part of the production process was redesigned and rebuilt, reducing the number of heating steps in the process from two to one (Figure 4).

This became possible through the development of a method for making a high temperature vacuum seal around the pump out tube using a demountable all-metal evacuation cup ([12] and Figure 5). Although very costly and time consuming, these changes greatly improved the viability of the technology by halving the post-assembly manufacturing time and significantly simplifying the manufacturing process.

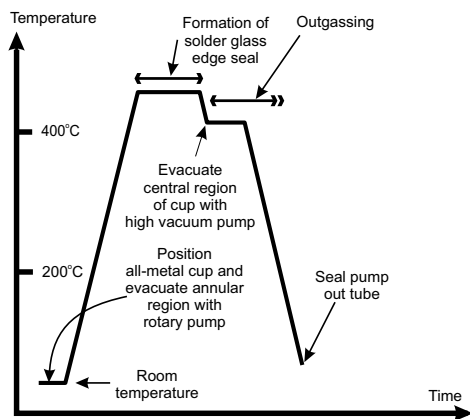


Figure 4 Single step manufacturing process

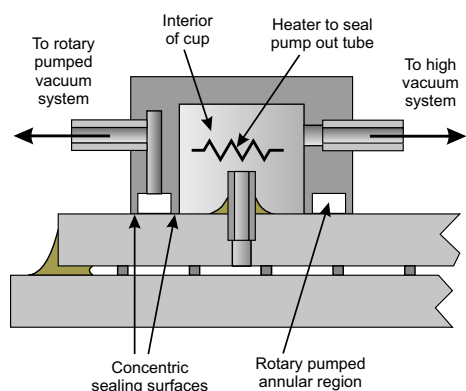


Figure 5 All-metal evacuation cup

A feature of this commercial development was the effectiveness of the interactions between NSG and the University. Both parties in the collaboration were completely open to each other about the information that was generated and the issues that needed to be addressed. The University's research program continued to provide new information of relevance to the product development at NSG. Much of the University's work was stimulated by issues that emerged from the production process. For its part, NSG was unshakable in its resolve to make the project succeed, even when significant technical challenges arose that required major changes in production processes. In hindsight, the decision by NSG to commercialise a VIG product must be regarded as very courageous. NSG committed to this goal at a time when many other companies

took the view that commercial development of the VIG concept was too risky and costly. As it turned out, the costs involved were much larger than originally anticipated, and the technological challenges were also much greater. Despite concerns about the viability on this enterprise, NSG chose to work these issues through, and over time this technology has become one of the company's premium products.

The demonstration of the technical and commercial feasibility of VIG stimulated several other organisations to commence work on VIG, leading to many publications and patents.

### 2001 to present

The past 16 years have been a period of consolidation of VIG technology. Several million VIG units have been manufactured by NSG, and have shown excellent reliability in many types of building. Several major research studies have been undertaken at other academic institutions, in government laboratories and by other companies. VIG products made by other manufacturers are in the market or under development. There has been extensive relevant publication and patenting. Current commercially available VIGs using annealed glass can have centre-of-glazing U-values as low as  $0.6 \text{ W m}^{-2} \text{ K}^{-1}$  in a structure 10 mm thick. VIGs are also being used in hybrid glazings and laminated assemblies. The International Standards Organisation (ISO) is developing Standards for this technology. This work is being undertaken by Working Group 10 (Glass in building – Product considerations – Vacuum glass) of ISO Technical Committee 160, Sub-committee 1. Part 1 of a draft Standard for measurement of the thermal insulating properties of VIG is in the process of ratification. Work has commenced on Part 2 relating to temperature-induced effects in VIG.

### Future prospects

Although VIG is now a well established technology, there is considerable scope for further development on many aspects of its design, manufacture and marketing. Several of these are listed below. Those currently under active development or consideration are indicated by an asterisk (\*).

#### Design

- VIG made with tempered glass\* offers the prospect of higher levels of thermal insulation, and broader areas of application. A major challenge for this design approach is the development of a relatively low temperature edge seal. Departures from planarity of the tempered glass sheets need to be accommodated

so that the mechanical load due to atmospheric pressure is uniformly distributed over the pillars.

- Performance improvements are also likely with innovative pillar designs, including pillars made from thermally insulating materials\*, high strength materials\*, and by melting small areas on the glass sheets\*. Pillars are under development with low friction bearing surfaces\*, and different geometries\*, that facilitate a small amount of relative lateral movement of the glass sheets.
- It is likely that the pillar separation in current VIGs with annealed glass can be increased\*, resulting in improved thermal insulation,
- VIGs with a flexible edge seal\* would experience very low stresses and bending under temperature differentials. However, in such designs the pillars must slide repetitively across the glass. Because of the high stresses in the glass sheets near the pillars, the author considers it unlikely that this type of edge seal will prove viable.

#### Production technology

- There are many alternative possibilities for making the edge seal, including low temperature solder glass\*, lead free solder glass\*, and metal\*. All currently available polymer materials are far too permeable for this application. In the author's opinion, this is unlikely to change.
- There are also many different design possibilities for the evacuation port of the device\*.
- VIG production technology is sufficiently well understood that a continuous manufacturing process can now be implemented\*. Although relatively capital intensive, such an approach would enable larger numbers of VIGs to be made, and this could result in significant cost reductions in the product.
- In principle, it is possible to form the edge seal in the VIG within a highly evacuated space, eliminating the need for a pump out port. Challenges in this approach include bubbling of the molten solder glass, vacuum degradation due to outgassing of the hot internal surfaces after sealing, and avoiding bending of the glass sheets in the edge region.

### Conclusion

The history of VIG is quite unusual for a technological development. There was an extraordinarily long period (75 years) between the initial patent describing the concept and its first realisation in the laboratory. This was followed by a relatively short period

(8 years) of research, development and technology transfer, leading to the launch of the first commercial VIG product. Over the subsequent 20 years, the development of the technology has continued, although most currently available products have much in common with early commercial designs. In addition, although sales of VIG have steadily increased and the product has exhibited high reliability in practical installations, only a few manufacturers are currently active in the field. NSG is in the process of completing a significant expansion of its VIG manufacturing capability. In addition, there is currently a high level of interest in the technology, both at the research level, and in product development programs by other manufacturers. It is therefore not unreasonable to expect that the next few years will see more manufacturers entering the VIG market, and substantially increased sales volumes. Should this occur, new and possibly better performing VIG products made using different processes will become available, and the cost of VIG will decrease.

The capital investment for a VIG manufacturing facility will always be greater than for a conventional IG plant of comparable capacity. The unit area cost of VIG is therefore always likely to be greater than for conventional IG. In large volume manufacture, however, materials cost should dominate, and the cost differential between the two technologies need not necessarily be large. The capability of VIG to achieve high levels of thermal insulation, the high reliability afforded by the hermetic edge seal, and the very small thickness of the structure, are likely to make VIG technology an increasingly attractive choice in the market for high performance thermally insulating glazing.

## Acknowledgments

VIG would not exist as it is today without the many contributions by the author's students at the University of Sydney, and his colleagues in the University's School of Physics, at NSG, and in other research laboratories. The author dedicates this paper to Stephen Robinson, whose student project led to the first practical VIG samples, and Hideo Kawahara, whose vision, dedication and tenacity enabled this technology to be commercialised successfully. Sadly, neither is alive today to reflect on the significance of their achievements.

## References

1. R E Collins, A C Fischer-Cripps and J-Z Tang, *Solar Energy* 49, 333-50 (1992)
2. R E Collins et al., *Building and Environment* 30, 459-92 (1995)
3. R E Collins and T M Simko, *Solar Energy* 62, 189-213 (1998)
4. A Zoller, German Patent No. 387655 (1913)

5. S J Robinson and R E Collins, ISES World Congress, Int. Solar Energy Soc., Kobe, Japan (1989)
6. T M Simko, A C Fischer-Cripps and R E Collins, *Solar Energy* 63, 1-21 (1988)
7. C J Dey et al., *Rev. Sci. Instr.* 69, 39-2947 (1998)
8. N Ng, R E Collins and C So, *J. Vac. Sci. Tech. A* 21, 1776-83 (2003)
9. C Kocer and R E Collins, *J. Amer. Ceram. Soc.* 84, 2585-93 (2001)
10. A C Fischer-Cripps and R E Collins, *Building and Environment* 30, 29-40 (1995)
11. Q-C Zhang et al., *Int. J. Heat Mass Transfer* 40, 61-71 (1997)
12. N Ng, R E Collins and M Lenzen, *J. Vac. Sci. Technol. A* 20, 1384-9 (2002)

# A Novel Glass Spacer for Vacuum Insulated Glazing

Dr Cenk Kocer  
University of Sydney, School of Physics, Sydney  
NSW Australia 2006

## Keywords

1 = Thermal insulation, 2 = Spacer, 3 = Vacuum insulated glazing

## Abstract

The vacuum insulating glazing (VIG) is a highly thermally insulating window technology that is thin in profile and light weight. It consists of two panes of glass separated by a sub-millimetre vacuum gap, with an array of high strength spacers located in the gap to prevent the glass panes from collapsing under atmospheric pressure. It is well-known that the VIG has the potential to reach thermal conductance levels as low as  $0.4 \text{ W m}^{-2} \text{ K}^{-1}$ .

A crucial part of the VIG which greatly impacts potential thermal performance and underpins ultimate mechanical strength are the spacers. The choice of spacer also greatly affects the production process, cost and the appearance of the VIG product. In this work a novel glass spacer is discussed, with the thermal and mechanical performance of the spacer outlined.

## Introduction

The conventional method of reducing heat loss through a single pane window has been to use an insulating window technology, such as double glazed, gas filled, windows where a standard configuration results in a thermal conductance between the inside and outside air of about  $1.5$  to  $2 \text{ W m}^{-2} \text{ K}^{-1}$  [1]. A unique alternative technology is the Vacuum Insulated Glazing (VIG). The glazing consists of two panes of glass separated by an evacuated gap, with an array of high strength spacers in the gap used to maintain separation between the glass panes under the action of atmospheric pressure. The first successful fabrication of a VIG unit was reported by the Collins group at the University of Sydney (USYD) [2-6]; Figure 1 is a schematic illustration of the USYD design; in this design as-received soda-lime glass panes, where one or both the panes are coated with a low emittance coating, are used, and the array of high strength spacers are cylindrical in shape and typically  $0.5 \text{ mm}$  in diameter and  $0.2 \text{ mm}$  in height. The two glass panes are

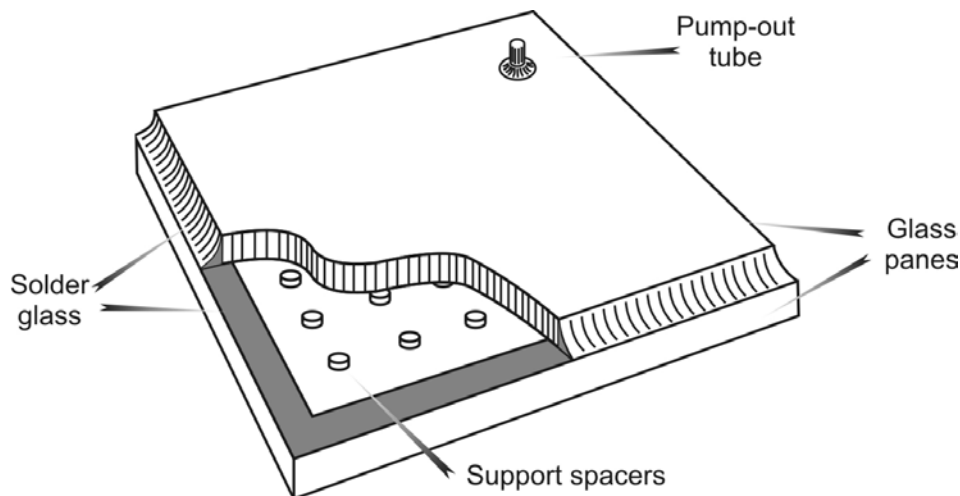


Figure 1: A schematic illustration of the vacuum insulating glazing invention from the University of Sydney.

hermetically sealed using a solder glass (glass frit) over the perimeter of the panes, and a pump-out tube on the top glass pane is used to evacuate the internal gap.

Heat flow through the VIG is due to, 1. conduction through the spacer array, 2. radiation between the internal surfaces in the vacuum gap, and 3. conduction through the solder glass edge seal; we assume the internal vacuum is low such that residual gas conductance is essentially zero. The overall heat transport for a window unit is typically given as the air-to-air heat conductance (or

U-value). To determine the U-value the heat transfer coefficient from the surfaces of the VIG to the inside and outside environments must be defined, and in this work we will use  $8.3 \text{ W m}^{-2} \text{ K}^{-1}$  and  $30 \text{ W m}^{-2} \text{ K}^{-1}$ , respectively, where the inside and outside temperatures are defined as  $+21.1 \text{ }^\circ\text{C}$  and  $-17.8 \text{ }^\circ\text{C}$ , respectively. These values are taken from the ASTM standards and were also employed in past works [5]. The detailed formulations for the different heat transfer pathways are not given here as a matter of brevity, they have been reported in detail in previous publications [2-6]. It is important to note that

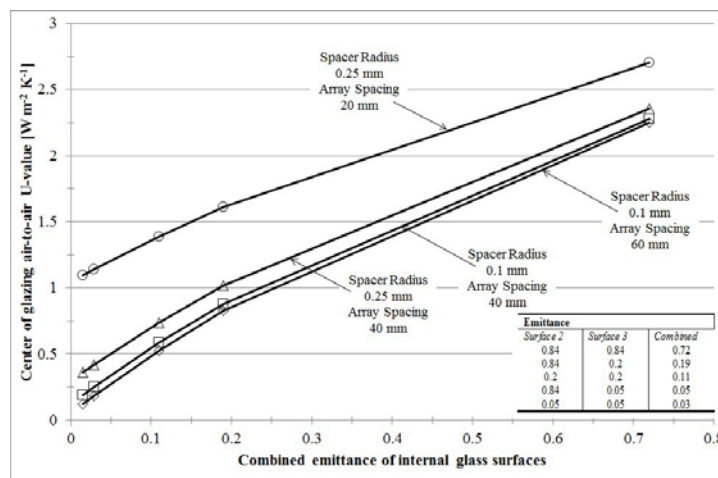


Figure 2: A plot of the VIG centre-of-glazing, air-to-air thermal conductance as a function of the combined surface emittance, for different combinations of the radius of the spacer and the spacer array separation (equivalent to the total number of spacers in the gap). The combined emittance is elucidated in inset table;  $\epsilon = 0.84$  is for soda-lime glass with no coating,  $\epsilon = 0.2$  for a conventional low emittance coating, and  $\epsilon = 0.03$  for a high performance low emittance coating [16].

the thermal conductance of VIG is not strongly dependent on the glass thickness. The thermal conductance is dominated by the surface-to-surface radiation between the glass panes and the conductance of the spacer array. Figure 2 is a plot of the VIG centre-of-glazing, air-to-air, thermal conductance as a function of the combined surface emittance, for different combinations of the radius of a spacer and the array separation (the distance between the spacers). What is particularly highlighted in figure 2 is the importance of the low emittance coating. Nevertheless, to reduce further the U-value of the VIG it is the spacer array contribution that is of most interest. Clearly, to reduce the overall VIG U-value through reductions in the spacer array, a reduction is needed in the thermal conductivity and/or the size and/or the number of spacers. For each option the critical issue is one of strength; reducing the diameter of contact produces high levels of bulk compressive stress in the spacer and high levels of surface stress in the underlying glass, and a lower number of spacers (equivalent to increasing the distance between spacers) results in higher forces on each spacer and a greater stress in the glass.

### Spacer Design Implications

The resistance to heat flow through a single spacer is related to; 1. the constrained flow that occurs because of the relative size difference between the supported glass area and the area of the spacer where this term is known as the *spreading resistance*, and only depends on the spacer size and the thermal conductivity of the glass and 2. the thermal resistance of the material of the spacer, which is determined from the length, area and thermal conductivity of the spacer material. The total resistance to spacer heat flow is then the series sum of these two terms and is expressed as,

$$R_{spacer} = \frac{1}{2k_{glass}r} + \frac{h}{k_{spacer}\pi r^2} \quad (1)$$

where  $r$  is the radius of the spacer,  $h$  is the height of the spacer,  $k_{glass}$  and  $k_{spacer}$  are the thermal conductivities of the glass and spacer, respectively [6,7,9]. Typically, for a spacer produced from a metal, such as stainless steel, the thermal spreading resistance dominates the conductance, and therefore, it is only the thermal conductivity of the glass, the radius of the spacer, and the number of spacers which determines the total contribution of the spacer thermal conductance. Figure 3 is a plot of the total contribution of the spacer array thermal conductance as a function of the spacer height, for different thermal conductivity values of the spacer material. Clearly, there is an advantage in producing spacers from materials of low

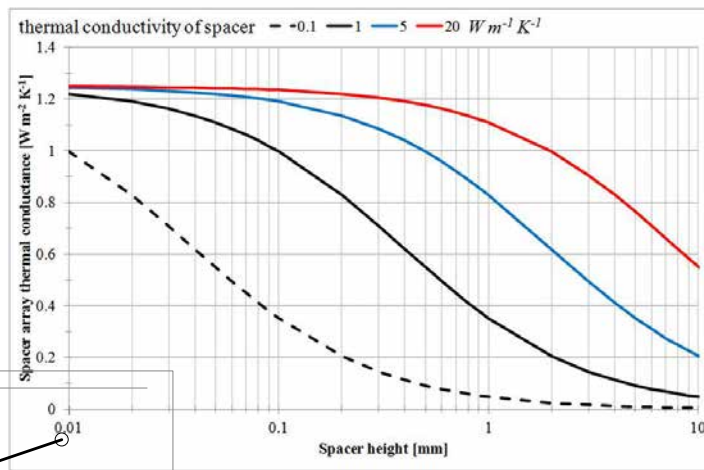


Figure 3: A plot of the total contribution of the spacer array thermal conductance as a function of the spacer height, for different thermal conductivity values of the spacer material. Here individual spacers are 0.5 mm in diameter, and the array spacing is 20 mm. The thermal conductivity of the underlying float glass is presumed to be  $1 \text{ W m}^{-2} \text{ K}^{-1}$ .

thermal conductivity, if the thermal conductivity is less than  $5 \text{ W m}^{-2} \text{ K}^{-1}$ .

As mentioned, the changes that can be made to the spacers and the spacer array dimension provide a significant impact on reducing the overall U-value of a VIG. Assuming that the edge seal of a VIG is well formed to reduce the local stresses to levels below the critical point of long term glass failure, the dominant changes of interest are directly related to the spacers; 1. compressive stress in the spacers, 2. the stress on the glass surface due to indentation of the spacers, and 3. the deformation of the glass between the spacers, which produces tensile stresses above spacers on the outside surfaces of the glass panes. Each of these stress fields is at a level that is directly related to the spacer shape, size, and distance of separation in the array. Table 1 presents the basic formulas that provide a good criterion for the potential failure of material due to these stress fields; the derivation and implications of these formulas is discussed in detail in the literature [6,9,10]. In each case it is assumed that for long term (+25 yrs) loading of the glass, the magnitude of stress should not exceed 8 MPa; this criterion of stress is taken from the ASTM standard. The allowable stress level in the case of indentation

of the spacers is not determined in the same way. The indentation process is further complicated due to the high gradients of the stress at the edge of the spacer contact [11,12]. Typically, the spacer can be produced from a stainless steel, such as type 304, which as a cylindrical spacer can exhibit a yield strength of about 1- 2 GPa.

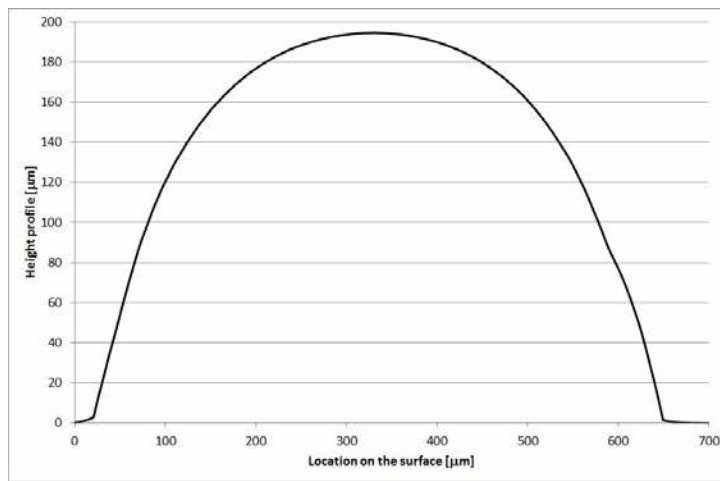
Clearly, the choice of spacer material, shape, size (height), and the spacer array design will play a significant role in defining the thermal and mechanical performance of a VIG unit. There are, however, other issues that must be considered. First, is the production of the spacer; good tolerances in size and shape must be adhered to; otherwise, localised differences in the forces and stresses may produce undesirable failures over long service lifetimes. In addition, this may impact on the visual appearance of the spacer array. Second, it is a non-trivial exercise when placing the spacers on the surface of the glass panes in manufacturing, where speed and accuracy will have significant knock on effects. If the placement process is slow the production costs will increase, and if accuracy is not well defined, as mentioned, localised differences in the forces and stresses may produce

| Basic Formulas for the allowable maximum stress before glass fracture occurs |                                  |   |
|--|----------------------------------|---|
| Compressive stress in a spacer   | Stress in glass above spacers    | Contact stress limit in glass at a spacer |
| $0.032 \frac{\lambda^2}{r^2} < 1000 - 2000$                                  | $0.11 \frac{\lambda^2}{t^2} < 8$ | $\lambda < 155r^{\frac{3}{4}}$            |

Table 1: The stress formulas for a VIG unit, where  $r$  is the spacer radius (cylindrical geometry assumed),  $\lambda$  is the array spacing, and  $t$  is the thickness of the glass sheet. Here the units are mm, MPa



(a)



(b)

Figure 4: (a) photograph, top view, of a laser spacer produced on soda-lime float glass, (b) the surface profile of the spacer.

undesirable failures over long service lifetimes, not forgetting undesirable visual effects. It is important to optimise the choice of the spacer parameters not only for VIG performance, but also the performance and reliability of the manufacturing process of the spacer and ultimately the VIG unit. In the following sections the detail of a novel spacer is presented. The spacer is not an independent component, in great contrast to traditional spacer designs; the spacer is produced on the glass surface and is a part of the glass pane. A method of laser irradiation is used to heat a local volume of the underlying glass pane. The heating process takes the glass to temperatures over 900°C for short periods, typically 1-2s. This process was invented at Corning Inc. USA [14,15]. Since the heated volume is confined by the surrounding mass of cold glass, it expands at the surface creating a surface feature that is spherical in shape. Figure 4a is an image, top view, of the surface feature produced on the glass surface. Figure 4b is a surface profile of the surface feature. This process has been demonstrated on several glass types [15], with the latest development including application of the process on as-received soda-lime float glass. In producing a surface feature on the glass surface that can be a spacer element, significant advantages can be gained in relation to several of the critical design issues mentioned above. The *laser spacer*, as it is termed in the remainder of this paper, can provide an advantage in the underlying lower thermal conductivity. It is in the following sections that the measurement of the total thermal conductance and the ultimate strength of the laser spacer are presented.

### The Thermal and Mechanical Performance of the laser spacer

As presented previously, figure 3 is a plot of the analytical solution of the total array thermal conductance for a typical cylindrical spacer. The plot highlights the advantage of increasing the height or decreasing the thermal conductivity of the spacer. Even though the laser spacer can be produced at different heights, it is the advantage of the lower thermal conductivity that is of interest. The data indicates an approximate 30% decrease in the total spacer array thermal conductance, when considering the difference between what would be a metal spacer and the laser spacer. To confirm that this is in fact the case, measurements on the laser spacers were performed. At the University of Sydney a small area guarded hot plate (GHP) was developed for measuring the thermal conductance through a single spacer [7]. Clear soda-lime float glass sheets, at a size of 350x350 mm, with an array of laser spacers were obtained from Corning Inc. USA [16]. These glass panels were then used to construct VIG units, the spacing of the array was 20 mm and the spacers were spherical in shape, about 180 µm in height and 600 µm in diameter at its base. Measurements were taken on several of the laser spacers and at several points between the spacers. In these samples the glass was not coated with a low emissivity coating and the unit was prepared with an internal volume pressure below  $10^{-3}$  Torr; at this pressure the residual gas thermal conductance is at a level of  $0.01 \text{ W m}^{-2} \text{ K}^{-1}$  or less.

As mentioned previously it is important that the spacer used in a VIG be strong since there is not only the continuous load of atmospheric pressure, but also the potential of additional forces on a spacer due to external loads, such

as thermal and wind loads. At the University of Sydney a simple and effective lever apparatus has been developed. Into the apparatus a single spacer, sandwiched between two small glass sheets, of size 30x30 mm, can be placed under load. Relative to the spacer the applied load can be a combination of a normal and shear load, up to a limit of about 500N. For these measurements 30x30 mm, 4 mm thick, glass coupons with a single laser spacer, located at the centre of the coupon, were obtained from Corning Inc. USA [16]. During typical measurements the load sequence on the spacer was continuously imaged and the load at the spacer was measured using appropriately placed load cells. In all tests the load on the spacer was applied at low rates and care was taken to identify all levels of damage. In general, regardless of the spacer type (that is, cylindrical or spherical shapes), as long as the contact area of the spacer is equal, the contact surface of the glass substrate will exhibit failure at the same normal/shear load combinations; cylindrical and spherical contacts, of the same contact area, exhibit a negligible difference in the contact surface stress [11,12]. It was not the focus of this work to characterise the failure limit of the underlying glass material. The object of the test was to determine the loads at which damage and/or failure of the spacer is observed, and thus, define simply the strength of the spacer. In all cases the glass was prepared to condition the surface to provide a contact friction as would be expected within the vacuum environment of the internal volume of the VIG. As the applied load on the spacer is increased the contact area also increases, and follows well the analytical contact mechanics definition of a spherical contact on a flat surface [11,12]. In the analysis

| Sample                     | Thermal conductance<br>[W m <sup>-2</sup> K <sup>-1</sup> ] | Ultimate strength<br>[GPa] |
|----------------------------|---|----------------------------|
| On as-received glass       | 0.6-0.7   | 8-10                       |
| After annealing of glass   | 0.6-0.7   | 6-7                        |
| 304 Stainless steel spacer | 0.9-1.2   | 1-2                        |

Table 2: The measured thermal and mechanical properties of the laser spacer, when produced on as-received soda-lime float glass and when the laser spacer has been annealed at 600°C for 1 hr. The measured stainless steel spacer is 304 grade and was cylindrical in shape, about 0.5 mm in diameter and 0.2 mm in height.

of the measurement data the linear elastic properties of glass-on-glass contact was taken into consideration. The laser spacer contact measurement was performed on as-received glass, thermally tempered glass, and on a Sapphire substrate.

Table 2 presents the results for a laser spacer that was produced on as-received soda-lime glass, and also results for the same spacer sample that has been annealed at a temperature of 600°C for 1 hr. In the case of the thermal conductance, a typical sample, of uncoated glass, provided a measured surface-to-surface thermal conductance of approximately 3.8 W m<sup>-2</sup> K<sup>-1</sup>. On the same VIG sample the thermal conductance of the array of spherical laser spacer was measured to be approximately 0.66 W m<sup>-2</sup> K<sup>-1</sup>, which is in good agreement with the analytical calculation result of 0.6 W m<sup>-2</sup> K<sup>-1</sup>. It is important to note that under the action of atmospheric pressure the contact radius of the laser spacer was about 0.18 mm during the measurement of the thermal conductance. The data provided in figure 3 was calculated for a spacer with a cylindrical contact radius of 0.25 mm. As mentioned previously, the advantage of the laser spacer in addition to a potentially smaller contact area, is the underlying lower thermal conductivity. Considering all parameters equal except for the thermal conductivity, the advantage for the laser spacer is about a 30% decrease in the total thermal conductance contribution as compared to that of a metal spacer array.

Even though the thermal conductance of the laser spacer is lower because of the underlying lower thermal conductivity, in most cases the fact that the spacer is glass would be a concern in terms of ultimate strength. Under an increasing applied load the laser spacer exhibited a much higher ultimate strength than expected. It is reasonable to suggest that the laser process has resulted in a significant

structural change; of which one part is a level of residual stress (temper) that has been locked into the structure. Typically, the force on a spacer due to atmospheric pressure increases as the array spacing is increased: that is, at a spacing of 20 mm the force is 40N, at 30 mm it is 90N and at 40 mm it is 160 N.

The ultimate strength of the spacer was measured to be at an applied load of about 500-600N. This translates to a mean contact pressure (compressive stress) of about 8 – 10 GPa. At the point of catastrophic failure, the fracture of the spacer exhibits fragmentation that is similar to that observed in thermally tempered glass sheets. This is shown in figure 5, an image of a coupon sample from the side. A simple test was performed to observe a change in the temper of the spacer. A coupon sample was annealed at 600°C for 1 hr.

The annealed laser spacer exhibited a negligible change in size and shape, and when loaded to failure, the ultimate strength decreased by about 25-30%. Interestingly, the previously observed fragmentation did not occur. Figure 6 is an image of an annealed coupon sample from the side, after failure. The spacer has disintegrated under load, with very little through thickness fragmentation. *that was annealed at 600°C for 1 hr, after catastrophic failure.*

## Summary

The Vacuum Insulating Glazing (VIG) is a highly insulating technology that has the potential to have a significant impact on energy use in buildings. The ultimate thermal conductance of the VIG is strongly dependent on the number, shape, and size, of the spacer array. The use of a method to produce a spacer on the surface of the glass pane, by using the underlying glass as the material for the spacer, produces an advantage in the lower thermal conductance of the spacer. Measurements performed show that this advantage in the lower thermal conductance is about 30%. Furthermore, even though the laser spacer is glass, the processing of the glass to form the spacer results in structural changes which lead to a higher ultimate strength. In this paper the background information and the initial thermal and mechanical measurements of a laser spacer were presented. Further work has been performed to detail the characteristic behaviour of shape changes, shear load effects, application in



Figure 5: (a) a side view image of a laser spacer after catastrophic failure, (b) a magnified image of the surface and bulk region of the spacer.



Figure 6: A side view image of a laser spacer,

panel size strength tests, and integration of tempered glass. In addition, numerical modelling to systematically detail the physical processes that govern the behaviour of the spacer has been undertaken. In future articles these results will be presented to provide a complete picture of the use of a laser spacer in the construction of a VIG device.

[16] Dr Alexander Streltsov, Corning Research & Development Corporation, Sullivan Park, SP-AR-02-05, Corning, NY 14831

## References

[1] D. Arasteh, S. Selkowitz, and J. Wolfe, The design and testing of a highly insulating glazing system for use with conventional window systems, *Journal of Solar Energy Engineering*, 111, 44-53, 1989.

[2] R. E. Collins et al., Vacuum glazing – A new component for insulating windows, *Building and Environment*, 30[4], 459-492, 1995.

[3] T. M. Simko et al., Temperature-induced stresses in vacuum glazing: Modeling and experimental validation, *Solar Energy*, 63[1], 1-21, 1998.

[4] R. E. Collins et al., Transparent evacuated insulation, *Solar Energy*, 49[5], 333-350, 1992.

[5] R. E. Collins et al., Current status of the science and technology of vacuum glazing, *Solar Energy*, 62[3], 189-213, 1998.

[6] C. F. Wilson et al., Heat conduction through the support pillars in vacuum glazing, *Solar Energy*, 63[6], 393-406, 1998.

[7] C. J. Dey et al., Design and validation of guarded hot plate instruments for measuring heat flow between evacuated plane-parallel glass surfaces, *Review of Scientific Instruments*, 69[8], 1998.

[8] H. Manz et al., Triple vacuum glazing: Heat transfer and basic mechanical design constraints, *Solar Energy*, 80[12], 1632-1642, 2006.

[9] R. E. Collins and A. C. Fischer-Scripps, Design of support pillar arrays in flat evacuated windows, *Australian Journal of Physics*, 44, 73-86, 1991.

[10] A. C. Fischer-Cripps et al., Stresses and fracture probability in evacuated glazing, *Building and Environment*, 30[1], 41-59, 1995.

[11] R. Mougnot and D. Maugis, Fracture indentation beneath flat and spherical punches, *Journal of Materials Science*, 20, 4354-4376, 1985.

[12] R. Mougnot, Crack formation beneath sliding spherical Punches, *Journal of Materials Science*, 22, 989-1000, 1987.

[13] Q-C. Zhang, T. M. Simko, C. J. Dey, R. E. Collins, G. M. Turner, M. Brunotte, A. Gombert, The measurement and calculation of radiative heat transfer between uncoated and doped tin oxide coated glass surfaces, *International Journal of Heat and Mass Transfer*, 40[1], 61-71, 1996.

[14] A. Streltsov, et al., Laser texturing of doped borosilicate glasses, *Proc. of SPIE Vol. 7584 75840S-3*, 2010.

[15] S. Loguno, et al., Laser-induced swelling of transparent glasses, *Applied Surface Science*, [257], 2011.

# Vacuum Insulated Glazing under the Influence of a Thermal Load

Dr Antti Aronen, Dr Cenk Kocer  
University of Sydney, School of Physics, Sydney  
NSW 2006, Australia

## Abstract

Vacuum Insulated Glazing (VIG) is a highly thermally insulating transparent flat panel that is constructed from two glass panes, separated by an evacuated sub-millimeter gap, and hermetically sealed around its perimeter. Typically, solder glass is used as the edge seal, which results in a narrow rigid bond between the glass panes. In-service, the VIG unit must withstand forces resulting from atmospheric pressure, and also survive temperature differences (thermal loads) that occur in extreme climates. In this paper a study of the finite element analysis of the deformations and stresses induced because of a thermal load are presented. The finite element model was validated with respect to measurements. Using the finite element model, results of the dependence of the thermally-induced stresses on the size of the VIG unit, the thickness of the glass panes, and the temperature field over the surfaces of the glass panes due to different heat transfer coefficients and thermal conductance of a VIG, are presented and discussed.

## Keywords

1=Vacuum insulated glazing,  
2=Thermal stresses,  
3=Numerical modeling,  
4=Heat transfer

## 1 Introduction

Vacuum Insulated Glazing (VIG), shown in Fig. 1, is a highly insulating double pane glazing, with its edges sealed hermetically using solder glass (a glass frit), and containing a thermally insulating internal vacuum. Typically the width of the edge seal is about 4-8 mm. Within the internal vacuum, between the glass panes, an array of small spacers is used to maintain the separation of the glass panes under the action of atmospheric pressure. Nevertheless, atmospheric pressure does cause local bending, and thus stresses, in the glass panes around and in between the spacers and close to the edge seal [1,2]. Additional stress in the VIG is induced by other external loads, including wind, impact and temperature differences.

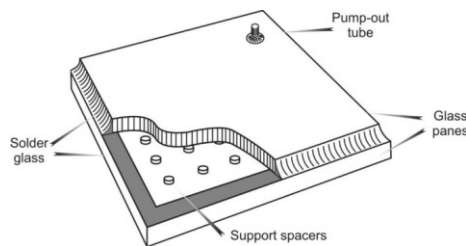


Fig. 1 An illustration of the Vacuum Insulated Glazing [3]

When under load the rigid solder glass edge seal prevents relative movement of the glass panes close to the edge seal. In particular, under a thermal load the differential expansion of the glass panes induces a moment of rotation which leads to mechanical stresses in the glass, and overall bending of the VIG panel. The amount of stress induced and the degree of bending in the VIG unit is highly dependent on several factors related to heat transfer properties, size parameters and the mechanical properties of the individual components. The purpose of this work is to present a finite element analysis which will accurately describe the deformations and stresses that are induced because of a thermal load on a VIG. In the following section a review of the background work is presented. Following this, the validation of the thermo-mechanical finite element model with respect to measurement data is presented. Finally, the finite element model is solved to determine the influence of the size of the VIG unit, the thickness of the glass panes, and the temperature field over the surfaces of the glass panes due to different heat transfer coefficients and thermal conductance of the VIG, on the deformations and thermally-induced stresses in the VIG unit.

### 1.1 Previous work

The thermal bending of a solid plate, in which the temperature is non-uniform through its thickness, has been studied extensively [4,5]. However, such work cannot be directly applied to the VIG case since the VIG is not a homogeneous monolithic plate. Specifically, the temperature profile through the thickness of the VIG structure is quite different and lateral heat flow in the vicinity of the edge seal results in lateral temperature variations in-the-plane of the VIG glass panes. The overall bending and resulting stresses in the VIG due to a thermal load have been

studied. Collins et al. [6] and Fischer-Cripps [7] reported analytical solutions for the structural deformations and stresses induced in a VIG based on the theory of bimetallic beams; theory originally developed by Timoshenko [8]. The finite element method was used in studies by Simko et al. [9], Wang et al. [10], Wullschlegel et al. [11] and Fischer-Cripps [7] to study thermal load effects. The Simko et al. [9] study also presented measurement results for overall bending and the mechanical strain in VIG units under well-defined thermal conditions. All of these studies have shown that the thermally induced stresses in each glass pane of a VIG unit vary through the thickness of the panes. The surface labeling to be referred to in the following discussion is defined in Fig. 2. For a VIG with an un-supported edge condition, the stresses remote from the edge seal over the outer surfaces of the hot side (surface 4) and cold side (surface 1) are found to be isotropic and of the same magnitude, but are tensile and compressive, respectively [1,6,7,9]. Closer to the edges of the glass panes, the stresses over the glass surfaces are anisotropic. The stresses normal to the edges approach zero near the edge, while the stresses parallel to the edge are approximately twice in magnitude than that found at the center of the glass panes; this is due to lateral temperature variations in the glass panes close the glass edge. On the inner surface of each glass pane (surfaces 2 and 3 for the cold and hot pane, respectively) the magnitude of the stress at the center is about twice that of the stress on the outer surface of the same pane and of opposite sign (that is, tensile and compressive, respectively); where the stress through the thickness of each pane varies linearly. It is well known that the rate of crack growth in glass, particularly soda-lime float glass, is highly dependent on the relative humidity of the surrounding environment to which the stressed crack tip is exposed [12]. Since the internal surfaces (surface 2 and 3) of the VIG are exposed to the vacuum cavity, for an equal magnitude and distribution of stress the probability of crack initiation at surfaces 1 and 4 would be significantly higher than that on surfaces 2 and 3. In addition, in all thermal load cases solved in this work, surface 4 will have the greater tensile stress field. Therefore, in this work, as a matter of brevity, only the stress field induced over surface 4 is considered.

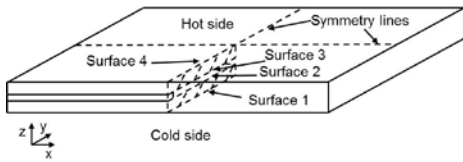


Fig. 2 An illustration of the mirror symmetry planes within the VIG and the labeling convention of the individual surfaces of the glass panes with respect to the hot and cold side. The local coordinate system is shown.

## 2 Results

The Finite Element Method (FEM) is used to simulate the thermal and mechanical behavior of the VIG under applied loads. The thermal model is a static model used to solve the temperature distribution over the VIG unit. In the model the spacers are modeled with all relevant material and contact properties included. Furthermore, surface-to-surface radiative heat transfer within the vacuum cavity and the temperature non-uniformity over the glass surfaces were included. On the outer surfaces of the VIG, convective boundary conditions are employed to simulate the heat transfer process between the inside/outside environment and the glass hot/cold surfaces, respectively.

In all cases the FEM solutions are performed with the initial step to determine the deformation/stress field due to atmospheric pressure only and then, in a subsequent second step, the total solution of atmospheric pressure plus the desired thermal load is solved. The thermal load solution is obtained by simulating the temperature distribution over the VIG unit first, and subsequently the mechanical strain over the VIG unit due to the thermal load is calculated. Since the temperature range of interest is not large, the mechanical solution is obtained for linear elastic behavior of the glass and spacers. The stress distribution over the VIG due only to the thermal load is calculated by subtracting the stress distribution due solely to atmospheric pressure from the final data of atmospheric pressure plus thermal load. As a matter of brevity the mechanical behavior is solved in this paper only for the case of an un-supported (unconstrained or free) edge support.

Therefore, to constrain the model from virtual full-body displacements, only the corner points (FEM model nodes) of the VIG model are fixed not to move in the z direction, only on surface 1 (cold side). To minimize the computational effort/time required to obtain a solution, the mirror symmetry planes are used to reduce the required model size to one quarter of the original full size VIG unit; along the symmetry lines appropriate boundary conditions are applied, Fig. 2 highlights these symmetry

planes. In all cases the finite element software package ANSYS version 17.0 was used to simulate thermal and mechanical behavior. In the following sections the FEM results are validated through direct comparison to measurements published by Simko et al. [9]. Following this, the typical stress and deformation results from the thermal load simulations are presented. This includes data of the effect of different VIG model parameters on the stresses and deformations.

### 2.1 Validation of the finite element model with respect to measurements

The results from the FEM are validated by direct comparison to measurement data. The overall bending and the mechanical strain (perpendicular and parallel to the edge) at different locations along a mirror symmetry line on the hot side (surface 4) of a VIG are presented in Fig. 3 and 4, respectively. The FEM simulations were performed using model parameters taken from the Simko et al. [9] work and are listed in Table 1.

The FEM simulation and measurement data in Figs. 3 and 4 are in good agreement. The

center deflection of the VIG from the FEM simulation is approximately 5 % higher as compared to the measured displacement. This is due mainly to the small difference in curvature close to the edge of the VIG unit. The specific edge constraints of the real VIG measurement setup cannot be exactly reproduced within the finite element model.

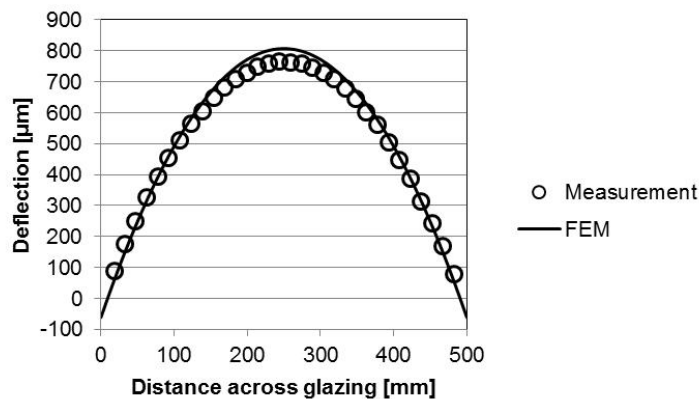


Fig. 3 Deformation results from FEM simulations and measurement.

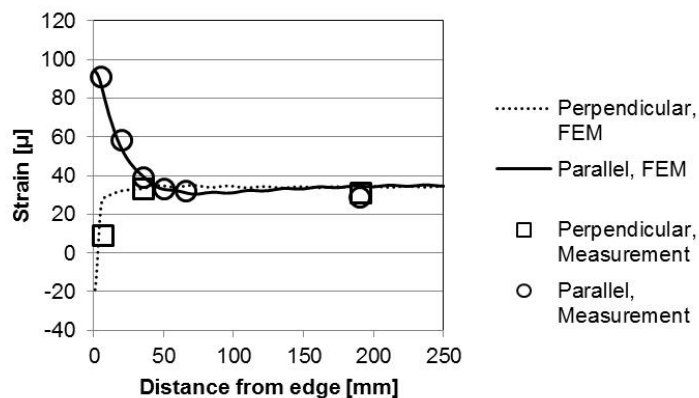


Fig. 4 Mechanical strain results from FEM simulations and measurement. center of the unit, is proportional to the square of the distance from the center.

| Parameter   | Simko et al. [9]  | Reference case    |
|---|-------------------|-------------------|
| Young's modulus [GPa]   | 74                | 70                |
| Poisson's ratio   | 0.23              | 0.22              |
| Thermal expansion coefficient [ $^{\circ}\text{C}^{-1}$ ]                                   | $8 \cdot 10^{-6}$ | $9 \cdot 10^{-6}$ |
| Thermal conductivity of glass [ $\text{W m}^{-2} \text{K}^{-1}$ ]                           | 1                 | 1                 |
| Length [mm]   | 500               | 350               |
| Width [mm]  | 500               | 350               |
| Glass-to-glass thermal conductance [ $\text{W m}^{-2} \text{K}^{-1}$ ]                      | 1.32              | 0.47              |
| Spacer array separation [mm]  | 25                | 40                |
| Glass thickness [mm]  | 4                 | 4                 |
| Vacuum cavity/spacer height [mm]  | 0.2               | 0.2               |
| Solder glass width [mm]   | 4                 | 4                 |
| Emissivity (surface 2/surface 3) [-]  | 0.25/0.25         | 0.03/0.837        |
| External heat transfer coefficient (hot side/cold side) [ $\text{W m}^{-2} \text{K}^{-1}$ ] | 5.7/6.7           | 8/8               |
| External temperature (hot side/cold side) [ $^{\circ}\text{C}$ ]                            | 44.5/13.2         | 20/10             |

Table 1. The material properties of soda-lime glass and the dimensions of a VIG unit, as used by Simko et al. [9], and as used in this work.

## 2.2 Behavior of VIG under thermal load

In the previous section, FEM and measurement data were shown to be in good agreement over the glass outer surface on the hot side (surface 4). In this section the FEM simulation results of the stresses and temperature field on a VIG (over different surfaces) are presented, where the model parameters (reference case) are listed in Table 1. First, the temperature profile along the mirror symmetry line is shown in Fig. 5. The temperature at the center of the VIG is dependent on the glass-to-glass thermal conductance of the VIG, the external heat transfer coefficients and the external inside/outside temperatures. Close to the edge the temperature changes exponentially from the temperature at the edge seal, to the temperature on the glass surface at the center of the glass pane. Even though the edge seal region is a thermal bridge the hot and cold side (surface 4 and 1, respectively) surface temperatures over the edge seal are not equal. There is a small temperature difference (approximately  $0.5^{\circ}\text{C}$  in Fig. 5) and therefore, a through thickness temperature profile at the edge seal.

The stress profile over each surface, parallel to the edge, is shown in Fig. 6. The stress profile at the edge is close to three times the magnitude of the stress remote from the edge (on surfaces 4 and 1), which was also the case as shown in Fig. 4. The stress remote from the edge on the inner surfaces is also close to three times the magnitude as compared to the stress remote from the edge on the outer surfaces. This result does not agree

with the previous published analytical results [1] discussed in section 1.1. In the published works the analytical solutions were obtained on the assumption that each glass pane is wholly at a defined constant temperature. The FEM stress field perpendicular to the edge, Fig. 7, is much more uniform along the symmetry line of the VIG unit than the stress parallel to the edge, Fig. 6. In Fig. 7, there is a significant spike in the magnitude of the stress close to the edge, at the inner surface. The spike in stress is wholly caused by a numerical singularity at the model node which is the point at which the glass pane and the rigid edge join together. In a "real" VIG unit the transition from the glass pane to the edge seal is smooth and there is no significant spike in stress, therefore, the spike in stress in Fig. 7 can be ignored.

The deflection of the VIG unit along the symmetry line calculated using FEM is shown in Fig. 8. The deflection at any point along the surface of the VIG unit, relative to the maximum deflection at the center of the unit, is proportional to the square of the distance from the center.

## 2.3 Case study using the Finite Element Method

Clearly, there are numerous parameters which affect the thermal and mechanical response of the VIG unit. In the following sections the results of FEM calculations looking into the effects of VIG unit size, glass pane thickness, overall thermal conductance, and external heat transfer coefficients, are presented. The

parameters employed in these calculations are listed in Table 1 as the reference case.

In the following discussion the stress distribution parallel to the edge seal is most relevant to the potential fracture of the glass panes, and thus, only the results of the stress field over surface 4 and close to the edge seal are considered.

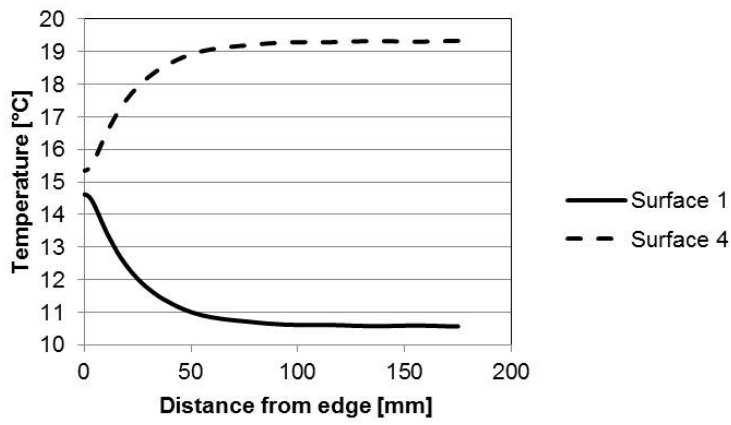


Fig. 5 Temperature profile over the symmetry line of a VIG unit, obtained from FEM.

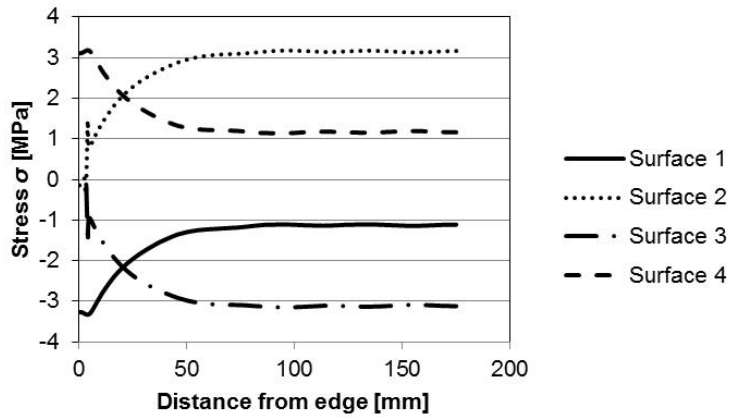


Fig. 6 Stress profiles parallel to an edge along the symmetry line obtained from FEM.

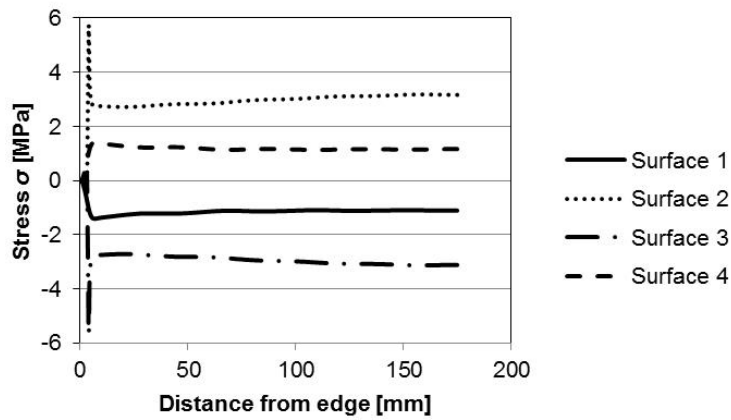


Fig. 7 Stress profiles perpendicular to an edge along the symmetry line obtained from FEM.

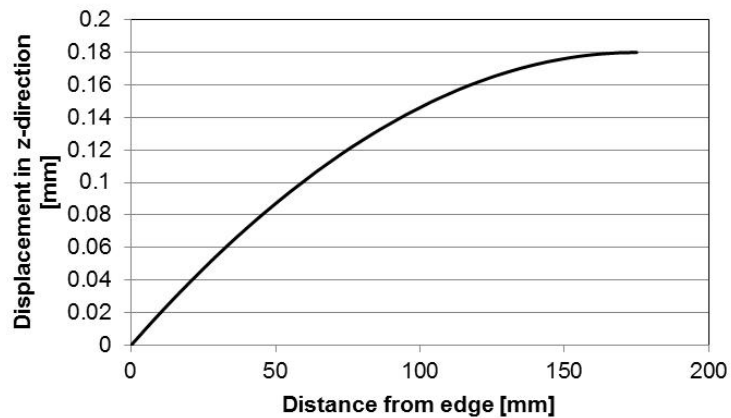


Fig. 8 Out-of-plane deflection profile of a VIG unit along the symmetry line obtained from FEM.

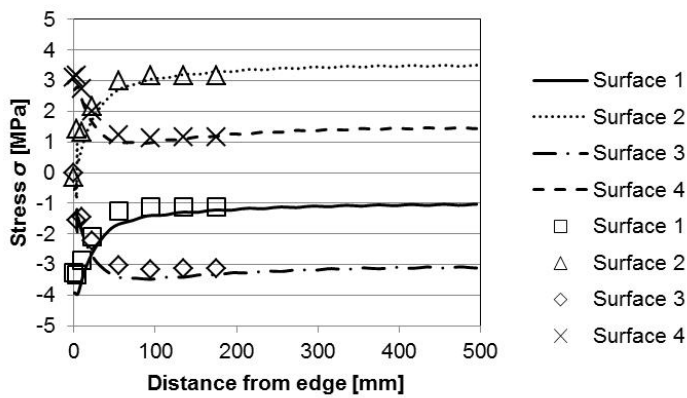


Fig. 9 The effect of the size of the VIG sample on the stresses parallel to the edge along a symmetry line. The lines are for a VIG of size 990 x 990 mm<sup>2</sup> and the points are for a VIG of size 350 x 350 mm<sup>2</sup>.

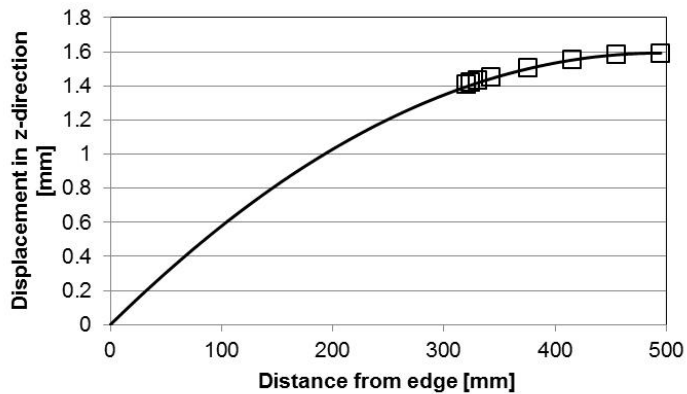


Fig. 10 The effect of the size of the VIG on the deformations along a symmetry line. The lines are for a VIG of size 990 x 990 mm<sup>2</sup> and the points are for a VIG of size 350 x 350 mm<sup>2</sup>. The maximum center deflections of the large and small VIG units are 1.6 and 0.2 mm, respectively.

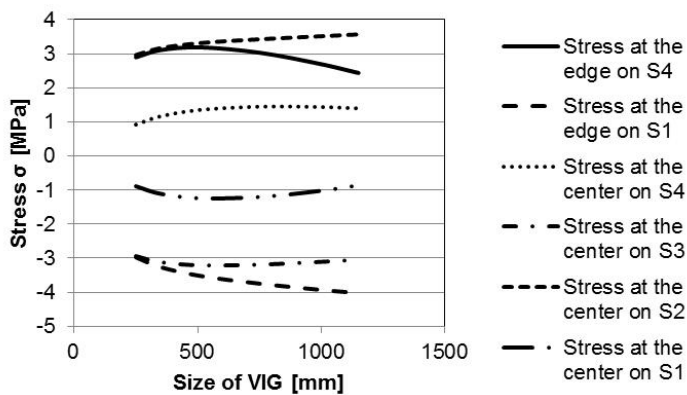


Fig. 11 The stress parallel to the edge seal, at the edge on the hot and cold surfaces (surface 4 and 1) and at the center on all surfaces (surface 1, 2, 3, and 4) as a function of the characteristic size (length and width) of a square VIG unit.

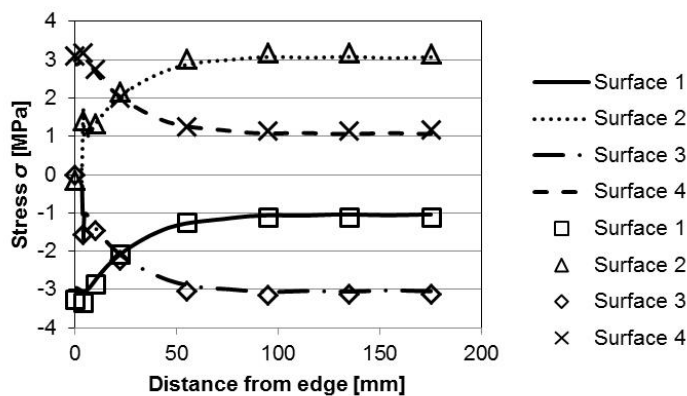


Fig. 12 The effect of the glass pane thickness on the stresses parallel to the edge seal, along the mirror symmetry line. The solid and dashed lines are for a VIG unit with 6 mm thick panes and the individual data points are for a VIG unit with 4 mm thick panes.

### 2.3.1 Effect of unit size

From the thermo-mechanical FEM simulations it was found that the VIG unit size has two effects on the distribution of stress. The first effect is due to changes in the temperature distribution over the VIG and the second is due to the non-linear effect of bending. Fig. 9 is a plot of the stress profile, along the symmetry line from the edge seal to the center-of-pane, for two unit sizes of 350 x 350 mm<sup>2</sup> and 990 x 990 mm<sup>2</sup>. As the unit size is reduced from 990 x 990 mm<sup>2</sup>, the temperature non-uniformity associated with heat flow through the edge seal occurs over a larger proportion of the surface area of the VIG unit. This decreases the average temperature difference between the glass panes, and correspondingly reduces the stresses at the outer surface (surface 4). Clearly, however, for larger unit sizes the maximum center deflection is larger, see Fig. 10, and thus, for the larger unit size the non-linear deformation of the plate must be taken into consideration. The effect of a non-linear deformation is discussed in greater detail by Wullschlegger et al. [11]. It is found that the non-linear effect produces an increase in stress at the center of the unit, and a decrease in stress close to the unit edge.

The deflection of the VIG unit, Fig. 10, is proportional to the square of the characteristic dimension of the sample if the curvature is constant; therefore, the maximum deflection of the VIG unit increases dramatically with increases in the unit size of the VIG. In order to directly compare the curvature of the deflected small and large unit, the data of the small unit, in Fig. 10, is shifted so as to make the center deflection of the small and large unit the same. Interestingly, the overall curvature of small and large VIG units is the same. The maximum center deflections of the large and small VIG units are 1.6 and 0.2 mm, respectively.

Fig. 11 is a plot of the stresses as a function of the characteristic length of a VIG unit. In the figure are shown the stresses parallel to the edge seal, at the edge, on the outer surfaces and at the center of all surfaces. The magnitude of the stress increases until the characteristic length reaches 500 mm. This is due to the influence of the lateral temperature profile of the edge region. At a length greater than 500 mm the lateral temperature distribution decreases and the effect of non-linear deformation dominates. At the edge the non-linear deformation results in a lower stress parallel to edge, with an increased stress remote from the edge. Due to the in-plane temperature distribution and the non-linear deformation the peak tensile stress at the edge on the outer surface of the hot pane (surface 4) occurs at a length of approximately 500 mm. It is important to note that the unit length at which the stress peaks is dependent

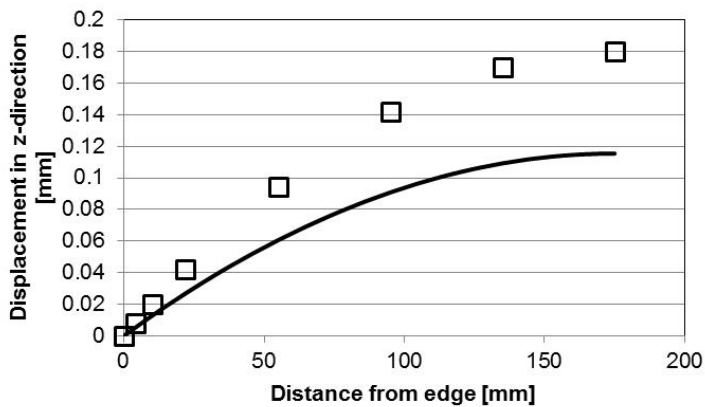


Fig. 13 The effect of the glass thickness on the overall VIG unit deflection (bending) along the mirror symmetry line. The solid line is for a VIG with 6 mm thick panes and the open squares are for a VIG with 4 mm thick panes.

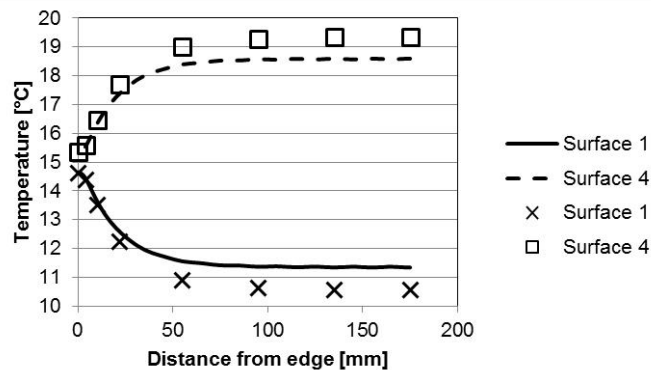


Fig. 14 The effect of the VIG U-value on the temperature profile along the mirror symmetry line. The solid and dashed lines are for a VIG glass-to-glass U-value of 1.38 W m<sup>-2</sup> K<sup>-1</sup> and the individual points are for a VIG glass-to-glass U-value of 0.47 W m<sup>-2</sup> K<sup>-1</sup>.

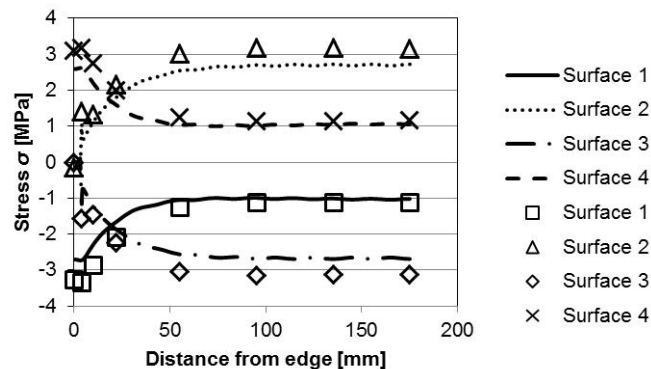


Fig. 15 The effect of the VIG U-value on the stresses parallel to the edge seal along the symmetry line. The solid and dashed lines are for a VIG glass-to-glass U-value of 1.38 W m<sup>-2</sup> K<sup>-1</sup> and the individual points are for a VIG glass-to-glass U value of 0.47 W m<sup>-2</sup> K<sup>-1</sup>.

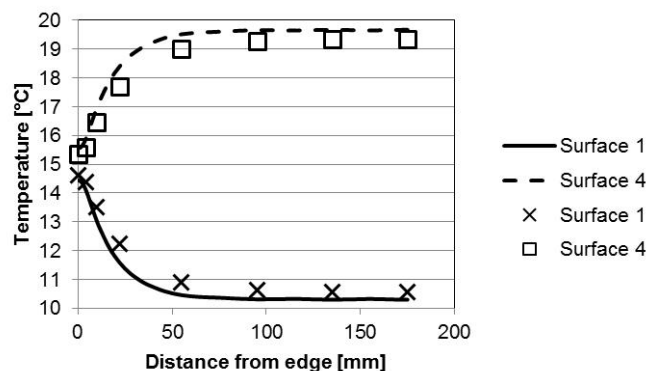


Fig. 16 The effect of the external heat transfer coefficient on the temperature profile along the mirror symmetry line. The solid and dashed lines are for an external heat transfer coefficient of 15 W m<sup>-2</sup> K<sup>-1</sup> on both sides and the individual points are for an external heat transfer coefficient of 8 W m<sup>-2</sup> K<sup>-1</sup> on both sides.

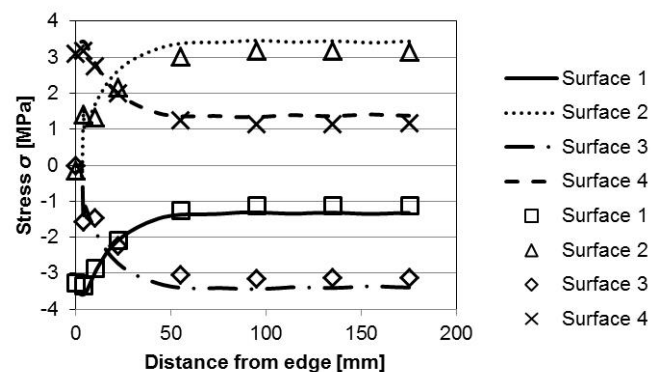


Fig. 17 The effect of the external heat transfer coefficient on the stress profile along the mirror symmetry line. The solid and dashed lines are for an external heat transfer coefficient of 15 W m<sup>-2</sup> K<sup>-1</sup> on both sides and the individual points are for an external heat transfer coefficient of 8 W m<sup>-2</sup> K<sup>-1</sup> on both sides.

on the external heat transfer coefficients and the thickness of the glass panes.

### 2.3.2 Effect of glass pane thickness

Fig. 12 compares the stress profile over the mirror symmetry line, from the edge seal to the center of glazing, for VIG units with either 4 or 6 mm thick glass panes, equal on both sides. The resulting deflection of the VIG unit is shown in Fig. 13. Clearly, the stress profiles over each surface do not change significantly relative to a change in the glass pane thickness. However, the overall deflection (bending) of the VIG unit is appreciably less for thicker glass panes, as would be expected.

### 2.4.3 Effect of the glass-to-glass, center-of-glazing, VIG thermal conductance (U-value)

The ultimate heat flow through a VIG unit will, clearly, be highly dependent on the U-value of the unit. Figs. 14 and 15 compare the temperature and stress profiles in VIG units where the U-values are 0.47 W m<sup>-2</sup> K<sup>-1</sup> and 1.38 W m<sup>-2</sup> K<sup>-1</sup>. The latter U-value is for a VIG with a 20 mm spacer array separation and a single internal low-E coating (0.03 hemispherical emittance). Due to the higher Uvalue the temperature difference between the hot and cold panes is less. This reduced temperature difference proportionally reduces the magnitude of induced stress; where a similar change is observed when the external temperatures are changed.

### 2.3.4 Effect of external heat transfer coefficients

Clearly, the magnitude of the external heat transfer coefficients defines the surface temperatures of the glass panes, and therefore, the induced stresses within the VIG unit. This is best illustrated in Figs. 16 and 17 where the VIG glass-to-glass U-value is 0.47 W m<sup>-2</sup> K<sup>-1</sup>. In each case, the external heat transfer coefficients were 8 W m<sup>-2</sup> K<sup>-1</sup> and 15 W m<sup>-2</sup> K<sup>-1</sup>, and equal on both sides of the VIG. The external heat transfer coefficient has a nonlinear effect on the temperature and stress distributions because of its influence on the lateral heat flow through the glass panes. Increasing the external heat transfer coefficient increases the temperature difference between the glass panes at the center region of the VIG. Furthermore, the in-plane temperature profile at the edge region now extends from the edge to center region over a shorter distance, and thus, the relative local temperature change close to the edge is larger as compared to that at the center-of-pane region.

### 3 Summary

In this paper the finite element method was employed to determine the deflections and stresses in a VIG unit which is subjected to a thermal load. The FEM gives results that are in good agreement with measurement data published in the literature. Specifically, the stress distribution found on each glass surface clearly highlights the effect of the whole area influence of the convection boundary condition of heat transfer used in the simulations. Over the outer surface (surface 1 and 4) the stress parallel to edge at the edge region is about three times the stress remote from the edge. It was also found that the magnitude of stress over the inner surface (on surface 2 and 3) remote from the edge is about three times the stress over the outer surface (on surface 1 and 4). The parameter study shows clearly that:

- Increasing the VIG unit size increases the magnitude of the stress until the effect of non-linear deformation dominates. Then the stress at the edge region decreases and at the center it increases,
- Change in the glass thickness in the VIG only affects the bending of the unit, since it does not affect the temperature distribution,
- Change in the external heat transfer coefficients, and also the unit glass-to-glass U-value, results in a change of the temperature profiles on the VIG. The increase in the glass-to-glass U-value decreases the temperature difference between the glass panes, which results in lower stresses,
- The external heat transfer also has a nonlinear effect on the stress and temperature distributions.

### Acknowledgements

The writers thank Richard Collins for valuable comments on the manuscript. The authors also acknowledge the University of Sydney HPC service at The University of Sydney for providing HPC and software resources that have contributed to the research results reported within this paper.

### References

- [1] Fischer-Cripps, A.C., Collins, R.E., Turner, G.M., Bezzel, E.: Stresses and Fracture Probability in Evacuated Glazing. *Build. Environ.* 30(1), 41-59 (1995).
- [2] Collins, R.E., Turner, G.M., Fischer-Cripps, A.C., Tang, J.-Z., Simko, T.M., Dey, C.J., Clugston, D.A., Zhang, Q.-C., Garrison, J.D.: Vacuum Glazing – A New Component for Insulating Windows. *Build. Environ.* 30(4), 459-492 (1995).
- [3] Kocer, C.: A discussion of highly insulating windows; a hybrid vacuum insulating glazing. In: *Glass Performance Days 2013*, Glaston, Finland, 447-450 (2013)

- [4] Hetnarski, R.B., Eslami, M.R.: *Thermal Stresses – Advanced Theory and Applications*. Springer (2009)
- [5] Boley, B.A., Weiner, J.H.: *Theory of Thermal Stresses*. Dover Publications (2012)
- [6] Collins, R.E., Fischer-Cripps, A.C., Tang, J.-Z.: Transparent Evacuated Insulation. *Sol. Energy* 49(5), 333-350 (1992).
- [7] Fischer-Cripps, A.C.: *Stresses and Fracture Probability in Evacuated Glazing*. Dissertation, The University of Sydney, Australia (1993)
- [8] Timoshenko, S.: Analysis of Bi-Metal Thermostats. *J. Opt. Soc. Am.* 11(3), 235-255 (1925).
- [9] Simko, T.M., Fischer-Cripps, A.C., Collins, R.E.: Temperature-Induced Stresses in Vacuum Glazing: Modelling and Experimental Validation. *Sol. Energy* 63(1), 1-21 (1998).
- [10] Wang, J., Eames, P.C., Zhao, J.F., Hyde, T., Fang, Y.: Stresses in Vacuum Glazing Fabricated at Low Temperature. *Sol. Energ. Mat. Sol. C.* 91, 290-303 (2007).
- [11] Wullschleger, L., Manz, H., Ghazi Wakili, K.: Finite Element Analysis of Temperature-Induced deflection of Vacuum Glazing. *Constr. Build. Mater.* 23(3), 1378-1388 (2009).
- [12] Lawn, B.: *Fracture of Brittle Solids*. 4th Ed. Cambridge University Press, Great Britain (1993)

# Laser-Grown Bumps on Window Glass

Alexander Streltsov, Jin Kim, Leonard Masters, and David Lance  
Corning Research & Development Corporation  
Corning, New York, USA

## Keywords

1=Laser 2=Glass 3=Swelling 4=VIG  
5=Soda-lime

## Abstract

The process of forming bumps on window glass with an ultra-violet nanosecond laser is described. Bump growth is caused by heating the glass to temperatures above the softening point. Directional flow carries the softened glass towards the surface forming a bump. The shape of the bump is mostly determined by the surface tension of the molten glass. We show that the height of the bumps, which are typically approximately 180  $\mu\text{m}$  tall, can be controlled with sub-micrometer accuracy and the shape can be altered from semi-spherical to flat-top. The time required for growing a bump is on the order of a second or less. These bumps may be an alternative to the metal posts in the incumbent vacuum-insulated glazing designs.

## Introduction

Vacuum Insulated Glazing (VIG) concept allows for a significant improvement of thermal insulation compared with the incumbent double-pane windows design.

Existing VIG designs incorporate pillars of stainless steel as spacers to prevent the glass panes from touching each other under atmospheric pressure. Some of the issues of metal pillars are 1) high thermal conductivity compared to other materials (e.g. ceramics, glass), 2) parts/material cost, and 3) manufacturing yield or throughput. For a VIG unit with window size of 1  $\text{m}^2$  and array spacing of 20 mm, about 2,000 pillars are required to be placed on a pane, adding significant cost to the VIG unit. Lastly, after metal pillars are placed on a pane, moving the pane carefully through the manufacturing process without disrupting the position of pillars compromises manufacturing yield and/or throughput.

Thermal conductivity: The spacers grown from glass pane have thermal conductivity significantly lower than that of metal. It is known that heat conduction through spacers is the major factor that determines overall insulation of a VIG unit [1]. So, changing the spacer material from metal to glass will significantly improve thermal insulation of a VIG unit.

VIG manufacturing cost can be significantly lowered with laser-grown bumps. Lower manufacturing cost is enabled by lower material cost, higher production yield, and higher throughput.

Material cost: VIG with laser-grown bumps does not use discrete materials for spacers, whereas VIG with metal pillars does use discrete materials, i.e., metal pillars, which increases material cost. For VIG with laser-grown bumps, glass spacers are grown out of the pane. For VIG with metal pillars, metal pillars are formed first by masking and etching a metal sheet and then introducing the pillars on the pane.

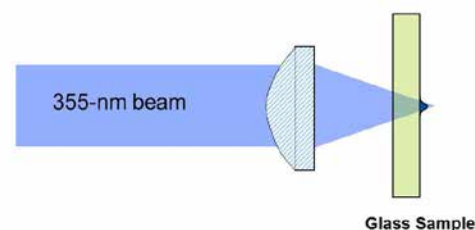
Manufacturing yield or throughput: For VIG with laser-grown bumps, the glass spacers are attached to (or a part of) the pane. This permanent bond prevents any movement throughout the production steps. In contrast, when metal pillars are placed on the pane, especially with anti-friction coating on them, careful handling is required in order to prevent pillars' movement, sacrificing manufacturing yield and/or throughput.

We propose to use laser-grown glass bumps as spacers for VIGs. Laser-grown glass bumps can solve many of the problems associated with metal pillars. The advantages come in terms of thermal conductivity, material cost, manufacturing yield, and throughput.

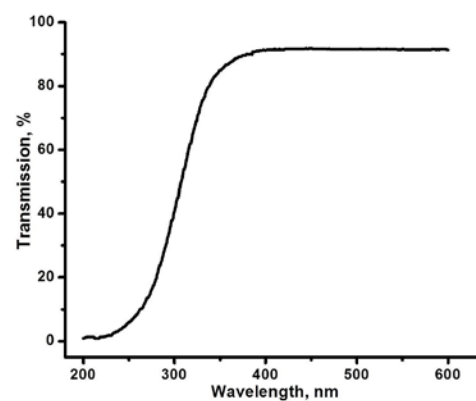
In the following sections, we will describe how glass bumps are made in various forms with high accuracy for the application to vacuum-insulated glazing.

## Bump Growth Process

The mechanism of creating bumps on transparent glasses is described in [2,3]. The output of a 355nm, nanosecond laser is directed through the soda-lime (window) glass substrate such that the focus is behind the rear surface (Fig. 1a). The substrate is kept at room temperature.



(a)



(b)

Figure 1: (a) Beam focusing setup; (b) Optical transmission in soda-lime glass.

Although the soda-lime glass is quite transparent at 355 nm (Fig. 1b), its absorption effectively increases when exposed with high-intensity laser radiation due to multi-photon absorption. This is why focused laser beam causes heating of the glass through increased absorption. Heating results in glass melting and its directional flow/expansion towards the rear surface of the glass thus forming a swelling. The shape of this swelling is defined by the surface tension of molten glass. When the laser is switched off, the swelling freezes first due to radiative cooling followed by quenching of the molten volume inside the glass.

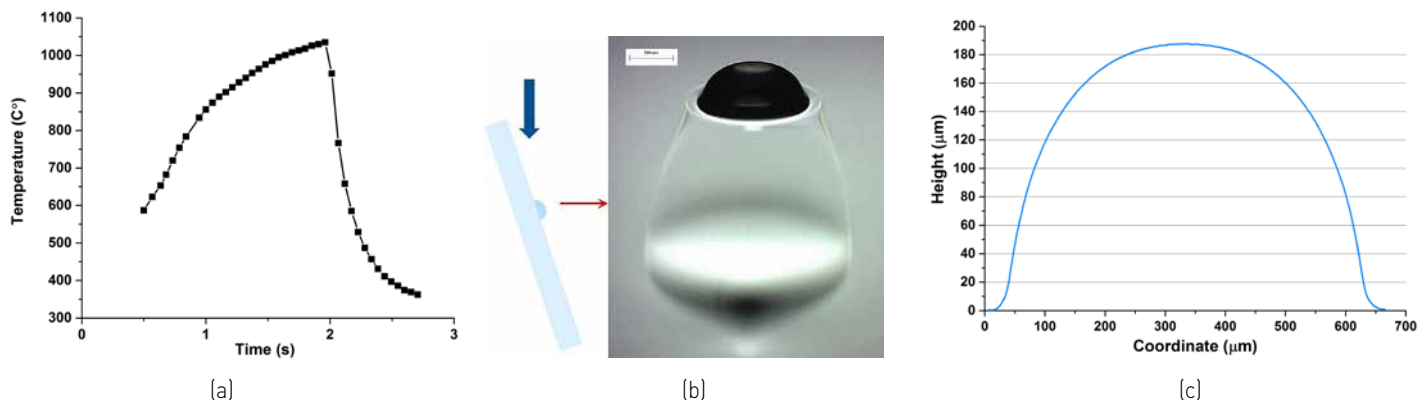


Figure 2: (a) Typical temperature dynamics of the bump vs. time as measured with a thermal camera; (b) Microscope photo of a ~190 μm bump (side view, 200 μm marker); (c) bump profile.

Fig. 2a shows the temperature of the glass surface where the bump is grown measured with a thermal camera. The glass is irradiated for approximately 2 s with a 15 W, 355 nm, nanosecond laser (Coherent AVIA-355-20) to the temperature above the working point of 1000 °C (corresponding to the  $10^4$  P viscosity). After the laser is switched off, the bump cools down to below the strain point (~ 400 °C) in less than 1 s.

Fig. 2b presents the microscope photo of the laser-grown bump on 4-mm thick soda-lime (window) glass. This side view shows the semi-spherical profile of the bump, which is about 190 μm tall and 500 μm in diameter. The characteristic ratio between the diameter and the height lies usually in the 2.5-3 range. The volume below the bump, which is visible because of the lower refractive index, is under tension. This tensile stress goes away when the glass article with bump(s) is brought above the annealing point. The bump profile is shown in Fig. 2c.

The maximum bump height depends on a number of factors: glass composition, thickness, and laser conditions. Thicker glass allows for taller bumps because of larger molten and expanding volume. Glass composition defines the visco-elastic, thermal, and optical properties of the glass. The role of viscosity is not fully understood at this moment; however, it is obviously easier to make bumps on low-temperature glasses compared with the refractory ones.

Optical properties, specifically linear and non-linear (laser intensity dependent) absorption, determine the requirements for the laser conditions. Higher laser power results in taller bumps unless excessive laser power causes glass ablation rather than swelling. Similar limitations are applied to exposure duration: long exposure may cause ablation or

re-melting of the bump and its reflow resulting in height decrease and in diameter increase. In general, increasing the laser power allows for shorter irradiation times for the same bump height. For a 4-mm thick window glass and 180 – 190 μm bumps, the lower limit for the irradiation time is around 0.75 – 1 s because of time required for heating the glass beyond the working point and giving time for it to flow. Shorter bumps require less time, although their height should not be less than approximately 150 μm. The minimum bump height is limited by the thermal conductance of the residual gas in the VIG and by evanescent coupling.

Bumps like these can be fabricated on a range of transparent glasses. Besides a regular soda-lime (window) glass bumps can be grown on Ultra-White window glass, which has lower iron content and does not have the typical greenish tint of the regular window glass. The heights of the bumps are basically the same as on the regular window glass.

### Bump Height Control

The glass pillars must have the same height in order to maintain uniform contact with the flat glass surface of the second glass pane. If the bump height variation is approximately greater than +/- 1 μm the stresses on the taller bumps will be significantly higher than on the shorter bumps. This uneven stress distribution caused by excessive bump height variation within the VIG unit will likely result in reduced thermo-mechanical performance and in lower mechanical strength overall.

We achieve improvement in height variance by using a feedback signal to control the duration of glass irradiation with a laser when growing a bump. The bump gets taller with longer laser irradiation duration and by adjusting this duration one can control the bump height.

However, depending on the variation of glass properties and the fluctuations of laser power, the bump size may vary even for fixed irradiation durations when the fixed interval is based on the opening and closing of a laser shutter. To overcome these perturbations, a controlling feedback signal is used, which is based on the bright flash of light coming from the rear side of the glass, where the bump is grown. The bright flash is registered by a photodiode. This flash takes place a fraction of a second after the laser exposure starts. It is this bright flash that marks the beginning of the fixed duration rather than the opening of the shutter. The glass is irradiated for a fixed duration of time after this flash thus controlling the exposure time in the regime where the bump is growing [4]. Controlling laser irradiation in this manner allows for a noticeable reduction in the variance of bump height.

In Fig. 3, an example of the feedback signal from a photodiode (as viewed on an oscilloscope) is shown. The profile shows a jump in signal when the laser shutter is first opened up. The time between shutter open and bump growth initiation is variable and may depend on glass material property variation as well as laser power variation among other factors. Once bump growth begins, a much stronger spike is registered and it is this signal that is used as a start time for the fixed irradiation interval. A threshold level is chosen that is ~50% of the typical height of the bump growth signal. Once that threshold is overtaken, then the timer begins. The fixed irradiation time is chosen according to the desired bump height.

Fig. 4 shows the results of growing two populations of bumps. One population is generated using the height control method and the second is generated without height control. It is readily apparent that the variation

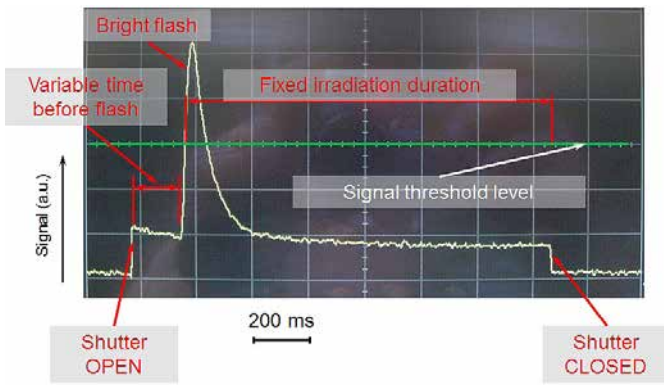


Figure 3: Typical glass fluorescence signal registered by a photodiode. The fixed irradiation duration is approximately 1.6 s.

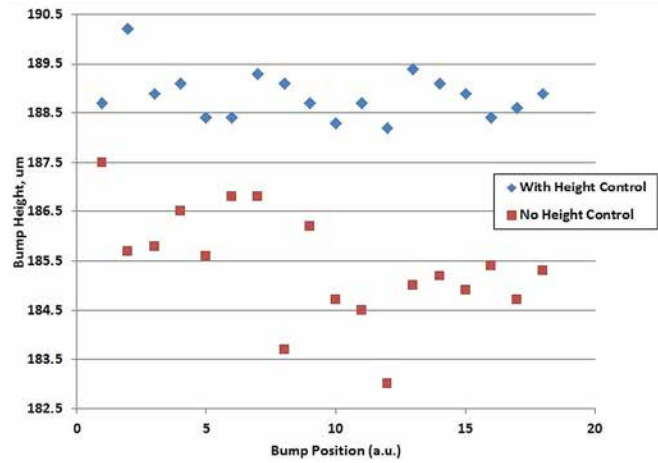


Figure 4: Results of bump growth with and without height control. The blue diamond series corresponds to the bumps grown with height control while the red square series corresponds to the bumps grown without height control.

in the bump height is noticeably reduced. The average height is also different between the two populations but that is ancillary to the experiment. Laser parameters could have been tweaked such that the average of the bump heights would be approximately equal. It is the variance reduction between the "no height control" population and the "with height control" population that is important. Table 1 below quantifies the statistics between the two populations.

| No Height Control |       | With Height Control |       |
|-------------------|-------|---------------------|-------|
| Max Dev           | 2.1   | Max Dev             | 1.3   |
| Min Dev           | -2.4  | Min Dev             | -0.7  |
| Average           | 185.4 | Average             | 188.9 |
| StDevP            | 1.1   | StDevP              | 0.5   |

(a)

(b)

Table 1: Height statistics (a) without height control and (b) with height control. Enabling height control reduces the standard deviation by more than 2x and significantly reduces maximum deviations as well.

Table 1 shows that the variance or standard deviation of bump height for the "with height control" population is reduced by more than half compared to that of the standard deviation of the "no height control" population. Also, the maximum deviations from the average height are also reduced.

### Flat-top bumps

Previous sections described growing quasi-spherical bumps on glass. These bumps have a limited contact area with a flat pane in the VIG, resulting in significant stresses in the flat pane. Flat-top bumps offer a means to reduce the stresses by increasing the contact area between the bump and the flat pane, resulting in improved mechanical performance. In fact, thermal performance may improve by allowing for larger bump array spacing.

Flat-top bumps were grown by placing a "stop" glass behind the window glass, on which the bump was grown. The glasses were separated by 100-150µm gap defined by the shims placed in between (Fig. 5a). The laser beam was focused behind the windows glass and, in the described configuration; its focus was inside the "stop" glass.

Fused silica was selected as the material for the "stop" glass substrate because of its high softening point and because molten window (soda-lime) glass will not wet fused silica and will not stick to it.

The intensity of the 15 W focused laser beam was high by itself and the additional focusing provided by the growing bump re-focused the beam onto the surface of the "stop glass". Even a polished fused silica substrate, having quite high laser damage threshold, developed a crater on the surface from surface ablation making it useless.

The problem was solved by grinding the top surface of the "stop" glass substrate flat and leaving a frosted polish. This prevented the damage of the "stop" glass and allowed for multiple reuses of the same spot for bump flattening (Fig. 5b). The resulting profile of the flat-top bump is shown in Fig. 5c. The bump height is about 130µm, which was determined by the 130µm shims in between of the glasses. The diameter of the contact area between the bump and the flat pane, which can be quantified as, say, the bump diameter at the -3% height, is ~ 260µm compared to ~ 70µm for the semi-spherical bump.

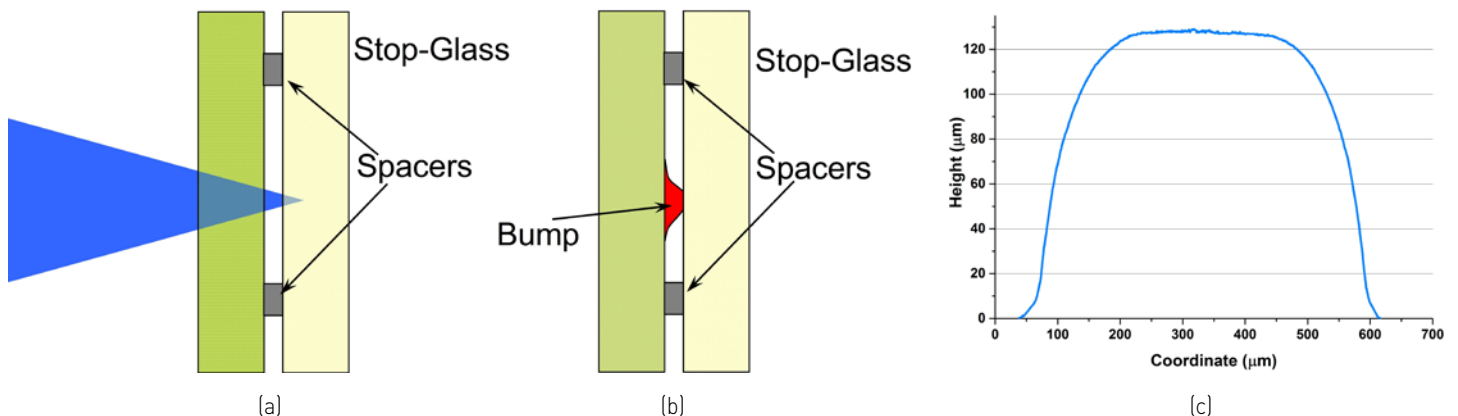


Figure 5: (a) Laser beam focused inside the stop-glass; (b) Flat-top bump between the sample glass and stop-glass; (c) Flat-top bump profile.

## Conclusion

We described the technique of making bumps (pillars) on window glass by laser-induced glass swelling. The bumps may be a cost-effective alternative to the incumbent metal pillars as spacers in VIG while their attributes and thermo-mechanical performance are on par or better than that of metal pillars. The bumps have potential to lower the material cost and improve the manufacturing yield associated with metal pillars.

## References

- [1]. C. Kocer. The thermal and mechanical performance of a vacuum insulated glazing. Glass Performance Days 2015 Conference Proceedings, (2015) 37-40.
- [2] S. Logunov , J. Dickinson, R. Grzybowski, D. Harvey, A. Streltsov, Laser-induced swelling of transparent glasses, Applied Surface Science, 257 (2011) 8883-8886.
- [3]. US patent 8,616,023 (2013). R. Grzybowski, S. Logunov, A. Streltsov. Raised features on transparent substrates and related methods.
- [4]. US patent 9,359,252 (2016). LT Masters and A. Streltsov. Methods for controlled laser-induced growth of glass bumps on glass articles.
- [5] US patent 9,346,710 (2016). R. Grzybowski, D. Harvey, A. Streltsov. Sheet glass product fabrication with growth-limited glass bump spacers.

# Analysis of the Uncertainties in Acoustic Insulation Performance of DGU: a Comparison in-between Products and Laboratories

Fabien Dalzin  
CRDC, Saint-Gobain

## Keywords

1=Acoustics 2=Insulation 3=Uncertainties  
4=Double-Glazing-Unit

## Abstract

Acoustic insulation performance is one of the main criteria for choosing Double Glazing Unit (DGU) product. Standardized acoustic measurements are performed in ISO10140-certified laboratories to determine the acoustic insulation of DGU. Nevertheless, measurement of a given DGU configuration in different ISO10140-certified laboratories does not lead to the same values of acoustic insulation. A question thus arises: is this difference due to the product uncertainties of a given DGU configuration and/or due to the laboratory uncertainties? This study aims at quantifying the relative impacts of both product and laboratory on the uncertainties in acoustic insulation measurement. Some testing campaigns in two different laboratories have been performed leading to the following main conclusions. No significant influence of the production line or the manufacturing site on acoustic insulation is found. Moreover, DGU elements like type of standard spacers or standard PVB interlayers provided by different suppliers, etc do not affect acoustic insulation. The major source of uncertainties actually comes from discrepancies between acoustic laboratories. Thus, some laboratories will measure higher acoustic insulation for a same DGU configuration, and this leads to a competitive advantage for both the acoustic laboratory and the DGU manufacturer that purchases the acoustic measurement to this laboratory. The latest modifications in EN ISO 10140 aim at decreasing the discrepancy of acoustic insulation values from different laboratories.

## Acoustic insulation of DGU

Acoustic insulation performance of Double Glazing Unit (DGU) needs to be performed in a dedicated acoustic laboratory. A DGU is described by the thicknesses of the two glass panes and the gas cavity. For example, 4(16)4 designates two 4-mm-thick glass

panes, 16-mm-thick air cavity apart. The acoustic laboratories considered in this study are certified against the standard ISO 17025 [1] and measurements are performed according to standards NF EN 10140 [2]. Glazing dimensions are 1480 mm x 1230 mm. The measured acoustic insulation of glazing is quantified as the Sound Transmission Loss (STL) in decibel (dB), for each third-octave-band frequency in the frequency range [100 Hz – 5 kHz]. As a reminder, audible frequency range of human ear is [20 Hz – 20 kHz], road traffic is a low frequency noise source around 200 Hz, whereas a baby's crying voice is a high frequency noise source around 2 kHz. An example of STL measured for a 4(16)4 sample is shown in figure 1. The higher the STL, the better the acoustic insulation of glazing.

The STL spectrum of DGU in figure 1 can be divided into three parts following the theory of double-leaf insulation detailed in [3-5]:

- At low frequencies around 200 Hz, the STL exhibits a dip. This insulation weakness, classically called "mass/spring/mass effect", is caused by a coupling between the two glass plates and air cavity.
- At mid frequencies in the frequency range [300 Hz – 2 kHz], the increase of insulation can be understood as a pseudo mass law.

The heavier the system, the better its acoustic insulation.

- A new STL dip occurs around 3 kHz. This phenomenon corresponds to the "coincidence effect" for which sound speeds in air and glass are identical. Energy transfer between the glass and the air is then optimal leading to insulation weakness.

This description can be generalized to any STL of DGU.

Three main indices  $R_W$ ,  $R_A$  and  $R_{A,tr}$  expressed in dB are derived from the detailed STL spectrum in order to get unified values of acoustic insulation for a given product. Their calculation in the frequency range [100 Hz – 3150 Hz] is described in ISO 717-1 [6]. Each of these indices highlights spectrum weighting at different frequency ranges.  $R_W$  index is the most common method of rating sound insulation in buildings and building elements.  $R_{A,tr}$  index should be used when the noise source in question is road traffic. For outside background noise it is better to use  $R_A$  index.  $R_A$  and  $R_{A,tr}$  indices are generally expressed from  $R_W$  index, by respectively adding from this index the negative correction factors  $C$  and  $C_{tr}$ .  $R_W$  is an integer number, whereas  $R_A$  and  $R_{A,tr}$  may be expressed with one decimal. Final DGU acoustic insulation is

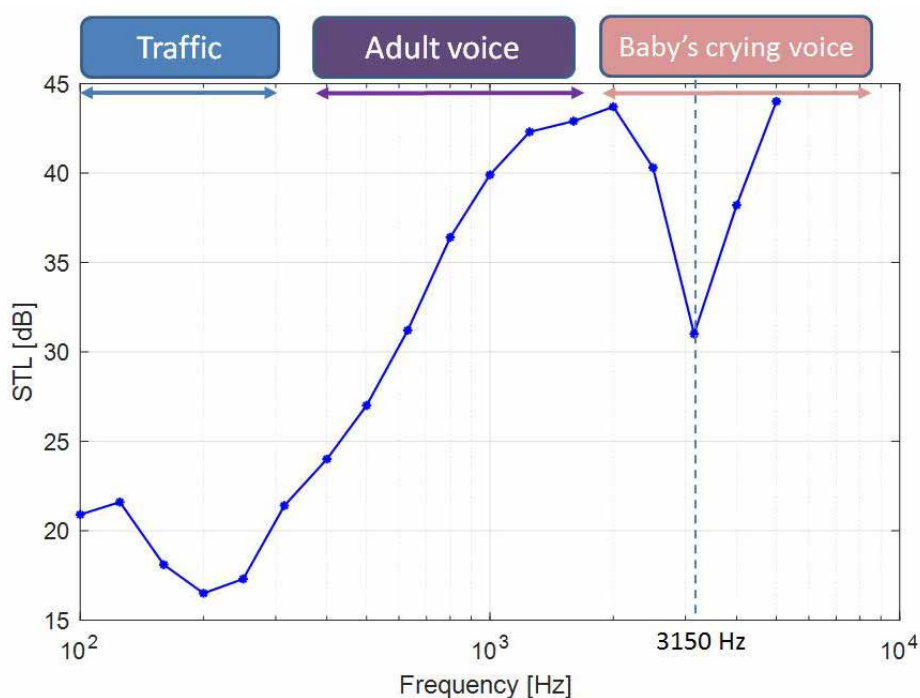


Figure 1 – Measured STL of a 4(16)4 sample.

expressed as follow:  $R_{W(C,C_{tr})}$ . As an example,  $R_{W(C,C_{tr})}=30[-1.0,-3.0]$  dB for a 4(16)4 DGU sample means  $R_W=30$ dB,  $R_A=29.0$  dB and  $R_{A,tr}=27.0$  dB.

DGU configurations can be easily ranked thanks to these three acoustic indices. For example, a 4(16AIR)10 sample exhibiting a  $R_{W(C,C_{tr})}=36[-1.0,-4.0]$  dB is more insulating than a 4(16AIR)4 sample with  $R_{W(C,C_{tr})}=30[-1.0,-3.0]$  dB. However, measurement of a same glazing sample in different laboratories does not lead to the same values of acoustic index. The discrepancy can reach 5 dB of  $R_{A,tr}$  variation for a given DGU [7]. The goal of this study is to determine the origin of this discrepancy between on the one hand, DGU uncontrolled variations of product element and manufacturing process and on the other hand, acoustic laboratories.

### Acoustic insulation variations due to DGU composition

The effects of DGU parameters, such as the origin of glass manufacturing site, the repeatability of production lines, the type of standard spacers, the supplier of standard PVB, are firstly investigated.

Tested DGUs are introduced in Table 1.

All the measurements are performed in a same ISO10140-certified acoustic laboratory.

Each considered parameter is being varied independently for the three following DGU

configurations 4(16)4, 4(10)10 and 44.2(16)4.  $\Delta R_W$ ,  $\Delta R_A$  and  $\Delta R_{A,tr}$  designate the maximal difference of acoustic indices between the samples for the variation of the considered parameter.

Obtained results are detailed in Table 2. We focus our analysis on the variation of acoustic index  $R_{A,tr}$ . The variation of 4(16)4 acoustic insulation coming from three different production lines of Saint-Gobain are  $\Delta R_{A,tr}=1.2$  dB. The supplier of standard spacer has also a negligible impact on 4(16)4 acoustic insulation with a difference  $\Delta R_{A,tr}=0.4$  dB for 4(16)4. The result of  $\Delta R_{A,tr}=0.2$  dB between samples manufactured by the same production line highlights a quasi-perfect process reproducibility. Regarding laminated DGU, the influence of standard PVB provider and PVB batches is analyzed. For both protect (PRO) and acoustic (SIL) PVB, there is no influence of standard PVB provider and PVB batch from a same supplier on the acoustic insulation of DGU. It may be concluded from this analysis that acoustic insulation does not depend on manufacturing process and type of product elements.

### Acoustic insulation variations due to acoustic laboratories

The same DGU samples are tested in another ISO10140-certified acoustic laboratory. Once again, no acoustic variation coming from the product has been observed in this second acoustic laboratory. However, the variations of acoustic insulation indices between the two laboratories are shown in Table 2. Maximal  $\Delta R_{A,tr} = 2.6$  is obtained for 44.2SIL(16)4. For 4(16)4 configuration,  $\Delta R_{A,tr}=2.4$  dB. The difference  $\Delta R_{A,tr}$  is higher than  $\Delta R_A$  and  $\Delta R_W$  leading to think that the main difference is mainly located in the low frequency range. This is indeed validated in Figure 2.

| DGU Configuration | $\Delta R_W$ [dB] | $\Delta R_A$ [dB] | $\Delta R_{A,tr}$ [dB] |
|-------------------|-------------------|-------------------|------------------------|
| 4(16)4            | 1                 | 1.8               | 2.4                    |
| 4(16)10           | 1                 | 1.8               | 1.8                    |
| 44.2PRO(16)4      | 1                 | 1.8               | 1.8                    |
| 44.2SIL(16)4      | 1                 | 1.8               | 2.6                    |

Table 2 - Variation of acoustic insulation indices obtained for the same DGU samples measured in two laboratories

| DGU       | Studied DGU parameter                | Number of tested samples | Sample size [L*h] |
|-----------|--------------------------------------|--------------------------|-------------------|
| 4(16)4    | From the same production line        | 4                        | 1480 mm x 1230 mm |
|           | From different manufacturing site    | 3                        | 1480 mm x 1230 mm |
|           | With different kind of spacer        | 3                        | 1480 mm x 1230 mm |
| 4(10)10   | From the same production line        | 5                        | 1480 mm x 1230 mm |
| 44.2(16)4 | With different protect PVB provider  | 2                        | 1480 mm x 1230 mm |
|           | With different acoustic PVB provider | 2                        | 1480 mm x 1230 mm |
|           | With different acoustic PVB batch    | 2                        | 1480 mm x 1230 mm |

Table 1 – Tested DGUs

| DGU       | Studied DGU parameter                   | $\Delta R_W$ [dB] | $\Delta R_A$ [dB] | $\Delta R_{A,tr}$ [dB] | Comments                     |
|-----------|---|-------------------|-------------------|------------------------|------------------------------|
| 4(16)4    | Repeatability in a same production line | 0                 | 0.4               | 0.4                    | 4 different samples          |
|           | Influence of manufacturing site         | 1                 | 1.2               | 1.2                    | 3 different production lines |
|           | Spacer type                             | 1                 | 0.6               | 0.4                    | 3 types of standard spacers  |
| 4(10)10   | Repeatability in a same production line | 0                 | 0.2               | 0.2                    | 5 different samples          |
| 44.2(16)4 | Protect PVB provider                    | 0                 | 0.4               | 0.4                    | 2 protect PVB providers      |
|           | Acoustic PVB provider                   | 0                 | 0.2               | 0.4                    | 2 acoustic PVB providers     |
|           | Acoustic PVB batch                      | 0                 | 0.2               | 0.2                    | 2 acoustic PVB batches       |

Table 2 - Effects of DGU parameters on the acoustic insulation indices. The measurements have been performed in a same acoustic laboratory.

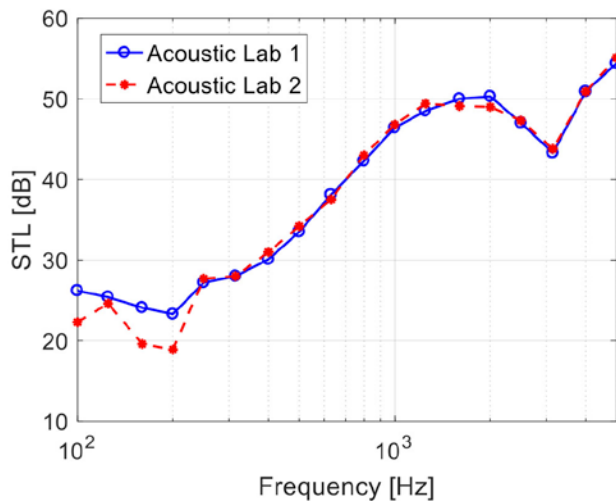


Figure 2 – STL obtained for a same DGU sample measured in two different acoustic laboratories. The main differences occur at low frequency (below 300 Hz).

This low frequency differences could be interpreted by the difference of room sizes between both laboratories. This room size difference implies that the room acoustic modes occurring at frequency lower than the so-called “Schroeder frequency”, estimated at around 300 Hz, will impact measurement values. Indeed, the main differences assessed between both laboratories occur below 300 Hz in figure 2.

### New standard updates of ISO 10140

An update of ISO 10140 has been published in November 2016 [2] in order to further reduce inter-laboratory uncertainty. Both acoustic laboratories analyzed in this study agree to improve their equipment in order to be in accordance with this update. According to this update, STLs of two referent DGUs, 6(16)6 and 44.2(16)10, have to be in a given range for each third-octave frequency band in order for laboratory to be certified against ISO 10140.

### Conclusion

No significant impact of site manufacturing, standard spacer type and standard PVB provider on acoustic insulation of DGUs has been found. The major source of uncertainty comes from the acoustic laboratory. The new version of EN ISO 10140 aims at decreasing this uncertainty.

### Acknowledgement

The completion of this study could not have been possible without the participation and the assistance of Gilles Battigelli, Fabien Bouillet, Christophe Cina, Laurent Courtin, Cécile Dalle-Ferrier, Marc Michau and Nicolas Nadaud.

### Bibliography

- [1] «ISO/IEC 17025:2005 General requirements for the competence of testing and calibration laboratories»
- [2] ISO 10140-1:2016 to ISO 10140-5:2013 «Acoustics – Laboratory measurement of sound insulation of building elements».
- [3] A. J. Tadeu et D. M. Mateus, «Sound transmission through single, double and triple glazing. Experimental evaluation» Applied acoustics, n°162, pp. 307-325, 2001.
- [4] C. Lesueur, «Rayonnement acoustique des structures», Eyrolles, 1988.
- [5] F. Fahy, «Foundations of Engineering Acoustics», Academic press, 2001.
- [6] «ISO ISO 717-1 Acoustics – Rating of sound insulation in buildings and of building elements – Part 1: Airborne sound insulation». 05 2013.
- [7] Analysis and conclusions of a Round Robin on glazings organized by joint WG CEN TC 126 129

# The Consequences of Panelisation on Visual Inconsistency of Curved Glazed Façades

Neesha Gopal  
Meinhardt Façade Technology

## Keywords

1 = Panelisation 2 = Cold bent 3 = Hot bent 4 = Visual distortion 5 = Quality 6 = Optimisation

## Abstract

Increasingly designers produce inspirational building images with seamless curved façades. The challenge is providing a visually consistent glazed façade allowing views out and light in with minimal distortion and interference. This study aimed to identify factors influencing panelisation of curved glazed façades, the subsequent impact on visual consistency and finally how quality may be improved. It illustrated that architectural division/panelisation for a curved façade can be achieved in different ways: triangulating flat elements; cold bending by forced or laminated methods or hot bending by radial or slump formed processes. The study appraised current specification methods and processes for production of flat and bent glass. This highlighted omissions and inconsistencies in standards/guidelines and inadequate visual assessment criteria. Defects/attributes for different glass and bending types vary and this can lead to visual inconsistency if different types are used simultaneously. Case studies illustrate the

challenges. A pilot survey to industry and designers was used to reaffirm the issues. A preliminary design roadmap was subsequently devised for informing design decisions. Finally, outline proposals for future investigations and studies to improve the overall specification, production and visual assessment of bent glass and curved glass buildings are identified.

## Introduction

This paper is based on my dissertation submission for the MSc in Façade Engineering at the University of Bath 2015. The purpose of the study was to illustrate that panelisation of curved glazed façades affects visual consistency. It identified potential visual differences between different types of glass and bending methods used and the particular attributes leading to visual inconsistency. The understanding and identification of visual manifestations was used to assist with the production of a preliminary design roadmap which illustrates how risk of visual inconsistencies might be better managed through an improved understanding of the characteristics of different glass types and bending methods.

## Curvature and Bending Types

The bending types generally considered for commercial buildings are cold bent using

forced or laminated methods or hot bent using radial/conical or free form slumped methods. These curved types are derived from flat glass initially. Visual issues arise when trying to achieve the panelisation by using different bending types together. Often the panelisation will also include areas of flat glass. The type of curvature can be grouped into certain families which for this study are defined as single point, 2 point radial/conical and doubly curved or free form curved. This categorisation informs the most appropriate bending type. Figure 1 indicates how differing panelisation can influence aesthetic. The starting point is flat glass. This will have a number of attributes depending on whether it is annealed or tempered. Further enhancements to the glass such as coating, laminating and insulating have further traits and then the process of bending will add further characteristics. The attributes for flat and bent glass identified are as follows:

|                      |  |
|----------------------|--|
| Visual defects:      | spots, scratches.  |
| Tempering defects:   | roller wave, edge lift, anisotropy.                            |
| Coating defects:     | soft/hard coating visual irregularity due to poor application. |
| Laminated defects:   | bubbles, delamination.   |
| Multi-layer defects: | lens effects.  |
| IGU defects:         | pillowing, Newton's rings, Brewster's fringes.                 |

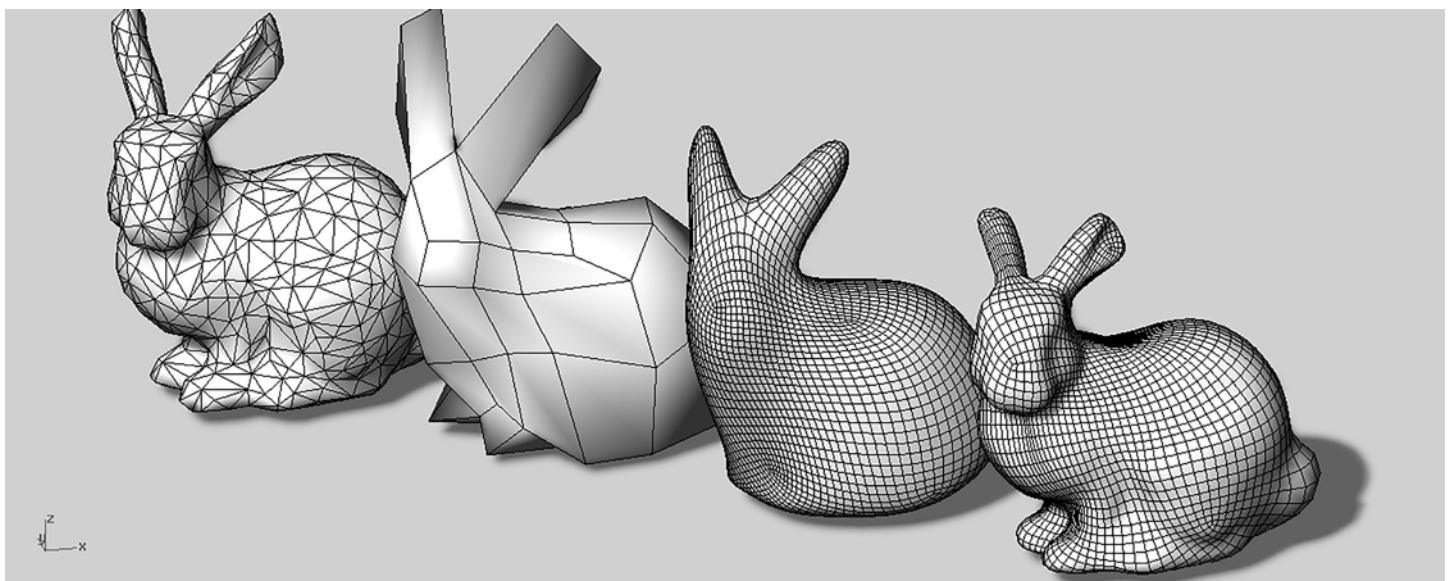


Figure 1: Examples of methods of panelisation. (grasshopper 3d, 2015)

Hot bent glass may be produced by radial forming on rollers or by slump forming on a mould. The following attributes can be considered:

Roll formed hot bent: Visual defects;

Tempering defects: Coating defects and discolouration of the coating: Laminated defects; Multi-layer defects; IGU defects.

Slump formed hot bent: Visual defects; Coating defects and discolouration of the coating: Laminated defects; inconsistencies due to mould marks. IGU defects.

Cold bent glass may be produced by forcing the flat glass into a form or by laminating the glass into a form. The following attributes can be considered:

Forced cold bent: Visual defects; Tempering defects: Coating defects: Laminated defects; Multi-layer defects; IGU defects; dishing/creasing due to over bending.

Laminated cold bent: Visual defects; Tempering defects: Coating defects: Laminated defects; Multi-layer defects; IGU defects; may suffer springback.

A review of the UK and European glass standards/guidance was carried out for flat and curved glass generally referred to in UK specification for visual/optical requirements and visual assessment. This was to identify if there were applicable criteria available and whether there were inconsistencies and omissions. The review confirmed that there is no consistent guidance for the different bent types and often the flat glass standards are reverted to.

The study of glass attributes for the flat and bent glass types was summarised:

- The production of flat glass and the enhanced processes affect visual characteristics.
- To achieve the building form different types of bending method may be required for the panelisation and each differ in performance and visual attributes.
- The visual characteristics vary between flat, cold bent and hot bent glass.
- The consequence of panelisation using several types is that visual inconsistency is more likely.
- There is very limited written guidance or industry standards to address the production and quality of curved glass or how to measure visual assessment.
- Visual acceptance criteria is subjective and not measurable.
- There is no guidance on managing the potential visual inconsistencies between different types.
- Different glass types are required to meet building performance – strength thermal acoustic requirements etc. This will impact the types possible to use.
- Good production methods and controlling

the tolerances of the material assist visual quality.

- The reflection properties of glass highlight visual inconsistency issues.

Examples of poor consistency between panels is shown in Figure 2 and 3



Figure 2: Distortion between curved panels



Figure 3: Inconsistency in coating colour

## Panelisation and Visual Consistency

The choice of the bending types can be considered against the key driver for the project – visual consistency/quality, cost and programme. The pilot survey carried out confirmed that preference for optimising visual consistency was to: re-panelise so all the glass is curved by the same method or keep the panelisation similar but optimise to reduce number of different types.

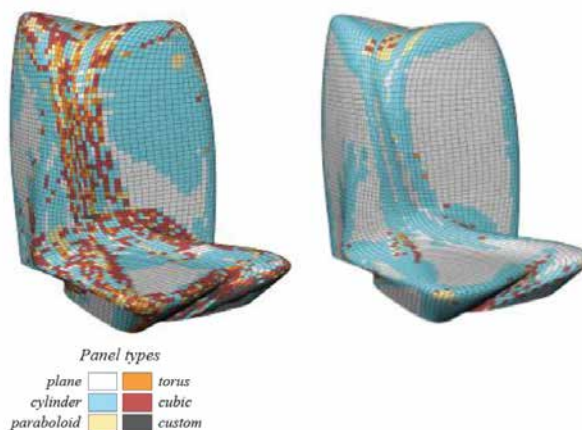


Figure 5: Interpretation examples of varying panelisation. National Holdings Headquarters Building, Abu Dhabi. (Stanford Graphics, 2015).



Figure 4: National Holdings Headquarters Building, Abu Dhabi. (Mathematics in industry, 2015)

Case studies show how the panelisation may be rationalised in order to reduce the bending types and therefore allow for better management of the visual consistency. Figure 4 is an example of a project in Abu Dhabi designed by Zaha hadid Architects with the rendering showing a seamless façade.

The project was not built, however a number of panelisation studies as illustrated in Figure 5 show how the panelisation might be rationalised.

## Panelisation Categorisation and Development of the Roadmap

Hypothetical examples considering panelisation categorisation were developed. These were used to inform the decision making process for a roadmap for improved specification of curved glass façades. The diagrams consider the panel geometry as well as the attributes due to the curving methods. Figure 6 illustrates the pros and cons of the different glass types when considering single bending with visual quality/consistency as the key driver. It shows which types of glass could be considered if visual quality/consistency is of low importance or high importance.

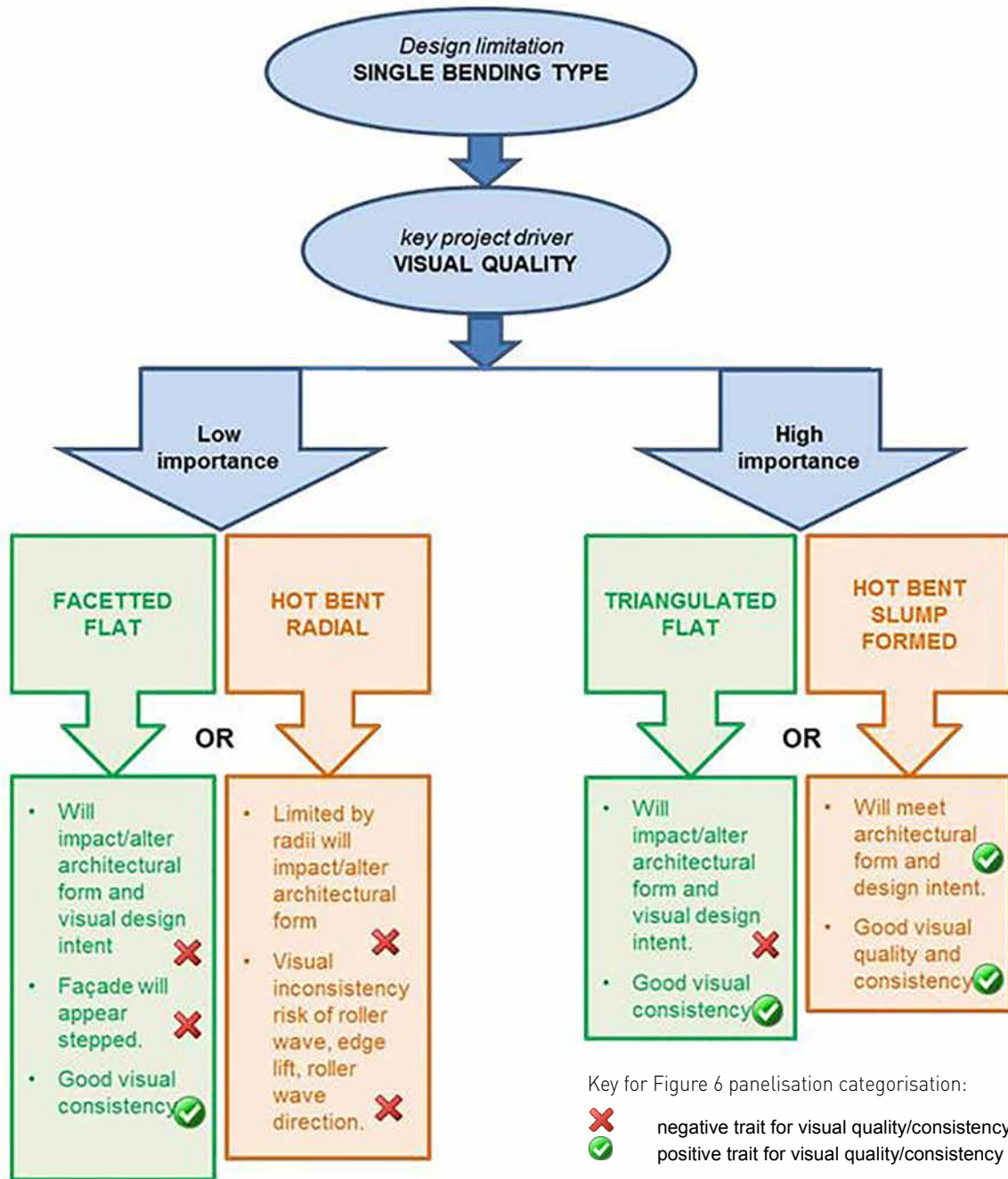


Figure 6: Single bending type with visual quality considered.

If more than one type is to be used, the types can be rationalised to have similar attributes as illustrated in Figure 7.

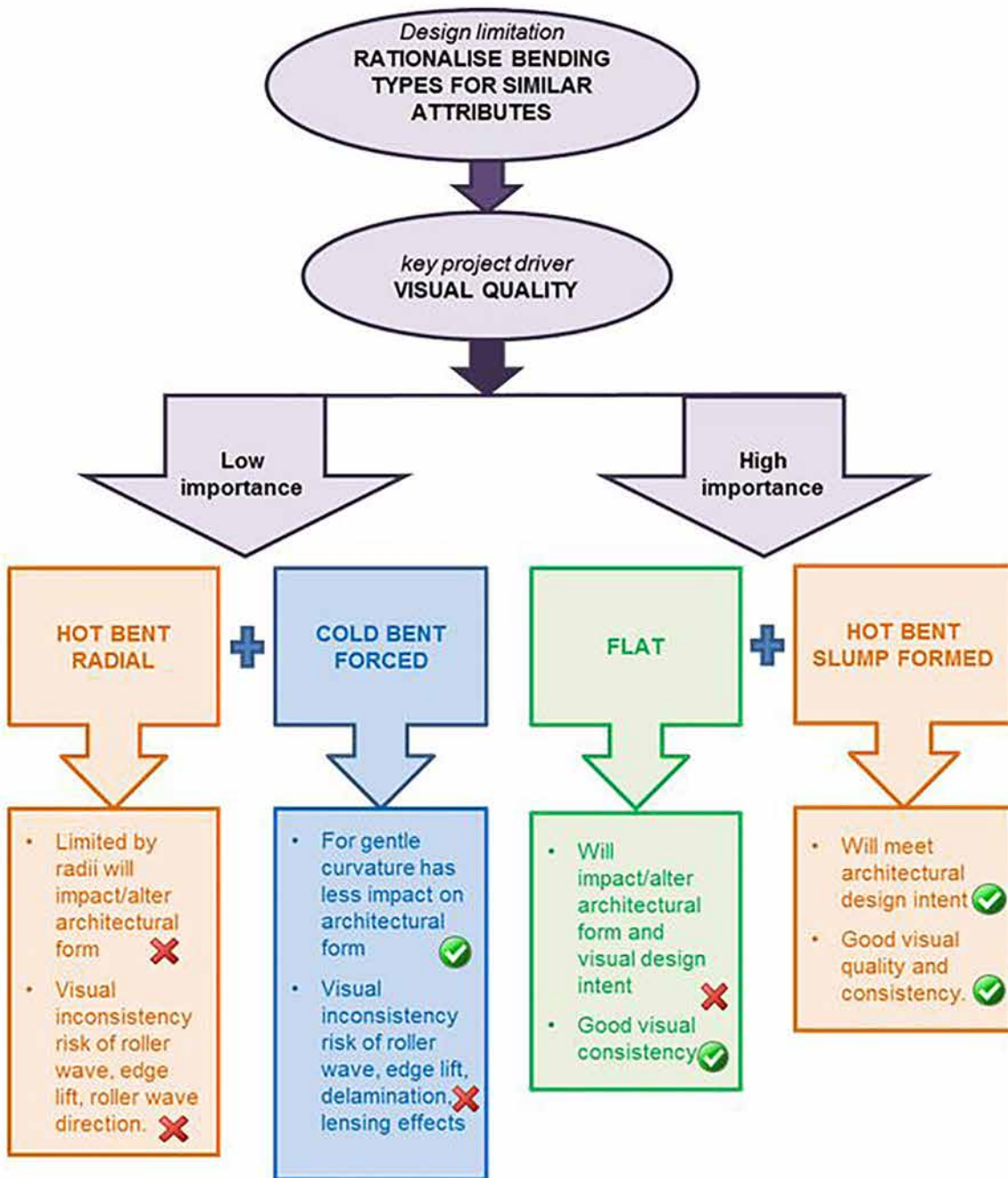


Figure 7: Rationalise bending types for similar attributes with visual quality considered.

The following preliminary road map for improved specification in Figure 8 was based on a typical design process flow and identified the key decision criteria that need to be considered during the stages.

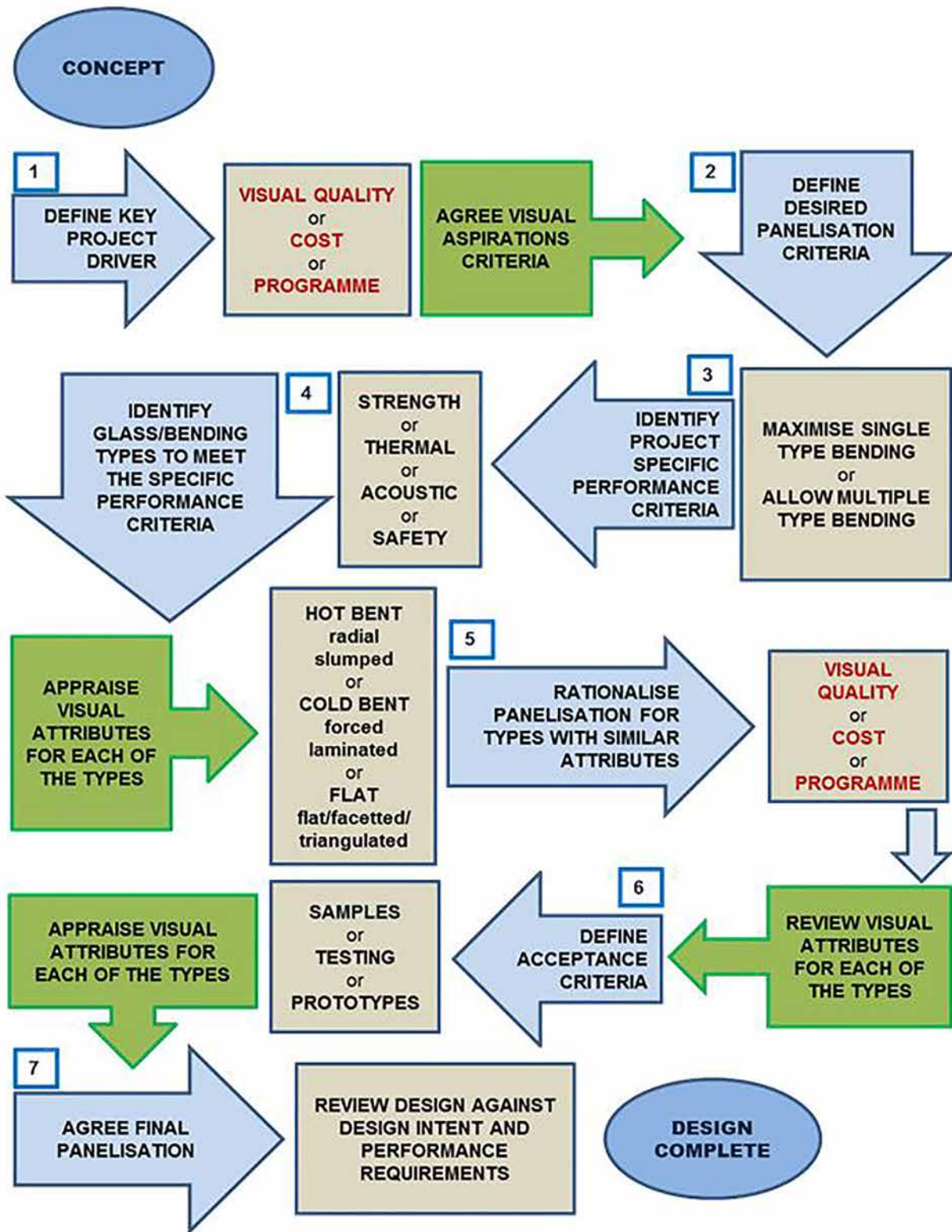


Figure 8: Preliminary road map parameters.

The map can be applied to the key performance criteria. The following example in Figure 9 is for limited budget as a key driver.

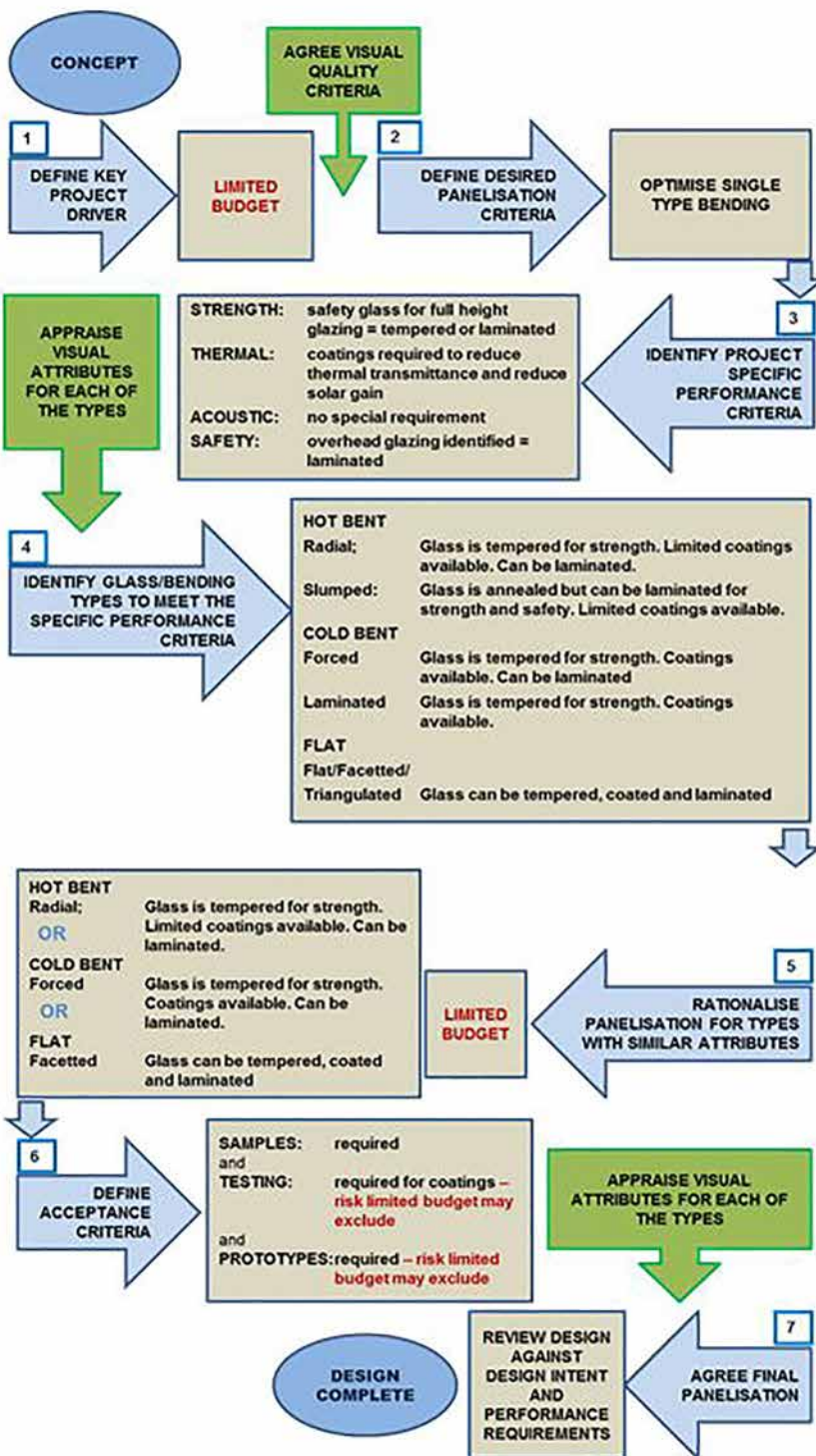


Figure 9: Limited budget is key driver

## Outcome of the Study and Future Developments

Using the knowledge gained from the study and the feedback from the survey, potential improvements to the specification of and visual quality of curved glass buildings were identified: These are summarised as follows:

- Improve standards/guidance.
- Ensure sampling and viewing in finished position.
- Agree tolerances and acceptance criteria early in the design stage.
- Improve production methods of hot bent glass.
- Improve durability and colour consistency of temperable coatings.
- Investigate bending methods used by other industries.
- Research new materials such as thin glasses that are being developed.
- Consider mathematical approach to resolving inconsistency issues.

# Approaching Hot Bent Annealed Glass

Dipl.-Ing. Timo Bühlmeier  
Josef Gartner GmbH

1=hot bent annealed glass  
2=curved glass 3=double curved glass  
4=complex geometry 5=testing 6=glass strength  
7= thermal loading 8=edge quality

## 1. Abstract

Contemporary architectural designs of transparent building skins with curved geometries challenge the industry. Approaches using geometry rationalization in combination with planar glazing, cold bent glazing or tempered hot bent curved glass are coupled with geometry constraints and are not always architecturally desired. Hot bent annealed glass opens up additional freedom in design, especially biaxial and more curvature in the building skin's glazing.

The paper will provide an overview of the currently applied engineering approach in the industry for curved hot bent glass in the absence of standards and codes. Design specifics of hot bent annealed glass applications will be highlighted and test results shown. It is an experience report of how innovative annealed curved glass applications can be realized with the currently available knowledge of research projects, engineering tools and project specific testing.

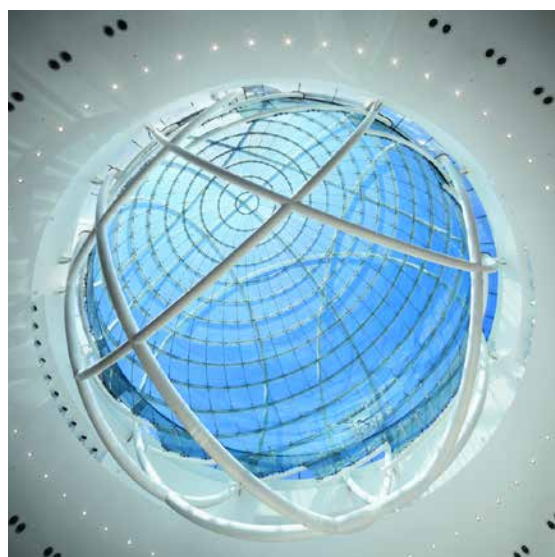


Figure 1 (left) Spherical hot bent annealed glass, Erin Mills Town Centre Mississauga (Canada) ©Tom Arban Photography



Figure 2 (right) Free-formed hot bent annealed glass, Musée des Confluences, Lyon (France) ©Karin Jobst

## 2. The need of hot bent annealed glass

Within the last years the façade industry is faced with the trend of curved building envelopes. Especially geometrically complex feature elements of buildings are predestined applications of curved glass with the intention to create unique and transparent enclosures (Figure 1 & 2). Even if recent technologies provide a broad range of opportunities to resolve curved envelopes, the use of hot bent annealed glass is essential to create extreme curvature as shown by the following limitations and approach-specifics:

1) Tempered curved glass: The overall glass sizes and producible radii are generally limited by the production process. Cylindrical curved glass is producible as heat strengthened glass and fully tempered glass if the radii are not too small (typically  $R > 1000\text{mm}$ ) and if the bending angle does not exceed certain limits [1]. Meanwhile double curved glass can also be produced as thermally tempered glass for large scale radii by few suppliers. The tempering process of curved glass products can be realized by adjustable rollers. Nevertheless, quenching and temperature control poses an increased difficulty to the production process compared to flat glass products. Therefore, geometry and size

limitations should always be verified in close collaboration with the glass supplier. Local distortions through processing reduce the visual glass quality which is mostly lower compared to annealed curved glass. Soft coatings and frits are typically solely feasible on the concave surface of curved tempered glass products (hard coatings also on the convex surface).



Figure 3 Double curved insulated glass units made of hot bent annealed glass, Concert Hall Elbphilharmonie, Hamburg (Germany)



Figure 4 Cold bent insulated glass units (4th point out of plane), Singapore Chancery, New York (USA)

2) Cold Bending (including cold warping): Typically planar tempered glass panes will be forced in the required shape on site. The bending process causes additional constraints in the glass built-up; consequently only low curvatures can be achieved (Figure 4). The degree of bending is either limited by additional long term stresses introduced in the glass, the mechanical and tightness properties

of the deformed edge seal in case of insulated glass units or by the mechanical properties of interlayer connections in the case of glass laminates. Additionally, geometry and stability effects need consideration using the cold bending approach.

Manufacturing of cold bending during lamination is a technology which also allows only for low-curvature glass [2] and is a factory-made product compared to cold bending on site. Due to the technological complexity (e.g. spring back effect after cold bending and lamination) the amount of suppliers is limited. The feasible degree of curvatures of both cold bending technologies, on site or factory-made, is within the same range. The major benefits of cold bending approaches are the high optical quality and the freedom of feasible glass configurations (frit, coating, etc.). General producibility limitations are similar compared to flat glass products.

3) Geometry Rationalization and Methods of Form Finding: Typically the approaches are applied to approximate and simplify the given curved geometry, to transform double-curved glazing elements into single curved or planar glazing elements. In the context of big scale projects those methods are essential due to their economic impact. However, the methods imply geometry and mesh modifications which are occasionally in conflict with the envisioned design intent and not desired for feature façade elements.

Chemically strengthened glass should also be mentioned at this point, although it is currently still a niche product within the building industry. The penetration of chemical tempering process affects only a very thin layer; consequently chemically strengthened glass is very sensitive to scratches and should be protected by adequate measures. All the before mentioned boundary conditions require consideration while finding reasonable project-specific approaches for curved geometries. The nearly limitless freedom in shape (spherical, paraboloid, hyperboloid,

etc.), especially bending along several axes are the driver to apply hot bent annealed glass products (Figure 3 & 5). However, a high visual quality is also achieved by omitting quench marks and distortions known as drawbacks from the tempering process. Additionally, the gravity bending production process of annealed glass in moulds allows bending in couples. The result is that several curved glass panels fit perfectly together (also different glass thicknesses).

Given the brittle failure behavior of hot bent annealed glass, the whole design, fabrication and installation process requires special attention and a holistic approach. The complexity is increased by the absence of product standards respectively application standards. Fundamental aspects and findings experienced in the last Josef Gartner projects with the product are explored in the present paper.

### 3. Approach to hot bent annealed glass

#### 3.1 Design & Engineering

The structural behavior of curved glass elements differs tremendously from flat glass elements. Arching and membrane effects are triggered without previous deflections under loads [3], creating very stiff and deformation resistant elements. However, the edges of curved glass elements are mostly prone to the main tensile stresses. The load paths are very similar to non-membrane elements respectively structural glass elements, for instance, in the case of a spherical curved annealed glass panel. Figure 6 shows the main tensile stresses at the free glass edges, an area with limited strength caused by edge flaws and the lack of residual compressive stress. Edge flaws are caused by edge processing and other mechanical damages during the life time of such glazing elements.

Depending on the stress distribution, the edges of curved annealed glass are often the

origin of fracture [4] as shown in Figure 7. The critical flaw initiates failure by propagation of an initial crack under tensile stresses [8]. The context of dealing with structural glass elements combined with the low strength of annealed glass products indicates already the evidence for special attention. Matters are complicated by the fact that currently most frequently used design methods (DELR and GFPM) do not provide verification formats for edge strength under in-plane loads [9]. Additionally, the actually existing edge flaw population is not considered in those methods. Even if using current standards, there is a lack of information on the material resistance side. The face surface strength and the edge strength of curved annealed glass are insufficiently documented in recently applied standards. However, the "Guidelines for Thermally Curved Glass" (Bundesverband Flachglas) [10] provide recommendations for reduced characteristic strength values underneath other fundamental orientation in the use of curved glass throughout all project stages. Herein the characteristic surface strength is given with  $f_k=40N/mm^2$  and the characteristic edge strength with  $f_k=32N/mm^2$ , verified by test series [10]. Nevertheless, if curved glass products without National Technical Approvals are used, it is recommended to verify the characteristic bending tensile strengths beforehand by testing [10].

But also the load side requires specific consideration. It could be observed that specific design loads like temperature loads or constraint forces induced by building movements or support conditions play a decisive role designing curved annealed glass elements (apart from impact loads and concentrated loads). It comes along that those loads need to be combined with general building design loads (dead load, wind load, snow loads, etc.) leading to further accumulation of tensile stresses mostly close to the curved glass elements edges. Due to those reasons it is crucial that



Figure 5 Double curved hot bent annealed glass, Baha'i Temple of South America, Santiago de Chile (Chile) © Jose Luis Stephens

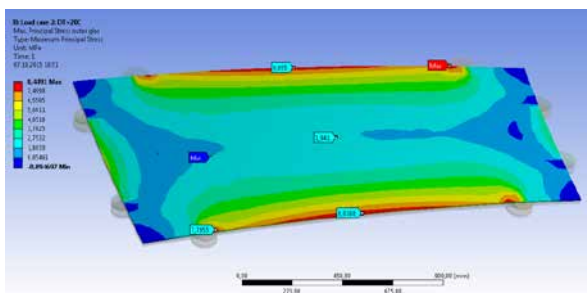


Figure 6 Edge Stresses spherical curved laminated glass (hot bent annealed) under thermal loading  $\Delta T [6]$

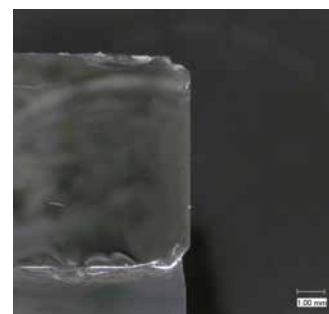


Figure 7 Microscopic view of failure origin [6]

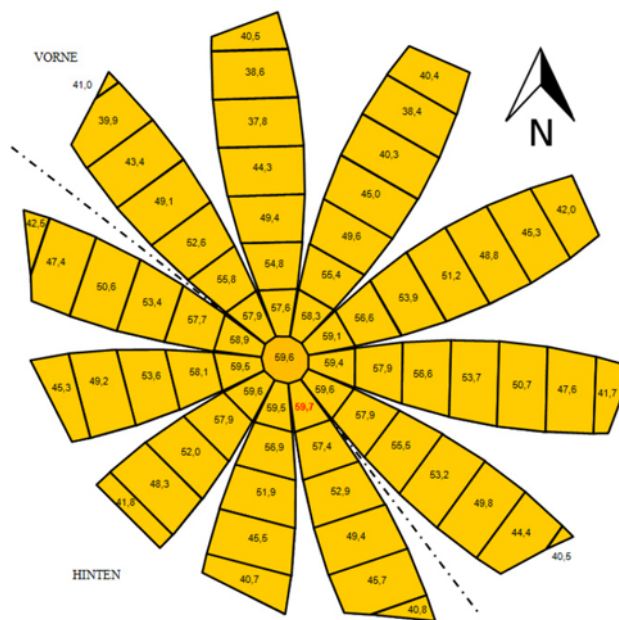


Figure 8 (left) Glass surface temperatures determined by dynamic building simulation [7]

temperature data of the glass surfaces are available. Dynamic building simulation using representative weather data including spectral data of solar radiation can provide the necessary information. Metallic coatings and fritted glass surfaces have particular significance in this context as they induce long-wave radiation exchange between glass surfaces. The more diverse the thermal outflow of a heated up glass element is, the higher are the temperature differences on the glass surfaces [7]. Consequently the thermal stress within the curved annealed glass element is higher. Figure 8 shows the surface temperature results of a dynamic building simulation.

In any case substructures serving as support for the curved annealed glass elements must be engineered under the perspective of possibly occurring constraints. Glass tolerances (increased for curved glass [10]), substructure tolerances, building movements and deflections of adjacent structural elements must be analyzed precisely as they might cause cold bending or in-plane forces in the curved annealed glass elements. Such additional forces should be avoided respectively minimized as far as possible by using appropriate support configurations of the glazing, as shown exemplary in Figure 9. Even constraint forces induced by climatic loads, typically occurring in curved double glazed units, can be reduced considerably by using flexible spacer systems [12]. Load conditions impacting the curved annealed glass infill elements require consideration within the structural glass analysis, including appropriate

material idealization. Spring stiffnesses or material models should consider the real support situation and load paths precisely [3].

### 3.2 Testing

The general approach to determine the edge strength is a four-point-bending test set-up. However, the EN ISO 1288-3 standard is solely valid for flat glass products. For this reason the research project PRÜFgbGLAS currently develops a testing method for cylindrically curved glass [13]. Geometries other than cylindrical can be tested by a simplified approach. The glass strength is determined either by the four-point-bending test set-up or the ring-on-ring-test with flat test specimens passed through the thermal cycles of the bending process of curved glass. Using the ring-on-ring tests allows separating the surface strength from the edge strength to determine impacts of the gravity bending process itself [4]. To examine residual surface stresses induced by insufficient or inhomogeneous heating after bending of hot bent annealed glass, photo elastic residual stress measurements [5] or cutting tests can be applied.

Nevertheless, for some cases it is beneficial to perform real size tests of hot bent annealed glass elements including the envisioned support situation, especially for a better understanding of the post-breakage behavior. Accompanied by the tests described above, microscopic and fractographic analysis provide further in-sights of the material quality and strength (e.g. fracture mirrors, failure origin, edge chipping, etc.) [6].

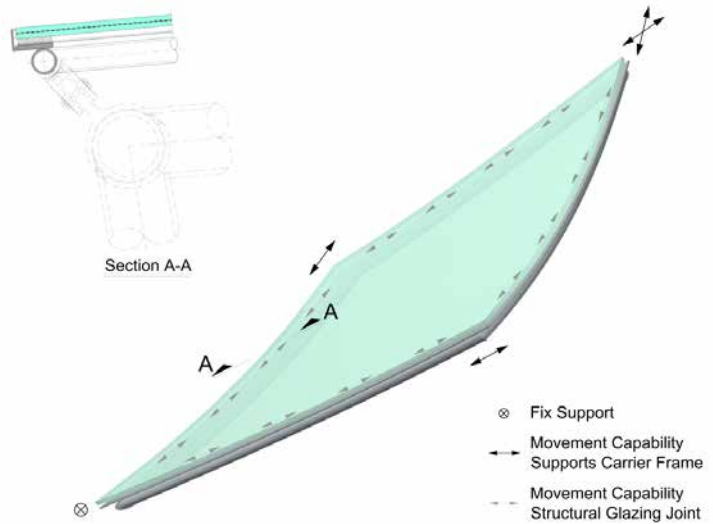


Figure 9 (right) Schematic example of the support situation of hot bent annealed glass (freeform geometry) with movement capability precautions

### 3.3 After Manufacturing

Once the hot bent annealed glass panels leave the production, still extreme caution is required. Already packaging and transportation need to consider the brittle behavior of the material. Load cases exceeding the planned conditions, from production up to the final boundary conditions on-site, must be omitted. Especially the edges of hot bent annealed glass should be protected sufficiently. Eventually occurring edge chipping might reduce the edge strength tremendously (refer to Chapter 3.1). However, also surface scratches should be avoided during the complete lifetime of annealed glazing elements.

## 4. Findings from various testing

To quantify some of the major influencing, project-specific parameters on hot bent annealed glass different testing series were executed as described below. Furthermore the aim was to establish a reliable planning basis in the partly non-regulated normative situation.

### 4.1 Glass surface strength depending on individual processing

Specimens of different glass suppliers and different base glasses (GS-1, GS-2 and GS-3) were tested to ensure the appropriate product quality of the hot bent annealed glazing used in a project. Concentric ring-on-ring tests were carried out to investigate the bending surface strength. "To quantify the influence of the individual processing steps both acid-etched glasses, non-etched glasses and glasses which passed the hot bending process (heat-up/cool-down process) were investigated" [7].

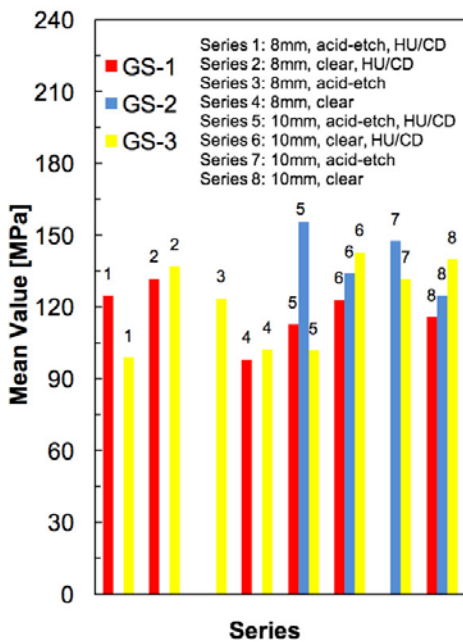


Figure 10 (left) Comparison of mean values of surface strength [17]

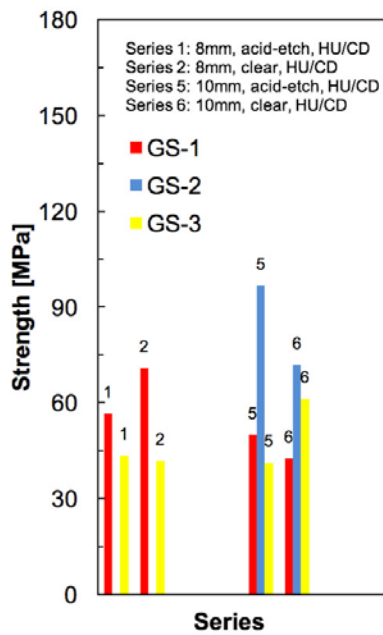


Figure 11 (right) Comparison of characteristic surface strength between series GS-1, GS-2 and GS-3 [17]

Test values were adjusted to the log-normal distribution (providing typically the best fit to evaluate material strength), the prognosis and confidence intervals for the regression were calculated (characteristic strength calculated based on 5%-quantile with a confidence level of 95%) [7].

The following findings could be observed in [17]: Depending on the source the results spread in a certain range. Both the mean values (Figure 10) and the characteristic

strength values (Figure 11) obtained by testing vary. The most promising results could be determined for the GS-2 series as shown in Figure 11. Both the GS-2 series as well as the GS-1 series are in accordance with the requirements of the relevant product standard EN 572-1 [14]. The herein postulated float glass bending strength is defined with 45MPa. Substantial influences on the glass strength caused by acid-etching or by thermal cycles of the hot bending process could not be indicated.

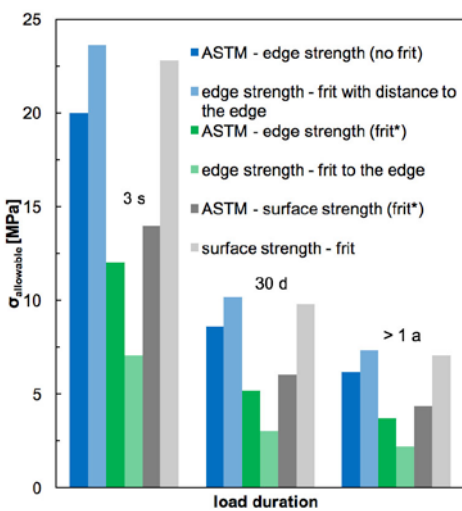


Figure 12 (left) Comparison of the allowable design stress according to ASTM 1300 [16] design methodology compared to the values determined by the bending test [6] Note: (frit\*) = values not given in ASTM 1300 [16] but calculated assuming a strength reduction of 0,6 for fritted glass compared to ASTM 1300 [16] values.

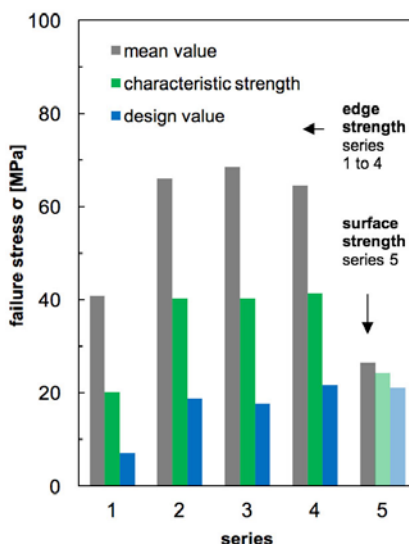


Figure 13 (right) Comparison of the mean strength, the characteristic strength and the design strength of the different test series

Photo elastic residual stress measurements and tests of the fracture pattern were performed in other test series on full size hot bent annealed glass elements to gain further knowledge of residual surface stresses caused by the annealing process. Measured residual surface stresses are in the range of conventional flat annealed soda-lime silicate glass and did not show irregular crack patterns [5].

#### 4.2 Edge Strength and Frit

Ceramic frit colors applied occasionally to glass surfaces pose additional challenges to hot bent annealed glass products. Beside the reduced characteristic bending strength of fritted annealed glass, which is not even regulated in product standards for planar glazing [15], dark frit colors may trigger thermal stresses by solar radiation. Some test series including subsequent evaluation were executed to compare the edge strength of polished edges with frit to the edge (series 1), polished edges without frit (series 2 & 3), grinded edges with surface frit in a distance to the edge (series 4) and the surface strength (series 5) [6]. All test specimens (dimension: L= 180mm, h= 32mm, t=7,8-8mm) went through the identical production process usually applied for hot bent annealed glass. Series 1 to 4 were examined in 4-point-bending-test and series 5 in a concentric ring-on-ring-test. In the statistical analysis the measured values of the testing were adapted to the Weibull distribution [6] which considers next to the material strength also other parameters (e.g. size effects). The design strength was calculated corresponding to a failure probability of 1/1000 according to the ASTM E 1300 standard [16].

Based on the results of Figure 12, the following conclusion could be drawn by [6]: The characteristic edge strength of specimens with frit was 50% less, compared to the characteristic edge strength of specimens without frit. The allowable edge stresses determined by tests are about 40% of the allowable edge stresses after ASTM 1300 (glass without frit) [16]. The characteristic edge strength of test specimens without frit is in the same range as test specimens with surface frit in a distance to the edge. The mean value of the edge strength (Figure 13) is significantly higher compared to the mean value of the surface strength. Nevertheless, considering the big variation of test values, the characteristic edge strength is lower. The test series above clearly indicate the required necessity of precise investigation and caution designing the edges of hot bent annealed glass elements. The following influences on the final edge strength are

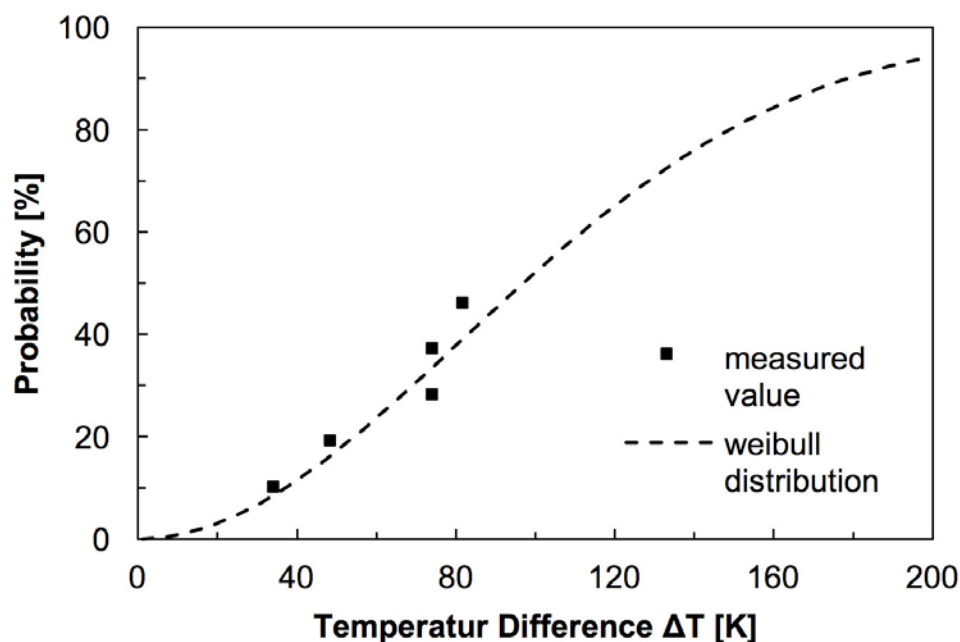


Figure 14 (left) Comparison between test data and Weibull distribution [11]

known: Edge finishing (cutting, grinding, polishing, etc.) [19], length of the edge (flaw population), load duration [20] and residual stress distribution. Frit seems to disturb the cooling process during glass production which reduces the final glass strength [15] [21].

#### 4.3 Thermal loading $\Delta T$

In many cases different surface temperatures on the inside surface and the outside surface of the glazing, expressed as thermal loading  $\Delta T$ , are the decisive criteria for the design of hot bent annealed glass elements. To predict influences of the above shown low edge strength of fritted glass, in combination with uneven thermal loading  $\Delta T$ , some element tests with different glass configurations were performed with the following test set up [11]: The interior glass surface (installed on the top) was heated by custom made silicone rubber heaters attached to the glass surface. The outer glass surface (bottom side) was cooled by a fan and sprinklers. The thermal stresses were measured by strain gauges (Figure 15). Different glass configurations comparing fully fritted glass, edge delete frit glasses and clear glasses (glass built up 3x8mm annealed double-curved hot bent glass with 1,52mm SGP Interlayer, frit #2, low-e coating #6) were investigated under various uneven thermal loading conditions  $\Delta T$ .

The following findings could be observed by [17] [18]: Nearly all glass breakages in the element tests started from the edge of the fully fritted glass. The measured stresses principally agree to the calculated stresses (by FEM Analysis). Breakages occurred solely for glasses with full frit to the edge on position

#2. The test results were fitted to the Weibull distribution to predict the failure probability as shown in Figure 14. A temperature difference of  $\Delta T=10$ [K] between exterior glass and interior glass showed a failure probability of 0,8 percent ( $\Delta T=21$ [K] showed a failure probability of 3,4 percent). Based on the temperature results of previous dynamic building simulation failure probabilities of the glazing can be determined in dependence on its orientation. In consequence, the failure probability obtained by evaluation of the tests described above, partly exceed the typically applied failure probabilities according to ASTM 1300 [16]. Such findings require modified glass configurations, or a mutually agreed shared risk policy for projects dealing with the material hot bent annealed glass.

#### 5. Conclusion

As long as there are no product codes and standardized test codes in place, project-specific testing will be crucial to establish a reliable basis for the design of projects using the highly sensitive material hot bent annealed glass. In several testing series for hot bent annealed glass, results show a huge variation in stress resistance, mainly depending on the glass configuration and the quality of the annealed curved glass product itself. A continuous control of the material quality and the production process is absolutely necessary, especially regarding edge strength with its fundamental role in the context of the glass fracture mechanics. Furthermore, hot bent annealed glazing requires very careful design and engineering. Given its brittle material



Figure 15 (right) Test setup of the component tests [18]

behavior and the absence of engineering standards, a holistic approach considering any boundary condition is essential to realize geometrically complex building envelopes. In general, a user friendly design method considering the material quality based on previous flaw detection as well as specific load conditions should be implemented.

#### 6. References

- [1] Haldimann M., Luible A., Overend M.: Structural Use of Glass, International Association for Bridge and Structural Engineering, Zürich, Switzerland, 2008.
- [2] Fildhuth T., Knippers, J.: Interior stress monitoring of laminated cold bent glass with fibre bragg sensors, Challenging Glass 4 & COST Action TU0905 Final Conference EPFL-Louter, Bos, Belis & Lebet (Eds), Lausanne, Switzerland, 2014
- [3] Schuler C., Elstner M., Illguth M., Stief S., Lorenz A.: Application of curved glass in architecture; Stahlbau Volume 81; Issue 3, March 2012
- [4] Hof P., Oechsner M.: General technical approval for curved annealed and curved tempered glass in Germany, Proceedings of Cost Action TU0905 Mid Term Conference on Structural Glass, Porec, Croatia, April 2013
- [5] Schneider J., Hilcken J.: Test report 1163/2017.07.01 30th January 2017, Heusenstamm, Germany
- [6] Schütz Goldschmidt Schneider – Ingenieurdienstleistungen im Bauwesen GmbH
- [7] Post H.: Report Dynamic Building Simulation, b+e Consulting Engineers for Building Climate and Energy Schemes, January 2016, Munich, Germany
- [8] Lindqvist M.: Structural Glass Strength Prediction Based on Edge Flaw Characterization; These No 5627 EPFL École Polytechnique Federale de Lausanne, 22. February 2013, Lausanne, Switzerland
- [9] Haldimann M.: Fracture Strength of Structural Glass Elements – Analytical and Numerical Modelling, Testing and Design, These No 3671, EPFL, Lausanne, Switzerland, 2006.

- [10] Bundesverband Flachglas, BF Merkblatt 009/2001, Guidelines for Thermally Curved Glass
- [11] Schneider J.; Hilcken J. Hagen B.: Test Report 1163/2016.44.02, 16th March 2017; Heusenstamm, Germany
- [12] Wellershoff F., Förch M., Minasyan, M.: Impact of Foam Spacer Systems on curved double glazed units under climatic loads; Engineered Transparency – International Conference at Glasstec, Düsseldorf, Germany, 2014
- [13] Bukieda P, Engelmann M., Elstner M., Weller B.: Research and Standardisation of Four-Point Bending Test for Thermally Curved Glass, Glasbau 2017, Dresden, Germany
- [14] EN 5721:2004 German version, Glass in building Basic soda lime silicate glass products Part 1: Definitions and general physical and mechanical properties
- [15] Weller B., Nicklisch F., Thieme S., Weimar T.: Glasbau-Praxis Konstruktion und Bemessung, 2010
- [16] ASTM E 1300 -04, Standard Practice for Determining Load Resistance of Glass in Buildings, July 2004
- [17] Schneider J.; Hilcken J.: Test Report 1119/2015.14.02, 28th April 2016, Heusenstamm, Germany
- [18] Schneider J.; Hilcken J., Müller Braun, S.: Test Report Nr. 102.01.16 TU Darmstadt - Institute for Structural Mechanics and Design (ISM+D), 15th April 2016; Darmstadt, Germany
- [19] Kleuderlein J., Ensslen, F., Schneider J.: Investigation of edge strength dependent on different types of edge processing, Proceedings engineered transparency, International Conference at glasstec, 21 and 22 October, Düsseldorf, Germany, 2014.
- [20] Vandebroek M., Lindqvist M., Belis J., Louter C.: Edge Strength of cut and polished glass beams, Glass Performance Days, 17 -20 June, Tampere, Finland, 2011
- [21] BergersM., NatividadK.; MorseS. M.,Scott NorvilleH.: Full scale tests of heat strengthened glass with ceramicfrit, Glass Structures &Engineering, Volume 1, Issue 1, June 2016"

# Free-Form Shape Cold-Bent Structural Silicone Glazed Façades - Design Concept and Challenges

Benjamin Beer  
 Technical Director  
 Meinhardt Façade Technology  
 Dubai, United Arab Emirates

## Keywords

1= Structural Silicone Glazing 2= Free-Form Cold-Bending 3= Single Corner Cold-Bending 4= Warp 5= Engineering Stress 6=FE Stress

## Abstract

Free-form cold-bent structural silicone glazed façades open the door to a new world of options for cost effective two-way curved and free-form shape façades. The design of the primary and secondary seal structural silicones is however a challenge as no design standards are available; even most of the major silicone suppliers currently do not have clear design guidelines for free-form cold-bent structural silicone glazed façades. Following up on the previous Glass Performance Days paper by the author with focus on the "single corner cold-bending" [1], this paper focusses on the "free form shape cold-bending" and presents a new design concept for the structural silicone design. In addition, various graphs are shown to provide theoretical background on façade panelisation options, various cold-bending geometries (e.g. spherical, anticlastic and concave/convex free-form), post-cold-bending glass edge rotation and silicone stress models for different cold-bending/edge warp modes.

## Introduction

After a series of realised projects, the so called "Single Corner Cold-Bending" process (Figure 02) became established within the façade industry to provide better architectural appearance compared to the "Fish Scale" principle (Figure 01). Taking the next step in the cold-bending process, the first façade using the new "Free-Form Cold-Bending" process is currently being installed in Dubai (Figure 03). Comparing to the panelisation options Fish Scale [outwards, centre-point and inwards] and the option Single Corner Cold-Bending" as explained in Figure 01, the Free-Form Cold-Bending option provides the best approximation to a perfectly curved façade – however with the downside of high complexity

| System Illustration | Fish Scale<br>(Glass panel flat, framing members inclined and linear) |  | Cold-Bent (Warped)<br>(Glass panels warped, framing members inclined and linear or curved) |  |
|---------------------|---|--|--|--|
|                     | Outwards Fish Scale   | Centre-Point Fish Scale                            | Single Corner Cold-Bending   | Free-Form Cold-Bending                                     |
| A)                  | Medium impact<br>(Fish scale triangles visible)                       | Low impact<br>(Small fish scale triangles visible) | Low impact<br>(glass panels warped)  | No impact<br>(glass panels warped)                         |
| B)                  | No impact<br>(glass panels flat)                                      | No impact<br>(glass panels flat)                   | High impact<br>(glass panels warped)   | Very high impact<br>(glass panels warped, mullions curved) |

Notes: A) Impact on architectural appearance (close to perfect curvature), B) Impact on structural silicone design (long term stresses)  
 For "Shifted Louvre" and "Inwards Fish Scale" panelisation options, see [02] © 2017, Meinhardt Façade Technology, Benjamin Beer

Figure 01: Comparison of Fish Scale and Cold-Bending panelisation options



Figure 02: Single corner cold-bending structural silicone glazed façades, Credit Libanais, Beirut



Figure 03: Free-form shape cold-bent structural silicone glazed façades (partially hot bent-glass is used)

in the structural silicone design. When considering the structural silicone design and guidance for a stress based design, both cold-bending processes mentioned above are not covered by national or internal design codes or standards – showing the need for in-depth research and discussions between industry experts. Whilst the single corner cold-bending process was discussed by the author in previous publication [01], [02]

including a proposal for a design concept, this paper focusses on a new structural silicone design concept for free-form shape cold-bent façades. This design concept uses a stress approach "FE Stress" (Finite Element Stress) vs. "Engineering Stress", in which a FE analysis with hyperelastic material constitutive modelling has been implemented for a reference project (Figure 03).

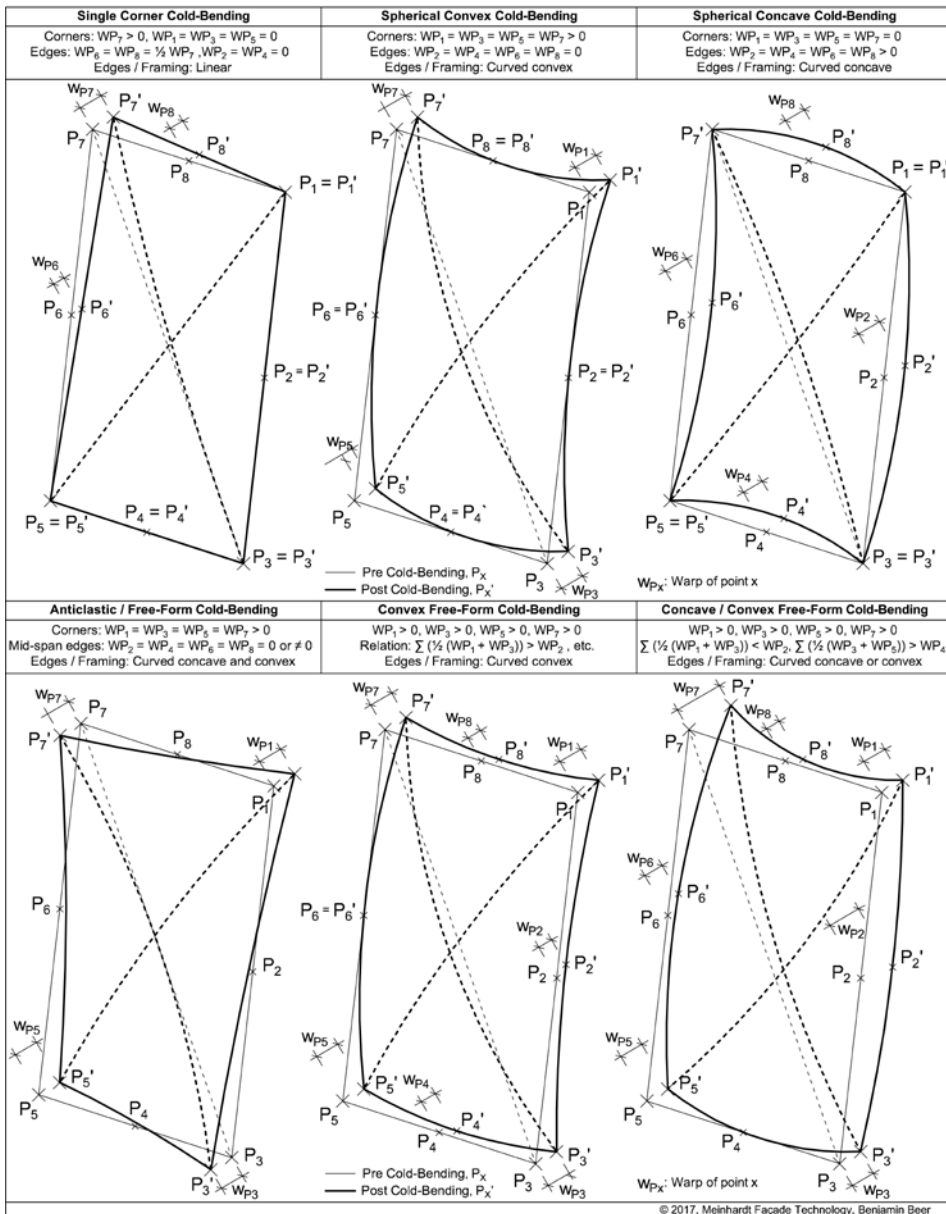


Figure 04: Principle overview of the most common cold-bending geometries

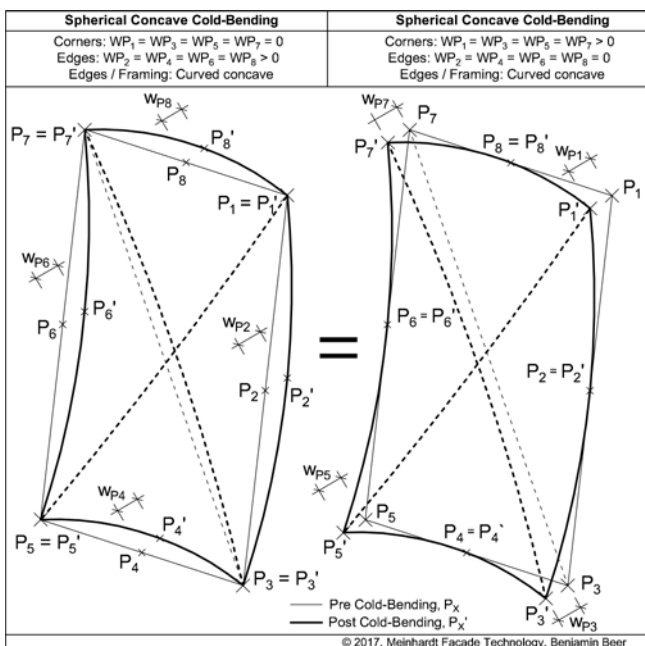


Figure 05: Inwards and outwards bending option for spherical concave cold-bending

## Single Corner Cold-Bending vs. Free-Form Cold-Bending

Figure 04 provides an overview of typical cold-bending geometries. The single corner cold-bending is the most common geometry being realised on various projects over the last approximately 10 years. Here, the aluminium framing members are linear and the glass is produced flat. All other cold bending geometries including spherical convex, spherical concave, anticlastic free-form, convex free-form and concave / convex free-form are based on curved framing members. The amount of warp at each corner ( $P_1, P_3, P_5$  and  $P_7$ ), at centre of the edges ( $P_2, P_4, P_6$  and  $P_8$ ) and the relation between the warp data ( $P_1$  to  $P_8$ ) defines the cold-bending geometry.

Most cold-bending geometries have an inwards and outwards mode as shown in Figure 05. Swapping in between these two modes can be done by exchanging the warp value of the corner points ( $P_1, P_3, P_5$  and  $P_7$ ) with the warp values of the centre of edges points ( $P_2, P_4, P_6$  and  $P_8$ ). The choice between inwards or outwards mode is usually dictated by the position of the framing members, typically located on the building's inside.

## Cold-Bent Structural Silicone Glazed Facades – Silicone Shear Stresses

The cold-bending process and resulting curvature causes shear deformations between the various layers of the façade panel assembly. The shear deformation is not constant and varies over the width and height of the panel, maximum values can be expected at the points of greatest shear deflections and are defined by the angle of rotation  $\varphi$ . Figure 06 provides system sketches indicating edge warp and edge rotation for the two key locations: corner and mid-edge.

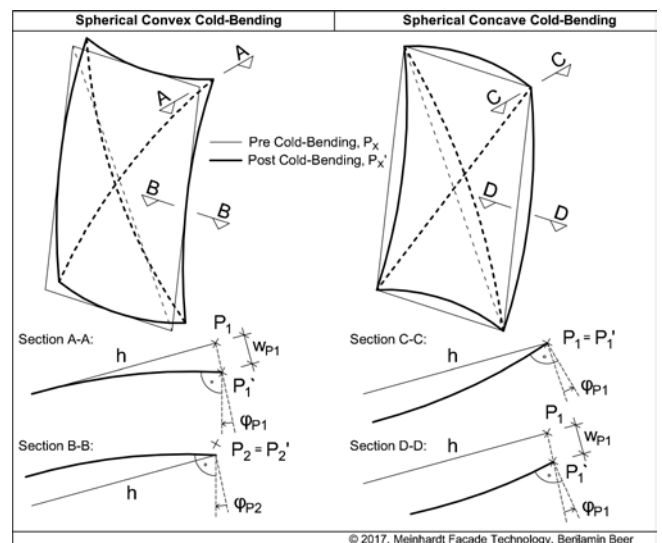


Figure 06: Comparison of edge warp and edge rotation due to cold-bending

Besides the permanent tensile forces in the structural silicone, the edge rotation angle and resulting permanent shear deformation is one of the key problems when designing cold-bent structural silicone glazed facades. This applies to both structural silicone seals (Figure 07):

- A) Primary Seal - between the IGU inner glass pane and aluminium frame
- B) Secondary seal - between IGU inner and outer glass pane

As per [4] and the corresponding European Technical Approval ETA's for typical two part structural silicones, the allowable long term silicone stress is only 1/10 of the allowable short term silicone stress. In an effort to reduce the silicone primary seal shear stresses for single corner cold-bent facades and firstly used for the Credit Libanais project in Beirut [1], the author developed the method "Workshop Cold-Bending & Site Re-Bending". A comparison of the two cold-bending options for single corner cold-bending is listed below:

A) Option A - Site cold-bending:

The glass panel and the framing members are produced flat, the structural silicone between glass panel and framing members is applied in the workshop. Once the silicone is cured, the flat façade panel is transported to site and forced into the cold-bent geometry during installation to the building's slab edges.

B) Option B - Workshop cold-bending and site re-bending:

The glass panel and the framing members are produced flat. While still in the workshop, the glass panel and the framing members are forced into the cold-bent geometry using a bending rack. Then the structural silicone between glass and framing member is applied. Once the silicone is cured, the cold-bent façade panel is transported to site in the bending rack. The lifting and installation of the panel requires the panel's release from the bending rack, for this temporary condition the panel will partially deform back from the cold-bent geometry and silicone shear stresses increase for that moment. The panel fixing to the building's slab edges will require the site re-cold-bending. After that process, the installation is finished and the silicone shear stresses are back to the post-cold-bending normal level.

Figure 07 compares the corner shear deformations and provides an overview table for the single corner cold-bending options A and B, as well as for the mode free-form cold-bending. As mentioned above, the single corner cold-bending option B results in lower shear stresses in the primary seal. Due to the pre-curved framing members used for free-

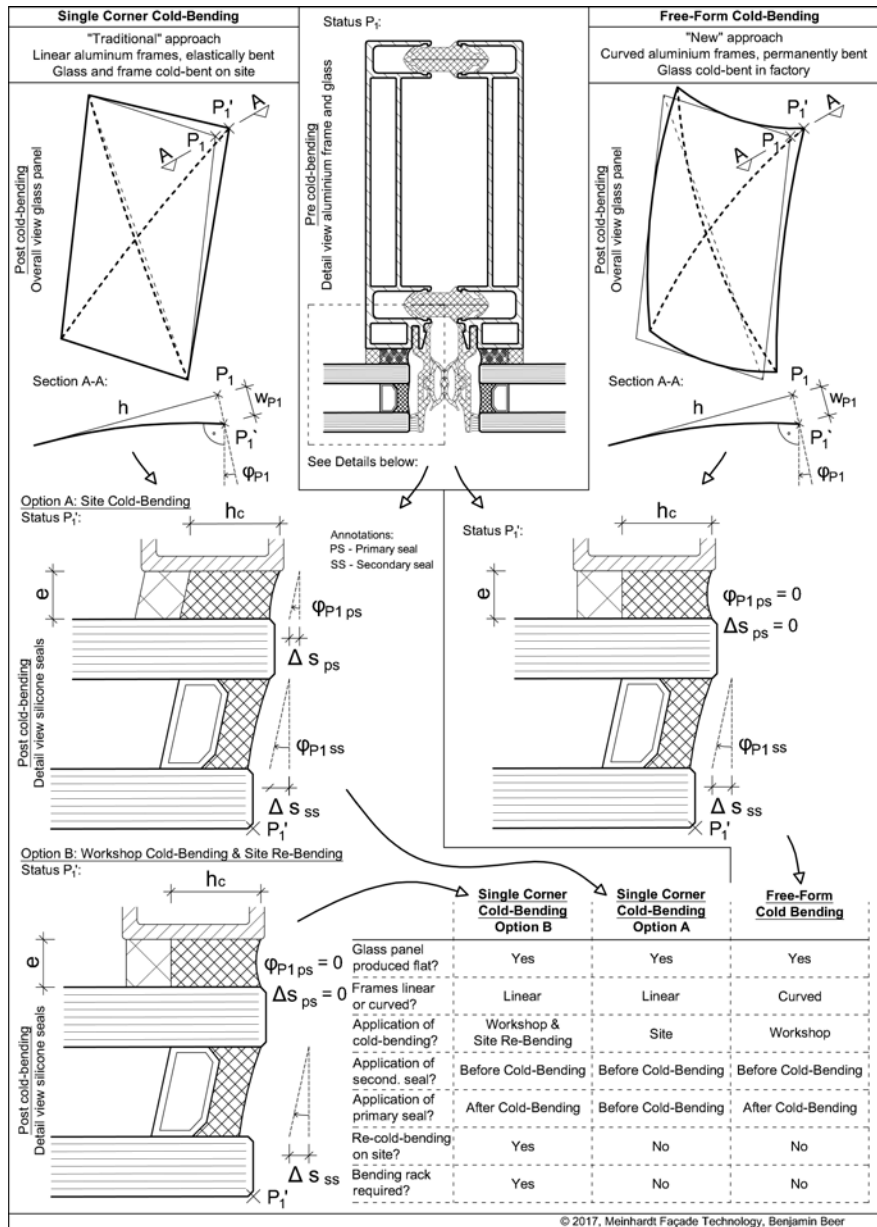


Figure 07: Single corner and free-form cold-bending – Mullion, glass and silicone details with shear deformation

form cold-bending, a similar effect with lower shear stresses in the primary seal is achieved. It shall be noted that for all options, the shear stresses in the secondary seal (between inner and outer glass pane) are not reduced as the insulating glass production is usually before façade panel assembly and cold-bending. An insulating glass unit production with application of the secondary seal structural silicone post-cold-bending might be technically feasible, would however require further research and is does not form part of this paper.

### Free-Form Cold-Bent Structural Silicone Glazed Facades – Silicone Tensile Stresses

As for the allowable silicone shear stress, also the tensile stress for long term loads can

be assumed to 10% of short term allowable stress. Due to the elastic cold-bending process and the glass trying to bend back into its original flat position, permanent (long term) tensile stresses act in the silicone. The distribution of the permanent silicone tensile stresses depends on the cold-bending geometry and the method of stress analysis: hand calculations or Finite Element (FE) analysis. Referring to the output of computational FE analysis and stress peaks often encountered in the results graphs, the evaluation requires substantial expertise and engineering judgement. The stress peaks are often localized in small areas and might be "cut-out" to avoid an overly conservative design - considering that these small overstressed areas will result in a localised higher elongation, which shall be no problem for the overall system. The concept of corner "cut-out"

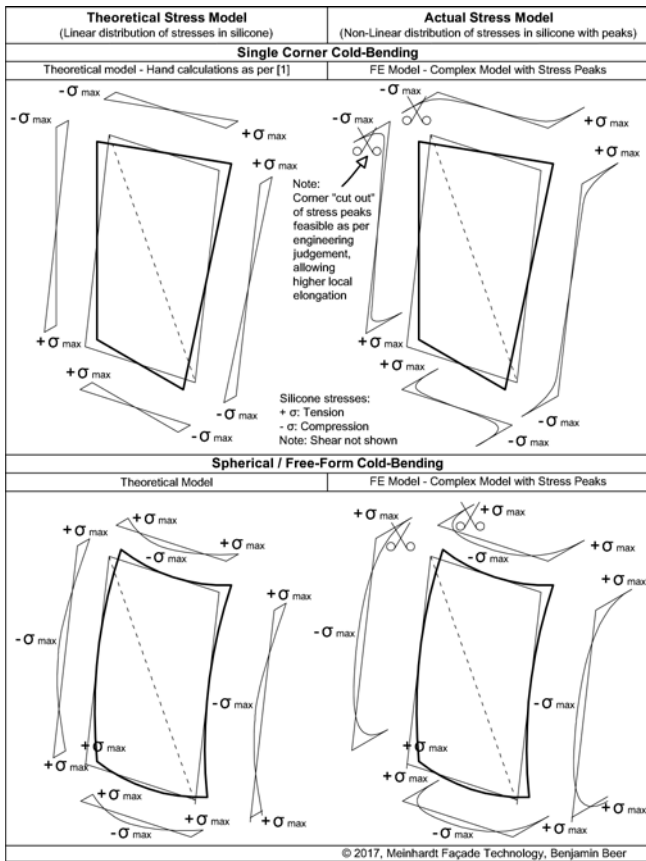


Figure 08: Silicone tensile stress models for single corner and free-form cold-bending

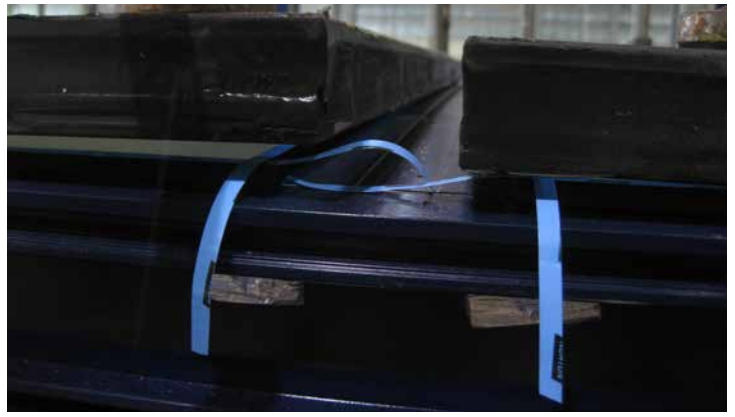


Figure 09: Free-form cold-bent structural silicone glazed unitized façade panel before glass cold-bending process, gap showing the corner warp



Figure 10: Free-form cold-bent structural silicone glazed unitized façade panel during glass cold-bending process, concave long edges and convex short edges

of local stress peaks was presented for single corner cold-bending in [1]. Figure 08 compares the theoretical stress models with actual models, both for single corner cold-bending and free-form shape cold-bending.

### Free-Form Cold-Bent Structural Silicone Glazed Façade – Project Example

As mentioned in the introduction, the first project using the free-form Cold-Bending process is currently under installation in Dubai (Figure 03). The curved facades use both hot-bent glass and cold-bent glass; the hot-bent glass is used for areas with high curvature where cold-bending limits would have been exceeded. Figure 09 shows the pre-cold-bending status with the open gap (corner warp) between glass and frame. Figures 10 and 11 show photos taken after cold-bending and prior to primary seal structural silicone application.

### Engineering Approach for the Structural Silicone Design Concept

Currently no international code or standard covers the structural silicone design of cold-bent structural silicone glazed systems. Guidance on the structural silicone design using FE models is given in [5] and [6], where

publication [5] presents the concept of True (FE) Stresses vs. Engineering Stresses and emphasizes the importance of deriving a conversion factor between both stresses (also see item B below).

This paper is based on an engineering approach using the following steps:

- A. Initial simplified assessment of the structural silicone seals assuming flat glass and flat framing (no cold-bending) using ETAG 002 "Structural Sealant Glazing Systems Part 1: Supported and Unsupported Systems" [4]. This is for initial guidance only and helps to assess the silicone's capacity available for additional (cold-bending) stresses.
- B. Set up and analyse a FE model to simulate the ETAG-002 [4] H-test model already tested by the silicone supplier as per ETA (European Technical Approval). This model acts as a validation model to derive a conversion factor between the true Finite Element (FE) Stress derived from the FE models, and the Engineering Stress as per the allowable design limit stress stated in the ETA of the silicone supplier.
- C. Set up and analyse a FE-Model for each free-form shape cold-bent glass panel. The structural models include 3D volume elements of the structural silicone and all loads including long term (e.g. cold-



Figure 11: Free-form cold-bent structural silicone glazed unitized façade panel during glass cold-bending process, concave long edge

bending) and short term loads (e.g. wind pressure and suction).

- D. Assessment of the FE-Stress results and conversion from "FE-Stress" to "Engineering Stress", result overview using the allowance stress approach as per [4]. Local stress peaks might be assessed using the "corner cut-out" method explained in [1].

### H-Test Model to Derive Conversion Factor "Engineering Stress" to "Finite Element Stress"

The H-test model FE analysis shall use identical boundary conditions as the laboratory tested H-test specimen as per [4]; the steel plate being 40 mm width, 50 mm length, 5 mm thickness and the silicone being 12 mm width, 12 mm height 50 mm length (Figure 12). These dimensions are in line with ETAG figures [4].

Stresses and strains are derived for this model and compared with the actual test results. This H-test FE model (Figure 12) shall use the same setting (analysis software Marc Mentat 12, setting, FE mesh density, etc.) as the FE models of the complete glass panels being cold-bent (Figure 20, 21). All FE models use shell elements for the glass panes, volume elements for the structural silicone sealants and the Neo-Hook material model for the silicones:

$$\sigma = G \left[ \lambda - \frac{1}{\lambda^2} \right], G = 0.67 \text{ MPa}$$

Two load cases were set up to derive the conversion factors for a typical 0.14 N/mm<sup>2</sup> silicone stress limit (as per silicone supplier's ETA), and a silicone overstress of 1.0 N/mm<sup>2</sup> (as the engineer's judgement). See data below:

- Load case 84 N tensile load to derive conversion factor for 0.14 N/mm<sup>2</sup> silicone stress:
  - Face load on upper steel plate: 84 N / (40 mm x 50 mm) = 0.042 N/mm<sup>2</sup>
  - Nominal tension stress in silicone: 84 N / (12 mm x 50 mm) = 0.140 N/mm<sup>2</sup>
- Load case 600 N tensile load to derive conversion factor for 1.0 N/mm<sup>2</sup> silicone stress:
  - Face load on steel plate: 600 N / (40 mm x 50 mm) = 0.3 N/mm<sup>2</sup>
  - Nominal tension stress in silicone: 600 N / (12 mm x 50 mm) = 1.0 N/mm<sup>2</sup>

The FE results are shown in Figure 13 to 15. Taking the Van Mises stress output of the load case 84 N and 600 N models, the following conversion factors "Engineering Stress" to "Finite Element Stress" can be derived:

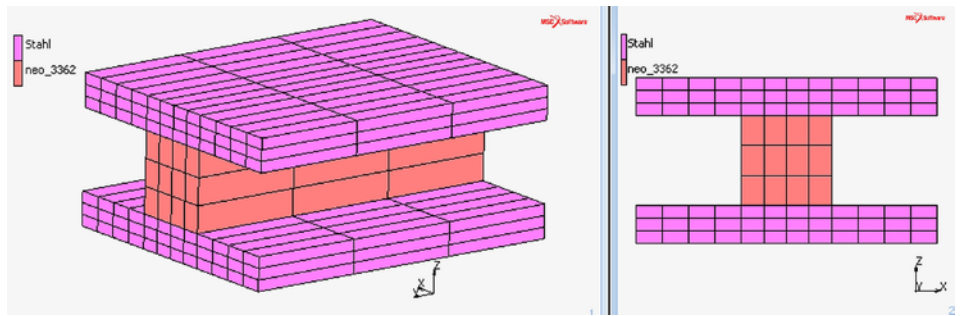


Figure 12: H-test specimen FE model to derive conversion factor "Engineering Stress" to "FE Stress"

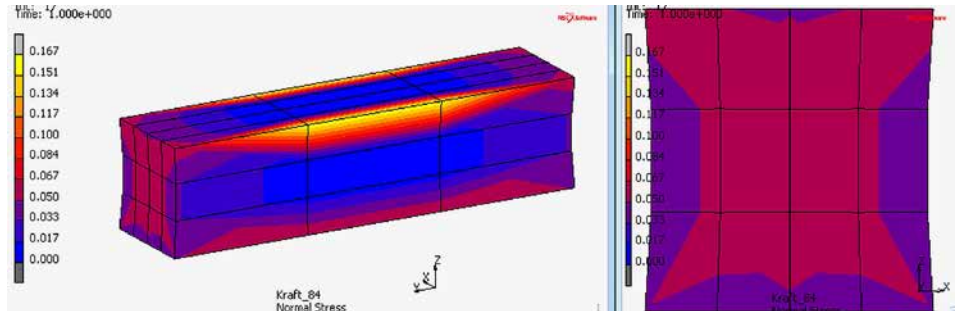


Figure 13: H-test specimen FE result for normal tensile stress, load case 84 N, course mesh

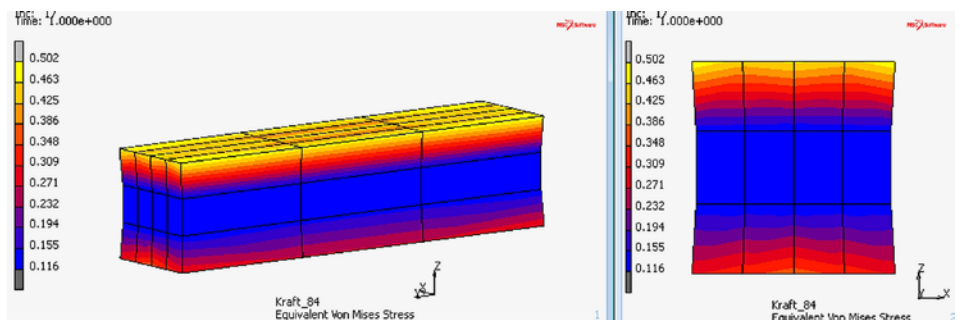


Figure 14: H-test specimen FE model result for equivalent von Mises Stress, load case 84 N, course mesh

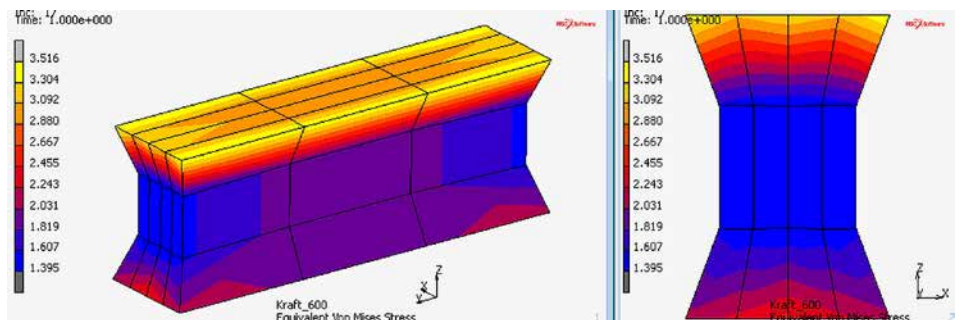


Figure 15: H-test specimen FE result for equivalent von Mises Stress for load case 600 N, course mesh

- Load case 84 N (equivalent to 0.14 N/mm<sup>2</sup> Engineering Stress): 3.59
- Load case 600 N (equivalent to 1.0 N/mm<sup>2</sup> Engineering Stress): 3.52

The above factor of 3.52 and 3.59 depends on the FE software, calculation model, mesh

density, stress type used and other items. Therefore, the above conversion factor varies from the factor shown in other publications [5]. It shall also be noted that [5] used the First Principle Stress, whereas the above calculations use the Van-Mises Stress.

Both stresses can be used and the difference in the conversion factors is almost neglectable (Figure 16).

## FE Mesh Density

The above H-Test models (Figure 13 to 15) use an identical FE mesh density as the actual models of the complete glass panels (Figure 21). This is important as the conversion factor Engineering Stress to FE Stress from the H-Test model will be used for actual calculations. The mesh density of the H-Test models above might be seen as coarse and not dense enough. This however should have no effect as the same mesh density is used for the actual calculations of the complete glass panels (Figure 21), nevertheless comparison calculations with higher FE mesh densities were carried out. When comparing the Van Mises stresses of the H-Test model with course mesh (Figure 13 to 15) and the Van Mises stresses of the H-Test model with fine and extra fine mesh (Figure 17 to 19), the difference in maximum Van Mises stress is as follows:

- Standard mesh density (course): 3.53 N/mm<sup>2</sup>
- Fine mesh density: 4.08 N/mm<sup>2</sup>
- Extra fine mesh density: 4.92 N/mm<sup>2</sup>

To keep the computing time within reasonable limits, the actual models of the complete glass panels use the standard mesh. As the H-Test model for calculation of the conversion factor uses the same mesh density, this standard mesh will not lead to significant differences in the stress results and is therefore acceptable.

## Full Scale FE Models of Free-Form Cold-Bent Structural Silicone Glazed Panels

The FE models are built in two stages; first the structural sealant with an ideal stiff bent frame (zero deflections under all load cases) and second the planar (flat) insulating glass unit. FE contact elements are placed between the insulating glass unit and structural sealant. The modelling and analysis process involves the following steps:

1. Set up of the initial pre-cold-bending model with curved framing and planar (flat) glass (Figure 20). Generate the FE mesh (Figure 21) with mesh density as per H-test model used to derive the conversion factor "Engineering Stress" to "Finite Element Stress".
2. The initial model with planar insulating glass is loaded at the edges, the glass is deformed until the edges get in contact with the structural sealant geometry (bent silicon, Figure 22).

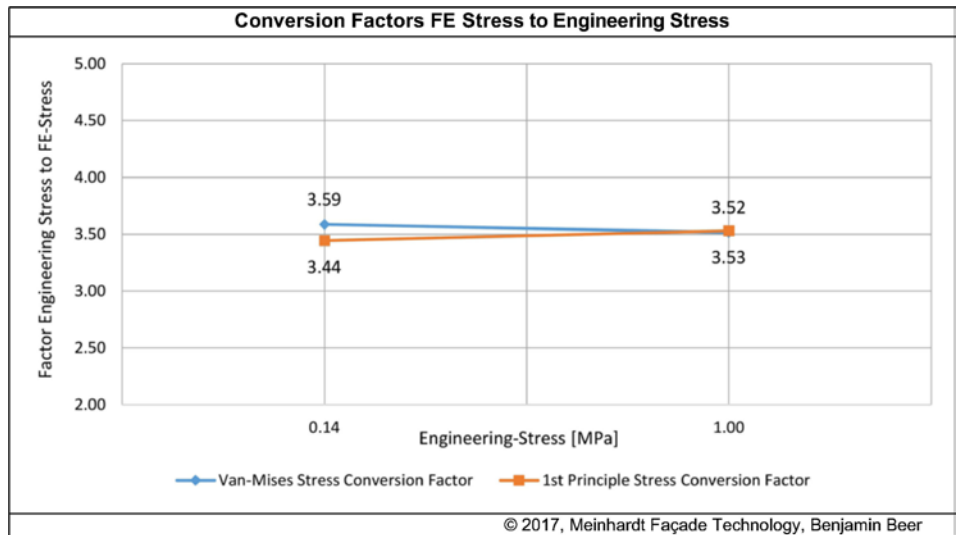


Figure 16: Conversion Factors for Van-Mises and Frist Principle Stress at 0.14 N/mm<sup>2</sup> and 1.0 N/mm<sup>2</sup> Engineering Stress

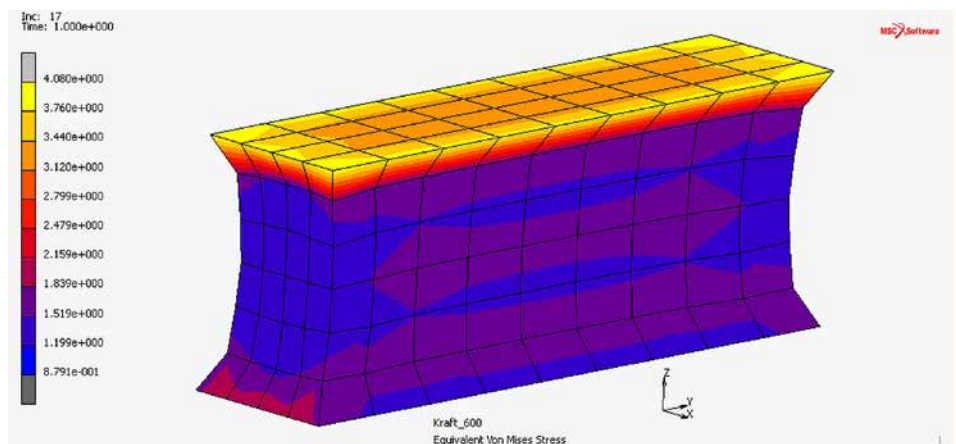


Figure 17: H-test specimen FE result for equivalent von Mises Stress for load case 600 N, fine mesh

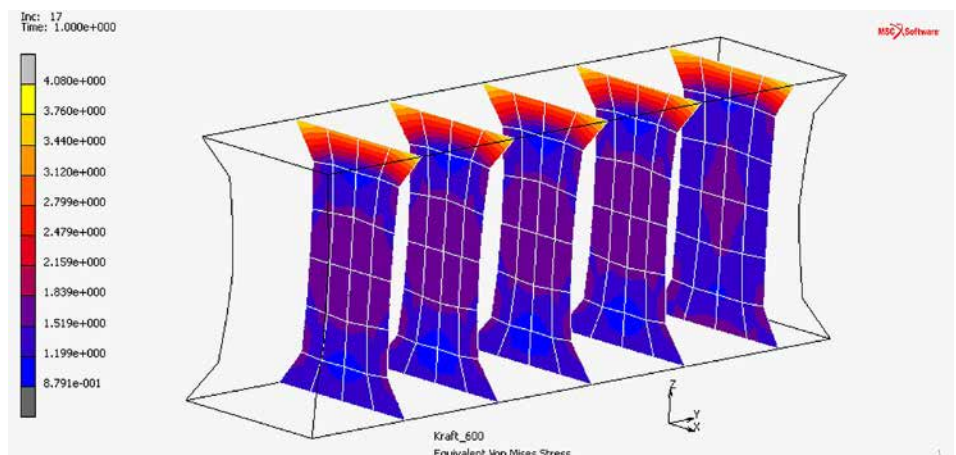


Figure 18: H-test specimen FE result for equivalent von Mises Stress for load case 600 N, fine mesh (five sections through silicone)

The contact elements are closed and will be "glued" for the other steps. This step considers that the primary structural silicone is applied after cold-bending of the glass, see also the illustration and table data for free-form cold-bending shown in Figure 07.

3. The edge loads required to achieve contact between the silicone and the curved frame are deleted. All glass elastic cold-bending loads are now transferred via the structural silicone; preventing the glass to bow back into its original flat (planar) geometry.
4. Load the model with the climatic loads (isochronic pressure in cavity) based on air pressure (hPa), temperature change in air cavity (°C) and the height difference (m) between glass manufacturer and site location.
5. Add the wind loads.

The process of load application at the edges during step 1 is iterative, the load amount and load spacing must be varied up to the status of continuous contact between the silicone and framing at all locations. Some FE programs allow coloured output plots for contact checks (Figure 23).

## Evaluation of FE Analysis Stress Outputs

FE analysis stress outputs for the following load cases (item 1 to 4) and load combinations (item 5) shall be checked to evaluate compliance to allowable stress limits:

1. Dead load - Long term load
2. Post-cold-bending (cold-bending forces released) - Long term load
3. Climate loads (isochronic pressure, summer or winter) - Long term load
4. Wind load (pressure or suction) - Short term load
5. Combinations of the above load cases including wind load case – Combination of long and short term loads

Item 5 refers to load combinations including short and long term loads. Here the results evaluation is further complicated by the different stress limits for long term loads and short term loads, where the stress limits for long term loads is usually 1/10 of the limit for short term loads. Due to the nature of the cold-bending process reflected in the steps during FE analysis, the short term load case 4 (wind load) can only be run in conjunction with the long term load case 2 (cold-bending forces released: post-cold-bending). For this load combination, the FE software provides just one stress plot "merging" the stress results for the long term and short term load case. An "manual" overlay of the short and long

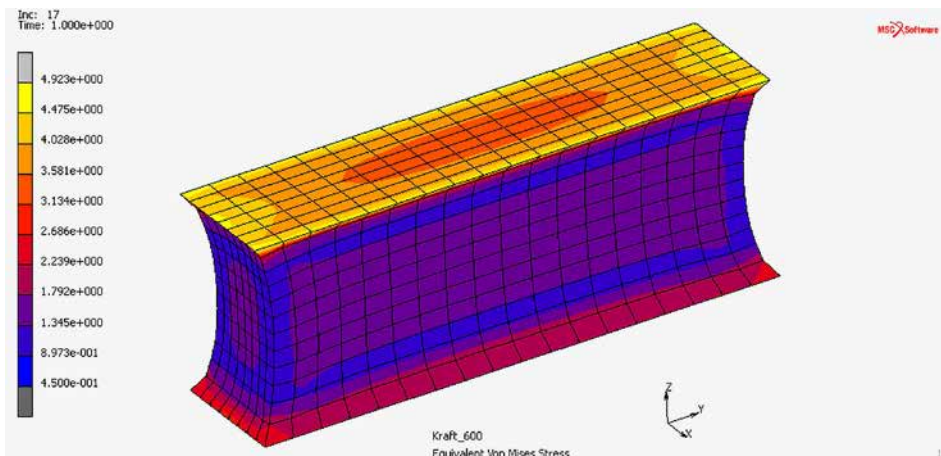


Figure 19: H-test specimen FE result for equivalent von Mises Stress for load case 600 N, extra fine mesh

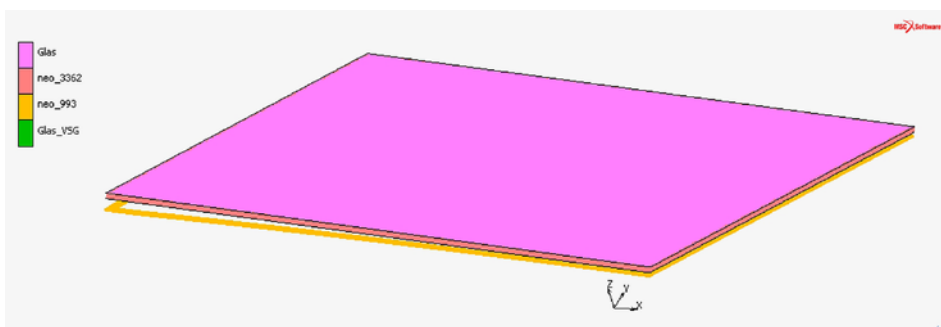


Figure 20: Example of full scale FE model at pre-cold-bending stage, overall view

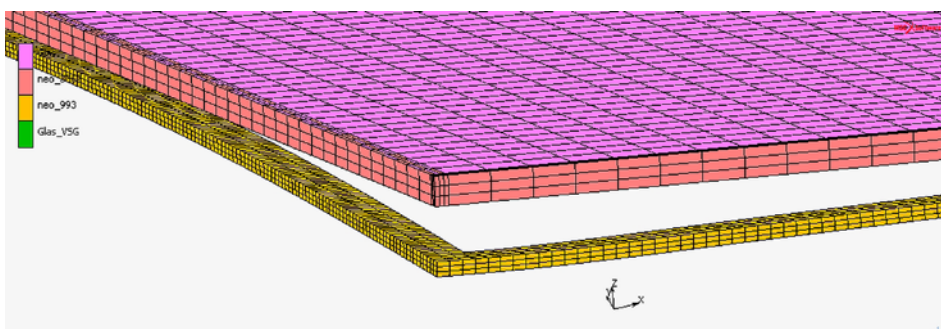


Figure 21: Full scale FE model at pre-cold-bending stage, detail

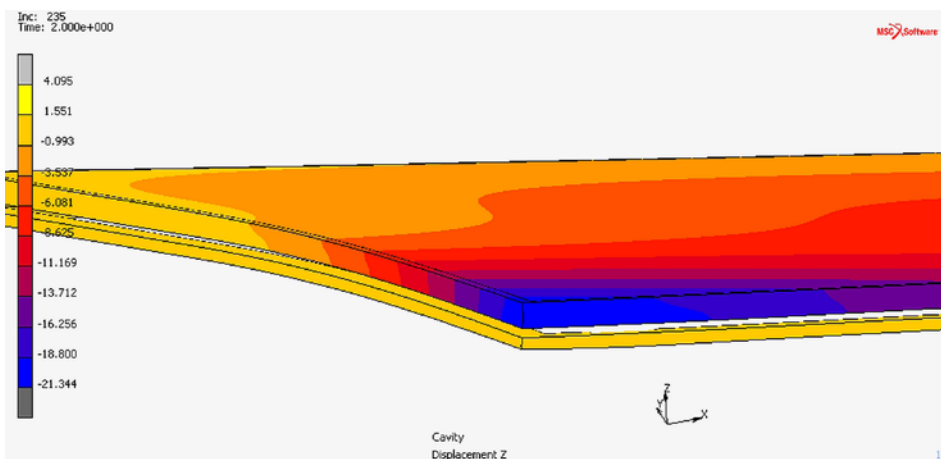


Figure 22: Full scale FE model at post-cold-bending stage, detail with deflection plot

term stress data for each FE mesh nodal point can be done, however this complex and time consuming method might not be preferred. Further research will be required to assess the best way how to easily evaluate these load combinations.

Looking at the overall stress plot for one glass panel, the evaluation of FE results can differentiate between "Overall", "Peak" and "Non-Peak" areas. For peak areas, the concept of cutting out stress peaks (Figure 08) can be used to avoid an overly conservative design. The definition of extent of corner cut-out requires engineering judgement and experience, as a local silicone overstress will be allowed. In the case of the secondary sealant, acting as the edge seal of insulating glass unit, the local overstress might lead to a locally reduced air tightness of the edge seal. A typical corner area with stress peaks is shown in Figure 24. Here, the concept of corner cut-out as shown in Figure 25 (non-peak plot) and in Figure 26 leads to a stress reduction of approx. 25%. Further information on the topic of long term performance of cold-bent insulating glass units can be found in [7], although no detailed information on stress limits is provided.

## Summary

To achieve a flush and capless outer glass appearance, many complex geometry cold-bent façade projects use structural silicone glazing systems to hold the glass panels in place. While this is architecturally a preferred and ideal solution, the façade engineering and structural designer is faced with the problem of long term tensile and shear forces on the structural silicone, caused by the glass intending to reverse the elastic glass cold-bending process and forming back to its initial flat position. This effect is unique to cold-bent facades and different to hot bent glass facades, where the glass bending process causes a permanent (non-elastic) curvature of the glass. Besides the presentation of various graphs for the most common cold-bending geometries and a recommendation for workshop cold-bending and site re-bending to reduce structural silicone primary seal shear stresses, a new design concept for the structural silicone design of free-form cold-bent structural silicone glazed panels is presented in this paper. To push this new design concept to an agreed standard within cold-bent façade specialists and silicone suppliers, the author welcomes feedback and technical comments.

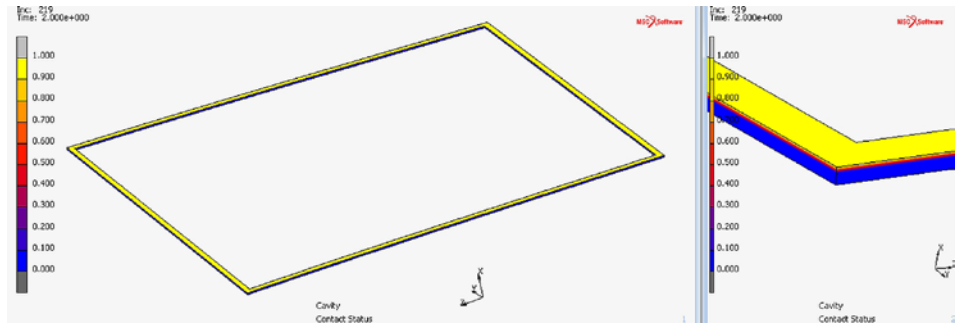


Figure 23: Full scale FE model, contact check of primary seal structural silicone to frame (yellow: 1 - full contact, blue: 0 - no contact)

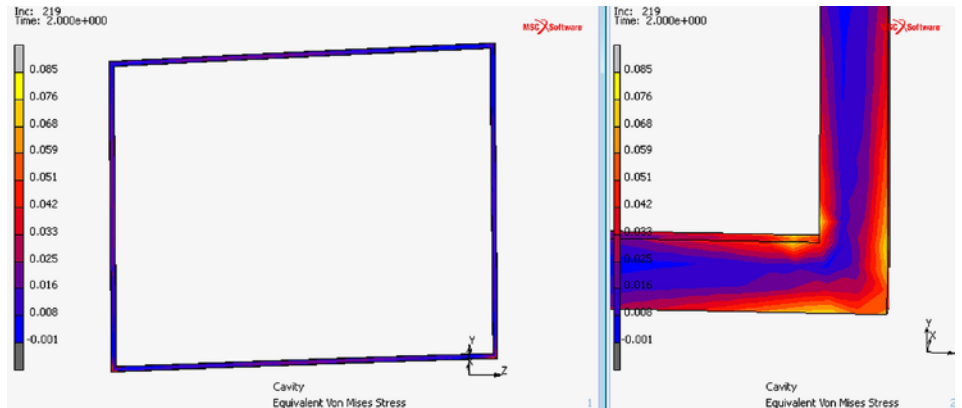


Figure 24: FE analysis stress plot of primary seal (Von Mises stress) for load case 1, showing local stress peaks

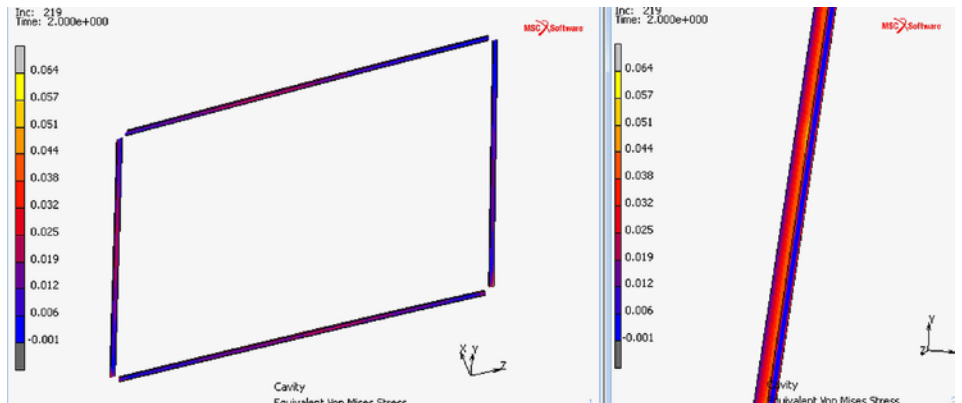


Figure 25: FE analysis stress plot of primary seal (Von Mises stress) for load case 1, excluding corner cut-out areas

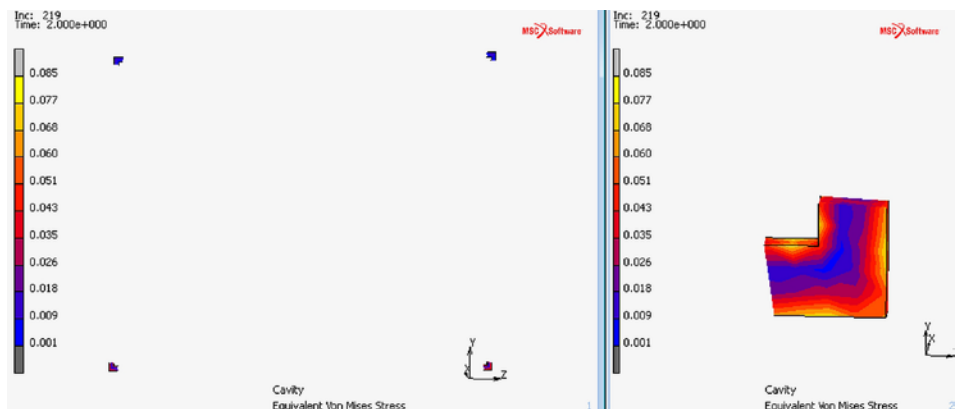


Figure 26: FE analysis stress plot of primary seal (Von Mises stress) for load case 1, corner cut-out areas

## Acknowledgements

The author kindly acknowledges Prof. Dr.-Ing. Eva Scheideler (University of Applied Sciences Ostwestfalen-Lippe, Germany) and her engineering office for their support in carrying out the hyperelastic Neo-Hookean material model analysis with MSC Marc Mentat 12.

- [1] Beer, B.: Structural Silicone Sealed Cold-Bent Glass – High-Rise Projects Experience Leading to a New Design Concept, Glass Performance Days, 2015
- [2] Beer, B.: Complex Geometry Facades – Introducing a New Design Concept for Cold-Bent Glass, Glass Performance Days, 2013
- [3] Datsiou, K.C., Overend, M.: The mechanical response of cold bent monolithic glass plates during the bending process, Engineering Structures 117 (2016) 575-590, 2016
- [4] EOTA (2012); ETAG 002 - Guideline for European Technical Approval for Structural Sealant Glazing Kits (SSGK), Edition November 1999, 3rd amendment May 2012
- [5] Descamps, P., Kimberlain, J., Bautista, J., Vandereecken, P.: Structural Glazing: Design under high windload, IGS Magazine, Summer 2016 Issue
- [6] Vandereecken, P., PowerPoint "Positioning on FEA analysis", Dow Corning, 2016
- [7] Besserud, K., Bergers, M., J. Black, A., Donald, L. D., Mazurek, A., Misson, D., Rubis, K.: Durability of Cold-Bent Insulating-Glass Units, Journal of ASTM International, Vol.9, No.3, 2012

# Structural Silicone Joints in Cold-Bent SSG Units

Viviana Nardini 1  
Florian Doebbel 1

1 Sika Services AG – Building Systems & Industry

## Keywords

Structural Silicone, Cold-Bending, SSG Units, Curved, Warped

## Abstract

Use of cold-bent and warped glass units in unitized curtain walling has been getting a state-of-the-art application for the last years. This creates special demands on appropriate design of glass units and frame members as well as on the elastic and load-bearing bonding joints in Structural Sealant Glazing applications. Depending on the approach of producing and installing these units as well as the geometrical boundary conditions, the structural silicone joints are affected by additional permanent load reactions and joint movements next to regular loading. Due to the warped or curved shape of the units, significant changes in load distribution, load sharing and stiffness can result and even load peaks in the elastic silicone joints can arise. This paper summarizes technical requirements and engineering rules as well as design aspects enabling appropriate design and calculation of structural silicone joints in cold-bent SSG units. Reflecting a reliable safety concept and the expected life cycle of these load-bearing bonding joints is part of the approach.

## 1. Introduction

The demand of emulating nature's complex and flowing layout by using curved or even biomorphic design combined with transparent panels and valuable surfaces is an increasing trend replacing conventional straight-lined and sharp-edged geometry in architectural design. While traditional design limits the architectural freedom as well as the value of recognition and building identity, curvilinear design offers an unlimited variety of custom-made and nonrecurring building shapes. Designs supported by advanced planning processes and computer-aided tools, which had been reserved for automotive industry, have been transferring to buildings and facades.

Considering that sophisticated designs of typical industrial products are implemented to a serial production using complex and dedicated tools, it's the façade engineer's and manufacturer's challenge to properly realize custom-made and mostly nonrecurring shapes within the given economical, technical and regulative restrictions and within acceptable timeframe.

Based on the fact that facades as face and skin of a building have to comply with functional, protective and architectural demands, glass and glazed units as a main part of the envelope have to comply with these demands, too. That means, glass units and their restraints have to fit curvilinear designs, what pushes the demand on curved and warped single glass, laminated glass as well as insulating glass units replacing more and more flat and polygonally installed or even cylindrically shaped glass units.

## 2. Curved Glass Elements Manufacturing

Curved architectural glass can be manufactured in the façade markets according to three main methods.

- Hot bending  
During thermal shaping of glass, a variety of cylindrical and spherical as well as asymmetrical and irregular bending shapes with smaller and larger bending radii can be achieved within the technical limits. The advantage lies in the exact and permanent setting of the required shape in the manufacturing process. The pre-sized float glass sheets are heated to just over the transformation temperature. Based on the desired geometry and manufacturing processes, the softened glass either can settle in the prefabricated and fire-resistant mold (bending by gravity) by its own weight or is shaped through mechanical molding. The resulting glass strength, fracture pattern and tolerances in the finished state are largely controlled by the cooling process itself. Glass coatings can't be applied on the shaped glass surfaces, after hot-bending. Due to the manufacturing process, required reflective of low-e coatings must be thermally stable and suitable for tempering. PVB interlayers, applied
- Cold-bending or cold-warping of flat glass elements  
If the use of slightly curved and uniformly or symmetrically bent geometries is required, the use of cold-bent glazing is usually recommended. Since cold-bent glazings are no longer heated up to the glass transformation temperature, the surface quality of smooth and leveled produced float glasses is maintained. Local distortions, as they arise during the transformation process of hot-bending, can be excluded during cold-bending. Tempering, frit-coating, printing and film coating can be done with standard equipment in flat condition without compromising properties, quality and variety. However, value and shape of the cold-bent unit are limited. Permanent glass stress, which is caused by cold-bending, has to be limited through imposed displacement and glass thickness. Heat-treated glass products are normally used to provide an adequate resistance to counter permanent stress conditions.
- Cold-bending by lamination  
Glass units cold-bent by lamination are similar to the condition of glasses, likewise cold-bent glazings. In contrast to normal cold-bending, the required bending shape is applied during the autoclave process using a corresponding bending device or mold on the overall package of glass and interlayers, before they are joined together to form a single unit. Thermal treatment in the autoclave is done far below the glass transformation temperature and thus has

between two bent glass lites after the hot-bending procedure, must be chosen in respect of thickness and material properties so that tolerance between the bent lites can be accommodated without constraining stresses. The assembling of the insulated glass unit or its connection to the façade element must also be stress-free. But especially for heavily curved units increased climatic effects, affecting the hermetically sealed cavity, as well as formation and distribution of reaction forces which differ significantly from the situation of flat glazing and non-curved insulating glass units have to be taken into account.

no effect on the properties of the glass products and existing coatings. Depending on the interlayer used, a specific elastic back flipping as well as a time-, load- and temperature-dependent creep of the organic interlayer have to be considered for the curved and laminated unit. The use of glasses bent by lamination is particularly advantageous when the use of laminated glass is required for other reasons too, or if an exact cylindrical or spherical design is targeted, which differs to a limited extent from the natural bending shape of the glazing. Cold-bending by lamination can significantly reduce permanent effects on laminated glass edges and glass supports.

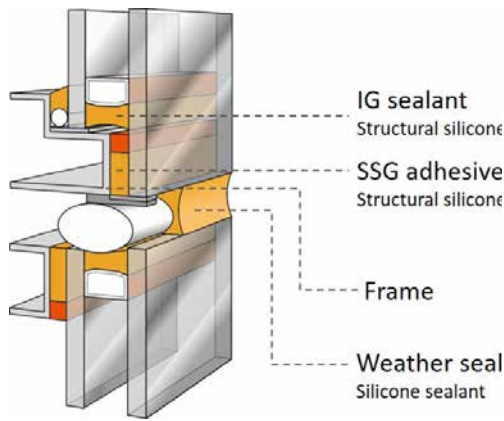


Figure 1: Typical SSG system.

Visual (aesthetic) demands, technical feasibility and actual availability usually drive the selection of the specific manufacturing process. In addition, regulative requirements, consultants' agreement and appropriate balance between costs, benefits and risks are important factors to be accounted for the selection.

Even if curved glass units are becoming standard elements of architectural design and project designers and glass and façade producers are getting more and more experienced, curved glass elements are still not standardized. As a consequence, related technical and economic risks lay on decision-makers and investors.

### 3. Structural Silicone Joints in Cold-Bent SSG Systems

Cold-bending and cold-warping of facade elements mainly consists in cold bending of monolithic glasses, laminated glasses or insulating glass units as well as the frames that retain them in the structure after they have been produced and assembled in a flat state. This technique drastically reduces the production costs of the curved façade elements and is very beneficial in projects where serial repetition is limited.

In the majority of international projects where transparency and flowing layouts are emphasized by curvilinear shapes, fixing of appropriate cold-formed glass panels in Structural Sealant Glazing (SSG) units is achieved by the load-bearing bonding provided by structural silicone adhesives (Figure 1). Their approvals and assessment are controlled in the European area by EOTA ETAG002 [3] and American area by ASTM C 1401 [4]. EOTA ETAG 002 [3] refers to exposure of the structural silicone joints to short-term wind loads (dynamic tensile stress), to cyclic thermal expansion between different components (dynamic shear stress) and to permanent dead load transfer (static shear stress). A

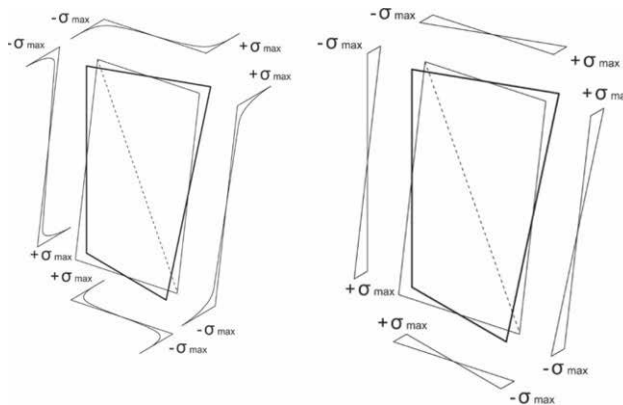


Figure 2: Tensile stress distribution in SSG-joints of cold-warped units according to Beer [2]: stress peaks at the corners based on non-linear FE analysis (left) and simplified uniform stress distribution (right).

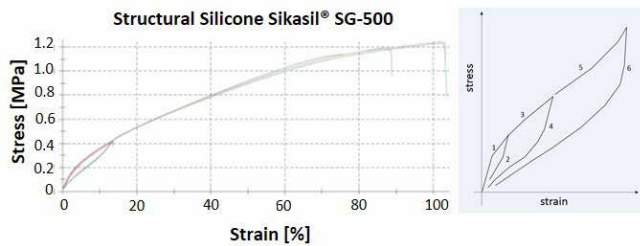


Figure 3: Mullins effect on structural silicone Sikasil® SG-500.

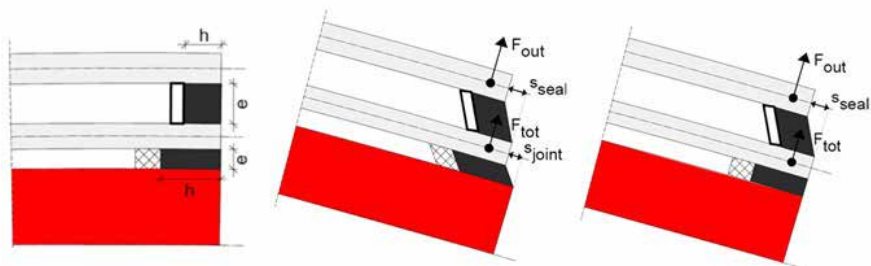


Figure 4: Long-lasting effects on elastic adhesive joints by SSG bonding and insulating glass edge seal: Flat situation (left). Insulating glass and frame bonded in a flat state and subsequently warped (center). Bonding of flat produced insulating glass unit on pre-shaped frame members (right). (© Sika)

similar concept is covered by ASTM C 1401 [4]. Stress from cold-bending of glass units and façade elements is not explicitly considered in [3] or [4] and thus requires careful and comprehensive engineering analysis. Significant reactions, which arise in the elastic silicone joints due to cold-bending, are:

• **Permanent tensile loads** – Stressing the SSG joint to bond the glass element to the frame (F<sub>tot</sub> – Figure 4) as well as the IG joint of any insulating glass units which is cold-bent (F<sub>out</sub> – Figure 4).

The permanent tensile stress is caused by restoring forces (back flipping) of displacement elastically applied on the flat produced glass unit and need to be properly withstood over the entire life cycle. Figure 2 shows the visualization of the distribution of the tensile stress caused by restoring forces of a cold-warped unit according to Beer [2]. High stress peaks at the element corners can be identified with precise simulation of the reaction forces in a non-linear finite element model based on hyper elastic bulk elements representing the elastic adhesive joints. Consideration about Mullins effect could be called upon to evaluate such stress peaks in the joints: the mechanical response of the silicone adhesive and its stress-strain curve depends on the maximum loading previously experienced (Figure 3) and can be idealized as an instantaneous and irreversible softening of the stress strain curve that occurs whenever the load increases beyond its prior all-time maximum value. Non-linear elastic behaviour prevails when the load is lower than a prior maximum, while Mullins softening is a viscoelastic effect mainly driven by friction of fillers and sliding of polymer chains. Therefore, it can be argued that short-term wind load superimposed to tensile load due to cold bending can produce a softening of the material and stress reductions. Nevertheless, the extent to which stress peaks can be regarded as a temporary effect and can be compensated due to relaxation in favor of a uniform stress distribution requires further investigation or a material-dependent clarification.

Under the assumption of a uniform distribution as shown in Figure 2 on the right, the restoring force of a representative glass unit could also be calculated or experimentally determined using a dummy load, which could then be distributed as an idealized triangular load on the edges of the panel. Depending on the relevant needs, the resistance of the elastic adhesive joints against the permanent load can be adjusted by increasing the joint bite as necessary.

• **Permanent shear movements** – affecting the SSG joint to bond the glass element to the frame (s<sub>joint</sub> – Figure 4) as well as the IG joint of any insulating glass units which is cold-bent (s<sub>seal</sub> – Figure 4).

Under the influence of shear forces caused by geometric-related and reverse movement imposed to the bonded surfaces, possibilities to control the stress level in the joint without a significant increase in its thickness (clearance of bonded surfaces) are limited. However, while the restoring forces acting out-of-plane of the cold-bent and cold-warped unit can only be reduced by decreasing the glass stiffness (glass thickness, glass size, elastic / viscous and thermo-elastic interlayers) or by using mechanical restraints, there are possibilities for actively influencing the reduction of shear movements in the elastic adhesive joints by evaluating different cold-bending procedures:

- A very effective option to remove the permanent shear stress in the SSG joints due to cold bending is using hot-bent frame members, so that only the glazing is cold-bent. The glass unit can be cold-bent on the pre-shaped frame and temporarily fix to it by mechanical devices; application of the SSG-joints can follow. After the adhesive is completely cured, mechanical devices can be removed. The introduction of significant shear movements in the SSG joints (s<sub>joint</sub> – Figure 4) is permanently prevented.
- An other option to limit the permanent shear stress in the SSG joints due to cold bending is to temporary fix by mechanical devices the glass unit to the frame and cold bent them; after that, application of the SSG joint can follow. When adhesive is completely cured, the mechanical temporary devices can be removed. Permanent tensile stress will arise in the SSG joints; shear stress will arise in the SSG joints too, but its duration will be limited to the timeframe from production to installation, when cold-bent shape will be restored.

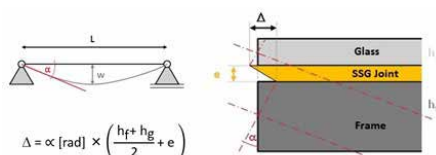


Figure 5: Effect of curvature and cross-sectional height on shear deformation of the SSG joints. (© Sika)

If one considers that the level of shear movements does not only depend on the displacement needed to set the curvature but also on the geometry of the bonded components, it is obvious that the system design itself could have important influence on limiting permanent forces in the adhesive joints without further increasing the effort and complexity of factory production and bonding of façade elements.

As shown in Figure 5, the degree of shear deformation is significantly influenced by the cross-sectional height of the bonded components and does not just depend on the displacement and the curvature of the cold-bent element. That means, the larger the cross-sectional height of frame and glass, the bigger the offset of the bending axis and surfaces of the bonded components and the bigger the reverse movement Δ of the bonding surfaces, whereas the accommodation of large shear movements within the allowable stress can only be realized by a massive increase of the adhesive joint thickness. In other words: permanent shear stress in the SSG joints can be significantly reduced by increasing the thickness of the structural silicone joint but also by a massive reduction of the cross-sectional height of the bonded components. This can be achieved e.g. by:

- Using flat slim frames mechanically connected to a load bearing frame in such a way that free in-plane relative displacements are allowed (Figure 6). The flat slim adapter frame can be bonded to the glass unit at the factory site; after joints are completely cured, application of required out-of-plane displacements for cold bending can occur on site.
- Using flat slim adapter frames which are bonded to the flat glass units at the factory site. After joints are completely cured, the bonded assembly can be cold-bent and fixed to a pre-shaped load bearing frame on site.

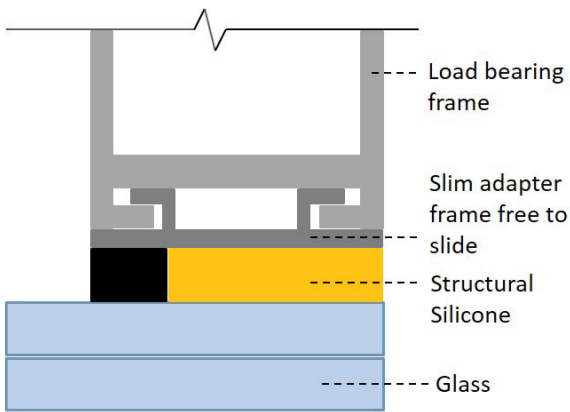


Figure 6: Slim adapter frame to minimize effects of imposed shear movements due to cold-bending.

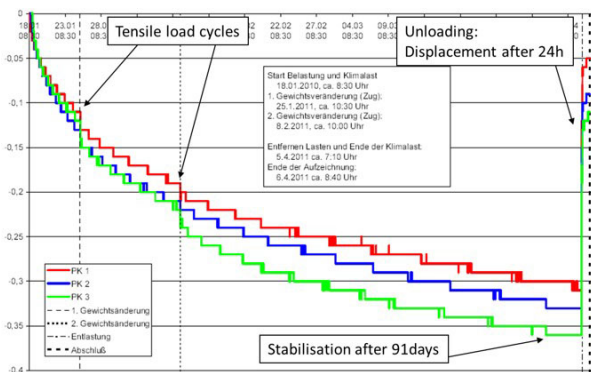


Figure 7: Documentation of creep test according to EOTA ETAG 002- 5.1.4.6.8 for Sikasil® SG-500. (© Sika)

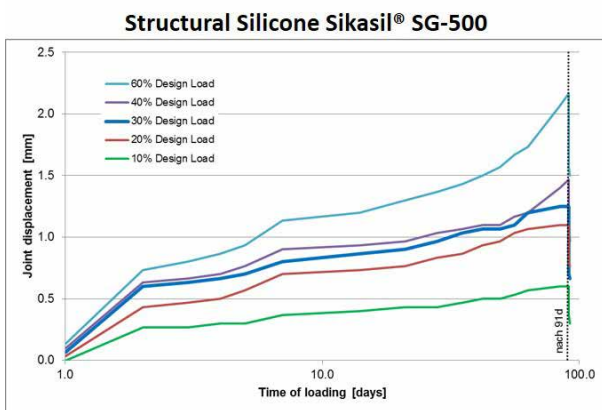


Figure 8: Creep test according to EOTA ETAG002 for different load levels. (© Sika)

#### 4. Permanent Effects on SSG Joints due to Cold Bending

After determining the permanent load reactions, which are created in the elastic adhesive joints by cold-bending or cold-warping of SSG units, the influence on the load-capacity and durability of the structural silicone bonding needs to be evaluated. ASTM C 1401 [4] requires a strong limitation of permanent load effects, such as dead-load shear, to maximum 1psi (0.007MPa), while European EOTA ETAG 002 [3] only gives partial guidance on how to proceed. The definition of a creep test under long-term shear in superposition with cyclic tensile loading in Section 5.1.4.6.8 of [3] helps to get an indication about the long-term performance of the structural silicone. It defines the influence of permanent shear stress on dead-load unsupported systems, what means that the total weight of the glass is permanently transferred by the structural silicone only. In addition to the creep test, which requires massive restriction on residual shear deformation after complete unloading besides an adequate material resistance under permanent loading, a creep factor of at least 10 is defined by [3] in the same section. The allowable shear stress has to be reduced by the creep factor in addition to the dynamic safety factor when the elastic adhesive joints are required to take the total dead load.

The procedure defined in [3] can be applied to the evaluation of elastic adhesive joints which are used in cold-bent SSG units only to a certain extent. Indeed, while creeping test defined by [3] analyzes the combined effect of permanent shear load and temporary or dynamic tensile load, the effects of cold-bending produces permanent tensile loads and limited-in-distance shear movement. Considering this, one could take over the approach of [3] and reduce the allowable stress for dynamic tensile loading by an additional creep factor  $\gamma_c \geq 10$ , with respect to the permanent action of the restoring forces and in order to permanently restrain the cold-bent and structurally bonded glass units. For evaluating permanent shear movement [3] has no practical approach since the use of the allowable static shear stress for this case would hardly lead to applicable joint thickness, in most cases. Moreover, it must be considered that the imposed displacement is indeed permanent but limited in magnitude, as related to a one-time setup and does not increase over the life cycle. Thus the risk of creep is structurally non-existent. Instead, a process must be found which eventually defines a maximum permissible level for the relaxation of permanently distorted joints. In this context,

it should be mentioned that an allowable relaxation of the adhesive joint in shear direction must not have effects in a reduction of material resistance.

For this purpose, following tests have been performed on structural silicone adhesives:

- Lap-shear tests with structural silicone joints loaded up to failure as per following conditions:
  - Lap-shear samples tested up to failure at 23°C / 50% relative humidity with no preliminary loading and used as reference
  - Lap-shear samples tested up to failure at 55° C / 95% relative humidity with no preliminary loading
  - Lap-shear samples loaded for 91 days under different levels of imposed shear movements and tested up to failure at 55° C / 95% relative humidity.

Comparison of results obtained from the above lap-shear samples shows that the ultimate strength of the joint does not decrease, if adhesive has previously experienced an imposed deformation up to maximum 30% design load set by [3].

- Creep tests according to EOTA ETAG002 [3], associated to permanent loading from 10% to 60% the design load defined by [3]. The test shows that up to maximum 30% the design load set by [3], joint movements are stabilized and do not increase further after 91 days, although residual deformation are recorded (Figure 8).

Based on above considerations and test series, extended design values could be proposed to include shear strength accounting for relaxation effects to use when shear movements are imposed to joints, but no permanent shear loads to be transferred. For an entire evaluation of the structural silicone joints, the influences of wind, live loads and climatic effects must be taken into account too. Short-term and permanent load combinations should be defined and combination of utilization levels out of existing stress and allowable stress should be evaluated with regard to relevant load directions and durations.

| Product                | EOTA ETAG 002        |                    |                    |         |                      |                           |
|------------------------|----------------------|--------------------|--------------------|---------|----------------------|---------------------------|
|                        | $\sigma_{des}$ (MPa) | $\tau_{des}$ (MPa) | $\tau_{rel}$ (MPa) | G (MPa) | $\sigma_{rel}$ (MPa) | $\tau_{rel, relax}$ (MPa) |
| Sikasil® SG-500        | 0.14                 | 0.105              | 0.0105             | 0.50    | 0.014                | 0.0315                    |
| Sikasil® SG-550        | 0.20                 | 0.13               | 0.013              | 0.63    | 0.020                | 0.039                     |
| Sikasil® IG-25         | 0.14                 | 0.101              | 0.010              | 0.73    | 0.014                | 0.030                     |
| Sikasil® IG-25 HM Plus | 0.19                 | 0.13               | 0.011              | 0.86    | 0.019                | 0.033                     |

Table 1: Extended range of design values

## Conclusions

A variety of criteria exists for optimizing the bending process of curved glass elements in façade applications, which take into account different design and manufacturing process and needs. Besides the preferably discussed visual, technical and cost-driven aspects, influences on the joint design of SSG units must also be considered. How the negative influence of large shear deformation can be significantly reduced on permanently loaded structural silicone joints through a clever system design and use of leaner adapter frame is shown in Section 3.

Furthermore, the relationship between EOTA ETAG 002 [3] and the stress of elastic adhesive joints in cold-bent units is established in Section 4. The observation shows that the existing approvals of structural silicone adhesives on the basis of [3] and [4] cannot or can only be consulted to a limited extent for the verification of cold-bent SSG units. More extensive guidelines are needed for evaluation and calculation methods of cold-bent elements, as well as definition of meaningful allowable stress.

## References

- [1] Dodd, G.; Thieme, S.: Comparison of curved glass and cold bent panels. GPD Glass Performance Days 2007, S. 83-86.
- [2] Beer, B.: Structural Silicone Sealed Cold-Bent Glass – High-Rise Projects Experience Leading to a New Design Concept. GPD Glass Performance Days 2015, S. 235-240.
- [3] EOTA ETAG 002-1, Structural Sealant Glazing Systems Part 1: Supported and Unsupported Systems, 1998.
- [4] ASTM C1401, Standard Guide for Structural Sealant Glazing, 2014.

# Chaoyang Park Plaza Tower: Design and Construction of Complex Geometry Facade

Yu Hui<sup>1</sup>, Nicolas Leduc<sup>2</sup>, Tan Hui<sup>1</sup>,  
 Florian Rochereau<sup>1</sup>, Jin Shihui<sup>1</sup>,  
<sup>1</sup> RFR Shanghai  
<sup>2</sup> T/E/S/S

## Keywords

Double Curved Façade, Geometry Optimization, Cylinder Glass Panel, Semi-Discretization

## Abstract

In this paper, we present the workflow of design and construction of Chaoyang Park Plaza tower façade located in Beijing, China, which is one of the most challenging façade system due to its complex double curved geometry from architectural scheme by MAD Architects.

The system is divided into two main zones one with purely cylindrical façade and the others with twisted roofs strips which blend smoothly into the tower faces.

The initial surface was rationalized with a cylindrical fitting algorithm. The goal is to find a panelized surface which keeps a very smooth appearance, while at the same time minimize cold bending amount. This optimization process also had to consider the unitized façade frames to obtain a buildable geometry with straight extrusion mullions and planar circles transoms, following to the parameters extracted from the reference surface. (Twisting angle to mullion, dihedral angles, etc.) The waterproofing design for sloped parts was specially investigated.

The design integrated a fully automated manufacturing process which included 7600 glass panels produced according to the limitation of size of the bending machine. A 3D BIM and an automated digital manufacturing technology were used to cut the frames with variable angles, which made possible to realize the 3-dimensional geometry of each component. These components were then assembled with a small amount of cold bending applied in factory.

## Introduction: Challenge and Strategy

Free-form façade has become more common in China. A series of technical improvements support this trend with new tools and methodology enabling to realized what has become commonly referred as complex



Figure 1 Chaoyang park plaza construction completed.

geometry.

In this paper, we are sharing the experience of designing and fabricating of Chaoyang park plaza tower, which is the most complex free-form high rise facade in china. RFR shanghai was contracted by the developer and has done the geometry optimization, the façade system design work which has started in 2014 and followed by the supervision of the whole construction process until its completion in 2016.

Chaoyang Park Plaza is in the central business district (CBD) of Beijing. A pair of asymmetrical towers up to 143m creates a dramatic skyline in front of the park. Vertical ridges and valleys define the shape of the exterior glass facade, as if the natural forces of erosion wore down the tower into a few thin lines, according to the architectural concept of MAD architects, the "Shanshui". The challenge is thus to translate this artistic intent into a design and fabrication process and to apply to it an actual tower with an industrial mass production process, cost-effective and with off the shelf fabrication technology.

The Challenges of Chaoyang project can be summarized as three aspects:

- Double curved geometry for the Glass;
  - Double curved geometry for the façade system;
  - Industry 3D design and production capacity
- First, the double curved geometry pushed the

limit of the current façade industry, especially for high-rise building. 54% of curved surface are highly doubled curved (radius <12m). The necessary geometry rationalization had not only to keep the smoothness of the surface desired by MAD, but also keep the glass panels within the constrain of standard production capacity and with the maximum curved glass sizes which could be produced at the time. After reviewing possible solutions for glass panels such as hot forming double curve glass, quadrangular flat panels, twisted panels (flat panel cold bended), we concluded that we should focus on a well-known approach but never applied at such scale: A cylindrical best fit optimization.

Learning from the experience of the foundation Louis Vuitton in Paris [1], the Eiffel tower pavilion [2] for the principle of cylinder fitting, and from Strasbourg TGV Station [3][4], Lille TVG station much earlier and Avignon TGV station for cold bending with single curvature, we decided to pursue the work and applied these principles to the Chaoyang project. In this case, the joint layout of the reference surface is horizontally rebuilt as planar arc, and vertically polygonized. The rebuilt semi-discretized surfaces are curved smoothly in the horizontal direction and leave minimal kinks at the adjacent floors, forming general cones at each floor, which gives the best results for local cylinder fitting. The deviation stays within

maximum 30mm between the rebuilt surface panel and the fitted cylinder panel. This deviation is even more reduced by applying a cold bending onto the glass to the frame. Second, the double curved geometry is also a challenge to the facade system design. To obtain a curved unitized façade with smaller deviation at the corners of each components, a common and cheap solution is to fabricate planar components and apply cold bending on site. But for Chaoyang project, the curvatures are big and geometry is freeform without repetition, a three-dimension frame system is therefore preferred. The frames are CNC cut with individual angles and assembled non-planar in the factory. It is not realistic to have all aluminum extrusion profiles curved and twisted, our solution aims to have straight extrusion mullions following average surface normal direction at each floor. In this way, straight and CNC profiles would provide the buildability and precision required by the system.

Moreover, the complexity of glass panels and frame components is demanding for the contractor's not only 3d design and fabrication capacity but also a very tight assembly precision. Today's automatic curving machine can produce perfect quality tempered glass with no repetition radius and edges. Computer Numeric Controlled machines are used to cut the frames with difference angles and carved the transoms in arc, which made possible to obtain the complex 3-dimentional geometry for each component. The contractor pursued the fabrication work with its own capacity and expertise under collaboration and supervision of RFR Shanghai.

## Geometry optimization

### Reference geometry

#### Reference surface and typologies

At the very beginning of the project are the "reference surfaces".

In the preliminary stages of design, the whole facade complex is modeled by simple surface patches with no thickness, so called "reference surfaces". It expresses the architectural design intent and thus represent a guideline shared by MAD architects and the engineering consultants working on the project. The reference surfaces are frequently updated as the project evolves over time.

The reference surfaces fulfil another important purpose: they guaranty the consistency of the geometrical design of all the facade components. Each part of the facade has a well-defined relationship with the surface, in terms of offset, orientation, etc.

The 21.300 m<sup>2</sup> of reference surfaces of the Chaoyang Park Tower can be described in

terms of geometry or facade technology. See in Figure 2 and Figure 3.

#### Reference jointing layout

The reference jointing layout is complementary to the reference surfaces for a precise definition of the facade components. It consists in a bidirectional network of curves located on the reference surface and represents the design intent for facade subdivision into panels. As shown in Figure 4.

Note that the intersection of these planes and the reference surface generates arbitrary planar curves.

#### Surface geometry: rationalization strategies

Facing the problem of construction of complex geometry, several strategies could be envisaged. Their relevance depends on many criteria such as the respect of the design intent, the cost or the technical performance. With no claim to be a rigorous classification, we propose three possible strategies: no rationalization, pre-rationalization and post rationalization.

#### No rationalization

This first option consists in building the surface "as it is", which often implies to build unique panels in their cutting patterns as well as their 3d shapes. The balustrades of A4-A7 buildings can be considered partly in this class. Changing partition direction can reduce the curvature of the panel, but it's not preferred by architect, part of the balustrades are still made of doubly-curved glass panels.

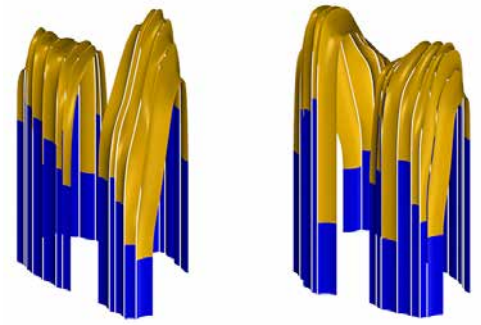


Figure 2 the surfaces are split into the geometric types based on the Gaussian curvature corresponding to increasing level of complexity: half of the area is generated with rotational cylinders (blue) and the rest is a free-form double curved surface (gold).

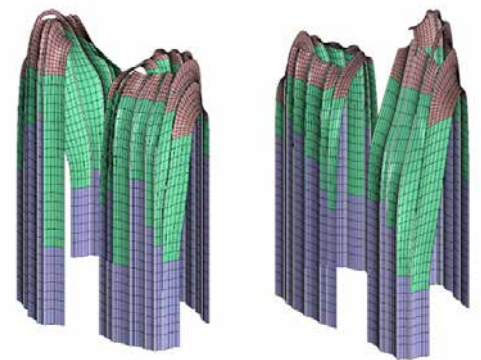


Figure 3 shows three facade technologies types: The blue part (46%) represents insolated vertical façade, the green part (38%) represents insolated sloped façade, the red part (38%) represents canopy single-glazed roof

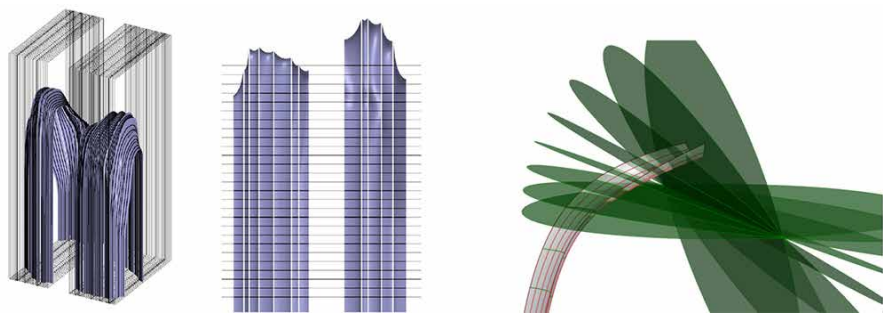


Figure 4 Reference surface jointing layout. Left: the vertical network is the result of the intersection of vertical planes and the entire reference surface. Middle: The horizontal network of the vertical and sloped part is aligned with the slab level. Right: The roof subdivision is the result of the intersection of a pencil of radial planes and the reference surface. This generating process allows a continuous transition between the last horizontal plane [between sloped and roof part] and the last plane of roof part.



Figure 5 Chaoyang Park Plaza A4-A7 buildings Balustrade partly made of double curved glass panels.

### Pre-rationalization

The pre-rationalization approach limits the design space to families of surfaces whose geometric properties provide technological benefits. Spheres, cylinders, cones and torus are obviously part of these surfaces. The 80's and 90's saw an extensive use of revolution, translational and homothetic surfaces that allowed more freedom than basic geometric primitives [See Figure 6 Shanghai ocean terminal].

It should be noticed that this kind of geometry is at the heart of contemporary research again. Mesnil et al propose intuitive tools that guarantee the planarity of quadrangular meshes from architectural sketches [5]. Another article widens the range of pre-rationalized surfaces with the ones of Monge while guaranteeing planarity of quadrangular faces and torsion free structural nodes at the same time [6].

### Post-rationalization

Post-rationalization is a most recent approach whose development has been enabled thanks to the extensive computing power and further progress in discrete differential geometry knowledge.

Based on optimization process, the discrete panel solution tries to best fit the reference surface of the architect. One must distinguish between two distinct kinds of approximation: local and global optimization. For local approximation (easier implementation and less computing-time consuming), each individual panel tries to fit as well as possible the reference surface. Since there is no adjacency relationship between two consecutive panels, this approach may

lead to a heterogeneous distribution of the performance.

On the contrary, a global optimization approach tries to minimize the divergences by relaxing the panel solution at a global scale under a set of control constraints (planarity, position and tangency continuity between panels, and closeness to the reference surface...). The optimization is no more driven by the best individual approximation of a common reference (the reference surface) but the best collective performance of a panel population. A global optimization approach is likely to homogenize the distribution of the performance and provide overall improvements.



Figure 6 Shanghai Ocean Terminal, planar-quad glass panels because of its homothetic surface

### Chosen approach

Let us explain why the selected approach for the facades of the Chaoyang Park towers has been oriented to a post-rationalized approach. Building the design surfaces as-is was deemed impossible due to economic feasibility reasons. The huge quantity of panels (more than 7000) could let us think that repeatability would make possible the use of a unique mold for several glass panels. Unfortunately, despite in depth studies, the numerous geometric degrees of freedom (in plane cutting pattern et 3d shape) did not allow an effective panel clustering under an acceptable tolerance. Figure 7 shows the study of panel's possibility of repetitive fabrication.

On the other hand, the complexity of the design surfaces could not be captured using surface primitives proposed by the pre-rationalization approach.

Thus, the architectural requirement about the respect of the design intent led us to adopt the post-rationalization approach. The state of the art of optimization tool, with further ad-hoc developments allowed us to approximate the design surface with a good fidelity while providing excellent technical properties to the panels and the support structure.

### Panel geometry: rationalization strategies

Once a rationalization option for the reference surface has been chosen at the global scale, another question rises at the panel scale. As we saw previously that unique doubly curved panels were not an economic option, a survey in the field of industrial fabrication of glass panels gives some clues. We examined three options: flat, twisted and cylindrical

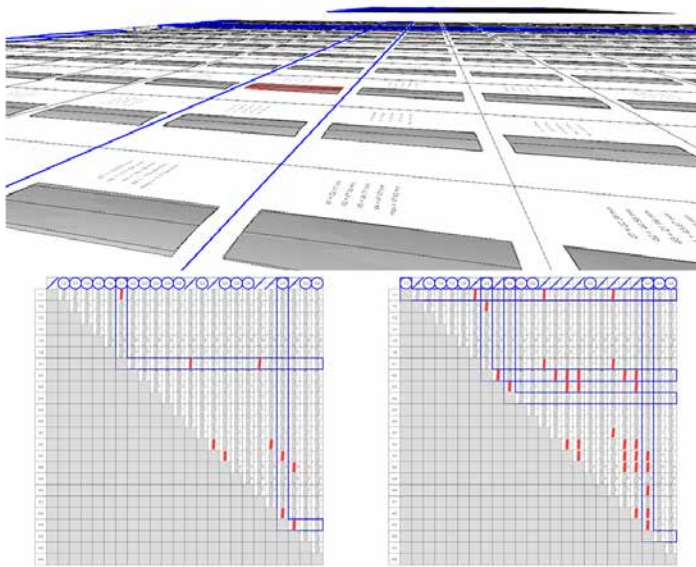


Figure 7 shows 24 pieces of most similar panels among 7600 panels were chosen to study their receptivity. Three parameters have to match to offer the repetition of cylinders: Curvature radius, Cutting pattern, direction of the cylinder. For the studied 24 reference panels, 18 different panels are needed for a tolerance of 10mm.

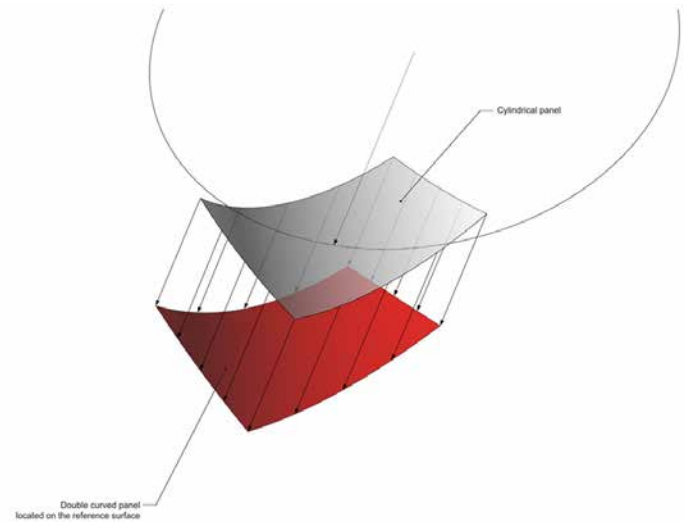


Figure 8 local approximation aiming at minimizing the distance from a cylinder glass panel (white) to the reference panel (red)

panels. From a geometrical point of view, the approximation quality (and complexity) of the reference surface is increasing from solution 1 to 3

#### Geometrical features and technical consequences for glass panels

A target panel is defined as a reference surface patch bounded by four curves of the reference jointing layout. The goal of the geometrical approximation being to minimize the distance between the target panel and the manufactured panel, we have to choose the most appropriate surface geometry. Quadrangular flat panels are of course the first option which comes in mind since it is a proven and reliable technology and from far the cheapest way to produce and assemble insulated glass panels. But the faceted aspect (discontinuity in tangency) was rather inappropriate when the reading of the curvature was a priority for MAD architects. Moreover, one should notice that on a given doubly-curved surface, four arbitrary point are not coplanar. Therefore, gaps between two consecutive panels (discontinuity in position) give a scale-like aspect to the facade, raising once more the question of architectural aspect. Furthermore, on a technical point of view, divergences between adjacent panels is a critical condition for the water-tightness of the facade which should be carried out by a non-standard technical detail.

In order to take advantage of the hardness of planar panels manufacturing while minimizing the waterproofing issues mentioned above, an option with twisted glass panels has been envisaged. This method forces the glazing unit

within its elastic domain to a target position defined by the reference surface. Special attention will be given in the specific case of double glazing. As a matter of fact, in addition to mechanical stress in the glass due to twisting, the shear strength in the sealing joint may damage the isolating performance of the panel. The twisting of the panel only improves slightly the faceted aspect of the facade. Increasing the geometrical degrees of freedom of the panel, and then its manufacturing complexity, let us approximate the target panel with lower tolerance. Such is the case with rotational cylinders which present a unique curvature radius for each panel. However, this unique radius can be different for each panel. The generatrices of the cylinder are parallel to each other but have an arbitrary direction regarding the edge of the panel. For this reason, this type of cylinder is called "arbitrary cylinder".

This option greatly enhances the visual aspect of the facade in that it respects the notion of curvature proper to the facade design. From a technological point of view, the divergences in position and tangency between two consecutive panels being minimized, the water-tightness technical details can be addressed in a more traditional way.

The use of rotational cylinders can be justified by an industrial reason. Today's bending machines enable the fabrication of cylindrical panels with variable radii without the use of individual mold for each panel. And these systems provide excellent quality tempered bent glass. Unfortunately, shapes like general cylinders or cones, which would increase the approximation performance are not available yet.

An arbitrary intersection of a cylinder and a plane is an ellipse portion. However, it exists two given planes along which the ellipse portion becomes an arc of circle and a straight line. Thus, a specific orientation of the cylinder enables to get peculiar geometric properties for the edges of the panel. For this reason, this type of cylinder is called "oriented cylinder". One should notice this slightly affects the quality of the approximation: it is not necessarily the optimal cylinder regarding the reference surface since a constraint has been imposed on the orientation of the generatrices.

#### Implications for support structure

The choices for the geometry of the panels have been taken, measuring the consequences they imply on the structure that holds the glazing units: two mullions (vertical direction) and two transoms (horizontal direction). The manufacturing complexity of these structural components is highly related to the geometrical complexity of the profile axis (plane or spatial curvature) and the geometrical behavior of the cross-section (torsion). The various options are summarized in the following table.

|                     | Mullions               | Transoms               |
|---------------------|------------------------|------------------------|
| Flats panels        | Straight / Not twisted | Straight / Not twisted |
| Twisted panels      | Straight / Twisted     | Straight / Not twisted |
| Arbitrary cylinders | Elliptic / Twisted     | Elliptic / Not twisted |
| Oriented cylinders  | Straight / Not twisted | Circular / Not twisted |

### Chosen approach

The chosen option is the oriented cylinder. It seems to represent the best possible accommodation between the architectural aspect and the technical performances of the facade panels and its support structure.

### Design process

#### Reference surface remodeling

In order to take advantage of the geometrical and technical properties of the panels (rotational cylinders) and the structural elements (straightness of mullions and circularity of transoms), the remodeling of the reference surfaces allows a better approximation. With reference to the rationalization strategies proposed earlier, we set up a hybrid approach (pre & post-rationalization) by applying panel optimization to new reference surfaces modeled between two floor levels.

Each edge of slab, initially defined as an arbitrary planar curve is rebuilt by an arc of circle. Through two arbitrary circles whose support planes are parallel, it is possible to generate a general cone. This set of surfaces is a semi-discretized representation of the reference surface. The newly constructed surface is smooth in the horizontal direction and polygonized in the vertical direction.

#### Cylinder approximation

The subdivision of the general cones by the reference jointing layout defines target panels to be approximated. A cylindrical local approximation is then performed for each panel.

Since the radii of curvature of two consecutive slab edge are quite similar, the cylinder approximation is of excellent quality. The minor divergences between the approximate cylinder and the semi-discrete reference surface are cancelled by cold-bending the panel.

#### Unrolling

The selected geometrical option is entirely based on automatic glass bending machines which are able to put the glass panel in shape and temper it without the use of molds. However, the bending bed size limitations and the large format of the panels of the towers required in-depth studies of the compatibility between unrolled cutting pattern and the available machines on the market

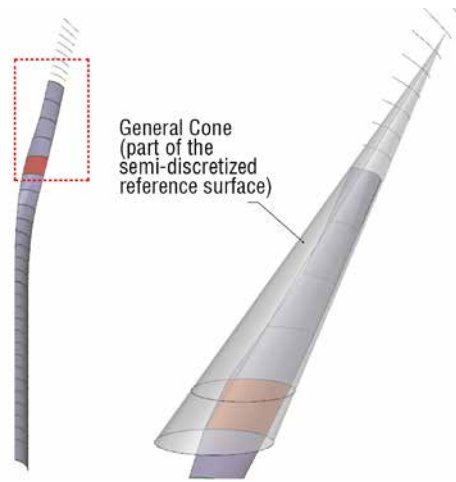


Figure 9 Semi-discretized reference surface: general cones

This work led to an iterative process with the architect to densify the jointing layout where needed. For the vertical and sloped part, the target panel is systematically horizontally subdivided in two parts: window and spandrel. For the roof part, no horizontal subdivision is performed. Additional vertical subdivisions are locally introduced where the panel is too large to fit maximal dimensions of the bending bed. At the end of the subdivision process, 7257 panels have been automatically unrolled in a format close shop-drawings, including graphical information (cutting pattern, orientation of the panel along bending axis of the machine, bounding box, ...) as well as textual information (location, panel naming, radius of curvature, ...)

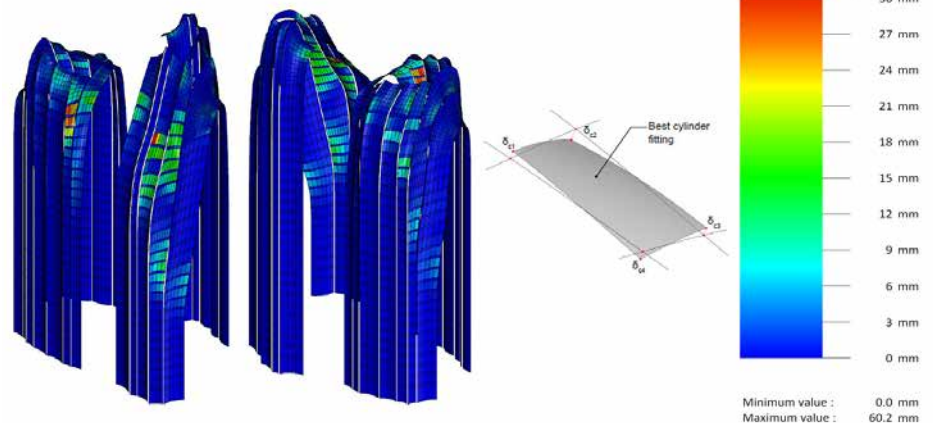


Figure 10 Cylinder fitting deviation

### Analysis: cartography and bill of quantities

These geometrical studies were supported by a quantitative analysis of the various geometrical parameters with help of cartography and statistic recurrence (extreme and median values, distribution of the population by class). This was very helpful to feed the other related studies and particularly the technical detail design. As an example, we can mention the dihedral angle between two panels. The data extraction of this geometrical parameter is directly linked to the range of variation the mullion or transom is likely to absorb. This quantitative approach has also proved its usefulness for reliable and fine pricing by sorting components and systems by class of complexity.

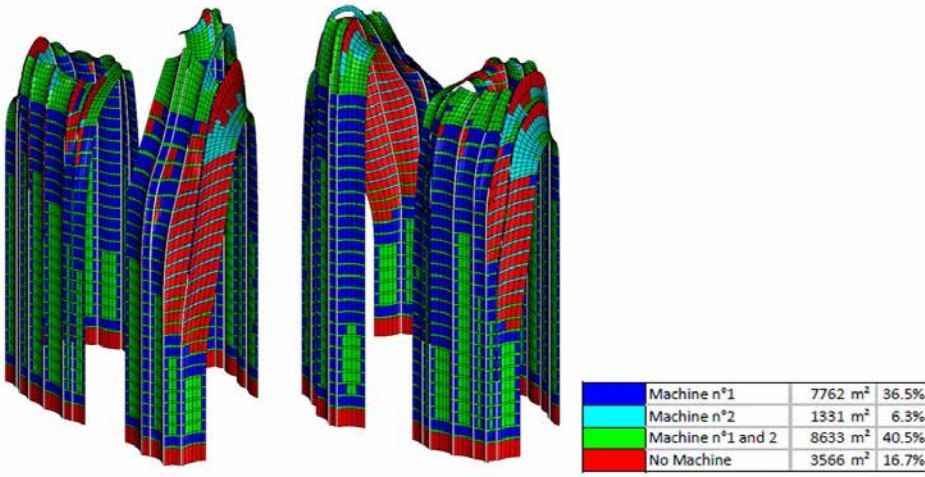


Figure 11 Compatibility with North Glass bending machines (before subdivision). Dimension of biggest bending bed available at the moment: Machine 1: Straight length 12.8m, Arc length 2.8m; Machine 2: Straight length 3.3m, Arc length 4.2m

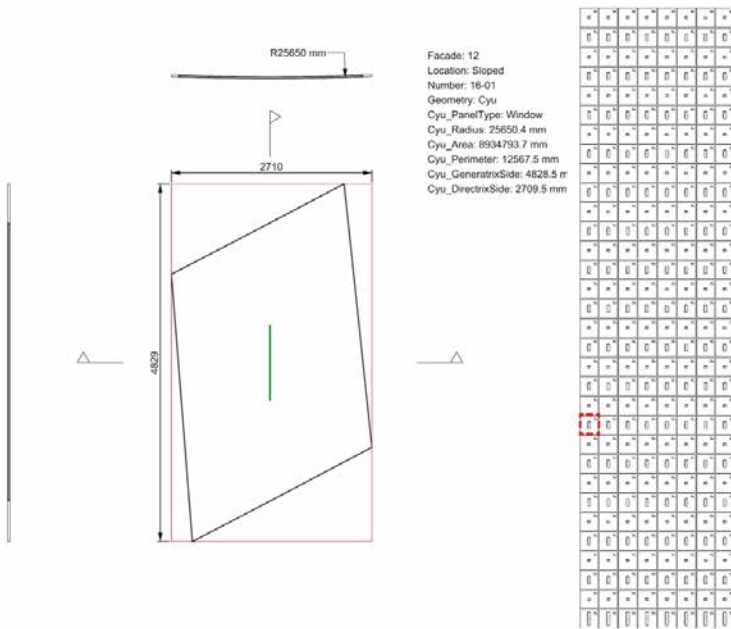


Figure 12 All the cylindrical panels have been unrolled in a sorted grid with the position of the panel and textual information.

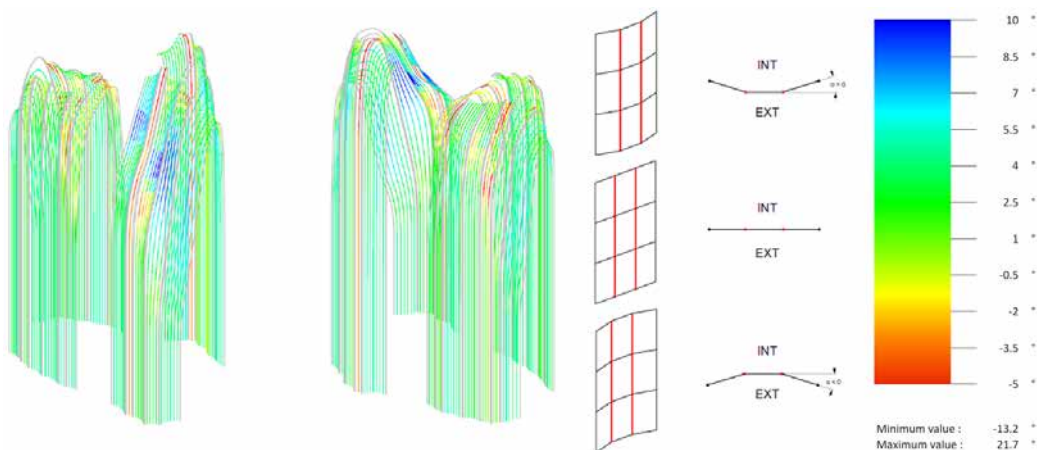


Figure 13 Dihedral Angle between two panels.

## Façade System Design

### Frame orientation

From the geometry optimization process, semi-discretized surfaces are generated with general cones and ruled surfaces whose generatrices are mainly vertically oriented. Mullions front axis, equivalent to the glass division lines, are the result of the intersection of these reference surfaces and vertical planes. 98% of these axes are within 5mm deviation from straight lines, so that mullions can be simplified to straight extrusions. As mentioned above, horizontal divisions are horizontal planar arcs which can be considered as planar circular extrusion transom. Both of these profiles are suitable for industrial mass production.

The solutions of straight, non-twisted extrusion and mullion orientation with normal of surface result in the mullion orientation solution shown in Figure 15 image on the right. Straight mullions are segmented and take average normal direction of surface of each floor, thus upper and lower floor mullions are oriented separately with continuous rotation center at mullion front axis.

On the left, the non-rationalized approach leads to smooth but double curved and twisting mullions not feasible for industrial production. Because of the normal difference which appears from one floor to another within one mullion strip, a clustering process has been studied to verify that the deviation induced by this twist was in acceptable range and taken with structural silicon. In practice, results show few mm deviation for the back of the mullion between floor  $n$  and floor  $n+1$ , 95% were less than 5 degrees difference.

### System detailing design

Once the principle of the façade system is defined, further studies have been made to optimized and achieve the required precision, and performance while fabrication cost is always considered in parallel.

Bending process for aluminum extrusions is not reliable in precision, so that we decide that main part of transoms are also kept straight but CNC cut in arc, only the small front part fixing the glass is bended and attached to the main part.

The solution of three-dimensional frame system provides buildability and precision, but there is an issue with inclined frames not meeting at the same point at joints. Figure 17 shows the variety of dihedral angles between adjacent transoms and between upper lower mullions.

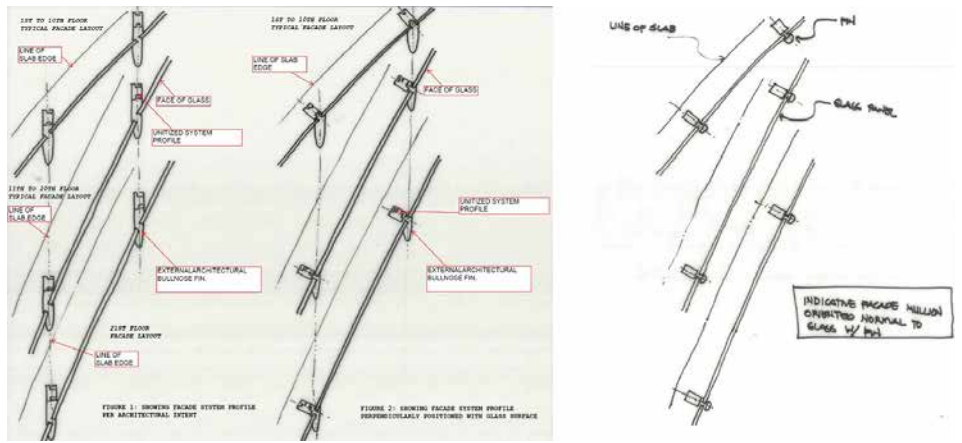


Figure 14 shows different options for mullion orientation with façade surface. Left and Middle is not feasible because the wide range of angle variation between mullion and façade surface. Mullion orientation should follow as much as possible the normal of the glass panel as shown on the right.

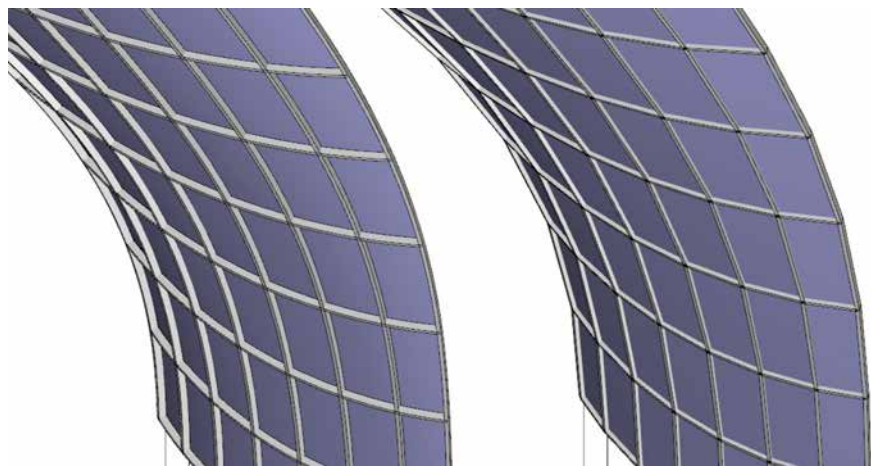


Figure 15 geometry of frame Left: Non-rationalized mullion approach right: straight mullion approach

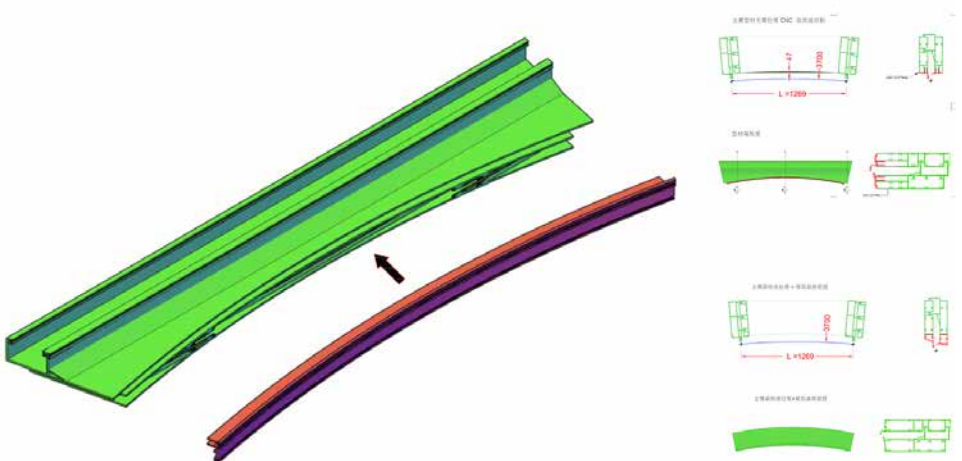


Figure 16 Straight transom cut in arc, coupled with small front frame bended.

Because of mullions inclination changing from one floor to another and the constant depth of the profiles, the resulted intersections with the transom plane have different length. An adaptable gutter integrated within the transom profiles has been designed to slide and match with the inner cavity of the mullion for waterproofing continuity.

A tolerance uptake was also introduced to reduce number of the dies. A clustering process has been applied to the frame geometry to minimize the number of die for mullions and transoms used on the overall project. Thanks to this process, with a step of 2.5 degree inclination of gutter between each die, only 2 dies were necessary for the mullions and 6 set of dies were necessary for the transoms.

Sleeve covers over the gap of transom gutter on site and is sealed with silicone. Rainwater occasionally coming into the inner cavity gathers in the transom gutter and flow through the holes into waterpipe then come outside.

In addition to typical unitized façade's drainage system, special treatment is used to secure waterproof performance. Because the slope angle of the façade with ground is very small at upper part of the tower, the façade is more working as a skylight. Structural silicon is used to fix glass panels and the frames while assembling in factory, and weather silicone was applied to the gaps of components after they are installed, leaving a few holes for air going through the balance pressure cavity and outside.

|               | Horizontal (mullions) |  | Vertical (Transoms) |  |
|---------------|-----------------------|--|---------------------|--|
| Vertical Part |                       |  |                     |  |
| Sloped Part   |                       |  |                     |  |
| Roof Part     |                       |  |                     |  |

Figure 17 Dihedral angles

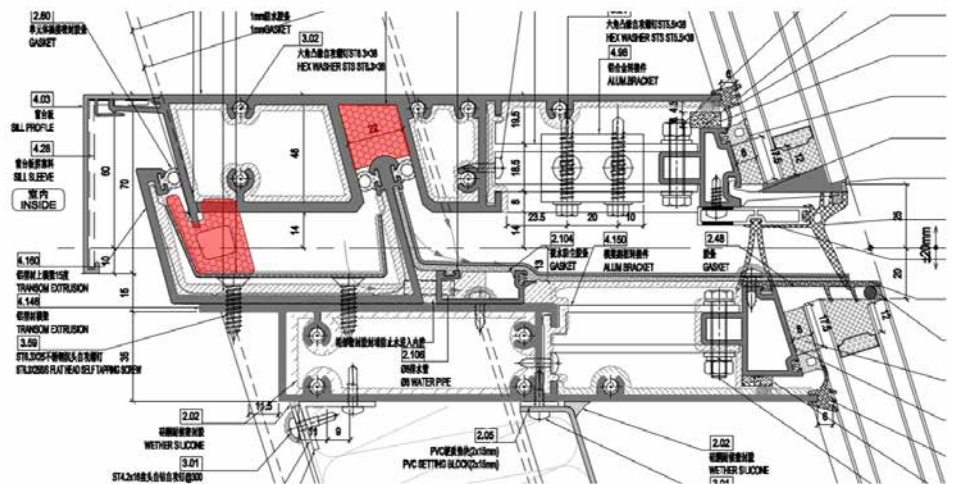


Figure 18 Transom construction drawing showing relation of adaptable gutter and sleeve with mullion inclination angle

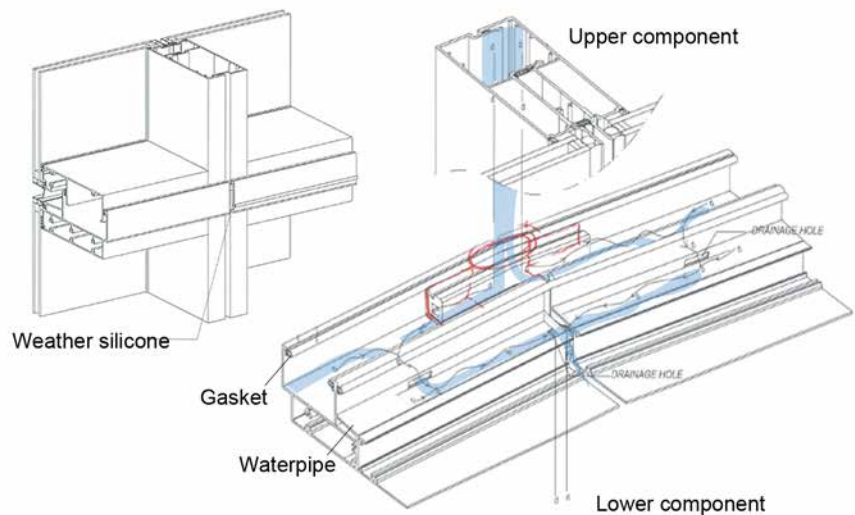


Figure 19 3D view for 4-way joint of the components

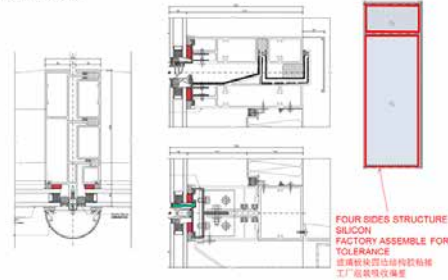
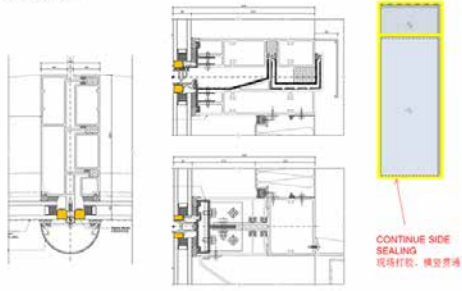


Figure 20 double layer silicon sealing

Realization

Façade contractor Jangho got involved in the project since Visual Mockup phase. Research and experiments were carried out, such as VMU, PMU, glass smoothness checking etc. With the help of 3d BIM, contractor defines more clear and detailed principles and parameters for fabrication and construction. Parameters such as: inclination angle of the mullion in relative and absolute coordinate, adaptable gutter position relative to transom, cutting angle of transom with inclined mullion, orientation plane of mullion, torsion angle of mullions between upper and lower levels, etc. are invested carefully to specify each component in 3D. After construction drawings and BIM models are checked and confirmed, it come to fabrication phase. Shop drawings are directly extracted from Jangho's customized Pro-E parametric system.

7600 pieces of glass panels are fabricated as the execution drawing mentioned above. Width of glass panel bounding box is set within 2.4 meters. Unrolled panel edge length and its difference with corresponding frame length are checked to make sure the glass can fit into the frame with enough margin for structure silicon. Arc height is increased a few millimeters so that when the glass panels are cold bended to the frame, the glass can attach more tightly to frame while cold bending. The components are assembled with one corner lifted in space and three other points lay planar, cold bending is applied along long edges. Small amount of cold bending doesn't deform the frame more than 5mm, so components are plugged together with little adjustments during on-site installation. Components are installed with bottom transoms plugged and fixed in position first and then top corners are pushed or pulled to the designed position, to erase the deformation caused by transportation and cold bending stress. Edges and joint sealing are applied at the same time.

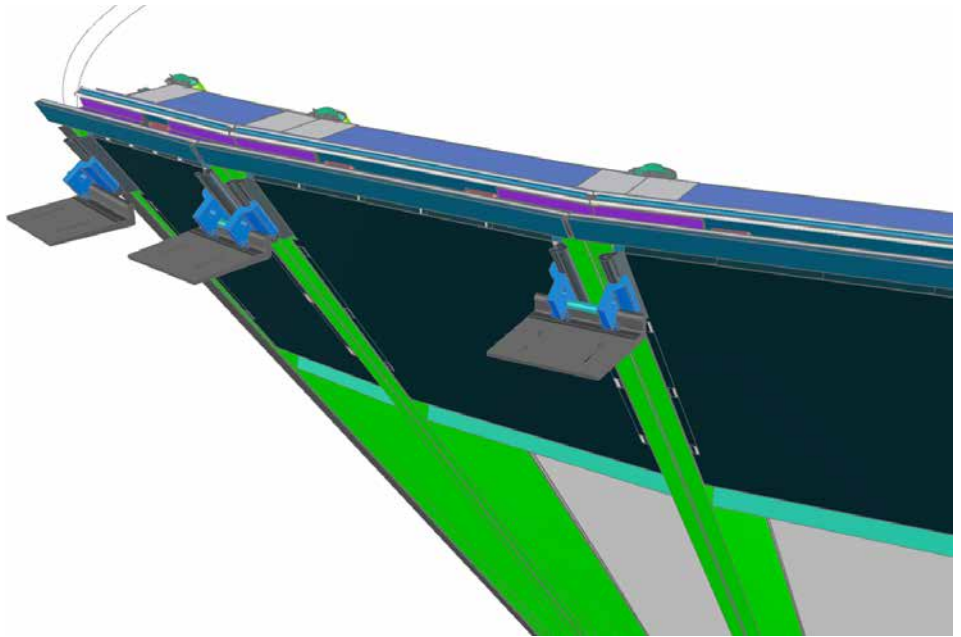


Figure 21 – BIM partial model of unitized façade

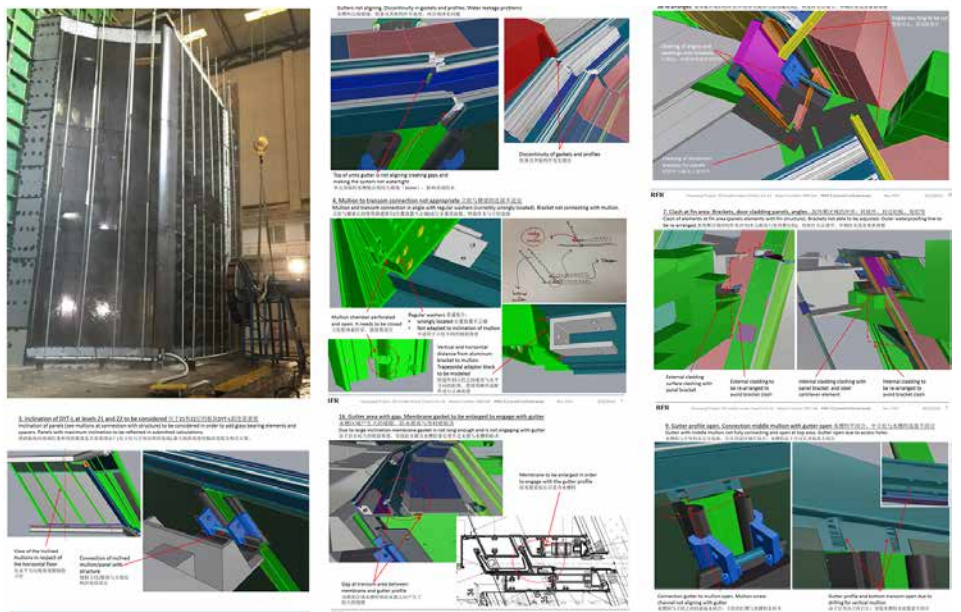


Figure 22 RFR's documentation of PMU checking and 3d BIM checking

## Conclusion

Chaoyang Park Plaza Tower represent today one of the most complex double curved façade build today not only in China, but also in the World. As described above, the most advanced research on geometry and fabrication processes have been applied to the project to achieve this great result. Results that would not be possible to be achieved with a close cooperation between Architects, Façade and Structure Consultants and Contractors.

## Acknowledgements

Façade consulting RFR Shanghai, with the team: PD: Yuhui, PM: Tanhui, team: 谭晖, Armin Kainz 于辉, Nicola Leduc, 金长发, 赵燕华, 王先锋, Florian Rochereau, 贺学峰, 朱申亚, Philippe Bompas, Nicolas LEDUC, currently at T/E/S/S, atelier d'ingénierie. PhD student at Laboratoire Navier. Geometry optimization of this project has been done when he was working at RFR sas Paris. The writing of this paper is funded by T/E/S/S and VIRY. Architect MAD; Façade contractor Jangho; 李剑星, 程宏波 from Jangho shared their experience of this project.

## References

- [1] RAYNAUD J VAUDEVILLE B. How irregular geometry and industrial process come together: A case study of the Fondation Louis Vuitton, Paris In Advances in Architectural Geometry 2012 Springer Vienna
- [2] Schiftner, A., Leduc, N., Bompas, P., Baldassini, N., & Eigensatz, M. (2013). Architectural geometry from research to practice: the Eiffel tower pavilions. In Advances in Architectural Geometry 2012 (pp. 213-228). Springer Vienna.
- [3] BLASSEL, J.F. AND PFADLER, A. 2008. La gare de Strasbourg. In Construction Métallique, n° 1, page 15-36.
- [4] Blassel, J.F. 2007. New Glass and Old Stones. Glass Performance Days 2007.
- [5] Mesnil R., Douthe C., Baverel O., Marionette Mesh From Descriptive Geometry to Fabrication-Aware Design, 5th Symposium on Advances in Architectural Geometry (AAG), 2016, p.62-81 ;
- [6] Mesnil R., Douthe C., Baverel O., Isogonal moulding surfaces: a family of shapes for high node congruence in freeform structures, Automation in Construction (2015) Vol 59, p.38-47;



Figure 23 Factory fabrication and Site Assembly

# Systematically Unique Facade Geometry

Oliver Hans 1  
Andreas Fuchs 2  
Stefan Peters 3  
Jörg Möhring 1  
1 Schüco International KG, Germany  
2 FAT LAB, Germany  
3 Graz University of Technology, Austria

## Keywords

1=parametric design 2=digital process 3=BIM  
4=mass customization 5=complex geometry

## Abstract

Today's parametric design tools allow for geometric variation throughout architectural projects, permitting the designer to manipulate i.e. an entire façade while controlling each element individually. The technical implementation of parametrically developed constructions is generally complex and demanding. Architects, engineers and fabricators are confronted with challenges of geometry, structural design, complicated detailing and varying software interfaces during design and production. With the Parametric System these problems have been addressed by developing a tested aluminium façade system based on a set of variable geometries that are parametrically adaptable and supported by a secure, dedicated digital process chain as well as embedded structural analyses and the mass customization of certain components.

## 1 Introduction

For over two decades and following a century of efficient, functional and often orthogonal architecture, we are experiencing the extensive search for ever more complex building geometries and expressive architectural forms. This development is shaped by a wide variety of motives which, from our point of view, could hardly be more different. In some projects it appears important to architects and clients to set themselves apart from the "formal" standard. At the same time designers declare solar radiation, shading and optimum lighting of the rooms to be "design parameters" and thus shape both the building form and the building envelope. Example projects, such as the C10 high-rise of Darmstadt University of Applied Sciences (German Façade Prize

2013 [1]) by Staab Architects and the Oxford Street Project in London by Future Systems show prismatic façades despite a different approach in the design process. If the objective in Darmstadt was clearly the fusion of design with solar shading functionality, then the project by Future Systems shines in its optical brilliance and inimitability. Both however are still shaped by the rhythmical repetition of the same units. If you were to implement such strategies on free-form architecture, there would be an almost infinite number of different unit geometries. Façade technology today therefore faces key challenges:

- Curtain-wall technology, now over 100 years old, is not a system that offers a strategic solution here. The classic glass curtain wall was developed against the backdrop of serial production for flat surfaces and is based on the addition of industrial, identical, mainly right-angled modules.
- Due to the progress and dissemination of modern parametric 3D planning tools in connection with Building Information Modelling (BIM), the aforementioned design strategies can be represented visually and geometrically, and in many respects successfully. However, this means that the standard market components must be forced into the desired form, which often makes each individual component a prototype.

### 1.1 Systematic approach

The desire for "free forms" requires "free construction products" in the sense of systems that can be manipulated parametrically. The fact that expensive individual solutions had to be used to implement nearly all the existing free-form designs of recent years is counterproductive and at odds with the creative will of the architects. To resolve this, SCHÜCO and FAT LAB began a joint research project entitled "Parametric Concept" in 2012, the objective of which was to develop a façade system to enable geometric freedom in both the individual façade unit and the entire system. The constructive structural processing during prototyping and product development was carried out by ENGELSMANN PETERS engineering. After the initial prototypes for BAU 2013 trade fair in Munich, the PARAMETRIC SYSTEM could be presented to visitors at BAU 2015 (Fig. 1). The systems concept is applicable and has a regulatory

function. However, thanks to the large number of possible combinations and geometric manipulations, the formal design variations are almost limitless. A distinction must be drawn at façade level between local and global manipulation:

Local manipulation can be understood as the geometric differentiation of the individual façade unit. In this way, for example, deliberately turning transparent surfaces away from the sun can considerably reduce solar heat gain. Conversely, the generation of energy can be improved by the targeted alignment of PV surfaces. Key here is that a SINGLE repetitive geometry is not the aim; instead, EVERY unit can be designed in accordance with its position and function.

We refer to the application on building structures which are not right-angled and extruded as global manipulation. Through the coupling of units, covering double fold surfaces with rhombic or diamond-shaped units becomes possible. The unit connectors take on the task of "flexible" joints.



Figure 1: Presentation of the Schüco Parametric System at BAU 2015.

The choice of profile geometry is an essential element of the system concept which is understood as a strategy for the solution of a diverse range of tasks. The round tube geometry joined by using customized, inserted and therefore invisible corner cleats is the basis of the "Parametric System". The selected geometries and intersections of individual transparent, translucent or opaque surfaces permit the angle within each individual unit to be determined almost completely at will. The infill units are bonded to an aluminium frame and installed onto an internal secondary adapter frame, creating the thermal seal of the building as a structural glazing façade.

The cutting-edge Parametric System exhibit for BAU 2015 plays with the overall and individual unit geometries as well as unit depths. The local distinction between transparent and translucent glass units as well as the global flexion of the entire surface suggest the future possibilities for façade design.

## 2 Structure

There are two notable innovations concerning the load-bearing structure of the façade:

- the parametric optimisation of the load-bearing structure
- the bonding of the insulating glass.

The modules of the Parametric System consist of a load-bearing aluminium unit frame which is fixed to the building structure at selective points and connects the modules structurally. Atop the unit frame is an aluminium tubular frame which, within the bounds of the module dimensions, geometrically defines and bears a three-dimensional, folded surface consisting of several panes of i.e. insulating glass (Fig. 2). To achieve structural rigidity, the aluminium tubes are connected using welded steel nodes (corner cleats) with multiple arms. The node arms are inserted into the aluminium tubes with a plastic adapter, form-fitted with metal adhesive and are force-fitted securely. Panes of insulating glass securely connect the fields of the three-dimensional frames constructed in this way. These panes of insulating glazing can be attached to the tubular frame using screws thanks to an adapter profile on the tubes and a frame bonded to the glass with two-component silicone. The panes are blocked to bear the dead load (Fig. 3).

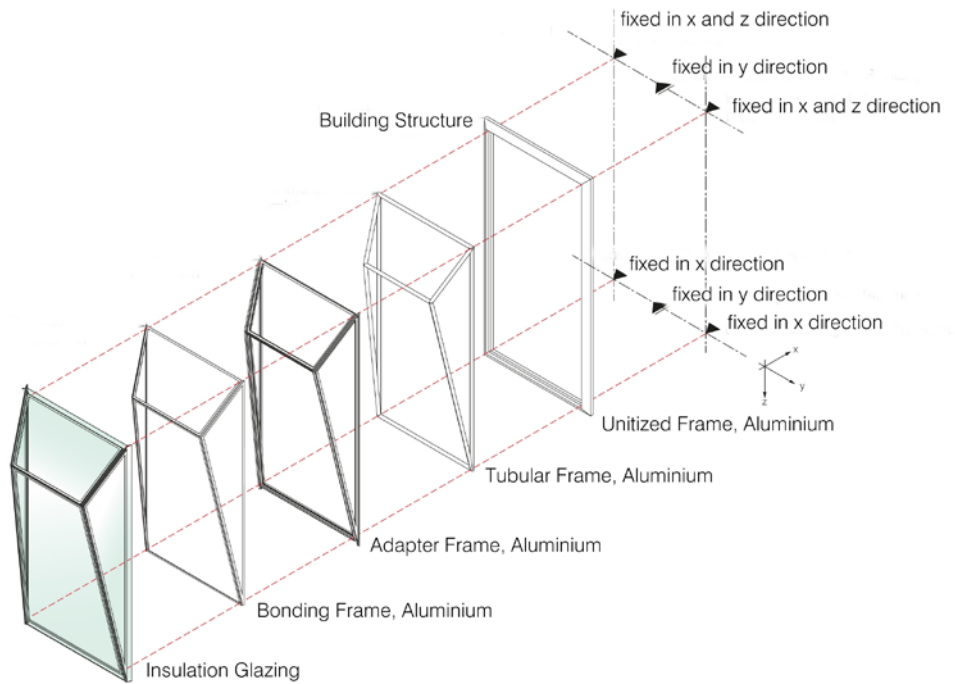


Figure 2: Modular construction and structural system of the Schüco Parametric System.

Figure 3: Construction detail of the Schüco Parametric System and the subjacent unit frame. The contour of the unit frame can be adapted to specific project requirements and the glazing thickness.

## 3 Digital process

The design and implementation of geometrically complex façade systems generally requires improved coordination and planning by everyone involved. Coordinated interfaces in the process chain are essential to ensuring the continuity of the geometries and reference points [2] [3]. The faultless transfer of model information from one planning stage or software tool to the next has to be ensured. The repeated checking, adjusting and creation of drawings would otherwise drastically increase the time required for design. Ultimately, and of no lesser importance, the implementation requires highly detailed and robust information to ensure the precise machining, reliable creation and subsequent installation of the components [4]. The Schüco Parametric System offers diverse ways to design façades geometrically. To ensure the simple, reliable and fast design and implementation of this potential diversity, in addition to the profile system, a continuous, closed software process has been developed from the first design stages through to fabrication. The use of a façade system rather than an individual solution is of benefit here as system rules and components can be used as a basis on which to build. Individual planning steps can thus be supported, automated and

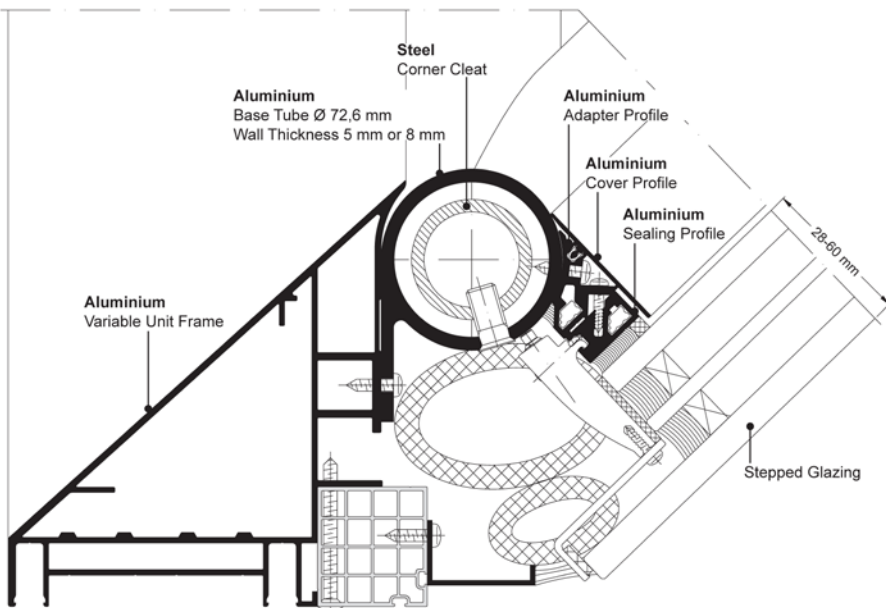


Figure 3: Construction detail of the Schüco Parametric System and the subjacent unit frame. The contour of the unit frame can be adapted to specific project requirements and the glazing thickness.

the complexity of the design process reduced through dedicated software components. The depth of information is adjusted in accordance to the planning stage in a Building Information Modelling (BIM) process.

### 3.1 Design phase

Two plug-ins are available for the design and form finding process which can be embedded into the Grasshopper [5] and Revit [6] CAD environments respectively. A library of intelligent base modules with intrinsic system conditions thus facilitates the draft design and negates the necessity to know the rules underlying the system. The modules can undergo additional parametric modelling through the use of further external software components. Developers therefore have diverse ways to generate and optimise shapes at their disposal. A systematic plausibility check inside the plug-ins ensures feasibility, whilst departing from the limits of the system remains possible. Special constructions beyond the system limits can therefore also be generated and subsequently implemented as a project solution. The models are simplified at this first level of design and do not contain all of the system components to prevent slowing the design process.

### 3.2 Detailing

The planning process is automated through the creation of detailed parametric detail models of the basic modules. The entire structure required are added to the designed geometries upon import into the Autodesk Inventor [7] software. An internal rule set forms the basis for generating the system and special components required, as well as their dimensions, processing and position. The plausibility of the models is tested again at this stage. Editing the detailed models, so that alterations and adjustments are ensured, remains possible.

### 3.3 Fabrication

The detailed model allows components and system profiles to be ordered directly via SchüCal, the manufacturer's preparation and ordering software. The contractors do not have to carry out own planning work to the base system. This is particularly significant in reference to the required stepped glazing (Fig. 4) and the system nodes (Fig. 5). Latter are manufactured as system articles on the basis of the geometry transferred while ordering in a mass-customisation process. When generating the detailed model they are also clearly marked to ensure their correct assignment and position in the units. The data for the precise computer-aided manufacturing



Figure 4: The length of the stepped glazing is dependent on the angles of the design geometry

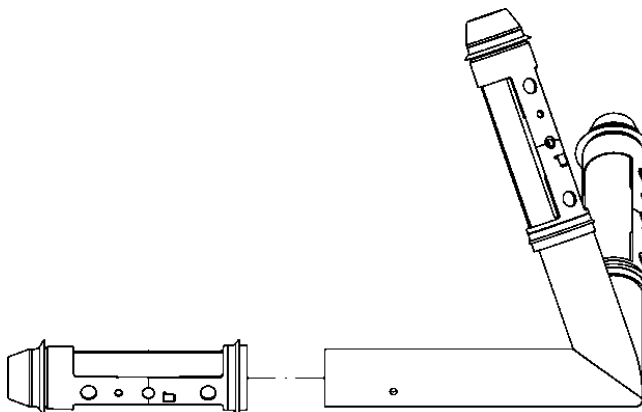


Figure 5: The Parametric System nodes or corner cleats are custom manufactured to suit the designed geometries. Centring sleeves aid the assembly and fixing of the tube joints.

is also stored here and allows the machining to be performed directly on a 5-axis processing centre, i.e. the Schüco DC500 or AF500.

Throughout the continuous software process, all the data constantly remains in a single geometric model (Fig. 6), which everyone involved in the project phase can access at the required level. Here, the possibilities for parameterisation are not only used in the first design phase but also in particular during detailing. Compared to conventional design, the process of implementation is therefore accelerated considerably and system reliability is also the idea behind the software process.

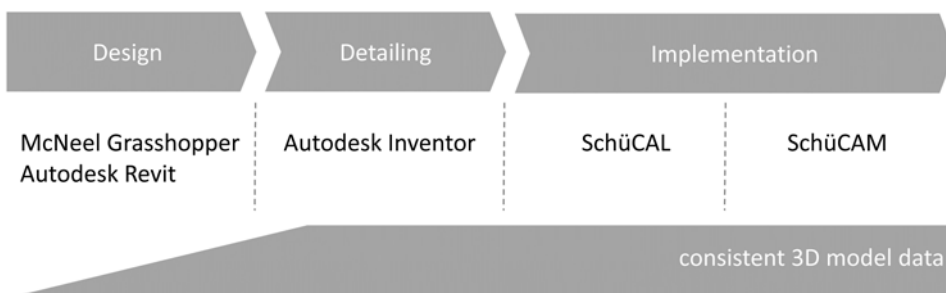


Figure 6: Construction detail of the Schüco Parametric System and the subjacent unit frame. The contour of the unit frame can be adapted to specific project requirements and the glazing thickness.

## 4 Optimisation of structural system

The fundamental challenge in the development and in particular the optimisation of material use of the load-bearing structure lies in the geometric freedom of the system. With 11 different static module geometry types as the starting point, an almost infinite number of geometric variations can be created through the flexible variation of the internal tubular frame nodes in the X, Y and Z axes. This naturally raises the question concerning which of the geometries is the least favourable in respect of the loads on the bars, nodes and connectors and which of the geometries should be used for the dimensioning of the components. The effects on the load-bearing structure of the façade include dead, wind, snow and temperature loads as well as live loads if the bottom of a structure is angled outwards. An approximate approach or a simplified estimate will not suffice here to ensure a structure that is really cost-efficient. A parametric model was therefore created and used for the structural design. This makes it possible to create any number of geometric variations to cover all areas of application. All these variations are then calculated automatically for the significant load combinations and pre-dimensioned via a programmed interface to a finite-element program. This makes it possible to precisely define geometric areas of application depending on the cross section dimensions sought and material strengths as well as to subsequently store them in a configuration tool.

The safety concept of the Parametric System envisages calculating the load-bearing capacity of the tubular frame. The stiffening effect of the bonded panes of insulating glass is initially not taken into account in the proof of the ultimate limit state. In contrast, the stiffening effect of the bonded panes of glass is taken into consideration for the serviceability limit state. The interaction between the effects of the supporting structure and the panes is recorded using a highly detailed finite-element model, taking into account the stiffness of the bonding joints, which ultimately also allows the load on the bonded joints to be recorded. On the basis of such calculated estimates and accompanying tests, the number of areas of application of load-bearing silicone bonds has increased dramatically over the past few years. Overhead glazing could therefore be supported and fixed exclusively using a bonded joint for the exhibit at the BAU 2015 trade fair on the basis of a precisely specified testing and monitoring concept. The lack of any retaining system for the glazing was granted individual case-specific approval.

## 5 Conclusion

Modern digital planning and fabrication technologies open new paths for architectural expression, though also require the planning process and construction methods to be rethought. In conjunction with the possibilities for reliably simulating and parametrically depicting complex relations, these new technologies provide important stimuli for overcoming the challenges of our time. The digital revolution certainly has the potential to help facilitate another evolutionary leap in construction comparable to the development away from solid structures and towards skeleton structures, which not only defined a new construction method but also fundamentally altered and shaped the architecture of the last century. Elementary research projects require close cooperation and a willingness to re-think existing approaches. This ensures constant technological development through innovative products and processes. The authors view the great interest and positive responses at BAU 2013 and BAU 2015 as the vindication of their endeavours to develop innovative solutions to future challenges.

## 6 References

- [1] FVHF, "Deutscher Fassadenpreis 2013 für vorgehängte hinterlüftete Fassaden (VHF)", Berlin, 2013.
- [2] Azhar, S., "Building Information Modeling (BIM): Trends, Benefits, Risks, and Challenges for the AEC Industry", Leadership Manage. Eng., vol. 11, no. 3, p. 241-252, 2011.
- [3] K. Vollmers, *Twist&Build creating non-orthogonal architecture*, 010 Publishers, 2001.
- [4] B. Kolarevic, "Architecture in the Digital Age - Design and Manufacturing.," Oxford, Taylor & Francis, 2003.
- [5] "Grasshopper 3D v1.0.," Robert McNeel & Associates, 2014.
- [6] "Revit 2015," Autodesk, 2014.
- [7] "Inventor 2015," Autodesk, 2014.

# Beauty and the Beast: The Wilshire Grand's Façade Design in L.A.'s Seismic Zone 4 Reality

Tammy Jow  
AC Martin

## Keywords

1=Skyline 2=Los Angeles 3=Seismic Hot Zone

## Abstract

Not since City Hall has a tall building truly addressed the issue of creating an iconic skyline for Los Angeles. The Wilshire Grand Tower is a building of our time; a contemporary contrast to a generation of flat top buildings composed of granite and inset windows. Fulfilling a design vision of glass in L.A.'s seismic Zone 4 environment will be examined in this manuscript.

Offering views never seen before in downtown Los Angeles, large format glass clads the tower to maximize visible light and openness. Factors that influenced the glass selection and stack joint design will be reviewed.

Reminiscent of Yosemite's Half Dome, the 73-story tower rises above a solid podium base. Bridging between these forms is a lyrical double curved skylight that provides the enclosure for the central Atrium. The challenges and innovative solutions involved in achieving this parametric building feature will be explored.

Finally, the design of the iconic Crown will be investigated. The signature top rises 10-stories above the tower's observation deck. Wrapped in glass, the Crown completes the architectural parti while responding to G4 forces.

## Introduction

In the heart of downtown Los Angeles, at the site formerly occupied by the Stadler Hotel, rises the new tallest building west of the Mississippi, the Wilshire Grand Center. It was Korean Air's vision to create a single, iconic tower – a symbol of the friendship between South Korea and the United States, an investment in Los Angeles – the city that hosts the second largest Korean population, next to Korea itself. The Wilshire Grand Center is comprised of a 900-room, four-star hotel that sits atop eighteen leasable office floors.

Its podium includes hotel convention spaces – ballrooms, meeting rooms, break-out areas, along with a health club, retail spaces and restaurants. Five underground parking levels are provided to meet local requirements and serve the guests and tenants of the Center.

There were five big design ideas set forth by the architects and designers at AC Martin. The first big idea was to change the Skyline of downtown Los Angeles, as shown in Figure 1. Acknowledging that the Wilshire Grand Center would be the first significant tower to be built in Los Angeles in over twenty years, the AC Martin team sought to create a building of our time. The downtown Los Angeles skyline is characterized by a generation of high-rise buildings with truncated flat tops, responding to the Los Angeles Fire Department's 1974 Ordinance requiring helipads for high-rise buildings. Taking into consideration lessons learned in the past 20-25 years, coupled with advances in fire suppression systems and exiting strategies, negotiations were successful with the Fire Department and project team to gain relief from the 1974 Ordinance.

The second big design idea was to create an accessible Sky Lobby. By locating the hotel's lobby at the top of the tower, all hotel guests would be treated to the never-seen-before views of downtown Los Angeles that could be experienced at the 70<sup>th</sup> floor. High speed, double-deck elevators transport guests at

1600 feet per minute from the ground floor to the 70<sup>th</sup> floor, facilitating high-volume vertical transportation.

Considering the fact that the project site is located in southern California, the next big idea was to take advantage of the temperate climate in Los Angeles. With average temperatures in the 70's (Fahrenheit), the building was programmed to maximize the use of outdoor spaces. Ballrooms have operable walls that open onto covered outdoor spaces. The hotel's porte cochere is a covered outdoor space that drives through the center of the site. A generous pool deck facilitates recreation and relaxation, while flanked by cabanas for more private gatherings.

Taking advantage of the Urban Context was the fourth big idea. The Wilshire Grand's site is located at the confluence of two major axes in downtown. The Figueroa corridor runs in the north-south direction. With L.A. Live to the south, the Wilshire Grand Center becomes the northern anchor to the rise of major building developments along the corridor. In the east-west direction, 7<sup>th</sup> Street has experienced a renaissance of restaurant and retail developments that lands at the front door of the Wilshire Grand Center.

The fifth big idea was to optimize efficiencies wherever possible. From the design of the mechanical systems for the tower to the



Figure 1 – Downtown Los Angeles Skyline

utilization of prefabricated restroom units throughout the hotel, the designers were challenged to be efficient while not sacrificing quality. The philosophy of efficient design is a backbone of Korean Air's success for generations, and the design team was highly encouraged to employ these principals in the design of the Wilshire Grand Center.

## The Main Text

The journey toward creating a towering icon involved poetry and practicality. The beauty of the form was derived from an array of architectural and artistic tools that spanned several generations. From the fluidity of water color paintings, to spastic collections of computer generated Rhino model forms, to 3-D printed models, to basic paper models, each tool contributed to the sculpting of the Wilshire Grand's aqueous forms. Viewing the building from various vantage points, the shape of the tower is sometimes reminiscent of Half Dome in Yosemite, and sometimes it is reminiscent of an airplane wing, a literal metaphor to Korean Air's aviation business.

The tower is a glassy expression of our time with a high performance skin, a departure from the granite inset windows characteristic of most buildings in downtown Los Angeles, as shown in Figure 2. The curtain wall was designed to maximize views and ceiling heights for the office and hotel uses. Employing large size glass panels, kiss mullions were provided to set a datum for finished ceilings. The composition of the tower's form was



Figure 2 – The Wilshire Grand Tower under construction. [1]

rationalized into measurable geometries, facilitating the use of repeatable units for constructability and to meet the project's cost parameters.

The rectangular, slender tower form challenged the structural engineers from Thornton Tomasetti and Brandow & Johnston to develop a structure that would not tip over, while responding to the inevitability of ground motion in a seismic zone four location, a seismic hot zone. The structural design involved a 17.5 feet deep mat foundation with over 6.6 million pounds of densely woven rebar and 21,200 cubic yards of concrete to set the stage for breaking a Guinness World Record for the largest continuous concrete pour in the world on February 16, 2014. Rising from the foundations is a concrete core with massive four feet thick walls, ascending and tapering to two feet thick walls at the top. At three strategic locations over the height of the tower, outriggers extend from the concrete core to capture the perimeter box columns. The outriggers are composed of bucking restrained braces (BRB's) that act as shock absorbers, resisting vertical and lateral forces. At the top and bottom outrigger locations, belt trusses of steel wide flange members encircle the floor plate to resist torsional movement.

The design of the curtain wall panels considered eight sources of structural movements [2]:

- 1 - Interstory drifts (lateral displacements) under lateral load conditions
- 2 - Vertical movements of horizontal framing members under live load
- 3 - Column shortening from construction load after panel installation
- 4 - Column shortening from imposed compatibility with concrete core creep and shrinkage
- 5 - Differential gravity and lateral movements at terminated columns near sloping columns
- 6 - Differential gravity movements at floor extensions at building ends
- 7 - Main tower column shortening and lengthening from lateral loads
- 8 - Thermal strains

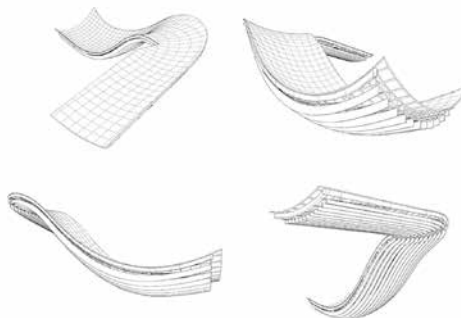


Figure 3 – Views of the Skylight from the Rhino model

Taking into account the largest of the anticipated movements, the stack joints of the unitized curtain wall system were designed for an open position of +7/8" and a closed position of -1 5/16". The profile of the stack joints was designed with a gentle curve to create a shadow line for visual depth.

Nestled between the 73-story tower and the solid podium base is the river that runs through it, a lyrical doubly curved skylight, as seen in Figure 3. Providing a glass roof enclosure for the hotel's central Atrium, the skylight stretches from one end of the property into the public plaza, as shown in Figure 4. It covers a volume that is 80 feet tall at its peak and 30 feet tall at its valley. Balconies from the hotel's convention floors look onto the Atrium. The light-filled space is the heart of the property, the central nucleus of circulation and wayfinding.

The poetic idea was one thing. Making it real was another thing. The design development process involved tackling major challenges, including cost, constructability and seismic movement. It was clear from the onset that the project could not support the cost and schedule implications of curved glass. The skylight was perpetually on the development manager's value engineering chopping block. If the skylight was to become a reality, it would take a great deal of persistence and innovation. The first challenge was to simplify the form while maintaining the larger design idea and aesthetic expression, the River of Glass. The complex geometries were rationalized into simple forms with manageable constraints, using Rhino and Grasshopper definitions. The use of flat glass was fundamental to the design. The glass size was limited to 5'-0" x 5'-0" maximum, a constructible size parameter provided by the glazing contractor, Benson Industries. Next, the maximum allowable warpage of the specified glass from Viracon was considered and constrained to a deflection value of L/100. Through the manipulations of the Grasshopper definitions the worst

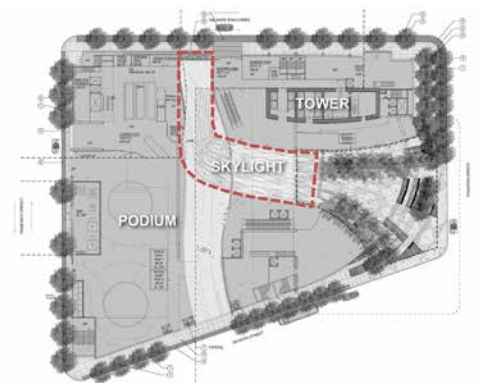


Figure 4 – Site Plan

performing panel ultimately had a deflection value of  $L/120$ .

Placing a delicate glass element between two massive building forms in a seismic hot zone was seemingly illogical. However, the notion became achievable when equally motivated professionals were teamed together to make it happen. The skylight was organized into clear components to identify layers of primary structure, the skylight's structure, and the glazing system. Seismic movements between the Tower and Podium were calculated and defined by Brandow & Johnston, the Structural Engineer of Record. Within the skylight's enclosure, it was necessary to consider the combined movements of the tower and podium in the "x" and "y" directions. The movements ranged from 13 inches at the 7<sup>th</sup> floor to 3 inches at the 1st floor. The skylight would be fixed to the podium side, and seismic motion would be addressed on the Tower side. To accommodate the range of movements between intersecting floors, slide bearings were designed to move within the constraints of keeper plates, attached to the Tower's perimeter box columns. Movements in the "z" direction, primarily for wind uplift, were addressed through the addition of steel tubes, welded to the tower's box columns that lock the skylight in place. Next, the structure of the skylight itself was addressed. Catena Engineers, structural engineers from Portland, Oregon analyzed the skylight's form and maintained the aesthetic by introducing drift joints and V-braces into the skylight's structural system of trusses and purlins. Large full-scale mockups of the skylight's frame were created by Columbia Wire & Iron, steel craftsmen also from Portland, Oregon, to ensure that the framing sections could be installed seamlessly, sequentially and without complications. The construction of the Atrium Skylight has since been completed and is a recognized captivating form in the City of Los Angeles, unlike anything that has preceded it in Downtown.

Taking into account the lessons learned through the design development of the tower and the skylight, the Crown was the final piece to be considered. The Crown is also referred to as a Sail because of its gentle curvilinear form, as shown in Figure 5. Its south-facing side curves both in plan and in section. Its north, west and east sides are both orthogonal and sloping planes. The signature top of the Tower rises 100 feet above the observation deck. It is open at the top and is a functional screen to conceal the building maintenance units, elevator machine rooms and mechanical equipment that reside within its enclosure. By utilizing Grasshopper definitions again,

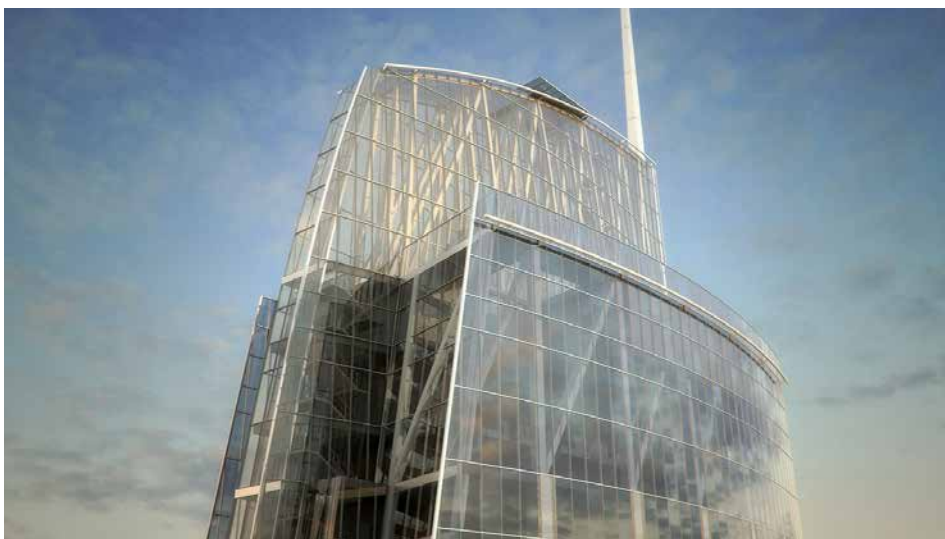


Figure 5 – Rendered View of the Crown

the doubly curved forms were rationalized to minimize warpage, allowing the unitized curtain wall panels to cover the glass screen, a visual extension of the Tower's fenestration.

The structure of the Crown was first envisioned to be light and lacy. It was about joinery and beauty, the iconic top to redefine the skyline of downtown Los Angeles, ultimately accented by a Spire that rises another 173 feet above the peak of the Crown. Upon further analysis by the structural engineers, it became apparent that an earthquake could produce 4G forces of acceleration at the top of the Tower. Gone was the notion of laciness and filigree. The Crown's structure became a statement of brute force. Paired vertical trusses were replaced by robust sized wide flange steel members and massive gusset plates. Despite the functional realities of the seismic forces and their implications on the structural design, the design team persisted to ensure that all beauty was not lost. The structure was organized and engaged with the overall design of the Crown.

## Conclusions and Summary

The Wilshire Grand Center will open for business in June 2017. The original design objectives will have been implemented: Skyline, Sky Lobby, Climate, Urban Context and Efficiency. The original building forms remain intact. Through the perseverance of the design, engineering and contracting team, beauty plays well with the beast.

## References

- [1] Wilshire Grand Center construction photo by Gary Leonard
- [2] Thornton Tomasetti Memorandum to Brandow & Johnston, "Structural Movements for Façade", June 18, 2013

# Banco Popular HQ - Auditorium, Madrid (Spain)

Miguel Ángel Ruiz<sup>1</sup>, Pedro Rodrigues<sup>1</sup>  
1 Martifer Metallic Constructions. Facade Contractor

## Keywords

1= structural glass 2=large panes 3=double skin 4=glass fins

## Abstract

The use of structural glass in Architecture has always been a challenge since the beginning of time, and despite Peter Rice's first great achievements in this field in the middle of the XX century, it is something that we should always try to improve and seek greater achievements. If we add the desire to achieve the largest possible glass dimensions that can be made with the greatest transparency (see figure 1) then the challenges are big.

The concept of architectural design in the Auditorium of the New Headquarters of the Banco Popular in Madrid (Spain) was made by Arquitectos Ayala and ENAR as part of the Architects team. It is a question of combining all the previously mentioned ingredients to achieve the Architect and Facade Consultant intention of creating a double skin glass with the fewest visible pieces as possible in order to eliminate the visibility of any supporting structure. By this way, we are able to have a fully "transparent box" for the enjoyment of the people who use this facility.

## Introduction

This document refers to a small explanation of the Auditorium execution process from the design and development of the technical solution, testing, manufacturing, to its final execution. As usual in this type of singular projects, the design and calculations were essential to ensure the correct functioning of the facade system. Obviously, to build a glass box, the first objective was to define the structural concept of the double skin and run the calculation of all elements that forms part of the entire system.

Once the calculations were done and the compositions of the glasses were defined, the next step was to test a real scale mock-up in a certified laboratory to check its feasibility. If



Figure 1. Architectural concept at initial design stage. Interior view

the results were as expected at structural and performance level then the manufacturing and assembly phase can begin.

Although the manufacture required a great control to avoid problems of lamination and finishing due to its large format, the biggest challenge was the installation due to the fact that the Auditorium is located between two large buildings with limited access to the glazing logistics and resources.

## Typical details

After reviewed the original drawings and specs, the initial idea was clearly defined. The exterior and interior glass should have a dimension of 2,600x9,500 mm (width x large) and both surfaces should be separated 700 mm with a 7,980 mm glass fin inside between them. A top gap (1800 mm) was required to allow the passage of two bespoke rail systems for future maintenance (see figure 2 below). All the glasses are composed with low iron glass to focus the transparency and laminated with standard PVB.

The inner and outer glass panes are fixed in its lower part in the 3 axes and supported on a hidden metallic substructure. However, in the upper end the glass are fixed in axes (x, z), leaving free movement in the vertical (figure 3). In relation to the glass fin, it is embedded 280 mm in its lower part by the use of screws, using polyamide, nylon and resins in the holes for proper operation.



Figure 2. 3D Image for small visual mock up to show the double skin of glazing

## Structure and analysis

The design calculation of the agreed solution was made by Autodesk Robot Structural Analysis, SolidWorks Simulation (figure 3) and SJ Mepla.

### Initial conditions:

Wind pressure:  $W_p = W_s = \pm 0,6$  KPa (typical bay) and  $W_s = -0,9$  KPa at corners (first 2,6 m)  
Horizontal live loads: 1,6 KN/m ( $h = 1,2$  m)  
Maximum displacement for outer/inner panes: L/65 or 50 mm  
Upper slab maximum deflection: 32 mm

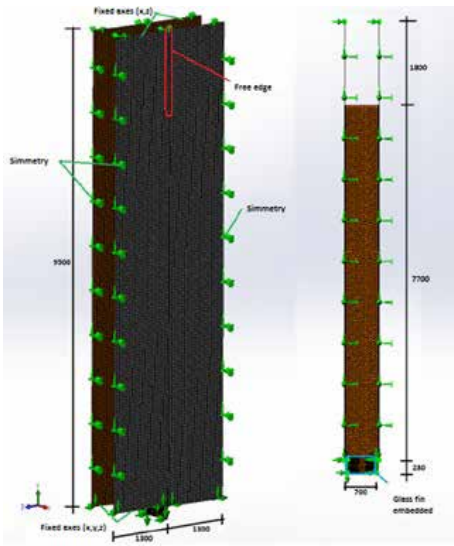


Figure 3. Auditorium structure, supports, dimensions and section

After all the calculations (SLS and ULS), the final glazing compositions are:

|                         | Dimensions   | Composition        | Heat Treatment    |
|-------------------------|--------------|--------------------|-------------------|
| Outer pane              | 2600x9500 mm | 10/2,28/10         | Heat-strengthened |
| Inner pane              | 2600x9500 mm | 10/2,28/10         | Heat-strengthened |
| Glass fin (typical bay) | 700x7980 mm  | 10/1,52/10/1,52/10 | Heat-strengthened |
| Glass fin (corner)      | 1000x7980 mm | 10/1,52/10/1,52/10 | Full tempered     |

Table 1. Final glazing composition

On the other hand all the joints required to bond the glass panels were designed, and tested is chemical and adhesion between all the elements. For example, the joint with the vertical aluminum profile (figure 4), the top horizontal edge and a special vertical joint at corners.

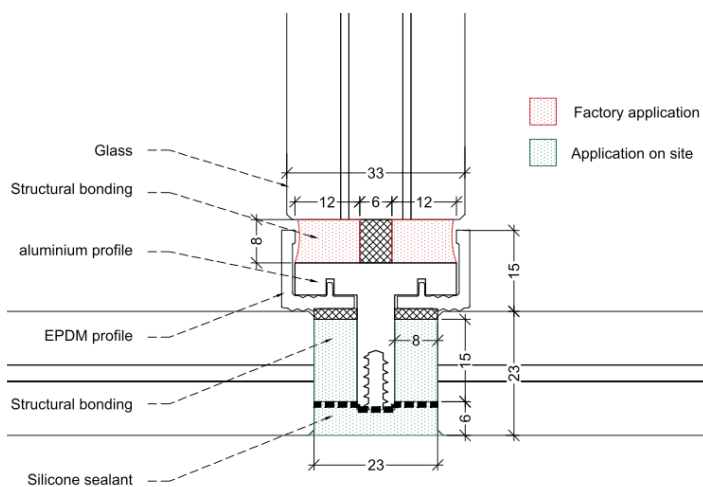


Figure 4. Joint between the main glasses (outer/inner pane and glass fin)

In figure 4 above we can see that the bond process of the aluminium profile to the glass fin were made in the factory, while the strings that join the side of the glass with the metal profile itself is made with the same material, but on site. The design allows Applying the silicone only with two surfaces contact. Finally the finishing silicone is applied also on site. As required by the Architect all aluminium profiles are hidden creating the desired effect of a completely "glass transparent box".

### Testing of prototype

Due to the large dimensions of this façade it was required to create a special chamber (first of its kind in the Iberian Peninsula) to perform the laboratory tests (see figure 5). Test for air permeability, watertightness, resistance to wind load and impact resistance were done according to the current regulations standards. As expected, the results were satisfactory (see table 2)



Figure 5. Image during the installation phase at the laboratory

Summary table of test results:

|                         | Test Method                      | Classification | Results       |
|-------------------------|----------------------------------|----------------|---------------|
| Air permeability        | UNE 12153:2000                   | UNE 12152:2000 | Class A4      |
| Water tightness         | UNE 12155:2000                   | UNE 12154:2000 | Class R7      |
| Resistance to wind load | UNE 12179:2000                   | UNE 13116:2001 | Class 600 Pa  |
| Impact test             | UNE 13049:2003<br>UNE 12600:2002 | UNE 14019:2004 | I3 (interior) |

Table 2. Test results and regulation applied.



Figures 6 and 7. Installation process and general view with some of the pieces protected

## Installation

As mentioned before, the installation process was a big challenge (see figures 6 and 7). A detailed 3D assembly sequence study was done to ensure a proper execution of the work. Due to the fact that bottom level of the different “cube faces” were different we had to double check the levelling of all supporting structure in order to ensure a perfect fit of the glass. Once the overloads of the areas near the final site were verified, the zone was modelled to analyse the installation tolerances for the future movements. It was very important because in addition to the glasses dimensions, each unit weighs more than 1,200 kg.

## Future opportunities for concepts development

Looking to the future, it would be interesting to collaborate in a new project with bigger panes. Why not use 16x3,21 m pieces to build a new glass box? Another aspect is the use of titanium inserts to make the joints between glasses, although sometimes the use of these pieces, even punctual, may not follow the architectural concept of self-supporting transparent structure without visible metallic profiles.

## Acknowledgements

Many thanks to our Client, Banco Popular, for the trust shown to Martifer during the development of project, and to believe on this type of singular constructions. To Ayala Arquitectos and ENAR for designing this type of structures that are so different and special that creates great technical challenges and make us overcome every day. Also grateful to BOVIS for the coordination during all this execution of this special project.

# Sustainable Facade Design for Glazed Buildings in a Blast Resilient Urban Environment

Guido Lori, Permasteelisa Group. Colin Morison, Colmor Consulting, Martin Larcher, European Commission, Joint Research Centre. Jan Belis, Ghent University

## Keywords

blast, facades, resilient, MDOF, dissipative, balance

**Extended Abstract** (The complete contribution will be published in the *Glass Structures and Engineering Journal*)

In facade construction the glazed elements have always been considered the most critical components for the minimization of hazards during a blast event. In today's blast events, terrorists have changed their mode of action and targets where the glass performance is weak have become even more of a concern. Therefore counter-terrorism offices (such as in the UK) have been introducing design guidelines for crowded places, making a compromise between safety and sustainability. This paper describes how it is possible to achieve a resilient urban environment, where glass is still the dominant element of the architectural scope.

The protection of buildings against explosive events is not standardised like the general structural building procedures in Europe [1]. The EUROCODES only contains some procedures concerning the protection against internal explosions. The protection against explosive events is in general undertaken for specific threat scenarios by numerical simulations together with or supported by experimental trials.

The facade is the first building component impinged by the blast wave and its behavior makes the difference in terms of building response and number of injuries during a bomb attack. Several buildings can suffer "facial" damages during a blast event; the most part of them are subjected to indirect loading. For public interest a first level of blast enhancement would be important for all the buildings, in the areas of the world with high risk. At this purpose counterterrorism offices are releasing guidelines for safe use of materials and components. Guidelines sometimes limit application of glass, when related to blast enhancement [2]. However a

certain degree of blast enhancement is always applicable, once the dominant engineering problem is understood, assessed and possibly upgraded. Resilience can be achieved preserving at the same time the major facade requirements, in terms of aesthetics, energy efficiency, comfort and other daily demand.

After bomb attacks against soft targets in UK and US during the 90's, curtain wall behavior under blast loading has been investigated through an intensive experimental campaign. Since the first outcomes, the resistance of the curtain wall facades appeared surprising [3], especially when subjected to low/mid threats, expected as more probable on a building when it is not a direct target of the bomb attack. This type of threats is also affecting the major area damaged during a blast event and is of primary importance when resilience plans are developed for a certain risk area. The available best practices have been strongly influenced by the military applications and still today the reference hazard scenario has not been properly updated. It is not just a lack for the right simulation of the typical hazard facade conditions, but it has a strong impact in design/calculation methods too. For instance into the typical sequential design methods, the facade is analyzed by means of numerical model sequence, each simulating one or more facade components. Sequential methods are in general not capturing the proper facade behavior, because for instance they neglect the deformability of the framing when the glazing behavior is assessed. In curtain wall design the deformability has an important effect in extending the life of the intact glass phase, favoring the 1 way spanning mode of deformation rather than the 2 way spanning, while this effect is somehow negligible for typical window design. An example of sequential design is given by the maximum capacity loading (also known as balanced design). Under that approach it must be proven that framing and connections are capable to withstand the load from the glazing (maximum capacity), as if the glazing fails under a load higher than expected, framing and connections must not fail, structural integrity being preserved. Usually the glazing is analyzed by a Multi DOF approach, under the hypothesis of rigid frame. This is on the safe side (although uneconomical) against the real coupled behavior glazing/frame. However

the estimated mullion behavior could be not on the safe side, as for instance the real behavior could preserve the glazing intact status, giving higher impulse edge reactions on the mullion if compared with the broken status, got by means of the rigid support hypothesis. This can occur especially for low/mid levels (first level of threat) of blast loads. The use of the sequential approach could be detrimental under those scenarios, as it moves the design towards a general upgrade of glazing thickness and mullion inertia. On the contrary the target should be to couple the glazing with the weakest mullion allowed by conventional load design, in order to extend as much as possible the life of the glass and then reduce the hazard level. This design approach is that one proposed by the authors, by means of a flowchart described as "balanced design chart" into an approach called "true balanced design", exactly in opposition to the classical sequential balanced design approach. Interesting option into this approach will be the integration in facade of dissipative components, which can absorb energy in excess with respect to the maximum absorbed by the glazing/frame system. The dissipative component, for instance at the bracket level, is another fundamental element for the facade dynamic equilibrium. When the dissipative principle is activated under the blast loading, the force remains constant for a defined plastic deformation of the bracket and the inertial effect of the full facade movement freezes the stresses on the facade components, allowing a reduction of the glazing and mullion deformation for the same glass thickness/mullion inertia combination.

In order to extensively apply a true balanced design approach in facade enhancement, a powerful and accurate calculation tool should be available, with sustainable computational effort within a typical design process. The finite element method (FEM) allows simulating the behavior of structures under different loadings [4]. It can be considered the referenced method for dynamic analysis too, but for several reasons its adoption is difficult in practical project design. On the other side Single Degree of Freedom (SDOF) methods of dynamic analysis are a traditional way of undertaking a fast but approximate analysis of the dynamic response of a member or system. In the 1950s, early numerical analysis by Newmark [5] produced charts of elastic-plastic response that could be

applied to ductile systems such as steel beams and RC beams and slabs. The Equivalent SDOF method used energy equivalence to calculate transformation factors for loading, resistance and mass and later for damping. The availability of nonlinear FE allowed glass panes under blast loading to be analyzed dynamically by SDOF. Moore [6] produced deflection and stress curves for large deflection glass panes of various aspect ratios and Morison [7] proposed an elastic-plastic PVB material model which produced a pressure-deflection curve. Subsequent analysis has shown this material model to be a good approximation of the PVB interlayer performance in blast trials [8]. 2DOF analysis can be extended into a Multi DOF analysis by including supporting transoms and mullions loaded by reaction from the glazing, and brackets loaded by reaction from the transoms and mullions.

Previous Multi DOF models were developed by the authors in order to assess the deformability contribution of bracket and mullion on the glazing behavior [9], including up to five degrees of freedom and considering simply supported mullions. By the proposed model extension, further degrees of freedom can be considered, each one for any surface area. The constraint function  $\Phi$  of the frame is expressed in terms of  $n$  angles  $\theta_i$ , representing for each surface area the relative slope of the mullion from transom to transom and giving in this way the 1 way spanning deformation of the glazing for that surface area. The application of the virtual work principle requires the knowledge of the constraint functions for glass and framing under dynamic conditions. The common assumption followed for the glass is that under a certain center deflection, the dynamic constraint function matches the static one with the same center deflection. The same principle has been applied to the frame constrain function, which can be found by means of the static function by the same combination  $\Phi(\theta_1, \theta_2, \dots, \theta_n)$ .

The authors have already undertaken sensitivity of the SDOF for variable glass thickness and blast loading [10], showing that higher modes of vibration can have a contribution on the peak of the glass deflection of around 5% in the typical range of the blast load duration  $t$  and first natural period of the glass  $T$ , even if for small load duration (highly impulsive loads) and large natural period (tall and narrow glass, with large aspect ratio) the error can be even higher than 10%. The proposed extended Multi DOF model results in errors consistent with the typical level of accuracy of the SDOF approach and has shown far superior estimations in comparison with sequential method and in general good accuracy against reference FEM analysis

results. Similar outcomes have been derived by the back-calculation from a series of experimental full scale open air arena testing. Further research will be conducted on the impact of the optimized reaction time histories on the design of local slab and in general about secondary and primary building structures.

## References

- [1] Larcher M; Arrigoni M; Bedon C; Van Doormaal A; Haberacker C; Hüsken G; Millon O; Saarenheimo A; Solomos G; Thamie L; Valsamos G; Williams A; Stolz A. Design of blast-loaded glazing windows and facades: a review of essential requirements towards standardization. *Advances in Civil Engineering* 2016.
- [2] Measures to improve the blast resistance of glazing, CPNI EBP 01/14: April 2014
- [3] PSDB Notes on Design for Glazing Protection, Home Office, Police Scientific Development Branch, 2004
- [4] M. Larcher, G. Solomos, Folco Casadei, and N. Gebbeken. "Experimental and numerical investigations of laminated glass subjected to blast loading". *International Journal of Impact Engineering*, 39:42-50, 2012
- [5] Newmark N M. "An engineering approach to blast resistant design", *American Society of Civil Engineers Transactions*, Paper No 2786, Vol 121 p45, 1956.
- [6] Moore D M. "Proposed method for determining the glass thickness of rectangular glass solar collector panels subjected to uniform normal pressure loads", JPL Publication, Pasadena, CA, October 1980.
- [7] Morison C "Response of glazed facades to blast loading", MSc dissertation, U of Westminster, 1999.
- [8] Morison C, Zobec M, Franceschet A. "The measurement of PVB properties at high strain rates, and their application in the design of laminated glass under bomb blast". *ISIEMS 12.1*, Orlando FL, 2007.
- [9] Zobec, M., Lori, Lumantarna, Ngo, T., Nguyen, "Innovative design tool for the optimization of blast enhanced façade systems", *Journal of façade Design and Engineering*, vol.2 n.3-4, 2015
- [10] Lori G., Zobec, M, Franceschet, A., Manara G., "The behavior of facades due to blast loads. A single degree of freedom performance evaluation approach", *Glass Processing Days*, 2009, Tampere

# Structural Silicone Glazing: Life Expectancy of more than 50 Years?

Andreas T. Wolf<sup>1</sup>  
 Christoph Recknagel<sup>2</sup>  
 Norman Wenzel<sup>2</sup>  
 Sigurd Sitte<sup>3</sup>

A&S SciTech Consulting, Hünstetten/Germany<sup>1</sup>  
 Federal Institute for Materials Research (BAM), Berlin/Germany<sup>2</sup>  
 Dow Corning GmbH, Wiesbaden/Germany<sup>3</sup>

## Keywords

Structural Sealant Glazing, silicone adhesive, durability, climatic simulation, artificial weathering, mechanical loading

## Abstract

Structural Silicone Glazing (SSG) is a curtain walling method that utilizes silicone sealants to adhere glass, ceramic, metal or composite panels to supporting framing members by means of a peripheral adhesive joint. In SSG curtain walls, silicone sealants serve not only as a weather seal, but also act as a structural bonding element, eliminating the need for exterior retainers and covers.

The paper discusses some essential findings of two recent research studies on the durability and service life of structural silicone glazing sealants and structures. The first study demonstrates, that specimens of a first generation 2-part silicone sealant taken from a SSG façade after 23+2 years of real life successfully passed the European ETAG002-1 performance criteria for residual strength. In a second study, a new performance-based durability test method was developed in partnership with the Federal Institute for Materials Research Berlin/Germany (BAM). This method is based on simultaneously exposing system test specimens to artificial weathering and complex, multiaxial mechanical loadings. 2-part structural silicone sealants of the first and of the second generation where subjected to this test, which is considered to correspond to an anticipated service life of 50 years.

## Introduction: Brief History of Structural Silicone Glazing

The SSG concept was developed in the USA during the mid-1960s. In the initial 'all-glass system', thick glass fins (mullions) were installed at regular intervals perpendicular to the face of the façade, then vision glass was adhered to these reinforcing elements using a transparent silicone sealant. The first building to use this type of glazing was constructed in 1964/65. As time continued, further systems were developed in which the glass fins between the glass panes were replaced by aluminum mullions located behind the panes. Two different designs emerged, referred to as 'two-sided' or 'four-sided' SSG, where the silicone sealant served as a structural adhesive between the glass and the supporting structure either on any two opposite or on all four edges of the glazing panel. By 1968, architects started designing seemingly uninterrupted, free-flowing strips of two-sided SSG. The two-sided SSG method became extremely popular and even today represents a widely used technique. By 1971, the first four-sided SSG curtain wall was installed on-site. On this project in Detroit (Fig. 1), the structural silicone sealant transferred all loads from the glazing panels to the supporting structure; however, cast-aluminum spiders were installed as supplementary safety retainers at the intersections of the aluminum framing members to prevent glass panes from falling in the event of a structural seal failure. Having performed successfully for more than 45 years, this building now has become famous as the 'granddaddy' of the industry.



Figure 1: 455 W Fort Street, Detroit, the world's first four sided silicone structural glazing project, 1971 designed by architects Smith, Hincham and Grylls. Photo courtesy of SmithGroupJJR

The first four-sided SSG project without a safety retention mechanism, the Chicago Art Institute, was completed in 1974. By 1978, this glazing technique began to spread more widely. Structural silicone sealants enabled the design of four-sided curtain walls with a completely flush appearance, resulting in smoother rain runoff, shedding of dirt, and easier cleaning. A real boom in the application of the four-sided glazing technique began towards the middle of the 1980s, when some ten years of experience had been gained with this system.

## Benefits of Structural Silicone Glazing

During the 1980s, the SSG curtain walling concept spread rapidly around the world, as this glazing method allowed architects new levels of design freedom and offered a unique aesthetic appearance. Today, SSG has become a resounding success with literally tens of thousands of projects demonstrating the aesthetic and performance benefits associated with this curtain wall technique. Nowadays, structural glazing is carried out almost exclusively using factory-produced (shop-glazed) unitized modules resulting in efficient fabrication, enhanced overall quality, increased speed of installation, and reduced on-site labor.

## The Challenge: Estimating the Technical Useable Life of SSG Curtain Walls

One major concern with adhesively assembled structures in general is the long-term integrity of the structural bond. Therefore and because of missing comprehensive verification methods, with the aim of ensuring public health and safety, building code authorities in countries like Germany, France or Austria still require additional mechanical fasteners for four-sided SSG curtain walls to provide safe retention of the infill panel in case of structural sealant failure.

Today there is a significant number of SSG curtain walls globally that have now reached 30+ years of service. Building owners and code authorities are faced with the task of estimating the residual service life of these structures. Ultimately, the underlying questions are, what is the technical usable life of a SSG curtain wall – is it 50, 75 or even 100 years

– and how exactly will a structural silicone sealant degrade and ultimately fail? In some countries, this uncertainty is responsible for inhibiting the wider use of the four-sided structural bonding technology. Therefore, important issues that remain to be addressed are the investigation of the regular functional behavior under superimposed loading, the prediction of the degradation behavior and the resulting long-term durability of adhesive-bonded structures. The essential challenge that researchers face today is twofold:

- a) How to develop durability test methods that provide a better representation of the actual service environment in the laboratory?
- b) And, how to calibrate laboratory durability test results against actual in-service performance of SSG adhesive joints?

Besides the potential of a more realistic investigation of the interaction of chosen design and material combinations the ultimate objective, then, is a more realistic prediction of the technical usable life of SSG curtain walls. Two recent studies constitute major steps forward in this direction and, for the first time ever, provide compelling scientific support for service life estimates of SSG structures significantly in excess of 25 years. The findings validate anecdotal evidence gathered from successful field-performance of SSG buildings that have now been in operation for more than 30 years [2].

### A Unique Opportunity: Calibrating ETAG002 Test Requirements Against Actual In-Service Performance

In 1985, the southwest facing bow front façade section of a building at IFT Rosenheim (Institut für Fenstertechnik e.V.), an internationally renowned authority in the testing of windows and façades, was installed using the then-novel 'hybrid' four-sided SSG system with glass sizes up to 1m x 3.2m (width x height). In this SSG design, special toggles engage in U-shaped glass edge spacers located at the periphery of insulating glass units. Rotating the toggles by 90° during installation of the insulating glass unit mechanically secures the inboard pane to the support structure. Regardless of their mechanical fixation to the substructure, toggle-glazed hybrid SSG designs still expose the insulating glass edge seal to structural loads; therefore, an approved structural silicone sealant must be used to adhesively bond the U-shaped retention channel to the adjacent glass panes. The three-story high toggle-glazed hybrid SSG system broke new ground, as it was installed (in regards to the outboard glass panes) without additional safety retainers and without dead load support for the outer glass.



Figure 2: structurally bonded façade of the IFT Rosenheim, 1985, Photo: @ift Rosenheim

Such a hybrid SSG design corresponds to Type IV Glazing listed in ETAG002, as the structural bond transfers not just dynamic external loads, such as wind load, but also the self-weight of the infill panel. However, different from the situation in a regular (non-hybrid) SSG design, the structural bond in a hybrid SSG system is also subjected to climatic loads, as changes in temperature, atmospheric pressure, and altitude influence the sealed gas volume trapped within the insulating glass unit. When the façade was refurbished for improved energy efficiency after 23 years of service, the disassembled SSG structure offered the opportunity of 'calibrating' the requirements

stated in the European approval guideline for SSG sealants and systems, ETAG002-1, which was developed by the European Organization for Technical Approvals (EOTA) in 1991 [3-5]. Its comprehensive range of tests and stringent assessment criteria makes ETAG002-1 a very demanding standard for SSG sealants. The standard defines key provisions for bonding strength and durability of bonding strength of the SSG sealant and, notably, mentions that *the provisions made in the ETAG002-1 are based on an assumed service life of the SSG structure of 25 years.*

In 2012, after the dismantled façade had been stored in an unheated warehouse for 2 years, an experimental and statistical evaluation of the natural aging behavior of the structural silicone sealant installed at the IFT Rosenheim façade in light of the ETAG 002-1 requirements was conducted by a B.Sc. study at the University of Regensburg [6]. In order to do so, a total of 200 test specimens were cut from the hybrid SSG units utilizing a water jetting process. The study was supported by the IFT Rosenheim institute, a fact that allowed to compare the results with the previously collected reference data.



Figure 3: Samples cut out from the IFT Rosenheim glass, Photo: @ift Rosenheim

| Type of test          | Test Temperature (°C) | Average Breaking Stress $X_{mean}$ (MPa) | Strength Retention Ratio $X_{mean,7} / X_{mean,+23}$ | Failure Mode (% cohesive) |
|-----------------------|-----------------------|--|--|---------------------------|
| Tensile               | +23                   | 0.75                                     | reference value                                      | 100                       |
|                       | -20                   | 1.1                                      | 1.47   | 100                       |
|                       | +60                   | 0.73                                     | 0.97   | 100                       |
|                       | +80                   | 0.58                                     | 0.77   | 100                       |
| Shear                 | +23                   | 0.67                                     | reference  | 100                       |
|                       | -20                   | 0.97                                     | 1.45   | 97                        |
|                       | +60                   | 0.67                                     | 1.00   | 94                        |
|                       | +80                   | 0.64                                     | 0.96   | 100                       |
| ETAG002-1 Requirement | -20 and +80           | -  | $\geq 0.75$  | $\geq 90$                 |

Table 1: Mechanical strength properties of structural silicone sealant after 23+2 years of natural aging (23 years of service exposure)

During its more than 23 years of service, the south- and southwest-facing SSG façade section had been exposed to harsh climatic conditions, with severe wind-driven rain exposure, high radiation heat gain (during days) and loss (during nights), and frequent freeze-thaw cycles. Over the period of 2004 to 2011, air temperatures of - 23.7 °C and +35.2 °C were recorded as seasonal extremes. Thermocouples, installed within the SSG curtain wall in the vicinity of the structural sealant, recorded extremes of -9.0 °C (corresponding to -23.1 °C outside air temperature) and +59 °C (at an outside air temperature 32.5 °C) during a 12-month period starting in December 1985. The façade also received high levels of solar radiant energy; based on historical meteorological data for the period from 2004 to 2011, the average annual global solar radiation exposure at the city of Rosenheim is 1100 kWh/m<sup>2</sup>.

A key consideration for determining Safety in Use and, thus, the suitability of a SSG sealant according to ETAG002, is the stability of cohesive and adhesive properties when exposed to different environmental and aging conditions. Therefore, an important question to ask is whether or not the structural sealant that had undergone 23+2 years of environmental exposure would still pass the requirements of 'Initial Mechanical Strength' and 'Residual Strength' (now applied to *natural aging*) as laid out in ETAG002-1 sections 6.1.4.1. and 6.1.4.2. The aim of the Initial Mechanical Strength tests is to evaluate the bonding strength of the structural sealant when subjected to tensile or shear forces acting on the joint at different temperatures. Temperature-induced variations in the sealant's properties may lead to a drop in mechanical and bonding strengths. Therefore, ETAG 002-1 stipulates that the mean tensile and shear strength values measured at -20 °C and +80 °C must not drop below a minimum of 75% of the corresponding values observed at +23 °C and that rupture must occur at an average cohesive failure mode of 90% or greater.

In the B.Sc. study, test specimens were subjected to destructive tensile and shear tests at -20 °C, +23 °C, +60 °C, and +80 °C. As can be seen in Table 1, across the board, the sealant passes both the above mentioned ETAG002-1 Initial Mechanical Strength requirements with flying colors.

The Residual Strength test is meant to determine the durability of the bonding strength. ETAG002-1 stipulates that the residual tensile strength after all types of accelerated aging tests must still equal or exceed 75% of the sealant's initial strength measured at 23 °C and that the failure mode after aging must be >90% cohesive in nature.

| Type of Test | Test Temperature (°C) | Average Breaking Stress $\chi_{\text{mean}}$ (MPa) |                            | Residual Strength Ratio | ETAG002-1 Requirement |
|--------------|-----------------------|--|----------------------------|-------------------------|-----------------------|
|              |                       | ITT (New)  | Natural Aging (23+2 Years) |                         |                       |
| Tensile      | +23                   | 0.95   | 0.75                       | 0.79                    | ≥ 0.75                |
|              | -20                   | 1.7  | 1.1                        | 0.65                    | -                     |
|              | +60                   | 0.81   | 0.73                       | 0.90                    | -                     |
| Shear        | +23                   | 0.94   | 0.67                       | 0.71                    | -                     |
|              | -20                   | 1.54   | 0.97                       | 0.63                    | -                     |
|              | +60                   | 0.71   | 0.67                       | 0.94                    | -                     |

Table 2: Tensile and Shear Strength Values in Initial Type Testing (1985) and after 23+2 Years of Natural Aging and Corresponding Residual Strength Ratios

Table 2 displays the tensile and shear strength values observed in the Initial Type Testing (ITT) and on the naturally aged product along with the corresponding residual strength ratios for all test temperatures. Despite 23+2 years of natural aging, the sealant successfully passes the ETAG002-1 criteria. Such strong performance against key performance indicators at the end of the 25-year service life assumed by ETAG002 is quite reassuring. It may give conservative building code authorities the added confidence they need to consider future four-sided SSG structures without supplementary safety retainers. The findings of this study are especially remarkable as the silicone sealant used in the IFT Rosenheim SSG application, Dow Corning Q3-3332 was commercialized as a first generation of neutral curing 2-part silicone long before the ETAG002 guideline was developed and failed to meet its stringent requirements, once this standard went into effect. The inability of this first generation 2-part silicone to meet the ETAG specification then triggered the development of Dow Corning 993, the 2<sup>nd</sup> generation, higher performance successor product, also neutral curing, which is capable of passing all SSG standards globally.

### Back to Basics: Developing a Performance-Based Durability Assessment for SSG Sealants

Inspired also by the results of the field study mentioned above the need for a generalized, repeatable and time-accelerated durability test methodology comes again in the focus of interests. In 2012, the German Federal Institute for Materials Research and Testing (BAM), a leading research institute for science and technology in Germany, picked up the challenge of developing a performance-based durability test method for SSG sealants that better reflects the actual service environment and activates both the relevant performance features and its durability. The project was executed between 2012 and 2015 and

accomplished the following major deliverables [7]:

- Derivation of a realistic environmental and mechanical loading function suitable for accelerated durability testing;
- Development of system test specimen that provide a better representation of the SSG joint;
- Design and realisation of a test facility capable of simultaneously imposing weathering and complex, multiaxial mechanical loadings on the test specimen;
- Evaluation of the durability of two 'benchmark' SSG sealants: 1st generation and 2<sup>nd</sup> generation.

The test was designed to reproduce typical environmental exposure and service conditions and is expandable with special load conditions like impacts or chemical loading. Consideration was given for the following loads [8,9]:

- Mechanical loads resulting from self-weight, temperature, wind and human impact loads;
- Climatic loads taking into account typical average and extreme temperatures, humidity, the number of rainy days and the average amount of precipitation and solar radiation per year;
- Chemical loads resulting from water (rain) or de-ionised water as solvent agent and cleaning agents (aqueous surfactant solution).

The deformation/stress loading was derived from parametric finite-element analyses (FEA) of a large-sized SSG glazing unit installed at a height of 50 meters on a building located in wind load zone II considering terrain categories II and III according to DIN 1055-4 [10]. The following assumptions were made in the parametric analyses:

- The SSG glazing module (2.5 m wide and 3.2 m high) is oriented vertically; the unit is structurally bonded on all four sides; the dimensions of the structural bond are 12 mm x 6 mm;
- The SSG system is glazed with either

single pane, insulating glass, or stepped insulating glass (3 options) and installed either with or without support of its own self-weight (types II and type IV according to ETAG002);

- The design stress ( $\sigma_{des}$ ) of the structural sealant is 0.21 MPa.

Furthermore, in order to simulate a human impact on the SSG module, a separate FEA study was conducted to investigate the effect of a pendulum impact test according to DIN 18008-4 on the relevant sealant's deformation/stress loading. The multitude of FEA studies of single or multi-superimposed associated load cases allowed the BAM researchers to derive the maximum tensile and shear deformations occurring in the SSG sealant for each loading event. In general, they assumed the worst-case combination of loads (and resulting movements). However, in order to derive deformation parameters for more regular load situations, they used the load distribution spectrum, as laid out in ETAG002-1 section 5.1.4.6.5 Mechanical Fatigue, as shown in Table 3.

| Load Reduction Factor          | Prevalence |
|--------------------------------|------------|
| 0 = 100% maximum deformation   | 1.9%       |
| 0.20 = 80% maximum deformation | 4.7%       |
| 0.40 = 60% maximum deformation | 93.4%      |

Table 3: Load Reduction Factors used in the Load Function for Deformations Resulting from Regular Loads and their prevalence in the Overall Deformation Spectrum

| Test Segment                     | Deformation |                          | Amplitude (mm) |                |                |
|----------------------------------|-------------|--------------------------|----------------|----------------|----------------|
|                                  | Number      | Type                     | Maximum        | 80% of Maximum | 60% of Maximum |
| Durability Cycle (repeated 50 x) | 2526        | Tensile (↑)              | 0.53           | 0.42           | 0.28           |
|                                  |             | Compression (↓)          | -0.67          | -0.54          | -0.38          |
|                                  |             | Shear (→)                | 2.03           | 1.62           | 1.22           |
|                                  |             | Shear (←)                | -1.31          | -1.08          | -0.79          |
| Human Impact Simulation          | 1           | Tensile/Compression (↑↓) | 1.33/-1.05     |                |                |
|                                  |             | Shear (←→)               | 0.95/-1.86     |                |                |
| Durability Cycle (repeated 2 x)  | As above    |                          |                |                |                |

Table 4: Durability Test Protocol (BAM Research): Deformations Enforced in System Test Specimen Joint

The reduction factors represent the ratio of test deformation to maximum deformation. For instance, deformations corresponding to 80% of the maximum deformation only occurred with a prevalence of 4.7% in the overall deformation spectrum.

Utilizing the knowledge of the life-cycle load profile that was established during the previous research, the BAM researchers subjected the test specimens to repetitive durability cycles. Each durability cycle, which exposed test specimens for 24 hours to simultaneous climatic and multiaxial mechanical loads, was designed to represent one year of actual service exposure. After the completion of 50 durability cycles, the test specimens were subjected to a rapid, complex deformation in order to evaluate the aged sealant's ability to sustain an accidental human impact on glass. The impact simulation was then followed by another two durability cycles (see Table 4).

Simultaneously to the complex, two-dimensional shear and tensile deformations, test specimens undergoing durability cycles were also exposed to temperatures of -10 °C to +60 °C, relative humidity ranging from 20% to 98%, rain events (intensified loading by use of distilled water) corresponding to 620 l/m<sup>2</sup> rain fall, and 1.4 MJ/m<sup>2</sup> of UV light (290 to 410 nm) simulating relevant seasonal climate variations. In order to investigate the effect of mechanical fatigue, additional test specimens were kept separately in the BAM weathering chamber of the complex test facility that were subjected only to weathering without movement.

For the realization of the identified relevant annual service exposure on representative system test specimen and its repetitions for durability aspects a new complex test facility has to be developed. This unique test facility, see Figure 4, consists of the main constituents:

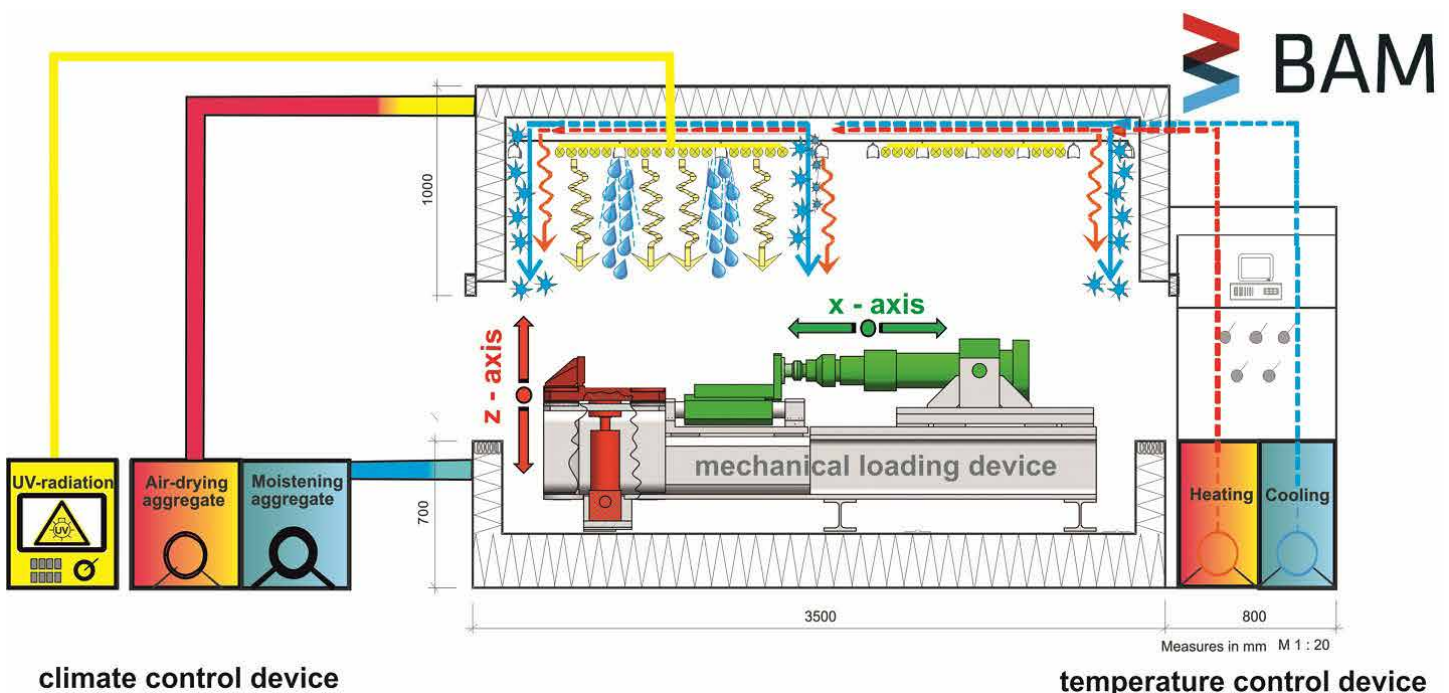


Figure 4: General illustration of the new test facility at the BAM institute

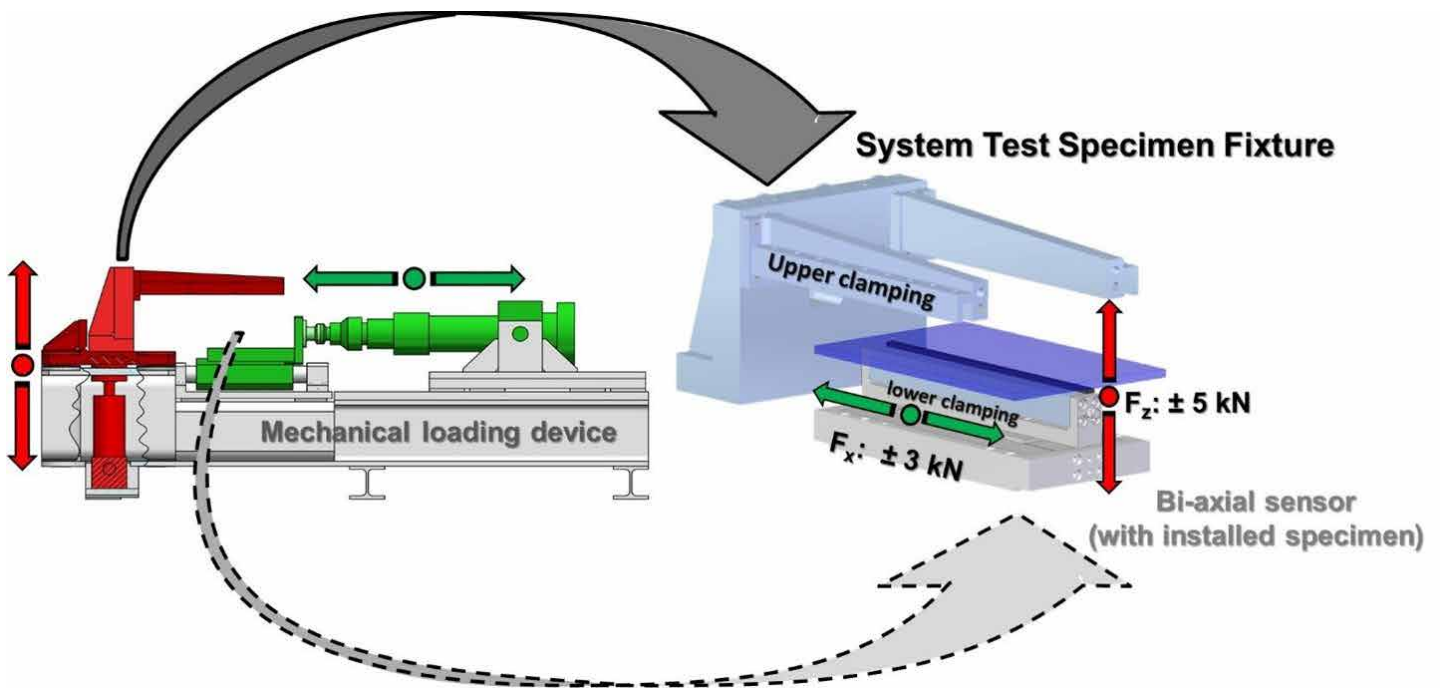


Figure 5: Detail illustration of the mechanical loading device

- mechanical loading device
- system test specimen fixture and bi-axial mechanical sensor
- climate control devices

The mechanical key component of the test facility is a biaxial mechanical loading device, see Figure 4 and 5. With it loading in z-axis [extension/compression of the SSG specimen] as well as x-axis [alternating shear loading of the SSG-specimen] is realized with the help of a vertical and horizontal sliding carriage mechanically powered by independent working servohydraulic cylinders. New developed 2-D mechanical sensors monitor the mechanical response of the SSG-specimen to the superimposed loading. The SSG-specimen - a section of the glass façade element representing a representative bond situation - is fixed between the upper clamping of the vertical sliding carriage and the 2-D mechanical sensor as lower clamping, see Figure 5.

The assessment methodology of this new test methodology offers different ways for performance conclusions regards to functionality and especially durability. The methodology offers direct and indirect assessment opportunities by

- discussion and assessment of the directly mechanical specimen response to loading by
  - cycle-dependent continuity of the monitored course of mechanical characteristics supported by
  - regular visual observation of

- surface characteristics and bond situation [adhesion; cohesion]
- assessment of durability by comparative discussion of test characteristics relevant to ETAG002, section 5 "Methods of verification" before and after complex loading acc. to our superimposed load function

In terms of methodology validation as well as for traceability the project's results to the actual technical guidelines both assessment ways were exercised on benchmark sealants

representing the 1<sup>st</sup> generation and the 2<sup>nd</sup> generation of 2-part Structural Silicone sealants.

From the discussion of the swelling dynamically induced force paths [extension/compression, shear] over all yearly seasons one can detect the general mechanical response of the sealants [e.g. detailed exploration of visco-elasticity], maximum stress states, temperature and humidity sensibility of the sealants and its mechanical consequences. With it also an individual system fingerprint is monitored.

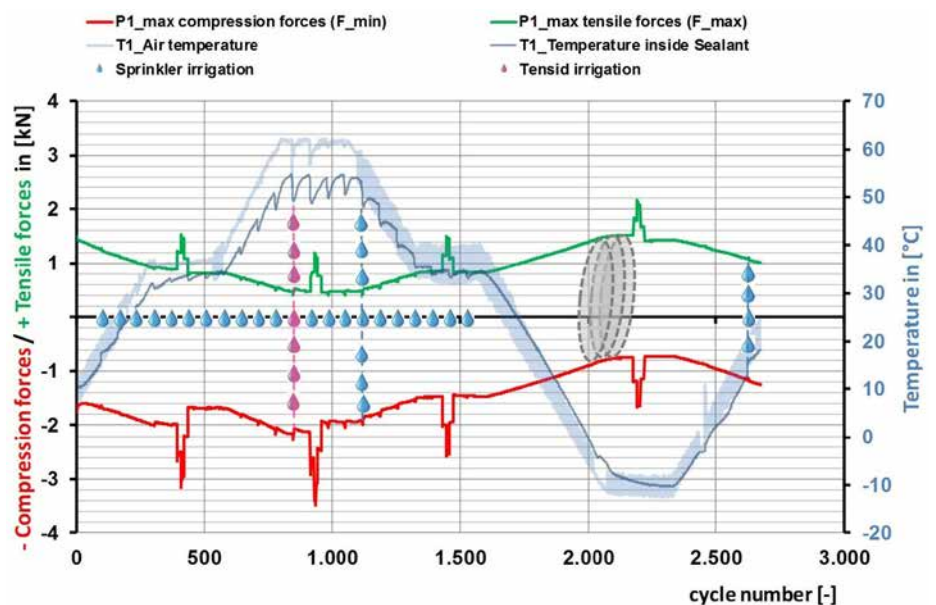


Figure 6: Schematic illustration of a typical force path (tensile/compression) over the first simulated year of service life

From the path of the compression/tensile reaction forces of 2<sup>nd</sup> generation sealant in a determined specific SSG-construction (see figure 6) following consequences for the functionality can be concluded:

- actual distribution of the visco-elastic mechanical response, system stiffness by dynamic moduli, damping
- maximum and regular mechanical bond stresses to be adopted
- consequences from stress depending material softening (e.g. Mullin's effect)
- specificity of thermal and hygroscopic sensibility (thermal elongation and/or thermoplasticity)

The typical service life time model for constructions and technical elements with 3 stadiums of deterioration [11] - adapted from the inflection points of a failure distribution (Hazard function) based on a bathtub curve - is presented in figure 7. The inflection point at the end of phase 2 represents the end of working life and the transition to the ultimate limit state.

According to the experiences in durability assessment so far (inter alia [11], [12]), this model represents our expectations in matters of the cycle depending course of mechanical characteristics.

For a performance-oriented life time assessment of SSG-constructions especially the bond behavior and its fatigue as well as ageing induced material changes are suitable criteria. Durability indicators (suitable mechanical characteristics) for the load depending deterioration may be detected especially from the course of system stiffness and its changes over repeated dynamic loading. Resulting from simulated 50 years of use with the BAM-methodology the course of dynamic moduli of typical and corresponding SSG-constructions with sealants of 1<sup>st</sup> and 2<sup>nd</sup> generation are monitored in figure 8. In terms of comparative description the 2<sup>nd</sup> generation system exhibits a remarkable higher stiffness. The range of temperature dependent stiffness variation determines a similar temperature dependency of both investigated systems.

Because of their continuously course no complete failure can be deduced for both SSG-systems from the slope of the monitored system reaction graphs (here: stiffness modulus  $E_{dyn.}$  defined by summarized force reaction related to the summarized compression and extension deformation load). At first glance, end of working life resp. beginning of phase III according to the life time model (figure 7) seems not yet attained. Only the course of  $E_{dyn.}$  for the 1<sup>st</sup> generation

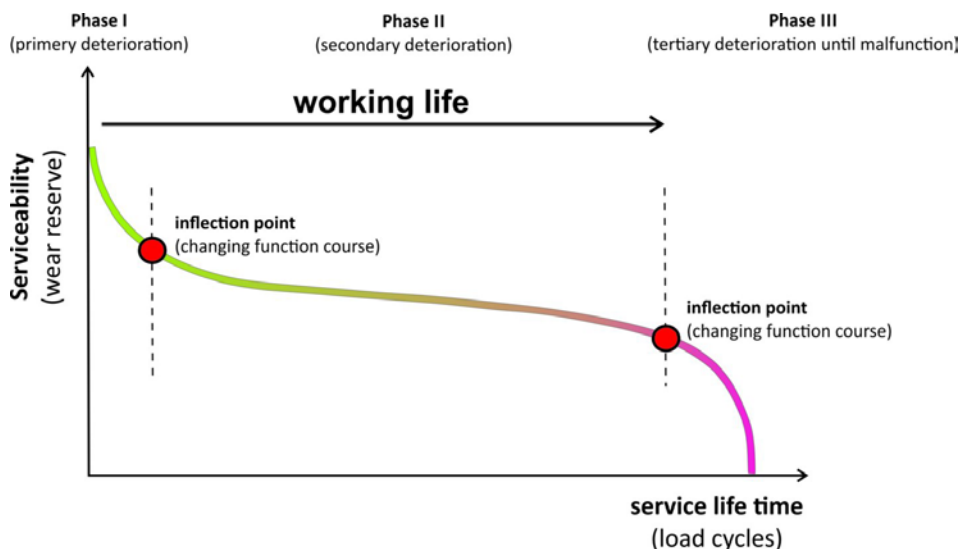


Figure 7: Typical lifetime model for constructions and technical elements (acc. to [11])

product gives indications for a changing negative function decrease at cycle numbers above 110.000 (suggested second inflection point) for higher stiffness reduction. Although both graphs show incipiently comparable mechanical behavior clear indication for different long-time behavior is indicated by the course of the  $E_{dyn.}$  graphs from cycle numbers above ~20.000. While the graph for the 2<sup>nd</sup> generation sealed SSG-system after a typically primary decrease with cycle numbers above 20.000 changes to constant slight decreasing the larger and growingly negative gradient for the 1<sup>st</sup> generation sealed SSG-system suggests higher sensibility under repeated loading. Additionally the course of  $E_{dyn.}$  for 1<sup>st</sup> generation at cycle numbers above 110.000 (suggested second inflection point)

gives indications for further and accelerated increase of stiffness reduction. What is reason for the different durability of the investigated sealants resp. SSG-systems? Is the durability behavior of the 1<sup>st</sup> generation SG-system more dominated by mechanical effects (fatigue and/or deterioration of bond) or by ageing effects of the sealant's material? Is there really an indication for generally affected system performance resp. is the end of working life reached? An attempt for a more detailed system exploration is a separate discussion of the mechanical system reaction under extension loading ( $E_{dyn.,extension}$ ) compared to the system reaction under compression loading ( $E_{dyn.,compression}$ ). Background for this approach is the assumption both bond

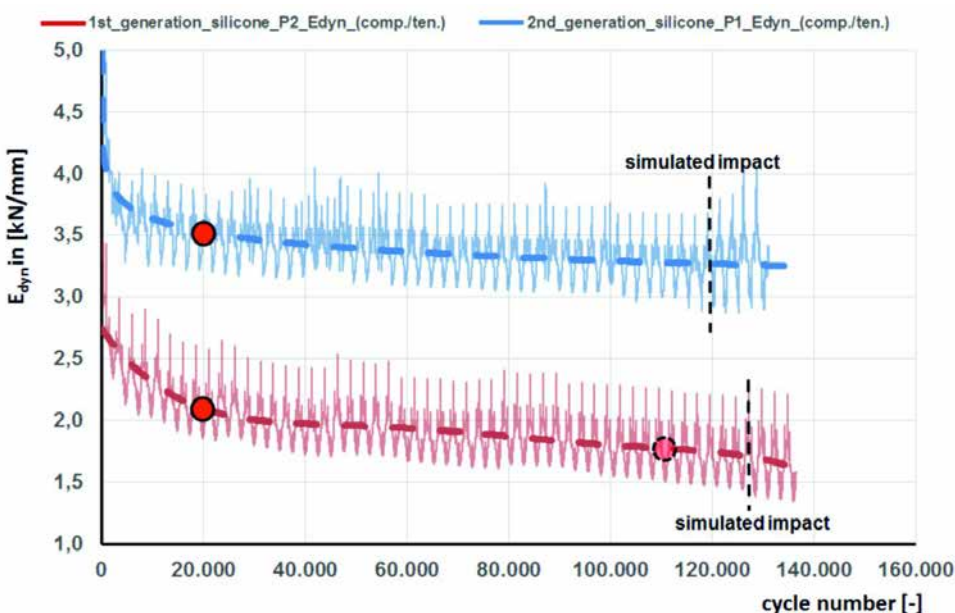


Figure 8: Comparison of stiffness course under superimposed compression/extension over simulated 50 years of use

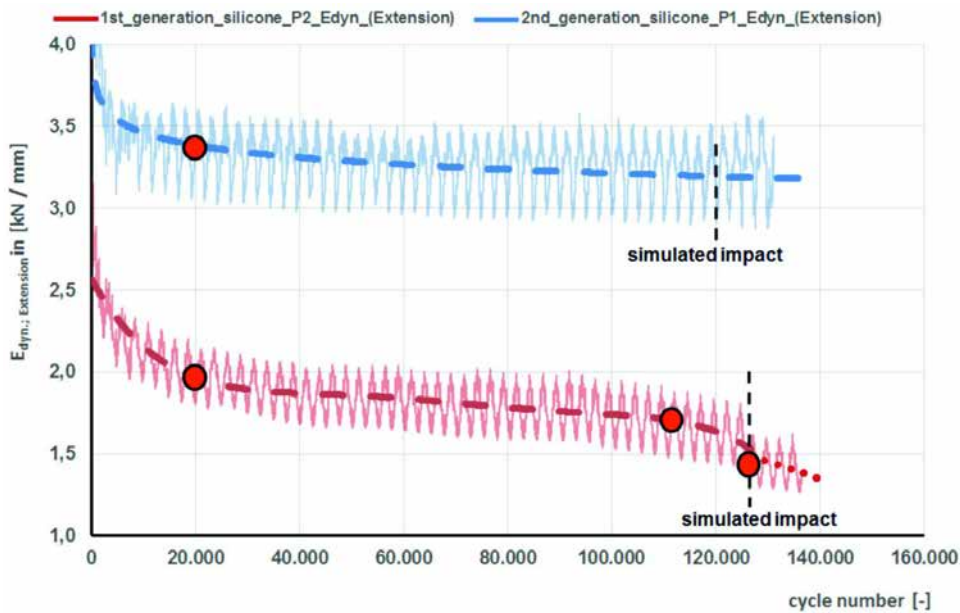


Figure 9: Separated comparison of stiffness course under tensile loading over simulated 50 years of use

and fatigue sealant characteristics will be predominantly addressed by dynamically repeated constant tensile loading. Meanwhile aging caused system changes (changes in sealants analytical structure) should especially be reflected under swelling compression loads because of eliminated bond effects. Although one can explore different ageing behavior of 1<sup>st</sup> generation silicone compared to 2<sup>nd</sup> generation silicone from the course of compression moduli (not figured in this paper) the growingly reduction of the 1<sup>st</sup> generation system stiffness (resistance) against repeated loading (see figure 8 and 9) seems to be obviously attributed to deteriorated bond by affected cohesion and/or adhesion. To clarify this hypothesis the course of stiffness under repeated tensile loading shall be discussed (figure 9).

Consistent with the graphs in figure 8 and 9 the 2<sup>nd</sup> generation system doesn't give indications for malfunctioning performance. Even after an extraordinary impact loading the further course of the stiffness under extension stays

unaffected and stable. This mechanical system reaction under superimposed mechanical and climatic loading indicates performance according to the requirements. The end of working life is not yet attained.

In contrast the accelerated stiffness reduction for the 1<sup>st</sup> generation system already incipient in figure 8 at cycle numbers above 110.000 seems to be caused by affected bond. A clear stiffness reduction as indicator of the mechanical resistance is indicated at cycle numbers above 110.000. After impact simulation a further abrupt stiffness loss under repeated extension with rapid ongoing reduction is monitored. Even a load transmission is still given, an affected performance by bond malfunction is to be accepted.

Utilizing the advantages of the new assessment methodology we found validation for the deduced mechanical performance from accompanying visual observations.

According to these results a performance and durability according to the requirements could be verified for the 2<sup>nd</sup> generation SSG

system. Opposite to this performance the 1<sup>st</sup> generation system shows higher sensibility to ageing as well as bond loading resulting in lower durability under complex loading. Without total collapsing our validation methodology indicates that the end of working life was attained.

To utilize the methodology potential for direct traceability to ETAG002 requirements, the system test specimens were cut after completion of the durability test by water-jetting into standard-sized ETAG002-1 samples, which were then tested for their residual strength. Table 5 displays the results observed initially (prior to testing) and after completion of the durability test. Tensile and shear strength values along with the corresponding residual strength ratios (after aging) are shown. The data gathered at the completion of the durability test differentiate between test specimens that had undergone simultaneous weathering and enforced movement and those that were subjected only to weathering.

As can be seen, 2<sup>nd</sup> generation sealant passes the ETAG002-1 criterion for residual tensile strength, while 1<sup>st</sup> generation sealant fails this requirement for test specimens that had undergone simultaneous weathering and enforced movement. The differentiation between these two sealants becomes even more apparent when considering the extent of interfacial (adhesion) failure observed in the system test specimens. While the 2<sup>nd</sup> generation sealant showed only marginal loss of adhesion, primarily at the corners of the specimen, interfacial failure of the 1<sup>st</sup> generation sealant was more pronounced and, in certain areas, extended through the whole depth of the sealant (see figure 10 and figure 11).

## Summary and Conclusions

Recently, two research studies focusing on the investigation of the durability and service life of SSG structures were completed. Both studies provide compelling scientific support for service life estimates significantly in excess of 25 years. The findings validate anecdotal evidence gathered from successful field-performance of SSG buildings that have now been in operation for more than 30 years. The first study demonstrated that the 1<sup>st</sup> generation 2-part structural silicone test specimens obtained from a SSG façade after 23+2 years of natural aging successfully passed ETAG002-1 key performance criteria for initial mechanical strength and residual strength. This finding is especially remarkable as the silicone sealant used on this project was commercialized long before the ETAG002-1 guideline was developed and failed to meet

| Specimen              | 1 <sup>st</sup> generation silicone sealant |                         |                      |                         | 2 <sup>nd</sup> generation silicone sealant |                         |                      |                         |
|-----------------------|---|-------------------------|----------------------|-------------------------|---|-------------------------|----------------------|-------------------------|
|                       | Tensile Strength [MPa]                      | Residual Strength Ratio | Shear Strength [MPa] | Residual Strength Ratio | Tensile Strength [MPa]                      | Residual Strength Ratio | Shear Strength [MPa] | Residual Strength Ratio |
| Initial               | 1.02  | -                       | 0.68                 | -                       | 1.59  | -                       | 1.18                 | -                       |
| Weathering            | 1.05  | 1.03                    | 0.84                 | 1.24                    | 1.52  | 0.95                    | 1.18                 | 1.00                    |
| Weathering + Movement | 0.63  | 0.62                    | 0.56                 | 0.83                    | 1.23  | 0.78                    | 0.98                 | 0.83                    |

Table 5: Tensile and Shear Strength Values and Residual Strength Ratios for 1<sup>st</sup> and 2<sup>nd</sup> generation silicone sealants observed in the BAM Durability Testing



Figure 10: Visual investigation of system bond after simulated 50 years of use (here: 2<sup>nd</sup> generation SSG)

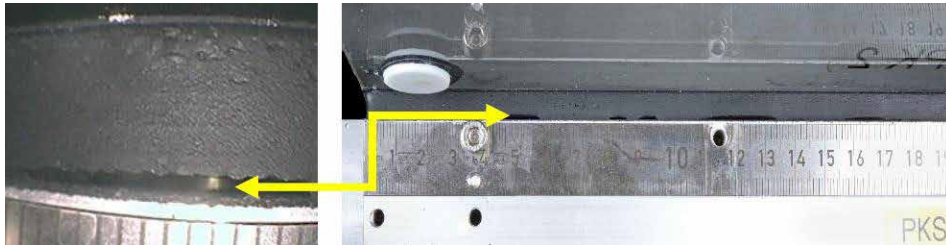


Figure 11: Visual investigation of system bond after simulated 50 years of use (here: 1<sup>st</sup> generation SSG)

its stringent requirements, once this standard went into effect. In the second study, two benchmark sealants, the 1<sup>st</sup> and the 2<sup>nd</sup> generation of 2-part structural silicones, were tested according to a newly developed performance-based durability test method based on simultaneously exposing system test specimens to artificial weathering and complex, multiaxial mechanical loadings. The test results help to explore the mechanical behavior and sealants reaction under mechanical and superimposed climatic loading over an annual cycle. The mechanical indicators are able to describe durability effects like ageing, fatigue and durable bond. It is a special advantage of the new methodology to complement the mechanical characterization by visual observations and traceability to the empirical ETAG002 requirements. After completion of this test, which is considered to correspond to an anticipated service life of 52 years, the today's structural 2-part silicone (2<sup>nd</sup> generation) still passed the ETAG002-1 criterion for residual tensile strength with only marginal loss of adhesion at the specimen corners; a result that demonstrates the outstanding bonding strength durability of this sealant. Such strong performance against key ETAG002-1 performance indicators after natural and accelerated exposure is quite reassuring. It may give conservative building code authorities the added confidence they need to consider future four-sided SSG structures without supplementary safety retainers. SSG has proven its reliability now for many years, which is a testament to the performance of the structural silicone sealants

involved and the implementation of effective quality assurance procedures. Nevertheless further results of the BAM-research project (see e.g. table 5) proof the evidence for a performance-related working life assessment under superimposed mechanical and climatic loading opposite to separated specimen conditioning similar to ETAG 002.

## References

- [1] Klosowski, J.M. and Wolf, A.T., Sealants in Construction, Second Edition, CRC Press (2015), ISBN 9781574447170.
- [2] Carbary, L.D., "A Review of the Durability and Performance of Silicone Structural Glazing Systems," Glass Performance Days 2007, J. Vitkala (ed.), 190-193
- [3] EOTA, ETAG 002 Structural Sealant Glazing Systems, Part 1: Supported and Unsupported Systems, European Organization for Technical Assessment, Brussels, Belgium (2012).
- [4] Lieb, K., "It Keeps Lasting and Lasting and Lasting – Structural Glazing Façade Undergoes Duration Test" ["Sie hält und hält und hält... Structural Glazing Fassade im Dauertest"], Rosenheimer Fenstertage 2013, ift Rosenheim, pp. 49-53.
- [5] Lieb, K. and Krewinkel, H., "23-Year Old Bonded Façade Undergoes Lab Testing – A Historical SG Façade is Subjected to Lab Testing After Actual Service and Displays Amazing Durability" ["23 Jahre alte geklebte Fassade im Labortest – Historische SG-Fassade kommt nach Realtest auf den Prüfstand und zeigt erstaunliche Haltbarkeit"], ift Rosenheim Publication
- [6] Graf, N., Durability of Structural Sealant Glazing Systems (SSGS) – Material-based, experimental study and statistical evaluation of an ift facade

subjected to natural aging in accordance with EOTA ETAG 002-1 [Beständigkeit von SSGS – Materialorientierte experimentelle Untersuchung und statistische Auswertung einer real gealterten ift-Fassade in Anlehnung an die EOTA ETAG 002-1], Bachelor dissertation, University of Applied Science Regensburg (2012).

[7] Anonymous, Structural Sealant Glazing – Evaluating the performance and durability of structural sealant glazing systems under combined mechanical and climatic loads.

[8] Kaatz, R. and Recknagel, C., "Advanced Evaluation of Structural Sealant Glazing Systems by a New System Test Approach", ASTM STP 1583 (2015), DOI: 10.1520/STP158320140074.

[9] Recknagel, C. and Kaatz, R., "Exploration and Evaluation of the Performance and Durability of SSG Systems by Dynamic-Mechanical System Testing", ASTM STP 1583 (2015), DOI: 10.1520/STP158320140064

[10] DIN 1055-4:2005-03, Action on structures – Part 4: Wind loads. Deutsches Institut für Normung e. V. (DIN), Beuth-Verlag, Berlin (2005)

[11] Ritter, F., „Lebensdauer von Bauteilen und Bauelementen“, Schriftenreihe der TU Darmstadt, Institut für Massivbau, Heft 22 (2011), 265 Seiten, ISBN 978-3-942886-00-0

[12] Ehrenstein, G.W.; „Hysteresis-Messverfahren – Verfahren der dynamischen Werkstoff- und Bauteilprüfung“; Schriftenreihe des Lehrstuhls für Kunststofftechnik der Universität Erlangen-Nürnberg; 273 Seiten; ISBN 3-9802740-4-7

# Silicone Opacifiers for Spandrel Glass Applications: Risk Mitigation in Thermal Stresses

Kris Vockler 1  
 Timothy Krytenberg 2  
 Scott Norville 3  
 Samir Blanchet 4  
 John Swanson 5  
 Chris Barry 6  
 Lawrence Carbary 7  
 Stephane Hoffman 8  
 George Torok 9  
 Christopher Fronsoe 10

1 I.C.D High Performance Coatings  
 2 I.C.D High Performance Coatings  
 3 Texas Tech University  
 4 Texas Tech University  
 5 I.C.D High Performance Coatings  
 6 Chris Barry Glass Consultant  
 7 Dow Corning Corporation  
 8 Morrison Hershfield  
 9 Morrison Hershfield  
 10 I.C.D High Performance Coatings

## Keywords

insulating glass units, ceramic enamel, silicone coatings, architectural glass, glass weakness, uniform lateral load, four-point bending, ball drop, glass strength

## 1. Abstract

Curtain wall design commonly uses insulating glass units for spandrel glazing to provide better visual harmony between vision and spandrel areas. Risks with this approach include higher thermal stresses, especially when low-emissivity coatings are used, and increased chance of spontaneous breakage by nickel sulfide inclusions if fully tempered glass is used to control thermal stress. The thermal stress control benefit of heat treated glass is reduced if a ceramic enamel frit opacifier -which induces a known strength reduction of up to 40%- is applied. Incidences of thermal stress related fracture have occurred with heat strengthened, ceramic enamel frit opacified spandrel glass.

Silicone coatings have been examined as a solution to prevent strength reduction in heat-treated glass when applied as a spandrel opacifier. Four-point bending tests were used to investigate the flexural strength of coated heat strengthened and fully tempered glass. Ball drop testing was used to investigate the impact resistance of coated fully tempered

glass. Silicone coatings have no adverse effect on the flexural strength or impact resistance of the substrate and, in some instances, improve it. These coatings also provide fallout protection in accordance with ASTM C1048 (ASTM, 2012). This suggests using a silicone opacifier on heat-treated spandrel glass could greatly reduce the risk of fracture resulting from thermally induced tensile stress, flexural stress, and impact related glass breakage and reduce the risk of injury from fallout if breakage occurs.

## 2. Introduction

Insulating glass (IG) units have been used in commercial and residential high-rise construction for many years to increase HVAC energy efficiency, and more recently, in the case of spandrel areas, to provide greater color and visual harmonization between vision and spandrel areas. Before the widespread use of IG units, the spandrel areas of a building were mostly monolithic glass applications.

In the world of façade glass, there are two types of glass: vision, and spandrel. Vision glass is transparent to provide viewing areas for occupants and daylight for the interior. Spandrel glass areas, where slab ends, vents, and mechanical parts reside, are opaque. As vision glass improved -greater light transmission and lower reflectance while increasing energy performance- it has become more difficult to visually harmonize the spandrel and vision areas. This difficulty has been intensified with the increasing prevalence of IG units over monolithic applications for spandrel areas as both tinted glass and colored spandrel coatings work together in combination for improved visual harmony between the areas.

Since the 1990's, the amount of spandrel glass on a building has fluctuated between 15-30% of a building's total glass area, as dictated by design trends. Still a sizable area of the building sides, spandrel glass not only contributes to the visual aspects of a building but its energy use as well since IG units improve the energy performance of the spandrel area. Recent energy codes, where the baseline building are governed by lower glazing ratios, are resulting in increased spandrel areas.

However, there are several risks associated with using IG units in a closed spandrel area.

One of the most important, commonly known to the industry, is that thermal stresses will increase, particularly in the opacified inboard lite. This is primarily due to heat gain that accumulates in an IG unit as the sun's rays strike it. The increased heat differential between glass center and edges, often exacerbated by the use of low-emissivity coatings or by dark colors in a spandrel cavity (Mognato and Barbieri, 2013), leads to thermal stresses which can result in fracture. The accepted rule is that 0.34 MPa (50 psi) hoop stress is created around the edge of a lite of glass for every 0.56°C (1°F) increase in temperature of the exposed area. Therefore, a center-to-edge temperature difference ( $\Delta T$ ) of 56°C (100°F) will create 34.5 MPa (5,000 psi) thermal stress.

Thermal stress issues are further aggravated from the use of ceramic enamel frit as a spandrel opacifier. In recent years, there has been increased awareness in the industry that ceramic enamel frit, used as a spandrel coating, lowers the flexural strength of both heat strengthened (HS) and fully tempered (FT) glass. The degree depends on glass coverage, the colors used, and even the formulation of the ceramic enamel frit itself (Maniatis and Elstner, 2016). There are several newly published works that discuss the weakness of various heat-treated (HT) products with an applied ceramic enamel frit opacifier; "full coverage black ceramic enamel...reduced the load resistance (LR) of FT glass and HS glass by approximately factors of 2.0" (Natividad et al., in press) and 37.5% reduction of strength (Krampe, 2014).

In summary: laboratory tests have shown significant flexural strength reductions in both new and artificially weathered glass, in both HS and FT glass, when fully covered with a ceramic enamel frit opacifier. Strength reductions, of approximately 50% to 20% have been measured in mean strength and in the 8 per 1000 probability of breakage strength, respectively. Bergers, et al. (2016) attributed the difference between mean strength values and design strength values to the fact that samples with ceramic enamel frit opacifiers have a much lower coefficient of variation, (CoV) than clear samples.

European product standards EN 12150-1 (2015) & EN 1863-2 (2004) address reductions in flexural strength of HT glasses resulting from the application of ceramic enamel frit.

These standards reduce the minimum surface flexural strengths of HT glass from 120 N/mm<sup>2</sup> (17400 psi) to 75 N/mm<sup>2</sup> (10900 psi) and from 70 N/mm<sup>2</sup> (10200 psi) to 45 N/mm<sup>2</sup> (6500 psi) for FT and HS glass with ceramic enamel frit, respectively.

The American standard, ASTM E 1300 "Load Resistance of Glass in Buildings" (ASTM, 2016), uses conservative 2X and 4X multiplying factors for the strength of HS and FT glass, when compared to annealed glass. As no field-breakage has been reported from flexural stress in enameled HT glass, there has been little immediate incentive to change the published uniform load strength values in ASTM E 1300-16 (2016).

However, there have been a significant number of thermal stress breakages in IG spandrel units with ceramic enamel frit (Barry and Norville, 2015). In all the reported cases the fracture origin is typically been located 13 mm (0.5") to 25 mm (1") in from the cut edge of the glass. Significantly, the fracture origin has always occurred on the glass surface in contact with the ceramic enamel frit and never on the uncoated glass surface. This clearly indicates a relatively large reduction of the tensile strength of HT, in-service, glass with an application of ceramic enamel frit.

In response to the thermal stress failures in the field, FT glass lites have been used in spandrel areas to mitigate thermally induced breakage. However, this increases the risk of spontaneous breakage from nickel sulfide inclusions in FT glass, unless the glass is heat soaked, with a consequent cost increase. Also, if inner lite breakage occurs and goes unnoticed, the LR of the IG unit decreases to where additional fracture may occur allowing glass shards to fall from the spandrel cavity. As such, there is an increasing need for a spandrel opacifier that does not weaken the glass, but ideally, increases its strength and offers fallout protection. Silicone coatings were examined as a solution to the strength reduction issue created by applying ceramic enamel frit to HT glass as a spandrel opacifier. Investigations were performed using four-point bending and ball drop test methods.

### 3. Experimental

#### 3.1 Four-Point Bending

Six samples of HS and six samples of FT 102 x 305 x 6 mm (4 x 12 x ¼ in.) flat glass beams were obtained, with each sample comprised of at least 30 specimens.

Specimens were coated using OPACI-COAT-300® a water borne silicone elastomer, or with OPACI-COAT-500® a 100% solids silicone elastomer. All coatings were applied to the air side of the specimen. A total of 193 specimens were tested. All coatings

| Sample | Sample Size | Glass Type | Coating         |
|--------|-------------|------------|-----------------|
| 1      | 34          | HS         | Clear           |
| 2      | 33          | HS         | OPACI-COAT-300® |
| 3      | 30          | HS         | OPACI-COAT-500® |
| 4      | 33          | FT         | Clear           |
| 5      | 33          | FT         | OPACI-COAT-300® |
| 6      | 30          | FT         | OPACI-COAT-500® |

Table 1. Samples tested via four-point bending

were black. OPACI-COAT-300® was applied via spray gun to 330 µm (13 mils) wet film thickness (WFT). OPACI-COAT-500® was applied via roll coat to 150 µm (6 mils) WFT. Specimens were tested in four-point bending using an MTS machine to provide load at a uniformly increasing rate as per ASTM C 1161-13 (ASTM, 2013). The MTS machine was certified by the American Association for Laboratory Accreditation (ASLA Cert. No. 11455.01) for the basis of the ISO/IEC 17025 international standards for calibration laboratories. During loading, a data acquisition (DAQ) system captured the load-time history from inception of loading to fracture for each specimen. Each specimen's load-time history was converted to an equivalent fracture load of three seconds (P<sub>3</sub>) using traditional beam theory to compute equivalent failure stresses (σ) coupled with the failure prediction model (Beason, 1980) using equation 1:

$$\sigma_3 = \left[ \int_0^{t_f} \frac{(\sigma(t) - RCSS)^{16} dt}{3 \text{ sec}} \right]^{1/16} + RCSS \quad [1]$$

Where,

σ<sub>3</sub> denotes the 3-second equivalent fracture stress

t<sub>f</sub> denotes time of fracture

σ(t) denotes stress at time, t

RCSS denotes the minimum observed residual compressive surface stress in a sample

All specimens were installed in the four-point testing mechanism with the float glass air side (coated side) facing down. This orientation induces tensile stresses in the float glass air side and compressive stresses in the float glass tin side during testing. Figure 1 displays a schematic diagram of the testing apparatus. The loading supports spanned 254 mm (10 in.) where each glass beam specimen was placed center to center (c-c) allowing 63.5 mm (2.5 in.) between each support and loading point. The four-point bending creates uniform stresses between the inside loading supports' 127 mm (5 in.) span.

Once installed each test consisted of loading a beam specimen at a rate of 2.54 mm per min (0.1 inches per min), an equivalent loading rate of 445 N per min (100 lbs per min), while the DAQ system recorded the load and time histories at a sampling rate of 10 Hz. Each test concluded with the fracture of the beam specimen, followed by inspection and measurement.

Using the Maximum Likelihood Estimation (MLE), the σ<sub>3</sub> values were used to fit a three parameter Weibull distribution to obtain cumulative distribution functions (CDFs) for the P<sub>3</sub> using equation 2:

$$P_f = 1 - \exp(-B) \quad [2]$$

$$B = k S_m^m$$

$$S_m = \sigma_{3sec}^m A_{surface}$$

Where,

m, k denote statistical parameters

A<sub>surface</sub> denotes the surface area

The CDF's allow direct comparison concerning LR of clear and coated beam specimens of the same glass type. In this work, LR for the glass beams is defined as the constant applied force with 3-second duration that leads to a probability of breakage equal to or less than 8 per 1000. Work by others (Bergers, et al., 2016) has indicated a reasonable correspondence between results from four-point bending tests and full scale test of rectangular lites.

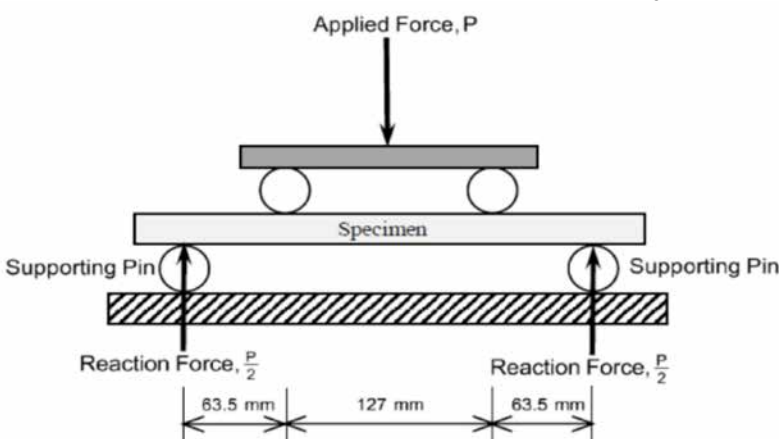


Figure 1. Schematic diagram of four-point bending test.

| Sample | Sample Size | Glass Type | Coating         |
|--------|-------------|------------|-----------------|
| 1      | 34          | FT         | Clear           |
| 2      | 34          | FT         | OPACI-COAT-300® |
| 3      | 31          | FT         | OPACI-COAT-500® |
| 4      | 33          | FT         | Ceramic Frit    |

Table 2. Samples tested via ball drop

### 3.2 Ball Drop

Four samples of FT 305 x 305 x 3 mm (12 x 12 x 1/8 in.) flat glass beams were obtained, with each sample comprised of at least 30 specimens.

Specimens were coated using OPACI-COAT-300® a water-borne silicone elastomer, OPACI-COAT-500® a 100% solids silicone elastomer, or with a ceramic enamel frit. All coatings were applied to the air side of the specimen. A total of 132 specimens were tested. All coatings were black. OPACI-COAT-300® was applied via spray gun to 330 µm (13 mils) WFT. OPACI-COAT-500® was applied via rollcoat to 150 µm (6 mils) WFT. Ceramic enamel frit was applied via screen print to 38 µm (1.5 mils) WFT.

Specimens were tested in a ball drop impact test frame following the parameters from a GANA Specification (GANA 76-12-10a, 2008), using a 50 mm (2 in.) diameter steel ball with 535 g mass weighing approximately 5.25 N (1.18 lbs).

Samples were loaded into the test frame, float glass air side (coated side) facing down. Impact height was increased until fracture occurred, at which point drop height was recorded and the specimen inspected.

## 4. Results and Discussion

### 4.1. Four-Point Bending

All specimen fracture origins lay between the load points on the beam specimens, that is, within the area of constant bending moment and flexural stress. No fracture origin was located on the edge of a specimen.

Table 3 summarizes the statistical results for the samples. Researchers used the minimum RCSS for each sample in calculations described.

The CoVs for samples of HS glass beams coated with OPACI-COAT-300® and OPACI-COAT-500® were relatively small. The small values of CoV led to large and similar values of the statistical parameter  $m = 17$  and

| Sample | Mean P3 (kN) | Std Dev (kN) | CoV (%) | Minimum RCSS (MPa) |
|--------|--------------|--------------|---------|--------------------|
| 1      | 2.19         | 0.23         | 10.5    | 50.2               |
| 2      | 2.35         | 0.16         | 6.67    | 52.0               |
| 3      | 2.36         | 0.17         | 7.26    | 52.9               |
| 4      | 2.75         | 0.15         | 5.48    | 104                |
| 5      | 2.74         | 0.16         | 5.76    | 104                |
| 6      | 2.77         | 0.11         | 3.81    | 82.6               |

Table 3. Sample statistics displaying mean P3, standard deviation, coefficient of variation, and minimum residual compressive surface stress of all samples.

$m = 18$  for Sample 2 and Sample 3, respectively, which were significantly larger than  $m = 10$  for Sample 1. One can make a similar observation concerning values of  $m$  and the CoVs for Samples 4, 5, and 6.

Figures 2 and 3 display the empirical values and CDFs for the  $P_3$  values for HS and FT samples respectively while Figures 4 and 5 present the lower portion of the CDFs for HS and FT samples respectively.

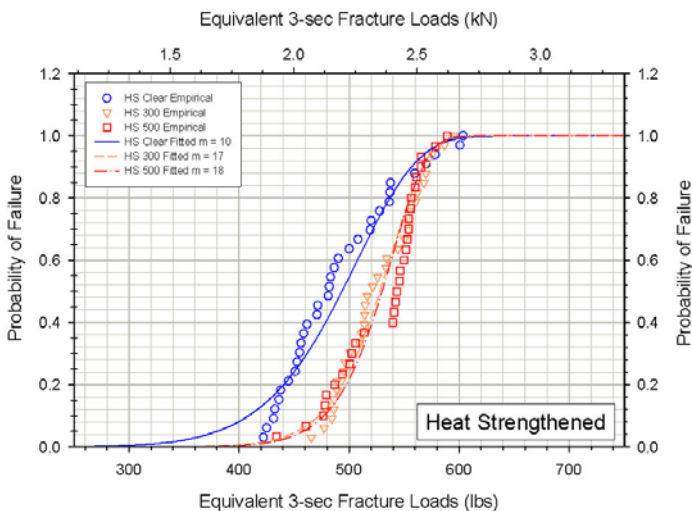


Figure 2. Cumulative distribution function for the probability of failure for clear HS, OPACI-COAT-300®, and OPACI-COAT-500® specimens.

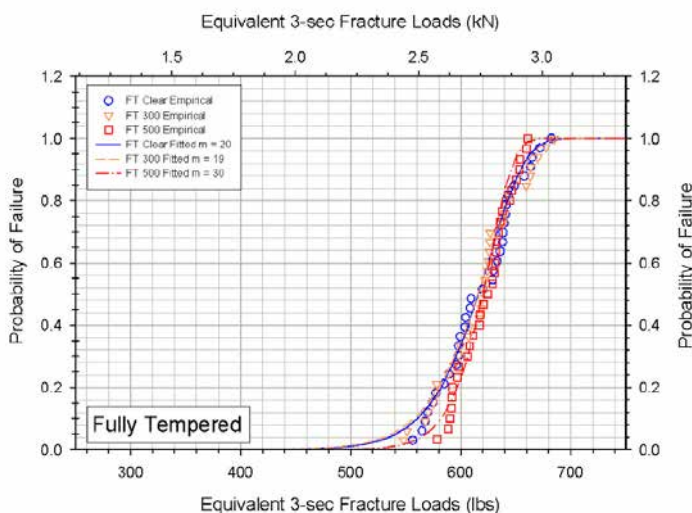


Figure 3. Cumulative distribution function for the probability of failure for clear FT, OPACI-COAT-300®, and OPACI-COAT-500® specimens.

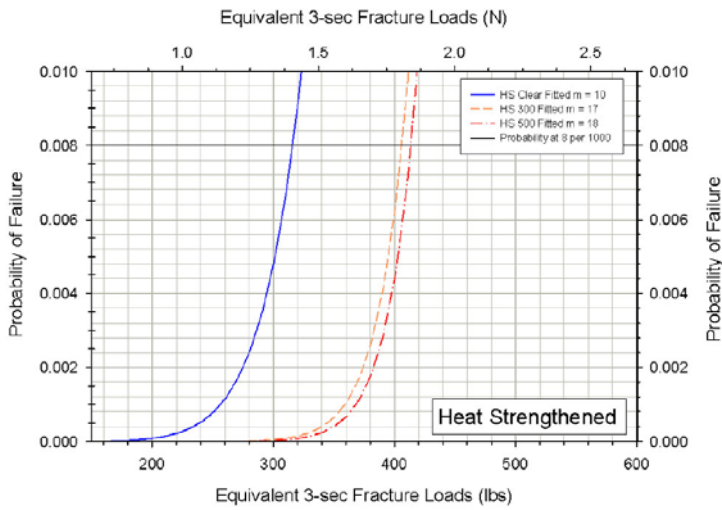


Figure 4. Fitted cumulative distribution function for the probabilities of failure less than or equal to 10 per 1000 for clear HS, OPACI-COAT-300®, and OPACI-COAT-500® specimens.

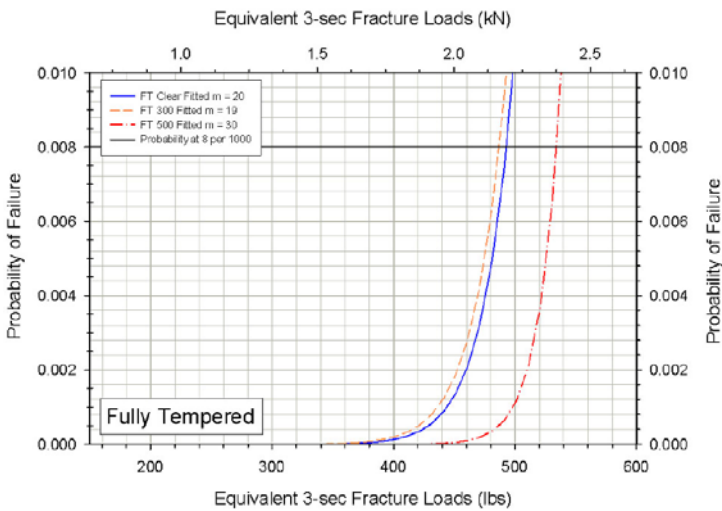


Figure 5. Fitted cumulative distribution function for the probabilities of failure less than or equal to 10 per 1000 for clear FT, OPACI-COAT-300®, and OPACI-COAT-500® specimens.

| Sample | $\Delta P_3$ (%) | $\Delta LR$ (%) |
|--------|------------------|-----------------|
| 2      | 7.28             | 28.50           |
| 3      | 7.66             | 30.90           |
| 5      | 0.16             | -1.20           |
| 6      | 0.75             | 8.36            |

Table 4. Change in  $P_3$  and LR relative to the associated clear samples.

| Sample | Mean Height |      | Std Dev |      | CoV  |
|--------|-------------|------|---------|------|------|
|        | (m)         | (ft) | (m)     | (ft) | (%)  |
| 1      | 1.42        | 4.65 | 0.36    | 1.17 | 25.3 |
| 2      | 2.13        | 7.00 | 0.72    | 2.36 | 33.7 |
| 3      | 2.06        | 6.76 | 0.84    | 2.74 | 40.6 |
| 4      | 0.44        | 1.43 | 0.05    | 0.17 | 11.8 |

Table 5. Sample statistics displaying mean fracture height, standard deviation, and coefficient of variation of all samples.

The CDFs in Figures 2 and 4 indicate that both OPACI-COAT-300® and OPACI-COAT-500® increased the strength of HS glass a statistically significant amount. This is demonstrated in mean  $P_3$  values and most prominently at a probability of breakage less than or equal to 8 per 1000. This data is summarized in Table 4.

In Table 4, Samples 2 and 3 are HS specimens coated with OPACI-COAT-300®, and OPACI-COAT-500® respectively, while samples 5 and 6 are FT specimens coated with OPACI-COAT-300®, and OPACI-COAT-500® respectively.

Fully tempered specimens coated with OPACI-COAT® however do not demonstrate a statistically significant change in either  $P_3$  or load resistance relative to uncoated specimens.

#### 4.2. Ball Drop

Table 5 summarizes the statistical results for the samples while Figure 6 displays the mean fracture height of all samples. Table 6 shows the statistical values associated with mean fracture heights relative to those of uncoated Sample 1. Figure 7 displays the percent change in fracture height of the sample means relative to that of uncoated Sample 1.

| Sample | $\Delta$ Height |       | $\Delta$ Height | P-value                 |
|--------|-----------------|-------|-----------------|-------------------------|
|        | (m)             | (ft)  | (%)             |                         |
| 2      | 0.72            | 2.35  | 50.6            | 7.9(10 <sup>-5</sup> )  |
| 3      | 0.64            | 2.11  | 45.5            | 22.2(10 <sup>-3</sup> ) |
| 4      | -0.98           | -3.21 | -69.2           | 6.1(10 <sup>-14</sup> ) |

Table 6. Sample statistics displaying change in mean fracture height relative to uncoated Sample 1, and associated P-value

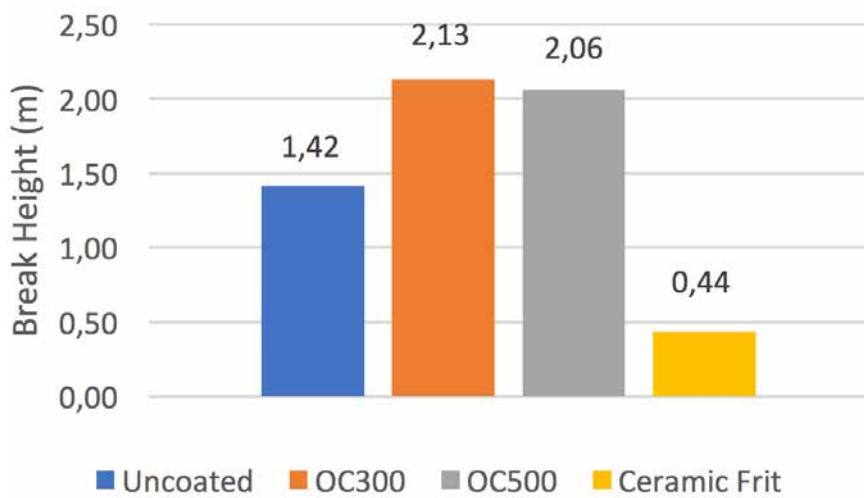


Figure 6. Mean fracture height of coated and uncoated specimens.

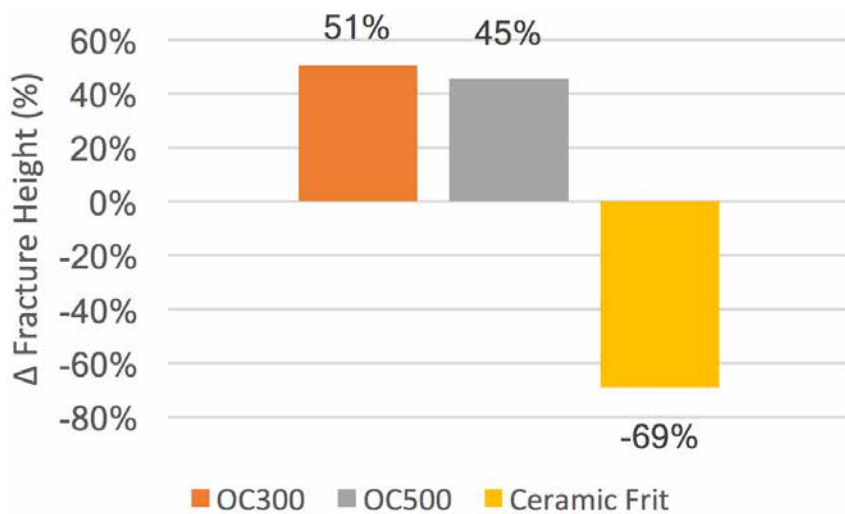


Figure 7. Percent change in fracture height of coated specimens relative to uncoated glass specimens.

Specimens coated with OPACI-COAT-300@ demonstrated a mean increase in fracture height of 0.72 m (2.35 ft.) while specimens coated with OPACI-COAT-500@ displayed a mean increase in fracture height of 0.64 m (2.11 ft.). This corresponds to increases of 50.6% and 45.5% respectively. Specimens coated with ceramic frit demonstrated a reduction in break height of 0.98 m (3.2 ft.), or 69.2%.

## 5. Conclusions

Four-point bending test results indicate OPACI-COAT@ coatings have a positive impact on the flexural strength of HS glass, and have little to no impact on the strength of FT glass. However, ball drop tests displayed a large increase in impact resistance for OPACI-COAT@ coated FT glass. Since four-point bending is generally considered a more precise flexural strength testing methodology those

results should be given greater weight.

It is clear silicone opacifiers, such as OPACI-COAT@ coatings, certainly do not decrease the LR of HT glass, unlike ceramic enamel frit. As such, silicone opacifiers should be considered instead of ceramic enamel frit as a spandrel opacifier when glass breakage from thermal or bending induced tensile stresses, or from impact loads, is a concern.

## 6. References

- ASTM (2012): "Standard specification for heat strengthened and fully tempered flat glass" ASTM C 1048-12e1, West Conshohocken, PA.
- ASTM (2013): "Standard test method for flexural strengths of advanced ceramics at ambient temperature." ASTM C 1161-13, West Conshohocken, PA.
- ASTM (2016): "Standard practice for determining the load resistance of glass in buildings." ASTM E 1300-16, West Conshohocken, PA.

Barry, C., Norville, H.S., (2015): Unexpected Breakage in Ceramic Enamelled (Frit) HS IG Spandrels. IGMA Winter Conference, FL, Feb 5.

Beason, W.L., (1980): "A Failure Prediction Model for Window Glass," Institute for Disaster Research, Texas Tech University, Lubbock (NTIS Accession No. PB81-148421), May.

Bergers, M., Natividad, K., Morse, S., Norville, H.S., (2016); Full Scale Tests of Heat Strengthened Glass with Ceramic Frit. In Glass Structures & Engineering; Springer: Switzerland, Vol. 1, Issue 1, p. 261.

EN 1863-2 (2004): "Glass in building – Heat strengthened soda lime silicate glass – Part 2: Evaluation of conformity/Product Standard" BSI, Brussels.

EN 12150-1 (2015): "Glass in building – Thermally toughened soda lime silicate safety glass" BSI, Brussels.

GANAs 76-12-10a (2008): "Fully Tempered Glass Uses Requiring Strength and Resistance to Temperature – Rev #1" Topeka, KS.

Krampe, P. (2014); The strength of enamelled glass. In Challenging Glass 4 & COST Action TU0905 Final Conference; Louter, C., Ed.; Taylor & Francis: London, p. 691.

Maniatis, I., and Elstner, M. (2016); Investigation on the mechanical strength of enamelled glass. In Glass Structures & Engineering; Springer: Switzerland, Vol. 1, Issue 1, p. 277.

Mognato, E., and Barbieri, A. (2013); The breakage of glass – Thermal shock and nickel sulfide inclusion. In COST Action TU0905, Mid-term Conference on Structural Glass; Mociobob, D. Louter, C., Ed.; CRC Press: Boca Raton, p. 155.

Natividad, K., Morse, S.M., and Norville, H.S. (In Press). "Tests of heat treated glass with full coverage ceramic frit." J. of Architectural Engineering, ASCE.

# Structural Glass Sandwich Panels

Graham Dodd, Arup

## Keywords

1 = Glass 2 = Honeycomb 3 = Sandwich  
4 = Desiccant 5 = Breather 6 = Climatic  
Abstract

To provide stiffness, shading and privacy with abundant daylight and a feeling of openness for restaurant extensions and an entrance canopy to a London hotel, we used glass sandwich panels with aluminium honeycomb core. Similar construction had been used on smaller scale for interior decorative panels and for some interior floor panels but without engineering development. Exterior glass sandwich panels need durable strength and stiffness with continuing clarity, so we developed a detailed set of tests and acceptance criteria for all aspects of the appearance and performance of the panels with a specialist façade contractor. The panels were over twice the area of previous examples and too large for the established sandwich panel manufacturers so the contractor developed a new production method. When sealed sandwich panels are exposed to the weather, they experience changes of pressure in the entrained air, so need to be allowed to equalise. We proposed to ventilate the panels through canisters of silica gel desiccant to dry incoming air sufficiently to avoid condensation. The technique is commonly used to condition the expansion airspace above insulating oil in electrical transformers but was not known in the glazing industry. The technique has wide potential for façade applications.

## Introduction

Rogers Stirk Harbour + Partners designed extensions of the bar and restaurant and created a new entrance canopy composed of clear glass panels supported by carbon fibre beams for The Berkeley Hotel in London's Knightsbridge. Project Partner, Amo Kalsi described the challenge to give guests the feeling of sitting in a bright, open space while being protected from the heat of the sun or the prying lens of the paparazzi. A reflective coating on the glass would prevent a view in during the day but would make the volumes look hard, heavy and monolithic from



*Fig 1 The Berkeley entrance*

outside rather than light and transparent. At night, a reflective coating would not prevent a view in but would reduce the view out, making the spaces feel closed. Patterns of ceramic frit could blur the view in either direction but provide little shading and detract from the intended clarity and sparkle.

## Honeycomb panel applications

Browsing our collection, comparing combinations of glass types and other materials, a number of shading and privacy devices, such as reflective louvers and plastic tube bundles, enclosed within double glazed units, seemed to offer some of what was required but none had the desired combination of clarity, privacy, sparkle and charm required. It was a combination that was as difficult to express as to achieve but when Amo referred to the marque "Bugatti" it became clear that we needed a combination of technology and craft serving performance objectives, from which the aesthetic would emerge. We found a small sample of clear plastic sandwich panel with an aluminium honeycomb core and had seen honeycomb panels with glass skins used as interior dividers and glass floors, in projects like the Light House in North London by Gianni Botsford Architects.

Playing with a variety of honeycomb sizes and seeing them sandwiched between glass, we noted the inevitable small variations in the geometry of the hexagonal cells that results from the process of stretching out the block from a stack of bonded foils. Far from being an undesirable 'defect' the variations lent interest and richness to the texture.

## Performance

Although the aluminium foil is only 50 to 70 microns thick, and therefore less than 0.8% of the cross sectional area, the thermal conductivity would be too high to form the insulating envelope of the building on its own. We did experiment with a Nomex paper honeycomb sample, which is a much better insulator, but the characteristic colour was not suitable in this case. Thermal insulation was provided by adding a conventional insulating cavity with laminated heat strengthened glass on the interior face of the structural honeycomb panels. The lower pane of the sandwich panel carried a durable solar reflective coating and the lower face of the insulating cavity had a low emissivity coating to minimise long-wave radiant heat gain from the honeycomb when exposed to direct sun, as well as to minimise heat loss.

The effective shading coefficient or total solar heat gain was complex to estimate because of the geometry of the aluminium honeycomb and was simulated in a variety of ways to converge on an estimate. The properties are expected to be dependent on the angle of insolation but more research is required to characterise such composites fully.

An advantage of using honeycomb bonded to the glass skins is that the resulting panel has much higher stiffness and strength than a simple laminated pane. This enabled the 4.5m high walls to be spanned vertically without mullions and the 1.9m wide roof panels to remain flat enough to allow a very shallow fall.

## Development of the criteria

Prior uses of glass honeycomb panels appeared all to be interior applications, where exposure to UV light and thermal changes were not so severe. In addition, the required sizes up to nearly 4.8m by 2.4m were too big for existing panel making facilities, so the appointed specialist contractor Bellpart elected to manufacture their own panels, which required selection of the clear adhesive and development of a production method for such large panels.

The newly made panels would not have a track record of performance in service based on previous production, so it was essential to carry out a programme of testing to verify the properties and durability. We worked with specialist contractor Bellpart to identify the various potential failure modes to test for, find or devise test procedures and agree acceptance criteria before testing commenced. [1]

The testing programme included:

- Yellowing under Xenon light 2000hr (EN-ISO 4892-2:2006);
- Chemical compatibility with butyl and silicone sealants;
- Fogging as a result of acrylate vapour condensation (by rapid cooling from 80oC to 12oC);
- Interaction between desiccants and acrylate vapour;
- Moisture ingress through perimeter seal and breather tubes;
- Accelerated ageing in high moisture environment (EN1279-6:2003 Annex B) followed by tests of flatwise tensile (BS 5350-C6), compression and four-point flexural strength (EN 1288-3);
- Cyclic temperature test to load the honeycomb with isochore pressure (based on EN1279-2);
- Impact strength, soft body, EN12600; and
- CWCT TN42 overhead glazing robustness.

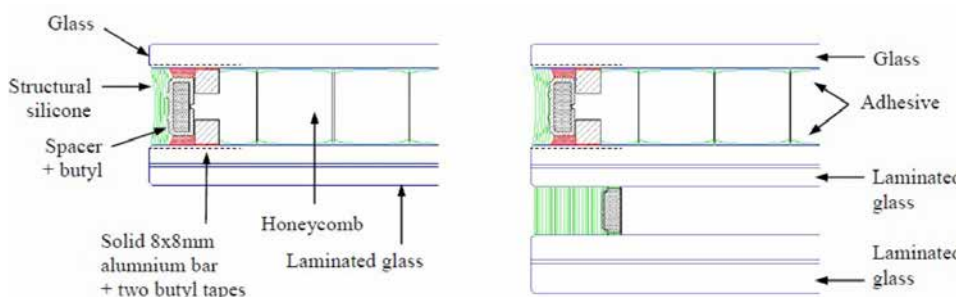


Fig 2 Canopy and roof panel cross sections with 8mm HST outer glass, 19mm honeycomb and 13.5mm and 17.5mm laminated HS glass. Diagram credit to Bellpart

The adhesive finally selected from the four initial possibilities performed excellently, maintaining its clarity and mechanical properties.

Bellpart developed a panel manufacturing cell complete with specially engineered mixing, de-airing and dispensing machinery to apply the adhesive to the glass panels and cure the assembly with UV light. The design was finalised in 2009 but construction was paused until 2015. [2]

## Climatic loads

When sealed sandwich panels are exposed to the weather, they experience changes of pressure in the entrained air according to the ideal gas law

$$pV = nRT$$

The honeycomb core prevents the glass skins from deflecting, so in a sealed panel the full isochore pressure would be developed, which

in this case would be up to 15kPa. [3]

The average stress applied to the edges of the aluminium honeycomb appears to be relatively low isochore pressure/cross section of aluminium = stress on aluminium edge.

$$15000/0.008 = 1.9N/mm^2$$

However, this would be additional to stresses arising from other structural loads, and would occur repeatedly over long periods. In fact, the production method does not make an adhesive bond simply to the edge of the honeycomb foil but forms a continuous fillet joint between the glass and the walls of the honeycomb. In that joint, the stress is distributed to some extent but remains concentrated at the root junction where the aluminium foil meets the glass. To maximise the durability of the panels and avoid the risk of premature deterioration as a result of vapour seal failure, it was decided to equalise them to external pressure. Perforated honeycomb was used to allow equalisation, a common strategy in aerospace applications. [4]



Fig 3 Perforated honeycomb bonded to glass

## Desiccant breather

Allowing the units to equalise to atmospheric pressure introduced the challenge of keeping the cavity dry enough to avoid condensation during cold conditions. Although the perforations in the honeycomb would allow slow equalization of pressure between cells, the rate of diffusion between parts of the cavity would be slowed significantly, so a simple capillary breather tube was not considered to be a reliable solution because transient condensation could be trapped for long periods and biological growth might occur inside the unit. [5]

Hydraulic systems, fuel systems, large gearboxes and oil-filled transformers all need to allow for flows of air to compensate volume changes and all need to avoid condensation from moist air drawn in, so a range of industrial desiccating breathers is available. These breather units contain silica gel granules, which are better than molecular sieves at releasing moisture into outgoing warm air, and inward and outward relief valves or an oil trap to keep the desiccant separated from external air until a small pressure difference exists to be relieved. Some systems even include moisture sensors, valves and a heater to re-generate the silica gel when it approaches saturation. In most cases, the low cost silica gel is replaced periodically. The air inside the system does not achieve the very low dew-point typical of a new hermetically sealed insulating glass unit but in most cases will be low enough to prevent transient condensation when the glass gets cold.

## Potential applications

Honeycomb sandwich panels are very suitable for glass floors, owing to their high strength to weight ratio, providing post failure resistance is provided by tough laminated glass. The inherent obscuration provides modesty and reassurance while maintaining brightness. We applied a similar breather system to the spherically curved insulating glass units on the Las Vegas High Roller observation wheel in Nevada, USA because the glass could not be thermally tempered and the climatic loads would have been excessive for annealed glass. [6]

Other reasons to equalise climatic load would be to avoid visual distortion arising from deflection of the glass, or excessive stress on edge seals.

Various curtain wall systems, especially those with large cavities, are also being studied for application of the same technique. More research is needed to understand the details of moisture movement within façade systems, using desiccant breathers and designs will need to take note of diffusion and convection effects, including the lower density of moist air, in order to realise the full potential.

The primary advantage is that because the desiccant can be replaced or regenerated remotely from the insulating glass, the life can be greatly extended. It may also be feasible to re-configure glazing design without the permanent bonding of panes, which would have advantages for upgrading in service and the re-use or recycling of materials at end of life.

## Conclusions and Summary

Structural glass sandwich panels with honeycomb core have been shown to be durable and to have unique architectural qualities including light transmission, shading, privacy and high stiffness to weight ratio. To maximise the durability of honeycomb panels, the desiccant breather technique was applied, which has applications where climatic loads need to be equalised or where it is advantageous not to bond panes permanently together.

## References

- [1] Teixidor, C. The Berkeley glass pavilion – Design and construction. GPD 2009, Tampere.
- [2] Teixidor, C. The Berkeley Glass Pavillion, Proceedings Engineered Transparency Conference on Glass in Architecture and Structural Engineering, 2016, Dusseldorf, Wiley, ISBN: 978-3-433-03187-2, pp. 317-326
- [3] Feldmeier, F.: Belastung des tragenden Randverbundes von Isolierglas bei Structural Glazing durch klimatische Einflüsse. Fraunhofer IRB Verlag, Stuttgart (1999)
- [4] Rinker, M.: Analysis of an Aircraft Honeycomb Sandwich Panel with Circular Face Sheet/Core Disbond Subjected to Ground-Air Pressurization NASA, Hampton, 2013
- [5] Rose, A. Pressure-equalised insulating glass units – a feasibility study, IFT Rosenheim, 2015
- [6] Smith, A. Atmospheric Loads and the Design of Curved Insulating Glass Units, GPD 2001, Tampere.



Fig 4 Desiccant breathers installed

# Tall Self-supporting Load Bearing Glass Structures

G. Vasilchenko-Malishev, Malishev Engineers  
www.malishevengineers.com  
tel. +44(0) 207 251 66 38  
gvm@malishevengineers.com

## Keywords

Curved glass, vertically stacked glass, tall glass structure

**1. Extended Abstract** (The complete contribution will be published in the *Glass Structures and Engineering journal*)

This paper describes the design, detailing and construction of an 8 storey high, 28m tall self-supporting lift enclosure for a residential property in Knightsbridge, London. The glass structure comprised of curved laminated glass cylinder of 1.4m diameter with cantilevered steel staircase wrapping around it. The glass shaft is split at each floor level with helical steel handrail which also acts as a splice joint between top and bottom glass panels. Lift shaft terminates with static and openable semi-circle roof lights as well as cylindrical roof top structure, independently supported of cantilevered structure. This is reduced version of the paper, full version and more technical details could be found in earlier published article "Design and construction of the 28 m tall self-supporting glass lift enclosure", *Glass Structures & Engineering*, Springer publishing June 2016, Volume 1, Issue 1, pp 233–246

## 2. Historic precedents

In our knowledge some of the first stacked load bearing glass walls started to be developed around late 1990s. One of the notable examples, from our point view, would be the Glass Cube Reading Room, Arab Urban Development Institute, Riyadh, Saudi Arabia, designed by Dewhurst Macfarlane and Partners (Macfarlane.T, *Architectural Review Middle East* 1999). In this project, 3 rows of 2.67m high façade panels are stacked (supported one on top of the other) rather than hung and are structurally bonded to the glass beams and columns to create a 8m cube. We have used the above precedent to develop load bearing technology further in our Bolton's Place residential development project in South West London and further still in our project of 28m tall lift enclosure in Knightsbridge.

Based on our experience with the above project we were approached by the main contractor (Walter Lilly) who were working on a major refurbishment of the a residential property with a triple basement in Knightsbridge, London where the architects (Tim Flynn architects, TFA) were designing a feature glass lift, Ø1.4m and spiral staircase around it in a very confined floor space, connecting 8 storeys with total height of around 28m.

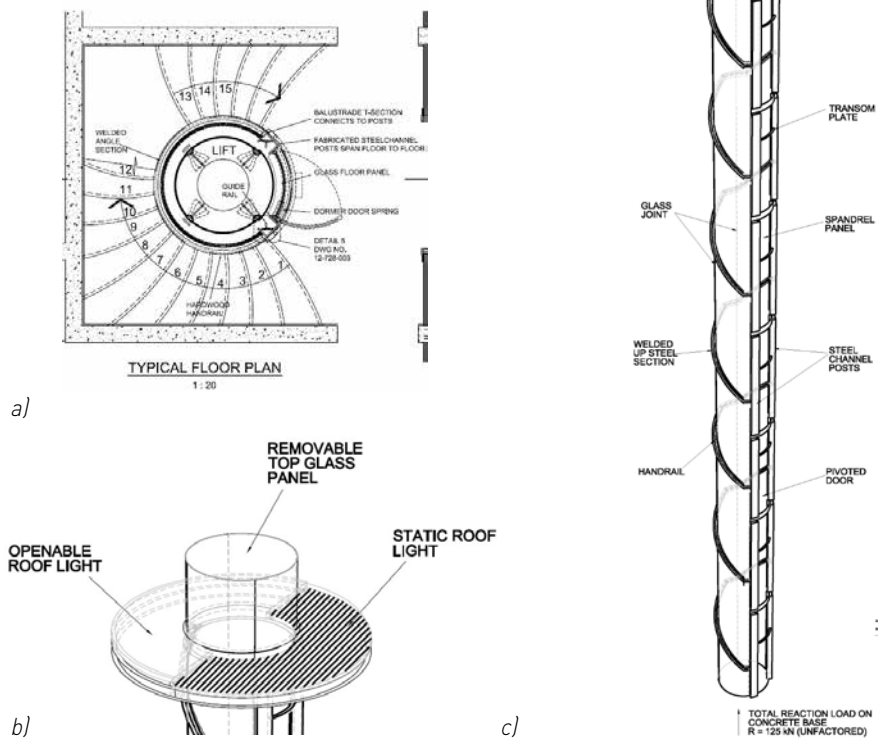


Fig. 4 a) Typical floor plan of the lift shaft b) Roof light c) axonometric general arrangement

## 3. Design of the main shaft enclosure

### 4. Construction

#### Installation of glass

Installation of glass began around March 2015 and took almost exactly one year to complete. Glass was lifted up with hoists using overhead gantry and down through the oculus of the openable roof light. Despite very tight working space none of the glass panels were damaged during installation process. Hydraulic ram lift was used as a working platform to facilitate the process of installation. Slow speed of installation ensured that grouting was properly cured before the next level of glass is received.



a)



b)



c)



d)



Fig.14 a) Crane lift to the roof b) through oculus c) down in the shaft d) installation of the openable roof light



## 5. Conclusion

In conclusion, after a long period of design, manufacturing and construction, 28m tall lift shaft was completed on the 29th March 2016, making this structure, in our view, tallest self-supporting glass structure in the world (Vasilchenko-Malishev, G. 2016), further pushing boundaries of edge bearing technology in glass.

## References

- Institution of Structural Engineers: Structural use of glass in buildings (1st ed). London, IStructE, (1999)
- Institution of Structural Engineers: Structural use of glass in buildings (2nd ed), London, IStructE, (2014)
- prEN13474, Glass in building - Determination of the load resistance of glass panes, replaced by prEN16612 (2013)
- Vasilchenko-Malishev, G.: Sustainable Design in Glass, Innovative Glazing Global Summit, Berlin, (2016)
- Vasilchenko-Malishev, G.: Design and construction of the 28 m tall self-supporting glass lift enclosure. Glass Structures & Engineering, Springer publishing June2016, Volume 1, Issue 1, pp 233-246



# Counter Selective Glazing for a Passive Building Concept

F. Weber, Arup  
M. Muoth, Glas Trösch AG, R&D Coatings  
P. Pecher, Glas Trösch AG, R&D Coatings

## Keywords

infrared transmission, selectivity, historic structure, passive comfort, glare

**Extended Abstract** (The complete contribution will be published in the *Glass Structures and Engineering Journal*)

## General

Exploring options for maximizing passive comfort from a thermal, glare and acoustic perspective lead to a dynamic facade concept with a highly unusual glazing approach for a large restoration project in Mediterranean climate. The very large and tall existing structure was to be re-skinned and house office spaces with actively controlled environment (or building "pods") surrounded by a passively controlled R&D workshop space or "deck" with assembly based tasks and minimal visual display.

## Design criteria and modelling

The design criteria for the office pods were to follow ASHREA 55, but the active systems were not part of the scope. The design team was to focus on the deck, because the space was impossible to control actively at reasonable cost and the aim to maximize passive comfort effected the performance criteria for the envelope. The design team and client agreed on a set of less stringent criteria that were informed by mockup testing. Thermal and glare assessments were carried out with an energy calculation script that was informed by a CFD model and RADIANCE model to investigate different envelope solutions that maximize passive comfort on the deck over the year. The design team studied envelopes of different opacity and solutions with fixed and dynamic shades. A solution with dynamic shades achieved the best thermal comfort, the shades could open in the morning to allow the sun to heat up the deck after the typically cold nights and then close for the rest of the day to avoid overheating. Dynamic

shades could also address the different passive heating requirements between the cold springs and mild autumns of the Bay Area climate.

## Façade concept

The façade concept featured internal louvers to control unwanted heat gain and avoid overheating during midday and afternoon in summer and autumn.

The design team identified the ideal material to be glazing that is selective towards infrared light transmission. The sloped glass was to maximize transmission in the infrared spectrum with a SHGC of ideally more than 80% to utilize passive solar gains whilst controlling the visual spectrum for glare comfort to  $40 < T_{vis} < 60\%$ . The weight of the original metal façade was 5psf (0.24kN/m<sup>2</sup>) and it was decided to use 2x3/16" (5mm) single laminated glass in lieu of double glazing to limit any strengthening of the existing primary and secondary steel. The glazing was to be supported off a sloped aluminum curtain wall system with mullions at that approximately 5ft centers.

## Counter selective glazing featuring high $T_{NIR}$ and reduced $T_{vis}$

The design team had identified a series of products that are opaque in the visible spectrum but are transmitting light in the infrareds spectrum, for example, chalcogenide glass (Schott), Paliogen pigment (BASF) or VOIRT inks (Epolin), but such product was not readily available for application on laminated glass. Glas Trösch AG assisted the team with technical expertise and developed a series of unique samples that investigate different coating approaches with 'IR-selectivity' and indicate an economic way to realize a large scale project with such a glazing approach. Colored PVB foils, interference filters, absorbers based on metal nitrides, on elemental and on compound semiconductors were evaluated regarding their transmission in the near infrared (NIR) for increased solar gain, and neutral color rendering. Optimized process parameters for reactively sputtered metal-based thin films where identified that enable desired absorption of visible light while solar transmission is increased compared to standard architectural glazing products. The absorber stack is economically thin (< 70 nm)

and provides a neutral appearance with good angular stability. Low-iron glass as substrate increased transmission, especially in the NIR range. Four different approaches where presented in form of A4 sized samples to the Architect and client for review:

1. elemental semiconductor & colored PVB foil
2. colored PVB foil (grey)
3. compound semiconductor,
4. elemental semiconductor

The client and Architect preferred samples 2 and 3 visually and these where intended to be produced at large scale. Unfortunately, the client changed his mind regarding the occupancy of the building and the second mockup stage was put on hold. The team could proof that this unusual facade approach is feasible, economical and efficient and is looking for other opportunities in the region to realize it.

## References

- McNeil, Andy: Applicability of DGP and DGI for evaluating glare in brightly daylight space. ASHRAE and IBPSA-USA SimBuild 2016. Salt Lake City, UT
- ASTM; Emery, K.: Reference Solar Spectral Irradiance: Air Mass 1.5 - ASTM G173-03 Tables: Direct Normal + Circumsolar. American Society for Testing and Materials (ASTM) Terrestrial Reference Spectra for Photovoltaic Performance Evaluation. <http://rredc.nrel.gov/solar/spectra/am1.5/> (2003). Accessed 14 March 2017
- Hody-Le Caër, V., Schüler, A.; Swissinso SA: Laminated glazing with coloured reflection and high solar transmittance suitable for solar energy systems. Patent application WO 2014045141 A2, (2014).
- Mertin, S., Hody-Le Caër, V., Joly, M., Mack, I., Oelhafen, P., Scartezzini, J.-L., Schüler, A.: Reactively sputtered coatings on architectural glazing for coloured active solar thermal façades. *Energy and Buildings*, 68, Part C, 764–770 (2014). doi: 10.1016/j.enbuild.2012.12.030

# La Maison des Fondateurs – Load Bearing Interlocking Glass Spiral as Building Structure

## Authors

J. Villiger, Ph. Willareth (Dr. Lüchinger+Meyer Bauingenieure AG)  
F. Doebbel, V. Nardini (Sika Services AG)

## Keywords

Load bearing glass, watch museum, IGU, glass, brass

## Abstract

The museum “La Maison des Fondateurs” in Le Brassus, Switzerland will represent the watch making manufacture Audemars Piguet. Audemars Piguet stands for the finest quality, precision as well as innovation based on traditional watchmaking expertise and craftsmanship.

BIG-Bjarke Ingels Group won the competition for the design of the museum in 2015. The design is based on interlocking spirals formed by glass walls evolving out of the rough, natural landscape. The spirals provide a perfect linear museum path for the building program.

Despite the severe loading and weather conditions and inspired by the high values of Audemars Piguet, the project team designed the building to the limits of what is technically possible. The curved and very large insulated façade glass units, as well as the curved glass partition walls of the interlocking glass spiral are forming the load bearing structure. All vertical and horizontal loads are transferred by

these glass components making solid columns and shear wall obsolete.

The article reflects the close collaboration of the designers, engineers, specialist contractor and industry. The global structural concept, transfer of the concentrated point loading into the curved structural glass elements as well as the structural bonding beyond standards and the context of energy efficiency are discussed and elaborated.

## Introduction

During 2013 Audemars Piguet launched an invited competition for a watch museum in Le Brassus, Switzerland. The competition team headed by BIG – Bjarke Ingels Group developed the successful project proposal in an intense, interacting design process. The design team focused on creating a building for Audemars Piguet, which is reflecting the company’s values, referring to the past and to the future as well as to strengthen the brand with an iconic, sculptural like building close to an architectural emblem. Many options and solutions have been investigated. Finally, the interlocking spiral has been created. The one-story tall spiral is located at the north side of the historical founders building and is directly linked to the new founder’s hall, which is positioned between the existing buildings.

The geometrically very strong spiral is providing a perfect linear museum path along the company’s history as well as watches, and shows a clear analogy to the mechanic of a

mechanical watch. Workshops and workplaces of the company’s best watchmakers are positioned along this museum path.

The materials and structural elements are reduced to the essentials. Glass, brass and cast stone are the predominantly, visually used materials.

Structurally, the lightweight roof is supported only by glass elements for the vertical and horizontal loading. This dematerialized glass structure ensures full transparency throughout the building and façade.

The development from the competition project throughout to the execution phase has been subject to many challenges, such as structural robustness, enhanced durability as well as energy efficiency and sustainability.

## Project Fundamentals and Design Process

The essential and most important parameter of the project is the shared vision to create the aspired load bearing all glass structure. This vision has been the base of the successful, interdisciplinary design process. A process, that has been exposed to conflicting parameters and focuses. But exactly the constant work on these parameters is the base of the current, successful execution. It is the execution of a carefully developed and enhanced competition project, preserving the original DNA of the design intent.

Due to the location in the Vallée de Joux with the particular, harsh micro climatic condition, the building is exposed to high snow loads



Figure 1: rendering of the spiral, founders hall and historic buildings (courtesy of BIG)



Figure 2: rendering of structural glass elements (courtesy of BIG)

above 5 kN/m<sup>2</sup>, even doubling locally, and very cold temperatures well below -20°C. Sustainability and energy efficiency are imperative design values. Audemars Piguet enhanced these values with a strong commitment to satisfy the Minergie label as minimum. Minergie is a very common Swiss label rating the energy efficiency but paying attention to the user comfort additionally. These main design drivers illustrate the design challenges. The building structure, formed by the glass elements, have to carry severe loading, and be highly insulated glass walls with premium optical performance. Furthermore, solar control devices have to be implemented to prevent overheating during the warm seasons.

All these objectives are literally wrapped up by an absolute transparent, crisp all glass façade. Triple glazed units (IGUs) are forming the weather skin, providing the water tightness, low air permeability and the thermal insulation. The inner leaves of these triple glazed units are activated as loadbearing elements, proving the vertical and horizontal structural capacity. As an additional element, a brass curtain shades the façade passively but never interfering with eye vision and therefore maintaining the full visual transparency. This brass curtain, a three-dimensional net of individually shaped weaves, is hung above eye level in front of the upper area of the glazing, providing just enough solar protection for comfort and required energy efficiency.

The outlined design shows very well how the best solution was developed on these most



Figure 3: rendering brass blind (courtesy of BIG)

important building parts and components, satisfying all major parameters. Iterative design steps, constant testing and improving and a dialogue of the designers and engineers based on expertise have been the key factors.

#### Material and surface qualities

The materialization, respectively the dematerialization is an important part of the project specific design language. The materialization aims for real, raw materials. Materials, that enhance in beauty by aging and building up a natural patina. Untreated brass has been chosen for the visual components such as sun shades and cladding parts, for example cover of roof edge, slabs etc. At the opening, these components will be shiny but darken in different grades due to the

natural patina. This patina is a great material characteristic, reducing cleaning demands but also creating esthetic qualities.

The dematerialization depends very much on the glass surface qualities. Surface flaws, such as surface anisotropies and visual distortions, eliminate the aspired dematerialization and transparency. Instead of the visually desired "nothing", visual errors "kill" the transparency and lead to a surface spiked with visual errors. Technically, these surface flaws or errors belong to the characteristic of processed glass and are mostly subject to thermally introduced surface stresses. Furthermore, the typical total reflection of glass at a particular viewing angle and mirror effect of the applied low e-coating work against the transparency.



Figure 4: First glass unit at works of Frener & Reifer in Brixen

the best possible annealed surface condition. The first assembled and inspected glass units prove to have an excellent appearance and are achieving the very much aspired and promised transparency.

### Thermal concept

The thermal concept of the façade and glazing is predominately defined by the Minegie criteria. The described exterior passive sun shades and the low g-value of 23% of the glazing is satisfying the energy demands in summer case and prevent overheating. The low u-value of 0.6 W/(m<sup>2</sup> K) in conjunction with heaters below the glazing ensures the user comfort, avoiding any down drift during the cold seasons. The energy demands in the winter case are within the set limits. The large, glazed areas are compensated by the highly insulated green roofs. Additionally, photovoltaics on the adjacent existing building are contributing to the strict overall energy assessments and good rating.

### Overall structural concept

The transparent design of the spiral did not allow placing columns or even walls inside the building. Therefore, it was decided to find a solution with load bearing glass walls. The façade as well as the interior separation walls would be used to transfer the vertical loads (dead load of the roof construction, snow load) and also the horizontal loads (wind load, seismic load). The horizontal loads have to be transferred through the rigid roof construction to the roof edge, from there as in-plane forces through the glass and eventually into the concrete foundation.

### Individual glass pane

The concept for the individual glass panes was designed as simple as possible. At the outer façade, where the IGU is carrying the loads, the innermost layer of the IGU acts as the loadbearing layer. The loadbearing glass consists of a three times laminated 12mm annealed glass with a SGP interlayer. The glass is bordered at the top and bottom edge with a steel shoe, that is bonded to the glass. The shoe transfers horizontal in-pane loads to the vertical edge of the glass and from there diagonally through the glass to the bottom support. The vertical loads are being transferred from the roof bracket directly through the steel shoe into the glass. The connection between the bracket and the shoe is only pinned. This ensures that bending moments are not being transferred from the roof into the glass pane. The outer layers of the IGUs are only being supported at the bottom.

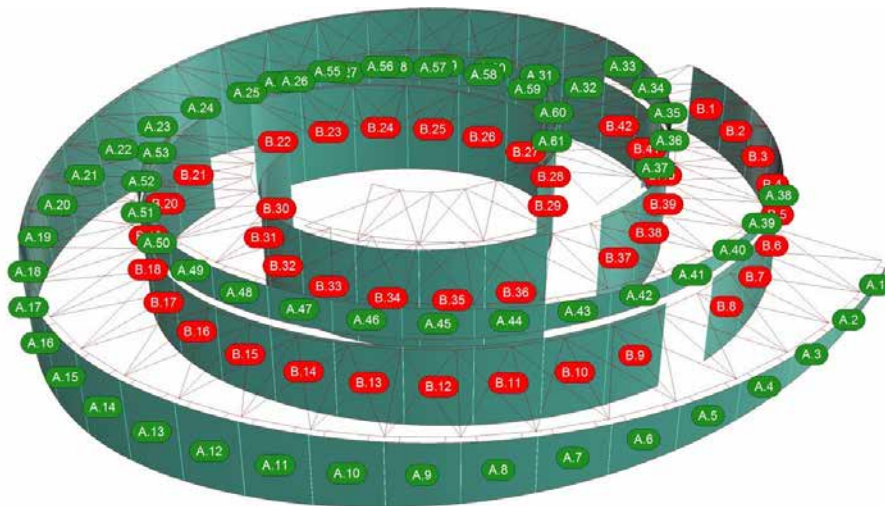


Figure 5: Schematical view of the loadbearing glass element and roof structure

Therefore, the dematerialization and transparency are partially opposed by physical laws. Taking on the challenge to get as close as possible to the wanted appearance, the following parameters have been subject to a challenging development. Firstly, the g-value had to be optimized in accordance to the passive shading devices described above. A g-value of 23% proved to be the upper limit in order to avoid the overheating of the building. Esthetically, the low g-values has been a not negotiable value and had to be accepted, as the passive shading devices should not have been extended in the area. Despite this low value, the samples and the first manufactured units show a nice appearance. The more challenging issue has been to tackle the surface errors. From an engineering point of view, the thermally introduced stresses are used to strengthen the glass. Fully toughened or heat strengthened glass provides a higher

load bearing capacity. Furthermore, the risk of failure due to thermally introduced stresses during service is obsolete. Optimizing the glass towards the annealed state (float condition) with the best possible surface condition requires a careful consideration of the loadbearing capacity under long term loading condition. Additionally, the risk of thermal breakage during service has been assessed carefully, taking into account the interface details, climatic exposure, the applied low e-coating, etc. The decision to use annealed glass on all layers in the triple glazing influenced the bending method fundamentally. Hot (roller) bending and lamination bending had to be eliminated as a processing option due to the introduced and, in case of the lamination bending, also required thermal stresses, respectively strengthening. Slump or gravity bending is the used bending method, ensuring

These supports take the dead load and reduce the permanent stress on the edge sealing, which now only has to carry the wind loads. The bearing concept of the inner glasses is exactly the same. Due to the larger forces in the centre of the spiral, the glass build-up increases to a maximum of five times 12mm annealed glass.

## Design specialities

**Geometry:** The main part of the building consists of two spirals rotating in opposite direction, that interlock in the centre. The way it was designed, only four different glass radii exist. This reduces the expenses of the formwork for the slump bent glasses significantly. The shape of the glasses is, however, always unique. The upper edge of the façade follows the design of the roof edge. The roof edge was designed in consideration of a consistent overall geometry as well as proper drainage paths.

**Durability:** Since the façade is the thermal envelope as well as a structural element in one, the durability of it became more relevant than usual. It is very important that as little moisture as possible passes through the edge seal. Additionally, the climatic loads in the cavity of a bended IGU cause higher stresses on the edge seal due to the higher stiffness of the glass. Typical IGU's are being tested for its durability with artificial aging procedures.

**Redundancy:** The brittle material behaviour of the glass calls for a certain redundancy in the load bearing structure. Although the use of annealed glass in the laminated glass does provide quite a high residual carrying capacity, different load cases with damaged glass plies have been defined for the analysis. Glass panes with one or two damaged glass plies are being calculated as well as the failure of an entire element.

**Testing:** Many design relevant details and structures with structural glass are not standardized. The few reference projects with similar structures served as an indication during the design phases. Nonetheless, additional testing was unavoidable. The load transfer from the shoe into the glass had already been tested in the design phase. This gave a certain security for the planners to continue with the all-glass design. Further tests, including tests of the IGU and the five times laminated glass, are going to be carried out in the near future with the contractor.

Load case: leading action snow + wind in x direction

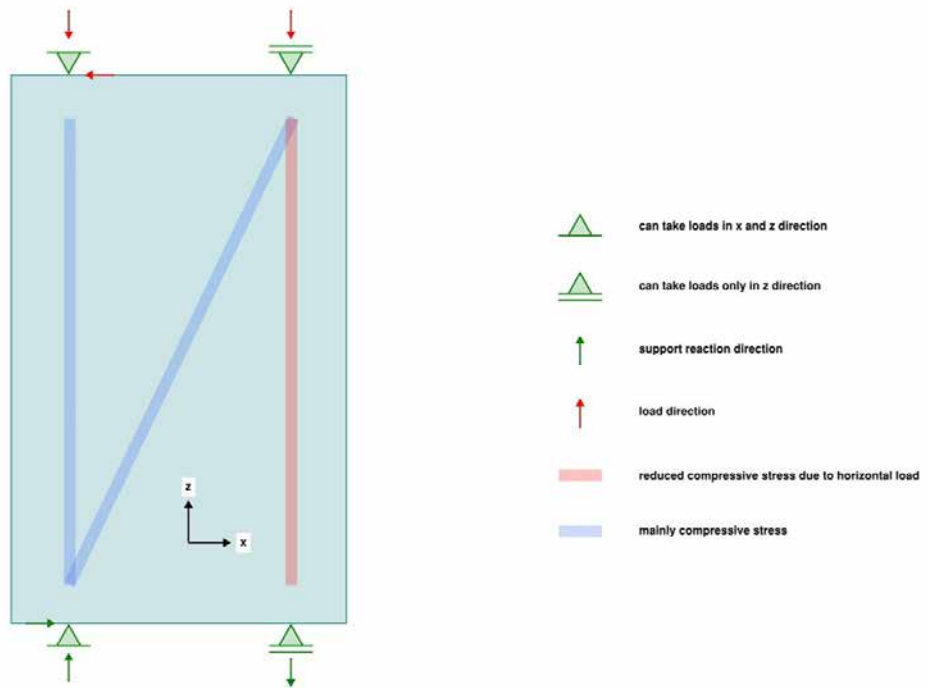
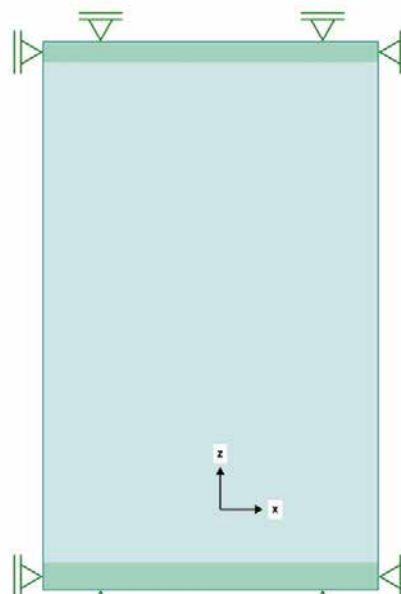


Figure 6: Structural boundary condition of glass elements and supporting components

Boundary conditions for glass



Boundary conditions for shoe

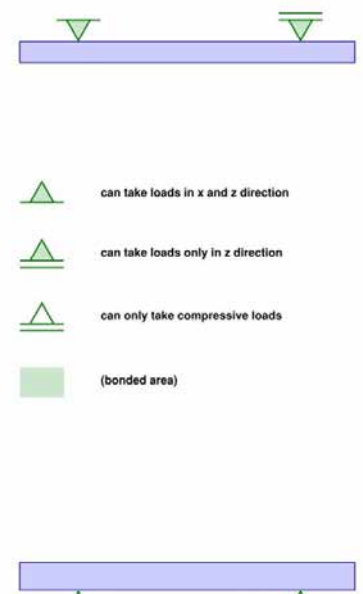


Figure 7: Structural principles of load bearing glass elements

## Anchoring of the Glass Units and Structural Bonding

The unique design of La Maison des Fondateurs challenges the engineering of details and solutions.

With regard to the top and bottom connections used to retain the curved IG units, a bonded anchoring system is developed beyond state-of-the-art, in order to answer to technical demands outside available Standards.

The anchoring system includes clamping profiles bonded to the glass edges by structural silicone Sikasil SG-500 (Refer to figure 4) and is designed to overcome the following challenges:

### Design Loads

Due to the curve shape, the severe vertical and horizontal loads applied to the glass components -representing the load bearing structure of the building- are converted into in-plane and out-of-plane reaction forces at the bonded connections.

From a structural point of view, the use of an elastic adhesive is ideal to transfer in-plane forces and redistribute them uniformly, without preventing differential thermal dilatation between glass and metallic support. Indeed, any alternative mechanical shear solution (e.g. boring holes through the glass or contact elements) would be critical limiting free dilatations and creating uncontrolled stress peaks into the system.

Compared to typical Structural Sealant Glazing (SSG) systems, where joints are mainly used in tension, embedding the glass panels into clamping profiles allows to maximize the available shear area and convert the out-of-plane reactions into contact compression forces on glass and adhesive. This allows to minimize the SG-joint dimensions while exploiting the compression behavior of the structural silicone Sikasil SG-500.

For comparison, Figure 8 and 9 provide behavior of a linear joint (50mm x 12mm x 12mm) tested in tension and behavior of a circular joint portion (D=46mm, H=20mm) loaded by unconfined compression respectively.

### SSG-Joints Life Expectancy

A 50-year life expectancy for the designed SSG system is required. This is beyond provisions given by EOTA ETAG002, which regulates SSG performances based on a design life expectancy of 25 years.

As a part of the concept set by EOTA ETAG002 for a 25-year life expectancy, it requires to test adhesion on original project substrates exposing them to artificial aging of 7 days at 23° C / 50% r.h. and 35 days of water

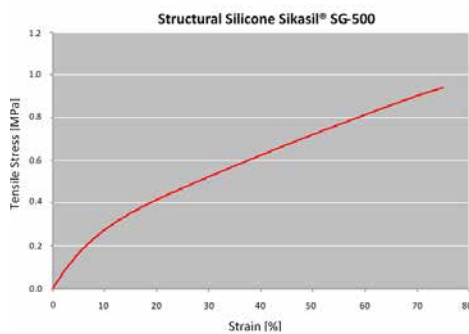


Figure 8: Tensile behaviour of Sikasil SG-500

immersion at 45° C.

For the project target of 50-year life expectancy, adhesion tests on the original project substrates are performed based on prolonged artificial aging consisting of 7 days at 23°C / 50% r.h. and 70 days of water immersion at 45° C. Test results confirm the excellent adhesion of Sikasil SG-500 on the substrates, if they are preliminarily grinded, pretreated by Sika Aktivator-205 and primed by Sika Primer-210.

Aforementioned adhesion tests are a precondition to release SSG-joints for extended life expectancy. However, the following additional project requirements must also be met:

- The load bearing concept for the whole façade must be designed for 50-year life expectancy;
- The design of the façade has to fulfill all other requirements of EOTA ETAG002;
- A working life time of 50 years must be granted for the substrates, including surface stability;
- Adhesive application must occur in factory and must comply with Sika guidelines and recommended production quality control schemes;
- The place of installation must be carefully checked and limitations may apply (e.g. acid rains, power plants proximity, saltwater, etc. must be excluded).

### Materials

Substrates approved by EOTA ETAG002 for structural bonding are stainless steel, anodized aluminum, coated aluminum and glass.

The specific project design requires that the support frames to retain the IG units are composed by galvanized steel plates, with the only exception of stainless steel outer plate used at the bottom connection.

This material selection is implemented to balance project costs and structural needs, while minimizing corrosion risks. As a matter of fact, stainless steel is used where contact to

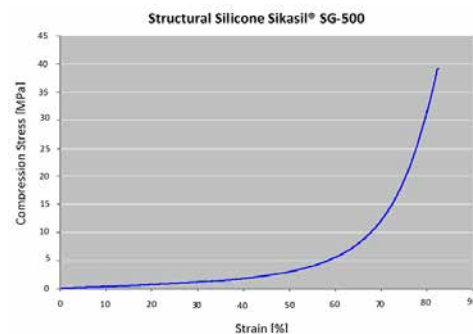


Figure 9: Unconfined compressive behaviour of Sikasil SG-500

ground and outdoor environmental conditions occur, drainage is more critical and risk of corrosion exists. Galvanized steel is used where exposure to outdoor environmental conditions is excluded and uniform indoor temperatures apply.

In addition to the technical considerations above, galvanized steel can be approved for structural bonding under confirmation that:

- The substrate corrosion protection is adequate to the service life of the bonding joints.
- The coating performances are adequate to the mechanical resistance of the silicone adhesive in the long-term, e.g. the coating must consist in a layer able to transfer loads from the joint to the core metallic substrate.

### Adhesive Application

The curing process of 2-component silicones generates by-products that must be released from the joint into air, in order to ensure a proper adhesion build-up. Experimental tests on Sikasil SG-500 show that maximum joint depth must be limited to 50mm to allow a complete by-products elimination, when access to air is limited to one side only of the joint.

Such a limitation is critical for the adhesive application in the project brackets, since design loads require joints up to approx. 200mm.

To overcome the by-product elimination issue, an alternative adhesive application method is recommended; unlike typical SSG application by gap filling from open side, adhesive viscosity of Sikasil SG-500 allows for injection through holes, regularly patterned along the metallic substrate. Brackets can be manufactured with holes drilled at a max. distance of 100mm throughout their height and length. Injection process requires to:

- Start adhesive injection from the first hole.
- When adhesive is visible in the adjacent holes, proceed sequentially with adhesive injection from there.
- Repeat procedure until all gaps between glass and plates are filled in. The visibility of injected adhesive from one hole to the adjacent ones is used as a proof for adequate gap filling.

This bonding procedure allows to compensate easily for manufacturing tolerances of curved parts and to assemble elements in the factory for direct installation, optimizing efforts on site and deglazing procedure.

## Project progress

Certainly, the project "La Maison des Fondateurs" will be taken to the GPD 2019 as a completed project and as a museum in service. Currently, the project is in execution. Beside the manufacturing and assembly of the steel and glass element, the bespoke test regime is executed at the Façade and Metal Engineering Center at Lucerne University as well as other test houses. The test regime covers important points such as the extended life span of the triple glazing, load transfer of the concentrated point loads up to 400 kN as well as a full scale ultimate load test .

The installation will start in early summer and the building is expected to be water tight by the end of autumn.

## Acknowledgement and project partner

Client: Audemars Piguet, Le Brassus

Architecture: BIG - Bjarke Ingels Group, New York

Local Architect: CCHE, Lausanne

Structural Engineering: Lüchinger+Meyer, Zürich

Façade Engineering: Lüchinger+Meyer, Zürich / Lüchinger+Meyer+Hermansen, Copenhagen

Building Physics: Estia, Lausanne

Specialist Façade Contractor: Frener & Reifer, Brixen

Glass Processor: SFL Glastechnik, Stallhofen

Thermal Glass Assessment: concept4glass, Regensburg

Full Scale Testing: Façade and Metal

Engineering Center, Lucerne University, Lucerne

# Exciting Architectural Case Studies From All Around the World

Sandro Casaccio  
Kuraray Europe GmbH

## 1. Abstract

The presentation aim to share how the new interlayers developments fit with the new construction challenges. Specifically in the field of safety, security, decorative and sound dumping issues. There are a growing number of interlayers for laminated glass aiming at meeting the evolving needs of architects and specifiers. This presentation describes thru some case studies which interlayers have been adopted in according to the specific requirements of these iconic projects. How those interlayers expand design possibilities, raise safety standards, provide new solutions. Standard PVB is still used in more than 70% of the application. Its primary function is to enhance safety or security performance of the glazing and at the same time improve the acoustic and UV protection performance in single and double glazed units. In the last years were developed structural Interlayers which are basically divided into 2 families: Inoplast interlayer, Stiff PVB (low plasticizer) which increased even more the design possibilities as:

- Transparency
- Splinter protection
- Impact resistance
- Residual capacity after breakage
- Noise protection
- UV light control
- Design

## 2. Introduction

Laminated-Safety Glass is widely used in architectural market. The requirements are challenging more than ever. The architectural market demands more and more the use of glass in construction that withstands human and load impacts and harsh climates, comfort and aesthetics. Superior structural performance can be obtained using laminated glass fabricated with interlayers. Enhanced post glass breakage characteristics increase safety factors for performance in case of accidental glass breakage.

## 3. Applications

### Façade & Curtain wall

Today's facades are engineered to deliver not only aesthetically pleasing and energy-saving daylight, but also increased safety, durability and design freedom. The façade of a building is often the most important from a design perspective, as it sets the tone for the rest of the building. When glass is used as the façade, a great advantage is that natural light can penetrate deeper within the building. The façade transfers horizontal wind loads that are incident upon it to the main building structure through connections at floors or columns of the building.

### Balustrades & Railings

When used in glass railings, balustrades and partitions, laminated safety glass helps keep people in safe places, while adding daylight, maintaining open views, and preventing injuries related to sudden glass failure. Open edges, fixturing, and outstanding structural performance are among the advantages of railings made with interlayer.

### Acoustic Glazing

Acoustic interlayer is a PVB film with outstanding sound protection properties. Compared to a glass assembly containing standard PVB film, the same assembly containing acoustic interlayer achieves improvements in sound insulation of up to 3 db. The production process for laminated safety glass containing acoustic interlayer is just as efficient and simple as for standard architectural glazing products. Laminated safety glass produced with acoustic PVB has outstanding product properties in terms of safety, long-term stability, light-fastness and appearance.

### Roof & Overhead Glazing

In architectural terms, overhead glazing or roof glazing is defined as glazing that has the potential to fall on breakage, causing safety and other related concerns. The glass is normally positioned over space that is occupied by humans. Examples of overhead glazing include roofs and skylights, as well as sloped overhead glazing. Other types of overhead glazing include canopies installed over the front door or entrance to a building.

### Glass Fins

The trend to open design invites more glass and less visible framing and structural support, with an increasing structural role for advanced laminated glass. Glass Fins provides support and backup structure for structural glass designs and to prevent buckling of the structural glazing.

### Screens & Louvers

Glass louver consists of parallel glass panels set in a frame. The louvers are locked together onto a track, so that they may be tilted open and shut in unison, to control airflow through the window. Main purpose of a louver: to form an outer skin for solar shading purposes. Typically, the glass panes can rotate to control the sunlight / shading. Screen constructions also exist, whose primary function is to provide partition glazing (exterior and interior applications).

### Floors, Stairs & Bridges

Worldwide, there is an increasing trend in the use of glass in both flooring and stairs in residential (private) buildings, commercial (offices) buildings and retail outlets. This trend is being driven by the increased desire to provide more open plan, unique, stylish designs. For load-bearing safety glass floors and stairs, laminates made with interlayers offer an extra level of deflection strength and structural integrity.

### Windows & Doors

More and bigger visible areas are requested by the market and windows and doors play a big role. As for the facade, a great advantage is that natural light can penetrate deeper within the building.

## 4. Conclusion:

Architects & Specifiers are continuing to improve freedom of design and reaching more and more tight norms/codes through new interlayers for safety glazing developments which is a continuous improvement to follow new construction market needs in terms of safety, security, comfort and aesthetics.

# Testing of Glass Laminates for Edge Stability

Julia Schimmelpenningh  
Eastman Chemical Company, United States  
of America

## Keywords

laminated glass, interlayer, edge stability, durability

Laminated glass is a high-performance construction material comprised of glass and polymer interlayer which is bonded together under a heat and pressure process. Laminated glass is typically subjected to performance testing meant to evaluate the capability of the material in its resistance to damage or attack. Edge delamination typically results from damage or attack originating at the edge of laminated glass where the interlayer is exposed. Edge delamination affects the aesthetics of laminated glass and may be described as a material characteristic known as edge stability.

Determination of the edge stability of a laminated glass construction is complex but can be examined through various methods of test. Exposure of the laminate to moisture and chemicals, specifically at the edge, is the basis of various test protocols that result in the development of edge stability ratings. This paper will present exposure protocols including natural weathering, sealants, salt fog and immersion that are used to determine the edge stability characteristic of laminated glass configurations. Rating processes and results will be discussed for various interlayers. The attending will be familiar with the test scope, purpose and results interpretation of the included testing. This information allows the specifier to make an informed choice in selecting installation methods, system design and laminated glass products.

## Natural Exposure

Edge stability is a performance property that indicates an interlayer's resistance to delamination when subjected to a hot and humid environment with exposed edges. For natural exposure, a commercially operated site near Miami, Florida (USA) for exposed edge stability testing was selected. Edge stability, as defined here, is a long-term test with the samples exposed to the natural outside environment. The edges are unprotected and consequently are wet in the early morning

(dew) and during episodes of fog or rain. It should be noted that Arizona is another natural exposure site that is used for durability testing of laminates. The purpose of this site tends to be for the evaluation of polymer degradation by UV radiation versus edge stability as the climate is hot and dry. As such, edge defects in PVB laminates are not commonly noted or analyzed for long term natural exposure in Arizona.

The Edge Stability Number (ESN) is a weighted sum of "percent defect lengths" where the weight increases as the square of the depth (expressed in sixteenths of an inch – rounded metric provided for reference only). The maximum ESN number is 2500 with a minimum number being zero, therefore the smaller the number the better the edge stability in this environment. This means that any product with 6 mm delamination band all the way around the sample would be rated at 2500 (Figure 1). Any product exhibiting an ESN of less than 500 is considered exceptional. The ESN number is the averaged rating for all specimens of the sample set using the following calculation method:

PCT1 = % defect length with depth < 1/16 inch (1.6 mm)  
PCT2 = % defect length with depth = 1/16 inch to < 1/8 inch (1.6 mm to 3 mm)  
PCT3 = % defect length with depth = 1/8 inch to < 3/16 inch (3 mm to 5 mm)  
PCT4 = % defect length with depth = 3/16 inch to < 1/4 inch (5 mm to < 6 mm)  
PCT5 = % defect length with depth =  $\pm$ 1/4 inch (> 6 mm)

$$\text{ESN} = 1 \cdot \text{PCT1} + 4 \cdot \text{PCT2} + 9 \cdot \text{PCT3} + 16 \cdot \text{PCT4} + 25 \cdot \text{PCT5}$$

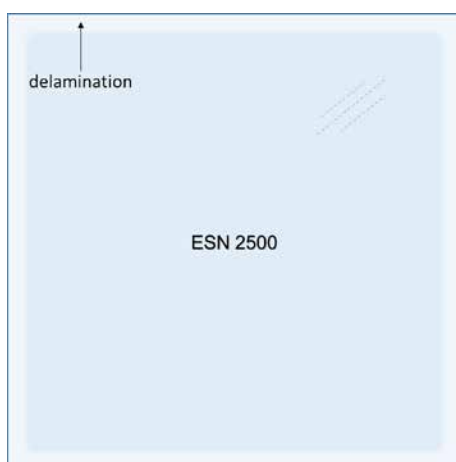


Figure 1: Depiction of laminate with ESN = 2500

A sample set typically consists of 10 laminates prepared using standard laboratory conditions. These specimens are mounted with exposed edges on a rack facing South with 45-degree slope in accordance with ASTM D1435. They are exposed for a set duration with on-site ratings every 6 months.

Figure 2 shows the difference between conventional PVB and structural PVB interlayers, both exposed at the above-mentioned site for the corresponding duration. Using the guideline that an ESN of 500 is considered exceptional, the performance of structural PVB at 52 months is outstanding. The conventional PVB exposure was complete at 46 months, however structural PVB interlayer is being exposed for a longer duration.

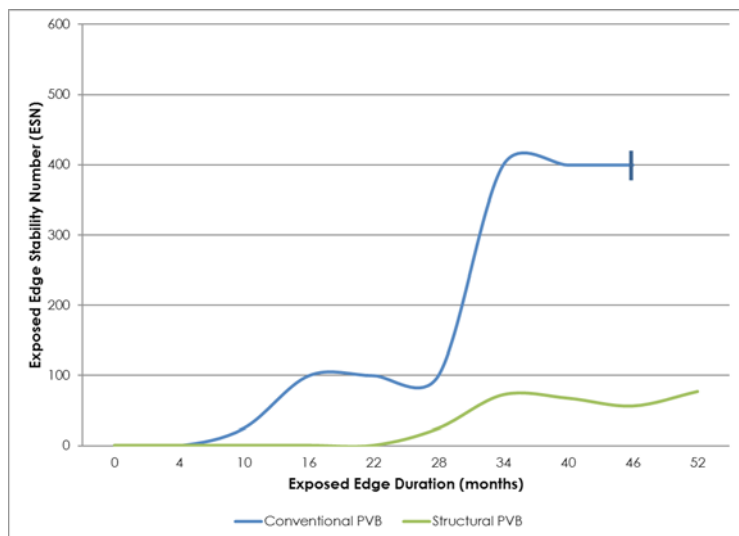


Figure 2: Edge Stability Numbers of conventional and structural PVB interlayers

Figure 3 is a magnified photograph of a laminate exposed with no edge protection in South Florida, USA with an ESN of approximately 100.

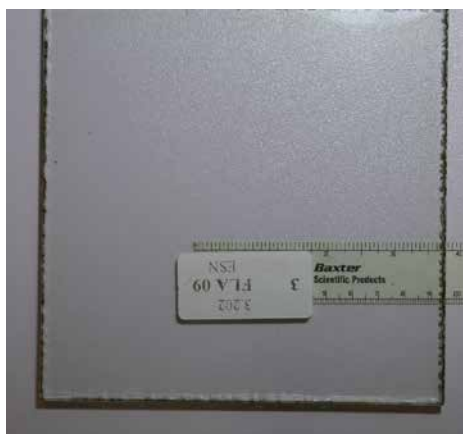


Figure 3: Exposed laminated glass sample with ESN 100

Data from Florida exposure programs continues to be gathered for various interlayers, it is impractical to keep the laminates exposed for longer than 5 years without compromising the edge with cleaning. The climate invites the growth of mold and fungus on the edge of the laminates, as seen

if Figure 3. To effectively clean the edges for proper rating, the edge may be altered providing a false ESN. Natural exposure tends to be the prevailing methodology to arrive at an ESN value, it however takes at least one year of exposure to discern existing or oncoming trends in product stability. The following sections describe alternate tests that serve as predictors or alternate mechanisms to evaluate the stability of a laminated glass edge upon exposure.

### Salt Fog Exposure

Salt fog testing exposes laminates to a saline fog which is expected to simulate South Florida environmental conditions. This test protocol is designed to determine the reaction of laminates to a simulated hot and humid environment and allow conclusions to be reached about their longer-term performance and use in marine-like climates. Salt fog testing does not include intentional or concentrated solar radiation exposure.

Laminated glass specimens are produced using standard laboratory practices with conventional and structural PVB interlayers.

The specimens are exposed in a salt-fog cabinet for 12 weeks and evaluated visually for edge blush and delamination. The test is run in accordance with ASTM B117-11 Standard Practice for Operating Salt Spray (Fog) Apparatus. The method involves placing specimens in a hot (35°C) environment where the entire specimen (except for the section protected by the holder/frame) is uniformly surrounded by a fog that is created from a 5% saline solution (Figure 4).



Figure 4: Laminated glass in exposure rack for Salt Fog testing

A sample set consists of 6 laminated specimens for each interlayer type which are constantly exposed to this environment for the selected duration (12 weeks). Table 1 includes the laminate characterization in terms of initial adhesion, moisture and interlayer thickness prior to the laminates beginning exposure in the salt fog cabinet. The exception is the time out of the cabinet to rate samples and chamber maintenance (~ 1hr per week). The specimens are rated visually for the appearance of edge blush and delamination. Corner edge blush or delamination was recorded diagonally from the corner while depth of blush or delamination from the straight edges was measured perpendicular to the edge. The depth and length of any edge effect was measured; average area and maximum depth are reported for the sample set in Table 2. The samples remained for 60 days at ambient condition and were re-evaluated with results shown in Table 3. Edge blush was no longer visible upon re-evaluation. The study indicates salt fog testing in accordance with ASTM B117 can generate edge blush and delamination in laminated glass samples in 12 weeks or less and may serve as an accelerated predictor test for ESN. Structural PVB interlayer in laminates

performed better than conventional PVB in laminates with regard to edge blush development in this study. Both interlayers when exposed to continuous marine-like climate, as simulated by salt fog testing, have good durability as demonstrated by minimal and reversible edge blush development. The results of this test also indicate that Structural PVB is not as susceptible as conventional PVB to the development of minor edge delamination after removal from salt fog exposure.

| Exposure Rating                 | Edge Effects <sup>(1)</sup> |              |                |              |
|---------------------------------|-----------------------------|--------------|----------------|--------------|
|                                 | Conventional PVB            |              | Structural PVB |              |
|                                 | Edge Blush                  | Delamination | Edge Blush     | Delamination |
| Maximum area (mm <sup>2</sup> ) | 21                          | 0            | 6              | 0            |
| Maximum Depth (mm)              | 7                           | 0            | 3              | 0            |

(1) Blush area calculated as diagonal depth \* 3mm as predominately corners.

Table 2: PVB interlayers - Salt Fog exposure 12-week exposure summary

| Post Exposure Rating            | Edge Effects                    |              |                |              |
|---------------------------------|---------------------------------|--------------|----------------|--------------|
|                                 | Conventional PVB <sup>(1)</sup> |              | Structural PVB |              |
|                                 | Edge Blush                      | Delamination | Edge Blush     | Delamination |
| Maximum area (mm <sup>2</sup> ) | 0                               | 15           | 0              | 0            |
| Maximum Depth (mm)              | 0                               | <1           | 0              | 0            |

(1) Delamination occurred on top edge < 1mm maximum depth

Table 3: PVB interlayers - Salt Fog exposure- 60 Day Post Exposure Rating

## Sealant Compatibility

Interlayers can react with non-compatible materials with which it may come in contact. As such, direct contact between interlayers with chemicals used in sealants or adhesives should be carefully examined and in some cases avoided. This test method aims at providing guidance information regarding sealant compatibility when the sealant is in direct contact with the laminate edge. Compatibility testing is conducted between commercially available sealants and interlayers as warranted by product introductions, product modifications or in the case of special projects.

Results are reported from testing, but sealant recommendation are not made by the interlayer manufacturers as variations and modifications in the sealants may occur from time to time. Tests are performed under a strict protocol allowing comparisons to be made between products tested. The test results may not reflect in-situ performance. A commercially available sealant that is consistently compatible with the laminated glass as tested following the prescribed

protocol has not been identified. Based on market trends, silicone sealants as a family seem to be most commonly used with laminated glass. Sealants may contain solvents that can be harmful to the interlayer. In most cases investigated, the sealants considered neutral in curing are routinely better performers in this compatibility assessment than those sealants that indicate acetoxy cure. Acetoxy cure sealants tend to have the highest incident of generating edge effects in laminated glass out of the silicone family of glazing sealants. Sealants and other adhesives are required to maintain intimate contact with the laminate edge throughout testing in order to be evaluated for edge effects. The procedure used for testing is documented and published both by Eastman and the Glass Association of North America (GANA) as Standard Test Method for Laminated Glass Edges when in Contact with Sealants and Glazing Tapes. The exposure calls for a UV condensation chamber with UV313 bulbs set to an irradiance of 0.71 W/m<sup>2</sup>. The continuous exposure cycle is 16 hours UV at 66°C followed by 8 hours of condensation at 60°C. The total exposure duration is 3500

hours with 500-hour rating intervals. Edge effects are normally seen as clear, very small, 2 mm – 3 mm (0.08 inch – 0.12 inch), edge bubbles, sometimes continuously occurring along an edge, other times very distinct and isolated. The extent of edge effects differs depending upon the sealant or adhesive. Edge effects from sealants and adhesives as seen in this testing are typically maximized in depth at approximately 10 mm (0.39 inch) from the edge, and often occur as a single bubble. Although a slight discoloration can occur with sulfide containing sealants and adhesives, normally the edge effect is clear and does not cause a color change in the interlayer.

Occasionally a test cycle will result in minimal to no interaction between the laminated glass and the sealant or adhesive. This does not guarantee the same results in field as application, environmental and material deviations can affect the reactions.

Sealants, adhesives, gaskets and setting blocks should be selected firstly on a basis for their desired performance (i.e.: compression, tensile strength, weatherproofing, structural, cosmetic), with edge effects being a consideration after a performance class or family has been established. Although gaskets and setting blocks can and do come in contact with the laminate edge, the data acquired using this test method is only valid when intimate contact with the laminated glass edge has been maintained for the full duration of the test.

The data reported from this test are visually rated using the following criteria (Figure 5):

**Average Depth Edge Effect:** The depth on average, as determined visually, at which bubbles, discoloration or haze were observed. This reading is taken from the laminate edge towards the center of the laminate and measured in millimeters (mm). This number is rated at each exposure interval

**Maximum Depth Edge Effect:** The greatest depth of a bubble, discoloration or haze as measured from the edge of a laminate toward the center. This is the highest number recorded off any edge during any rating interval of a laminate in the set. Maximum depth is reported at the completion of the testing in millimeters (mm).

**Length Affected:** The sum of the length of the laminate edge to which sealant is applied, measured in millimeters, of which bubbles, discoloration, or haze were observed during the exposure interval.

**Percent Length Affected:** The average length affected by edge effects divided by the total length of the laminate to which the sealant was applied. The overall length of the laminate with sealant applied is and weathered is 580 mm.

**Average Area Affected:** The average depth of edge effect observed multiplied by the average length.

**Delamination Plateau:** Maximum and Average depth consistent for last two rating periods.

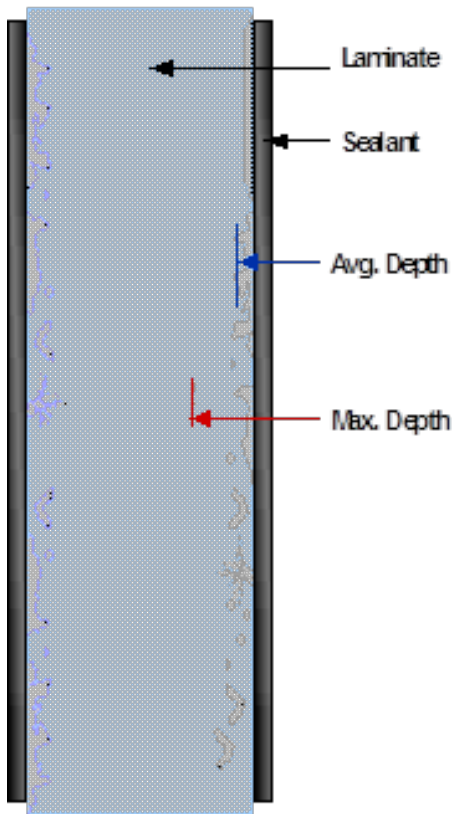


Figure 5: Rating Diagram for Sealant Compatibility Reporting

Edge effects can “move” throughout the test and may vary from interval to interval. The maximum depth seen at any time throughout the exposure program is the reported value independent of the maximum depth at the termination of the testing.

The data in Figure 6 shows a data presented in a typical manner for structural PVB and a structural sealant. The summary data in Table 4 shows consolidated data by general silicone product type and laminated glass compatibility of both conventional PVB and structural PVB. The data shown should be used as a reference and guide for sealant selection but should not be deemed as a guarantee of performance.

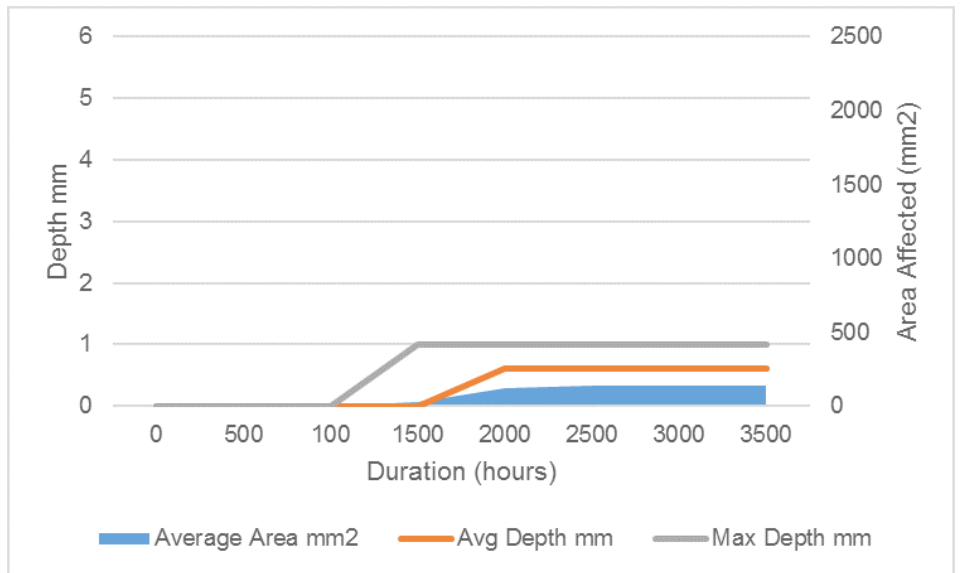


Figure 6: Typical data for structural PVB and a structural sealant

| Sealant Type          | PVB Interlayer | Depth of Edge Effect (mm) |   |   |   |   |   |
|-----------------------|----------------|---------------------------|---|---|---|---|---|
|                       |                | 1                         | 2 | 3 | 4 | 5 | 6 |
| Silicone Hybrid       | Conventional   |                           |   |   |   |   |   |
|                       | Structural     | zero                      |   |   |   |   |   |
| Silicone Neutral Cure | Conventional   |                           |   |   |   |   |   |
|                       | Structural     |                           |   |   |   |   |   |
| Silicone 2-Part Cure  | Conventional   |                           |   |   |   |   |   |
|                       | Structural     |                           |   |   |   |   |   |
| Silicone Acetoxy Cure | Conventional   |                           |   |   |   |   |   |
|                       | Structural     |                           |   |   |   |   |   |

Table 4: Select silicone and laminated glass compatibility data

### Immersion Testing

The immersion testing protocol involves the submersion of laminate specimens in various liquids for a total of 60 days plus controls that are kept in an ambient dry state. The laminates are inspected at various intervals to determine if any edge degradation occurs. The objectives for this test are to: 1.) determine if contact of various liquids with exposed laminate edges has a detrimental effect on visual appearance of the laminate and edge quality, 2.) determine if cut edges versus polished edges are affected differently, 3.) evaluate laminates after storage for long duration to determine adverse effects from absorbed chemicals and 4.) determine test applicability as an accelerated ESN predictor. This test did not review repetitive submersion after extended drying. There is no known national consensus standard that covers this type of testing, therefore the specifics of the test are provided.

The specimen construction consisted of laminated annealed glass with conventional PVB interlayer. The specimen size was nominal 10 cm x 10 cm. Lamination was performed using standard assembly and autoclave techniques. Half of the specimens were further fabricated after autoclaving by polishing edges. A zero-time rating for visual cloudiness and edge effects was performed. The specimens were then divided so that two of each edge type were placed in the various liquids. The specimens were stacked horizontally on their flat surfaces in plastic containers with sufficient undiluted liquid to cover the tops of the laminates. Edges of the laminates were completely free of the containers edge to ensure maximum exposure to the cleanser (Figure 7).

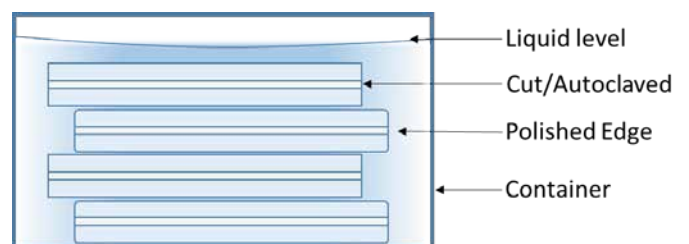


Figure 7: Laminated Glass Stacked in Test Container with Fluid

The specimens sat at ambient temperature covered by the respective liquids for a set period. The specimens were briefly removed from the liquid, rinsed with water to remove any residual cleanser and wiped dry with towel prior to examination. The specimens were rated in this manner each day for one week, then at 14, 21, 28 and 60 days. The rating consisted of recording the ambient temperature, visual inspection for cloudiness, haze, discoloration, plus recording of maximum depth, average depth and length of any edge let goes. Any blemish was measured in mm. Immediately following the rating of the specimens, they were placed back in the liquid cleanser until the next rating interval. This technique was repeated at each interval until 60 days elapsed.

Upon the final rating the rinsed and dried laminates were stacked and placed horizontally on top of the respective containers and allowed to equilibrate with the ambient atmosphere. The specimens were rated at 1 day and 1 week in the same manner as previously reported except for the rinse and dry step. Liquids used for exposure were: bleach, laundry detergent, glass cleaner, dish detergent and water. In general, no blemishes of any kind formed in the specimens before the 14-day rating. At the 14-day rating period very slight edge blush (whitish "fog") was seen on the bleach, glass cleaner and water specimens. The maximum depth of this blemish was 1 mm for the bleach and water and 2 mm for the glass cleaner. All specimens except the dry control exhibited some form of edge blush by the 21-day rating period. No edge let goes were seen during the entire 60 days of the submersion portion of the test. The edge blush continued to invade the laminate with time, but at no time during this testing did the edge blush exceed 4 mm (as seen on the glass cleaner specimens). The average depth of the blush was 2 mm.

Upon removal of the specimens from the submersion portion of the test, it was noted at the 1 day rating that most of the edge blush had greatly diminished or disappeared completely. There was still no edge delamination. At the 7 day, dry rating, minor edge haze was seen on the glass cleaner specimen and the water control. The let goes on all specimens were also restricted to the edge and in some cases, so small they were difficult to see. The only exception to this is specimen number 9, glass cleaner, cut/autoclaved specimen which had a visible delamination in the lower right hand corner of the specimen. The delamination was amebic

in shape, located 15 mm from each edge with the leading front of the delamination 20 mm diagonal from the corner. The delamination was approximately 3 mm in diameter.

All specimens except the dry controls exhibited some form of edge blush during the exposure period. This edge blush essentially disappears on most specimens within one day of removal from the liquid. Most specimens developed a slight edge let go (release) after 1 week of sitting in ambient conditions after submersion. There does not appear to be a significant difference between the cut and polished edges, although some of the polished edges had lower levels of edge let go after drying. During the testing and subsequent drying it was obvious that the window cleaner was the harshest of the liquids with regard to laminate attack.

After six (6) years of laminates sitting in an ambient environment without light, the laminates were re-evaluated. All signs of blush were gone from every laminate. In the case of chlorine bleach, water and untreated edges all samples showed no defects for delamination or blush – even when edge delamination was recorded during testing. The other samples had typically uniform let-go around the edge with no sample having a delaminated depth of more than 4 mm. The samples did not develop deeper penetration of the delamination area, however the delamination area did in most cases become uniform around the edge, if it existed.

There was no significant difference between the cut/autoclaved edge and the polished edge specimens. However, the overall edge effect numbers are so small it is difficult to determine if there was any improvement or detriment to polishing the edges in this test. From the survey of products tested it appears that glass cleaner is the harshest cleanser from both and edge blush and a delamination perspective. It is not known if repetitive submersion and drying would alter these results or if exposure to other solvents or exposure at temperatures higher than ambient would have any effect. Note that no adhesion or other mechanical testing has been completed on these samples.

Based on the results of this testing it can be determined that limited (casual) contact with the tested liquids will not have a dramatic adverse effect on the visible acceptability of laminated glass made with conventional PVB interlayer. This test may also serve as a predictor for ESN performance.

## Summary

It is clear that the four tests described have different delivery mechanisms to infuse the interlayer with moisture or chemicals that could in turn react and cause a delamination at the edge. Laminated glass is a high-performance construction material comprised of glass and polymer interlayer which is bonded together under a heat and pressure process. Although this paper looks at the test methods to assess edge stability, it should be noted that causes of delamination, at the edge or in the body of the laminate, can be caused by many variables and are usually present in combinations rather than a single factor. Laminated product with PVB and non-PVB interlayers can be susceptible to delamination if not properly designed and laminated. Causes of delamination can be interlayer type and thickness, glass warp, edge kink of glass, contamination, improper processing, storage and handling, or inappropriate installation and many other variables. A low ESN alone is not a guarantee against delamination, just as a heat soak test is not a guarantee against spontaneous breakage of tempered glass. ESN is a rating that allows the user to make a decision regarding basic acceptability of a product for a given application. Edge delamination affects the aesthetics of laminated glass whereas center delamination can affect the impact characteristics and safety performance of the glazing at the time of impact, or after impact, should glass shards not be retained by the interlayer. Determination of the edge stability of a laminated glass construction is complex but as demonstrated, can be examined through various test methods. An overall assessment of interlayer and laminated glass performance should be completed for each project to ensure the materials are capable of meeting the desired characteristics in-situ. Laminated glass offers many benefits from safety and security through UV screening, acoustic damping, structural and vibrant design options. This information allows the specifier to make an informed choice in selecting installation methods, system design and laminated glass products.

# Edge Stability and Potential Cause of Blemishes in Laminated Safety Glass

Vaughn Schauss 1,  
Stefan Hiss 2,  
1 Kuraray America Inc.  
2 Kuraray Europe GmbH

## Keywords

1 = Laminated Glass 2 = Edge Blemishes 3 = Edge Stability 4 = Polyvinyl Butyral, PVB 5 = Ionoplast

## Abstract

The use of laminated safety glass in outdoor applications continues to increase, and as a result, questions about edge stability often arise. This is especially true where exposed edges are required to eliminate any sightline obstructions. Although the vast majority of laminated glass will never experience any edge blemishes, sometimes it does happen. This paper will focus on the edge stability of PVB and ionoplast laminates and address the potential causes of blemishes.

## Introduction

The role of glass in building construction has drastically changed in recent years. Laminated glass is now being used for safety, security, structural, and decorative components of buildings. With the increased application of laminated glass, as well as the recent code changes for balustrades in North America, laminated glass is being specified more and more for exposed edge applications. Although the vast majority of exposed edge laminates will never experience issues, sometimes blemishes around the edges may occur. When these do appear, they can compromise the visual appeal of laminated glass. There are a few reasons edge blemishes may appear, including the lamination process, compatibility with other building components, and the choice of the right interlayer for the application. This paper will focus on edge stability and discuss the potential causes of edge blemishes in laminated glass.

## Background

What is edge stability of laminated glass? Edge stability is defined as the ability for the edges of laminated glass to resist discoloration, bubbling, delamination, or other blemishes over time when exposed

to environmental conditions. In addition to natural and accelerated weather via different test methods or regulations such as ANSI Z97.1, or ISO 12543-4, similar tests may be initiated to investigate the performance of the laminates in regards to specific installation conditions, such as high temperature, salt (fog) spray, or compatibility to sealants, grouts, and glass coatings. Laminates with ionoplast interlayer have repeatedly performed well in edge stability testing. While laminates with traditional PVB have also performed well, they are more likely to experience edge blemishes. Although it may be difficult to determine the exact cause of the blemish after the fact, the potential reasons may be classified into two areas, the lamination process and the application conditions.

### Lamination Process and Edge Defects

The lamination process brings together heat and pressure, or vacuum, to remove the air and melt the interlayer between the lites of glass. Throughout the process, there are a few variables that play an important role in the edge stability of a laminate. These variables are adhesion of the interlayer to the glass, the quality of the glass, and edge seal.

## Adhesion

The adhesion of the interlayer to the glass plays a major role in the edge stability of the finished laminate. As the adhesion level lowers, the likelihood for blemishes increases. During the lamination process, there are many factors that may affect the adhesion level. The first factor is the cleanliness of the glass. When the glass arrives at the laminator, it can have cutting oil, release agents, dust, and other impurities on the surface. The glass must first be cleaned before lamination may begin. Modern glass washing machines are equipped with rotating brushes that clean the glass exceptionally well with only water. Since the cleanliness of the glass surface and the quality of the water affect the adhesion of the interlayer to the glass, only demineralized water is recommended. The water should have a conductivity less than 20 $\mu$ S. Water from natural or municipal sources contains dissolved salts that impart hardness to the water. These salts are typically composed of Ca<sup>++</sup>, Mg<sup>++</sup>, Na<sup>+</sup>, and K<sup>+</sup> ions. The former two negatively affects adhesion even in low concentrations, while the latter two have a lesser but still measureable effect. The loss of

adhesion, especially at the edge, may lead to edge bubbles or delamination. Moisture content of the interlayer is the second key factor for adhesion. PVB is hygroscopic, and its adhesion to glass is inversely related to its moisture content. It is produced with an optimum moisture content around 0.4%, and then the roll is hermetically sealed in a foil bag to prevent moisture absorption. Once the foil packaging is open though, the PVB will start to absorb moisture from the air until an equilibrium is reached. To prevent this, any open rolls of PVB should be stored in an environment with a relative humidity between 25-30%. It is also recommended to replace the foil packaging and seal it, especially if the storage conditions are not adequate. For ionoplast interlayer, it too absorbs moisture, but at a much slower rate. Because its optimum moisture content is lower than PVB though, it is recommended to always reseal the foil packaging, unless it is stored in the clean room below 10% relative humidity. The effects of either interlayer absorbing moisture is a reduction in the adhesion and potentially bubbles. The adhesion between the interlayer and the glass is governed heavily by the ability of the polar groups from the interlayer to bond with the polar groups of the glass surface. Figure 1 depicts how good adhesion is formed through the hydrogen bonds between the polyalcohol groups of the PVB interlayer and the silanol groups of the glass. In contrast, figure 2 shows how moisture content and ions from the wash water can reduce the adhesion by blocking the hydrogen bonds. Reduced adhesion at the edges may result in water ingress, blushing, bubbles, and or delamination.

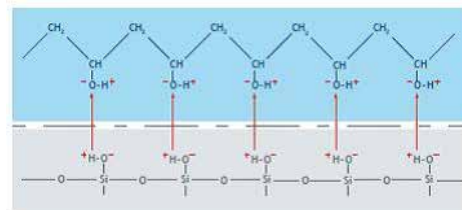


Figure 1 Example of good adhesion

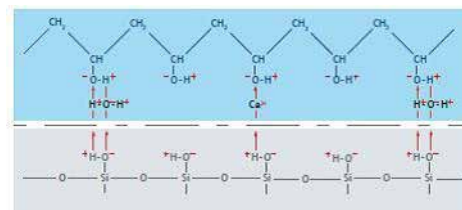


Figure 2 Example of poor adhesion caused by moisture and ions

## Quality of the Glass

Most of the glass used for lamination today is produced by the float process. Although standard float glass, also referred to as annealed glass, is of high quality and very flat, it is not considered safety glass since it breaks into large, sharp, dangerous pieces. The bending tensile strength of annealed glass is also relatively weak. To make it safer and stronger, the glass is subjected to a thermal strengthening process. The annealed glass is heated to approximately 600°C, and then cooled rapidly with jets of air. The rate of cooling determines the degree of strengthening by locking the surface of the glass in a state of compression. The faster the cooling, the higher the compression, and the stronger and safer the glass becomes. Fully tempered glass is cooled faster than heat-strengthened glass making it much stronger and giving it a smaller, safer break pattern. For lamination though, the potential issue with thermally strengthened glass is the inherent distortion imparted on it from the process. When the glass is heated that hot, it can start to deform and become wavy. This distortion can result in an overall waviness, a general or local bow, or edge curl. Figure 3 depicts the typical distortions. There has been a great improvement over the last few years with tempering furnaces, and some of the newer furnaces can produce exceptionally flat glass, but care must be taken to use the flattest glass possible for lamination. Even the values specified in ASTM C1048 are not tight enough for lamination. A general rule is that the deviation of flatness should be below 10% of the interlayer thickness. For a 0.76 mm interlayer, the maximum flatness deviation would be 0.076 mm. A deviation larger than this tolerance on the edge has the potential to develop bubbles or delaminate.

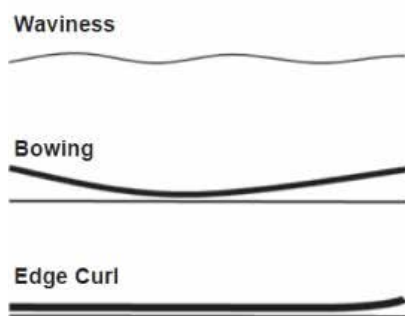


Figure 3 Typical distortions of heat treated glass

A laboratory study was initiated to determine the effect that edge curl has on the finished laminate. Two types of laminates were prepared using tempered glass with edge curl, see figure 4. Orientation A matched the curls together so that they were nested, while

orientation B placed the curls in opposite directions. The gap between the two lites of glass was measured and sample A had a gap of 0.05mm whereas sample B had a gap of 0.65mm. The samples were then laminated using 0.76mm PVB and autoclaved together. After the autoclave, the samples were stored under high heat and humidity for several months at 85°C and 85% relative humidity. Samples with orientation A showed no visible blemishes, however, orientation B had numerous edge bubbles, see figure 5.

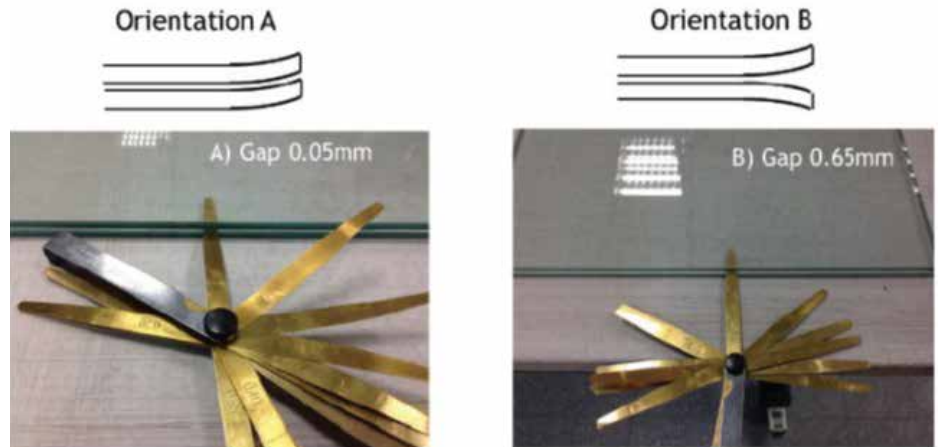


Figure 4 Orientation of edge curl in tested samples



Figure 5 Edge bubbles after weathering of orientation B sample

## Edge Seal

The autoclaving process is the last step in the production of laminated glass. The conditions inside the autoclave allow for viscous flow of the interlayer resulting in an intimate contact with the glass. Any remaining air is dissolved and dispersed creating a clear laminate. Once the laminates have been de-aired, they are placed on autoclave racks. There should be space between the laminates to allow channels for air flow to ensure even heating and cooling. The glass should be secured in position on the racks so there is very little movement during the autoclave cycle. Excessive movement may lead to glass breakage. When securing the laminates, care must be taken to avoid excessive localized pressure. The localized pressure may lead

to the interlayer extruding from the edges, creating a thinning of the interlayer at that point. This could lead to edge bubbles or delamination.

Once on the racks, the laminates should be placed as quickly as possible in the autoclave. Excessive delays could result in the edges beginning to separate, especially if the edge seal was not good. The autoclave is then heated to 135-145°C while pressurizing to 12-15 bars. Once top heat and pressure is reached, it is held for at least 30 minutes, but the length of time is dependent on the glass thickness and load size. After the hold time is up, the glass is allowed to cool down while still under pressure. The pressure should not be released until the interlayer/glass temperature is below 50°C, otherwise, small champagne or finger-like bubbles may start to appear, see figure 6.



Figure 6 Edge bubbles present after autoclave

**Application Conditions and Edge Blemishes**  
Besides the conditions of the laminating process, how and with what the laminate is installed with may potentially cause edge blemishes. There are a variety of different ways to install laminated glass, while different, there are some basic precautions that should be followed for all installations. The first of which is contact with water. Even with the best lamination conditions, laminated glass should not be allowed to sit in water for an extended period of time. For applications where the laminate has captured sides, weep holes or other ways for any accumulated water to drain should be included. For exposed edge applications, drainage should be adequate enough as to not allow standing water to remain in contact with the laminate. This is also true for point supported glass. If the

point supports are not sealed properly, water can infiltrate the opening and may lead to delamination, as seen in figure 7.



Figure 7 Delamination around point support fitting

In addition to water, any other chemical that may be in contact with the edge of the laminate should be tested for compatibility. This is especially relevant to sealants and grouts. Incompatibility of the sealant and grouts with the interlayer may result in edge bubbles, discoloration, or delamination. There are a variety of sealants on market. While most are compatible with ionoplast laminates, PVB laminates may experience some minor edge blemishes. It is best to contact the sealant or interlayer manufacturer to determine compatibility. As North America begins to move toward laminated glass for balustrades, and away from monolithic tempered glass, the topic of grouts has become increasingly popular. As discussed in the 2007 GPD paper "Outdoor glass baluster – new challenges," cement-based grouts are not recommended for contact with laminated glass.

The last potential cause of edge blemishes is the environmental conditions where the laminate is installed and what interlayer is used. Is the laminate indoors, or outdoors? Is it in a dry environment, or a wet one? Is it close to an ocean? Is PVB used or ionoplast? Based upon these answers, different edge stability levels may be achieved. For example, can ionomer laminates be installed in an open edge balustrade by the beach? To answer this question, salt spray testing was performed.

### Salt Spray (Fog) Testing

Salt Spray (Fog) Test, is a standard corrosion test usually done on coated metal products in the architectural industry. However, it is starting to be requested for laminated glass railing applications in exposed edge conditions for coastal climates. The testing is an accelerated weathering test based on ASTM B117 "Standard Practice for Operating Salt Spray (Fog) Apparatus." The samples are exposed to 3,000 hours at 35°C while misted with a 5% NaCl water solution. The samples

are removed and inspected at 500 hour increments and then returned to the chamber. Four laminates were prepared with one being the control sample and three subjected to the weathering. The results were as predicted for the ionoplast laminates. After 3,000 hours, there were no visible edge defects noticed, figure 8. Standard PVB however, began to experience a clouding of the edges around 1,000 hours, figure 9. In addition to standard PVB, our high adhesion grade PVB was also tested. As stated earlier, adhesion is a key factor in edge stability, and after 3,000 hours, the high adhesion PVB showed no signs of cloudiness or other edge defects, figure 10.

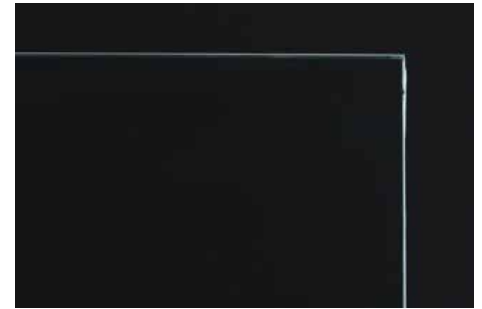


Figure 8 SentryGlas® ionomer after 3,000 hours in the salt spray test



Figure 9 Standard PVB after 1,000 hours in the salt spray test

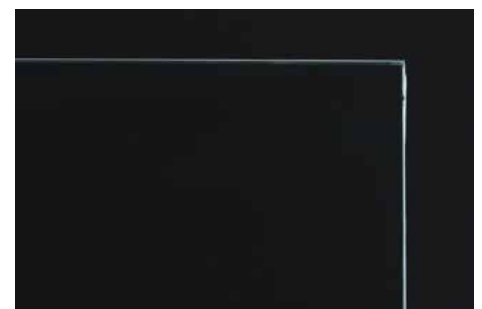


Figure 10 Trosifol BG R20 high adhesion PVB after 3,000 hours in the salt spray test

## Conclusion

The use of laminated glass for exposed edge applications is increasing, and as such, so are the questions about edge stability. While the majority of laminates will never experience edge blemishes, it can sometimes happen. Edge blemishes can be attributed to the lamination process, compatibility of materials, and choosing the right interlayer. When properly laminated and installed, the potential for edge blemishes decreases, leaving a clearer view.

## References

- [1] Kuraray Trosifol: Technical Manual, The Processing of PVB Film, Sixth edition, Kuraray Europe GmbH, 2012
- [2] Keller, U. & Mortelmans, H.: Adhesion in Laminated Safety Glass – What makes it work?, Conference Proceedings, Glass Performance Days, pp. 353-356, 1999.
- [3] Kuraray Glass Laminating Solutions: SentryGlas® Ionoplast Interlayer Technical Manual For Structural Engineers, Kuraray, 2014
- [4] Schmidt, M. & Nugent, W.: Outdoor Glass Baluster – New Challenges, Conference Proceedings, Glass Performance Days, pp. 206-209, 2007.

# Post-lamination Response of Warm-bent Laminated Glass

Laura Galuppi<sup>1</sup>,  
Gianni Royer Carfagni<sup>1,2</sup>  
1 Department of Engineering and Architecture,  
University of Parma, Italy  
2 Construction Technologies Institute - Italian  
National Research Council (ITC-CNR), Milano,  
Italy

## Keywords

1=Laminated glass 2=Warm-bending 3=Shape optimization 4=Time-dependent response 5=Delamination phenomena 6=Gradual release

## Abstract

Warm-bent laminated glass is obtained by elastically curving glass plies against a constraining negative mould and by performing, in this condition, the lamination process in autoclave. After removing the constraints, the laminate holds its curved geometry because of the shear coupling from the polymeric interlayer. Curved panels so obtained are called "warm bent" to distinguish them from "cold-bent" panels, where flat glass is forced into a curve on site and restrained by a frame. An analytical study is presented to describe how, after removal of the constraint, the laminate maintains the curvature only partially, suffering an initial spring-back followed by a long-term relaxation. The model problem considered here is that of two Euler-Bernoulli beams coupled by a thin viscoelastic adhesive layer. Within a variational approach, we analytically describe the relationship between the initial constrained shape and the shape of the curved beam, which is time-dependent due to the viscosity of the interlayer. Localized contacts and stress concentrations may occur, depending upon the type of profile that is initially imposed. Comparison of the cases of instantaneous or gradual release of the contact with the mould evidences a remarkable reduction of the transient state of stress in the second case.

## Introduction

Glass has been used for building purposes since the early nineteenth century, yet this is still a dynamic product that has far from exhausted its potential. The use of curved laminated glass, produced through either hot-bent or cold-bent, is constantly growing

and represents the leading feature of a modern architectural trend. Traditional hot-bent laminated glass is produced, first, by heating glass sheets up to the softening point and curving them against a negative form; secondly, by performing the lamination process in autoclave. A crucial issue in this process consists in obtaining glass plies that fit together perfectly, with curvatures only slightly different one another. Cold-bending consists in forcing in the desired position initially-flat glass, laminated with the standard process in autoclave, so that the curvature is produced through elastic straining. It allows to construct low-cost free-form glazed surfaces, being the expensive negative forms not necessary, but it requires a strong structural frame to withstand the constraining forces necessary to elastically bend the element, forces without which the glass would return to be straight.

A recent and promising technique to obtain curved laminated glass, that combines the benefits of the aforementioned process, is *Warm-Bending*, also known as *Cold-Lamination-Bending*. This process consists in three different phases [1, 2], schematically shown in Fig. 1.

**Phase I, distortion.** The yet-not-coupled package composed by glass plies and polymeric sheets is elastically deformed into the desired shape by means of provisional constraints. In this phase, schematically represented in Fig. 1a, there is a relative shear-slip between the glass plies and the polymeric interlayer. The lamination process in autoclave, at high pressure and temperature, is performed in this deformed configuration.

**Phase II, release.** When lamination is completed, the constraints are released (Fig. 1b), either instantaneously or gradually, but the now coupled laminated package partially maintains the deformed shape through the interlayer. However, the curved laminate suffers an initial springing back and a relaxation due to the viscosity of the interlayer. Because of this, the state of stress may strongly depend upon the history of the release process.

**Phase III, final placement.** Finally, the laminated glass panel is fixed *in situ* in the desired location (Fig. 1c). Again, the viscoelastic behavior of the interlayer causes a redistribution of stress in the glass plies, and the state of stress may further vary because

there might be an interaction with the final constraints to the underlying structure, if such constraints are such to prevent the free deformation of the panel.

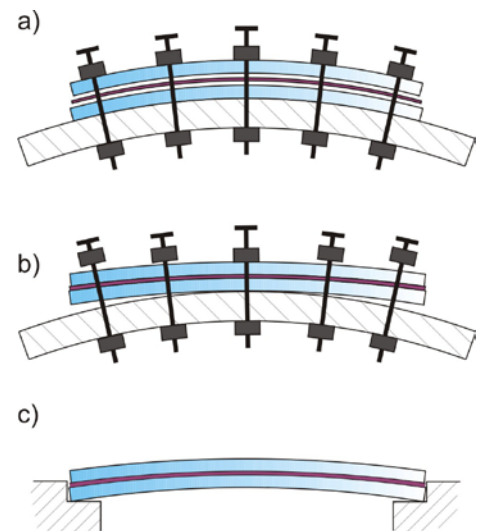


Figure 1 Warm-Bending process.

a) Phase I: cold bending of the uncoupled package;  
b) Phase II: gradual release after lamination;  
c) Phase III: final placement.

In such a way, much of the curvature is preserved, so that the result is similar to a hot-bent glass, because no constraining forces are needed, but the production cost is much lower, because the process at high temperature is skipped.

A major issue in the warm-bending process that still needs clarification is how to precisely model the phase when bending takes place and the successive transient relaxation. Here, a simple analytical model is proposed, that can contribute to the understanding of the importance of the various parameters to achieve an optimal design, with particular regard to the prescribed geometry and the kind of release (instantaneous or gradual). Second, as confirmed later on, stress concentrations may arise in some cases, but this information gets lost in standard finite element analyses, because the use of regular shape functions smears the critical states on the size of the finite element (mesh dependence).

The single-curvature warm-bending of a laminated glass panel is here analyzed by using sandwich beam theory, developing for this particular case a method originally proposed by Newmark *et al.* [2]. The proposed

approach allows finding the relationship between the prescribed deformation in Phase I and the time-evolution of the deformed shape of the panel, and the consequent indication of the spatial and temporal distribution of the stress in both glass plies and interlayer. Here, we will focus on the first and second phase only. The two paradigmatic cases of circular (constant-curvature) and sinusoidal profile are considered and, for both of them, the transient state during either an instantaneous or a gradual release of the element from the constraining mould is analyzed in detail. Comparisons are made between "stiff" interlayers (like IonoPlasts IP) and "soft" interlayers (like PVB).

## Analytical model for Warm-Bending of laminated glass

Let us consider the laminated glass beam schematically shown in Fig. 2a, of length  $L$  and width  $b$ , composed by two glass layers with elastic modulus  $E$ , bonded by a thin polymeric interlayer with shear modulus  $G(t)$ , which is time-dependent due to the viscoelasticity of the polymer. Let  $H$  denote the distance between the centroids of the two glass panels. By denoting by  $\bar{v}(x)$  the prescribed vertical displacement of the beam in the distortion phase, i.e. the mould shape, the shear distortion due to the relative slip between the faces of the glass plies in contact with the interlayer can be modelled as a *distributed shear dislocation* in the interlayer, denoted by  $\bar{\gamma}(x)$  and highlighted in Fig. 2b.

As discussed in [1, 2], the equilibrium equation in  $y$  direction of the beam takes the form

$$EIv''''(x,t) + b\tau'(x,t)H - M''(x,t) = 0 \quad [1]$$

where ' denotes differentiation with respect to  $x$ ,  $v(x,t)$  is the vertical displacement of the beam in Phase II and  $M(x,t)$  is the applied overall bending moment, related with the constraint reaction forces per unit length of the constraints (that is null in case of instantaneous release, but time-decreasing in the case of a gradual release of the laminate). The time-dependent shear stress in the interlayer,  $\tau(x,t)$ , which provides the shear coupling of the glass plies, is related with the shear strain due to the springing back and relaxation, represented by the difference between the actual shear strain  $\gamma(x)$  and  $\bar{\gamma}(x)$  i.e.,

$$\tau(x,t) = G(t)[\gamma(x,t) - \bar{\gamma}(x)], \quad \bar{\gamma}(x) = \frac{H}{h} \bar{v}'(x), \quad \gamma'(x,t) = \frac{EI_{tot} v''(x,t) - M(x,t)}{EhHA^*} \quad [2]$$

where  $I_{tot}$  represents the moment of inertia of the cross sections of the laminate at the monolithic limit (shear-rigid interlayer).

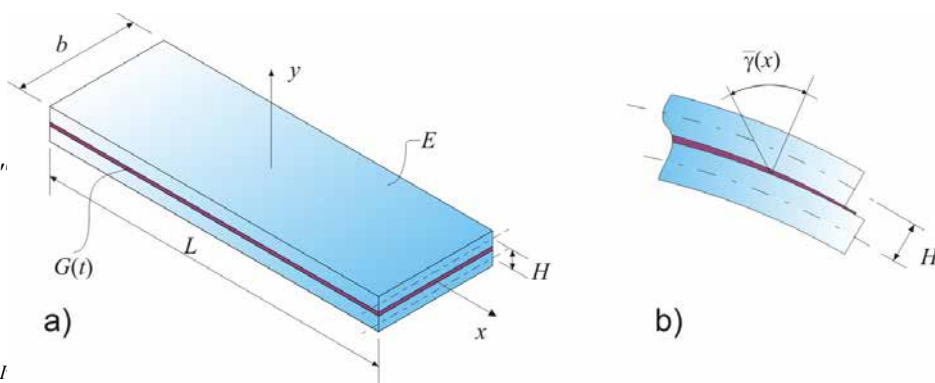


Figure 2 Laminated glass beam and shear distortion due to warm bending.

By expressing  $\gamma(x)$  as a function of  $v(x,t)$  and  $M(x,t)$  (see [1] for the details), and by substituting [2] into the equilibrium equation (1), an analytical relationship can be found among the prescribed shape in Phase I and the time-evolution of the deformed shape of the beam. Once  $v(x,t)$  is known, the shear stress transmitted across the interlayer may be evaluated through eq. (2), as illustrated in [2, 3]. In the sequel, different shapes for the warm-bent panel and different kind of release, gradual and instantaneous, will be considered. Furthermore, a comparison is made between the most common commercial polymeric films, i.e., PolyVinyl Butyral (PVB) and IonoPlastic Polymers (IP), which represent paradigmatic examples of a "soft" and a "stiff interlayer", respectively. Their viscoelastic properties are accounted for by evaluating the typical values of their secant shear modulus  $G(t)$  at 20°C, for different durations of the load according to the Prony's series recorded in [4].

## Effect of the mould shape

As well known, the most common shape for warm bending of laminated glass is the constant curvature one (circular bending). Here, the most common shape for warm bending, i.e. the constant curvature one (circular bending) and the (co)sinusoidal one, i.e.,

$$\bar{v}(x) = v_{max} \left( 1 - \left( \frac{2x}{L} \right)^2 \right), \quad \bar{v}(x) = v_{max} \cos \left( \frac{\pi x}{L} \right), \quad [3]$$

respectively, are now considered. Comparison will be made in terms of both time-dependent evolution of the panel shape and of stress arising both in glass plies and interlayer.

Remarkably, for standard geometric parameters, the difference between these two configurations cannot be appreciated with the naked eye, and consequently the aesthetics is not compromised.

Let us consider, as an illustrative example, the cold-bending of a beam of length  $L = 2400$  mm, width  $b = 800$  mm, composed by two glass plies of thickness 6 mm bonded by an interlayer of thickness 1.52 mm whose the time-dependent shear modulus  $G(t)$  is calculated according to [4]. The beam is warm-bent with a mould shape given by eq. (3) with  $v_{max} = 144$  mm, and then *instantaneously* released. Both stiff (IP) and soft (PVB) interlayers are analyzed. Figure 3 Vertical displacement of the beam at various times, for constant-curvature Warm-Bending.

Fig.3 shows the vertical displacement of the beam, as a function of  $x$ , in Phase II, i.e. its deformed shape, at different times after the forcing of the beam in the desired position for the case of constant-curvature Warm-Bending, and for PVB and IP interlayers. Fig.4 is its counterpart for (co)sinusoidal Warm-Bending. It is evident that the time-dependent deformed shape of beams subjected to constant-curvature and sinusoidal are very similar. Observe the immediate elastic springing-back and the curvature that is maintained due to the shear coupling offered by the interlayer. Afterwards, the viscosity of the interlayer leads to an overall relaxation of the beam, until the long-term equilibrium configuration is reached. It is evident that the shear modulus of a IP interlayer is high enough to maintain the deformation in practice for the whole lifetime of the laminated glass element (50 years). On the other hand, much of the initial curvature is lost if one uses a PVB interlayer.

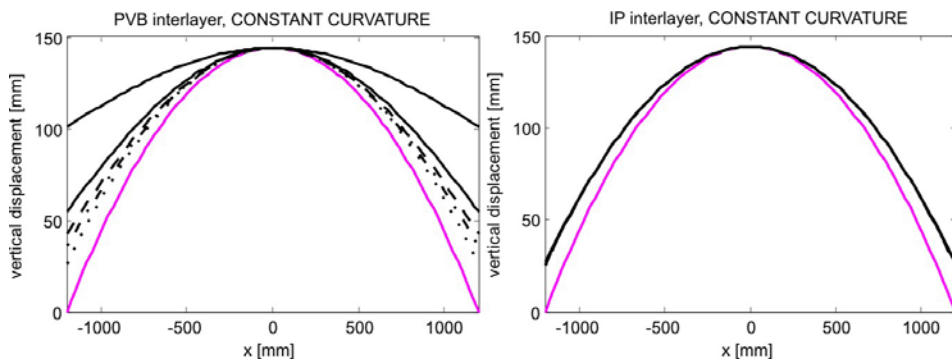


Figure 3 Vertical displacement of the beam at various times, for constant-curvature Warm-Bending.

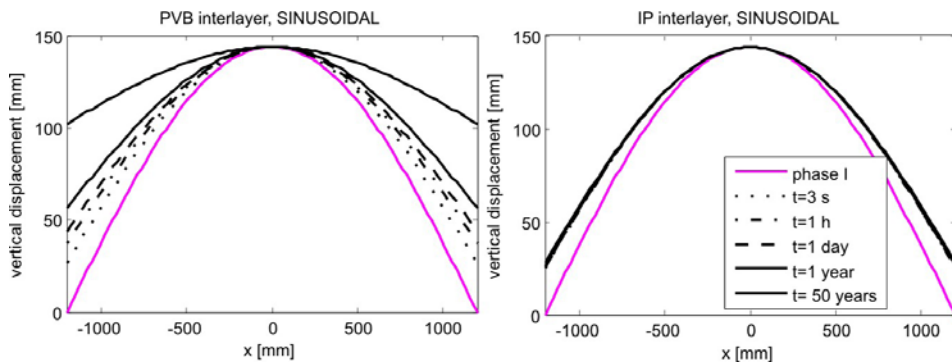


Figure 4 Vertical displacement of the beam at various times, for sinusoidal Warm-Bending.

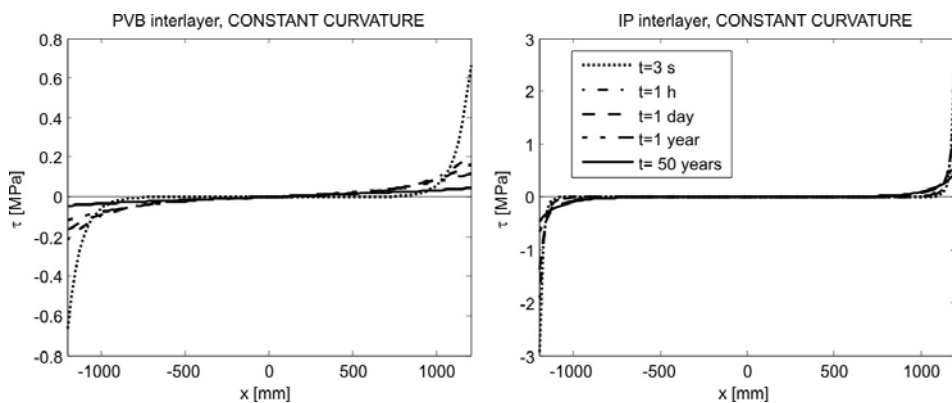


Figure 5 Shear stress in the interlayer at various times for PVB and IP interlayers (not in the same scale) for constant-curvature Warm-Bending.

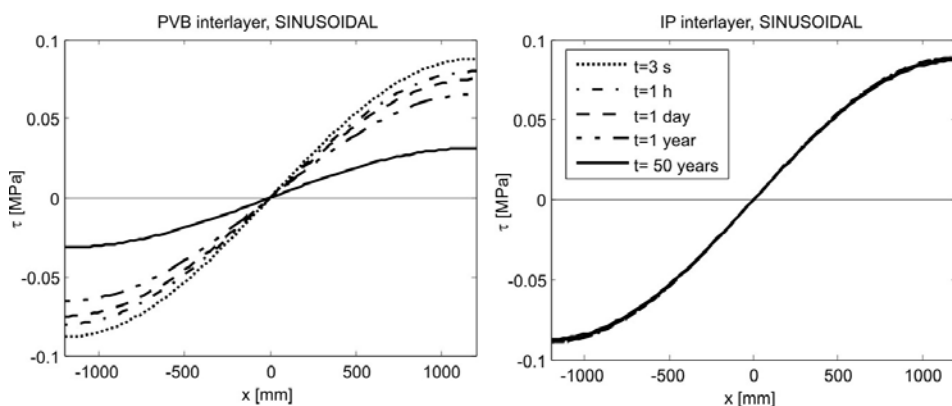


Figure 6 (Co)Sinusoidal CLB. Shear stress in the interlayer for various times for PVB and IP interlayers for sinusoidal Warm-Bending.

Figures 5 and 6 show the shear stress transmitted by the interlayer, as a function of  $x$ , at various times after the removal of the provisional constraints, for PVB and IP interlayers, respectively, for Warm-Bent beams with constant and sinusoidal curvature, respectively. Observe that the stress state is more critical and that the time-decay of the shear stress is slower for stiff (IP) than for soft (IP) interlayers.

Notice that, in the former case, the shear stress tends to concentrate in the neighbourhood of the beam ends. This may represent a risk of delamination, as sometimes observed in practice.

On the other hand it is evident that, in the latter case, the stress peaks are smoothed out with respect to the case of constant-curvature, even when the shear modulus of the polymer is high. In particular, from comparison of Figures 5 and 6, notice that the sinusoidal Warm-Bending produces a decrease in terms of maximum shear stress of more than one order of magnitude for PVB interlayers, and of about two orders of magnitude for IP interlayers. It may be verified [3] that the maximum axial stress in the glass plies is in general slightly higher in the case of sinusoidal Warm-Bending with respect to constant curvature one, but the difference is not relevant. For example, changing the prescribed deformed shape from constant-curvature to sinusoidal, for the previously defined glass beam with IP interlayer, 3 s after the releasing of the beam, the obtained axial stress increases approximately 20% higher, but, on the other hand, the maximum shear stress in the interlayer is less than 5% of the previous case. Indeed, the most remarkable advantage consists the reduction of the shear stress in the interlayer.

Accurate comparisons between numerical and analytical results [2] have confirmed the accuracy of the proposed model for the evaluation of both the time evolution of the beam shape and of the shear stresses.

### Effect of the type of release

As discussed in [3], noteworthy advantages in terms of stress state can be obtained not only through the optimization of the mould profile, but also by designing a *gradual release* of the laminated beam.

In the framework of the proposed model, the gradual release may be modelled by means of time-decreasing external constraining forces pressing the beam on the mould, that are supposed to linearly decrease from the initial value to zero in a time  $t^*$ , producing a progressive decrease of the beam-mould

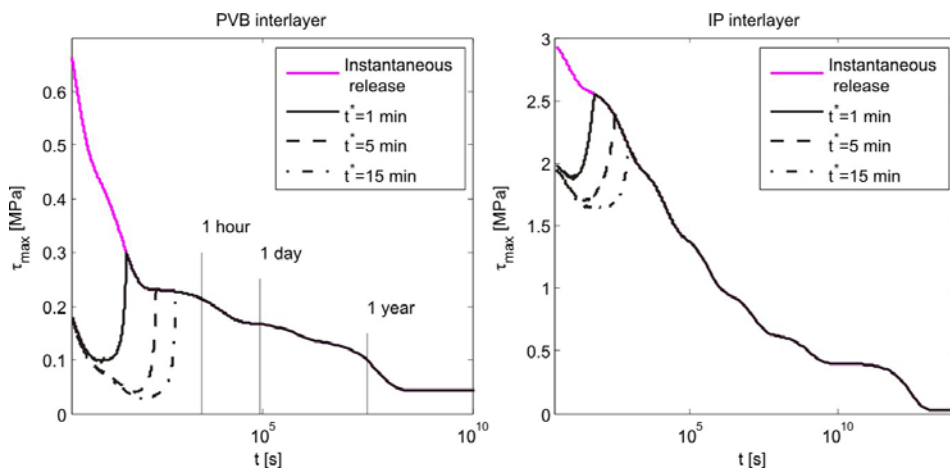


Figure 7 Time-evolution of maximum shear stress in the interlayer for constant-curvature Warm-Bending with instantaneous and gradual release. Case of PVB and IP interlayers.

contact area, until the laminate is completely released.

Figure 6 shows the maximum shear stress in the interlayer, as a function of time  $t$ , in correspondence of the beam's extremities, for a warm-bent laminated glass beam with PVB and IP interlayer, for the case of constant-curvature mould shape. Comparison is made among the case of instantaneous release and gradual release performed in 1, 5 and 15 minutes.

Obviously, the graphs corresponding to instantaneous and gradual release link up on to each other at  $t = t^*$ , i.e. at time at which the element gets free of constraints, while for  $t < t^*$ , the maximum shear stress in the interlayer is always lower in the latter than in the former case.

In other words, the gradual release allows to bypass the initial phases in which the polymer is quite stiff, allowing the viscoelastic effects to soften the material and mitigate the peak stress, while it has no effect in the long- and mid-term stress state. For this reason, it may be noticed that in the PVB case the beneficial effect of the gradual release is more relevant, because the time-decrease of the shear modulus  $G(t)$  of PVB is faster than of IP and, hence, the relaxation occurring in the first minutes is higher. For example, a gradual release performed in 5 minutes leads to a reduction, with respect to the case of instantaneous release, of the maximum shear stress of more than 60% and of the order of 20% for PVB and IP interlayers, respectively, with no considerable increase of the axial stress in the glass plies. Obviously, the beneficial effect is more noticeable for high values of the release duration. However, since the stress is much higher in IP than in PVB, the major advantages are for IP cold-lamination-bent glass beam. Of course, also in the case of sinusoidal

Warm-Bending the shear stress can be further reduced with a gradual release, but since there are no critical states of stress, the polymer viscosity has a weaker influence than in the circular case, and the benefit is less relevant.

## Conclusions

Warm-Bending is a promising technique to obtain curved glazed surfaces. It consists, first, in the elastic deformation of packages made of glass plies and polymeric interlayers and, afterwards, in producing the bond in autoclave between glass and polymer. It allows to obtain permanently bent shapes due to the shear coupling of the glass plies through the polymeric interlayer. Due to the polymer viscoelasticity, the laminated element suffers an initial spring-back, followed by a long-term relaxation, whose effects needs to be evaluated for a proper design.

An analytical approach is here proposed, which accounts for the distributed shear dislocation produced by laminating the beam in the deformed configuration. It allows to evaluate the relationship between the design shape and the time-dependent state of stress in both glass and interlayer, that are strongly dependent upon the prescribed warm-bent shape, as well as on the viscoelastic properties of the interlayer and on the kind of release of the beam from the mould.

A comparison between "soft" and "stiff" interlayers has demonstrated that the latter are able to maintain the beam in the deformed shape also in the long term, for the whole lifetime of the element [50 years]. Remarkably, this study demonstrates that the constant-curvature shape, indeed the most used, is perhaps one of the worst that could be selected, because it produces shear stress concentrations at the end of the laminated glass element, which may possibly be a source of delamination. The higher is the shear

modulus of the polymer forming the interlayer, the most critical is the corresponding state of stress, and hence the risk is higher for beams with Ionoplastic interlayers.

A very effective way to reduce the peak stress in the interlayer is to slightly change the shape of the mould. Remarkably, the sinusoidal shape, which for typical values of the deformation only slightly differs from the circular one, seems to be optimal for distributing and smoothing the shear stress in the interlayer. In general, for the same sag of the laminated glass beam, the shear stress in the interlayer is consistently lower than in the aforementioned cases.

It has been also demonstrated that another way to mitigate the delamination risk is to perform a gradual release of the laminated glass from the mould, bypassing the initial critical states occurring when the release is instantaneous, which are the most critical in terms of stress. The relevance of this effect depends upon the viscoelastic properties of the interlayer.

## References

- [1] L. Galuppi, G. Royer-Carfagni, 2014. Rheology of cold-lamination-bending for curved glazing, *Eng Struct* 61, pp. 140-152.
- [2] L. Galuppi, G. Royer-Carfagni, 2015. Cold-lamination-bending of glass: sinusoidal is better than circular. *Compos Part B - Eng* 79, pp. 285-300.
- [3] L. Galuppi, G. Royer-Carfagni, 2015. Localized contacts, stress concentrations and transient states in bent-lamination with viscoelastic adhesion. An analytical study. *Int. J Mech Sci* 103, pp.275-287.
- [4] S.J. Bennisson, I. Stelzer, 2009. Structural properties of laminated glass. Short Course, Glass Performance Days, Tampere (Finland).

# Thermal Radiation Compared with Forced Convection Heating in a Flat Glass Laminating Oven

Dr. Mikko Rantala  
Glaston Finland Oy

## Abstract

In a flat glass laminating oven, glass-film sandwiches are located on rotating rollers and conveyed through a heating chamber in a continuous flow. The PVB-film should be heated up to a temperature of about 60°C before it enters into a nip roll at the end of the oven. Usually, heating is arranged with conventional heating resistors located in a heating chamber. In some ovens, the heating is based on forced convection. In these, hot air jets are blown toward the glass-film sandwich. Glass and PVB have low thermal conductivity. So, it takes time to transfer heat to the inner film in a multi-film layer sandwich. The spokespersons of the radiation ovens catch of the problem and express that radiation heating helps, because the radiation penetrating through the glass is absorbed by the film. The statement that clear and low-e coated glass-film sandwiches can be processed with the same speed is given as an advantage of convection heating. Thus, there exist various kinds of argument as to how heating should be arranged. The paper aims to end the speculation. It shows theoretical results for how various glass-film sandwiches heat up in radiation and convection ovens.

## 1. Introduction

In a glass laminating process, sheets of glass are stuck together with a polyvinyl butyral (PVB) film between them. A typical PVB-film thickness is 0.76 mm. At first, PVB is placed between glasses in a laminating room. Then, the whole sandwich containing glasses and films is heated up in a de-airing conveyor in which heating is arranged with thermal radiation and/or forced convection. In a flat glass de-airing conveyor, i.e. a laminating oven, glass-film sandwiches are located on rotating rollers and conveyed through a heating chamber in a continuous flow. There is a nip roll before and after the oven. Even lines without the first nip roll exist. The air from glass-film interfaces is pressed out when a sandwich goes through the nip. The major function of the de-airing, in addition to sticking and air removal, is edge sealing, which prevents air re-penetration into a

sandwich. Next, the bond between glass and film is stabilised in an autoclave, which is a hot pressure chamber. Autoclaving presses and breaks remaining air bubbles into smaller sizes and then dissolves them into the film. In a flat glass laminating oven, glass-film sandwiches are heated up to a temperature of about 60-70°C measured from the surface, when a sandwich comes out of the oven (nip roll) to the unloading table. Surface temperatures above 90°C are avoided. Usually heating is arranged with conventional heating resistors located near the ceiling and roof in a heating chamber. Also, so-called quartz tube heaters, emitting near- and mid-infrared radiation, are used in some ovens. In the ovens mentioned above, heating is based on the radiation heat transfer. In some ovens, the heating is based on forced convection. In these, fans circulate hot air inside the oven, and hot air jets are blown toward the glass-film sandwich. Both materials, i.e. glass and PVB, have low thermal conductivity. So, it takes time to transfer heat into the inner film in a multi-film layer laminate, when at the same time the overheating of the outer film must be avoided. That limits the heating speed of multi-film layer laminates. As to heat transfer, an interesting detail is that glass and PVB are semi-transparent for thermal radiation, and both materials have their own spectral absorption properties.

There are various kinds of beliefs as to how heating in lamination oven should be arranged. The spokespersons of the radiation ovens claim that the most efficient means for heating the glass-film sandwich is to use near- or mid-infrared radiation, which penetrates through the glass but is absorbed into the film. The statement that clear and low-e coated glass-film sandwiches can be processed at the same speed is given as an advantage of convection heating. The paper aims to end the speculations. It shows the theoretical results how various glass-film sandwiches heat up in radiation and convection ovens.

## 2. Emission from a black surface

All objects emit radiation on the basis of their temperature, which is called thermal radiation. An ideal black surface has complete

emission and absorption of incident radiation at all wavelengths, and from all directions. The spectral distribution of the hemispherical emissive power of a blackbody is given as a function of a wavelength and absolute temperature ( $K = ^\circ C + 273$ ) by

$$e_b(\lambda, T) = \frac{C_1}{\lambda^5 (e^{C_2/\lambda T} - 1)} \quad (2.1)$$

This is known as Planck's spectral distribution of blackbody emissive power. In Eq. (2.1)  $C_1 = 2\pi^5 hc^2 = 3.7419 \times 10^{-16} \text{ Wm}^2$  and  $C_2 = hc_0/k = 14,388 \text{ } \mu\text{mK}$ , where  $k$  is Boltzmann's constant and  $h$  is Planck's constant. Eq. (2.1) is solved for three surface temperatures in Figure 2.1.

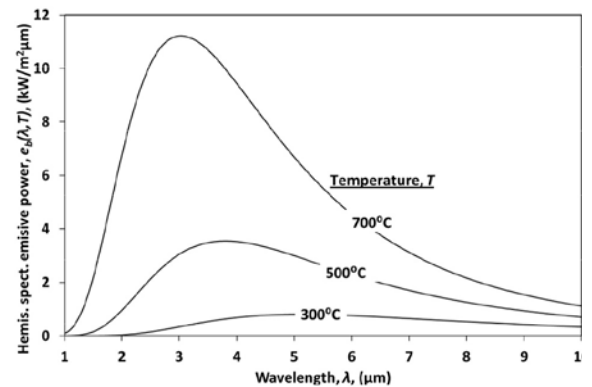


Figure 2.1 Hemispherical spectral emissive power of a blackbody at various blackbody temperatures.

As seen in Figure 2.1, the spectral distribution of the emissive power shifts towards shorter wavelengths when the temperature of a blackbody increases. The wavelength  $\lambda_{peak}$  at the peak of the spectral distribution can be calculated from Wien's displacement law

$$\lambda_{peak} T = C_3 \quad (2.2)$$

where  $C_3 = 2897.756 \text{ } \mu\text{mK}$ . In Figure 2.1 the area between curves and the wavelength-axis is equivalent to the total emission of a blackbody, and is obtained from the Stefan-Boltzmann equation

$$e_b(T) = \int_0^{\infty} e_b(\lambda, T) d\lambda = \sigma T^4 \quad (2.3)$$

in which  $\sigma = 5.6703 \times 10^{-8} \text{ W/(m}^2\text{K}^4)$ .

### 3. Absorption of thermal radiation in a glass-film sandwich

In Figure 3.1, the behaviour of incident radiation hitting a glass-film sandwich is shown schematically. At air-glass interface, a proportion of the radiation is reflected. The reflectivity depends on the hitting angle and the wavelength [1]. Because of the low reflectivity (typical direction-averaged value is 0.09) of a clear glass surface, the main proportion of radiation goes through the interface. The radiation to which glass is opaque is absorbed to a glass surface. The radiation to which glass is transparent penetrates deeper into glass, and the proportion of it absorbed into the glass. The rest of the radiation meets the glass-film interface, where a second reflection occurs. Without air at the interface, i.e. after the de-airing, the reflectivity of the interface is minimal, because glass and PVB have almost the same refractive indices. In the spots where air is between glass and film, the reflection occurs from glass-air and air-film interfaces. It is apparent that the reflectivity of the interface decreases during heating in a laminating oven, because the contact between glass and film is getting better. Now, value  $\rho_{\text{Aint}} = 0.10$  is used in the modelling.

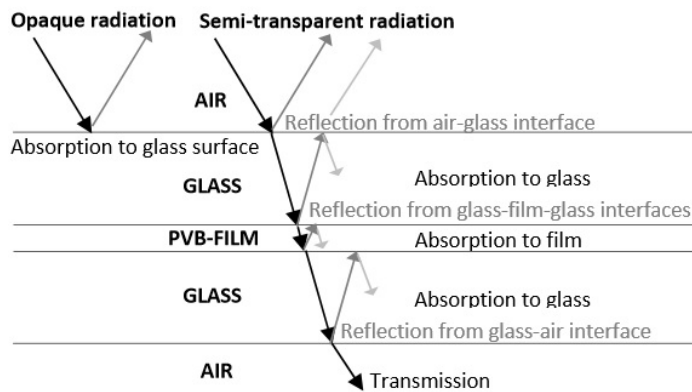


Figure 3.1 Behaviour of incident opaque and transparent radiation beam in the glass-film sandwich

Due to absorption, the intensity of the radiation attenuates when it propagates in glass. Bouguer's law is the mathematical relation describing the reduction in intensity of radiation as it travels along a path of finite length within a medium. The intensity of radiation after a path distance  $x$  in a medium is

$$i_x = i_0 e^{-\kappa x} \quad (3.1)$$

where  $i_0$  is the intensity at the surface and  $\kappa$  is the absorption coefficient, which is the property of a medium that describes the amount of absorption of thermal radiation per unit path length within the medium.

Figure 3.2 shows the spectral absorption coefficient of clear soda-lime glass and PVB-film. Soda-lime glass has two cut-off wavelengths, at which its absorption coefficient undergoes a major change. Practically speaking, glass is opaque for thermal radiation when the wavelength is over  $4.5 \mu\text{m}$ , whereas for wavelengths under  $2.75 \mu\text{m}$ , glass is very transparent. At wavelengths between  $2.75$  and  $4.5 \mu\text{m}$ , the absorption coefficient is about  $4 \text{ cm}^{-1}$ , which is still a relatively high value. At wavelengths between  $1$  and  $2.75 \mu\text{m}$ , the absorption coefficient is about  $0.3 \text{ cm}^{-1}$ . The spectral transmissivity through  $3 \text{ mm}$  (=typical minimum glass thickness in a flat glass laminating oven) thick glass is about 28%, when  $\kappa_\lambda = 4 \text{ cm}^{-1}$ , and 84%, when  $\kappa_\lambda = 0.3 \text{ cm}^{-1}$  (hitting angle =  $0^\circ$ ). The absorption coefficients at wavelengths below  $4.5 \mu\text{m}$  are higher when the concentration of iron oxide in glass increases. Such a glass has a greener colour, and its light transmission is also lower than it is for clear glass.

As shown in Figure 3.2 PVB-film has a much higher absorption coefficient at wavelengths between  $1$  and  $4.5 \mu\text{m}$  than glass. The curves in the figure easily gives the impression that the wavelength band  $2.75$ - $4.5 \mu\text{m}$  is the optimal in order to get radiation through glass to the PVB-interlayer. Well, this is true if the glass is very thin, but as given above even  $3 \text{ mm}$  glass absorbs the major proportion of such a radiation before it reaches the PVB. So, the wavelength band  $1.7$ - $2.75 \mu\text{m}$  can be classified as the best for the purpose above. The absorption coefficients of the PVB-film above  $4.5 \mu\text{m}$  have not any effect on the heating speed of glass-film sandwich, because such radiation is absorbed by the surface glass.

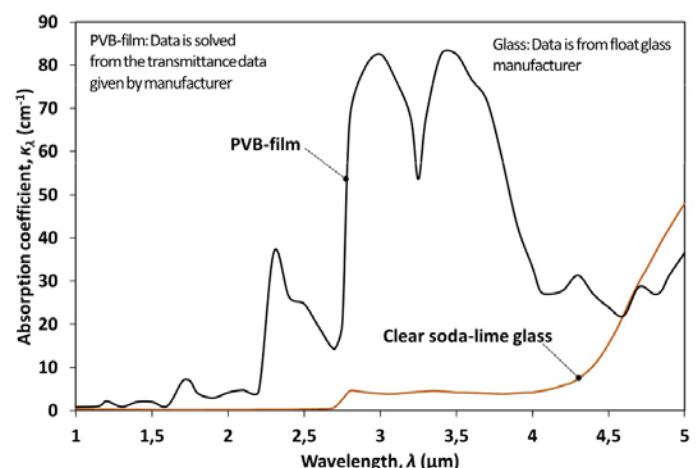


Figure 3.2 Spectral absorption coefficient of clear soda-lime glass and the PVB-film.

With the directional spectral reflectivity, spectral absorption coefficient and Bouguer's law Eq. (3.1) it is possible to formulate the directional spectral absorptance of a layer in glass-film sandwich. For total absorptances, the integration over the polar angle  $0-90^\circ$  is needed. Now, the Averaged Net Radiation method developed in [1] for clear and coated glass is applied in solving spectral total absorptances of layers in a glass-film sandwich. In this method, instead of the complicated integration, the special direction-averaged values are used for spectral reflectivity and penetration angle in a sandwich. The integration over wavelengths is covered by using wavelength bands inside which the radiative properties are quite wavelength-independent, which is a common method in the literature of the field. The radiative properties of some low-e coatings are given with details in [1], from which the following main points are chosen. A low-e coating changes glass surface reflectivity selectively. For visible light ( $0.4 < \lambda < 0.7 \mu\text{m}$ ), reflectivity remains almost constant, but at slightly longer wavelengths, reflectivity increases sharply to 0.8 - 0.97 depending on the coating. The coating itself also absorbs radiation, and its absorptivity is slightly dependent on wavelength.

#### 4. Description of the heat transfer problem

Figure 4.1 shows the schematic of a glass-film sandwich inside a laminating oven. The sandwich is exposed to radiation, and convection heat transfer between hot air and glass affects both surfaces. In Figure 4.1 the radiative heat flux is divided to two proportions. The proportion  $F_{G-R} \sum F_b(\lambda_i, \lambda_j, T) \sigma T_r^4 = q_{r2}$  stands for the radiative heat flux from the radiant heaters and the proportion  $(1-F_{G-R}) \sigma T_\infty^4$  stands for the radiative heat flux from other inside surfaces of the oven toward to the sandwich. Above  $F_{G-R}$  is the view factor from the sandwich to heaters, and  $F_b(\lambda_i, \lambda_j, T_r)$  is the fraction of radiative energy of a blackbody between the wavelengths  $\lambda_i$  and  $\lambda_j$  at temperature  $T_r$ . The division of radiative heat flux above is needed, because in some ovens the temperature of radiant heaters is clearly higher than the temperature of other surfaces. Then, the proportions consist of clearly different kinds of thermal radiation. Heaters emit shorter wavelength radiation, which can partly penetrate deeper into the sandwich. The radiation emitted by other surfaces affects only the outer surfaces of the sandwich alike convection. At  $200^\circ\text{C}$ , which is quite typical control temperature of a laminating oven, 91% of the radiative energy emitted is opaque for glass ( $\lambda < 4.5 \mu\text{m}$ ). In a laminating oven,

the sandwich is always so cold that only its outer surfaces are emitting radiation, and the emission increases when the glass gets hotter. Thermal conduction transfers heat from hotter to colder layers inside the glass-film sandwich. The problem is to solve the development of the thickness-wise temperature profile in a glass-film sandwich during heating in a laminating oven.

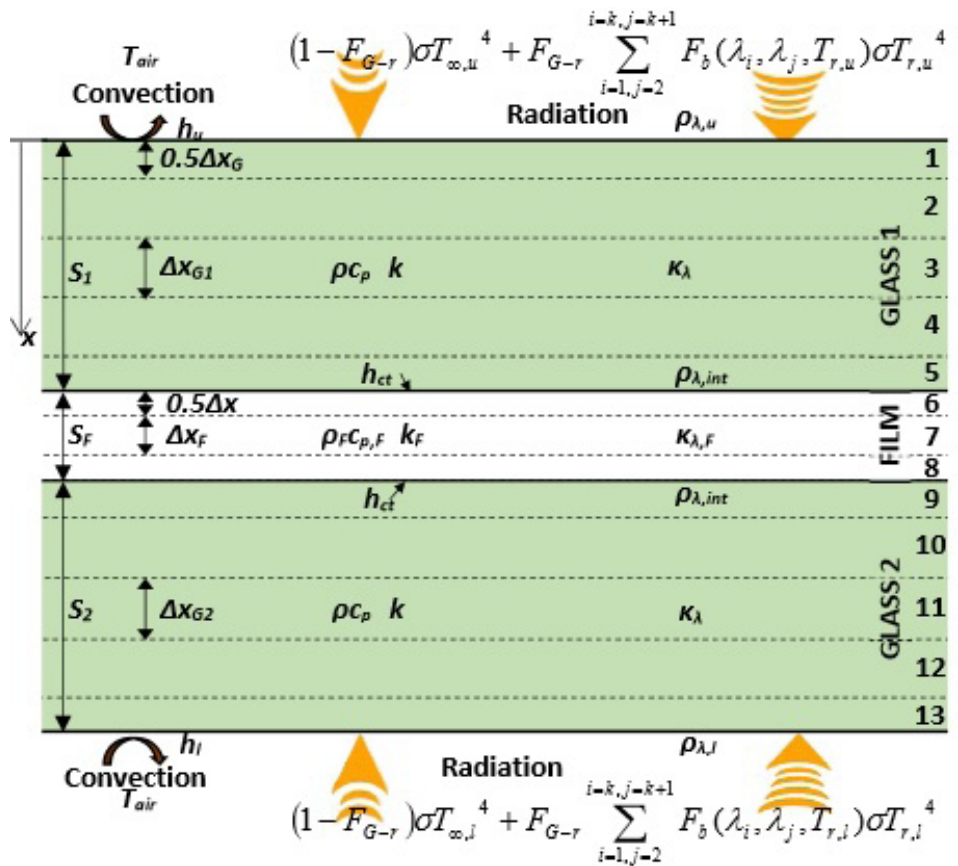


Figure 4.1 One-dimensional computation model for heating of a glass-film sandwich with radiation and convection

#### 4.1 Solving method

In the explicit finite difference method, the glass is divided into layers (volume elements), the calculation proceeds by time-step  $\Delta t$  at once and the results after the last time-step are used as initial data for the next time-step. In Figure 4.1, both glass thicknesses ( $S_1$ ,  $S_2$ ) are divided into five layers, and the film thickness  $S_F$  to three layers. The thickness of each surface layer is one half the thickness of the inner layer. Thus, the thickness step  $\Delta x$  in glass 1 is  $S_1/4$  and in film  $S_F/2$ . Glass density  $\rho = 2530 \text{ kg/m}^3$  and film density  $\rho_F = 1060 \text{ kg/m}^3$ . Now, specific heat  $c_p = 920 \text{ J/(kgK)}$  stands for the glass and  $c_{p,F} = 2100 \text{ J/(kgK)}$  for the film. In the inner layers of glasses and film heat transfer occurs by conduction between

adjoining layers and absorption of radiation emitted by heating resistors. Thermal conductivity  $k = 1 \text{ W/(mK)}$  stands for the glass and  $k_f = 0.25 \text{ W/(mK)}$  for the film. For instance, the energy balance for the inner layer 4 in Figure 4.1 can be written as

$$\rho c_p \frac{T_4^{p+1} - T_4}{\Delta t} \Delta x = k \frac{T_5 - T_4}{\Delta x} + k \frac{T_3 - T_4}{\Delta x} + S_{4,u} + S_{4,l} \quad (4.1)$$

where superscript  $p+1$  indicates the future after time-step  $\Delta t$ . In the energy balance, the temperature  $T_4$  covers the whole layer, but its accurate coordinate is in the middle of layer 4 at the thickness of  $3\Delta x$  from the glass upper surface. Net radiation is taken into account with source terms  $S_4$  written separately to upper and lower side radiation. The source terms for each layer in a glass-film sandwich in Figure 4.1 can be formulated in a corresponding way as in [1] for the clear and low-e coated glass.

In addition to conduction and radiation, convection also occurs in glass surface layers. Convective heat flux  $q_c$  can easily be specified using a convection heat transfer coefficient and temperature difference between air and glass surface  $q_c = h_u(T_a - T_l)$ . The evaluation of the correct value of the convection mean heat transfer coefficient is often difficult. Now, the convection mean heat transfer coefficient  $h_u = h_l = 50 \text{ W/(m}^2\text{K)}$  is used in the modelling of a convection oven, the value of which is based on measurements from Glaston ProL convection oven.

The efficiency of conduction from the glass to PVB-interlayer depends on the purity of the contact between them. In this method, the heat transfer through the interface between the upper glass and PVB-interlayer, for instance, is calculated from the equation  $q_{ct} = h_{ct}(T_5 - T_6)$ , where  $h_{ct} = 1000 \text{ W/(m}^2\text{K)}$  is the contact heat transfer coefficient. The value above is based on the measurements, which indicated that the value can be even higher. The exact value is not important for the accuracy of the modelling results in the next chapter, because the value is great anyhow.

## 5. Results

The ovens modelled are convection oven (oven 1), typical radiation oven (oven 2) and special radiation ovens with two kinds of radiant heaters (ovens 3 and 4). In oven 1, the convection heat transfer coefficient and heating air set temperatures are as in the Glaston ProL oven. The typical radiation oven is equipped with conventional heating resistors, keeping the oven temperature control thermocouple at a set value. In the special radiation ovens, extra heating resistors are forced on when the glass-film sandwich is in

their heating zone. It assumed that, when they are turned on, resistors instantly reach the heater temperature used in the modelling. This is certainly true in oven 4, because in practice a heater temperature of  $2,000^\circ\text{C}$  enables resistors to be thin filaments inside a quartz tubes alike in a light bulb. The operation of such a heating resistor is treated in detail in [2]. Now, the heaters are just black surfaces at given temperatures in the modelling. Table 5.1 defines the circumstances in the ovens modelled.

Table 5.1 Circumstances in the ovens modelled, when the glass-film sandwich is thin or thick.

| Oven                         |            |       | 1   | 2   | 3   | 4    |                      |
|------------------------------|------------|-------|-----|-----|-----|------|----------------------|
| Convection heat trans. coef. | $h$        | Thin  | 50  | -   | -   | -    | W/(m <sup>2</sup> K) |
|                              |            | Thick | 50  | -   | -   | -    |                      |
| Surface temperature          | $T_\infty$ | Thin  | 180 | 250 | 180 | 180  | °C                   |
|                              |            | Thick | 140 | 250 | 140 | 140  |                      |
| Air temperature              | $T_{air}$  | Thin  | 180 | -   | -   | -    | °C                   |
|                              |            | Thick | 140 | -   | -   | -    |                      |
| Extra heater temperature     | $T_r$      | Thin  | -   | -   | 500 | 2000 | °C                   |
|                              |            | Thick | -   | -   | 500 | 2000 |                      |
| Extra Heater power           | $q_{r2}$   | Thin  | -   | -   | 8   | 8    | kW/m <sup>2</sup>    |
|                              |            | Thick | -   | -   | 4   | 8    |                      |

The thin glass-film sandwich modelled consisted of two sheets of 3 mm glass and a PVB-film between them (Thin = 3 + 0.76 + 3 mm). The thick sandwich modelled consisted of four sheets of 4 mm glass and film layers between them (Thick = 4 + 0.76 + 4 + 0.76 + 4 + 0.76 + 4 mm). Three different cases for both sandwiches were modelled. In the first glasses were clear, in the second the top side and in the third the bottom side of the uppermost glass was low-e coated. In the modelling of the third case above, the radiative properties of the low-e coating against the PVB-film were assumed to be the same as in air interface. Ovens 1 and 2 represent the ovens on the market, so the comparison of their results gives practical information for those who are planning to invest in a lamination line, for instance. Ovens 3 and 4 are more theoretical. In these, the extra heater power was set as the same as the convection heating power at the beginning of the heating in oven 1, when the thin sandwich was modelled. The temperature of inside surfaces of the oven (excluding extra heaters) was also kept the same in ovens 1, 3 and 4. In the case of the thick sandwich with clear glasses (first case) the initial convection heating power in oven 1, and the extra heating power in ovens 3 and 4, was as high as possible to avoid uppermost glass top surface temperatures above  $85^\circ\text{C}$ . The heating powers was kept the same, when the sandwiches with a low-e coated glass (second and third case) were modelled. The maximum was limited to

8 kW/m<sup>2</sup> used with the thin sandwich. Such a procedure aimed to keep the comparison between convection and radiation heating more practical and comparable. In oven 1, the set air temperature was lowered from 180°C to 140°C to keep the temperature of the top surface of the thick sandwich below the limit above. The heating was assumed to be ready, i.e. the sandwich proceeds to the nip roll after the oven, when all PVB-film layers were above 60°C.

Figures 5.1-5.3 show the development of thickness-wise temperature profiles in the thin glass-film sandwich. Temperature profiles are given for heating times of 10, 20, 31 and

41 s, and the latest profile in each figure is taken when the heating is ready. Thus, convection oven 1 heats up the thin sandwich with clear glasses in 44 s, typical radiation oven 2 in 100 s, and so on. Special radiation oven 4 is 25% slower than special radiation oven 3, because it emits shorter wavelength radiation penetrating more through the thin sandwich. In all cases, the uppermost glass surface temperature is clearly below the limit above. The temperature profiles in oven 4 are clearly smoother because of short wavelength radiation absorbed by the film and glass interior. In it, the film clearly absorbs the radiation, because its temperature is higher

than the glass inner surface temperature. As seen from Figure 5.2, the low-e coating on the top surface of the upper glass has a very high impact on the heating speed of the sandwich in radiation ovens 2-4. Additionally, the temperature profile becomes very asymmetrical. For convection oven 1, the heating speed in Figure 5.2 is close to the heating speed without low-e coating in Figure 5.1.

If the low-e coating is in the bottom surface of the upper glass, as in Figure 5.3, its effect on heating speed is insignificant.

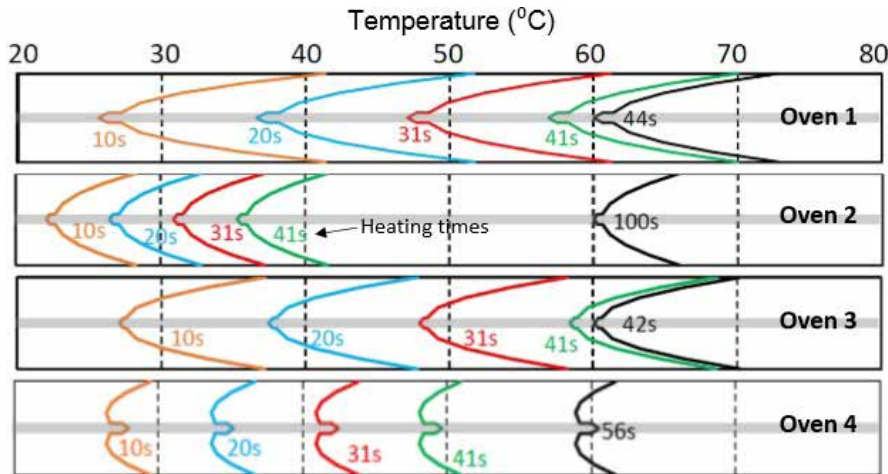


Figure 5.1 Calculated development of the thickness-wise temperature profile in thin (3+0.76+3mm) glass-film sandwich in ovens 1-4.

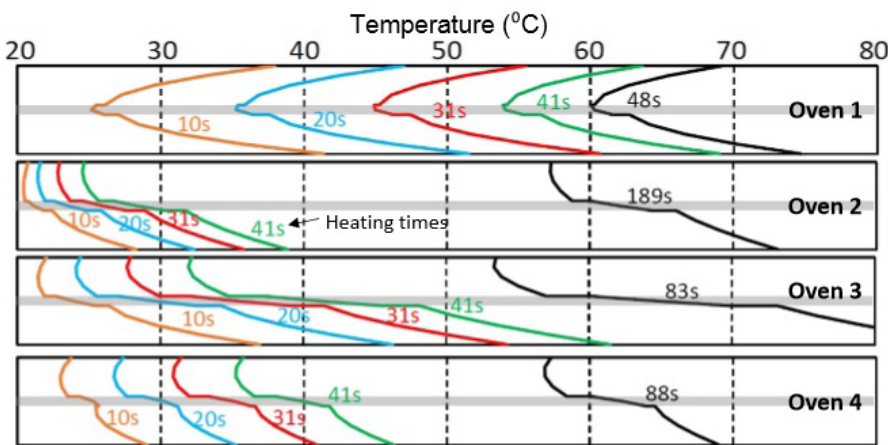


Figure 5.2 Calculated development of the thickness-wise temperature profile in thin (3+0.76+3mm) glass-film sandwich in ovens 1-4. The top surface of the upper glass is low-e coated.

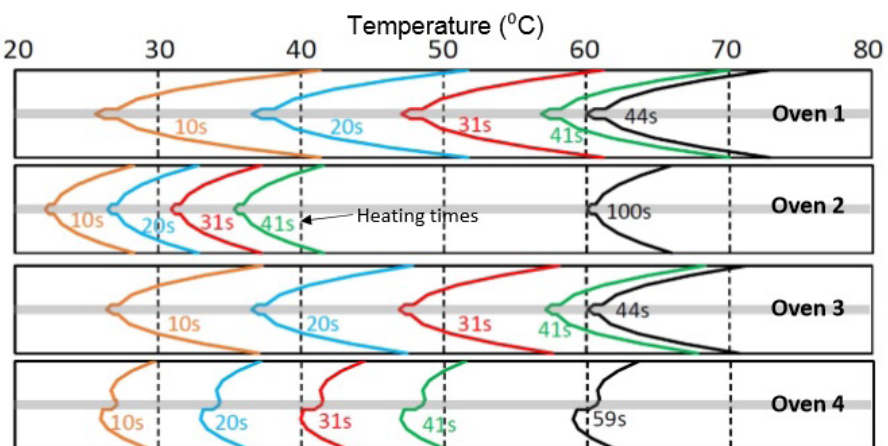


Figure 5.3 Calculated development of the thickness-wise temperature profile in thin (3+0.76+3mm) glass-film sandwich in ovens 1-4. The bottom surface of the upper glass is low-e coated.

Figures 5.4-5.6 show the development of thickness-wise temperature profiles in the thick glass-film sandwich. Temperature profiles are given for heating times 31, 92 and 153 s, and the latest profile in each figure is taken when the heating is ready. Thus, convection oven 1 heats up the thin sandwich with clear glasses in 231 s, typical radiation oven 2 in 315 s, and so on. The special radiation oven 4 is now the fastest, because only in it could the extra heating power be kept as the same as with the thin sandwich. Despite of that the surface temperatures of the sandwich are clearly lower as the ones in ovens 1 and 3. So, the extra heating power in oven 4 could still be raised. The thick sandwich is so thick that the short wavelength radiation emitted by the radiant heaters at 2,000°C is absorbed effectively into it. According to Figure 5.5, oven 4 is almost as fast as the convection oven 1 even for sandwich

in which top surface of the uppermost glass is low-e coated. In practice, the speed difference is higher, because the bottom surface temperature of the sandwich in oven 4 is clearly higher than the limit above. So, to keep the comparison balanced, the extra heating power in oven 4 should be cut by shutting down some heaters. If the low-e coating is on the bottom surface of the upper glass, as in Figure 5.6, its effect on the heating speed in ovens 1-3 is minimal. In oven 4, the heating time increases +12%, which in practice is still quite insignificant.

The results above match for the glass-film sandwich area excluding the area near the edges, where heat transfer is two or three (corners) dimensional. The edge area tends to heat up more quickly than the mid areas of the sandwich, because the surfaces in the

oven radiating heat above and below the mid-areas of the sandwich are more loaded by the cold glass-film sandwich, and cool more than other surfaces during heating. The edges of the sandwich are also an extra heat transfer surface, whose effect increases with sandwich thickness. It is unavoidable that the edge area heats up more quickly, but it is also desirable to ensure that edges are sealed, when the nip roll after the oven presses the sandwich. On the other hand, in de-airing it is important that the edges are not sealed before the nip roll, so that air can be pressed out from the sandwich. So, the temperature difference between the edge area and mid area of the sandwich is desirable only to certain limit. Now, only the following two sentences can be written considering the level of the edge heating problem above in radiation and convection ovens. The intensity ( $W/m^2$ ) of radiation heat transfer on the edge surface (thickness-wise

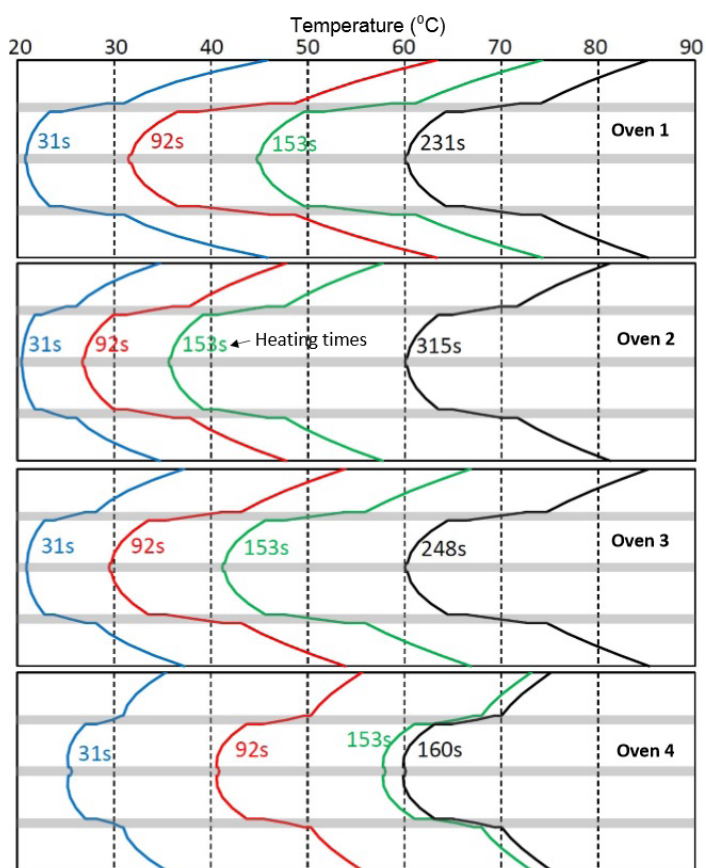


Figure 5.4 Calculated development of the thickness-wise temperature profile in a thick (4+0.76+4+0.76+4+0.76+4mm) glass-film sandwich in ovens 1-4.

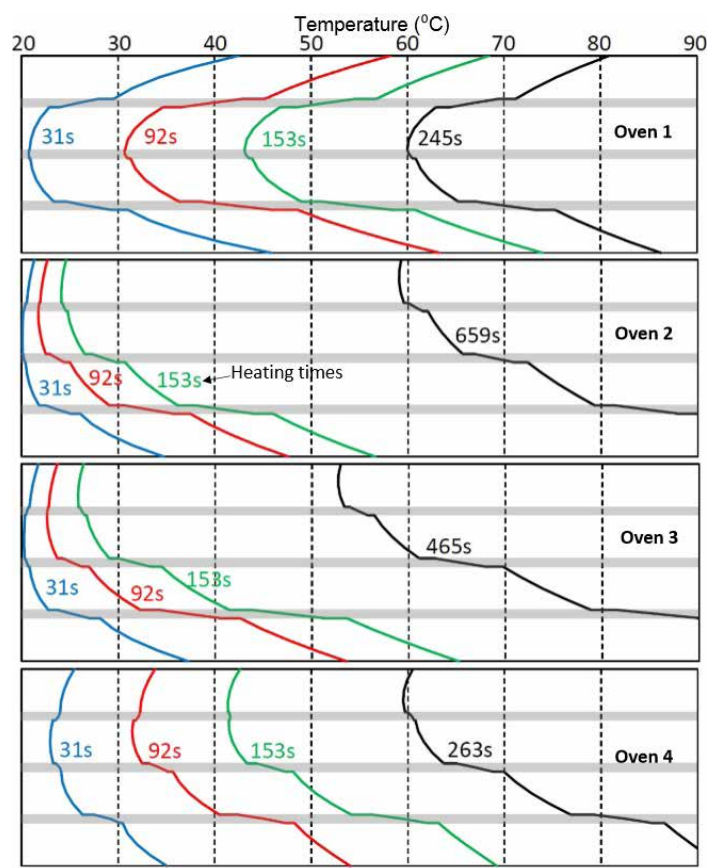


Figure 5.5 Calculated development of the thickness-wise temperature profile in a thick (4+0.76+4+0.76+4+0.76+4mm) glass-film sandwich in ovens 1-4. The top surface of the uppermost glass is low-e coated.

surface) is at least equal to the intensity on the main surfaces. The forced convection heat transfer coefficient is clearly smaller at the edges than at the main surfaces to which air jets are focused.

## 6. Conclusions

Forced convection heating in a laminating oven is the optimal solution particularly for thin glass-film sandwiches in which the convection heat is quickly conducted from surfaces through a glass to a PVB-film. Convection heating enables high line speed and/or short oven length, and is easy to control. As to heat transfer, a typical radiation oven equipped with relatively low temperature radiant heaters does not have any benefits compared with the convection oven modelled.

The wavelength band 1.7-2.75  $\mu\text{m}$  is the optimal to get radiation through the glass

to the PVB-film, and in such a way speed up the heating in a laminating oven and keep the thickness-wise temperature gradient in a sandwich smooth. Such a radiation helps particularly when the sandwich has more than two film layers. This benefit of radiation heating as opposed to forced convection heating can be utilized only with the heaters in which the resistor is a thin and hot filament in a protective gas inside a quartz glass tube. The filament temperature in such a heater should rather be about 2,000°C. A notable part of the radiation at the wavelength band above gets through a thin glass-film sandwich, which reduces the heating speed.

The glass-film sandwiches with clear and low-e coated surfaces can be processed with the same heating recipe when the rate of the forced convection is high enough, as in the convection oven modelled. In all kinds of radiation ovens, the line speeds must be

slowed down dramatically, when an outer surface of the sandwich is low-e coated. A low-e coating on the inside interface of the sandwich does not affect the line speeds.

## References

- [1] Rantala, M., Heat Transfer Phenomena in Float Glass Heat Treatment Processes. Tampere University of Technology. Publication, Vuosikerta. 1355, Tampere University of Technology, 2015.
- [2] Petterson, M. and Stenström, S., Modelling of an electric IR heater at transient and steady state conditions - Part 1: model and validation, International Journal of Heat and Mass Transfer, p. 1209-1222, 2000.

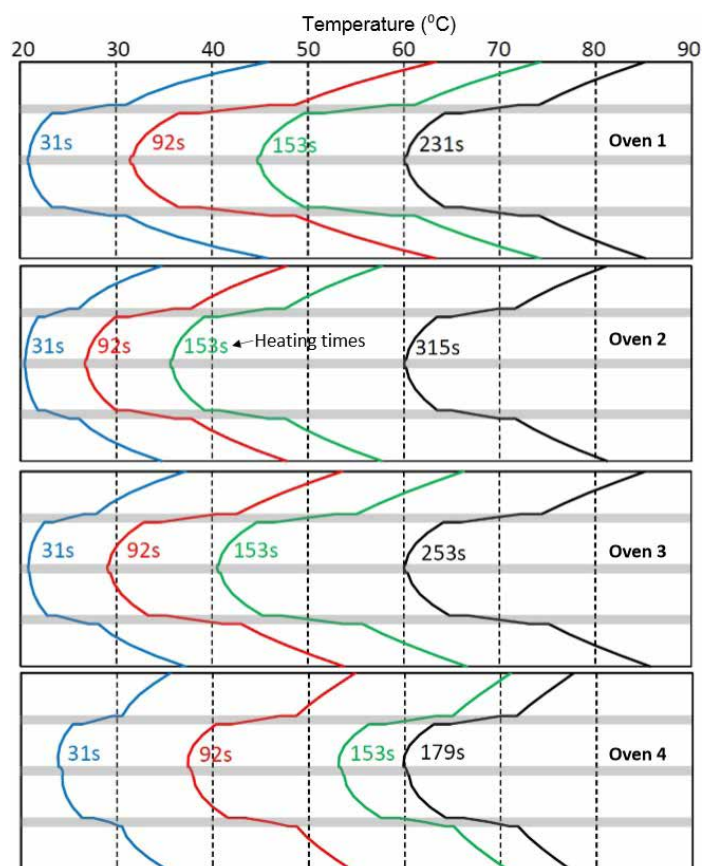


Figure 5.6 Calculated development of the thickness-wise temperature profile in a thick  $[4+0.76+4+0.76+4+0.76+4\text{mm}]$  glass-film sandwich in ovens 1-4. The bottom surface of the uppermost glass is low-e coated.

# Testing of Adhesion on Laminated Glass Using Photometric Measurements

Dr.-Ing. Peter Hof 1  
Prof. Dr.-Ing. Matthias Oechsner 2  
1,2 Technische Universität Darmstadt, MPA/IfW  
Darmstadt, Grafenstraße 2, 64283 Darmstadt

## Keywords

laminated glass, adhesion, photometric measurement, comparison

## 1 Abstract

The use of laminated safety glass instead of single glass sheets is especially important in order to mitigate the risks of potential post-breakage behaviour and thus for the fixation of glass fragments in case of damage to the glass. As well the whole component shall not fall out of the construction either. In Addition to this safety aspect, the utilization of the compound effect also allows a more economical design of the glass.

When the compound effect resulting from the bond is applied to laminated safety glass, the adhesion strength between the laminated foil and the glass pane must fulfil certain requirements, which have to be verified experimentally.

The presented paper reports on the results of various possibilities for determining the adhesion properties of laminated safety glass. The tests are carried out with one particular type of polyvinyl butyral (PVB) interlayer. The results of the well-known and commonly used pummel test are compared to a defined pull test as well as to results achieved by assessing the transmission of using photometric measurements. The transmission behaviour of light can be correlated to the moisture content of the PVB interlayer, using a phenomenologically based mathematical calculation rule in conjunction with a calibration standard.

The comparison of the results shows a good correlation between the adhesion strength value achieved by the pull test and the moisture content of the interlayer. Both results correspond also well to the results achieved by the established pummel test.

## 2 Introduction

Laminated safety glass products are commonly used in and on buildings. In particular, they are frequently utilized in overhead glass

constructions and glazings with fall-through protection.

Laminated safety glass is constructed using two or more discrete glass layers with an interlayer made of a specific type of plastic material positioned between the glazing sheets. The plastic interlayer causes several positive results for the product [3, 4]. First, by considering the compound effect, it provides the opportunity of achieving a more economical design of the laminated safety glass.

Second, laminated safety glass possesses the important property of sticking the glass fragments together, in case the glass sheet is damaged and broken. The post-breakage behaviour of the laminated safety glass provides damage tolerance to the laminated glass, improving its safety properties.

In order to be able to count on these positive effects, a reliable and robust verification method regarding the adhesive behaviour between the glass sheet and the plastic interlayer is an important issue. The producer of the laminated safety glass should be able to check this property during the production process.

As outlined below, there are several possibilities for monitoring the adhesion level. The so-called pummel test and the pull test are common approaches to check the adhesion behaviour directly. An alternate test method is based on measuring the light transmission of the laminated safety glass. From the transmission behaviour, the moisture content of the interlayer can be obtained, utilizing a calculation approach as well as a calibration standard. This moisture content is a direct indication factor for the adhesive strength. The glass structure was identical for all test samples. The test samples consisted of a multilayer glass structure with 2 x 4mm (nominal thickness) float glass and a foil (PVB) with a nominal thickness of 0.76mm.

## 3 Testing methods and results

### 3.1 Light transmission by spectrophotometry

#### 3.1.1 Method description

Using a spectrophotometer, the light transmission of multilayer glass panes has been determined. Initially, the light transmission of reference samples with three different moisture contents (measured by Karl Fischer Titration) was determined and converted to an absorption ratio (AR) using a

calculation method.

The transmission behaviour depends on the wavelength of the light. In addition, it also depends on the water content of the interlayer. Therefore it is possible to obtain the moisture content of the interlayer by the transmission rate. The absorption ratio was calculated from the light transmission values of four special wavelengths, which were local minimum (wavelength about 1700 nm and 1925 nm) and maximum values (wavelength about 1650 nm and 1875 nm).

The absorption A will be calculated as

$A(\text{wavelength}) = \log_{10}(100/\%T)$   
with T as transmission value.

The Absorption Ratio AR is defined as

$AR = [A(1925) - A(1875)] / [A(1700) - A(1650)]$ .

Details on the calculation procedure are given in [1].

In order to obtain a calibration standard, reference samples of 100mm x 100mm (length x width) with a thickness of 8.5 mm were investigated, which were delivered with a stated moisture content. Those reference samples were sealed around the edges of the pane by a self-adhesive aluminium strip as a moisture barrier. By correlating the measured absorption ratio to the stated moisture content, a regression line could be determined (Figure 1). To determine the moisture content in the test specimens, again 100mm x 100mm (length x width) samples were utilized. The photometric measurements on those test samples yielded AR values, which could be converted to the moisture content using the previously determined regression curve.

All samples were measured at two spots and from both sides of the pane. The mean value of those four determined absorption ratios for each sample was then used for further calculations.

The slit width of the measurement setup in our study was 2nm. The wavelength increment for the analysis was defined as 5nm.

Details on the experimental approach is described in the protocol "Measuring the moisture content in multilayer glass with a spectrophotometer" from the company Eastman, Issue August 2014, Rev. 5.[1]

## Reference Samples

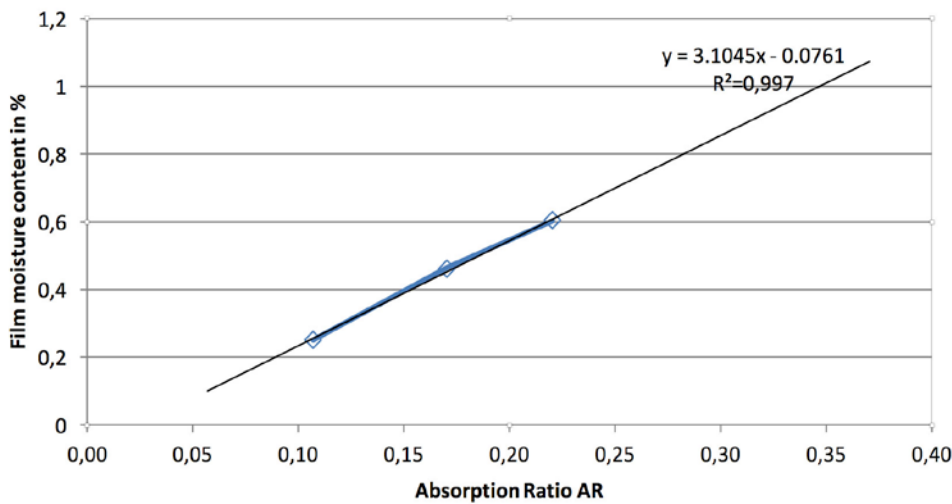


Figure 1: Results of the reference samples with linear regression

| Sample Name | Moisture as labelled in % | Averaged AR value (x) | Calculated moisture content in % (y) | Value of the difference between labelled and determined moisture in % |
|-------------|---------------------------|-----------------------|--------------------------------------|---|
| A214        | 0.214                     | 0.09319               | 0.213                                | 0.001   |
| B214        | 0.214                     | 0.09806               | 0.228                                | 0.014   |
| A449        | 0.449                     | 0.16339               | 0.431                                | 0.018   |
| B449        | 0.449                     | 0.16949               | 0.450                                | 0.001   |
| A648        | 0.648                     | 0.22279               | 0.616                                | 0.032   |
| B648        | 0.648                     | 0.22484               | 0.622                                | 0.026   |
| A798        | 0.798                     | 0.27646               | 0.782                                | 0.016   |
| B798        | 0.798                     | 0.26921               | 0.760                                | 0.038   |
| A1012       | 1.012                     | 0.34743               | 1.003                                | 0.009   |
| B1012       | 1.012                     | 0.33867               | 0.975                                | 0.037   |

Table 1: Results of the moisture content determination using photometric measurements

## Results of Pummel test in accordance to moisture content

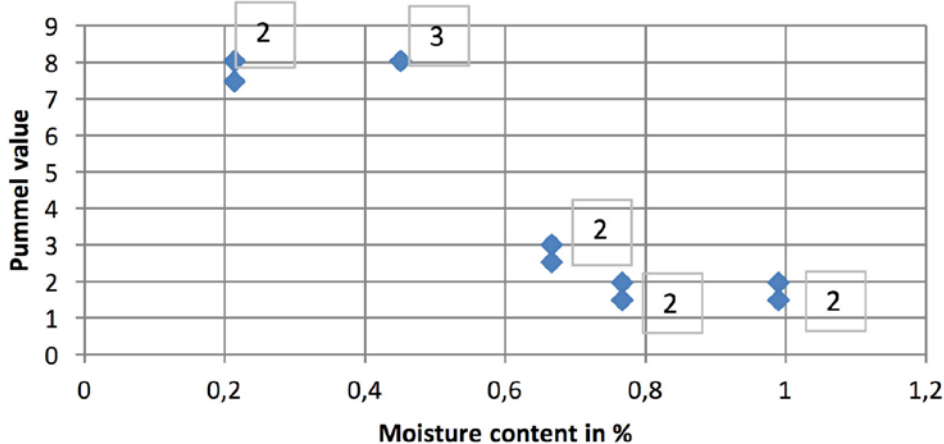


Figure 2: Results of the Pummel test, (The number in the box at the digit gives the number of the results for this pummel value.)

### 3.1.2 Results

A comparison of the moisture content determined by the transmission spectroscopy and by Karl Fischer Titration revealed deviations of less than 0.038 % in all specimens tested (Table 1), indicating an outstanding capability of the taken approach.

### 3.2 Pummel test

#### 3.2.1 Method description

The pummel tests were performed according to the instructions "ATAC Procedure P0006 Saflex DG Pummel Procedure 021114", dated 2014-02-13 [2]. Because of the stiffness of the used PVB interlayer the time between removal from the climate controlled environment (-18 °C) and the test was increased to seven to nine minutes. When testing earlier the high stiffness of the interlayer in addition with the low temperature could result in a brittle fracturing of the interlayer.

The samples were 100mm x 200mm (width x length). The samples' thickness was about 8.5mm.

The specimens were struck with hammer blows on both sides.

#### 3.2.2 Results of Pummel test

For glass specimens of five different moisture contents three pummel tests were carried out, respectively.

The results of the pummel test indicate approximately two regimes in Pummel value. While the specimens containing moisture below 0.67% show a high levels in Pummel value (7-8) specimens containing moisture of 0.67% and above show low Pummel values (<3).

### 3.3 Pull test

#### 3.3.1 Method description

Pull tests were performed to determine the adhesive strength again on five series of laminated glass samples of different film moisture contents. The dimensions of those test samples were 10mm x 40mm. The samples' length and width were measured to determine the relevant cross sectional area. The test samples consisted of a multilayer glass structure consisting of two panes of 4mm nominal thickness float glass bonded by a polyvinyl butyral interlayer of 0.76mm nominal thickness. An example of the experimental setup is shown in Figure 3 (a,b). The glass samples were glued to dove-tailed metal sliding blocks.

Because of the increased sensitivity of the film to moisture caused by the small sample size, the samples were delivered wrapped in film. To prevent moisture ingress during the time before the test, the exposed edges of the film were sealed with a self-adhesive aluminium strip. The strip was applied directly after



Figure 3: Experimental setup, a) overview, b) detail

unpacking the specimens.

The pull tests were performed on a universal testing machine with a crosshead speed of 0.5mm / min.

### 3.3.2 Results

Nearly all samples failed between the film and glass and thus could be assessed as "valid". The results of the mean values of the calculated tension of adhesive strength and the standard deviation are given for the five different moisture levels in Table 2. The adhesive strength in relation to the moisture content of the film is shown as well in Figure 4.

As shown in Figure 4, the pull test indicates a decrease in adhesive strength with increasing moisture content. This decrease can be approximated by a linear regression line. The sensitivity of the results of the pull tests was investigated with the statistical software R including all single values for the pull tests. The slope of the linear regression line for this data is -6.73 MPa/(% moisture). The standard deviation of this slope is calculated to  $\pm 0.8$ . This deviation together with a p-value of  $2.7 \cdot 10^{-8}$  for this analysis verifies the correlation between the moisture content and the adhesive strength. The coefficient of determination,  $R^2$ , is calculated to 0.943 regarding the mean values, which allows to explain the supposed inconsistency indicated by a lower adhesion strength for the lower moisture content of 0.65 % compared to the higher adhesive strength at the higher moisture content of 0.8 %.

| Moisture content of film in % | Number of specimens with valid failure | Adhesive strength in MPa |                    |
|-------------------------------|--|--------------------------|--------------------|
|                               |  | Mean value               | Standard deviation |
| 0.215                         | 5                                      | 18.58                    | 1.37               |
| 0.453                         | 5                                      | 17.15                    | 1.41               |
| 0.650                         | 5                                      | 14.66                    | 0.5                |
| 0.811                         | 5                                      | 14.77                    | 1.13               |
| 0.989                         | 4                                      | 13.42                    | 0.64               |

Table 2: Result of the pull tests

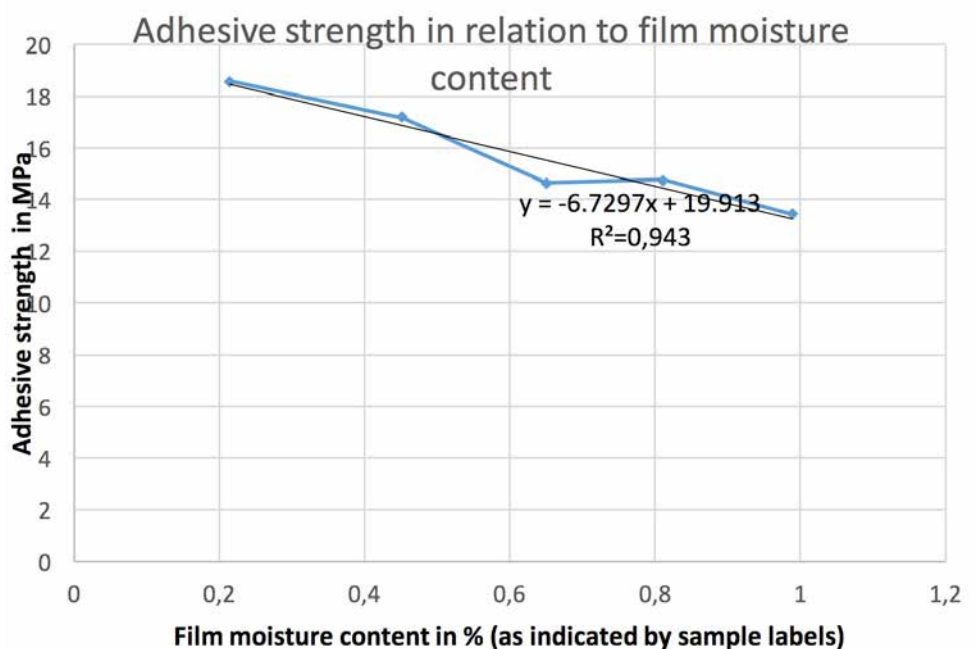


Figure 4: Adhesive strength in relation to film moisture (pull test)

## 4 Summary and Conclusion

Three experimental methods to determine the moisture content in laminated glass have been compared. All methods investigated have been demonstrated to be sensitive towards the moisture content. While the results obtained by the Pull test provide a direct measure of the adhesive strength of the interface, the results of the Pummel test and in particular the result of the light transmission spectroscopy allow only an indirect correlation to the adhesion properties.

Regarding the dependency of the measured signal on the moisture content, the Pull test and the light transmission spectroscopy indicate a linear correlation between the achieved value - Adhesive Strength and Absorption Rate, respectively - and the moisture content. This linear correlation is not seen at the Pummel test. Here, a high level and low level regime in Pummel value is indicated correlating low moisture contents to high Pummel values - and consequently to a better adhesive behaviour - and vice versa. These results, and the fact that the results for the moisture content measured via light transmission with an additional calculation routine are very precise, show that the measurement of the light transmission is an appropriate way to determine the existing moisture content in the laminated glass, and also therefore constitute an essential piece of information on the adhesive strength. This information is, in fact, paramount in assessing the performance of laminated safety glass as it relates to the safety aspect. It is also worth mentioning that the light transmission spectroscopy is the only approach investigated allowing a non destructive measurement of the glass panes, and thus might provide advantages regarding the capability of incorporating the measurement approach as a quality tool during production.

## 5 References

- [1] Measuring the moisture content in multilayer glass with a spectrophotometer, Eastman, Issue August 2014, Rev. 5.
- [2] ATAC Procedure P0006 Saflex DG Pummel Procedure 021114, Eastman, Issue 2014-02-13
- [3] Franz J., Schneider J., Untersuchung zum Resttragverhalten von Verbundglas, 2.Darmstädter Ingenieurkongress Bau und Umwelt, Darmstadt, Germany,
- [4] Butchart, C., Overend, M. Delamination in fractured laminated glass, Engineered Transparency 2012, Düsseldorf, Germany

# Which Interlayer for Which Glazing Application?

Björn Sandén  
Kuraray Europe GmbH

## 1. Introduction

Laminated glass as we know it today was originally produced with PVB which was developed and patented exactly 80 years ago. Its original application was to increase the safety of automotive windscreens by combining the properties of glass with the properties of a thermoplastic polymer modified with a plasticizer.

The first requirement for the PVB interlayer was enhanced safety through glass shard retention and later on impact performance. To achieve this, polymer chemistry and interlayer thickness were modified consecutively to meet the increasing requirements of the automotive windscreen. For the first 50 years this was the only application for PVB with well-defined requirements and specifications: 0.76mm caliper, a controlled adhesion to meet the impact performance and in some cases tinting of the interlayer for esthetical and shading requirements.

The use of laminated glass in architectural application started to develop about 35 years ago. It was originally driven by the following requirements of the building industry:

- Increased daylighting in building through more glass surfaces
- Development of safety standards in building codes

More recently, new requirements have added challenges to the performance of laminated glass:

- UV filtration performance
- Acoustic performance
- Larger glass panes and minimally supported glass.
- Post breakage performance
- Enhance glazing system performance for:
  - Blast and ballistic resistance
  - Very high wind load and debris resistance for hurricane sensitive areas
- Concerns about the safety performance of tempered glass
- Durability and performance in open edge and silicone sealed applications.
- Changes in colour and transparency/translucency
- Material inclusion and combination with glass coatings

Laminated glass is also increasingly challenged to help meet the energy control requirements imposed on new and retrofitted buildings.

These requirements have led to a dramatic increase of interlayer solutions. At the beginning some of these challenges were met through modification of the original "automotive" PVB: Interlayer thickness ranging from 0.38mm up to 4.56mm or more, sheet size increase and introduction of colors for architectural applications including translucency.

However, as the architectural laminated glass market was maturing, the original PVB recipe proved to have its limitations for architectural applications. This led to the modification of the PVB recipe for applications such as enhanced acoustics, and the development of other polymers such as ionomers and EVA. The paper "Laminated Glass and interlayers – Breaking the Myths" by Ir.-Arch. Reinout Speelman and Dr. Gerard Savineau presented at GPD 2013 gives an overview of the main interlayers used in modern laminated glass. In this paper I will be covering more in details the applications of laminated glass.

## 2. Lamination process, quality and cost:

While laminated glass and its interlayer have considerably evolved during the last 80 years, so did the lamination process. This was important to increase the product availability, allow innovation through new products and improve the cost position of laminated glass for the construction industry

### a) Roller line:

Most of the laminated glass produced worldwide is produced on this type of line. The improvements in this technology together with improvement on the processability of the interlayer have led to automated lines with high yield and high throughput. This allowed the production of laminated glass up to 321cmx600cm at very competitive costs and price. These lines have been the main driver for the high growth of laminated glass in Europe.

Following this process, the glass needs to be autoclaved to complete the lamination process.

### b) Vacuum bag and vacuum ring line:

More complex laminated glass constructions, such as curved glass, some types of multi-layered make-ups and less conventional glass shapes and geometries will require this type of lamination process. It is more labor intensive and has a lower productivity, but gives a high level of flexibility and yields which can be important when high value glass and interlayer are used.

This process generally also includes a vacuum cycle, but some lamination line manufacturers also offer a system without autoclave, a solution generally selected for its low investment.

The lamination costs is an important part of the total cost.

Another recent factor on cost and price is the latest generation of structural interlayer that allows to down gage the glass thickness under specific load conditions reducing the total cost of the construction. With glass price increasing exponentially with thickness, this feature is important at high load conditions and for reduced glass support conditions.

## 3. Which interlayer is used for which application?

### a) Standard PVB:

This interlayer is still used in more than 70% of the applications. Its primary function is to enhance safety or security performance of the glazing and at the same time improve the acoustic and UV protection performance in single and double glazed units. Its main application is in traditional four side supported glazing in windows and façade systems. It is still used in special glazing application such as overhead, floor and balustrade applications, but is getting increasingly replaced by more performant interlayers for those applications.

### b) Structural interlayers:

There are basically 2 families of structural interlayers:

- Ionoplast interlayers
- Stiff PVB (low plasticizer)

These interlayers with much higher shear and elastic modulus enhance the coupling between the glass panes increasing the strength of the laminate. Stress and deflection are reduced which will allow the use of lower laminated glass thickness and/or increased glass span. The extra stiffness of the interlayer does also enhance post breakage performance, especially in tempered laminated constructions which is a limitation with standard PVB. These enhancements make these interlayers particularly well suited for structural applications such as:

- Minimally supported glass constructions
- Overhead glazing
- Structural balustrade systems.
- Replacement of glazing systems made-up with a monolithic tempered glass system (Eliminate risks related to nickel-sulfide spontaneous breakage)

Mechanical properties of the interlayer are dependent of temperature and load duration. For applications with longer load duration and/or higher temperature the ionoplast structural interlayer will have higher mechanical properties and is therefore generally selected.

#### c) EVA:

EVA which is only processed in a vacuum bag process is mainly used for the encapsulation of photovoltaic cells and decorative materials such as fabrics.

## 4. Other performance enhancing interlayers

### a) Acoustics

Although standard PVB already provides acoustic improvement vs a monolithic glass, the increasing noise issues in our society has led to the development of highly performant acoustic PVB interlayers. Separate paper by Dr.B. Koll does give more details about these interlayers.

### b) Security enhancing interlayers (Blast, Intrusion, Ballistic, Anti-Spalling)

Laminated glass solutions for these applications are generally specially tailored for a specific application. The quality of the glass is only a part of the solution. Framing systems and other hardware will contribute to an effective system for the defined threat. For blast performance, A large number of testing data from arena and shock tube testing has been generated for standard PVB and ionoplast. Engineers and consultants have been selecting between these two interlayers depending on the level of compliance or rigidity needed after glass breakage. For ballistic applications, the codes require the

glazing to stop the specified ammunition, and to also stop the glass spalls to be projected from the back glass into the room. Bi-layers composed of a interlayer coupled to a polyester film and laminated as a cladding on the back glass will offer that extra protection. The polyester film is coated with a hard coat to enhance scratch resistance.

Polycarbonate combined with a Polyurethane interlayer is another combination used between glass or as back cladding for high security applications.

### c) Natural disaster glazing

Codes in Florida have driven the use of laminated glass to meet the testing requirements developed to resist the flying debris and the wind pressure caused by hurricanes. Different classification levels will define the glass type and the window system design required. Ionoplast interlayers with a 2.28mm thickness will resist the higher classification. Standard PVB will meet the lower classifications.

### d) High and low UV transmission requirements

Standard interlayer block UV radiation up to 380 nm. In some cases an extra protection up to 400 nm is required and can be achieved through PVB interlayers with a higher level of protection. A typical application for this type of interlayer is glazing for museums. Other applications will require the full UV spectrum to pass through the glazing. This is for example the case for greenhouses. Special grades of PVB or Ionomer interlayer with high UV transmission should be used in this case.

### e) Durability

Durability of laminated glass will depend of a number of factors:

- Quality of the lamination process.
- Quality of the glass. Specifically in tempered glass the level planarity is a critical factor.
- Procedure and quality of the glass installation.
- Glass fixation system.
- Interlayer selection: Type and thickness.
- Exposure of the glass edges to moisture, temperature and sealants.

Durability requirements in building applications are increasing. In the past 20 years the composition of the interlayers has been improving to meet these requirements. There are however still differences in performance, especially with regard to the sensitivity to develop defects at the edges. Interlayer suppliers should be consulted to understand these differences and select the right interlayer for the specific application.

### f) Low iron glass(extra clear) applications

When laminated glass made out of low iron glass is specified, it is generally to obtain a neutral glass color. Choosing an interlayer which will match the clarity of the glass is in this case very important. This can be achieved by selecting a high clarity PVB or Ionomer interlayer

### g) Coated glass application

Including a coated glass in a laminated glass application is possible. It may require some adjustment to the lamination process since some of the coatings will affect the ability of the glass sandwich to absorb the heat in the laminating oven.

If the coating is required to be laminated against the interlayer, compatibility between the coating and the interlayer needs to be evaluated to avoid issues of discoloration or loss of performance.

### h) Colored and decoration enhancing interlayers

Most of the commercial interlayer have the possibility to be colored. Tinted interlayers can be used to avoid the use of a tinted glass, but are also developed to meet the growing requests by architects and specifiers for custom colors.

Commercial tinted interlayer range from transparency, though different levels of translucency to full opacity and have been developed to meet architects color requirements in a durable way.

Inclusion of materials to be sandwiched between two interlayers is possible such as polyester mesh. The choice of the right type of interlayer is often based on a qualification program to ensure the right quality.

### i) Intelligent glass:

Special layers such as a photochromic layer can be embedded between 2 interlayers. This glass is used to vary the level of shading in the building.

## 5. Codes and glass thickness design and selection:

The first calculation methods for laminated glass were assuming zero coupling transmitted by the interlayer between the glasses. This very conservative approach has led in many cases to too thick glass specifications for the specific load requirement. Recent research work has led to a better characterization of the strength of laminated glass which was eventually reflected in national and international codes. The introduction of structural interlayers has also driven the code bodies to introduce differentiation within the laminated glass "family". In the USA, ASTM 1300 has already

design charts for Ionoplast structural interlayer and there is a similar development going on in China.

In Europe the CEN norm on glass strength EN16612 and EN16613 are still in development. Laminated glass is characterized by an equivalent thickness which is calculated by a factor Omega. Interlayers are grouped in families based on their mechanical properties. The structural interlayer will be classified in the highest class resulting in the highest equivalent thickness. This code will however also allow the use of E and G modulus which is preferred by engineering offices for more complex glass design cases. As the standard is not yet approved, special general approval has already been delivered for ionoplast structural interlayers for Germany and France.

## 6. 'Conclusion:

Modern construction without laminated glass is no more an option to meet the architect and specifiers need and at the same time meet codes and regulations in place. At the same time global challenges of the our industrial world are calling for some new glazing solutions. Interlayer suppliers have been able to address some of these challenges through innovative products and will continue to do so in the coming years.

# Effect of different sources of interlayer modulus data for glass design: the structural PVB case

Wim Stevels  
Eastman Chemical Company

## Keywords

1=Laminated glass 2=PVB interlayer  
3=Structural PVB 4=Torsion 5=Glass design  
6=Modulus

## Abstract

Interlayer modulus influences the stress laminated glass experiences under load. The determination of interlayer modulus data is complex, and the design engineer would rely in most cases on interlayer modulus properties as determined on the foil, as published by the interlayer producers.

For a structural PVB type interlayer, the modulus values of the interlayer as expressed in laminated glass, have now been determined using torsional glass laminate testing on specimens of 360 \* 1100 mm. Load cases at 0 °C, 23 °C and 40 °C have been studied for durations up to one month, covering many conventional load scenarios as experienced by buildings. In addition, allowable modulus values for design for this PVB type have become available through a recent German national approval for fixed load scenarios, and more flexibly for other load scenarios, through a Prony-series approach.

This paper aims to present the different type of modulus data that have recently become available in terms of conventional load scenarios, and analyze the effect of different modulus data sources on effective thickness. This allows the design engineer to make an informed choice around modulus data used for modelling, and choose values as appropriate for specific project design.

## Introduction

Interlayer modulus properties are typically determined through measurements on the interlayer film directly using some form of dynamic mechanical analysis. Data are collected at various temperatures, over a range of frequencies e.g. typically in a 0.1 to 100 Hz range, see e.g. ISO 6721 [Plastics - Determination of dynamic mechanical properties] [1], or specifically for interlayers in prEN 16613 [Determination of interlayer mechanical properties] [2]. Some specific

recommendations have been made based on a comparison of different methodologies for interlayer materials [3, 4, 5], and references cited therein. As interlayers are viscoelastic materials, the modulus of the material is a function of time (load duration) and temperature. The combined results of the measurements are translated to a so-called mastercurve of the material at a specific temperature using time-temperature superposition. This allows the determination of interlayer modulus values under load durations that far exceed the frequency domain over which the measurements took place. For this approach to be valid, it is important that the materials are rheologically simple, and no combination of physical processes, such as moving through both a glass-transition and melting temperature, should take place during the measurement or in the time-temperature range to which the properties are transposed [6]. Schneider et al. [7] concluded that poly(vinylbutyral) (PVB) materials are rheologically simple in contrast to some other interlayer materials e.g. poly(ethylene-co-vinylacetate) or poly(ethylene-co-methacrylic acid).

Structural or stiff PVB interlayers have only recently found wider use in structural and other glass applications [8]. Thus far, no data are available that compare the modulus properties as determined on the interlayer to values determined directly in laminated glass for this class of materials. Torsion tests are one test procedure that can be used for the determination of interlayer modulus values as a function of time and temperature. Other forms of testing are available, such as 3- or 4-point bending studies, or deformations in a circular geometry (ring clamping), but torsion testing has the advantage that it leads to very uniform deformation of the specimens, and clamping effects can be minimized. After installing, aligning and fixing a 3600 \* 1100 mm laminated glass pane, a specimen is torsion twisted using displacement-controlled loading up to a twist angle of 2°. A schematic representation is given in Figure 1. The twist angle  $\alpha$  is maintained for the duration of the experiment and at the same time, the corresponding reduction of the applied force necessary to maintain the angle is measured digitally. This methodology was developed by Kasper [9], and improvements were proposed later [10]. Experiments of this nature were

executed for a structural PVB interlayer at 0 °C, 23 °C (up to one month) and 40 °C (one hour). This comprises a wide range of potential load scenarios for buildings.

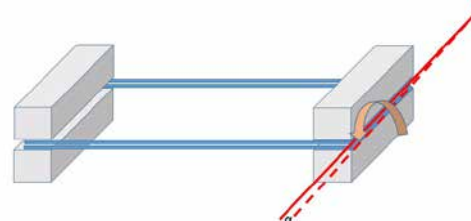


Figure 1. Schematic representation of a laminate torsion test. The glass laminate specimen is clamped stationary on the left, whereas the clamping of the right can be torqued over angle  $\alpha$ .

With modulus data available from different sources, such as different DMA methods, methods using glass laminates and data provided in standards in standards and national approvals, it becomes important to develop an understanding of the relevance of different modulus values for glass design. Therefore, this paper will examine the effect of different interlayer modulus data sources on effective thickness.

## Experimental

To prepare the experimental glass laminates for torsion testing, two nominally 6 mm glass panes of 3600 \* 1100 mm were laminated with two layers of 0.76 mm Saflex® DG41 structural interlayer to a total thickness of 1.52 mm interlayer in a nip-roll process.

Two different test set-ups for the execution of the torsion measurements were used at two different independent research institutes, one with the glass laminates mounted horizontally (set-up 1, experiments at 23 and 40 °C, annealed glass (EN 572)) and one with laminates mounted vertically (set-up 2, 0 and 23 °C, strengthened glass (EN 1863)). In both cases, experimentation was executed in a temperature controlled, isolated chamber. Temperature control to within 1.5 °C was achieved, and multiple temperature monitoring points were set-up for use during experimentation. At least 3 samples were tested under each measurement condition. In both set-ups, monolithic glass specimens of 12 mm thickness were used as control species,

specifically for slip during experimentation. A detailed description of the experimental test-ups, data treatment and individual experiments is beyond the scope of this article. In general, the approach taken in [9] was taken. The results of the two test-ups at 23 °C were very similar. The data of set-up 2 were used for this article for the experiments at 23 °C. Dynamic mechanical analysis (DMA) was used to measure modulus values directly on the film using a Discovery HR-2 hybrid rheometer using an 8 mm plate/plate characterization. An extensive overview of measurement details and data transformation was published [4].

## Results and discussion

### 1. Torsion test data

An overview of the modulus data generated using the torsion set-up on laminates, and the data generated using DMA is given in Figure 2. Data for torsion relaxation under one minute are not readily accessible using torsion testing, as during the time required to apply the angle, relaxation also occurs. Therefore, data are presented for durations of one minute and longer.

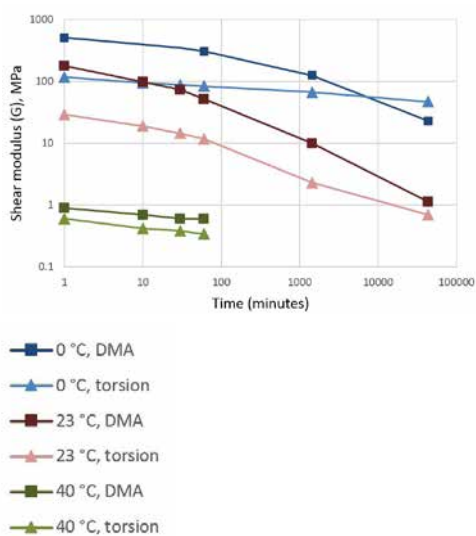


Figure 2. Modulus data of Saflex® DG structural PVB interlayer generated using DMA (squares) and laminate torsion (triangles) type measurements. Data points were collected at 1 minute, 10 minutes, 30 minutes, 1 hour, 1 day and 1 month.

A viscoelastic reaction of the interlayer can be seen in all torsion tests. The generic shape of the curves at 23 and 40 °C is very similar in nature to the shape of the curves from the DMA measurements, whereas the torsion curve at 0 °C is relatively flat. It is unclear at this point why this would be the case, but the high rigidity of the assembly under the measurement conditions may play a role. From

a glass design perspective, the interlayer in glass at 0 °C still behaves very rigid in a glass laminate, and essentially full shear transfer is a realistic assumption for durations up to at least 1 month, whichever measurement method is used.

In general, the modulus values determined in torsion testing of laminates are lower than those determined using DMA directly on the film. Given the very different nature of these experiments in terms of sample size, type of deformation applied, time scale of the experiment and data treatment, it is not surprising that differences would occur. Rather than trying to consolidate the data, we wanted to explore the effect of different modulus data sources on glass design and different load scenarios will be assumed, each at their specific duration and temperature. The required modulus data are not always available from the torsion test data as they are non-continuous in nature. Generating curves over a wide range of temperatures is very cumbersome and requires lengthy experimentation. Even if this effort made, the short term modulus values are not accessible because of the experimental constraints. Therefore, we decided to use the data from a German nation approval as a conservative proxy for the torsion test data. This is illustrated in Figure 3.

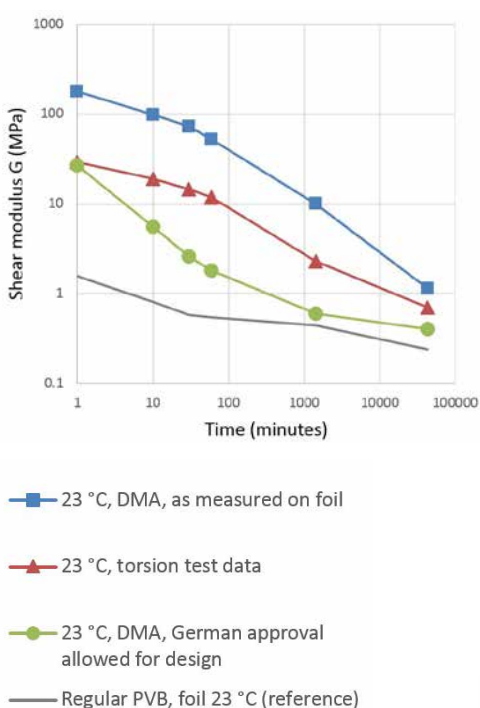


Figure 3. Modulus data of Saflex® DG structural PVB interlayer at 23 °C generated using DMA (squares) and laminate torsion (triangles) type measurements, and as derived from a German National approval (circles) and a regular PVB foil as reference. Data points were collected or calculated at 1 minute, 10 minutes, 30 minutes, 1 hour, 1 day and 1 month.

The data from the German national approval were always more conservative than the torsion test data, and since a Prony series is provided, modulus values can be calculated with any load scenario, as long as the boundary conditions for time and temperature are respected. Over the entire duration range, the data of structural PVB are significantly higher than of a regular PVB type, even if the conservative German data are taken. As compared to the data measured in a glass laminate, the difference is close to a decade in modulus values over the entire duration, even more for the data obtained in the same way, directly measured on the foil. This is a clear indication of the design possibilities of structural PVB's.

### 2. Modulus and effective thickness

Before exploring the effect of different sources of modulus data on the design, it is helpful to develop an understanding of the effect of interlayer modulus on glass behavior. This can be done using FEM modelling, or analytically in an effective thickness approach. In the effective thickness approach, the thickness of a monolithic glass is calculated that would behave as the laminate for stress or deflection. Details of this well-known approach are e.g. provided in their basic form in standards such as ASTM 1300 Annex X9 [12] and prEN 16612 [13]. More refined approaches are available [14, 15]. In contrast to FEM methods, the results are readily reworked by others. In Figure 4, the effective thickness for stress and deflection is plotted as function of interlayer modulus for a 66.2 configuration with a short side of 2 m as calculated per ASTM 1300 Annex X9.

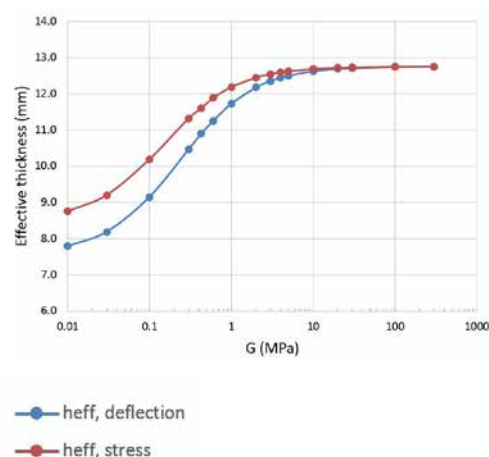


Figure 4. Effective thickness for stress and deflection calculated per ASTM 1300 X9 for a 66.2 interlayer configuration with a short side of 2 m

It can be calculated that 70 % of the potential increase of effective thickness for stress is achieved at a modulus of around 0.4 MPa, and 90 % of the potential increase of effective thickness at 2 MPa. For a configuration with short side of 1 m, these values would be 1.5 and 5 MPa respectively, and for a relatively unfavorable scenario of 1212.4 configuration with a short side of 1 m, these values would be 5 and 20 MPa respectively. Although the values of 70 and 90 % have been chosen arbitrarily, high absolute interlayer modulus values are not required to drive significant increases in effective thickness, and ultimately glass design.

### 3. Selecting modulus data for design

To assess the effect of using different sources of modulus data for structural PVB, load scenarios had to be assumed. Although these tend to vary by applicable standard and code, use class, and other building related aspects, common load scenarios include wind loads, live loads, snow loads and climate loads. As a reference, the load scenarios provided in prEN 16612 were used as general guidance [13]. An overview is provided in Table 1. As structural PVB can be classified as an interlayer from the highest stiffness family, the associated default shear transfer coefficient is listed for each load scenario for this stiffness family.

| Number | Load Scenario                                    | Duration   | Temperature interval (°C) | Default $\omega$ |
|--------|--|------------|---------------------------|------------------|
| 1      | Wind gust load (Mediterranean areas)             | 3 seconds  | 0 to 35                   | 0.5              |
| 2      | Wind gust load (other areas)                     | 3 seconds  | 0 to 20                   | 0.7              |
| 3      | Wind storm load (Mediterranean areas)            | 10 minutes | 0 to 35                   | 0.1              |
| 4      | Wind storm load (other areas)                    | 10 minutes | 0 to 20                   | 0.5              |
| 5      | Personnel balustrade loads - normal duty         | 30 seconds | 0 to 30                   | 0.5              |
| 6      | Personnel balustrade loads - crowds              | 5 minutes  | 0 to 30                   | 0.3              |
| 7      | Maintenance loads                                | 30 minutes | 0 to 40                   | 0.1              |
| 8      | Snow load - external canopies                    | 3 weeks    | -20 to 0                  | 0.3              |
| 9      | Snow load - roofs of heated buildings            | 5 days     | -20 to 20                 | 0.1              |
| 10     | Climatic loads on insulating glass units: summer | 6 hours    | 20 to 40                  | 0.1              |
| 11     | Climatic loads on insulating glass units: winter | 12 hours   | -30 to 20                 | 0.3              |

Table 1. Overview of load scenarios in prEN 16612\* and associated default shear transfer coefficient  $\omega$

\* load scenarios taken from the latest draft version available to the author, subject to change

Table 2 lists the different values of the modulus associated with each of these load scenarios as available from 1) DMA data as provided by the producer, 2) calculated allowable for design values from a German national approval, 3) minimum values for G required for classification in stiffness family 3. In the latter case, the relation between Young's modulus E and shear modulus G was taken as  $G = E/3$ , assuming a Poisson ratio of 0.5 for the interlayer.

| Load Scenario, Number | Shear modulus (G) Saflex DG41, MPa |                                  |                                    |
|-----------------------|------------------------------------|----------------------------------|------------------------------------|
|                       | Producer film data                 | Allowed for design, Germany [11] | Min. value stiffness family 3 [12] |
| 1                     | 27                                 | 5.3                              | 6.7                                |
| 2                     | 341                                | 147                              | 33                                 |
| 3                     | 0.9                                | 0.6                              | 0.3                                |
| 4                     | 180                                | 15                               | 6.7                                |
| 5                     | 39                                 | 4.9                              | 6.7                                |
| 6                     | 6.8                                | 1.2                              | 3.3                                |
| 7                     | 0.6                                | 0.4                              | 0.3                                |
| 8                     | 23                                 | 25.7                             | 3.3                                |
| 9                     | 6.5                                | 0.6                              | 0.3                                |
| 10                    | 0.5                                | 0.1                              | 0.3                                |
| 11                    | 37                                 | 1.0                              | 3.3                                |

Table 2. Overview of modulus values from different sources for the load scenarios of Table 1 for a structural PVB interlayer.

The absolute values can differ substantially, with the absolute values almost always the highest for the directly measured material properties, as expected. The allowed values for design in Germany and the minimum required in European standard are relatively close in most cases. Since the absolute modulus values do not drive glass design, but rather the extent to which the modulus values are high enough to drive shear transfer between the glass design, these modulus values were translated to effective thickness increases. The load scenarios of Table 1 were used to calculate the effective thickness increase of a 1212.4 configuration with a 1 m short side using the modulus values in Table 2, except in the case of prEN 16612, where the default  $\omega$  values were used. The configuration used is one where the conditions for shear transfer are relatively unfavorable (thick glass, thick interlayer, smaller pane), as a conservative approach. These results were expressed as a fraction of the maximum effective thickness increase as calculated for hypothetical modulus values of  $G = 0.001$  MPa for the lower limit and  $G = 1000$  MPa as the upper limit. These values correspond to an effective thickness for stress of 17 and 25.5 mm, respectively. The results are expressed in Figure 5.

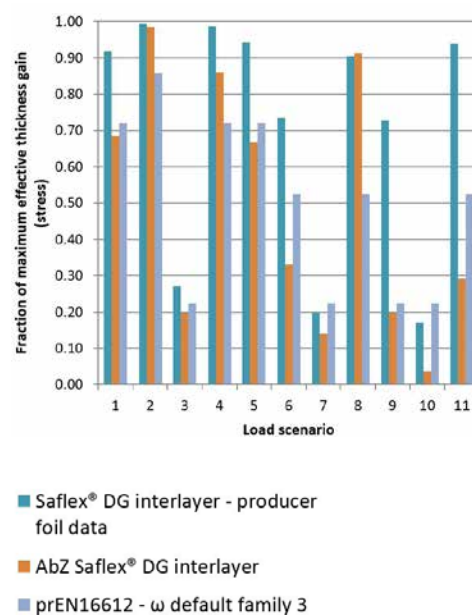


Figure 5. Effective thickness increase for stress calculated per ASTM 1300 Annex X9 for a 1212.4 glass configuration with a short side of 1 m, as fraction of the maximum gain, for the load scenarios 1-11 of able 1.

Although the effective thickness gains vary as a function of the data source, the variation is far smaller than the variation in the modulus values themselves, because of the non-linear relation between modulus and effective thickness. In most cases, any of the three data sources could have been used, without major impact on the glass design. The one exception is likely the load case of snow loads of heated buildings, where the film data are above the threshold for significant shear transfer, and the more conservative values are below (load scenario 9). In case like this, some additional design space may be created by reviewing the actual glass temperature of the glass pane under load, or a further review of load scenario in terms of the duration or value of the snow load. Significant effective thickness increases are observed for most of the load scenarios, as an effective thickness increase of 25 %, in this case corresponding to 2 mm glass, bridging the gap to the thickness of the next available thinner glass grade (12 to 10 mm). Of course, the benefits are relatively smaller for longer duration and/or higher temperature load scenarios. In these cases, it is important to review if these load scenarios are also the design limiting load scenarios and/or review the calculations for the actual glass configuration and dimensions, as Figure 5 was generated as a conservative example.

## Conclusions

The rigidity of structural PVB interlayers as characterized by their shear modulus could be confirmed in laminated glass specimens through torsion testing. The torsion test values are in between the data measured directly on the foil, and the modulus data in the German national approval or the minimum values in prEN 16612 for a structural interlayer. Torsion testing is less suitable to generate modulus values for a broad range of load scenarios because of limitations in duration (short term loads) and lengthy experimentation at each temperature of interest.

For most design situations, there is limited impact of the choice of source for modulus data for structural PVB, and data are available from independent resources. This should help design engineers and others involved with glass design to explore the benefits of this class of relatively new materials with confidence.

## References

- [1] International Organization for Standardization: ISO 6721-1 Plastics – Determination of Dynamic Mechanical Properties\_Part 1-12 (2011).
- [2] European Committee for Standardization: prEN 16613 Glass in Building – Determination of interlayer mechanical properties (2013).
- [3] Kuntsche, J.; Schuster, M.; Schneider, J.; Langer, S.: Viscoelastic properties of laminated glass interlayers – theory and experiments. In: Proceedings Glass Performance Days (Tampere Finland), 2015, pp. 143-147
- [4] Zhang, P., Stevels, W., Haldeman, S., Schimmelpenninck, J.: Shear modulus measurements of structural PVB interlayer and prEN 16613. In: Proceedings Glass Performance Days (Tampere Finland), 2015, pp. 148-152.
- [5] Stevels, W.; D'Haene, P.; Zhang, P.; Haldeman, S.: A comparison of different methodologies for PVB interlayer modulus characterization. In Proceedings Challenging Glas 5, Bos, F.; Louter, C.; Belis, J. (eds), Gent, 2016.
- [6] Ferry, J.D.: Viscoelastic properties of polymers. 3rd Ed. Wiley, New York, 1980
- [7] Schneider, J.; Kuntsche, J.; Schuster, M.: Mechanical behavior of polymeric interlayers. In: Proceedings Glas im konstruktiven Ingenieurbau 14 (Munich Germany), 2016, Chapter 16.
- [8] Stevels, W., Haller, M.: Glasdesign mit steifen PVB-folien für den konstruktiven Glasbau: Eine aktuelle Perspektive. In Glasbau 2017 (Dresden, Germany) 2017
- [9] Kasper, R.: Tragverhalten von Glasträgern. Dissertation RWTH Aachen, Aachen Germany 2003
- [10] Callewaert, D., Belis, J., Van Impe, R., Lagae, G., Vanlaere, W.: refined set-up for pure torsion of laminated glass. In: Proceedings Glass Performance Days (Tampere Finland), 2007, pp. 118-121
- [11] German building institute: Verbund-Sicherheitsglas aus der Produktfamilie Saflex DG mit Schubverbund. Generic building approval Z-70.3-230, Berlin 2016
- [12] ASTM International: ASTM E1300 -12a: Standard Practice for determining the load resistance of glass in buildings (2012).
- [13] European Committee for Standardization: prEN 16612 Glass in Building – Determination of the load resistance of glass panes by calculation and testing (2013).
- [14] Galuppi, L., Royer-Carfagni, G.: The effective thickness of laminated glass plates. Journal of Mechanics of Materials and Structures, 7: 375-400, 2012
- [15] Galuppi, L., Manara, G., Royer-Carfagni, G.: Practical expression for the design of laminated glass. Composites, part B: engineering, 45: 1677-1688, 2013

# Enhanced Structural Integrity of Laminated Glass Balustrades

Malvinder Singh Rooprai 1,  
Ingo Stelzer 2

1. Kuraray India Pvt. Ltd.  
2. Kuraray Europe GmbH

## Keyword:

Ionomer Interlayer, Balustrades, Post-Breakage Strength,

## Abstract:

Glass balustrades are a common application of laminated glass, wherein the glass panel acts as a structural member that is required to sustain lateral design loads as stipulated by building regulations.

Rising awareness about safety related to glass usage instigated by accidents due to human impact is the driving factor for evolution of safety regulations for usage of glass in a building. Singapore building authorities look for a solution that complies with the most stringent safety criteria, limiting the induced deflection in a free standing balustrade, in "all layers broken" condition to a limit that is deemed to be safe against "fall through". Live load testing of a balustrade, laminated with ionomer interlayer, was done with a leading railing system supplier. The test concluded that the glass balustrade can be designed for sustaining the design loads, not only in "pre-breakage" but also for "post breakage" condition, thus providing a very high redundancy in balustrade design.

## Introduction

A balustrade can be defined as a system designed to keep people from (in most cases unintentionally) straying into dangerous or 'off-limit' areas. Most public places are fitted with guard rails as protection against accidental falls. Any abrupt change in elevation (where the higher portion is accessible) makes a fall possible. Due to this responsibility and liability, rails are placed to protect people using the premises. According to most of the building standards, railings are generally required where there is a drop of 30" or more. There are many types of guard railings in a building, and are mandatory per the building codes in many circumstances. Railings along stairways are common, and balconies are

also lined with them. The most common residential balustrade is usually a wood railing around the deck. However, nowadays glass is becoming more and more integral component of any modern day building. As a result, glass balustrades open the view while still providing safety, as at the Grand Canyon Skywalk in USA. Depending on the support conditions, glass may act only as an infill material or as a structural component. Whenever glass acts as a structural component, it becomes necessary for the engineer to ensure a reasonably high degree of redundancy in the design. Fig 1(a),(b) & (c) illustrate common types of balustrades where glass is acting as a structural component for sustaining the imposed lateral loads [1].

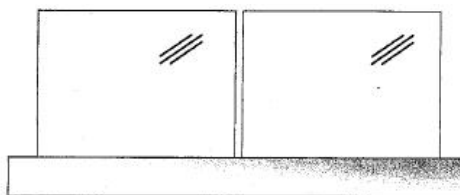


Figure 1(a) Glass Balustrade, supported only at the bottom edge.

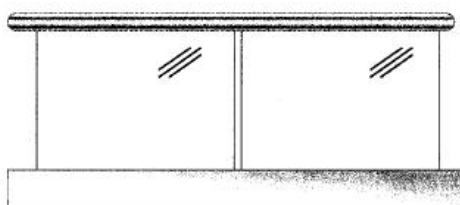


Figure 1(b) Glass Balustrade with a protective top rail, supported only at the bottom edge.

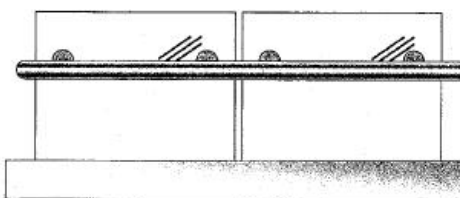


Figure 1(c) Glass Balustrade with a bolted/attached hand rail, supported only at the bottom edge.

## Global Standards on Balustrades

Major countries like USA, UK, Australia, Germany and EU have their relevant standards for design of balustrades. Others follow the criteria laid down by these countries or have their standards derived from them. All of these

standards specify a minimum lateral imposed load that should be sustained by a balustrade and the desired performance when it is subjected to impact loads.

## ASTM - E2353 - 06

The standard requires shot bag test, pendulum test, horizontal and vertical static load tests for the balustrades. The performance of the panel under impact is classified as follows:

- (i) Unbroken
- (ii) Broken & retained
- (iii) Broken & not retained

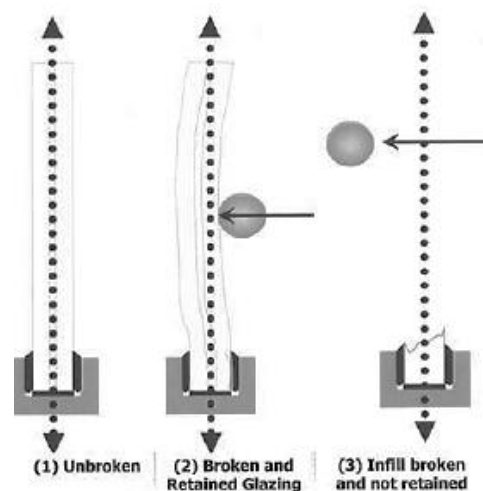


Fig 2: Glass Retention in Balustrades

The standard requires broken glass to be strong enough not to allow a spherical steel ball of diameter 75 mm when pushed with a force of 18 N.

## AS 1288 - 2006

The Australian standard permits cantilevered balustrades that have an interlinking hand rail. The handrail is non-load-supporting, unless a panel breakage occurs, and is connected to adjacent panels of glass, or the building, where the adjacent panels are at least 1000 mm wide and three or more panels of glass form the balustrade. If any one panel fails, then the remaining panels and handrail are required to be capable of resisting the design load [2]. Building authorities in Australia permit "free standing" balustrades (without interlinking hand rails) only on a project by project basis, through an "Alternate Solution" per Building

Code of Australia(BCA)-2015. As per BCA 2016, the same is known as "Performance Solutions" that involves rigorous assessment methods[3]. Singapore too, has a similar regulation that bars "free standing" balustrades.

### German TRAV Guideline – 2003

Germany has its TRAV Guideline for Balustrades. So far it does not allow cantilevered balustrades, or only with a structural top-railing cap. For balustrades without top-cap a project specific approval and test scenario is required. Similar to Australia, the approval criteria depends on the project and local authority involved (could differ from one state to another).

### BS 6180 – 2011

Depending on the type of occupancy of the building, the British Standard has requirements of sustaining below design loads for barriers

1. Uniform distributed loads of 0.5KN/m<sup>2</sup>, 1.0 KN/m<sup>2</sup> & 1.5 KN/m<sup>2</sup>
2. Linear live loads of 0.36 KN/m, 0.74 KN/m, 1.5 KN/m & 3.0 KN/m
3. Concentrated Live Loads of 0.25KN, 0.5 KN & 1.5 KN

Additionally, the standard requires the glass to be Class A safety glass. However, there are no criteria for post breakage strength [4].

The review of the above important standards & building regulations conclude that Australia & Singapore in particular have a critical approach towards free standing balustrades without any interlinking hand rail. The approach highlights the concern of the authorities for human safety. Clearly, the intent of authorities is to ensure the highest safety level in post glass breakage scenario.

### Post Breakage Strength Test for Laminated glass

Does glass has a strength after it has broken? It all depends on what type of glass and interlayer has been chosen for laminate construction and its boundary conditions. A tempered glass laminate construction with PVB interlayers in a balustrade application may have the desired structural strength but has poor post breakage strength depicted by "blanket effect". This justifies the safety concerns of Building authorities in Australia & Singapore. Ionomer interlayers, rightly address this problem by not only enhancing the stiffness of the glass laminate construction but bring in additional benefits of a very high edge stability compared to standard PVB. Singapore

building authorities look forward to elevating the balustrade safety standards by requiring the broken laminate construction, to resist the design live loads within a safe deflection limit of maximum 150 mm when a design load of 1.5 KN/m is applied with all glass layers broken. Clearly, no parallel can be drawn to such a high performance standard of glass balustrade. In 2015, Kuraray attempted a post breakage strength test on a balustrade having a 2 x 12mm Tempered Glass laminated with 2.28 mm Ionomer Interlayer. The test was conducted at an ambient temperature of 33°C, at TUV Singapore. In the test, the broken tempered laminate construction provided sufficient post breakage strength against a "collapse". However, the broken glass construction was not strong enough to meet the Building Construction Authority (BCA) of Singapore's requirements as the top edge deflections far exceeded 150 mm when 1.5 KN/m linear load was applied at the top edge. Although, this test was a failure, it provided two key learnings – 1. Tempered glass laminate does not have the required post breakage strength. 2. The base of the balustrade need to be made perfectly rigid to mitigate the base mobility issues observed in the built up U Channel base holding the glass panel. In 2016, Kuraray & Q Railings together, ventured out to develop a solution that meets the intents of not only the architects but the building authorities (BCA) as well in Singapore. The same test was repeated at an in house testing lab of Q Railings at Mumbai in India, which concluded that Ionomer interlayers with heat strengthened laminated glass constructions can achieve a very high structural strength capable of safely resisting the design loads in post breakage condition too.



Fig. 3 Test Set for the Post Breakage Strength Test

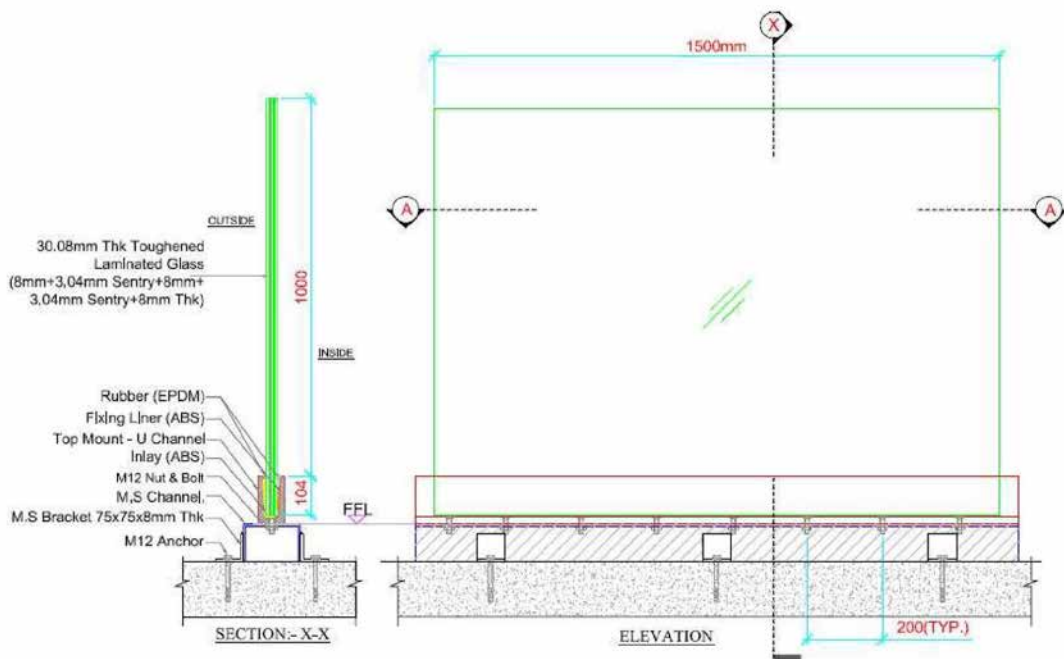


Fig. 4 Triple Layer Laminated Glass Balustrade with Ionomer interlayer rigidly supported at the base.

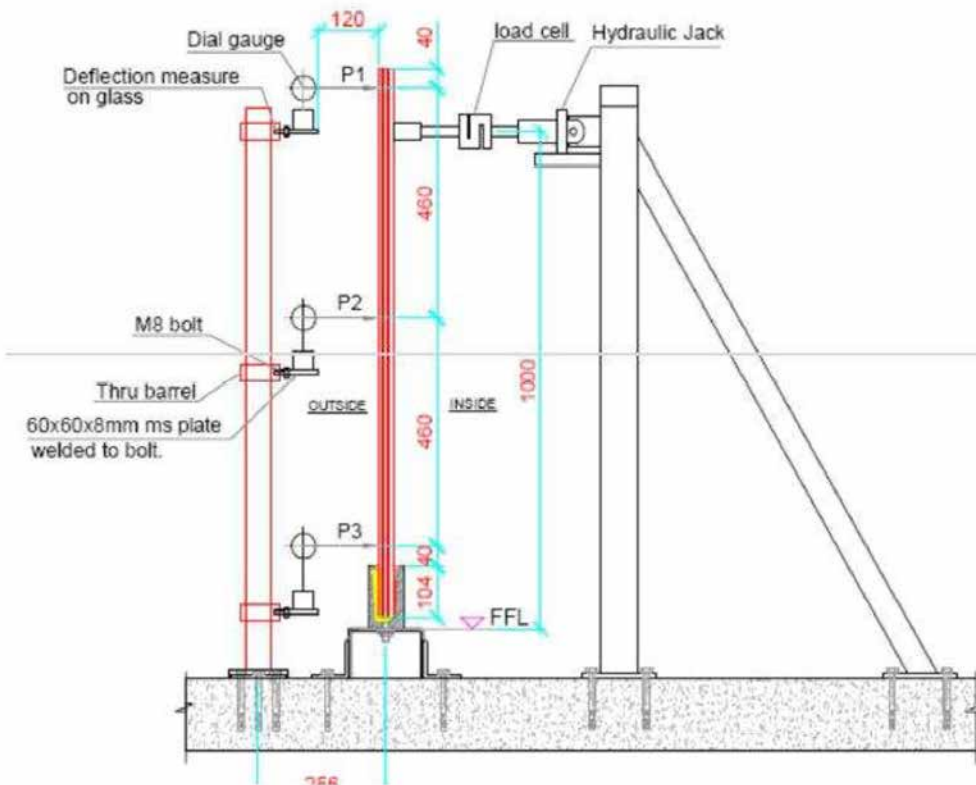


Fig. 5 Sectional view of the test set up

The U Channel base with *Acrylonitrile Butadiene Styrene* (ABS) Fixing Liner ensured a perfectly rigid base to the balustrade. The glass construction was also changed to a triple laminate construction made with heat strengthened glass instead of tempered glass, with a hope that the middle glass layer "interlocked" between outer glass layers would improve the post breakage strength.

#### Laminated Glass Construction Details –

8mm Heat Strengthened + 3.04 mm Ionomer Interlayer + 8mm Heat Strengthened + 3.04 mm Ionomer Interlayer + 8mm Heat Strengthened

#### Test Methodology

The glass panel was applied horizontal linear loads with hydraulic jack and load cell arrangements as shown in Fig 5. The entire test was conducted in an uncontrolled temperature (33-35°C) environment.

To ensure a linear load distribution, the load was applied at two locations at the top edge. The dial gauges for measuring the panel deflection at the top, centre and at the top of the rigid support were used. The load was gradually ramped up from zero to 1.5 KN/m. One specimen (Number 2) out of three had an unexpected breakage at 1.5 KN/m. Deflections were recorded for 1.5 KN/m and 3.0 KN/m load. The load was gradually ramped up to ultimate load capacity of the panel. Post to the breakage of glass, a linear of 1.5 KN/m was applied and deflections recorded after one minute. The test results are tabulated below.

Specimen #2 had an unexpected breakage, probably due to less surface compression stress. The deflections in the Specimens # 1 & 2 in pre breakage conditions for 1.5 KN/m were bit on the higher side because a full rigidity of the bottom edge could not be achieved for the non-standard glass thickness with combination of two different standard ABS wedges. For Specimen # 3, the base stiffness was enhanced

by Q Railings, using slightly thicker ABS wedges which resulted in significant reduction in top edge deflections of the panel in pre and post breakage condition [5].

#### Conclusions

1. Advanced Structural Interlayers like Ionomers, when used in a triple layer heat strengthened glass laminate construction, significantly enhance the structural integrity of the glass balustrades to resist the design loads in post breakage condition as well, thus meeting the most stringent safety norms laid down by countries like Singapore & Australia.
2. The test was done only for laminates made with Ionomer Interlayer. PVB Laminates although not tested but have little or no chance to pass the post breakage performance requirement achieved in the test because shear modulus value for PVB is almost one hundredth of the value for Ionomer.

#### Future Testing

Stiff PVB has a shear modulus comparable to Ionomer interlayers up to a temperature of 30°C. Future tests can be aimed at exploring how Stiff PVB laminates perform in comparison to Ionomer interlayers.

#### Acknowledgements

The authors would like to extend a special thanks to Mr. Vijay Sawant, Head (Technical) of Q Railings India Pvt. Ltd. and his team for their support in conducting the post breakage strength test at their facility.

#### References

- [1] ASTM E 2353 - Performance of Glass in Permanent Glass Railing Systems, Guards, and Balustrades
- [2] AS 1288 - 2006 - Glass in Buildings - Selection & installation
- [3] Building Code of Australia - 2015, 2016
- [4] BS 6180 - 2011 - Barriers in and about Buildings - Code of Practice
- [5] Testing of Glass Balustrade System, free standing without cap rail / handrail by Q Railing India for Kuraray India Pvt. Ltd.

| Specimen No. | Max. Deflection in the glass ( pre breakage condition) |                       | Result @ 3.0 KN/m            | Max. Deflection in the glass panel (post breakage condition) for 1.5 KN/m load. |
|--------------|--|-----------------------|------------------------------|---|
|              | @1.5 KN/m  | @3.0KN/m (Proof Load) |                              |   |
| Specimen 1   | 44.0 mm  | 64 mm                 | No breakage of glass         | 56.0 mm   |
| Specimen 2   | 49.6 mm  | NA                    | Glass Broke at 1.5 KN/m load | 56.0 mm   |
| Specimen 3   | 24.3 mm  | 69.6 mm               | No breakage of glass         | 41.0 mm   |

Table 1 – Deflection measurements for 3 different specimens in pre breakage and post breakage condition

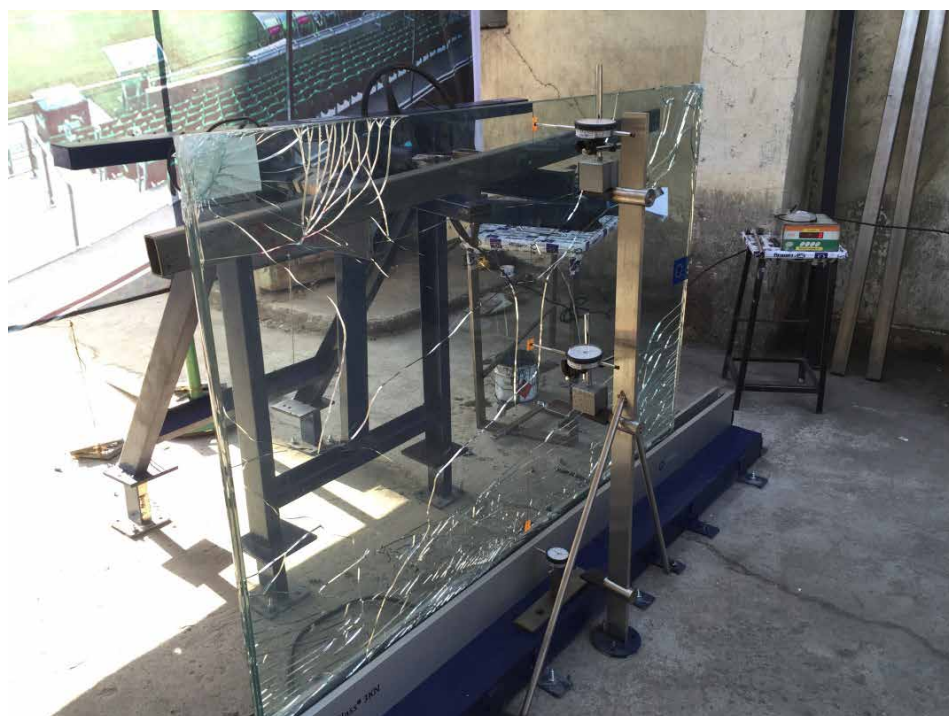


Fig. 6 1.5 KN/m load applied on broken laminate construction

# On the Causes of Optical Defects in Laminated Glass

Peer reviewed.  
Published in  
Glass Structures  
& Engineering  
Journal  
no.40940

**Extended abstract** (The complete contribution will be published in the Glass Structures & Engineering journal)

The development of visual defects, such as bubbles, local delamination, cloudiness and discoloration in laminated glass are unwanted phenomena that negatively affect the visual quality of a laminate but do not affect its structural safety. These defects can arise due to numerous influences during the production of a laminate and/or can be triggered during its lifetime. To get a better understanding of the defect formations, several laminated glass specimens were deliberately produced erroneously to promote these unwanted phenomena. Subsequently, the specimens were subjected to durability tests such that the link between a production fault, a triggering mechanism and the resulting defect pattern could be investigated. The tests are conducted on laminates with a PVB interlayer.

## Keywords

Laminated glass; PVB interlayer; bubbles; delamination; durability testing

## Authors

Prof. Jan Belis, PhD, corresponding author

- 1) Ghent University – LMO, Department of Structural Engineering, Technologiepark-Zwijnaarde 904, 9052 Ghent, Belgium
- 2) Eindhoven University of Technology, Structural Design Unit, Eindhoven, The Netherlands

E: [jan.belis@ugent.be](mailto:jan.belis@ugent.be)

T: +32 479 235 100

ORCID: 0000-0001-9248-2171

Pieter Raes, MSc

Former student, Ghent University, Department of Structural Engineering, Technologiepark-Zwijnaarde 904, 9052 Ghent, Belgium

Gérard Savineau, PhD

Independent Glass Consultant, Antwerp, Belgium

# Architectural Acoustic Glazing – Fundamentals of Sound Transmission and Acoustic Interlayers

Hengyi Ju  
Advanced Research Scientist  
Advanced Materials - Interlayers Technology  
Eastman Chemical Company

## Keywords

Sound insulation, acoustic interlayer, laminated glass, architectural glazing

## Abstract

Tranquility is an important element to our well-being in everyday life. When it comes to sound insulation, achieving indoor quietness can be a challenge, especially for urban areas with dense population and heavy street traffic. In buildings, windows are generally more susceptible to noise penetration than other partitions because of their lower surface mass. Fortunately, acoustically engineered interlayers in laminated glass can effectively dampen sound propagation and reduce the overall sound transmission. In this paper, the interlayer technology involved in acoustic glazing is presented from a physics perspective. The mechanism of sound transmission through a solid panel is reviewed at a fundamental level, and the technical approaches to enhance sound transmission loss of laminated glass are discussed. Lab tests and numerical simulations are conducted for verifying the performance of acoustic glazing constructions as well as making predictions.

## Mechanism of sound transmission

To establish a basic understanding of sound transmission, it is useful to assume a simplified geometry as shown in Figure 1. Here the solid panel is infinitely large in the vertical plane. Air fills the rest of the space on both sides of the solid. On one side of the panel, sound waves are generated and they come at the panel from arbitrary directions. As sound waves impinge upon the solid, the acoustic energy goes three ways: the first part of the energy gets reflected back to the air; the second part couples into the solid material and induces vibration and/or sound propagating in the solid structure; the third part penetrates through the panel into the air on the other side, becoming transmitted sound waves. Apparently the third energy fraction is of the most interest

as it reflects the ability of the solid panel to block sound. Conventionally, transmittance is used to quantify how much sound energy is transmitted, defined as

$$T = I_t/I_i = p_t^2/p_i^2, \quad (1)$$

where  $p$  and  $I$  are the amplitude of sound pressure and intensity, respectively; subscripts  $i$  and  $t$  stand for the incident and transmitted sound waves, respectively. The reciprocal of sound transmittance is the sound transmission loss (STL). As human hearing exhibits sensitivity on a logarithmic scale, the STL is usually presented in decibels (dB), defined as

$$STL = -10\log_{10}(T). \quad (2)$$

Given the time-frequency representation of sound waves and the problem being in the linear dynamic range, one may decompose a sound field of any temporal profile, frequency content, angular directivity and spatial intensity distribution into a summation of continuous, monochromatic plane waves. Therefore, the fundamental problem can be further simplified to the sound transmission through an unbounded panel by a plane wave propagating at a certain frequency and along a certain direction (i.e. a constant wavenumber vector) in the air.

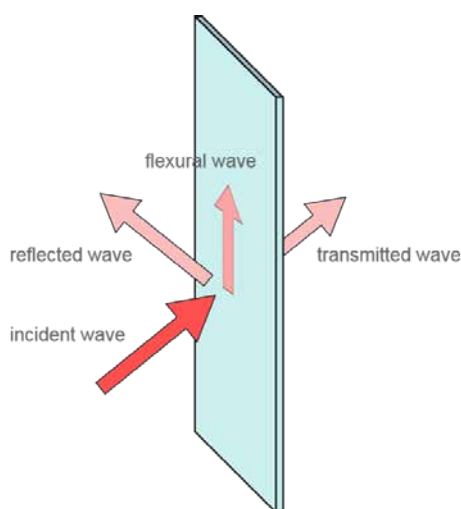


Figure 1. Geometry of an unbounded solid panel subjected to an incident sound wave.

The mechanism of sound transmission varies depending on how the panel thickness compares to the wavelength of the incident sound wave. At audible frequencies (20 Hz - 20 kHz), the acoustic wavelengths are most likely greater than the thickness of a glazing panel. At very low frequencies where the panel thickness can be considered infinitesimal, the solid material along the entire thickness dimension moves along with the incident wavefront. In such case the incident sound wave forces the panel to vibrate and radiate sound waves back to the air. Sound transmission in this frequency range is dominated by the inertia of the panel to external excitations. The sound intensity transmittance is found to be inversely proportional to the product of sound frequency, density of the solid and thickness of the panel. The STL therefore increases linearly with logarithmic frequency at a slope of 6 dB/octave while the vertical offset of the STL curve is determined by the surface density of the solid panel. This linear correlation is usually referred to as the "mass law", whereas these low frequencies comprise the mass-controlled frequency regime, as shown in Figure 2.

At higher frequencies, the acoustic wavelength in the air approaches the panel thickness, and it becomes possible that sound will propagate in the solid in the form of plate waves [1]. The dominating mode to which the majority of the acoustic energy will be distributed is the zero-order asymmetric mode, also known as the flexural wave [2]. Such mode exists in plate wave propagation as resonance exists in structural vibration, like a pendulum swing or ringing of a bell. Upon generation from an impulse excitation, a flexural wave ends up following the free propagation mode as dictated by the mechanical properties of the solid material and the thickness of the panel. The wavenumber of a free flexural wave can be described as

$$k_b = \omega^{1/2}(m/B)^{1/4}, \quad (3)$$

where  $\omega$  is radial frequency;  $m$  and  $B$  are the surface density and bending stiffness of the panel, respectively. If the panel consists of

only one material, the bending stiffness can be described in a simple expression as

$$B = Eh^3 / 12(1 - \nu^2), \quad (4)$$

where  $h$  is the panel thickness;  $E$  and  $\nu$  are Young's modulus and Poisson's ratio of the solid material. Although a free mode is preferred by the flexural wave, under the settings to our sound transmission problem, the entire panel is subjected to an incident plane wave of a certain wavenumber. Therefore, only the flexural wave of the same frequency and wavenumber as the projected incident wave on the panel will be allowed to propagate in the solid. In many occasions when the "forced" flexural wave does not fit into the free propagation mode, the sound transmittance will be inversely proportional to the product of bending stiffness and cubic frequency. These frequencies comprise the stiffness-controlled regime, where the STL increases linearly with logarithmic frequency at a slope of 18 dB/octave, and the curve is vertically shifted by bending stiffness.

There is a third frequency regime where the forced flexural wave does match the free propagation mode. When this critical condition is met, a unique phenomenon, termed the coincidence effect, kicks in during the course of sound transmission. As the incident sound field engages, the solid panel exhibits pronounced displacements as if the resistance for generating flexural waves is reduced. Moreover, along the path of the incident sound wave, it would seem that the mechanical motion behaved by the panel becomes so cooperative to the incident field that a greater proportion of the acoustic energy is allowed through the panel.

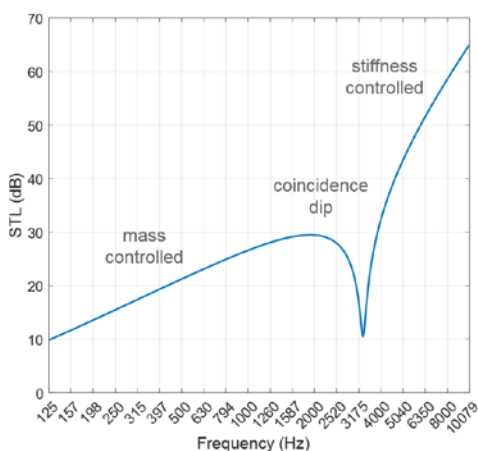


Figure 2. Calculated STL of a 4-mm glass panel as a function of frequency at a 70-degree angle of incidence.

Despite the term "coincidence", this effect can be seen in the STL spectra of most glazing constructions. The dispersive nature of the flexural wave dictates that for any angle of incidence above 0 there is a frequency at which coincidence will occur. In real-world scenarios, a window panel is exposed to incident sound waves from all directions with equal probability [2]. Consequently, coincidence will take effect within a continuous frequency band, to which the span can be substantial. Figure 3 shows the calculated STL of a monolithic glass panel as a function of frequency from incident plane waves at various angles. It is clear that the spectra show steep STL drops covering frequencies from 3 kHz to 10 kHz and beyond. As the spectra superimpose onto one another during a practical test, these drops add up to a collective coincidence dip as seen in the overall STL signature for the panel.

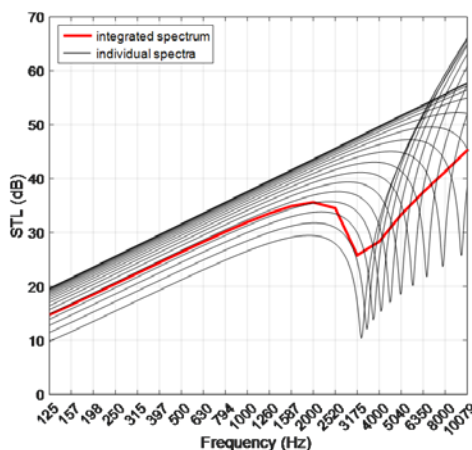


Figure 3. Calculated STL of a 4-mm glass panel as a function of 1/3 octave frequency. The black curves represent STL spectra at individual incident angles from normal (top) to oblique (bottom) incidences. The red curve is the integrated STL spectrum over all incident angles.

## Material damping and sound deadening

As the physical picture of sound transmission becomes clear, it is important that we divide the entire audio frequency range into the three regimes when evaluating the acoustic performance of glazing materials. At both ends of the spectrum, i.e. in the mass- and stiffness-controlled regimes, the assessment is rather straightforward. The major indicator for acoustic performance, the STL, will be predominantly influenced by glass. Simply utilizing thicker glass will benefit sound insulation at both frequency extremes. On the flip side, however, once the overall panel thickness is decided, there is very little room

left for sound barrier engineering, since the density and modulus of glass are relatively stable.

A silver lining emerges when it comes to dealing with the third frequency regime. In this regime, we look to recover the acoustic performance that has been compromised by the undesirable coincidence effect. An effective way to achieve this goal is to introduce damping to the solid. Damping by nature represents the loss of mechanical energy and it roots from the imaginary part of a material's elasticity. Having an outstanding damping factor in the solid will facilitate the attenuation of flexural wave propagation and the transform of acoustic energy into heat. As flexural waves decay, the incident sound wave will be greeted with less cooperative motions by the panel, and the coincidence transmission will be reduced. It should be noted that glass by itself has a damping coefficient of almost zero in the audible frequency range at room temperature. Therefore, damping is usually added to the panel via lamination, where a comparatively soft interlayer is sandwiched between two pieces of glass. The interlayer material, regardless of its formulation or intended application, usually increases the damping factor of the composite due to its intrinsically lower glass-transition temperature than glass. As a result, laminated glass usually exhibits a shallower coincidence dip than monolithic glass of the same overall thickness.

Engineered acoustic interlayers give rise to further improved STL over nonspecific interlayers in the damping-controlled frequency regime. The viscoelasticity of acoustic interlayers is tailored such that damping is maximized at frequencies where it is most beneficial. For example, laminated glass constructed with two pieces of 3-mm glass and a standard PVB interlayer exhibits a collective coincidence dip around 2 kHz and a damping factor of less than 0.1 at this frequency. Replacing the standard PVB with acoustic PVB, the damping factor of the composite will be more than doubled at 2 kHz and neighboring frequencies, leading to up to 10-dB increase in the acoustic performance as well as a less steep coincidence dip in the STL spectrum.

## Numerical simulations

A numerical model has been established to simulate the physical process of sound transmission through an unbounded panel. Figure 4 shows the simulated sound pressure distribution in the air and mechanical motion throughout the panel, at a certain angle of incidence and sound frequency. The panel

is constructed with a monolithic layer of annealed glass of 4 mm thickness. The two graphs demonstrate sound transmission at a 70-degree angle of incidence at coincidence (5 kHz) and non-coincidence (7 kHz) frequencies, respectively. Above the panel the incident and reflected sound waves interfere and form the checkered pattern as seen in the pressure field. Underneath the panel the transmitted sound wave carries itself along the same direction as the incident wave but with a discounted pressure amplitude. It is clear from the comparison that the amplitude of both the flexural wave displacement in the solid and the transmitted sound pressure in the air gets enhanced when coincidence happens. Following Eqns. (1) and (2), the sound transmittance for a certain combination of incident angle and sound frequency can be calculated by taking the ratio between the averaged sound intensities on the upper and lower surfaces of the panel. Using this model, one can take a step further and derive the overall STL spectrum for a given panel structure by integrating sound transmittance over all the incident angles and scanning through a range of audio frequencies.

Further verification of the model was conducted comparing the simulated STL with the actual measurement, as shown in Figure 5. These measurements were taken from laboratory acoustic testing on samples of a finite size following ASTM E90 [3]. The dash lines in the figures represent the mass law as determined by the surface density of the panel. Note that the measured STL tends to exceed what is limited by the mass law at frequencies below 500 Hz. This should not be considered violations to the law of physics, but rather a result of complication to the physical processes at lower frequencies. As the sound frequency comes down to a point where the acoustic wavelength is not significantly smaller than the panel size, the generation of vibration or wave propagation in the panel is affected not only by the weight of the material in the thickness dimension but also by the boundary conditions at the edges of the panel in the lateral plane. At frequencies over 500 Hz the measurement conforms to the mass law, indicating that the boundary effect diminishes and the test piece becomes practically unbounded to the sound waves with short wavelengths. It can be seen from the figure that the simulation faithfully describes the physical process thus providing on-point STL prediction for the majority of the audible spectrum.

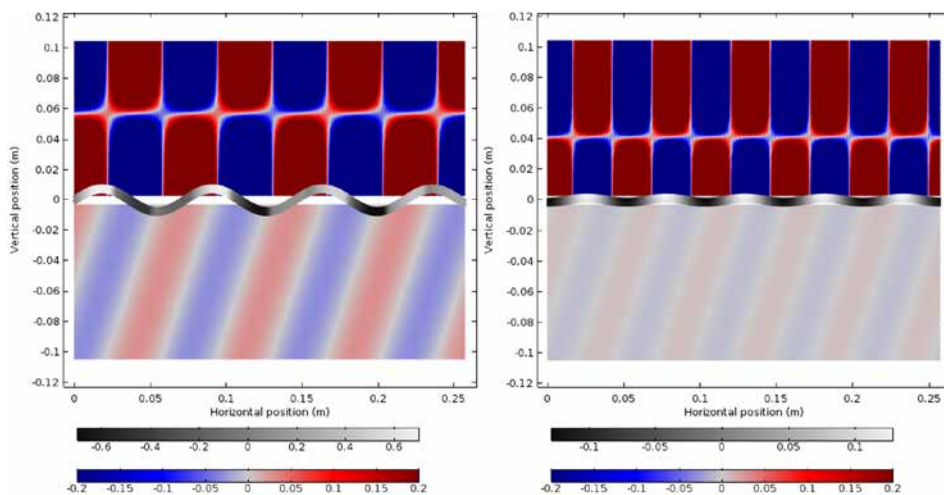


Figure 4. Distributions of sound pressure (color) in the air and displacement (gray) in the solid during plane-wave sound transmission through a 4-mm glass panel. The angle of incidence is 70 degrees for both plots. The sound frequencies are 5 kHz (left) and 7 kHz (right).

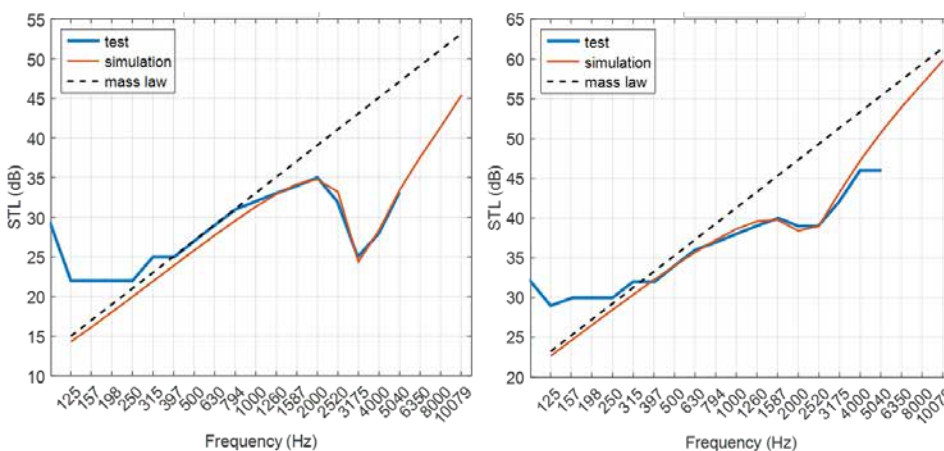


Figure 5. Measured and simulated STL spectra of monolithic (left) and laminated (right) glass panels. The thickness of the monolithic glass panel is 4 mm. The laminate is constructed with two pieces of 5-mm glass panels sandwiching an acoustic PVB interlayer (0.76 mm).

Using the same model, a case study was carried out demonstrating the difference in sound insulation characteristics between standard and acoustic PVB. The results are shown in Figure 6 depicting the STL spectra of laminated glass with a variety of glass thicknesses. An obvious feature to pick up in this graph is that thicker laminates outperform thinner ones because of the extra weight and stiffness as discussed in preceding sections. Apart from the baseline shift, the laminates using standard PVB all show a prominent coincidence dip in the STL curves. In other words, none of them is really effective keeping the acoustic performance. It is worth mentioning that the center frequency where the coincidence dip is located is determined by the bending stiffness of the composite [2]. The higher the bending stiffness, the lower the coincidence frequency. As seen in Eqn. (4), the bending stiffness increases with thickness. It

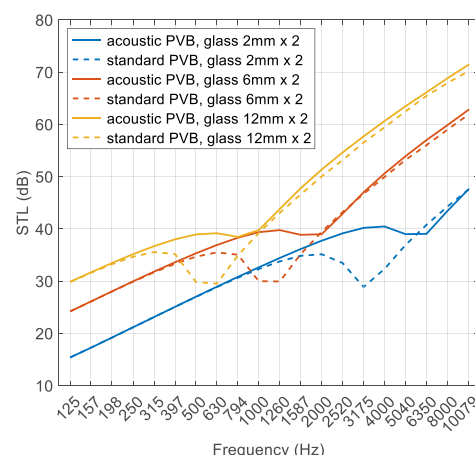


Figure 6. Calculated STL spectra of laminated glass using standard (dash lines) or acoustic (solid lines) PVB in several symmetrical glass configurations.

is therefore expected that the coincidence dip in the STL spectrum move to a lower frequency as the laminate becomes thicker. Even though the coincidence frequency may shift, it is still confined between 500 Hz and 10 kHz for common glazing thicknesses (3-25mm). From a human perception point of view, our hearing sensitivity does not change much (< 2 dB) in this frequency range, therefore the excess noise the laminate lets through within the coincidence frequency band will still be noticeable.

Laminates containing acoustic PVB, on the other hand, do a much better job at dealing with the coincidence effect. The acoustic PVB brings two benefits to the table: first, the softer material reduces the bending stiffness of the laminate, moving the coincidence frequency up by approximately one octave band thus extending the portion of the curve under the mass law; second, the material features high damping factor covering a wide range of audio frequencies, hence less damage done to the STL when coincidence takes effect. In light of both mechanisms, the performance of acoustic-specific laminates surpasses their nonspecific counterparts under the same glass configuration. At frequencies where the latter is at the bottom of the coincidence dip, the STL can be improved by as much as 10 dB owing to the acoustically engineered interlayer. This improvement can also be seen in single-number ratings [4]. As shown in Table 1, one can gain as much as 6 units in the sound transmission class (STC) rating when making the interlayer upgrade from standard PVB to acoustic PVB.

| Interlayer \ glass thickness | 2mm x 2 | 4mm x 2 | 6mm x 2 | 8mm x 2 | 10mm x 2 | 12mm x 2 |
|------------------------------|---------|---------|---------|---------|----------|----------|
| Acoustic PVB (0.76mm)        | 32      | 37      | 39      | 41      | 42       | 43       |
| Standard PVB (0.76mm)        | 31      | 33      | 34      | 35      | 36       | 37       |

Table 1. Calculated STC ratings in various laminate constructions

## Conclusions

In this paper, the physics of sound transmission through a glazing panel is reviewed. Three frequency regimes are defined based on the length scale of the problem, and the physical processes associated with each frequency regime are carefully analyzed. Following proper understanding of the physical problem, a numerical model is established and implemented for predicting the sound transmission loss signature of glazing panels. Comparisons are drawn amongst monolithic and laminated glass panels as well as laminates using standard and acoustic PVB. Results show that acoustically engineered PVB unlocks superior sound insulation performance compared to what nonspecific interlayers have to offer. The acoustic product also shows versatility as improvement in noise reduction can be seen in a variety of glass configurations.

## References

- [1] H. Lamb, "On Waves in an Elastic Plate," Proc. Roy. Soc. London, Ser. A 93, 114-128, 1917
- [2] F. Fahy, P. Gardonio, "Sound and Structural Vibration," 2nd Ed., Academic Press, 2007
- [3] ASTM Standard E90, 2009, "Standard Test Method for Laboratory Measurement of Airborne Sound Transmission Loss of Building Partitions and Elements," ASTM International, West Conshohocken, PA, 2009, DOI: 10.1520/E0090-09
- [4] ASTM Standard E413, 2010, "Classification for Rating Sound Insulation," ASTM International, West Conshohocken, PA, 2010, DOI: 10.1520/E0413-10

# Recent Developments of Laminating Films as Contribution for Energy Efficient Buildings and façades

Steffen Bornemann, Kristin Riedel, Jasmin Weiss  
Folienwerk Wolfen GmbH

## Keywords

Laminating film, EVA, interlayer, laminated glass, energy-efficient buildings

## Abstract

The reduction of greenhouse gases is one of the most important goals of the international climate policy. Today, roughly one third of all greenhouse gas emissions is created by urban population.

Modern architecture is focusing on new solutions to energy-efficient buildings. Nowadays, heat exchange systems by use of smart windows are under development to actively control the climate conditions in the buildings. Furthermore, it is possible to harvest solar energy by building integrated photovoltaics. Such technologies require high demands on the glass structures which can be achieved by new material combinations. New approaches from recent developments of Folienwerk Wolfen GmbH and its scientific partners offer the possibility to match these requirements. The presentation will focus on the effect of the crosslinking of polymeric interlayer or laminating films on the performance of laminated glass structures. Mechanical and safety properties under hard climate conditions, compatibility of the interlayer films to chemicals as well as life-time stability of the glass structures and the final products will be discussed. Furthermore, some new glass structures for the achievement of the requirements will be introduced.

## Introduction

Today, urban life is requiring huge resources. Buildings, part of our culture, are still demanding a lot of energy. In modern architecture, the skins of the buildings are used mostly for representative purposes. The more urban life is moving into cities, more and more buildings with large façades and roofs are being built. Why not use these large areas of the skin for more than aesthetic purposes? New architectural concepts are including energy relevant topics into the development of

new buildings.

Such new projects and concepts for energy-efficient buildings have reached popular science, too. For example, articles about future trends in urban life discuss energy harvesting façades or windows which store heat and energy. [1]

There is a huge market for energy efficient buildings and façades along the so called "sunbelt" of our planet. Prosperous megacities, growing and ambitious economies, as well as progressive nations are located in these areas. Due to the high solar radiation, the geographic regions in the "sunbelt" are offering tremendous possibilities for energy harvesting technologies like photovoltaics or intelligent façades. However, besides the high solar radiation, the other climate conditions are challenging: high differences in temperature between day and night, condensing fog in the morning hours, arid climate conditions as well as strong wind or sand storms have to be considered during development of materials for energy-efficient buildings and façades. The use of laminated structures is a powerful tool for the development of tailor-made materials for such environmental challenges.

Laminated glasses consist of glass panes which are bonded together by an adhesive material. Such adhesive material can be a glue or a polymeric interlayer film. The requirements of the film are manifold: good adhesion to the glass, long lifetime without loss of functionality, outstanding resistance to outdoor effects, or high transparency have to be achieved in combination with easy processing and justifiable costs. These days, the manufacture of laminated glasses by polymeric interlayers is a state-of-the-art process all over the world.

## Polymeric interlayer films

For the manufacture of laminated glasses, different polymeric films can be used: The standard interlayer film in the glass industry is consisting of polyvinyl butyral (PVB). However, other polymeric interlayer films have entered the market successfully, especially for niche applications: interlayer films consisting of ionomers (i.e. Sentry glass) are used for safety applications with high static

requirements, while polyolefin, silicone or ethylene-vinyl acetate (EVA) based interlayer films offer significant advantages, especially for applications under humid climate. The market of photovoltaic applications has been dominated by EVA based interlayer films for a long time.

Depending on the applications, different EVA interlayer films can be chosen: For the fabrication of photovoltaic modules, EVA films were developed for fast processing speed and special performance in the vacuum lamination process. Contrary to this, EVA interlayer films for the manufacture of laminated safety glasses for façade or architectural applications have to fulfill the requirements of the glass industry, including verifiable certification of the building industry.

## EVA interlayer film:

Compared to the other polymeric films, EVA interlayer film behaves differently. Under the effect of temperature and time, the polymer chains of the EVA will create a three-dimensional network structure due to a crosslinking step. This crosslinking step is initiated by peroxides. The peroxide is part of the formulation of EVA interlayer films like evguard®, the interlayer film developed and produced by Folienwerk Wolfen GmbH. The process of the crosslinking can be described as followed: The peroxide will decompose, creating radicals. In the next step, these radicals will activate carbon-hydrogen bonds at the polymer chains by abstraction of hydrogen atoms. By recombination of such activated polymer chains or fragments thereof, a three-dimensional polymeric network will be achieved. The formation of the crosslinked polymeric network, as well as the properties of the resulting material, can be controlled by varying the formulation of the EVA film, and the process parameters.

The crosslinking speed of an EVA interlayer film during the lamination process is shown in figure 1. Due to the crosslinking, the viscosity, as well as the viscous and storage modulus of the polymer melt will change. The conversion of the crosslinking at different temperatures was measured by means of a rheometer (Malvern Kinexus Ultra). Measurement was carried out by plate-plate equipment, under isothermal conditions. The change of the viscous and storage modulus was used for

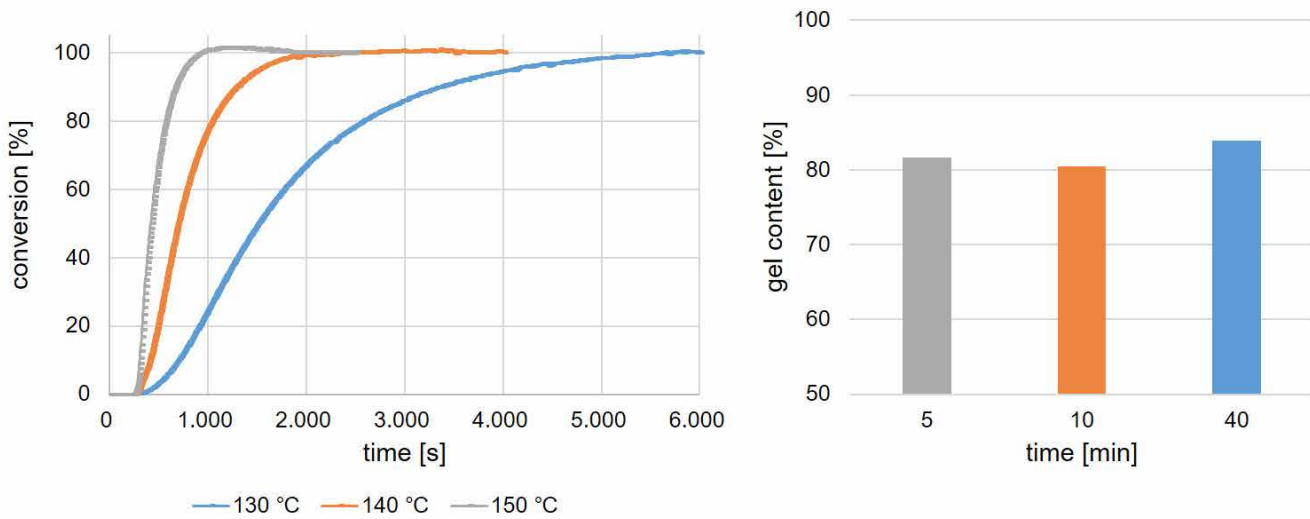


Figure 1. Conversion of the crosslinking of EVA interlayer film (left), and resulting gel rate (right), at different temperatures

determination of the crosslinking conversion. The gel-rate, representing the amount of the crosslinked EVA polymer chains, was analysed by extraction in xylene. The conversion of the crosslinking is shown for three different temperatures. For achieving safety properties of laminated glasses, a crosslinking degree of at least 80% is required. As can be seen (figure 1, right diagram), an increase of the temperature from 130°C to 150°C reduces the conversion time to achieve a crosslinking level of at least 80% from approx. 40 min. to 5 min.

The crosslinking step changes the behaviour of the EVA interlayer film. This is important for the properties of the film, and the laminated glass, too. The effect of the crosslinking on the mechanical properties of the EVA interlayer film can be shown easily by the tensile test. In figure 2, the mechanical properties of uncured (left) and crosslinked (right) evguard® EVA interlayer film are shown. Neat, uncured EVA interlayer film is characterized by a stress of up to 12 N/mm<sup>2</sup> and an elongation of more than 700%. Slightly different curves can be seen depending on the orientation of the film. The stress-strain curves of machine oriented EVA film typically show less elongation than the curves measured for transversal specimen. Such behaviour is well known for films made of thermoplastic materials. In contrast to uncured EVA, the crosslinking yields in a significantly stronger, stiffer film. This is shown in figure 2 (right). Stress values more than 20 N/mm<sup>2</sup> and elongation values of about 600 % are detected for the crosslinked EVA interlayer film. No effect of the film orientation can be seen now, all curves are showing similar course.

Due to the change of the EVA film properties by crosslinking, the properties of the laminated glasses can be modified considerably by this kind of interlayer. As an example of the effect of the crosslinking rate, results of the pendulum impact test are shown in figure 3. The pendulum test was carried out according to DIN EN 12600, drop height 1200 mm. Laminated glasses of the structure 44.2 were tested. The EVA interlayer film was crosslinked to different extent. When the EVA interlayer film was crosslinked to low level only, the pendulum test failed. A long crack can be seen as a typical result. Compared to this, a

laminated glass with high crosslinked EVA interlayer film passed the pendulum test. As can be seen in figure 3 (right), no crack of the glass occurs. The shown pictures in figure 3 are exemplarily for these observations.

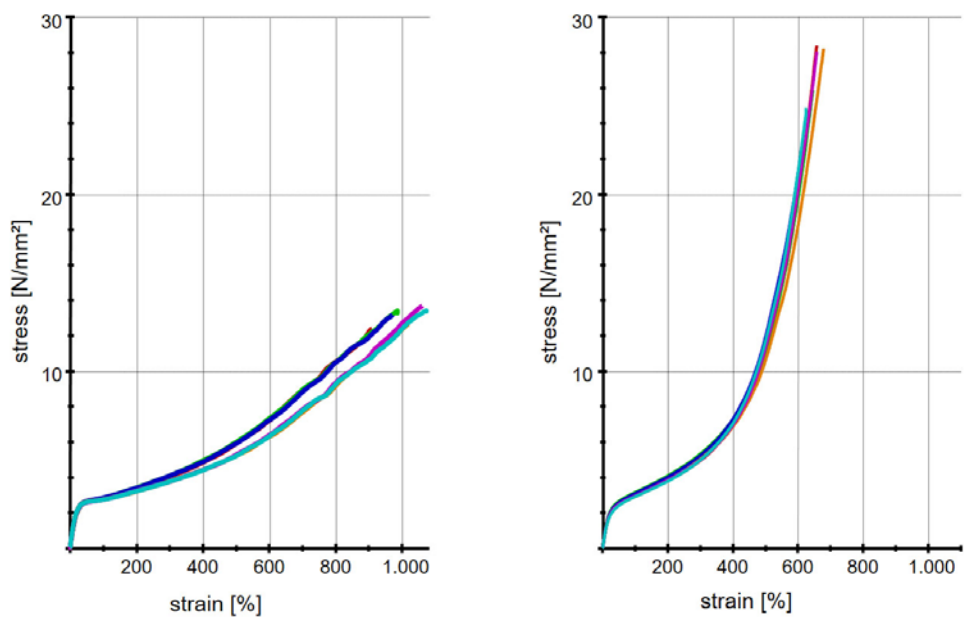


Figure 2. Stress-strain curve of neat (left) and crosslinked (right) EVA interlayer film



Figure 3. Pendulum test according to DIN EN 12600 on laminated glasses with EVA interlayer. Result for low crosslinking (left) and high crosslinking (right)

### Use of EVA interlayer films for composite capillary glasses

Within the EU Horizon 2020 funded project Lawin (large area fluidic window), ultra-thin composite capillary glasses are under development. [2] The capillaries of the glass will be created by a rolling process during float glass processing. The structured float glass will be connected with a thin, strengthened cover glass, to achieve a composite structure. The result is a flat-panel laminate with thickness adapted to a single glass sheet in conventional windows. A fluid is flowing through the capillaries, allowing absorption or release of heat. By combination with a heat exchanger, these composite capillary glasses will be used in isolating glass units or façades for absorption, storage or transfer of heat. Key market of the product is the use for climate controlled windows and façades. [3] The structure of such composite capillary glass for use as large area fluidic window is shown in figure 4.

During the project, different approaches for the connection of the structured float glass and the thin, strengthened cover glass were investigated. Both gluing and lamination technologies were tested for the manufacture of the required composite capillary glass. Visual appearance, durability and thermal performance under various climate conditions are the key requirements for the product, as listed in Tab. 1.

Laminated glass samples of different size and structure were subjected to a defined test program, including chemical, mechanical and optical measurements. The test specimens were exposed to cyclic and climatic conditions to access the long-term behaviour of the bonded areas. [4]

The use of glues as well as interlayer films as adhesive for the manufacture of the composite capillary glass was investigated. From the first results of the tests, the EVA interlayer film was found to be a material with well-balanced performance profile. The EVA interlayer film offers the following advantages:

- Good adhesion: Composite capillary glasses were laminated using strips of the EVA interlayer. A side view parallel to the capillaries is shown in figure 5. As can be seen, the EVA interlayer film strips bond the capillary glass and the ultra-thin cover glass only at the connecting zones. This allows a maximum cross section of the capillaries which is needed for constant flow of the fluid.

- Resistance to the fluid: In case of glues or thermoplastic interlayer films like PVB, the contact of the fluid with the adhesive will possibly lead to brittleness, negatively affecting the safety properties. In case of glues, the formation of cracks was found, possibly enforcing the brittleness. For PVB interlayer films the contact to the fluid may cause a leaching of softeners from the polymer. Compared to this, the crosslinked EVA remains stable for a longer time. It is also free of softeners, showing significantly

| Visual properties  | Chemical resistance   | Mechanical requirements  |
|--|---|--|
| <ul style="list-style-type: none"> <li>- high transparency;</li> <li>- refractive index similar to glass and close to fluid;</li> <li>- even distribution of the polymeric adhesive</li> </ul> | <ul style="list-style-type: none"> <li>- chemical resistance of the adhesive to the used fluid;</li> <li>- non-hygroscopic adhesive;</li> <li>- non-toxic in case of leakage</li> </ul> | <ul style="list-style-type: none"> <li>- long term stability under various climate conditions;</li> <li>- no leakage;</li> <li>- stability at high temperatures;</li> <li>- high tensile strength and elasticity;</li> <li>- high safety level achievable</li> </ul> |

Tab. 1. Key requirements for the laminated capillary glasses

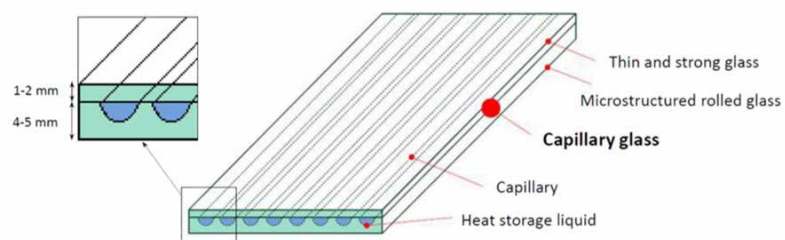


Figure 4. Scheme of a Lawin composite capillary glass



Figure 5. Side view of a composite capillary glass

improved resistance in contact to the fluid of the capillary glass.

- Exposure to high temperatures: Used at the façade of a building, the composite capillary safety glass will be exposed to high temperatures. Due to the crosslinked nature of the EVA film, such material has sufficient performance also at temperatures above 50°C.

- Edges: At the edges of the capillary glass, the bonding material is in contact both to the fluid in the inside the capillaries and the external sealant. Good compatibility to the different materials is required at this sensitive area. The EVA based interlayer film also reduces the risk of delamination at this critical part of the composite capillary glass.

- Safety properties: The selected EVA interlayer film is certified by various German, European and American certifying bodies for use as laminated safety glass.

### Environmental conditions

All components of energy efficient buildings and façades or building integrated photovoltaic modules for the sunbelt areas have to resist the challenging climate conditions. Compared to central European climate, the temperatures, differences in day-night temperatures, and solar radiation are significantly higher. Only selective materials can resist the harsh climate conditions, especially the high UV radiation, in combination with wind and sand load.

In another cooperation project, test scenarios for the investigation of glass laminates or solar modules under challenging climate conditions

in combination with geographical aspects were developed. [5]

Based on the international standard IEC 61215:2016, test programs were extended or newly generated. [6] Temperature changes over the season can be used to prepare thermal cycling tests, while day-night temperature changes are needed to prepare test programs especially for thermally sensitive materials like wires or inlays. The differences in solar radiation between the various climate zones have to be considered in relation to humidity and other effects. To estimate the mechanical stress of glass laminates or façades for building integrated photovoltaics, the wind load has to be considered. Following these considerations, three different models were defined as basis for the test programs: tropical climate (temperature always above +18°C), desert climate (extremely dry conditions), as well as moderate climate as reference (central European climate). In moderate climate zone, the temperature of the cold season is in the range of -3°C to +18°C, deposits are at a level higher than in dry environment. For each climate model zone, typical geographical areas can be identified.

Different polymeric materials, usable as interlayers for laminated glasses or photovoltaic modules, are currently under investigation using the developed test methods. First results indicate, that special polyolefin materials are offering very good ageing properties. [7]

However, EVA based interlayer films are

also showing durable performance under the test conditions. EVA interlayers are also an advantage, if effects of wind have to be considered. Due to the crosslinked polymeric network, EVA films can withstand wind loads, especially at high temperatures better than most of the thermoplastic materials. This performance strongly depends on the formulation of the EVA interlayer film. The selection of the EVA needs to be focused on the content of vinyl acetate, and the melt flow index. [8] These factors influence the melting behaviour of the film during extrusion and lamination, as well as the optical properties of the final laminated glass or photovoltaic module. The selection of the optimum additive formulation is the second important key to a successful interlayer film. Some basics are well-known, but mainly focusing on solar applications. [9-11] For application in energy efficient buildings, further developmental work is required. This is the focus of current work of the Folienwerk Wolfen GmbH and its research partners.

### Conclusions

Modern architecture requires new concepts for energy-efficient buildings. Due to the large surfaces, façades, roofs and windows are offering the possibility to generate and store heat or energy. To bring in such functionalities, laminated structures can be used. Glass laminates are an advantage both of regarding aesthetics and functionality.

As an example for façade and window application, results of a research project for the development of composite capillary glasses were discussed. The key targets for such laminated capillary glass include visual appearance, chemical resistance, as well as mechanical and safety requirements.

For fulfilling the needs, an adhesive with well-balanced properties is required for the laminated glass. Different adhesion systems were examined. From the results, the evguard® EVA interlayer film has shown good performance for the requirements. Potential markets for energy-efficient buildings are along the sun-belt of our planet. However, the solar energy gain in these areas is combined with harsh environmental conditions. The temperatures, differences in day-night temperatures, load of wind and sand, as well as UV radiation are significantly higher, demanding materials which can withstand the challenges of the climate conditions. The development of materials for such regions requires ambitious test methods. Some initial results of such test methods for laminated glasses for architectural and photovoltaic applications are shown.

## References

- [1] Nat. Geographic magazine, German Ed., Nov. 2015, p. 100
- [2] [www.lawin.uni-jena.de](http://www.lawin.uni-jena.de)
- [3] B.P.V. Heiz, Z. Pan, G. Lautenschläger, C. Sirtl, M. Kraus, L. Wondraczek, Adv. Sci. 2017, 4, 1600362
- [4] C. Sirtl, M. Kraus, C. Hadlich, A. Osburg, L. Wondraczek, in: B. Weller, S. Tasche (Eds.): Glasbau 2017, Ernst & Son, 2017, p. 305
- [5] E. Heyer, Witterung und Klima – Eine allgemeine Klimatologie, B.G. Teubner Verlagsgesellschaft, 1988, p. 169 ff.
- [6] S. Dietrich, M. Pander, M. Sander, S.H. Schulze, M. Ebert, in: N.G. Dhere, Bellingham, WA: SPIE, 2010 (Proceedings of SPIE 7773) Paper 77730F
- [7] S.H. Schulze, M. Wendt, C. Ehrich, S. Henning, R. Meitzner, Proc. EU PVSEC 2014, p. 3138 – 3141
- [8] D.C. Anderson, „EVA overview: Global demand, regional market capacities and trends“, 2nd Symposium Polymer Apps in Photovoltaic, Leipzig, 12./13.03.2012
- [9] F.J. Pern, Angew. Makromol. Chemie, 252 (1997), 195
- [10] S.M. Tamboli, S.T. Mhaske, D.D. Kale, Indian Journal of Chemical Technology 11 (2004) S. 853
- [11] S.H. Schulze, A. Apel, R. Meitzner, M. Schak, C. Ehrich, J. Schneider, Proc. EU PVSEC, 2013, p. 503 - 507

## Acknowledgements

The authors kindly acknowledge financial support from the European Commission through its Horizon-2020 framework program (Grant Agreement GA 637108). The financial support of the Federal Government of Saxony-Anhalt (project number 1604/00008) is also gratefully acknowledged. Many thanks to all members of the projects for fruitful discussion and collaboration.

# Minimum Energy Performance Requirements for Window Replacement in the 28 EU Member States

Cédric Janssens  
Glass for Europe

## Keywords

1=energy performance 2=windows 3=building  
4=minimum requirements 5=energy efficiency  
6=energy saving

## Abstract

In the European Union, Member States are allowed to set minimum performance requirements to construction products available on their market. It is preferred not to have EU wide performance requirements, so that individual Member States regulate such performance individually taking into account their own building stock and climate specificities.

In Member States that have correctly and timely implemented the European Energy Performance of Buildings Directive (EPBD) (2010) there are requirements related to the energy performance (holistic approach) of new buildings and buildings receiving major renovation. This should in theory be complemented by prescriptive energy performance requirements for building components with a very strong influence on the energy performance of the whole structure, such as windows.

In 2017, the European Union reviews the EPBD which represents an opportunity to assess the state-of-play in the Member States and, eventually, propose measures to improve the assessment of the energy performance of windows in national schemes. A study for Glass for Europe provides a clear picture of the minimum requirements for window replacement in the residential sector across the different Member States and reflects on if/how the European framework could be improved to further support the Member States with additional guidance.

## Introduction

The potential of energy savings in the European Union's (EU) building sector through

efficient building products is well known<sup>1</sup> and acknowledged by the European Commission in its Energy Union framework strategy (European Union, 2015). In a recent study commissioned by the European Commission<sup>2</sup>, windows in the EU are considered responsible for 24% of the EU heating demand and 9% of the cooling demand. These high figures can be explained by the percentage of sub-optimal windows installed in EU residential sector. A recent study estimates that over 85% of glazed areas in EU buildings are equipped either with single glazing or uncoated double glazing (TNO, 2011). When considering that over 1 billion of new windows will be sold by 2030 in the European Union, according to market forecasts available in the same European Commission study, the energy saving potential for the European building is substantial.

Despite the priority given to energy efficient buildings in Europe and the vast amount of energy that can be saved if consumers opt for energy-efficient windows, putting in place meaningful regulatory measures at EU level to foster building renovation and push the market has shown to be a challenging task.

The Energy Performance of Buildings Directive (EPBD) is the main EU policy driver affecting the energy use in buildings. Member States that have correctly and timely implemented the EPBD introduced energy performance (holistic approach) requirements for new buildings and buildings receiving major renovation. These do not exclude the existence of prescriptive requirements for building components with a very strong influence on the energy performance of the whole structure (or components with relatively long lifetimes), including windows. In other words, under the EU legislative structure, it is preferred not to have EU wide performance requirements, so that individual Member States can set minimum performance requirements to construction products available on their market, taking into account their own building stock and climate specificities.

A recent study commissioned by Glass for Europe to Ecofys (figure 1), in the context of

the current revision of the EPBD, shows that all Member States but one (i.e. Estonia) have introduced such requirements for windows. The Glass for Europe's study by Ecofys is based on existing studies, legal national documents, and interviews with contact person from all Member States, including the three Belgium regions and four UK regions. The findings of the study highlight divergences between Member States in terms of methodology, ambition and effective implementation. The present paper will present these key differences and reflect on if/how the European framework could be improved to further support the Member States with additional guidance.

| Member State          | Legal requirements                           |             |             |
|-----------------------|--|-------------|-------------|
|                       | U <sub>w</sub> - value<br>W/m <sup>2</sup> K | g - value   | Last update |
| Austria               | 1.2  | -           | 2015        |
| Belgium - Brussels    | 1.8 (U <sub>2</sub> : 1.1)                   | -           | 2014        |
| Belgium - Flanders    | 1.5* (U <sub>2</sub> : 1.1)                  | -           | 2016        |
| Belgium - Wallonia    | 1.5 (U <sub>2</sub> : 1.1)                   | -           | 2017        |
| Bulgaria              | 1.4*   | -           | 2015        |
| Croatia               | 1.6 / 1.8*                                   | -           | 2015        |
| Cyprus                | 2.9*   | -           | 2017        |
| Czech Republic        | 1.5  | -           | 2011        |
| Denmark               | -*   | -           | 2015        |
| Estonia               | -*   | -           | 2013        |
| Finland               | 1.0*   | -           | 2012        |
| France                | 2.3 / 2.6*                                   | -           | 2008        |
| Germany               | 1.3  | -           | 2014        |
| Greece                | 2.6..3.2*                                    | -           | 2010        |
| Hungary               | 1.6*   | -           | 2006        |
| Ireland               | 1.6*   | -           | 2011        |
| Italy                 | 1.7..3.2*                                    | 0.35*       | 2015        |
| Latvia                | 1.3.k / 1.8.k*                               | -           | 2015        |
| Lithuania             | 1.6.k*                                       | -           | 2014        |
| Luxembourg            | 1.5*   | -           | 2016        |
| Malta                 | 4.0*   | 0.89        | 2015        |
| Netherlands           | 2.2  | -           | 2015        |
| Poland                | 1.1*   | -           | 2017        |
| Portugal              | 2.2..2.8*                                    | 0.10..0.56* | 2016        |
| Romania               | 1.5*   | -           | 2016        |
| Slovak Republic       | 1.0  | 0.60        | 2016        |
| Slovenia              | 1.3*   | 0.50        | 2010        |
| Spain                 | 2.5..5.7*                                    | -           | 2013        |
| Sweden                | 1.2*   | -           | 2012        |
| UK - England          | 1.6*   | -           | 2016        |
| UK - Wales            | 1.6*   | -           | 2014        |
| UK - Northern Ireland | 1.6*   | -           | 2013        |
| UK - Scotland         | 1.6*   | -           | 2016        |

Figure 1: Overview about legal requirements for replacement of windows in residential buildings by Member State – Ecofys for Glass for Europe - 2017

<sup>1</sup>See for instance the International Energy Agency study on "Capturing the Multiple Benefits of Energy Efficiency"

<sup>2</sup>Preparatory study on window energy label (2015) – preparatory study (Lot32)

## Main learnings

### Calculation of the windows' energy performance

In 27 EU Member States (out of 28) minimum requirements for windows have been introduced. These requirements can be regrouped in three categories: minimum requirements based on the U-value (being  $U_w$ -value or  $U_g$ -value), on the  $U_w$ -value and g-value separately or on the energy balance combining both the  $U_w$ -value and g-value.

A vast majority of Member States have introduced in their national legislations minimum requirements for windows based solely on the heat transition coefficient for the whole window (glass and frame); i.e.  $U_w$ -value (see table 1). In total, 18 EU Member States make use of this value only; i.e. Austria, Bulgaria, Croatia, Cyprus, Czech Republic, Finland, France, Germany, Greece, Hungary, Ireland, Luxembourg, Netherlands, Poland, Romania, Spain and Sweden. For the three Belgian regions, Latvia and Lithuania the minimum requirements are based solely or partially on the  $U_g$ -value (heat transition coefficient for the transparent area).

Only five countries include legal requirements for the total energy transmittance factor of glazing system, i.e. g-value, to complement the requirement based on a  $U_w$ -value: Italy, Malta, Portugal, Slovak Republic and Slovenia. Despite significant yearly solar irradiance levels, countries from the South of Europe and Central Europe (Western or Eastern Europe) such as Spain, Greece, France, Germany, Czech Republic or Bulgaria are not considering the solar heat gains in their energy performance calculations and minimum requirements.

Only Denmark applies minimum requirements for windows based on the energy balance approach combining both the solar heat gains and heat losses of the window into a single value (figure 2). However, the United-Kingdom allows legal requirements to be met either by way of meeting minimum requirements based on the  $U_w$ -value (i.e. 1.6 W/m<sup>2</sup>K) or band of the Window Energy Rating label (i.e. Band C or better) which is calculated based on the energy balance approach.

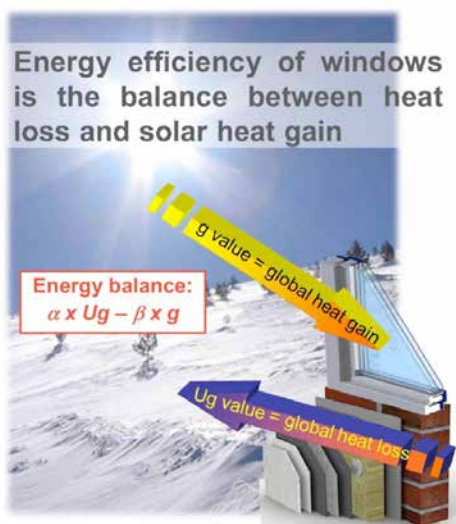


Figure 2: Energy balance<sup>3</sup> – Glass for Europe

*Despite the fact that the energy balance has been widely recognized by window professionals has the only effective way to assess the energy performance of a window, e.g. eco-design preparatory study Lot 32 on windows<sup>4</sup>, this methodology is only applied in Denmark and the United-Kingdom. A vast majority of Member States focuses the requirements on the sole  $U_w$ -value, not taking into account the energy gains from passive solar irradiance; while five Member States introduced additional separated requirements based on the g-value which does not provide a balance between the heat gains and heat losses over one year.*

### Minimum requirements based on the $U_w$ -value

As underlined previously, Estonia is the only EU Member States which does not have set minimum legal requirements for replacement of windows in the residential buildings. All other EU Member States have introduced minimum requirements based on the  $U_g$ -value, being by way of a  $U_w$ -value,  $U_g$ -value (i.e. three regions in Belgium) or integrated in the energy balance calculation (i.e. Denmark and United-Kingdom WER label).

From a formalistic point of view, all Member States are compliant with the EU legislation prescriptions. However, when looking at the minimum requirements set in the national legislations, two fundamental problems arise in an important number of Member States: the sub-optimal minimum requirements set in the national regulation and the absence of updates.

As mentioned in the introduction of this paper, under the European legislation (EPBD), it is the Member States' responsibility to set the minimum requirements for building components with a strong influence on the energy performance of the whole structure. The flexibility given to Member States is meant to give room for national regulations to take into account their own building stock and climate specificities. However, when looking at the requirements set for windows in some countries, one can hardly argue that the very low minimum requirements are resulting from national climate or building stock. For instance, two of the EU founding countries, namely France and the Netherlands, have set minimum requirements respectively at 2.3 W/m<sup>2</sup>K and 2.2 W/m<sup>2</sup>K. In comparison, Germany minimum requirements for windows is set at 1.3 W/m<sup>2</sup>K. At the moment, the two countries with the most demanding minimum requirements are the Slovak Republic and Finland with a  $U_w$ -value of 1.0 W/m<sup>2</sup>K.

As one could expect, the minimum requirements are usually most demanding in the North compared to the South of Europe. What is more interesting is that for the Center of Europe, the requirements set in the ten Central and Eastern European countries which joined the EU in 2004 and 2007 are often more ambitious than in the founding members' countries. For instance, in Poland, the minimum requirements are set at 1.1 W/m<sup>2</sup>K compared to 1.3 W/m<sup>2</sup>K in Germany.

Another fundamental problem highlighted by the Ecofys findings is the absence of updates in the legal requirements. Eight countries have not updated their building codes minimum requirements for at least five years: Czech Republic, France, Finland, Greece, Hungary, Ireland, Slovenia and Sweden. In the case of minimum requirements for windows, the absence of updates is expected to be even more important since an update of building code does not necessarily implies an update of the minimum performance requirements of all the building elements. For instance, in England, the minimum requirements for windows remained the same despite the revision of the building code in 2016.

It is interesting to note that two countries have put in place an automated update of their minimum performance requirements for windows to anticipate the increase in the energy performance of windows available on

<sup>3</sup> $\alpha$  and  $\beta$  in the Energy balance equation refer to climate data specific to the location of the building; i.e. typical outdoor temperature and solar irradiance across the year

<sup>4</sup>Preparatory study on window energy label (2015) – preparatory study (Lot32)

their national market: Poland and Bulgaria. In Bulgaria, the current minimum  $U_w$ -value is set at  $1.4 \text{ W/m}^2\text{K}$  for windows with PVC frames and shall decrease to  $1.1 \text{ W/m}^2\text{K}$  by 2018 and  $0.6 \text{ W/m}^2\text{K}$  by 2020. In Poland, the current minimum  $U_w$ -value is set at  $1.1 \text{ W/m}^2\text{K}$  and shall decrease to  $0.9 \text{ W/m}^2\text{K}$  by 2021.

*In this section of the paper only extreme cases were used to illustrate the sub-optimal minimum requirements set in Member States and the absence of updates. While extreme cases were used, the same two loopholes that negatively affect the minimum requirements apply to a majority of countries (see table 1).*

## Scope and implementation of the legal requirements

A third finding of the study is the problem related to the scope and implementation of the legal requirements for windows in national regulations. It is important to note here that the Glass for Europe's study by Ecofys report (table 1) shows the minimum performance requirements for window replacement in the residential sector when these exist. In practice, their implementation and scope differ due to conditions added in the national regulations, generating de facto loopholes in the regulation. It results that, in those countries, windows not meeting the minimum requirements could be installed under certain conditions.

Glass for Europe's study by Ecofys shows that in only 11 Member States (out of 28) the minimum requirements for windows apply to single window replacement; i.e. Austria, Cyprus, Denmark, France, Hungary, Lithuania, Luxembourg, Romania, Spain and the United-Kingdom. It results that the residential market in those countries is limited to windows with a performance equal to the minimum requirements or higher.

For 11 Member States, the Glass for Europe's study by Ecofys shows that conditions are set for the application of the minimum requirements to window replacement; i.e. Belgium, Croatia, Czech Republic, Estonia, Finland, Germany, Greece, Ireland, Italy, Poland and Portugal. In other words, windows for the residential sector with a performance below the minimum requirements could still be installed. These conditions to the application of the minimum requirements are often based on the need for town permit prior to the renovation or minimum area to be renovated. For instance, in Belgium, the minimum performance requirements apply only if a town planning permit is required. Another example is Germany, where the minimum requirements

apply only if 10% or more of the building component area is concerned.

It is worth to note here that Finland reported that, despite the conditions allowing windows with a lower level of performance to be installed in the residential sector, almost 100% percent of the renovation market fulfil the minimum requirements as manufacturers do not produce windows below those requirements. No other countries reported the same market trend in the research.

For six Member States out of the 28, the study has not been able to confirm if conditions apply to the minimum requirements for window replacement; i.e. Bulgaria, Latvia, Netherlands, Slovak Republic and Slovenia.

*The Glass for Europe's study by Ecofys highlights that when minimum requirements for windows exist in national regulations they are often conditional. One may reasonably consider that the conditions applying to the minimum requirements limit the push to the market for window replacement.*

## Conclusion

Minimum performance requirements are in many countries not what drives the market towards energy efficient products, since they often refer to sub-optimal choices and apply under certain conditions. To make minimum performance requirements a driver, the EU legislative framework currently under revision (EPBD) could be improved to be more effective. Glass for Europe's study by Ecofys tend to demonstrate that although the legislative framework forces Member States to set minimum requirements it fails on two aspects: the lack of guidance on how to best assess the energy performance of windows (i.e. energy balance) and its flexibility which allows Member States not to properly implement it.

In view of the current EU political context, it is unlikely that the EPBD could be strengthened and be made more stringent vis-à-vis Member States in its current revision. Therefore, the work to improve the minimum requirements for windows needs necessarily to be made in countries, with national authorities.

This paper identifies three elements that need to be improved to achieve that objective: Firstly, when outdated, sub-optimal or based on the sole U-value or separated U-value and g-value, minimum requirements should be reviewed and be based on the energy balance approach. Secondly, national legislations could include milestones with automated

update/review of the window minimum requirements to anticipate the increase in the energy performance of windows available on their national market. Thirdly, minimum requirements for windows shall apply to new buildings, major renovation down to single window replacement.

## References

- Buildings Performance Institute Europe (2011) "Europe's Buildings under the Microscope. A country-by-country review of the energy performance of buildings".
- European Union (2010), "Directive 2010/31/EU of the European Parliament and of the Council of 19 May 2010 on the energy performance of buildings", 2010/31/EU, 19 May.
- European Union (2015) "Communication from the Commission to the European Parliament, the Council, the European Economic and Social Committee, the Committee of the Regions and the European Investment Bank, A Strategy for a Resilient Energy Union with a Forward-Looking Climate Change Policy". COM(2015) 80 final, 25 February.
- European Commission (2016), "Proposal for a directive of the European Parliament and of the Council amending Directive 2010/31/EU on the energy performance of buildings", COM(2016)675 final, 30 November.
- International Energy Agency (2015), "Capturing the Multiple Benefits of Energy Efficiency".
- Glass for Europe study by Ecofys (2017) "Minimum performance requirements for window replacement in the residential sector".
- TNO Built Environment and Geosciences (2011), "Glazing type distribution in the EU building stock", - February 2011.

## Websites

- Preparatory study on window energy label (2015) – preparatory study (Lot32)

# Applicability of Design Thinking to the Construction Industry

Olavi Uusitalo  
Holmark

## Keywords

1=Design thinking 1=Customer experience  
2=Construction industry

## Abstract

The aim of the paper to apply design thinking to the construction industry via recent case studies. Design thinking, first used to make unique products, is now being applied to complex, intangible issues, such as how a customer experiences a service and in company strategy. A company-wide focus on it offers good opportunities for humanizing technology and for developing emotionally resonant services. A collaborative design-thinking may solve several supply chain problems such compatibility of components, right information and good communication. The paper employees several cases from the construction industry.

## 1. Introduction

Customer relationship management (CRM) has been used for decades. It should collect information from each customer and share the information in the organization. CRM seems to work only for marketing people but not over the all organization. CRM systems are not necessarily user friendly. They probably need expensive tailoring for small and medium size firms (SMEs).

The aim of the design is to reduce the everyday complexities. People need help making sense of them. People need their interactions with technologies and other complex systems to be simple, intuitive, and pleasurable. Design thinking's principles -empathy with users, a discipline of prototyping, and tolerance for failure for instance - are the best tools for creating simple, intuitive and neat interactions and for developing a responsive, flexible organizational culture. A focus on design thinking offers unique chances for humanizing technology and for developing emotionally resonant products and services. Adopting this perspective isn't easy. But doing so helps create a workplace where people want to be, one that responds quickly to troubles on deliveries and changing business dynamics

and empowers individual contributors. And because design is empathetic, it implicitly drives a more thoughtful, human approach to business. [1]

Once people try the design thinking tools and see the benefits, they get excited. That's where the second challenge kicks in: You cannot master any skill just by doing a workshop; you need to practice it until it becomes second nature. Internal acceptance comes only with proven results. Start small with an initiative that has good odds of success (few internal stakeholders, not a lot of dependencies, fairly clear success criteria). [2].

The aim of the paper is to find out whether design thinking could help firms to form a comprehensive view of their products and processes. This means to enlarged the focus on customer experience even in small things and understand how good customer experience is made and how it is destroyed. The focus is SMEs in the construction industry. However, I try to take ideas from large firms experience of design thinking. I use several case examples to illustrate the situation where I think design thinking could have been helpful. The rest of the paper has three parts. First, the idea, the content and the process of design thinking are briefly discussed. Second, the recent empirical cases from the construction industry are illustrated. Third, in the conclusion an example, balcony and terrace glazing from the glass process and the managerial implication are given.

## 2. Design thinking

### 2.1. The idea and the content of design thinking

Firms must focus on users' experiences, especially their emotional ones. To build empathy with users, a design thinking organization let employees to observe behaviour and make conclusions about what customers want and need. These conclusions may be very hard to express in quantitative language. Instead, organizations that identify design use emotional language (desires, aspirations, engagement, and experience) to illustrate products and users. Design thinking, first used to make physical objects, is increasingly being applied to complex, intangible issues, such as how a customer experiences a service and also company strategy. Design thinkers tend to use physical

models, also known as design artifacts, to explore, define, and communicate. Those models—primarily diagrams and sketches—supplement and in some cases replace the spreadsheets, specifications, and other documents that. [1]

In a firm emphasizing efficiency and engineering rigor the designers had little status or influence. In 1996 Samsung made a change and started to create design lead culture and recruited a lot of designers (now 1600 designers). The innovation process begins with research conducted by multidisciplinary teams of designers, engineers, marketers, ethnographers, musicians, and writers who search for users' unmet needs and identify cultural, technological, and economic trends. Although designers have strong support from top management they face continuously challenges coming from the company's deep-rooted efficiency-focused management practices. Design must co-operate intensively with suppliers to get new designs for both products and services. [2].

In many ways, the idea of intervention design is very relevant for B2B companies. Because B2B customer relationships are often very intimate, rapid iterative prototyping in collaboration with the customer— which makes the customer more confident in the change as the intervention design goes on— is easier to do. Recently a food manufacturer applied a collaborative design-thinking approach to solve supply chain challenges with its supermarket customers. [3]

Pepsi reinforces the importance of finding the right person to launce design thinking and make a change. The company pushes design thinking through entire system from product creation to packing and labelling to how a product looks on the shelf and how consumers interact with it. According to CEO their products look like they're tailored to the right cohort groups, and our packaging looks great, too. She defined a well-designed product as one you fall in love with. Pepsi pays a lot more attention to user experience focusing on crunch, taste, and everything else now pushes us to rethink shape, packaging, form, and function. All of that has consequences for what machinery we put in place—to produce, say, a plastic tray instead of a flex bag. It forces the design thinking both back in the supply chain and forward to marketing channel. Pepsi's retailers fell in love with the person

responsible for design thinking and invited him to their shops to talk about how to reset their shelves. [4].

## 2.2. The Design Thinking process

The design thinking process (Figure 1) has four stages: Immersion, Analysis and synthesis, Ideation and Prototyping [5]. The first one is broken down into two parts: Preliminary Immersion (PI) and In-Depth Immersion (I-DI). PI seeks an initial understanding of the problem and, if needed, to reframe it. I-DI tries to identify the needs of the stakeholders (for instance in renovation of apartment buildings) involved in the project, and the opportunities that are likely to arise from an understanding of their experience regarding the issue under scrutiny. Analysis and Synthesis tries to organize the data visually so as to indicate patterns that will help to provide an understanding of the whole (including the relevant stakeholders) and identify opportunities and challenges. Analysis and Synthesis with the other stages described in Figure 1 is not as a step in a linear process, but rather as a part of a tangled whole, where each stage impinges on other stages. For instance, Analysis may occur during Immersion and act as a support for the next phase, Ideation. In Ideation innovative ideas are tried to generate through collaborative activities. In Synthesis solutions (on the topic under scrutiny) are generated by using tools developed in Analysis. The ideas/solutions generated are then selected – on the basis of business goals, technological feasibility and, naturally, the human needs that are to be met – for validation in the Prototyping stage. [5]

## 3. Empirical cases

The empirical cases come from the construction industry. I have myself experienced them and they took place during the last ten years. Design thinking is not a new thing. In the travel business people have unwittingly used it. The first case illustrates this. It comes from the travel business and from the late 1990s. The second case is an illustration of a six-year assembly process of a geotherm heating system in a private house. The third case tackles bathroom renovations. The last case is story of the missing bolts of a chimney cover.

### 3.1. Experience from Australia

Twenty years ago I travel to Australia. I arrived the hotel at midnight. At the entrance door I just happened to count the hours, 30, I had travelled from my home door. At the reception the lady said politely that I had to wait for my room another half an hour. Since I knew my travel hours it was easy for to say: "That is not a big deal. It does not matter whether I travel 30 hours or 30.5 hours" Immediately she switched the tone by saying that there is a honeymoon sweet waiting for you. For eight days I lived in a large, nice sweet having living room with TV, bedroom with TV and balcony to the north, bathroom with jacuzzi and kitchenette.

### 3.2. Where is the expertise and service?

Everything started six years ago, when I visited the construction exhibition to get acquainted with geotherm systems for private houses. I had considered switching from oil to geotherm. In addition to the three offers received in the exhibition I asked a fourth one on the web pages of a domestic supplier (later on the original equipment manufacturer / OEM). The OEM never replied. About a year later in March 2012 I met in another occasion the management of the OEM. They presented me

the equipment I had been interested in. Next month a local dealer chosen by the OEM made me an offer.

In early June I asked for an offer for a more powerful unit. I neither got a new offer nor a contact to the dealer until August. I got a new offer, accepted it and fixed the drilling and assembly dates which were a month later than planned. This mixed up my schedule since I had planned to make the necessary renovation work between my two trips. The assembly went almost without any troubles. The physical size (larger than expected) of the heating unit caused extra work. The lack of electrical drawings prevented me from making the electrical installations. The first technician from the OEM made them in the next day while I was on trip. The system seemed to work. As the days got cooler the troubles started. The heating unit was connected directly to radiators without any buffer cylinder. This made the radiators creak while they cooled and warmed up. Usually a buffer cylinder is installed in the heating system as the water circulating continuously through the buffer cylinder is approximately at the same temperature which prevent the radiators making noise. The lights started to flicker all over the house because of the high ignition current taken by the compressor. This was fixed on March 2013 by the second OEM technician. The next trouble occurred when the expansion container stopped working. The replacement of it the container took half a year regardless of several contacts. Troubles continued. By Christmas 2013 the heating in the bathroom did not work. One pump was not on. In February 2014, the third OEM technician noticed that the assembly of the bathroom floor heating was wrong. At the same time, he noticed (ok) that the main pump of the floor heating had been off since the original assembly one and a half year ago. The wrong connection prevented the sensor and the adjusting valve working properly. The bathroom was still cold. By moving the sensor as far as possible from the valve I managed to get this circuit to function. In September 2014 I called the moral seller of the equipment, the person from OEM management who, with his charisma, had sold the equipment to me back in March 2012. The fourth OEM technician came on September. He understood the problems well. I got an offer from him for a buffer container, the fixing of the wrong connection and a promise that another dealer chosen by them will contact me. I accepted the offer. Nothing happened. In December 2014 I informed the OEM about this. In January 2015 a person from the second dealer contacted and we agreed to revert this after winter. In April 2015 we agreed on how to proceed. For a month, I asked for a plan and a

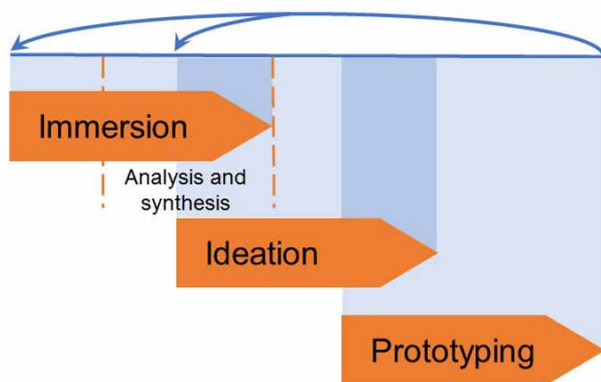


Figure 1. Design Thinking process [5]

drawing from him, in vain. The hectic time had prevented him from doing his job. After a half year, in November 2015 I contacted the OEM who promised to take care of this. I informed the dealer what I wanted from the system and asked him to make an assembly drawing and a list of needed devices. A couple of months passed, again. In January 2016, I called the dealer's representative, who said that he had not enough knowledge to make a plan or a drawing. He promised to ask for help from the OEM. I waited for a month, again, until I wrote an article on a newspaper. Somebody at the OEM had deduced from the article that I was their customer. This info reached the dealer, as well. Nothing happened. In April 2016, I called the dealer. An unknown person to me, the owner- manager, promised to take care of my project. Nothing happened. One month later, I tried to call the contact person at OEM. I left a message to him. Nothing happened. Three weeks later, I left a message relating to several matters, one being this heating system problem, to the person in the management. After this message in June the OEM contact person visited, asked R&D unit to make an assembly drawing, which I received later. We also booked a seven-day time lot for assembly. He promised that the dealer would fix the date with me. After checking the drawing with my neighbor, I sent my acceptance and the list of necessary control sensors and devices. In the early August, the OEM notified me about the assembly. I did not receive any info about

the coming assembly from the dealer. In this situation, I thought that the assembly would start on first day of suggested time lot. Nothing happened. After informing the OEM, the dealer called and the date was fixed. The dealer's technician had a wrong assembly drawing. I gave him the right one. The 2012 control unit was not compatible with the 2016 devices. The third OEM technician fetched a compatible device from the warehouse. The electrician from a third firm installed an ordinary thermostat in the bathroom, although the list provided to the OEM had a dampproof one. In the early September, the heating did not function. During a phone call to the third OEM technician I could not fix the problem. The house was without heating during my two-week trip. The fifth OEM technician found that two thermostats had been connected to wrong heating circuits. Thermostats were switched to the right circuits. The heating was on and the house was warm. However, I could not find the bathroom circuit in the remote controller. It has not been set there. During a phone call with the fifth OEM technician, I could fix this last? problem. What went wrong? How to improve performance?

### 3.3. Bath room repair

The bathrooms are usually at least in old flats or houses very small. The small size asks for a proper repair design. Every centimetre should be used. In our case the installation of the waste water outlet pipe on the middle of

the space of the washing machine (not in the empty lots of the space of toilet seat) took the washing machine 8 centimetre closer to the sink. Every morning you feel in your feet the machine. The heating unit was without the thermostat. In the summer time the bathroom was extremely hot. A comprehensive view of the renovation of the bathroom was missing. The safety aspect is very important in electrical installations. However, it should not be the only design criteria. The design should take in the account also the customer experience while using the flat after renovation. Usually in bathroom repairs the design focus is solely on bathroom. In this case, necessary sockets (loading mobile phones, laptops, etc., light for a mirror lamp etc.) in the hall through which electricity wiring was taken anyway could have been installed. I have seen several halls which missed sockets after the bathroom repair. Kitchen needed also sockets; easily they could have been installed since kitchen shared the wall with bathroom. Moreover, the extra switchboard took the place of an important piece of furniture, the chair, to be used while phoning. The switchboard could have been installed up just under the ceiling.

### 3.4. Chimney cover

A chimney cover keeps precipitation from entering the chimney flue and protects the inside of the chimney. It was made of two steel plates (one glides inside the other one), which gives the adjustable length. The width is adjusted by placing the feet of the cover



Figure 2. Assembling the chimney cover [Photo: Olavi Uusitalo].

according to the collar of the chimney. The long rods tighten the feet of the cover against the collar. The cover is relative simple to install if one has enough rods, bolts and nuts (Figure 2). While assembling the chimney cover the package lacked about twelve dip-zincd 8 mm nuts. Very seldom there is in a private house that many such bolts. It was the last the last day of my stay in that house that time. The way to the nearest hardware store was 15 kms. The daylight was disappearing, as well. Everything was against me. I was lucky to find several equipment in the garage which had 8 mm bolts. I managed to get the missing ones.

#### 4. Conclusion

The balcony and terrace glazing is one example from the glass processing business. What is the use of balcony or terrace. Is it for year-round use? What is expected from glazing. It prevents dust, dirt, wind and rain from reaching the balcony or terrace, protects terrace structures and units as well as suppresses noise. Glazed balconies terraces add safety and comfort to private- as well as apartment houses. In apartment houses the width of balconies increased in the 1908s so that a balcony can be used as an extra room. Every terrace should be planned well. It is not only glazing. What else than glazing can be the unidentified needs to increase the comfort of the uses? Is electricity needed for radios, lights, laptops, tablets or heating? Where should sockets be assembled to avoid the use of loose cables? Can you use the glazed balcony for heating purposes (intake of the air to the heating system)?

What can get from the cases. In the first one the receptionist in the hotel understood at once the traveller's situation solve the troubles. Supposedly she had been in this kind of situation earlier i.e. she had prototyped it. Anyway, a great user experience since I keep talking on it after 20 years. In the second case, nobody was interested either in the user experience or a comprehensive picture of the delivery (not even after three years). The OEM did not have CRM. I doubt whether it would have helped. According to Pepsi design thinking helps the co-operation in the value chain. It may have helped also in the second case to improve communication, to avoid noncompatible components and to create a comprehensive picture of the delivery. In bathroom repair the design thinking process could have helped. First, to figure out what are needs of people in the 2010s? Second, a visit to the flat (=prototyping) see the most important aspect: the save of space both in the hall and bathroom. The user would have paid extra for having the waste water outlet giving room for washing machine and the extra switchboard for

the chair. The user lives with these "mistakes" for the next 20 years. In the last case, the manufacturer blamed the subcontractor for the fault. Then I realized how important it is for a manufacturer to know the worst-case scenario if something is missing from the delivery. It should have been prototyped together with the subcontractor, which would have made the packer emphatic for the end user and focused to put all necessary bolts in the package.

These matters hopefully help to understand the power of design thinking in small things within SMEs. Design thinking is not only for large firms. It helps to get out from the tunnel vision of the business. What else for instance the glazing of terrace can give for the user. It also helps to when a process (for instance delivery) sucks and enables quick action to fix it. Design thinking helps people and organizations cut through complexity. It's great for innovation. It works extremely well for imagining the future. "Design thinking is an essential tool for simplifying and humanizing. It can't be extra; it needs to be a core competence". [1].

#### References:

- [1] Kolko, J. "Design Thinking Comes of Age The approach, once used primarily in product design, is now infusing corporate culture", Harvard Business Review, September, 66-71, 2015.
- [2] Yoo, Y and Kim, K. "How Samsung Became became a Design Powerhouse", Harvard Business Review, September, 72-78, 2015.
- [3] Brown, T. and Martin, R. "Design for Action How to use design thinking to make great things actually happen", Harvard Business Review, September, 56-64, 2015.
- [4] Ignatius, A. "Spotlight Interview How Indra Nooyi Turned Design Thinking into Strategy", Harvard Business Review, September, 80-85, 2015.
- [5] Vianna, M, Vianna, Y., Adler, I. K., Lucena, B. and Russo, B. "Design Thinking Business Innovation", MJV Press, 2011.

# The Advantages of Digitalization in the Glass Industry

Bernhard Saftig  
Siemens AG

## Keywords

1=Digitalization 2=Integrated Engineering  
3=Integrated Operations 4=Integrated Services  
5=Siemens 6=Glass Industry

## Abstract

From Integrated Engineering to Integrated Operations and Services: digitized solutions along the entire value chain make glass plant operators and equipment suppliers more efficient, more flexible, better and faster. Digitalization will change the face of the glass industry as much as electrification and automation did in earlier times. The result will be huge leaps in productivity.

## Introduction

A Europe-wide study [1] by German industry association VDMA and McKinsey forecasts that more than ten percent of revenue in the mechanical engineering industry alone will be generated using data-based business models by 2020 (Figure 1). Open standards, powerful communication networks and integrated automation and drive technologies are also of great importance to the glass industry in this regard, as it heads toward Industrie 4.0.

## Main text

What does it actually mean when plant operators and equipment suppliers in the glass industry digitize their businesses? "In figurative terms we think of two directions, horizontal and vertical," explains Bernhard Saftig, head of Glass Business, Process Automation, at Siemens in Karlsruhe. "Horizontal refers to the digitalized value chain, which is why we say 'From Integrated Engineering to Integrated Operations and Services,' to describe consistency throughout the process – from designing the production facility and engineering to commissioning and operation, and the necessary services." In the vertical direction, on the other hand, "Integrated Operations" describes the link between the real and the virtual worlds in the operating phase, in other words the connection between



Figure 1: Data-based business models are also becoming increasingly relevant to the glass industry.

the field, automation and management levels, all the way to the Cloud.

## Digitizing the value chain, step by step

Anyone dealing with the digitalized value chain will observe that consistency always implies consistent data. Plant operators and equipment suppliers that use a standardized data platform like Comos to integrate their engineering stages reach the operating phase, and thus the market, much faster. The fact that multiple planning stages can be executed simultaneously saves both time and costs.

## Digital twin: a virtual copy of the plant

The result of Integrated Engineering is what's known as the "digital twin" – a virtual copy of all or part of the plant. At the heart of this digital twin is a consistent data model that operators and equipment suppliers can use to run plant simulations for training purposes, for example. In turn, the data gathered while the plant is in actual operation is fed back into the data model. This keeps the digital

twin up to date and maintains it as a one-to-one representation of actual plant status throughout the entire life cycle.

## Benefits of Integrated Engineering

A further benefit of the digital twin is that, even before the plant goes into real operation, operators and equipment suppliers can view it using 3D visualizations and even walk through it at a virtual level. This has the advantage that employees can be trained at an early stage and, for example, test whether all the vital parts of the plant are readily accessible. Comos Walkinside is an example of software that makes these functions a possibility. Another example that shows the advantages offered by Integrated Engineering: at the click of a mouse, all the data relevant to automation can be transferred directly from an engineering and design tool like Comos into a process control system, such as Simatic PCS 7. This can save up to 60 percent of the time normally spent on configuring the automation structures. And working with consistent data also improves the quality of the engineering. Product data can also be easily and rapidly

integrated at this point using libraries, and much more besides.

## Benefits of Integrated Operations

Simulation software like Simit can also directly acquire automation data from the process control system and the engineering and design tool. This allows all automation and process control functions to be tested ahead of time, so potential faults can be rectified prior to real-world commissioning. This, too, saves time and costs, since the real commissioning process will then run smoothly and can take place much earlier, in parallel with further configuration work. The simulation software can also be used to provide early training to operating personnel. Testing can be performed to identify wiring or programming errors. And it makes work safer for the operating personnel. During plant operation itself, too, changes in process control can be fed back into the engineering and design tool. That means you have access to up-to-date plant and process documentation at all times. A digital twin that is kept up to date saves time and costs, compared to documentation that has to be laboriously drawn up by hand or may not be available at all.

Maintenance and servicing are other aspects that are better resolved digitally during the operating phase: operators can use the process control system to convey their requirements directly and easily to the service personnel. If the service personnel use maintenance software like Comos MRO in conjunction with the opportunities offered by 3D visualization using Comos Walkinside, these requirements can be directly located and correctly assessed using the up-to-date plant and process documentation. The standardized database keeps all participants equally up to date, enabling them to arrange the necessary action in direct consultation. As a result, machines and devices can be kept perfectly maintained before any outages occur. The system works even faster if the employees can view the relevant information directly using tablet PCs. Here, too, the digital twin is brought up to date again once the process is complete.

Operations Intelligence, known as XHQ at Siemens, is another handy application in the operating phase: to make the best possible decisions, glass manufacturers must take data relating to the plant, process and economic efficiency into account. Operations Intelligence delivers all this data and these KPIs clearly and in real time, from all kinds of systems. The data can be played back on customized cockpits or dashboards with the desired level of detail. This may involve an overview of

particularly cost-intensive assets, for example. Or benchmark analyses in the plant. Or even global comparisons between different plants at different locations.

## Benefits of Integrated Services

For services, too, digitized solutions prove handy: "Software as a Service," for example. This means that equipment suppliers can obtain a time-limited license for specific software rather than purchasing it. They can then access a complete engineering environment via the Cloud, for example, without having to own and update it. Plant equipment suppliers benefit from having pre-tested packages they can use to perform these simulations, which again save time and money during the real commissioning process. Software-based employee training can also be provided ahead of commissioning.

## Cloud solution as a foundation for new, data-based business models

It is obvious that all activities containing the keyword "digitalization" will involve the use of a database. What's new is that today, the data must be available everywhere, at all times, for quite different users, if all the various businesses involved are to benefit. Cloud solutions meet all these requirements. MindSphere is one example of a Cloud-based, open Industrial Internet of Things (IIoT) operating system. Being scalable, it supports the digital transformation of companies regardless of size or industry. It can be considered as a foundation for new, data-based business models.

Anyone using the platform ("Platform as a Service – PaaS") can improve plant performance, for example, by recording and analyzing large volumes of production data. This means MindSphere is the basis for applications and data-based services from Siemens and third-party providers, e.g. in the area of predictive maintenance, energy management, or resource optimization. At the same time, platform users benefit from a development environment in which they can integrate their own applications, services, and thus implement and offer new business models.

## Smart Motors Cloud application

One of these applications involves the Smart Motors concept, a completely new generation of communications-capable drive technologies. The data recorded using integrated sensors (e.g. temperature or vibration data) can be read out quickly and easily and analyzed in Cloud

environments. This means that users can improve both efficiency and plant availability, as well as optimizing their servicing and maintenance activities. For example, they can see that not all fan motors need to run at full speed if they are not currently needed. Converters can provide a simple solution here.

## Defense in Depth

Anyone talking about the Cloud must also be able to provide state-of-the-art security concepts. To provide industrial plants with end-to-end protection against cyber attacks from both inside and outside, a simultaneous approach is needed at all levels, from operating level to field level, from access controls to copy protection. To do this, Siemens uses an in-depth defense structure – "Defense in Depth" – as an overarching protection strategy in accordance with the recommendations of ISA99/IEC 62443, the leading standard for security in industrial automation.

## Conclusions and Summary

"From Integrated Engineering to Integrated Operations and Services": digitized solutions along the entire value chain make glass plant operators and equipment suppliers more efficient, more flexible, better and faster. Digitalization will change the face of the glass industry as much as electrification and automation did in earlier times. The result will be huge leaps in productivity. "Take the first step, start with a small, easy-to-follow data analysis and review the benefits. After all, there is no manual for digitalization. It needs daring players among the plant operators and equipment suppliers who are prepared to test things at a small level and then build up step by step to larger and larger tasks," Saftig concludes.

## References

[1] <https://www.vdma.org/viewer/-/article/render/16241528>

# New Possibilities for Windshield Bending

Reinhold Senft  
Grafotec Spray Systems GmbH

## Keywords

1=Bending 2=windshield 3=Kieselguhr  
4=Diatomaceous earth 5=powderapplicator  
6=powdersprayer

## Abstract

The author compares different existing and new application systems for interleaving material for bending windshields. The comparison of existing application systems e.g. roller applicators, nozzle applicators as well as dry or liquid spray nozzle systems which are used worldwide to apply the interleaving material required to bend a windshield will be introduced and advantages as well as disadvantages are discussed. Attending this session will enable you to take a decision for the "right" application system fitting your production line.

## Introduction of interleaving material used for windshield bending

Before understanding the application equipment, it seems to be of advantage to know something about the interleaving material.

The most common interleaving material is "Kieselguhr" or "Diatomaceous Earth - DE" or "Diahydro" or "Celite". These materials are all naturally occurring, soft, chalk-like sedimentary rock that is easily crumbled into a fine, white powder. It has an abrasive feel, is very light due to its high porosity. It is very well heat resistant. The typical chemical composition is about 85% silica, about 5% sodium, about 3% magnesium and about 2% iron.

It is clearly stated, that the interleaving material used for windshield bending is a material nobody wants to work with. Because of the small particle size ( $< 20\mu$ ) it has very poor flow characteristics – therefore it is difficult to handle with the common application equipment. If used in a dry application system, the flow characteristic is a problem, if used in a wet or liquid application system sedimentation is a problem.

## Introduction of existing application systems

The interleaving application machine market knows two ways to apply the interleaving material:

Dry:  
with a dry applicator working with a "roller"  
with a dry applicator working with "air-nozzles"

Wet:  
with a liquid applicator working with "air and liquid through spray-nozzles"  
with a liquid applicator working with "liquid through spray-nozzles"  
with a liquid applicator working with a "liquid through spray-roller"

## Dry application machines

### Dry application – through "roller" application

The dry application method has the most experience and has established a large community working with such devices. When geometries become more difficult, the technical ability to distribute the interleaving material as the geometry needs is reaching the limit quickly. Then the wet application systems came into the game and established themselves as the more precise and modern way to apply the interleaving. Both methods do have advantages and disadvantages, which I want to introduce to the auditorium.

FIGURE 1

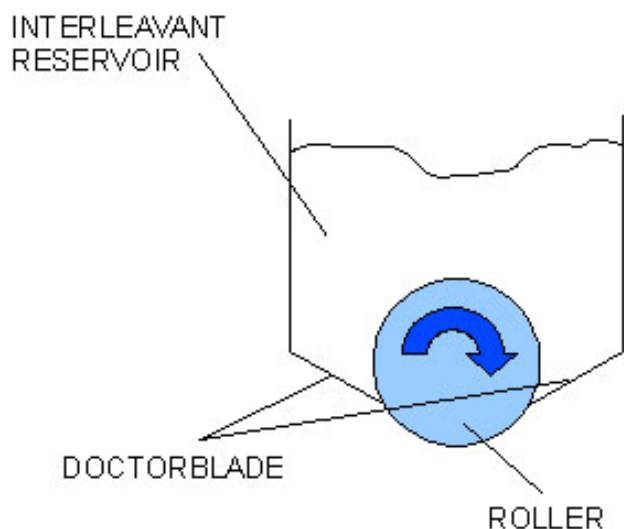
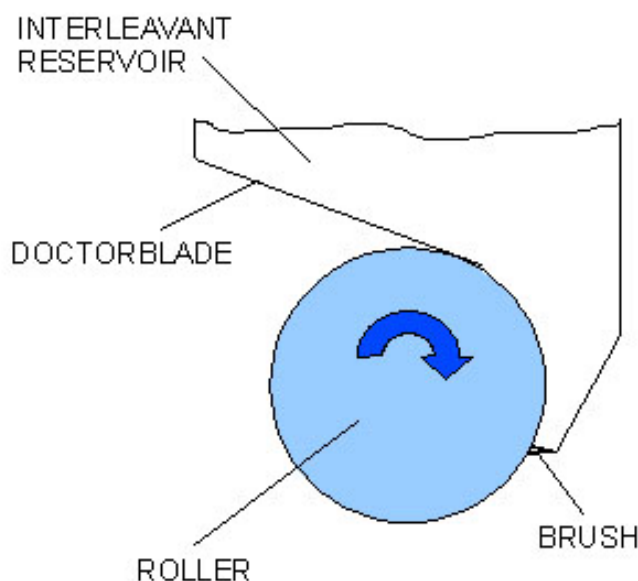


FIGURE 2



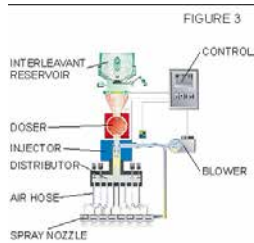


FIGURE 3

The standard technology is the “DRY ROLLER APPLICATOR” - where an engraved roller is turning in the interleaving material itself. The material was hold back from either 2 doctor blades on the side of the roller (Figure 1) or 1 doctor blade from the top of the roller and a brush from the bottom side (Figure 2). Both technologies depend on gravity, both systems are equipped with some kind of electrostatic devices trying to increase the particle adhesion to the windshield. Both systems essentially need an enclosure to ensure that air draft cannot blow away the interleaving material.

#### Dry application – through “air-nozzle” application

Transferred from the printing machinery manufacturing, air-nozzle systems (Figure 3) are much more flexible than “roller” systems. The air is used as transporter and transfers the interleaving material from the reservoir through plastic air hoses and different kind of nozzles (Figure 4) onto the glass. Due to their fast reaction time, the interleaving spill – beside the glass – is minimized. An enclosure might not be necessary without having the environment too much polluted. Because of local conditions many of the users install an enclosure to protect the spray from the wind draft, so that the distribution quality of the interleaving material appears quite good.

#### Liquid application machines

##### Liquid application – two component nozzles - air and liquid through “spray-nozzle” application

Like the air-nozzle systems the wet application with two component nozzles (Figure 5) uses air as a transporter. The liquid – or better suspension – is getting mixed with the air either inside the nozzle or right before the nozzle. Under pressure and due to the geometry of the nozzle a spray curtain

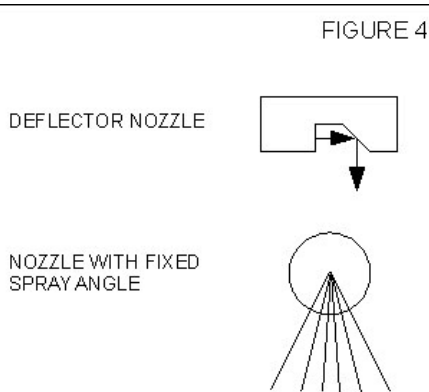


FIGURE 4

containing fine aerosols appears. Normally 2 of these nozzles are used for standard windshields. Surrounded from an enclosure, the spray falls onto the glass. Due to the number of aerosols, the control of the spray curtain is very difficult so that all these systems need an enclosure.

##### Liquid application – liquid through “spray-nozzle” application

Same principle as the two-component nozzle system, just working with only one media under pressure (Figure 6).

The suspension is pressurized and the nozzle produces the fine mist, which falls down onto the windshield.

The standard design for such machinery is containing 2 spray nozzles covered from an enclosure.

The production of aerosols is almost identical to the two-component nozzle.

##### Liquid application – liquid through “roller” application

This system (Figure 7) is not using nozzles nor working with a separate media as a transporter. The spray curtain is produced due to a roller turning at high speed and its very specific surface (Figure 7-A).

The geometry of the surface takes the suspension and throws it out of the housing. A shutter opens a gap through which the suspension is released.

After introducing the individual systems we can discuss about advantages, disadvantages and problems of the systems

#### Advantages

##### Dry application machines

###### ROLLER application system

- Price-wise very attractive
- Robust systems with rare breakdown

###### Air nozzle system (dry interleaving air operated application)

- Price-wise attractive
- Robust systems

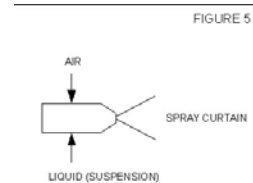


FIGURE 5

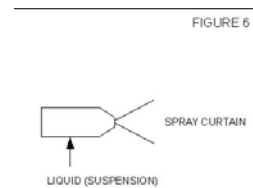


FIGURE 6

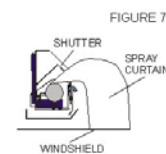


FIGURE 7

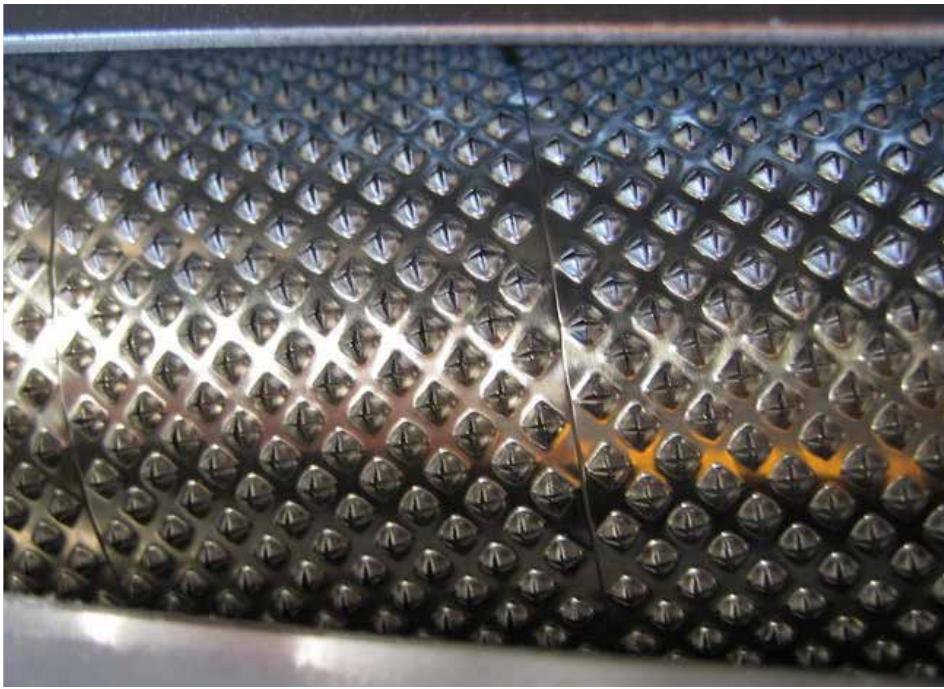


Figure 7-A

#### Liquid application machines

##### Two component nozzle system

- Price-wise very attractive
- Very fine distribution of interleaving

##### Spray nozzle (pure liquid) system

- Price-wise very attractive
- Fine distribution of interleaving

##### Roller spray system

- Fine distribution of interleaving
- Enclosure not essentially needed
- No deposit of interleaving material in the area (even in an enclosure) – relatively clean conveyor
- Absolutely no spitting effect – even after long operation time
- Highly resistant against wear-off effects
- Nozzle-free system
- No change in application quality
- Little need of maintenance

#### Disadvantages

##### Dry application machines

##### ROLLER application system

- Accumulation of interleaving material on the underside of the applicator → “fall-off” and lumps
- Interleaving distribution quality decreasing over operation time
- Vagrant interleaving material all over → needs an enclosure and/or dust extraction
- Need for maintenance (cleaning) is very high

##### Air nozzle system (dry interleaving air operated application)

- Accumulation of interleaving material on the underside of the applicator → “fall-off” and lumps
- “Spitting” effect occasionally seen
- Vagrant interleaving material all over → needs an enclosure and/or dust extraction
- Need for maintenance (cleaning) is high

##### Liquid application machines

##### Two component nozzle system

- Enclosure is essential – otherwise contamination of environment and conveyor
- Accumulation of interleaving material on the inside of the enclosure → “fall-off” and lumps
- “Spitting” effect after some time
- Wear-off of the nozzle mouth results in bad distribution and uneven deposit of interleaving
- Need of maintenance becomes more critical the longer in operation

##### Spray nozzle (pure liquid) system

- Enclosure is essential – otherwise contamination of environment and conveyor
- Accumulation of interleaving material on the inside of the enclosure → “fall-off” and lumps
- “Spitting” effect after some time
- Wear-off of the nozzle mouth results in bad distribution and uneven deposit of interleaving
- Need of maintenance becomes more critical the longer in operation

##### Roller spray system

- Price-wise unattractive
- Little maintenance

#### Problems

##### Dry application machines

##### ROLLER application system

Operators report that they need two applicator systems to operate continuously. Whilst one unit is in production, the second one is under maintenance.

Due to the roller design and the high voltage distribution, lumps are uncontrolled falling off the underside very frequently. This increases the rejection rate.

The high voltage feature needs more replacing as the operators like.

The control of the powder amount is not so good as it is mostly done through a potentiometer. A digital setting method would help to control the powder amount much better.

Interleaving adhesion to the glass is not so good, meaning that some of the interleaving is lost during handling – depending on the process.

Pairing right after the interleaving application seems to be the best process step, but the risk of plate movement during transportation is quite high.

Over-spray contaminates the application area – especially below the glass.

##### Air nozzle system (dry interleaving air operated application)

Operators report that the accumulation of interleaving on the underside and around the nozzles is causing problems, because the interleaving falls off uncontrolled and leaves lumps on the glass.

Occasionally operators report that “stripes” can be seen in the distribution of the interleaving, without quality effects in bending.

“Stripes” are commonly indicating worn-off nozzles. After replacing the “stripes” are gone.

The risk of plate movement is also present.

Over spray contaminates the application area – especially below the glass.

##### Liquid application machines

##### Two component nozzle system

The major problem with all nozzle systems is “spitting” and the “area contamination”. Depending on the

quality of the spray nozzle the “spitting” effect occurs earlier or later, but no nozzle design can overcome this problem.

Most of the operators of nozzle systems have an enclosure for the spray system. The biggest problem with it is maintenance. What happens is that the spray curtain also reaches the walls of the enclosure on the inside. The interleaving accumulates and falls-off after some time. Only frequent maintenance (cleaning) helps out of this problem.

Another reported problem is sedimentation. All the liquid application machines face the problem to keep the suspension agitated.

Over-spray contaminates the application area – especially below the glass.

#### **Spray nozzle (pure liquid) system**

Again, “spitting” and “area contamination” is the most common problem reported.

Most of the operators of nozzle systems have an enclosure for the spray system. The biggest problem with it is maintenance. What happens is that the spray curtain also reaches the walls of the enclosure on the inside. The interleaving accumulates and falls-off after some time. Only frequent maintenance (cleaning) helps out of this problem.

Over spray contaminates the application area – especially below the glass.

#### **Roller spray system**

Some operators claim that the application area is dirty because of the “overspill” - same as with the dry application systems.

Other operators claim, that the applicator unit becomes dirty after some time – cleaning is necessary.

### **Report from a windshield manufacturer**

Our customer requested a complicated (small bending radii, deep sag bending) windshield from us. With our standard dry roller application system, we found a rejection rate of 47% due to bending faults. We immediately established a liquid spray nozzle system where we could drop the rejection rate to below 30%. Modifications to the systems allowed us to retrieve a rejection rate of 27% as our best result. Then we tried the liquid roller spray system and found a rejection rate of 8% due to bending faults. This was now satisfactory to us. Turkish car glass manufacturer.

### **Conclusion**

There are 3 points we have to focus if we want to establish a rank list:

- Application quality
- Cost for housekeeping
- All over investment cost

Concerning application quality, I only can advise the liquid roller spray system as it supplies constant quality conditions in matters of even interleaving distribution and amount control, followed by the liquid nozzle spray systems which are weak in constant quality performance and finally the dry nozzle spray system followed by the dry roller spray system. Housekeeping cost is completely neglected from purchasers as this is a different account, but together with the machine investment it is the true system cost to be paid for.

The lowest housekeeping expenses is to find with the liquid roller spray system, followed from the liquid spray nozzle systems, the dry spray nozzle system and the dry roller application system.

The liquid roller spray application system offers the best performance in regards of application quality, housekeeping and life-cycle-cost, followed by the liquid spray nozzle systems, the dry spray nozzle system and the dry roller application system.

# Energy Efficiency of Different Windscreen Bending Furnaces

Juha Karisola,  
Glaston Finland Oy

Energy efficiency is one of the key criteria when considering investment in new processing equipment. The global trend towards sustainable and environmental friendly solutions increase steadily energy price. This affects windshield producer in 2 ways: the energy efficiency of the processing equipment itself is becoming increasingly important. Secondly, energy saving features of the product itself set new requirements on the processing technologies.

The most energy-intensive part of the windscreen production is the bending process. The energy consumption of the whole windshield forming process depends on a variety of factors: on the furnace, glass, mold as well as the process. Once the furnace and it's construction has been chosen, there is little what can be done to improve its efficiency. Therefore the features and solutions, which improve energy efficiency must be considered when designing the equipment. On the other hand, much can be done to improve the efficiency of the tooling and process itself. The best result can be achieved by using a variety of different measures.

This presentation explains the energy consumption of different type of furnace and different measures, which can be used to improve energy efficiency in the current production.

# The Effective Stiffness of Broken Laminated Glass. A Homogenized Approach

Laura Galuppi<sup>1</sup>,

Gianni Royer Carfagni<sup>1,2</sup>

<sup>1</sup>Department of Engineering and Architecture,  
University of Parma, Italy

<sup>2</sup>Construction Technologies Institute -  
National Research Council of Italy (ITC-CNR),  
Milano, Italy

## Keywords

1=Post-breakage response 2=Laminated glass  
3=Tension stiffening 4=Effective stiffness

## Abstract

Due to the tension stiffening of the polymeric interlayer resulting from the adhesion with the glass shards, laminated glass maintains significant stiffness and strength even when all glass plies are broken.

A homogenized approach is presented that fits the case of broken tempered glass, characterized by small shards approximately of the same size. The tension stiffening is evaluated as a stress perturbation, determined within a class of shape functions through complementary energy minimization. This provides accurate estimates for the post-breakage in-plane effective-stiffness, which strongly depends, besides the interlayer stiffness, upon fragment size and glass-to-polymer adhesion. An extension of the model to the case of broken laminated glass plates under equi-biaxial loading.

The strength of the proposed method consists in the possibility of accounting for the stress diffusion phenomena in simple mathematical terms, allowing to reach simple formulas for the estimation of the effective stiffness of laminated glass in the post-breakage phase. Comparisons with numerical experiments confirm the accuracy of the proposed homogenized approach.

## Introduction

When used for structural purposes, glass is often of a safety type, a category that includes laminated glass, a composite formed by two (or more) glass plies bonded by thin polymeric interlayers with a process at high temperature and pressure in autoclave. The role of the interlayer is twofold. In the pre-glass breakage phase it allows the transfer of shear stresses between the glass plies, ensuring that the

flexural inertia of the laminated glass element is higher than the sum of the inertiae of the isolated glass plies. In the *post-glass breakage phase*, the glass shards remain attached to the polymer so that the assembly maintains a certain cohesion. This provides a small but significant load bearing capacity, avoiding injuries due to catastrophic collapse.

A large number of theoretical and experimental studies have been devoted to the evaluation of the properties of sound laminated glass, while very few are the contributions for the post-breakage response, although this is strongly associated with the safety requirements, mainly ruled by impact and dynamic performance.

Indeed, many standards prescribe to use for structural glass the *fail safe* design approach, typical in aircraft design, where it is accepted that one or more components may fail in extreme situations, but without compromising the overall stability of the structural system. Its goal is to verify that, in case of partial or total fragmentation of glass components as a result of accidental actions, a sufficient stiffness and strength is maintained to withstand self-weight and dead loads, as well as a fraction of the live loads, thereby preventing danger from falling materials.

The laminated glass response in the post-critical phase is highly dependent on the bridging between adjacent glass fragments ensured by the polymer, and results from a combination of the elongation of the interlayer and the delamination from the glass shards near the cracks. Henceforth, factors that influence the post-breakage response are

- glass-interlayer adhesion properties;
- interlayer stiffness, depending upon polymer type, temperature and load duration;
- size and shape of the glass fragments, which are influenced by the type of glass, treatments to which it has been subjected,

glass thickness, type of load, loading rate and type of constraints.

Remarkably, the adherence with the glass fragments produces the tension stiffening of the polymeric film, which otherwise would present negligible mechanical performance.

In [1] an innovative method, based on a proper development of the perturbation approach first proposed by Hashin [2], is presented to evaluate the post-breakage effective stiffness of laminated glass panels under uniaxial in-plane loading, i.e., to find the elastic modulus of an equivalent homogeneous body with the same tensile properties of the broken laminated element. The considered scenario is specifically representative of thermally toughened and heat strengthened glass, characterized by the presence of small fragments, invading the entire panel, and accounts for the glass-interlayer delamination.

The proposed model starts from the analytical evaluation of the stress state in the interlayer, that turns out to be strongly influenced by the contact with the glass shards. In [3], the study has been extended to the case of broken laminated glass under equi-biaxial state of stress.

## Broken laminated glass under tensile stress. The model problem

In the post-glass-breakage phase, thermally-toughened and heat-strengthened laminated glass can be regarded as a composite formed by the interlayer to which randomly distributed glass shards remain adherent (Fig. 1a), with homogeneously distributed fragmentation. As shown in Fig. 1b, we will consider first the case in which the element is uniaxially loaded approximately in the same direction of the dominant cracks. Clearly, the cracks whose

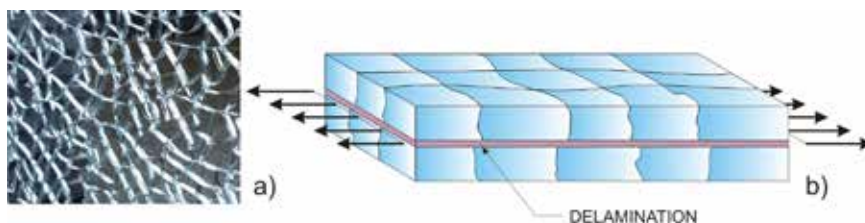


Figure 1 (a) Cracked laminated-glass panel and (b) schematic view of a cracked laminated glass under uniaxial tension.

plane is parallel to the direction of loading are subject to null or negative opening stress (due to the lateral contraction of the interlayer), so that they do not influence the tensile response. Therefore, one can consider only the effects of the cracks orthogonal to the tensile stress and the problem may be studied as a two-dimensional case, in plane stress or plane strain.

The considered reference geometry is a broken laminated glass element composed by two glass plies of the same thickness, bonded by a polymeric interlayer of thickness  $2t$  and Young's modulus  $E_p$ . Let us consider, as reference element, the region comprised between two consecutive cracks, of length  $2a$ , shown in Fig. 2. Any two consecutive glass fragments are bridged by the ligament of the polymeric interlayer and the tensile response is governed by the interlayer stiffness and adhesion.

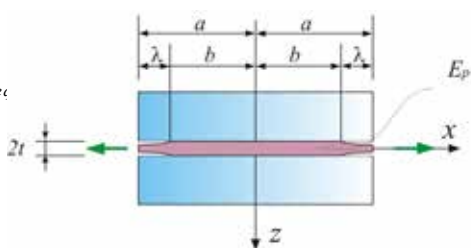


Figure 2 Elementary portion comprised between two crack planes.

The same figure also evidences that each glass fragment is assumed to be symmetrically detached at its ends for a length  $\lambda$  and, hence, bonded to the interlayer in the central zone of length  $2b = 2(a - \lambda)$ .

To our knowledge, the only formula available in the literature [4] defines the equivalent Young's modulus  $E_{eq}$  of cracked laminated glass, stiffened by the adhesion with the glass shards, as a function of the interlayer modulus  $E_p$ , of the fragment size  $L$  and of the glass/polymer debond length  $\lambda$ , in the form

$$E_{eq} = E_p \frac{a}{\lambda} \quad (1)$$

The underlying hypothesis in this approach is that the strain in the interlayer is null in the bonded zones, and uniaxial in the remaining parts. In our approach, we will instead consider the stress diffusion between the bonded and unbonded parts.

## Evaluation of the stress state in the interlayer

Since the elastic modulus of glass (70 GPa) is much higher than that of the interlayer (strongly dependent on temperature and load duration, but of the order of 10 MPa), the glass shards can be considered rigid with respect to the polymer and the analysis may focus on the interlayer only. In particular, the isolated interlayer may be regarded as the *reference* configuration, in which it is subjected to a homogeneous state of stress  $\bar{\sigma}$  while the actual state of stress  $\sigma$  is the sum of the reference stress and a perturbation stress arising from the contact with the glass fragments, i.e.,

$$\sigma = \bar{\sigma} + \sigma \quad (2)$$

The perturbation stress is evaluated in [1], under the simplifying assumption of constant-through-the thickness axial stress, by means of energy minimization methods. Fig. 3a shows a qualitative plot of the obtained solution, according to which the mean axial stress in the interlayer turns out to be constant in the external detached zones, where the presence of the glass fragments does not lead to stress perturbations. The stress distribution is characterized by a stress diffusion phenomena inside the bonded region, which depends upon the bond length, the interlayer thickness and its Poisson's ratio.

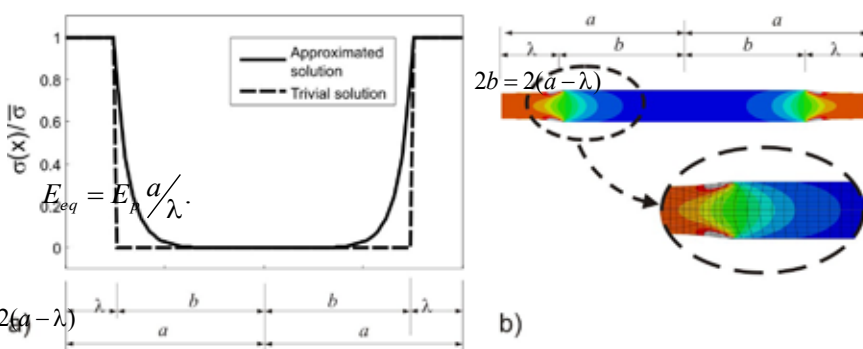


Fig. 3 (a) Average axial stress in the region between two crack. Comparison between the trivial solution and the proposed approximation; (b) Plot of the numerically evaluated axial stress with evidence of the stress diffusion inside the bonded zone.

In the same figure, a trivial solution is plotted for the sake of comparison. This solution, leading to the simplified formula (1) for the effective stiffness of the beam, considers that only the detached zones of the interlayer contribute to the elongation of the element, while the contact with the glass fragments prevents the elongation of the interlayer in the bonded zones. Obviously, this approach completely neglects the stress diffusion phenomena, that, on the other hand, are confirmed by numerical experiments, as shown by Fig.3b.

Comparisons of the obtained average stress with that evaluated numerically, by means of accurate analyses performed with the code Abaqus, are shown Fig. 4 and discussed in detail in [1], for different values of the fragment size and of the delamination length.

In general, the stress diffusion phenomenon is the more important the lower the length of the glass shards is.

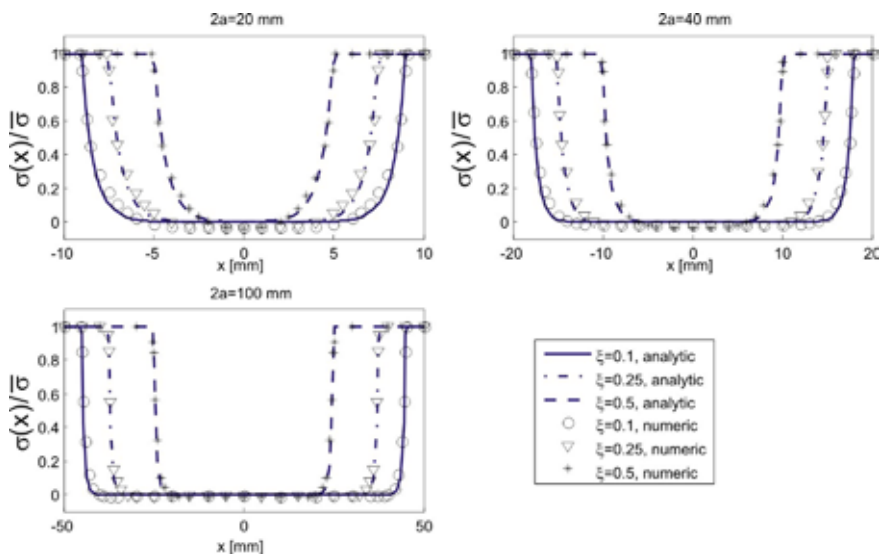


Figure 4 Average axial stress in the region comprised between two consecutive crack, for different values of the glass fragment size and detachment length. Comparison between analytical and numerical results for plane stress condition.

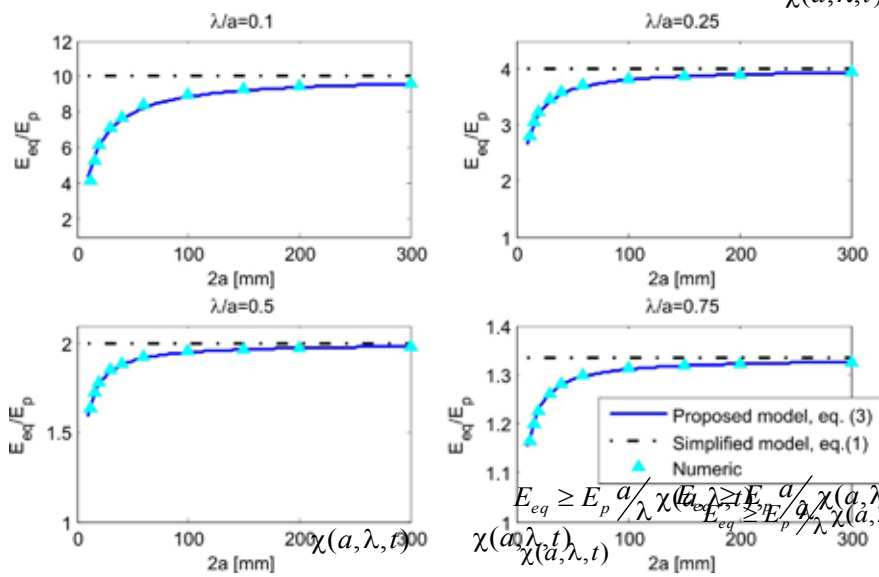


Figure 5 Effective elastic modulus for plane stress condition  $E_{eq}$ , normalized by the interlayer elastic modulus  $E_p$ , as a function of the fragment length  $2a$ , for different values of  $\lambda/a$ .

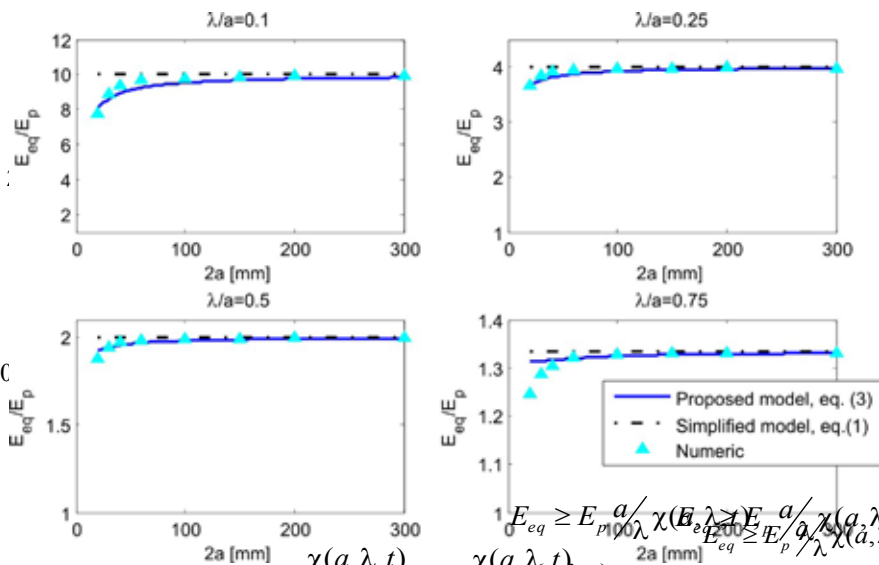


Figure 6 Effective elastic modulus for plane strain condition  $E_{eq}$ , normalized by the interlayer elastic modulus  $E_p$ , as a function of the fragment length  $2a$ , for different values of  $\lambda/a$ .

## Effective stiffness of the broken laminated glass element under tensile load

To facilitate the structural calculations, it is convenient to introduce average properties of the damage elements. Here, we define the effective stiffness of the cracked laminate under tension as the stiffness of a homogeneous body with the same geometry of the interlayer, presenting the same tensile properties in terms of elongation. It is determined by introducing the effective Young's modulus  $E_{eq}$ .

As discussed in [1], a lower bound for the effective stiffness may be found, starting for the perturbed stress state [2], by means of energy theorems, in the form

$$E_{eq} \geq E_p \frac{a}{\lambda} \chi(a, \lambda, t), \quad (3)$$

where  $\chi(a, \lambda, t)$  is a non-dimensional quantity, depending on the detachment length, the glass fragment size and the interlayer thickness. It may be regarded as a corrective coefficient for formula (1). Accurate charts for the determination of such a coefficient are proposed in [5].

The graphs of Fig. 5 and Fig. 6 show  $E_{eq}$ , normalized by the interlayer elastic modulus  $E_p$ , as a function of the fragment length  $2a$  for different values of  $\lambda/a$  (representing the percentage of detached interlayer) for interlayer thickness of 1.52 mm, and for plane stress and plane strain conditions, respectively. Numerical results, obtained by means of numerical analyses performed with the program Abaqus, and values from the simplified model of (1) are compared in the same graphs. By comparing those Figures, it may be observed that, for plane strain conditions, the dependence of the effective modulus on the fragment length is less pronounced than in the plane stress conditions.

Observe that the simple model of eq. (1) provides values of  $E_{eq}$  independent of the glass fragment length, which are correlated only with the parameter  $\lambda/a$ . In general the corresponding estimate is not accurate. On the other hand, it is evident that the estimate from (3) is very close to the numeric results. The mean error, considering the range  $2a = [20\text{mm} \div 300\text{mm}]$  and  $\lambda/a = [0.1 \div 0.9]$ , is less than 4% for plane stress, and of the order of 1% for plane strain conditions. It may be observed that the analytic prediction for the lower bound of  $E_{eq}$  results to be higher than the numerical calculation for high values of  $\lambda/a$  and low values of  $a$ . Here, the model indicates a stiffening of the element, which is not predicted by the numerical analysis.

This discrepancy is associated with the phenomenon of stress diffusion in the bonded zone of the interlayer: when the bond length is very small the two stress-diffusion zones tend to merge, so that part of the axial load directly flows through the interlayer, with no need of being transferred to the adherent glass fragments. The proposed analytical model, based upon the constant-in-the-thickness axial stress approximation, cannot correctly capture this effect. However, this is a limit condition, certainly of minor practical interest.

### Response under equi-biaxial loading

Let us consider now a cracked laminated glass panel subjected to equi-biaxial loading, as shown by Fig. 7a, assuming that the fragmentation is homogeneously distributed, so that all the cracks are subjected to the same positive opening stress. The representative element, shown in Fig. 7b, comprised between cracks, is assumed to be the square,  $2a \times 2a$ , while the shape of the central bonded region has been evaluated by means on numerical experiments [3] and turns out to be circular, with radius  $R$ .

Following a procedure similar to that described for the case of beam under tensile load, the perturbed stress state in the interlayer is evaluated through a perturbation approach, while a lower bound for the effective stiffness of the broken laminate may be obtained by means of energetic methods, and reads

$$E_{eq} \geq E_p \chi(a, R, t) \quad (4)$$

where, again,  $\chi(a, R, t)$  is a non-dimensional coefficient, depending on the fragment size, the radius of the bonded region and the interlayer thickness.

With respect to the case of beam under tensile load, for the 2D problem of plate under equi-biaxial load, the interaction among adjacent

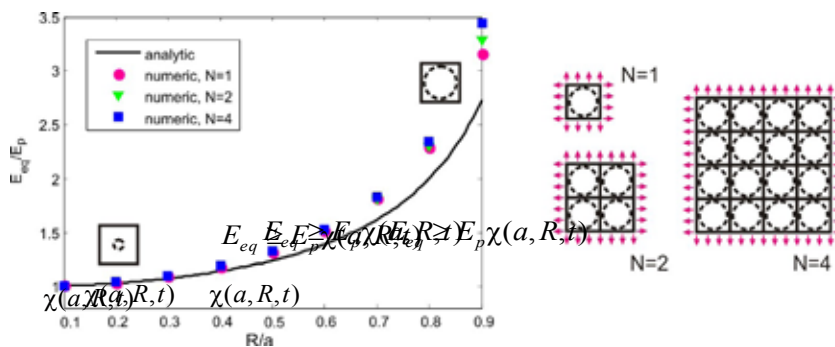


Figure 8 Ratio between effective elastic modulus  $E_{eq}$  and interlayer modulus  $E_p$ , as a function of  $R/a$ , for fragment lengths of  $2a = 100$  mm. Comparison between analytical and numerical results for different number of elements.

cells represents an important issue. This is shown in Fig. 7, where the numerical results, in terms of effective elastic modulus  $E_{eq}$  (normalized by the interlayer modulus  $E_p$ ) are plotted as a function of  $R/a$ , for fragment lengths of 100 mm and for different numbers of elementary cells  $N$ . Results obtained through equation (4) are plotted in the same graphs.

The numerical analyses show that, by increasing  $N$ , the effective stiffness increases, being the phenomenon more pronounced for high values of  $R/a$ . This is due to the fact that, when the number of elements is high, the stress state of the detached zones turns out to be perturbed by the presence of the adjacent fragments and, hence, the stiffening actions of the glass fragments interact one other. This effect is more marked for high values of  $R/a$  because the different bonded regions are closer one another. Phenomena of this kind cannot be caught by the analytical approach. However, it may be verified that of the error in the evaluation of  $E_{eq}$  with the analytical approach strongly depends upon  $R/a$ , while its dependence on  $N$  is less evident. In practice, if the approximation for the effective stiffness is considered to be acceptable for a given value of  $R/a$ , it is acceptable independently of the

panel size. Analogous analyses performed by considering different values of the glass fragment size confirm that the cracked element response is almost independent of the glass fragment size, as found analytically.

### Conclusions

An innovative method has been presented to evaluate the post-breakage effective stiffness of laminated glass panels under uniaxial tensile loading, either in generalized plane stress or plane strain conditions. The polymeric interlayer foil is stiffened by the contact with the adherent glass shards, but partial delamination is supposed to occur at the interface. The model can take into account the complicated stress distribution from the detached zones, in which the shards are bridged by the interlayer-ligament only, to the regions where glass is bonded to the interlayer. Such a phenomenon, which does not seem to have been properly considered in previous studies, provides a stiffening effect for the cracked laminated glass that depends upon the interlayer thickness, the characteristic size of the glass shards and the length of the bonded zone. The method has been extended to the study of the response of broken laminated glass plates under equi-biaxial state of stress. In both cases, the proposed model allows a simple evaluation of the effective stiffness of broken laminated glass element under tension, permitting to reach simple expressions for the elastic modulus of a homogeneous body with the same tensile properties. This study has confirmed that the response of the damaged panel is governed by the presence of the delaminated regions, and by the interface conditions with the bonded zone, as well as on the interlayer properties and thickness.

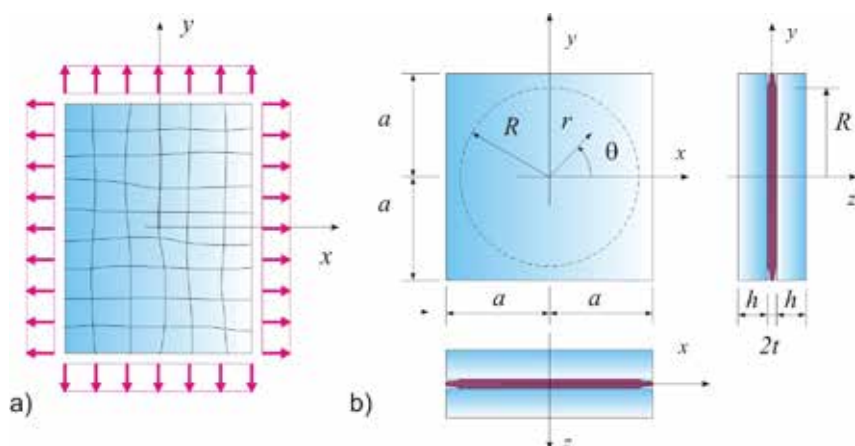


Figure 7 (a) Schematic of a broken laminated glass panel under equi-biaxial stress and (b) Schematic of the representative element.

Comparisons of the obtained results with accurate numerical experiments confirm the accuracy of the proposed approach. The errors in the considered case-studies are of the order of a few percentage.

This study is certainly propaedeutic for the analysis of the bending response of laminated glass beams, as well as of damaged glass panels under out-of-plane equibiaxial flexure, like the situation occurring in the ring-on-ring testing methods for glass strength suggested by standards EN-1288-2 and EN-1288-5.

## References

- [1] L. Galuppi, G. Royer-Carfagni, 2016. A homogenized model for the post-breakage tensile behavior of laminated glass. *Compos Struct* 154, pp. 600–615.
- [2] Z. Hashin, 1985. Analysis of cracked laminates: a variational approach. *Mech Mater* 4(2), pp. 121-136.
- [3] L. Galuppi, G. Royer-Carfagni, 2017. A homogenized analysis à la Hashin for cracked laminates under equi-biaxial stress. Applications to laminated glass. *Compos Part B – Eng* 111, pp. 332-347.
- [4] S.J. Bennison, I. Stelzer, 2009. Structural properties of laminated glass. Short Course, Glass Performance Days, Tampere (Finland).
- [5] L. Galuppi, G. Royer-Carfagni, 2017. Modelling the post-breakage response of laminated glass. Analogies with reinforced concrete mechanics. Submitted.

# Simple Statistics Shows that Heat-treated Glass is much Stronger than Expected

Gabriele Pisano<sup>1</sup>,  
Gianni Royer Carfagni<sup>1</sup>,  
<sup>1</sup> Department of Engineering and Architecture,  
University of Parma, Italy.  
<sup>2</sup> Construction Technologies Institute - Italian  
National Research Council (ITC-CNR), Milano,  
Italy.

## Keywords

1=Glass strength 2=Heat-treated glass  
3=Weibull 4=Statistics 5=Failure 6=Verification  
formulae

## Abstract

In structural design the bending strength of pre-stressed glass (HTGS) - heat-strengthened or tempered - is usually formulated as the sum, weighted with correction coefficients, of the values for pristine-material strength (PMS) and surface pre-compression (SPC), induced by the thermal treatment. Characteristic values are associated with the 5% fractiles of the corresponding statistical distributions, but since they are different for PMS and SPC, the 5% fractile for the distribution of HTGS may be much higher, due to statistical interference, than the simple sum. Assuming for PMS a two-parameter Weibull distribution and for SPC a Gaussian distribution, as suggested by experiments, the probability density function for HTGS is obtained by statistical convolution. Several aspects, such as test set-up, can affect the difference between the sum of the fractiles of the operant distributions and the fractile of the compound distribution. This finding suggests that the formulas presented in most standards for HTG strength may be too much conservative. Of course, an ad hoc experimental campaign is necessary to corroborate this theoretical finding that, if confirmed, could permit a much better use of the material, with incommensurable savings in construction works.

## Introduction

During last decades, the increasing architectural desire for transparency has enforced the use of load-bearing glass elements such as beams, columns, and frames. Glass is the brittle material par excellence, it is homogeneous and isotropic, and its behavior is linear elastic up to failure.

Micro-cracks are unavoidably present on the external surfaces of panes because of manufacturing process, later handling and aging. The combination of flaw size and opening tensile stress (in mode I) govern the occurrence of collapse. As a consequence of the random nature in terms of size, location and orientation of micro-cracks, failure probability of a glass pane turns out to be dependent upon size of loaded surface and type of applied stress. The edges represent the weakest part of glass plates since additional defects are there present due to cutting process. Moreover, the *subcritical crack growth*, according to which cracks can grow over time even at stress level much lower than the critical threshold, is another peculiar phenomenon related to glass.

Much researchers are engaged in characterizing the mechanical properties of this material. Glass can be considerably strengthened through a heat treatment followed by a rapid cooling, because this generates a residual surface compressive stresses. Thus, the resulting eigenstress state due to out-of-plane loading is such that the tensile stresses due to bending are algebraically reduced, if not annihilated. Therefore, since the compression strength of glass is much higher than its tensile strength, the failure load for a heat-treated glass plate is much higher than for an untreated elements. The heat-strengthened and the tempered glass constitute the two main types of heat-treated glass, the difference between the two is correlated with the rapidity of the cooling process. In heat-strengthened glass the cooling process is slower than in tempered glass and, consequently, the state of induced surface compression milder.

The sum of residual surface compression (in absolute value) and pristine float glass strength gives the ultimate strength for heat-treated glass. In general, the 50% fractile of the distribution of strengths for prestressed glass is generally evaluated by summing up the 50% fractile corresponding to glass strength before thermal treating and the 50% fractile associated with the prestress state. Anyway, several experimental campaign (Norville Sheridan and Lawrence 1993, Zaccaria and Overend 2016, Veer Louter and Boss 2009, Veer et al. 2013, Veer and Rodichev 2014) have shown that thermal-treated glass strength is higher (in some cases it could be much

higher) than the simple sum of the prestress and of the pristine material strength. We will show that the statistical interpretation of the interaction between the residual compressions and the additional stress state due to bending may explain this finding.

## The statistical distribution for heat-treated glass strength

A micro-mechanically motivated analysis of interaction between surface pre-compressions and tensile stresses due to bending leads to the analytical formulation for the population of heat-treated glass strength.

## Pristine glass strength

How to statistically characterize float glass strength is a matter of much debate in the scientific world, thus several statistical models have been analysed and proposed. The two-parameter Weibull statistics (Weibull 1951), based on the weakest-link-in-the-chain rationale, is certainly the most widely used for what concerns design of glass components. However, during last years, its applicability has been questioned, and arguments were presented (Ballarini Pisano and Royer 2016) which support the existence of a lower bound for glass strength due to strict production control for optical and aesthetic reasons. Anyway, reference will be made to the most classical two-parameter Weibull distribution, whose simple analytical form gives noteworthy analytical advantages. A reliable interpretation of glass strength population can be reached through such statistics if the tails of the distribution play a secondary role (Pisano and Royer 2015) and, in any case, it certainly provides estimates on the safe side. According to this formulation, the failure probability of annealed float glass subjected to a generic state of stress reads

$$P(\sigma_{\perp}) = 1 - \exp \left[ - \int_A \left( \frac{\sigma_{\perp}}{\eta_0} \right)^m dA \right], \quad (1)$$

where  $A$  is the loaded area,  $\eta_0$  and  $m$  are the scale and shape parameters of the distribution, respectively, while  $\sigma_{\perp}$  is the component of stress at right angle with crack axis, which can be written

$$\sigma_{\perp} = [\sigma_1 \cos^2 \psi + \sigma_2 \sin^2 \psi], \quad (2)$$

where  $\sigma_1$  and  $\sigma_2$  are the principal components of tensile stress. By considering an uniform and isotropic defectiveness, an equivalent stress could be defined of the form

$$\sigma_{eq} = \left[ 2/\pi \int_0^{\pi/2} (\sigma_1 \cos^2 \psi + \sigma_2 \sin^2 \psi)^m d\psi \right]^{1/m}, \quad (3)$$

while, once defined  $\sigma_{max}$  as the maximum tensile stress in the tensile area and the effective area as

$$A_{eff} = \frac{\int_A \frac{\sigma_{eq}^m dA}{\sigma_{max}^m}, \quad (4)$$

which summarily takes into account the effect of the type of stress state, the probability of failure for a float glass pane may be written as

$$P_a(\sigma_{max}) = 1 - \exp \left[ -A_{eff} \left( \frac{\sigma_{max}}{\eta_0} \right)^m \right]. \quad (5)$$

### Residual compressions

The eigenstress state due to heat treatment on the glass surfaces may be strongly inhomogeneous, but the industrial practice, such as the oscillation of glass panes during cooling and/or the increase of the cooling rate, allow to mitigate this phenomenon [Chen et al. 2013]. Hence, it is acceptable, at least at a first order approximation, to assume that, at a certain distance from the borders, the residual stress state is equibiaxial and homogeneous [Aben et al. 2013]. Although a limited number of data is available in technical literature, the Gaussian distribution can be reasonably used for interpreting residual compressions variability from plate to plate [Pisano and Royer 2016]. Thus, the assumed probability density function for thermal-induced pre-stresses reads

$$f_p(|\sigma_{pc}|) = \frac{1}{\sigma\sqrt{2\pi}} \exp \left[ - \frac{(|\sigma_{pc}| - \mu)^2}{2\sigma^2} \right], \quad (6)$$

where  $\mu$  and  $\sigma$  represent the mean value and the standard deviation, respectively, and  $\sigma_{pc}$  is the surface pre-compression.

### Compound probability distribution

It is certainly customary to schematize heat-treated glass strength  $\sigma_{htg}$  as

$$\sigma_{htg} = \sigma_{ann} + |\sigma_{pc}|, \quad (7)$$

where  $\sigma_{ann}$  represents glass strength before heat treatment. This formulation is not correct when terms represent stochastic variable, and statistical interference between  $\sigma_{ann}$  and  $\sigma_{pc}$  should be taken into account. Let  $f_p(|\sigma_{pc}|)$  and  $f_a(\sigma_{ann})$  be the probability density functions associated with the residual compressive stress state and with the float glass strength, respectively. The function  $f_t(\sigma_{max})$  associated with the failure of a heat-treated glass pane can be obtained through convolution of the density functions of the operant distributions in the form

$$\begin{aligned} f_t(\sigma_{max}) &= (f_a * f_p)(\sigma_{max}) \\ &= \int_{-\infty}^{+\infty} f_a(\sigma_{max} - |\sigma_{pc}|) f_p(|\sigma_{pc}|) d|\sigma_{pc}|. \end{aligned} \quad (8)$$

The cumulative distribution function reads

$$\begin{aligned} F_t(\sigma_{max}) &= P(\sigma_{ann} + |\sigma_{pc}| \leq \sigma_{max}) \\ &= \int_{-\infty}^{+\infty} F_a(\sigma_{max} - |\sigma_{pc}|) f_p(|\sigma_{pc}|) d|\sigma_{pc}|, \end{aligned} \quad (9)$$

which, by using the above-described statistics, becomes

$$\begin{aligned} F_t(\sigma_{max}) &= \int_0^{\sigma_{max}} \left\{ 1 - \exp \left[ - \int_A \left( \frac{\sigma_{max} - |\sigma_{pc}|}{\eta_0} \right)^m dA \right] \right\} \\ &\quad \left\{ \frac{1}{\sigma\sqrt{2\pi}} \exp \left[ - \frac{(|\sigma_{pc}| - \mu)^2}{2\sigma^2} \right] \right\} d|\sigma_{pc}|. \end{aligned} \quad (10)$$

Observe that, here, it is assumed that the intrinsic properties of glass are not influenced by the thermal treatment and, hence,  $\sigma_{ann}$  and  $\sigma_{pc}$  can be considered independent.

### Extremal cases: Equibiaxial versus uniaxial strength

The dependence of float glass strength upon acting stress state has been deeply discussed in technical literature, but the same cannot be said for what concerns heat-treated glass. Two extremal cases are here reported: the equibiaxial stress state, which represents the most severe case since the maximum tensile stress is always at right angle with crack axis, and the uniaxial one, which is approximately reached through four- or three-point bending tests. For the sake of simplicity, we here assume that state of stress is uniform.

### Equibiaxial state of stress

Approximately, an equibiaxial stress state is reached by testing glass panes under coaxial double ring tests. Moreover, as it has been mentioned in Section 2.2, even the compressive state of stress acting on the external surface of the pane due to heat-treatment can be considered equibiaxial, albeit in its core part. Thus, the effective area reads  $A_{eff} = A$ , where  $A$  is the whole area under tensile stress, and it is easy to manipulate convolution integral (10), to reach the expression

$$\begin{aligned} F_t(\sigma_{ebx}) &= \int_0^{\sigma_{ebx}} \left\{ 1 - \exp \left[ -A \left( \frac{\sigma_{ebx} - |\sigma_{pc}|}{\eta_0} \right)^m \right] \right\} \\ &\quad \left\{ \frac{1}{\sigma\sqrt{2\pi}} \exp \left[ - \frac{(|\sigma_{pc}| - \mu)^2}{2\sigma^2} \right] \right\} d|\sigma_{pc}|. \end{aligned} \quad (11)$$

### Pure bending

The uniaxial stress state is associated with the lowest probability of finding the critical crack at right angle with the maximum tensile stress, i.e., it leads to the lowest failure probability for a glass pane. From the simple analysis of the Mohr circle associated with the pure bending (stress state due to bending is uniaxial), one finds that all cracks whose plane inclination is comprised between a certain angle  $-\beta$  and  $\beta$  are compressed [Pisano and Royer 2016]. Hence, a certain number of cracks is not subjected to opening stress and cannot cause failure. For the same value of  $\sigma_{unx}$ , the higher the absolute value of  $\sigma_{pc}$ , the higher is the number of *inactive* cracks and the lower is the probability of failure for a bended glass plate. By taking  $\sigma_1 = \sigma_{unx} - |\sigma_{pc}|$  and  $\sigma_2 = -|\sigma_{pc}|$ , and by assuming isotropic defectiveness again, equivalent stress  $\sigma_{eq}$  of equation (3) assumes the form [Pisano and Royer 2016]

$$\frac{1}{\pi} \int_{\frac{\pi}{2} - \beta}^{\frac{\pi}{2} + \beta} [(\sigma_{unx} - |\sigma_{pc}|) \cos^2 \psi - |\sigma_{pc}| \sin^2 \psi]^m d\psi, \quad (12)$$

and the probability of failure of the annealed glass at the stress  $\sigma_{unx} - |\sigma_{pc}|$  becomes

$$\begin{aligned} F_a(\sigma_{unx} - |\sigma_{pc}|) &= 1 - \exp \left\{ \int_A - \left[ \left( \frac{\sigma_{unx} - |\sigma_{pc}|}{\eta_0} \right)^m \right. \right. \\ &\quad \left. \left. \int_{\frac{\pi}{2} - \beta}^{\frac{\pi}{2} + \beta} [(\sigma_{unx} - |\sigma_{pc}|) \cos^2 \psi - |\sigma_{pc}| \sin^2 \psi]^m d\psi \right] dA \right\}, \end{aligned} \quad (13)$$

$$\text{where } \beta = \frac{1}{2} \arccos \left[ 1 - 2 \frac{|\sigma_{pc}|}{\sigma_{unx}} \right].$$

Finally, by considering a homogeneous state of stress acting within an area, the convolution integral (10) becomes

$$\begin{aligned} F_t(\sigma_{unx}) &= \int_0^{\sigma_{unx}} \left\{ 1 - \exp \left[ - \left( \frac{\sigma_{ebx} - |\sigma_{pc}|}{\eta_0} \right)^m \frac{A_t}{\pi} \right. \right. \\ &\quad \left. \left. \int_{\frac{\pi}{2} - \beta}^{\frac{\pi}{2} + \beta} [(\sigma_{unx} - |\sigma_{pc}|) \cos^2 \psi - |\sigma_{pc}| \sin^2 \psi]^m d\psi \right] \right\} \\ &\quad \left\{ \frac{1}{\sigma\sqrt{2\pi}} \exp \left[ - \frac{(|\sigma_{pc}| - \mu)^2}{2\sigma^2} \right] \right\} d|\sigma_{pc}|. \end{aligned} \quad (14)$$

## Discussion and conclusions

In accordance with an expression of the type (7), structural standards generally assume that the design value for heat-treated glass resistance is the sum of the design value for the annealed glass and the contribution from the prestress. For example, the project of European norm PrEN 16612 suggests the formula

$$\sigma_{max,d,\tau} \leq \frac{k_{mod,\tau} f_{g,k}}{\gamma_M} + \frac{f_{b,k} - f_{g,k}}{\gamma_{M,v}}, \quad (15)$$

where  $f_{b,k}$  and  $f_{g,k}$  represent the characteristic strengths of heat treated glass and of annealed glass, respectively, which can both be considered representative of the 5% fractile. The coefficient  $k_{mod,\tau}$  takes into account the effects of subcritical crack growth, while  $\gamma_M$  and  $\gamma_{M,v}$  represent the partial safety factors. Even though such expression is on the safe side, the underlying rationale is not correct and has to be questioned.

It is very unlikely that both the statistical functions that interpret the strength of annealed glass and the thermal prestress, respectively, attain their lowest values simultaneously, that is why the stochastic variable obtained as the sum of two independent stochastic variables leads to lower probabilities of failure, with respect to its deterministic counterpart. The 5% fractile of the resulting distribution of strength is hence higher than the sum of the 5% fractiles of the operant distributions.

Experimental data recorded in the technical literature allow to claim that the state of residual prestress due to thermal treating can be considered approximately uniform and equibiaxial, whereas its variation from one specimen to another can be assumed to follow a normal distribution. On the other hand, the population of float glass strength before treatment has been interpreted through the most classical two-parameter Weibull distribution. Even though many questions arise about such statistics ability of interpreting float glass strength variability, it can provide quite reliable results if one is interested in statistical descriptors far from the tails. Finally, the analytical formulation for the probability density function associated with the failure of a bended heat-treated glass specimen is obtained through the statistical convolution of the density functions of the operant distribution (pristine material strength and prestress). Obviously, the resulting compound probability function turns out to be highly sensitive to the variation of Weibull parameters, in particular for what concerns the shape parameter  $m$ . The proportion of benefic effect due to thermal treating strongly depends upon the type of applied stress. In fact, since glass strength is

governed by the opening in mode I of surface cracks, when stress state due to bending is uniaxial, a certain number of cracks will remain always inactive, whatever the level of the applied load is. This phenomenon together with the statistical interference between float glass strength and prestress have never been considered in the computation of heat-treated glass strength and make heat-treated glass much stronger than generally expected. The most common approach in the verification formulae proposed in structural standards consists of computing the characteristic strength of heat-treated glass as the simple sum of the characteristic values of annealed glass strength and surface prestress. This procedure is certainly on the safe side, but we believe that a revision of such verification formulae could lead to an optimization of the use of the material, bringing noteworthy benefits to the building industries.

## References

- Aben H., Anton J., Paemurru M., Ôis M., 2013. A new method for tempering stress measurement in glass panels. *Estonian Journal of Engineering* 19(4): 292-297.
- Ballarini R., Pisano G., Royer-Carfagni G., 2016. The lower bound for glass strength and its interpretation with generalized Weibull statistics for structural application. *ASCE Journal of Engineering Mechanics* 142(12): 04016100, 20pp.
- Chen Y., Lochegnies D., Defontaine R., Anton J., Aben H., Langlais R., 2013. Measuring the 2d residual surface stress mapping in tempered glass under the cooling jets: the influence of the process parameters on the stress homogeneity and isotropy. *Strain* 49: 60-67.
- Norville H.S., Sheridan D.L., Lawrence S.L., 1993. Strength of new heat treated window glass lites and laminated glass units. *ASCE Journal of Structural Engineering* 119(3): 891-901.
- Pisano G., Royer-Carfagni G., 2015. The statistical interpretation of the strength of float glass for structural application. *Construction and Building Materials* 98: 741-756.
- Pisano G., Royer-Carfagni G., 2016. Statistical interference of material strength and surface prestress in heat-treated glass. *Journal of the American Ceramic Society*. Available from: <http://onlinelibrary.wiley.com/doi/10.1111/jace.14608/full>.
- Veer F., Louter P.C., Bos F.P., 2009. The strength of annealed, heat-strengthened and fully tempered float glass. *Fatigue & Fracture of Engineering Materials & Structures* 32(1): 18-25.
- Veer F., Oikonomopoulou P., Riemsdag T., Carvalho P., Cruz P., Rodichev Y., 2013. Consistency of pre-stress and bending strength of annealed, heat-strengthened and tempered glass. *Conference Proceedings, Glass Performance Days*, pp. 538-544. Tampere, Finland.
- Veer F., Rodichev Y., 2014. The relation between pre-stress and failure stress in tempered glass. *Challenging Glass 4 & COST Action TU0905 Final Conference*, pp. 731-738. Taylor & Francis, London, U.K.
- Weibull W., 1951. A statistical distribution function of wide applicability. *Journal of Applied Mechanics* 18: 293-297.

Zaccaria M., Overend M., 2016. Thermal healing of realistic flaws in glass. *Journal of Material in Civil Engineering* 28(2): 04015127, 9pp.

## Acknowledgement

The authors acknowledge the partial support of the Italian *Dipartimento della Protezione Civile* under project ReLUIS-DPC 2014-2018.

# Zaryadye Park, Glass Grid Shell Roof

G. Vasilchenko-Malishev, Malishev Engineers

www.malishevengineers.com

tel. +44(0) 207 251 66 38

gvm@malishevengineers.com

## Keywords

glass beams, grid shell structure

## Abstract

This paper will describe the design, detailing, testing and construction of structural glass beams as part of load bearing grid shell structure in the newly built Zaryadye Park in Moscow, Russia, situated short distance from Red Square and the Kremlin.

Glass beams (72 in total) are fixed into the main steel grid shell structure measured around 120m long by 60m wide and measured around 3m long by 0.2m deep. Glass beams were designed to accommodate extreme weather conditions with snow drift loads of up to 350 kg/m<sup>2</sup>, as well as differential movement of the main structure which required sophisticated analysis with more than 100 load combinations as well as full scale testing to gain approvals from the authorities. Due to lack of legislation on use of structural glass in Russia, so called "special technical standard" was created with our help to cover technical aspects of glass and it's performance, which formed part of approval documents



Fig. 1 Artist impression of the completed grid shell structure



Fig. 2 Situation plan of the Zaryadye Park

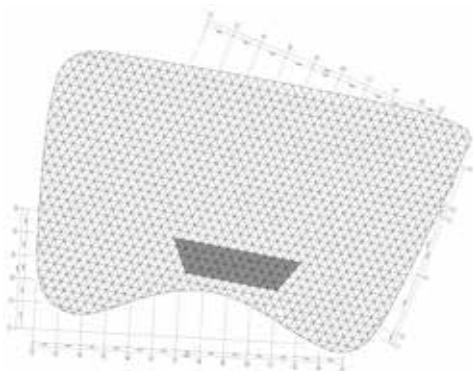


Fig. 3 general arrangement plan of the grid shell structure with highlighted area representing structural glass beams as part of the main structure



Fig. 4 General arrangement plan of the glass beams, each approximately 3m long. Roof panels are not shown for clarity



Fig. 5 Artist impression of the desired view

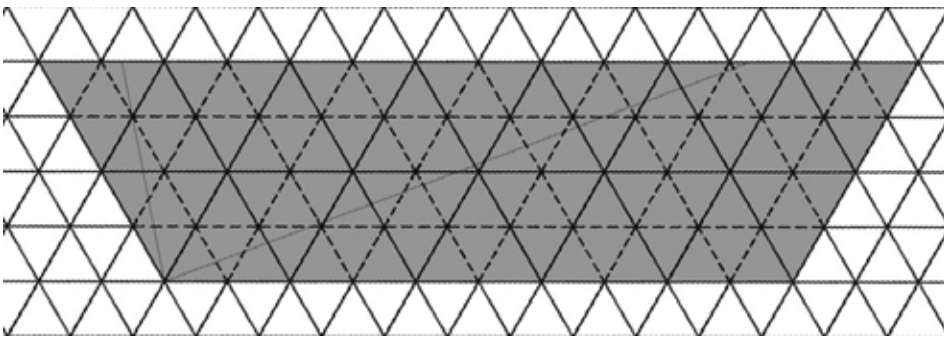


Fig. 6 Dotted lines indicate proposed structural glass beams.

| Glass type        | Design strength (short term-wind), MPa | Design strength (mid. Term-snow), MPa | Design strength (long term), MPa | Edge strength (long term), MPa |
|-------------------|--|---------------------------------------|----------------------------------|--------------------------------|
| Annealed glass    | 25                                     | 14                                    | 8.15                             | 6.5                            |
| Toughened glass   | 79                                     | 75                                    | 70                               | 56                             |
| Heat Strengthened | 40                                     | 34                                    | 29                               | 23                             |

Table 1: glass properties adopted, based on prEN13474, replaced by prEN16612

| Material              | Compression strength, MPa | Tensile strength, MPa | Young's modulus, MPa | Shear Strength, MPa |
|-----------------------|---------------------------|-----------------------|----------------------|---------------------|
| Stainless steel, S304 | 210                       | 210                   | 200000               | 126                 |
| DC895                 | 0.14                      | 0.14                  | 1                    | 0.33                |

Table 2: other materials properties

## Design

### 3.1 Concept

The grid shell structure was designed to follow the curve of artificially created hill as an open structure (not enclosed), hence subject to thermal movements as well as snow loading and wind. The main structure is comprised of structural steel elements of approximately 3m long and 300mm deep. However in certain locations clear less obstructed views were required, hence more transparency in the structure was necessary. Initially glass clad cable structure was proposed by the architect, however due to significant snow drifts high prestress forces were required which proved to be difficult to achieve hence different solution needed to be found.

### 3.2 Design loadings

Scaled model of entire project was wind tunnel tested to ascertain wind loads and possible snow drifts associated with that. Resulting loads are shown on the right:

In total there were 19 load cases which included: 3 cases for dead load, 5 variations on snow, 9 load cases for wind and 2 cases for the thermal movement. All those load cases generated over hundred different load combinations.

### 3.3 Load combinations used

Load combinations taken in accordance with Eurocode 0&1:

$$\text{ULS: } 1.35G_k + 1.5 Q_{k1} + 1.5 \Psi_0 Q_{k2}$$

$$\text{SLS: } G_k + Q_{k1} + \Psi_0 Q_{k2}$$

### 3.4 Glass selection

Based on draft version of European standard for use of glass in structures, following design values were adopted for this project, see table 1&2 on the left:

Glass beam thickness was adopted as 5x10mm toughened glass laminated with PVB interlayer each 1.5mm thick.

### 3.5 Other materials used in the construction

| Load type  | Characteristic load | Normative reference  |
|--|---------------------|--|
| <b>Нормативные нагрузки на конструкции стеклянной кровли</b> |                     |  |
| Snow UDL $\mu_1 = 0.4$                                       | 0.56кПа             | СП20.13330.2011, wind tunnel test Kucherenko institute, 2016 |
| Snow UDL $\mu_2 = 0.8$                                       | 1.12кПа             | СП20.13330.2011, wind tunnel test Kucherenko institute, 2016 |
| Snow UDL $\mu_3 = 1$   | 1.4кПа              | СП20.13330.2011, wind tunnel test Kucherenko institute, 2016 |
| Snow UDL $\mu_4 = 1.2$                                       | 1.68кПа             | СП20.13330.2011, wind tunnel test Kucherenko institute, 2016 |
| Snow UDL $\mu_5 = 2.4$                                       | 3.36кПа             | СП20.13330.2011, wind tunnel test Kucherenko institute, 2016 |
| <b>Нормативная Ветровая нагрузка</b>                         |                     |  |
| Wind Load (structure)  | +0.25кПа/-0.6кПа    | СП20.13330.2011, wind tunnel test Kucherenko institute, 2016 |
| Wind Load (cladding fixings)                                 | -1.2кПа             | СП20.13330.2011, wind tunnel test Kucherenko institute, 2016 |

| <b>Климатические воздействия, г. Москва</b>                                   |             |                 |
|---|-------------|-----------------|
| Average temperature through the elements summer/winter $t_w / t_c$            | +42°C/-34°C | СП20.13330.2011 |
| Max temperature summer/winter $\Delta t_w$ и холодное $\Delta t_c$ время года | +46°C/-48°C | СП20.13330.2011 |

### 3.8 Computer modelling

Node coordinates were imported from the main engineer's model with associated deformations under individual load cases. Node deformations were combined with individual loadings for each glass beam and then analysed. Over 100 different load combinations were generated and analysed.

### 3.9 Bracket design

Initially, bolted connection was assumed however from more detailed analysis and assessment it was clear that relatively rigid bolt connection details causing glass overstress in various locations. Hence softer, more flexible joint details was required. Detailed analysis of node deformations in glass fixing points was carried out and summarized in Fig 13 on the right side. Based on this, nodes are predicted to be rotating approximately 1 degree around each axis. One rotation requirement was established, joint stiffness could be calibrated to minimize stress concentrations in glass.

To model and predict stresses within flexible joint, non-linear solid modelling was carried out using Mooney-Rivlin behavior model and stress strain curve tabulated data based on information from silicone manufacturer. Adopted model has shown silicone behaving within allowable stress range, see fig. 14 on the right side.

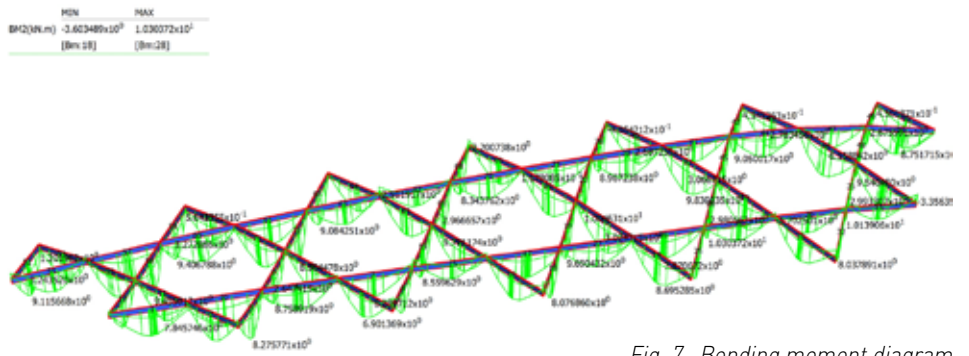


Fig. 7 Bending moment diagram

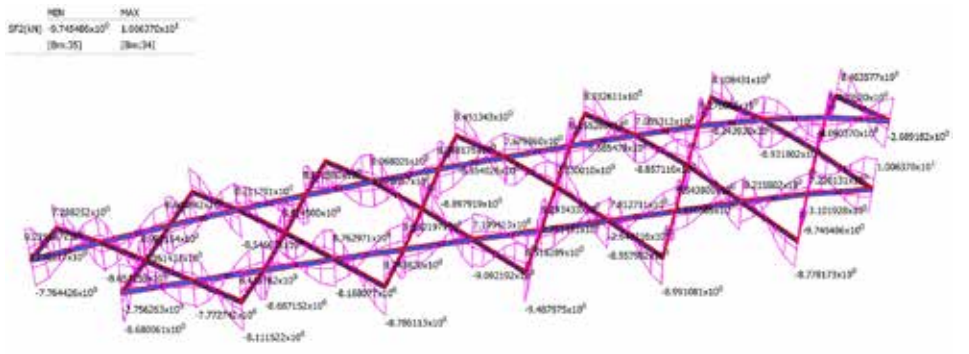


Fig. 8 Shear force diagram

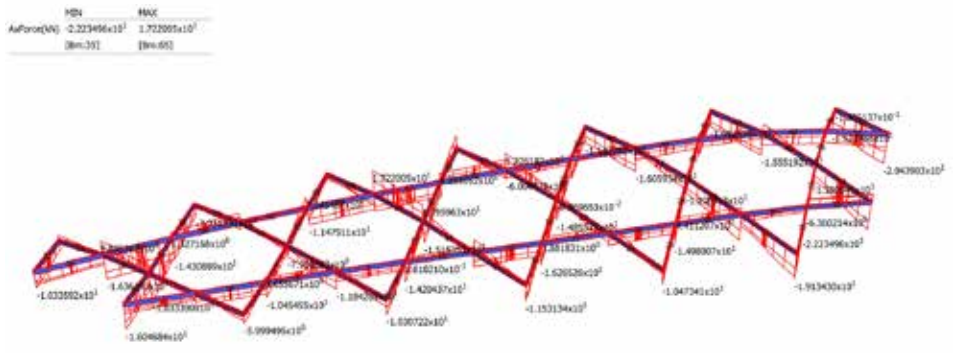


Fig.9 Axial forces

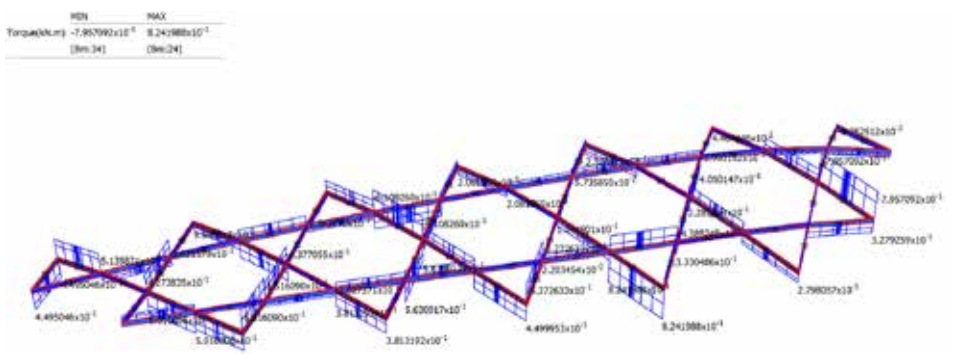


Fig.10 Torsion

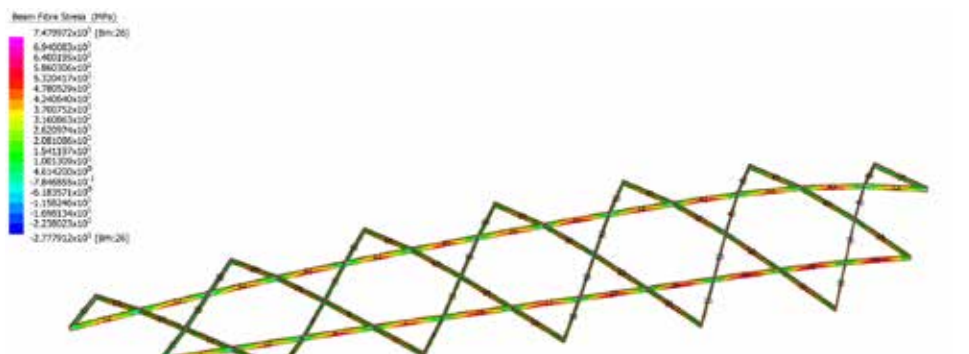


Fig.11 Max stress

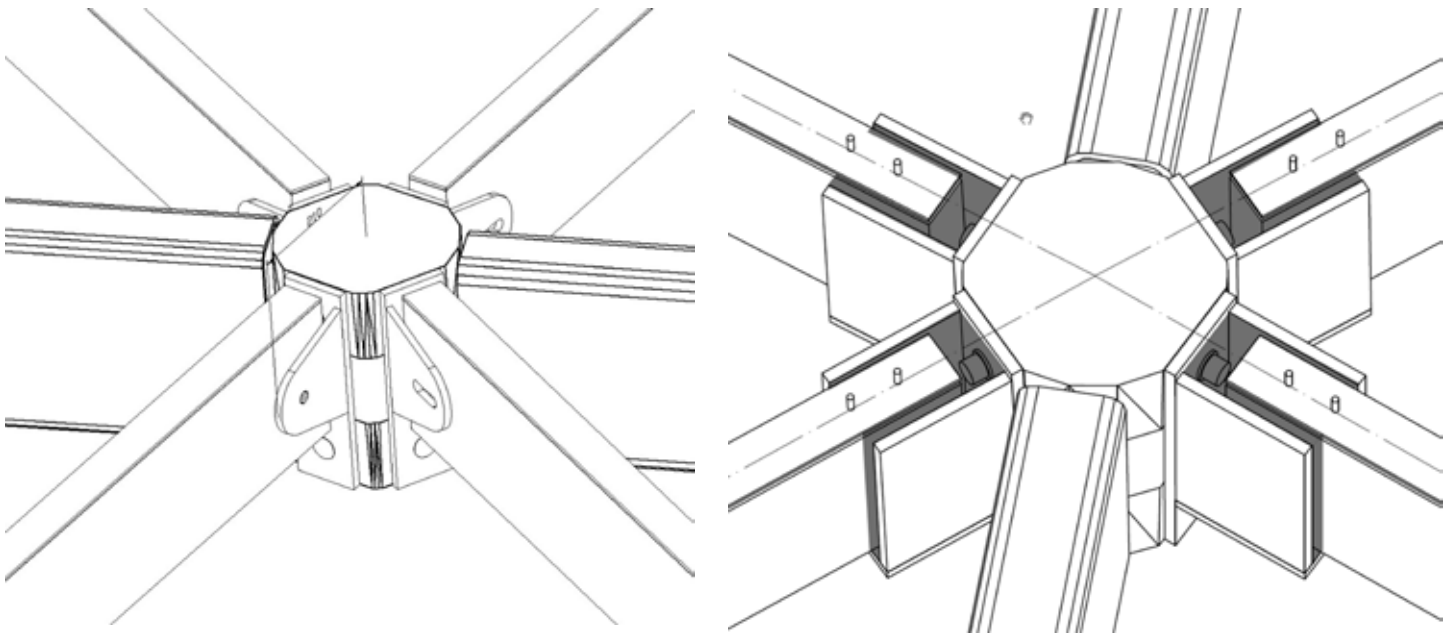


Fig.12 Fixing detail options a) original bolted solutions b) flexible joint

| MaxiumValues                  |           |           |             |             |             |
|-------------------------------|-----------|-----------|-------------|-------------|-------------|
| X<br>(MM)                     | Y<br>(MM) | Z<br>(MM) | UX<br>(Deg) | UY<br>(Deg) | UZ<br>(Deg) |
| 43.212                        | 22.536    | 15.393    | 1.137       | 0.954       | 0.808       |
|                               |           |           |             |             |             |
| Original Values (SW Included) |           |           |             |             |             |
| X<br>(MM)                     | Y<br>(MM) | Z<br>(MM) | UX<br>(Deg) | UY<br>(Deg) | UZ<br>(Deg) |
| 47.31873                      | 22.82347  | 17.72615  | 1.280207    | 1.076145    | 0.91037     |

Fig.13 Angular displacement of a node to be acomodated by the connection

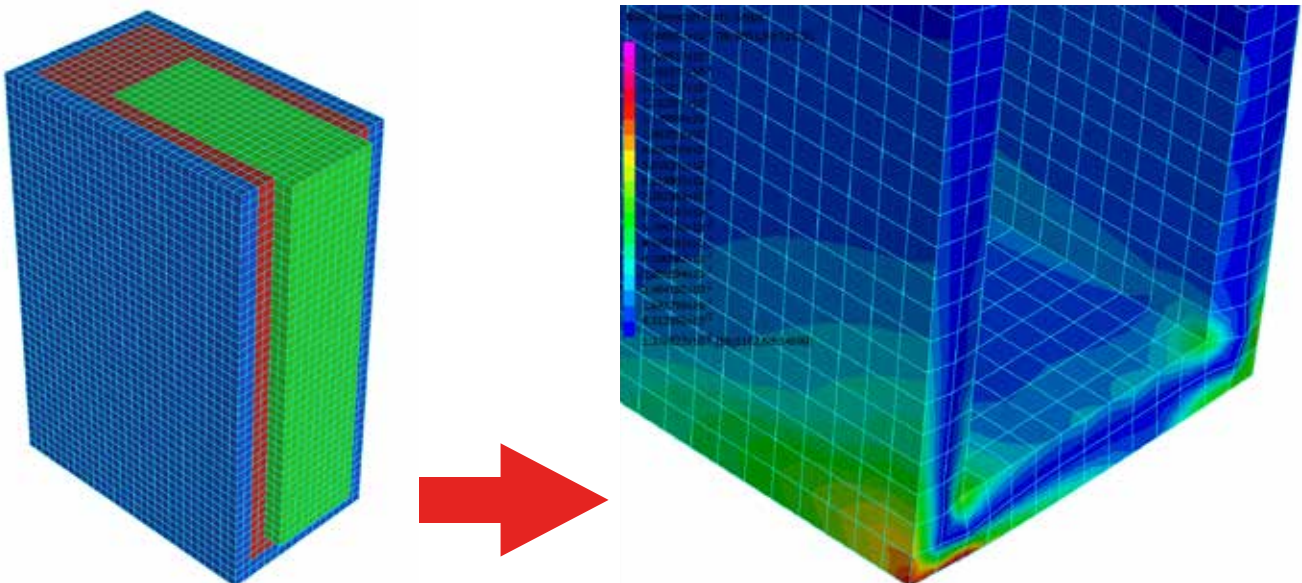


Fig.14 Non-linear analysis of the silicone joint was carried out to ascertain stresses and deforemtions

## Testing

### 4.1 Full scale mock up

Due to unprecedented nature of the project in this country, it has been decided that full scale testing mock up is necessary. The tests were carried out in the Glass Institute facilities in Moscow, on the 26<sup>th</sup> April 2017

## Production

### 5.1. Glass production

Glass production was carried out during the course of April 2017 by Modern Glass Ltd, Chelyabingks, Russia with installation due to start on site in May-June 2017.

## Conclusion

In conclusion, this project is our first experiment with use of structural glass beam element in grid-shell type construction which in our view has a potential to be scaled up.

## References

Institution of Structural Engineers: Structural use of glass in buildings (1<sup>st</sup> ed). London, IStructE, (1999)

Institution of Structural Engineers: Structural use of glass in buildings (2<sup>nd</sup> ed), London, IStructE, (2014)

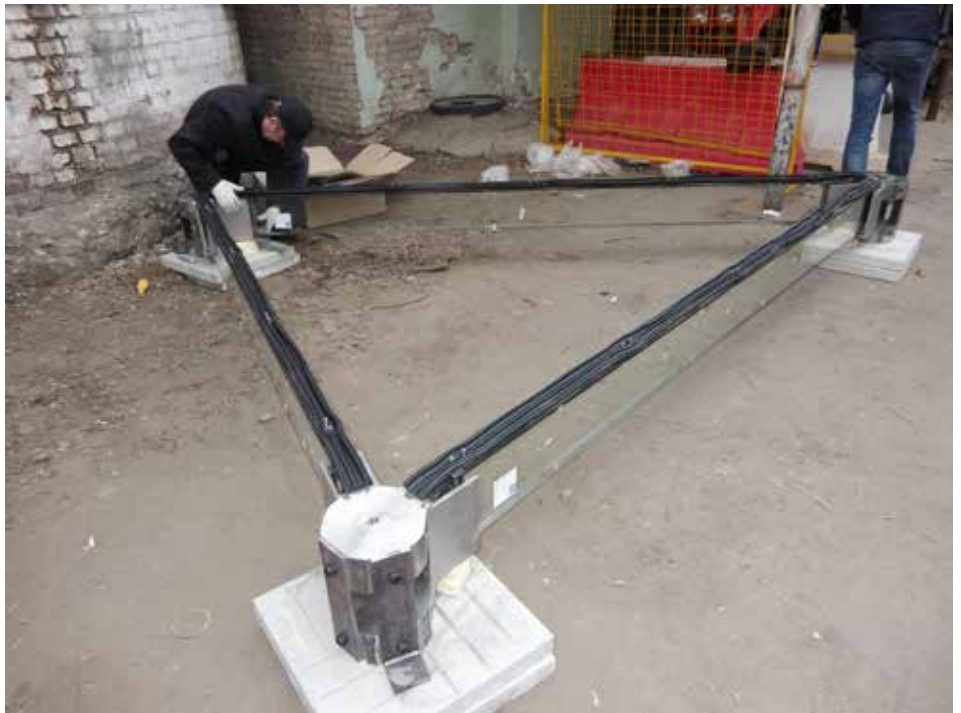


*Fig.15 typical triangular bay assembly*



*Fig.16 fully loaded mock up, taking 3 tonnes of sand bags.*

# Will the US Impose Tariffs on Imported Flat Glass Again?

Olavi Uusitalo  
Holmark

## Keywords

1=US flat glass industry 2=Tariffs 3=Industry structure

## Abstract

By 1960 imports supplied 25% of US sheet glass market. Local producers failed to fill the gap between the higher demand and the limited supply. In the mid-1960s local strikes and the devaluation of several European currencies helped the foreign supply. In 1962 tariffs doubled to 26%. In 1967 they were reduced to 16%. The protection on sheet glass last until 1972. One WTC building opened in 2014 in New York has Chinese glass in its first 20 floors. This event ignited a discussion of tariffs on imports of flat glass. Last year the US added further tariffs on Chinese steel imports. Donald Trump, the President of the US, had urged the US companies to bring their production back and to impose tariffs for instance on imported cars. By analysing the evolution of the NAFTA flat glass industry the paper tries to answer whether tariffs are needed.

## 1. Introduction

In the 1960s the US imposed tariffs on imported sheet glass. The local industry was incapable to compete with foreign suppliers which were said to have lower labour and raw material costs. Exporters had the advantage of devaluation of their home currencies. However, the US manufacturers applied very strict, several-layer marketing channel [1]. Now republicans debate to change the tax code so that it would see exporters and firms bringing profits home paying less tax than before, while firms shifting production abroad would face tariffs. Early this year Ford, a carmaker, decided to cancel a new plant in Mexico and invest more home [2].

In 2009 the One World Trade Center (to be built on the site of the destroyed WTC twin towers) construction project ordered for the first 20 floors of the tower's facade from China, Beijing Glass. PPG Ind. lost the deal. "This is going to be an iconic U.S. building that will have Chinese glass in it," said PPG

Ind.'s spokesman [3]. In Trade Center bidding Guardian won as the supplier of the intricately layered flat glass for the upper 85 floors [4]. However, in an interview Russell J. Ebeid, Guardian's chairman, said that "Those who are looking through the rearview mirror, waiting for the glass industry in this country to come back, should know it isn't going to come back, not the way it was," [4].

We will not have as many workers as we did in the early 2000s said one of the Guardian's plant manager. That is partly because of increased efficiency, but also because imported glass now in 2009 accounts for almost 24% of domestic market, up from 21% four years ago. What's more, the industry's biggest customers — the car and the construction industries — are not likely to raise production to the levels achieved before the credit crisis [4]. China's excess industrial capacity for instance in steel, cement, aluminium and flat glass causes troubles within its trading partners. In 2008 and 2014 the capacity utilisation rates for flat glass were 88 and 79 %, respectively. Moreover, it is said that the Chinese flat glass industry is heavily subsidised. [5].

In March 2016, the US increased further tariffs on Chinese steel imports. The 522% duty applies to cold-rolled flat steel, which is used in the production of cars among other things. The domestic demand for steel in China has fallen. The US and other countries accuse China of filling markets with cheap exports to keep its mills going. The China expressed "strong dissatisfaction" with the US' tariff decision. [6]

In his campaign, Trump's trade policy was an alarming mixture of coruscating complaints and fierce treats of protectionist retaliation. His trade strategy document has a preference of bilateral trade deals over multilateral ones and he used a tone: "It is time for a more aggressive approach". There is also an indication of how a Trump administration might take a trade fight to China by using sections 201 and 301 of the Trade Act of 1974. The first one (201) allows tariffs to be imposed as a safeguard to protect American producers from surge of imports. Affected local firms have to show that they have suffered "serious injury", but they have not to prove any unfair practice by the foreign firms. The other one (301) implies that the Trump administration might start going outside the global rules of World Trade Organisation's rules. The approach may

be a similar one to that of Ronald Reagan in the 1980s when the target was Japan. [7]. The research method is a qualitative case study with multiple cases in the North American Free Trade Agreement (NAFTA) flat glass industry. The main data source to cover the years 1950-1995 is [1] which uses several information sources: company and industry histories, books on the flat glass technology, trade journals (such as the Glass Industry and Ceramic Industry Magazine issues for 1961-1984; the American Glass Review, and Chemistry and Industry), business magazines (The Economist, Fortune, International Management, Management Today), and business books. The illustration for the years 1995-2005 is based companies' information and news clippings from newspapers and trade journals such as Glass-Technology International, Glass Online, and Glass for Europe. Some of the most relevant articles are cited.

The aim of the paper is to find out whether the US will impose tariffs on imported flat glass again as it did in the 1960s when three Presidents, Kennedy, Johnson and Nixon were involved. In the analysis, I compare the industry structure in the NAFTA countries, Canada, Mexico and the U.S., by 1960 to that of by 2017. The rest of the paper has four sections. First, the structural changes of the US sheet glass industry in 1960-1975 is illustrated. Second, I tackle the evolution of the NAFTA flat glass industry to the present structure of it. Third, analysis is given and fourth, the conclusions with managerial implications are given.

## 2. The US Sheet Glass Industry in 1960-1975

In the early 1960s, all three major plate glass manufacturers, Pittsburgh Plate Glass (PPG), Libbey Owens Ford (LOF) and Ford Motor Co. (Ford), produced also sheet glass. The newcomer in plate glass, American St. Gobain (ASG), produced sheet glass in its three plants, as well. Ford used all the sheet glass it produced internally. Fourco Glass Co. and Mississippi Glass Co. were smaller producers. [1].

In the early 1960s sheet glass known as 'Premium Pennvernon,' was free from distortion. It was expected to find a high degree of acceptance among architects, automobile manufacturers, and manufacturers of flat

glass specialty products [8]. In 1961 the Tariff Commission (TC) recommended to the President Kennedy that the tariffs for sheet glass should be increased. In 1950 domestic producers supplied 98 per cent of the demand. Ten years later imported sheet glass had taken a 25% share of the market. Sale of imported glass at lower price had weakened the domestic price structure. In 1960 four companies accounting for the bulk of the domestic output of sheet glass had shown a net loss of \$1.2 million while five years earlier the aggregate net profit in the industry had been \$30 million. According to the commission, the principal factors leading to the import trend were periodic shortages, availability of thinner and cheaper single- and double-strength glass from foreign manufacturers and the reluctance of U.S. producers to bypass their direct factory-distributor customers to sell directly to other large volume distributors and industrial users. [1].

In 1962 higher tariffs for imported sheet glass were in use. The increase corresponded to a 6% increase in the selling price. In 1964 it was said that float glass cannot compete with sheet glass, since float glass is not so much better than sheet glass as to merit paying the price differential. PPG took its Premium Pennvernoff the market because of too high quality. The sheet glass market was highly price-sensitive. The following reasons were identified for the current difficulties of local sheet glass manufacturers [8]:

- the successive reductions in rates of duty applicable to sheet glass
- the great disparity between wage rates paid to sheet glass workers in the US and Europe
- the European manufacturers had cost advantage (15%) in raw materials
- the companies which imported to the U.S. were large, well performing organizations.

Sheet glass producers in North America invested heavily in their plants. ASG's modernization its plants in 1962. In 1964-1967 PPG improved warehousing at the Mount Vernon plant and added two drawing machines twice (increasing the capacity first by 50 % and then 33%) at the Mount Zion plant. In the opening speech, the vice president of PPG said that further expansion would depend on action taken by TC. In 1967 PPG opened in Fresno, California a plant with six drawing machines. The plant was considered one of America's most modern facility and it 'is serving as a model for glass plants the PPG will build elsewhere'. Next year PPG open a plant with six drawing machines in Canada. [1]

In 1967 TGI wrote: "it would appear that President Johnson's decision to reduce and partly eliminate the escape-clause duties on sheet glass is based on obsolete information,

and not on the facts of today". The tariff should not have been reduced in the first place. The tariffs would have to be reinstated immediately if the imports were to increase. LOF's sheet glass operation was 'in a struggle to stay alive'. In 1966, 1967 and 1968 the share of the annual imports of sheet in US sheet glass consumption were 25, 27 and 33%, respectively. In 1969 U.S. sheet glass manufacturers again urged TC to prevent sharply rising glass imports from capturing a major share of the American market. In 1969, PPG introduced a new vertical manufacturing technology which enabled the company to produce new, thin (1/8" and less) sheet glass, Vertiglass, that would compete in quality and cost with float glass. Combustion-Engineering Inc. (C-E Glass) was the first company in the sheet glass industry to be granted a float glass licence in 1970. The company entered the sheet glass business by acquiring Mississippi Glass Co. In 1970 Pilkington produced float glass of 2 mm thick. In the same year float glass (4 mm thick) competed with sheet glass in the Canadian market. "Keep your eyes on these float glass developments - both in technology and marketing. There may be some surprises ahead". [1].

In 1970 St. Gobain sold its US plants to local investors who formed ASG Ind. Same time Guardian and Ford sold float glass at sheet glass prices. Ford shut down its sheet glass operations. According to Ford anyone who thinks float glass will not compete directly with sheet glass in the future is "quite mistaken". In 1971 Asahi Glass Co. (Asahi), a Japanese company, introduced a new vertical drawing process. The same time LOF closed one of its window glass plants because of sheet glass imports and high union wage and benefit demands [OU]. Next year a politician from Pennsylvania said that the President Nixon "has driven another nail in the coffin of the domestic glass industry" by his approval of a three-step reduction in import duties for window glass. In 1971, PPG increased the sheet production capacity of its plant in California. The company was the largest local sheet glass producer. In 1973 PPG advocated its Pennvernoff sheet glass method. In 1974-1977 C-E Glass, ASG Ind. and Fourco Glass shut down their sheet glass plants while PPG in 1976-1980. LOF followed in 1980. In 1979 Asahi acquired a sheet glass plant in the US to utilize its new vertical drawing process. Three years later it shut down the plant. In the meantime, the investment in float glass production soared. [1].

### 3. The evolution of the structure of the NAFTA flat glass industry in 1975-2017

By 1977, there were seven local float glass manufacturers, PPG Ind., LOF, Ford, Guardian, ASG Ind., C-E Glass and Fourco Glass in the U.S. PPG Ind. and Pilkington had plants in Canada while the local Vitro in Mexico. In 1978 Fourco Glass merged ASG Ind. to form AFG Ind. (AFG). In the early 1980s Pilkington withdrew from Canadian by selling the plant to Ford while C-E Glass sold its two float glass plants to AFG and Guardian. In 1984-1988 AFG opened two lines in Tennessee and one in California, and bought Ford's Canadian operations. In 1986 LOF was sold to Pilkington. Three years later Pilkington sold 20% of LOF to Nippon Sheet Glass (NSG), the second Japanese producer. In 1980-1992 in the US flat glass the share of imports to the apparent consumption varied from 5% to 9%. In 1992 Asahi acquired AFG Ind. At the end of 1970s Ford had three float glass plants (Nashville, Dearborn and Tulsa) in the US. In 1989 Ford and Central Glass, a third Japanese producer, formed a joint venture, Carlex, to supply automotive glass in the US. Six year later Ford sold its part of Carlex to Central Glass. In 1992 Cardinal, an insulating glass manufacturer, started float glass production to supply raw glass for its own use. [1]

In Europe in 1979-1981 BSN, another French flat glass producer sold Flachglas, the German subsidiary with three float glass lines (FGLs), to Pilkington, Glaverbel, the Belgium and Holland subsidiary with two FGLs, to Asahi, and Boissois, the French subsidiary with two FGLs, to PPG Ind. In Germany, the local cartel officials denied Pilkington to acquire Glaverbel while in France St. Gobain was denied for buying Boissois. At the same time, Guardian started float glass production, Luxguard, in Luxembourg. In 1983-1984 Asahi, PPG Ind. and Pilkington converted their last sheet glass plants to the float process in Italy, Holland and Finland, respectively. In 1983 Pilkington's, St. Gobain's, PPG's, and Asahi's market shares in Europe were 35, 30, 13, and 11%, respectively. The remaining 11% was distributed to Luxguard and the Italian S.I.V. In the 1980s Guardian opened FGLs in Luxemburg and Spain, where St. Gobain had by 1980 three lines. By 1993 Guardian had eight foreign float glass plants on three continents and the world market shares of flat glass were as follows: Pilkington 19, Asahi 18, Saint-Gobain 14, PPG Ind. 12, Guardian 8, Ford 4, NSG 3, Central Glass 2%. [1].

In 2000 Ford arranged its glass business into a spin off company, Visteon. Five years later, it acquired them back under the entity, Automotive Components Holdings (ACH). In 2007 Zeledyne bought flat glass business

(including Nashville and Tulsa plants) from ACH and invested \$4 million in the Tulsa plant for a new cutting system, and rebuilt the other float line. In 2010 the company exited the glass business because of "continuing difficulties in the economy." In 2011, Carlex bought from Zeledyne the Nashville float glass and automotive fabricated glass plants, and the replacement glass distribution center. In 2012 Ford bought and demolished the idling Tulsa plants plus sold the land. In 2014 Central Glass acquired two (one from the US and one from Europe) automotive product subsidiaries from Guardian.

In 2006 NSG acquired Pilkington. In 2007-2014 the industry closed nine FGLs in the US and Canada. There is no flat glass production in Canada. In 2017 Guardian operates seven FGLs in the US and another 21 abroad. In 2014 Fuyao Glass, a Chinese flat glass manufacturer, bought Mt. Zion plant from PPG Ind., while in 2016 Vitro, a Mexican flat glass manufacturer, the rest of PPG Ind.'s flat glass, safety glass and distribution operations in the US and Canada. This year Guardian was sold to Koch Industries. St. Gobain withdrew from the US flag glass industry in 1970. In 1997 and 2006 it opened two FGLs in Mexico. In Mexico Vitro started float glass production in Mexico in 1968 and have now four lines in operation.

In 2003-2007 in the US flat glass the share of imports to the market was around 15%. The export was at the size as import. In 2015-2016 import accounted about 12%. By 2017 the local producers, Cardinal and Guardian, had 12 lines while 10, seven and two lines were owned by Japanese Asahi, NSG and Central Glass, Mexican Vitro, and Chinese Fuyao Glass, respectively. In Mexico Vitro, the local one, run four lines, St. Gobain two lines and Guardian one line [9]. In 2011 throughout the EU there were 61 FLGs operating close to both the markets and raw materials. This meant almost 15 million tons total annual capacity. Moreover, there were six other FGLs in Turkey. In 2014, close to 8.5 million tons of float glass was produced in the 55 FGLs. China is the biggest flat glass producer in the world. About 50 % of the world-wide float glass demand is filled by the Chinese capacity (about 240 FGLs). In 30 years, China's flat glass production capacity has increased over 40 times. The largest producers are Kibing, China Glass, Fuyao Glass, Xinyi Glass, CGS, and Shandong Jinjing.

#### 4. Analysis

By 1960 the world stock of foreign direct investment (FDI) reached \$60 billion. By 1980 it was more than \$500 billion. In these decades, the term "multinational company (MNC)" was invented, and when economic theorists turned their attention to explaining their existence.

In 20 years from 1945 the US accounted for around 85% of all new FDI flows. By 1980 it held 40% of total stock. In the same time both German and Japanese FDIs remained low, but after growth in the 1970s they both had an overall share of world FDI of 7-8%. By 1980 more than 65% of world FDI was located in Western Europe and North America. [10]. The NAFTA flat glass industry experienced the similar evolution as was illustrated above. By 1950 the domestic companies produced the flat glass. Since the early 1950s Pilkington had manufactured sheet glass in Canada for the local use. By 1960 the imports mainly from Europe accounted 25% of the flat glass market. St. Gobain entered the US in the mid-1950s. In 1962 it as American St. Gobain (ASG) opened a plate glass plant. In the late 1960s Pilkington built two FGLs in Canada. In the 1980s Asahi, a Japanese manufacturer (acquired a sheet glass manufacturer), and Pilkington (acquired LOF) entered the US flat glass industry. [1]. By 2017 foreign firms. MNCs, operated 23 out of 38 NAFTA FGLs.

Before 1960 the flat glass industries (both sheet and plate) were able live in peace. The US and European plate glass industries, which had high entry barriers, had shared the market already in the 1930s. The industry structure with many layer distribution channel was tight. In the late 1950s some firms started to by-pass the rigid distribution system by importing sheet glass. This was a new thing for the local sheet industry which in general thought that the US is the centre of the world. The Xerox co-operation with the Rank, from UK, illustrates this well. Xerox made 50-50 joint venture, Rank-Xerox, with Rank and let it take care of the global market since there was supposed to be nothing compared to the US. The US government could not help Xerox but it could help local sheet glass producers by imposing tariffs. The plate glass industry was not involved and it could concentrate on the float glass plants investments. Float glass was licensed exclusively to the plate glass producers, PPG, LOF and Ford. Soon they faced a problem, a similar one, the sheet glass industry had: the by-pass of the distribution. The second shake-up came by William Davidson, the owner of Guardian, who was fed up with high prices local float glass producers charged for. The firm needed raw material for its safety glass plant. He hired a float glass specialist and few other people from Ford's glass division and built a plant without a license from Pilkington. This episode opened the way for other licensees in the US. The next licensees were Combustion-Engineering (C-E Glass), Guardian, ASG Ind. (a firm created to buy ASG from St. Gobain) and Fourgo Glass. By 1975 seven companies operated 24 FGLs in the U.S. while Pilkington operated two lines

in Canada. The incumbent firms and Guardian (built three lines in the 1970s) did well, but three other newcomers were struggling. The third shake-up had similar features as the earlier ones, shortage of raw material. In the 1960s one entrepreneurial person, Dee Hubbard, had run auto service company and windscreen reseller, Safelite. The windscreen price increase forced Safelite to manufacture them itself. For ten years Safelite made windscreen of purchased glass until Hubbard was asked whether Safelite considered the acquisition of Fourgo Glass. Fourgo Glass, almost in bankruptcy, was bought. Hubbard hired the very float glass specialist from Guardian and put the technology in work. Next, he merged Fourgo Glass with another loser, ASG Ind. and formed AFG Ind. (AFG). At once Hubbard reconstructed marketing department. He formed inside sales-service operation which solved everyday customer problems on the phone, thus freeing the outside sales force to concentrate on selling. AFG increased flexibility and reduced response and delivery times. Customers contacted the same person. The sales team worked on a straight salary plus bonus basis. Hubbard passed his lean and hungry attitude on to his sales team. His favorite quote was that 80% of all sales are made after the fifth call, yet 90 % of salesmen give up after fourth one. The team was also motivated by company cars, diesel Mercedes-Benz 240Ds. The salesman of the year qualified for Mercedes-Benz 300D as a company car. AFG was much more flexible than established firms like PPG Ind. in which orders could go through four steps. On the contrary PPG applied strong advertising campaigns to gain customers. In 1981 AFG bought its third float glass plant from C-E Glass. In the 1980s AFG opened four plants and bought a plant in Canada. AFG changed the industry towards customer orientation. The industry seemed not to recognize this since, for instance, the CEO of PPG Ind. was worried the way Guardian operated but not the way AFG operated. In the early 1980s Pilkington withdrew from Canada. The competition on its home market (about 40% of the market was imported) made it to think of a closer co-operation with LOF, a strong player on the automotive sector. The owner, Gulf & Western Industries, was ready to leave the industry. In 1983 Pilkington bought 30% of LOF and in 1986 the rest. Pilkington worked more closely with NSG and sold 20% of LOF to NSG. In Canada PPG Ind. continued its operation while Ford resold Pilkington's plant to AFG. PPG Ind. and Guardian built three FGLs in the US and four abroad. In the 1990s a newcomer, Cardinal, came in 1992. Guardian built two plants in the US and nine outside. Asahi bought AFG (which had eight FGLs) and built a plant in Canada. Ford

started co-operation with Central Glass. By 1992 there were in the U.S. three large local manufacturers and two foreign MNCs. During the restructuring of the industry in 1978 to 1992 the firms served the local market well enough to keep imports low (only 5-8% of consumption). In 1997-2000 PPG Ind. made 18 acquisitions outside the flat glass or related industries. In 2000 its flat glass business was 28% of its total revenue.

In the 2000s Guardian built plants all over the world (in Mexico, too). Cardinal supplied glass to its fabrication plants from five lines built in 1992-2006. Ford struggled with its glass business. Finally, in 2011 the former Ford float glass plant got a stable owner, Central Glass, after 5 owners in 12 years [11]. Central Glass intensified its strategic move to the auto part business by acquiring two subsidiaries from Guardian. In 2006 NSG acquired Pilkington. In 2014, Fuyao Glass, a large auto part manufacturer, came closer to its US customers by buying a plant from PPG. Vitro became a remarkable supplier by acquiring the rest (including seven FGLs) of PPG Ind.'s business. Vitro and St. Gobain built more lines in Mexico. Local customers have been quite satisfied with the services since the imports have been in the last 15 years 12% to 15% of the US market.

## 5. Conclusion

By 1960 three large firms acted both on the sheet glass and plate glass industries. The industry structure and business environment had been reasonable stable and nice for decades. It cannot last forever. Shake-ups in the form of new technology, a by-pass of the distribution, newcomers, an introduction of new management systems and foreign firms, MNCs, etc. took place.

The strict distribution and delivery problems created the need for sheet glass imports. Float glass changed the industry. Pilkington's licensing policy made it possible for float glass to enter the U.S. and to safeguard the existing plate glass industry long enough. The next shake-ups came by newcomers, Guardian and AFG. These entrepreneurial companies took on the establishment [12,13]. Guardian questioned the robber baron attitude of the existing float glass suppliers. It demonstrated also the commitment and ability to build a global company, a MNC. AFG introduced key account management in the industry. In the 1980 and 1990s the flat glass industry became global. In the NAFTA area local manufacturers, LOF and AFG, were sold to foreign MNCs. An entrepreneurial newcomer, Cardinal, came in. These changes shook up the industry, again. In the 2000s and the 2010s Mexico got three lines more while Canada lost all. Three committed foreign MNCs bought the operations of

uncommitted local ones, Ford and PPG. I do believe that Guardian's new owner, Koch Industries, is committed in the industry and let Guardian also operate in its entrepreneurial way.

In the 1980s during the recession and the invasion of the Japanese products the shake-ups kept the industry alert. There was no need for such protection (tariffs on import motor cycles) as Harley-Davidson got during Ronald Reagan's term. As we saw the healthy shake-ups have kept the industry flexible. The system has worked. The last structuring in 2005-2017 was welcomed to keep the industry awake for the next 15 years. There is neither a need to break NAFTA nor intervene in the forms of tariffs the industry. The President Donald Trump should act as Americans use to act: "Do not touch the process if it works."

## References

- [1] Uusitalo, O. "Float Glass on the Flat Glass Industry", SpringerBriefs in Applied Sciences, Springer, Heidelberg, 2014.
- [2] "Briefing Multinationals The retreat of the global company", The Economist, Jan 28th 2017, 14-17.
- [3] Seltzer, R. "Cumberland County company loses bid to produce Trade Center glass", The Patriot-News, April 02, 2009 [http://www.pennlive.com/midstate/index.ssf/2009/04/ppg\\_loses\\_bid\\_to\\_produce\\_world.html](http://www.pennlive.com/midstate/index.ssf/2009/04/ppg_loses_bid_to_produce_world.html)
- [4] Uchitelle, L. "Glassmaking Thrives Offshore, but Is Declining in U.S.", New York Times, Jan. 18, 2010
- [5] "Business this week", The Economist, May 21st, 2017, 7.
- [6] "Industry in China; the March of the Zombies, China's excess industrial capacity harms its economy and riles its trading partners", The Economist, Feb 27th, 2016, 52-53.
- [7] "American trade policy; Plan of action", The Economist, March 4th, 2017, 59-60.
- [8] Barker, R. F. "Report to the U.S. Tariff Commission", The Glass Industry, August, 1964, 426-7 & 444.
- [9] World of glass <http://worldofglassmap.com/map>
- [10] Jones, G. "Multinationals and Global Capitalism: From the Nineteenth to the Twenty-First Century", Oxford. University Press, 2015
- [11] Chappel, L. "The state of suppliers After 5 owners in 12 years, a former Ford glass plant finally has a stable owner", Automotive News, August 1, 2011.
- [12] Kleinberg, E. "AFG takes on establishment", Industrial marketing, July 1981, 14.
- [13] Kinkead, G. "The Raging Bull of Glassmaking", Fortune, April 5, 1982, 58-64.

# Analysis of Float Glass' Development by Design Envelope

Olavi Uusitalo  
Holmark

## Keywords

1=Innovation 2=Float glass 3=Design envelope  
4=Positioning

## Abstract

In the 1950s the flat glass industry had two separate products and sub-industries: plate glass and sheet glass. Float glass merged these two industries. Since the mid-1990 flat glass has had two separate products again: high quality float glass and lower quality float glass. The aim of the paper is first to explain how float glass could merge the sub-industries and second to analyze the situation of lower quality float glass in the industry. The modified design envelope model is applied to demonstrate the technological competence and especially strategic thinking concerning to understanding of the markets and positioning the product. The envelope model helps companies building scenarios for responses if new unexpected innovations are introduced. The analysis of lower quality float glass with modified design envelope rise the question: Should there be a lower quality float glass available?

## 1. Introduction

In the late 1970s the flat glass industry had two separate industries, sheet/window (later on sheet) glass and plate glass. The float glass innovation has its origins from both industries. It aimed to have optical quality of plate glass and "fire-finished" manufacturing method from sheet glass. The R&D process of float glass in Pilkington, that time a UK based family owned company, took seven years. During it the company made a strategic decision to position float glass as a readymade product in the plate glass industry and not too quickly in between two industries. In the 1960s Pilkington developed the float glass technology, so that float glass could compete also with sheet glass (see Figure 1.).

The aim of the paper is to explain how Pilkington was able to revolutionize the flat glass industry. This involved both high technological competence and also strong

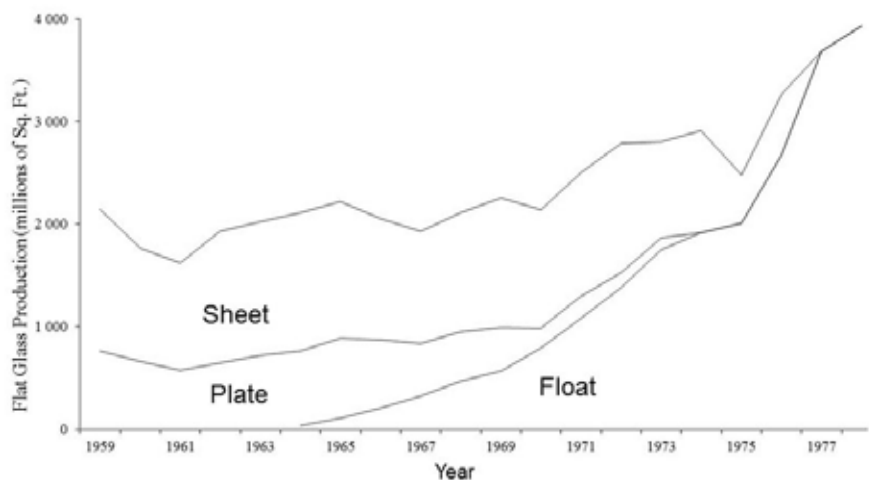


Figure 1. Flat Glass Production in the U.S., 1964-1980 (Millions of Sq. Ft.) [1].

strategic thinking concerning to understanding of the markets and positioning the product. I use a modified version the design envelope model (DEM) [2] for analyzing the emergence of float glass innovation and to demonstrate the reasons beyond the revolutionary change in the flat glass industry. The DEM is also applied in the analysis of lower quality float glass. The study applies a longitudinal and contextual approach with the use of a multiple case study method.

The rest of the paper has three parts. First, the DEM is presented. Second, the emergency of float glass as the dominant design is illustrated by applying the modified DEM. This includes also illustration to the Chinese lower quality float glass. Third, conclusion and managerial implications are given.

## 2. The Design Envelope Model (DEM)

A technological innovation, which later may be thought of as the capture of design dominance (DD), depends heavily on the degree to which market structure and market needs are understood [2]. To link the market structure and technological deployment decisions, a DEM is proposed for analyzing the complex closed or open systems. Based on the analysis of float glass innovation I draw conclusions from positioning of it. [2] Positioning is a matter of corporate strategy not sales tactics [3]. The purpose of the authors is threefold: first, to develop a comprehensive business strategy according to which the top managers needs

an intimate understanding of product class evolution (especially the emergency of DDs), i.e. technology as an outcome of community dynamics (variation, selection and retention), second, to offer a perspective suggesting that emergencies of DDs may be explained in terms of 'lumpiness' of markets which have finite and limited customer bases and, third, to identify the mechanisms through which executive teams shape technology strategy, and to identify the processes which affect the scope, direction and quality of technology strategy decisions. [2]

The focus is primarily on systemic technologies, because these more complex technologies are influenced much more heavily by social, organizational, and political processes. Since it is the rare technology, which clearly dominates across all possible dimensions of merit, a process of compromise and accommodation between suppliers, vendors, customers, and government becomes important in adjudicating among feasible options. The achievement of a DD can thus be seen to be driven by the strategic decisions made by organizations interacting with other organizations and with practioner communities. [2].

Technological merit is crucial. A difficulty with this concept of technological evolution is that the DD can only be identified ex post, and at an industry level. How a DD can be created in an industry for a firm? It might be useful to develop a framework for thinking about the drivers of DD in complex, interdependent

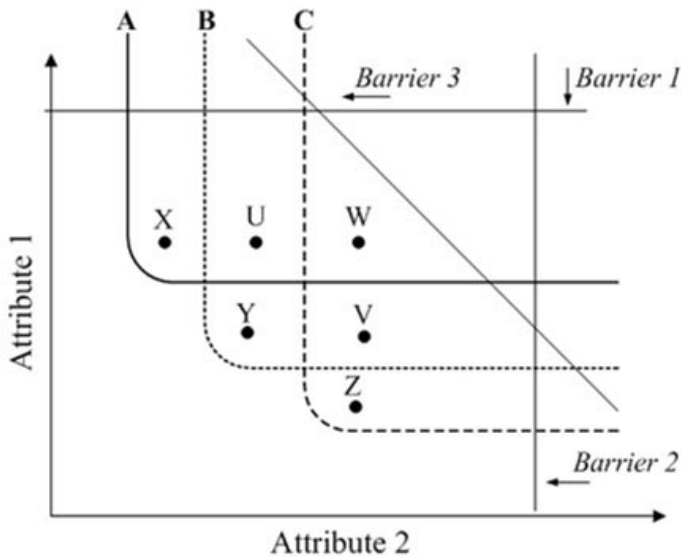


Figure 2. Combined Effects of Market 'Lumps' and Technology [2]

systems. This requires a more specific definition of DD, which both captures the industry level ex post construct but also allows strategist ex ante, and through the linkage between the firm's technology strategy and the way it wishes to attack its markets [2].

The two-dimensional model (bases on two product attributes) is in Figure 2. The edges of the 'design envelope' are defined by the current limits of technology. Designs are constrained by a multiplicity of technological barriers, in much the same way as linear program solution is held within a multidimensional envelope of constraints. The edges are defined as Barrier 1, Barrier 2 and Barrier 3. [2].

Customers make trade-offs between attributes depending on the price charged for it. In virtually all real markets, uneven concentrations of customers clustered around different attribute preferences create disparate sub-populations who each make their own trade-offs in product attribute space. These unevenly concentrated groups of customers are defined as lumps or 'market knolls'. For instance, group A (or market knoll A) may require only attribute 1, while group C prefers attribute 2. For group B both attributes are equally stressed. At a given price level, each group would have its own isoprice line (Figure 2), which suggests that at the given price, the group A would buy any design to the north and east of line A and so on. [2].

The area north and east of lines A, B and C are the knolls. Standard marketing treatments divide the market into niches and each knoll is being handled separately. In the light of the potential for very rapid and substantial changes in technology, however, firms usually focus exclusively on developing niche products that serve only one of the knolls (a product

at a price in points X for group A, Y for B and Z for C). However, companies could use technology to design products at points U, V and W in which case each of the niche players will find their products obsolete on their niche attributes, while at the same time the new entrants reaps the benefits of a larger market size than any of the niche players with now obsolete designs. As new designs advances north and east in an attribute space, the number of sub-populations that are attributed by that design increases. This means that there might emerge a design that captures all the market knolls lying to the south and west of the design. This highlights the specific conditions that determine the viability of a niche, as well as its fragility. 'It is only for as long as technological barriers confine designs within specific market knolls that these knolls can be thought of as niches. Since technology advances can create a design that lies to the north and east of whole groups of niches, niches are strictly tactical in the long run'. [2].

A revised definition of DD captures the strategic problem of attempting to develop such a design ex ante and at firm level. "A DD in any market knoll is that design that lies the most northeast in that knoll's product attribute space." Executive teams should shape technology strategy as follows: "Executive teams must put in place the processes that will drive technology development in the appropriate directions, so that the firm can navigate from its current design to a future design that gives the maximum increase in market access per unit development cost." [2].

The challenge of executive teams is to help establish key dimensions of merit both by managing environmental relations and by managing intraorganizational dynamics

to produce a system that dominates in the targeted product space. The more complex the product is, the more complex the intra- and extraorganizational strategic and managerial challenges are. Their definition of the concept of DD lets them to contribute in two ways: first, to develop a more precise understanding of the factors that lead one particular design to dominate another, and second, to begin to think through the strategic implications of managing technological investments to capture DD. [2].

#### 4. The Flat Glass Industry and the Float Glass Innovation

In the 1940s (and as late as 1975) the flat glass industry had two separate industries: the sheet glass and plate glass industries. Sheet glass was subject to inhomogeneities and sheep while plate glass was free of optical distortions and expensive. Float glass was launched in 1959 and it changed the whole flat glass industry globally. [4] Later on China and its float glass technology took a large share in the world market [5].

##### 4.1. Flat Glass Manufacturing in 1930-1960

To make plate, molten glass was rolled into a plate and then ground and polished both surfaces were smooth and parallel. The process was noisy and created a lot of dirty. Plate glass was used in more sophisticated applications such as mirrors and the large windows used for retail displays and architectural effects, where the inhomogeneities and optical distortion were not acceptable. The plate glass industry was characterized by high quality and high price products. Sheet glass was drawn into a ribbon through a block floating on the surface of the molten glass. The ribbon passed vertically upward through an asbestos roller and then into a cutting room where the cooled, hardened glass was cut and stacked. It was suitable for ordinary windows used in construction. [4].

In Figure 3 the plate glass and sheet glass industries are illustrated in a modified DEM. The X-axis is the unit price (descending) and the Y-axis is the optical quality of glass. I call my model a modified version since the price is on the X-axis. Thus, I do not have isoprice lines as the original model has [2]. On the other hand, unit price could be seen as an attainable attribute due to the technology. These attributes are offered to the customers, i.e. the glass producers, with certain costs of acquisition (comparable to isopricelines) [4].

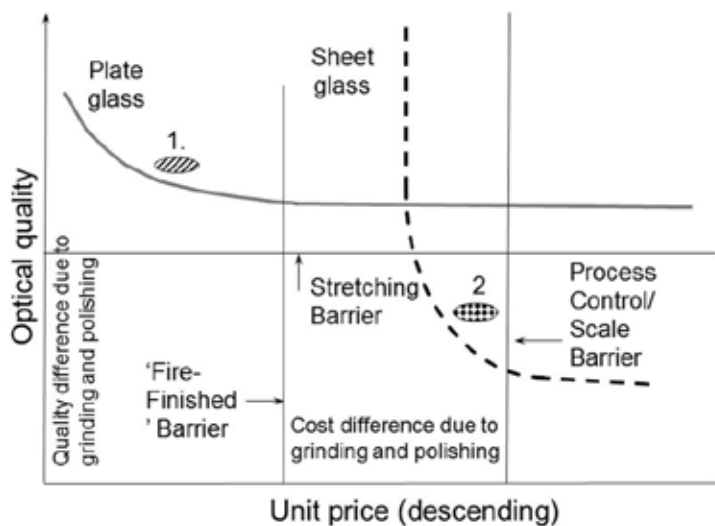


Figure 3. The plate and sheet glass industries illustrated by the means of modified DEM.

The plate glass line (solid) in Figure 3 tells that customers preferred high quality products and as cheap as possible, i.e. customers were above the plate line (this refers to a market knoll). The plate glass industry in the early 1930s was located on the left upper corner, Area 1, since a technology barrier, 'Fire Finished' Barrier (i.e. the need of grinding and polishing) was the constraint for the cost (price) reduction of plate glass. There was no technology barrier for quality of plate glass, since quality depended on the amount of grinding and polishing. The drawing processes allowed producing 2-12 mm thick flat glass. The customers valued cheap products and as high quality as possible, i.e. customers were right and above the sheet line. Sheet glass was 'fire-finished' (i.e. no processing after cooling) and thus beyond the 'Fire-Finished' Barrier for plate glass. The quality of sheet glass was, however, constraint by another technology barrier, Stretching Barrier (i.e. if a glass ribbon is drawn from molten glass without any continuous support the ribbon has optical distortion). Since sheet glass has partly manual control the Process Control / Scale Barrier limited for the cost reduction. The sheet glass industry by 1950 was in Area 2 in Figure 3. [4].

The industries targeted different customers and were quite different. The plate glass industry was much more concentrated because of high investment requirements and large production capacities. Large flat glass companies produced both sheet glass and plate glass. However, the companies although they developed technologies in both industries kept the products and their applications separate. They also started safety glass production in the 1920s. Since then the

car industry was the main customer for plate glass. In 1935 Pilkington introduced a 'twin' grinding to grind both sides of a plate glass ribbon at the same time. This lowered the cost of plate glass [6]. The company licensed twin grinding technology (referred to as the I licensing in Figure 4) to the plate glass producers [6]. The plate glass industry moved to Area 3. [4]

#### 4.2. Float Glass Innovation

The float glass development started in 1952. Two years later Pilkington decided to launch float glass only if it could replace plate glass (not on Area crossed). The cost of float, if successful, estimated to be closer to those of sheet glass than those of plate glass. In 1959 the process was launched. Float glass is "fire finished" having no grinding and polishing phases. Its quality is equal to that of plate, but the investment and production costs were much less than those of plate glass. First the only possible thickness was 6.5 mm, luckily suitable for side panes in cars. Pilkington moved over the 'Fire Finished' Barrier to Area 4. Float glass was above the Stretching Barrier since the molten tin gave continuous support to floating glass. There was, however, a new barrier, the Ribbon Speed Barrier, which prevented manufacturing of thinner float glass and thus, prevented float glass entering the laminated windscreens and the sheet glass industry. Pilkington by licensing float glass technology (III licensing) inside the plate glass industry let the whole industry to move to Area 4. Pilkington worked also with the further development of float glass and it could move the Ribbon Speed Barrier further north east. [4]. In 1970 Pilkington produced 2 mm thick float glass. Float glass started to compete with

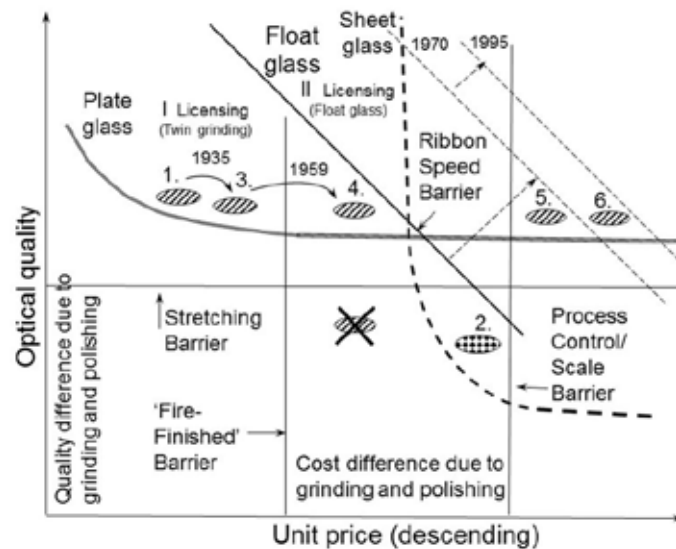


Figure 4. Introductions of twin grinding and float glass plus the evolution of float

sheet glass. Ultimately float glass went beyond the Process Control / Scale Barrier (Area 5) of sheet glass. In the mid-1970s float glass took over sheet glass. As Pilkington positioned float glass clearly in the high cost plate industry, and not in between two subindustries, it was able concentrate on one 'market knoll' with prevailing technological competence. Sheet glass was not challenged before float glass was cost-effective enough to replace the existing technology. The US situation (Figure 1) illustrates well, how float glass made these two subindustries obsolete one by one. By 1995 large scale operation had decreased the manufacturing cost of float glass and it moved to Area 6. [4].

#### 4.3. China's float glass

In the 1960s the Chinese scientific and technical workers began to study float glass process. In 1971 the first industrialized test line for float glass production was built in Luoyang. In 1981 the process was named "China Luoyang Float Process". Since then China float process has been third process among Pilkington and PPG processes. In the 1990s the development focused the capacity. The progress from 90t/d to 700 t/d. By 2006 the capacity reached 900 t/d with glass ribbon width up to 5.2 meters. Since then China has been one of the few countries in the world capable to build super tonnage float glass lines. In 1980s China established float glass quality standard. The quality of float glass made by the China float glass technology has increased with better equipment and raw material. This has narrowed the gap with the international advanced level greatly. The super grade product meets the needs of automotive glass, mirror glass and other fabricated



Figure 5. Lower quality float glass in modified DEM

glass. The national standard is the lowest quality target. More and more companies have taken as their objective to satisfy the market demands on high quality flat glass products. [5].

In 2002 the global flat glass market was about 35 million tons of which 22, and 7 million tons were high quality float glass and lower quality float glass produced mainly in China, respectively [7]. Two years later the numbers were 38 (flat glass), 23 and 10 million tons, respectively [8]. In 2009 the numbers were 52 (flat glass) 29 and 19 million tons, respectively [9]. Although the Chinese government tries to eliminate the lower quality float glass capacity and tighten the capacity expansion, these policies have execution risks [10]. The fluctuating oil price in was the main cause for the difficulties facing the Vietnamese flat glass industry in 2008-2009. Moreover, the increase in imports of flat glass, a decrease in domestic demand due to the global economic crisis and commercial fraud (low-quality float glass sold with labels of high-quality products) contributed to the injury to the domestic industry [11].

Basically, Chinese float glass was lower quality at global scale depending on the supplier. There were clear category difference with leading companies like CSG (China Southern Glass), Xinyi and Jinjiang. There were differences in the basic technologies and how did companies monitor the process. Costs were reduced by using low cost of materials, low cost labor, local incentives from local administration to employ more people. In quality sense for instance the nominal thickness could have 15-20 % difference. Lower quality float glass was/is used by customer segments with home appliances,

furniture etc. products. Whether lower quality float glass will disappear is a question of the cost difference and investments. [12] Based on the previous information I can place the lower quality float glass on the modified DEM (Area 7 in Figure 5). There are again two types of glass as in the 1950s, but for how long. It seems that every Chinese manufacturer also like to produce high quality float glass [5].

## 5. Conclusion

The ultimate goal of float glass was based on the combination of the attributes of products of two separate industries, the sheet glass and plate glass industries. Pilkington positioned float glass clearly in the high cost plate industry and not in between the sheet glass and plate glass industries. This left no chance for creative imitators [13]. Had Pilkington introduced float glass as a semi-finished product in between sheet glass and plate glass it would have been difficult for them to persuade plate glass users to buy lower quality and sheet glass users to pay higher price. More over there would have been a risk that another company, a creative imitator, would have taken (by further development) float glass to the plate glass industry. With careful licensing policy Pilkington managed the interorganisational dynamics world-wide. The great differences between plate glass and sheet glass justified the merge of the two industries.

In China there has been / is problems with the quality as we saw above. This situation has created confusion in the industry. On the one hand, large established manufacturers seem to devalue lower quality float glass, but on the other hand, the Vietnam case showed

that some manufacturers try or have tried to cheat with lower quality float glass. However, it seems that every firm in the industry aims to produce high quality glass. Flat glass will / has become a commodity without any room for differentiation, segmenting and thus different prices. Savaète calls this a mistake the flat glass industry has done [14]. It seems that while flat glass being a commodity the service is the only way to differentiate in the flat glass market. Should it be so? There are several types of float glass: tinted, self-cleaning, extra clear etc. for special purposes. The float glass manufacturing process seems to be well understood and managed. It should not be difficult on purpose manufacture lower quality float glass on lower cost (and thus on lower selling price) for less demanding applications. Luoyang Glass is in a sense advocating this [15]. As we saw, before float glass there were two types, plate and sheet, of flat glass for different applications. All big manufacturers produced both types of glass and kept reasonable well the industries separate. Could it be possible in the float glass era? Last April I visited my friend's elegant villa on the lake and built by 1960. It was both cool and nostalgic to see 2 \* 2 meter<sup>2</sup> windows made by Lahti Glassworks' Fourcault machines. Naturally the optical quality difference between high quality and low quality float glass is much less than that of plate glass and sheet glass. Generally speaking, if a technology to be used in manufacturing a simple product (the manufacturing process can be the most sophisticated one just as the case of float glass) occupies a position of dominant design there is a risk of the product becoming a commodity which means that there is only one universal product with the same price for a demanding and nondemanding applications. There is now room for differentiation of product and segmenting the market for charging different prices. In a sense the DEM should be worked in reverse way. This finding is a theoretical contribution for DEM.

## References

- [1] Edge, K. C. "Section 11, Flat Glass Manufacturing Processes (Update)" in Tooley, F. (ed.) Handbook of Glass Manufacture, 3rd Edition, Volumes I & II, Books for the Glass Industry Division, Ashlee Publishing Co., New York, pp. 714/1-21, 1984
- [2] McGrath, R., MacMillan, I. C. and Tushman, L. M. "The Role of Executive Team Actions in Shaping Dominant Designs: Towards the Strategic Shaping of Technological Progress", Strategic Management Journal, Vol. 13, pp. 137-161, 1992.
- [3] Kalafatis, S. P., Tsogas, M.H., and Blankson, C. "Positioning strategies in business markets", Journal of Business & Industrial Marketing, Vol. 15 No. 6, pp. 416-437, 2000.
- [4] Uusitalo, O. "A Revolutionary Dominant Design - The Float Glass Innovation in the Flat Glass Industry", dissertation A-108, Helsinki School of

Economics, Helsinki, 1995.

[5] Peng, S. "Present Status and Internationalization Prospect of China Float Glass Technology", Boletín de la Sociedad Española de Cerámica y Vidrio Nota Técnica, 47(2), 117-121, 2008.

[6] Barker, T. C. "The Glassmakers. Pilkington: the Rise of an International Company 1826-1976," Weidenfeld and Nicholson, London, 1977.

[7] Som, A. "Saint-Gobain: The Expansion Options", International Journal of Case Method Research & Application, 17(4), 477-487, 2005.

[8] Industry Overview [www.hkexnews.hk/listedco/listconews/SEHK/2006/.../EWP111.pdf](http://www.hkexnews.hk/listedco/listconews/SEHK/2006/.../EWP111.pdf), 2006 (read 25.4.2017).

[9] Pilkington "Pilkington and the Flat Glass Industry", 2010.

[10] UOBKayHian, China "Update Glass Sector New Demand Emerging", March, 2013, [ustrade.com.hk/en/blue-top/315201344036PM524953.pdf](http://ustrade.com.hk/en/blue-top/315201344036PM524953.pdf), (read 25.4.2017).

[11] Layton, D. W. and McConkey, M. "Vietnam issues final determination in country's first trade remedy case", March 10, Mayer Brown LLP, 2010 <http://www.lexology.com/library/detail.aspx?g=36f0ad52-6253-409e-a5f2-48b45b6521e3>, (read 25.4.2017).

[12] Nieminen, P. Answers to a questionnaire. April 2, 2017.

[13] Drucker, P. "Innovation and Entrepreneurship", Pan Books, London, 1985.

[14] Savaète, B. "25 Years (1992 - 2017) in the flat glass industry - What did we get during last 25 years in the flat glass industry (1992-2017) and what could we expect for tomorrow? in the chapter "Main mistakes we have made during last 25 years" @ BJS. Différences [Document in preparation for GPD 2017 at Tampere]

[15] Luoyang Glass Company Limited <http://lygoverseas.en.hisupplier.com/about-us.html>

# Morphological and Structural Special Features of the Gold Nanolayer Sputtered on the Glass Surface Modified by Surface Ion Exchange and Chemical Etching

Olga N. Sidelnikova<sup>1</sup>, Aleksey N. Salanov<sup>2</sup>,  
Dmitry A. Yatsenko<sup>2</sup>, Aleksandra N. Serkova<sup>2</sup>  
1 - Institute of Solid State Chemistry and  
Mechanochemistry, Novosibirsk, Russia,  
e-mail: ol\_sideln@mail.ru  
2 - Bokeskov Institute of Catalysis, Novosibirsk,  
Russia

## Key words

glass, ion exchange, chemical etching,

## X-ray structure analysis

The research data are related to X-ray structure analysis of the gold nanolayers (50, 100 and 200 nm thick) on glass surface modified by the surface ion exchange, chemical etching or by treatment combining two indicated above methods. The soda lime silica glass has been modified by the special Surface Ion Exchange Paste (SIEP) [1-3]. Na<sup>+</sup>/Li<sup>+</sup> ion exchange with SIEP has included next stages: glass surface degreasing and washing; the SIEP laying on the glass surface; thermal treatment at ~ 300° C for 15 – 20 min.; washing with running and distilled water. The chemical etching of glass have been carried out with the composition containing hydrofluoric acid [4]. The glass surface morphology has been observed by the SEM JSM-6460 (Jeol, Japan); the gold nanolayers were deposited on the glass surface by the special device JVC-1600 (Jeol, Japan).

X-ray data have been measured with diffractometer D8 Advance (CuK $\alpha$  radiation, one-dimensional detector Lynx-Eye with nickel filter). The range of the measurement was  $2\theta = 10 - 120^\circ$  with step  $0,02^\circ$  and acquisition interval 35,4 c. The program Topas 4.2 (Bruker AXS, Germany) and initial structural data of inorganic base ICSD, FIZ Karlsruhe, Germany have been also used in calculations.

Morphological special features of the gold nanolayer on the glass surface modified by surface ion exchange and chemical etching are presented in Figures 1 and 2.

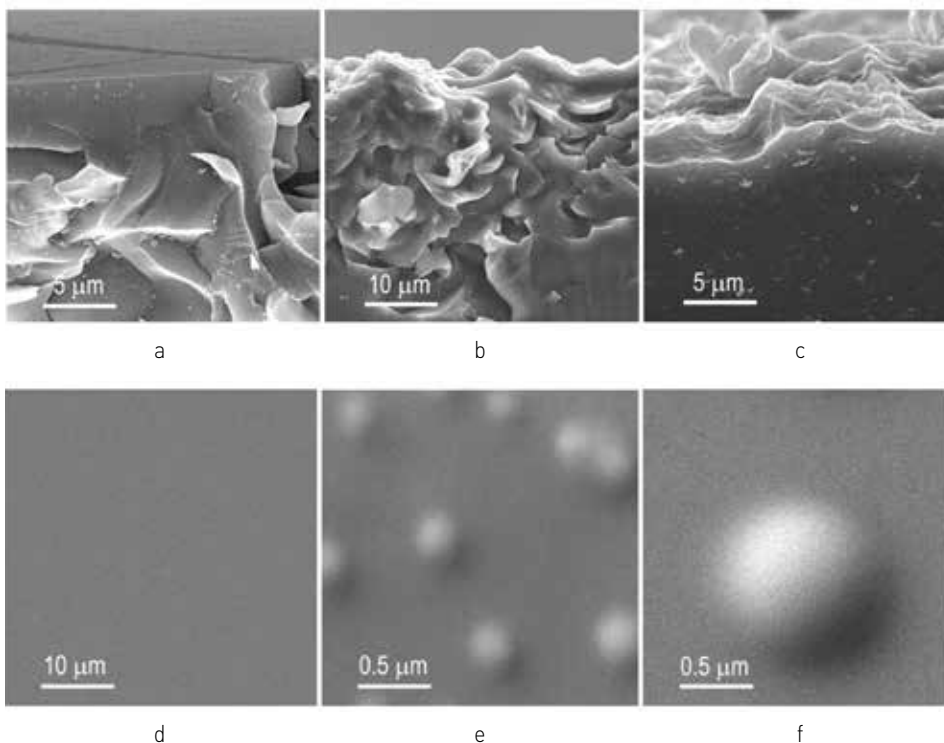


Figure 1. Morphology of gold surface nanolayer on glass: a – glass surface modified by the special Surface Ion Exchange Paste (SIEP); b – glass surface modified by treatment combining two indicated methods; c – glass surface modified by chemical etching; d – morphology of the thin gold nanolayer on the glass substrate without treatment; e, f – morphology of the gold nanolayer with hemispherical gold nanocrystals on the glass substrate without treatment.

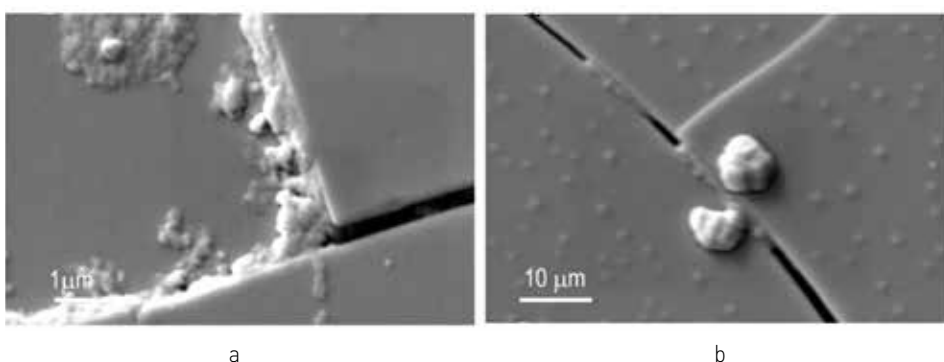


Figure 2. Morphology of gold surface nanolayer on glass: a, b – morphology of gold agglomerates on the gold surface nanolayer sputtered on the glass substrate.

X-ray data analysis allows make conclusion that the surface modification of the soda lime silica glass by the surface ion exchange and chemical etching has a substantial influence upon the size of gold crystal grains (Figure 3). Gold crystal grains have elongated shape in direction  $\langle 111 \rangle$ . The increase of the gold nanolayer thickness leads to decreasing of the crystal grains size. The least size have been related to gold nanolayer 200 nm thick on glass surface modified by combined method indicated above: in direction  $\langle 111 \rangle$  average calculated grains size is  $\sim 14.7$  nm; grains size averaged in directions  $\langle 200 \rangle$ ,  $\langle 220 \rangle$  and  $\langle 311 \rangle$  is  $\sim 6.8$  nm. Authors express thanks to N.V. Bulina for technical support.

### References

1. A.A. Sidel'nikov, D.V. Svistunov, O.N. Sidel'nikova Patent RF 2238919, (2004) 1-3.
2. O.N. Sidel'nikova, A.N. Salanov Glass and Ceramics, 64 (2007) 425 - 428.
3. O.N. Sidel'nikova, G.A. Pozdnyakov, A.N. Salanov A.N., A.N. Serkova A.N. Glass Tech.: European J. of Glass Sc. and Tech. Part A, 52 (2011) 15 - 22.
4. E.K. Lazareva, T.M. Chelsova, A.A. Vernyj Inventor's certificate USSR 948926A (1982).

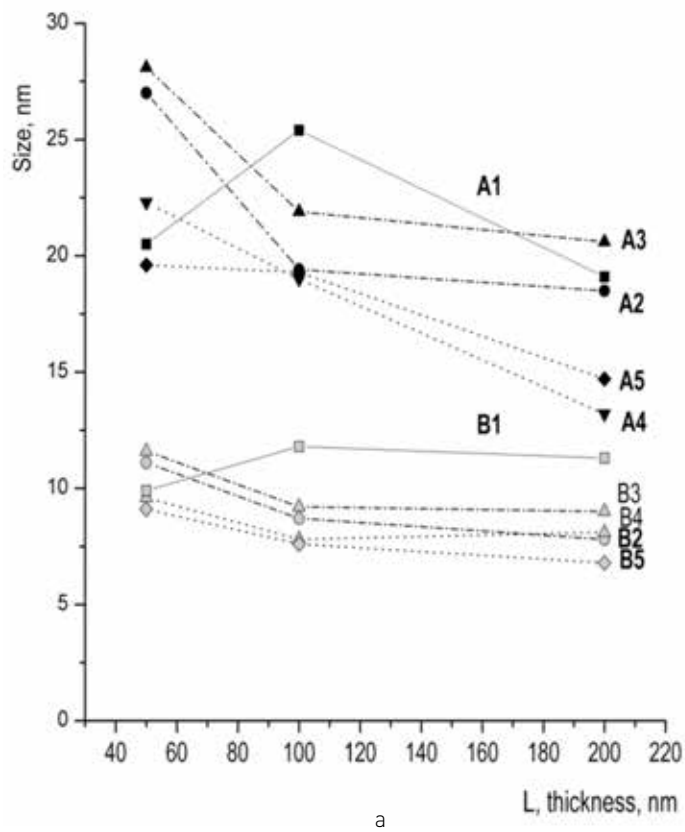


Figure 3. Dependence of the grains size on the gold nanolayer thickness: curves A1-A5 - grains size in direction  $\langle 111 \rangle$ ; curves B1-B5 - grains size averaged for directions  $\langle 200 \rangle$ ,  $\langle 220 \rangle$  and  $\langle 311 \rangle$

## Platinum sponsors

**glaston**



**kuraray** **trosifol™**  
world of interlayers

**TECNOGLASS**



## Gold sponsors

**EASTMAN**



**SIEMENS**  
*Ingenuity for life*

## Silver sponsors

**Eckersley  
O'Callaghan**



**MERCK**



Software for  
Glass + Windows



Construction Hardware Expert



The conference is supported by the following trade fairs and associations:



INTERNATIONAL TRADE FAIR FOR GLASS  
PRODUCTION - PROCESSING - PRODUCTS

[www.glasstec-online.com](http://www.glasstec-online.com)



January 14-19 - Munich

[www.bau-muenchen.com](http://www.bau-muenchen.com)



abrapidro



GANVA



Glass and Glazing  
Federation



GlassBuild  
AMERICA



Italian Glass Processing  
Machinery and Accessory  
Supplier's Association



National Glass Association



Glass Technology



VITRUM

NÜRNBERG MESSE

